DOE/WIPP 91-005
Revision 6

# Resource Conservation and Recovery Act Part B Permit Application

## Volume III of XIII

Appendix D1

**Waste Isolation Pilot Plant**
**Carlsbad, New Mexico**

# APPENDIX D1

# SITING REPORTS

THIS PAGE LEFT BLANK INTENTIONALLY

THIS DOCUMENT COPIED FROM BEST AVAILABLE ORIGINAL

THIS PAGE LEFT BLANK INTENTIONALLY

# SUMMARY OF SITE CHARACTERIZATION STUDIES CONDUCTED FROM 1983 THROUGH 1987 AT THE WASTE ISOLATION PILOT PLANT (WIPP) SITE, SOUTHEASTERN NEW MEXICO

(Lappin, A. R.)

THIS PAGE LEFT BLANK INTENTIONALLY

SANDIA REPORT
SAND88—0157 • UC—70
Unlimited Release
Reprinted January 1989

# Summary of Site-Characterization Studies Conducted From 1983 Through 1987 at the Waste Isolation Pilot Plant (WIPP) Site, Southeastern New Mexico

A. R. Lappin

Prepared by
Sandia National Laboratories
Albuquerque, New Mexico 87185 and Livermore, California 94550
for the United States Department of Energy
under Contract DE-AC04-76DP00789

SF2900Q(8-81)

Issued by Sandia National Laboratories, operated for the United States Department of Energy by Sandia Corporation.

**NOTICE:** This report was prepared as an account of work sponsored by an agency of the United States Government. Neither the United States Government nor any agency thereof, nor any of their employees, nor any of their contractors, subcontractors, or their employees, makes any warranty, express or implied, or assumes any legal liability or responsibility for the accuracy, completeness, or usefulness of any information, apparatus, product, or process disclosed, or represents that its use would not infringe privately owned rights. Reference herein to any specific commercial product, process, or service by trade name, trademark, manufacturer, or otherwise, does not necessarily constitute or imply its endorsement, recommendation, or favoring by the United States Government, any agency thereof or any of their contractors or subcontractors. The views and opinions expressed herein do not necessarily state or reflect those of the United States Government, any agency thereof or any of their contractors or subcontractors.

Printed in the United States of America
Available from
National Technical Information Service
U.S. Department of Commerce
5285 Port Royal Road
Springfield, VA 22161

NTIS price codes
Printed copy: A13
Microfiche copy: A01

SAND88-0157
Unlimited Release
Printed May 1988
Reprinted January 1989

Distribution
Category UC-70

# SUMMARY OF SITE-CHARACTERIZATION STUDIES CONDUCTED FROM 1983 THROUGH 1987 AT THE WASTE ISOLATION PILOT PLANT (WIPP) SITE, SOUTHEASTERN NEW MEXICO

A. R. Lappin
WIPP Earth Sciences Division, 6331
Sandia National Laboratories
Albuquerque, NM 87185

## ABSTRACT

The Waste Isolation Pilot Plant (WIPP) is being constructed at a depth of 650 m in bedded halites of the Salado Formation. The geologic setting of the WIPP site has been active for at least 250 million years, and is presently responding to the end of the last pluvial period, within the 10,000-year time scale of regulatory interest. Both construction of the WIPP facility and WIPP site-characterization activities impose additional transient effects, some of which will last until the hydrologic and structural closure of the facility.

The Bell Canyon Formation beneath the WIPP facility contains shales, siltstones, and sandstones. Studies suggest that no channel sandstone is present in the Bell Canyon beneath the WIPP site. Fluid movement would be downward if drilling interconnected the Bell Canyon with the Rustler Formation, the first water-bearing zone above the WIPP facility.

The Salado and Castile Formations contain abundant bedded halites and anhydrites, and deform in response to gravity. Fluids play a major role in this deformation, although the regional permeabilities of both units are extremely low. Pressurized brines may be present within the Castile Formation 200 m or more beneath the WIPP waste-emplacement panels. The hydrologic and structural characteristics of the Salado change within an altered zone extending a few meters from the WIPP underground workings.

The permeability within this altered zone is enhanced, and deformation includes local opening of preexisting fractures in anhydrite and formation of new fractures in halite. Within a few meters of the facility the Salado characteristics become those of the far field, in which permeability is extremely low and deformation is dominated by creep. Brine seepage into the WIPP facility is extremely slow, and involves transient behavior resulting from the combined effects of deformation, low permeability, and ventilation.

At the WIPP site, the hydrology and geochemistry of the Rustler Formation and younger units overlying the Salado are dominated by confined flow within the Culebra dolomite. Rustler karst is not present at the WIPP site, but is present in and near Nash Draw. The combination of modern heads and transmissivities of units other than the Culebra indicates the potential for limited vertical flow within the Rustler, and from the Salado into the Rustler, but is not consistent with infiltration of water from the surface to the Rustler carbonates at the WIPP site. Isotopic studies indicate that surficial water was required for formation of secondary gypsum veins within the Dewey Lake Red Beds overlying the Rustler. The distribution of hydrochemical facies in Culebra groundwaters and the results of stable-isotope, radiocarbon, and uranium-disequilibrium studies are all consistent with the interpretation that there is no modern recharge to the Rustler at the WIPP site, and that a change of flow directions in the Culebra dolomite has occurred over approximately the last 10,000 years.

The transmissivity of the Culebra dolomite varies by approximately 6 orders of magnitude at and near the WIPP site. The transmissivity in the central portion of the site, including the locations of all four WIPP shafts, is low (less than $10^{-6}$ $m^2/s$). Higher Culebra transmissivities are found south, northwest, and west of the site, especially in Nash Draw. Fracturing within the Culebra affects local hydrology and contaminant transport, but is not significant in regional-scale behavior at and near the site, at least so long as the present distribution of head potentials is not significantly disturbed.

## SUMMARY

The Waste Isolation Pilot Plant (WIPP), which is designed for receipt, handling, storage, and permanent isolation of defense-generated transuranic wastes, is being excavated at a depth of approximately 655 m in bedded halites of the Permian Salado Formation of southeastern New Mexico. Site-characterization activities at the present WIPP site began in 1976. Full construction of the facility began in 1983, after completion of "Site and Preliminary Design Validation" (SPDV) activities and reporting. Site-characterization activities since 1983 have had the objectives of updating or refining the overall conceptual model of the geologic, hydrologic, and structural behavior of the WIPP site and providing data adequate for use in WIPP performance assessment.

This report has four main objectives:

1. Summarize the results of WIPP site-characterization studies carried out since the spring of 1983 as a result of specific agreements between the U.S. Department of Energy and the State of New Mexico.

2. Summarize the results and status of site-characterization and facility-characterization studies carried out since 1983, but not specifically included in mandated agreements.

3. Compile the results of WIPP site-characterization studies into an internally consistent conceptual model for the geologic, hydrologic, geochemical, and structural behavior of the WIPP site. This model includes some consideration of the effects of the WIPP facility and shafts on the local characteristics of the Salado and Rustler Formations.

4. Discuss the present limitations and/or uncertainties in the conceptual geologic model of the WIPP site and facility.

The objectives of this report are limited in scope, and do not include determination of whether or not the WIPP Project will comply with repository-performance criteria developed by the U.S. Environmental Protection Agency (40CFR191). When combined, the results of recent and previous geologic studies of the WIPP site form a conceptual model, summarized below. The model presented is limited to aspects relevant to WIPP site characterization and, ultimately, performance assessment.

The overall geologic and hydrologic setting of the WIPP site area has been transient (not steady-state) since before the beginning of deposition of the Bell Canyon Formation, approximately 250 million years ago, and will continue to be transient after effective closure of the WIPP facility. Some events, such as crystallization of secondary minerals within the Salado Formation approximately 200 million years ago and formation of the Mescalero caliche 400,000 to 500,000 years ago, have taken place on a very long time scale relative to WIPP performance assessment, which must consider only a 10,000-year time frame. Two types of transient response

have occurred or are occurring at and near the WIPP site within the 10,000-year time frame of regulatory interest. These are: a) the continuing natural response of the geologic and hydrologic systems to the end of the last pluvial period (period of decreased temperatures and increased precipitation) in southeast New Mexico; and b) the continuing responses to hydrologic, geochemical, and structural transients resulting from WIPP site characterization and facility construction. The transient responses induced by the presence of the WIPP underground workings will continue until reequilibration following effective structural and hydrologic closure of the facility.

The Bell Canyon Formation, consisting largely of shales, siltstones, and sandstones, contains the first relatively continuous water-bearing zone beneath the WIPP facility. In some parts of the northern Delaware Basin, the unit contains permeable channel sandstones that are targets for hydrocarbon exploration. Recent studies suggest that the upper Bell Canyon at the WIPP site does not contain any major channel sandstone. This decreases the probability of the Bell Canyon serving as a source of fluids for dissolution of overlying evaporites at the WIPP. These same studies indicate that the final direction of fluid flow following interconnection of the Bell Canyon, Salado, and Rustler Formations within a drillhole would be downward into the Bell Canyon, after accounting for density increases in the fluids due to dissolution of halite within the Salado. It is assumed here that the measured hydrologic characteristics of the Bell Canyon Formation are more significant to WIPP performance assessment than those of underlying units. The head distribution within the upper Bell Canyon near the WIPP site indicates flow towards the northeast.

Both regional studies and studies within the WIPP facility indicate that the Castile and Salado Formations, both of which are made up predominantly of layered anhydrites and halites, should be considered as low-permeability units that deform regionally in response to gravity. In general, permeabilities and fluid-flow rates in both units are very low and are insensitive to stratigraphy. Formation permeabilities in the Castile and Salado Formations remote from the WIPP excavations are generally less than 0.1 microdarcy, and the regional water content of Salado halites is up to 2 weight percent. Exceptions include local brine occurrences in Castile anhydrites and gas occurrences in the Salado Formation, both of which are fracture-controlled, can be large in volume, and can be under pressures high enough to cause fluid flow to the surface. No major gas occurrence within the Salado Formation has been encountered at the WIPP site. In fact, where it has been possible to measure far-field brine pressures within the Salado, the pressures, permeabilities, and available brine volumes combine to indicate the potential for only very limited fluid flow upwards into the overlying Rustler Formation. It is not certain that the Castile and Salado Formations are hydrologically saturated regionally.

Pressurized Castile brines have been encountered in Castile anhydrite in hole WIPP-12, approximately 1.5 km north of the center of the WIPP site. Geophysical studies indicate that Castile brines may be present beneath a portion of the WIPP waste-emplacement panels, consistent with earlier assumptions. These brines are stratigraphically 200 m or more below the

WIPP facility horizon and are not of concern except in the case of human-intrusion breach of the facility.

In the western part of the Delaware Basin, extensive halite dissolution has apparently taken place in both the Castile and Salado Formations. However, much of the variability in structure and internal stratigraphic thicknesses within the Castile and Salado Formations results from deformation and original depositional variability, rather than from evaporite dissolution. Regional or far-field deformation of the Castile and Salado Formations involves pressure solution as a major mechanism, due to the presence of intergranular fluids, but occurs too slowly to be of future concern to the WIPP Project. Structures within hole DOE-2 result from deformation rather than dissolution.

The hydrologic and structural characteristics of the Salado Formation in the disturbed zone generated by the presence of the WIPP facility are different than those in the far field. Formation permeability within a couple of meters of the underground workings at the facility horizon increases significantly. Near-field deformation of the Salado Formation involves both the opening of preexisting fractures in anhydrite beneath the facility horizon (Marker Bed 139) and generation of new fractures in halite. Fluid contents in the disturbed zone at the facility horizon decrease in response to facility ventilation and/or deformation. Within a few meters of the underground workings, both hydrologic and structural behavior of the Salado Formation become essentially those of the far field. Brine seepage into the WIPP facility includes a significant transient phase, which will probably last until effective facility closure. The results of preliminary hydrologic testing in the Salado Formation adjacent to the WIPP air-intake shaft indicate extremely low permeabilities, with no apparent stratigraphic variability. The results also indicate that development of a disturbed zone around the WIPP shafts is less extensive than at the facility horizon. The extent, characteristics, and importance of the disturbed-rock zones around the WIPP shafts and at the facility horizon remain to be determined in detail.

At and near the WIPP site, the Rustler Formation should be considered as a layered unit of anhydrites, siltstones, and halites, containing a thin and variably fractured carbonate unit, the Culebra dolomite. The Culebra dolomite is the first continuous water-bearing unit above the WIPP facility and, at the WIPP site, is at least an order of magnitude more permeable than other members of the Rustler Formation, including the Magenta dolomite. The transmissivities of Rustler anhydrites at the WIPP site are too low to measure. As a result, the Culebra dominates fluid flow within the Rustler Formation at the WIPP site and is the most significant pathway to the accessible environment from the WIPP facility, except for direct breach to the surface by human intrusion. The transmissivity of the Culebra varies by approximately six orders of magnitude in the region containing the WIPP site. The Culebra transmissivity in the central portion of the site, including the locations of all four WIPP shafts, is low. Higher Culebra transmissivities are found in areas southeast and northwest of the central part of the site. Fluid flow rates within the Culebra are very low at the site center and in regions to the east, but

relatively high within Nash Draw. Modern flow in the Culebra is confined and largely north-south in the area of the WIPP site.

Fluid flow and geochemistry within the Culebra dolomite and shallower units are in continuing transient response to the marked decrease or cessation of local recharge at approximately the end of the last pluvial period. Both bulk chemistry and isotopic relations within Culebra fluids are inconsistent with modern flow directions if steady-state confined flow is assumed. Because of the relative head potentials within the Rustler Formation at and near the WIPP site, there must be a small amount of vertical fluid flow between its members, even though the permeabilities of Rustler members other than the Culebra dolomite are quite low. Where measured successfully, the modern head potentials within the Rustler prevent fluid flow from the surface downward into the Rustler carbonates. These results do not prohibit either the modern movement of fluids from the underlying Salado Formation upwards into the Rustler Formation or the downward movement of Dewey Lake waters into the Rustler Formation during or even after the cessation of local recharge at the end of the last pluvial period. They do, however, suggest that recharge from the surface to the Rustler Formation is not now occurring at the WIPP site. The results of stable-isotope, radiocarbon, and uranium-disequilibrium studies are also consistent with the interpretation that there is no measurable modern recharge to the Culebra dolomite from the surface at and near the WIPP site. The transient hydrologic response of the Rustler Formation to the end of the last pluvial period has involved at least some change in flow directions in the Culebra dolomite. Although the modern flow is largely north-south, the results of uranium-disequilibrium studies suggest that flow was more easterly during previous recharge.

Within and near Nash Draw, evaporite karst is operative within the Rustler, as evidenced by the continuing development of small caves and sinkholes in near-surface anhydrites and gypsums of the Forty-niner and Tamarisk Members. There is no evidence of karstic hydrology in the Rustler at and near the WIPP site. However fracturing of some portions of the Culebra dolomite is sufficient at the site to strongly affect both hydraulic and transport behavior on the hydropad scale, i.e., over distances of approximately 30 m. Interpretation of multipad interference tests conducted both north and south of the center of the WIPP site indicates that this fracturing need not be incorporated into numerical modeling of the regional-scale hydraulic behavior of the Culebra east of Nash Draw. Similarly, detailed transport calculations indicate that effects due to fracturing are not significant in regional-scale transport within the Culebra dolomite at and near the WIPP site, at least as long as the modern head distribution is not significantly disturbed and the calculated flow directions and transport properties are representative.

The Dewey Lake Red Beds overlying the Rustler Formation consist largely of siltstones and claystones, with subordinate sandstones. In tested locations, the Dewey Lake may be hydrologically unsaturated, but is too low in permeability for successful hydrologic testing. South of the WIPP site, near an area where the unit may be receiving modern recharge, sandstones within the Dewey Lake locally produce potable water. In general, water

levels within the Dewey Lake Red Beds, like those in the underlying Rustler Formation, must be in transient response to the end of the last pluvial period. Isotopic relations suggest that surficial waters have been involved in the formation of secondary gypsum veins within the Dewey Lake, but that the Dewey Lake and Rustler hydrologic systems are largely separate.

The major near-surface units at the WIPP site are the Gatuna Formation and Mescalero caliche. The sandstones and stream-channel conglomerates within the Gatuna indicate that major changes in local climate have occurred over (at least) the last 600,000 years. The widespread preservation of the Mescalero caliche indicates not only the relative structural stability of the Livingston Ridge surface (on which the WIPP surface facilities are sited) over the last 400,000 years, but also that infiltration over this same time period has not been sufficient to dissolve a layer of carbonate 1 to 2 m thick.

## ACKNOWLEDGMENTS

Thanks to all authors of the detailed technical documentation upon which this report is based, particularly those authors who carefully reviewed portions of this report. Special thanks are extended to Regina Hunter and Dennis Powers for their additional editorial reviews.

Thanks also to Jo Ryan, Ellen Cronin, Georgia Bowens, Tina Johnson, and Dan Garber for their assistance in preparing the text, tables, and figures.

CONTENTS


Page

1.0 INTRODUCTION..... 1

1.1 Report Objectives..... 5
1.2 Structure of Report..... 5
1.3 General Stratigraphic Setting of the WIPP Site and Facility..... 6
1.4 Technical Issues of Interest in WIPP Site and Facility Characterization..... 10

1.4.1 Transient Versus Steady-State Geologic, Hydrologic, and Geochemical Setting of the WIPP..... 10
1.4.2 Dissolution of Evaporitic Rocks at and near the WIPP Site..... 11
1.4.3 Directions of Fluid Flow to Be Expected if the Rustler and Bell Canyon Formations Are Interconnected..... 16
1.4.4 Distribution and Origin of Brine Occurrences within Castile Anhydrites..... 16
1.4.5 Deformation of the Castile and Salado Formations..... 18
1.4.6 Fluid Flow within the Salado Formation..... 19
1.4.7 Present-Day Hydrology, Transport Behavior, and Geochemistry of the Rustler Formation..... 20

2.0 BELL CANYON FORMATION..... 22

2.1 Potential for the Bell Canyon Formation to Serve as a Source of Fluids for Dissolution of Evaporites in the Castile and Salado Formations..... 22
2.2 Expected Directions of Fluid Flow Between the Bell Canyon and Rustler Formations..... 23

2.2.1 Results from Hole Cabin Baby-1..... 24
2.2.2 Results from Hole DOE-2..... 26

3.0 CASTILE AND SALADO FORMATIONS..... 28

3.1 Regional and Local Variability, Deformation, and Dissolution of the Castile and Salado Formations..... 29

3.1.1 Regional Relationships and Behavior..... 29
3.1.2 The DOE-2 Structure..... 37

3.2 Occurrence and Origin of Pressurized Brines within Anhydrites of the Castile Formation..... 38
3.3 Recent Hydrologic, Geochemical, and Structural Studies of the Salado Formation..... 43

CONTENTS (Continued)

Page

3.3.1 Regional-Scale and Near-Facility Hydrology of the Salado Formation..... 43

3.3.1.1 Hydrologic Testing from the Surface and at the Facility Horizon..... 43
3.3.1.2 Hydrologic Testing Adjacent to the WIPP Air-Intake Shaft..... 47
3.3.1.3 Brine Contents and Brine Seepage into the WIPP Facility..... 52

3.3.2 Geochemical and Mineralogical Studies of the Salado Formation Near the Facility Horizon..... 56
3.3.3 Marker Bed 139 and the Structural Behavior of the Salado Formation near the WIPP Facility..... 61

4.0 RUSTLER FORMATION AND YOUNGER UNITS..... 66

4.1 Hydrologic Testing of the Rustler Formation and Dewey Lake Red Beds..... 66

4.1.1 Single-Hole Hydraulic Testing and Interpretation..... 68

4.1.1.1 Transmissivity Distribution within Individual Units..... 68
4.1.1.2 Head Distribution within the Rustler Formation and between the Rustler, Dewey Lake, and Salado..... 79

4.1.2 Single-Pad Interference Testing..... 82

4.1.2.1 Interference Testing at the H-3 Hydropad.... 82
4.1.2.2 Interference Testing at the H-11 Hydropad and Comparison with Results at the H-3 Pad.. 84

4.1.3 Multipad Interference Testing..... 88

4.1.3.1 The H-3 Multipad Interference Test and the Regional Culebra Model of Haug et al. (1987)..... 89
4.1.3.2 The WIPP-13 Multipad Interference Test and the Regional Culebra Model of LaVenue et al. (1988)..... 110

4.2 Pad-Scale and Regional-Scale Studies of Contaminant Transport within the Culebra Dolomite..... 130

4.2.1 Hydropad-Scale Transport of Conservative Tracers at the H-3 and H-4 Hydropads..... 131

CONTENTS (Continued)

Page

4.2.1.1 Conservative-Tracer Tests at the H-3 Hydropad..... 132
4.2.1.2 Conservative-Tracer Tests at the H-4 Hydropad..... 141

4.2.2 Regional-Scale Contaminant Transport in the Culebra Dolomite under Low-Pressure Conditions..... 146

4.3 Geochemical Studies in the Rustler Formation and Shallower Units..... 155

4.3.1 Solute Geochemistry and Delineation of Hydrochemical Facies within the Culebra Dolomite..... 156

4.3.1.1 Hydrochemical Facies..... 156
4.3.1.2 Normative Salt Assemblages of Rustler Waters..... 169
4.3.1.3 Saturation Indices and Factor Analysis of Culebra Waters..... 171
4.3.1.4 Estimated Oxidation-Reduction Potentials of Culebra Waters..... 176
4.3.1.5 Mineralogy of the Culebra Dolomite..... 178

4.3.2 Recent Stable-Isotope Studies of Groundwaters from the Rustler Formation and Younger Units..... 181

4.3.2.1 The Character of Modern Recharge in the Northern Delaware Basin..... 181
4.3.2.2 The Hydrology of the WIPP Site and Vicinity Relative to Modern Recharge..... 185

4.3.3 Recent Isotopic Studies with Emphasis on Radiocarbon..... 194
4.3.4 Uranium-Disequilibrium Studies in the Culebra Dolomite..... 201

4.4 Recent Studies Addressing Near-Surface Geology and Hydrology at and near the WIPP Site..... 208

4.4.1 Recent Studies of Near-Surface Stratigraphy at and near the WIPP Site..... 209
4.4.2 Recent Studies of Evaporite Dissolution and/or Vertical Fluid Movement within the Rustler and Younger Formations..... 215

4.4.2.1 General Geologic Studies..... 215
4.4.2.2 Isotopic Studies..... 220

CONTENTS (Concluded)


Page

5.0 SUMMARY OF WIPP SITE-CHARACTERIZATION ACTIVITIES, 1983 THROUGH 1987 ..... 228

5.1 General Conceptual Model for the Geologic Behavior of the WIPP Site and Facility ..... 228

5.2 Individual Conclusions and Discussions ..... 231

5.2.1 Conclusions Concerning the Overall Geologic and Hydrologic Setting of the WIPP Site and Vicinity ..... 232

5.2.2 Conclusions Concerning the Bell Canyon Formation ..... 235

5.2.3 Conclusions Concerning the Castile and Salado Formations ..... 236

5.2.4 Conclusions Concerning the Rustler Formation and Younger Units ..... 241

6.0 REFERENCES ..... 251

## Figures


Page

1.1: Setting of the WIPP site relative to the northern Delaware Basin..... 2

1.2: Boreholes at and near the WIPP site referred to in text..... 4

1.3: Lateral distribution and thicknesses of channel sands in the informal Ramsey member of the Bell Canyon Formation in the northern Delaware Basin, including holes DOE-2 and Cabin Baby-1..... 7

1.4: Generalized distribution of the Castile and Salado Formations in the Delaware Basin, with emphasis on distribution of halites..... 13

1.5: Generalized halite distribution within the Rustler Formation at and near the WIPP site..... 15

1.6: Generalized distribution of Castile brine occurrences and approximate extent of the Castile "Disturbed Zone" in the northern Delaware Basin..... 17

3.1: Generalized stratigraphic cross section of the Salado and Castile Formations between holes Cabin Baby-1 and WIPP-11..... 30

3.2: Hole locations used in Figure 3.1..... 31

3.3: Deformation map for halite, assuming all deformation is anhydrous..... 34

3.4: Deformation map for halite, assuming fluids present and considering pressure solution as a major deformation mechanism..... 35

3.5: Contour map of apparent depth to first major deep conductor in survey including area of WIPP waste-emplacement panels, in meters..... 40

3.6: Cross section of apparent depth to first major deep conductor, showing brine locally present in both the Bell Canyon and Castile Formations..... 41

3.7: Summary of formation conductivities determined in 1987 testing in the WIPP waste-handling shaft..... 50

3.8: Summary of fluid formation pressures determined in 1987 testing in the WIPP waste-handling shaft..... 51

3.9: Apparent variation in water content of Salado halite at the WIPP facility horizon with depth into the wall..... 53

Figures (Continued)


Page

3.10: Compositional variability of Salado fluids from fluid inclusions and macroscopic brine occurrences in the WIPP facility..... 57

3.11: Stable-isotope composition of fluids from the Rustler/Salado contact and deeper evaporite zones at the WIPP site..... 59

3.12: Generalized stratigraphic and structural cross section of MB139..... 62

3.13: Variations in approximate overburden pressure at the WIPP facility horizon as a function of time..... 64

4.1.1: Measured and simulated response of H-3b1 to pumping of hole H-3b2..... 69

4.1.2: Transmissivity of the Culebra dolomite in relation to the distribution of halite within the Rustler Formation..... 74

4.1.3: Head relations among units in the Rustler Formation and between the Rustler, Dewey Lake Red Beds, and Salado at the WIPP site..... 80

4.1.4: Physical layout of the H-3 hydropad..... 83

4.1.5: Physical layout of the H-11 hydropad..... 86

4.1.6: Pumping and observation wells for the H-3 multipad interference test..... 90

4.1.7: Observed drawdown versus the square root of time in hole H-3b2 during the H-3 multipad interference test..... 93

4.1.8: Comparison of measured and simulated responses at H-11 and DOE-1 during the H-3 multipad interference test, assuming perfectly linear flow..... 94

4.1.9: Initial kriged Culebra transmissivities, based on data available as of April 1986..... 96

4.1.10: Estimation error in initial kriged Culebra transmissivities, based on data available as of April 1986..... 97

4.1.11: Best estimate of pre-shaft Culebra freshwater equivalent heads, based on data available as of April 1986..... 98

4.1.12: Best calculated distribution of Culebra transmissivities, based on pressure calibration to head distribution shown in Figure 4.1.11..... 99

Figures (Continued)


Page

4.1.13: Best estimate of density distribution of Culebra fluids, based on information available as of April 1986..... 101

4.1.14: Calculated steady-state, brine-density distribution within the Culebra Dolomite, based on data available as of April 1986..... 103

4.1.15: Difference between calculated steady-state brine density distribution within the Culebra (Figure 4.1.14) and the estimated distribution shown in Figure 4.1.13..... 104

4.1.16: Final calculated Culebra transmissivities and flow directions, based on data available as of April 1986..... 108

4.1.17: Pumped and observation wells for the WIPP-13 multipad interference test..... 111

4.1.18: Measured and simulated hydrologic response of WIPP-13 during the pumping phase of the WIPP-13 multipad interference test..... 112

4.1.19: Initial kriged Culebra transmissivities, based on data available as of November, 1987..... 116

4.1.20: Estimation error in initial kriged Culebra transmissivities (one standard deviation), based on data available as of November 1987, assuming no uncertainty in individual measurements..... 117

4.1.21: Estimation error in initial kriged Culebra transmissivities (one standard deviation), including estimated uncertainty in individual measurements..... 118

4.1.22: Measured density distribution of Culebra fluids, based on information available as of November 1987..... 120

4.1.23: Estimate of pre-shaft, freshwater-equivalent heads in the Culebra dolomite, based on data available as of November 1987..... 122

4.1.24: Calculated Culebra transmissivities at and near the WIPP site, based on steady-state calibration against freshwater-equivalent head distribution shown in Figure 4.1.23, fixing in place the fluid-density distribution shown in Figure 4.1.22..... 124

4.1.25: Calculated pre-shaft, freshwater-equivalent head distribution in the Culebra dolomite, based on calibrated transmissivity distribution shown in Figure 4.1.24..... 126

Figures (Continued)


Page

4.1.26: Difference between calculated Culebra head distribution (Figure 4.1.25) and measured pre-shaft head distribution (Figure 4.1.23) ..... 127

4.1.27: Calculated Darcy-velocity vectors in the Culebra dolomite, assuming the transmissivity distribution shown in Figure 4.1.24 and head distribution shown in Figure 4.1.25 ..... 128

4.1.28: Calculated particle flowpaths and flow times within the Culebra dolomite, assuming steady-state and the transmissivity and head distributions shown in Figures 4.1.24 and 4.1.25 ..... 129

4.2.1: Observed tracer behavior during the convergent-flow test at the H-3 hydropad ..... 133

4.2.2: Best-fit simulation of measured transport behavior along the the H-3b1 - H-3b3 flow path, assuming matrix tortuosity of 0.15 ..... 136

4.2.3: Best-fit simulation of measured transport behavior along the H-3b1 - H-3b3 flow path, assuming matrix tortuosity of 0.45 ..... 137

4.2.4: Best-fit simulation of measured transport behavior along the H-3b2 - H-3b3 flow path, assuming matrix tortuosity of 0.15 ..... 138

4.2.5: Best-fit single-porosity and dual-porosity simulations of tracer behavior along the H-3b1 - H-3b3 flow path when both simulations are forced to match the time of peak concentration ..... 139

4.2.6: Calculated total masses of tracer m-TFMB in matrix and fractures as a function of time after injection ..... 140

4.2.7: Physical layout of the H-4 hydropad ..... 143

4.2.8: Best-fit simulation of m-TFMB behavior during testing at the H-4 hydropad, assuming effective injection and stability of 1 kg of tracer and control of behavior by the specified numbers of high-permeability zones ..... 145

4.2.9: Release points into the Culebra Dolomite and flow paths to the accessible environment considered by Reeves et al. (1987) ..... 148

Figures (Continued)


Page

4.2.10: Comparison of base-case, regional-scale transport behavior of a conservative contaminant in the Culebra dolomite under discrete-fracture, dual-porosity, and porous-medium assumptions..... 150

4.2.11: Estimated effect of variations in diffusion time on breakthrough, otherwise assuming base-case Culebra properties.... 152

4.2.12: Variations in calculated breakthrough times to the boundary of WIPP zone 3 as a function of assumed matrix retardation, otherwise assuming base-case Culebra properties..... 154

4.3.1: Summary of hydrochemical facies and local flow directions in the Culebra dolomite..... 167

4.3.2: Piper (trilinear) diagram for analyzed Culebra fluids..... 168

4.3.3: Variation in calculated halite saturation indices of Culebra waters as a function of ionic strength..... 172

4.3.4: Variation in calculated gypsum and anhydrite saturation indices of Culebra waters as a function of ionic strength.... 173

4.3.5: Variations in calculated dolomite saturation indices of Culebra waters as a function of calculated gypsum indices (Figure 4.3.4)..... 174

4.3.6: Variability in approximate redox potential of waters from several Culebra wells..... 177

4.3.7: Fence diagram of variations in bulk mineralogy of core samples of the Culebra dolomite along the east-west section including holes WIPP-29, H-7, and H-10..... 179

4.3.8: Available stable-isotope analyses of waters from the unconfined portion of the Capitan limestone in Carlsbad Caverns, New Mexico..... 183

4.3.9: Recent stable-isotope analyses of surficial and near-surface waters in the northern Delaware Basin..... 184

4.3.10: Stable-isotope compositions of waters from the Culebra and Magenta dolomites at and near the WIPP site..... 186

4.3.11: Comparison of stable-isotope character of waters from unconfined and confined portions of the Capitan limestone... 187

4.3.12: Relationship between oxygen fractionation and chloride content for analyzed fluids from the Culebra, Magenta, and Rustler/Salado contact..... 190

Figures (Continued)


Page

4.3.13: Stable-isotope character of waters from the Rustler/Salado contact, compared with modern precipitation in the northern Delaware Basin..... 191

4.3.14: Possible derivation of Carlsbad Caverns waters from modern precipitation..... 193

4.3.15: Relationship between calculated percent modern carbon (PMC) and bicarbonate in analyzed fluids..... 195

4.3.16: Relationship between $^{13}C$ fractionation and bicarbonate for analyzed fluids..... 197

4.3.17: Relationship between percent modern carbon and $^{13}C$ fractionation for analyzed fluids..... 198

4.3.18: $^{234}U/^{238}U$ activity ratios in analyzed Culebra fluids..... 203

4.3.19: Contours of $^{234}U/^{238}U$ activity ratios in analyzed fluids, relaxing constraint of linear variation between data points..... 205

4.3.20: Total dissolved uranium content of analyzed fluids..... 207

4.4.1: Distribution and thickness of the Gatuna Formation at and near the WIPP site..... 210

4.4.2: Probable distribution of stream channels and flow directions at and near the WIPP site during Gatuna time..... 211

4.4.3: Distribution and thickness of Triassic rocks at and near the WIPP site..... 212

4.4.4: Distribution and thickness of the Dewey Lake Red Beds at and near the WIPP site..... 213

4.4.5: Columnar cross section across the WIPP site, showing lithologic correlations and variability of units in the Rustler Formation..... 218

4.4.6: Hole locations used in Figure 4.4.5..... 219

4.4.7: $^{87}Sr/^{86}Sr$ in Ochoan and related rocks at and near the WIPP site..... 221

4.4.8: $^{87}Sr/^{86}Sr$ in coexisting mineral pairs from veins and Ochoan host rocks at and near the WIPP site..... 223

Figures (Concluded)

Page

4.4.9: Deuterium distribution of the waters of crystallization of gypsums from the Dewey Lake Red Beds (squares) and Rustler Formation (circles) at and near the WIPP site, as a function of variations in rock/water ratio involving only Rustler-type water, the range in deuterium content of which is taken from Figure 4.3.10 ..... 224

4.4.10: Deuterium distribution of the waters of crystallization of gypsums from the Dewey Lake Red Beds (squares) and Rustler Formation (circles) at and near the WIPP site, as a function of variations in rock/water ratio involving only surface-type water, the range in deuterium content of which is taken from consistent data in Figures 4.3.8 and 4.3.9 ..... 225

## Tables


Page

1.1: Generalized stratigraphic column of the Delaware Mountain Group and younger sedimentary rocks at and near the WIPP site ..... 3

1.2: Generalized stratigraphy of the Rustler Formation at and near the WIPP site ..... 9

2.1: Summary of hydrologic test results from the Bell Canyon Formation in Cabin Baby-1 and DOE-2 ..... 25

3.1: Summary of known Salado gas occurrences and measured wellhead pressures from surface drilling ..... 44

3.2: Summary of Salado hydrologic properties interpreted in hydrologic testing from surface ..... 45

3.3: Summary of results of 1987 hydrologic testing in the WIPP waste-handling shaft ..... 49

4.1: Transmissivity data bases used in numerical modeling of the Culebra dolomite in Barr et al. (1983), Haug et al. (1987), and LaVenue et al. (1988) ..... 70

4.2: Detailed summary of recent single-well test results in the Culebra dolomite ..... 71

4.3: Summary of available transmissivity information for members of the Rustler Formation in holes H-14, H-16, and DOE-2 ..... 78

4.4: Summary of single-pad interference testing results for the Culebra dolomite at the H-3 and H-11 hydropads ..... 85

4.5: Summary of apparent hydraulic anisotropy of the Culebra dolomite ..... 88

4.6: Summary of results of analytical interpretation of H-3 multi-pad interference test ..... 91

4.7: Summary of analytical interpretation of results of the WIPP-13 multipad interference test ..... 113

4.8: Summary of observed tracer behavior during the convergent-flow test at the H-3 hydropad ..... 134

4.9: Input and best-fit calibration parameters from interpretation of the conservative-tracer test at the H-3 hydropad ..... 135

4.10: Summary of observed tracer behavior during the convergent-flow, conservative-tracer test at the H-4 hydropad ..... 144

Tables (Concluded)

Page

4.11: Base-case Culebra transport properties and ranges of properties considered in regional-scale transport within Culebra dolomite..... 149

4.12: Estimated importance of different parameters in regional-scale contaminant transport within the Culebra dolomite..... 153

4.13a: Major solutes and other parameters in analyzed groundwaters from the Culebra, Magenta, Dewey Lake, and Bell Canyon..... 157

4.13b: Minor and trace solutes and other parameters in analyzed groundwaters from the Culebra, Magenta, Dewey Lake, and Bell Canyon..... 161

4.14: Summary of possible rock-water reactions affecting compositions of Culebra fluids..... 181

4.15: Results of application of different interpretative models to available radiocarbon analyses, including corrections involving dolomite..... 200

THIS PAGE LEFT BLANK INTENTIONALLY

# SUMMARY OF SITE-CHARACTERIZATION STUDIES CONDUCTED FROM 1983 THROUGH 1987 AT THE WASTE ISOLATION PILOT PLANT (WIPP) SITE, SOUTHEASTERN NEW MEXICO

## 1.0 INTRODUCTION

The Waste Isolation Pilot Plant (WIPP) in southeastern New Mexico (Figure 1.1) is designed for the receipt, handling, storage, and disposal of defense-generated transuranic (TRU) wastes. The WIPP underground facilities are currently being constructed at a depth of approximately 655 m in bedded halites in the lower portion of the Salado Formation (Table 1.1). First receipt of waste is scheduled for October 1988.

WIPP site-characterization activities began in 1976 with the drilling of hole ERDA-9 near the center of the site (Sandia National Laboratories and United States Geologic Survey, 1983) (Figure 1.2). As used here, the term "WIPP site" specifically refers to the sixteen square miles of T22S, R31E contained within WIPP Zone 3 and shown in Figure 1.2. This terminology is used for internal consistency within the report. Construction of the WIPP facility and monitoring of its underground structural and hydrologic behavior began in 1981, with construction of two shafts and limited underground workings.

WIPP site-characterization and facility-characterization studies through March 1983 are documented in several reports, including: 1) the WIPP Geologic Characterization Report (Powers et al., 1978); 2) the WIPP Final Environmental Impact Statement (FEIS) (U.S. Department of Energy, 1980); and 3) both summary and topical reports completed as part of the WIPP Site and Preliminary Design Validation (SPDV) effort (e.g., Beauheim et al., 1983a; Borns et al., 1983; Lambert, 1983; Popielak et al., 1983; Weart, 1983; Wood et al., 1982).

After the SPDV studies were completed and documented, the U.S. Department of Energy and the State of New Mexico agreed to several additional site-characterization activities, which, with one exception, were scheduled for completion by January 1988. The specific studies are described in Appendices I and II to the "Agreement for Consultation and Cooperation Between [the U.S.] Department of Energy and the State of New Mexico on the Waste Isolation Pilot Plant" (1981), and are referred to here as "C&C studies." Some non-C&C studies, such as a major regional-scale interference test of the Culebra dolomite, have also been carried out since 1983. A reactive-tracer experiment in the Culebra dolomite, originally a C&C study, was deleted during 1987, by agreement between DOE and the State of New Mexico. Studies agreed to in lieu of the reactive-tracer experiment should, with a few exceptions, be completed and reported by approximately December 1988.

Thus, formal WIPP site-characterization activities will end approximately December 1988. However, understanding of the geologic, hydrologic, and geochemical behavior of the WIPP facility (and site) will continue to

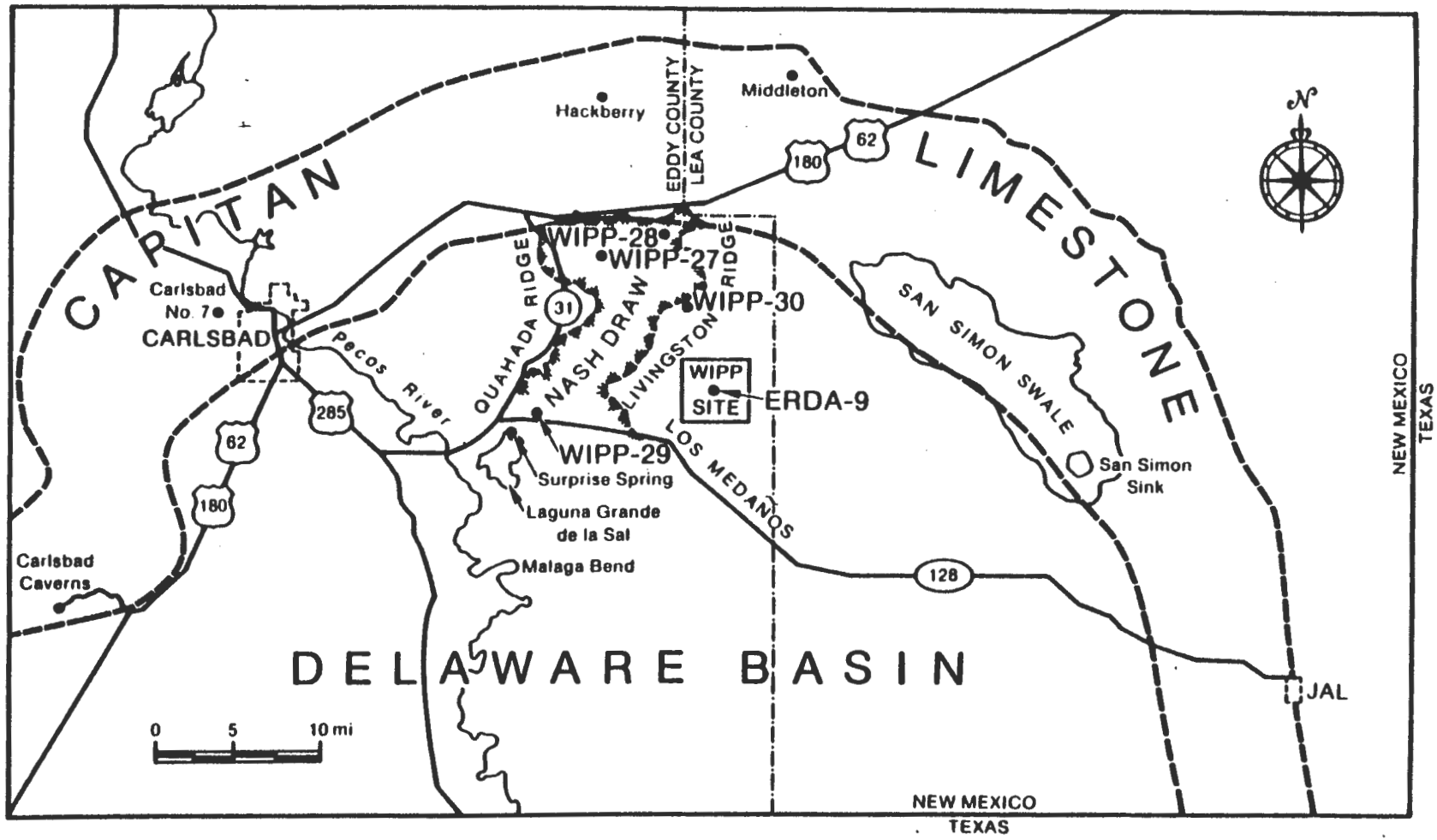


Figure 1.1: Setting of the WIPP site relative to the northern Delaware Basin. Selected geomorphic features and some holes referred to in text but not shown in Figure 1.2 are also included. Modified from Figure VI-1 of Lambert (1983).

Table 1.1: Generalized stratigraphic column of the Delaware Mountain Group and younger sedimentary rocks at and near the WIPP site. Figure 2-1 of Beauheim (1987c).

| SYSTEM | SERIES | GROUP | FORMATION | MEMBER |
|---|---|---|---|---|
| RECENT | RECENT | | SURFICIAL DEPOSITS | |
| QUATER-NARY | PLEISTO-CENE | | MESCALERO CALICHE | |
| | | | GATUNA | |
| TRIASSIC | | DOCKUM | UNDIVIDED | |
| PERMIAN | OCHOAN | | DEWEY LAKE RED BEDS | |
| | | | RUSTLER | Forty-niner |
| | | | | Magenta Dolomite |
| | | | | Tamarisk |
| | | | | Culebra Dolomite |
| | | | | unnamed |
| | | | SALADO | |
| | | | CASTILE | |
| | GUADALUPIAN | DELAWARE MOUNTAIN | BELL CANYON | |
| | | | CHERRY CANYON | |
| | | | BRUSHY CANYON | |

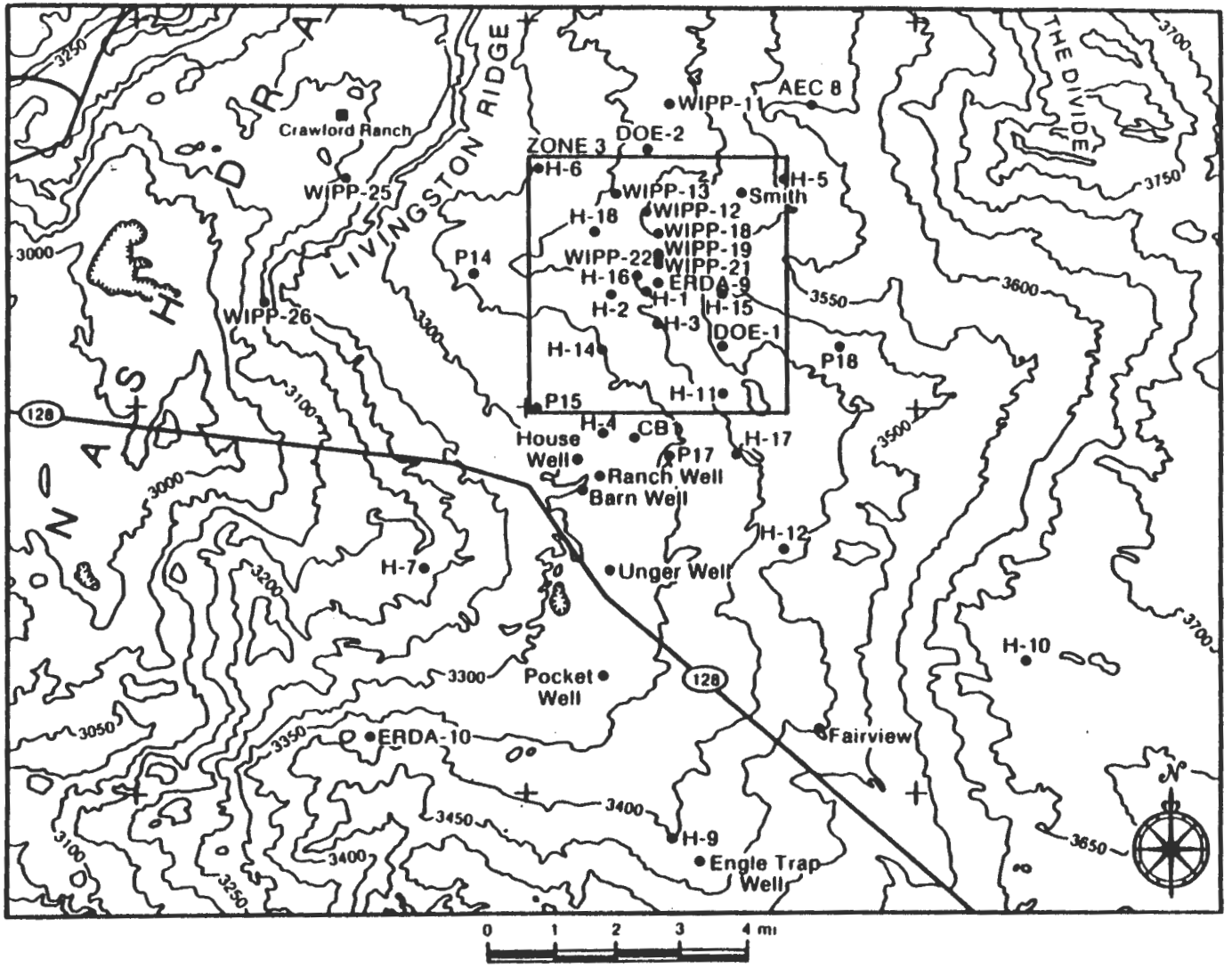


Figure 1.2: Boreholes at and near the WIPP site referred to in text. Holes were drilled as part of the site-characterization of the WIPP, as ranchers' wells, or as potash or hydrocarbon exploration holes. Only exploration holes which have been hydrologically tested are included.

develop after that time. Geotechnical work in and near the WIPP facility will extend into the period of operational demonstration, especially to complete characterization of the hydrologically and structurally disturbed zones around the underground workings and access shafts, in direct support of WIPP performance assessment. Data collected during these studies must support a full evaluation of expected facility performance against criteria developed by the U.S. Environmental Protection Agency (40CFR191) in their present or revised form. The structural, hydrologic, and nuclide-containment behavior of the WIPP facility, including potential far-field paths of nuclide release to the accessible environment, will be monitored throughout the WIPP operational period.

## 1.1 Report Objectives

This report has four main objectives. These are to:

1. Summarize the results of C&C studies carried out since the Spring of 1983.

2. Summarize the results and/or status of site-characterization and facility-characterization studies carried out since 1983 but not mandated by the C&C Agreement.

3. Compile the results of WIPP site-characterization studies into an internally consistent conceptual model for the geologic, hydrologic, geochemical, and structural behavior of the WIPP site. This model includes preliminary consideration of the local effects of the WIPP facility and shafts on the Salado and Rustler Formations.

4. Discuss the present limitations and/or uncertainties in the conceptual geologic model of the WIPP site and facility.

The objectives of the report are limited in scope and do not include determination of whether or not the WIPP Project will comply with repository-performance criteria developed by the U.S. Environmental Protection Agency (40CFR191). Whether or not the WIPP will comply with 40CFR191 must be demonstrated by the WIPP performance-assessment activity within five years following first emplacement of waste. The objective of this report is to develop as complete a conceptual model as possible for use in the required performance assessment.

## 1.2 Structure of Report

The remaining parts of this section (1.0) contain:

1. A general discussion of the stratigraphic setting and variability of sedimentary rocks within the northern Delaware Basin that have been of interest during WIPP site characterization (Section 1.3).

2. A general discussion of the technical issues of interest in WIPP site (and facility) characterization (Section 1.4). Emphasis in this discussion is on technical areas of site characterization which have been actively pursued since 1983.

The sections making up the body of the report (2.0 through 4.0) are generally ordered in stratigraphically upward sequence. This structure is a matter of convenience, and is not intended to imply relative priorities of the different issues and units discussed.

Within each technical section, recent studies in the formation(s) of interest are discussed in relation to the topics or issues outlined in Section 1.4. The final section of the report, Section 5.0, attempts to compile the results of the three preceding sections into an internally consistent conceptual model for the geologic, hydrologic, structural, and geochemical behavior of the WIPP site.

## 1.3 General Stratigraphic Setting of the WIPP Site and Facility

As shown in Figure 1.1, the WIPP site is located in southeastern New Mexico, in the northern portion of the Delaware Basin. The generalized stratigraphy in the vicinity of the WIPP is summarized in Table 1.1. Regional stratigraphic relationships and characteristics are discussed in detail in Powers et al. (1978).

The Delaware Basin became a distinct structure by the late Pennsylvanian Period to early Permian Period, approximately 280 million years ago. Approximately 250 million years ago, the reef now represented by the Capitan limestone began to grow around the margins of the developing basin, and the sandstones, shales, and carbonates now making up the Delaware Mountain Group (DMG) were deposited within the basin. Most of the Capitan limestone is relatively massive. Some portions of the unit are hydrologically active and support local karst hydrology, including the formation of large cavities such as Carlsbad Caverns. The Delaware Mountain Group, which is limited to the basin, contains three major subdivisions, the Brushy Canyon, Cherry Canyon, and Bell Canyon Formations (in ascending stratigraphic order). Only the Bell Canyon Formation is considered here, as it is the first regionally continuous water-bearing formation beneath the WIPP facility. The hydraulic behavior of the Bell Canyon Formation is assumed to be more significant than that of any underlying units in WIPP breach scenarios.

The Bell Canyon Formation is divided into five informal members, the Hays sandstone, Olds sandstone, Ford shale, Ramsey sandstone, and Lamar limestone (in ascending stratigraphic order). The individual members vary in thickness and lithology. As shown in Figure 1.3, the upper Bell Canyon sandstones tend to be elongated and laterally discontinuous, in the nature of "channel sands." Individual sands are separated laterally by stratigraphically equivalent siltstones and/or shales. Near the WIPP site, the Bell Canyon Formation consists of a layered sequence of sandstones, shales/siltstones, and limestone 300 m or more in thickness (Powers et al., 1978).

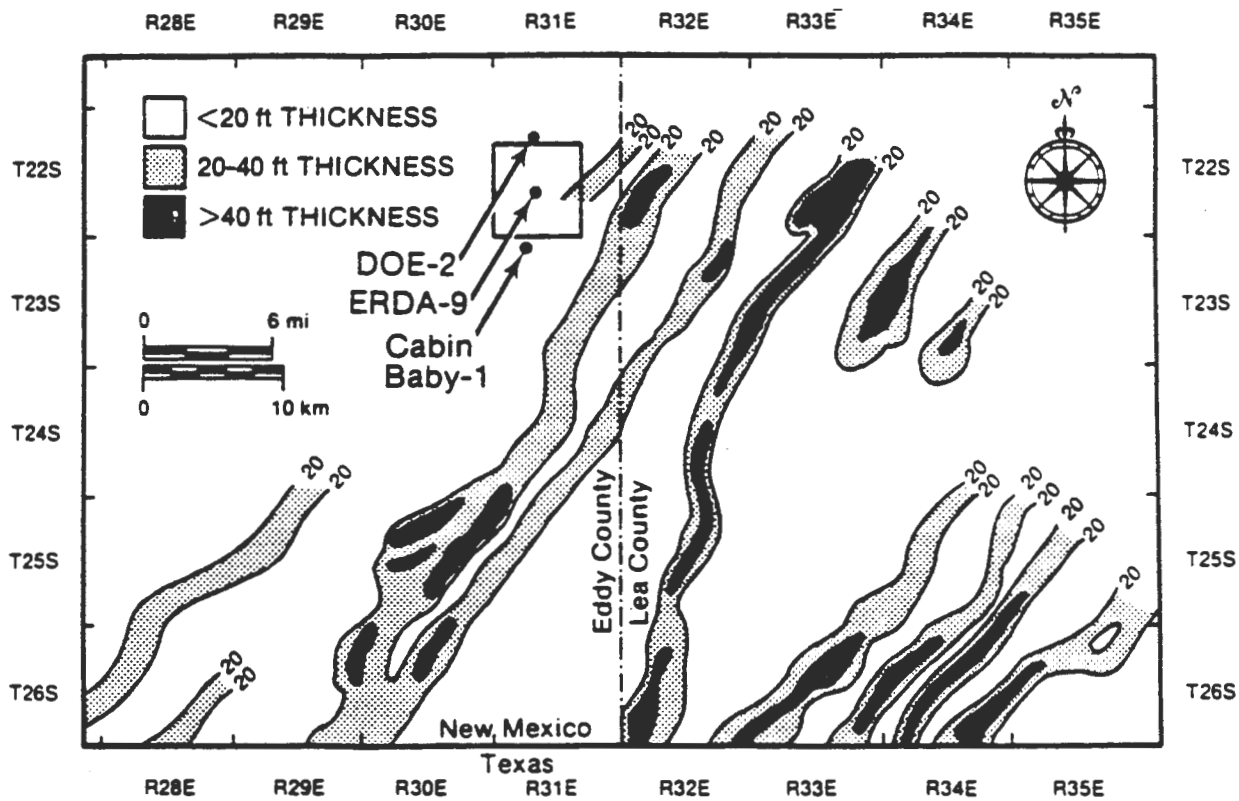


Figure 1.3: Lateral distribution and thicknesses of channel sands in the informal Ramsey member of the Bell Canyon Formation in the northern Delaware Basin, including holes DOE-2 and Cabin Baby-1. Simplified from Figure 2-2 of Davies (1983).

Within the northern Delaware Basin, the sandstones and shales of the Bell Canyon Formation are overlain by the thick-bedded sequence of anhydrites and halites of the Castile Formation, also of Permian age. As shown in Table 1.1, the Castile Formation near the WIPP site normally contains three relatively thick anhydrite/carbonate units and two thick halites. Both anhydrites and halites contain abundant anhydrite and/or carbonate laminae, may be strongly deformed internally, and are variable in local thickness. The thickness of the Castile Formation near the WIPP site is approximately 400 m.

The Salado Formation, of Late Permian (Ochoan) age, is 530 to 610 m thick at and near the WIPP site, and is generally bedded on a scale of 0.1 m to 1 m. It contains 45 numbered "anhydrite" marker beds of variable thickness (MB101 through MB145 with increasing depth). Between marker beds, the Salado consists of layered halites of varying purity and accessory mineralogy; anhydrite ($CaSO_4$), clays, and polyhalite ($K_2MgCa_2(SO_4)_4 \cdot 2H_2O$) are dominant accessory minerals. The WIPP facility horizon is between MB138 and MB139.

The Salado Formation is overlain by the Rustler Formation, also of Ochoan age. As shown in Table 1.2, the Rustler contains five members. Two, the Magenta and Culebra dolomites, are somewhat variable gypsiferous dolomites. The Culebra and Magenta dolomites vary mainly in the concentration of fractures and the local occurrence of silty zones. The other three members of the Rustler (unnamed lower member, Tamarisk Member, and Forty-niner Member in upward succession) consist of varying proportions of anhydrite, siltstone/claystone, and halite. The major mineralogical variability within the Rustler Formation as a whole is in the degree of alteration of anhydrite to gypsum and the presence or absence of halite, both generally interpreted to result from evaporite dissolution. Some of this variability, however, may reflect original depositional patterns. The Rustler ranges from 83 m to 130 m in thickness at the WIPP site, depending on the extent of evaporite dissolution and/or depositional variability.

The Culebra dolomite is the first laterally continuous unit above the WIPP facility to display significant permeability. Barring direct breach to the surface, the Culebra dolomite provides the most direct pathway between the WIPP facility and the accessible environment. The hydrology and fluid geochemistry of the Culebra dolomite are quite complex. The unit displays wide ranges in hydraulic properties, local flow and transport mechanisms, and geochemistry. As a result of these factors, the Culebra has received a great deal of study in WIPP site characterization, both before and since 1983.

The Rustler Formation at the WIPP is overlain by the Dewey Lake Red Beds (the uppermost unit of the Ochoan Series) consisting largely of siltstones and claystones, with subordinate sandstones. The unit is approximately 30 m to 170 m thick at and near the WIPP site, varying at least in part due to post-depositional erosion. Where relatively thick and hydraulically unsaturated, the Dewey Lake Red Beds form a low-permeability buffer zone between the surface and relatively soluble carbonates and/or sulfates in the underlying Rustler Formation. In some areas, however, the unit is

thinned by local erosion and/or is hydraulically saturated. Where sufficiently thin, the Dewey Lake may not present an effective barrier to vertical fluid movement from the surface into the Rustler, depending on the local fluid pressures within and above the Rustler Formation. Where saturated, the Dewey Lake may, in some areas, serve as a source of fluids to the underlying Rustler Formation. The depositional age of the Castile, Salado, and Rustler Formations, as well as the Dewey Lake Red Beds, ranges approximately from 245 million to 230 million years. Over approximately the eastern half of the WIPP site, the Dewey Lake Red Beds are overlain by the (undivided) Dockum Group of sandstones and shales of Triassic age.

Table 1.2: Generalized stratigraphy of the Rustler Formation at and near the WIPP site. Adapted from Snyder (1985).

| Age | Member | Approximate Thickness (m) | Generalized Character in "Unaltered" Sections |
|---|---|---|---|
| Permian/ Ochoan | Forty-Niner | 45± | Anhydrite<br>Halite and Siltstone<br>Anhydrite |
| | Magenta Dolomite | 6-9 | Thinly Laminated Gypsiferous Dolomite; Local Anhydrite |
| | Tamarisk | 65± | Anhydrite<br>Halite and Siltstone<br>Anhydrite |
| | Culebra Dolomite | 6-10 | Finely Crystalline, Vuggy, Gypsiferous Dolomite; Local Siltstone |
| | Unnamed | 44± | Alternating Halite, Siltstone, Anhydrite<br>Laminated Siltstone |

The shallowest and youngest stratigraphic units at the WIPP site proper, except for recent surficial sands, are the Gatuna Formation, the Mescalero caliche, and the Berino soil. The Gatuna Formation, the upper part of which is approximately 600,000 years in age, consists of siltstones, sands, and stream-laid conglomerates, deposited in a wetter climate than is now present in southeast New Mexico. The Mescalero caliche, 410,000 to 510,000 years in age, is relatively continuous in the vicinity of the WIPP site and supports the Livingston Ridge surface on which the site is located (Figure 1.1). The Berino soil, approximately 250,000 years old, is a thin horizon, and is much less widespread than either the Gatuna or the Mescalero. Together, the Gatuna Formation, Mescalero caliche, and Berino soil indicate

some of the variability of the climate in southeastern New Mexico over the last 600,000 years and the relative structural stability of the Livingston Ridge surface over the last 400,000 to 500,000 years.

Localized gypsite-spring deposits, approximately 25,000 years in age, occur along the eastern flank of Nash Draw, but are not currently active. Around the northwest margin of the Delaware Basin, packrat middens indicate that the climate approximately 10,500 years ago was significantly wetter than that at present. The recent surficial windblown sands at and near the WIPP site are almost all stabilized by vegetation. South of the site, however, there is an area in which surficial dunes appear to be active. It is from these dunes that the area has derived its name, "Los Medanos."

## 1.4 Technical Issues of Interest in WIPP Site and Facility Characterization

This section contains brief discussions of several technical issues of general interest in site characterization of the WIPP, including some consideration of the WIPP facility itself. The most general issues are discussed first. After that, the approach is generally stratigraphic, in parallel with the structure of the report as a whole. Detailed referencing of individual technical studies is not included here, but is included in Sections 2.0 through 4.0, where appropriate.

### 1.4.1 Transient Versus Steady-State Geologic, Hydrologic, and Geochemical Setting of the WIPP

In order for the expected behavior of the WIPP facility to be evaluated against the EPA's repository-performance guidelines (40CFR191), it must be demonstrated that the structural, hydrologic, geochemical, and transport behavior of the WIPP facility and environs are adequately understood to provide satisfactory predictions over at least the 10,000-year time frame of regulatory interest. "Structural behavior," as the term is used here, includes both far-field and near-field mechanical deformation of stratigraphic units. Far-field structural behavior is behavior independent of the presence of the WIPP facility, especially the underground workings. Near-field behavior is the behavior of the portions of the Salado and Rustler Formations that have been disturbed by the presence of the WIPP facility. "Hydrologic behavior" includes description of the distribution of hydrologic properties, fluid pressures, and directions of fluid flow. As the term is used here, however, it does not include investigation of chemical equilibrium between fluid and rock. "Geochemical behavior" includes both bulk chemistry and isotopic relations resulting from rock-water interaction, but is largely limited to consideration of natural chemical transport and reactions between rocks and fluids, independent of waste. "Transport behavior" includes consideration of the mechanisms of contaminant transport in Rustler groundwaters and the relative importance of different transport mechanisms; it does not include consideration of any specific radionuclides that will or will not be a part of the WIPP radionuclide inventory.

Two basic assumptions are possible concerning the overall geologic setting of the WIPP site. The simplest assumption, implicitly made in the WIPP FEIS (U.S. Department of Energy, 1980), is that the entire geologic system at the WIPP is at steady state on the time scale of regulatory interest. Under this assumption, the geology, hydrology, and geochemistry of the WIPP site should be constant with (or independent of) time for at least the period of regulatory concern to waste isolation.

However, the overall geologic and hydrologic settings of the WIPP site have been transient (not steady-state) since before the beginning of deposition of the Bell Canyon Formation, approximately 250 million years ago, and will continue to be transient long after effective closure of the WIPP facility. Some events, such as crystallization of secondary minerals within the Salado Formation approximately 200 million years ago and formation of the Mescalero caliche 400,000 to 500,000 years ago, have taken place on a very long time scale. Two types of transient response are occurring at and near the WIPP site within the 10,000-year time frame of regulatory interest. These are: a) the continuing natural response of the geologic and hydrologic systems to the end of the last pluvial period (period of decreased temperatures and increased precipitation) in southeast New Mexico; and b) the responses to man-induced hydrologic, geochemical, and structural transients resulting from site characterization and facility construction.

Thus, there is abundant evidence that the overall setting and behavior of the WIPP site are transient on at least three geologic and two human-induced time scales. The time scales of transient behavior range from at least tens of millions of years in the cases of secondary mineralization and fracture formation within the Salado Formation (independent of the WIPP facility) to tens of years in the case of pressure transients imposed on the Rustler Formation by shaft construction and hydrologic testing. The evidence for transient behavior of the WIPP site comes from a broad range of geologic, hydrologic, geochemical, and structural studies. The WIPP performance-assessment activity will ultimately determine which transient phenomena are significant to the long-term performance of the WIPP facility.

### 1.4.2 Dissolution of Evaporitic Rocks at and near the WIPP Site

Evaporite dissolution, i.e., dissolution or alteration of halite, anhydrite/gypsum, and/or the sulfatic carbonates of the Rustler, Salado, or Castile Formations by groundwaters, has been an issue of major interest in WIPP site characterization. The fundamental reason for this has been the need to evaluate the possibility that, although the Permian evaporites at the WIPP site have been in existence for approximately 240 million years, they might be regionally or locally dissolved on the 10,000-year time scale of regulatory interest. If this occurred, then evaporite dissolution could play a major role in breach of the WIPP facility, by short-circuiting the transport of radionuclides from the facility to the accessible environment.

There are four settings in which evaporite dissolution is or has been of interest in WIPP site characterization. These include:

1. Regional-scale stratabound dissolution of evaporites, especially halite, within the Castile and Salado Formations. In stratabound dissolution, fluid movement is predominantly parallel to bedding. Stratabound dissolution has probably taken place in the western part of the Delaware Basin, as indicated by the absence of halite from both the Castile and Salado Formations in Figure 1.4. If stratabound dissolution within the Castile reached the WIPP site, mechanical collapse of the overlying Salado Formation would occur, possibly resulting in direct breach of the facility. If stratabound dissolution within the Salado reached the WIPP, direct breach of the facility might result.

The possibility of stratabound dissolution reaching the WIPP site itself on the 10,000-year time scale of interest was evaluated as part of site-characterization activities prior to 1983. There is general agreement that stratabound dissolution of the Castile and/or Salado Formations will not reach the WIPP facility in the 10,000-year time frame of interest. In addition, recent interpretations indicate that much of the variability in the thicknesses of the Castile and Salado Formations is due to deformation and original depositional variability, rather than to evaporite dissolution. This should result in slower estimated dissolution rates.

2. Dissolution of Castile and/or Salado halites by localized upward intrusion of halite-unsaturated fluids from the upper portion of the Bell Canyon Formation into the overlying units. If such dissolution occurred immediately beneath the WIPP site, the resulting mechanical subsidence might directly breach the WIPP facility. If this dissolution mechanism is in fact feasible, the locations at which it might occur in the future are not predictable with the present understanding of hydrology in the northern Delaware Basin.

At the WIPP site, one basinal structure within the Salado Formation was proposed in 1983 as a possible result of subsidence resulting from point-source dissolution of Castile and/or Salado halites. This structure has since been investigated by the drilling, coring, and hydrologic testing of hole DOE-2 (Figure 1.2). No evidence of evaporite dissolution was found in hole DOE-2. The DOE-2 structure is the result of syndepositional and postdepositional deformation of the Castile and Salado Formations, rather than of evaporite dissolution. This conclusion, together with earlier studies indicating that the only proven "breccia pipes" in the northern Delaware Basin result from dissolution within the Capitan limestone and occur only directly above this unit (Snyder and Gard, 1982), indicates that point-source dissolution of Castile and/or Salado evaporites is not operative either within the main part of the basin or at the WIPP site.

3. Dissolution of halite from within the Rustler Formation by stratabound flow. East of the WIPP site, the Rustler Formation contains abundant halite (salt) in the Forty-niner, Tamarisk, and unnamed members. West of the WIPP site, for example in Nash Draw, the Rustler

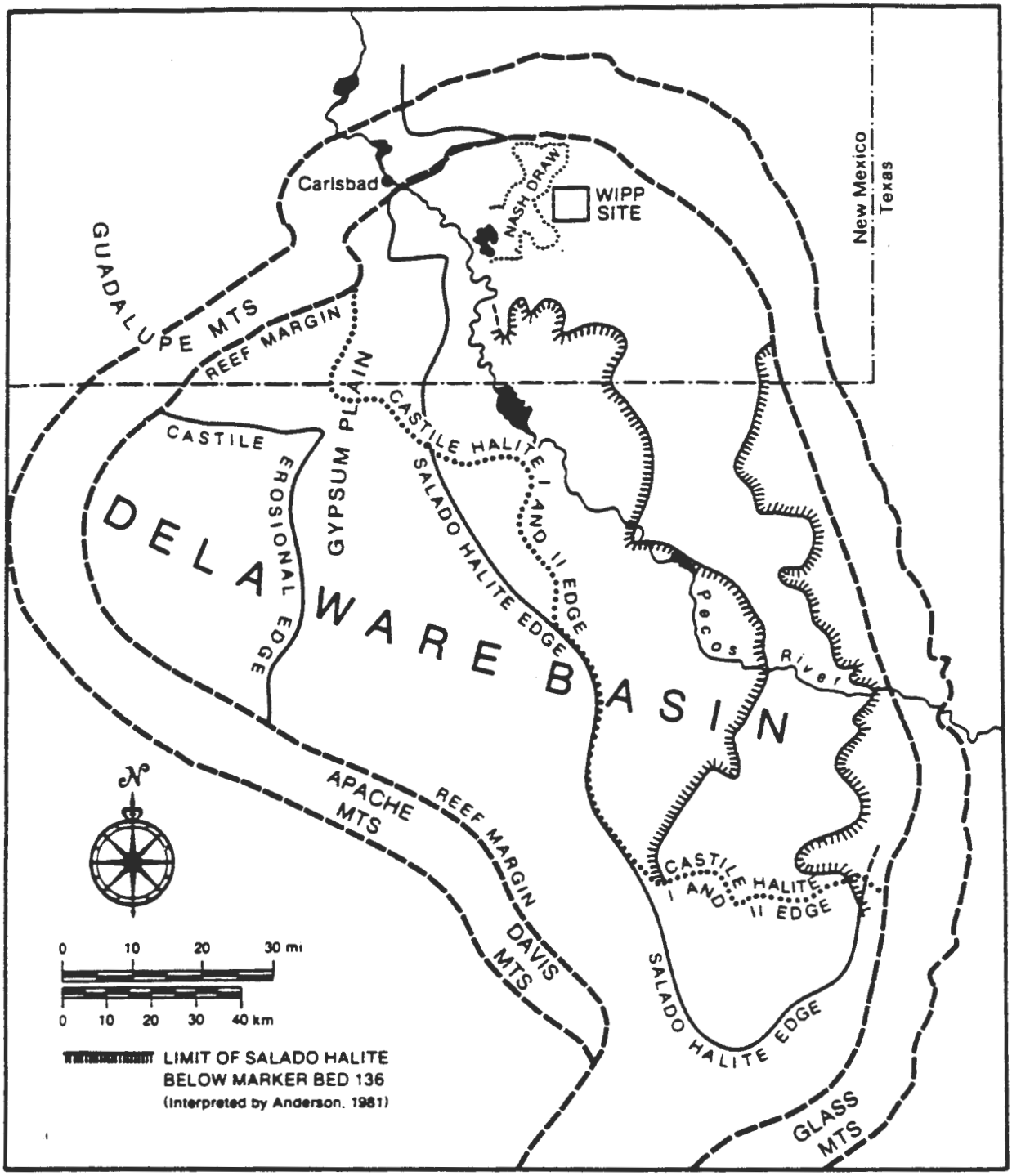


Figure 1.4: Generalized distribution of the Castile and Salado Formations in the Delaware Basin, with emphasis on distribution of halites. Slightly modified from Figure VII-1A of Lambert (1983) and including, in part, the interpretation of Anderson (1981).

Formation is totally devoid of halite (Figure 1.5). If Rustler variability is due to evaporite dissolution and if stratabound dissolution reached the WIPP site within 10,000 years, the overburden at the WIPP would be significantly reduced, perhaps leading to breach.

The variability within the Rustler Formation has conventionally been thought to result from regional-scale stratabound evaporite dissolution, based on the assumption that the distribution of halite was originally uniform. It has also traditionally been assumed that dissolution of Rustler evaporites was a recent phenomenon, linked to the growth of Nash Draw over the last 600,000 years. These two assumptions maximize both the total amount of halite dissolved from the Rustler and the rate at which this dissolution occurs. There is considerable disagreement concerning the uniformity and amount of stratabound evaporite dissolution within the Rustler Formation. However, even with the two "conservative" assumptions outlined above, i.e., assumptions thought to maximize the potential impact to the WIPP, it does not appear feasible for the Nash Draw structure to extend to the WIPP site on the time scale of regulatory interest.

4. Evaporite dissolution within the Rustler Formation as a result of vertical fluid flow. This second potential evaporite-dissolution mechanism involving the Rustler Formation at and near the WIPP site requires local recharge, from the surface to the Rustler Formation, of waters unsaturated in halite and anhydrite/gypsum. If this vertical movement of unsaturated fluids occurs to a significant degree, the resulting local evaporite dissolution within the Rustler might result in local high-permeability channels or pathways within the Rustler Formation. The final result of such dissolution would be the generation of a "karstic" hydrologic system. In such a system, the hydrology and transport behavior would be dominated by relatively narrow high-permeability pathways or channels, even though most of the unit would consist of low-permeability "blocks." The hydrology of at least part of the Rustler Formation within Nash Draw, where the Rustler is exposed at the surface, is known to be karstic, and includes the continuing formation of small caves and sinkholes in anhydrites of the Forty-niner and Tamarisk Members. Such a hydrologic and transport system within the Rustler Formation at the WIPP site itself might provide a means for rapid transport of nuclides from the WIPP facility to the accessible environment.

A comprehensive approach has been taken to the question of Rustler karst at the WIPP site. Field studies have evaluated the surface-geological evidence for and against significant surface infiltration and possible development of karstic cavities below. Hydrologic measurements, including regional-scale pumping tests, have characterized the present distribution of hydraulic properties and relative head potentials within the Rustler at and near the WIPP. Isotopic studies have estimated the isolation or residence times of Rustler waters, estimated the relative importance of vertical and stratabound fluid flow within the Rustler and Dewey Lake, and evaluated the extent to which the entire Rustler hydrologic setting is transient.

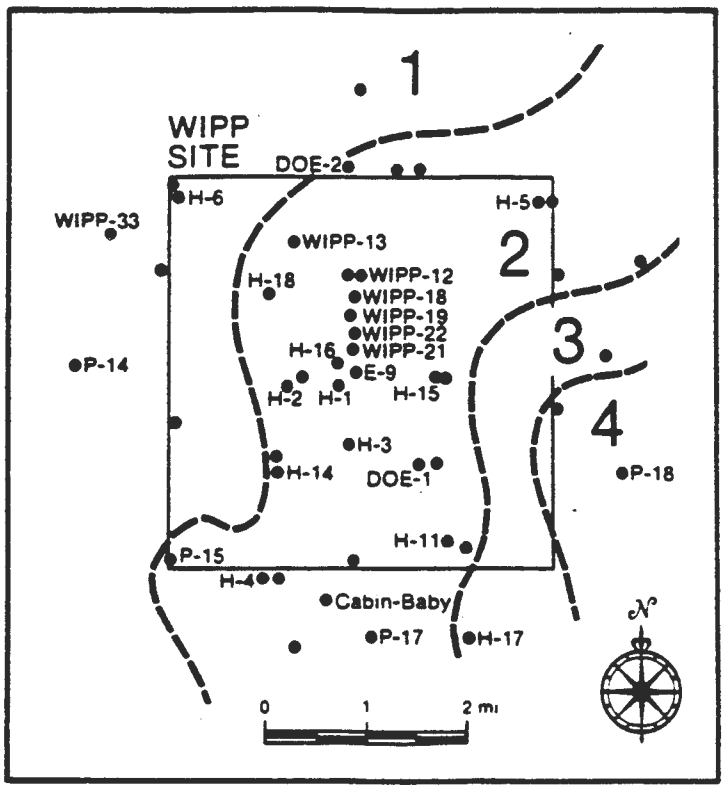


Figure 1.5: Generalized halite distribution within the Rustler Formation at and near the WIPP site. Slightly modified from Figure 9 of Chaturvedi and Channell (1985). Zone 1: no halite present within the Rustler Formation; Zone 2: halite present only below the Culebra Member; Zone 3: halite present between Culebra and Magenta Members; Zone 4: halite present above the Magenta Member.

The combined results of these studies indicate that vertical recharge from the surface to the Rustler is not active at the WIPP site. Where measured successfully, the calculated residence or isolation time of Rustler groundwaters at the WIPP site is greater than 10,000 years. There must have been changes in flow directions within the Culebra dolomite within the last (approximately) 10,000 years. The isotopic results do indicate that some vertical fluid flow has taken place, especially within the Dewey Lake Red Beds. In addition, local development of karstic channels or porosity within Rustler anhydrites does appear to have been a consequence of vertical infiltration of fluids from the surface in the WIPP-33 structure, approximately 1 km west of the western boundary of Zone 3. However, the WIPP-33 structure is unique at and near the WIPP site and is not now significantly active. Regional-scale pumping tests of the Culebra dolomite have not identified any major or dramatic high-transmissivity structures similar to those expected if Rustler karst involving the Culebra were present at the WIPP site.

### 1.4.3 Directions of Fluid Flow to Be Expected if the Rustler and Bell Canyon Formations Are Interconnected

In the effort to be "conservative," i.e., to not underestimate the impact of breaches of the WIPP facility, it was assumed in the WIPP FEIS (U.S. Department of Energy, 1980) that fluid flow in the event of interconnection of the Rustler and Bell Canyon Formations would be upward into the Rustler. This issue, as well as the distribution of hydrologic properties within the Bell Canyon Formation, has since been investigated in testing of the holes Cabin Baby-1 and DOE-2, near the southern and northern boundaries of the WIPP site, respectively (Figure 1.2).

The results of hydrologic testing in both Cabin Baby-1 and DOE-2 suggest that the WIPP site is not directly underlain by a high-permeability channel sand in the upper part of the Bell Canyon (Figure 1.3). If such a sand is present, it must be more narrow than those shown in Figure 1.3. This decreases the potential, already concluded by Wood et al. (1982) to be negligible, for any significant upward migration of Bell Canyon fluids into overlying evaporites in the absence of a drillhole. In addition, the fluid pressures and brine densities measured in both Cabin Baby-1 and DOE-2 indicate that, in the event of interconnection of the Bell Canyon, Salado, and Rustler Formations within a drillhole, the final direction of fluid flow would be downward into the Bell Canyon Formation. This conclusion assumes that both Bell Canyon and Rustler fluids become saturated as a result of local halite dissolution within the Salado Formation.

### 1.4.4 Distribution and Origin of Brine Occurrences within Castile Anhydrites

In the northern Delaware Basin, highly pressurized brines have been encountered locally in fractured anhydrites of the Castile Formation during drilling from the surface. The known distribution of these Castile brine occurrences as of 1983 is shown in Figure 1.6. Castile brines have been

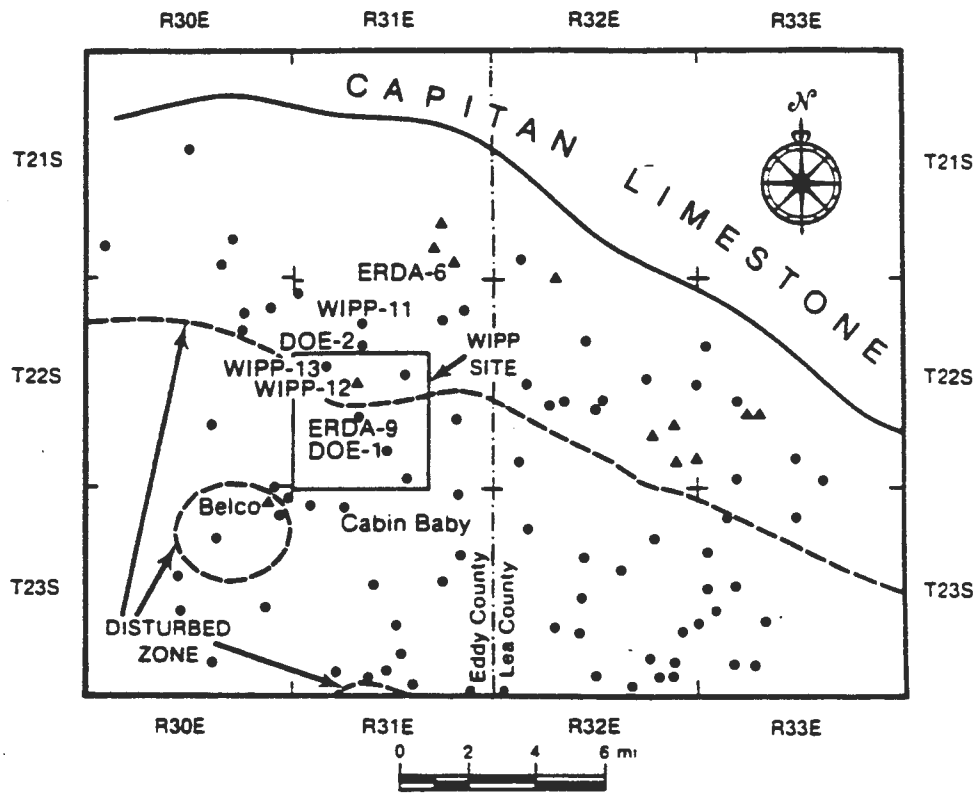


Figure 1.6: Generalized distribution of Castile brine occurrences and approximate extent of the Castile "Disturbed Zone" in the northern Delaware Basin. Distribution of Castile brines is simplified from Figure G-11 of Popielak et al. (1983). Approximate boundaries of Castile "Disturbed Zone" are from Figure 1-1 of Borns et al. (1983). Closed triangles represent holes in which Castile brines have been encountered. ERDA-9 is included for reference, but does not penetrate Castile Anhydrite III completely.

encountered largely in hydrocarbon-exploration drillholes both north and northeast of the WIPP site (i.e., between the WIPP site and the margin of the basin). However, brine was also encountered southwest of the WIPP site, at the Belco well. During WIPP site characterization, Castile brines have been encountered in hole WIPP-12, approximately 1.6 km north of the site center, and in ERDA-6, approximately 8 km northeast of the site center.

Two basic hypotheses have been put forward to explain the origin of Castile brines, namely that the occurrences are due to:

1. Migration of connate Castile fluids from halites into anhydrites fractured as a result of local deformation.

2. Isolation of meteoric waters within the fractured Castile anhydrites, following episodic lateral hydrologic connection of the Castile Formation and the Capitan limestone.

Because of the localized but widely distributed occurrence of Castile brines in the vicinity of the WIPP site, it has previously been assumed for purposes of performance assessment that Castile brine is present beneath the WIPP facility itself. Since the upper Castile anhydrite is stratigraphically 200 m or more beneath the WIPP facility horizon, this brine is of concern only in the event of a drilling intrusion which connects the brine occurrence with the facility. A recent surface-geophysical survey over an area including the WIPP waste-emplacement panels is consistent with the presence of Castile brines beneath a portion of the panels.

### 1.4.5 Deformation of the Castile and Salado Formations

Borns et al. (1983) define a structurally "Disturbed Zone" (DZ) (Figure 1.6) within the Castile Formation, based largely on the systematic loss of coherent seismic response. The deformation of the Castile Formation within the DZ involves both anhydrites and halites, and is associated with the known occurrences of Castile brines. Although the overall mineralogies of the Salado and Castile Formations are similar, the two units are layered on different scales. Regional deformation of the Salado Formation is largely in response to regional deformation of the underlying Castile Formation.

Recent results indicate that fluids and pressure-solution mechanisms play a major role in far-field deformation of both the Castile and Salado Formations. This has been investigated both theoretically and by examination of core collected in hole DOE-2. The time scale of regional deformation of the Salado and Castile Formations is from thousands to millions of years, too long to be of concern in evaluation of the future performance of the WIPP facility.

Construction of the underground WIPP facility, resulting in generation of a large void space at a depth of 650 m within a stratigraphic section that is predominantly halite, results in a strong local mechanical response within the Salado Formation. The near-field mechanical response of the Salado

Formation around the WIPP facility involves both higher stresses and deformation rates than expected in natural or far-field deformation. At least during early closure, near-field creep deformation appears to involve mechanisms such as dislocation climb. It is presently not known when, or if, pressure solution will become a dominant mechanism in creep closure of the WIPP facility.

Creep, however, is not the only near-field process involved in closure of the WIPP facility. Marker Bed 139 (MB139), approximately 1 m below the WIPP facility horizon, is fractured from pre-excavation processes, i.e., processes not related to excavation of the WIPP facility. The opening of these fractures, in addition to formation of fractures within Salado halites, plays a significant role in the near-field structural response to excavation of the WIPP facility.

Monitoring of these structural "excavation effects" is ongoing, and will continue through the operational phase of the WIPP. The time scale of near-field mechanical effects began with the beginning of construction of the WIPP facility and will continue until structural reequilibration following complete closure of the facility. Therefore, the time of interest may be 100 years or more, depending on both the long-term behavior of the facility and the types and amounts of both waste and backfill that are emplaced.

### 1.4.6 Fluid Flow within the Salado Formation

Salado halites were assumed to be anhydrous at the time of the WIPP FEIS and SPDV activities, with the exception of small amounts of fluid inclusions and water bound up in hydrous minerals. Fluid flow into the WIPP facility under this assumption would be very small in volume, directly stress-related, and transient. Long-term steady-state fluid flow would be zero.

Recent hydrologic measurements from the surface and within the WIPP facility, combined with geochemical studies within the facility, indicate that grain-boundary fluids are present within the Salado Formation, and that the unit should be considered as a very low-permeability material in which fluid residence times in the far field are on the order of millions of years. There are, however, major increases in both permeability and fluid-pressure gradients within the Salado Formation within a few meters of the WIPP facility at and near the facility horizon. The recent results suggest that, while there are major stress-related transient effects, long-term fluid flow into the facility will reach some very low but non-zero steady-state rate, and will continue until effective hydrologic closure of the facility. On the basis of preliminary hydrologic testing results, the development of an altered or disturbed zone around the WIPP shafts appears to be much more limited than at the facility horizon.

### 1.4.7 Present-Day Hydrology, Transport Behavior, and Geochemistry of the Rustler Formation

The Culebra Dolomite Member of the Rustler Formation is the first laterally continuous water-bearing zone above the WIPP facility. Transport within the Culebra dolomite constitutes the major transport mechanism from the WIPP facility to the accessible environment, except for direct transport to the surface. Therefore, there is great interest in determining the modern distribution of hydraulic and nuclide-transport properties within the Culebra.

The hydrologic characteristics of the Culebra dolomite are complex. The transmissivity of the unit varies by approximately four orders of magnitude at and near the WIPP site, with relatively high-transmissivity regions both southeast and northwest of the site center. However, the center of the WIPP site, including all four shaft locations, is in a region of low Culebra transmissivity (permeability). The relatively transmissive parts of the Culebra contain fractures that dominate both hydraulic and transport behavior on the scale of individual three-hole hydropads (approximately 30 m between holes). If these fractures were to dominate flow and transport behavior on the "regional" scale considered here, i.e., over the 3.2-kilometer distance between the center of the WIPP site and the boundary of WIPP Zone 3 (Figure 1.2), nuclide-transport times to the accessible environment would be greatly decreased relative to times estimated without considering fractures.

Numerical modeling of Rustler hydrology through 1983 was based on testing only at single holes and individual three-hole hydropads, and ignored possible fracturing. Since 1983, two regional-scale interference tests have been conducted in the Culebra, one centered at the H-3 pad and one at hole WIPP-13 (Figure 1.2). Hydraulic effects of fracturing have been evaluated in detail at the H-3 and H-11 hydropads. The interpretation of the regional-scale multipad interference tests indicates that fracturing need not be included in modeling simulation of Culebra hydrologic behavior at this scale, since test calculations with and without fractures have produced very similar results.

In addition, detailed calculations completed in 1987 indicate that although fracturing plays a major role in local or pad-scale contaminant transport within parts of the Culebra, radionuclide transport to the accessible environment can realistically be modeled using the porous-medium approximation, at least so long as the present pattern of head distributions within the Culebra is not significantly perturbed and the transport properties and flow paths assumed in the calculations are representative. This conclusion may or may not be valid in the case of a breach involving a Castile brine reservoir at high fluid pressures.

Through 1983, numerical modeling of Rustler hydrology also ignored both the geochemical variability of Rustler fluids and possible effects of variable fluid density on directions of fluid flow. Both numerical methods and data bases for evaluation of groundwater flow in the region of the WIPP site have developed significantly since that time. Recent groundwater-flow calculations, which include effects of variable brine density, indicate

that modern fluid flow within the Culebra dolomite is generally north-south in the vicinity of the WIPP site. Flow rates vary greatly, being rapid down the axis of Nash Draw, but extremely slow across the WIPP site proper. While the assumption of hydrologic steady state appears adequate for modeling of head potentials within the Culebra dolomite, groundwater flow across the WIPP site within the Culebra is sufficiently slow to make the assumption of hydrologic steady-state inadequate for detailed modeling of long-term flow directions and rates. However, the changes in flow rates and directions as a function of time appear not to be dramatic at the WIPP site itself. Groundwater flow is quite slow in this area.

As noted, Culebra fluids are quite variable. Recent work indicates that they can be broken into four distinct geochemical facies. The general distribution of fluid compositions is inconsistent with steady-state confined fluid flow in the present flow directions. The mineralogy of the Culebra dolomite is widely variable, but without sharp regional distinctions, since dolomite, clays, and gypsum/anhydrite are all widespread. Halite has not been reliably identified in Culebra core, except for that which may have been introduced during drilling. The analyzed Culebra fluid compositions form a variable but continuous population, all of which reflect exposure to evaporitic rocks.

## 2.0 BELL CANYON FORMATION

The Delaware Mountain Group is divided into the Brushy Canyon, Cherry Canyon, and Bell Canyon Formations, all of which are predominantly of shales, siltstones, and sandstones. Only the Bell Canyon is considered here, since it is the first regionally continuous water-bearing zone beneath the WIPP facility. The hydraulic behavior of the Bell Canyon is assumed here to be more significant than that of underlying units in WIPP breach scenarios.

There have historically been two reasons for interest in the Bell Canyon Formation in WIPP site characterization. First, the Bell Canyon has been proposed by some as a source of fluids for local or point-source dissolution of halite in the overlying Castile and Salado Formations. This mechanism and general conclusions regarding its validity at the WIPP site are summarized in general terms in Section 2.1, based on work completed through 1983. Second, it must be assumed for purposes of performance assessment that at least one drillhole from the surface will penetrate the WIPP facility. It may then be important to estimate the distribution of permeable zones within the Bell Canyon at the WIPP site and to estimate directions of fluid flow that might result from an open borehole penetration that connected the Bell Canyon with fluid-bearing zones within the Rustler Formation, especially the Culebra dolomite. The character of the Bell Canyon and expected directions of fluid flow between the Culebra and the Bell Canyon at the WIPP site are discussed in Section 2.2.

### 2.1 Potential for the Bell Canyon Formation to Serve as a Source of Fluids for Dissolution of Evaporites in the Castile and Salado Formations

Anderson (1978, 1981) and Davies (1983) have proposed a major role for the Bell Canyon Formation in point-source dissolution of overlying evaporites. The proposed mechanism involves: 1) recharge of halite-unsaturated fluids to the Bell Canyon Formation from the Capitan limestone; 2) upward movement of these fluids into (at least) the lower halite of the Castile Formation; 3) halite dissolution within the Castile Formation; 4) subsidence and disruption of the Castile and overlying Salado Formations as a result of halite dissolution; 5) downward flow of halite-saturated brines back into the Bell Canyon Formation; and 6) removal of brines through the Bell Canyon Formation. An important characteristic of this hypothesis proposal is that it is not possible to predict localities of future point-source evaporite dissolution.

Wood et al. (1982), as part of the WIPP SPDV studies, addressed the potential for fluids within the upper Bell Canyon Formation to dissolve evaporites within the Castile Formation. For this evaluation, it is assumed that: 1) a permeable sandstone is present at the top of the Bell Canyon Formation, i.e., a Ramsey channel sand (Figure 1.3); 2) the effective thickness of the sandstone is 30 m; and 3) the transmissivity of the sandstone ranges from $1.0 \times 10^{-6}$ to $2.8 \times 10^{-6}$ $m^2/s$. Any decrease in sandstone permeability or shifting of the sandstone to positions below the

top of the Bell Canyon would reduce the potential for dissolution of overlying evaporites.

For the range of hydraulic properties and gradients considered, and assuming the Ramsey sand is at the top of the Bell Canyon, Wood et al. (1982) conclude that:

1. Except at locations adjacent to the Capitan limestone, only diffusional dissolution is possible directly above the Bell Canyon. Salt directly above the top of the Bell Canyon, assuming diffusional processes, is calculated to dissolve at a vertical rate of approximately 0.003 m per 10,000 years. This would have negligible effect on the WIPP facility.

2. Allowing for an order-of-magnitude increase in flow velocities within the Bell Canyon Formation, dissolution would still be too slow to maintain open cavities within Castile halites at depth. Such cavities are required to maintain the high-permeability pathways necessary for dissolution due to the density-flow mechanism outlined above.

3. Even allowing for the maximum potential dissolution rates at the top of the Bell Canyon from both diffusive and convective mechanisms, no significant evaporite dissolution as a result of fluid flow from within the Bell Canyon should be observed at the WIPP facility for at least 10,000 years.

In addition, Lambert (1983) concludes that the Bell Canyon Formation itself shows no evidence of either modern hydraulic connection with a source of halite-unsaturated fluids (such as the Capitan limestone) or any effective path for brines to exit the Delaware Basin. Instead, Lambert interprets the Bell Canyon fluids as having very long residence times and concludes that their compositions reflect extensive rock-water interaction, evolving isotopically and geochemically away from compositions representative of meteoric recharge.

Thus, studies at the end of the WIPP SPDV phase indicated that the Bell Canyon Formation was not dissolving evaporites near the WIPP site. As discussed in Section 3.0, however, this question was later investigated directly by the drilling, coring, and hydrologic testing of hole DOE-2, near the northern boundary of WIPP Zone 3 (Figure 1.2).

### 2.2 Expected Directions of Fluid Flow Between the Bell Canyon and Rustler Formations

The information on freshwater-equivalent heads in the Rustler and Bell Canyon Formations available through 1983 is summarized in Mercer (1983). At that time, the freshwater head within the Bell Canyon Formation at the center of the WIPP site, approximately 1040 m AMSL, was 120 m greater than the expected freshwater head in the Culebra dolomite at the same location,

approximately 920 m AMSL. (All elevations here are given relative to mean sea level.) This is consistent with the assumption made in the WIPP FEIS (U.S. Department of Energy, 1980) that fluid flow would be upwards into the Rustler if the Bell Canyon and Rustler were interconnected in an open hole. However, this "conservative" assumption, i.e., the assumption with most apparent impact to WIPP performance assessment, neglects: a) the original density of fluids in the Bell Canyon and Culebra; b) possible increases in both Bell Canyon and Culebra fluid densities due to dissolution of halite within the Salado Formation; c) possible effects of fluid potentials within the Salado Formation or elsewhere within the Rustler Formation; and d) possible changes in fluid density as a result of entrainment of waste from within the WIPP facility.

In the event of a drillhole breach interconnecting the Bell Canyon, Castile, Salado, and Rustler Formations, it is reasonable to assume that local dissolution of halite within the Salado Formation would take place, resulting in an average fluid density of approximately 1.2 $g/cm^3$, the approximate density of saturated NaCl brine. Under this assumption, Bell Canyon brine at the center of the WIPP site would stand to an elevation of approximately 835 m in an open hole, some 445 m above the WIPP facility, but approximately 210 m below land surface, and more than 200 m lower than the Bell Canyon freshwater-equivalent head of approximately 1040 m. Assuming that local halite dissolution within the Rustler or upper portion of the Salado Formations led to a final density of Culebra brine of 1.2 $g/cm^3$, the Culebra near the center of the WIPP site would support a column of brine to an elevation of approximately 900 m, 20 meters below the freshwater-equivalent head within the Culebra, but some 65 m higher than supported by the underlying Bell Canyon Formation.

Therefore, if brine saturation by halite dissolution is considered, the data available as of 1983 are consistent with the interpretation that interconnection of the Bell Canyon Formation and the Culebra dolomite in an open drillhole through the WIPP facility should result in downward movement of contaminated brine into the Bell Canyon Formation. However, the calculated direction of fluid flow depends on assumed fluid densities. Fluid might move upward until the Bell Canyon and Culebra fluids were saturated with halite, at which time downward flow would begin. In addition, these results depend on the assumption that no significant fluid or gas pressures are generated within the Salado Formation or WIPP facility. As of 1983, however, predicted directions of fluid flow were limited in reliability, because heads and fluid densities in the Culebra dolomite and Bell Canyon Formation had not been measured together in the same hole. Two holes penetrating the Bell Canyon Formation very near the WIPP site have since been drilled and/or hydrologically tested. The results from hole Cabin Baby-1 are discussed in Section 2.2.1, and those from hole DOE-2 in Section 2.2.2.

### 2.2.1 Results from Hole Cabin Baby-1

Cabin Baby-1, a hydrocarbon exploration hole, was originally drilled through the Castile Formation and the upper 35 m of the Bell Canyon

Formation in 1974 and 1975. At that time, all of the Ramsey and part of the Olds members of the Bell Canyon were penetrated. The hole depth at that time was 1265 m below land surface. As described in Beauheim et al. (1983b), the hole was deepened to a total depth of 1308 m in 1983 to allow hydrologic testing, fluid sampling, and monitoring of Bell Canyon fluid levels. The deepening allowed testing of most of the Hays sandstone member underlying the Olds, in addition to all of the Olds and Ramsey members.

The results of hydrologic testing of the Bell Canyon in Cabin Baby-1 and DOE-2 are summarized in Table 2.1. Only the lowermost "sand" member of the Bell Canyon, the Hays, is significantly permeable in Cabin Baby-1, with an interpreted transmissivity of between $1.7 \times 10^{-7}$ and $5.1 \times 10^{-7}$ $m^2/s$. The description of the Hays member by Beauheim et al. (1983b) indicates that it is siltstone. The estimated transmissivities of the overlying Olds and Ramsey members are less than $10^{-8}$ $m^2/s$. Core from the Ramsey member is not available from Cabin Baby-1.

Table 2.1: Summary of hydrologic test results from the Bell Canyon Formation in Cabin Baby-1 and DOE-2. Data from Table 6 of Beauheim et al. (1983b) and Table 7-2 of Beauheim (1986).

| Effective Test Interval (m blg) | Unit | K(md) | T($m^2/s$) |
|---|---|---|---|
| Cabin Baby | | | |
| 1230-1246 | Lamar | $6 \times 10^{-4}$ | $5.7 \times 10^{-11}$ |
| 1247-1257 | Ramsey | $2.3 \times 10^{-2}$ - $8.7 \times 10^{-2}$ | $1.7 \times 10^{-9}$ - $6.3 \times 10^{-9}$ |
| 1259-1269 | Olds | $2.2 \times 10^{-2}$ - $8.2 \times 10^{-2}$ | $2.1 \times 10^{-9}$ - $7.9 \times 10^{-9}$ |
| 1271-1308 | Hays | 0.57 - 1.7 | $1.7 \times 10^{-7}$ - $5.1 \times 10^{-7}$ |
| DOE-2 | | | |
| 1263-1272 | Ramsey | $8.4 \times 10^{-2}$ - $9.4 \times 10^{-2}$ | $5.8 \times 10^{-9}$ - $6.5 \times 10^{-9}$ |
| 1276-1285 | Olds | $9.8 \times 10^{-2}$ - 0.11 | $7.1 \times 10^{-9}$ - $8.2 \times 10^{-9}$ |
| 1297-1318 | Hays | 2.3 - 2.4 | $5.7 \times 10^{-7}$ - $6.0 \times 10^{-7}$ |

Fluid samples were successfully collected from the Hays and Olds members of the Bell Canyon in Cabin Baby-1, as was a mixed sample from the entire exposed Bell Canyon. The presence of the tracer added to the drilling

fluid indicates that all of the water samples are slightly contaminated with drilling fluid. Therefore, the reported specific gravity of fluid from the Hays sandstone (1.120 - 1.134) may be slightly too high (Beauheim et al., 1983b).

At the end of operations in 1983, the penetrated portion of the Bell Canyon in Cabin Baby-1 was isolated by a packer emplaced in the lower anhydrite of the Castile Formation, and a monitoring tube was installed to the surface to allow long-term monitoring of a composite Bell Canyon fluid level. As of October 1986, the composite Bell Canyon fluid level in Cabin Baby-1 was stabilized at an elevation of approximately 920 m (Saulnier et al., 1987). Assuming that a specific gravity of 1.12 represents Bell Canyon fluids in the hole, and that the fluid column is supported by the effective pressure at the top of the Hays member at an elevation of -255 m, the calculated pressure at this elevation is 12.81 MPa. This pressure in the Bell Canyon in Cabin Baby-1 would support a column of brine having a density of 1.20 $g/cm^3$ to an elevation of 842 m.

Culebra fluid pressures and properties in Cabin Baby-1 are contained in LaVenue et al. (1988). These results indicate a Culebra freshwater-equivalent head of approximately 913 m. At the elevation of the base of the Culebra in this hole, approximately 856 m, this requires a fluid pressure of approximately 0.55 MPa. Assuming a final brine density of 1.2 $g/cm^3$ after halite dissolution, this is equivalent to a brine column supported to an elevation of 903 m.

The expected saturated-brine head in the Culebra in Cabin Baby-1, 903 m, is 61 m higher than the composite saturated-brine head in the Bell Canyon in the same hole, 842 m. Thus, under the assumptions used here and consistent with extrapolations from regional data available as of 1983, the final direction of fluid flow in the event of an open drillhole interconnecting the Bell Canyon and Salado Formations with the Culebra dolomite at Cabin Baby-1 would be downward.

### 2.2.2 Results from Hole DOE-2

Hole DOE-2, located near the center of the northern boundary of WIPP Zone 3 (Figure 1.2), was drilled in two stages to a total depth of 1318 m, between August 1984 and June 1985 (Mercer et al., 1987). In addition to the shallower units in the hole, the Ramsey, Olds, and Hays "sandstone" members of the Bell Canyon Formation were hydrologically tested (Table 2.1), as described by Beauheim (1986).

The results of testing in DOE-2 are similar to those in Cabin Baby-1, in which the lower "sand," the Hays, is the only unit with appreciable permeability or transmissivity. Estimated transmissivities for the Hays in DOE-2 range from $5.7 \times 10^{-7}$ to $6.0 \times 10^{-7}$ $m^2/s$, similar to the upper estimate of transmissivity for the same zone in Cabin Baby-1. Estimated transmissivities of the Ramsey and Olds members in DOE-2 range only from $5.8 \times 10^{-9}$ to $8.2 \times 10^{-9}$ $m^2/s$, similar to the upper range of estimated transmissivities for the same members in Cabin Baby-1. The lithologic log

contained in Mercer et al. (1987) indicates that all three members are fine-grained sandstones, rather than siltstone.

After hydrologic testing, the Bell Canyon in DOE-2 was isolated for monitoring of a composite fluid level (Beauheim, 1986). As of March 1986, the composite fluid level had "stabilized" at an elevation of approximately 925 m. Assuming that the measured specific gravity of 1.10 (Mercer et al., 1987) is representative for the Bell Canyon fluids, and that the composite Bell Canyon head is controlled by fluid pressures at the top of the Hays member at an elevation of -243 m, this requires a fluid pressure of 12.5 MPa at this elevation. This pressure would support a column of brine having a density of 1.2 $g/cm^3$ to an elevation of approximately 827 m.

The Culebra freshwater-equivalent head in DOE-2 is approximately 934 m (LaVenue et al., 1988). Using the measured fluid density of 1.04 $g/cm^3$ (Uhland et al., 1987) for the Culebra in DOE-2, a freshwater-equivalent head of 934 m requires a pressure of 1.47 MPa at the base of the Culebra, at an elevation of 784 m. Assuming a final Culebra brine density of 1.2 $g/cm^3$ following halite dissolution, the Culebra-fluid pressure at DOE-2 would support a brine column of density 1.2 $g/cm^3$ to an elevation of approximately 909 m, 82 m higher than supported by the composite Bell Canyon head in the same hole. Under the assumptions used here, the final direction of fluid flow in the event of an open hole interconnecting the Bell Canyon, Salado, and Culebra at DOE-2 would be downward.

Wood et al. (1982) estimate that the transmissivities of sandstones within the Bell Canyon Formation normally range from $1.0 \times 10^{-6}$ to $2.8 \times 10^{-6}$ $m^2/s$, although they report a maximum value of $1.7 \times 10^{-5}$ $m^2/s$. This range is approximately one order of magnitude greater than the transmissivity of the Hays member in Cabin Baby-1 and DOE-2, and more than two orders of magnitude greater than the transmissivities measured in the Olds and Ramsey members in the same holes. Therefore, the Ramsey member in Cabin Baby-1 and DOE-2 does not appear to be part of one of the channel sands shown in Figure 1.3. Given that Cabin Baby-1 and DOE-2 are the only two holes very near to WIPP Zone 3 that penetrate the Bell Canyon, this result does not guarantee that no channel sandstone is present in the Bell Canyon beneath the WIPP site. Given the general trend of the channel sands shown in Figure 1.3, it does suggest that any channel sand present would have to be at least as narrow as the sand shown at the eastern edge of the WIPP site. Cabin Baby-1 lies along the trend of this sand, however, indicating that this channel is not continuous towards the southwest.

The recent results in both DOE-2 and Cabin Baby-1 are consistent with the conclusion that the final direction of fluid flow resulting from interconnection of the Bell Canyon Formation and the Culebra dolomite at or near the WIPP site would be downwards into the Bell Canyon, contrary to assumptions maintained in the WIPP FEIS. There are some limitations to this conclusion. There might be upward fluid movement until the Bell Canyon and Culebra fluids became essentially saturated with halite, at which time downward flow would begin. In addition, these results depend on the assumption that flow rates within the Bell Canyon and Culebra dominate any fluid pressures generated within the Salado Formation. This assumption appears generally valid, however, given the low fluid-flow rates normally encountered within the Salado Formation (Section 3.0).

## 3.0 CASTILE AND SALADO FORMATIONS

The major halite-bearing units at and near the WIPP site are the Castile and Salado Formations. Both units contain halites of varying purity and thickness. The two halites within the Castile Formation are normally thick, contain abundant sulfate/carbonate laminae, and are separated by two relatively thick anhydrites. The bedded halites within the Salado Formation contain accessory minerals such as polyhalite, clay, and anhydrite, and are separated by numerous anhydritic marker beds and related clay seams. Locally the middle portion of the Salado Formation contains commercial potash mineralization, at a level some 300 m stratigraphically above the WIPP facility horizon. The underground workings in the WIPP facility are being developed at a depth of approximately 655 m within bedded halites and anhydrites in the lower Salado. The halitic interval containing the WIPP facility horizon is approximately 8 m thick, and is situated between anhydrite marker beds MB138 and MB139. The Castile and Salado Formations are discussed together here, since halite is a major component of both, and many of the processes of interest involve both units.

The Castile Formation overlies the Bell Canyon Formation (Delaware Mountain Group). Near the WIPP site, the Castile normally contains a sequence of three thick anhydrites (Anhydrite I at the bottom and Anhydrite III at the top), separated by two thick halites (Halites I and II). The thickness of the Castile Formation at and near the WIPP site is approximately 400 m. Anderson et al. (1972) provide a general stratigraphic description of the Castile, including the more than 200,000 sulfate/carbonate laminae that occur throughout both halites and anhydrites within the unit. Bedding within Castile anhydrites ranges from massive (approximately 30 m) to laminar (see, for example, Mercer et al., 1987). Individual beds in the Salado are often 1 m thick or less. The unit nominally contains 45 anhydrite marker beds, numbered from Marker Bed 101 (MB101) to MB145 with increasing depth. The Salado Formation is about 600 m thick at the WIPP site.

In some areas, both total thickness and the thickness of stratigraphic intervals within the Castile and Salado Formations are variable. The origin and timing of this variability are discussed in Section 3.1. This variability has played a significant role in WIPP site characterization, since variable halite (and anhydrite) thicknesses could have at least three origins:

1. Initial depositional variability (e.g., Lambert, 1983; Borns and Shaffer, 1985).

2. Gravity-driven deformation, in which dense anhydrites sink into less dense halites, with compensating formation of salt-cored domes or anticlines (Borns et al., 1983; Borns and Shaffer, 1985).

3. Evaporite dissolution, by which halites are preferentially dissolved by contact with unsaturated groundwaters (Anderson, 1978; Davies, 1983).

Significant volumes of fluid are not normally encountered in drilling either the Castile or Salado. There are exceptions, however. Highly pressurized brines have been encountered in the uppermost Castile anhydrite in some hydrocarbon-exploration and stratigraphic test holes near the WIPP site (Figure 1.6). These fluids are under sufficient pressure to flow to the land surface. The origin and distribution of Castile brines at and near the WIPP site is discussed in Section 3.2.

As mentioned previously, the WIPP facility is presently being developed within the bedded halites and anhydrites of the lower Salado Formation. In order to place the WIPP facility within a proper regional perspective, it is necessary to characterize the behavior of the Salado Formation on both the regional scale and adjacent to the WIPP facility itself. The characteristics of the Salado are locally different as a result of "excavation effects" from construction of the WIPP facility. These transient effects demonstrably occur on time scales of interest in performance assessment. Recent studies examining the structural, hydrologic, and geochemical characteristics of the Salado Formation in and near the WIPP facility are discussed in Section 3.3. These studies are progressing, and will play a critical part in monitoring the behavior of the WIPP facility during the operational phase. The discussion of these activities is preliminary.

## 3.1 Regional and Local Variability, Deformation, and Dissolution of the Castile and Salado Formations

### 3.1.1 Regional Relationships and Behavior

As mentioned above, both aggregate and internal thicknesses within the Castile and Salado Formations vary locally. The variability near the WIPP site is shown in Figure 3.1. Holes WIPP-12, DOE-2, and WIPP-11 lie within the southern part of the Castile "Disturbed Zone" (DZ) shown in Figure 1.6, while hole Cabin Baby-1 lies outside this zone. Since ERDA-9 penetrates only the upper portion of the Castile Formation, the possible extension of the DZ beneath the WIPP facility has not been determined by drilling. The Castile and Salado Formations in hole Cabin Baby-1 are assumed here to represent the "undisturbed" character of these units near the WIPP site.

In the cross section shown in Figure 3.1, the total thickness of the Castile is known only in holes Cabin Baby-1 and DOE-2. The Castile is 409 m thick in Cabin Baby-1 and 302 m thick in DOE-2. The apparent thickness of Anhydrite I is 72 m in Cabin Baby-1 and 80 m in DOE-2. Therefore, we assume here that the thickness of Anhydrite I is not significantly variable on the scale of the WIPP site, and that, south of DOE-2, Anhydrite I is not strongly involved in structures within the Castile and overlying Salado. Apparent stratigraphic thicknesses from the top of the Castile to the top of Anhydrite I range from 222 m at DOE-2 to 372 m at WIPP-11. The assumed undisturbed thickness, that at Cabin Baby-1, is 337 m.

Much of the variability within the Castile Formation in Figure 3.1 is in halite thickness. For example, the anomalously thick Castile at WIPP-11 includes a thickness of 311 m for Halites I and II, compared with a

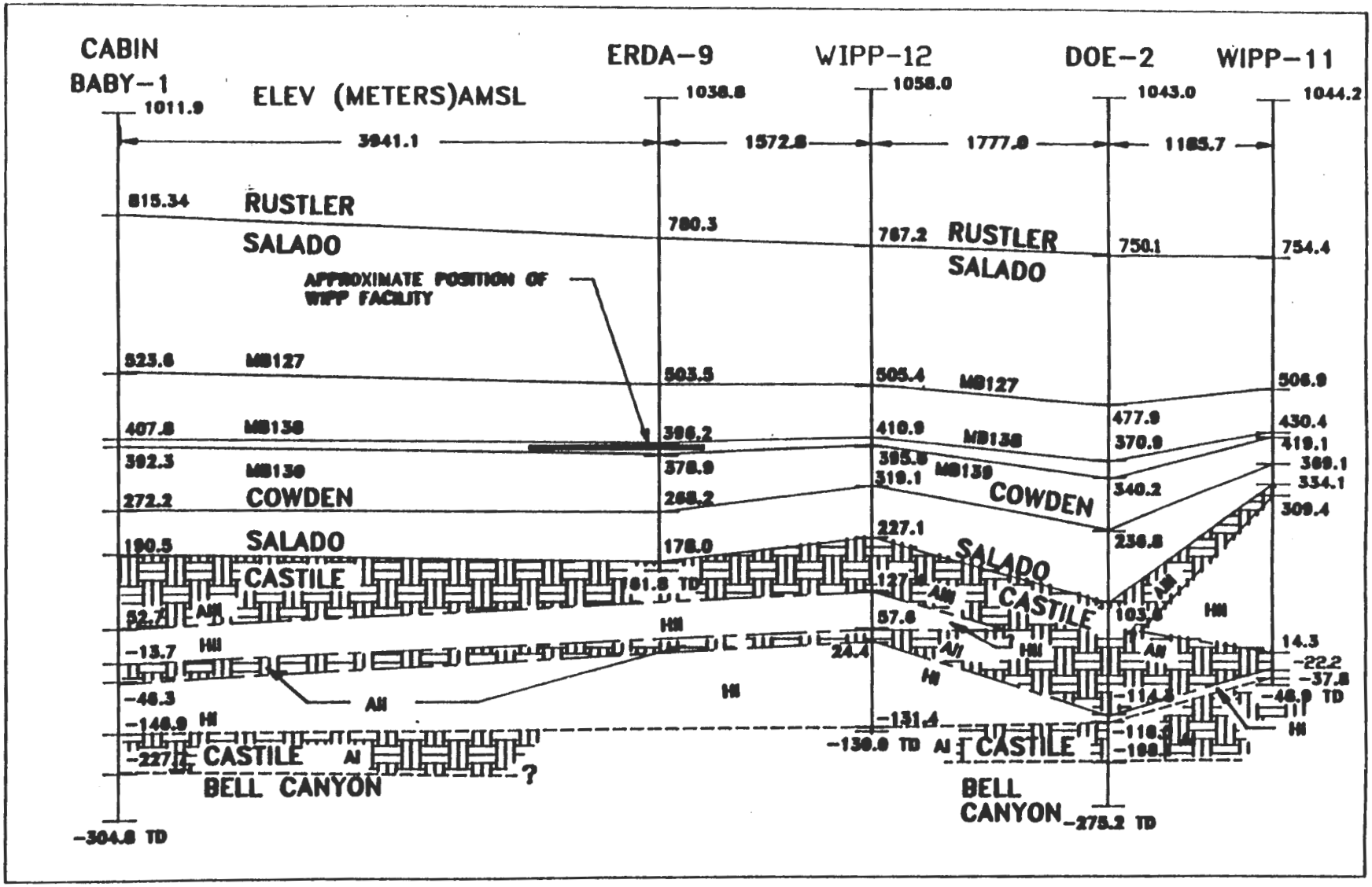


Figure 3.1: Generalized stratigraphic cross section of the Salado and Castile Formations between holes Cabin Baby-1 and WIPP-11. Hole locations used are shown in Figure 3.2. Elevations and hole spacings are in meters.

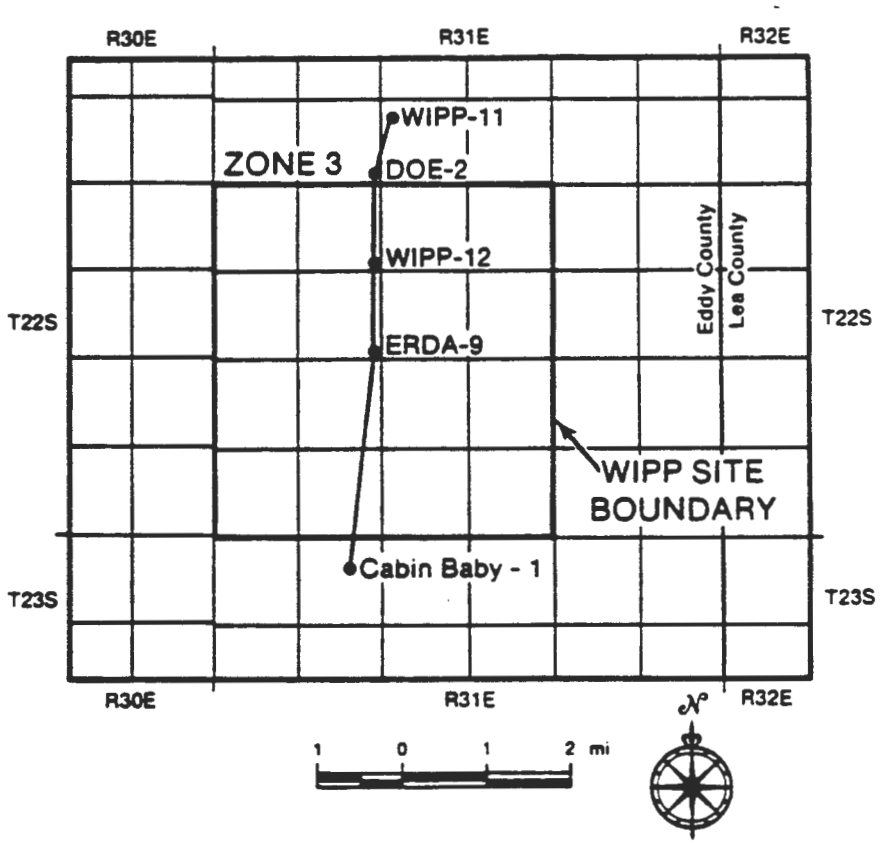


Figure 3.2: Hole locations used in Figure 3.1.

thickness of 167 m for the same units in Cabin Baby-1. At the other extreme, a total of only 2 m of Castile halite is present in DOE-2; Halite II is completely missing.

However, Anhydrites II and III also vary in thickness. Their total apparent thickness (drilled thickness, ignoring dip) in WIPP-11 is 61 m, compared to 219 m in DOE-2. Both values differ significantly from the total thickness of the two units in Cabin Baby-1, 170 m. These relationships indicate that, at least locally, anomalously thick halites within the Castile Formation are combined with anomalously thin anhydrites. Conversely, anomalously thin Castile halite, as in DOE-2, is combined with anomalously thick anhydrite. These results are inconsistent with halite dissolution being the only cause of variability in the thickness of the Castile Formation at the WIPP site.

Locally, the antithetic relations between anhydrite and halite thicknesses within the Castile are consistent with a similar relationship between overall thicknesses of the Salado and Castile Formations. The Salado is 625 m thick at Cabin Baby-1 and 602 m thick in ERDA-9. However, at WIPP-11 and WIPP-12, where the underlying Castile is anomalously thick, the Salado is unusually thin, 420 and 540 m, respectively. On the other hand, the Castile is relatively thin at DOE-2, and the apparent thickness of the Salado at DOE-2 is 647 m, greater than at either Cabin Baby-1 or ERDA-9.

Thus, the variable thicknesses of the combined Salado and Castile Formations at and near the WIPP site appear due to internally compensating variations in thicknesses of both anhydrites and halites. The origin of compensating anhydrite and halite thicknesses may be either depositional, as suggested by Lambert (1983) and Borns and Shaffer (1985), or a consequence of later gravity-driven deformation, as discussed in Borns et al. (1983). The Castile and Salado variability considered here at the WIPP site proper is very similar to that considered by Borns and Shaffer (1985) at the Poker Lake structures well south of the WIPP.

There is considerable evidence for both syndepositional and postdepositional deformation within the Castile Formation, as summarized by Borns et al. (1983) and Borns (1983). These authors distinguish three stages of deformation, listed in the sequence of development:

1. Formation of discontinuous isoclinal folds interpreted to be approximately syndepositional in age, i.e., to have occurred in soft sediments. These structures include displacive crystal growth in both anhydrites and carbonate laminae. Characteristically, the syndepositional structures are confined to a single layer, and may include disruption of the affected layer.

2. Asymmetric folding, including formation of crenulation cleavage, boudinage (separation) of carbonates, and convolute folding of anhydrite stringers within halites. Borns (1983) attributes a widespread subhorizontal fabric within Castile halites to folding at this stage. The axial planes of convolute folds in anhydrite stringers within Halites I and II are also subhorizontal. Borns (1983) interprets these relations to indicate that major deformation within the Castile often involves lateral movement of halite.

3. Late-stage near-vertical fractures and veins, which cross-cut earlier structures. These fractures may be either open, or filled with halite, anhydrite, and/or gypsum.

Syndepositional deformation was probably driven by gravity acting on original depositional slopes, or by responses to density contrasts within still-soft sediments. Borns et al. (1983) attribute later deformation to some combination of direct gravity-driven deformation resulting from deposition of dense anhydrites over less-dense halites and regional tilting of the Delaware Basin. On the large scale, the gravitic driving force for internal deformation of the Castile and overlying Salado Formations is clear. Above Anhydrite I, the Castile includes two thick anhydrites, with densities of approximately 2.95 $g/cm^3$. Each unit was deposited above thick halite with a density of 2.2 to 2.25 $g/cm^3$. Modeling discussed in Borns et al. (1983) indicates that, for the relatively thick-bedded Castile, these density contrasts should be sufficient to drive deformation in which the anhydrites effectively sink into underlying halites. Layering within the Salado is too thin to support such deformation; the Salado structures appear essentially to follow those in the underlying Castile as a relatively passive marker.

However, a driving force for deformation can be effective only if there are appropriate deformation mechanisms operating in the rocks involved. There have been three major studies into possible deformation mechanisms within the halites of the Castile and Salado. Munson (1979) assumed that deformation within the units is anhydrous. Munson concludes (Figure 3.3) that deformation under generic conditions for either a high-level-waste or TRU facility in halite would occur by an undefined mechanism, except at relatively high stress levels. At high stress levels, deformation would be dominated by creep mechanisms involving dislocation climb.

In contrast, Borns et al. (1983) associate structures within deformed portions of the Castile and Salado with the presence of fluids, and conclude that pressure solution plays a major role in controlling the regional deformation of both units. During pressure solution, deformation proceeds as a result of the migration of mineral constituents from regions of high stress to regions of low stress by means of diffusion through grain-boundary fluids. In the interpretation of Borns et al. (1983), the participation of fluids during deformation of the Castile and Salado Formations is indicated by veins containing both halite and anhydrite, as well as by anhydrite recrystallization in stress shadows. Recent studies of fluid contents within Salado halites indicate contents of as high as 2 weight percent (see Section 3.3), more than required for pressure solution to be operative (Borns, 1987b).

Borns (1987b) estimates deformation fields for halite, including pressure solution as a deformation mechanism (Figure 3.4). Field "C" in this figure includes the temperature and stress regimes estimated for regional deformation at and near the WIPP site by Borns et al. (1983), while field "B" is an analogous field for natural deformation of halites estimated by Carter and Hansen (1983) and Heard (1972). Pressure solution plays a major role in halite deformation within the conditions of both fields and assumed

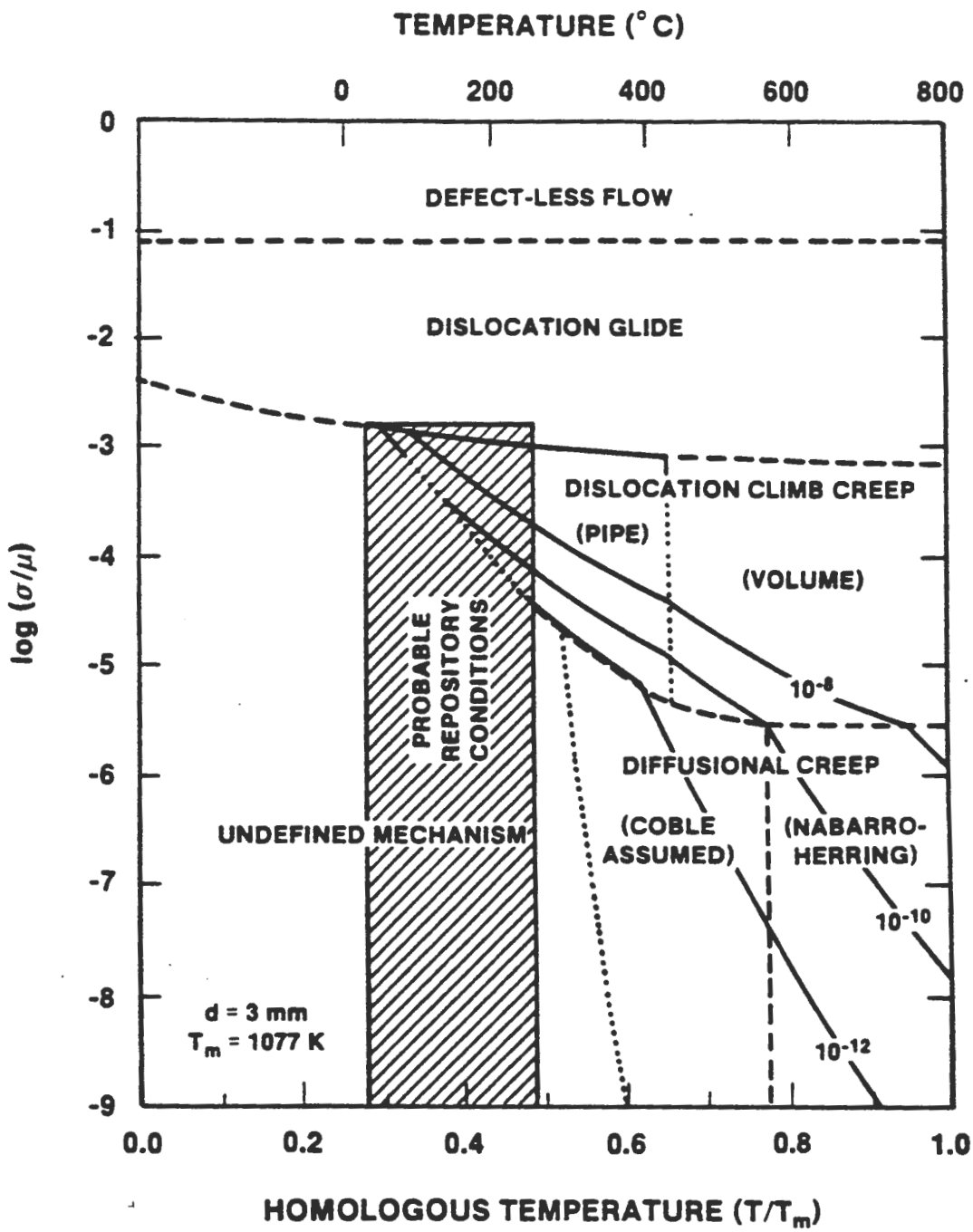


Figure 3.3: Deformation map for halite, assuming all deformation is anhydrous. Figure 2 of Borns (1987b). Homologous temperature ($T/T_m$) is the ratio between temperature and the dry melting temperature of halite. The stress axis is the log ratio of differential stress to halite shear modulus.

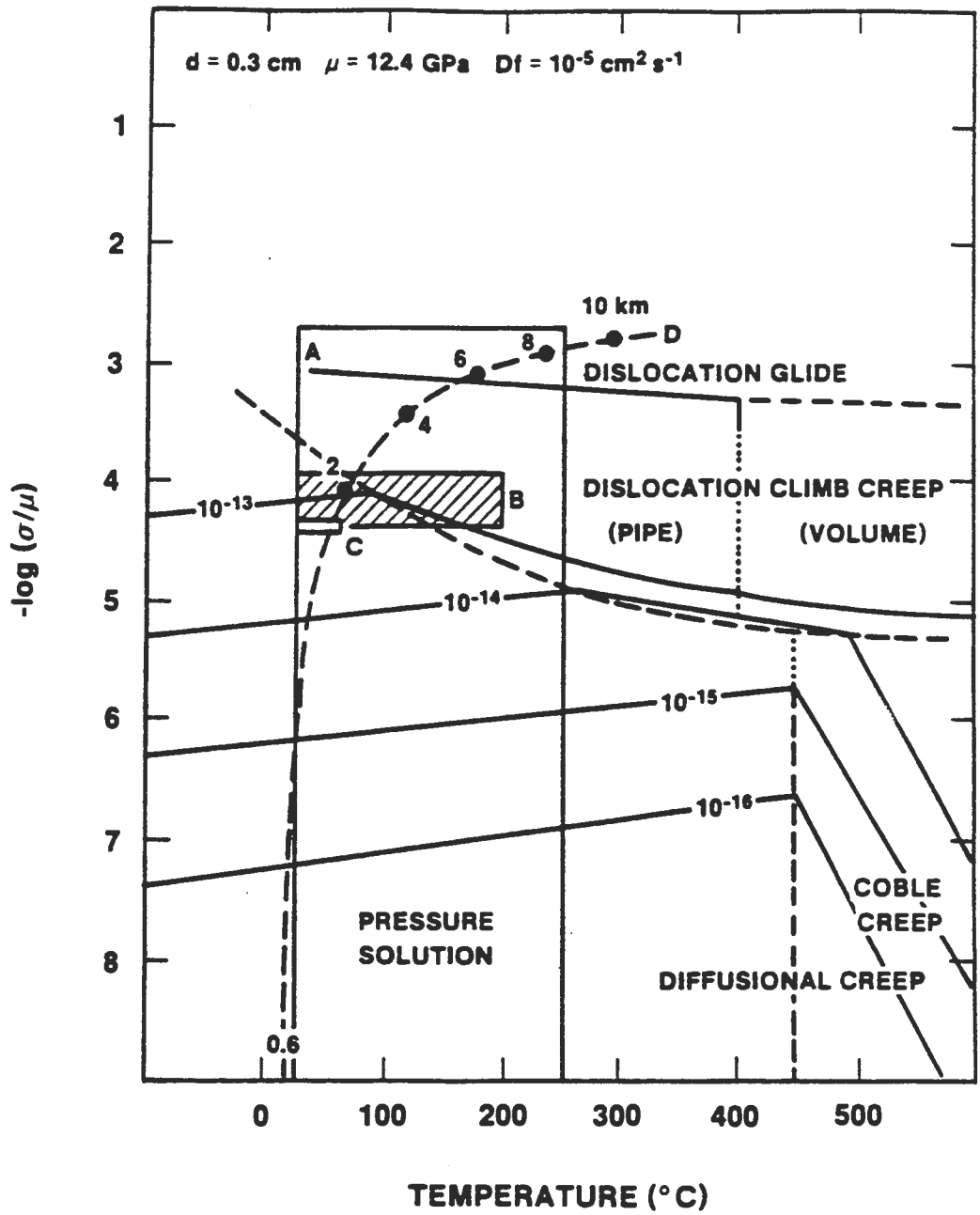


Figure 3.4: Deformation map for halite, assuming fluids present and considering pressure solution as a major deformation mechanism. Figure 4 of Borns (1987b). In this figure, viscous effects on grain boundaries are ignored. Field A is the field of "probable repository conditions" shown in Figure 3.3. Field B is the range of stress and temperature conditions estimated for natural rock-salt deformation (Carter and Hansen, 1983; Heard, 1972). Field C is the range of stress and temperature conditions for gravity-driven deformation at the WIPP site (Borns et al., 1983). Curve D is the estimated stress and temperature path for a Gulf Coast salt dome at the indicated depths (Carter and Heard, 1970).

material properties, so long as the volumetric strain rate is not greater than approximately $10^{-13}$ $s^{-1}$. As discussed by Borns (1987b), the maximum strain rates at which pressure solution is a dominant deformation mechanism depend on the character and thickness of the grain-boundary fluids.

The estimated strain rates for far-field deformation at the WIPP site, not including near-field deformation around the WIPP facility itself, are consistent with pressure solution. Based on a range of estimated strain rates of between $3 \times 10^{-14}$ and $10^{-16}$ $s^{-1}$, the range of times calculated for formation of the WIPP-12 anticlinal structure, estimated to have undergone 1% volumetric strain, is $1.1 \times 10^4$ to $10^6$ years (Borns et al., 1983). Near an underground facility such as the WIPP facility, however, early-time strain rates are probably too rapid for pressure solution to be a major deformation mechanism. Reported volumetric strain rates in such a setting are as high as $10^{-11}$ $s^{-1}$ (Borns, 1987b), and may be even higher during initial transient closure.

In summary, the understanding of far-field deformation within the Castile and Salado Formations is consistent with the interpretations that:

1. Pressure solution, in which deformation results from mineral constituents being transported from high-stress to low-stress domains by means of an intergranular fluid or film, plays a major role in regional deformation of evaporites at and near the WIPP site. Since only approximately 0.2 volume percent (0.1 weight percent) fluid is required for pressure solution to be operative in halite, more than enough fluid is present within the Salado and Castile Formations at and near the WIPP site.

2. Much of the deformation within the DZ may have been effectively syndepositional (i.e., Permian) in age, although this is not the last period of deformation that has taken place.

3. The driving force behind regional-scale evaporite deformation at and near the WIPP is gravitational, due to the depositional emplacement of dense anhydrites over less dense halites. There is, however, a regional overprinting due to Pleistocene tilting of the entire northern Delaware Basin.

4. Deformation such as that known to occur within the DZ, even if it does progress toward the WIPP, is unlikely to reach the WIPP site within $10^4$ years, the minimum estimated time required for formation of the WIPP-12 structure.

5. It is not known whether or when pressure solution will become an important mechanism in closure of the WIPP facility itself. At early times close to the facility, i.e., at relatively high stresses and deformation rates, mechanisms involving dislocation climb (and fracturing) should dominate. At later times and/or at greater distances from the underground workings, i.e., at lower stresses and deformation rates, pressure solution may dominate.

### 3.1.2 The DOE-2 Structure

The recognition of gravity as a driving force for regional-scale deformation of the Castile and Salado Formations and the probable role of pressure solution in such deformation does not rule out the possibility of halite removal by dissolution. The absence of halite within the Castile in the western part of the Delaware Basin (Figure 1.4) is interpreted as partly due to halite dissolution in response to regional tilting and uplift of the basin. However, as summarized by Neill et al. (1983), there is generally agreement that blanket or stratabound dissolution within the Castile and Salado Formations is not a feasible mechanism for breach of the WIPP facility on the regulatory time frame. Regional-scale evaporite dissolution within the Castile and Salado Formations is not discussed further here.

Both Anderson (1978, 1981) and Davies (1983) proposed that evaporites in the Castile and/or Salado Formations may be locally dissolved by halite-unsaturated fluids moving upwards from the Bell Canyon Formation (see Section 2.0). Subsidence of the overlying evaporites, especially the Salado Formation, would result. Hole DOE-2 was drilled specifically to investigate a depression in MB124 in the middle portion of the Salado Formation (Figure 3.1; see also Figure 2-2 of Mercer et al., 1987). However, the DOE-2 structure is interpreted as being due to lateral and vertical deformation of the Castile and Salado Formations, rather than evaporite dissolution.

The expected position of the top of the Castile Formation (Anhydrite III) in DOE-2 was at an elevation of between 230 and 260 m. However, the top of the Castile in DOE-2 was actually at an elevation of 102 m, more than 120 m lower. The base of the Castile in DOE-2, at an elevation of -199 m, is consistent with regional trends, indicating that the structure does not extend below the top of Anhydrite I.

Laminae within the upper Castile anhydrite in DOE-2 are strongly deformed, with vertical bedding and discontinuous folds at various depths (Mercer et al., 1987; Borns, 1987a). These structures are consistent with syndepositional deformation. Other structures seen in the Salado and Castile Formations in DOE-2, such as pull-apart structures and fibrous vein infillings, are interpreted by Borns as postdepositional. As noted by Borns (1987a), removal of Castile halite from DOE-2 by dissolution should have left in place many of the anhydrite "laminae" originally present in Halites I and II. No such dissolution residues were identified in core collected in hole DOE-2. The very thin Castile halite in DOE-2 (approximately 2 m) is compensated by unusually thick halites within the overlying Salado Formation. As shown in Figure 3.1 and noted in Table 3-3 of Mercer et al. (1987), halites within the informal lower member of the Salado Formation (from MB126 to the top of the Castile) in hole DOE-2 are 96 m thicker than in the same stratigraphic interval in hole WIPP-12, and 204 m thicker than in WIPP-11.

The DOE-2 structure is interpreted as being due to both lateral and vertical deformation of the Castile and Salado Formations, rather than to evaporite dissolution. The structural understanding of the Salado and

Castile does not allow prediction of where such a structure might develop in the future. Drilling and testing of hole DOE-2 indicates that no such structure remains unexamined at and near the WIPP site. Estimated times required for 1% strain in the structure at WIPP-12 indicates, however, that the time required for generation of a significant structure as a result of gravitationally driven deformation probably exceeds the 10,000-year time frame of regulatory interest.

### 3.2 Occurrence and Origin of Pressurized Brines within Anhydrites of the Castile Formation

Uncertainties about the original thicknesses, rates of gravity-driven deformation, and regional and local dissolution rates of Castile halites relate to natural phenomena affecting the reliability of long-term extrapolations of WIPP performance. One issue, the possible presence of pressurized Castile brines beneath the WIPP facility itself, plays a direct role in evaluation of the possible consequences of human intrusion into the WIPP facility. This is because, when encountered in drillholes, such brines can rise to the land surface; they would be capable of directly transmitting entrained waste to both the Rustler and the land surface. A geophysical survey conducted in 1987 indicates that Castile brines may be present beneath a portion of the WIPP waste-emplacement panels, consistent with previous assumptions made in WIPP performance assessment.

The known occurrences of Castile brines in the northern Delaware Basin as of 1983 (Figure 1.6) are taken from Popielak et al. (1983). Brines have been encountered in fractured Castile anhydrites in several hydrocarbon-exploration drillholes both north and northeast of the WIPP site, between the WIPP site and the margin of the Delaware Basin. In addition, Castile brines were encountered southwest of WIPP in the Belco well, approximately 6.5 km from the center of the site. During WIPP site characterization, pressurized Castile brines have been encountered in holes WIPP-12, approximately 1.6 km north of the site center, and ERDA-6, approximately 8 km northeast of the site center.

Brine volumes in the two occurrences have been estimated on the basis of flow tests and drillstem testing, but remain somewhat uncertain because of limited early flow data and the assumptions necessary concerning both fracture porosity and rock-mass compressibility in the absence of observation holes. Estimated brine volumes in the two occurrences range between $9.5 \times 10^3$ and $10^5$ barrels for ERDA-6 and between $5 \times 10^6$ and $17 \times 10^6$ barrels for the WIPP-12 occurrence (Popielak et al., 1983; Neill et al., 1983).

Because of the apparent large volume of the WIPP-12 reservoir, it is reasonable to postulate that this reservoir extends beneath all or part of the WIPP facility. However, geophysical studies prior to 1983 were unsuccessful in determining whether or not Castile brines were present beneath the WIPP facility (Borns et al., 1983). Nonetheless, as a result of the occurrence of Castile brine in WIPP-12, it was assumed through 1983 that these brines were present beneath the WIPP facility (Channell, 1982; Bard, 1982; Case et al., 1982). A geophysical survey using transient

electromagnetic methods was made directly over the WIPP waste-emplacement panels in 1987 (Earth Technology, 1987), to determine the presence or absence of Castile brines beneath the facility. The results contained in Earth Technology (1987) are summarized in Figures 3.5 and 3.6.

As discussed in Section 2.0, the WIPP is underlaid by the Bell Canyon Formation. While the permeability of the upper portion of the Bell Canyon Formation is variable, the entire unit appears to be a good electrical conductor. Therefore, the dominant conductive layer beneath the WIPP facility appears to be the Bell Canyon. However, the apparent variations in depth to the first major conductor appear to exceed the estimated depth uncertainty for the geophysical method used, 75 m (Figure 3.6). At some of the locations, the interpreted depth to the first major conductor lies significantly above the depth of the top of the Bell Canyon Formation, i.e., within the Castile Formation. On the basis of this interpretation, brine may be present within the Castile Formation under part of the area outlined by the WIPP waste-emplacement panels (Earth Technology, 1987).

However, the combination of the depths to the first major conductor indicated in Figure 3.5 and stratigraphic depths indicated in Figure 3.1 suggests that the brine occurrence is limited. The depth to the top of the Bell Canyon is 1230 m in Cabin Baby-1 and approximately 1250 m in ERDA-9 (assuming linear variation between Cabin Baby-1 and DOE-2). Therefore, conductor depths greater than 1300 m in Figure 3.5 almost certainly reflect the Bell Canyon Formation. At the other limit, the depth to the bottom of the Salado is 861 m in ERDA-9 and 821 m in Cabin Baby-1. Since the minimum interpreted depth to the conductor is 988 m, the conductor does not appear to be within the Salado Formation anywhere in the surveyed area. The depth to the bottom of Anhydrite III is 959 m in Cabin Baby-1, and is assumed to be approximately 950 m in ERDA-9. Assuming 75 m vertical uncertainty in the geophysical soundings, this implies that apparent conductor depths of less than approximately 1025 m are consistent with brine occurrence within Anhydrite III. This interpretation suggests that brine is present within Anhydrite III under only the furthest northern and northeastern parts of the waste-emplacement panels. To date, pressurized Castile brines have been found only within fractured portions of the uppermost anhydrite present, Anhydrite II in ERDA-6 and Anhydrite III in WIPP-12.

The results shown in Figure 3.5 are based on one-dimensional modeling. Preliminary attempts at three-dimensional interpretation of the results indicate that the lateral resolution of the interpretation cannot be improved by more complex modeling approaches. Therefore, the "conservative" interpretation is that Castile brines are present beneath at least the northern portion of the WIPP waste-emplacement panels, consistent with both the most recent work and earlier assumptions.

Two basic hypotheses have been put forward to account for the occurrences of Castile brines:

1. Migration of connate Castile fluids into fractured anhydrites as a result of local deformation (Borns et al., 1983; Popielak et al., 1983).

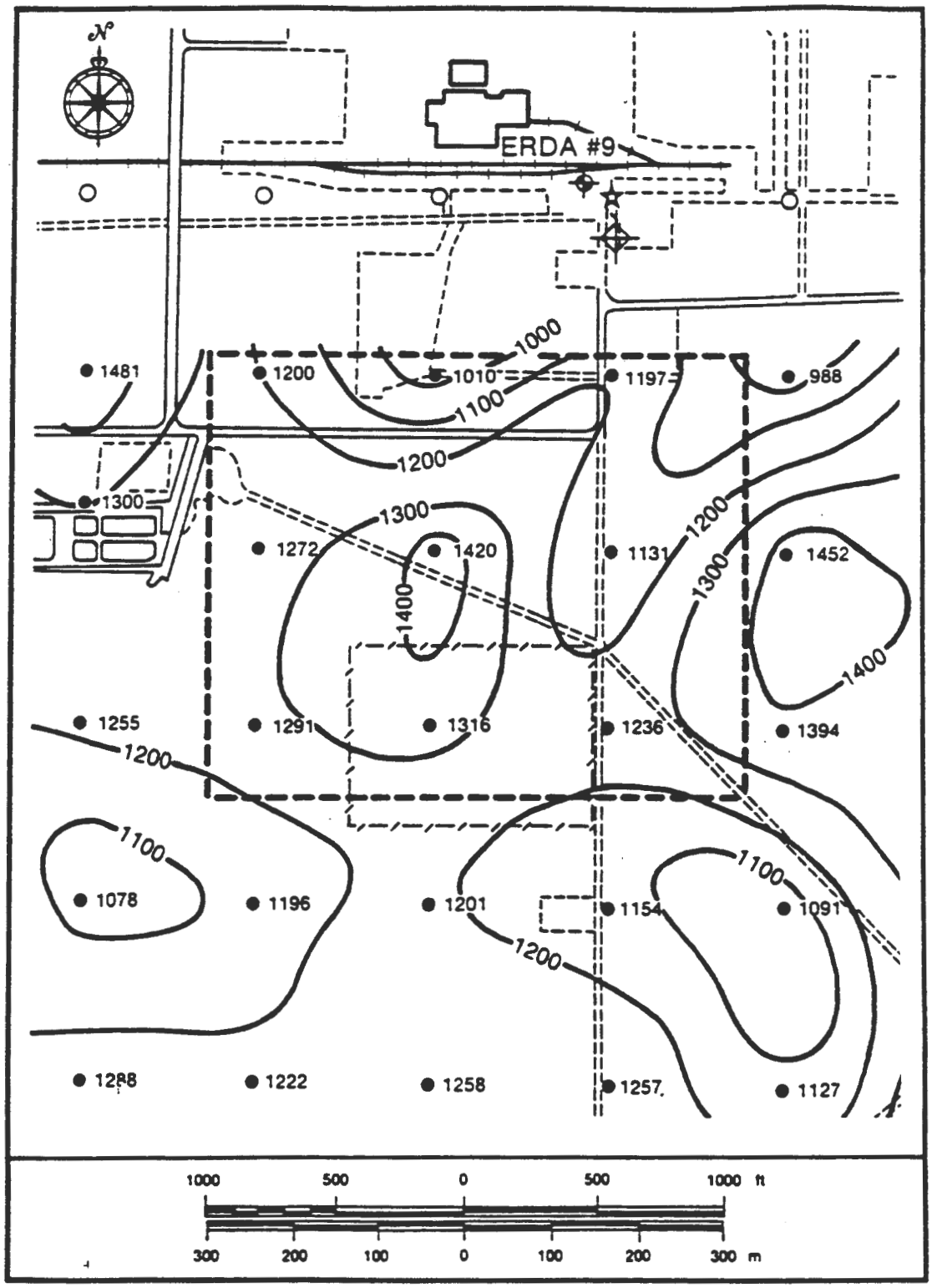


Figure 3.5: Contour map of apparent depth to first major deep conductor in survey including area of WIPP waste-emplacement panels, in meters. The heavily dashed rectangle outlines the surface projection of the WIPP waste-emplacement panels. Simplified from Figure 3-3 of Earth Technology (1987).

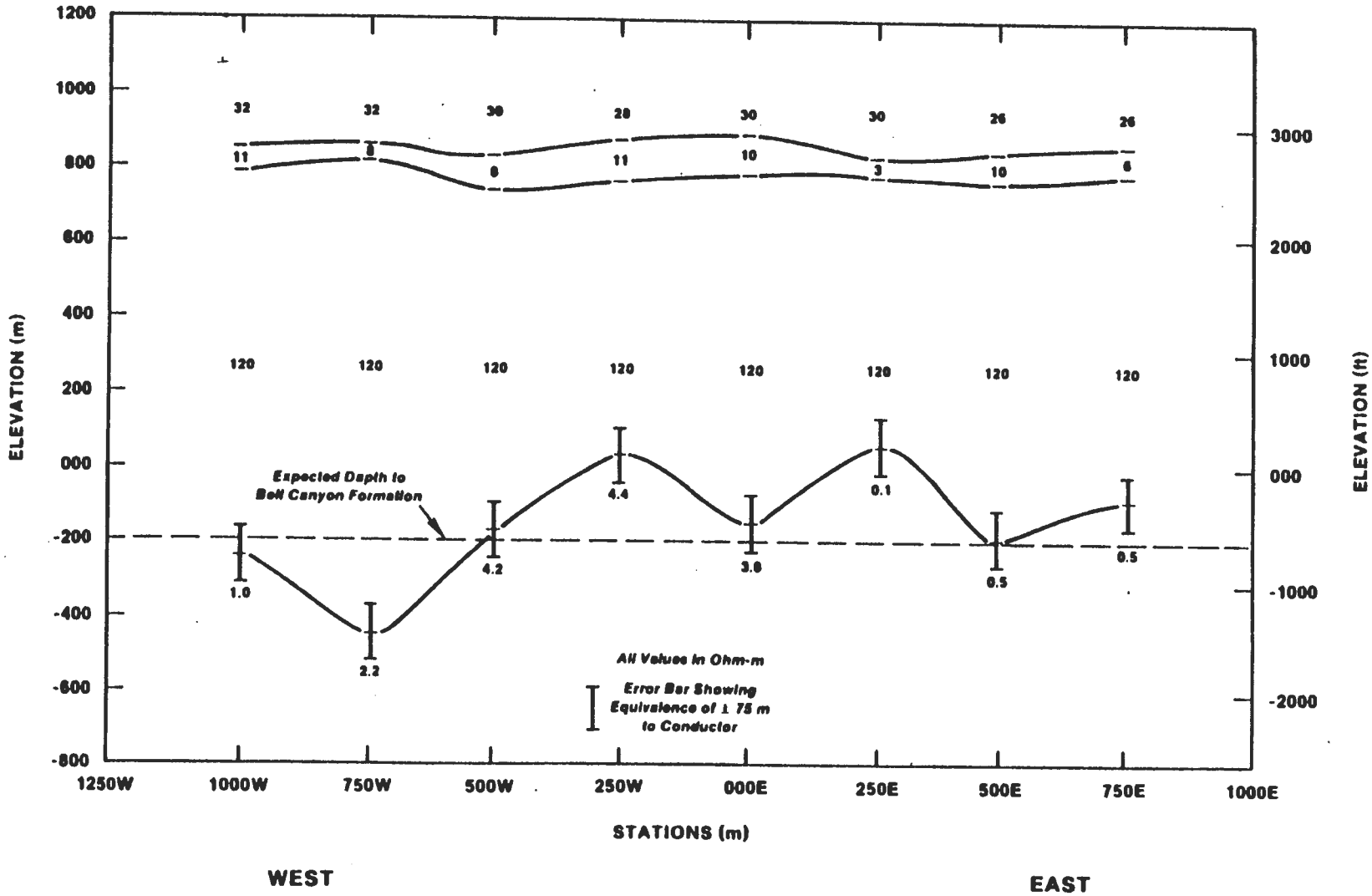


Figure 3.6: Cross section of apparent depth to first major deep conductor, showing brine locally present in both the Bell Canyon and Castile Formations. Line of section is along the north side of the WIPP waste-emplacement panels. Figure 4-11 of Earth Technology (1987).

2. Isolation of meteoric waters within fractured anhydrites following episodic hydrologic connection of the Castile with the Capitan limestone (Lambert and Carter, 1984).

According to the first hypothesis, the brines would be localized by deformation of the Castile Formation. The brines would occur in relatively low-pressure areas, such as the crests of domal or anticlinal structures similar to those encountered at WIPP-12 and ERDA-6. Such brines might continue to be generated by slow gravitationally driven deformation during and after the WIPP operational phase. Borns (1983) estimated that the reduction of porosity of the Castile halites by 0.2% required to generate the volumes of brine encountered in the WIPP-12 domal structure would likely be indistinguishable in bulk-property measurements. As pointed out by Borns (1987b), mechanical displacement and/or fluid movement during gravity-driven deformation need not be continuous. From a mechanical point of view, the emplacement of Castile brines appears consistent with either continuous or episodic deformation, and would result in indistinguishable changes in the properties of surrounding Castile halites. However, as discussed in Section 3.1, regional deformation within the Castile Formation is probably too slow to be of concern in the performance of the WIPP facility.

Lambert and Carter (1984) conclude, on the basis of uranium-disequilibrium studies, that the Castile brine occurrences were neither in-place nor remobilized connate Castile fluids. They conclude that the brine occurrences are the result of isolation of waters resulting from intermittent or episodic lateral hydraulic connection of the Capitan limestone and Castile anhydrites. Local fracturing of the Castile anhydrites is still required. Lambert and Carter (1984) specifically conclude that:

1. The residence or isolation times for the Castile brines at ERDA-6 and WIPP-12 are between 360,000 and 880,000 years.

2. The extent of buildup in $^{234}U/^{238}U$ ratios expected to result from continuous exposure of fresh rock to fluids during gravity-driven deformation is not seen.

3. Therefore, the mode of emplacement of the Castile brines must be episodic in character. The relevant episodic feature of the system is interpreted by Lambert and Carter (1984) to be hydraulic connection between the Castile anhydrites and the Capitan limestone. Any future brine generation, according to this interpretation, would require hydrologic reconnection of the Capitan and Castile.

In summary, recent geophysical studies indicate that brines are probably present within Castile anhydrites under a portion of the WIPP waste-emplacement panels. The brines are 250 m or more stratigraphically below the WIPP facility horizon. Although the detailed distribution of the brines remains unknown, this is not of special concern, since the presence of Castile brines beneath at least a portion of the WIPP facility has been and will continue to be assumed in WIPP performance assessment. The

mechanism(s) giving rise to Castile brine occurrences are not completely known. However, both mechanisms proposed, fluid migration in response to episodic deformation and isolation of fluids resulting from episodic interconnection of the Capitan limestone and Bell Canyon Formation, are unlikely to generate significant additional brine beneath the WIPP facility in the 10,000-year time scale of regulatory interest.

## 3.3 Recent Hydrologic, Geochemical, and Structural Studies of the Salado Formation

As mentioned above, the WIPP facility is presently being developed within bedded halites and anhydrites of the Salado Formation, at an average depth of approximately 655 m. This section attempts to place the WIPP facility within a proper perspective relative to both local and regional-scale hydrologic and structural behavior of the Salado Formation. Differences in Salado behavior as a result of the presence of the WIPP facility are considered as "excavation effects."

Section 3.3.1 discusses the hydrologic behavior of the Salado Formation as interpreted from testing conducted from the surface and within the WIPP facility. Section 3.3.2 describes the present understanding of the fluid geochemistry and mineralogy of the Salado Formation, based on recent and ongoing studies within the WIPP facility. Section 3.3.3 discusses the interim results of ongoing investigations into the structural behavior of the Salado Formation adjacent to the WIPP facility, with emphasis on Marker Bed 139 (MB139), a relatively thick anhydritic marker bed approximately 1 m below the WIPP facility horizon.

### 3.3.1 Regional-Scale and Near-Facility Hydrology of the Salado Formation

3.3.1.1 Hydrologic Testing from the Surface and at the Facility Horizon--Unlike the case in the Castile Formation, significant brine flows have not been encountered in hydrologic testing of the Salado Formation from the surface. However, two anomalous phenomena have been encountered in the Salado. First, pressurized gas has been encountered in some holes drilled from the surface and near the mining face in WIPP excavations. In the most dramatic case, nitrogen gas was encountered in the upper portion of the Salado in hole AEC-8, at a depth between 335 m and 391 m, during reworking of the hole approximately one year after original drilling (Table 3.1; Mercer, 1987). The gas pressure was sufficient to partially remove the drillstem from the borehole. A large volume of gas, approximately 6 x $10^5$ $m^3$, was allowed to flow to the surface without apparent depletion of the reservoir (Mercer, 1987). Gas has also been locally encountered during construction of the WIPP facility, as described in Deal and Case (1987). To date, all gas occurrences within the WIPP facility have been small, although the largest such occurrence did result in a 0.4-m diameter disk being blown out of the face being mined. Second, as shown in Table 3.1, long-term monitoring at some holes penetrating the Salado Formation indicates a slow buildup of fluid pressure. The maximum pressure measured to date is 3.3 MPa (472 psig) at WIPP-12. This pressure is generated within the Salado, since it was measured before the hole was deepened into

Table 3.1: Summary of known Salado gas occurrences and measured wellhead pressures from surface drilling. Gas-occurrence data are modified from Table 2 of Mercer (1987). Fluid-pressure data are from the text of Mercer (1987).

A. Gas Occurrences

| Hole | Comments |
|---|---|
| ERDA-9 | At 430 m; trace of $H_2S$ |
| ERDA-6 | At 561 m; blew for 30 min. |
| AEC-7 | At 491 m; blew for 1 hour |
| AEC-8 | At 335-391 m; blew for several months |
| P-7 | Many kicks |
| P-12 | Hole unloaded fluid over weekend |
| P-20 | Slight blow at TD of 608 m |

B. Pressures Measured at Surface

| Hole | Comments |
|---|---|
| Cabin Baby | 1.4 MPa |
| WIPP-12 | 2.94 MPa, <u>before</u> deepening |
| WIPP-13 | 2.93 MPa, hole open to Castile and Salado |
| WIPP-11 | 0.12 MPa |
| DOE-2 | 0 |
| AEC-7 | 0 |

the Castile Formation and intersected Castile brines (Section 3.2). The rate at which Salado brine pressures build up is very slow and, as noted by Mercer (1987), the pressures appear to be supported by only very small volumes of fluid. Complete reduction of the 1.6 Mpa (228 psig) pressure at the WIPP-12 wellhead in 1985 was achieved by release of approximately 5 gallons of brine. In some holes, for example DOE-2 and AEC-7, no long-term pressure buildup has been observed.

The published results of "successful" hydrologic tests of the Salado from the surface (Table 3.2) indicate permeabilities from approximately 0.01 microdarcy to a high of 25 microdarcies. Ongoing evaluation indicates that, as a result of instrumentation limitations, testing-time limitations or problems with pressure or flow stabilization, data from the Salado in DOE-2 are the most reliable, indicating a maximum permeability of 0.3 microdarcies. It has not been possible in testing from the surface to identify any discrete sources for this fluid or to determine any stratigraphic effects.

Table 3.2: Summary of Salado hydrologic properties interpreted in hydrologic testing from surface. Modified from Tables 3 through 9 of Mercer (1987). Ongoing interpretation indicates that only results from hole DOE-2 are reliable.

| Hole | Comments |
|---|---|
| AEC-7 | 550.8-581-3 m; MB 126; gas perm. 3 x $10^{-6}$ D |
| AEC-7 | 672.7-703.2 m; MB 139; gas perm. 12-21 x $10^{-6}$ D |
| ERDA-9 | 436.8-452.9 m; MB 118, 119; perm. 0.1-0.7 x $10^{-6}$ D |
| ERDA-9 | 613.9-638.3 m; MB 136, 137; perm. 0.6-3.2 x $10^{-6}$ D |
| ERDA-9 | 765.7-798 m; Cowden, lower Salado; perm. 1.6-2.2 x $10^{-6}$ D |
| ERDA-9 | 799.5-876 m; lower Salado; perm 0.4-6.5 x $10^{-6}$ D |
| ERDA-9 | 799.5-826.9 m; lower Salado; perm. 0.7-25 x $10^{-6}$ D |
| Cabin Baby | 230.7-828.2 m; entire Salado; perm. 0.01-0.1 x $10^{-6}$ D |
| DOE-2 | 669-703.8 m; MB 138, 139; perm. $\leq$0.3 x $10^{-6}$ D |

However, there has been only limited "success" in field testing of the Salado from the surface. There appear to be two causes for this. First, the formation permeability appears in many cases to be below the testable minimum for the equipment used, approximately 0.01 to 0.1 microdarcy. For example, testing of all intervals in holes AEC-8, ERDA-10, and WIPP-12 was unsuccessful due to the low permeability and limitations to the test equipment. The most recent results included in Table 3.2, based on testing in Cabin Baby-1 in 1983 and DOE-2 in 1985, suggest an upper permeability

limit of approximately 0.3 microdarcies. As noted by Mercer (1987), it is not clear that any of the successful tests indicate the permeability of undisturbed halite, since the test intervals almost always include one or more interbeds. Second, in the case of hole WIPP-12, hole "ageing" during the seven years between hole completion and attempted testing of the Salado made it extremely difficult to find locations in the borehole that allowed successful setting of packers to isolate intervals for drillstem testing. The tentative interpretation is that this ageing involves loosening of grain boundaries in halites, with a concomitant increase in local permeability around the borehole.

Flow testing of the Salado Formation within the WIPP facility is still in its early stages. Preliminary results indicate that the presence of the WIPP facility has a strong impact on the hydrologic behavior of nearby portions of the Salado Formation. The results of initial gas-flow testing in the WIPP facility are described by Stormont et al. (1987). Interpretation of this testing indicated that apparent gas permeabilities are very low at distances of greater than approximately 2 m from the underground workings, with no distinguishable stratigraphic variability. Stormont et al. (1987) calculate a "far-field" permeability of less than 1 microdarcy for the Salado.

Stormont et al. (1987) identify a zone of markedly increased permeability within approximately 2 m of the underground workings, on the basis of marked increases in gas flow rates at constant injection pressure. The apparent increases in permeability are especially dramatic near room center lines, in both room roofs and floors. In addition, the magnitude of the local increases in permeability appear to be a function of both time and room width. Stormont et al. (1987) note that their measurements are consistent with time-dependent development of a dilatant or "damaged" zone around the underground workings, and that this zone may well be only partially saturated. Finally, Stormont et al. (1987) indicate that the interpretation of their tests was complicated by uncertainties in the degree of saturation of the Salado, pressure-threshold effects inherent in gas-flow testing in either a partially or fully saturated medium, and local flow inhomogeneities due to fracturing in the disturbed or altered zone near the facility.

Recent brine-flow testing within the WIPP facility described by Peterson et al. (1987) has eliminated some of the problems inherent in gas-flow testing. Peterson et al. (1987) describe the results of long-term (240-day) shut-in brine-flow tests in two holes. One hole penetrated "intact" halite and the other "intact" anhydrite in MB139, both at a distance of 8 to 9 m from the underground workings. Assuming complete saturation within the tested zones, the results indicate far-field permeabilities of approximately 0.001 microdarcy for intact halite, and 0.01 microdarcy for MB139. In addition, apparent steady-state "pore" pressures of 8.3 MPa and 10.3 MPa were measured in the two holes. Peterson et al. (1987) note that there is some uncertainty in both estimated permeabilities and fluid pressures, due to the long test times required.

Gas-flow testing of the same two holes prior to brine-flow testing, at a gas-injection injection pressure of 2.1 MPa, indicated halite and marker-bed permeabilities approximately one order of magnitude greater than

indicated in the later brine-flow testing. These higher permeabilities are similar to those reported by Stormont et al. (1987). Gas-flow testing after brine-flow testing indicated effectively zero permeability. The reasons for this complexity are not clear. It may well be that initial gas-flow testing utilized unsaturated flow paths resulting from near-hole dilatancy, and that these flow paths were later saturated during brine-flow testing.

However, it is not clear that the Salado Formation is completely saturated, even in the far-field. For example, the gas "blows" locally encountered in drilling the Salado from the surface (see Table 3.1) indicate that high-pressure gases occur locally within the unit. Unfortunately, it cannot be determined whether the initial pressures in these occurrences represent regional partial saturation or are a result of exsolution of dissolved gases as a result of stress release around drilled holes. The large gas flow in the Salado in hole AEC-8 occurred approximately one year after initial hole completion. Experience during the development of the WIPP facility also indicates the local occurrence of gas within the Salado at high pressure, perhaps approaching the local lithostatic pressure of 16 MPa. Release of gas concentrated along a fracture nearly parallel to the facility working face resulted in a small blowout during mining operations, as described by Deal and Case (1987). Later drilling in front of the same working face encountered gas at a depth of approximately 3 m. However, because gas occurrences within the WIPP facility have all been near faces being actively mined, it cannot be demonstrated that they were at lithostatic pressure before release. They may result from exsolution of dissolved gases during stress release near the excavation. Other observations by Deal and Case, such as the widespread exsolution of gas from brines collected within the WIPP facility and local bubbling of brine seeps on ribs within the facility, further suggest that gas may play a major role in at least the near-field hydrologic behavior of the Salado Formation.

Thus, the results of recent permeability testing within the Salado Formation, both within the WIPP facility and from the surface, are generally consistent with a far-field permeability of approximately 0.001 to 0.1 microdarcy. It is not certain whether the Salado is saturated or partially saturated regionally; in the altered zone near the WIPP facility, it appears to be partially saturated. There are marked near-field increases in Salado permeability near the WIPP facility, resulting from fracturing and possibly matrix dilatancy. The development of a hydrologically altered zone around workings at the WIPP facility horizon appears to depend on both time and geometry. The ultimate extent of this zone and the rate or extent of its elimination or reduction during the final stages of facility closure remain unknown at present, but will be examined carefully during the early operational phase.

3.3.1.2 Hydrologic Testing Adjacent to the WIPP Air-Intake Shaft--Barring a direct breach of the WIPP as a result of human intrusion, the successful long-term performance of the facility largely depends on the success with which the facility shafts are plugged or sealed. Present planning calls for emplacement of shaft seals in both the Salado Formation and the unnamed

lower member of the Rustler Formation. Therefore, it is important to know the distribution of hydrologic properties within both units adjacent to the WIPP shafts. A preliminary series of hydrologic tests was conducted at several levels in the WIPP waste-handling shaft during 1987. Additional testing and monitoring of the hydrologic characteristics of both the Rustler and Salado Formations adjacent to the WIPP air-intake shaft is planned.

The objectives of the preliminary hydrologic testing adjacent to the WIPP waste-handling shaft, results of which are described in Saulnier and Avis (1988), were to:

1. Determine if a significant fractured or altered zone had developed around the concrete shaft liner in the shaft since its completion.

2. Estimate the radial extent of the hydrologic cone of depression resulting from construction of the waste-handling shaft.

3. Determine "far-field" hydrologic properties for previously untested zones in the lower unnamed member of the Rustler Formation and levels in the Salado Formation at which it is anticipated that plugs might be placed at the end of the WIPP operational phase.

Testing in the waste-handling shaft was carried out in subhorizontal drillholes, using three distinct test zones. The detailed experimental instrumentation is described in Stensrud et al. (1988). Zone 1 extended from the hole "bottom" approximately 7.9 m outside the shaft to a depth of some 5.7 m, Zone 2 from approximately 4.8 m to 3.7 m, and Zone 3 from approximately 2.9 to 1.6 m. There was, however, some variability in both test-zone depths and the relationship between Zone 3 and the shaft liner. No shaft liner was present below the 850-foot level. The shaft liner was thin enough in the lower Rustler for Zone 3 to test entirely within the rock mass. At the 850 level, however, the thickened shaft liner in the keyway dictated that Zone 3 in one hole included the interface between rock and shaft liner. (English depth units are used here for consistency with depth records within the shaft).

The results of the preliminary testing in the waste-handling shaft are summarized in Table 3.3 and Figures 3.7 and 3.8. Tested lithologies include mudstone and claystone in the unnamed lower member of the Rustler (at the 782 and 805-foot depths, respectively) and halites, an anhydrite, and a polyhalite within the Salado Formation (850 and 1320-foot depths). All of the tested intervals are extremely low in permeability. Hydraulic conductivities listed in Table 3.3 range only from $10^{-14}$ to $10^{-13}$ m/s. This corresponds to an approximate range in permeability of one order of magnitude,[1] from 0.001 to 0.01 microdarcy. There is no consistent increase in conductivity towards the shaft (from Zone 1 to Zone 3) in any of the rock types tested, except at the 850-ft level. In the 850W hole, pressurized fluids flowed into the borehole at the liner/rock interface. The precise origin of these fluids remains to be determined.

Table 3.3: Summary of results of 1987 hydrologic testing in the WIPP waste-handling shaft. From Saulnier and Avis (1988).

| Borehole | Lithology | Test Zone Depth Int. (Feet from Shaft Wall) | Test Period | Pressure Pulse (psi) | Hydraulic Conductivity (m/s) | Formation Pressure (psi) |
|---|---|---|---|---|---|---|
| W782W | Silty Mudstone | 1) 18.6-26.0 | 07/18-22/87 | 113.3 | 1.0 E-13 | 90 |
| | | 2) 12.3-15.9 | 07/20-22/87 | 108.3 | 1.0 E-14 | 140 |
| | | 3) 5.4- 9.5 | 07/21-22/87 | 99.4 | 1.0 E-14 | 140 |
| W805W | Silty Claystone | 1) 18.6-26.0 | 07/11-15/87 | 94.5 | 5.0 E-14 | 225 |
| | | 2) 12.3-15.9 | 07/13-15/87 | 105.1 | 1.0 E-14 | 140 |
| | | 3) 5.4- 9.5 | 07/14-15/87 | 97.8 | 1.0 E-14 | 110 |
| W805SW | Silty Claystone | 1) 18.6-26.5 | 08/28-31/87 | 102.9 | 6.0 E-15 | 275 |
| | | 2) 12.3-15.9 | Not Tested | | 1.0 E-14* | 90* |
| | | 3) 5.4- 9.5 | 08/29-31/87 | 92.6 | 2.0 E-14 | 70 |
| W850W | Halite | 1) 18.6-26.0 | 07-30/08-03/87 | 97.6 | 1.0 E-13 | 40 |
| | | 2) 12.3-15.9 | 08/2-3/87 | 116.5 | 1.0 E-13 | 40 |
| | | 3) 5.4-9.5 | 07-31/08-3/87 | 90.39 | Not Analyzable* | |
| W850SE | Halite | 1) 23.2-36.0 | 08/19-24/87 | 103.5 | 3.0 E-14 | 50 |
| | | 2) 16.8-20.5 | 08/21-24/87 | 103.1 | 3.0 E-14 | 30 |
| | | 3) 10.0-14.1 | 08/22-24/87 | 100.7 | 2.0 E-14 | 90 |
| W1320E | Halite/ Anhydrite Polyhalite | 1) 18.6-41.8 | 08/11-17/87 | 173.3 | 2.0 E-14 | 550 |
| | | 2) 12.3-15.9 | 08/14-17/87 | 52.6 | 3.0 E-14 | 450 |
| | | 3) 5.4- 9.5 | 08/15-17/87 | 53.0 | 3.0 E-14 | 100 |

*Zone 2 analysis from pressure buildup after shut-in, August 28 to 31, 1987.

Physical limitations to the testing system dictated that Zone 3 not extend any closer than approximately 1.6 m from the inside of the shaft. Therefore, even if the one or two holes tested at each level are representative and adequately characterize the permeability at the tested levels, it can only be argued that the results indicate that no damaged zone presently extends more than 2 m into the rock mass. This includes any damage zone resulting from blasting during construction of the shaft. In addition, because of scheduling constraints, all of the testing was relatively short-term. Longer-term testing might identify changes in hydraulic properties near the shaft.

The permeabilities listed in Table 3.3 indicate no significant stratigraphic variability. All of the tests indicate extremely low permeability, roughly one order of magnitude less than estimated from measurements from the surface. One reason for this may be that the holes tested here were nearly horizontal; as a result, at least part of the fluid flow was vertical, perpendicular to layering. The results may imply that vertical

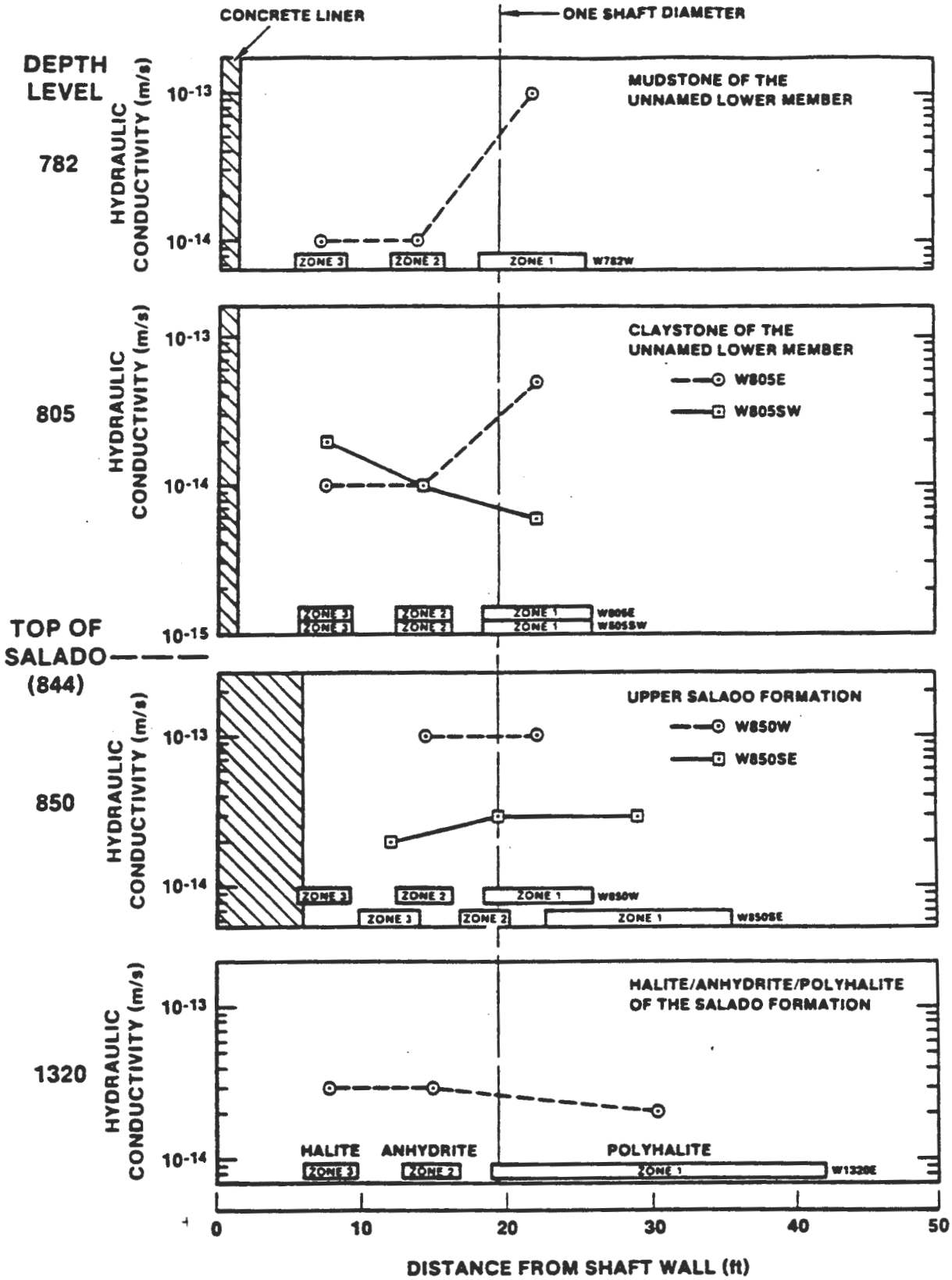


Figure 3.7: Summary of formation conductivities determined in 1987 testing in the WIPP waste-handling shaft. Figure 6.3 of Saulnier and Avis (1988).

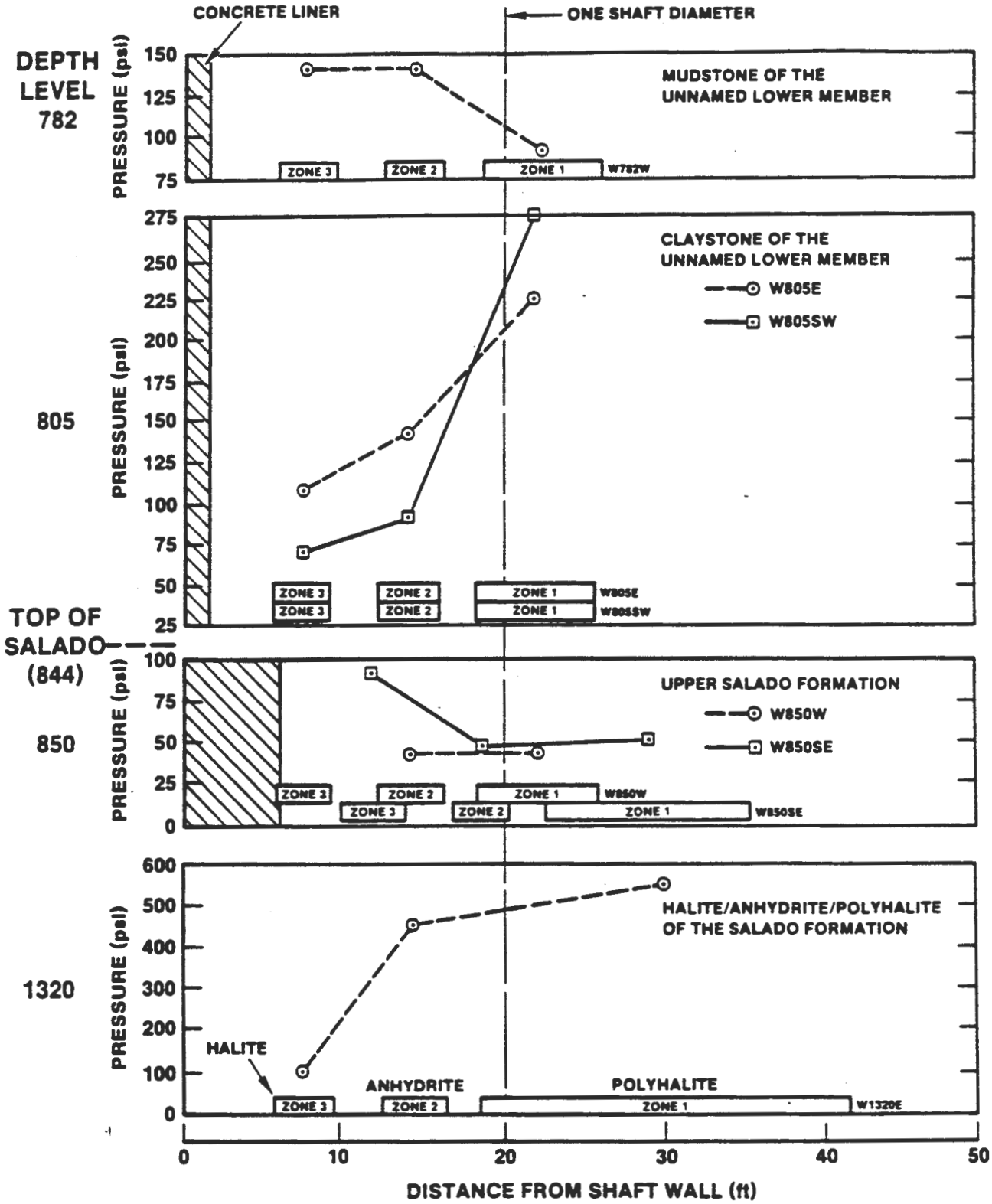


Figure 3.8: Summary of fluid formation pressures determined in 1987 testing in the WIPP waste-handling shaft. Figure 6.1 of Saulnier and Avis (1988).

permeability in both the lower part of the Rustler Formation and the Salado Formation is less than horizontal permeability, consistent with experience in other layered rock types.

Testing adjacent to the waste-handling shaft did indicate a distinct zone of decreased fluid pressures around the shaft at the 805-foot and 1320-foot levels, in claystone and halite/anhydrite/polyhalite, respectively (Figure 3.8). The cone of fluid-pressure depression apparently extends outward to greater than one shaft diameter at these levels. The fluid-pressure profiles at the 782-foot and 850-foot levels may be indeterminate because of effects of equipment compliance (Saulnier and Avis, 1988). The generation of a hydraulic cone of depression around the shaft was expected, consistent with responses noted earlier in the Culebra dolomite to construction of the WIPP exploratory shafts (see Haug et al., 1987). The behavior of this zone outside the Culebra as a function of time remains unknown.

Interpretation or prediction of long-term flow behavior into the shaft would require an observation hole, so that fluid storativities within affected units could be estimated. A nearby observation hole does not exist for the waste-handling shaft. However, hole H-16 was drilled and instrumented in 1987, approximately 17 m from the centerline of the WIPP air-intake shaft, specifically to investigate the near-field hydraulic response of all members of the Rustler Formation to construction of the shaft, and to provide monitoring data adequate for long-term predictions.

The hydrologic testing completed to date adjacent to the waste-handling shaft is preliminary, as is the interpretation of test results. The results to date allow limited fracturing, since only one or two holes was tested at each level. To better determine the presence or absence of fracturing by direct hydrologic measurement, arrays of three or more holes would be needed at each level. The fact that fluids were encountered at the liner/rock interface in one hole at the 850-foot level demonstrates that fluid movement at the shaft-liner/rock interface is possible locally, and that a single drillhole is not sufficient to characterize the source or behavior of these fluids. Non-intrusive geophysical methods similar to those described in Section 3.3.1.3 may aid in characterization of any altered zone around the WIPP shafts.

3.3.1.3 <u>Brine Contents and Brine Seepage into the WIPP Facility</u>--Geophysical studies within the WIPP facility aimed at characterization of the near-field disturbed rock zone are interim, and will continue during the early part of the WIPP operational phase. The presently available results, summarized in Borns and Stormont (1987) and Pfeifer (1987), indicate both that there is near-field variability in the water content and hydrologic properties of the Salado Formation and that water contents of Salado halites in the far-field are approximately twice that estimated at the time of the WIPP SPDV studies.

The results of a series of electrical conductivity measurements within the WIPP underground workings (Pfeifer, 1987) are shown in Figure 3.9. Two

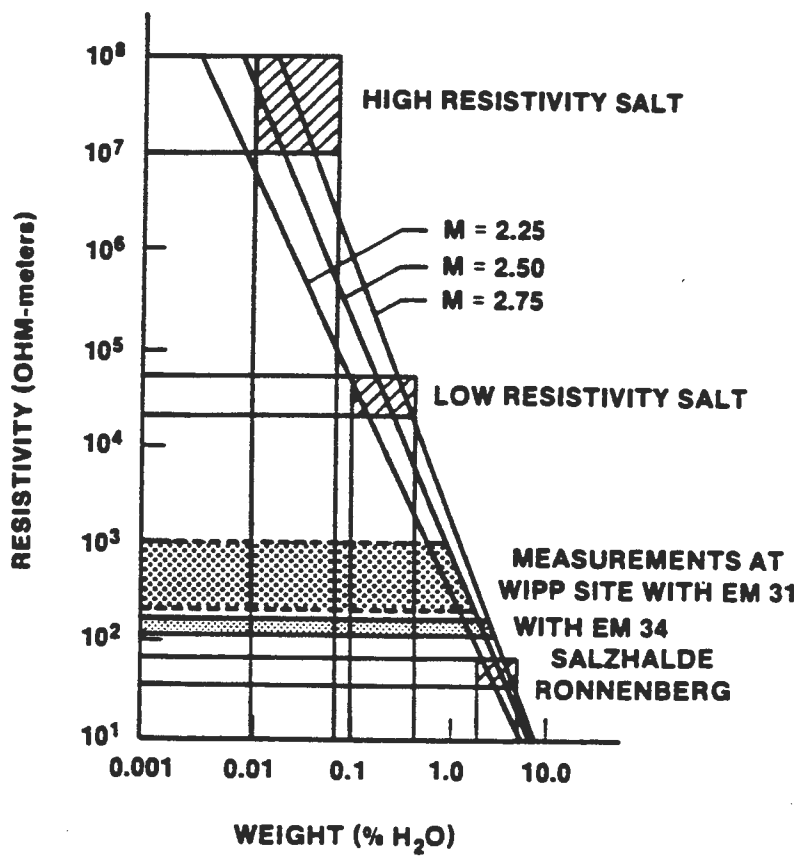


Figure 3.9: Apparent variation in water content of Salado halite at the WIPP facility horizon with depth into the wall. The EM31 survey investigates conductivity up to approximately 2 m depth and the EM34 survey to a depth up to 20 m. Figure 9 of Pfeifer (1987).

different instrumentation systems were used in these measurements. The EM31 system investigates the effective electrical conductivity to a depth of approximately 2 m, the EM34 system to a depth of up to 20 m into the adjacent rock mass. The apparent conductivity near the underground workings, measured with the EM31 system, is lower (resistivity is higher) than that measured at greater depth with the EM34 system. In Figure 3.9 this variation in resistivity is compared with a published correlation between water contents and resistivities of halites. The results are consistent with a water content of approximately 1% (by weight) near the mine opening and 2% or greater in the far field. Recent geophysical moisture and density measurements within the WIPP facility (Hudson, 1987) also are consistent with water contents of approximately 2 weight percent in Salado halite in the far field.

The recent results indicate that far-field water contents within the Salado Formation, estimated to average approximately 2 weight percent, are greater than previously expected. For example, estimated water contents of samples analyzed during SPDV activities ranged from a mean of 0.6 weight percent to a maximum of 1.8 weight percent, compared to mean and maximum values of 0.22 and 1.06 weight percent estimated from measurements on core from hole ERDA-9 (Beauheim et al., 1983a). The earlier estimates were made either on core material or on hand specimens collected during mining.

The combination of significant interconnected fluid contents and non-zero permeabilities within the Salado Formation in both the far-field and near the WIPP facility dictates that there be some fluid flow into the facility until effective hydrologic closure of the facility takes place. Two studies, both in their early stages, investigate the amounts and characteristics of fluid flow into the facility. One study, summarized in Deal and Case (1987), is a long-term study to characterize flow into the WIPP facility (exclusive of shafts) at ambient temperature. The second study, summarized in Nowak and McTigue (1987), is part of an experimental program using electrical heaters to simulate emplacement of defense-generated high-level waste (DHLW). A knowledge of ambient-temperature behavior is required in this study as a baseline for interpretation of later superimposed thermal effects.

Two lines of evidence summarized by Deal and Case (1987) indicate the complexity of ambient-temperature fluid flow into the WIPP facility from the Salado Formation. First, brine "seeps" often form within a few days on mined faces, and are indicated by the development of localized salt crusts or efflorescences on the walls. The seeps often appear to stop flowing after approximately one month. However, investigation of the salt deposits indicates that fluid flow may only decrease rather than ceasing entirely, and that the rate at which mine ventilation removes water locally exceeds the inflow rate at long times. Second, highly variable amounts of both brine and dissolved gas are intersected in drillholes within the WIPP facility. Minimum flow rates are apparently zero. The maximum flow rate was approximately 0.5 liter per day. One hole has produced approximately 235 liters of brine, and produced at a roughly steady-steady rate of 0.2 liters per day (Deal and Case, 1987). However, this hole apparently intersects numerous near-field fractures in MB139 related to the construction of the WIPP facility, and is unusual. Most of the measured

flow rates range from a few hundredths to a few tenths of a liter per day. Deformation near the facility strongly influences fluid flow. Deal and Case (1987) note that fluid flow into most holes within the WIPP facility is initially zero or nearly zero. This phase is normally followed by a relatively rapid rise to some maximum flow rate, after which flow slowly reduces to some relatively steady-state but decreasing value.

Work summarized in Nowak and McTigue (1987) investigates flow into one 0.9-m (36-inch) and three 0.76-m (30-inch) diameter holes emplaced as part of experiments simulating and overtesting emplacement of DHLW. Water was continuously removed from the holes by use of dry nitrogen. A baseline ambient-temperature flow of 5 to 15 grams/day was collected in each hole after an initial transient phase. The average flow of 10 grams per day extrapolates to a steady-state flux of approximately 1.6 $cm^3/day/m^2$ of excavation wall. After the heaters were turned on, there was a rapid increase in flow rate to some peak value, followed by a reduction to near steady-state flow. Apparent steady-state flow rates were 50 to 80 g/day in the two holes containing 1.5 kW heaters, and 8 to 10 g/day in the two holes containing 470 W heaters. The integrated fluid flow into the most strongly heated holes was 36 to 38 kg of fluid after 600 days. This mass is significantly greater than the 0.1 kg collected after two years in similar experiments conducted in domal salts at the Asse Mine, Germany (Nowak and McTigue, 1987). The difference suggests a significant difference between fluid flow in domal salts and in bedded salts, such as those at the WIPP.

Parametric numerical modeling described by Nowak and McTigue (1987) indicates that:

1. Pore-pressure measurements in both the near-field and far-field domains of the Salado Formation are needed to determine far-field and near-field flow behavior, since the observed transient effects resulting from seepage appear at present to be limited to the very near-field domain.

2. The transient stage of flow into the WIPP waste-emplacement rooms will last until connected pore space in both the rooms and any altered zone around the facility is either effectively eliminated or comes to pore-pressure equilibrium with the surrounding Salado. The calculations indicate that transient flow, ignoring closure, might last for more than 5000 years.

3. The rock volume effectively involved in flow within the Salado may be limited, rather than a significant portion of the formation. However, the affected volume must increase with time.

In summary, recent hydrologic results in the Salado Formation indicate that the unit has a far-field permeability of less than 0.1 microdarcy. It has not been possible to determine either stratigraphic effects or the presence of effective fracturing in the far-field environment. The brine content of Salado halites appears to be up to 2 weight percent in the far-field, roughly twice that previously expected. Where it has been possible to measure Salado brine pressures, the calculated heads indicate very limited fluid flow upwards into the overlying Rustler Formation. The permeability

of the Salado locally increases markedly within two meters of excavations at the WIPP facility horizon. The increase in permeability appears to be both time-dependent and geometry-dependent, and to involve significant fracturing. The Salado Formation may be only partially saturated in both the near-field and far-field environments. The low permeability of the Salado Formation, mine ventilation, and rapid mechanical deformation near the WIPP facility result in markedly transient fluid flow into the underground workings. At present, the time-scale of transient flow, volume of the Salado involved in flow, and final fluid volumes to be expected within the WIPP facility remain to be precisely determined.

### 3.3.2 Geochemical and Mineralogical Studies of the Salado Formation Near the Facility Horizon

The mineralogy and stratigraphy of the Salado Formation are somewhat complex. The general mineralogy of the units is summarized by Bodine (1978), and mineralogy near the WIPP facility horizon by Stein (1985). Bodine (1978) noted that Salado clays were unusually depleted in aluminum and enriched in magnesium. The recent work by Stein (1985) does not include detailed clay mineralogy, but does indicate the nearly ubiquitous occurrence of authigenic quartz and magnesite near the WIPP facility horizon, in addition to widespread occurrence of anhydrite, gypsum, and polyhalite as accessory minerals within halites.

As mentioned in Section 3.3.1, it has not been possible to sample Salado fluids during drilling or testing from the surface. However, Salado fluids have been sampled within the WIPP facility, and are continuing to be collected, as described in Deal and Case (1987). The compositional results available to date for Salado fluids collected within the WIPP facility are described in Stein and Krumhansl (1986), and directly address both the character of fluids within the Salado Formation and the validity of assumptions held through 1983 concerning the types of fluids within the unit.

It was assumed through 1983 that Salado halites were anhydrous, with the exception of fluid inclusions and the water of hydration of hydrated minerals such as clays and polyhalites. Both the compositions and ages of fluid inclusions within Salado halites were poorly constrained. The compositional results for Salado fluid inclusions and macroscopic brine occurrences within the WIPP facility, summarized by Stein and Krumhansl (1986), are shown in Figure 3.10. The open and half-open squares in Figure 3.10 represent the compositions of individual fluid inclusions extracted from crystals of halite. The circles and crosses represent the compositions of macroscopic fluids collected from the WIPP facility, respectively from brine "seeps" on the walls and holes in the floor.

The fluid-inclusion compositions and compositions of fluids from seeps and holes form two distinct populations in terms of their respective Na/Cl and K/Mg weight ratios. Therefore, fluids encountered within the WIPP facility cannot primarily arise from the migration of fluid inclusions. Stein and Krumhansl (1986) relate the compositions of fluid-inclusion Groups I (half-open squares in Figure 3.10) and II (open squares) to alteration of brines

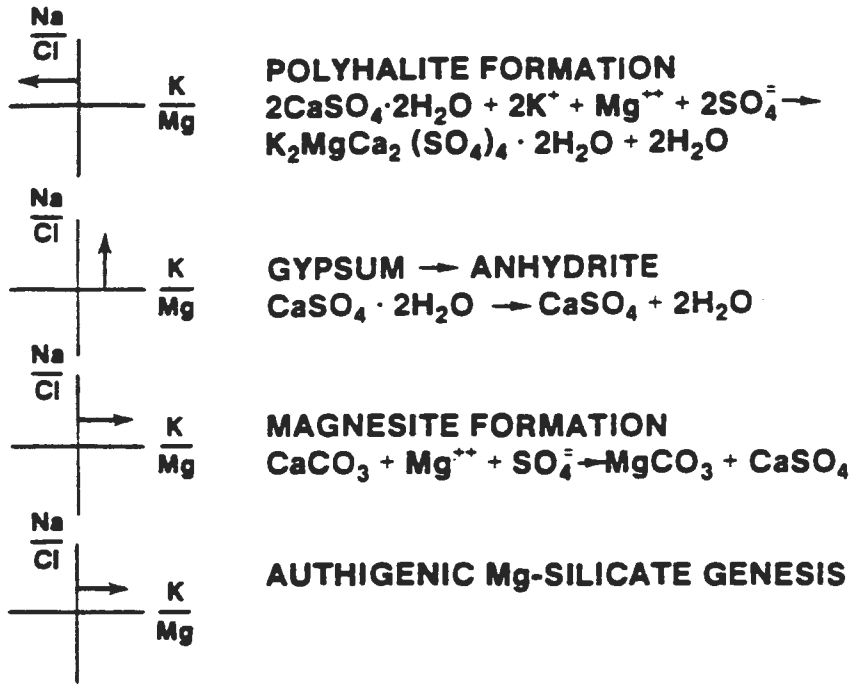


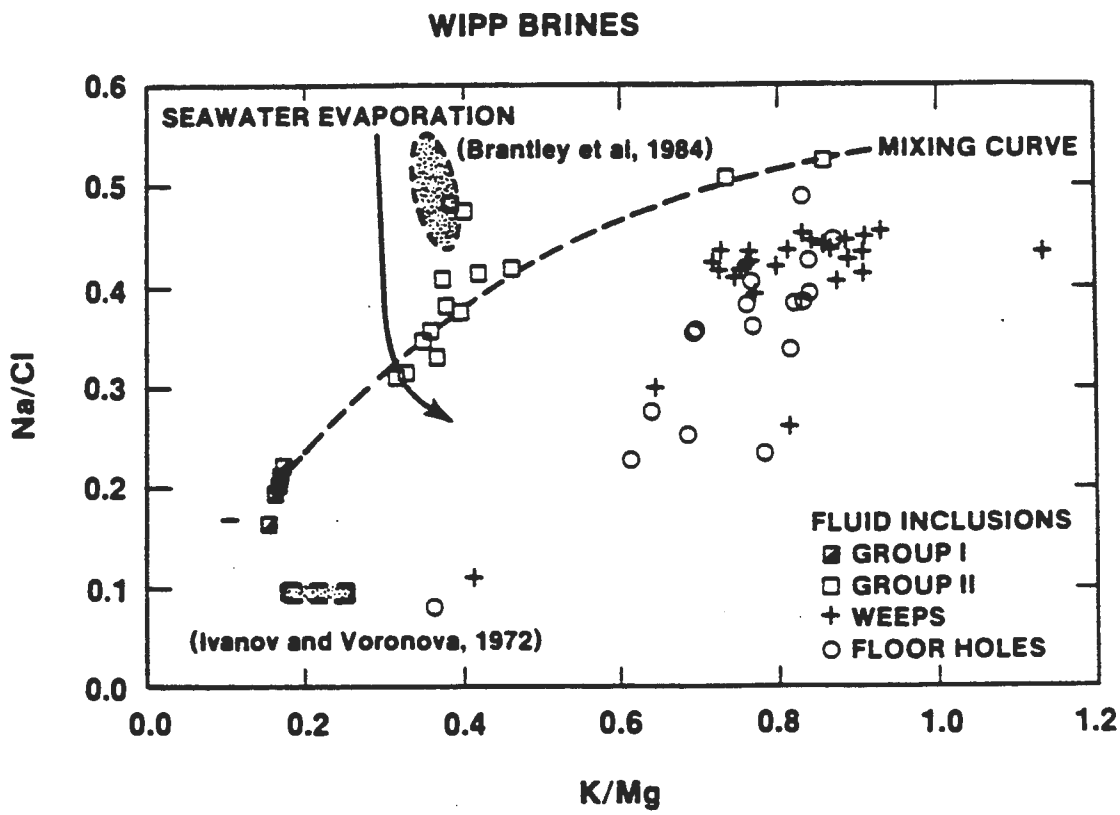


Figure 3.10: Compositional variability of Salado fluids from fluid inclusions and macroscopic brine occurrences in the WIPP facility. Figure 9 of Stein and Krumhansl (1986). Effects of individual reactions on fluid composition are also indicated.

originally resulting from evaporation of seawater. They interpret the controlling mechanisms to be crystallization of polyhalite and magnesite. Polyhalite formation drives fluid compositions to the left of the seawater-evaporation line in K/Mg space (Group I), while formation of magnesite drives fluid compositions to the right (Group II). The compositional effects of these reactions are summarized in the reactions included as part of Figure 3.10.

Both polyhalite and magnesite are widespread accessory minerals within Salado halites (Stein, 1985). Radiometric age dating of polyhalites from the WIPP (Brookins and Lambert, 1987) indicates crystallization ages of from 195 to 216 million years, i.e., from approximately 25 to 45 million years after deposition. The age of magnesite formation is unknown, but is assumed to be similar to that of polyhalite. On this basis, Stein and Krumhansl (1986) conclude that brines contained in fluid inclusions from samples near the WIPP facility horizon are roughly 200 million years old.

The fluids from weeps and seeps in the WIPP facility are enriched in potassium relative to both fluid inclusions and fluids expected from seawater evaporation (Figure 3.10). As discussed by Stein and Krumhansl and noted by Bodine (1978), the Salado clay-mineral assemblage is unusually Mg-rich. Stein and Krumhansl (1986) conclude that the relatively K-rich composition of fluids from weeps and seeps reflects the effects of the growth of these Mg-enriched silicates on grain-boundary fluids. While it is not possible to place a specific age on the grain-boundary fluids, it is known that the kinetics of such reactions are very slow. Therefore, Stein and Krumhansl (1986) conclude that the residence time of grain-boundary fluids within the Salado Formation must be at least several million years. The marked variability of fluids as a function of stratigraphy near the WIPP facility horizon, noted by Stein and Krumhansl, is consistent with there being little or no vertical fluid movement.

There is additional geochemical evidence for both the presence and timing of rock-water interactions involving fluids from the Rustler/Salado contact and deeper evaporite horizons at and near the WIPP. As summarized by Lambert and Harvey (1987), there is a body of consistent radiochronological evidence indicating the absence of any pervasive recrystallization of the evaporite section in approximately the last 200 million years. The internally consistent evidence consists of: a) K-Ar dating of polyhalites ($K_2MgCa_2(SO_4)_4 \cdot 2H_2O$); b) Rb/Sr isochrons on sylvites (KCl); and c) both Rb-Sr and K-Ar ages on langbeinite ($K_2Mg_2(SO_4)_3$). Apparent ages on leonite ($K_2Mg(SO_4)_2 \cdot 4H_2O$) are younger than ages on other minerals. Both Rb-Sr and K-Ar ages of clay minerals are significantly greater than the depositional age of the enclosing evaporites, suggesting that secondary reactions involving the clays have not completely altered their compositions. Thus, while the accessory magnesite near the WIPP facility horizon has not been dated, there is abundant radiometric evidence that the last major recrystallization of the Salado Formation occurred approximately 200 million years ago.

Available isotopic evidence for strong rock-water interactions in evaporitic rocks at and below the Rustler/Salado contact is summarized in Figure 3.11. These data and their implications for fluid flow are

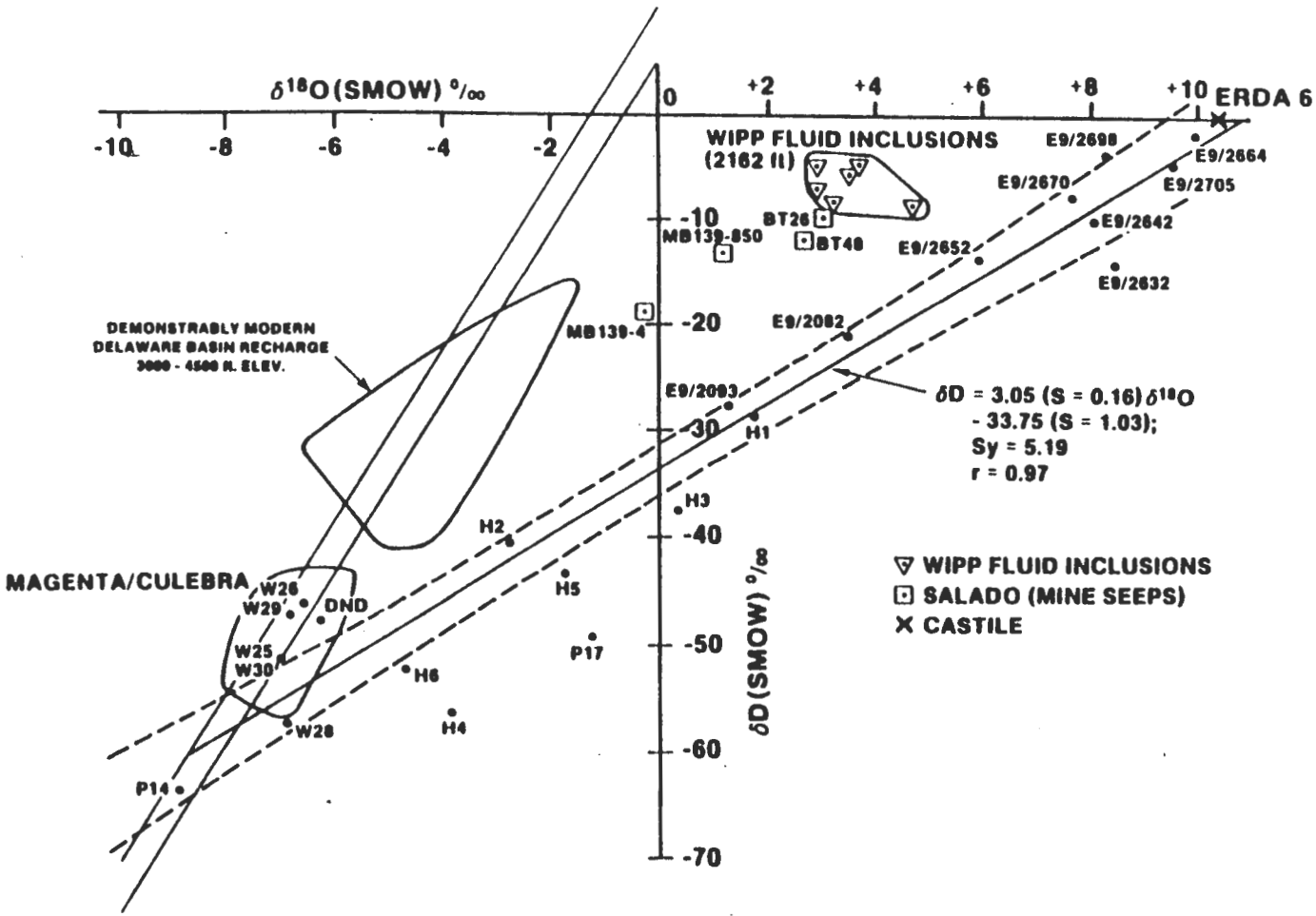


Figure 3.11: Stable-isotope composition of fluids from the Rustler/Salado contact and deeper evaporite zones at the WIPP site. Figure 25 of Lambert and Harvey (1987). Figure includes data from hole ERDA-9 (E9) of O'Neil et al. (1986) and fluid-inclusion data from the WIPP facility horizon (Knauth and Beeunas, 1986), in addition to original data from Lambert and Harvey. Lambert and Harvey data from the Rustler/Salado contact are indicated by hole designations, and those from MB139 by the appropriate prefix. Samples from seeps within the Duval Mine are indicated by the prefix BT (see Lambert and Harvey, 1987, for additional detail).

discussed by Lambert and Harvey (1987) relative to interpretations made by both O'Neil et al. (1986) and Knauth and Beeunas (1986).

O'Neil et al. (1986) consider the linear relationship between the isotopic composition of Castile brines (represented by brines from ERDA-6), fluid inclusions from the lower Salado in hole ERDA-9, and "modern meteoric water" (represented by fluids from Nash Draw and the western part of the WIPP site). They conclude that the trend reflects varying amounts of (vertical) mixing of Castile brines and modern near-surface waters. Lambert and Harvey (1987) conclude that large-scale mixing of fluids should involve major recrystallization of the evaporite section. They conclude, based on the radiometric-dating results discussed above, that such recrystallization has not taken place in the last 200 million years. Since they also concluded that large-scale mixing of fluids within an evaporite section would require recrystallization, the lack of significant recrystallization within the Salado is taken to indicate that there is no significant modern vertical mixing of Castile and surface fluids (Lambert and Harvey, 1987).

Instead, Lambert and Harvey (1987) consider the Castile fluids from ERDA-6, ERDA-9 fluid inclusions, and numerous fluids sampled from the Rustler/Salado contact as a single group (Figure 3.11). They conclude that these fluids form a variable population reflecting a mechanism by which increasing deviation of fluids from the meteoric compositional field results from increasing rock/water ratios, with resulting increasing interaction of fluids with hydrous minerals, especially clays, gypsum, and polyhalite. However, the isotopic character of rock-water reactions involving both gypsum and polyhalite are partially undefined at present.

One group of data shown in Figure 3.11 is not consistent with any single mechanism or trend of rock-water interaction within the Salado Formation. As noted, the trend including data from ERDA-6 brines, ERDA-9 fluid inclusions, and Rustler/Salado fluids appears to be continuous. However, fluids sampled directly in holes penetrating MB139 (samples MB139-850 and MB139-4) and in weeps within the nearby Duval Potash Mine (samples BT26 and BT48) are quite distinct. The isotopic composition of Salado fluid inclusions at the WIPP facility horizon reported by Knauth and Beeaunas (1986) are distinct and different from the character of inclusions from the Salado in ERDA-9. The reasons for the distinctions in fluid-inclusion analyses are not known, but may, as noted by Lambert and Harvey (1987), involve the different fluid-extraction techniques used by the different authors. The reason for the apparently distinct isotopic character of fluids from MB139 is not known at present. The available data indicate only a small isotopic distinction between fluid inclusions and macroscopic fluids collected at the WIPP horizon, in spite of the significant compositional differences between the two types of fluids noted by Stein and Krumhansl (1986).

In summary, the recent geochemical and hydrologic studies of the Salado Formation are generally internally consistent, but are incomplete at the present time. Hydrologic measurements indicate a far-field Salado permeability of less than 0.1 microdarcy. This indicates that, independent of local complications caused by the presence of the WIPP facility itself, fluid flow within the Salado is non-zero but extremely slow. The work by

Stein and Krumhansl indicates that the brine in fluid inclusions within Salado halites is on the order of 200 million years old, and is not the major source of fluid in the WIPP facility. Rather, the variable fluids in the WIPP underground workings appear to be grain-boundary fluids which have residence times within the Salado Formation of at least several million years. The variability in fluid compositions near the WIPP facility horizon is consistent with there being little or no vertical fluid movement. The isotope systematics and radiometric age dating of the Salado brines and minerals, considered together, are not consistent with derivation of Salado brines by modern large-scale vertical mixing of Castile and surficial waters.

### 3.3.3 Marker Bed 139 and the Structural Behavior of the Salado Formation near the WIPP Facility

Marker Bed 139, an anhydritic marker bed about 1 m in average thickness, occurs approximately 1 m or less below the WIPP facility horizon. Detailed study of MB139 began in 1983, because of concern that undulations on the top of the unit might be the result of deformation at some time after deposition or diagenesis (Jarolimek et al., 1983). If this were true, it is conceivable that such deformation might impact the WIPP facility during either the operational or regulatory time frames. The results of both Jarolimek et al. (1983) and Borns (1985) indicate, however, that the undulations on the upper surface of MB139 are depositional in origin.

Recent interest has focused on the mechanical and hydrologic fluid-flow behavior of MB139 near the WIPP underground workings. Observed behavior in room closure to date, especially in the oldest or "SPDV" rooms, indicates time-dependent opening of fractures in both MB139 and the halitic interval between MB139 and the room floors. It may be necessary to excavate MB139 in some areas before the end of operations, to provide an unaltered locality for emplacement of seals at the facility level. The mineralogy and structure of MB139 also provide information concerning long-term mechanical and fluid behavior within anhydritic portions of the Salado Formation, independent of the WIPP facility. Work examining MB139 and its role in excavation effects near the WIPP facility horizon is progressing; therefore, the discussion here is preliminary.

Borns (1985) investigated the stratigraphy and structure of MB139 in some detail, using core from a five-hole array drilled specifically for this purpose. The general level of internal complexity within MB139 is shown in Figure 3.12. The unit is bounded above and below by irregular contact zones. The lower contact zone (Zone V), often referred to informally as a "clay seam," is clay-rich and locally indicates some erosion and embayment of the top of the underlying polyhalitic halite. The upper contact zone (Zone I) is quite irregular in thickness, and contains structures indicative of shallow water deposition, such as mounds of halite hopper crystals. Borns (1985) concludes that the irregularities on the upper surface of MB139 are primary or depositional in origin, resulting from shallow-water depositional processes such as wave traction. This conclusion is in agreement with conclusions originally reached by Jarolimek et al. (1983).

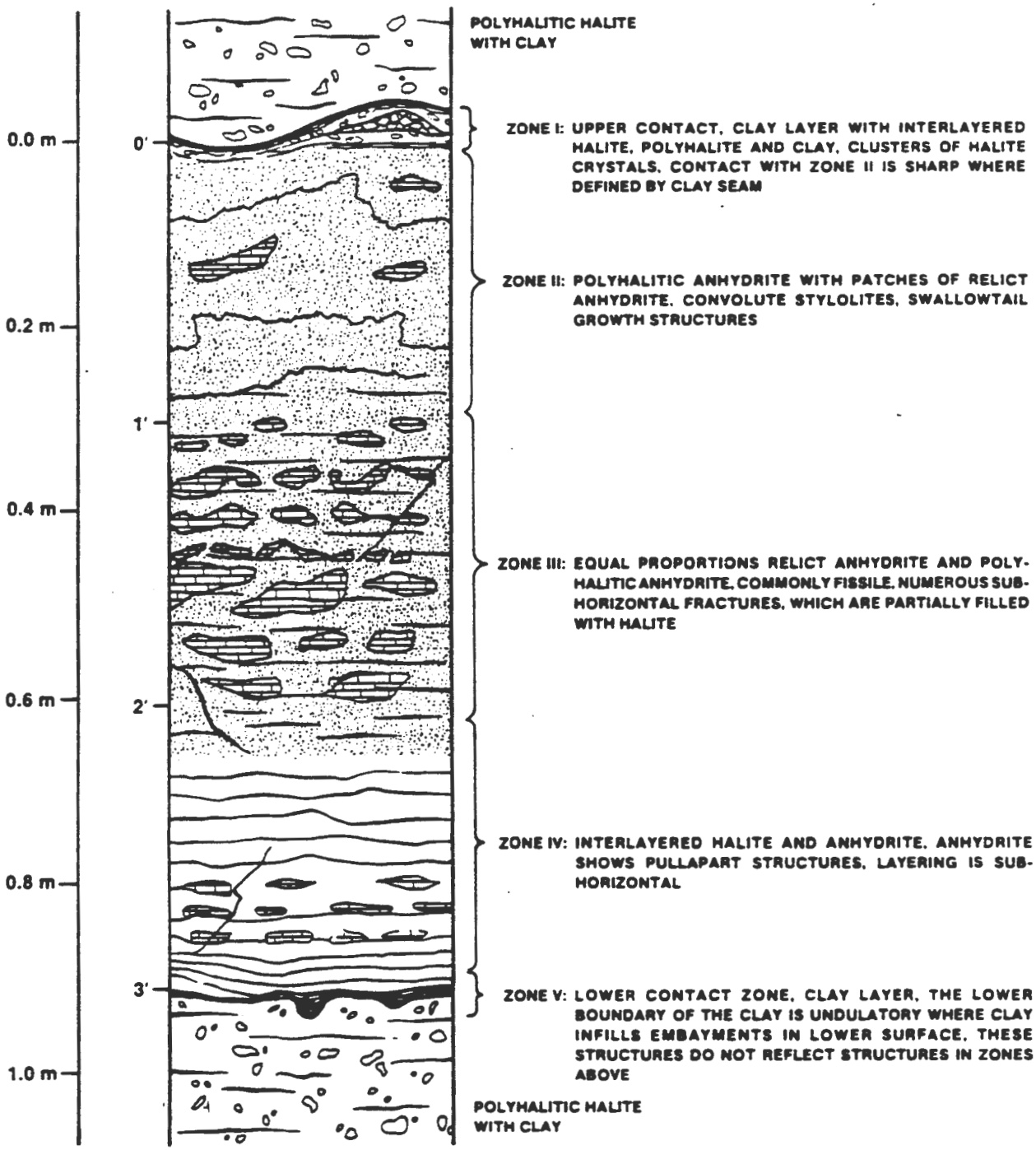


Figure 3.12: Generalized stratigraphic and structural cross section of MB139. The figure demonstrates the internal variability of the unit and the character of both upper and lower contacts. Figure 3 of Borns (1985).

The detailed investigations by Borns also revealed significant internal zonation and variability within the body of MB139. An upper zone within the unit (Zone II) is characterized by extensive replacement of original anhydrite by polyhalite (Figure 3.12), and by the presence of convoluted stylolites. Both features are interpreted to result from fluid movement after deposition. Based on the available radiometric ages on Salado polyhalites (Section 3.3.2), it may be that the formation of polyhalite MB139 occurred as much as 45 million years after deposition. However, polyhalites from within MB139 have not yet been dated. Zone IV, the internal zone directly above the basal contact, contains interlayered halite and anhydrite, with some replacement of anhydrite by later halite, again indicating fluid movement at some time. Anhydritic laminae in this zone show pull-apart structures with horizontal extension.

Within Zone III, the central portion of MB139, replacement of anhydrite by polyhalite is less complete than in Zone II. This zone also contains numerous sub-horizontal fractures, which are partially filled with halite and polyhalite. In some cases, inclined fractures extend from Zone III into or across the overlying Zones I and II. The cores investigated by Borns (1985) were drilled with air; halite was probably not removed from the fractures in Zone III during drilling. On this basis, Borns (1985) concludes that the partially healed subhorizontal fractures in the central part of MB139 predate the construction of the WIPP facility.

The time of formation of the fractures in MB139 is not known in detail. Borns (1985) suggests that they may have formed in response to long-term variations in the overburden pressure at the stratigraphic level of the WIPP facility. Alternatively, as noted by Borns (1985), the fractures may be a response to previous and/or ongoing gravity-driven deformation of the underlying Castile Formation. The horizontal orientation of most of the partially healed fractures favors an origin related to unloading.

An estimate of the variations in overburden pressure at the WIPP facility horizon, extrapolated from estimated variations in overburden at the contact between the Rustler and the Dewey Lake, is shown in Figure 3.13. The overburden pressure at the WIPP facility horizon is estimated to have varied between approximately 16 and 42 MPa since the end of deposition of the Dewey Lake Red Beds. The estimated overburden pressure at the end of the Cretaceous period, 42 MPa, is 2.6 times that at present. Based on stratigraphic interpretations, the reductions in overburden near the ends of the Cretaceous and Tertiary Periods appear to have been relatively sudden. If the interpretations of Borns (1985) are correct, and the sub-horizontal fractures within Zone III of MB139 formed by unloading in response to rapid erosion and removal of overburden, it follows that the formation of the fractures and at least initial movement of the halite-saturated fluids which resulted in their partial healing are probably either early Tertiary or early Pleistocene in age, i.e., that both fracture formation and fluid movement occurred either approximately 60 million or approximately 2 million years ago.

The mineralogical variability of MB139 and the occurrence of partially healed fractures within the central part of the unit have implications for both fluid flow and structural behavior of the unit. The widespread

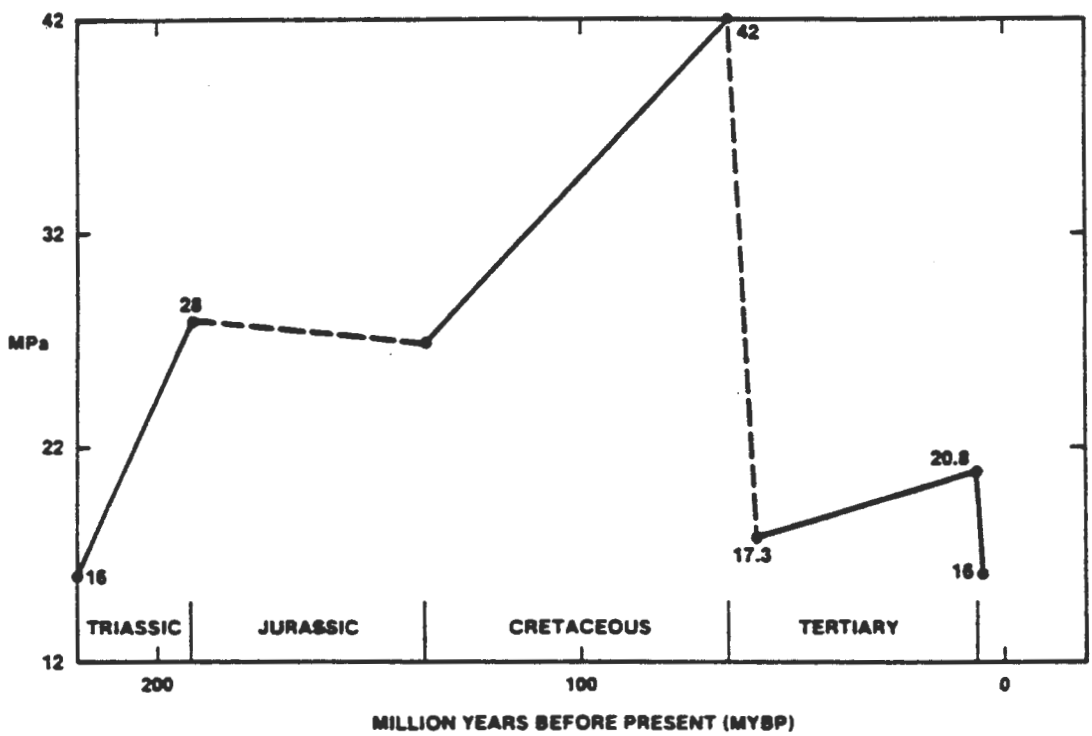


Figure 3.13: Variations in approximate overburden pressure at the WIPP facility horizon as a function of time. Overburden estimates (in MPa, 1 MPa = 145 psi) derived from Figure 10 of Borns (1985) by addition of constant 12 MPa overburden resulting from assumed constant thickness of interval between WIPP facility horizon and Rustler-Dewey Lake contact.

replacement of anhydrite by polyhalite indicates significant fluid movement, possibly some 45 million years after deposition. The replacement of anhydrite and partial healing of fractures by halite may indicate a second period of fluid movement at least 2 million years ago. The available hydrologic information for the Salado Formation at the WIPP site indicates that the far-field permeability within MB139 (and other anhydrite marker beds) is not significantly greater than that of the Salado halites themselves.

Pre-existing fractures within MB139 provide pre-existing planes of weakness that control or influence the near-field mechanical response around the WIPP excavation. Ongoing studies indicate that these fractures open locally in response to excavation. In the near-field altered zone, the resulting permeability is quite high. In the far-field, the permeability of MB139 appears no greater than that of surrounding halites. For confidence in plugging or sealing at the level of the WIPP facility horizon, it must ultimately be demonstrated either that fractures in MB139 will eventually reheal as a result of facility closure, or that damaged portions of the unit have been removed or grouted before seal emplacement. Characterization and delineation of the hydrologically and/or structurally altered zones around the WIPP facility horizon and shafts are ongoing, and will continue into the early operational phase of the facility.

# 4.0 RUSTLER FORMATION AND YOUNGER UNITS

As noted previously, much effort in WIPP site characterization has been focused on the Culebra Dolomite Member of the Rustler Formation, because this unit is the first laterally continuous water-bearing zone above the WIPP facility. The Culebra has continued to receive attention since 1983. However, work since 1983 has included other members of the Rustler Formation as well as shallower units. Section 4.0 discusses all units above the Salado as a group. Section 4.1 discusses hydrologic testing of the Rustler Formation and Dewey Lake Red Beds, and Section 4.2 discusses both field and numerical studies of the transport properties of the Culebra dolomite. Together, Sections 4.1 and 4.2 constitute a conceptual model of the modern flow and transport behavior within the shallow part of the WIPP stratigraphy, with emphasis on the Culebra dolomite. Section 4.3 discusses geochemical studies addressing both bulk-compositional and isotopic variability within the Rustler Formation and Dewey Lake Red Beds. Section 4.4 discusses studies into the overall geologic behavior of the Rustler and shallower formations at and near the WIPP site. Together, Sections 4.3 and 4.4 summarize available evidence concerning the transient geologic behavior in the region of the WIPP site for units above the Salado Formation.

## 4.1 Hydrologic Testing of the Rustler Formation and Dewey Lake Red Beds

The Rustler Formation at and near the WIPP site has been hydrologically tested and interpreted at three geometric scales, which are discussed sequentially from the smallest to the largest scale in this section. The smallest-scale of testing is conducted in single holes. Recent single-hole hydrologic testing has provided: 1) local or point transmissivity values for all members of the Rustler Formation except the Tamarisk Member, but with emphasis on the Culebra dolomite; 2) indications of the presence or absence of local hydraulically effective fracturing and wellbore damage within the Culebra; 3) information on relative head potentials within the Rustler; and 4) some indication of the distribution of properties and degree of hydraulic saturation within the Dewey Lake Red Beds. As discussed by Beauheim (1987b), single-hole testing is carried out by means of pumping, drillstem, slug-injection, slug-withdrawal, or pressure-pulse tests, depending on the local permeability or transmissivity. Single-hole testing is interpreted here in terms of transmissivities (in units of $m^2/s$). Use of this term assumes that the unit being tested is homogeneous across the tested interval. This assumption has been examined directly at hole H-14, in which two separate but overlapping intervals were tested in the Culebra dolomite. The results at H-14 indicate a factor of about 2 in vertical variability in transmissivity within the Culebra within a given hole. Recent single-hole testing of the Rustler Formation and Dewey Lake Red Beds is discussed in Section 4.1.1.

Single-hole tests do not indicate the extent to which either point transmissivity values or fracturing effects can be extrapolated laterally. Hydraulic behavior within the Culebra dolomite is, therefore, also examined at the "hydropad" scale. WIPP hydropads nominally contain three holes, located at the corners of an equilateral triangle 30 m on a side. Hydrologic information at the pad scale is collected by "interference"

testing. During this type of testing, at least two of the three holes on the pad are pumped sequentially in separate tests; the two unpumped holes in each test are used for observation. The objectives of interference hydrologic testing at the pad scale are to collect average or effective hydrologic-property data over distances of some 30 m, and to determine if fracturing effects are significant at this scale.

In the region of the WIPP site, single-pad hydraulic interference tests have been completed at the H-2, H-3, H-4, H-5, H-6, H-7, H-9, and H-11 hydropads. Detailed interpretation including evaluation of the effects of fracturing has been completed only for tests at the H-3 and H-11 hydropads, discussed in Section 4.1.2. Interference testing at the H-3 and H-11 pads has been interpreted using a "dual-porosity" approach, in which the Culebra is assumed to consist of an array of matrix blocks (primary porosity), separated by regularly spaced fractures (secondary porosity).

At some "large" scale, assuming that fracture spacing and properties are not too irregular, the effects of fracturing should become insignificant, i.e., it should become possible to model the flow and/or contaminant-transport behavior of a fractured rock unit such as the Culebra adequately using the porous-medium assumption. The scale at which this simplification is valid, however, may vary significantly with different rock types in different geologic or hydrologic settings. During WIPP site characterization, possible regional hydraulic effects of fracturing have been investigated by "multipad interference testing" of the Culebra dolomite. In this type of testing, one hole is pumped for a relatively long period of time, generally a month or more, while surrounding holes are used to observe hydraulic responses over an area of several square miles. Depending on the distances and extent of fracturing involved, effects due to fracturing may or may not be evident between the pumped hole and some of the observation holes.

Interpretation of multipad interference testing allows estimation of transmissivities and storativities within the tested area, provides information concerning the regional relationship between fluid densities and flow directions, and has allowed investigation of the interaction between WIPP shafts and the Culebra. Two major multipad interference tests, centered at the H-3 hydropad and at hole WIPP-13, have been carried out to date at the WIPP. Additionally, regional hydraulic information has been collected by observing hydrologic responses to WIPP shaft-sinking and shaft-sealing operations. Regional-scale hydrologic interpretation of the Rustler Formation, with emphasis on the Culebra dolomite, is discussed in Section 4.1.3. Interpretation on the regional scale indicates that fracturing need not be incorporated into regional-scale simulation of fluid pressures (head potentials) within the Culebra at and near the WIPP site, because pressure responses are relatively rapid, even on this scale. The assumption of steady state is adequate in modeling the modern Culebra head potentials. However, groundwater flow times are slow enough in the vicinity of the WIPP site to make the assumption of steady-state confined flow within the Culebra inadequate for simulation of long-term flow paths and flow times.

### 4.1.1 Single-Hole Hydraulic Testing and Interpretation

4.1.1.1 Transmissivity Distribution within Individual Units--Prior to 1985, hydrologic testing at and near the WIPP site was either interpreted using the porous-medium assumption or did not identify significant effects due to fracturing (e.g., Barr et al., 1983). More recently, Beauheim (1986, 1987b) has identified significant fracture effects in hydraulic testing of several holes, using the code INTERPRET. As described in detail by Beauheim (1986, 1987b), INTERPRET utilizes a "pressure-derivative" technique to determine whether or not significant pressure responses due to fracturing are present. In this approach, hydraulically effective fracturing is indicated by a flexure in the plot of dimensionless pressure derivative or drawdown versus dimensionless time (Figure 4.1.1). This flexure reflects a transition from "early" times, in which fluids are effectively produced only from within the fractures, to "late" times, in which fluid is produced from both fractures and matrix, but in which fluid release from the matrix to the fractures is generally the rate-limiting process. The transmissivity interpreted from behavior after this transition is referred to as "system" transmissivity.

At the time of the WIPP FEIS (U.S. Department of Energy, 1980) the suitability of the WIPP site was evaluated largely on the basis of possible releases from the site to Malaga Bend, on the Pecos River approximately 26 km from the WIPP site (Figure 1.1). Requirements for repository performance developed by the Environmental Protection Agency (40CFR191) were released in 1985. Although they may not be in their final form, these requirements place increased emphasis on evaluation of possible releases of radionuclides to the "accessible environment" near the facility. The definition of the accessible environment is not yet final. The WIPP Project has greatly increased the size and reliability of the hydrologic data base for the Rustler Formation since 1985, especially for the Culebra dolomite at and near the WIPP site. Table 4.1 contains the best local estimates of transmissivity used in modeling the hydrology of the Culebra dolomite from 1983 through 1987 and demonstrates the growth in this data base. Table 4.2 summarizes the results of recent single-hole testing in the Culebra dolomite.

Estimated Culebra transmissivities at the WIPP site area and within Nash Draw range over approximately six orders of magnitude, from 2.15 x $10^{-9}$ $m^2/s$ at P-18 to 1.34 x $10^{-3}$ $m^2/s$ at WIPP-26 (Tables 4.1 and 4.2). In addition to the growth in the Culebra data base evident in Table 4.1, many of the holes have been retested over the last five years. In some cases recent testing and interpretation have significantly changed earlier estimated transmissivities. However, the more recently estimated Culebra transmissivities are not consistently higher or lower than older values. At H-1 and DOE-2, recent data and interpretation indicate a significantly higher Culebra transmissivity. At H-3 and DOE-1, recent work indicates a lower local transmissivity than estimated earlier. In cases such as P-15, P-17, H-4, and WIPP-30, retesting and/or reinterpretation of earlier results has not resulted in any significant change in estimated Culebra transmissivity. In all cases, however, the more recent data and interpretations are better documented than older work, as a result of the

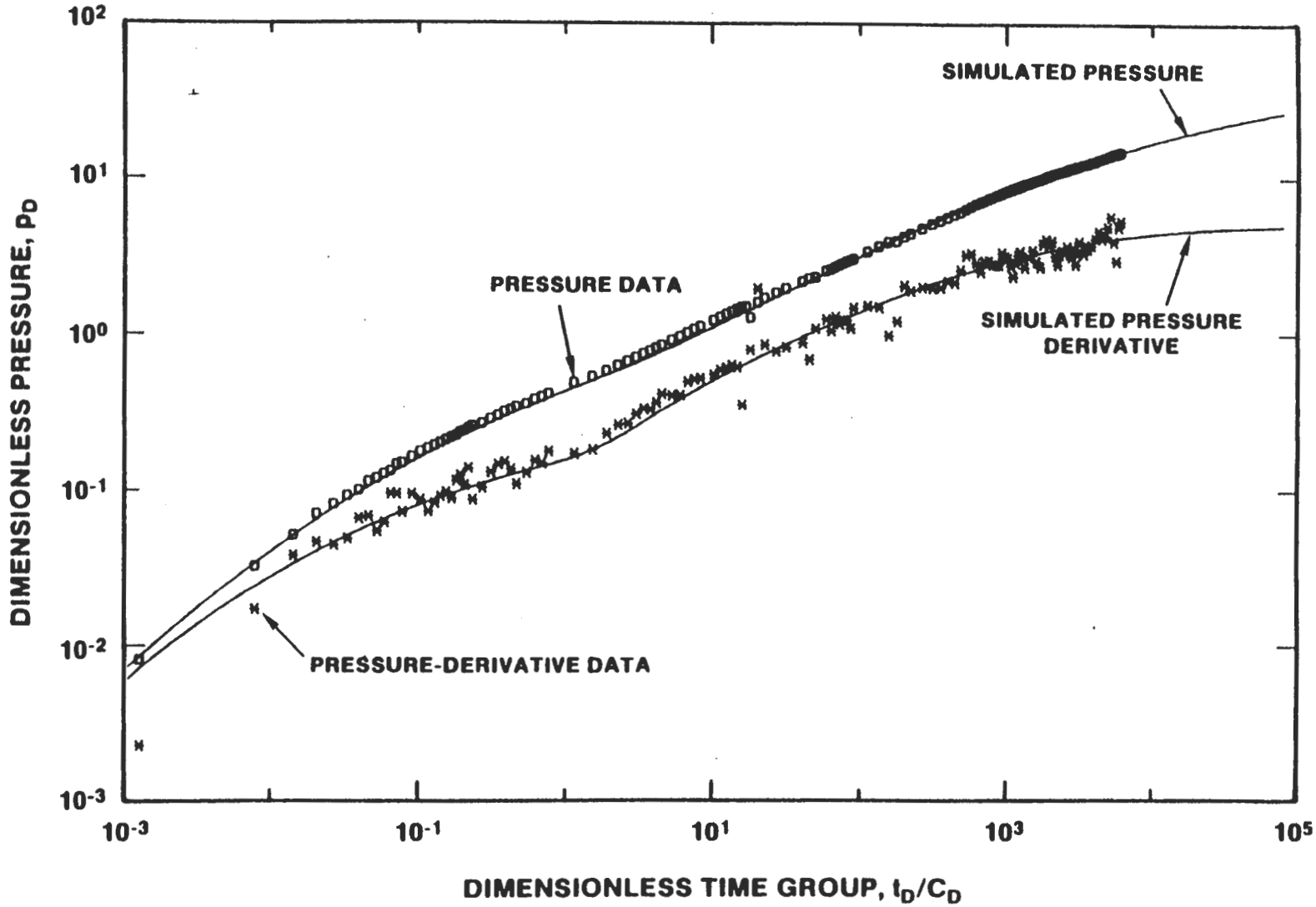


Figure 4.1.1: Measured and simulated response of H-3b1 to pumping of hole H-3b2. The presence of dual-porosity effects due to fracturing is indicated by the inflection in both measured and simulated pressure-derivative curves, in this case at a value of the dimensionless time group of approximately one. Simplified from Figure 6-11 of Beauheim (1987a).

Table 4.1: Transmissivity data bases used in numerical modeling of the Culebra dolomite in Barr et al. (1983), Haug et al. (1987), and LaVenue et al. (1988).

| Well | Barr et al. (1983) Transmissivity ($ft^2$/day) | Haug et al. (1987) Transmissivity ($ft^2$/day) | LaVenue et al. (1988) Transmissivity ($ft^2$/day) | Transmissivity ($m^2$/sec) |
|---|---|---|---|---|
| H-1 | 0.07 | 0.07 | 0.8 | $8.60 \times 10^{-7}$ |
| H-2 | 0.4 | 0.56 | 0.52 | $5.59 \times 10^{-7}$ |
| H-3 | 19 | 3.7 | 2.3 | $2.47 \times 10^{-6}$ |
| H-4 | 0.9 | 1.1 | 0.95 | $1.02 \times 10^{-6}$ |
| H-5 | 0.2 | 0.16 | 0.14 | $1.51 \times 10^{-7}$ |
| H-6 | 73 | 74 | 74 | $7.96 \times 19^{-5}$ |
| H-7 | >1000 | 1120 | 1030 | $1.11 \times 10^{-3}$ |
| H-8 | 16 | 6.7 | 8.2 | $8.82 \times 10^{-6}$ |
| H-9 | 230 | 170 | 160 | $1.72 \times 10^{-4}$ |
| H-10 | 0.07 | 0.07 | 0.07 | $7.53 \times 10^{-8}$ |
| H-11 | -- | 10 | 26 | $2.80 \times 10^{-5}$ |
| H-12 | -- | 0.04 | 0.18 | $1.94 \times 10^{-7}$ |
| H-14 | -- | -- | 0.31 | $3.33 \times 10^{-7}$ |
| H-15 | -- | -- | 0.12 | $1.29 \times 10^{-7}$ |
| H-16 | -- | -- | 0.7 | $7.53 \times 10^{-7}$ |
| H-17 | -- | -- | 0.2 | $2.15 \times 10^{-7}$ |
| H-18 | -- | -- | | |
| WIPP-12 | -- | -- | 0.03 | $3.23 \times 10^{-8}$ |
| WIPP-13 | -- | -- | 69 | $7.42 \times 10^{-5}$ |
| WIPP-18 | -- | -- | 0.3 | $3.23 \times 10^{-7}$ |
| WIPP-19 | -- | -- | 0.6 | $6.45 \times 10^{-7}$ |
| WIPP-21 | -- | -- | 0.25 | $2.69 \times 10^{-7}$ |
| WIPP-22 | -- | -- | 0.37 | $3.98 \times 10^{-7}$ |
| WIPP-25 | 270 | 270 | 270 | $2.90 \times 10^{-4}$ |
| WIPP-26 | 1250 | 1250 | 1250 | $1.34 \times 10^{-3}$ |
| WIPP-27 | 650 | 650 | 650 | $6.99 \times 10^{-4}$ |
| WIPP-28 | 18 | 18 | 18 | $1.94 \times 10^{-5}$ |
| WIPP-29 | 1000 | 1000 | 1000 | $1.08 \times 10^{-3}$ |
| WIPP-30 | 0.3 | 0.3 | 0.3 | $3.22 \times 10^{-7}$ |
| P-14 | 140 | 233 | 214 | $2.30 \times 10^{-4}$ |
| P-15 | 0.07 | 0.08 | 0.09 | $9.68 \times 10^{-8}$ |
| P-17 | 1 | 1.7 | 1.3 | $1.40 \times 10^{-6}$ |
| P-18 | 0.001 | 0.002 | 0.002 | $2.15 \times 10^{-9}$ |
| DOE-1 | -- | 33 | 11 | $1.18 \times 10^{-6}$ |
| DOE-2 | -- | 36 | 89 | $9.57 \times 10^{-6}$ |
| ERDA-9 | -- | -- | 0.47 | $5.06 \times 10^{-7}$ |
| CABIN BABY | -- | -- | 0.28 | $3.01 \times 10^{-7}$ |
| ENGLE | -- | -- | 43 | $4.62 \times 10^{-5}$ |
| USGS-1 | 515 | 515 | 515 | $5.54 \times 10^{-4}$ |
| | 21 Values | 25 Values | 38 Values | 38 Values |

Table 4.2: Detailed summary of recent single-well test results in the Culebra dolomite. Slightly modified from Table 5-3 of Beauheim (1987b).

| Well | Culebra Interval m (ft) | Interval Tested m (ft)* | Test Type | Transmissivity ($ft^2$/day) | Transmissivity ($m^2$/s) | Skin Factor |
|---|---|---|---|---|---|---|
| H-1 | 206-213.1 (676-699) | 205.7-214.3 675-703) | slug #1 | 1.0 | $1.1 \times 10^{-6}$ | -- |
| | | | slug #2 | 0.83 | $8.9 \times 10^{-7}$ | -- |
| | | | slug #3 | 0.83 | $8.9 \times 10^{-7}$ | -- |
| | | | slug #4 | 0.83 | $8.9 \times 10^{-7}$ | -- |
| H-4c | 149.4-157.3 (490-516) | 150.6-158.5 (494-520) | slug | 0.65 | $7.0 \times 10^{-7}$ | -- |
| H-8b | 179.2-187.1 (588-614) | 175.0-190.2 (574-624) | pumping | 8.2 | $8.8 \times 10^{-6}$ | -7.2 |
| H-12 | 250.9-259.1 (823-850) | 249.9-271.3 (820-890) | slug #1 | 0.18 | $1.9 \times 10^{-7}$ | -- |
| | | | slug #2 | 0.18 | $1.9 \times 10^{-7}$ | -- |
| H-14 | 166.1-174.3 (545-572) | 162.5-167.9 (533-550.7) | DST/FBU | 0.096 | $1.0 \times 10^{-7}$ | -0.8 |
| | | | DST/SFL | 0.10 | $1.1 \times 10^{-7}$ | -- |
| | | | DST/SBU | 0.10 | $1.1 \times 10^{-7}$ | -1.3 |
| H-14 | 166.1-174.3 (545-572) | 162.5-175.0 (533-574) | DST/FBU | 0.30 | $3.2 \times 10^{-7}$ | -1.1 |
| | | | DST/SBU | 0.31 | $3.3 \times 10^{-7}$ | -1.8 |
| | | | slug | 0.30 | $3.2 \times 10^{-7}$ | -- |
| H-15 | 262-4-269.1 (861-883) | 260.0-271.3 (853-890) | DST/FBU | 0.15 | $1.6 \times 10^{-7}$ | 2.6 |
| | | | DST/SBU | 0.15 | $1.6 \times 10^{-7}$ | 2.9 |
| | | | slug | 0.10 | $1.1 \times 10^{-7}$ | -- |
| H-16 | 213.4-221.0 (700-725) | 212.4-223.7 (697-734) | DST/FBU | 0.85 | $9.1 \times 10^{-7}$ | 0.0 |
| | | | DST/SBU | 0.85 | $9.1 \times 10^{-7}$ | -0.3 |
| | | | slug | 0.69 | $7.4 \times 10^{-7}$ | -- |
| H-17 | 215.2-222.8 (706-731) | 214.3-224.0 (703-735) | DST/FBU | 0.21 | $2.3 \times 10^{-7}$ | -1.5 |
| | | | DST/SBU | 0.22 | $2.4 \times 10^{-7}$ | -1.2 |
| | | | slug | 0.22 | $2.4 \times 10^{-7}$ | -- |

Table 4.2: Detailed summary of recent single-well test results in the Culebra dolomite. Slightly modified from Table 5-3 of Beauheim (1987b). (Continued)

| Well | Culebra Interval m (ft) | Interval Tested m (ft)* | Test Type | Transmissivity ($ft^2$/day) | Transmissivity ($m^2$/s) | Skin Factor |
|---|---|---|---|---|---|---|
| H-18 | 210.3-217.3 (690-713) | 208.8-217.6 (685-714) | DST/FBU | 2.2 | $2.4 \times 10^{-6}$ | -0.2 |
| | | | DST/SBU | 2.2 | $2.4 \times 10^{-6}$ | -1.0 |
| | | | slug | 1.7 | $1.8 \times 10^{-6}$ | -- |
| WIPP-12 | 246.9-254.5 (810-835) | 248.4-256.0 (815-840) | slug #1 | 0.10 | $1.1 \times 10^{-7}$ | -- |
| | | | slug #2 | 0.097 | $1.0 \times 10^{-7}$ | -- |
| WIPP-18 | 239.9-246-3 (787-808) | 239.0-245-7 (784-806) | slug | 0.30 | $3.2 \times 10^{-7}$ | -- |
| WIPP-19 | 230.4-237.4 (756-779) | 229.8-237.7 (754-780) | slug | 0.60 | $6.5 \times 10^{-7}$ | -- |
| WIPP-21 | 222.2-229.5 (729-753) | 221.6-228.9 (727-751) | slug | 0.25 | $2.7 \times 10^{-7}$ | -- |
| WIPP-22 | 226.2-232.9 (742-764) | 228.0-234.7 (748-770) | slug | 0.37 | $4.0 \times 10^{-7}$ | -- |
| WIPP-30 | 192.3-199.0 (631-653) | 191.7-199.6 (629-655) | slug #1 | 0.18 | $1.9 \times 10^{-7}$ | -- |
| | | | slug #2 | 0.17 | $1.8 \times 10^{-7}$ | -- |
| P-15 | 125.9-132.6 (413-435) | 125.0-133.5 (410-438) | slug #1 | 0.090 | $9.7 \times 10^{-8}$ | -- |
| | | | slug #2 | 0.092 | $9.9 \times 10^{-8}$ | -- |
| P-17 | 170.1-177.7 (558-583) | 170.1-178.6 (558-586) | slug #1 | 1.0 | $1.1 \times 10^{-6}$ | -- |
| | | | slug #2 | 1.0 | $1.1 \times 10^{-6}$ | -- |
| P-18 | 277.1-285.9 (909-938) | 277.1-286.5 (909-940) | slug | $4 \times 10^{-3}$ | $7 \times 10^{-5}$ | -- |
| ERDA-9 | 214.6-221.6 (704-727) | 214.9-221.9 (705-728) | slug #1 | 0.45 | $4.8 \times 10^{-7}$ | -- |
| | | | slug #2 | 0.47 | $5.1 \times 10^{-7}$ | -- |

Table 4.2: Detailed summary of recent single-well test results in the Culebra dolomite. Slightly modified from Table 5-3 of Beauheim (1987b). (Concluded)

| Well | Culebra Interval m (ft) | Interval Tested m (ft)* | Test Type | Transmissivity ($ft^2$/day) | Transmissivity ($m^2$/s) | Skin Factor |
|---|---|---|---|---|---|---|
| Cabin baby-1 | 153.3-161.2 (503-529) | 153.3-161.2 (503-529) | slug #1 | 0.28 | $3.0 \times 10^{-7}$ | -- |
| | | | slug #2 | 0.28 | $3.0 \times 10^{-7}$ | -- |
| DOE-1 | 250.2-256.9 (821-843) | 249.9-256.9 (820-843) | pumping/ drawndown | 28 | $3.0 \times 10^{-5}$ | -5.1 |
| | | | recovery | 11 | $1.2 \times 10^{-5}$ | -6.0 |
| Engle | 200.9-207.6 (659-681) | 197.5-208.2 (648-683) | pumping | 43 | $4.6 \times 10^{-5}$ | 4.2 |

*Actual intervals open to the wells.

increase in documentation requirements over the ten-year span of WIPP site characterization. The interpreted test data from recent single-hole testing at and near the WIPP site are included in Beauheim (1987b). Raw data, test histories, and test instrumentation for all hydrologic testing at the WIPP for approximately the last five years are contained in a series of six hydrologic data reports: Hydro Geo Chem (1985); INTERA and Hydro Geo Chem (1985); INTERA (1986); Saulnier et al. (1987); Stensrud et al. (1987); and Stensrud et al. (1988).

Transmissivities listed in Tables 4.1 and 4.2 are not identical in all cases. Transmissivity estimates included in Table 4.1 from three-hole hydropads, such as the H-4 pad, are effective transmissivities. In single-hole tests, this is the same as the measured value. In the case of three-hole hydropads, however, the effective transmissivity is the square root of the product of the estimated maximum and minimum transmissivities on the pad. The calculated effective transmissivity, which is used in regional-scale modeling (Section 4.1.3), generally does not correspond directly to any of the measured single-hole values on the same pad.

As mentioned above, Culebra transmissivities at and near the WIPP site and within Nash Draw range over approximately six orders of magnitude, from more than $10^{-3}$ $m^2/s$ to less than $10^{-8}$ $m^2/s$. However, this variability is not random. A large area of low transmissivities (less than approximately $10^{-6}$ $m^2/s$) is present near the center of the WIPP site, extending to the east, southeast, and southwest (Figure 4.1.2). This zone includes holes WIPP-12, 18, 19, 21, and 22; H-1, 2, 4, 5, 10, 12, 14, 15, 16, and 17;

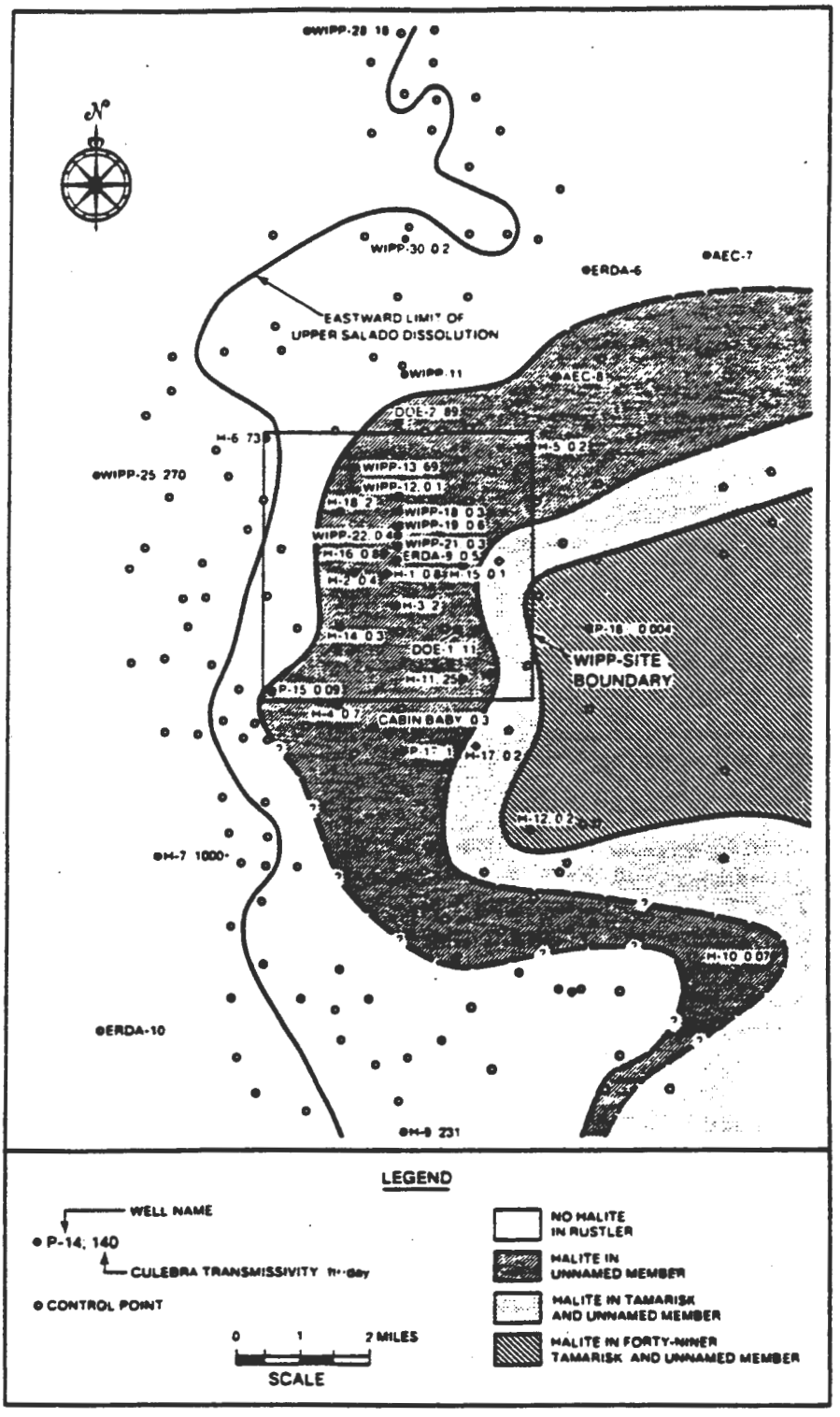


Figure 4.1.2: Transmissivity of the Culebra dolomite in relation to the distribution of halite within the Rustler Formation. Figure 6-2 of Beauheim (1987b). Halite distribution modified from Snyder (1985). Transmissivities in this figure are given in units of $ft^2$/day. Multiply by $1.075 \times 10^{-6}$ to get transmissivities listed in Table 4.1 in $m^2$/s.

P-15, 17, and 18; ERDA-9, and Cabin Baby-1 (see also Figure 1.2). Within this low-transmissivity region, relatively high Culebra transmissivities (greater than approximately $10^{-5}$ $m^2/s$) have been measured southeast of the site center, in holes DOE-1 and H-11. The transmissivity measured on the H-3 pad ($2.0 \times 10^{-6}$ $m^2/s$) is transitional between transmissivities at H-11 and DOE-1 and those in the low-transmissivity domain north and southwest of H-3.

A continuous zone of variable but high Culebra transmissivity appears to be present northwest, west, and south of the site center. This zone includes holes H-6, 7, and 9; WIPP-13, 25, 26, 27, 28, and 29; DOE-2 and P-14; and the Engle well (see Figures 1.1 and 1.2). The Culebra transmissivity in hole H-18 ($1.8 \times 10^{-6}$ to $2.4 \times 10^{-6}$ $m^2/s$) is transitional between those in adjacent higher-transmissivity and lower-transmissivity domains.

There are some limitations in the Culebra data base, in spite of the fact that Culebra transmissivities have now been estimated at 39 separate localities at and near the WIPP site and within Nash Draw. For example, although the low-transmissivity zone near the site center is interpreted here to be continuous to the southwest, there is no direct measurement of Culebra transmissivity in the interval between holes H-14 and H-2. At present there is also no direct field evidence of connection between the region containing holes DOE-1 and H-11 and the region to the south containing hole H-9. Quantitative integration of point data into a regional transmissivity pattern for the Culebra and evaluation of some of the uncertainties mentioned here are discussed in Section 4.1.3.

Single-hole Culebra tests in which the system transmissivity is less than $10^{-6}$ $m^2/s$ generally do not show signs of fracturing, while holes with higher transmissivity do. To a first approximation, fracturing within the Culebra (and the Rustler as a whole) appears to be related to the removal of halite. As discussed by Mercer (1983), Snyder (1985), and Beauheim (1987b), there is a general correlation between the distribution of halite within the Rustler Formation (Figures 1.5 and 4.1.2) and transmissivity of Rustler members, especially the Culebra dolomite. The distribution of halite within the Rustler Formation is briefly discussed in Section 4.4.2.

However, the correlation between halite distribution and Culebra transmissivity is neither unique nor completely reliable. With the exception of WIPP-30 and possibly H-10, the Culebra in holes in which there is no halite in the unnamed lower member of the Rustler are highly transmissive. In WIPP-30, there is no halite within the Rustler, and the Culebra transmissivity is quite low. Without exception, the Culebra transmissivity is low if Rustler halite is present above the Culebra. Where there is Rustler halite present only beneath the Culebra, the correlation is not completely reliable, perhaps because of complications involving the response of the Culebra to evaporite dissolution in the upper part of the Salado Formation. For example, holes DOE-2 and WIPP-13, in the western part of the region in which halite is present beneath the Culebra (Figure 4.1.2), are highly transmissive, but hole H-18 is not. In the southeastern part of the WIPP site, holes P-17 and H-3 are relatively low in transmissivity, but the transmissivity at H-11 and DOE-1 is greater than $10^{-5}$ $m^2/s$. As discussed by Beauheim (1987b), examination of the detailed

Rustler isopachs summarized in Snyder (1985) does not indicate any consistent reason for the high transmissivities at H-11 and DOE-1.

The significance of the distinction between dual-porosity (fractured) and porous-medium behavior in single-hole hydraulic testing is not completely straightforward. The apparent absence of fracturing in a test does not indicate a total absence of fractures, nor does fracturing in single-hole hydraulic testing indicate that far-field or long-term hydraulic or transport behavior near a given hole is or would be dominated by fracture effects. At one extreme, very local fracturing in a very low-transmissivity test interval may play a role in the very early pressure responses, but may not be evident because of wellbore-storage and fluid-flow surge effects at the beginning of a test. Any low-transmissivity hole listed in Tables 4.1 and 4.2 may contain fractures which are not apparent because of the testing techniques and instrumentation used. However, the effects of these fractures should be extremely localized. At the other extreme, intense fracturing may lead to high transmissivity, but result in such small block sizes that fluid flow from the matrix blocks is "immediately" the rate-limiting step. Dual-porosity effects would not be evident during testing at such a site, and the tested interval would behave hydraulically as an equivalent porous medium. This type of behavior may be applicable, for example, in the highly-transmissive portions of the Culebra within Nash Draw; however, testing results in Nash Draw have not yet been investigated using INTERPRET. The hydraulic behavior of the highly-transmissive Culebra in the Engle well ($4.6 \times 10^{-5}$ $m^2/s$) does not show dual-porosity effects. However, this behavior is tentatively attributed by Beauheim (1987b) to wellbore and near-wellbore conditions, rather than to extreme fracturing of the test interval.

In addition, the fact that testing at a given hole does not indicate local fracturing does not guarantee that there is not fracturing nearby. Single-hole testing at WIPP-21 indicates a Culebra transmissivity of $2.7 \times 10^{-7}$ $m^2/s$, with no dual-porosity effects. This hole responded strongly and rapidly to both the H-3 multipad interference test and activities in both the waste-handling and exhaust shafts. This behavior probably reflects the presence of a "low-storativity" structure, which could be a single fracture or fracture zone connecting the region near WIPP-21 with the two WIPP shafts, but not intersecting WIPP-21 itself.

Single-hole testing may also be strongly affected by drilling-induced near-well effects, which can make the test hole appear either more or less transmissive than the surrounding rock mass. As discussed by Beauheim (1986, 1987b), marked examples of such "skin" effects were found in testing in holes DOE-2 and WIPP-13. In the extreme example of hole DOE-2, the initial estimate of minimum transmissivity was $2.4 \times 10^{-5}$ $m^2/s$. The calculated "skin factor" was +31 (Beauheim, 1986). For comparison, a hole so badly damaged that it would not produce fluid at all would have a skin factor of plus infinity. At the WIPP, positive skin factors have, in some cases, been reduced by acid treatment. Treatment of hole DOE-2 with hydrochloric acid removed the near-hole damage effects, and increased the interpreted transmissivity by a factor of 4, from $2.4 \times 10^{-5}$ $m^2/s$, to $9.6 \times 10^{-5}$ $m^2/s$ (Table 4.1). The calculated skin factor at DOE-2 decreased from +31 to -4.7. A skin factor of less than zero indicates good connection of

the physical wellbore with fractures within the rock mass and results in an apparent well radius greater than that of the physical diameter of the hole. The Culebra in several holes listed in Table 4.2 exhibits negative skin factors, indicating good connection of the test hole with the surrounding rock mass.

As mentioned above, the presentation of data in terms of transmissivity explicitly assumes that the tested interval is vertically homogeneous. Data included in Table 4.2 indicate that Culebra transmissivity at H-14 varies with vertical position within the unit. While drilling this hole, it was possible to find a packer seat within the Culebra. Testing of the upper Culebra was then followed by testing of the entire unit. The calculated transmissivity of the upper 1.7 m of the Culebra is $1.1 \times 10^{-7}$ $m^2/s$, while that of the entire 8.2 m thickness of the unit is $3.3 \times 10^{-7}$ $m^2/s$. This indicates that the transmissivity of the lower 6.5 m of the Culebra in hole H-14 is approximately $2.2 \times 10^{-7}$ $m^2/s$. The results at H-14 indicate that the Culebra cannot be assumed to be vertically homogeneous, since the transmissivity of individual zones within the unit vary by a factor of about 2. The results at H-14 are in qualitative agreement with the variability indicated by results of tracer-injection tests at holes H-1, H-2c, H-3, and P-14 (Mercer and Orr, 1979).

Because the Culebra dolomite is generally more permeable than the Magenta dolomite at and near the WIPP site, less testing of the Magenta has been completed at the WIPP. Older transmissivity data for the Magenta dolomite are contained in Mercer (1983) and Gonzalez (1983a). The results of recent testing of the Magenta dolomite in H-14, H-16, and DOE-2 are included in Table 4.3. Overall, reported Magenta transmissivities range from approximately $5.9 \times 10^{-9}$ $m^2/s$ in hole H-14 to $4.0 \times 10^{-4}$ $m^2/s$ in WIPP-25. Magenta transmissivities greater than approximately $10^{-6}$ $m^2/s$ are known only in and near Nash Draw and the small valley south of the WIPP site (Figure 1.2).

As mentioned in Section 1.0, modeling of Rustler hydrology through 1983 assumed that the Culebra and Magenta dolomites were completely confined. This is equivalent to assuming that the unnamed lower, Tamarisk, and Forty-niner members of the Rustler have zero permeability. Indeed, standard hydrologic testing techniques are inapplicable to these units at the WIPP site because of their low permeabilities. Recent advances in testing, data-collection, and interpretation techniques have allowed meaningful examination of these units at three locations: DOE-2, H-14, and H-16 (Table 4.3). Even in the recent testing, however, it has only been possible to test the transmissivities of claystones and siltstones within the non-carbonate members of the Rustler. The claystones and siltstones in the Tamarisk and Forty-niner Members occur near the center of each unit, and are separated from the Magenta or Culebra by a zone of anhydrite/gypsum (Table 1.2). The anhydrites within the Rustler still cannot be tested from the surface, since their in situ transmissivities are less than approximately $10^{-11}$ $m^2/s$ (Beauheim, 1986; 1987b). In addition, it still has not been possible to measure the transmissivity of the Tamarisk claystone, due to its low transmissivity.

Table 4.3: Summary of available transmissivity information for members of the Rustler Formation in holes H-14, H-16, and DOE-2. Slightly modified from data contained in Tables 5-2 and 5-3 of Beauheim (1987b) and Table 7-2 of Beauheim (1986).

| | Zone depth (m) | Test interval (m) | Transmissivity ($m^2/s$) |
|---|---|---|---|
| H-14 | | | |
| Forty-niner "claystone" | 118.9 - 123.4 | 116.1 - 124.7 | $3.2 \times 10^{-8}$ - $7.6 \times 10^{-8}$ |
| Magenta | 129.2 - 136.6 | 128.0 -136.6 | $5.7 \times 10^{-9}$ - $6.0 \times 10^{-9}$ |
| Culebra | 166.1 - 174.3 | 162.5 - 175.0 | $3.2 \times 10^{-7}$ - $3.3 \times 10^{-7}$ |
| H-16 | | | |
| Forty-niner "claystone" | 171.6 - 175.0 | 170.7 - 177.1 | $2.4 \times 10^{-10}$ - $6.0 \times 10^{-9}$ |
| Magenta | 179.8 - 187.8 | 179.5 - 189.3 | $2.6 \times 10^{-8}$ - $3.0 \times 10^{-8}$ |
| Culebra | 213.4 - 221.0 | 212.4 - 223.7 | $7.4 \times 10^{-7}$ - $9.1 \times 10^{-7}$ |
| Unnamed member siltstone | 237.1 - 256.6 | 225.2 - 259.4 | $2.4 \times 10^{-10}$ - $2.9 \times 10^{-10}$ |
| DOE-2 | | | |
| Forty-niner "claystone" | 204.2 - 207.5 | 202.4 - 209.1 | $2.7 \times 10^{-9}$ - $1.2 \times 10^{-8}$ |
| Magenta | 213.1 - 220.1 | 213.4 - 220.1 | $1.1 \times 10^{-9}$ |
| Culebra | 251.2 - 257.9 | 251.2 - 257.9 | $9.6 \times 10^{-5}$ |

The transmissivity of the Magenta at H-14, H-16, and DOE-2 is $1.1 \times 10^{-9}$ to $3.0 \times 10^{-8}$ $m^2/s$ (Table 4.3). The transmissivity of the claystone in the overlying Forty-niner in the same holes is comparable, $5.6 \times 10^{-9}$ to $1.2 \times 10^{-8}$ $m^2/s$. The siltstone within the unnamed lower member of the Rustler has been successfully tested only in hole H-16, in which it has an estimated transmissivity of between $2.4 \times 10^{-10}$ and $2.9 \times 10^{-10}$ $m^2/s$. The transmissivity of the Culebra in DOE-2, H-14, and H-16 ranges from $1.1 \times 10^{-7}$ to $9.6 \times 10^{-5}$ $m^2/s$, at least one order of magnitude greater than that of any of the surrounding units.

The results at H-14, H-16, and DOE-2 indicate that the Culebra is the most significant water-bearing unit within the Rustler at and near the WIPP site, consistent with earlier assumptions, although in some holes (H-10, WIPP-12, P-15) the Culebra transmissivity is similar to the Magenta transmissivities measured at H-14, H-16, and DOE-2. However, the recent results are inconsistent with previous assumptions, in that they suggest that stratabound fluid flow within the portion of the Rustler above the Culebra dolomite may occur as much through the Forty-niner claystone as through the Magenta, except where the Magenta is significantly fractured. At and near the WIPP site, both the Magenta and the Forty-niner claystone are more transmissive than the bounding anhydrites; no data are available concerning the transmissivity of the Tamarisk claystone. There must be a qualitative increase in the transmissivities of the Tamarisk and Forty-niner anhydrites somewhere between the WIPP site and Nash Draw, however, since evaporite karst in and near Nash Draw involves formation of small caverns and sinkholes within the Tamarisk and Forty-niner Members, as briefly discussed in Section 4.4.

4.1.1.2 Head Distribution within the Rustler Formation and between the Rustler, Dewey Lake, and Salado--As mentioned previously, numerical modeling of Rustler hydrology through 1983 assumed the Culebra and Magenta were completely confined, and that the transmissivities of other units within the Rustler were negligible. The results discussed in the preceding section indicate that the transmissivities of claystones or siltstones within the Rustler are locally measurable at the WIPP site, and are similar in magnitude to that of the Magenta dolomite, except where the Magenta is fractured. However, the transmissivity of the Culebra dolomite is normally at least one order of magnitude greater than that of other units within the Rustler at and near the WIPP site, and the transmissivities of Rustler anhydrites at and near the WIPP site are too low to measure. These results suggest that flow within the Culebra dolomite, parallel to layering, is the dominant factor in the hydrology of the Rustler Formation at the WIPP site. However, as discussed briefly in this section, fluid pressures and densities have been measured locally in units both above and below the Culebra.

Therefore, unless the Rustler anhydrites and/or Tamarisk claystone have absolutely zero permeability, there must be some vertical fluid flow within the Rustler. The amount of this flow is not known quantitatively, and cannot be measured directly in the field. At one extreme, vertical fluid flow may be completely negligible relative to stratabound flow within the Culebra dolomite. At the other extreme, "karstic" hydrology might occur within the Rustler Formation at the WIPP site, involving surficial recharge from the surface to the Rustler carbonates and/or anhydrites. In order for fluid flow to take place from the surface to the carbonate members of the Rustler Formation, the head potential within the Forty-niner must be greater than that within the underlying Magenta dolomite, regardless of the head potential or state of saturation within the Dewey Lake Red Beds. The relationships among the effective hydraulic heads of the various members of the Rustler Formation, the Salado, and the Dewey Lake in the central portion of the WIPP site are shown in Figure 4.1.3. The flow directions indicated include the expected effects due to variable brine densities.

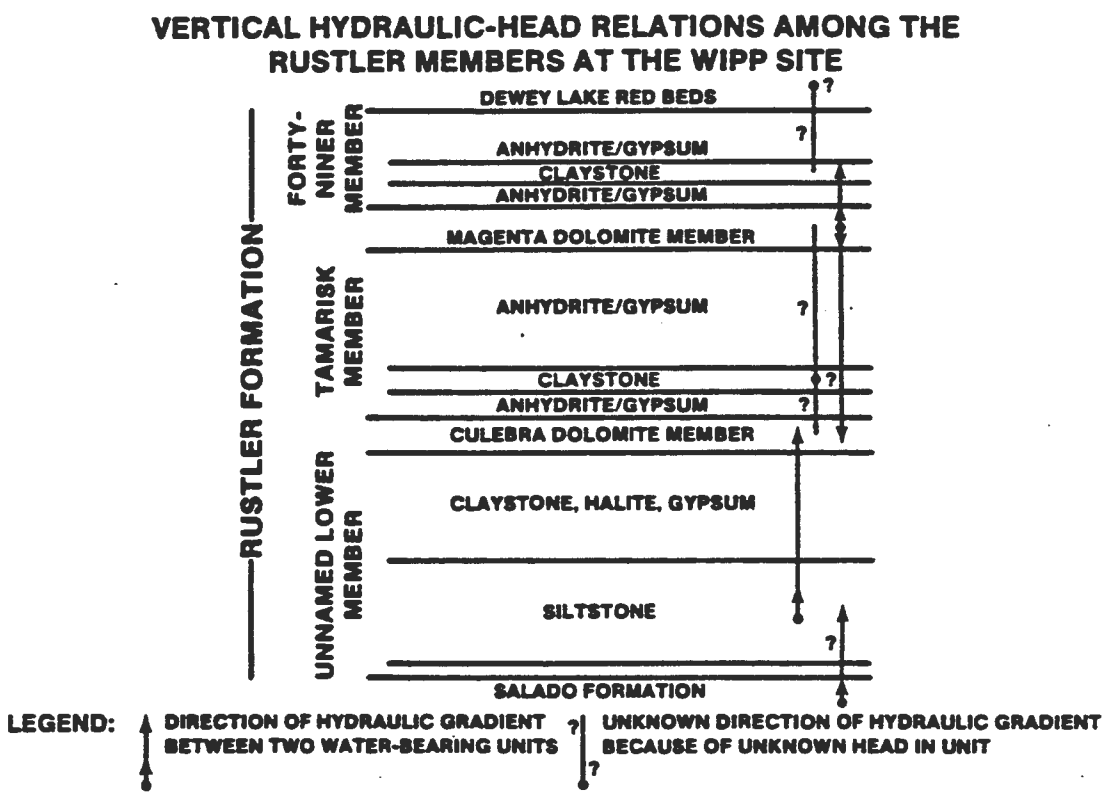


Figure 4.1.3: Head relations among units in the Rustler Formation and between the Rustler, Dewey Lake Red Beds, and Salado at the WIPP site. Figure 6-3 of Beauheim (1987b).

Figure 4.1.3 is based, in part, on testing of the Rustler and lower Dewey Lake Red Beds at H-14, H-16, and DOE-2. The transmissivity of the lower Dewey Lake was too low for successful testing, i.e., less than approximately $10^{-11}$ $m^2/s$. In fact, testing was unable to determine whether the Dewey Lake is hydraulically saturated. The regional pattern of hydrologic saturation within the Dewey Lake is not well known (Mercer, 1983); only very limited evidence has been found for local saturation at the WIPP site. South of the WIPP site, water is locally produced from the Dewey Lake, perhaps from lenticular sands within the unit (Mercer, 1983). Wells probably producing from within the Dewey Lake include the Pocket, Fairview, and Ranch wells indicated in Figure 1.2. As noted by Mercer (1983) the region east of the Ranch well includes thick active dune sands, and may serve as a location for local recharge to the Dewey Lake (see also Section 4.3.2).

In holes H-14 and H-16, consistent with the relationships shown in Figure 4.1.3, the Magenta head is greater than the head in the Forty-niner claystone (Beauheim, 1987b). Therefore, modern fluid flow between these two members is upward, rather than downward. Since water at these two holes is not moving from the top of the Rustler downwards into the Magenta, it cannot be moving from the surface down into the Magenta dolomite.

The Dewey Lake Red Beds at H-14 and H-16 may not be saturated. If not, fluid flow from the surface to the Forty-niner claystone is not likely. Given the uncertainty in regional saturation and head potentials within the Dewey Lake Red Beds the results at H-14 and H-16 do not rule out fluid movement from the surface downward into the Forty-niner claystone or the upper anhydrite in the Forty-niner and/or into the Magenta dolomite in some areas; i.e., where the Dewey Lake is saturated. Also, these results do not eliminate the possibility of flow between the Dewey Lake Red Beds and the Rustler carbonates in the past, if heads within the Dewey Lake Red Beds and Forty-niner were higher at that time relative to heads within the Magenta.

Magenta heads near the center of the WIPP site are greater than Culebra heads (Figure 4.1.3), consistent with downward flow between these two units. As indicated in Figures 17 and 18 of Mercer (1983), the difference in heads between the two units tends to increase towards the east and decrease towards the west, primarily due to a general east-to-west decrease in Magenta heads. Within and near Nash Draw, the heads within the two units are similar; in some places in and near Nash Draw, (H-7a, WIPP-26, WIPP-28), the Magenta is unsaturated (Mercer, 1983).

Vertical flow from the Magenta to the Culebra has been considered in regional-scale modeling of Culebra hydrology (Section 4.1.3.1). However, as noted above and indicated in Figure 4.1.3, it has not been possible to measure either transmissivities or head potentials within either the claystone or anhydrites in the Tamarisk at or near the WIPP site. Vertical flow between the Magenta and Culebra is discussed further by Mercer (1983) and Beauheim (1987b). The possible consequences of such flow, as considered in numerical modeling of Culebra hydrology (Haug et al., 1987), are briefly considered in Section 4.1.3.1.

As noted by Mercer (1983) and Beauheim (1987b), the head potentials in the silty portion of the unnamed lower member of the Rustler are greater than within the Culebra over much of the area of the WIPP site. Thus, fluid flow into the Culebra from the underlying unnamed member and possibly the Salado Formation is possible at both of these locations. However, as indicated in Figure 4.1.3, it has not been possible to measure either transmissivities or head potentials within the claystone, halite, or gypsum/anhydrite in the upper part of the unnamed lower member. The possible implications of vertical fluid flow from the unnamed member into the Culebra in numerical modeling of Culebra hydrology are briefly discussed in Section 4.1.3.1.

### 4.1.2 Single-Pad Interference Testing

Interference testing at the scale of a single hydropad is designed to provide data concerning the hydrologic effects of both fracturing and "anisotropy" at a geometric scale of some 30 m. If the test interval behaves as a porous medium at the hydropad scale, interference testing yields an "anisotropy tensor," which indicates local directions of maximum and minimum transmissivities. If, however, the porous-medium assumption is not valid at this scale, i.e., if fracturing effects are significant, testing at this scale normally provides average system transmissivities and storativities along the independent pairs of flow paths. Section 4.1.2.1 describes the detailed results of single-pad interference testing at the H-3 hydropad, and Section 4.1.2.2 the detailed results of testing at the H-11 pad. Detailed interpretation of pad-scale interference testing has only been completed to date for these two locations. Interpretation of results obtained at the H-2, H-4, H-5, H-6, H-7, and H-9 pads is ongoing.

4.1.2.1 Interference Testing at the H-3 Hydropad--Beauheim (1987a) interprets hydraulic data collected at the H-3 hydropad (Figure 4.1.4) during single-hydropad testing in 1984 and the H-3 multipad interference test conducted in 1985 and 1986. Hole H-3b3 was the pumped hole during the 1984 test, and H-3b2 the pumped hole during the H-3 multipad test.

The characteristic drawdown response in both pumped and observation holes at the H-3 pad is shown in Figure 4.1.1. As noted in Section 4.1.1, the inflection in dimensionless pressure at early dimensionless times indicates fracturing at H-3. In fact, the responses of observation holes on the H-3 pad to the beginning of pumping during both single-pad and multi-pad testing tests were practically instantaneous. Observation holes H-3b1 and H-3b3 responded within five seconds to the beginning of pumping in H-3b2 during the multipad test. The peak drawdowns in the observation holes were 90% or more of the drawdown in the pumped hole, even in the relatively short 1984 test. As a result, it was necessary to interpret the responses of observation holes on the H-3 pad as if these holes were a part of the pumped hole. This conclusion is supported by the fact that the calculated effective hydraulic radius of the pumped well in the 1984 testing (H-3b3) is approximately 146 m (Beauheim, 1987a). This interpretation, however, makes it impossible to determine storativities along the flow paths at the H-3 pad.

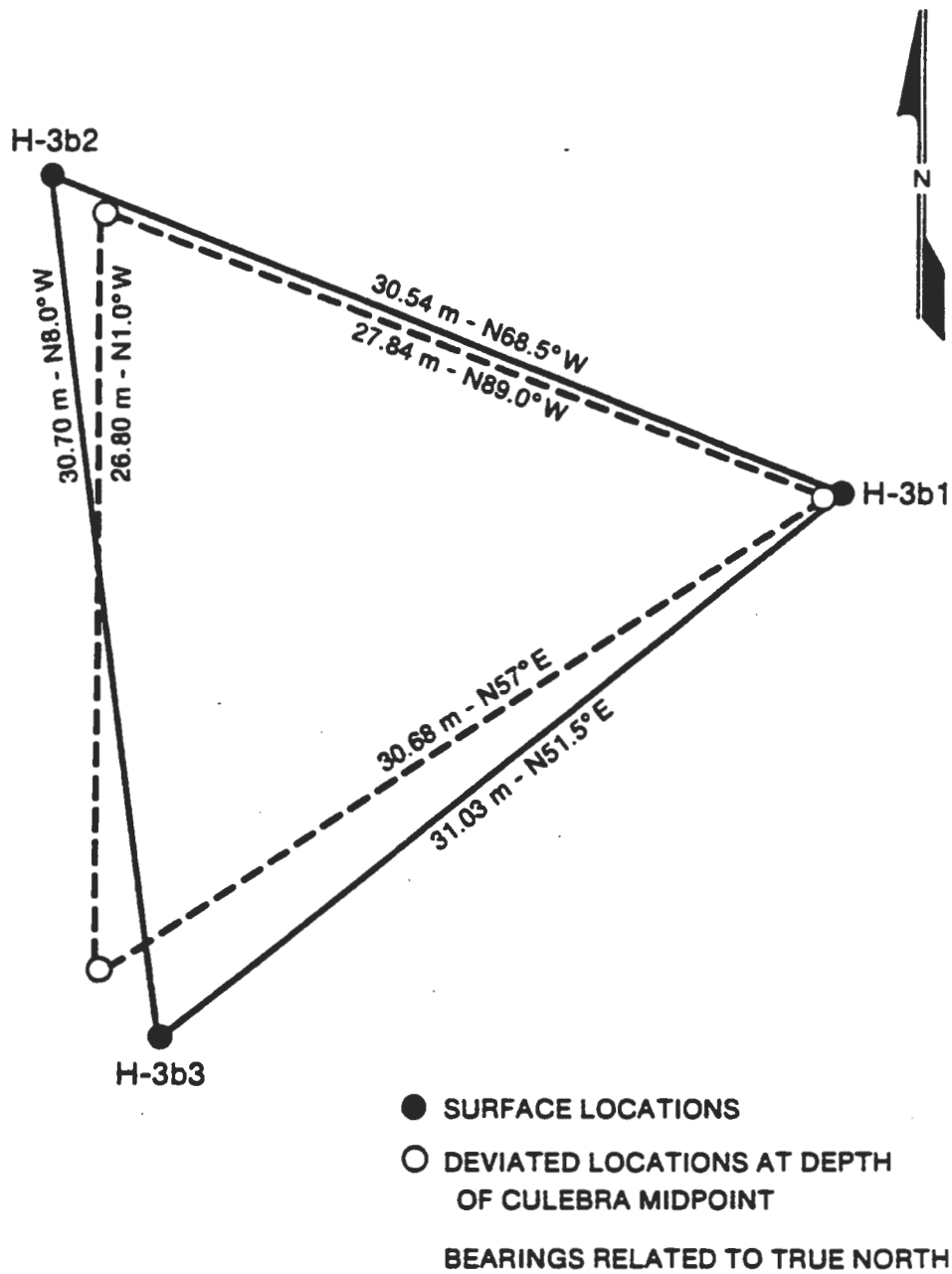


Figure 4.1.4: Physical layout of the H-3 hydropad. The figure is a plan view, showing positions and distances between wells both at the surface and where penetrating the Culebra dolomite. Figure 4.1 of Kelley and Pickens (1986).

The results of interference testing on the H-3 pad are summarized in Table 4.4. There is no significant difference between the interpreted transmissivities of the three holes on the H-3 pad, since the range in values is only from 3.1 to 3.2 x $10^{-6}$ $m^2/s$ for the 1984 testing and 1.8 to 1.9 x $10^{-6}$ $m^2/s$ for the multipad test. Therefore, there is no apparent anisotropy in the hydraulic properties at H-3. There is, however, a decrease of approximately 50% between the average transmissivity at H-3 interpreted from the 1984 testing, in which the pumping phase lasted 14 days at an average pumping rate of 4.0 gpm, and that interpreted from the H-3 multipad interference test, in which the pumping phase lasted 62 days, at an average rate of 4.8 gpm. Beauheim (1987a) attributes this difference to either a real difference in transmissivity between holes H-3b3 and H-3b2, the specific wells pumped in the two tests, and/or to the fact that the average transmissivity of the relatively large volume investigated during the long-term H-3 multipad test is lower than the average transmissivity of the volume investigated in the shorter-term 1984 testing. Consistent with this latter interpretation, the original H-3(b1) transmissivity of 2.0 x $10^{-5}$ $m^2/s$ reported by Mercer (1983) is based on a combination of bailing/recovery and slug tests, both of short duration.

Table 4.4 includes estimates of both "skin factor" and the "storativity ratio" for individual holes on the H-3 pad. Calculated skin factors range from -7.3 to -8.1. As discussed by Beauheim (1987a), the strongly negative skin factors indicate direct connection of all three wellbores with fractures, consistent with the interpreted effective radius of 146 m for hole H-3b3. Although the storativities of the observation holes on the H-3 pad could not be calculated, Beauheim (1987a) does calculate "storativity ratios" (omegas), the ratio of fluid storativity within the fractures (secondary porosity) to that of the entire system of matrix plus fractures (primary plus secondary porosity). The calculated values range from 0.03 to 0.25. As noted by Saulnier (1987), most fractured-rock systems have a storativity ratio less than 0.1. The storativity ratios at the H-3 pad indicate unusually high storage within fractures, perhaps due to the vugginess of the Culebra.

4.1.2.2 <u>Interference Testing at the H-11 Hydropad and Comparison with Results at the H-3 Pad</u>--Saulnier (1987) summarizes the interpretation of pad-scale interference testing carried out at the H-11 hydropad (Figure 4.1.5) in 1984 and 1985. During 1984, holes H-11b1, H-11b2, and H-11b3 were each pumped in individual tests lasting from 12 to 21 hours. The 1985 test, in which H-11b3 was the pumped hole, lasted for 32 days. However, complications with instrumentation during the 1985 testing resulted in four distinct pumping and recovery periods. The resulting superposition of effects complicates interpretation of the 1985 results.

The results of interference testing at H-11 are included in Table 4.4. The interpreted transmissivities for pumped holes and for flow paths between pumped and observation holes on the H-11 pad range from 1.2 x $10^{-5}$ to 3.0 x $10^{-5}$ $m^2/s$. With the exception of the interpreted transmissivity of H-11b1 during 1984 pumping the range is only 2.5 x $10^{-5}$ to 3.0 x $10^{-5}$ $m^2/s$.

Table 4.4: Summary of single-pad interference testing results for the Culebra dolomite at the H-3 and H-11 hydropads. Slightly modified from data contained in Tables 6-1 and 6-3 of Beauheim (1987a) and Table 6.1 of Saulnier (1987).

| | Transmissivity ($m^2/s$) | Skin Factor | Storativity | Storativity Ratio ($\omega$) | Flow Ratio($\lambda$) |
|---|---|---|---|---|---|
| H-3(1) | | | | | |
| H-3b3 (1984) pump | $3.1 \times 10^{-6}$ | -7.8 | - | 0.07 | - |
| H-3b1 (obs.) | $3.2 \times 10^{-6}$ | -7.3 | - | 0.25 | - |
| H-3b2 (obs.) | $3.2 \times 10^{-6}$ | -7.6 | - | 0.04 | - |
| H-3b2 (1986) pump | $1.8 \times 10^{-6}$ | -8.1 | - | 0.03 | - |
| H-3b1 (obs.) | $1.9 \times 10^{-6}$ | -7.7 | - | 0.25 | - |
| H-3b3 (obs.) | $1.9 \times 10^{-6}$ | -8.0 | - | 0.10 | - |
| H-11(2) | | | | | |
| H-11b1 (1984) pump | $1.2 \times 10^{-5}$ | -3.3 | - | 0.01 | $1.3 \times 10^{-9}$ |
| H-11b2 (obs.) | $2.5 \times 10^{-5}$ | - | $8 \times 10^{-4}$ | 0.35 | $2.0 \times 10^{-6}$ |
| H-11b3 (obs.) | $2.8 \times 10^{-5}$ | - | $5.5 \times 10^{-4}$ | 0.35 | $1.3 \times 10^{-6}$ |
| H-11b2 (1984) pump | - | - | - | - | - |
| H-11b1 (obs.) | $2.7 \times 10^{-5}$ | - | $6.1 \times 10^{-4}$ | 0.43 | $2.0 \times 10^{-6}$ |
| H-11b3 (obs.) | $2.6 \times 10^{-5}$ | - | $4.5 \times 10^{-4}$ | 0.40 | $3.8 \times 10^{-6}$ |
| H-11b3 (1984) pump | $2.8 \times 10^{-5}$ | -4.4 | - | 0.01 | $2.3 \times 10^{-6}$ |
| H-11b1 (obs.) | $2.7 \times 10^{-5}$ | - | $6.3 \times 10^{-4}$ | 0.30 | $1.3 \times 10^{-6}$ |
| H-11b2 (obs.) | $2.6 \times 10^{-5}$ | - | $7.2 \times 10^{-4}$ | 0.30 | $1.3 \times 10^{-6}$ |
| H-11b3 (1985) pump | $3.0 \times 10^{-5}$ | -4.6 | - | 0.01 | $3.7 \times 10^{-7}$ |
| H-11b1 (obs.) | $2.7 \times 10^{-5}$ | - | $2.9 \times 10^{-3}$ | 0.07 | $5.0 \times 10^{-6}$ |
| H-11b2 (obs.) | $2.8 \times 10^{-5}$ | - | $2.6 \times 10^{-3}$ | 0.07 | $5.8 \times 10^{-6}$ |

(1) All holes H-3 pad interpreted as part of pumped hole; therefore, storativities not available, but skin factors and point transmissivities available for all holes.

(2) Observation holes on H-11 pad well-behaved; therefore, transmissivities, except for pumped hole, are averages between observation and pumped hole.

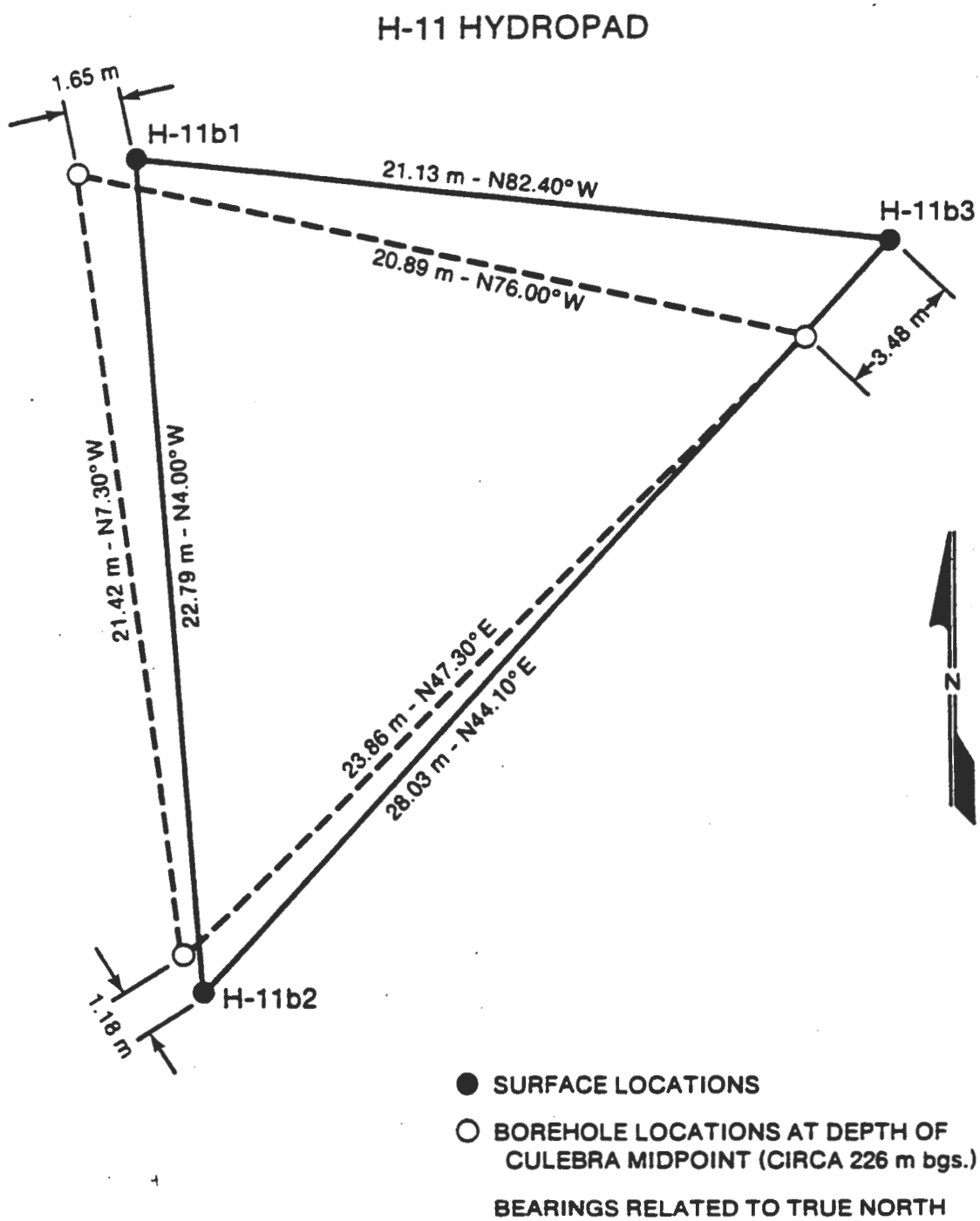


Figure 4.1.5: Physical layout of the H-11 hydropad. The figure is a plan view, showing positions and distances between wells both at the surface and where penetrating the Culebra dolomite. Modified from Figure 3.1 of Saulnier (1987).

The behavior of observation holes on the H-11 pad is consistently different than that observed on the H-3 pad. Although the observation holes on the H-11 pad displayed dual-porosity behavior, their response to the beginning and ending of pumping was sufficiently delayed to allow interpretation as observation holes, rather than as part of the pumped well. The calculated effective hydraulic radius of H-11b3, consistent with the behavior of the observation holes, is 4.9 m (Saulnier, 1987), as compared to an effective radius of 146 m at the H-3 pad (Beauheim, 1987a).

Comparison of the hydrologic behaviors at the H-3 and H-11 pads indicates that the hydraulic effectiveness of fracturing at a given site need not be proportional to the transmissivity. The interpreted transmissivity of H-11b3 during pumping of this hole in 1984 is 2.8 x $10^{-5}$ $m^2/s$, as compared to a transmissivity of 3.1.x $10^{-6}$ $m^2/s$ for hole H-3b3 in 1984 testing at the H-3 pad. However, the effective radius of H-3b3 is 146 m, while that of H-11b3 is 5 m. In addition, the observation holes at the H-3 pad had to be treated as part of the pumped well, while observation holes at the H-11 pad behaved properly as observation wells. As shown in Table 4.3, the calculated skin factors at the H-3 pad, which range from -7.3 to -8.1, are consistently more negative than those at the H-11 pad, which range from -3.3 to -4.6.

Interpretation of behavior along the assumed radial flow paths between observation and pumped wells on the H-11 pads indicates average hydraulic storativities between 4.5 x $10^{-4}$ and 2.9 x $10^{-3}$, with the higher values interpreted from testing in 1985. These storativities are higher than regional storativities calculated by Beauheim (1987a) from multipad testing at the H-3 pad (7.4 x $10^{-6}$ to 3.0 x $10^{-5}$, see Table 4.6). As at the H-3 pad, calculated storativity ratios at H-11 range from 0.01 to 0.43, higher than normal for fractured media.

Calculated interporosity-flow parameters (lambdas) at H-11 range from 1.3 x $10^{-9}$ to 5.8 x $10^{-6}$ (Table 4.4). As noted by Saulnier (1987), the definition of the parameter lambda includes the ratio of the matrix permeability (permeability of the primary-porosity system) to permeability of the fractures (secondary-porosity system). Therefore, the calculated results indicate that there is a strong contrast between matrix and fracture permeabilities at the H-11 pad. As also indicated by Saulnier (1987), interpretation of the calculated lambda values at the H-11 pad is consistent with effective block or slab dimensions of 0.3 to 1.0 m. The available information on the effective block size in fractured portions of the Culebra dolomite is discussed further in Section 4.2, based on the results of testing with conservative tracers at the H-3 hydropad.

Using the system transmissivities interpreted from 1984 testing and an average storativity of 6.3 x $10^{-4}$, Saulnier (1987) estimates the extent and orientation of hydraulic "anisotropy" at H-11. The calculated maximum transmissivity vector of 3.3 x $10^{-5}$ $m^2/s$ is oriented 5.8 degrees north of east, and the calculated minimum transmissivity vector of 2.1 x $10^{-5}$ $m^2/s$ 5.8 degrees west of north (Table 4.5). The calculated ratio of 1.6:1 between maximum and minimum transmissivities at H-11 indicates only a small degree of anisotropy. However, the presence of fractures at this site indicates that these results are only qualitative; because of the

fractures, directional variations in properties are almost certainly not continuous. Also, since the indicated directions of maximum and minimum transmissivity do not coincide with any direct flow paths on the H-11 pad, there is no guarantee that either the maximum or minimum values are reliable.

Table 4.5: Summary of apparent hydraulic anisotropy of the Culebra dolomite. Compiled from results contained in Saulnier (1987) and Gonzalez (1983b).

| | $T_{MAX}$ ($m^2/s$) | $T_{MIN}$ ($m^2/s$) | $T_{MAX}/T_{MIN}$ | Orientation of $T_{MAX}$ |
|---|---|---|---|---|
| Site | | | | |
| H-4(1) | $2.9 \times 10^{-6}$ | $1.1 \times 10^{-6}$ | 2.6 | N76W |
| H-5 | $2.4 \times 10^{-7}$ | $9.7 \times 10^{-8}$ | 2.5 | N25W |
| H-6 | $1.1 \times 10^{-4}$ | $5.2 \times 10^{-5}$ | 2.1 | N29W |
| H-11(2) | $3.3 \times 10^{-5}$ | $2.1 \times 10^{-5}$ | 1.6 | N84E |

(1) Data for H-4, H-5, and H-6 from Gonzales (1983b).
(2) Data for H-11 from Saulnier (1987).

The available interpretations of anisotropy within the Culebra dolomite are summarized in Table 4.5. Earlier interpretations at the H-4, H-5, and H-6 pads all explicitly make the porous-medium assumption (Gonzalez, 1983b). The interpretation of Saulnier (1987) is based on the calculated system transmissivities. The available interpretations indicate transmissivity ratios between 1.6:1 and 2.6:1, with a direction of between N84E and N76W for the major transmissivity vector. For calculated major Culebra transmissivities between $2.4 \times 10^{-7}$ $m^2/s$ and $1.1 \times 10^{-4}$ $m^2/s$ and minor transmissivities between $9.7 \times 10^{-8}$ and $5.2 \times 10^{-5}$ $m^2/s$ there appears to be less than a factor of three hydraulic anisotropy. The available results indicate that there is no consistent orientation of maximum Culebra transmissivity.

### 4.1.3 Multipad Interference Testing

As noted in the introduction to Section 4.0, the best method of estimating the regional distribution of properties within a variable hydrologic unit is by regional-scale testing and interpretation. At the WIPP site, two regional-scale multipad interference tests of the Culebra dolomite have been completed, centered at the H-3 hydropad and at hole WIPP-13. The H-3

multipad interference test and related analytical interpretation and regional-scale modeling of Culebra hydrology are discussed in Section 4.1.3.1. The WIPP-13 test and related interpretative and modeling studies are discussed in Section 4.1.3.2.

4.1.3.1 The H-3 Multipad Interference Test and the Regional Culebra Model of Haug et al. (1987)--The pumping phase of the H-3 multipad interference test (Figure 4.1.6) extended from October 15, 1985, to December 16, 1985. Recovery monitoring continued until April 16, 1986, when the data-acquisition system at the H-3 pad was turned off. Raw data from the test are included in INTERA (1986). Analytical interpretations of both detailed results at the H-3 pad and average or apparent transmissivities and storativities between H-3b2 (the pumped hole) and the numerous observation holes are reported by Beauheim (1987a). Analytical interpretation of regional flow patterns generated in response to the test, with emphasis on evaluation of a linear-flow regime at holes H-3, H-11, and DOE-1, is reported by Tomasko and Jensen (1987). Numerical calculation or simulation of Culebra transmissivities, heads, and fluid densities on the regional scale are reported by Haug et al. (1987), as well as modeling of the transient pressure responses to the H-3 multipad test.

Beauheim (1987a) describes the analytical (as opposed to numerical) interpretation of hydraulic data collected during the H-3 multipad interference test. Results on the H-3 pad itself are discussed in Section 4.1.2. The regional distribution of Culebra properties, based on Beauheim's analytical interpretation, is summarized in Table 4.6. The analytical approach used to interpret responses at observation holes necessarily assumes both radial flow into the pumped hole and homogeneous or average properties between pumped hole and individual observation holes (Beauheim, 1987a). Therefore, transmissivity values listed in Table 4.6 are apparent average values for an assumed radial flow path between H-3b2 and the listed observation hole. Beauheim (1987a) found it necessary to correct both pre-test and post-test heads for the relatively long-term transient behavior of some water levels at and near the WIPP site (Table 4.6). This transient behavior is in response to some combination of hydrologic testing, shaft sinking and sealing operations, and a possible regional transient.

Observation-hole responses to the H-3 multipad test fall into three general categories. First, on the H-3 pad itself, hydraulic fracturing was sufficient to require that Observation holes H-3b1 and H-3b3 be considered as part of the pumped hole (Section 4.1.2). Second, Observation holes DOE-1 and H-11b1, respectively 1606 and 2423 m southeast of H-3b2 (Figure 4.1.6), responded rapidly to both the beginning and ending of pumping. Drawdown in DOE-1 began 48 hours into the test, and that in H-11b1 only three hours later (Table 4.6). The average transmissivities interpreted along flow paths between H-3b2 and DOE-1 and H-11b1 are $5.9 \times 10^{-6}$ $m^2/s$ between DOE-1 and H-3b2 and $7.3 \times 10^{-6}$ $m^2/s$ between H-11b1 and H-3b2. Calculated apparent storativities along the same flow paths are $1.0 \times 10^{-5}$ and $7.4 \times 10^{-6}$, respectively. Beauheim (1987a) concludes that the rapid responses at DOE-1 and H-11b1 and relatively high calculated transmissivities along flow paths between these holes and H-3b2 indicate a

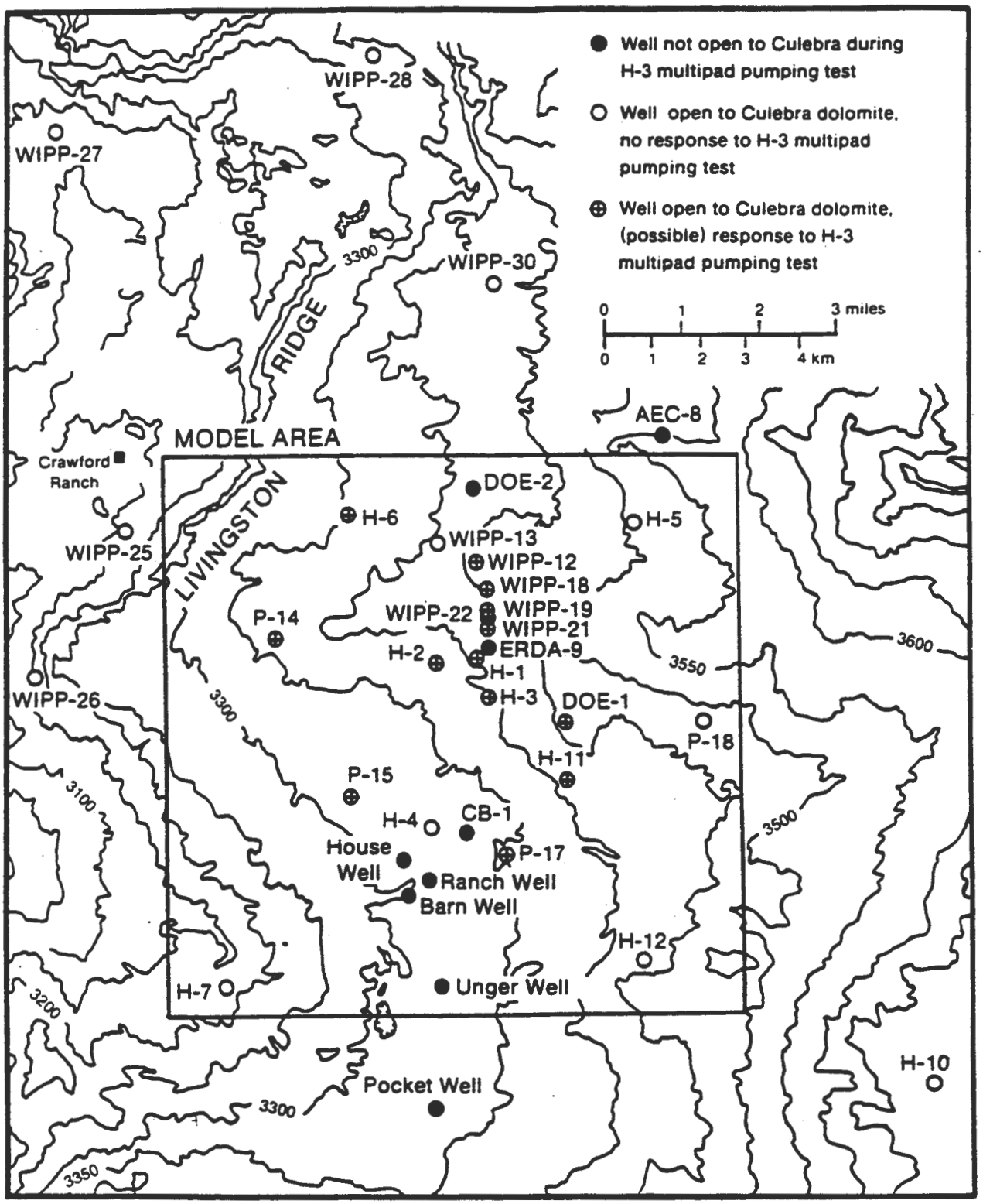


Figure 4.1.6: Pumping and observation wells for the H-3 multipad interference test. Figure 3.2 of Haug et al. (1987).

Table 4.6: Summary of results of analytical interpretation of H-3 multipad interference test. Slightly modified from data contained in Tables 3-1, 5-1, and 6-4 of Beauheim (1987a).

| Well | Distance(m)(1) | Direction | First Obs.(2) Drawdown (hrs) | Delay in Max. Drawdown (hr) | Unmodified Interpretation T($m^2$/s)(3) | Unmodified Interpretation S | Modified Interpretation T($m^2$/s) | Modified Interpretation S | Head Modification (m/day) |
|---|---|---|---|---|---|---|---|---|---|
| H-11b1 | 2423 | S42E | 79 | 51 | $1.4 \times 10^{-5}$ | $6.6 \times 10^{-6}$ | $7.3 \times 10^{-6}$ | $7.4 \times 10^{-6}$ | $8.6 \times 10^{-3}$ |
| DOE-1 | 1606 | S68E | 57 | 48 | $9.9 \times 10^{-6}$ | $9.2 \times 10^{-6}$ | $5.9 \times 10^{-6}$ | $1.0 \times 10^{-5}$ | $5.5 \times 10^{-3}$ |
| H-1 | 815 | N19W | 488 | 1423 | $8.9 \times 10^{-7}$ | $3.9 \times 10^{-5}$ | $4.9 \times 10^{-7}$ | $2.7 \times 10^{-5}$ | $2.64 \times 10^{-2}$ |
| H-2b2 | 1270 | N54W | 433 | 1393 | $2.7 \times 10^{-6}$ | $4.5 \times 10^{-5}$ | $1.3 \times 10^{-6}$ | $3.0 \times 10^{-5}$ | $1.16 \times 10^{-2}$ |
| WIPP-19 | 1875 | N2E | 1207 | 1855 | $3.1 \times 10^{-6}$ | $2.9 \times 10^{-5}$ | - | - | - |
| WIPP-21 | 1437 | N3E | 437 | 678 | $1.2 \times 10^{-6}$ | $9.0 \times 10^{-6}$ | - | - | - |
| WIPP-22 | 1739 | N2E | 990 | 727 | $1.7 \times 10^{-6}$ | $1.7 \times 10^{-5}$ | - | - | - |

(1) Distances and directions measured from H-3b2 to the indicated well.
(2) First drawdown and delay in maximum drawdown are given relative to times at which pump was turned on and off, respectively.
(3) Unmodified and modified transmissivities (T) and storativities (S) are apparent average values between H-3b2 and indicated well, assuming radial flow to H-3b2.

preferential connection between the H-3 pad and the southeast portion of the WIPP site. He further concludes, consistent with single-pad interference testing at both H-3 and H-11 (see Section 4.1.2), that this connection is related to fractures. Third, holes north and northwest of H-3b2 were much slower to respond to the H-3 multipad test, indicating relatively poor and variable hydraulic connection in this direction. Hole H-1, 815 m from H-3b2, did not respond to pumping until approximately 488 hours into the test. The best estimate of the average transmissivity between H-3b2 and H-1 is $4.9 \times 10^{-7}$ $m^2/s$. H-2b2, slightly further from H-3b2 than hole H-1, responded earlier (433 hours). The slightly higher apparent transmissivity between H-2b2 and H-3b2 ($1.3 \times 10^{-6}$ $m^2/s$) than between H-1 and H-3b2 indicates local variability within the Culebra dolomite, even in the low-transmissivity domain containing H-1, H-2, and H-3. In contrast to behavior at and southeast of the H-3 pad, there is no indication that regional-scale flow or pressure response between H-3 and either H-2b2 or H-1 involved fractures. Holes WIPP-19, 21, and 22 are north of the WIPP facility (Figure 4.1.6). Therefore, their response to any pumping test at H-3 will be influenced by the intervening WIPP shafts, unless the sealing of these shafts is perfect. There was, in fact, considerable uncertainty about the rates of leakage from the Culebra into the WIPP exhaust and waste-handling shafts during the H-3 test. As a result, interpreted transmissivities for flow paths extending north of the center of the WIPP site, i.e., between H-3b2 and holes WIPP-19, 21, and 22, may be inaccurate (Beauheim, 1987a).

Several observation holes did not respond measurably during the H-3 multipad test, including H-4, P-14, P-15, and P-17. Therefore, only minimal transmissivities could be calculated for areas south and southwest of H-3, based on the lack of response. Beauheim (1987a) estimates that the average transmissivity between H-4 and H-3b2 would need to be less than $1.0 \times 10^{-6}$ $m^2/s$. As indicated in Table 4.2, drilling and testing of hole H-14 has since yielded results consistent with this bounding interpretation.

Tomasko and Jensen (1987) note a strikingly linear relationship between the observed drawdowns and the square root of time in holes H-3b2, H-11b1, and DOE-1 during the H-3 multipad test, and conclude from this that much of the response to the test in this area was a result of "linear flow," in which flow is largely confined to a linear high-transmissivity structure between less-permeable boundaries. Their interpretation is a second line of evidence for a high-transmissivity structure in the southeastern part of WIPP Zone 3. Figure 4.1.7 shows the nearly linear response of H-3b2 versus the square root of time during the pumping phase of the H-3 multipad test. Tomasko and Jensen (1987) interpret the limited curvature shown in Figure 4.1.7 to reflect the fact that the high-transmissivity structure containing H-3b2 is finite in width.

Figure 4.1.8 compares observed drawdowns and recoveries at H-11 and DOE-1 with those calculated assuming linear flow in a high-transmissivity structure oriented N29W. There is good agreement during the pumped phase, even with a model that used a simplified transmissivity distribution. Although calculated drawdowns exceed those measured, the shape of both drawdown and recovery curves agree well. This linear-flow approach yielded average transmissivities of $2.2 \times 10^{-6}$, $9.7 \times 10^{-6}$, and $2.0 \times 10^{-5}$ $m^2/s$ for

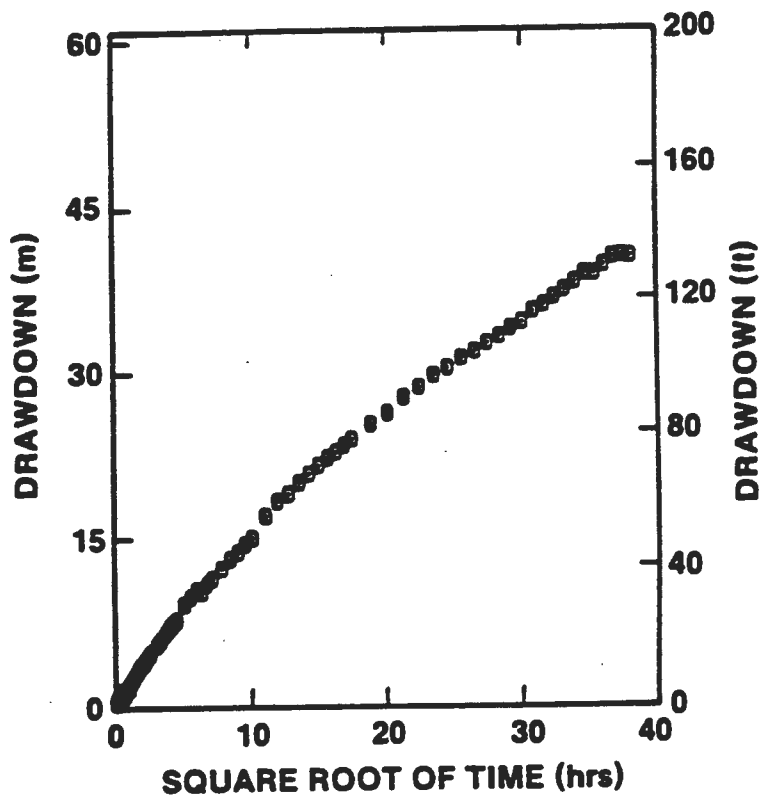


Figure 4.1.7: Observed drawdown versus the square root of time in hole H-3b2 during the H-3 multipad interference test. Slightly modified from Figure 15 of Tomasko and Jensen (1987).

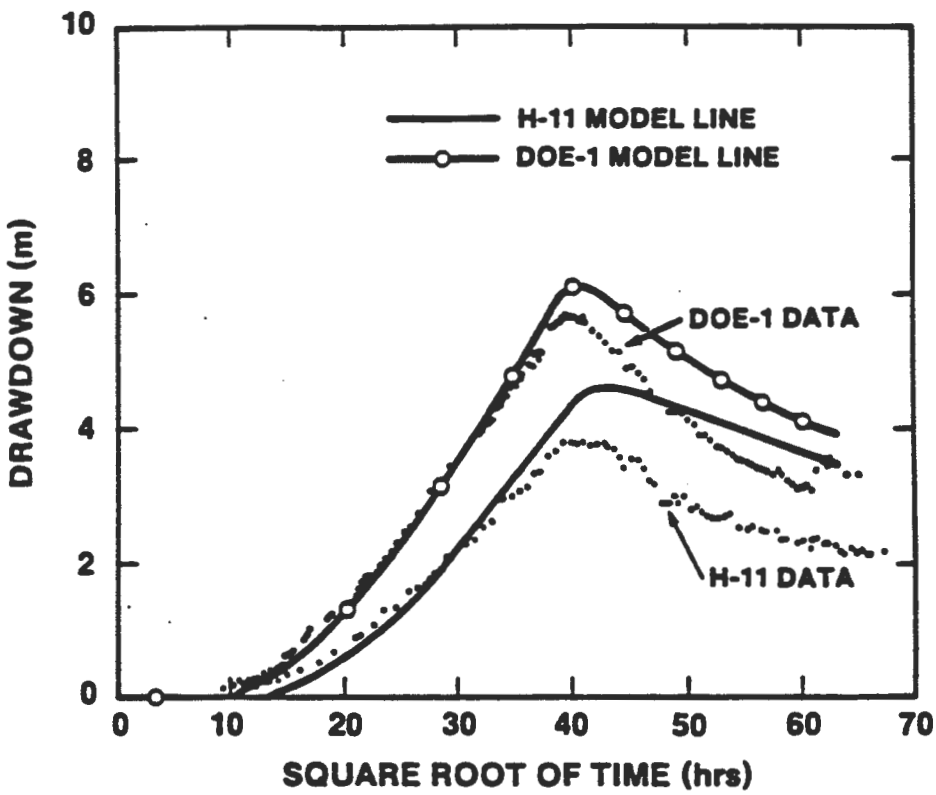


Figure 4.1.8: Comparison of measured and simulated responses at H-11 and DOE-1 during the H-3 multipad interference test, assuming perfectly linear flow. Figure 25 of Tomasko and Jensen (1987).

the H-3 pad and between H-3 and DOE-1 and H-11, respectively. These results are in qualitative agreement with the results of Beauheim (1987a) discussed above ($2.0 \times 10^{-6}$, $5.9 \times 10^{-6}$, $7.3 \times 10^{-6}$ $m^2/s$, respectively).

The analytical approaches discussed thus far involve specific assumptions, some of which pose real limitations in interpretation of testing on this geometric scale within a unit as complex as the Culebra dolomite. These include:

1. Regional-scale flow is assumed to be either perfectly radial or perfectly linear.

2. Transmissivities are either assumed uniform between pumped hole and observation hole, or a simplified transmissivity distribution is assumed.

3. Constant fluid density is assumed.

4. The Culebra dolomite is assumed to be completely confined.

In contrast, the approach taken by Haug et al. (1987), using the code SWIFT II (Reeves et al., 1986a; Reeves et al., 1986b), is fully numerical, and includes consideration of: a) a more complex pattern of regional flow, based on calculation of transmissivities between measurement points; b) variable fluid densities; and c) vertical fluid flux into or out of the Culebra. The modeling approach of Haug et al. (1987) assumes steady-state boundary conditions.

The results of non-directional kriging of the April 1986 Culebra-transmissivity data base (Figures 4.1.9 and 4.1.10) provide a quantitative indication of the statistical reliability of the data base at that time, independent of geologic and hydrologic judgement. The limited size of the data base resulted in the kriged transmissivity pattern consisting largely of "circles" around measured data points (Figure 4.1.9). The roughly circular areas within which the uncertainty in transmissivity (defined here as one standard deviation) was less than one order of magnitude were centered on individual hydro holes and approximately one kilometer in diameter (Figure 4.1.10). The only regions in which the areas of one-order-of-magnitude uncertainty overlapped was in the regions H-1 - H-2 - H-3 and H-11 - DOE-1. This finding provided strong impetus for testing of additional holes within WIPP Zone 3, as indicated by the large number of holes in Table 4.1 for which data have been collected or revised since April 1986.

One major emphasis of Haug et al. (1987) is consideration of the regional hydrologic behavior of the Culebra, independent of transient effects imposed by the WIPP facility. This required estimation of Culebra head potentials as they existed prior to the sinking of the WIPP shafts (Figure 4.1.11). Figure 4.1.12 shows the simulated or calculated Culebra transmissivity distribution resulting from calibration of downhole pressures within the Culebra against the "measured" pre-shaft freshwater-equivalent head potentials shown in Figure 4.1.11. The calibration effort

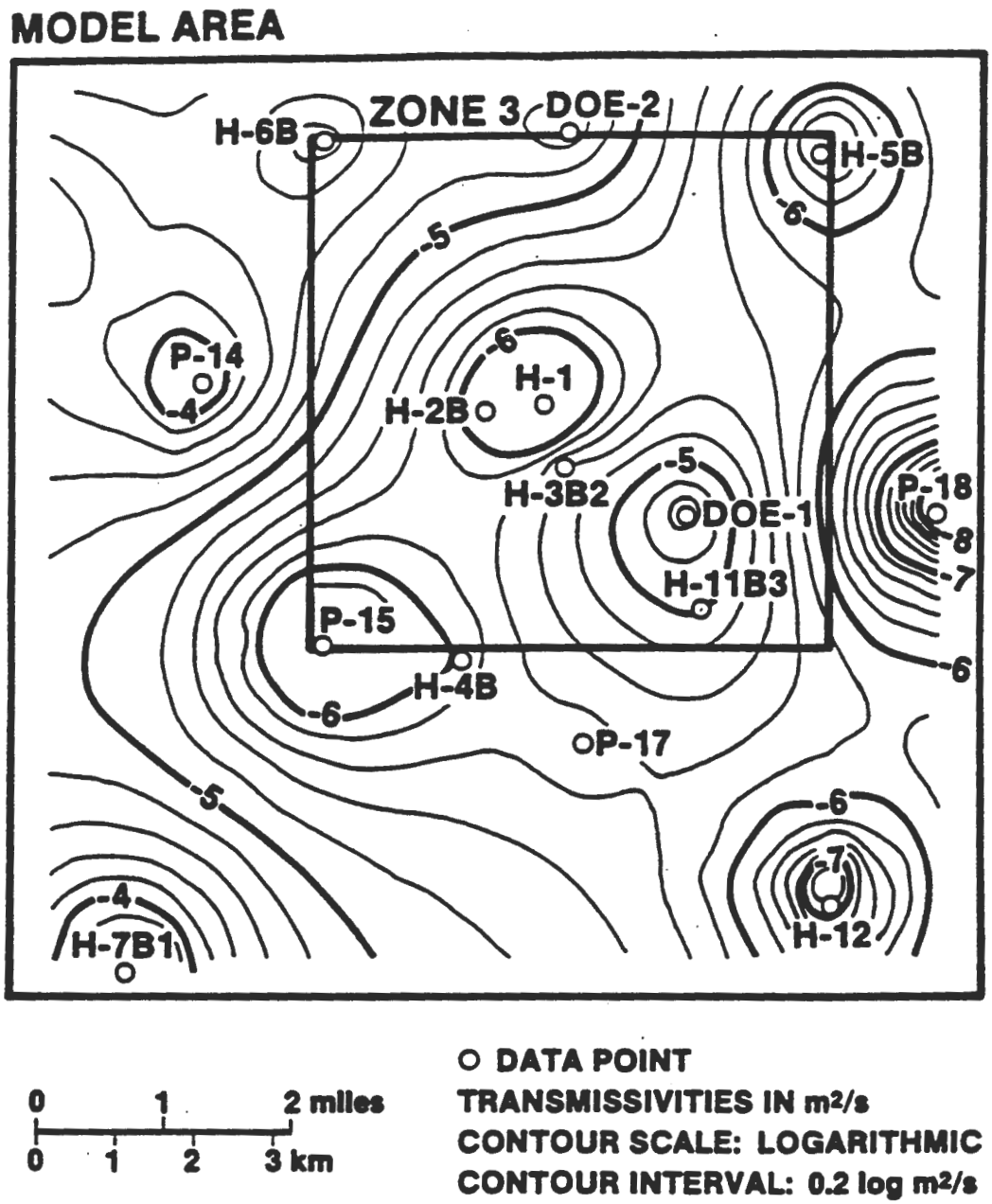


Figure 4.1.9: Initial kriged Culebra transmissivities, based on data available as of April 1986. Slightly modified from Figure 3.7 of Haug et al. (1987).

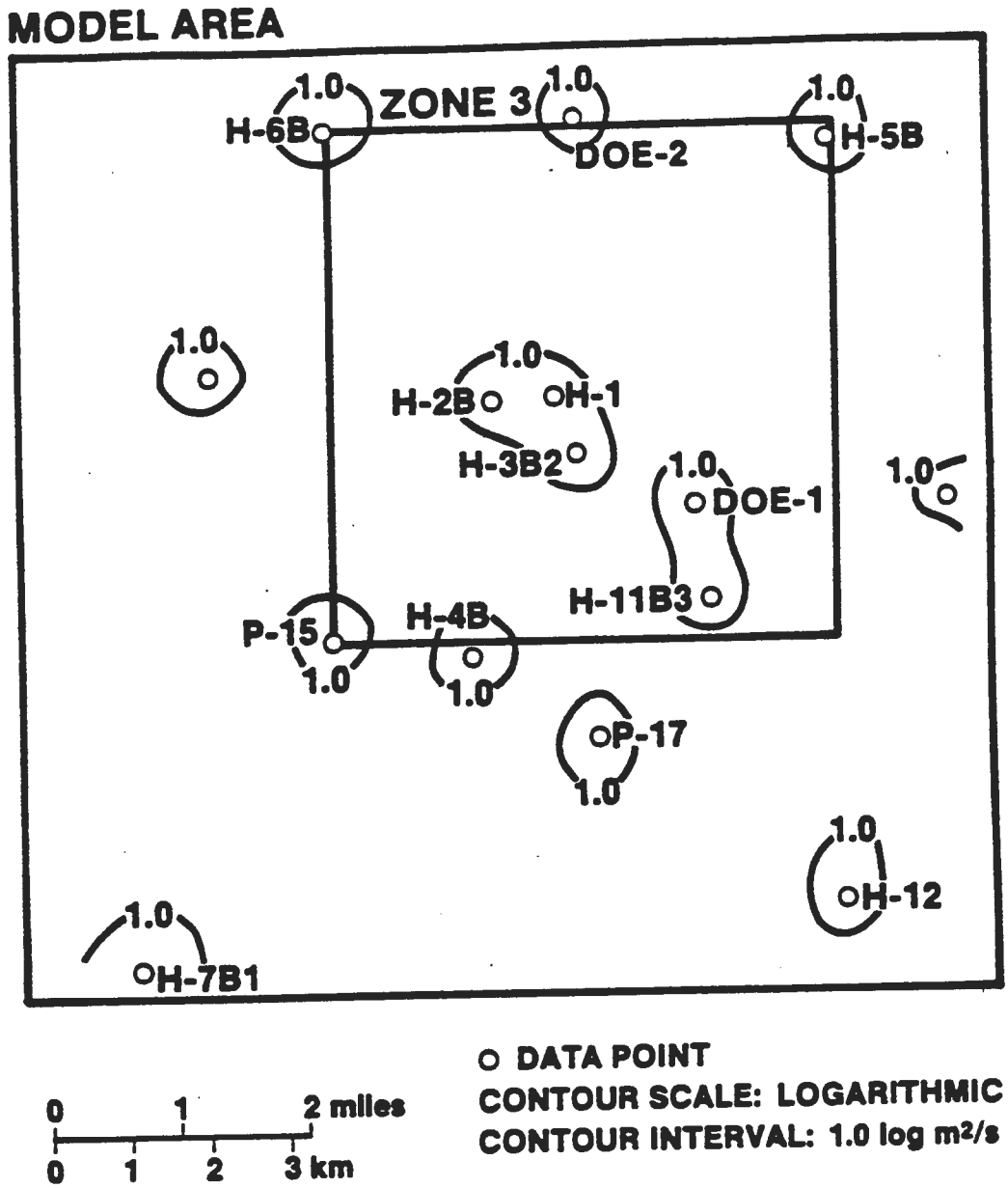


Figure 4.1.10: Estimation error in initial kriged Culebra transmissivi ties, based on data available as of April 1986. Slightl modified from Figure 3.8 of Haug et al. (1987).

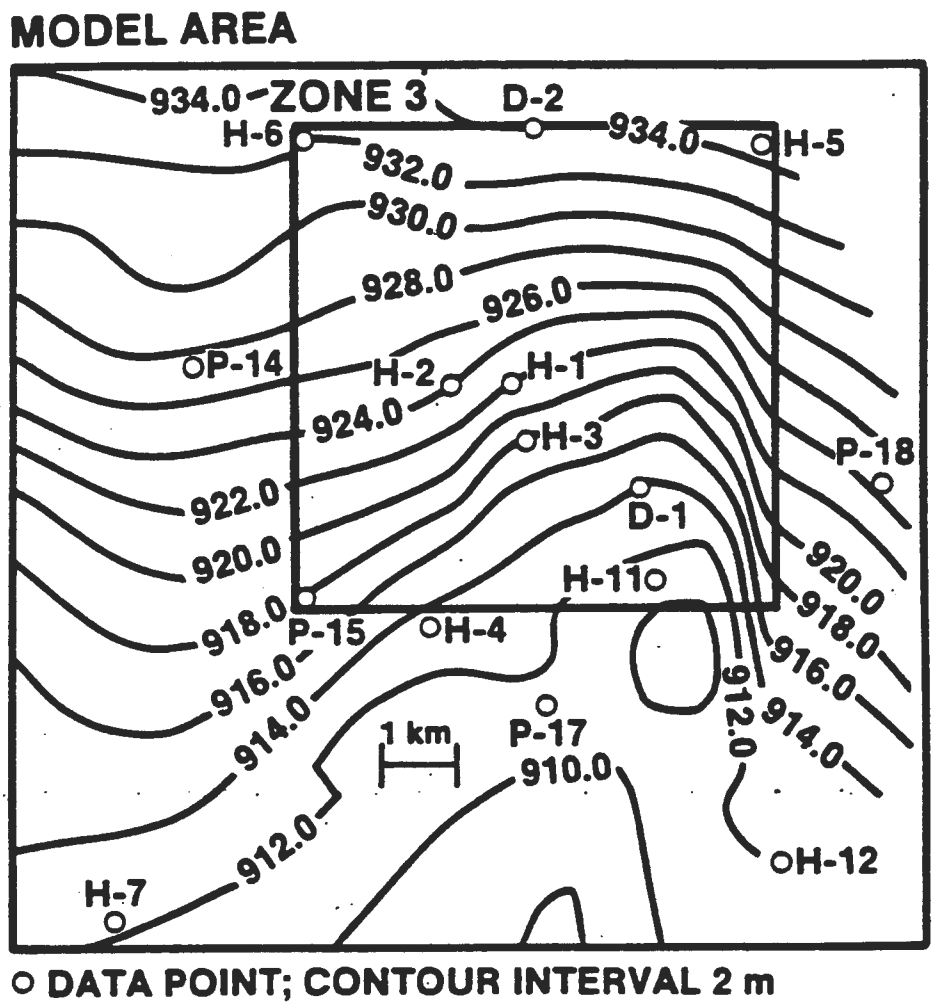


Figure 4.1.11: Best estimate of pre-shaft Culebra freshwater equivalent heads, based on data available as of April 1986. Slightly modified from Figure 3.9 of Haug et al. (1987).

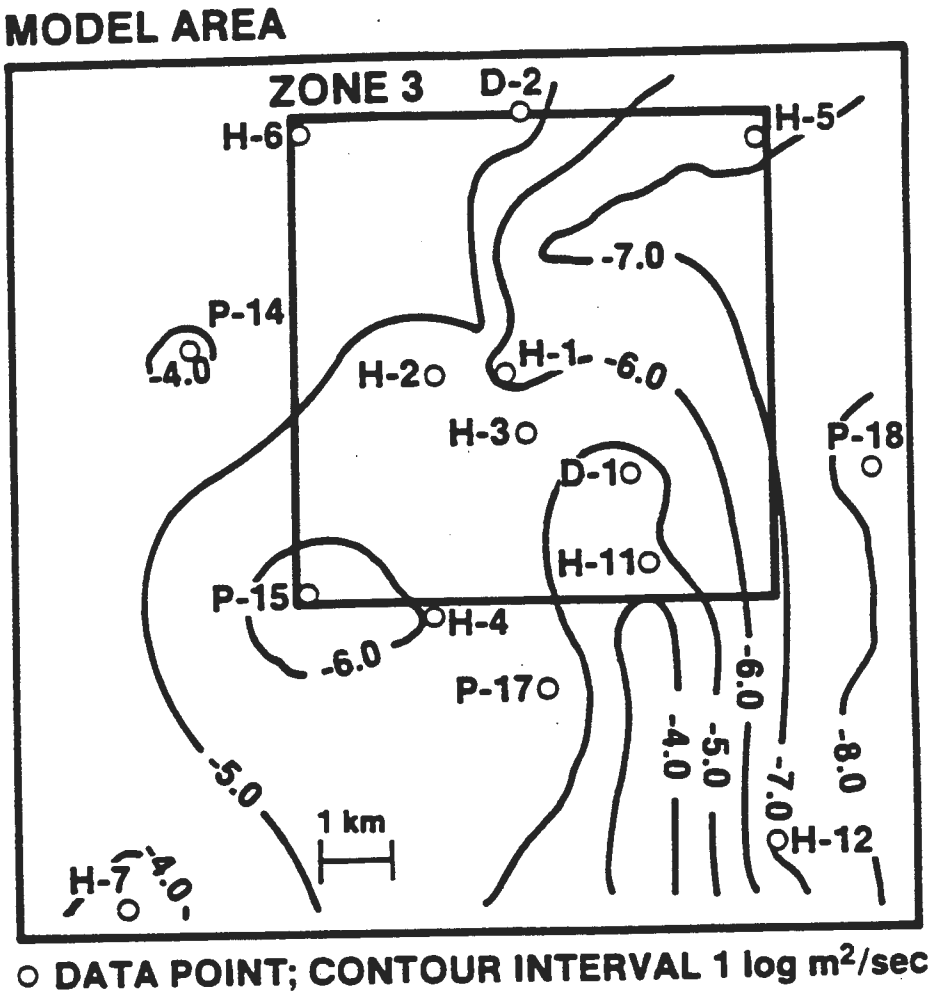


Figure 4.1.12: Best calculated distribution of Culebra transmissivities, based on pressure calibration to head distribution shown in Figure 4.1.11. Slightly modified from Figure 4.4 of Haug et al. (1987).

involved use of "pilot points" in some locations between measured data. At the pilot points, transmissivities were assigned, consistent with the uncertainty in initial kriged values. Evaluation of the statistical properties of the expanded data base including the pilot-point transmissivities indicated that the statistical properties of this data base were consistent with those of the measured data.

The transmissivity distribution in Figure 4.1.12 is marked by four main features:

1. A large and apparently continuous zone of relatively low transmissivity ($T<10^{-6}$ $m^2/s$) including the site center, the locations of the WIPP shafts, and extending to the east and northeast.

2. An apparently isolated region of low transmissivity in and near the southeastern portion of the site, in the region P-15 - H-4 - P-17. As noted in Section 4.1.1, it is not clear from existing point data whether or not this zone is connected to the low-transmissivity zone closer to the site center.

3. A narrow high-transmissivity zone ($T>10^{-5}$ $m^2/s$) in the region containing H-11 and DOE-1, and extending to the south. This zone was largely required in the model to account for the relatively low heads observed at H-11 and DOE-1 (Figure 4.1.11).

   The central portion of the high-transmissivity zone is defined in Haug et al. (1987) only by several pilot points, since no data from within the zone were available as of April 1986. The zone is consistent with results of both Beauheim (1987a) and Tomasko and Jensen (1987). Model transmissivities in the central part of the zone, approximately $3.0 \times 10^{-4}$ $m^2/s$, are similar to the transmissivities at H-9b ($1.7 \times 10^{-4}$ $m^2/s$) and P-14 ($2.3 \times 10^{-4}$ $m^2/s$), but lower than the transmissivity at H-7b ($1.1 \times 10^{-3}$ $m^2/s$) (Table 4.1). The assigned value was chosen in the effort to be reasonably "conservative," i.e., to have the zone contain as high a transmissivity as was reasonable.

4. A relatively large and apparently continuous high-transmissivity zone in the western part of the modeled area. As of April 1986, the high-transmissivity zone included measured data only at holes H-6, DOE-2, P-14, and H-7. The need to define the relationship of this high-transmissivity zone to the low-transmissivity zone containing the center of the WIPP site was a major driving force behind multipad interference testing at WIPP-13 (Section 4.1.3.2).

The calculated transmissivity distribution (Figure 4.1.12) served as a basis for further model calibration (Haug et al., 1987). The distribution of Culebra fluid densities measured as of April 1986 is shown in Figure 4.1.13. Culebra fluids in the vicinity of the WIPP site range in density from approximately 1.00 to greater than 1.10 $g/cm^3$ (see Section 4.1.3.2). Two main features of Figure 4.1.13 are of note:

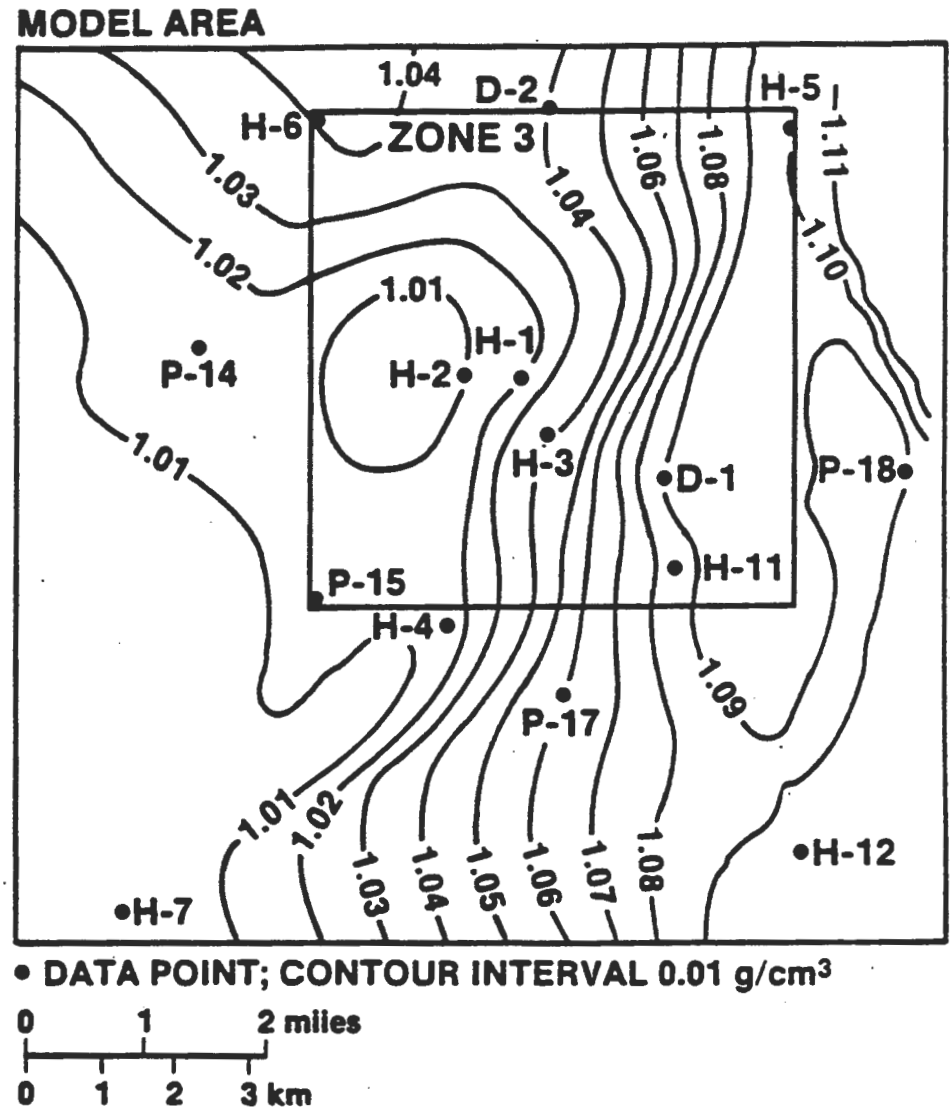


Figure 4.1.13: Best estimate of density distribution of Culebra fluids, based on information available as of April 1986. Figure 3.10 of Haug et al. (1987).

1. A linear zone of steep gradient in fluid density separates a large area of high fluid density (1.08 $g/cm^3$ or greater) east of the site center from an analogous area of relatively low fluid density (1.04 $g/cm^3$ or less) west of the site center.

2. Major curvature in the lines of fluid densities 1.01 through 1.04 $g/cm^3$ in the northwest part of the modeled area. As of April 1986, only measured density data from H-6, DOE-2, H-2, and P-14 provided control for this curvature.

During calibration of Culebra transmissivities against fluid densities, the interpolated brine densities near the boundaries of Figure 4.1.13 were first used as initial boundary conditions in simulation of assumed variable-density steady-state confined flow within the Culebra (Haug et al., 1987). The results of this approach were not satisfactory (Figures 4.1.14 and 4.1.15). Calculated brine densities at steady state are too low in the eastern portion of the model. The density contrasts in the eastern portion of the model (with the exception of the region near P-17) were adjusted successfully by slightly increasing the transmissivity in the northeastern portion of the model, without significantly changing fluid densities assigned at the boundaries. Over the western portion of the model, the problem was more severe. At steady state, a large area, including holes H-1, H-2, P-17, P-15, and P-14, was calculated to have fluid densities between 1.04 and 1.05 $g/cm^3$, compared to measured densities of 1.06 $g/cm^3$ at P-17 and less than 1.03 $g/cm^3$ at the other holes. The high calculated brine densities over the western portion of the site reflect the southward movement of the relatively dense brines at H-6 and DOE-2 required by steady-state confined flow (Haug et al., 1987).

These results are taken by Haug et al. (1987) to be consistent with at least three possibilities:

1. The interpolated brine densities along the northern boundary of the model are incorrect, except for the measured value at H-6. This possibility is considered in detail by Haug et al. (1987). Because of the recent increase in brine-density data in the northwest portion of the modeled area, the possibility is not considered further here (see Section 4.1.3.2).

2. There is enough vertical fluid leakage into and/or out of the Culebra to significantly affect fluid densities within the unit. This possibility is considered further by Haug et al. (1987), and is discussed below (see also Section 4.1.1).

3. The Culebra hydrologic regime is not at steady state on the time scale required for water flow across the modeled area. Transient boundary conditions for the hydrology of the Rustler Formation are consistent with recent geologic and isotopic results discussed in Sections 4.3 and 4.4, but have not yet been modeled directly, and are not considered further here.

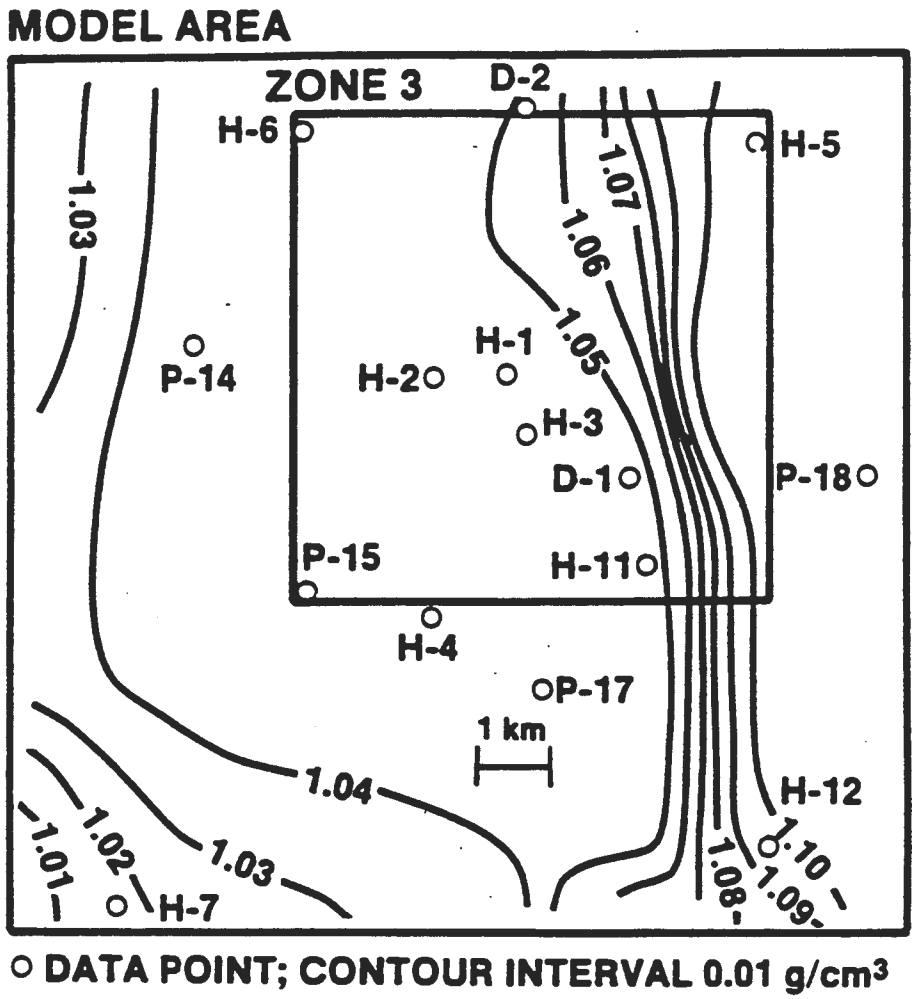


Figure 4.1.14: Calculated steady-state, brine-density distribution within the Culebra dolomite, based on data available as of April 1986. Slightly modified from Figure 4.7 of Haug et al. (1987).

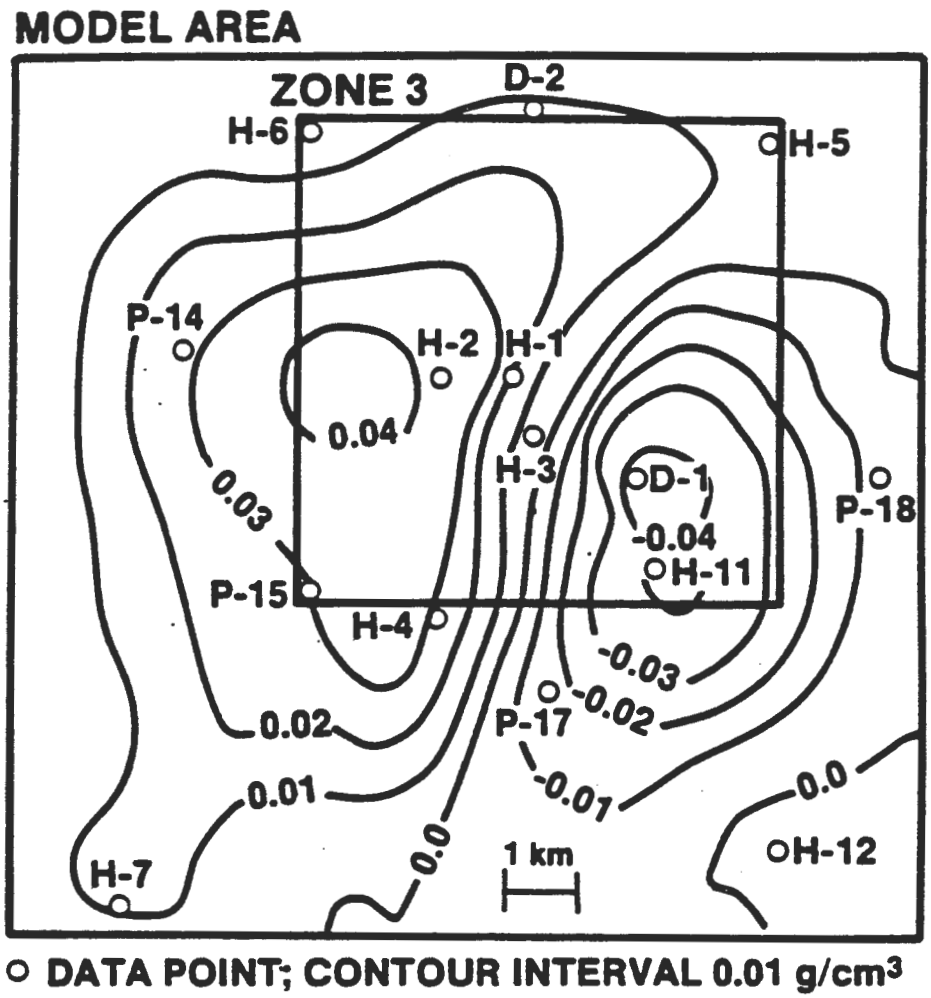


Figure 4.1.15: Difference between calculated steady-state brine density distribution within the Culebra (Figure 4.1.14) and the measured estimated distribution shown in Figure 4.1.13. Slightly modified from Figure 4.8 of Haug et al. (1987).

Haug et al. (1987) initially addressed the density contrast over the western portion of the modeled area by assuming that brine densities along the northern boundary of the model were incorrect; therefore, calibration against fluid density did not change interpolated transmissivities in this area. In the vicinity of hole P-17, however, better agreement between calculated and measured fluid densities was obtained by shifting the location of the southern high-transmissivity zone in Figure 4.1.12 closer to P-17.

Haug et al. (1987) then considered the possibility of vertical fluid flow into and/or out of the Culebra dolomite in two areas:

1. At and near P-17, where measured brine densities were 0.04 $g/cm^3$ higher than those calculated. Upward flow of relatively dense brine from the Rustler/Salado contact zone, through the unnamed lower member of the Rustler, into the Culebra dolomite was considered at this location, consistent with known head relationships (see Section 4.1.1).

2. Over the western and southwestern part of the modeled area, in which measured fluid densities are significantly less than modeled densities. Uniform downward flow of relatively fresh (low-density) fluids from the Magenta into the Culebra was considered in this area.

Assuming a brine density of 1.19 $g/cm^3$ for the Rustler/Salado contact zone and/or unnamed lower member of the Rustler in the region near P-17, Haug et al. (1987) estimate that a vertical flux of $10^{-12}$ $m^3/m^2s$ would be sufficient to result in a calculated brine density within the Culebra of 1.06 $g/cm^3$, the measured value. Given the approximate vertical gradient of 0.18 m/m at this location, based on head relations shown in Mercer (1983), this flux would require a vertical hydraulic conductivity of 5.7 x $10^{-12}$ m/s in the unnamed member. This is within the range thought reasonable (Haug et al., 1987), but slightly higher than recently measured adjacent to the WIPP waste-handling shaft (Section 3.3.1.2). Thus, a very small upward flux into the Culebra in the vicinity of P-17 appears to be largely consistent with known data, and improves agreement between measured and calculated brine densities in the area. However, it is not feasible to measure the small flux in a reasonable time in the field.

In considering fluid flow from the Magenta dolomite downward into the Culebra over the western portion of the modeled area, Haug et al. (1987) assumed a brine density of 1.00 $g/cm^3$ for the Magenta. Addition of a small but constant vertical flux of 5 x $10^{-12}$ $m^3/m^2s$ over the western portion of the model led to two qualitatively different responses:

1. In areas of low Culebra transmissivity, the resulting freshwater-equivalent heads were increased significantly, causing unacceptable disagreement between calculated and observed heads. In these areas, however, the assumed flux did significantly decrease the calculated brine densities within the Culebra.

2. In areas of high Culebra transmissivity, addition of the vertical flux did not significantly harm the agreement between calculated and

measured freshwater heads, nor did it significantly improve the agreement between measured and calculated brine densities within the Culebra.

Vertical flux from the Magenta downward into the Culebra dolomite over the western portion of the modeled area is consistent with known head and fluid-density relationships in some areas (Section 4.1.1.2). However, the flux, if real, must be laterally variable rather than constant, and the vertical conductivity of the Tamarisk claystone and anhydrites between the Magenta and Culebra may simply be too low at and near the site. The modeling results of Haug et al. (1987) suggest that vertical flow rates must be higher in regions in which the Culebra is more transmissive, and lower in regions where it is less transmissive. This amount of coupling of Culebra transmissivity with that of the overlying Tamarisk and Magenta members has not been identified in the regional variations in transmissivities of the different members of the Rustler at and near the WIPP site. For example, the transmissivity of the Tamarisk claystone, between the Magenta and Culebra, is too low for measurement at and near the site; the transmissivity of the Tamarisk anhydrites may be even lower. Given enough modeling time and effort, it appears that excellent agreement between measured and calculated brine densities within the Culebra dolomite could be obtained by calibration against both transmissivity distribution in the Magenta, Tamarisk, and Culebra and vertical flux, assuming steady-state boundary conditions. However, this agreement would not in any way be unique, and might not be consistent with the inability to measure properties within the Tamarisk. This is not to say that vertical flow is not occurring within the Rustler Formation (see Sections 4.1.1 and 4.4), simply that data are not adequate to model it precisely. The extremely low transmissivity of the Tamarisk claystone and anhydrites, relatively high transmissivity of the Culebra, and geochemical relationships within the Rustler (Section 4.4) suggest that transient confined flow within the Culebra dominates Rustler hydrology at and near the WIPP site.

In summary, model calibration to the Culebra pre-shaft head distribution by Haug et al. (1987) largely met with success, but also indicated uncertainties in the understanding of Culebra and Rustler hydrology. Calibration to the freshwater head distribution was successful to within one meter of measured values. Assuming steady-state confined flow, however, the resulting Culebra transmissivity distribution was not successful in simulating the measured brine-density distribution. In the eastern portion of the model, the required adjustment in transmissivity was minor. Over the western portion of the model, the results of Haug et al. (1987) indicated that: 1) the April 1986 understanding of brine densities may be qualitatively incorrect; 2) there may be regional-scale vertical flow within the Rustler Formation; and/or 3) the hydrologic setting of the Rustler Formation may be transient on the time scale required for groundwater flow across the modeled area.

The next step in model calibration by Haug et al. (1987) was simulation of transient stresses within the modeled area, assuming steady-state boundary conditions. Several transient activities were simulated, including: 1) sinking and grouting of the three existing WIPP shafts; 2) three pumping

tests and slug tests at H-2; 3) convergent-flow tracer testing at H-3; 4) a step-drawdown hydraulic test at H-3; and 5) the multipad interference test at H-3.

Responses to shaft sinking and grouting (both occurring before the H-3 multipad test) were well simulated using the density-calibrated transmissivity distribution estimated by calibration to the pre-shaft head distribution. From this, Haug et al. (1987) concluded that the transmissivity distribution in the region containing H-1, H-2, H-3, DOE-1, and H-11 was approximately correct.

Responses in the WIPP shafts and in holes WIPP-19, 21, and 22 during and after the H-3 multipad test could not be simulated closely unless additional leakage in the shafts was assumed to have occurred during the test. This conclusion, while coincidental, is supported by the fact that the hydraulic responses to sinking and initial grouting of the shafts were well simulated using the "steady-state" transmissivity distribution, while the later H-3 test itself was not.

The final calculated Culebra transmissivity distribution and fluid-flow velocities estimated on the basis of data available as of April 1986 and including adjustment for fluid-density effects in the eastern half of the model are shown in Figure 4.1.16. Four features are of note in this figure:

1. Fluid flow (presented as Darcy velocities) is extremely slow in the area H-12 - H-5 - WIPP-12. Calculated Darcy velocities in this area are $10^{-9}$ m/s or less.

2. Fluid flow in the southeastern portion of the model is strongly dominated by the high-transmissivity zone in the area H-11 - DOE-1 - P-17. Flow in this area is largely north-south, with Darcy velocities of approximately $10^{-8}$ m/s.

3. Flow in the northwest and western portions of the modeled area is rapid and largely north-south. Darcy velocities in this area range approximately from $5 \times 10^{-9}$ to $1 \times 10^{-8}$ m/s.

4. The region near the center of the WIPP site (WIPP-12 - P-15 - P-17) has relatively low Darcy velocities, approximately $1 \times 10^{-9}$ to $3 \times 10^{-9}$ m/s. The high-transmissivity zone to the southeast forces fluid flow in the region between H-4 and the center of the site to be northwest-southeast, in effect connecting the two high-transmissivity zones southeast and northwest of the site center. The control for this flow at the time of the H-3 multipad test was limited, since hole H-14 did not exist at that time.

As discussed in Section 4.1.2, interference testing at the H-3 and H-11 hydropads indicates the strong local influence of fracturing on hydraulic response. Haug et al. (1987) investigate whether or not a dual-porosity formalism is required to model regional-scale responses within the Culebra dolomite by examining times required for pressure equilibration between matrix blocks and fractures.

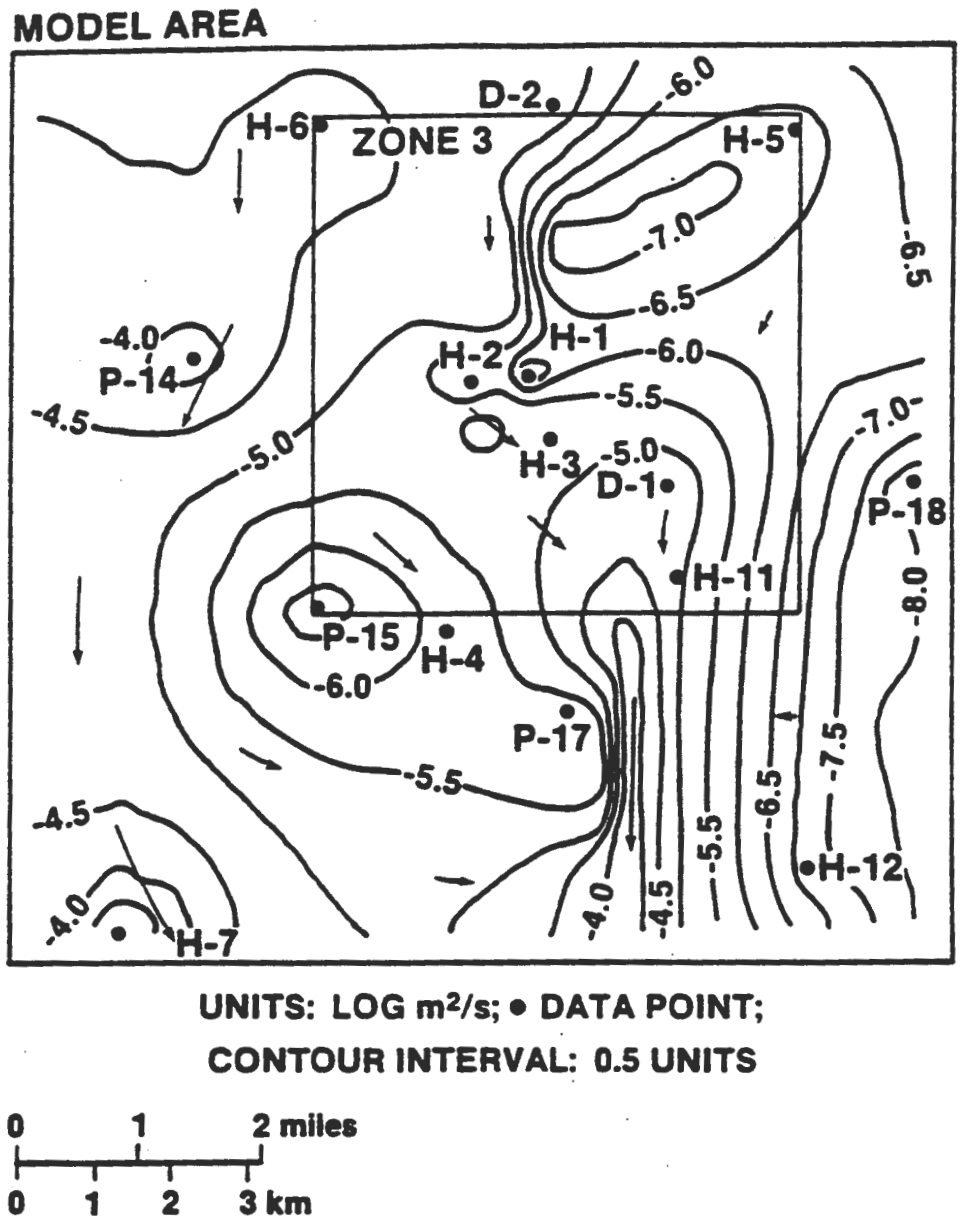


Figure 4.1.16: Final calculated Culebra transmissivities and flow directions, based on data available as of April 1986. Slightly modified from Figure 4.11 of Haug et al. (1987).

The time required for pressures in the fracture and matrix in a fractured medium to equilibrate to within 1% is proportional to the square of matrix block size and linearly proportional to the fluid diffusivity within the matrix. For a range of Culebra matrix block sizes (fracture spacings) between 1 and 8 m and a representative range of matrix compressibilities, matrix porosities, and matrix conductivities, Haug et al. (1987) calculate a maximum pressure-response time of 26 days. For the base-case properties interpreted from conservative-tracer testing at the H-3 pad (Section 4.2) the calculated pressure response time is only six hours. Based on these preliminary calculations, Haug et al. (1987) conclude that a dual-porosity formalism is not needed in modeling the regional-scale hydraulic responses within the Culebra dolomite at and near the WIPP site. Haug et al. (1987) modeled the transient hydraulic responses at the H-3 hydropad to both shaft sinking and sealing and the H-3 multipad interference test using both dual-porosity and porous-medium formalisms to examine this conclusion further. Consistent with their conclusion that use of the dual-porosity formalism is not needed at a regional scale, the maximum difference between the transient freshwater heads calculated using the two approaches is 0.02 m.

However, the validity of this conclusion is somewhat limited by the range of fracture spacings considered. The correlation between fracturing and transmissivity within the Culebra discussed in Section 4.1.1 indicates that fracturing is significant in areas of transmissivity greater than approximately $10^{-6}$ $m^2/s$. The approximate fracture spacing at the H-3 pad, with a transmissivity of $2 \times 10^{-6}$ $m^2/s$, is 0.25 to 1 m (Section 4.2). Zones of higher transmissivity presumably have smaller effective block sizes. The preliminary calculations of Haug et al. (1987) indicate that it is in zones of otherwise low transmissivity, in which fracturing is not evident in single-hole testing, and in which fracture spacings may significantly exceed the thickness of the Culebra, that hydraulic behavior on something approaching the regional scale might be controlled by fracturing. However, there is no evidence of any discrete fracture structures within low-transmissivity portions of the Culebra dolomite at or near the WIPP site.

In summary, fielding and interpretation of the H-3 multipad interference greatly increased the understanding of the hydrology of the Culebra Dolomite Member of the Rustler Formation. It emphasized the role of fracturing and lack of hydraulic anisotropy within the H-3 hydropad. The analytical interpretation by Beauheim (1987a) indicated the presence of a high-transmissivity region in the vicinity of H-11 and DOE-1, suggested strong directional dependence of responses to the test, and suggested that transmissivities between H-3 and H-4 were probably less than $10^{-6}$ $m^2/s$, an interpretation later confirmed by drilling and testing of hole H-14. The interpretation of Tomasko and Jensen (1987) indicated that regional-scale flow in the southeastern portion of the WIPP site was probably controlled by a linear high-transmissivity zone. Numerical modeling of the site area by Haug et al. (1987) yielded a more complete estimate of the lateral distribution of Culebra transmissivities, qualitatively consistent with the interpretations of Beauheim (1987a) and Tomasko and Jensen (1987). A high-transmissivity region in the vicinity of H-11 and DOE-1 was interpreted to be present, in addition to a largely separate high-transmissivity zone west and northwest of the site center. Large areas northeast, east, and

southwest of the site center appeared to have low transmissivity. The interpretation of Haug et al. (1987) indicated both that fluid flow on the WIPP site proper was largely controlled by the high-transmissivity zone containing holes H-11 and DOE-1, and that the effects of this zone included northwest to southeast flow across the area including H-4 and the site center itself. Consideration of discrete fractures or inclusion of dual-porosity formalism appears not to be required to model the regional-scale hydrologic behavior of the Culebra dolomite at and near the WIPP site.

Limitations to interpretation of the H-3 multipad test strongly influenced hydrologic field activities in 1986 and 1987. On a regional scale, the information gained through the H-3 test supported fielding and interpretation of a test centered at WIPP-13, which is discussed in the next section. In preparation for this test, updated and more-reliable data on the Culebra were collected at DOE-2, and a series of WIPP holes (13, 18, 19, 21, and 22). The paucity of reliable data in the southern half of Zone 3 led to the drilling and testing of H-14 and H-15, as well as to reentry and testing of the Culebra in P-17, H-4c, P-14, P-15, Cabin Baby-1, and ERDA-9. The scarcity of head-potential and hydraulic-property data from members of the Rustler other than the Culebra led to testing of all members in holes H-14, and H-16. H-16 itself was sited primarily to address the problem of linkage between all five members of the Rustler Formation and the WIPP air-intake shaft.

4.1.3.2 <u>The WIPP-13 Multipad Interference Test and the Regional Culebra Model of LaVenue et al. (1988)</u>--The second regional-scale or multipad interference test of the Culebra dolomite was centered at hole WIPP-13 (Figures 1.2 and 4.1.17). The pumping phase of the WIPP-13 test lasted from January 12, 1987, to February 17, 1987. Water levels were monitored continuously in 17 surrounding wells, at distances ranging from 1280 to 6248 m. Analytical interpretation of the WIPP-13 multipad test is discussed by Beauheim (1987c). Numerical simulation of Culebra transmissivities and pre-shaft heads in an area including that examined in the WIPP-13 test is the primary focus of LaVenue et al. (1988). This effort includes evaluation of long-term transient hydrologic data at and near the WIPP site. Detailed modeling of transient effects of the WIPP-13 multipad test will be combined during 1988 with calibration of the transient effects of a planned multipad interference test at the H-11 hydropad and emplacement of the WIPP air-intake shaft.

The effects of dual-porosity behavior were quite strong in WIPP-13 during the pumping phase of the WIPP-13 test (Figure 4.1.18). The Culebra in WIPP-13 has an estimated transmissivity of $7.4 \times 10^{-5}$ $m^2/s$ (Beauheim, 1987c). The Culebra in and near WIPP-13 is best thought of as a double-porosity medium with unrestricted interporosity flow (Beauheim, 1987c).

The analytical interpretation by Beauheim (1987c) indicates that WIPP-13 lies within a relatively homogeneous fractured region, which includes WIPP-13 and DOE-2, as well as the H-6 hydropad (both H-6a and H-6b were monitored during the WIPP-13 test). DOE-2, at a distance of 1475 m from WIPP-13, responded within one hour to the beginning of pumping, while H-6b, at a distance of 2188 m, responded within 8 hours (Table 4.7). The

## LOCATIONS OF THE WIPP SITE AND OBSERVATION WELLS

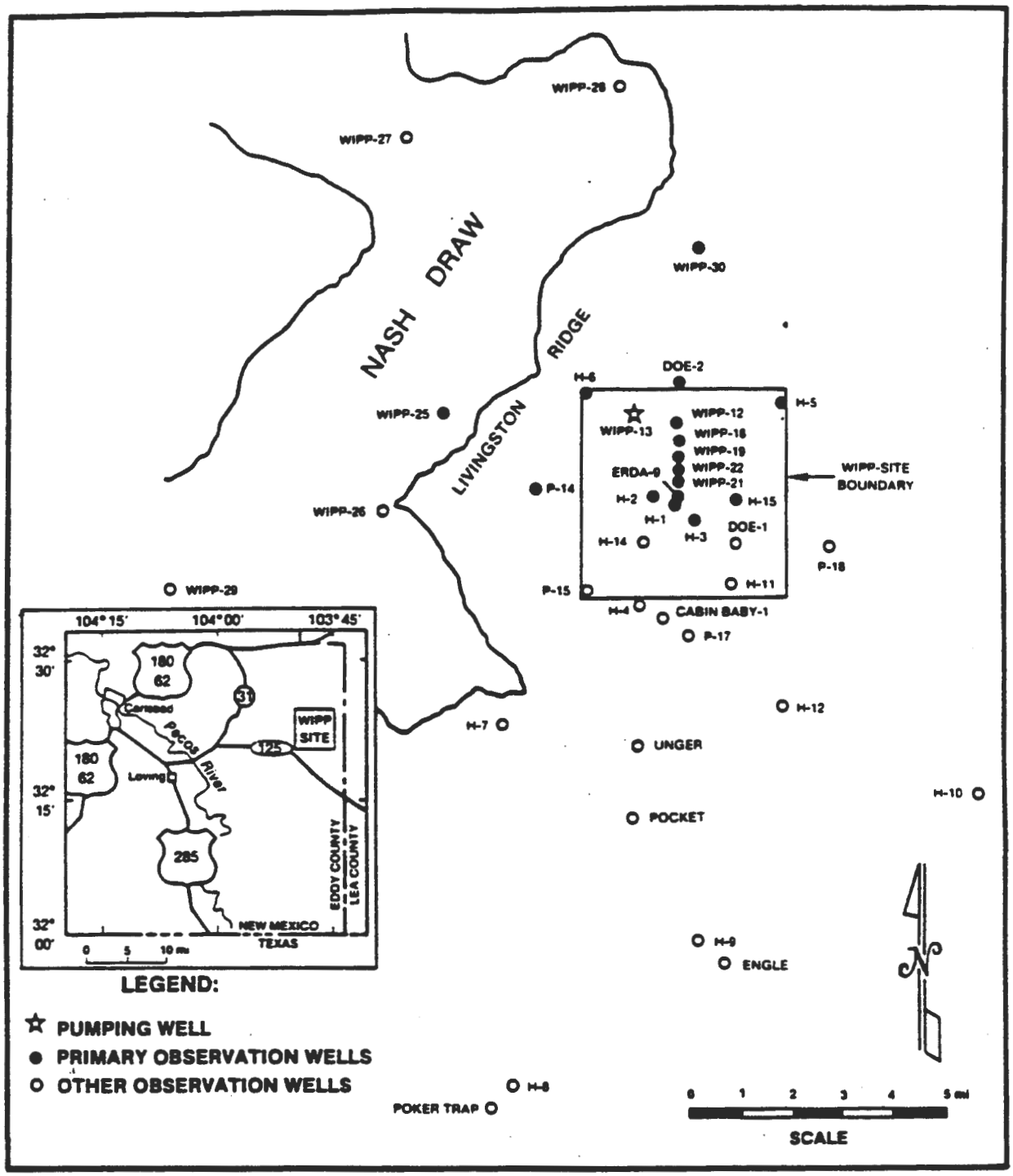


Figure 4.1.17: Pumped and observation wells for the WIPP-13 multipad interference test. Figure 1-1 of Beauheim (1987c).

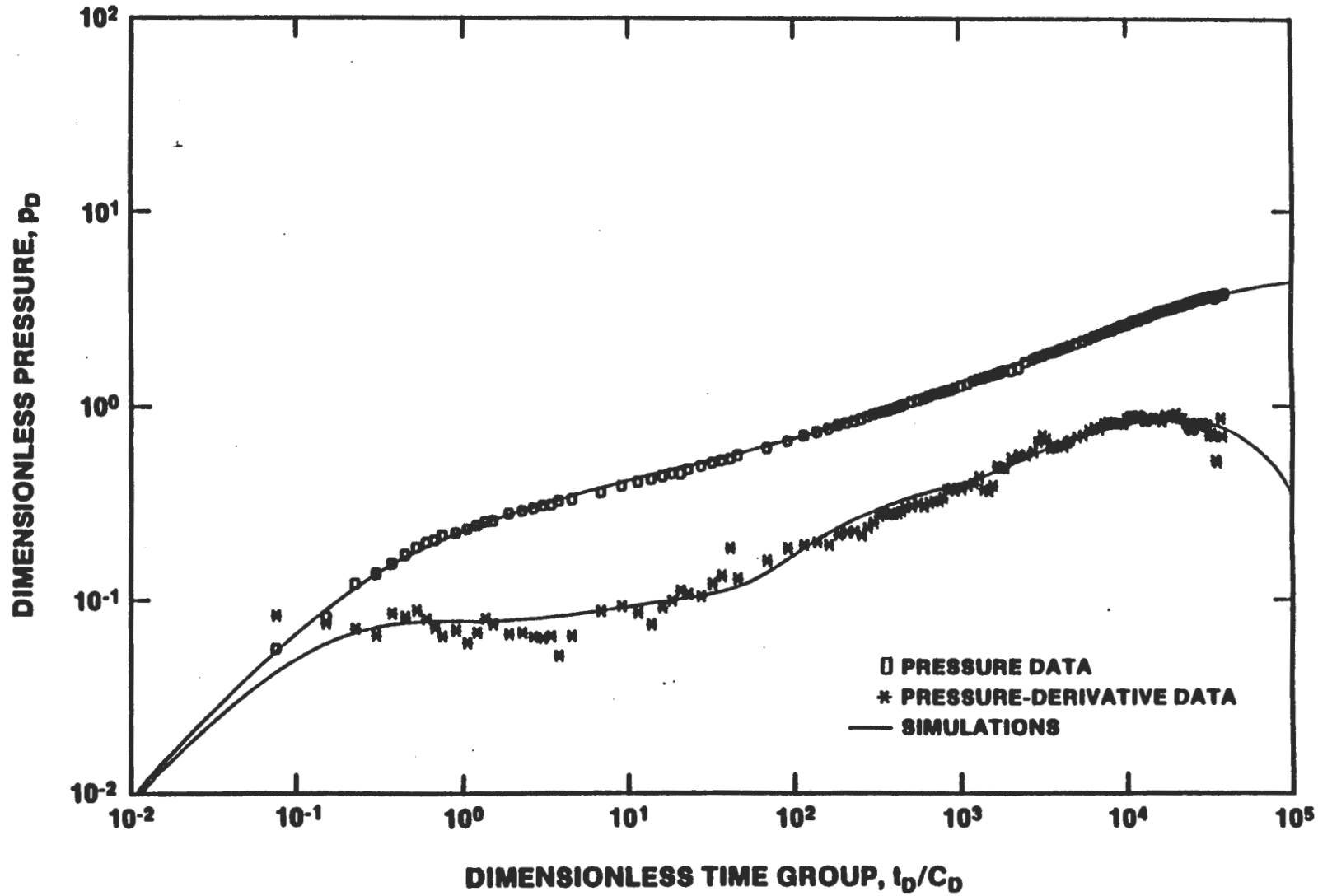


Figure 4.1.18: Measured and simulated hydrologic response of WIPP-13 during the pumping phase of the WIPP-13 multipad interference test. Slightly simplified from Figure 6-1 of Beauheim (1987c).

Table 4.7: Summary of analytical interpretation of results of the WIPP-13 multipad interference test. Slightly modified from data conatined in Tables 3-1, 5-1, and 6-1 of Beauheim (1987c).

| Well | Distance(m)(1) | Direction | First (2) Drawdown (hrs) | Delay in Max. Drawdown (hr) | Maximum Drawdown (Psi) | T($m^2$/s)(3) | S | Water-Level Modification (m/day) |
|---|---|---|---|---|---|---|---|---|
| WIPP-13 | 0 | - | 0 | 0 | | $7.4 \times 10^{-5}$ | - | - |
| DOE-2 | 1475 | N45E | 1 | 1 | 17.3 | $6.1 \times 10^{-5}$ | $5.1 \times 10^{-6}$ | - |
| H-6a | 2192 | N20W | 8 | 5 | 7.7 | $7.6 \times 10^{-5}$ | $8.2 \times 10^{-6}$ | - |
| H-6b | 2189 | N20W | 8 | 5 | 7.9 | $7.4 \times 10^{-5}$ | $7.9 \times 10^{-6}$ | - |
| WIPP-30 | 5587 | N12E | 61 | 136 | 4.9 | $3.0 \times 10^{-5}$ | $5.6 \times 10^{-6}$ | $5.3 \times 10^{-3}$ |
| WIPP-12 | 1283 | S55E | 74 | 186 | 11.9 | $8.5 \times 10^{-6}$ | $3.6 \times 10^{-5}$ | $4.5 \times 10^{-3}$ |
| WIPP-18 | 1521 | S45E | 74 | 86 | 9.3 | $2.5 \times 10^{-5}$ | $4.0 \times 10^{-5}$ | $3.6 \times 10^{-3}$ |
| WIPP-19 | 1823 | S37E | 102 | 186 | 7.2 | $2.6 \times 10^{-5}$ | $4.0 \times 10^{-5}$ | $7.6 \times 10^{-3}$ |
| WIPP-21 | 2216 | S29E | 133 | 396 | 3.6 | $2.4 \times 10^{-5}$ | $5.3 \times 10^{-5}$ | $1.7 \times 10^{-2}$ |
| WIPP-22 | 1933 | S34E | 102 | 286 | 5.7 | $2.0 \times 10^{-5}$ | $4.7 \times 10^{-5}$ | $8.2 \times 10^{-3}$ |
| H-1 | 2676 | S16E | 600 | 2086(?) | 1.1 | $2.2 \times 10^{-5}$ | $1.3 \times 10^{-4}$ | $1.4 \times 10^{-2}$ |
| H-2b2 | 2597 | S0W | 445 | 986 | 1.4 | $1.7 \times 10^{-5}$ | $7.3 \times 10^{-5}$ | $6.0 \times 10^{-3}$ |
| ERDA-9 | 2518 | S24E | 550 | 396 | 2.0 | $2.4 \times 10^{-5}$ | $5.4 \times 10^{-5}$ | $1.6 \times 10^{-2}$ |
| Exhaust shaft | 2414 | S26E | 400 | 336 | 3 | $3.0 \times 10^{-5}$ | $5.5 \times 10^{-5}$ | $2.9 \times 10^{-2}$ |
| P-14 | 4228 | S58W | 71 | 56 | 0.8 | $2.8 \times 10^{-4}$ | $5.2 \times 10^{-5}$ | - |
| WIPP-25 | 6264 | S88W | 76 | 26 | 0.3 | $7.0 \times 10^{-4}$ | $6.4 \times 10^{-5}$ | - |

(1) Distance and direction from WIPP-13.
(2) Time relative to beginning and ending of pumping phase.
(3) Apparent and effective transmissivity (T) and storativity (S) assume homogenous properties between WIPP-13 and given well, as well as radial flow into WIPP-13.

apparent average transmissivities between WIPP-13 and holes DOE-2 and H-6b are 6.1 x $10^{-5}$ $m^2/s$ and 7.4 x $10^{-5}$ $m^2/s$, respectively. The rapid responses at DOE-2 and H-6b and the low apparent storativities between these holes and WIPP-13, 5.1 x $10^{-6}$ and 7.9 x $10^{-6}$, respectively, suggest that the hydraulic response in this region is strongly affected by fracturing (Beauheim, 1987c).

The boundaries of the zone containing WIPP-13, DOE-2, and H-6 are complex. To the north, the zone appears to extend nearly to hole WIPP-30 (Beauheim, 1987c). This interpretation is based largely on the fact that WIPP-30, with a reported transmissivity of only 3.2 x $10^{-7}$ $m^2/s$ (Beauheim, 1987b; Mercer, 1983) and at a distance of 5587 m from WIPP-13, responded within 61 hours to the beginning of pumping. In addition, the apparent average storativity between WIPP-13 and WIPP-30, 5.6 x $10^{-6}$, is similar to that calculated between WIPP-13 and both DOE-2 and H-6b. Analytical interpretation of the response of DOE-2 to pumping of WIPP-13 requires addition of a low-permeability boundary; i.e., the response at DOE-2 shows the effects of a low-permeability region nearby. A change from high to low Culebra transmissivities must occur somewhere between DOE-2 and WIPP-12, as well as between DOE-2 and H-5.

Results contained in Beauheim (1987b) indicate a Culebra transmissivity of approximately 1.0 x $10^{-7}$ $m^2/s$ in WIPP-12 (Table 4.2). The apparent average transmissivity between WIPP-13 and WIPP-12 is 8.5 x $10^{-6}$ $m^2/s$ (Beauheim, 1987c). WIPP-12, only 1283 m from WIPP-13, did not respond to pumping of WIPP-13 until 74 hours into the test. Thus, by analogy with arguments concerning the response of WIPP-30, the boundary between the high-transmissivity zone containing WIPP-13 and the low-transmissivity zone containing WIPP-12 must lie relatively close to WIPP-13.

South of WIPP-12, the boundary between high-transmissivity and low-transmissivity domains probably lies further away from WIPP-13. Holes WIPP-18, 19, 21, 22; H-1, 2; and ERDA-9 all have estimated Culebra transmissivities of 1.0 x $10^{-6}$ $m^2/s$ or less (Table 4.1). The apparent effective average transmissivities between WIPP-13 and these holes range from 1.7 x $10^{-5}$ to 2.6 x $10^{-5}$ $m^2/s$ (Table 4.7), while that between WIPP-13 and the WIPP exhaust shaft is 3.0 x $10^{-5}$ $m^2/s$. Times required for the first response to pumping of WIPP-13 range from 74 to 600 hours, including the exhaust shaft. The high-transmissivity zone containing WIPP-13 is consistently represented as a high-permeability boundary in interpretation of the response of these observation holes (Beauheim, 1987c). The apparent behavior between WIPP-13 and the WIPP exhaust shaft is consistent with that between WIPP-13 and nearby observation holes. Beauheim (1987c) notes that the responses in both ERDA-9 and the exhaust shaft appear to be complicated by activities within the shaft.

The relatively homogeneous zone containing WIPP-13, DOE-2, and H-6 appears to be bounded on the west by a zone of higher transmissivity extending into the main portion of Nash Draw (Beauheim, 1987c). Apparent transmissivities between WIPP-13 and holes P-14 and WIPP-25 are 2.8 x $10^{-4}$ and 7.0 x $10^{-4}$ $m^2/s$, respectively. Hole WIPP-25, at a distance of 6264 m from WIPP-13, was the most distant monitoring hole used in the test (Figure 4.1.17).

The presence of both higher-transmissivity and lower-transmissivity domains outside the WIPP-13 - DOE-2 - H-6 region is consistent with the fact the analytical interpretation of the hydrologic behavior at WIPP-13 required the addition of both low-permeability and high-permeability boundaries (Beauheim, 1987c). In addition, a linear-flow interpretation of the flow near WIPP-13 analogous to that completed for the H-3 multipad test by Tomasko and Jensen (1987) was not successful.

The numerical simulation of Culebra hydrology over a large area, including the region stressed in the WIPP-13 test, is discussed and summarized in LaVenue et al. (1988). The emphasis in LaVenue et al. (1988) is on simulation of the Culebra hydrology as it existed before construction of the WIPP shafts, i.e., prior to 1981. Detailed numerical interpretation of the transient hydrologic stresses imposed by the WIPP-13 multipad test, sinking of the WIPP air-intake shaft, and a combined multipad interference test and conservative-tracer test at the H-11 pad will be conducted in 1988.

As noted in Section 4.1.1, there has been a significant increase in the Culebra transmissivity, head, and fluid-density data base since April 1986. In addition, as evident in Figure 4.1.19, the area included in modeling described in LaVenue et al. (1988), 24 x 25 km, is significantly larger than that included in Haug et al. (1987) (see Figure 4.1.6). As a result, the total data base considered in LaVenue et al. (1988) is much larger than that considered only 1.5 years earlier. Culebra transmissivity data from 38 individual wells or hydropads are considered in the 1988 report, as opposed to 24 locations in the 1987 report (Table 4.1). Compilation of the data base used by LaVenue et al. (1988) was significantly more complex for the data base used by Haug et al. (1987), both because of the increased number of holes and because of the increased awareness and concern about transient phenomena in Rustler hydrology. For example, development of the baseline water-level data required consideration of long-term transients, even in holes not directly affected by hydraulic testing at and near the WIPP site. In addition, some well locations were resurveyed (LaVenue et al., 1988); most Culebra fluid densities were revised as a result of recent sampling (Uhland et al., 1987), and were evaluated by detailed pressure-density surveys (Crawley, 1987).

The initial kriged Culebra transmissivities of LaVenue et al. (1988) are shown in Figure 4.1.19, based on data available as of November 1987. The general pattern is different from that indicated in Haug et al. (1987) (Figure 4.1.9). The increase in the available data base results in the initial kriged distribution in Figure 4.1.19 varying smoothly across much of the site area. The kriged transmissivities tend to be higher towards the west and lower towards the east, with an isolated zone of higher transmissivities at H-11 and DOE-1. In Figure 4.1.9, with the exception of the hole pairs H-1 - H-2 and H-11 - DOE-1, each data point tends to define a separate transmissivity zone.

The effects of the increased number of measurements on the Culebra transmissivity data base are demonstrated more clearly by comparison of Figure 4.1.10 with Figures 4.1.20 and 4.1.21. Kriging of the transmissivity data base available as of April 1986 (Figure 4.1.10) indicated that regions of

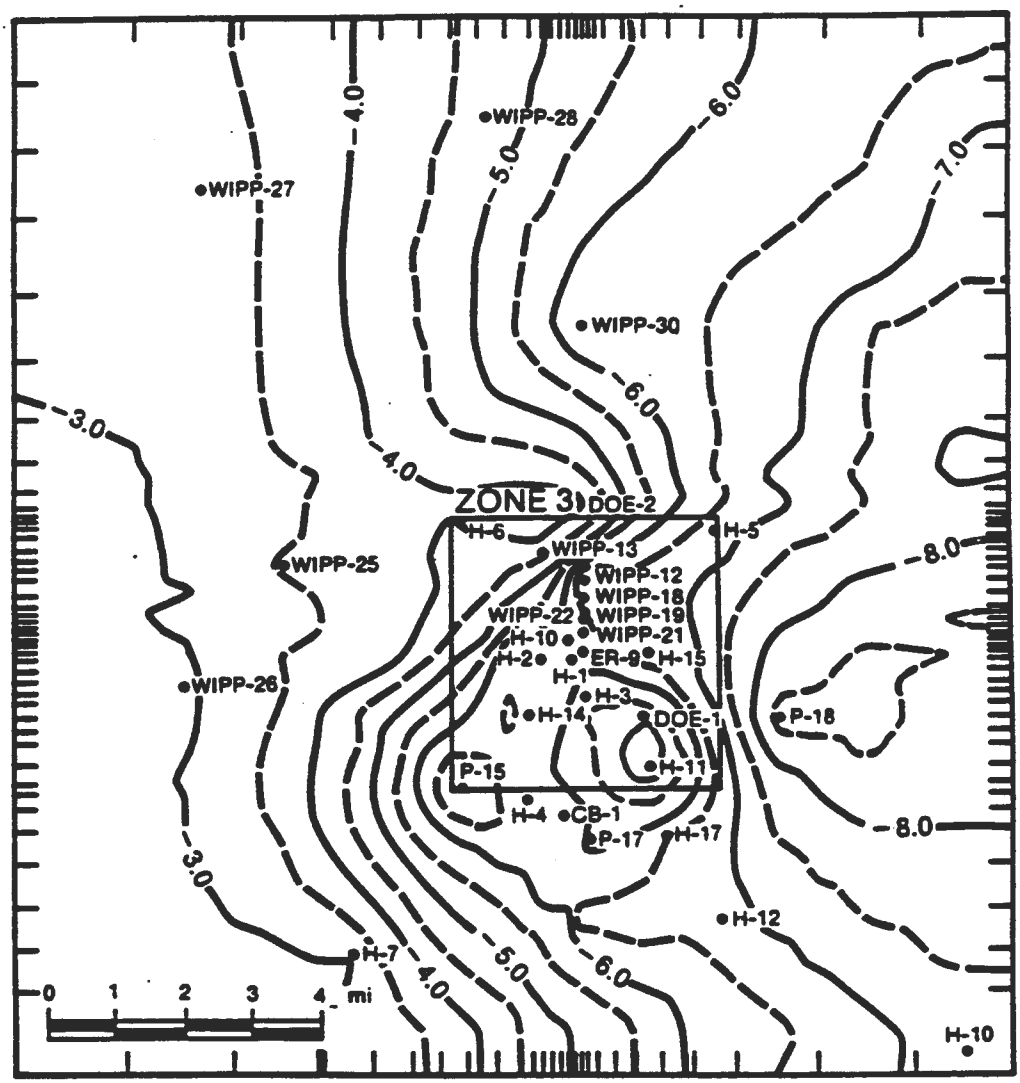


Figure 4.1.19: Initial kriged Culebra transmissivities, based on data available as of November, 1987. Values kriged with code AKRIP. Figure 3.12A of LaVenue et al. (1988).

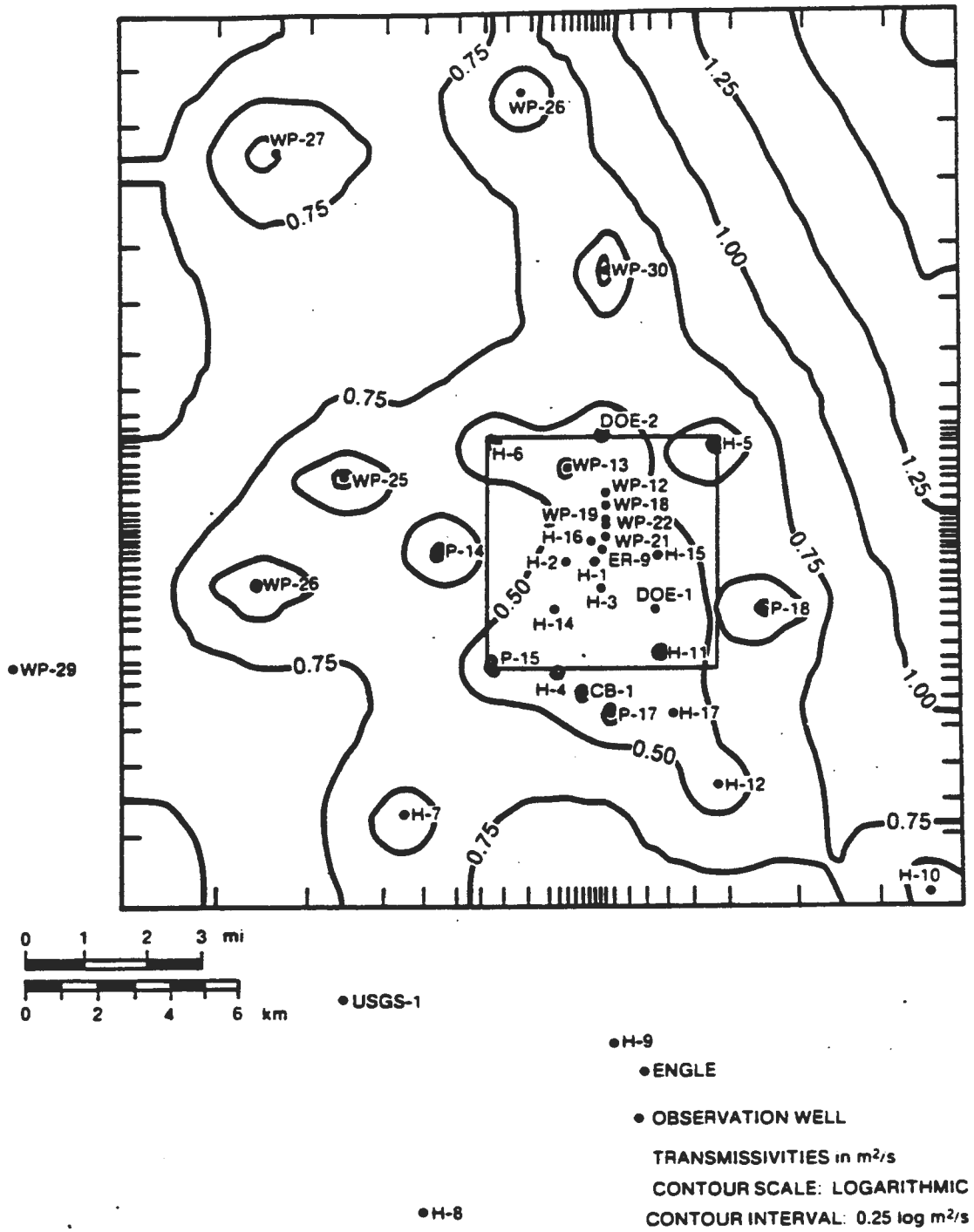


Figure 4.1.20: Estimation error in initial kriged Culebra transmissivities (one standard deviation), based on data available as of November 1987, assuming no uncertainty in individual measurements. Values kriged using code AKRIP. Figure 3.12B of LaVenue et al. (1988).

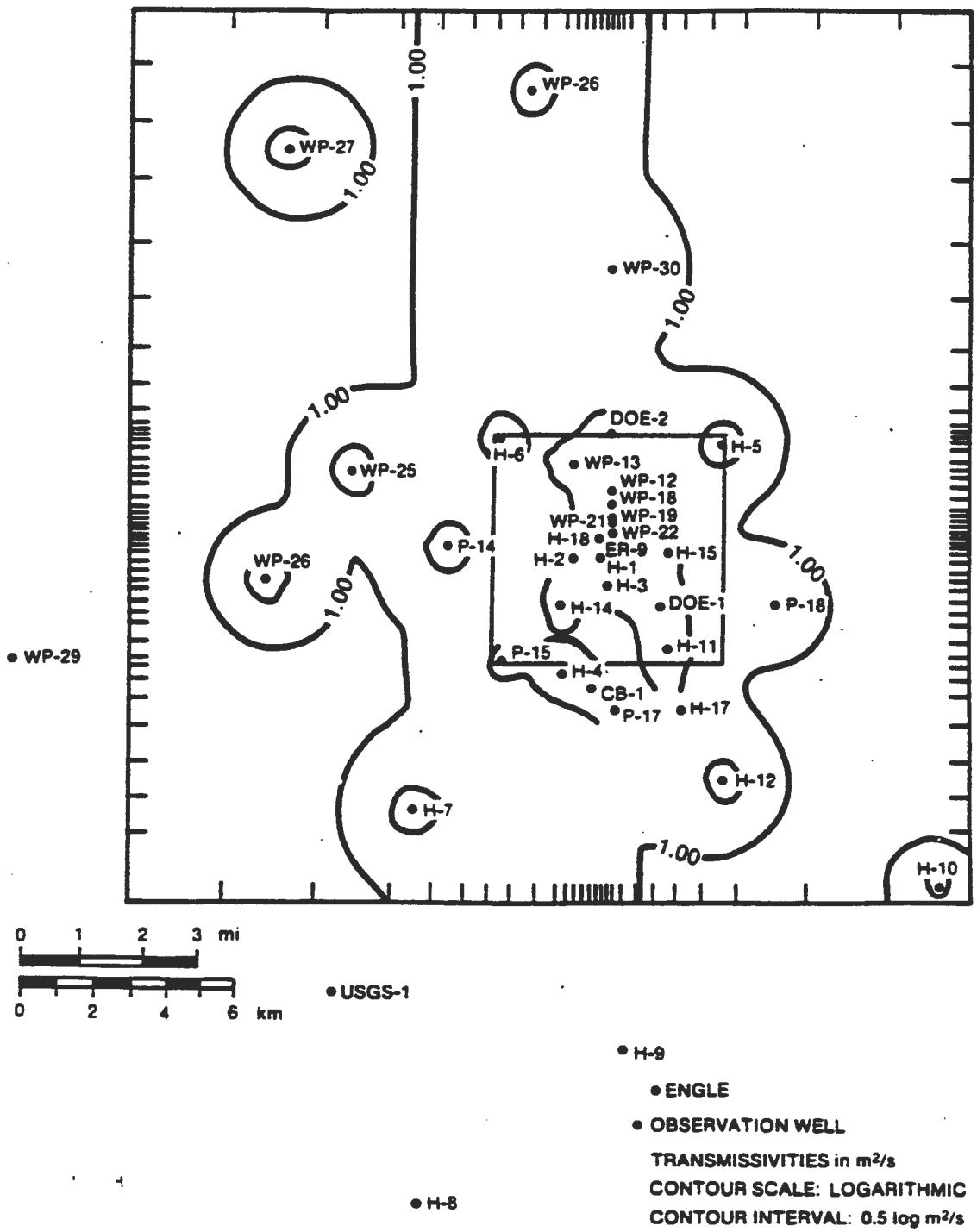


Figure 4.1.21: Estimation error in initial kriged Culebra transmissivities (one standard deviation), including estimated uncertainty in individual measurements. Values kriged using code K603. Figure 3.11B of LaVenue et al. (1988).

one order of magnitude uncertainty (defined at one standard deviation) did not overlap, except in very limited areas. Because of the limited data base available at that time, it was not possible for Haug et al. (1987) to consider either an underlying regional trend in the data or uncertainty in the measured data.

LaVenue et al. (1988) apply two kriging techniques to the Culebra transmissivity data in order to consider both the regional west-to-east decrease in transmissivities (Figure 4.1.19) and uncertainties in the measured data. Kriging of the enlarged data base using the AKRIP code, which fits a polynomial surface to the regional trend, but does not consider uncertainty in the measured data (LaVenue et al., 1988), indicates that the uncertainty in Culebra transmissivities over a large area, including most of Zone 3, should be less than 0.5 log unit at one standard deviation and less than one order of magnitude (1.0 log unit) at two standard deviations (Figure 4.1.20). Within the smaller area including both the center of the WIPP site and the locations the WIPP shafts, the uncertainty at two standard deviations is 0.5 log units or less; i.e., Culebra transmissivities should be estimated to within a factor of approximately three in this region, if it is assumed that field measurements are precise.

Results analogous to those in Figure 4.1.20, calculated by LaVenue et al. (1988) using the K603 code, which applies a linear trend surface to regional data, but allows consideration of uncertainty in measured data, are shown in Figure 4.1.21. LaVenue et al. (1988) estimate the uncertainty in measurements of Culebra transmissivities to be 0.25 log unit when transmissivity is estimated from pumping tests and 0.5 log units when estimated from other tests. Inclusion of these estimated uncertainties in individual measurements, combined with a simplified regional trend surface, suggests (Figure 4.1.21) an estimation error (one standard deviation) of 0.5 log unit or less within most of Zone 3. These results indicate that the uncertainty in Culebra transmissivities at two standard deviations within much of Zone 3, i.e., in a region extending from DOE-2 in the north to beyond H-11 in the south, is less than an order of magnitude, even including the estimated uncertainties in field measurements.

Such statistical approaches must not be overinterpreted, because they include no direct consideration of geologic processes. However, comparison of Figures 4.1.20 and 4.1.21 with Figure 4.1.10 provides a direct impression of the qualitative increase in both the size and reliability of the Culebra data base since April 1986.

The present distribution of measured Culebra fluid densities (LaVenue et al., 1988) is shown in Figure 4.1.22. Although the overall pattern is similar to that estimated on the basis of data available in April 1986 (Figure 4.1.13), with a general west-to-east increase in density, there are two significant differences. The density distribution in the west half of Zone 3 in Figure 4.1.13 is strongly non-linear, due to relatively high densities at H-6 and/or DOE-2. The variation in fluid densities in the region H-1 - DOE-2 - H-6 - P-14, based on data available as of November 1987 (Figure 4.1.22), is less irregular, and the regional trend is more consistent with the general west-to-east increase in density. Fluid

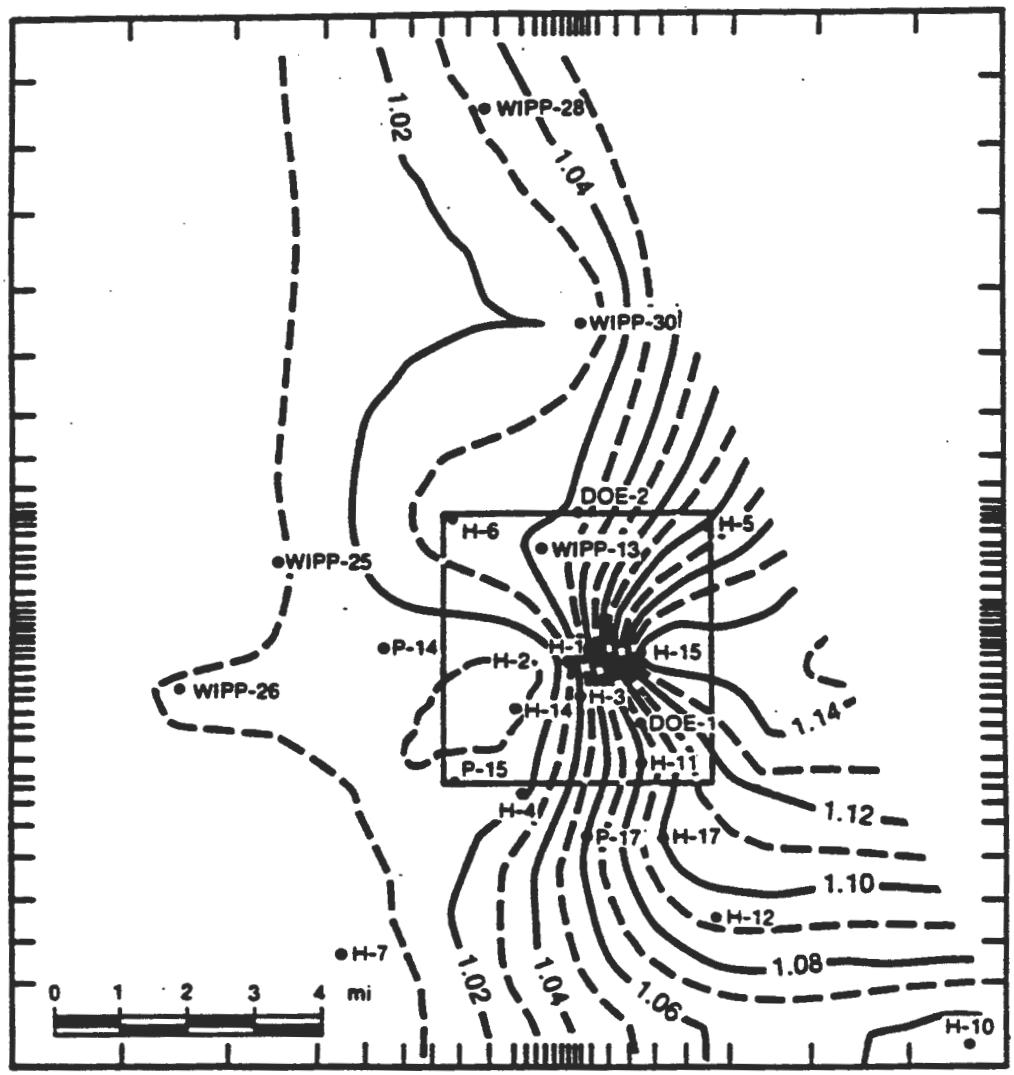


Figure 4.1.22: Measured density distribution of Culebra fluids, based on information available as of November 1987. Figure 3.15 of LaVenue et al. (1988).

densities in the region H-14 - H-2 - P-14 still appear to be anomalously low. The brine density distribution in the eastern part of Zone 3 (Figure 4.1.22) is also somewhat different than in Figure 4.1.13. In Figure 4.1.13, a general north-south trend of constant-density lines extends largely across the WIPP site west of holes DOE-1 and H-11. The distribution is more complex east of these holes. In Figure 4.1.22, the estimated brine density of approximately 1.14 g/cm$^3$ at hole H-15 causes significant curvature in the density distribution in the eastern portion of Zone 3. Nonetheless, the overall pattern of the distribution of Culebra brine densities based on data available as of November 1987 is simpler than previously estimated.

The present understanding of the distribution of pre-shaft freshwater-equivalent heads within the Culebra dolomite is shown in Figure 4.1.23. The general pattern is similar to that estimated by Haug et al. (1987), with a north-south head gradient of approximately $10^{-3}$ m/m across the area of the WIPP site. Gradients within the Culebra both south and north of the site are lower, approximately $10^{-4}$ m/m.

There is, however, one significant difference between the head distributions shown in Figures 4.1.23 and 4.1.11. Head contours form a sharp embayment in the southeastern portion of Zone 3 in Figure 4.1.11, extending at least as far north as the east-center of the site. Interpretation of water-level and fluid-density data available to November 1987 indicates (Figure 4.1.23) that there is little evidence of an embayment in Culebra freshwater-equivalent heads within WIPP Zone 3, except for the 913-m contour in the extreme southern part of the zone. Within the modeled area, head contours up to 919 m elevation do define a broad embayment south and east of the WIPP site. Expansion and improvement of the data base for calculation of Culebra freshwater-equivalent heads during 1986 and 1987 has resulted in significant smoothing of the estimated head distribution, especially within Zone 3.

In calibration efforts by Haug et al. (1987), it was assumed that Culebra fluid pressures and fluid densities were at steady state before construction of the WIPP shafts. As discussed in Section 4.1.3.1, assumption of steady state is adequate for simulation of pre-shaft Culebra heads or fluid pressures. The results in Haug et al. (1987), however, indicated problems with the assumption of steady-state confined flow in simulation of Culebra brine densities. The calibration approach taken by LaVenue et al. (1988) differed from that taken earlier. LaVenue et al. (1988) assumed that the fluid-density distribution remains fixed on the time scale required for pressure equilibration, and no calibration against the brine-density distribution was attempted. The calculations do take account of the variable fluid density at each point within the Culebra; they assume that effects of variable brine density on the modern flow directions can be estimated reliably fixing the modern fluid-density distribution in place. The results of calibration of Culebra transmissivities against the freshwater-equivalent head distribution shown in Figure 4.1.23, assuming that the fluid-density distribution shown in Figure 4.1.22 remains fixed (LaVenue et al., 1988), are shown in Figure 4.1.24.

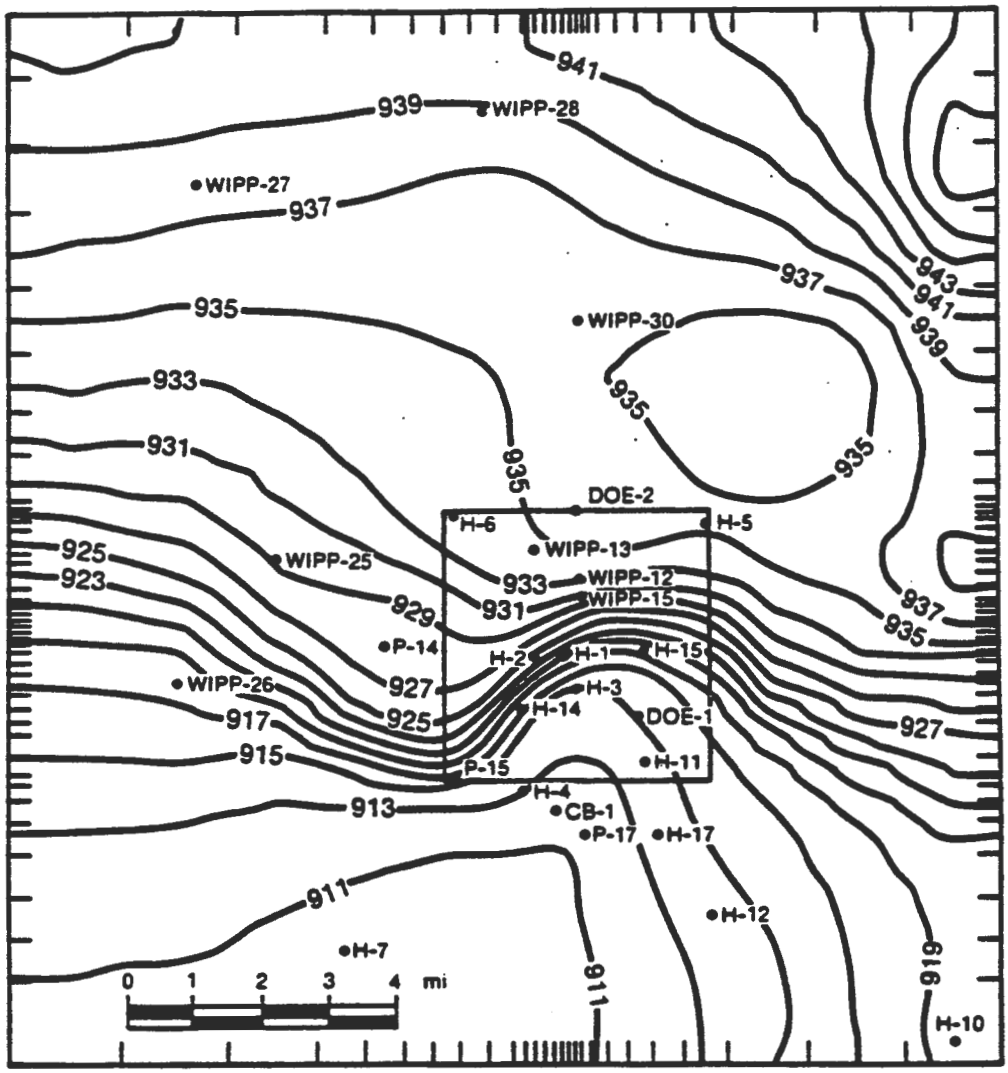


Figure 4.1.23: Estimate of pre-shaft, freshwater-equivalent heads in the Culebra dolomite, based on data available as of November 1987. Figure 3.14 of LaVenue et al. (1988).

The overall distribution of calibrated transmissivities (Figure 4.1.24) is not greatly different from the initial kriged distribution (Figure 4.1.19). The general trend of decreasing transmissivities from west to east is preserved. During calibration, transmissivities west of WIPP-30 and WIPP-28 were increased. Transmissivities in the area containing H-6, P-14, and WIPP-25 were generally decreased slightly, while those in the southern part of Nash Draw were increased. The low-transmissivity domain in WIPP Zone 3 ($T < 10^{-6}$ $m^2/s$) is expanded in the more recent interpretation (Figure 4.1.24). This region, including the center of the WIPP site, is now expected to be continuous from H-5 in the northeast to P-15, H-4, and Cabin Baby-1 to the southwest.

Calibration in the region between holes H-17, H-11, P-17, and extending to the south, required significant adjustment to the kriged distribution. Transmissivities in this region were increased from kriged values, similar to changes required during calibration by Haug et al. (1987). In order to simulate the low heads at H-11 and DOE-1 and the sharp head embayment in the southern part of Zone 3 expected on the basis of April 1986 data (Figure 4.1.11), Haug et al. (1987) included a narrow high-transmissivity zone east of P-17 (Figure 4.1.16). During calibration by Haug et al., a maximum transmissivity of approximately $3 \times 10^{-4}$ $m^2/s$ was assigned in this zone. The calibrated transmissivity distribution of LaVenue et al. (1988) in this region does not include as marked a high-transmissivity structure (Figure 4.1.24). Relatively high transmissivities are still required in the area, because of both the relatively low heads at H-11 and DOE-1 and the low gradients south of the WIPP site. However, the maximum transmissivity assigned at the pilot points shown in Figure 4.1.24 is approximately $5 \times 10^{-5}$ $m^2/s$, only a factor of two greater than the effective transmissivity of $2.8 \times 10^{-5}$ $m^2/s$ calculated at the H-11 pad (Table 4.1).

LaVenue et al. (1988) investigate the need for the high-transmissivity zone by making calibration runs in which the increase in transmissivities south of H-11 was not incorporated, as well as runs in which the assigned heads along the southwestern part of the model were increased slightly. In all cases, the fit between calculated and estimated heads was worse than when increased transmissivities south of H-11 were included. Thus, a region of relatively high transmissivities is still expected to be present south of H-11. Transmissivities within this zone may be approximately twice as great as those measured at H-11. Both the lateral extent of the zone and the contrast between the high-transmissivity zone and surrounding regions are expected to be smaller than estimated in Haug et al. (1987). The zone is still expected to connect with the high-transmissivity region further to the south.

The changes in estimated transmissivities within and near the WIPP site are a direct result of the increase in the Culebra data base since April 1986 (Table 4.1). For example, hole H-14 was drilled and tested in 1986, specifically to examine transmissivities southwest of the site center (Section 4.1.1). Holes P-15, H-4, H-15, H-16, P-17, Cabin Baby-1, ERDA-9, and WIPP-12 have all been tested or retested since April 1986 (Table 4.2). Hole H-17 was drilled and tested specifically to evaluate the high-transmissivity zone east of P-17. Transmissivities at both DOE-1 and H-11 have been interpreted in detail since 1986, as discussed in Section 4.1.1.

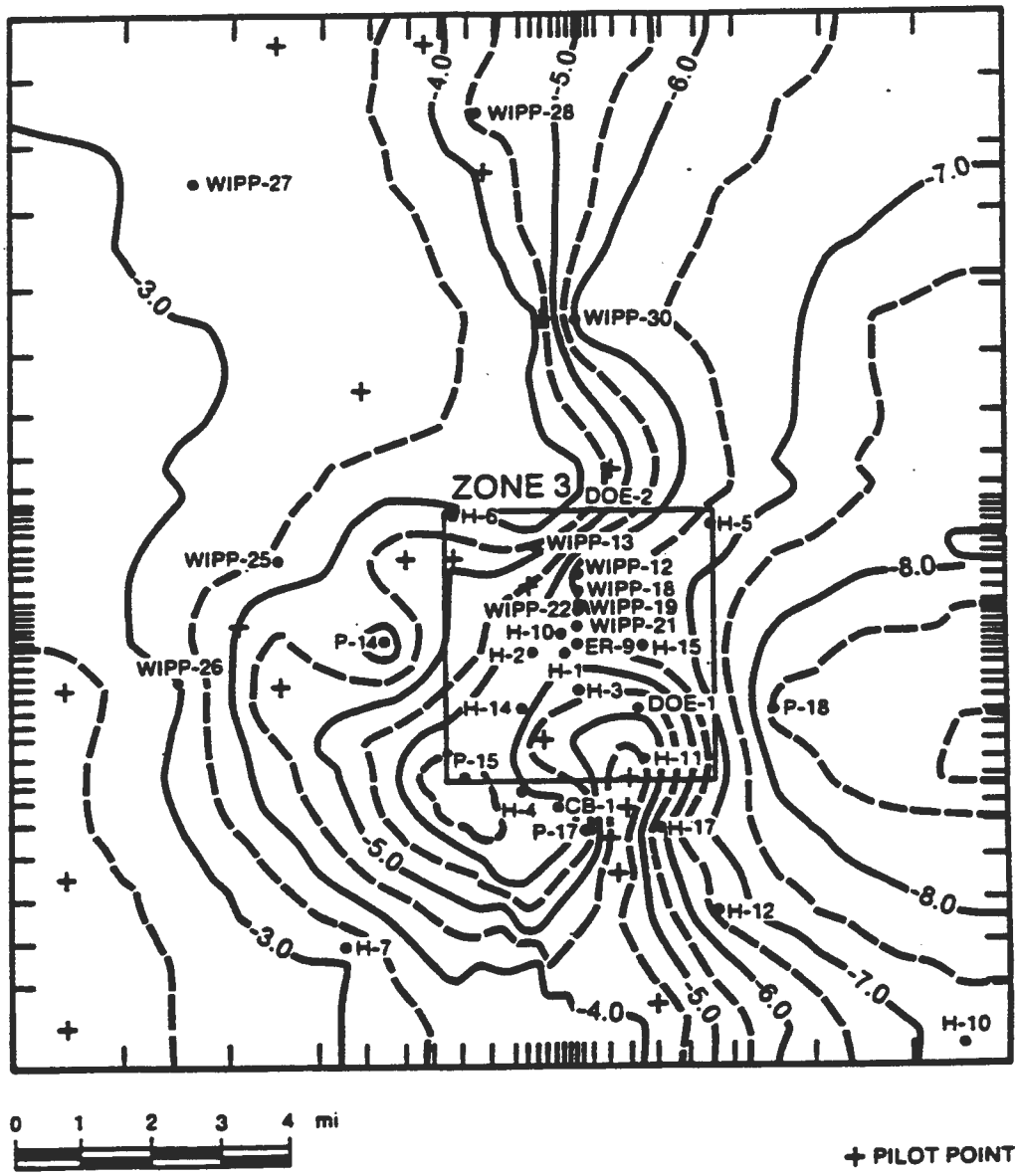


Figure 4.1.24: Calculated Culebra transmissivities at and near the WIPP site, based on steady-state calibration against freshwater-equivalent head distribution shown in Figure 4.1.23, fixing in place the fluid-density distribution shown in Figure 4.1.22. Figure 4.3 of LaVenue et al. (1988).

The distribution of Culebra pre-shaft head potentials calculated using the calibrated transmissivity distribution shown in Figure 4.1.24, is shown in Figure 4.1.25. Differences between calculated heads and those estimated on the basis of field data (Figure 4.1.23) are shown in Figure 4.1.26. The agreement is excellent, generally to within 1 m. This is less than the estimated uncertainty in freshwater-equivalent heads at individual wells, approximately 2 meters (LaVenue et al., 1988).

The modern flow directions and Darcy velocities within the Culebra dolomite at and near the WIPP site calculated by LaVenue et al. (1988) are shown in Figure 4.1.27. Darcy velocities do not include consideration of effective porosity; therefore, they do not represent actual groundwater particle velocities. Flow within the Culebra at and near the WIPP site is largely north-south, except in relatively low-transmissivity areas directly affected by either the high-transmissivity zone south of H-11 or by Nash Draw. Calculated Darcy velocities vary by six orders of magnitude, from $10^{-12}$ m/s ($m^3/m^2s$) east of the WIPP site to as high as $10^{-6}$ m/s along the axis of Nash Draw. In the region between WIPP-12 and the WIPP shafts, calculated Darcy velocities range from 2.5 to 7.5 x $10^{-10}$ m/s, and flow is north-south. LaVenue et al. (1988) note that calculated flow directions in the vicinity of DOE-2 appear unreliable due to local irregularities in the structure of the Culebra. As a result of the high-transmissivity zone south of H-11, flow in the vicinity of H-14 is towards the southeast, with a Darcy velocity of less than $10^{-9}$ m/s. Flow within the zone south of H-11 is to the south, with a Darcy velocity of approximately 2.5 x $10^{-9}$ m/s. The Darcy velocities shown in Figure 4.1.27 assume completely confined flow within the Culebra, and also assume steady-state heads and fixed brine-density distribution (LaVenue et al., 1988). They provide a realistic indication of modern flow directions.

Particle flowpaths and flowtimes calculated within the modelled area, assuming that the effective porosity of the Culebra is uniform at 16% are shown in Figure 4.1.28. As noted in Section 4.2, measured porosities within the Culebra range from 0.07 to 0.30. The effective in situ porosity is not known, but must be variable. It is not clear that assumption of confined flow within Nash Draw is valid. In addition, as discussed in Sections 4.3 and 4.4, Culebra hydrology is not at steady state, and there has probably been at least some change in flow directions within the Culebra within the last 10,000 years; the magnitude of the change remains uncertain. The travel times shown in Figure 4.1.28 must be taken only as an indication of the effects of relative variability in estimated particle flow rates.

Calculated particle velocities within Nash Draw are quite high, and calculated flow times across the entire modeled area are quite short in this region. Calculated travel times along paths A, B, and C (Figure 4.1.28) increase from west to east, from a low of 450 years to a high of 2800 years. Changes in Rustler water levels within Nash Draw since the beginning of potash mining approximately 50 years ago, described by Hunter (1985), indicate that the steady-state assumption is not realistic in this region, even on this relatively short time scale. At the other extreme, flow of a groundwater particle from H-5 to the southern boundary of the modeled area of LaVenue et al. (1988) is calculated to take more than one

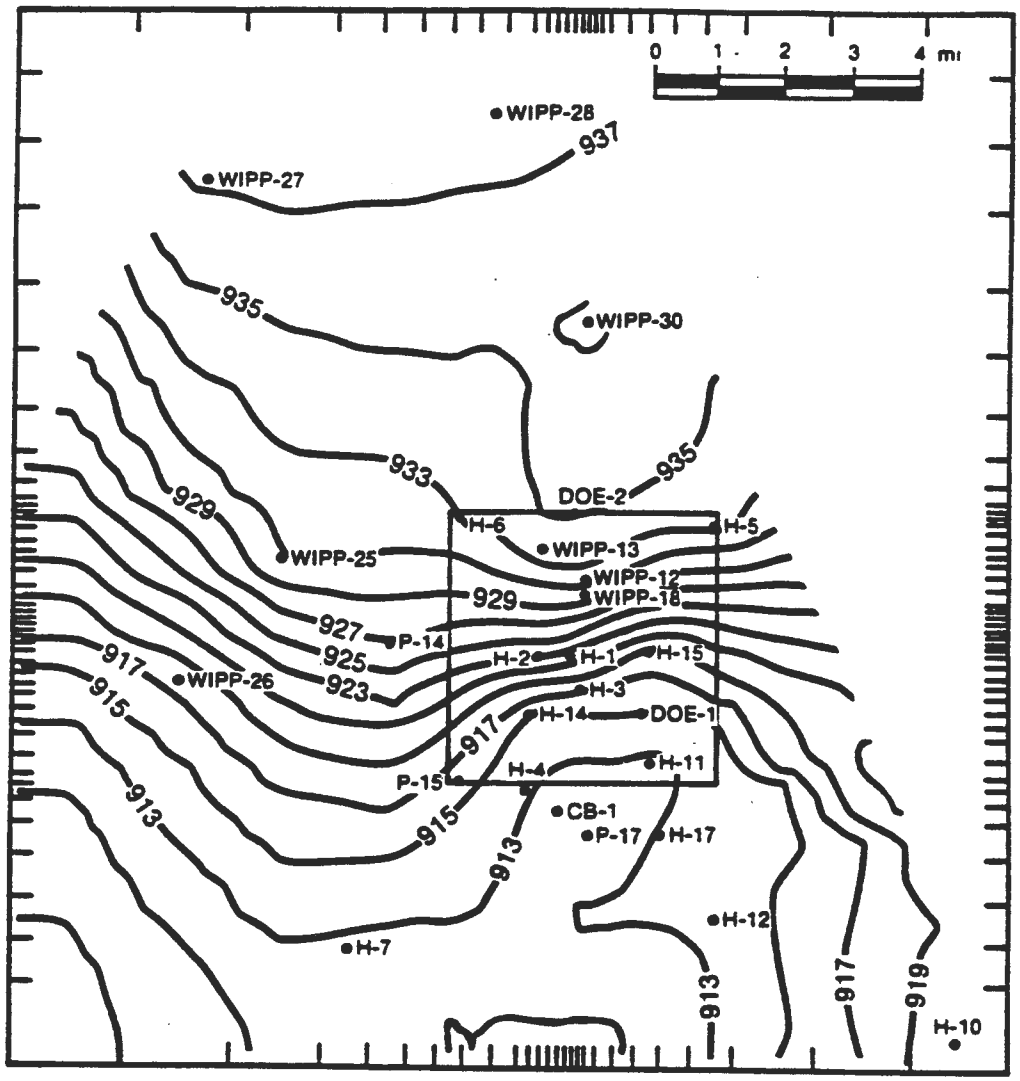


Figure 4.1.25: Calculated pre-shaft, freshwater-equivalent head distribution in the Culebra dolomite, based on calibrated transmissivity distribution shown in Figure 4.1.24. Figure 4.5A of LaVenue et al. (1988).

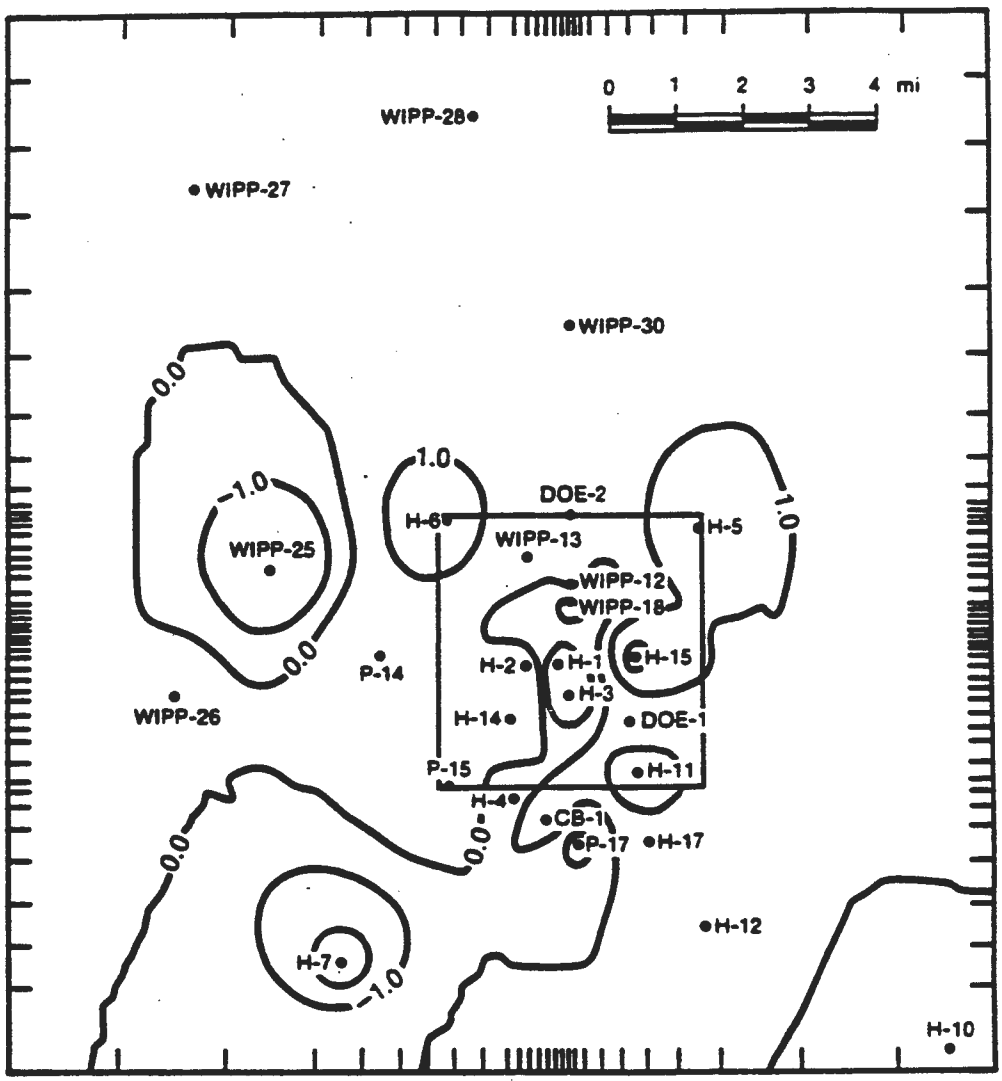


Figure 4.1.26: Difference between calculated Culebra head distribution (Figure 4.1.25) and measured pre-shaft head distribution (Figure 4.1.23). Figure 4.6 of LaVenue et al. (1988).

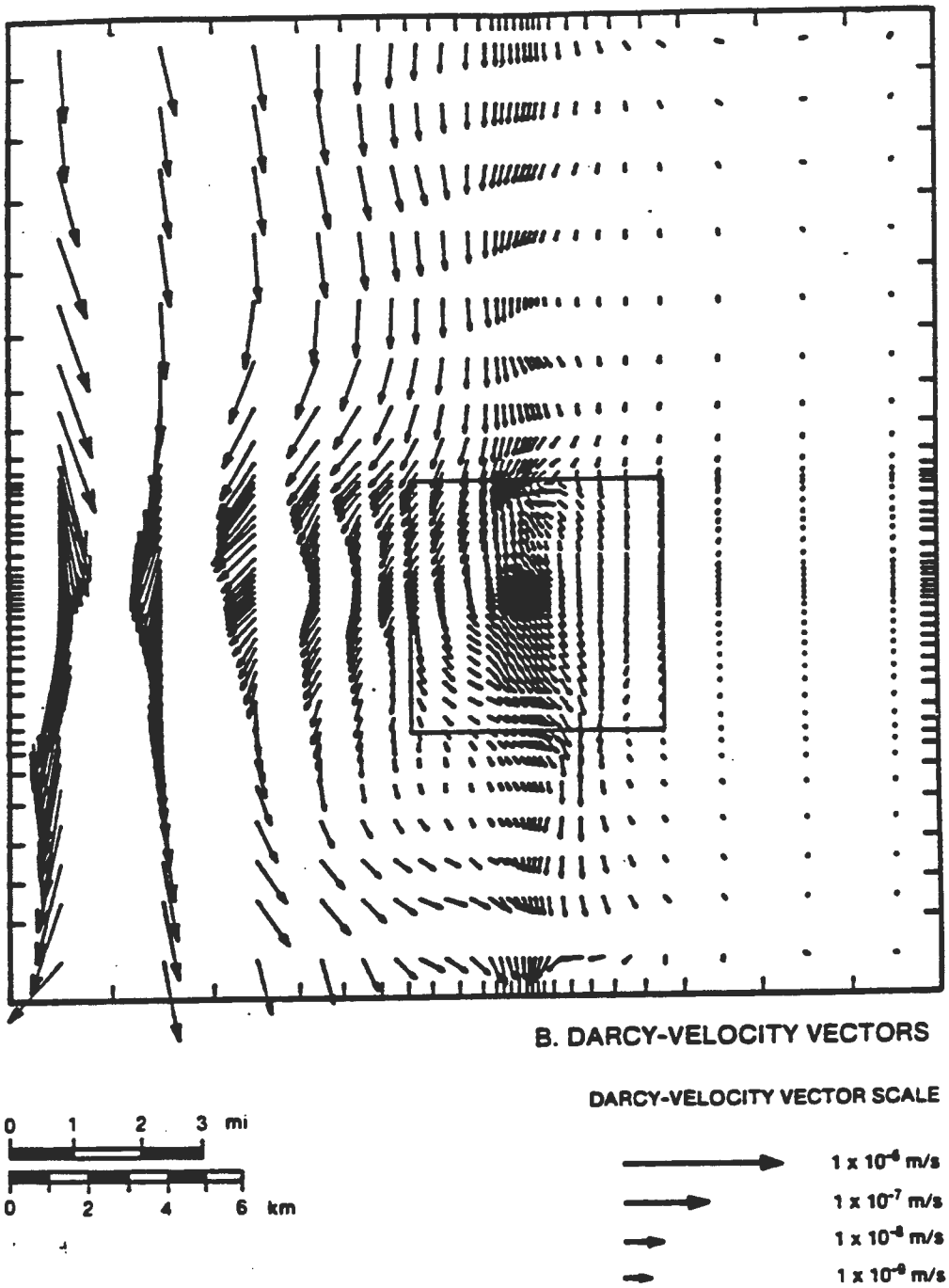


Figure 4.1.27: Calculated Darcy-velocity vectors in the Culebra dolomite, assuming the transmissivity distribution shown in Figure 4.1.24 and head distribution shown in Figure 4.1.25. Figure 4.5B of LaVenue et al. (1988).

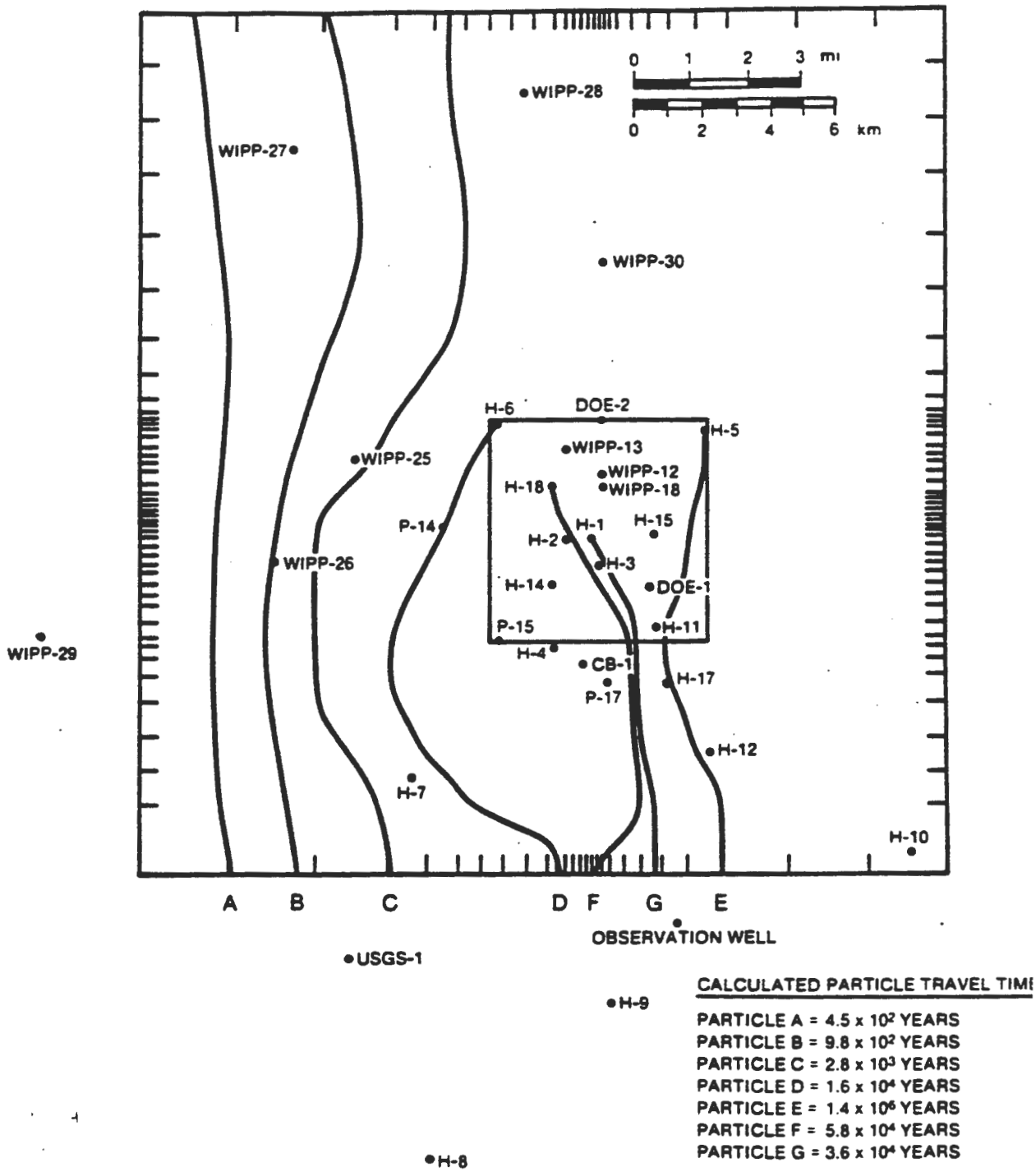


Figure 4.1.28: Calculated particle flowpaths and flow times within the Culebra dolomite, assuming steady-state and the transmissivity and head distributions shown in Figures 4.1.24 and 4.1.25. Figure 4.17 of LaVenue at al. (1988).

million years. Given that Culebra hydrology is in transient response to the end of the last pluvial period, it is not realistic to expect steady-state flow within the unit on a time scale of 106 years (LaVenue et al., 1988). The result indicates, however, that groundwater flow within the Culebra on the eastern part of the WIPP site is extremely slow.

Figure 4.1.28 also demonstrates an important consequence of the recent changes in the understanding of the distribution of Culebra transmissivities. Path G represents assumed steady-state flow from a position above the center of the WIPP waste-emplacement panels, analogous to the flowpath used in the detailed generic transport calculations contained in Reeves et al. (1987) (Section 4.2). Reeves et al. (1987) used the Culebra transmissivity distribution calculated by Haug et al. (1987), which included higher transmissivities south of H-11 than estimated by LaVenue et al. (1988) (Figure 4.1.24). The groundwater travel time calculated by LaVenue et al. (1988) for flow from directly above the center of the waste-emplacement panels to the southern boundary of the model shown in Figure 4.1.24 is 36,000 years. The calculated flow time from the release point of path G to the southern boundary of the WIPP site (Zone 3) is approximately 13,000 years, roughly 2.5 times that estimated by Reeves et al. (1987) along an analogous flowpath, but assuming the transmissivity distribution shown in Figure 4.1.16. The changes in interpreted Culebra transmissivities and head potentials since April 1986 have significantly increased expected groundwater flow times across the WIPP site within the Culebra dolomite. However, given the uncertainties in effective porosities, flowpaths, and transmissivities within the Culebra dolomite, the recent results must be considered approximate.

## 4.2 Pad-Scale and Regional-Scale Studies of Contaminant Transport within the Culebra Dolomite

For purposes of WIPP performance assessment, contaminant (radionuclide) transport within the Culebra dolomite is of concern in two general types of breach scenario. Section 4.2 discusses contaminant-transport results at both the hydropad and regional scale, under "low-pressure," relatively undisturbed conditions. Low-pressure conditions correspond to a release of fluids from the WIPP facility that does not disturb the pre-existing head distribution in the Culebra. "High-pressure" conditions, for which studies have not yet been completed, represent a breach involving effective connection of the Culebra dolomite with a pressurized brine in the Castile Formation beneath the WIPP facility (see Section 3.2) for a long enough period of time to significantly change the head gradients within the Culebra.

Detailed field testing of transport properties in the Culebra dolomite has been carried out only at the hydropad scale and is discussed in Section 4.2.1. Recent interpretation of conservative-tracer testing at the H-3 hydropad indicates that fracturing plays a major role in pad-scale contaminant transport in the transmissive (fractured) portions of the Culebra. In low-transmissivity areas, such as at the H-4 pad, pad-scale transport within the Culebra is best modelled using the equivalent-porous-medium assumption.

For purposes of performance assessment, however, the critical scale for transport within the Culebra dolomite is not the hydropad, but rather the distance between the point of breach into the Culebra and the boundary to the accessible environment. For purposes of consistency within this report, the boundary of WIPP Zone 3 is assumed to represent the boundary to the accessible environment. Contaminant transport over the 3.2 km from the center of the WIPP site to the boundary of Zone 3 is not amenable to field testing on a reasonable time scale. It is thus necessary to estimate the "regional-scale" transport behavior within the Culebra by numerical modeling. Section 4.2.2 discusses the regional-scale transport behavior of the Culebra dolomite at and near the WIPP site. The results in Section 4.2.2 indicate that, at least as long as the Culebra heads are not significantly disturbed and the assumed flow paths and material properties within the Culebra are reasonably representative, numerical simulation of regional-scale transport within the Culebra at and near the WIPP site need not include effects due to fracturing.

### 4.2.1 Hydropad-Scale Transport of Conservative Tracers at the H-3 and H-4 Hydropads

Convergent-flow tracer tests operated at the H-3 hydropad in May and June 1984 and at the H-4 hydropad between October 1982 and October 1984 are interpreted by Kelley and Pickens (1986). The interpretations are summarized here, with the objectives of examining the relative importance of dual-porosity or fracture-flow effects on the hydropad scale at two separate locations and discussing the ranges of transport parameters at the two locations.

The first stage of a convergent-flow tracer test is to establish approximate steady-state gradients between the observation holes and the pumped well. Tracers are then injected into the observation wells and their transport to the pumped well monitored. The fluorinated organic tracers meta-trifluoromethylbenzoate (m-TFMB) and pentafluorobenzoate (PFB) were used in testing at the H-3 pad. These same tracers were used at the H-4 pad, in addition to para-fluorobenzoate (p-FB) and thiocyanate (SCN). It is generally assumed that the tracers are chemically stable throughout a test, and that they do not interact with the surrounding rock mass except by diffusion (Kelley and Pickens, 1986).

The interpretation of the H-3 and H-4 tracer tests was done using the code SWIFT II (Reeves et al., 1986a; 1986b). SWIFT II handles the hydraulic and transport behavior of fractured media by means of a "dual-porosity" formalism, in which the composite medium is assumed to consist of an array of porous matrix blocks (primary porosity) and regularly spaced fractures (secondary porosity). The fractures and matrix are allowed to interact. The matrix-block geometry is idealized as either uniform slabs (parallel non-intersecting fractures) or cubes (three orthogonal fracture sets). In interpretation, radial flow towards the pumped hole was assumed.

Interpretation assuming the presence of three orthogonal sets of fractures and the assumption of radial flow are both equivalent to the assumption of isotropy. As mentioned in Section 4.1.2, however, interpretation of

hydraulic interference testing at the H-4, H-5, H-6, and H-11 hydropads indicates some directional dependence of Culebra hydraulic properties. In contrast, interpretation of the hydraulic behavior on the H-3 pad (Beauheim, 1987a) indicates effectively isotropic behavior. The results contained in Kelley and Pickens (1986) must be considered approximate.

4.2.1.1 Conservative-Tracer Tests at the H-3 Hydropad--The observed tracer behavior during convergent-flow testing at H-3 is shown in Figure 4.2.1, and is summarized in Table 4.8. Hole H-3b3 was the pumped hole in this test. Meta-trifluoromethylbenzoate (m-TFMB) injected in hole H-3b1 was first detected in hole H-3b3 ("breakthrough") approximately 0.92 days (22 hrs) after injection, and reached a well-defined peak concentration approximately 2.6 days (62.4 hrs) after injection. After this time, tracer concentration decreased rapidly towards a relatively steady-state value. In contrast, the pentafluorobenzoate (PFB) injected into hole H-3b2 travelled to the sampling hole much more slowly, was first detected approximately 3.76 days (90.2 hrs) after injection, reaching a very broadly defined peak concentration (if any) after approximately 23 days (552 hrs).

Thus, there is a marked difference between the apparent directional dependence of hydraulic behavior and transport behavior at the H-3 pad. Hydraulic anisotropy at the H-3 pad is negligible. However, m-TFMB breakthrough along the H-3b1 - H-3b3 path was four times more rapid than PFB breakthrough along the H-3b2 - H-3b3 path. The preliminary interpretation of a convergent-flow conservative-tracer test at the H-6 pad (Gonzalez, 1983b) also indicates a discrepancy between the directional dependence of hydraulic and transport behavior within the Culebra. In testing at H-6, PFB injected into H-6b arrived at H-6c 16 times more rapidly than did m-TFMB injected into H-6a (Gonzalez, 1983b). These results suggest that the apparent difference between the behaviors of m-TFMB and PFB at the H-3 pad reflects differences in transport behavior along the two flow paths, rather than inherent differences in the behavior of the two tracers.

Parameters resulting from calibration to the observed behavior of the H-3 test are shown in Table 4.9. In calibration, varying input parameters are used to simulate the observed tracer behavior until satisfactory agreement is reached. Because these same parameters were used in regional-scale transport calculations (Section 4.2.2), it is important to understand the character of the parameters listed in Table 4.9.

Three parameters, solute free-water diffusion coefficient, matrix tortuosity, and longitudinal dispersivity, were taken by Kelley and Pickens (1986) from ranges of published values, not based on WIPP-specific information. Specifically, values of 0.15 and 0.45 for matrix tortuosity were used as variable input to calculations. The matrix porosity value shown in Table 4.9 (0.20) is the approximate average of a series of six helium-pycnometer measurements made on Culebra core from holes H-3b2 and H-3b3.

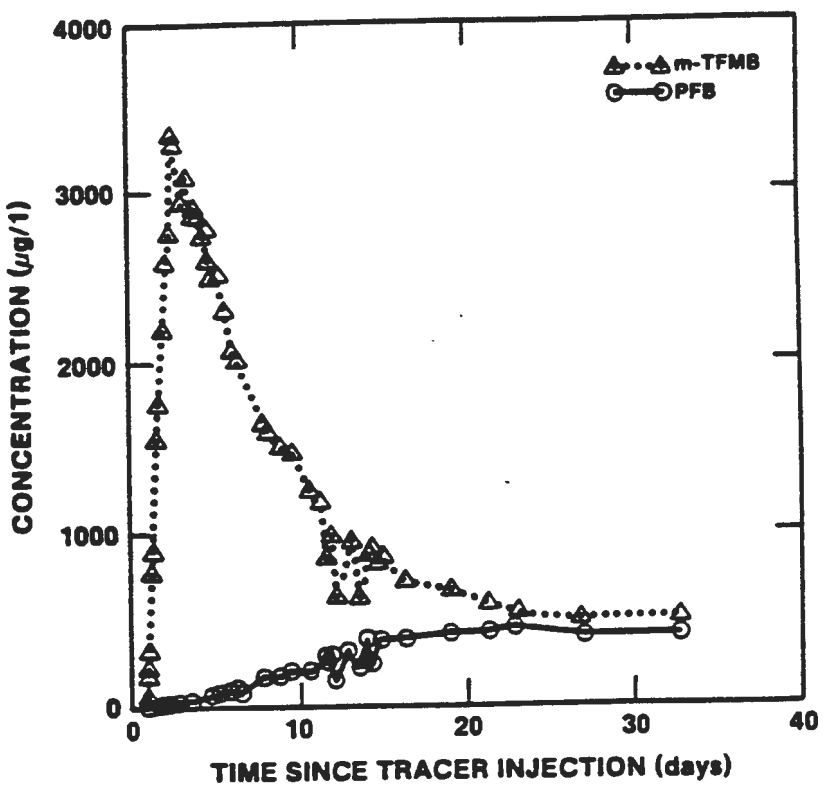


Figure 4.2.1: Observed tracer behavior during the convergent-flow test at the H-3 hydropad. Figure 4.5 of Kelley and Pickens (1986).

Table 4.8: Summary of observed tracer behavior during the convergent-flow test at the H-3 hydropad. Slightly modified from Table 4.2 of Kelley and Pickens (1986).

| Parameter | Tracer | |
|---|---|---|
| | m-TFMB | PFB |
| 1. Flow path | H-3b1 to H-3b3 | H3b2 to H-3b3 |
| 2. First detection (days) | 0.92 | 3.76 |
| 3. First reported concentration (mg/ℓ) | 56 | 20 |
| 4. Time of peak concentration (days) | 2.59 | 23.04 |
| 5. Peak concentration (mg/ℓ) | 3379 | 444 |
| 6. Relative Peak Concentration ($m/m_o$) | $3.3 \times 10^{-6}$ | $4.3 \times 10^{-7}$ |
| 7. Total tracer mass recovered ($m/m_o$) | 0.53 | 0.15 |
| 8. Apparent fracture porosity | 0.0019 | 0.019 |

Fracture porosity and matrix block length are specific outputs of the calculations, for the specific input values of other variables. Thus, in extrapolation of H-3 transport properties to other locations, only matrix block lengths and fracture porosities are based on the results of the H-3 tracer test; other values were input to interpretation of the H-3 testing based on either literature review or laboratory measurements.

The calculated fracture porosity of 0.19% along the H-3b1 - H-3b3 flow path (Table 4.9) was estimated directly from the relationship among pumping rate, H-3b1 - H-3b3 path length assuming direct radial flow, Culebra thickness, and time required for m-TFMB to reach peak concentration (22 hrs). Similar analysis along the H-3b2 - H-3b3 path yields an estimated fracture porosity of 1.9%. A fracture porosity of .19% was used in sensitivity studies, and was assumed to be applicable along both flowpaths on the H-3 pad (Kelley and Pickens, 1986).

Figures 4.2.2 and 4.2.3 show the best-fit simulations of transport behavior along the H-3b1 - H-3b3 flow path as a function of the specified input parameters. There is excellent agreement between measured and simulated results, with two different effective block sizes (1.2 and 2.1 m) being

Table 4.9: Input and best-fit calibration parameters from interpretation of the conservative-tracer test at the H-3 hydropad. Slightly modified from Table 4.3 of Kelley and Pickens (1986).

| | Tracer | |
|---|---|---|
| | m-TFMB | PFB |
| Flow path | H-3b1 to H-3b3 | H-3b2 to H-3b3 |
| Input Parameters | | |
| 1. Diffusion coefficient for solute-free water ($m^2/s$) | $7.4 \times 10^{-10}$ | $7.4 \times 10^{-10}$ |
| 2. Matrix tortuosity | 0.15, 0.45 | 0.15, 0.45 |
| 3. Longitudinal disporsivity (m) | 3.0 | 1.5 |
| 4. Matrix porosity | 0.20 | 0.20 |
| 5. Fracture porosity | - | $1.9 \times 10^{-3}$ |
| Output Parameters | | |
| 1. Fracture porosity | $1.9 \times 10^{-3}$ | $(1.9 \times 10^{-2})$ |
| 2. Matrix-block length (m) | 1.2, 2.1 | 0.25, 0.44 |

calculated as a function of two different input matrix tortuosities (0.15 and 0.45, respectively). Figure 4.2.4 shows the analogous best-fit simulation for the H-3b2 - H-3b3 flowpath, assuming a matrix tortuosity of 0.15. The calculated effective block size along the H-3b2 - H-3b3 flowpath, 0.25 to 0.44 m, is smaller than along the path H-3b1 - H-3b3. As mentioned earlier, the calculated block sizes are only qualitative although, as noted by Kelley and Pickens (1986) they are consistent with observation of both Culebra core and exposures within the WIPP shafts. Thus, conservative-tracer testing at the H-3 pad indicates both the strong role of fracturing in transport at this scale (at least in some directions) and the strong directional dependence of estimated transport parameters such as effective block size.

The role of both matrix and fractures in pad-scale contaminant transport of conservative (non-sorbing) trace contaminants in the Culebra dolomite at the H-3 pad is emphasized in Figures 4.2.5 and 4.2.6. If dual-porosity and single-porosity simulations are both adjusted to match the time of peak

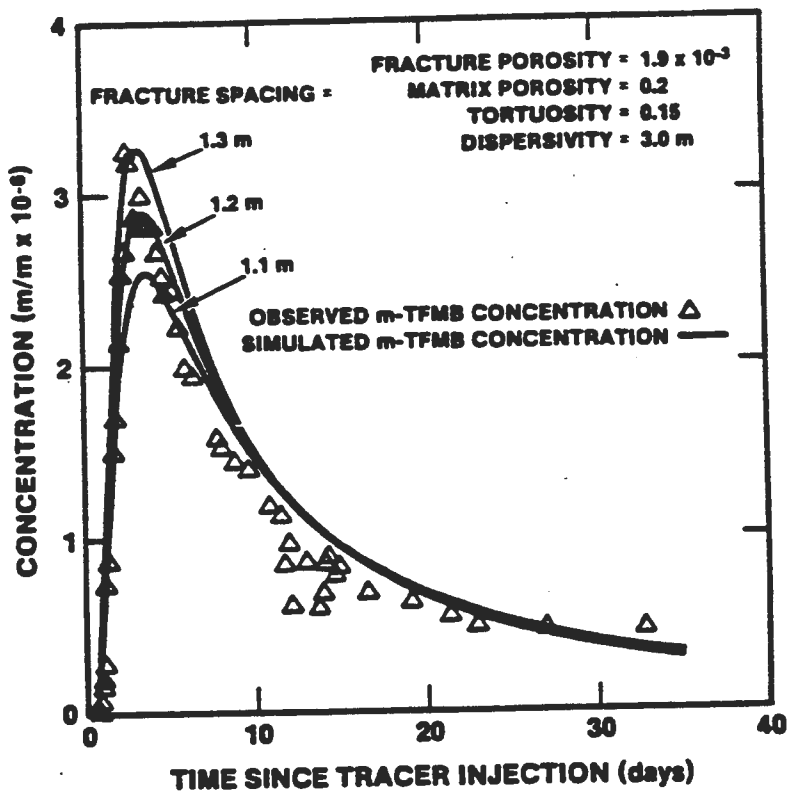


Figure 4.2.2: Best-fit simulation of measured transport behavior along the H-3b1 - H-3b3 flow path, assuming matrix tortuosity of 0.15. It is assumed that 1 kg of m-TFMB was successfully injected, and remained stable throughout the test. Figure 4.10a of Kelley and Pickens (1986).

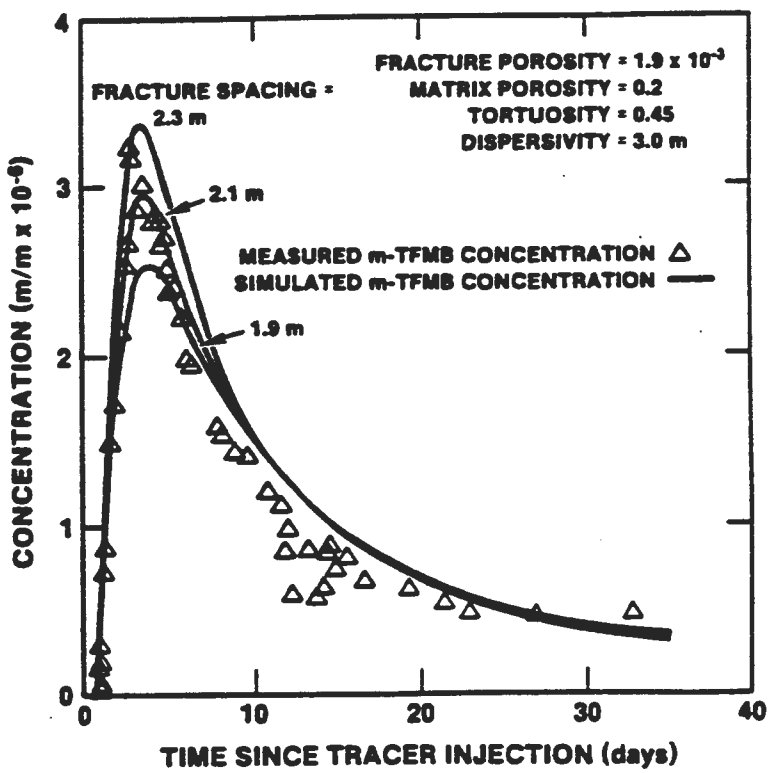


Figure 4.2.3: Best-fit simulation of measured transport behavior along the H-3b1 - H-3b3 flow path, assuming matrix tortuosity of 0.45. Figure 4.10b of Kelley and Pickens (1986).

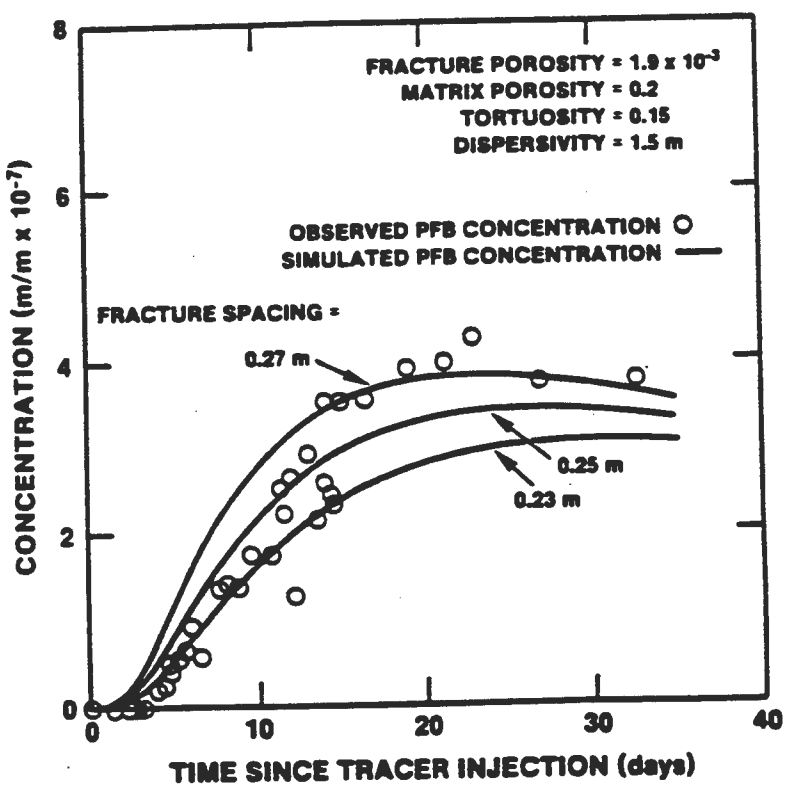


Figure 4.2.4: Best-fit simulation of measured transport behavior along the H-3b2 - H-3b3 flow path, assuming matrix tortuosity of 0.15. Fracture porosity is assumed to be the same as calculated for the flow path H-3b1 to H-3b3. Figure 4.11a of Kelley and Pickens (1986).

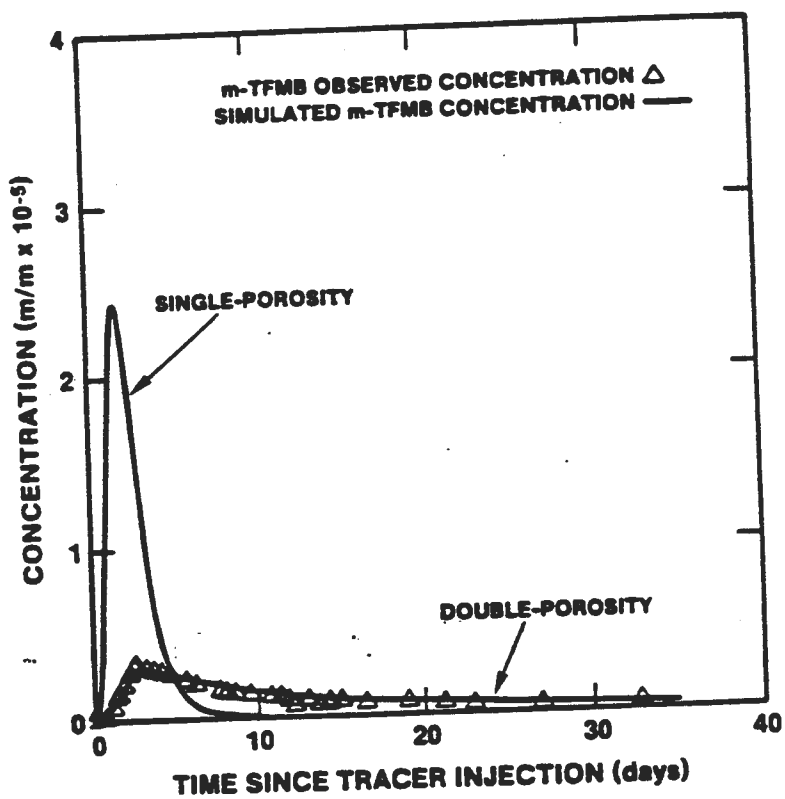


Figure 4.2.5: Best-fit single-porosity and dual-porosity simulations of tracer behavior along the H-3b1 - H-3b3 flow path when both simulations are forced to match the time of peak concentration. Figure 4.12 of Kelley and Pickens (1986).

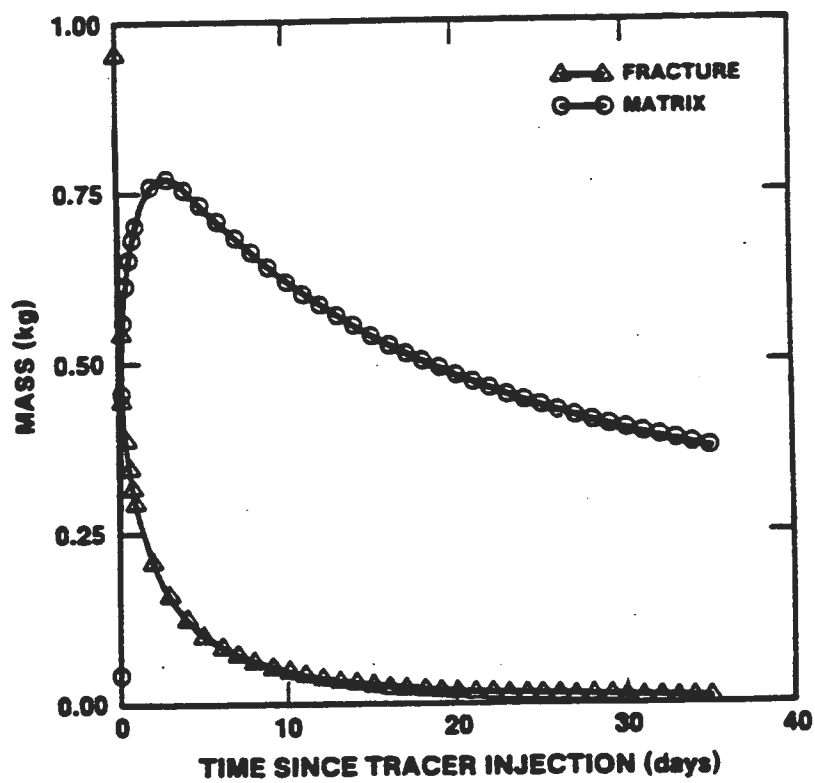


Figure 4.2.6: Calculated total masses of tracer m-TFMB in matrix and fractures as a function of time after injection. The fact that the total mass is less than 1 kg after approximately 2.5 days into the test reflects removal of tracer at the sampling hole, H-3b3. Figure 4.13 of Kelley and Pickens (1986).

concentration for m-TFMB transport along the path H-3b1 - H-3b3 (Figure 4.2.5), the post-peak behavior of the two simulations is qualitatively different. In the single-porosity simulation, the effective rock-mass porosity required to match the time of peak concentration is 0.0019, equivalent to the estimated fracture porosity in the dual-porosity simulation. The single-porosity simulation is thus equivalent to assuming no interaction between fractures and matrix, i.e., it is a "discrete-fracture" simulation, in which interaction between fractures and matrix is negligible. The peak concentration in the single-porosity simulation, which is overestimated by a factor of approximately eight, drops off very quickly, approaching zero, eight days after tracer injection. In contrast, the best-fit dual-porosity simulation matches both the time and magnitude of the tracer peak concentration well. In addition, both the observed tracer concentrations and those calculated with the best-fit dual-porosity parameters are above the detection limit more than 30 days after injection.

The conclusion by Kelley and Pickens (1986) that both the short-term and long-term transport behavior at the H-3 pad are affected by interaction of fractures and matrix is also supported by Figure 4.1.26. This figure indicates the total masses of m-TFMB calculated to be present in the matrix and fractures as a function of time since tracer injection. Initially, all of the injected tracer is contained in the fractures, and the total tracer mass in the matrix is zero. After approximately 0.5 days, however, tracer storage within the matrix blocks dominates as a result of diffusion from the fractures. At early times, storage within the matrix decreases both the concentration and the total mass of tracer in the fractures, consistent with the lower peak concentration calculated using the dual-porosity formalism (Figure 4.2.5). At longer times, the concentration of material within the matrix is greater than that within the fractures. Therefore, material diffuses from the matrix into the fractures, effectively keeping the concentration within the fractures from rapidly decreasing to zero as it does in the single-porosity simulation.

Interpretation of the H-3 conservative-tracer experiment provided the first estimates of Culebra transport parameters (fracture porosity and effective matrix block size) in fractured portions of the Culebra dolomite. There are unavoidable uncertainties in these estimates, however, due to both the need to assume radial flow in the interpretation and uncertainties in parameters such as effective matrix porosity. Regardless of these limitations, the conservative-tracer test at the H-3 pad provides direct evidence of the role of matrix diffusion in contaminant transport in fractured portions of the Culebra dolomite. This evidence is critical in supporting assumptions made in calculation of regional-scale transport within the Culebra (Section 4.2.2).

4.2.1.2 <u>Conservative-Tracer Tests at the H-4 Hydropad</u>--Conservative-tracer testing at H-3 investigated pad-scale contaminant transport where the Culebra is known to be effectively fractured (transmissivity approximately $2 \times 10^{-6}$ $m^2/s$). At the H-4 pad, however, the transmissivity is lower ($10^{-6}$ $m^2/s$ or less; Tables 4.1 and 4.2), and there is no evidence of dual-porosity behavior in hydraulic testing.

The physical layout of the H-4 hydropad is shown in Figure 4.2.7. During steady-state, convergent-flow tracer testing at the pad between October 27, 1982, and October 15, 1984, H-4c was the pumped hole (at nominal rates of $1.66 \times 10^{-2}$ and $3.33 \times 10^{-2}$ l/s), and tracers were injected into holes H-4a and H-4b. Due to the very long test time at the H-4 pad, detailed interpretation of tracer behavior is hampered by pumping-rate fluctuations and pump breakdowns, as well as by questionable tracer stability (Kelley and Pickens, 1986).

The observed tracer behavior during testing at H-4 is summarized in Table 4.10. The first tracer detected in H-4c was m-TFMB travelling along the path H-4b to H-4c. However, the tracer was not detected until 262 days after injection. Tracer recovery was very limited during the test, the greatest being 37% of the total mass of m-TFMB injected. Because of the limited tracer recovery, the emphasis here is on m-TFMB behavior.

The calculated effective matrix or fracture porosities controlling first arrival of m-TFMB and PFB (Table 4.9), analyzed in the same method as in testing at the H-3 pad, are 0.033 and 0.053, respectively. Lab-measured total porosity for samples from the H-2, H-3, H-4, and H-6 pads range from 0.07 to 0.30, with an average value of 0.16 (Reeves et al., 1987). The two Culebra samples from hole H-4b have reported total porosities of 0.20 and 0.30. Therefore, the apparent porosities calculated from peak-concentration behavior in the H-4 tracer test may indicate that the hydraulically effective porosity of the Culebra at H-4 is significantly less than total porosity, that the tracers used did not remain stable and non-reactive for the two-year duration of the test, and/or that the Culebra core samples from H-4 are not representative.

Kelley and Pickens (1986) applied three different interpretative models to the behavior of m-TFMB at the H-4 pad: 1) a single-porosity model; 2) a dual-porosity model; and 3) a layered porous-medium model. The first two models are analogous to those used in interpretation of conservative-tracer testing at the H-3 pad. The third model is different in that it assumes that the Culebra consists of a specified number of parallel high-permeability and low-permeability porous layers. In this approach, unlike the dual-porosity approach, the total surface area available for diffusive transport between high-permeability and low-permeability zones is fixed by the specified number of high-permeability zones.

The simulation of m-TFMB behavior shown in Figure 4.2.8 assumes specified numbers of high-permeability zones and stability of 1 kg of tracer for the duration of the test. The time of peak concentration (388 days) is matched with an effective porosity of 0.04. However, the peak concentration is overestimated by a factor of approximately two if the Culebra is assumed to be uniform (one high-permeability zone). Kelley and Pickens (1986) note that improved agreement between observed and calculated behavior resulted if it was assumed that only 0.5 kg of tracer was effectively injected, rather than the nominal 1.0 kg.

A dual-permeability formalism was also used by Kelley and Pickens (1986), assuming that both low-permeability and high-permeability zones had an

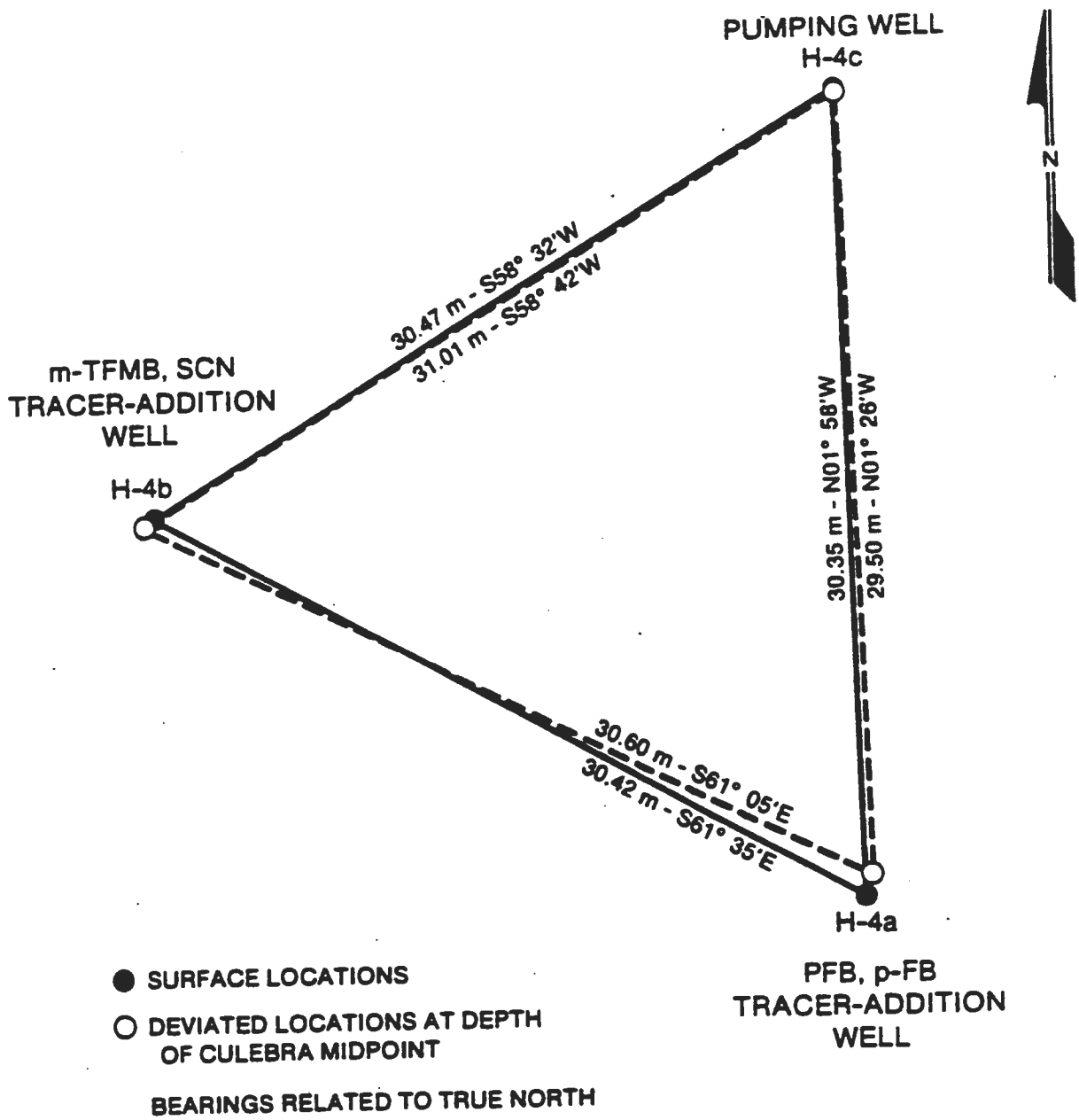


Figure 4.2.7: Physical layout of the H-4 hydropad. The figure includes orientations and spacings between holes, both at the surface and at the depth of the Culebra dolomite. Figure 6.1 of Kelley and Pickens (1986).

Table 4.10: Summary of observed tracer behavior during the convergent-flow, conservative-tracer test at the H-4 hydropad. Slightly modified from Table 6.2 of Kelley and Reeves (1986).

| Parameter | Tracer | |
|---|---|---|
| | m-TFMB | PFB |
| 1. Flow path | H-4b to H-4c | H-4a to H-4c |
| 2. First detection (days) | 262.2 | 501.1 |
| 3. First reported concentration (mg/ℓ) | 78 | 48 |
| 4. Time of peak concentration (days) | 388.2 | 507 |
| 5. Peak concentration (mg/ℓ) | 723 | 54 |
| 6. Relative peak concentration ($m/m_o$) | $7.1 \times 10^{-7}$ | $5.3 \times 10^{-8}$ |
| 7. Tracer Mass recovered ($m/m_o$) | 0.37 | 0.022 |
| 8. Apparent fracture porosity from peak concentration | 0.033 | 0.053(1) |

(1) Apparent porosities for SCN = 0.024; p-FB = 0.064.

effective porosity of 0.20. The number of high-permeability zones was allowed to vary. It was assumed that 1.0 kg of m-TFMB remained stable throughout the test. The presence of increasing numbers of interfaces between high-permeability zones and "matrix" zones, in which only diffusive transport is allowed, effectively decreases the simulated peak concentration (Figure 4.2.8). The best fit was obtained for five or six high-permeability zones, although none of the fits were satisfactory (Kelley and Pickens, 1986), in part because they overestimate tracer concentrations at longer times. In order to improve the long-term fit, it would have to be assumed that there was some tracer degradation at longer times.

In summary, interpretation of the conservative-tracer test at the H-4 pad, while not successful in developing detailed estimates of transport parameters in unfractured portions of the Culebra, does indicate important considerations in both tracer testing at the pad scale and interpretation of regional-scale modeling of transport behavior. Both tracer and hydraulic behavior during the test are consistent with porous-medium behavior, indicating that fracturing need not be considered in evaluation of pad-scale or regional-scale transport in areas of relatively low Culebra

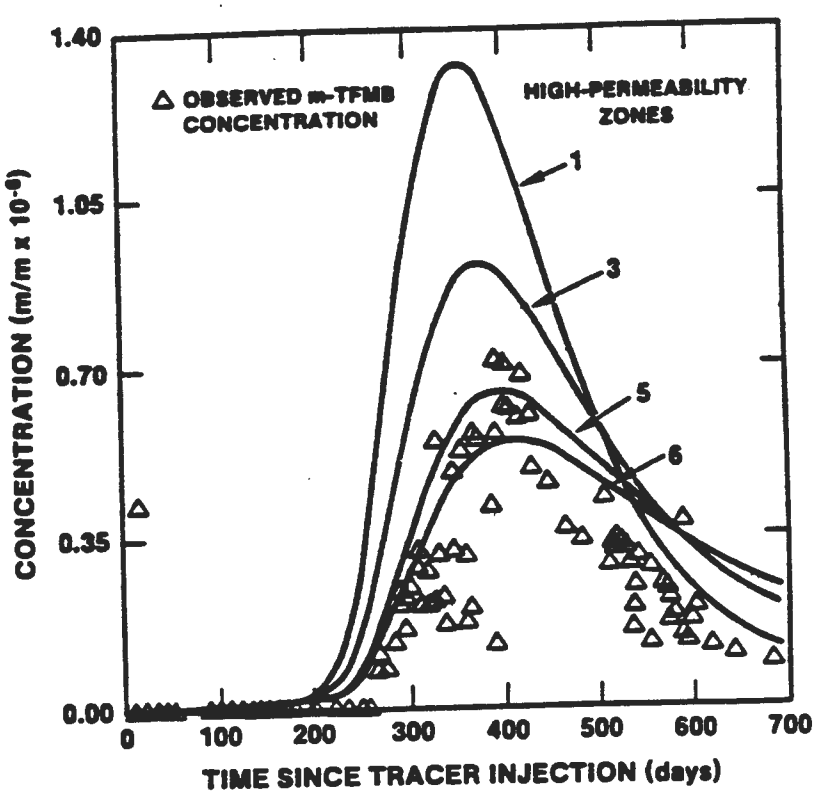


Figure 4.2.8: Best-fit simulation of m-TFMB behavior during testing at the H-4 hydropad, assuming effective injection and stability of 1 kg of tracer and control of behavior by the specified numbers of multiple high-permeability zones. Figure 6.11 of Kelley and Pickens (1986).

transmissivity ($T \leq$ approximately $10^{-6}$ $m^2/s$). If it is assumed that the Culebra at H-4 is vertically homogeneous and that the tracers used were stable and non-reactive for the duration of the test, then the hydraulically effective matrix porosity of the Culebra may be significantly less than the total porosity. Given the long duration of the H-4 test, however, it is probable that the tracers degraded during the test.

### 4.2.2 Regional-Scale Contaminant Transport in the Culebra Dolomite under Low-Pressure Conditions

Regional-scale contaminant transport within the Culebra dolomite under the low-pressure type of breach scenario, i.e., under conditions which do not disturb the head distribution within the Culebra, has been examined by Reeves et al. (1987). Significant transport under these conditions might be expected in the event of failure of the WIPP shaft seals in the absence of human intrusion, or in the event of an imperfectly plugged human-intrusion breach involving a high-pressure brine source within the Castile Formation. Calculations are ongoing to investigate behavior following a second type of breach, in which fluids are assumed to be injected at high pressures into the Culebra for long enough to dominate the local head potentials and flow rates.

The calculations in Reeves et al. (1987) investigate: 1) the significance of the interactions between matrix and fractures seen in tracer and hydraulic testing at the H-3 pad in regional-scale transport within fractured portions of the Culebra dolomite; and 2) the relative importance of several transport and material parameters of the Culebra in regional transport within fractured portions of the Culebra. The calculations in Reeves et al. (1987) were made using the following approach and/or assumptions:

1. Contaminants were assumed to be continuously injected into the Culebra dolomite at points directly above the WIPP waste-emplacement panels at a constant rate after time zero. The injection was slow enough not to disturb the "natural" (pre-WIPP-shaft) gradient or transmissivity distribution.

2. The boundary of WIPP Zone 3 was assumed to represent the boundary of the accessible environment.

3. Effects of radioactive decay and lateral dispersion were assumed negligible, and were not included. If lateral dispersion were included in the calculations, it would effectively slow down transport. The effects of lateral dispersivity on total integrated release to the accessible environment have not been quantified.

4. Material properties and flow velocity were assumed homogeneous between the point of entry into the Culebra and the accessible environment. The analysis was done in terms of an average Darcy velocity yielding groundwater travel times equivalent to those calculated from the flow model described in Haug et al. (1987). Fluid

flow and contaminant transport were controlled by the transmissivity and head distributions estimated by Haug et al. (1987), and were calculated along the flow paths shown in Figure 4.2.9.

5. As a result of the strong interactions between fractures and matrix observed in the conservative-tracer test conducted at the H-3 hydropad (Section 4.2.1), the double-porosity formalism was initially assumed to be appropriate for modeling of transport within fractured portions of the Culebra. However, a major objective of the report was to examine the consequences of both the "discrete-fracture" and "equivalent-porous-medium" end-member behaviors in regional transport.

6. The base-case values and ranges of properties shown in Table 4.11 were assumed to be representative for fractured portions of the Culebra dolomite. The Culebra transport properties estimated in conservative-tracer testing at the H-3 pad were taken as the base-case properties.

7. "Breakthrough," defined by Reeves et al. (1987) as the time at which the calculated contaminant concentration at the boundary to WIPP Zone 3 equaled 10% of the injected concentration, was assumed to provide a meaningful measure of transport behavior. Conclusions in the report are specifically evaluated on the basis of this assumption.

8. It was assumed that retardation effects within the Culebra dolomite can be realistically modeled as a linear process, i.e., that chemical reactions are "fast" relative to flow times within fractures, are reversible, and reflect local equilibrium within the matrix. Thus, it was assumed that chemical retardation within the matrix of the Culebra dolomite can be represented realistically by using an appropriate "matrix distribution coefficient," $k_d$.

9. The possible presence of mineralogical "skins" on matrix blocks was ignored, as were advective transport within the matrix and sorption on fracture surfaces. These assumptions appear to be generally "conservative," i.e., they should bias the calculations towards greater fracture flow, except for the case of mineralogical skins inhibiting diffusion into the matrix.

Figure 4.2.10 compares the average calculated travel times for a conservative contaminant from positions above the WIPP facility to the southern boundary of WIPP Zone 3, along the flow paths shown in Figure 4.2.9, according to three different assumptions. Using the dual-porosity formalism and assuming uniform distribution of the base-case material properties estimated at the H-3 pad, the time predicted for "breakthrough" of a conservative (non-sorbing) contaminant at the boundary of WIPP Zone 3 is 3490 years after the beginning of continuous injection. This is approximately 90% of the 3730 years predicted by single-porosity calculations in which the porosity is set equal to the sum of the base-case matrix and fracture porosities, 16.2%. In the absence of chemical retardation of the contaminant, the role of the matrix in transport is largely one of storage due to diffusion from fractures into/out of matrix blocks (Section 4.2.1).

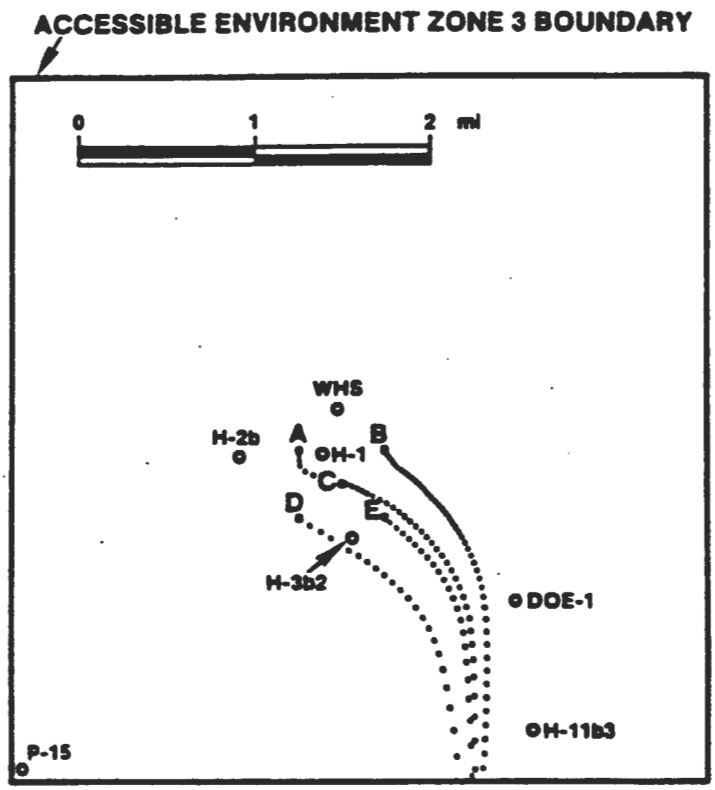


Figure 4.2.9: Release points into the Culebra dolomite and flow paths to the accessible environment considered by Reeves et al. (1987). Points A-E are vertical projections of the corners and center of the WIPP waste-emplacement panels upwards onto the Culebra dolomite. The small crosses extending from points A-E to the southern boundary of Zone 3 are equal-time marks along the flow paths. Slightly modified from Figure 1.7 of Reeves et al. (1987).

Table 4.11: Base-case Culebra transport properties and ranges of properties considered in regional-scale transport within Culebra dolomite. Slightly modified from Table 2.2 of Reeves et al. (1987).

| Parameter | Units | Symbol | Base-Case | Range in Values | Relative Range (2) |
|---|---|---|---|---|---|
| 1. Free-water diffusivity | $cm^2/s$ | $D'$ | $2 \times 10^{-5}$ | $4 \times 10^{-6}$ to $9 \times 10^{-5}$ | 4.30 |
| 2. Matrix tortuosity | - | $\theta'$ | 0.15 | 0.05 to 0.50 | 3.00 |
| 3. Matrix-block length | $2L'$ | $m$ | 2.4 | 0.25 to 7.0 | 2.81 |
| 4. Matrix porosity | - | $\phi'$ | 0.16 | 0.07 to 0.30 | 1.44 |
| 5. Fracture porosity | - | $\phi$ | $2 \times 10^{-3}$ | $2 \times 10^{-4}$ to $2 \times 10^{-2}$ | 9.90 |
| 6. Longitudinal dispersivity | m | $\alpha$ | 100 | 50 to 300 | 2.50 |
| 7. Specific matrix flux | $m^3/m^2s$ | $u$ | $3.2 \times 10^{-9}$ | $2.2 \times 10^{-9}$ to $4.7 \times 10^{-9}$ | 0.78 |
| 8. Matrix distribution coefficient | $m\ell/g$ | $k_d$ | (1) | (1) | - |
| 9. Fraction distribution coefficient | $m\ell/g$ | $k_d$ | 0 | 0 | - |

(1) Calculations done with fixed values of $k_d' = 0.0, 10, 10^2, 10^4\ m\ell/g$.
(2) Range divided by base-case value.

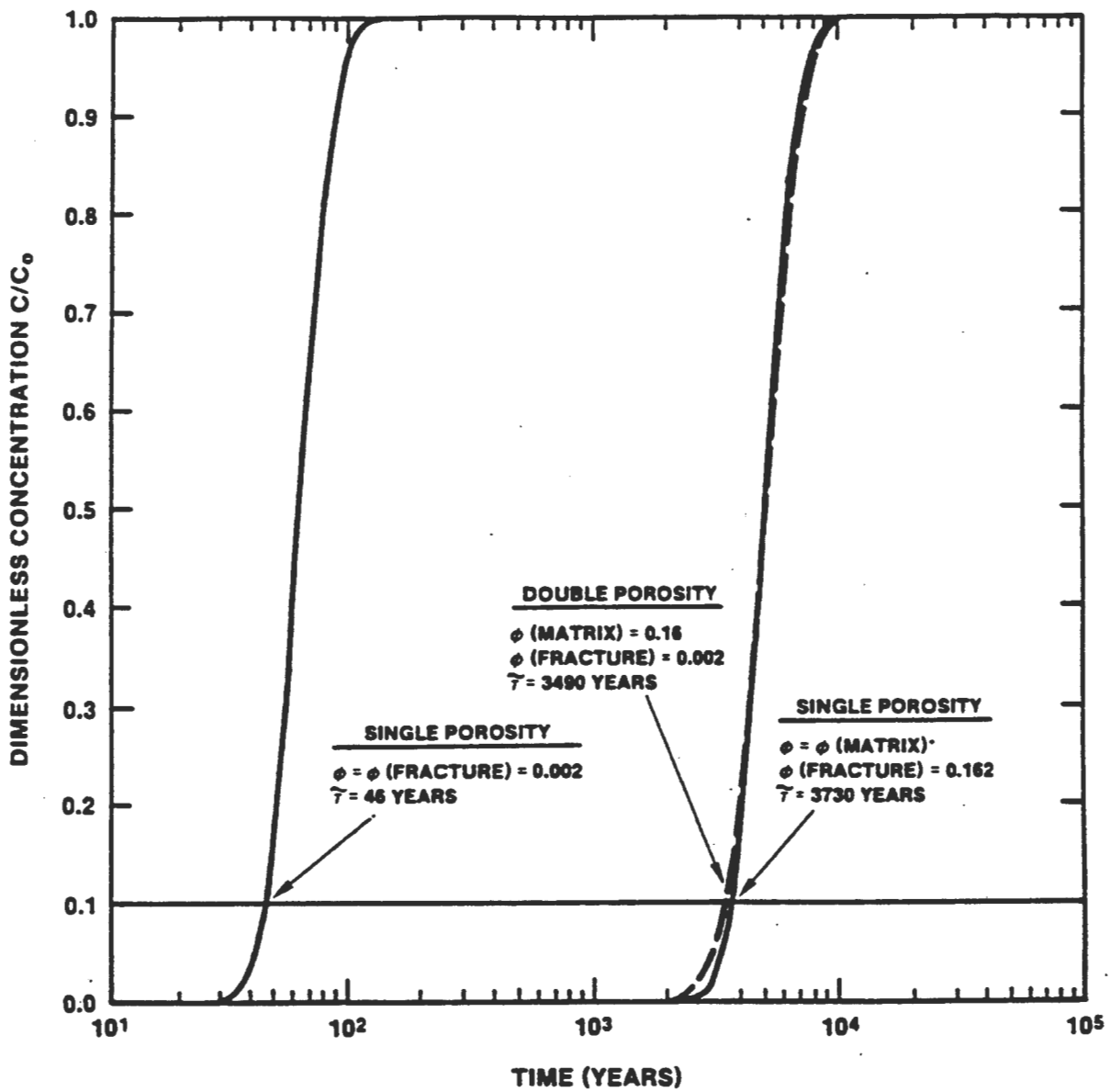


Figure 4.2.10: Comparison of base-case, regional-scale transport behavior of a conservative contaminant in the Culebra dolomite under discrete-fracture, dual-porosity, and porous-medium assumptions. Breakthrough is defined here as the time at which the concentration at the boundary of WIPP Zone 3 equals 10% of the injected concentration. Figure 5.1 of Reeves et al. (1987).

In effect, the single-porosity curve on the right-hand side of Figure 4.2.10 assumes instantaneous diffusion into and equilibration with the matrix.

At the other extreme, diffusion time into the matrix is infinite in fracture flow if it is assumed that fractures and matrix do not interact. The breakthrough time calculated (Figure 4.2.10) assuming that transport occurs only within fractures, assuming a fracture porosity of 0.2%, is 46 years (Reeves et al., 1987).

The experimental results at the H-3 hydropad (Section 4.2.1.1) and the calculated variations in breakthrough time at the boundary of WIPP Zone 3 shown in Figure 4.2.11 indicate the importance of matrix diffusion in both pad-scale and regional-scale transport in the Culebra dolomite. As described by Reeves et al. (1987), a diffusion time means that 1000 years is required for contaminant concentration in the center of matrix blocks to reach approximately 68% of the concentration at fracture surfaces. The base-case diffusion time (Figure 4.2.11) is 152 years. Even for diffusion times significantly greater than the base case value, a large benefit is gained from diffusion of non-sorbing contaminants into matrix blocks (Figure 4.2.11). Base-case transport properties were assumed in the calculations summarized in Figure 4.2.11, except for diffusion into matrix blocks.

Thus, the effective transport behavior within the Culebra dolomite for transport between any breach point directly above the WIPP emplacement panels and the boundary of Zone 3, assuming the breach does not disturb the head distribution within the Culebra, appears to be nearly that of an equivalent porous medium having a porosity equal to the sum of matrix plus fracture porosities. Inclusion of the dual-porosity formalism at this scale, given the assumed properties and flow paths, does not change calculated travel times by more than approximately 10%.

The conclusions supported by results shown in Figures 4.2.10 and 4.2.11 only apply directly to calculations assuming the base-case transport and material properties for the Culebra, which are based largely on interpretation of the conservative-tracer test at the H-3 pad (Section 4.2.1.1). Therefore, Reeves et al. (1987) examined the sensitivity of the results to variations in parameters. The relative importance of several transport parameters in regional-scale transport in the Culebra estimated by Reeves et al. (1987) is summarized in Table 4.12. Reeves et al. (1987) define importance in terms of both the sensitivity of calculated behavior to uncertainty in a given parameter and the estimated range of uncertainty of that parameter in the Culebra dolomite at and near the WIPP site. Thus, a highly sensitive parameter that was known with perfect precision would have zero importance. In contrast, a relatively insensitive parameter could be very important if its range of uncertainty was large.

Reeves at al. (1987) conclude that five parameters are most important in controlling "breakthrough" time to the southern boundary of WIPP Zone 3 in the Culebra dolomite. These are: 1) the matrix retardation (K'), where K' is proportional to $(1 + k_d')$ and $k_d'$ is the matrix distribution

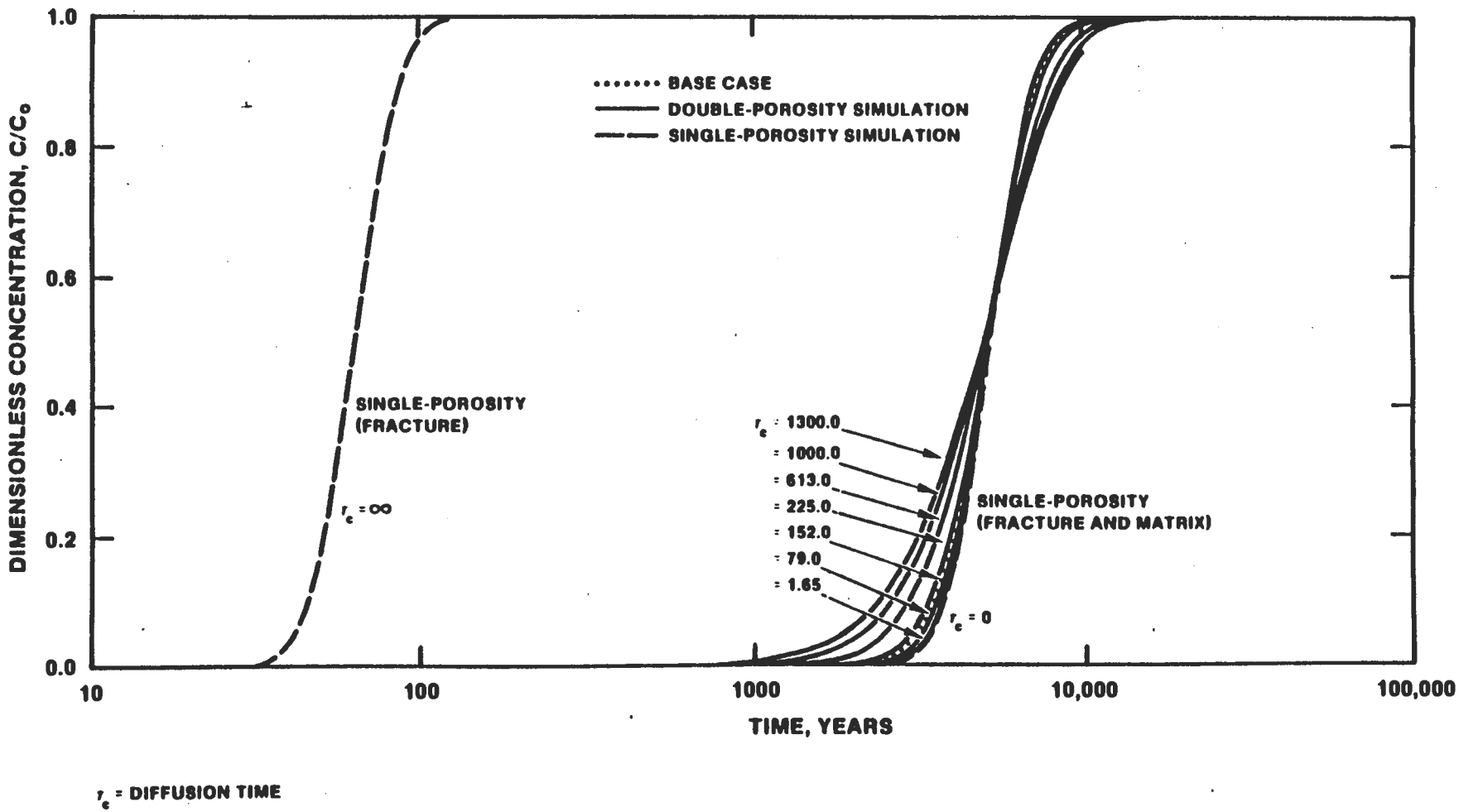


Figure 4.2.11: Estimated effect of variations in diffusion time on breakthrough, otherwise assuming base-case Culebra properties. The diffusion time is the time required for contaminant concentration at the center of matrix blocks to equal approximately 68% of the concentration in fractures. Modified from Figure 4.3 of Reeves et al. (1987).

Table 4.12: Estimated importance of different parameters in regional-scale contaminant transport within the Culebra dolomite. Table 4.5 of Reeves et al. (1987).

| Parameter | Symbol | Sensitivity[a] | Importance Coefficient[a] | Importance Ranking |
|---|---|---|---|---|
| Free water diffusivity | D' | 0.064 | 0.28 | 5 |
| Matrix tortuosity | θ' | 0.064 | 0.19 | 6 |
| Matrix-block length | 2L' | -0.13 | 0.36 | 4 |
| Matrix porosity | ϕ' | 1.1 | 1.58 | 1 |
| Fracture porosity | ϕ | 0.013[b] | 0.13 | 7 |
| Fracture dispersivity | α | -0.17 | 0.43 | 3 |
| Fracture flux | u | -1.1 | 0.86 | 2 |

(a) Results are valid for retardations K' = 1, $1.50 \times 10^2$, $1.49 \times 10^3$, and $1.49 \times 10^5$.
(b) Upper-bound estimate.

coefficient; 2) the effective matrix porosity; 3) the Darcy flux within the fractures (defined as a specific flux $m^3/m^2s$); 4) the dispersivity in the fractures; and 5) the effective matrix-block size. Reeves et al. (1987) conclude that four parameters are relatively unimportant in controlling regional transport within the Culebra. These include: 1) free-water diffusivity; 2) matrix tortuosity; 3) fracture porosity; and 4) retardation in the fractures (not shown in Table 4.12).

The linear dependence of calculated breakthrough time on matrix retardation (K') is indicated in Figure 4.2.12. This behavior also indicates the effective porous-medium behavior on the regional scale, since for an ideal porous medium the dependence of breakthrough time on retardation is strictly linear. Breakthrough to the southern boundary of Zone 3 should not occur within 10,000 years after release for any matrix distribution coefficient ($k_d$) greater than approximately 0.2 mL/g for the assumed base-case Culebra material properties.

Valid use or extrapolation of the results contained in Reeves at al. (1987) depends on the assumptions listed at the beginning of this section, especially the representative character of the base-case transport properties and range of properties used in the calculations. The validity of the results is also dependent on the validity of the transmissivity and head distribution within the Culebra dolomite between the calculated

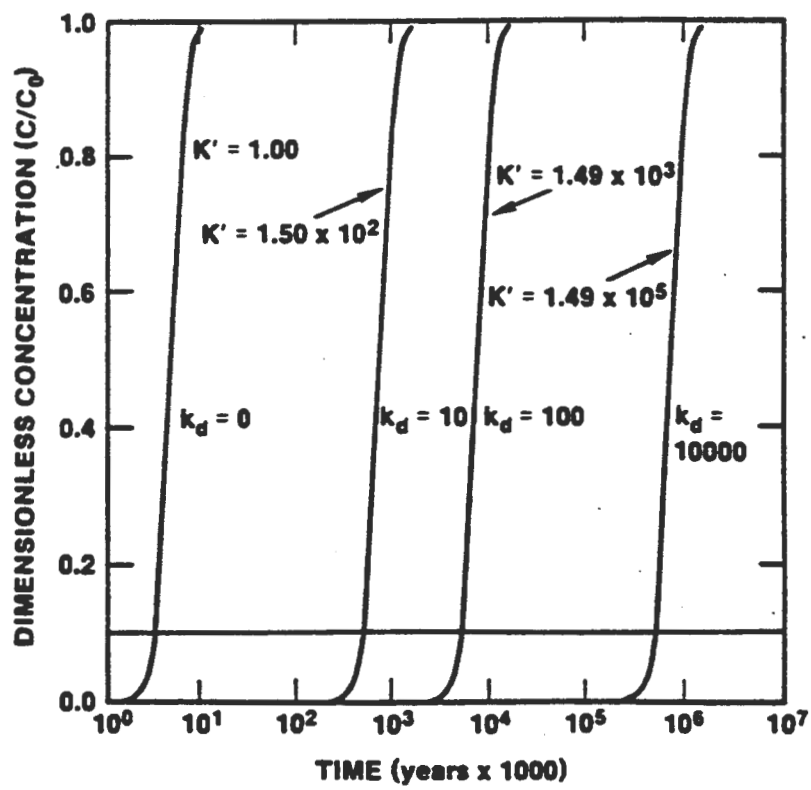


Figure 4.2.12: Variations in calculated breakthrough times to the boundary of WIPP zone 3 as a function of assumed matrix retardation, otherwise assuming base-case material properties. Matrix retardation (K') is proportional to $1 + k_d'$. Therefore, for a matrix distribution coefficient ($k_d'$) of 0, K'=1.0. Slightly modified from Figure 4.1 of Reeves et al. (1987).

release points and the southern boundary of Zone 3. The results of LaVenue et al. (1988) discussed in Section 4.1.3.2 indicate that groundwater and contaminant travel times in the southern part of WIPP Zone 3 may be even slower than calculated by Reeves et al. (1988), so long as flow directions and rates within the Culebra are not affected too greatly by the continuing transient response of the Culebra to the end of the last pluvial period.

Effective matrix diffusion within fractured portions of the Culebra may be possible only because of the relatively slow flow velocities calculated assuming an undisturbed Culebra head distribution. In the event of a brine-reservoir breach of the WIPP facility, the volumes of brine injected from the Castile Formation into the Culebra dolomite might be sufficient to redefine the head distribution within the Culebra, greatly increase hydraulic gradients, and decrease flow times to the accessible environment. Calculations are underway to determine if the dual-porosity formalism is required to evaluate transport within the Culebra under these conditions.

## 4.3 Geochemical Studies in the Rustler Formation and Shallower Units

The hydrologic studies discussed in Section 4.1 and transport studies discussed in Section 4.2 largely ignore both geochemical behavior within the Rustler Formation and the overall geologic behavior of the WIPP site, except for interaction between the Culebra dolomite and trace contaminants. The status and present conclusions of geochemical studies within the Rustler Formation and shallower units are discussed in this section. The results of these studies, summarized by Siegel et al. (1988a), help place constraints on the relationship between the modern geochemistry and flow directions within both the Culebra dolomite and the Rustler Formation as a whole.

Section 4.3.1 describes the status of geochemical studies of major and minor solutes, in which Culebra groundwaters have been divided into four hydrochemical facies that may be diagnostic of natural interactions between Culebra waters and the matrix of the Culebra dolomite. The results, when compared with modern flow directions within the Culebra, indicate that the geochemistry of Culebra fluids is inconsistent with steady-state confined flow.

Section 4.3.2 discusses the expansion of the stable-isotope results and interpretations contained in Lambert (1983) to interpretations contained in Lambert (1987b) and Lambert and Harvey (1987). Stable-isotope studies themselves do not provide any information concerning the absolute ages of groundwaters. The studies can, in some cases, indicate whether different bodies of water were recharged under similar or different climatic conditions. The results of the recent stable-isotope studies indicate that the isotopic composition of Rustler groundwaters at and near the WIPP site is distinct from that of modern meteoric precipitation at similar elevations in the northern Delaware Basin.

Section 4.3.3 summarizes studies examining the lengths of time groundwaters in the Rustler/Salado contact zone, Rustler Formation, and Dewey Lake Red

Beds in the region of the WIPP site may have been isolated from contact with atmospherically derived components such as radiocarbon, tritium, and chlorine-36 (Lambert, 1987a). At the WIPP site, the applicability of such "environmental isotopes," which occur in ultratrace amounts, is unavoidably limited by the variability of the rock types present, as well as by the ages of both rocks and groundwaters. Specifically, no detectable $^{36}Cl$ above background has been detected in Rustler fluids, because of the large chlorine background inherent in fluids which have been involved in dissolution of halite from within the Rustler Formation. Nor have tritium levels significantly above background been identified in Rustler fluids, except in hole WIPP-29, interpreted on other grounds to be contaminated by potash mining. Radiocarbon studies met with only limited success, because the normal techniques used in drilling hydrocarbon-exploration and hydrologic test holes at and near the WIPP have resulted, in many cases, in some contamination with organic materials. The limited number of minimally contaminated radiocarbon results, however, indicate that the Culebra dolomite and part of the Dewey Lake Red Beds at the WIPP site have been isolated from atmospheric carbon sources for at least 12,000 years.

Section 4.3.4 discusses fluid-flow directions and rates within the Culebra dolomite, as interpreted from uranium-disequilibrium studies (Lambert and Carter, 1987). The results provide an effectively independent check of conceptual models derived from other studies. Although the present uranium-disequilibrium data base is limited, allowing considerable uncertainty in flow directions, the results indicate that there must have been a significant change in flow directions within the Culebra dolomite, on a time scale generally consistent with the end of local recharge indicated by radiocarbon studies.

### 4.3.1 Solute Geochemistry and Delineation of Hydrochemical Facies within the Culebra Dolomite

This section summarizes the currently available data and hypotheses (Siegel et al., 1988a) concerning the origin and compositions of waters in the Culebra dolomite. These authors delineate Culebra fluids into various hydrochemical facies, consider the compatibility of these facies with modern flow patterns derived from stratigraphic and hydrologic studies, and examine the interactions of Culebra solutes and host-rock mineralogies. Although Siegel et al. (1988a) emphasize the Culebra, relevant preliminary results of work on fluids from the Magenta dolomite, Rustler/Salado contact zone, and Dewey Lake Red Beds are included. One section of Siegel et al. (1988a), Bodine et al. (1988), was prepared as a summary interpretation of a separate study (Bodine and Jones, 1988), based on an independent data base. Data used in estimation of oxidation potentials (Eh) (Myers et al., 1988) were collected as part of the WIPP Water-Quality Sampling Program.

4.3.1.1 Hydrochemical Facies--The analytical ranges of compositions of Culebra waters and compositions used in calculations contained in Siegel et al. (1988a) are included in Table 4.13; major solutes are listed in Table 4.13a, minor and trace solutes in Table 4.13b. Individual data sets

Table 4.13a: Major solutes and other parameters in analyzed groundwaters from the Culebra, Magenta, Dewey Lake, and Bell Canyon. From Siegel et al. (1988b).

| Well(s) | Collection Date(1) | Lab(2) | Total Dissolved Solids (mg/L)(7) | Ionic Strength (molal)(8) | Bromide (mg/L as Br) | Fluoride (mg/L as F) | Iodide (mg/L as I) | Boron (mg/L as B) | Lithium (mg/L as Li) | Strontium (mg/L as Sr) | Silica (mg/L as $SiO_2$) | Iron (mg/L as Fe) | Manganese (mg/L as Mn) |
|---|---|---|---|---|---|---|---|---|---|---|---|---|---|
| Culebra | | | | | | | | | | | | | |
| DOE-1 | 4/85 | UNC | 131200 | 2.53 | 56 | - | - | 37 | 0.64 | 26 | 8.4 | 0.28 | - |
| DOE-1 | (2) | avg | | | 60 | 1.2 | - | 36 | 0.64 | 21 | - | - | - |
| DOE-1 | (2) | rng | | | 56-64 | 1.0-1.7 | - | 35-37 | (1) | 16-26 | 8-24 | - | - |
| DOE-2 | 3/85 | UNC | 60400 | 1.19 | 34 | 1.7 | 0.22 | 16 | 0.47 | 38 | 17 | 0.036 | 0.30 |
| DOE-2 | (2) | avg | | | 35 | 1.6 | 0.22 | 18 | 0.47 | 29 | - | - | - |
| DOE-2 | (2) | rng | | | 34-36 | 1.2-2.2 | (1) | 14-24 | (1) | 22-38 | 17-24 | - | - |
| H-2A | 4/86 | UNC | 12900 | 0.27 | 5.6 | 2.2 | 0.081 | 10 | 0.22 | 9.5 | 13 | 1.1 | 0.055 |
| H-3B3 | 6/84 | UNC | 55000 | 1.08 | 29 | 2.1 | 0.13 | 30 | 0.53 | 23 | 9.8 | 0.57 | 0.13 |
| H-3B3 | 2/85 | UNC | 55800 | 1.08 | 26 | 1.9 | 0.14 | 26 | 0.40 | 30 | 11 | 0.20 | 0.12 |
| H-3B2, H3B3 | (4) | avg | | | 31 | 1.8 | 0.14 | 28 | 0.41 | 25 | - | - | - |
| H-3B2, H3B3 | (4) | rng | | | 26-39 | 1.5-2.1 | 0.13-0.14 | 21-34 | 0.30-0.53 | 23-30 | 9-20 | - | - |
| H-4B | 5/81 | UNC | 21700 | 0.46 | 42 | - | - | 18 | 0.39 | 14 | 11 | - | - |
| H-4C | 8/84 | UNC | 21200 | 0.45 | 48 | 2.1 | 0.23 | 20 | 0.49 | 18 | 13 | 2.2 | 0.20 |
| H-4B | 7/85 | UNC | 20200 | 0.42 | 43 | 2.7 | - | 14 | 0.40 | 14 | 14 | 0.32 | 0.11 |
| H-4B, H-4C | (4) | avg | | | 44 | 2.2 | 0.23 | 18 | 0.42 | 15 | - | - | - |
| H-4B, H-4C | (4) | rng | | | 43-48 | 1.7-2.7 | (1) | 14-23 | 0.39-0.49 | 13-18 | 11-30 | - | - |
| H-5B | 6/81 | UNC | 154400 | 2.99 | 62 | - | - | 33 | 0.77 | 32 | 6.2 | - | - |
| H-5C | 10/81 | UNC | 154500 | 3.00 | 64 | - | - | 35 | 0.77 | 31 | 5.8 | - | - |
| H-5B | 8/85 | UNC | 152600 | 2.97 | 49 | 2.0 | 0.19 | 34 | 0.81 | 29 | 7.1 | 2.9 | 0.29 |
| H-5B, H-5C | (4) | avg | | | 58 | 1.3 | 0.19 | 33 | 0.78 | 31 | - | - | - |
| H-5B, H-5C | (4) | rng | | | 49-64 | 0.8-2.0 | (1) | 29-35 | 0.77-0.81 | 29-32 | 5-36 | - | - |
| H-6B | 5/81 | UNC | 59300 | 1.18 | 34 | - | - | 11 | 0.44 | 32 | 20 | - | - |
| H-6B | 9/85 | UNC | 57400 | 1.13 | 34 | 1.9 | 0.096 | 10 | 0.45 | 30 | 18 | 0.094 | 0.13 |
| H-6B | (3) | avg | | | 34 | 1.6 | 0.096 | 9.5 | 0.44 | 28 | - | - | - |
| H-6B | (3) | rng | | | 34-35 | 1.3-1.9 | (1) | 7-11 | 0.44-0.45 | 24-32 | 18-43 | - | - |

Table 4.13a: Major solutes and other parameters in analyzed groundwaters from the Culebra, Magenta, Dewey Lake, and Bell Canyon. From Siegel et al. (1988b). (Continued)

| Well(s) | Collection Date(1) | Lab(2) | Total Dissolved Solids (mg/L)(7) | Ionic Strength (molal)(8) | Bromide (mg/L as Br) | Fluoride (mg/L as F) | Iodide (mg/L as I) | Boron (mg/L as B) | Lithium (mg/L as Li) | Strontium (mg/L as Sr) | Silica (mg/L as $SiO_2$) | Iron (mg/L as Fe) | Manganese (mg/L as Mn) |
|---|---|---|---|---|---|---|---|---|---|---|---|---|---|
| H-7B1 | 3/86 | UNC | 3220 | 0.089 | 0.57 | 1.5 | 0.052 | 0.76 | 0.10 | 8.5 | 47 | 0.056 | 0.050 |
| H-7B1 | (3) | avg | | | 0.57 | 1.4 | 0.052 | 0.77 | 0.11 | 7.7 | - | - | - |
| H-7B1 | (3) | rng | | | (1) | 1.2-1.5 | (1) | 0.34-0.80 | 0.10-0.12 | 5.8-8.7 | 47-92 | - | - |
| H-8B | 1/86 | UNC | 2830 | 0.083 | 0.085 | 2.5 | 0.14 | 0.48 | 0.12 | 6.9 | 29 | 0.036 | 0.021 |
| H-8B | (2) | avg | | | 0.085 | 2.4 | 0.14 | 0.49 | 0.12 | 6.7 | - | - | - |
| H-8B | (2) | rng | | | (1) | 2.1-2.5 | (1) | 0.48-0.50 | 0.12 | 5.9-7.4 | 29-56 | - | - |
| H-9B | 11/85 | UNC | 3080 | 0.087 | 0.24 | 3.3 | 0.11 | 0.63 | 0.18 | 7.5 | 27 | 0.032 | 0.015 |
| H-9B | (2) | avg | | | 0.24 | 3.0 | 0.11 | 0.66 | 0.18 | 7.2 | - | - | - |
| H-9B | (2) | rng | | | (1) | 2.6-3.3 | (1) | 0.63-0.70 | 0.17-0.18 | 7.0-7.5 | 27-39 | - | - |
| H-10B | 3/80 | GS | 65700 | 1? | - | 1.3 | - | 13 | - | - | 1.5 | - | - |
| H-11B3 | 6/85 | UNC | 117400 | 2.23 | 47 | - | - | 32 | 0.62 | 25 | - | 0.14 | 0.22 |
| H-11B3 | (2) | avg | | | 48 | 1.3 | - | 31 | 0.50 | 20 | - | - | - |
| H-11B3 | (2) | rng | | | 47-48 | 1.0-1.6 | - | 30-32 | 0.38-0.62 | 18-25 | 25-32 | - | - |
| H-12 | 8/85 | UNC | 140500 | 2.72 | 76 | - | - | 39 | 1.2 | 31 | 7.2 | 0.22 | 0.087 |
| H-12 | (2) | avg | | | 76 | 1.5 | - | 38 | 0.85 | 29 | - | - | - |
| H-12 | (2) | rng | | | 76-77 | 1.1-2.3 | - | 35-39 | 0.61-1.2 | 18-38 | 7-96 | - | - |
| P-14 | 2/86 | UNC | 24900 | 0.58 | 72 | 1.7 | 0.42 | 0.72 | 0.28 | 51 | 30 | 2.0 | 0.18 |
| P-14 | (2) | avg | | | 72 | 1.5 | 0.42 | 0.72 | 0.28 | 50 | - | - | - |
| P-14 | (2) | rng | | | (1) | 1.2-1.7 | (1) | (1) | (1) | 48-51 | 30-69 | - | - |
| P-17 | 3/86 | UNC | 86500 | 1.67 | 72 | 1.9 | 0.18 | 38 | 0.87 | 29 | 8.5 | 4.0 | 0.87 |
| P-17 | (2) | avg | | | 70 | 1.6 | 0.18 | 35 | 0.87 | 31 | - | - | - |
| P-17 | (2) | rng | | | 69-72 | 1.2-1.9 | (1) | 32-38 | (1) | 28-36 | 0-8.5 | - | - |
| P-18 | 10/77 | GS | 118300 | 2.5? | - | 1.2 | - | 100 | - | - | 1.0 | - | - |

Table 4.13a: Major solutes and other parameters in analyzed groundwaters from the Culebra, Magenta, Dewey Lake, and Bell Canyon. From Siegel et al. (1988b). (Continued)

| Well(s) | Collection Date(1) | Lab(2) | Total Dissolved Solids (mg/L)(7) | Ionic Strength (molal)(8) | Bromide (mg/L as Br) | Fluoride (mg/L as F) | Iodide (mg/L as I) | Boron (mg/L as B) | Lithium (mg/L as Li) | Strontium (mg/L as Sr) | Silica (mg/L as $SiO_2$) | Iron (mg/L as Fe) | Manganese (mg/L as Mn) |
|---|---|---|---|---|---|---|---|---|---|---|---|---|---|
| WIPP-13 | 2/87 | avg | - | - | 39 | 1.4 | - | 11 | 0.35 | 25 | - | - | - |
| WIPP-25 | 8/80 | UNC | 12100 | 0.26 | 2.6 | - | - | 1.5 | 0.20 | 12 | 34 | - | - |
| WIPP-25 | 8/80 | avg | | | 2.6 | - | - | 1.5 | 0.20 | 12 | - | - | - |
| WIPP-25 | 8/80 | rng | | | (2) | - | - | (1) | (1) | (1) | (1) | - | - |
| WIPP-25 | 2/86 | UNC | 13600 | - | 3.4 | 1.7 | 0.042 | 1.7 | 0.22 | 17 | 33 | 0.50 | 0.11 |
| WIPP-25 | 2/86 | avg | | | 3.8 | 1.6 | 0.042 | 1.7 | 0.22 | 17 | - | - | - |
| WIPP-25 | 2/86 | rng | | | 3.4-4.2 | 1.6-1.7 | (1) | 1.7 | (1) | (1) | 33-67 | - | - |
| WIPP-26 | 8/80 | UNC | 15100 | 0.33 | 3.2 | - | - | 1.4 | 0.24 | 17 | 33 | - | - |
| WIPP-26 | 8/80 | avg | | | 3.2 | - | - | 1.4 | 0.24 | 17 | - | - | - |
| WIPP-26 | 8/80 | rng | | | (1) | - | - | (1) | (1) | (1) | (1) | - | - |
| WIPP-26 | 11/85 | UNC | 17600 | 0.37 | 3.9 | 1.7 | 0.070 | 1.6 | 0.23 | 20 | 35 | 0.026 | <0.01 |
| WIPP-26 | 11/85 | avg | | | 3.9 | 1.5 | 0.070 | 1.6 | 0.23 | 18 | - | - | - |
| WIPP-26 | 11/85 | rng | | | (1) | 1.3-1.7 | (1) | (1) | (1) | 17-20 | 35-65 | - | - |
| WIPP-27 | 9/80 | UNC | 134700 | 2.57 | 28 | - | - | 2.3 | 0.33 | 51 | 23 | - | - |
| WIPP-27 | (2) | avg | | | 28 | - | - | 2.1 | 0.33 | 51 | - | - | - |
| WIPP-27 | (2) | rng | | | (1) | - | - | 1.9-2.3 | (1) | (1) | 13-23 | - | - |
| WIPP-28 | 9/80 | UNC | 46600 | 0.90 | 7.2 | - | - | 5.8 | 0.30 | 16 | 36 | - | - |
| WIPP-28 | 9/80 | avg | | | 7.2 | - | - | 5.8 | 0.30 | 16 | - | - | - |
| WIPP-28 | | rng | | | (1) | - | - | (1) | (1) | (1) | (1) | - | - |
| WIPP-29 | 8/80 | UNC | 245400 | 4.91 | 45 | - | - | 4.4 | 0.78 | 29 | 22 | - | - |
| WIPP-29 | 8/80 | avg | | | 45 | - | - | 4.4 | 0.78 | 29 | - | - | - |
| WIPP-29 | 8/80 | rng | | | (1) | | | (1) | (1) | (1) | (1) | - | - |
| WIPP-29 | 12/85 | UNC | 324100 | 6.57 | 61 | 4.6 | 0.38 | 5.2 | 0.70 | 13 | 15 | 1.1 | 1.7 |
| WIPP-29 | 12/85 | avg | | | 61 | - | 0.38 | 5.5 | 0.70 | 11 | - | - | - |
| WIPP-29 | 12/85 | rng | | | (1) | 0.9-4.6 | (1) | 5.2-5.8 | (1) | 9-13 | 15-110 | - | - |
| WIPP-30 | 9/80 | UNC | 29100 | 0.58 | 10 | - | - | 6.1 | 0.27 | 18 | 6.5 | - | - |
| WIPP-30 | 9/80 | avg | | | 10 | - | - | 6.1 | 0.27 | 18 | - | - | - |
| WIPP-30 | 9/80 | rng | | | (1) | | | (1) | (1) | (1) | (1) | - | - |

Table 4.13a: Major solutes and other parameters in analyzed groundwaters from the Culebra, Magenta, Dewey Lake, and Bell Canyon. From Siegel et al. (1988b). (Concluded)

| Well(s) | Collection Date(1) | Lab(2) | Total Dissolved Solids (mg/L)(7) | Ionic Strength (molal)(8) | Bromide (mg/L as Br) | Fluoride (mg/L as F) | Iodide (mg/L as I) | Boron (mg/L as B) | Lithium (mg/L as Li) | Strontium (mg/L as Sr) | Silica (mg/L as $SiO_2$) | Iron (mg/L as Fe) | Manganese (mg/L as Mn) |
|---|---|---|---|---|---|---|---|---|---|---|---|---|---|
| Engle | 3/85 | UNC | 3270 | 0.09 | 0.27 | 2.8 | 0.12 | 0.97 | 0.17 | 8.4 | 29 | 0.59 | 0.060 |
| Engle | 3/85 | avg | | | 0.27 | 2.8 | 0.12 | 0.87 | 0.17 | 7.7 | - | - | - |
| Engle | 3/85 | rng | | | (1) | 2.8-2.9 | (1) | 0.77-0.97 | (1) | 7.0-8.4 | 29-54 | - | - |
| Magenta | | | | | | | | | | | | | |
| H-3B1 | 7/85 | UNC | 8560 | - | 5.8 | 2.4 | 1.2 | 2.0 | 0.32 | 17 | 10 | 0.11 | 0.028 |
| H-3B1 | (3) | rng | | | 5.8-6.0 | 1.8-2.6 | 1.2-2.0 | 2.0-4.5 | 0.32 | 13-18 | 10-26 | - | - |
| H-4C | 11/86 | UNC | 23900 | - | 5.9 | 2.4 | 0.31 | 12 | 0.46 | 12 | 9.1 | 0.71 | 0.29 |
| H-4C | (2) | rng | | | 5.9-7.5 | 2.2-2.6 | (1) | 11-12 | 0.41-0.46 | 12-14 | 9-26 | - | - |
| H-5C | 10/86 | UNC | 6980 | - | 0.93 | 2.5 | 0.31 | 11 | 0.20 | 10 | 11 | 1.5 | 0.020 |
| H-5C | 10/86 | rng | | | (1) | 2.5 | (1) | 10-11 | 0.20 | 8-10 | 11-26 | - | - |
| H-6C | 10/86 | UNC | 4540 | - | 2.3 | 1.5 | 0.086 | 2.2 | 0.21 | 9.8 | 11 | 0.26 | 0.010 |
| H-6C | 10/86 | rng | | | 1.0-2.3 | 1.5-1.7 | (1) | 2.2-2.4 | 0.19-0.21 | 7.1-9.8 | 11-28 | - | - |
| Dewey Lake Red Beds | | | | | | | | | | | | | |
| Ranch | 6/86 | UNC | 2520 | - | 2.3 | 0.82 | 0.13 | 0.10 | 0.12 | 5.9 | 52 | 0.024 | <0.01 |
| Ranch | 6/86 | rng | | | 2.3 | 0.8-1.0 | (1) | 0.10-0.19 | (1) | 3.2-5.9 | 52-86 | - | - |
| Twin-Pasture | 1/86 | UNC | 401 | - | 0.17 | 0.58 | <0.01 | 0.13 | <0.05 | 1.1 | 47 | <0.01 | <0.01 |
| Twin-Pasture | 1/86 | rng | | | (1) | 0.5-1.4 | (1) | 0.13-0.16 | (1) | 0.6-1.1 | 47-90 | - | - |
| Bell Canyon Frm. | | | | | | | | | | | | | |
| DOE-2 | 7/85 | UNC | 149500 | - | 250 | 1.1 | 6.4 | 54 | 5.8 | 150 | 2.5 | 11 | 28 |
| DOE-2 | 7/85 | rng | | | (1) | 0.4-1.4 | 6.4-7.9 | 54-61 | 2.8-5.8 | 150-300 | 2-30 | - | - |

Table 4.13b: Minor and trace solutes and other parameters in analyzed groundwaters from the Culebra, Magenta, Dewey Lake, and Bell Canyon. From Siegel et al. (1988b).

| Well(s) | Collection Date(1) | Lab(2) | Zone(3) | Sodium (mg/L as Na) | Potassium (mg/L as K) | Calcium (mg/L as Ca) | Magnesium (mg/L as Mg) | Chloride (mg/L as Cl) | Sulfate (mg/L as $SO_4$) | Bicarbonate (mg/L as $HCO_3$)(4) | $pCO_2$(5) | pH(4) |
|---|---|---|---|---|---|---|---|---|---|---|---|---|
| Culebra | | | | | | | | | | | | |
| DOE-1 | 4/85 | UNC | A | 45800 | 1100 | 1730 | 1610 | 73600 | 7350 | 45 | -2.60 | 7.1 |
| DOE-1 | (2) | avg | A | 46000 | 1100 | 1700 | 1600 | 75000 | 7400 | - | | - |
| DOE-1 | (2) | rng | A | 45000-46000 | (1) | (1) | (1) | 73000-77000 | (1) | 45-46 | | 7.1 |
| DOE-2 | 3/85 | UNC | C | 18400 | 410 | 1960 | 1060 | 34600 | 3950 | 67 | -2.33 | 7.0 |
| DOE-2 | (2) | avg | C | 18000 | 420 | 1900 | 1000 | 33000 | 3700 | - | | - |
| DOE-2 | (2) | rng | C | 17000-19000 | 410-420 | 1900-2000 | 900-1100 | 32000-35000 | 3400-4000 | (1) | | (1) |
| H-2A | 4/86 | UNC | C | 3570 | 93.5 | 743 | 167 | 5310 | 2980 | 57 | -3.38 | 8.0 |
| H-3B3 | 6/84 | UNC | C | 17400 | 495 | 1550 | 829 | 29500 | 5130 | - | -2.83 | 7.4 |
| H-3B3 | 2/85 | UNC | C | 18000 | 425 | 1470 | 783 | 30300 | 4820 | 52 | -2.86 | 7.4 |
| H-3B2, H-3B3 | (4) | avg | C | 18000 | 440 | 1400 | 760 | 29000 | 4800 | - | | - |
| H-3B2, H-3B3 | (4) | rng | C | 17000-19000 | 360-500 | 1200-1600 | 690-830 | 27000-31000 | 4600-5200 | 50-52 | | 7.4 |
| H-4B | 5/81 | UNC | C | 6080 | 215 | 700 | 455 | 7980 | 6230 | 71 | -3.35 | 8.0 |
| H-4C | 8/84 | UNC | C | 6150 | 222 | 698 | 505 | 7950 | 5700 | 75 | -3.11 | 7.8 |
| H-4B | 7/85 | UNC | C | 5850 | 210 | 691 | 427 | 7480 | 5520 | 69 | -3.04 | 7.7 |
| H-4B, H-4C | (4) | avg | C | 6000 | 220 | 690 | 450 | 7700 | 5700 | - | | - |
| H-4B, H-4C | (4) | rng | C | 5800-6200 | 180-260 | 690-700 | 400-510 | 7400-8000 | 5500-6300 | 68-75 | | 7.6-8.0 |
| H-5B | 6/81 | UNC | A | 52400 | 1290 | 1710 | 2140 | 89500 | 7360 | 80 | -3.21 | 7.9 |
| H-5C | 10/81 | UNC | A | 52300 | 1300 | 1720 | 2150 | 89500 | 7570 | 86 | -3.17 | 7.9 |
| H-5B | 8/85 | UNC | A | 54100 | 1350 | 1700 | 2170 | 85400 | 7840 | 50 | -2.86 | 7.4 |
| H-5B, H-5C | (4) | avg | A | 53000 | 1300 | 1700 | 2200 | 87000 | 7600 | - | | - |
| H-5B, H-5C | (4) | rng | A | 52000-55000 | 1200-1400 | 1700-1800 | 2100-2200 | 84000-90000 | 7300-7900 | - | | - |
| H-6B | 5/81 | UNC | C | 18600 | 450 | 2150 | 1080 | 33000 | 3980 | 96 | -2.16 | 7.0 |
| H-6B | 9/85 | UNC | C | 18000 | 375 | 2040 | 1040 | 32300 | 3570 | 94 | -2.07 | 6.9 |
| H-6B | (3) | avg | C | 18000 | 420 | 2000 | 1100 | 33000 | 3600 | - | | - |
| H-6B | (3) | rng | C | 17000-19000 | 370-450 | 1900-2200 | 1000-1200 | 32000-34000 | 3300-4000 | 90-96 | | 6.9-7.2 |

Table 4.13b: Minor and trace solutes and other parameters in analyzed groundwaters from the Culebra, Magenta, Dewey Lake, and Bell Canyon. From Siegel et al. (1988b). (Continued)

| Well(s) | Collection Date(1) | Lab(2) | Zone(3) | Sodium (mg/L as Na) | Potassium (mg/L as K) | Calcium (mg/L as Ca) | Magnesium (mg/L as Mg) | Chloride (mg/L as Cl) | Sulfate (mg/L as $SO_4$) | Bicarbonate (mg/L as $HCO_3$)(4) | $pCO_2$(5) | pH(4) |
|---|---|---|---|---|---|---|---|---|---|---|---|---|
| H-7B1 | 3/86 | UNC | B | 207 | 7.0 | 587 | 130 | 320 | 1850 | 120 | -2.20 | 7. |
| H-7B1 | (3) | avg | B | 210 | 7.0 | 570 | 130 | 320 | 1800 | - | | - |
| H-7B1 | (3) | rng | B | 200-210 | 7.0 | 540-590 | 130 | 300-350 | 1700-1900 | 120 | | 7.3-7.4 |
| H-8B | 1/86 | UNC | B | 55.1 | 3.83 | 548 | 157 | 30.5 | 1950 | 96 | -2.70 | 7.3 |
| H-8B | (2) | avg | B | 54 | 3.9 | 540 | 170 | 32 | 1800 | - | | - |
| H-8B | (2) | rng | B | 51-56 | 3.7-4.1 | 520-550 | 150-180 | 30-33 | 1600-2000 | 93-96 | | 7.2-7.3 |
| H-9B | 11/85 | UNC | B | 146 | 6.85 | 590 | 137 | 194 | 1900 | 110 | -2.43 | 7.4 |
| H-9B | (2) | avg | B | 150 | 7.2 | 580 | 150 | 190 | 1800 | - | | - |
| H-9B | (2) | rng | B | 140-150 | 6.8-7.6 | 560-620 | 130-170 | 170-200 | 1700-1900 | 110 | | 7.3-7.4 |
| H-10B | 3/80 | GS | C | 21000 | 520 | 1600 | 1000 | 36000 | 5600 | 45 | - | 8.3 |
| H-11B3 | 6/85 | UNC | A | 40400 | 943 | 1700 | 1320 | 65900 | 7180 | 54 | -2.63 | 7.2 |
| H-11B3 | (2) | avg | A | 39000 | 940 | 1600 | 1300 | 66000 | 7200 | - | | - |
| H-11B3 | (2) | rng | A | 37000-41000 | (1) | 1500-1700 | 1300-1400 | 65000-67000 | (1) | 54-55 | | 7.2-7.3 |
| H-12 | 8/85 | UNC | A | 49200 | 1270 | 1760 | 1980 | 79000 | 7210 | 53 | -2.61 | 7.2 |
| H-12 | (2) | avg | A | 50000 | 1300 | 1800 | 2000 | 80000 | 7200 | - | | - |
| H-12 | (2) | rng | A | 49000-51000 | (1) | 1700-1900 | 1900-2000 | 78000-80000 | (1) | 53-62 | | 7.2 |
| P-14 | 2/86 | UNC | C | 4360 | 37.9 | 3520 | 840 | 14500 | 1590 | 110 | -1.81 | 6.8 |
| P-14 | (2) | avg | C | 4100 | 41 | 3700 | 800 | 14000 | 1600 | - | | - |
| P-14 | (2) | rng | C | 3700-4400 | 37-45 | 3500-3900 | 760-840 | 13000-15000 | 1500-1700 | 100-110 | | 6.8-6.9 |
| P-17 | 3/86 | UNC | C | 28300 | 782 | 1620 | 1460 | 48200 | 6020 | 64 | -2.90 | 7.5 |
| P-17 | (2) | avg | C | 28000 | 820 | 1600 | 1500 | 49000 | 6000 | - | | - |
| P-17 | (2) | rng | C | 28000-29000 | 780-880 | 1500-1700 | 1400-1600 | 48000-51000 | 5900-6100 | 61-64 | | 7.5 |
| P-18 | 10/77 | GS | A | 9200 | 6200 | 5600 | 16000 | 80000 | 980 | 310 | - | 7.2 |

Table 4.13b: Minor and trace solutes and other parameters in analyzed groundwaters from the Culebra, Magenta, Dewey Lake, and Bell Canyon. From Siegel et al. (1988b). (Continued)

| Well(s) | Collection Date(1) | Lab(2) | Zone(3) | Sodium (mg/L as Na) | Potassium (mg/L as K) | Calcium (mg/L as Ca) | Magnesium (mg/L as Mg) | Chloride (mg/L as Cl) | Sulfate (mg/L as $SO_4$) | Bicarbonate (mg/L as $HCO_3$)(4) | $pCO_2$(5) | pH(4) |
|---|---|---|---|---|---|---|---|---|---|---|---|---|
| WIPP-13 | 2/87 | avg | C | 19000 | 340 | - | - | 36000 | 4500 | ~120 | - | ~6.6 |
| WIPP-25 | 8/80 | UNC | C | 3160 | 73.5 | 905 | 260 | 5250 | 2500 | 210 | -1.69 | 6.9 |
| WIPP-25 | 8/80 | avg | C | 3200 | 74 | 900 | 260 | 5200 | 2500 | - | | - |
| WIPP-25 | 8/80 | rng | C | (1) | (1) | (1) | (1) | 5200-5300 | (1) | (1) | | (1) |
| WIPP-25 | 2/86 | UNC | C | 3180 | 102 | 1140 | 315 | 6320 | 2380 | 130 | - | 7.2 |
| WIPP-25 | 2/86 | avg | C | 3300 | 100 | 1100 | 330 | 6200 | 2400 | - | | - |
| WIPP-25 | 2/86 | rng | C | 3100-3400 | 100-110 | 1100-1200 | 310-340 | 6200-6400 | 2300-2400 | (1) | | (1) |
| WIPP-26 | 8/80 | UNC | C | 3620 | 170 | 1240 | 355 | 7200 | 2480 | 140 | -1.86 | 6.9 |
| WIPP-26 | 8/80 | avg | C | 3600 | 170 | 1200 | 360 | 7000 | 2500 | - | | - |
| WIPP-26 | 8/80 | rng | C | (1) | (1) | (1) | (1) | 6900- | (1) | (1) | | 6.9 |
| WIPP-26 | 11/85 | UNC | C | 4220 | 343 | 1340 | 380 | 8770 | 2420 | 120 | -2.14 | 7.1 |
| WIPP-26 | 11/85 | avg | C | 4100 | 350 | 1300 | 390 | 8600 | 2400 | - | | - |
| WIPP-26 | 11/85 | rng | C | 3800-4300 | 340-360 | 1200-1400 | 370-430 | 8400-8800 | 2300-2500 | (1) | | (1) |
| WIPP-27 | 9/80 | UNC | D | 39200 | 8060 | 3210 | 1900 | 78500 | 3830 | 120 | -1.33 | 6.4 |
| WIPP-27 | (2) | avg | D | 39000 | 8100 | 3200 | 2000 | 78000 | 3900 | - | | - |
| WIPP-27 | (2) | rng | D | 39000-40000 | (1) | 3100-3300 | 1900-2000 | 77000-79000 | 3800-3900 | (1) | | 6.4 |
| WIPP-28 | 9/80 | UNC | C | 15200 | 485 | 1180 | 555 | 24800 | 4380 | - | -0.76 | 6.5 |
| WIPP-28 | 9/80 | avg | C | 15000 | 480 | 1200 | 560 | 24000 | 4400 | - | | - |
| WIPP-28 | 9/80 | rng | C | (1) | (1) | (1) | (1) | 24000-25000 | (1) | - | | - |
| WIPP-29 | 8/80 | UNC | D | 71400 | 15600 | 950 | 5480 | 138000 | 14000 | 210 | -0.87 | 6.1 |
| WIPP-29 | 8/80 | avg | D | 71000 | 16000 | 880 | 5600 | 140000 | 14000 | - | | - |
| WIPP-29 | 8/80 | rng | D | (1) | (1) | 810-950 | 5400-5700 | 130000-140000 | 13000-14000 | (1) | | 6.1 |
| WIPP-29 | 12/85 | UNC | D | 94900 | 23300 | 413 | 6500 | 179000 | 20000 | 160 | -0.75 | 5.9 |
| WIPP-29 | 12/85 | avg | D | 92000 | 22000 | 410 | 6400 | 180000 | 18000 | - | | - |
| WIPP-29 | 12/85 | rng | D | 90000-95000 | 20000-24000 | (1) | 6300-6500 | 179000-180000 | 17000-20000 | (1) | | (1) |

Table 4.13b: Minor and trace solutes and other parameters in analyzed groundwaters from the Culebra, Magenta, Dewey Lake, and Bell Canyon. From Siegel et al. (1988b). (Concluded)

| Well(s) | Collection Date(1) | Lab(2) | Zone(3) | Sodium (mg/L as Na) | Potassium (mg/L as K) | Calcium (mg/L as Ca) | Magnesium (mg/L as Mg) | Chloride (mg/L as Cl) | Sulfate (mg/L as $SO_4$) | Bicarbonate (mg/L as $HCO_3$)(4) | $pCO_2$(5) | pH(4) |
|---|---|---|---|---|---|---|---|---|---|---|---|---|
| WIPP-30 | 9/80 | UNC | C | 8570 | 255 | 1140 | 460 | 14600 | 4120 | 40 $HCO_3$ | -4.41 | 8.8 |
| WIPP-30 | 9/80 | avg | C | 8600 | 260 | 1100 | 460 | 15000 | 4100 | 17 $CO_3$ | | - |
| WIPP-30 | 9/80 | rng | C | (1) | (1) | (1) | (1) | 14000-15000 | (1) | (1) | | (1) |
| Engle | 3/85 | UNC | B | 200 | 5.60 | 588 | 152 | 231 | 1990 | 110 | -2.44 | 7.4 |
| Engle | 3/85 | avg | B | 190 | 5.5 | 580 | 140 | 230 | 1900 | - | | - |
| Engle | 3/85 | rng | B | 180-200 | 5.4-5.6 | 570-590 | 130-160 | 220-240 | 1800-2000 | (1) | | (1) |
| Magenta | | | | | | | | | | | | |
| H-3B1 | 7/85 | UNC | Mag | 1520 | 34.5 | 1000 | 292 | 3360 | 2310 | 47 | - | 8.0 |
| H-3B1 | (3) | rng | Mag | 1500-1600 | 34-36 | 1000 | 270-300 | 3300-3400 | 2200-2400 | 45-47 | | 7.7-8.0 |
| H-4C | 11/86 | UNC | Mag | 7110 | 85.1 | 651 | 411 | 8460 | 7100 | 70 | - | 8.4 |
| H-4C | (2) | rng | Mag | 7100-7300 | 85-99 | 610-660 | 390-420 | 8400-8500 | (1) | 70-85 | | 8.1-8.4 |
| H-5C | 10/86 | UNC | Mag | 1480 | 33.6 | 550 | 173 | 1070 | 3620 | 56 | - | 8.0 |
| H-5C | 10/86 | rng | Mag | 1400-1500 | (1) | (1) | 170-190 | 1000-1100 | (1) | (1) | | (1) |
| H-6C | 10/86 | UNC | Mag | 642 | 16.6 | 546 | 160 | 428 | 2700 | 51 | - | 7.7 |
| H-6C | 10/86 | rng | Mag | (1) | (1) | (1) | 160-170 | 420-430 | 2400-2700 | (1) | | (1) |
| Ranch | 6/86 | UNC | DL | 200 | 4.0 | 420 | 202 | 418 | 1100 | 220 | - | 7.0 |
| Ranch | 6/86 | rng | DL | 180-200 | 3.6-4.0 | (1) | 190-210 | 390-420 | 920-1100 | (1) | | (1) |
| Dewey Lake Red Beds | | | | | | | | | | | | |
| Twin-Pasture | 1/86 | UNC | DL | 25.4 | 3.85 | 80.4 | 22.5 | 44.1 | 75.1 | 230 | - | 7.8 |
| Twin-Pasture | 1/86 | rng | DL | 24-26 | 3.7-4.3 | 80-81 | 22-25 | 44-47 | 70-76 | (1) | | (1) |
| Bell Canyon | | | | | | | | | | | | |
| DOE-2 | 7/85 | UNC | BC | 49600 | 885 | 5910 | 1330 | 89700 | 2020 | 48 | - | 6.8 |
| DOE-2 | 7/85 | rng | BC | (1) | (1) | (1) | (1) | 89000-90000 | (1) | (lab) | | (1) |

Footnotes for Tables 4.13a and 4.13b

*Solute values from various labs have been rounded as follows:

| | |
|---|---|
| -Na, K, Ca, Mg, CL, $SO_4$ from UNC | : 3 significant figures |
| -all others from UNC | : 2 sig. figs |
| -all solutes from GS | : 2 sig. figs |
| -all "avg" values | : 2 sig. figs |
| -all minimum 'rng' values | : down to 2 sig. figs |
| -all maximum 'rng' values | : up to 2 sig. figs |
| -all total dissolved solids (TDS) | : to nearest 100 mg/L or to 3 sig. figs (for TDS<10000) |
| -all bicarbonate values | : to 2 sig. figs |
| -all pH values | : to 0.1 pH unit |
| -all $pCO_2$ values | : to 0.01 unit |
| -all ionic strength values | : to 0.01 molal |

(1) Collection date: a number in parentheses indicates that values in that row are averages or ranges of data for up to that number of samples

(2) avg - average of one or more values from one or more laboratories; used to calculate element ratios and generate contour plots (Siegel and others, 1988)
rng - range of values from one or more laboratories; gives a crude estimate of the uncertainties associated with the data. A single value in the range row means that all values were indentical. A "(1)" in the range row means that only one reliable value was available
GS - USGS Central labs
UNC - UNC Geotech (before Oct. 1, 1986, Bendix Field Engineering Corp.), Grand Junction, Co.

(3) zone - hydrochemical facies zone described by Siegel and others (1988). Applies only to Culebra.

(4) Bicarbonate and pH values were measured in the field when the samples were collected. (Exception: $HCO_3$ in the DOE-2 Bell Canyon sample was measured in the lab)

(5) $pCO_2$ - calculated using PHRQPITZ (Siegel and others, 1988)

(6) Stratigraphic horizon: BC - Bell Canyon Formation
DL - Dewey Lake Red Beds
Mag - Magenta Dolomite

(7) Total dissolved solids - calculated by summing the major solutes

(8) Ionic strength - calculated using PHRQPITZ (Siegel and others, 1988)

evaluated in compiling the table and methods for evaluating the data are discussed in Robinson (1988), Lambert and Harvey (1987), and Siegel et al. (1988b). The data in Tables 4.13a and 4.13b were used by Siegel et al. (1988a) in facies assignments of Culebra fluids, saturation-index calculations, and factor analyses, as well as in plotting of element-ratio contours.

On the basis of the available major-solute analyses (Table 4.13a), Culebra waters can be combined into four hydrochemical facies (Figure 4.3.1). These include:

1. Zone A (H-5, H-11, H-12; DOE-1, P-17, P-18(?)), containing saline NaCl brines (about 2 to 3 molal) with a Ca/Mg weight ratio near unity. These waters are found in the eastern third of the WIPP site and further east, in a region roughly coincident with the region of lowest Culebra transmissivity. In the western part of Zone A, halite is present only in the unnamed lower member (Figure 1.5); in the eastern part of the zone, halite is present throughout the Rustler.

2. Zone B (H-7, H-8, H-9, Engle), containing relatively fresh waters (<0.1 molal) in which $Ca^{++}$ and $SO_4^{=}$ are the dominant solutes. These waters are found only south of the WIPP site. No Rustler halite is present in this zone. Data from the South and Indian wells (Bodine and Jones, 1988) suggest that these wells should also be classified as part of Zone B.

3. Zone C, containing waters of variable compositions, low to moderate ionic strength (about 0.3 to 1.1 molal), and Ca/Mg weight ratios greater than 1.5:1. These waters extend from the central part of the WIPP site to the eastern part of Nash Draw, in regions of low to high Culebra transmissivity. In the eastern part of the zone, halite is present in the unnamed lower member; on the western side of the zone, Rustler halite is absent. In general, the most saline brines in Zone C are found in the eastern part of the zone.

4. Zone D, containing waters of anomalously high salinities (about 3 to 7 molal) and K/Na mole ratios (about 0.2) relative to other sampled fluids (3 molal or less; K/Na mole ratios of 0.01 to 0.09) This zone is apparently confined to western Nash Draw, and contains only holes WIPP-27 and WIPP-29. Fluid compositions at WIPP-29 have have changed over the course of seven years of monitoring, probably in response to nearby potash refining operations.

The chemical characteristics of the defined Culebra fluid facies can be summarized graphically in a Piper (trilinear) diagram (Figure 4.3.2). This plot generalizes the relationships between several major solutes, i.e., those in the Na-K-Mg-Ca-Cl-$SO_4$-$CO_3$ system. Relative proportions of cations and anions are shown in the triangular plots in the bottom half of the figure, relative ratios of divalent to monovalent cations and chloride to (sulfate plus carbonate) in the parallelogram portion of the figure.

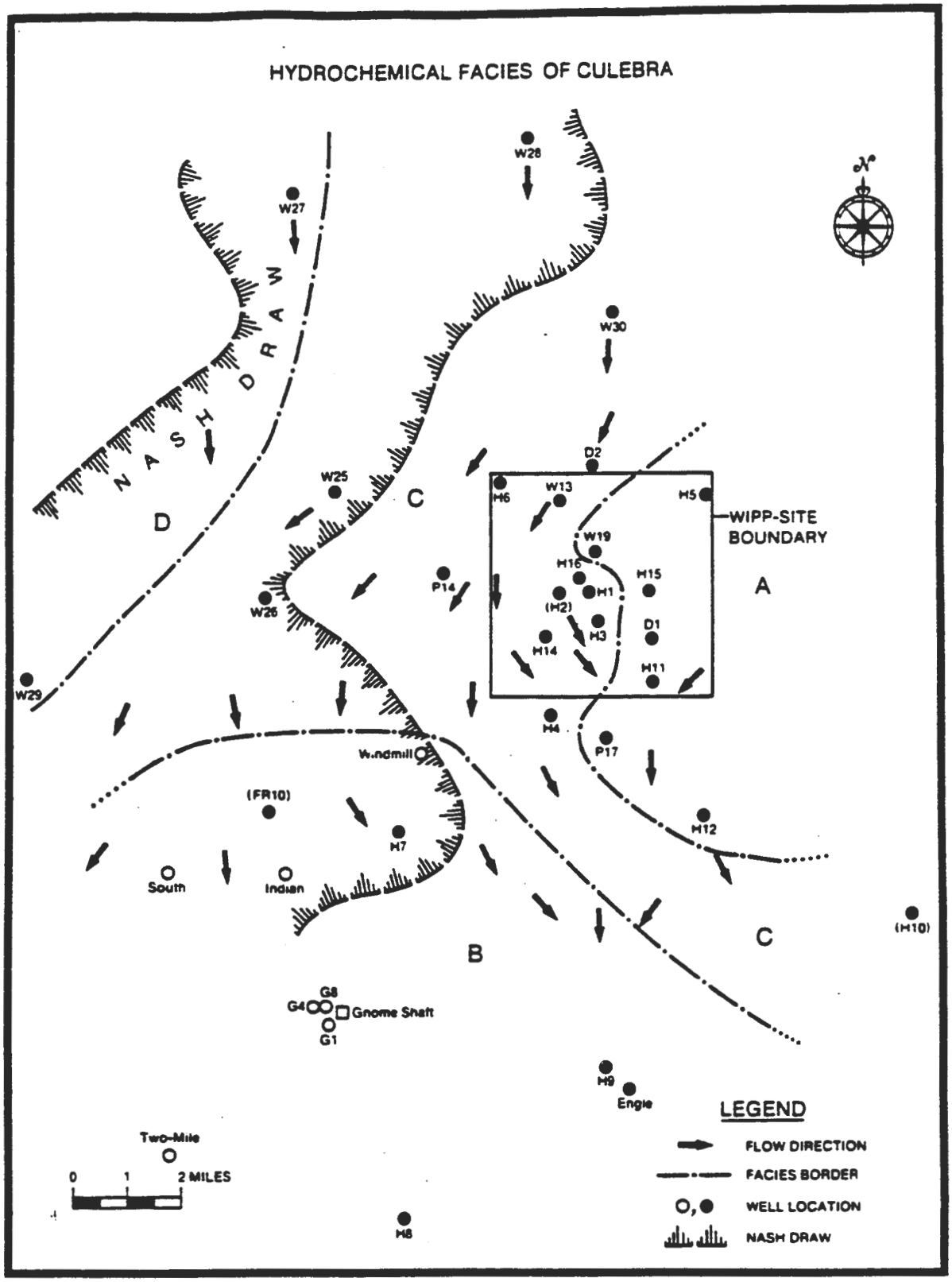


Figure 4.3.1: Summary of hydrochemical facies and local flow directions in the Culebra dolomite. Facies boundaries from Siegel et al. (1988a); modern flow directions from Figure 4.5B of LaVenue et al. (1988).

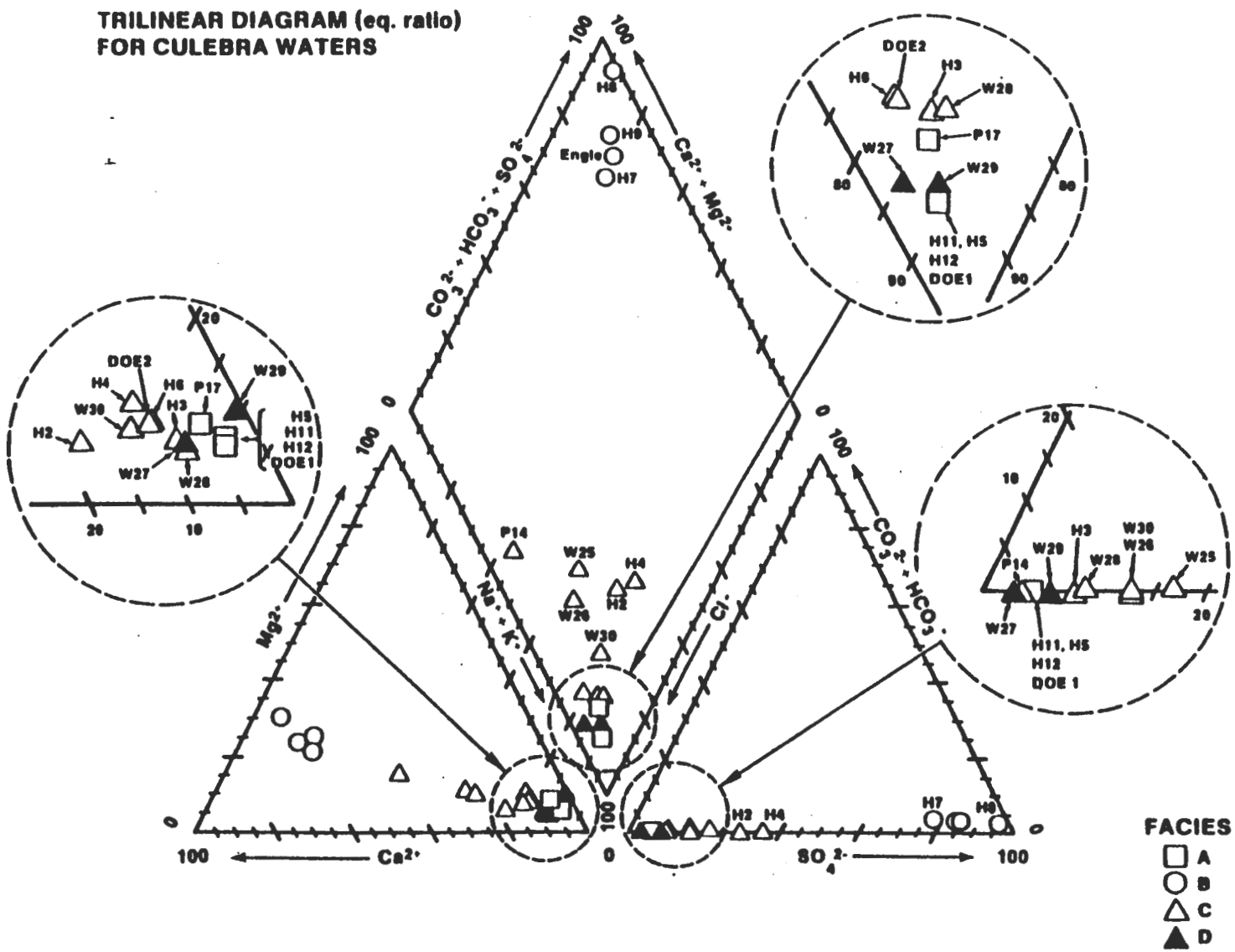


Figure 4.3.2: Piper (trilinear) diagram for analyzed Culebra fluids. Analyses are represented in terms of equivalents per liter. From Siegel et al. (1988b).

The analyses from Zone A have nearly identical ionic proportions (Figure 4.3.2), and plot very near the Na-Cl corner in both parts of the figure. In contrast, the analyses of the dilute fluids from Zone B all plot near the Ca-Mg-$SO_4$ corner in the upper part of the figure. Analyses from Zone C are variable, and those groundwaters closer to the Na-Cl corner of the plot are similar to waters from Zone A. Zones A and C are distinguished primarily on the basis of Ca/Mg ratio and ionic strength. Waters from Zone D have similar ionic ratios as fluids from Zone A except for K/Na; Zone D is distinguished primarily on the basis of its high K/Na ratios.

The overall interpretation of the facies distribution (Siegel et al., 1988a), assuming that the Culebra is relatively confined, is that flow directions within the Culebra must be transient. The inconsistency of Culebra fluid densities and steady-state confined flow was noted in Section 4.1, based on numerical modeling studies of Haug et al. (1987) and LaVenue et al. (1988). Ramey (1985) noted that modern flow directions within the Culebra do not appear consistent with the modern salinity distribution. This inconsistency is also evident in Figure 4.3.1, which is based on a larger and more reliable data base than considered by Ramey (1985). The most striking evidence is that fluids in Zone B, a facies with low salinity, lie down-gradient from more saline waters in Zone C. It is difficult to explain the origin of fluids presently in Zone B by steady-state confined flow through Zone C (Figure 4.3.1). One alternative to steady-state flow, based on isotopic studies (Sections 4.3.2, 4.3.3, and 4.3.4), is that there has been a significant change in flow directions within the Culebra dolomite in the last (approximately) 12,000 years. This is consistent with geologic evidence indicating the transient geologic and hydrologic setting of the WIPP site (Section 4.4).

4.3.1.2 Normative Salt Assemblages of Rustler Waters--The chemical variability of Culebra fluids has also been evaluated on the basis of normative salt assemblages, as summarized by Bodine et al. (1988). The normative salt assemblage (salt norm) of a given water is the equilibrium assemblage of salts that would precipitate from the water if it were evaporated to dryness under standard conditions (25 degrees C, 1 atmosphere pressure). In this interpretation, the SNORM code (Bodine and Jones, 1986) was applied by Bodine et al. (1988) to a different data base than that shown in Table 4.13.

The interpretations of the derivation of Culebra fluids based on hydrochemical facies, isotopic data, and physical hydrology are not in all cases consistent with those based on interpretation of salt norms. Siegel and Lambert (1988) conclude that the overall hydrologic setting of the Culebra is transient. Bodine et al. (1988) conclude that the present distribution of salt norms within the Rustler Formation is, when considered alone, generally consistent with the modern Culebra flow field. These authors relax the vertical confinement of the Rustler. On the basis of solutes alone, their interpretation cannot exclude dilution of primitive-diagenetic brines at P-14 and in the low-permeability, halite-rich zones of the Culebra east of WIPP Zone 3 (for example at P-18) by water that has infiltrated from the surface and dissolved both halite and anhydrite or gypsum. With increasing distances from P-18 and P-14, increasing amounts

of solutes from recharge are interpreted to have mixed with primitive-connate Culebra solutes.

Based on salt-norm calculations, Bodine et al. (1988) suggest four end-member fluid compositions from evaporitic rocks at the WIPP site. These are:

1. Brines containing alkaline earth (Ca, Mg, Ba, Sr, etc) chloride salts in their normative assemblages, combined with relatively low Cl/Br weight ratios (<300). These brines could arise as primitive-diagenetic fluids, for example when connate waters are involved in dolomitization. The data base supporting this end member is limited.

2. Dilute alkali-bearing carbonate waters, produced during recharge by carbonic-acid dissolution of detrital silicates in the zone of infiltration.

3. Dilute sulfate-rich waters, produced when meteoric waters dissolve anhydrite and/or gypsum, but little else.

4. Variably saline halite-rich fluids or brines, produced when meteoric waters dissolve both anhydrite/gypsum and halite in the Rustler and upper Salado Formations.

Bodine et al. (1988) conclude that the solutes in most waters in the Rustler Formation can be produced by mixing of these four end members. Water produced by dewatering of gypsum is not precluded by the solute assemblages. However, the stable-isotope compositions of confined Culebra and Magenta waters (Section 4.3.2) are characteristically meteoric, indicating that gypsum dewatering has not played an identifiable role in their derivation. Bodine et al. (1988) conclude that, if analyzed solutes from the Culebra at P-18 are representative, the Culebra water from P-18 has the highest proportion of apparent primitive-diagenetic brine. They also suggest that some components of the water from P-14 may be primitive, if it is assumed that there has been no mixing or contamination. Waters from the Rustler-Salado contact zone at H-5 and H-6 contain the highest proportion of the primitive-connate solutes. According to Bodine et al (1988), the relative proportion of recharge-type solutes to primitive-diagenetic solutes within the Culebra increases from the WIPP site towards the north, west, and south.

The interpretative model of Bodine et al. (1988) relies heavily on the compositions of Culebra fluids at P-18 and P-14. As noted by Siegel et al. (1988b), the representative character of samples of Culebra fluids from P-18 is suspect, i.e., the analyses appear reliable, but may not represent actual Culebra fluids at this location. Hydrologic considerations also weigh against the reliability of these data. The Culebra transmissivity at P-18 ($7.5 \times 10^{-11}$ to $4.3 \times 10^{-9}$ $m^2/s$, Table 4.2) is the lowest yet measured at or near the WIPP site. Therefore, while the Culebra at P-18 intuitively seems likely to contain connate brine, consistent with the norm-based interpretation of Bodine et al. (1988), the very fact that the Culebra is

so low in transmissivity at P-18 permeability makes it extremely difficult if not impossible to collect a meaningful fluid sample from the hole. In P-14, the situation is reversed. The Culebra in P-14 is extremely transmissive ($2.3 \times 10^{-4}$ $m^2/s$, Table 4.1). The preservation of original connate or diagenetic fluids in such a permeable region does not seem possible or consistent with expected rates of fluid flow in the vicinity (Figure 4.1.28). In addition (Section 4.3.2), the stable-isotope composition of Culebra waters from P-14 is meteoric, suggesting that P-14 fluids have not been involved in extensive diagenetic reactions. However, the analyses of Culebra waters from P-14 do appear reliable. The cause of the apparent primitive-diagenetic component in these fluids is not known.

The salt-norm interpretation also relies heavily on vertical recharge from the surface to provide fluids for dilution of the interpreted primitive-diagenetic signature of Culebra fluids, especially south of the WIPP site. However, the isotopic evidence, discussed in later parts of Section 4.3 and in Section 4.4, as well as the measured head and transmissivity distributions within the Rustler, discussed in Section 4.1, suggest that vertical recharge to the Culebra from the surface is not currently active at and near the WIPP site. The Culebra dolomite is confined at and south of the site, while the Dewey Lake Red Beds, where tested, are effectively impermeable. Finally, as discussed in Section 4.4, the preservation of large amounts of anhydrite in the Tamarisk Member overlying the Culebra, suggests that vertical infiltration of dilute solutions through the Tamarisk has been minimal. These relationships do not indicate that there has been no vertical fluid movement within the Rustler Formation or between the Dewey Lake and the Rustler, but that such movement is limited, and does not currently extend from the surface down to the Culebra.

4.3.1.3 Saturation Indices and Factor Analysis of Culebra Waters--Saturation indices of several evaporite minerals in analyzed Culebra waters have been calculated using the code PHRQPITZ (Plummer et al., 1988), and are summarized in Siegel et al. (1988a). The variation in halite saturation index as a function of ionic strength is shown in Figure 4.3.3. All fluids are undersaturated with respect to halite and Na and Cl concentrations vary widely. There is a consistent increase in halite saturation index with increasing ionic strength.

The variations in calculated gypsum and anhydrite saturation indices with ionic strength are shown in Figure 4.3.4. The data are internally consistent and indicate both a general saturation with respect to gypsum and an increase in anhydrite saturation with increasing ionic strength. However, with the exception of WIPP-29 (Zone D) all samples are undersaturated with respect to anhydrite. As a result, almost all Culebra waters are capable of converting into gypsum any anhydrite with which they might come into contact.

Most calculated dolomite saturation indices for Culebra fluids indicate saturation or apparent supersaturation (Figure 4.3.5). The relationships between saturation indices, pH, and calculated $pCO_2$ suggest, as discussed in Siegel et al. (1988b), that loss of $CO_2$ during sample collection may be

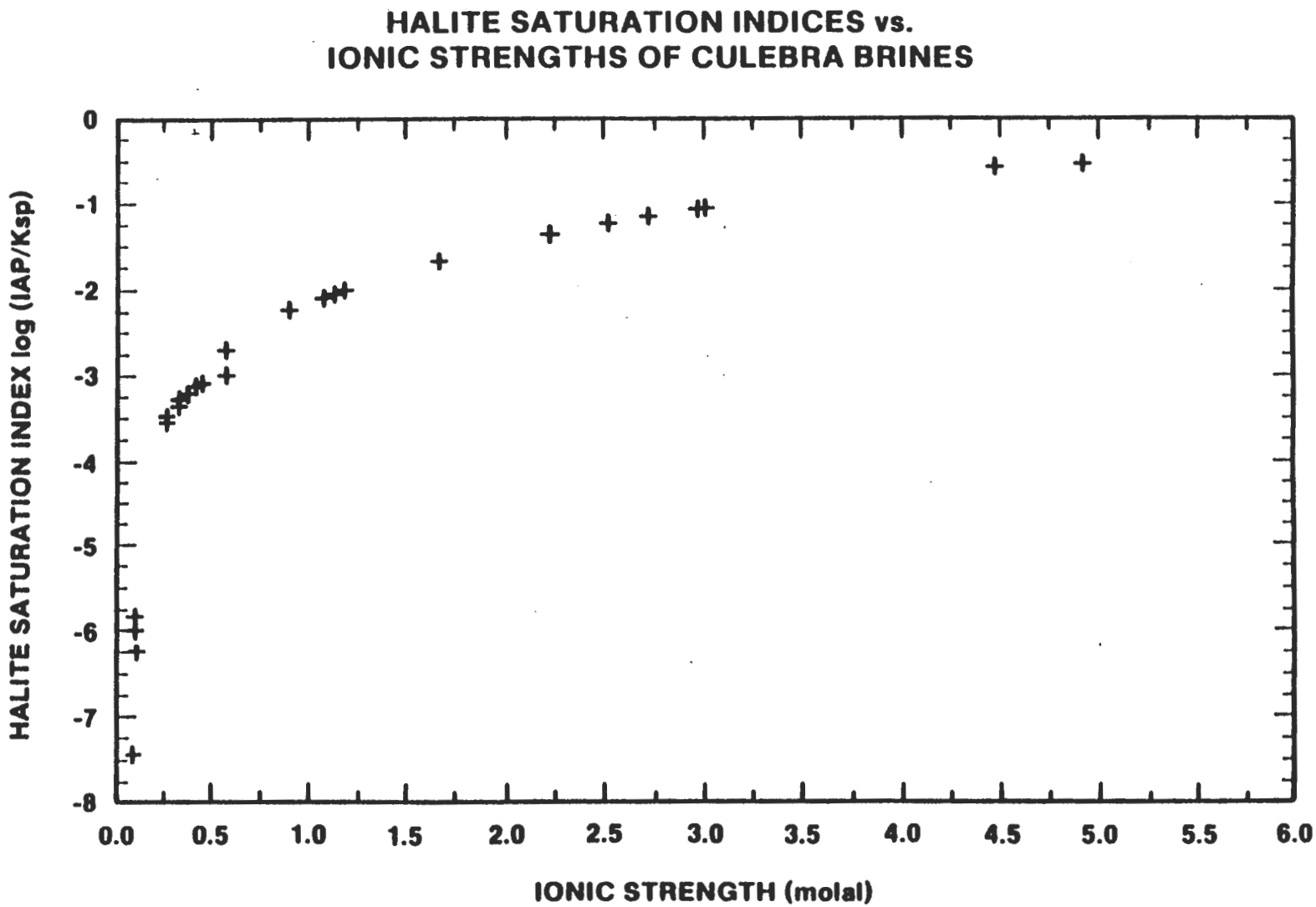


Figure 4.3.3: Variation in calculated halite saturation indices of Culebra waters as a function of ionic strength. From Siegel et al. (1988b).

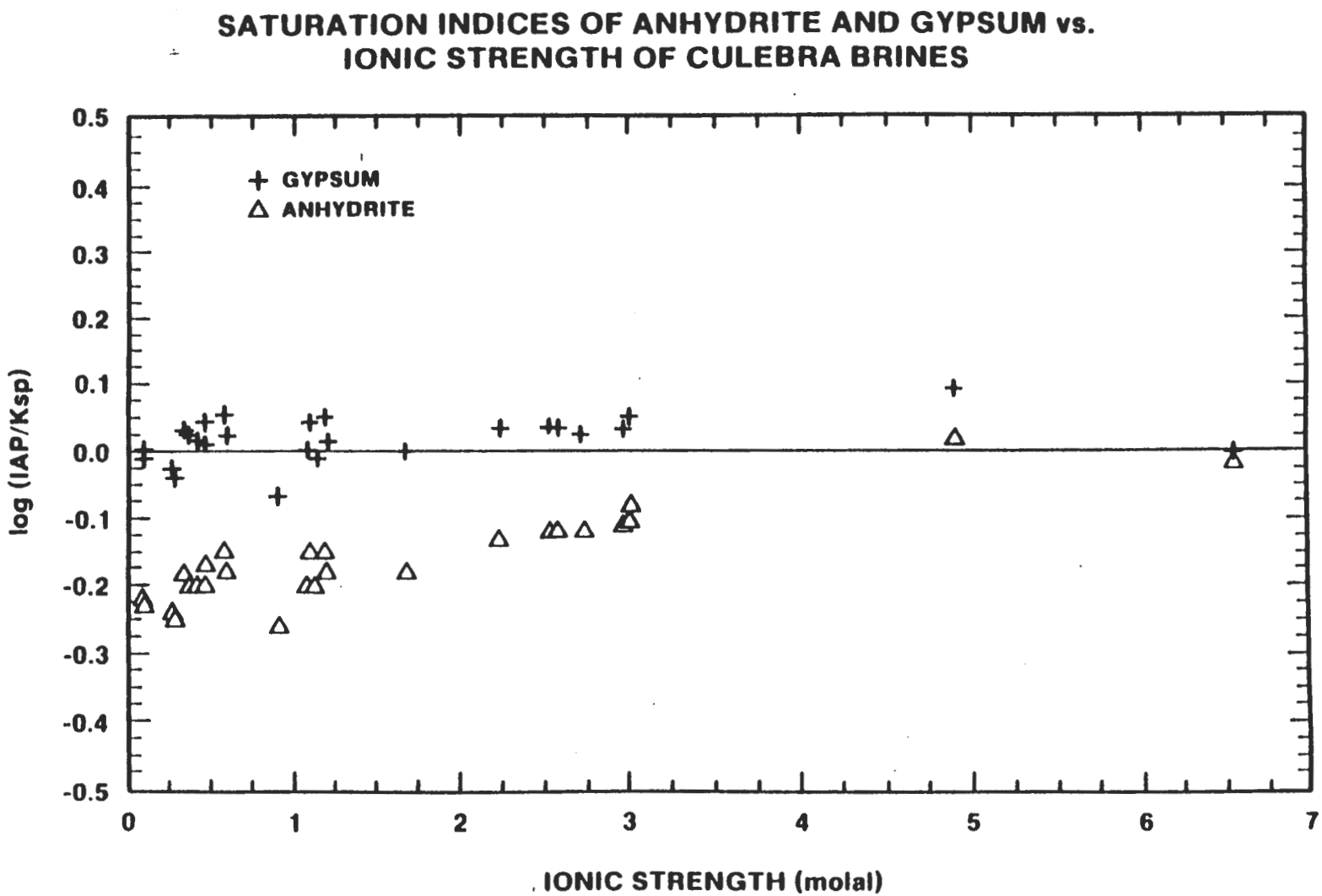


Figure 4.3.4: Variation in calculated gypsum and anhydrite saturation indices of Culebra waters as a function of ionic strength. From Siegel et al. (1988b).

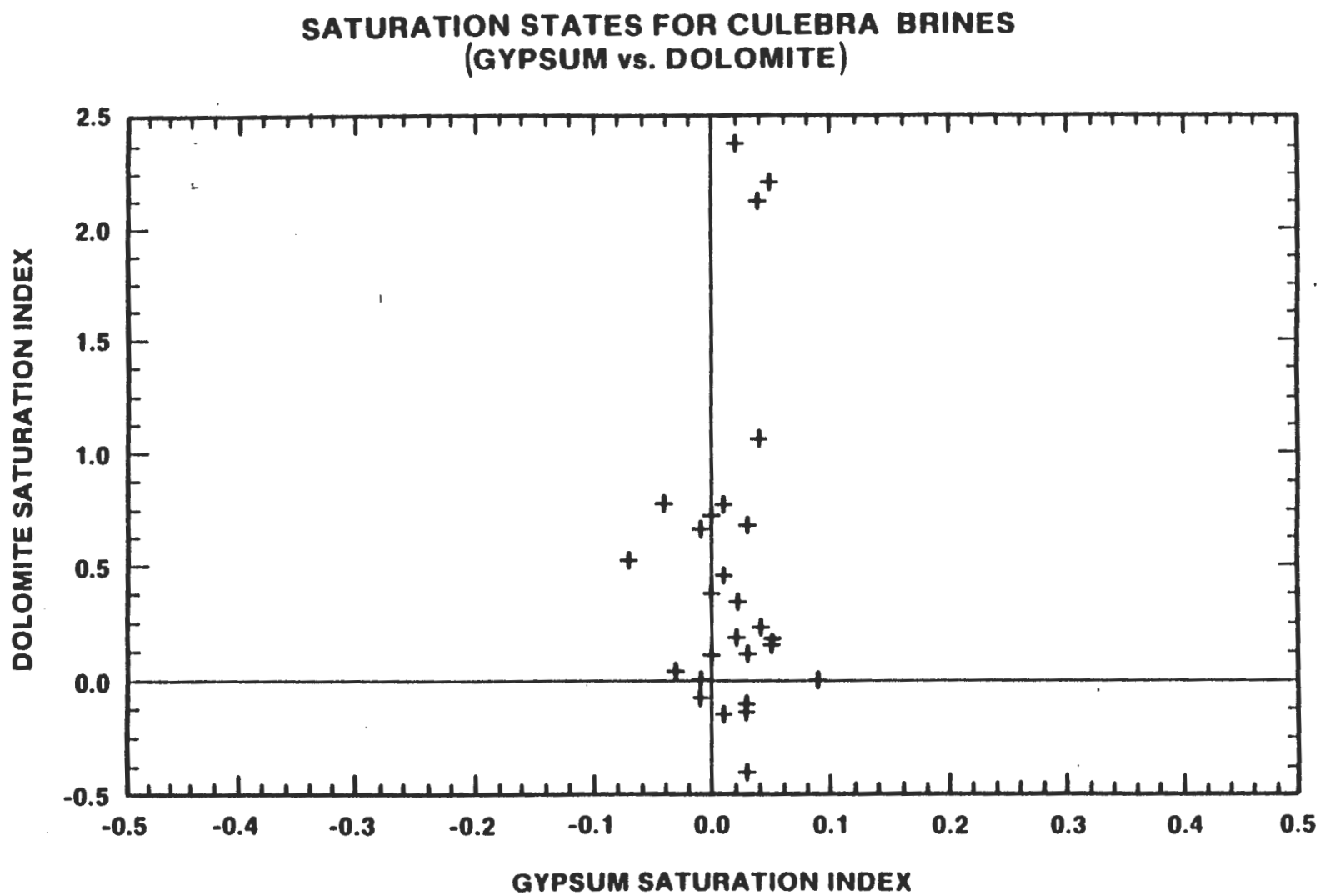


Figure 4.3.5: Variations in calculated dolomite saturation indices of Culebra waters as a function of calculated gypsum indices (Figure 4.3.4). From Siegel et al. (1988b).

responsible for the apparent supersaturation; other potential sources of error include use of an inappropriate free energy for dolomite and analytical error. The wide scatter in dolomite saturation indices gives some indication of the apparent effect of degassing on calculations involving dolomite. The origins of the high original $pCO_2$ in Culebra waters is not known, but may include carbonate dissolution and/or microbial action (see Section 4.3.3).

In addition to the major solutes used in defining hydrochemical facies and in calculating saturation indices considered thus far, there are consistent trends in both major-element (Ca, Mg, Na, K, Cl, and $SO_4$) and minor-element (Br, I, Sr) ratios in Culebra fluids. These trends, which are discussed in more detail in Siegel et al. (1988b) include the following:

1. The Na/Cl ratios of fluids south of the WIPP site are higher than would be produced by simple dissolution of halite, suggesting the importance of dissolution of Na-silicates at some time in the derivation of fluids in this area. This is consistent with the norm-based end member of dilute meteoric alkali-bearing carbonate waters discussed in Section 4.3.1.1.

2. At WIPP-27 and WIPP-29, the K/Na ratios and Na, K, Mg, Cl, and $SO_4$ concentrations are significantly higher than at other wells in Nash Draw or west of the site, suggesting that potash refining operations have significantly contaminated these locations. This is consistent with the definition of hydrochemical facies "D" in Section 4.3.1.1.

3. Both ratios and concentrations of several elements are anomalous in samples collected from P-14, compared to surrounding wells. For example, concentrations of Ca, Sr, and I are anomalously high at P-14, and K and $SO_4$, low. The Na/Cl, K/Na. and Mg/Ca ratios are somewhat low, and the Cl/Br ratio distinctly low at this well. The "primitive-diagenetic" salt norm at P-14 is anomalous (Section 4.3.1.1).

4. Regionally, the Cl/Br weight ratios are highest in Nash Draw, intermediate through the center of the WIPP site and to the south, and lowest at P-14 and H-4.

Examination of the relations between element ratios discussed above indicate that correlations between elements are not simply linear. For this reason, the data in Table 4.13 were also examined using Principal Component Analysis (PCA). The technique is described in detail in Siegel et al. (1988b). The purposes of PCA are to determine if the fluids come from a single or continuously variable population, and to delineate the different independent ways (factors) by which major and minor elements are correlated.

The preliminary results of factor analysis of Culebra fluids indicate that, on a regional scale, the samples are all drawn from a single chemical population; i.e., their chemistry is controlled by a consistent set of components. The most important component shown by R-mode PCA is dominated

by Na, K, Mg, Br, and Cl. All solutes except $SiO_2$, alkalinity, and pH exhibit positive correlation with this factor. The second major factor also includes Na and Cl, but is dominated by Ca, $HCO_3$, and Sr. Overall, the data are interpreted to suggest that the two fluid-compositional factors describing the variability of Culebra waters represent addition of solutes by dissolution of halite, gypsum/anhydrite, and carbonates (Siegel et al., 1988b).

However, because the amount of solute added by halite dissolution is so large relative to that added by other reactions, i.e., because halite solubility is much greater than that of other minerals considered, other chemical correlations may be masked. For this reason, a second set of PCA was carried out by Siegel et al. (1988b), using a method designed to be independent of total dissolved solids and hence halite dissolution. The primary component determined in this analysis contains two groups of elements that are inversely correlated. One group contains Mg, bicarbonate alkalinity, and $SiO_2$; the other group contains Na, pH, B, and Li. This pattern of element association is tentatively interpreted by Siegel et al. (1988b) to reflect clay diagenesis or silicate hydrolysis. The apparent uniformity of the compositional factors describing the variability of Culebra waters does not identify a discrete mechanistic or mineralogical delineation between the hydrochemical facies defined in Section 4.3.1.1.

4.3.1.4 Estimated Oxidation-Reduction Potentials of Culebra Waters--Many of the transuranic elements to be emplaced in the WIPP facility have multiple valence states. Therefore, given the possible role of the Culebra dolomite in transport to the accessible environment, it is important to estimate oxidation potentials (redox potentials, Eh) within the unit. Available measurements of redox potentials in Culebra waters are described in detail by Myers et al. (1988), and are summarized in Figure 4.3.6. Myers et al. (1988) conclude that the calculated potentials summarized in Figure 4.3.6, based on the data from Pt electrodes and redox pairs involving N, I, As, and Se, are fairly insensitive to assumptions concerning activity-concentration relationships, reasonable uncertainties in analytical data, and errors introduced by uncertainty in field pH. Absolute potential measurements made with Pt electrodes are not generally considered highly reliable; they are included here only for purposes of inter-well comparison. Nonetheless, many of the data are internally inconsistent.

The internally consistent values, indicated in Figure 4.3.6 by the vertical shaded bars, are interpreted by Myers et al. (1988) to bracket the redox potentials for the wells in Zone B (H-7, H-8, H-9, and Engle) between +330 and +630 mv (or higher). A similar range is indicated for WIPP-26 (Zone C) in the eastern part of Nash Draw. Data for the nitrogen couple in hydrochemical facies A and C (Figure 4.3.1), except for WIPP-26, indicate less oxidizing conditions, with an estimated Eh of less than approximately +330 mv.

Quantitative data are not available from within most of Nash Draw. The internally consistent data from WIPP-26 indicate a similar range of redox potential to that at H-7, H-8, and H-9. The platinum-electrode

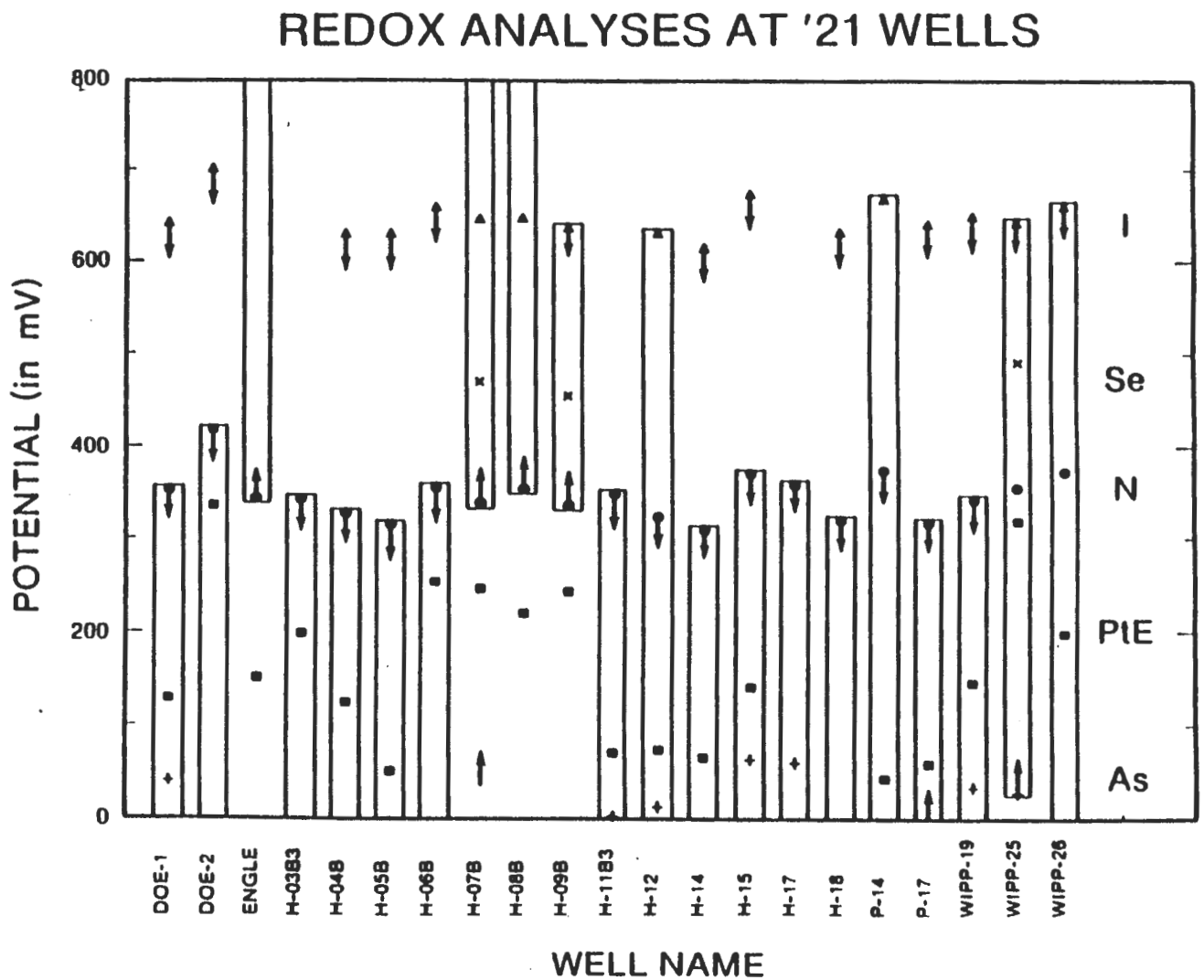


Figure 4.3.6: Variability in approximate redox potential of waters from several Culebra wells. Symbols: + = AsIII/AsV; □ = platinum electrode; o = $NH_3/NO_3^-$; x = SeIV/SeVI; ▲ = $I^-/IO_3^-$. Arrows indicate upper or lower limits resulting from one member of pair being present at levels below the detection limit. From Siegel et al. (1988b).

measurements in H-7, H-8, H-9 and WIPP-26 (Figure 4.3.6) are higher than those at most other locations. The apparent range of consistent potentials in WIPP-25 is large. Lambert and Robinson (1984) note, however, that WIPP-25 evolved $H_2S$ during fluid sampling, suggesting that these results are suspect. Relative measurements with Pt electrodes (Lambert and Robinson, 1984), also indicate that redox potentials in the Culebra in Nash Draw are higher than those in the underlying Rustler/Salado contact zone.

Thus, there appear to be consistent variations in redox potential within the Culebra dolomite, with more reducing conditions to the northeast and more oxidizing conditions toward the southwest. This regional variation in the modern oxidation potential plays a significant role in interpretation of uranium-disequilibrium studies discussed in Section 4.3.4.

4.3.1.5 Mineralogy of the Culebra Dolomite--It has already been noted that both the composition and density of Culebra fluids vary considerably at and near the WIPP site. One objective of studies summarized in Siegel et al. (1988a) was to determine whether or not variations in Culebra mineralogy correlate with variations in Culebra fluid compositions. Accordingly, detailed mineralogical studies of Culebra samples from ten different locations along three east-west traverses have been conducted, and are described by Sewards et al. (1988).

Figure 4.3.7 shows a mineralogical cross section of the Culebra dolomite from Nash Draw towards the east, south of the WIPP site proper, as interpreted from sampled core (Sewards et al., 1988). As in any core study, especially in a locally fractured unit such as the Culebra, it cannot be demonstrated that the sampled core has been in contact with flowing groundwater. Mineralogical contents estimated by Lambert (1988) during preparation of rubbled material selected for isotopic analysis of Culebra matrix and veins (Section 4.4.2) differ somewhat from analyses summarized in Figure 4.3.7. The mineralogy at H-7 and H-10 (Figure 4.3.7) is probably representative of intact core samples at the WIPP. The dominant mineral in the selected cores is fairly pure dolomite, comprising about 85% of the bulk rock (by weight). Minor amounts of gypsum, calcite, and clay are observed throughout the sampled cores, but their distribution is heterogeneous both vertically and laterally. Fractures, which are present in most cores, are most commonly lined with clay and gypsum. Gypsum ($CaSO_4 \cdot 2H_2O$) occurs as both fracture and vug fillings. Available analyses indicate that it is nearly pure. Both the composition and textural features suggest that it is secondary in origin. Calcite from the upper portion of the Culebra in WIPP-29 is also interpreted to be secondary. Minor amounts of pyrite, magnesite, quartz, and authigenic feldspar have been observed in some cores. Finally, a dark optically-amorphous and X-ray-amorphous material is present in some abundance in Culebra samples examined, and has been tentatively identified as organic matter. It is generally associated with clays, and often occurs in algal structures or haloes surrounding vugs, the origin of which is attributed to biological activity.

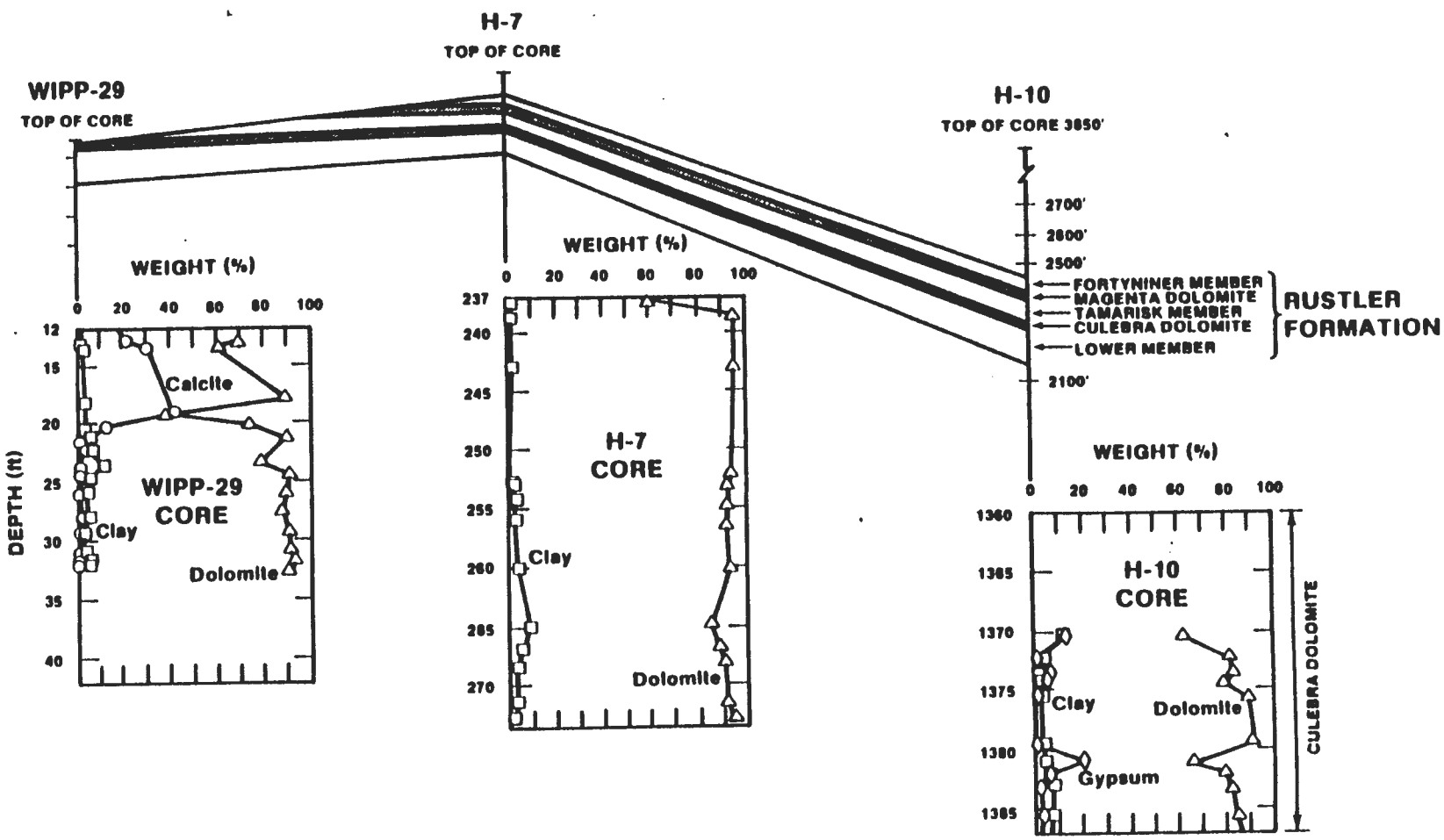


Figure 4.3.7: Fence diagram of variations in bulk mineralogy of core samples of the Culebra dolomite along the east-west section including holes WIPP-29, H-7, and H-10. From Siegel et al. (1988a).

In the intact cores examined by Sewards et al. (1988), corrensite, an ordered mixed-layer illite-smectite clay, is the second most abundant mineral within the Culebra after dolomite. In addition to occurring along fractures, clays are also present in the matrix of all Culebra samples, and commonly make up 3 to 5 weight percent of the bulk sample. The dominant clay minerals are corrensite, illite, chlorite, and a serpentine-like mineral, tentatively identified as amesite.

The recent mineralogical studies in the Culebra indicate that the unit is vertically and laterally heterogeneous. The dominant variation in Culebra fluids, variation in Na and Cl (Section 4.3.1.1), is not reflected in the presence or absence of halite in Culebra core. Dolomite, clays, and gypsum are ubiquitous, and calcite local in occurrence. Table 4.14 summarizes potential rock/water reactions that may influence the chemistry of Culebra waters. With the exception of halite, all of the minerals involved in reactions listed in Table 4.14 occur in the Culebra throughout the area at and near the WIPP site. Halite that has definitely not been introduced during drilling has not been reliably identified in any Culebra core. With the exception of halite dissolution, any of the reactions indicated in Table 4.14 can occur in any of the Culebra hydrochemical facies zones defined. Examination of potential rock/water reactions affecting fluids within the Culebra has not yet identified unique or discontinuous relationships between matrix mineralogy and fluid composition that can be used to place additional constraints on either present or past directions of fluid flow.

In summary, the highly variable fluids within the Culebra dolomite can be divided into four facies. The distribution of these facies is not consistent with modern regional flow directions estimated from hydrologic measurements, if steady-state confined flow is assumed. Zone B, containing lower-salinity fluids lies down-gradient from Zone C, which contains more saline waters. An internally consistent interpretation of the variability of Rustler fluids is possible on the basis of salt norms if large-scale vertical recharge is assumed in some areas. However, some of the analyses used in this interpretation do not appear to be representative, and both isotopic and hydrologic evidence suggest that such vertical fluid movement is not now operative at and near the WIPP site. The mineralogy of core samples from the Culebra dolomite is consistent only in its variability. It cannot be demonstrated that sampled fluids at a given well have been in contact with a given piece of core; therefore it cannot be directly demonstrated that rock/water interactions identified on the basis of a given core sample control or affect the local fluid composition. The available data cannot identify any unique relations between Culebra matrix mineralogy and major-solute or minor-solute compositions of Culebra waters that can themselves be used to place constraints on either past or present flow directions within either the Culebra or the Rustler Formation as a whole. As discussed in Section 4.4.2, however, the isotopic compositions of some minerals within the Rustler, especially gypsums, can be used to place constraints on vertical fluid flow.

Table 4.14: Summary of possible rock-water reactions affecting compositions of Culebra fluids. From Siegel et al. (1988a).

| Chemical Process | Potential Effect on Culebra Water |
|---|---|
| Halite Dissolution | increase Na, Cl, Br, Li; decrease Cl/Br; increase solubility of carbonates and sulfates up to 3 molal NaCl and then decrease solubility causing changes in Ca, Mg, $SO_4$, $CO_3$ |
| Precipitation/dissolution of gypsum | decrease/increase Ca, $SO_4$ |
| Precipitation/dissolution of calcite and dolomite | decrease/increase Ca, Mg, $CO_3$ |
| Dolomitization: calcite + Mg -> dolomite + Ca | decrease Mg/Ca |
| Dedolomitization: dissolution of gypsum and dolomite with concurrent precipitation of calcite. | decrease pH, alkalinity/$SO_4$; maintain Mg/Ca molar ration < 1 |
| Ion exchange involving Mg, K-rich clays in NaCl brines | loss of Na, gain of Mg, K by solution |
| Mixing of connate hypersaline formation water with recharge water that has dissolved gypsum, | increase Mg, Ca, K, Na, Cl; decrease $SO_4$, Cl/Br |
| Incongruent dissolution of polyhalite | increase Mg, K, $SO_4$; decrease Ca, Cl/Br |

### 4.3.2 Recent Stable-Isotope Studies of Groundwaters from the Rustler Formation and Younger Units

4.3.2.1 The Character of Modern Recharge in the Northern Delaware Basin--As mentioned above, stable-isotope studies do not provide direct information concerning the age of groundwater. Rather, they may indicate whether or not two or more bodies of water were recharged under similar climatic conditions and whether or not one of the bodies of water is modern. At the WIPP site, the approach requires both determination of the isotopic character of modern recharge in the region and determination of

whether or not the isotopic character of groundwaters in the Rustler Formation and younger units is consistent with that of modern precipitation. Recent stable-isotope studies of groundwaters in the northern Delaware Basin conducted as part of WIPP site-characterization activities are summarized by Lambert and Harvey (1987).

The present stable-isotope data base for waters from Carlsbad Caverns (Lambert and Harvey, 1987), is summarized in Figure 4.3.8. Samples were collected from active drips or pools in portions of the cavern system well above the modern water table. Depending on assumptions concerning seasonal averaging of fluid compositions during infiltration and possible evaporation within the caverns, these waters may or may not be representative of modern meteoric recharge in the northern Delaware Basin at elevations similar to that of the surface of the WIPP site.

Lambert and Harvey (1987) conclude that, with one possible exception (sample "GS"), evaporation and rock-water interaction do not play a significant role in derivation of the waters shown in Figure 4.3.8. This is because the waters fall in or near the "meteoric field," defined by the compositional space between the statistical world-wide precipitation trends calculated by Craig (1961) and by Epstein et al. (1965, 1970). Therefore, the isotopic character of the waters (Figure 4.3.8) is interpreted as consistent with that of modern meteoric recharge in the northern Delaware Basin.

The character of modern precipitation in the northern Delaware Basin also rests on other analyses. In 1983, waters from Carlsbad Caverns were essentially the only waters interpreted to represent this recharge. As shown in Figure 4.3.9, most of the more recent measurements on surficial waters and some on shallow groundwaters in the vicinity of the WIPP site and at similar elevations are consistent with measurements on unconfined waters from the Capitan limestone. Samples from a local storm (August 26, 1980) fall within the Carlsbad Caverns field, as do samples from the Dewey Lake Red Beds at the James Ranch and Quaternary alluvium at WIPP-15. The character of the water from the Dewey Lake Red Beds in the James Ranch well is consistent with the interpretation that the Dewey Lake is experiencing modern recharge at this location. The well at the James Ranch (identified as "ranch well" in Figure 1.2) is close to a locally active dune field south of the WIPP site; WIPP-15 was drilled specifically to investigate San Simon Sink (Figure 1.1), an active collapse feature over the Capitan limestone. The measured deuterium/hydrogen ratios of nine water-table samples from the Ogallala Formation in southeastern New Mexico are consistent with the lighter end of the Carlsbad Caverns field in Figure 4.3.9. Heavier Ogallala samples also high in tritium, discussed by Lambert (1988), are consistent with this field. Thus, Lambert and Harvey (1987) base the isotopic composition range of their field of "demonstrably modern precipitation" used in discussions below and in later figures in this section on measurements at several localities, and in several different geologic units. Additional information, especially concerning both the deuterium and tritium characteristics of groundwaters in the High Plains of Texas and the northern Delaware Basin of New Mexico is contained in Lambert (1988).

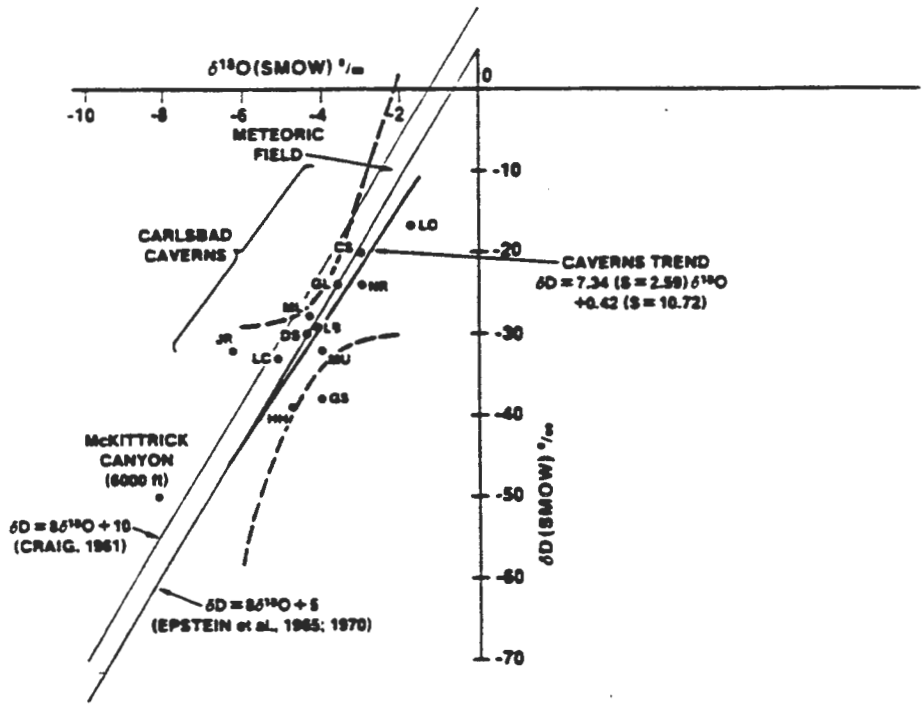


Figure 4.3.8: Available stable-isotope analyses of waters from the unconfined portion of the Capitan limestone in Carlsbad Caverns, New Mexico. The two-letter identification of individual samples is fully explained in Table 3 of Lambert and Harvey (1987). The meteoric field is defined as the area between the statistical correlation lines of Craig (1961) and Epstein et al. (1965, 1970). Slightly modified from Figure 6 of Lambert and Harvey (1987).

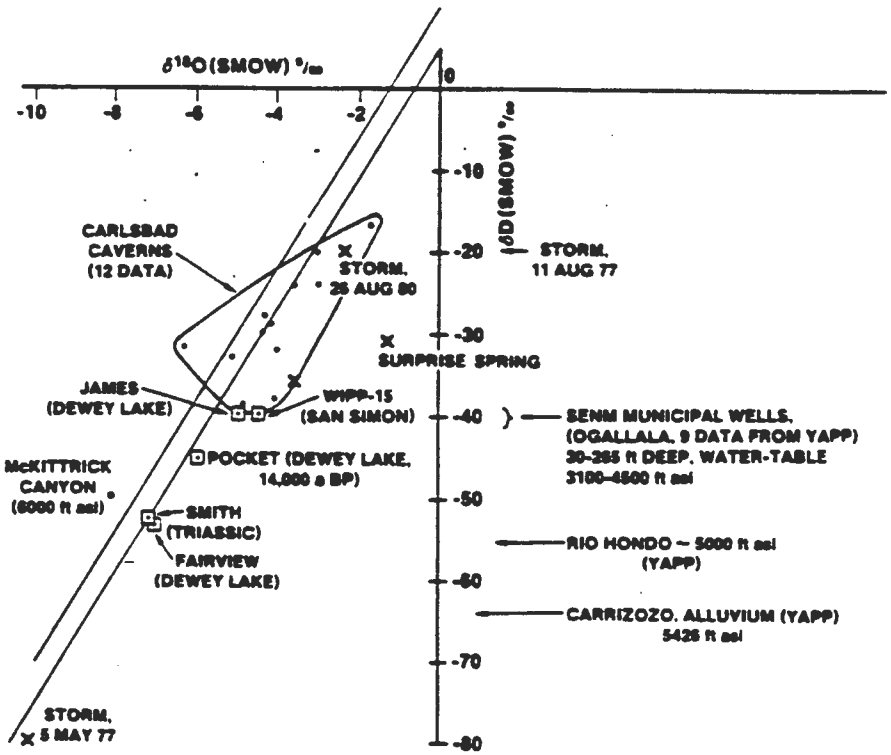


Figure 4.3.9: Recent stable-isotope analyses of surficial and near-surface waters in the northern Delaware Basin. Slightly modified from Figure 9 of Lambert and Harvey (1987).

Stable-isotope data from both the travertine deposit in McKittrick Canyon and a local storm (May 5, 1977) are much lighter than the Carlsbad Caverns field shown in Figure 4.3.9. The isotopic character of these samples is interpreted by Lambert and Harvey (1987) to be due to local elevation effects and point-data variability of individual storms. A similar elevation-dependent argument is made concerning the deuterium data available for Rio Hondo and at Carrizozo (see Lambert and Harvey, 1987 for discussion and detailed sample locations).

Not all data from stratigraphic units above the Rustler fall in the Carlsbad Caverns field in Figure 4.3.9. Water from the Dewey Lake Red Beds at the Pocket well is relatively light. This water has a calculated minimum radiocarbon age of 14,000 years (Section 4.3.3). The ages or isolation times of the relatively light waters from the Smith and Fairview wells are not known. The available stable-isotope results indicate complexity within the Dewey Lake Red Beds. The James Ranch well appears to contain "modern" water, and is located near an active dune field. The Pocket and Fairview wells, which both contain water isotopically distinct from the Carlsbad Caverns field in Figure 4.3.9, are both located near the southwestern lobe of Nash Draw.

4.3.2.2 <u>The Hydrology of the WIPP Site and Vicinity Relative to Modern Recharge</u>--Figure 4.3.10 summarizes the available stable-isotope data for groundwaters from the Magenta and Culebra dolomites at and near the WIPP site. In this figure, the isotopic character of these waters is contrasted with the Lambert and Harvey (1987) estimate of "demonstrably modern Delaware Basin recharge at 3,000 - 4,500 feet elevation," discussed above. The compositionally distinct waters from WIPP-29 and Surprise Spring, both of which are distinct from the meteoric field (Figure 4.3.8) are discussed separately below.

There is no overlap between the Culebra/Magenta data near the meteoric field and the interpreted compositional field representing modern recharge (Figure 4.3.10). On the basis of the consistent compositional distinctions shown in Figure 4.3.10, Lambert and Harvey (1987) conclude that: 1) the stable-isotope compositions of Culebra and Magenta groundwaters do not reflect modern meteoric recharge of the Rustler Formation; 2) there is no significant modern recharge to the Magenta and Culebra dolomites at and near the WIPP site; and 3) the waters presently contained within the Magenta and Culebra at and near the WIPP site were recharged under different climatic conditions than those at present. Therefore, at least some aspects of the hydrology of the Rustler Formation must be transient on some time scale.

The Rustler Formation is not the only unit in the northern Delaware Basin that contains older water. There is also significant variability in the isotopic character of fluids within the Capitan limestone (Figure 4.3.11). The heavier samples defining the "Carlsbad Caverns" compositional field in this figure, which is almost identical to the modern recharge field in Figure 4.3.10, are from the unconfined and partially saturated hydrologic system within Carlsbad Caverns. The lighter samples are from wells drilled

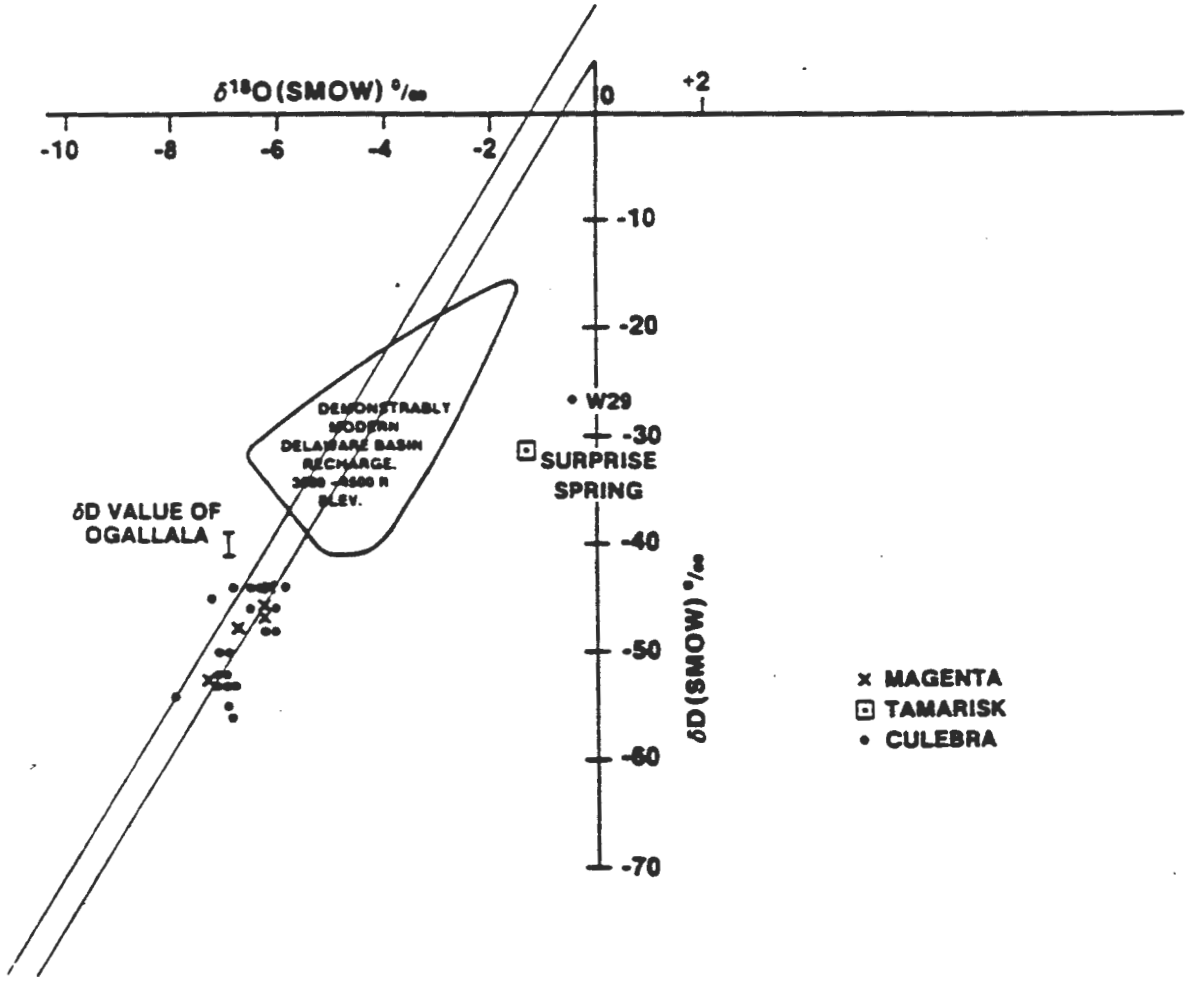


Figure 4.3.10: Stable-isotope compositions of waters from the Culebra and Magenta dolomites at and near the WIPP site. The "modern recharge" field is defined by the Carlsbad Caverns field and other consistent data contained in Figures 4.3.8 and 4.3.9. Note the anomalous character of samples from WIPP-29 and Surprise Spring. Slightly modified from Figure 14 of Lambert and Harvey (1987).

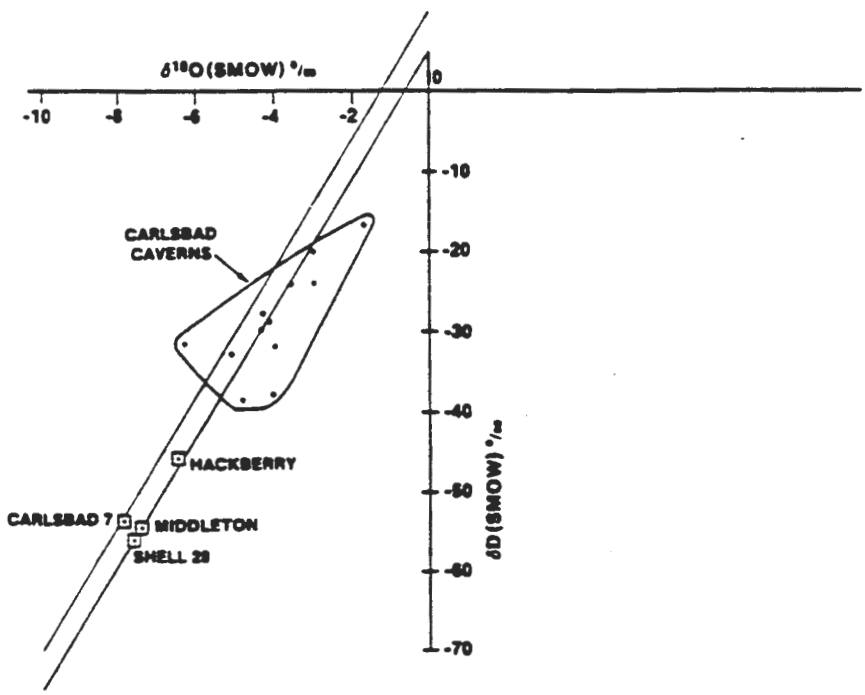


Figure 4.3.11: Comparison of stable-isotope character of waters from unconfined and confined portions of the Capitan limestone. Slightly modified from Figure 10 of Lambert and Harvey (1987).

into confined regions of the Capitan. The signatures of samples from confined portions of the Capitan limestone fall within the same compositional field as most Rustler fluids. Based on uranium-disequilibrium studies, Barr et al. (1983) estimate the isolation times for the Capitan waters from the Middleton and Hackberry wells (Figure 1.1) as $5.8 \times 10^5$ and $1.05 \times 10^6$ years, respectively.

Thus, stable-isotope measurements in the Rustler Formation, Dewey Lake Red Beds, and Capitan limestone are consistent with the conclusion that the hydrology of the northern Delaware Basin is transient. The fundamental conclusions of Lambert and Harvey (1987) and Lambert (1988) concerning the hydrologic setting of the northern Delaware Basin are:

1. The isotopic compositions of waters from unconfined portions of the Capitan limestone, the Ogallala Formation, and several other unconfined sampling locations at elevations similar to that of the WIPP site are representative of modern meteoric recharge within the northern Delaware Basin.

2. The general isotopic composition of samples from the Culebra and Magenta dolomites of the Rustler Formation at and near the WIPP site, as well as of samples from confined portions of the Capitan limestone, is distinct from that of modern meteoric precipitation within the northern Delaware Basin.

3. The Culebra and Magenta dolomites at and near the WIPP site, in addition to part of the Dewey Lake Red Beds and confined portions of the Capitan limestone, were recharged under climatic conditions different from those effective at the present time.

4. Therefore, the hydrology of the northern Delaware Basin is transient on some time scale. The stable-isotope technique itself provides no information concerning the possible times or time gaps between two interpreted recharge intervals or events, nor does it necessarily provide information concerning where recharge might have taken or be taking place. In the specific case of the Rustler Formation, however, the stable-isotope technique does indicate that significant modern meteoric recharge to the Culebra or Magenta is not taking place at any of the sampled localities.

One site-specific focus of Lambert and Harvey (1987) is the determination of whether or not southeastern Nash Draw, specifically the area including hole WIPP-29 and Surprise Spring (Figure 1.1), is a major point of discharge for Rustler fluids flowing across the WIPP site. Lambert and Harvey (1987) evaluate the question by comparison of the solute and isotopic characteristics of fluids from hole WIPP-29 and Surprise Spring with those of other Rustler fluids. As shown in Figure 4.3.10, the isotopic signatures of fluids from both WIPP-29 and Surprise Spring are quite distinct from the meteoric field. Lambert and Harvey (1987) conclude that the solute characters of WIPP-29 and Surprise Spring waters are also distinct.

In general, the modern flow directions within the Culebra in Nash Draw are roughly parallel to the axis of Nash Draw (Section 4.1). This suggests that, if Surprise Spring is to be a major point of Culebra discharge, fluids must first flow through the region of hole WIPP-29. Rustler groundwaters have been sampled at both Surprise Spring and WIPP-29. It is essentially impossible to derive Surprise Spring waters from evaporation of WIPP-29 Culebra waters, since the lower chloride content at Surprise Spring (Figure 4.3.1) indicates major dilution relative to WIPP-29. The same argument applies to derivation of Surprise Spring waters from Culebra waters at both H-5 and H-6 at the WIPP site, and at many holes within Nash Draw itself. Further, as noted by Lambert and Harvey (1987), Surprise Spring appears to discharge from the Tamarisk Member of the Rustler, rather than from either the Culebra or Magenta.

In addition, the Cl/K (weight) ratios for fluids from holes WIPP-27 and WIPP-29 are distinctly lower than those of other Rustler fluids both in and outside Nash Draw, including Surprise Spring (Section 4.3.1.1). Culebra groundwaters from WIPP-27 and WIPP-29 have Cl/K ratios of ten and nine, respectively, compared to ratios generally from 38 to 73 in holes outside Nash Draw, and a value of 52 at Surprise Spring. Hole WIPP-27 is downslope from the tailings ponds of Mississippi Chemical Corporation's potash refinery in Nash Draw, while WIPP-29 is downslope from the tailings ponds of the International Minerals and Chemicals refinery (Lambert and Harvey, 1987).

Lambert and Harvey (1987) interpret these relationships and the fact that the isotopic compositions of waters from WIPP-29 and Surprise Spring are both distinct from the meteoric field to indicate that:

1. The hydrology of Surprise Spring is essentially isolated and independent from that of the Culebra at WIPP-29, and is not dominated by confined Rustler groundwaters from elsewhere. Surprise Spring discharges from the Tamarisk Member of the Rustler. Nearby exposures of the Tamarisk serve as a likely recharge area for Tamarisk discharge at Surprise Spring, and may or may not be contaminated by local potash-refining operations. The isotopic compositions of groundwaters at both WIPP-29 and Surprise Spring appear to have been derived from surface-type water by partial evaporation.

2. Surprise Spring is not at present a significant point of discharge for Culebra and/or Magenta fluids flowing across the WIPP site.

3. As indicated by the relatively low Cl/K weight ratios in fluids from WIPP-27 and WIPP-29, local potash refining has a major impact on Rustler geochemistry and hydrology within Nash Draw (Section 4.3.1.1).

Lambert and Harvey (1987) conclude that the isotopic character of fluids collected from the Rustler/Salado contact zone (Figure 4.3.13) is strongly affected by rock-water interaction (isotope shift). The extent of this effect generally increases with increasing distance from Nash Draw, paralleling a general decrease in permeability (Section 4.1) and increase in rock-water ratios.

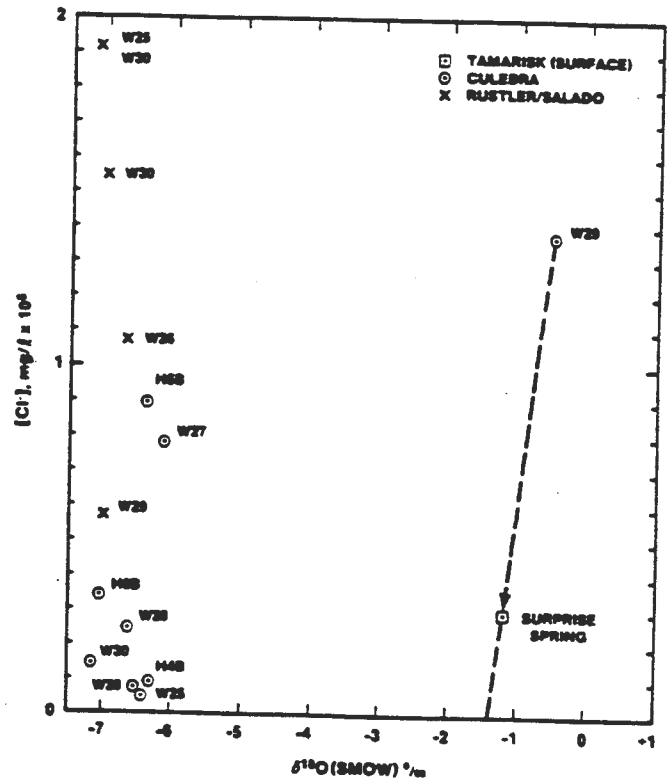


Figure 4.3.12: Relationship between oxygen fractionation and chloride content for analyzed fluids from the Culebra, Magenta, and Rustler/Salado contact. Figure 21 of Lambert and Harvey (1987).

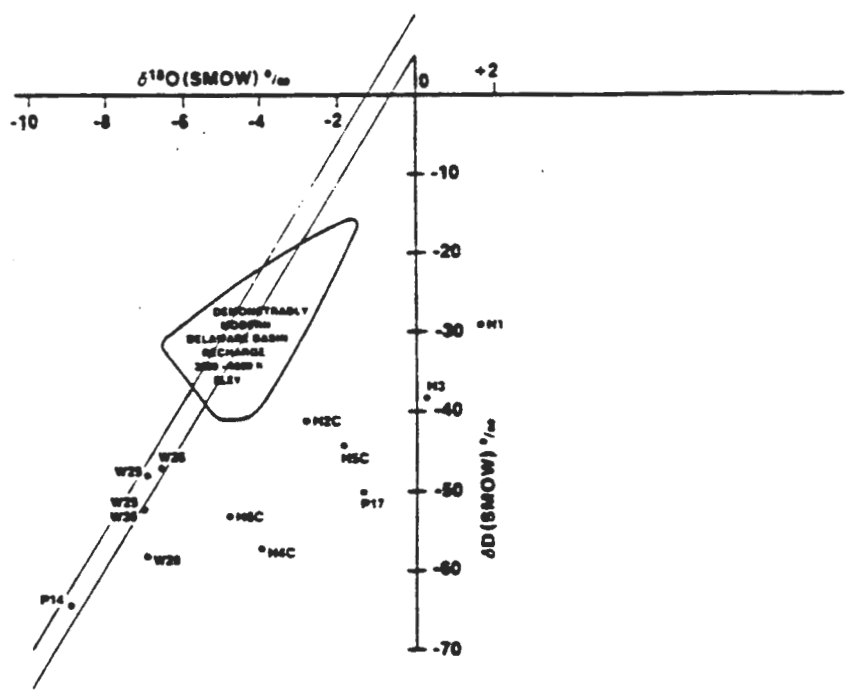


Figure 4.3.13: Stable-isotope character of waters from the Rustler/Salado contact, compared with modern precipitation in the northern Delaware Basin. The "modern recharge" field is defined as in Figure 4.3.10. Figure 15 of Lambert and Harvey (1987).

The interpretations of Lambert and Harvey (1987) and Lambert (1987b) are not consistent with some conclusions contained in Chapman (1986), which is based on review of much of the data contained in the two later reports. The fundamental disagreement lies in interpretation of the distinctions between waters from unconfined portions of the Capitan limestone, modern precipitation, and Rustler waters from at and near the WIPP site. The logic behind a portion of the disagreement is shown in Figure 4.3.14. Chapman (1986) concludes that the isotopic character of modern meteoric recharge in both the northern Delaware Basin and the Roswell Basin is represented by the weighted mean precipitation for the town of Roswell, calculated by Hoy and Gross (1982) (Figure 4.3.14), and that meteoric variability in both areas is closely represented by the trend line of Craig (1961). If these assumptions are valid, then it is possible to derive most of the isotopic compositions of unconfined waters collected within Carlsbad Caverns by "high-humidity" evaporation (line B in Figure 4.3.14) of water representing the calculated Roswell-weighted mean precipitation. Under this interpretation, the unconfined waters from Carlsbad Caverns would be secondary, and would not represent modern meteoric precipitation. As shown, the weighted mean precipitation used by Chapman to derive unconfined Capitan waters is also distinct from the compositional field defined by most Rustler, Dewey Lake, and confined Capitan waters. Chapman (1986) attributes this difference to a "seasonal or amount effect."

Chapman (1986) also notes that, if only stable-isotope relationships are considered, the isotopic character of waters from Surprise Spring can be derived by partial near-surface evaporation of Rustler groundwaters (Line A in Figure 4.3.14); i.e., that Surprise Spring could be a major point of discharge for Rustler waters at and near the WIPP site. While this appears to be theoretically possible on the basis of stable-isotope relationships alone, the solute-composition relationships described in Lambert and Harvey (1987) and summarized above preclude this possibility.

The disagreement between the interpretations contained in Lambert and Harvey (1987) and Chapman (1986) concerning the overall nature of the hydrology in southeastern New Mexico is fundamental, and cannot be resolved by stable-isotope studies alone. However, these studies do clarify the differences in opinion. Chapman (1986), in effect assumes that the hydrology of southeastern New Mexico is at steady state (or, alternatively, that its response to changing climatic conditions is effectively instantaneous). She assumes that the weighted mean precipitation for Roswell and the statistical correlation of Craig (1961) are significant by themselves, and demonstrates that it is possible, based on these assumptions, to generate unconfined waters from Carlsbad Caverns by evaporation. By Chapman's interpretation, the unconfined Capitan waters do not represent modern recharge. However, the field of demonstrably modern Delaware Basin recharge defined by Lambert and Harvey (1987) includes or is consistent with analyses from several other locations in addition to Carlsbad Caverns. The weighted mean precipitation used by Chapman to derive unconfined Capitan waters by evaporation is also distinct from the compositional field defined by most Rustler, Dewey Lake, and confined Capitan waters. Chapman (1986) attributes this difference to a "seasonal or amount effect." The

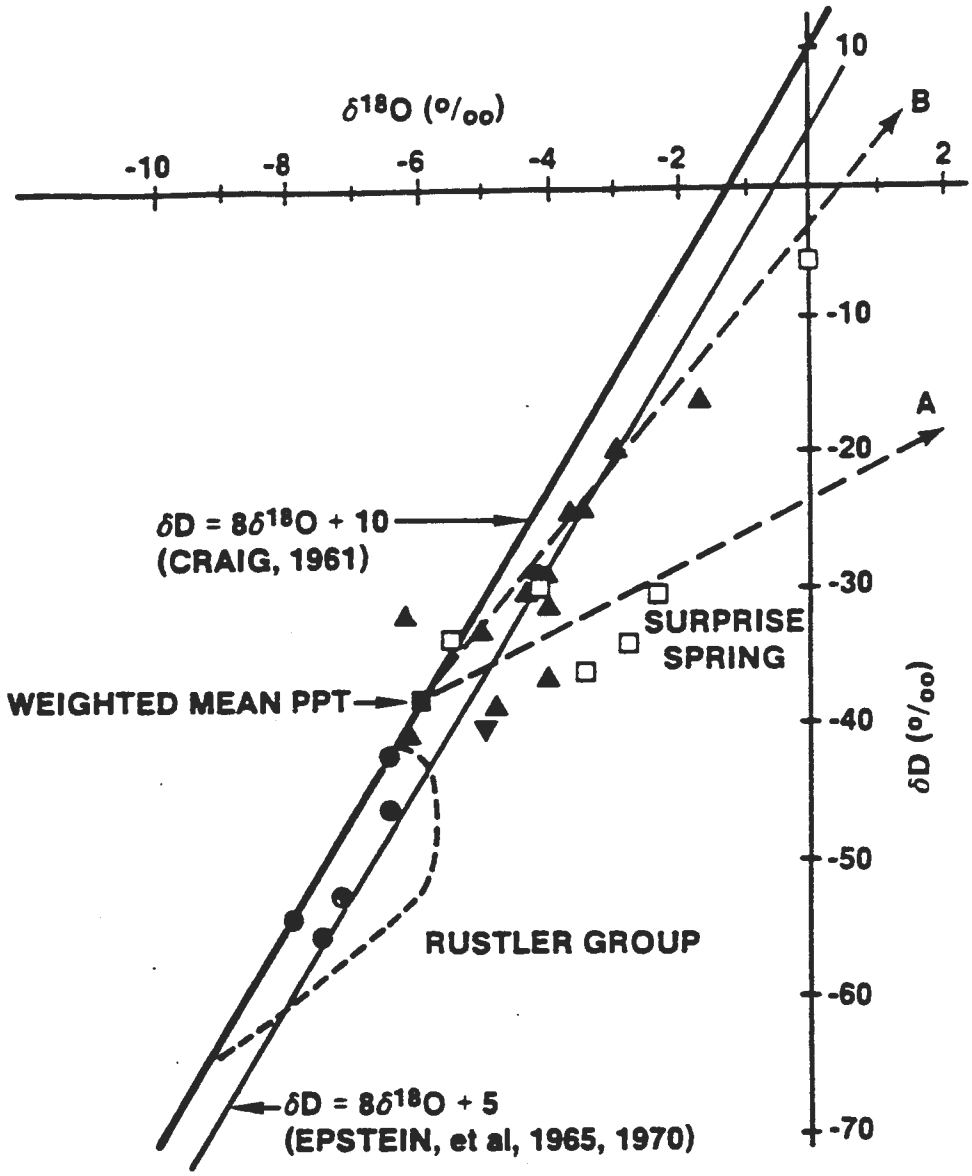


A: TREND FOR "LOW-HUMIDITY" EVAPORATION
B: TREND FOR "HIGH-HUMIDITY" EVAPORATION

- ● CAPITAN AQUIFER
- ▼ SHALLOW AQUIFERS: SANTA ROSA, DEWEY LAKE
- □ SURFACE WATER
- ▲ CARLSBAD CAVERNS
- ■ WEIGHTED MEAN PPT

Figure 4.3.14: Possible derivation of Carlsbad Caverns waters from modern precipitation. Modified from Figures 13 and 14 of Chapman (1986), by addition of the statistical correlation line for meteoric precipitation of Epstein et al. (1965, 1970) and deletion of waters from the Roswell Basin.

operation of this effect on Rustler, Dewey Lake, and confined Capitan waters, as well as Ogallala water from the High Plains is not explained.

Lambert and Harvey (1987) do not assume that the hydrology of southeastern New Mexico is at steady state. They do assume that significant departure in isotopic signature from the meteoric field defined by the compositional space between the statistical correlations of Craig (1961) and Epstein et al. (1965, 1970) is required before any recourse to evaporation is justified. Unconfined Capitan waters (and others, such as Ogallala fluids and samples from alluvium at WIPP-15) are interpreted by Lambert and Harvey (1987) to represent modern meteoric recharge in the northern Delaware Basin. The demonstrably different isotopic character of most Rustler, Dewey Lake, and confined Capitan waters from the field they interpret to represent modern recharge in the northern Delaware Basin is taken to reflect recharge under conditions distinctly different from those controlling modern recharge. Since steady state is not assumed, no single weighted mean precipitation is either defined or deemed relevant. The conclusions of isotopic studies discussed in Sections 4.3.3, 4.3.4, and 4.4.2 are consistent with the interpretation of a transient hydrologic setting of the Rustler Formation and shallower units at and near the WIPP site.

### 4.3.3 Recent Isotopic Studies with Emphasis on Radiocarbon

Studies investigating the applicability of several environmental isotopes (isotopes generated primarily within the atmosphere), especially radiocarbon, to the shallow stratigraphic units at the WIPP are summarized by Lambert (1987a, 1988). Although the emphasis in these studies was on radiocarbon, tritium, and chlorine-36 were briefly evaluated. No $^{36}Cl$ above background could be identified, nor could tritium values significantly above background be identified except in hole WIPP-27. The high chlorine background is to be expected in fluids in a halite-bearing evaporite section. The tritium at WIPP-27, consistent with the major-solute composition of Culebra groundwaters from WIPP-27 (Section 4.3.1.1), is interpreted to be due to contamination by potash-refining operations. Radiocarbon studies indicate that many of the sampled wells have been contaminated by organic materials during drilling, casing, and/or hydrologic testing. The successful radiocarbon measurements indicate isolation times of at least 12,000 to 16,000 years for three Culebra waters and one Dewey Lake water. Two of the four measurement points lie on nearly opposite sides of the WIPP site.

The relationship between calculated "percent modern carbon" (PMC) and the bicarbonate content of most of the fluids analyzed to date, including three samples from the Rustler/Salado contact zone, is summarized in Figure 4.3.15. PMC is carbon counts relative to 1950 wood. As shown in Figure 4.3.15, there is a strongly linear relationship between PMC and bicarbonate. The apparent end members are: a) a 0-PMC fluid with a bicarbonate content of approximately 60 mg/l, i.e., groundwater in equilibrium with carbonate, assuming bicarbonate is equal to total carbonate; and b) a 100-PMC fluid with a bicarbonate content of approximately 300 mg/l.

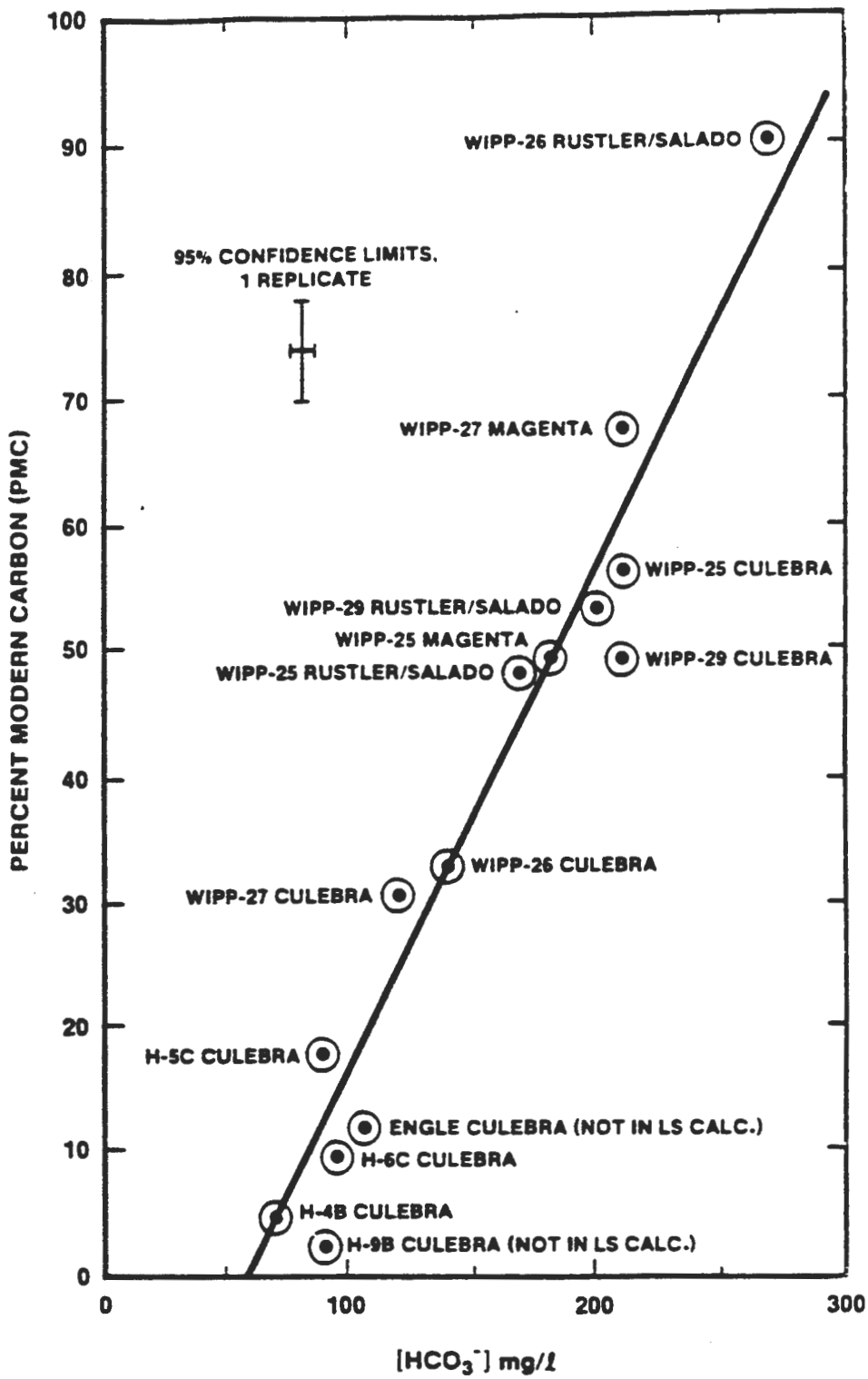


Figure 4.3.15: Relationship between calculated percent modern carbon (PMC) and bicarbonate in analyzed fluids. Figure 3 of Lambert (1987a).

If, as is commonly the case in radiocarbon studies, it is assumed that recharge groundwaters initially containing small amounts of atmospherically derived $CO_2$ (PMC near 100) equilibrate fairly quickly with carbonate minerals underground, it is difficult to explain waters in Figure 4.3.15 having greater than approximately 60 mg/l bicarbonate. In other words, one would expect the slope in Figure 4.3.15 to be negative rather than positive if this slope reflected increasing equilibration with underground carbonates with increasing time (decreasing PMC) (Lambert, 1987a). By this logic, the high-PMC samples in Figure 4.3.15 do not represent modern infiltration.

Regardless of the origin of high-PMC contents, a linear relationship should result from evaluation of any two compositional variables for the same fluids, if the data distribution in Figure 4.3.15 is a result of linear mixing of two fluid components. This is not the case for the analyzed fluids since the relationship between $^{13}C$ fractionation and bicarbonate (Figure 4.3.16) is statistically random. This result suggests that at least three fluid components may be involved in mixing to develop the indicated $^{13}C$ distribution. In such mixing, unique delineation of the mixing relationships and the ages or isolation times of the specific groundwater components involved is most likely impossible (Lambert, 1987a).

The relation between percent modern carbon (PMC) and $^{13}C$ fractionation for the samples on which adequate data are presently available is shown in Figure 4.3.17. The sampled fluids fall into two relatively distinct groups: a) a small group containing samples with less than approximately 10 PMC; and b) a larger group with from 10 to greater than 90 PMC. Data from H-5c and Engle could be included with the low-PMC group shown in Figure 4.53, though, as noted by Lambert (1987a), the statistical correlations within both data groupings are stronger if the four low-PMC samples (H-4b, H-6c, H-9b, and Pocket) are considered as a separate group. Of the four low-PMC samples, all but that from the Pocket well are for fluids from the Culebra dolomite; the Pocket sample is from the Dewey Lake Red Beds.

The definition of two distinct data groupings (Figure 4.3.17) leads to identification of three carbon-isotopic compositional components apparently involved in mixing within Rustler, Dewey Lake, and Rustler/Salado fluids. These are:

1. Dissolved carbon from Permian marine carbonates. Because the Permian carbonates are more than 200 million years old, this carbon is no longer measureably radioactive.

2. $CO_2$ derived from modern organic materials injected in variable amounts into the sampled holes during drilling and/or casing activities. Lambert (1987a) found it pointless to attempt dating of almost all of these contaminated samples, as discussed below.

3. $CO_2$ derived from Pleistocene and older organics during recharge. The location of this recharge cannot be specified on the basis of these studies. Because of the possible contamination of all these samples by small amounts of $CO_2$ from the modern reservoir, calculated PMC values

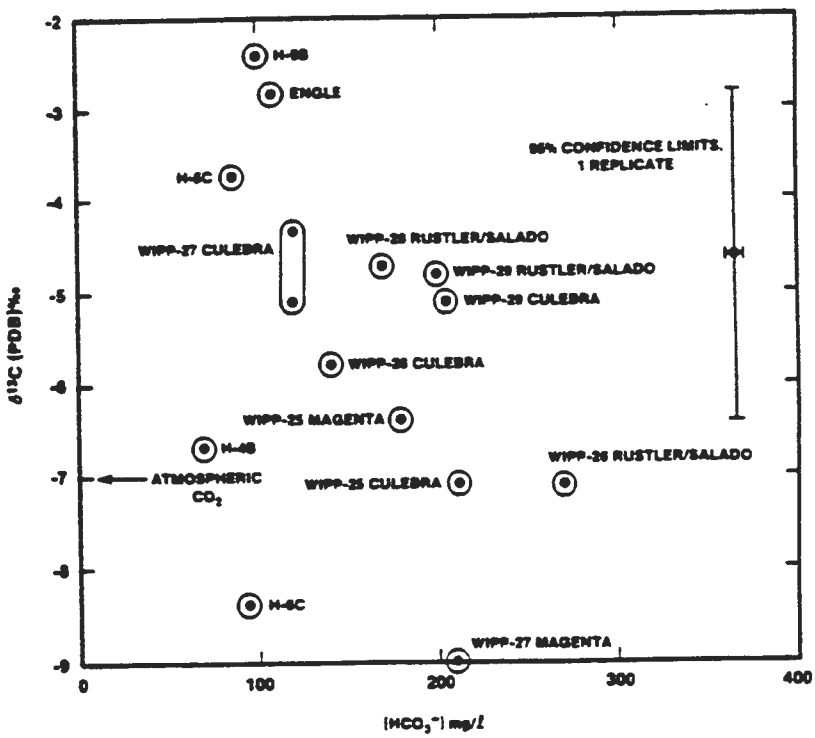


Figure 4.3.16: Relationship between $^{13}C$ fractionation and bicarbonate for analyzed fluids. Figure 4 of Lambert (1987a).

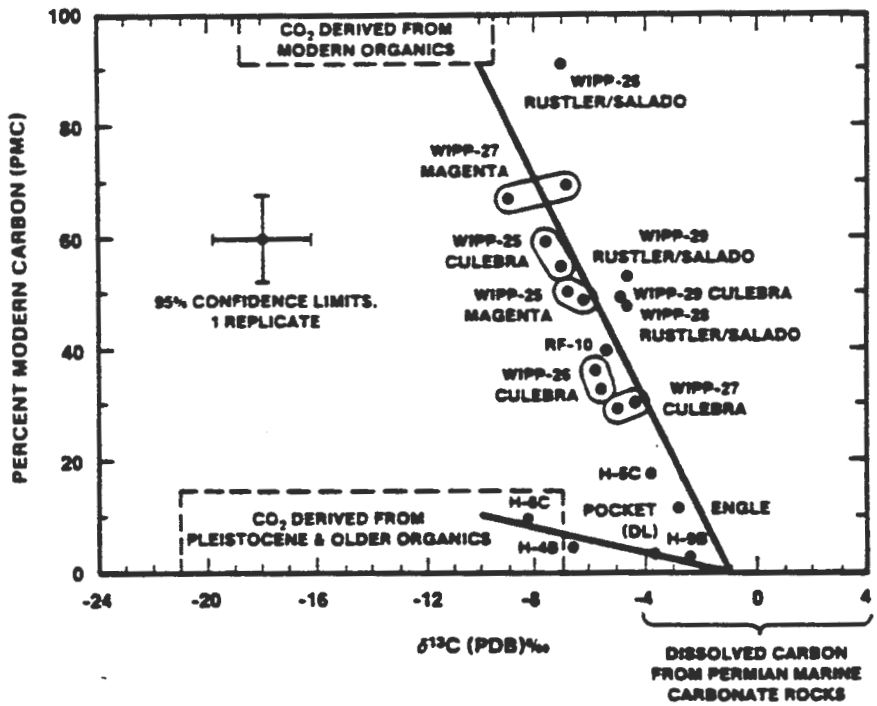


Figure 4.3.17: Relationship between percent modern carbon and $^{13}C$ fractionation for analyzed fluids. Three-component mixing is a plausible explanation for carbon-isotope characteristics of sampled Rustler and Dewey Lake fluids. In addition to "dead" carbon resulting from interaction with Permian carbonates, all samples may contain both $CO_2$ derived from Pleistocene and older organics and an unresolved component of $CO_2$ derived from modern organics. Figure 9 of Lambert (1987a).

in the four low-PMC samples shown in Figure 4.3.17 must be upper limits. Conversely, calculated ages or residence times for the fluids must be lower limits.

Lambert (1987a) applied several different numerical models to the analyzed groundwaters. The results, summarized in Table 4.15, indicate calculated isolation times of the sampled waters from any significant component of atmospherically derived carbon. The ages do not indicate that the fluids have been in their present location for the indicated time, simply that they have been isolated from a near-surface environment for approximately the time indicated. For the samples on which application of the models of Tamers (1975), Pearson and Swarzenki (1974), Mook (1976), and Evans et al. (1979) were generally successful, i.e., the four low-PMC samples (H-4 Culebra, H-6 Culebra, H-9 Culebra, and Pocket Dewey Lake), the results indicate isolation times of between 10,600 and 25,700 years, depending on both sample and model used. The different models used vary in the correction mechanisms assumed to effect fluid interaction with the rock. Lambert (1988) notes that it is not possible to reliably separate the effects of natural isotope evolution from effects of contamination for any data lying off the two-component mixing lines in Figure 4.3.17, i.e., within the three-component mixing triangle.

Because of the method it uses in correcting for equilibration between groundwater and carbonates, and because it involves only a limited number of empirically-derived inputs, Lambert (1987a) concludes that the model of Evans et al. (1979) is the available model most applicable in the WIPP environment. One conclusion arising from the presence of Permian marine carbonates in the Rustler and use of the model of Evans et al. (1979) is that any groundwater sample with greater then 50 PMC must either be contaminated, or must be assumed to have had very limited exposure to the carbonates present. Application of the model of Evans et al. (1979) to the entire data set results in: a) calculated isolation times of 12,100 to 16,100 years for the four low-PMC samples identified in Figure 4.3.17; and b) physically impossible negative model ages for all samples on and near the trend including modern organics in Figure 4.3.17, with the exception of samples from H-5c (Culebra) and Engle (Culebra). These two samples yield model ages of 714 and 2,410 years, respectively, but lie within the three-component mixing triangle shown in Figure 4.3.17.

Based on radiocarbon studies, Lambert (1987a) concludes that:

1. The four interpretable radiocarbon ages on Rustler and Dewey Lake fluids, i.e., those calculated on minimally contaminated samples using the model of Evans et al. (1979), indicate that some Culebra and Dewey Lake fluids present in the vicinity of the WIPP site were isolated from atmospheric radiocarbon at least 12,000 to 16,000 years ago. The relatively tight cluster of ages may suggest some type of recharge episode, rather than a gradient resulting from continuous recharge.

2. Because of there being no consistent directional age gradient in calculated ages in such old groundwaters, the radiocarbon technique provides no information concerning directions or rates of fluid flow within either the Rustler Formation or the Dewey Lake Red Beds in applications to date on WIPP groundwaters.

Table 4.15: Results of application of different interpretative models to available radiocarbon analyses, including corrections involving dolomite. Part of Table 4 of Lambert (1987a).

| Locality | PMC | $\delta^{13}C$ | Tamers (1975) | Pearson and Swarzenki (1974) | Mook (1976) | Evans et al. (1979) |
|---|---|---|---|---|---|---|
| H-4 | 4.82 | -6.7 | 19300 | 17300 | 12000 | 16100 |
| H-6 | 9.7 | -8.4 | 13600 | 12600 | 10600 | 12100 |
| H-9 | 2.22 | -2.4 | 25700 | 20200 | indet. | 14900 |
| Pocket | 3.67 | -3.8 | 21600 | 17400 | indet. | 14000 |

3. To date, most radiocarbon measurements on Rustler fluids collected in hydrologic drillholes are invalidated by unknown amounts and types of organic contamination occurring during and after drilling. Most fluids have a carbon-isotopic signature apparently reflecting nonresolvable three-component mixing among inorganic carbon, organic carbon from a past period of surficial recharge, and modern organic contamination introduced during drilling. All samples collected may be contaminated at some level; therefore, most calculated groundwater ages are lower limits.

4. Application of several models to calculate radiocarbon ages indicates that the best useable model is that of Evans et al. (1979), which accounts for both congruent dissolution of carbonates and possible continuing exhange of radiocarbon between the diluted groundwater solution and the surrounding country rock.

While the radiocarbon studies described by Lambert (1987a; 1988) were partially successful and indicate lower-limit isolation times for sampled fluids at four specific locations, extrapolation of the results must be done carefully. The results do not: a) mean that the sampled fluids have been in residence at the sampling sites for the indicated lengths of time; b) provide any information about where major recharge occurred when it did take place; or c) rule out small but indeterminate amounts of modern vertical recharge to the Rustler and Dewey Lake at the WIPP site. The available radiocarbon data can be interpreted consistently to mean that "steady-state" recharge of the Rustler and Dewey Lake is an actively ongoing process only at locations removed from the WIPP site, and that flow times from the point(s) of recharge to the sample localities are at least 12,000 to 16,000 years. However, the results mean that surficial recharge at the WIPP site, if significant at some time in the past, effectively stopped at the sampled localities at least 12,000 to 16,000 years ago. Two of the sampling localities, H-4 and H-6 lie close to and on nearly opposite sides of WIPP Zone 3.

Lambert (1987a) also concludes that measured $^{36}Cl$ and tritium contents on minimally contaminated Rustler fluids at and near the WIPP site cannot be discriminated from background values. Because of the high chlorine background in fluids that have been in contact with halite present in the Rustler and/or in surficial deposits in southeast New Mexico, no measurable $^{36}Cl$ was detected. No tritium content greater than 0.2 tritium units (TU) was found in any fluid that was demonstrably minimally contaminated, in contrast to a reasonable "background" level of 3 - 7 TU. The highest measured tritium content in Culebra water is 6.9 TU from WIPP-27 (Lambert, 1987a). However (Section 4.3.1.1) the Culebra at WIPP-27 is interpreted to be contaminated by potash-refining operations, on the ground of major-solute chemistry. Therefore, Lambert (1987a) concludes that there is no advantage in pursuing either technique further in the Rustler Formation at the WIPP site.

### 4.3.4 Uranium-Disequilibrium Studies in the Culebra Dolomite

The radiocarbon studies summarized in Section 4.3.3 indicate that the recharge age of groundwaters presently in the Culebra dolomite and part of the Dewey Lake Red Beds at and near the WIPP site is at least 12,000 to 16,000 years. While these results indicate that, independent of flow path, travel times from recharge to their present location are long, they indicate nothing about the flow directions or distances involved. The uranium-disequilibrium technique discussed in this section addresses some questions which cannot be addressed by radiocarbon or stable-isotope techniques, such as apparent directions of fluid flow. The basic principles of the uranium-disequilibrium method are discussed in both Lambert and Carter (1984) and Lambert and Carter (1987).

Interpretations of uranium-disequilibrium data can only be as reliable as the number and quality of the samples from which the data are derived, and are also limited by the applicability of the principles involved in the interpretations. There are two specific constraints to interpretation of uranium-disequilibrium data at and near the WIPP site. First, data east of Nash Draw are extremely limited in number, since values are known at only four locations, H-4, H-5, H-6, and WIPP-30. As a result, there is considerable uncertainty in both contouring of results and inferred flow directions east of Nash Draw. Second, as noted by Lambert and Carter (1987), there is no known trace component of Rustler fluids which reliably indicates whether or not any sampled groundwater is representative with respect to either total uranium content or uranium-disequilibrium "activity ratio" (A.R.). The activity ratio considered here is in terms of relative decay rates of the $^{234}U$ and $^{238}U$ isotopes, not the ratio of chemical activities. Two measurement trends have been noted which help evaluate the extent of approach to steady-state fluid composition during serial sampling and/or indicate the direction from which the sampled fluid may approach or bound a representative state for groundwater at the sampling locality. Uranium is a trace contaminant, at concentrations greater than normal for evaporitic rocks, in drilling and sampling apparatus, especially casing. Therefore, total uranium in the sampled fluid generally decreases with increasing pumping rate and/or total pumping time (Lambert and Carter, 1984), as the amount of contamination is reduced. Measured total uranium

contents in Culebra waters should represent upper bounds. The measured $^{234}U/^{238}U$ activity ratio in sampled fluids generally increases with total pumping volume and rate; i.e., with decreasing contamination from the casing and/or sampling apparatus (Lambert and Carter, 1984). This is presumably because the contamination present in sampling apparatus and casing has an Activity Ratio (A.R.) very near 1.0. Any measured A.R. in a sampled fluid should thus represent lower bounds.

As noted in Lambert and Carter (1987), interpretation of uranium-disequilibrium studies involves additional assumptions. During recharge, an initial A.R. equal to or not much greater than 1.0 (generally 1 - 3) is assumed to be fixed at the edge of the oxidation zone. There are several generalized sequences of behavior that can follow infiltration. The conceptual and numerical model used is essentially that of Osmond and Cowart (1976). The variability can be simplified by considering the relationship between A.R. and total uranium in the analyzed fluid. Under reducing conditions, the total uranium content of the fluids remains low, and the A.R. normally increases along the direction of fluid flow. This increase is a result of the preferential leachability of the $^{234}Th$ resulting from the alpha decay of $^{238}U$ within the country rock, relative to the leachability of $^{238}U$ (Lambert and Carter, 1984; 1987). Thus, the combination of low total uranium content and elevated A.R. is interpreted to reflect flow along a flow path under relatively reducing conditions or locally "stagnant" flow conditions, both occurring on a time scale for which the technique is applicable, approximately 2,000,000 years (Lambert and Carter, 1984). In contrast, a measured groundwater A.R. near 1.0 is taken to indicate one of three things: 1) approach to secular equilibrium after a lengthy period of radioactive decay; 2) sampling of fluids soon after recharge; and/or 3) possible "swamping" of a higher A.R. by dissolution of rock uranium having an A.R. very near 1.0. A strong correlation of increasing total uranium content of sampled fluids with decreasing fluid A.R. along an inferred flow path favors the third interpretation. This can only occur under relatively oxidizing conditions under which the congruent solubility of uranium is enhanced.

The available data for the $^{234}U/^{238}U$ A.R.s in Culebra fluids at and near the WIPP site are summarized in Figure 4.3.18. The figure shows a general eastward or southeastward increase in A.R.s east of Nash Draw. Contour lines shown in Figure 4.3.18 are based on the assumption that variations in A.R. are approximately linear between data points. From the resulting contours, it was inferred by Lambert and Carter (1987) that the most likely region of recharge for Culebra groundwaters is in or near the upturned edge of the Rustler units within Nash Draw. This interpretation reflects a major easterly or southeasterly component of flow from a recharge region within Nash Draw, assuming that high A.R.s such as measured in the WIPP site area at H-4, WIPP-30, and H-5 are generated by downgradient flow under relatively reducing conditions.

The flow directions implied by the contouring in Figure 4.3.18 are not unique, because of both the limited data east of Nash Draw and uncertain relationships between flow directions and directions in which A.R.s increase. All that is certain is that, unless no reaction is taking place, fluid flow must be at some angle to the lines of constant A.R., but need

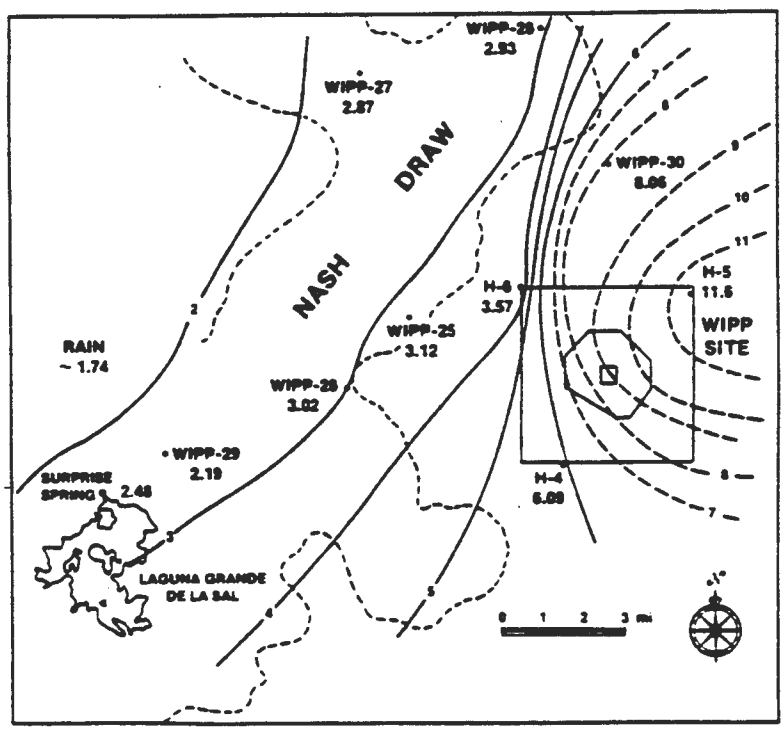


Figure 4.3.18: $^{234}U/^{238}U$ activity ratios in analyzed Culebra fluids. Figure 3 of Lambert and Carter (1987).

not be perpendicular to these lines. By analogy, groundwater flow in a fractured or anisotropic medium need not be perpendicular to potentiometric contours. If fluid flow is assumed to be perpendicular to the A.R. contours in Figure 4.3.18, flow is required to have taken place from regions of (present) high permeability in Nash Draw towards regions of (present) low permeability east of Nash Draw, such as the vicinity of H-5.

In addition, there is considerable freedom in the contouring of A.R. values themselves. An indication of this is shown in Figure 4.3.19. In the interpretation shown in Figure 4.3.19, the assumption of roughly linear variation in A.R. between data points is relaxed, and contours are rotated into a more north-south position. Under this interpretation, since the flow direction must be inclined to A.R. contours, the present A.R. distribution would be consistent with flow towards the south or southeast following recharge, i.e., at a lower angle to both the axis of Nash Draw and the very loose regional zonation of permeability within the Culebra (Section 4.1) than implied in Figure 4.3.18. However, flow towards the axis of Nash Draw is not consistent with the data.

While the uranium-disequilibrium method is not always capable of identifying the recharge area, it is capable, unlike radiocarbon applied to Rustler groundwaters, of estimating flow directions following recharge. The higher-permeability areas within the Rustler Formation in Nash Draw seem a more likely paleorecharge area than either the surface of the WIPP site area or the low-permeability areas east of WIPP-30. Therefore, flow within the Culebra following recharge probably had at least some easterly component.

Regardless of the estimated fluid-flow directions following recharge, the flow times estimated for the buildup to measured A.R.s east of Nash Draw depend on both the measured or assumed original uranium content of the host rock and the measured or assumed total uranium content of the groundwater fluid immediately after recharge. This buildup is a result of a combination of differential leachability of $^{234}Th$ and $^{238}U$ under reducing conditions and radioactive decay. In general, estimated flow times towards a measured high A.R. are inversely proportional to the initial uranium content of the groundwater and proportional to the estimated uranium content of the country rock. For example, Lambert and Carter (1987) found it impossible to generate calculated A.R.s greater than 3.4 using the mean present-day U concentration in Culebra core ($0.9 \times 10^{-6}$ g/g) and the lowest measured U concentration in Culebra fluid ($0.134 \times 10^{-9}$ g/g) as input. They interpret this inability to indicate that: (a) the present uranium concentration of the available Culebra core samples is probably not representative of the rock controlling A.R. buildup; and (b) the lowest measured uranium concentration in the fluid phase has been increased by at least some congruent dissolution.

Lambert and Carter (1987) estimated flow times to H-5, assuming that the original U content of Culebra fluids was the same as the lower value measured in fluid from the Rustler/Salado contact in hole WIPP-30 ($0.024 \times 10^{-9}$ g/g). Calculated travel times are approximately 550,000 and 30,000 years, for an assumed low-uranium and high-uranium Culebra matrix, respectively. The low-uranium matrix was taken as the average value

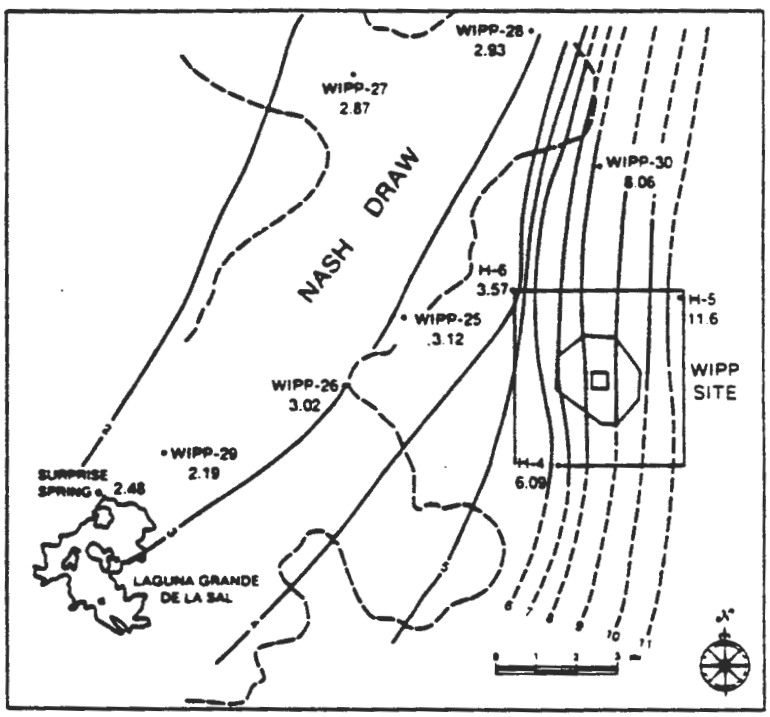


Figure 4.3.19: Contours of $^{234}U/^{238}U$ activity ratios in analyzed fluids, relaxing constraint of linear variation between data points. Modified from Figure 3 of Lambert and Carter (1987).

measured on core ($0.9 \times 10^{-6}$ g/g), and the high-uranium matrix ($9.0 \times 10^{-6}$ g/g) was assumed. The assumed value is similar to that measured in a silty zone found within a Permian limestone in Carlsbad Caverns. In the WIPP site area, local high U contents within Culebra are supported by a known (but uncored) occurrence of a silty zone in hole P-15, indicated by geophysical logging to be rich in (uranium + thorium + potassium). A final A.R.-evolution path, assuming the initial uranium content in the fluid was the same as that measured in Carlsbad rain, $0.01 \times 10^{-9}$ g/g, yields estimated flow times to H-5 of 140,000 and 12,000 years, respectively for the low-uranium and high-uranium Culebra matrices.

Thus, the minimum estimated times required for ingrowth of $^{234}U$ to give the measured high A.R.s at H-5, assuming a uranium-rich Culebra matrix, are qualitatively consistent with the estimated minimum recharge ages based on radiocarbon studies reported in Lambert (1987a). Analyzed Culebra core has a lower uranium content than assumed in these calculations. Therefore, flow times from the position of recharge to H-5 were almost certainly much greater. The measured A.R. of greater than 11.0 at H-5 is inconsistent with any significant modern recharge in this area. A minimum flow time of at least several thousand years is required under reducing conditions to generate such an A.R., regardless of assumptions concerning initial fluid and rock-matrix properties, location of recharge, and directions of fluid flow.

The ingrowth of A.R.s cannot be considered independently of the total dissolved uranium in the fluid phase. Figure 4.3.20 indicates a westerly or northwesterly increase in the amount of uranium in Culebra waters, from the WIPP site towards Nash Draw. Although there is uncertainty in the contouring of total uranium contents, the general direction of increase correlates with a general decrease in A.R. in a similar direction (Figure 4.3.18 or 4.3.19).

It is difficult to explain how any easterly flow of oxidized fluids involved in significant evaporite dissolution could maintain both high A.R.s and low total uranium contents measured east of Nash Draw, as would be required by any interpretation involving steady-state flow directions consistent with A.R. contouring in either Figure 4.3.18 or 4.3.19. During such flow, uranium would have to be precipitated within the Culebra dolomite. No evidence for elevated uranium concentrations has been found within the Culebra, except in hole P-15; the P-15 occurrence may in fact be a detrital accumulation. Measured uranium contents of bulk Culebra core are too low to account for the measured A.R.s.

A logical explanation of the combination of measured A.R.s and total uranium contents of Culebra groundwaters at and near the WIPP site involves a change of flow directions, after development or ingrowth of the elevated A.R.s measured east of Nash Draw (Lambert and Carter, 1987). In this interpretation, an early flow system with at least some component of easterly flow under reducing conditions, would later be changed, resulting in some component of westerly flow. The magnitude of the required change in flow directions within the Culebra is not well defined at present. Combination of the contours in Figure 4.3.19 and 4.3.20 requires something like a 60-degree change, assuming recharge occurred in the northern part of

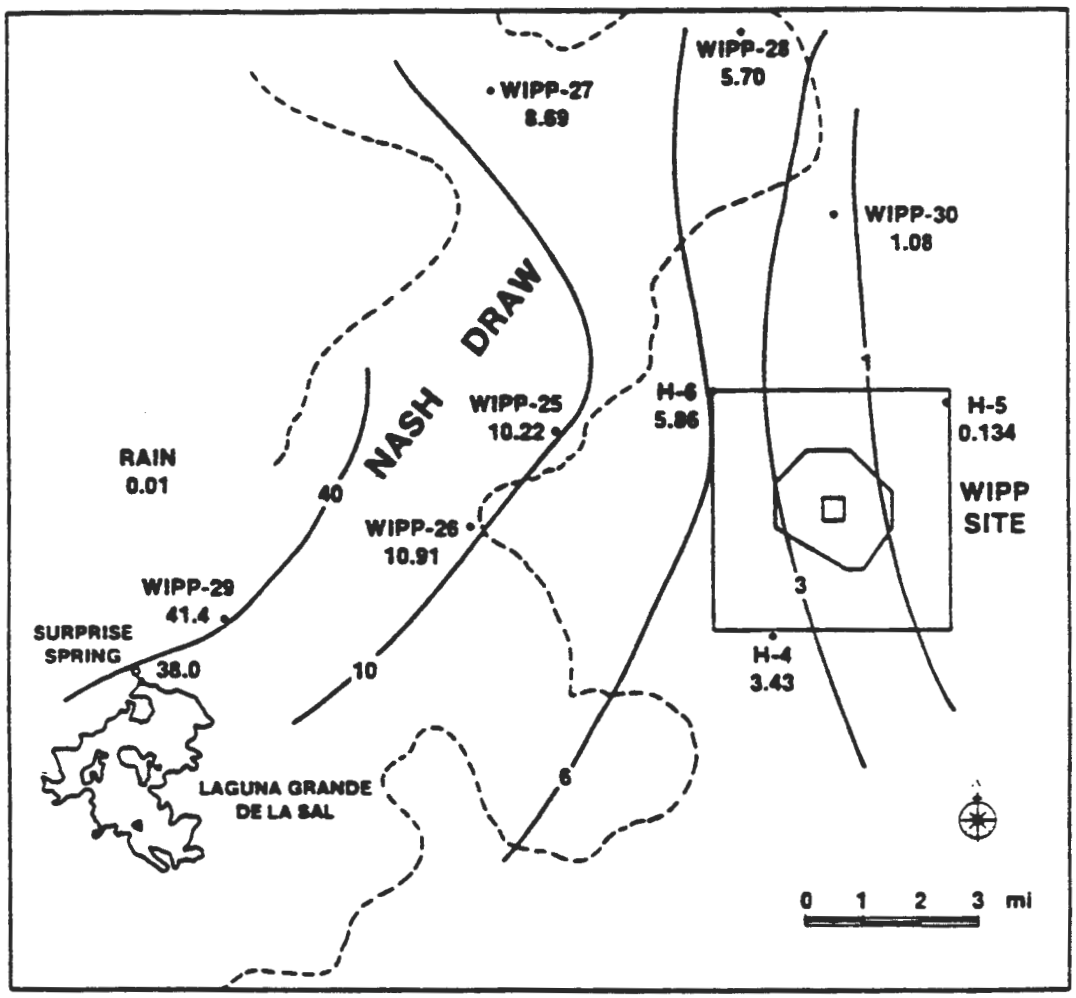


Figure 4.3.20: Total dissolved uranium content of analyzed fluids. Figure 2 of Lambert and Carter (1987).

Nash Draw. Combination of the contours in Figure 4.3.18 and Figure 4.3.20, assuming recharge within the main part of Nash Draw, implies a more marked "reversal" of flow directions.

Because of the general westward increase in total uranium in the Culebra groundwaters, the process resulting in a change in flow directions within the Culebra must include a general westward increase in oxidation potential, with resulting increase in uranium solubility. The mechanism for such an increase in oxidation potential, while not well defined at present, would presumably be related to the continuing exhumation of the Rustler Formation within Nash Draw (Lambert and Carter, 1987). Consistent with this interpretation, the redox measurements discussed in Section 4.3.1.4 generally indicate more oxidizing conditions within the Culebra south of the WIPP site and within at least part of Nash Draw than at the WIPP site.

Regardless of the detailed interpretation of transient flow directions within the Culebra, the uranium-disequilibrium studies of Lambert and Carter (1987) place strong constraints on some aspects of Culebra hydrology at and near the WIPP. These include the three constraints that:

1. Culebra fluid residence times at or flow times to sampling localities east of Nash Draw (H-4, H-5, H-6, and WIPP-30) are at least several thousand years. The shortest calculated residence or flow times are consistent with minimum groundwater isolation times estimated in radiocarbon studies (Section 4.3.3).

2. Regardless of the high Culebra head potentials in the area (Figure 4.1.23), no significant recharge is occurring in the vicinity of H-5. This conclusion is indicated by the high A.R. and low total fluid uranium in this area.

3. A significant amount of evaporite dissolution, under relatively oxidizing conditions appears to have taken place in and near Nash Draw, as indicated by the relatively high dissolved uranium contents in this area.

## 4.4 Recent Studies Addressing Near-Surface Geology and Hydrology at and near the WIPP Site

Considerable emphasis since 1983 has been given to evaluation of near-surface processes at the WIPP site. The primary objective of this effort has been evaluation of the potential for evaporite dissolution within the Rustler Formation. Regardless of conclusions concerning evaporite dissolution within the Rustler, studies of near-surface processes and stratigraphy at the WIPP demonstrate the transient nature of the climate and near-surface hydrologic setting in southeastern New Mexico. Section 4.4.1 summarizes recent studies of the near-surface stratigraphy and general geologic and hydrologic setting of southeastern New Mexico. Section 4.4.2 briefly summarizes recent studies concerning the extent of rock/water interactions and evaporite dissolution within the Rustler Formation.

### 4.4.1 Recent Studies of Near-Surface Stratigraphy at and near the WIPP Site

Recent studies of the near-surface stratigraphy at and near the WIPP site summarized in Bachman (1985) were conducted as part of the evaluation of possible near-surface evaporite dissolution. The present distribution of the Gatuna Formation at and near the WIPP site is shown in Figure 4.4.1. An ash bed relatively high in the Gatuna is between 500,000 and 600,000 years in age (Bachman, 1980). Since the Gatuna is overlain by the Mescalero caliche, which began to form approximately 500,000 years ago (Bachman, 1980), Bachman (1985) concludes that the Gatuna is ". . . at least as old as Middle Pleistocene and may contain some much older deposits." While preparing the isopachs shown in Figure 4.4.1, Bachman determined that the Gatuna along Livingston Ridge, on the east side of Nash Draw (Figure 1.1), contains cross-bedded channel deposits and conglomerates deposited by westward-flowing streams. The Bachman (1985) interpretation of the probable courses of streams at and near the WIPP site during Gatuna time is shown in Figure 4.4.2. Areas near the WIPP site presently overlain by Gatuna gravels were occupied approximately 600,000 years ago by moderate-energy stream channels. Based on comparison of the isopach maps for the Gatuna (Figure 4.4.1), Triassic rocks (Figure 4.4.3), and the Dewey Lake Red Beds (Figure 4.4.4), Bachman (1985) concludes that the Gatuna streams flowed across and eroded both Triassic and Dewey Lake Red Beds strata. In contrast, the present climate and surface-hydrologic setting at the WIPP site does not support any moderate-energy streams.

The Mescalero caliche, which overlies the Gatuna, is interpreted by Bachman (1985) as reflecting a slow process of soil formation on a stable geomorphic surface. The caliche is well-developed, and, in locations where the ". . . laminar horizon and the dense plugged horizons within the caliche are at the surface," contributes to ". . . rapid runoff and even to flooding during periods of heavy rainfall" (Bachman, 1985). Radiometric measurements indicate that the basal and upper portions of the Mescalero caliche began to form approximately 510,000 and 410,000 years ago, respectively (Bachman, 1980). The Mescalero surface on which the Mescalero caliche formed, encompasses the Livingston Ridge surface at and near the WIPP site (Figure 1.1). The widespread occurrence of the Mescalero caliche indicates relative structural stability of the Livingston Ridge surface over at least the last 400,000 years.

The Berino soil, a locally distributed paleosol up to approximately 1 m thick, is interpreted by Bachman (1985) as a remnant soil sequence that originally included the older Mescalero caliche. Local survival of the Berino, which began to form approximately 350,000 years ago, is interpreted to require ". . . a long period of tectonic and geomorphic stability within a limited climatic regime" (Bachman, 1985).

There is widespread evidence that the hydrologic setting of the vicinity of the WIPP site has changed at least once over the last 600,000 years. The Gatuna Formation, including moderate-energy stream gravels and conglomerates, was deposited at least 600,000 years ago in a setting which included actively eroding streams. Since approximately 350,000 years ago, the Livingston Ridge surface developed on the Mescalero caliche has remained

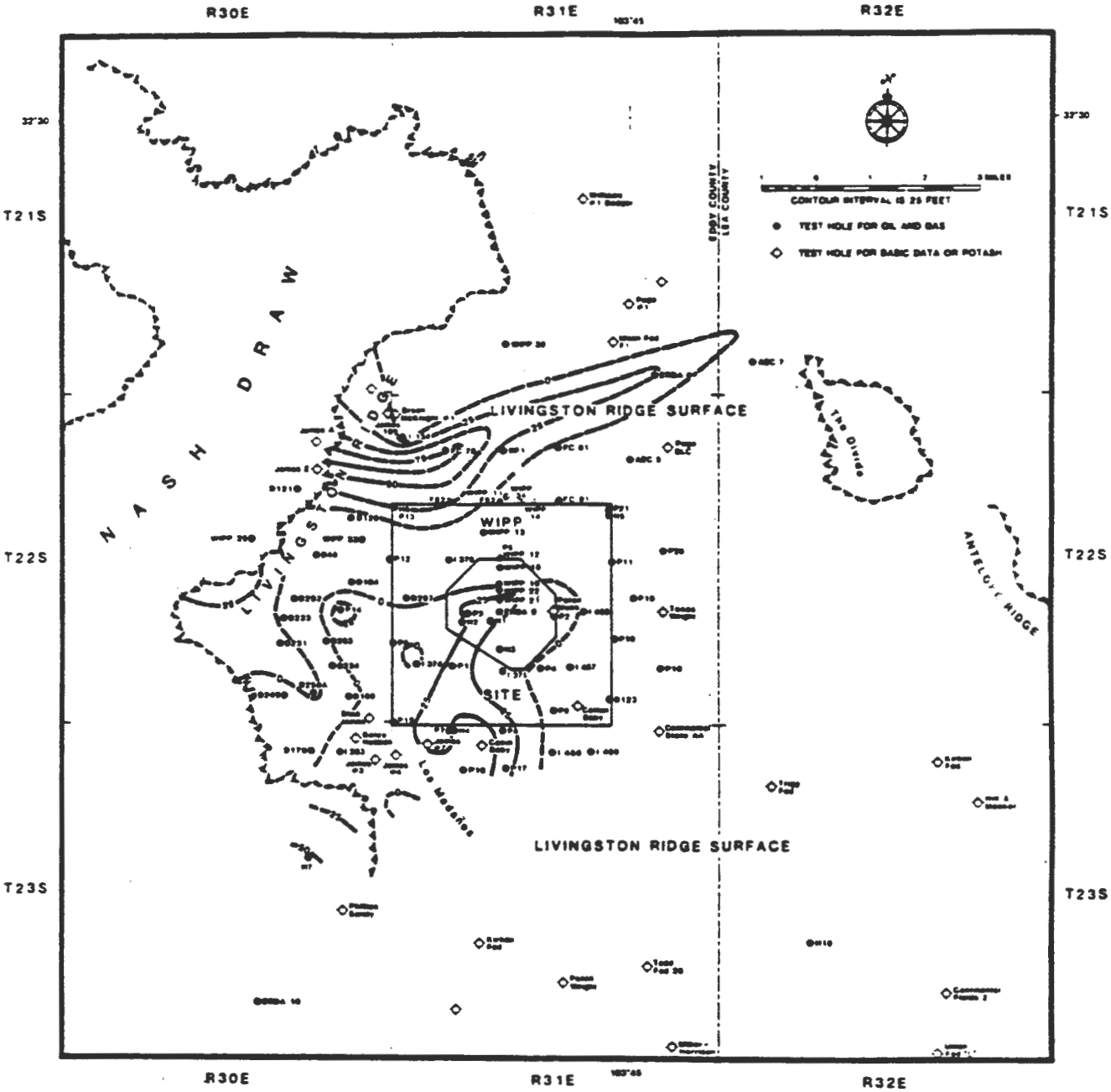


Figure 4.4.1: Distribution and thickness of the Gatuna Formation at and near the WIPP site. Figure 4 of Bachman (1985).

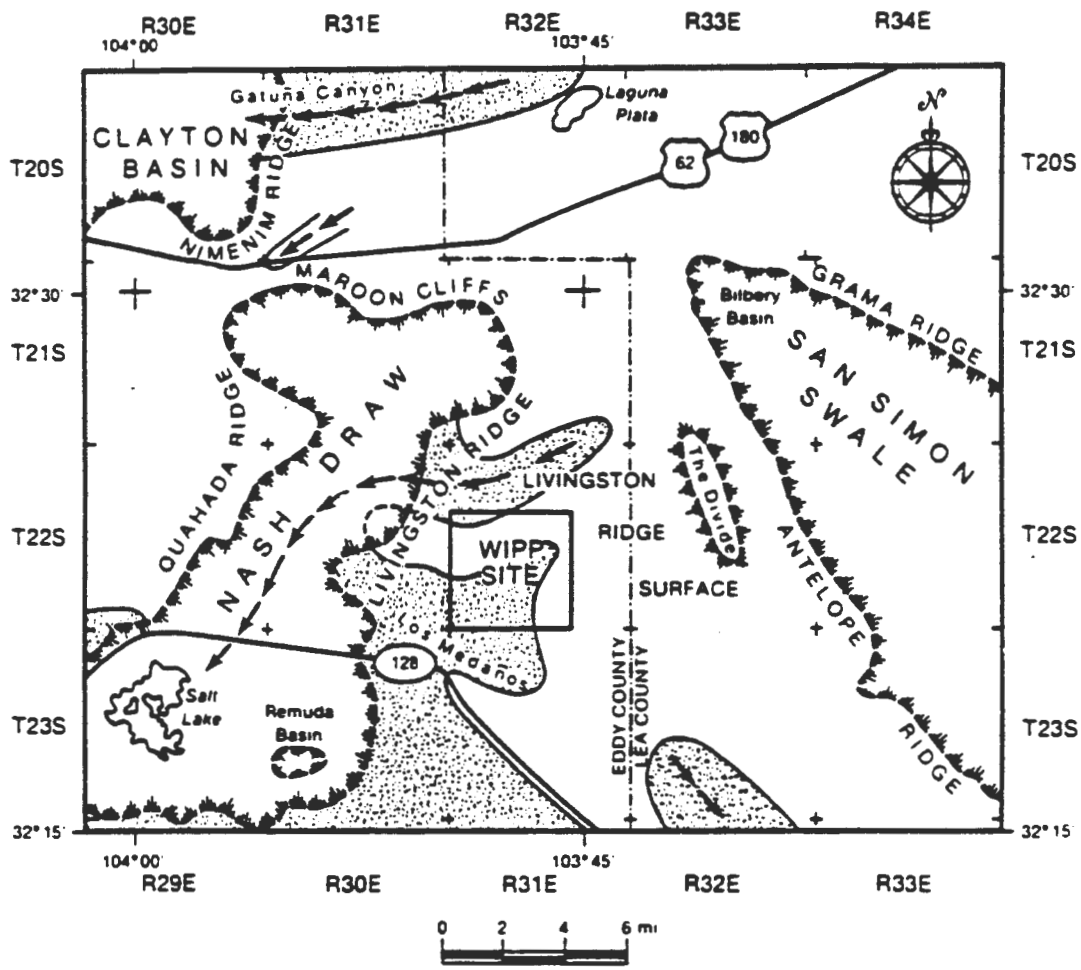


Figure 4.4.2: Probable distribution of stream channels and flow directions at and near the WIPP site during Gatuna time. Figure 11 of Bachman (1985). The present distribution of the Gatuna Formation is indicated by the stippled pattern.

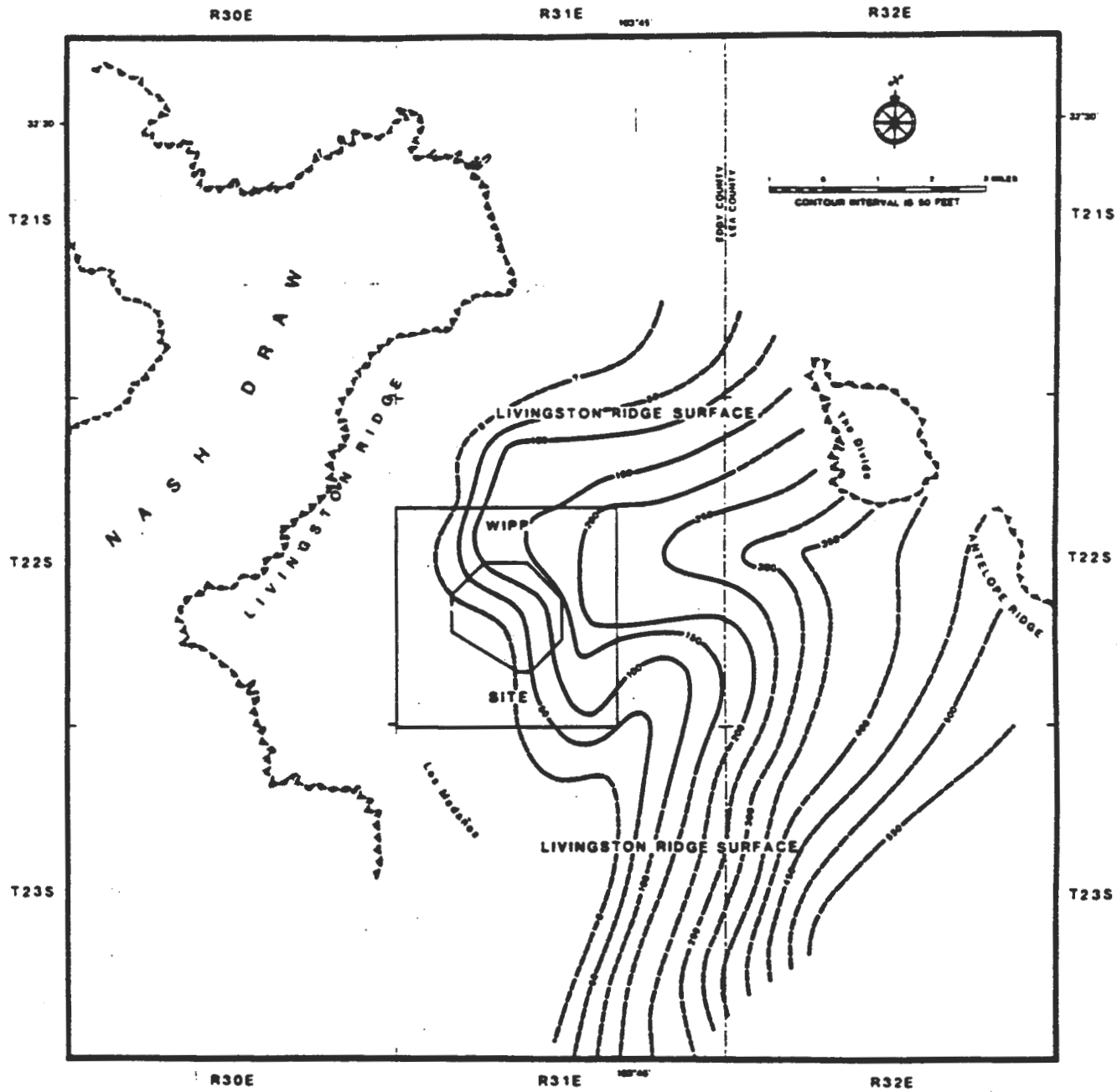


Figure 4.4.3: Distribution and thickness of Triassic rocks at and near the WIPP site. Figure 5 of Bachman (1985).

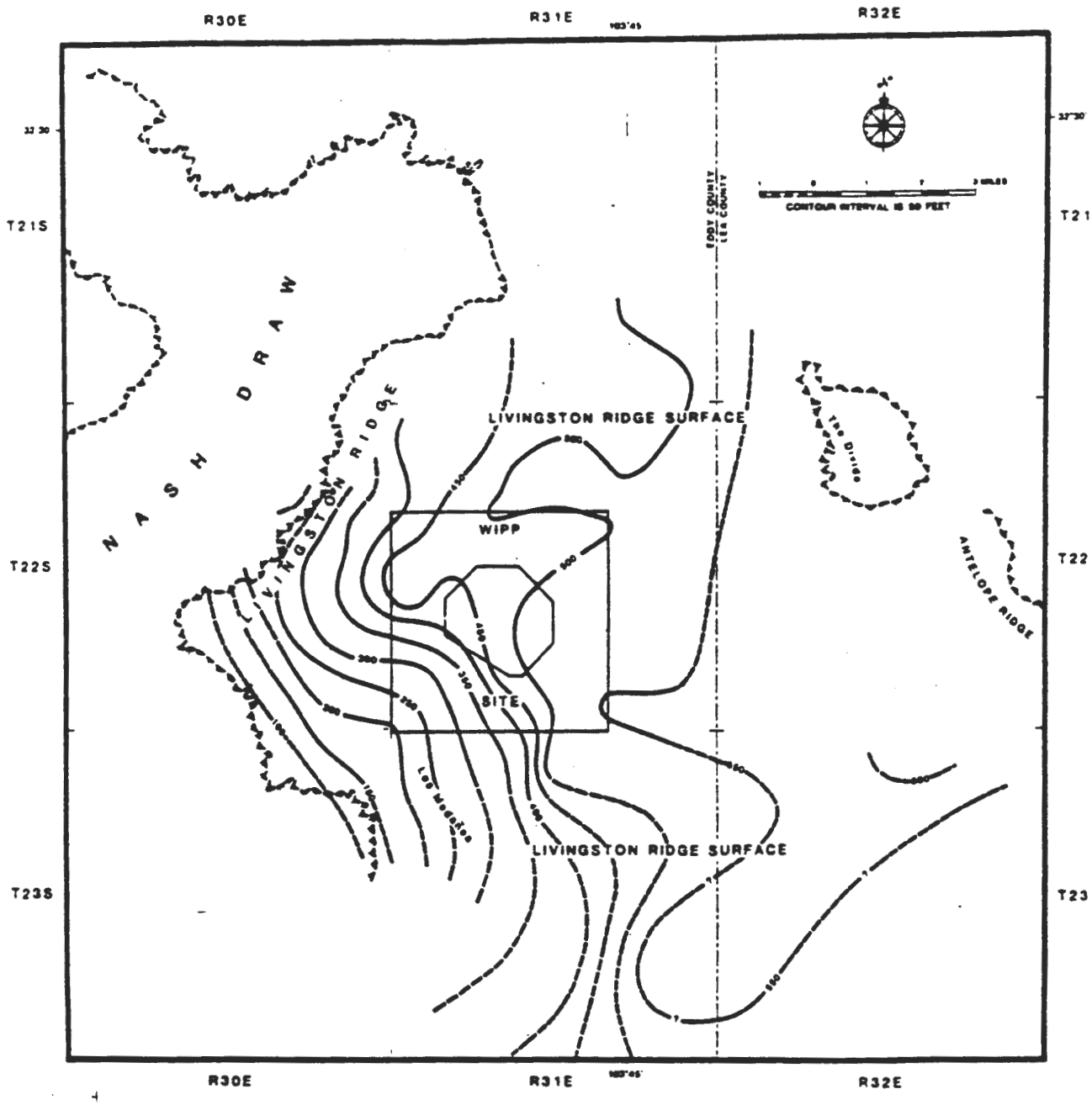


Figure 4.4.4: Distribution and thickness of the Dewey Lake Red Beds at and near the WIPP site. Figure 6 of Bachman (1985).

relatively stable; i.e., stable enough for local survival of the thin, 350,000-year-old Berino soil. The time scale of the climatic change between the Gatuna and Mescalero, however, is more than an order of magnitude greater than most groundwater residence, flow, and/or recharge times discussed in Section 4.3.

There is, however, evidence of local surface-water activity near the WIPP site, ending some 25,000 years ago (Bachman, 1980; 1985). This evidence consists of gypsite (calcium sulfate) spring deposits along the east side of Nash Draw. The fact that these springs are no longer active is interpreted by Bachman (1985) to indicate that ". . . the groundwater regime originally responsible for dissolving underground beds of gypsum and depositing spring deposits is no longer active." Bachman (1985) interprets the spring activity as ". . . part of a paleokarst system resulting from a much different [wetter] climatic regime" than the present regime in southeastern New Mexico.

There is limited evidence of regional climatic variability in southeastern New Mexico on approximately the same time scale as the gypsite springs in Nash Draw. As noted by Lambert (1987a), ". . . additional evidence for [a] wetter local climate is given by VanDevender (1980). From studying packrat middens in Rocky Arroyo, northwest of Carlsbad, New Mexico (about 35 miles northwest of the [present] study area . . . he determined that a juniper-oak community was present in the early Holocene (10,500 to 10,000 radiocarbon years ago), where now desert scrub communities exist." The presence of these middens is taken by Lambert and Harvey (1987) to indicate that ". . . in the immediate vicinity of the Delaware Basin, a wetter climate prevailed more than 10,000 years ago; the present desert scrub-plant communities have been stable in the last 4,000 years." Unfortunately, the data presented by VanDevender (1980) provide no information concerning variations in the climate in the area between approximately 10,000 and 4,000 years ago.

There is strong evidence for both climatic and hydrologic changes having occurred since at least 600,000 years ago in the vicinity of the WIPP site, and limited evidence for a "wetter" climate than present approximately 10,000 years ago. Unfortunately, there are broad time gaps in the regional information that is available. For example, no deposits are known at or near the WIPP site that are intermediate in age between the Berino soil and the gypsite springs in Nash Draw (Lambert, 1988).

The stratigraphic and paleoclimatic studies discussed in this section are not alone in indicating a transient hydrologic setting for the WIPP site and vicinity. Fluid-density and flow-time relations discussed in Sections 4.1.3.1 and 4.1.3.2, as well as hydrochemical facies discussed in Section 4.3.1 are all inconsistent with steady-state confined flow. The isotopic studies discussed in Sections 4.3.2, 4.3.3, and 4.3.4 indicate a transient hydrologic setting for the Rustler. The time scale of transience is generally consistent to within less than an order of magnitude with the time scale of the climatic change indicated by the gypsite springs in Nash Draw (Bachman, 1980; 1985) and the packrat-midden studies of Van Devender (1980).

### 4.4.2 Recent Studies of Evaporite Dissolution and/or Vertical Fluid Movement within the Rustler and Younger Formations

4.4.2.1 General Geologic Studies--As mentioned above, the Mescalero caliche is relatively continuous at and near the WIPP site. Where continuous, it plays a major role in limiting modern infiltration of precipitation. As noted by Bachman (1973), however, the unit is not completely continuous, since it is locally pierced by conical structures, roughly 1 m or less in diameter, resulting from localized caliche dissolution by humic acid released by plant roots. The structures generally do not completely penetrate the caliche (Bachman, 1973). Where these structures do completely penetrate, local infiltration through the Mescalero caliche may occur, at least to the depth of plant roots. The widespread presence of the Mescalero caliche on the Livingston Ridge surface must be taken to indicate structural stability of the surface, not to indicate the impossibility of localized infiltration. The widespread preservation of the caliche does indicate that not enough infiltration on a regional scale has taken place since its formation to result in its wholesale dissolution.

As discussed in Section 4.1.1 and 4.1.3, the measured head relations and relative transmissivities of members of the Rustler indicate only limited vertical fluid flow within the Rustler Formation. While there is limited vertical movement, stratabound or confined flow within the Culebra dolomite dominates the hydrology of the Rustler Formation at and near the WIPP site. If, however, vertical flow were to extend from the surface to the Rustler, through both the Mescalero caliche and the Dewey Lake Red Beds, the hydrologic setting of the Rustler Formation at and near the WIPP site might be "karstic." In such a system, vertical fluid movement both from the surface to the Rustler and within the Rustler might result in formation of solution channels or cavities. If karstic hydrology dominated within the Rustler at and near the WIPP site, transport rates to the accessible environment would be significantly increased (e.g., Chaturvedi and Channell, 1985). The presence of karstic cavities within the Rustler at the WIPP site has been proposed by Barrows et al. (1983) to explain apparent gravity patterns in the vicinity of holes WIPP-14 and WIPP-34 (Figure 4.4.1). Two additional structures have been interpreted by some to indicate the extension of the evaporite-karst behavior within Nash Draw over the WIPP site itself (see Neill et al., 1983). The first, a depression and related breach of the Mescalero caliche at hole WIPP-33, is interpreted (e.g., Bachman, 1985) as having originated by downward infiltration from the surface to sulfatic portions of the Forty-niner and Tamarisk Members of the Rustler immediately above and below the Magenta dolomite. The second is a relatively large but shallow depression in the SW1/4, SW1/4, Sec.29, T22S, R31E (see Figure 3.2 for general location), examined directly by Bachman. Bachman (1985) concludes that this structure is a result of wind erosion.

One approach used in arguing in favor of karstic hydrology in the Rustler at and near the WIPP (e.g., Barrows, 1982) is based on the assumption of an idealized water budget or water balance, independent of the presence or absence of specific structures indicating infiltration of surface recharge to the required depths. In such an approach, values of variables such as

infiltration, precipitation, and evapotranspiration are assumed to be known with high precision and accuracy. Any excess of estimated precipitation over estimated evapotranspiration is then attributed to vertical recharge from the surface to the Rustler, i.e., to karstic hydrology. As shown by Hunter (1985), however, the uncertainties in precipitation, infiltration, evapotranspiration and Rustler-discharge data at and near the WIPP site are so large that water-budget techniques cannot be used either to determine the amount of recharge or to determine that recharge is occurring. The detailed water budget described by Hunter (1985) is, in fact, not inconsistent with the conclusion (Sections 4.3.2, 4.3.3, 4.3.4) that no recharge is now occurring at and near the WIPP site. The evaluation of the potential for karst hydrology within the Rustler at and near the WIPP site must be by means of hydrologic and geochemical studies (see Sections 4.1, 4.3, and 4.4.2), rather than by an idealized water budget. The recent hydrologic and isotopic studies discussed in Sections 4.1, 4.3, and 4.4.2 place serious constraints on the plausibility of karstic recharge presently being active at the WIPP site.

If surface waters are to infiltrate to the level of the Rustler Formation, they must penetrate the Dewey Lake, after having penetrated both surficial sands and the Mescalero caliche. The presence of local structures penetrating the Mescalero indicates that localized infiltration is possible, although these structures generally do not completely penetrate the caliche and contain secondary laminar deposits resulting from infilling. Extensive studies of local surface depressions at and near the WIPP site led Bachman (1985) to conclude that:

1. Breaches of the Mescalero significantly larger than those represented by the structures resulting from dissolution by humic acid are required for more than extremely localized infiltration, i.e., for development of karstic structures or hydrology in underlying units. The Mescalero caliche continues underneath the depression in the SW1/4, SW1/4, Sec.29, T22S, R31E examined at the specific request of the New Mexico Environmental Evaluation Group (Neill et al., 1983). Therefore, Bachman (1985) concludes that the depression is a surface structure resulting from wind erosion.

2. The relatively large breach of the Mescalero beneath the surficial depression examined by drilling of hole WIPP-33 (Figure 4.4.1) in 1979 (Snyder and McIntyre, 1981) is a result of infiltration, but is unique at and near the WIPP site. The vicinity of WIPP-33 is the only region near the WIPP site in which vertical infiltration from the surface to the Rustler and resulting development of karstic hydrology and structures in the Rustler is reasonable.

Bachman (1985) does suggest that the gypsite springs along the east side of Nash Draw are the result of removal of anhydrite/gypsum from within the Rustler and development of a local flow system connecting WIPP-33 with the eastern side of Nash Draw. Either cavernous porosity or very soft clay-rich debris was encountered in Forty-niner and Tamarisk anhydrites directly above and below the Magenta dolomite in WIPP-33, but not in either the Magenta or Culebra dolomites. The depth of burial of the Forty-niner anhydrite in WIPP-33 is approximately 120 m.

The apparent WIPP-33 structure within the Rustler is consistent with interpretations that:

1. Rustler dolomites are nearly the last rock type to be significantly affected by evaporite dissolution (Snyder, 1985).

2. Because of the relative mechanical weakness of gypsum, the maintenance of open karstic structures within gypsum is possible only at relatively shallow depths. Bachman (1987) examines the regional distribution and impact of the dissolution of anhydrite and gypsum at relatively shallow depths. Certainly, sulfate dissolution has taken and is taking place within the Rustler Formation in Nash Draw, as evidenced by the continuing formation of small caves and sinkholes in the gypsums/anhydrites of the Tamarisk and Forty-niner Members.

3. The only Rustler carbonate from a water-bearing zone in the region to have recrystallized in response to input of meteoric water is at WIPP-33 (Lambert, 1988).

There is no consensus concerning the amount of evaporite dissolution within the Rustler east of Nash Draw. Two schools of thought exist. One approach, most recently summarized by Snyder (1985) and Lowenstein (1987), basically assumes an original laterally homogeneous halite distribution within the Rustler. By this assumption, lateral variability within the Rustler, especially the presence or absence of halite within the claystone portions of the unnamed lower member, Tamarisk, and Forty-niner Members, is due to halite dissolution. A simplified representation of halite distribution within the Rustler is shown in Figure 1.5. A representative cross section showing the variations in thicknesses and lithologies of individual members of the Rustler is shown in Figure 4.4.5.

As shown in Figure 4.4.5, the progressive east-to-west decrease in halite in successively lower members of the Rustler is reflected largely in decreasing thickness of the affected member. The thickness of the Culebra and Magenta dolomites varies only slightly across the area of the WIPP site. In fact, as shown by changes in Rustler thickness between holes WIPP-25 and BLM-1 (Figure 4.4.6), advanced stages of evaporite dissolution within the Rustler involve alteration/dissolution of anhydrite and gypsum rather than dolomites. The interpretations contained in Snyder (1985) and Lowenstein (1987) maximize both the total amount of halite originally present within the Rustler Formation and the amount of later dissolution. The conclusion in the WIPP FEIS (1980) that evaporite dissolution within the Rustler Formation was not of concern to the WIPP Project was based largely on extrapolation of vertical dissolution rates required to generate the depth of Nash Draw in the approximately 600,000 years since deposition of the Gatuna Formation (Bachman, 1974).

In contrast, Holt and Powers (1984; 1987) conclude on the basis of sedimentological arguments and structures that many structures within the Rustler Formation interpreted by authors such as Snyder (1985) and Lowenstein (1987) as resulting from halite dissolution are a result of primary depositional variability. By this interpretation, the amount of

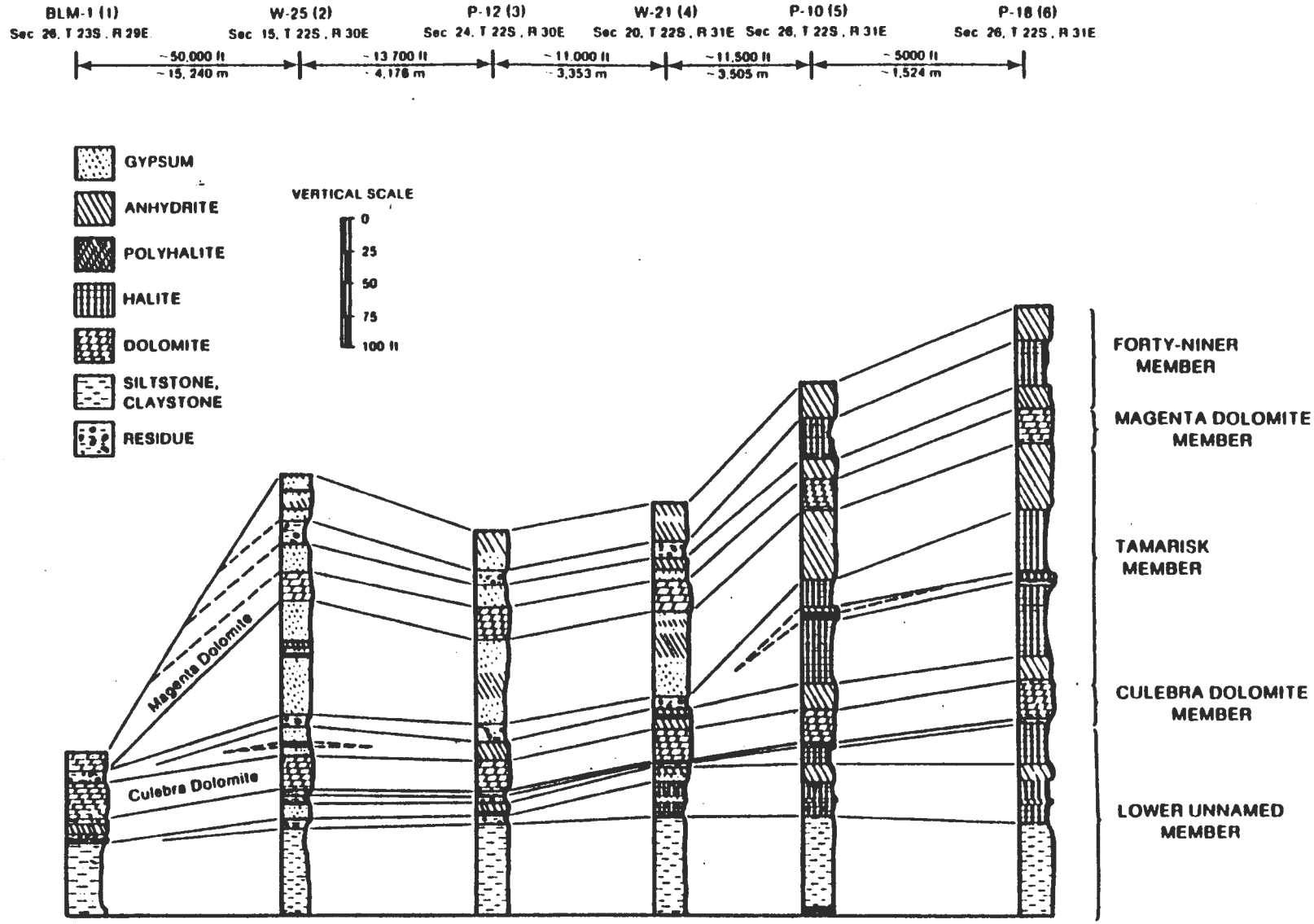


Figure 4.4.5: Columnar cross section across the WIPP site, showing lithologic correlations and variability of units in the Rustler Formation. Figure 2 of Snyder (1985).

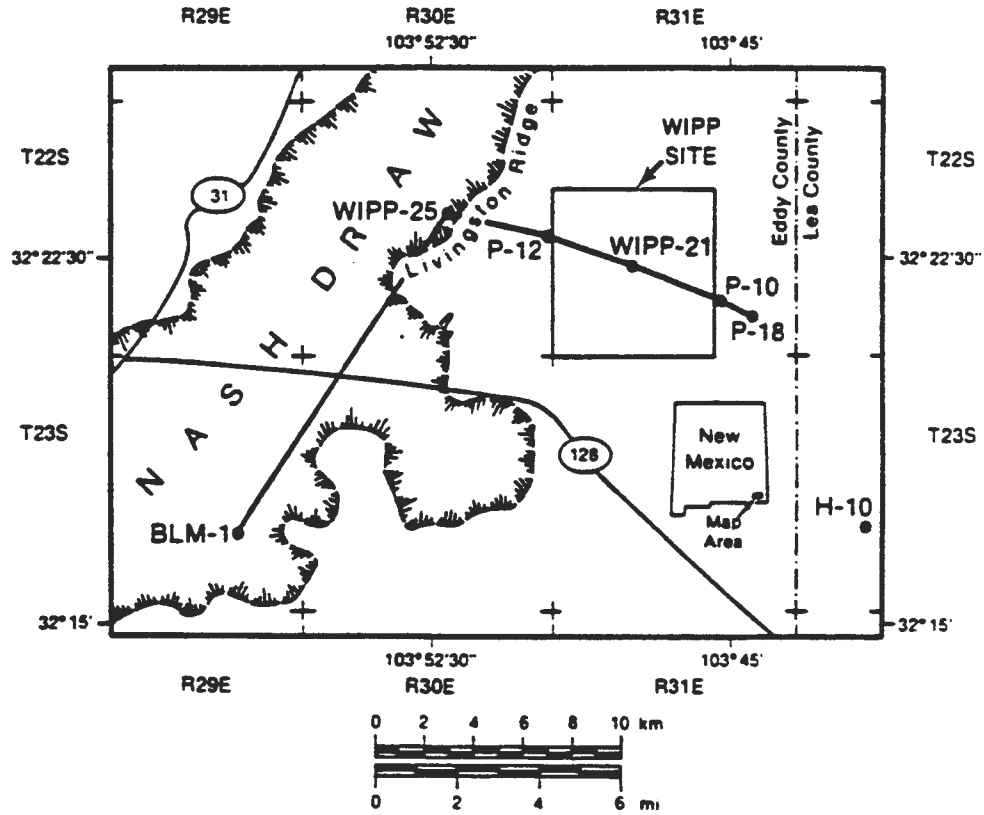


Figure 4.4.6: Hole locations used in Figure 4.4.5. Figure 1 of Snyder (1985).

halite later removed from the Rustler by evaporite dissolution is reduced. Since extrapolation of the estimated rates of dissolution within Nash Draw (Bachman, 1974) indicate that there is no need for concern at the WIPP site over the next 10,000 years, the differing interpretations do not directly affect the expected reliability of the WIPP facility. However, as discussed in Beauheim (1987b), primary depositional variability within the Rustler weakens the present understanding of the correlation between halite distribution within the Rustler, fracturing, and the transmissivity of the Culebra dolomite.

The conclusion that some of the gypsum observed within the Rustler is primary, rather than being due to alteration of preexisting anhydrite, is part of the interpretation by Holt and Powers (1984; 1987). Thus, little movement of water outside the Culebra or Magenta members might be required to account for gypsum observed in the Forty-niner or Tamarisk Members. At the other extreme, the assumption that infiltration from the surface to the Rustler is presently operative at the WIPP site, i.e., that karstic hydrology is important in the Rustler Formation east of Nash Draw or WIPP-33, requires that alteration within the Rustler and overlying formations involves surficial waters. At least localized flow through the anhydritic portions of the Forty-niner and Tamarisk Members is required by this assumption. Recent isotopic studies summarized by Lambert (1988) place constraints on the extent to which waters and hydrated minerals within the Rustler and Dewey Lake Red Beds reflect connate fluids, fluids resulting from stratabound movement, and fluids involved in vertical infiltration.

4.4.2.2 Isotopic Studies--Figure 4.4.7 summarizes $^{87}Sr/^{86}Sr$ measurements (Brookins and Lambert, 1988) on sulfates (anhydrites and gypsum) and carbonates from several evaporitic zones at the WIPP, as well as the Dewey Lake Red Beds. The isotopic signatures of samples from both the Nash Draw gypsite springs and the Mescalero caliche (see Section 4.4.1) are interpreted to represent surficial components; i.e., high $^{87}Sr/^{86}Sr$ ratios resulting from surficial weathering. At the other extreme, the markedly different and internally homogeneous isotopic signature of the anhydrites from throughout the Castile and Salado Formations is interpreted to imply that there has been no distinguishable input of surficial components to these rocks. Anhydrites and gypsums from the unnamed lower member, Tamarisk, and Forty-niner indicate only a very limited input of surficial material, presumably by solute transport by either vertical or stratabound flow.

The Magenta dolomite, which is significantly less permeable than the Culebra in most areas (see Section 4.1.1) is also more similar in $^{87}Sr/^{86}Sr$ character to the surrounding anhydrites and gypsums than is the Culebra. This implies, consistent with conclusions reached in Sections 4.1 and 4.3, dominantly stratabound fluid flow within the Rustler, with the Culebra dolomite being predominant. If the apparent surficial component of the Culebra were a result of vertical infiltration, rather than stratabound flow of originally surficial waters, the infiltration would be expected to alter the overlying portions of the Rustler. Instead, there is much less overlap between $^{87}Sr/^{87}Sr$ ratios measured in the Magenta, Tamarisk, and

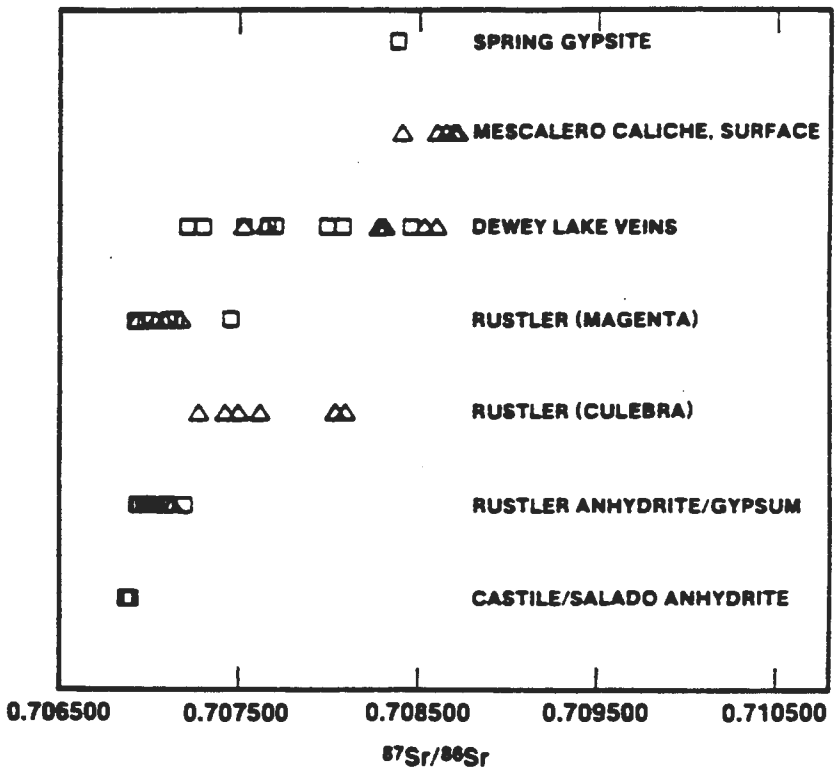


Figure 4.4.7: $^{87}Sr/^{86}Sr$ in Ochoan and related rocks at and near the WIPP site. Squares are anhydrites or gypsums; triangles are carbonates. All samples from the Dewey Lake are from veins. Samples from other units include both matrix and veins. Figure 17 of Lambert (1988).

Forty-niner Members with those measured in the Dewey Lake Red Beds than between the ratios measured in the Culebra and in the Dewey Lake.

Results contained in Figure 4.4.8 indicate further that the hydrologic system in the Dewey Lake Red Beds is significantly distinct from that of underlying units. With the exception of the Dewey Lake Red Beds, this figure summarizes the $^{87}Sr/^{86}Sr$ relationships between coexisting mineral pairs in evaporitic host rocks and in gypsum and/or calcite veins in the same unit. The question is whether these veins are locally derived or result from fluid movement over relatively long-distances. The matrix of the Dewey Lake Red Beds, however, is made up of silicic siltstones and sandstones. Therefore, carbonates and sulfates are rare in the matrix and analyses of Dewey Lake matrix materials are not included in Figure 4.4.8. The gypsum veins within the Dewey Lake probably cannot be locally derived. The strontium-isotopic character of the Dewey Lake gypsum veins (Figure 4.4.8) spans the range from surficial values represented by caliche and spring deposits in Figure 4.4.7 to isotopic values from underlying units. Since effectively none of the Dewey Lake veins can be locally derived, the range in their isotopic character indicates varying degrees of mixing of surficial waters and waters driven upward from the underlying evaporitic zones, consistent with modern head relationships discussed in Section 4.1.1.

Without exception, the strontium-isotope characters of coexisting mineral pairs from veins and host rock in units beneath the Dewey Lake are statistically identical to each other (Figure 4.4.8), indicating that the isotopic character of the vein material is controlled by that of the accompanying host rock, and not by a pervasive hydrologic system interconnected with veins in the Dewey Lake. This is even true for the one sample pair from the Culebra. These results indicate that there is little or no input of surficial material transported by groundwater below the Dewey Lake Red Beds, even into veins. All units below the Dewey Lake Red Beds considered here are evaporitic, i.e., they contain significant carbonates and/or sulfates in their matrix. Therefore, the local derivation of vein carbonates or sulfates is internally consistent.

Figures 4.4.9 and 4.4.10 indicate some constraints in rock-water ratios during gypsum crystallization or recrystallization in the Rustler and Dewey Lake. The dashed lines in Figures 4.4.9 and 4.4.10 represent the ranges in deuterium/hydrogen characteristics of Rustler water and modern surface-meteoric waters identified by Lambert and Harvey (1987) and Lambert (1988). At a sufficiently high rock/water ratio, i.e., when all of the available water is consumed in gypsum formation, for example during alteration of preexisting anhydrite, the deuterium characteristics of the resulting gypsum water of crystallization are constrained to be the same as that of the water added to the system. Therefore, the dashed fields in Figures 4.4.9 and 4.4.10 also represent the expected isotopic character of secondary gypsums formed under conditions involving very high rock/water ratios (Lambert, 1988). At equilibrium with a large excess of water, the deuterium/hydrogen ratio in gypsum is approximately 20 parts per thousand less than that of the coexisting water (Lambert, 1988). Therefore, the fields outlined by solid lines in Figures 4.4.9 and 4.4.10 are decreased from the fields outlined by dashed lines by 20 per mil and represent the

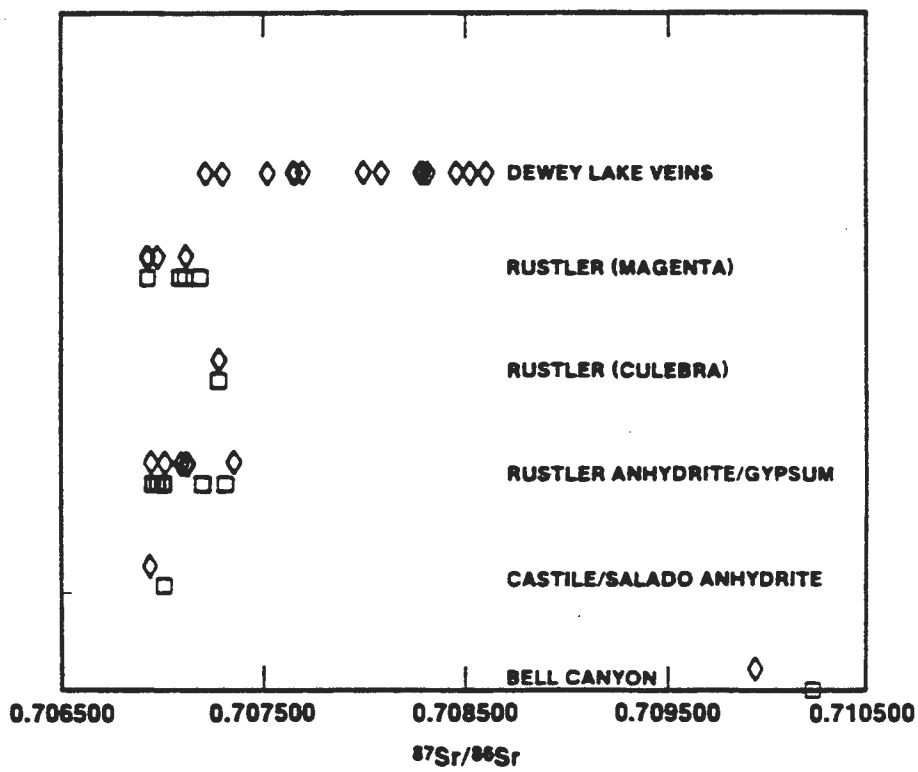


Figure 4.4.8: $^{87}Sr/^{86}Sr$ in coexisting mineral pairs from veins and Ochoan host rocks at and near the WIPP site. Squares are host rocks; diamonds are veins. Figure 18 of Lambert (1988).

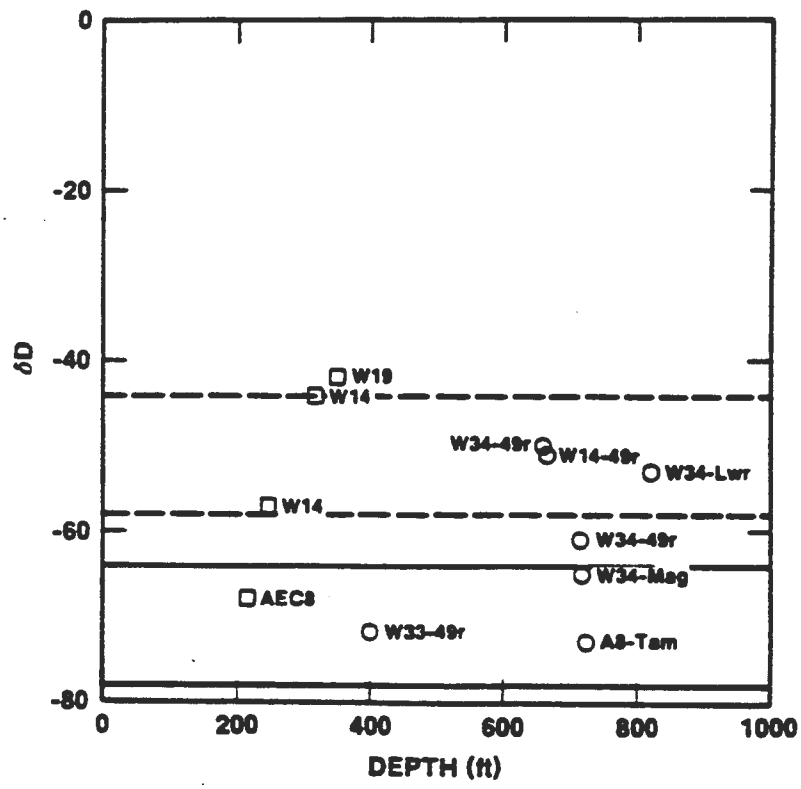


Figure 4.4.9: Deuterium distribution of the waters of crystallization of gypsums from the Dewey Lake Red Beds (squares) and Rustler Formation (circles) at and near the WIPP site, as a function of variations in rock/water ratio involving only Rustler-type water, the range in deuterium content of which is taken from Figure 4.3.10. Solid lines are for crystallization in the presence of a large amount of water, dashed lines for crystallization under conditions involving a very high rock/water ratio, in which all of the water is consumed in gypsum formation. Figure 19A of Lambert (1988).

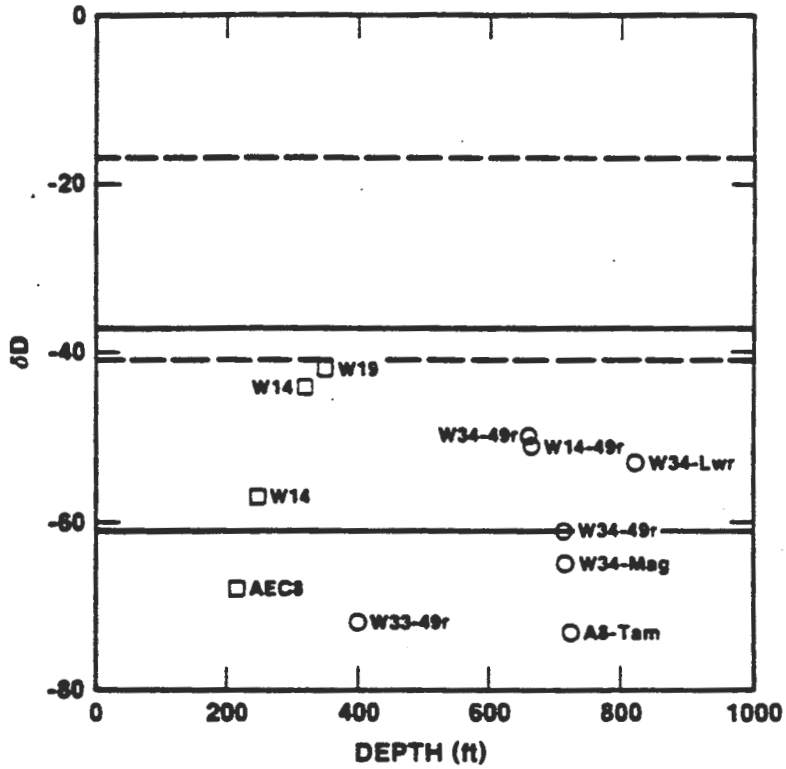


Figure 4.4.10: Deuterium distribution of the waters of crystallization of gypsums from the Dewey Lake Red Beds (squares) and Rustler Formation (circles) at and near the WIPP site, as a function of variations in rock/water ratio involving only surface-type water, the range in deuterium content of which is taken from consistent data in Figures 4.3.8 and 4.3.9. Solid lines are for crystallization in the presence of a large amount of water, dashed lines for crystallization under conditions involving a very high rock/water ratio, in which all of the water is consumed in gypsum formation. Figure 19B of Lambert (1988).

expected hydrogen-isotopic character of gypsums crystallized in the presence of excess amounts of Rustler-type and modern surface-meteoric waters, respectively.

The relationships shown in Figure 4.4.9 are consistent with crystallization of all of the analyzed gypsums with varying amounts of Rustler-type water, with the possible exception of vein material from the Dewey Lake in WIPP-19. Formation of the Dewey Lake gypsum veins in WIPP-19 apparently required infiltration of waters with the same isotopic character as those interpreted by Lambert and Harvey (1987) to represent modern meteoric precipitation. The character of the gypsum from WIPP-33 indicates crystallization in the presence of a large excess of Rustler-type water, but is not consistent with crystallization in the presence of any amount of modern-type water (Figure 4.4.10). [If it is assumed that the Magenta dolomite is more porous (permeable) than surrounding zones within the Rustler at this location, the isotopic variations in the vein gypsums from hole WIPP-34 are consistent with gypsum crystallization under varying ratios of rock to Rustler-type water.] The isotopic relationships (Figure 4.4.9) are consistent with crystallization of gypsums within the unnamed lower and Forty-niner members in response to vertical fluid flow upwards and downwards from the Magenta, assuming increasing effective rock/water ratio with increasing distance from the Magenta. This interpretation is also consistent with modern Rustler head relationships shown in Figure 4.1.3.

While results shown in Figure 4.4.9 are generally consistent with gypsum crystallization in equilibrium with varying amounts of Rustler-type waters, the results in Figure 4.4.10 indicate that this need not be the case for all samples. In Figure 4.4.10, the dashed field represents expected gypsum compositions for crystallization using modern surface-meteoric water, at a very high rock/water ratio, the solid field crystallization in the presence of greatly excess water. The hydrogen-isotopic relations indicate that it is impossible to form the gypsum from the Forty-niner Member at WIPP-33 with modern surface-meteoric water. This conclusion is consistent with the interpretations of Bachman (1980) that the gypsite springs in Nash Draw, which he believes to be the discharge for the WIPP-33 structure, are not presently active. The relations shown in Figure 4.4.10 also indicate that it is not possible to form the gypsum from the Magenta dolomite in WIPP-34 with surface-meteoric waters. The internally consistent interpretation of vertical variations in rock/water ratios within the Rustler Formation in WIPP-34, evident in Figure 4.4.9, breaks down if surface-meteoric waters are assumed to be involved.

The isotopic results summarized by Lambert (1988) indicate that there has been significant involvement of surficial waters in formation of gypsum veins within the Dewey Lake Red Beds. These same results indicate that the hydrologic behavior of the Dewey Lake is largely distinct from that of the underlying units and that there has been some upward movement of fluids into the Dewey Lake from the underlying Rustler Formation, consistent with the modern head relationships discussed in Section 4.1. Isotopic relations within secondary gypsums in the Rustler and Dewey Lake are somewhat ambiguous. In many cases, a given gypsum may have crystallized in equilibrium with either Rustler-type or modern surficial-meteoric waters,

depending on the rock/water ratio that is assumed to have been effective at the time of crystallization. The isotopic variability of gypsums from hole WIPP-34 is, however, best explained by local vertical movement of Rustler-type waters out of the Magenta dolomite, without the vertical karst channel system proposed for this locality by Barrows et al. (1983). It appears impossible to have crystallized secondary gypsum veins from the Dewey Lake at hole WIPP-19 without input of modern surface-meteoric waters. At WIPP-33, where the best physical evidence exists for vertical fluid movement from the surface downwards to the Rustler at depth, the isotopic character of analyzed vein gypsum from the Forty-niner indicates that this movement and related gypsum crystallization does not involve modern surface-meteoric water, i.e., that the WIPP-33 structure is essentially no longer active.

## 5.0 SUMMARY OF WIPP SITE-CHARACTERIZATION ACTIVITIES, 1983 THROUGH 1987

This section summarizes the present understanding of major aspects of WIPP site characterization, including some effort to place the WIPP facility in a regional hydrologic, structural, and geochemical prespective. A general conceptual model for the geologic behavior of the WIPP site and facility vicinity is presented in Section 5.1. Later sections describe more specific inclusions and briefly discuss remaining uncertainties or limitations. It must not be assumed either that any uncertainty discussed is significant to performance of the WIPP facility, or that any given uncertainty could be significantly reduced by further work. It is ultimately the role of the WIPP performance-assessment activity to determine which uncertainties are expected to be significant in evaluation of the short-term and long-term performance of the WIPP facility. The effort here is to provide as complete a conceptual model as possible for these decisions.

### 5.1 General Conceptual Model for the Geologic Behavior of the WIPP Site and Facility

The overall geologic and hydrologic setting of the WIPP site area has been transient (not steady-state) since before the beginning of deposition of the Bell Canyon Formation, approximately 250 million years ago, and will continue to be transient long after effective closure of the WIPP facility. Some events, such as crystallization of secondary minerals within the Salado Formation approximately 200 million years ago and formation of the Mescalero caliche 400,000 to 500,000 years ago, have taken place on a very long time scale relative to WIPP performance assessment, which must consider only a 10,000-year time frame. Two types of transient response have occurred or are occurring at and near the WIPP site within the 10,000-year time frame of regulatory interest. These are: a) the continuing natural response of the geologic and hydrologic systems to the end of the last pluvial period (period of decreased temperatures and increased precipitation) in southeast New Mexico; and b) the continuing responses to hydrologic, geochemical, and structural transients resulting from WIPP site characterization and facility construction. The transient responses induced by the presence of the WIPP underground workings will continue until reequilibration following effective structural and hydrologic closure of the facility.

The Bell Canyon Formation, consisting largely of shales, siltstones, and sandstones, contains the first relatively continuous water-bearing zone beneath the WIPP facility. In some parts of the northern Delaware Basin, the unit contains permeable channel sandstones that are targets for hydrocarbon exploration. Recent studies suggest that the upper Bell Canyon at the WIPP site does not contain any major channel sandstone. This decreases the probability of the Bell Canyon serving as a source of fluids for dissolution of overlying evaporites at the WIPP. These same studies indicate that the final direction of fluid flow following interconnection of the Bell Canyon, Salado, and Rustler Formations within a drillhole would be downward into the Bell Canyon, after accounting for density increases in the fluids due to dissolution of halite within the Salado. It is assumed

here that the measured hydrologic characteristics of the Bell Canyon Formation are more significant to WIPP performance assessment than those of underlying units. The head distribution within the upper Bell Canyon near the WIPP site indicates flow towards the northeast.

Both regional studies and studies within the WIPP facility indicate that the Castile and Salado Formations, both of which are made up predominantly of layered anhydrites and halites, should be considered as low-permeability units that deform regionally in response to gravity. In general, permeabilities and fluid-flow rates in both units are very low and insensitive to stratigraphy. Formation permeabilities in the Castile and Salado Formations remote from the WIPP excavations are generally 0.1 microdarcy or less, and the regional water content of Salado halites is up to 2 weight percent. Exceptions include local brine occurrences in Castile anhydrites and gas occurrences in the Salado Formation, both of which are fracture-controlled, can be large in volume, and can be under pressures high enough to cause fluid flow to the surface. No major gas occurrence within the Salado Formation has been encountered at the WIPP site. In fact, where it has been possible to measure far-field brine pressures within the Salado, the pressures, permeabilities, and available brine volumes combine to indicate the potential for only very limited fluid flow upwards into the overlying Rustler Formation. It is not certain that the Castile and Salado Formations are hydrologically saturated regionally.

Pressurized Castile brines have been encountered in Castile anhydrite in hole WIPP-12, approximately 1.5 km north of the center of the WIPP site. Geophysical studies indicate that Castile brines probably are present beneath a portion of the WIPP waste-emplacement panels, consistent with earlier assumptions. These brines are stratigraphically 200 m or more below the WIPP facility horizon and are not of concern except in the case of human-intrusion breach of the facility.

In the western part of the Delaware Basin, extensive halite dissolution has apparently taken place in both the Castile and Salado Formations. However, much of the variability in structure and internal stratigraphic thicknesses within the Castile and Salado Formations results from deformation and original depositional variability, rather than from evaporite dissolution. Regional or far-field deformation of the Castile and Salado Formations involves pressure solution as a major mechanism, due to the presence of intergranular fluids, but occurs too slowly to be of future concern to the WIPP Project. Structures within hole DOE-2 result from deformation rather than dissolution.

The hydrologic and structural characteristics of the Salado Formation in the disturbed zone generated by the presence of the WIPP facility are different than those in the far field. Formation permeability within a couple of meters of the underground workings at the facility horizon increases significantly. Near-field deformation of the Salado Formation involves both the opening of preexisting fractures in anhydrite beneath the facility horizon (Marker Bed 139) and generation of new fractures in halite. Fluid contents in the disturbed zone at the facility horizon decrease in response to facility ventilation and/or deformation. Within a few meters of the underground workings, both hydrologic and structural

behavior of the Salado Formation become essentially those of the far field. Brine seepage into the WIPP facility includes a significant transient phase, which will probably last until effective facility closure. The results of preliminary hydrologic testing in the Salado Formation adjacent to the WIPP air-intake shaft indicate extremely low permeabilities, with no apparent stratigraphic variability. The results also indicate that development of a disturbed zone around the WIPP shafts is less extensive than at the facility horizon. The extent, characteristics, and importance of the disturbed-rock zones around the WIPP shafts and at the facility horizon remain to be determined in detail.

Where not extensively altered, the Rustler Formation should be considered as a layered unit of anhydrites, siltstones, and halites, containing an important and variably fractured carbonate unit, the Culebra dolomite. The Culebra dolomite is the first continuous water-bearing unit above the WIPP facility and, at the WIPP site, is at least an order of magnitude more permeable than other members of the Rustler Formation, including the Magenta dolomite. The transmissivities of Rustler anhydrites at the WIPP site are too low to measure. As a result, the Culebra dominates fluid flow within the Rustler Formation at the WIPP site and is the most significant pathway to the accessible environment from the WIPP facility, except for direct breach to the surface by human intrusion. The transmissivity of the Culebra varies by approximately six orders of magnitude in the region containing the WIPP site. The Culebra transmissivity in the central portion of the site, including the locations of all four WIPP shafts, is low. Higher Culebra transmissivities are found in areas southeast and northwest of the central part of the site. Fluid flow rates within the Culebra are very low at the site center and in regions to the east, but relatively high within Nash Draw. Modern flow in the Culebra is confined and largely north-south in the area of the WIPP site.

Fluid flow and geochemistry within the Culebra dolomite and shallower units are in continuing transient response to the marked decrease or cessation of local recharge at approximately the end of the last pluvial period. Both bulk chemistry and isotopic relations within Culebra fluids are inconsistent with modern flow directions if steady-state confined flow is assumed. Because of the relative head potentials within the Rustler Formation at and near the WIPP site, there must be a small amount of vertical fluid flow between its members, even though the permeabilities of Rustler members other than the Culebra dolomite are quite low. Where measured successfully, the modern head potentials within the Rustler prevent fluid flow from the surface downward into the Rustler carbonates. These results do not prohibit either the modern movement of fluids from the underlying Salado Formation upwards into the Rustler Formation or the downward movement of Dewey Lake waters into the Rustler Formation during or even after the cessation of local recharge at the end of the last pluvial period. They do, however, suggest that recharge from the surface to the Rustler Formation is not now occurring at the WIPP site. The results of stable-isotope, radiocarbon, and uranium-disequilibrium studies are also consistent with the interpretation that there is no measurable modern recharge to the Culebra dolomite from the surface at and near the WIPP site. The transient hydrologic response of the Rustler Formation to the end of the last pluvial period has involved at least some change in flow

directions in the Culebra dolomite. Although the modern flow is largely north-south, the results of uranium-disequilibrium studies suggest that flow was more easterly during previous recharge.

Within and near Nash Draw, evaporite karst is operative within the Rustler, as evidenced by the continuing development of small caves and sinkholes in near-surface anhydrites and gypsums of the Forty-niner and Tamarisk Members. There is no evidence of karstic hydrology in the Rustler at and near the WIPP site. However fracturing of some portions of the Culebra dolomite is sufficient at the site to strongly affect both hydraulic and transport behavior on the hydropad scale, i.e., over distances of approximately 30 m. Interpretation of multipad interference tests conducted both north and south of the center of the WIPP site indicates that this fracturing need not be incorporated into numerical modeling of the regional-scale hydraulic behavior of the Culebra east of Nash Draw. Similarly, detailed transport calculations indicate that effects due to fracturing are not significant in regional-scale transport within the Culebra dolomite at and near the WIPP site, at least as long as the modern head distribution is not significantly disturbed and the calculated flow directions and transport properties are representative.

The Dewey Lake Red Beds overlying the Rustler Formation consist largely of siltstones and claystones, with subordinate sandstones. In tested locations, the Dewey Lake may be hydrologically unsaturated, but is too low in permeability for successful hydrologic testing. South of the WIPP site, near an area where the unit may be receiving modern recharge, sandstones within the Dewey Lake locally produce potable water. In general, water levels within the Dewey Lake Red Beds, like those in the underlying Rustler Formation, must be in transient response to the end of the last pluvial period. Isotopic relations suggest that surficial waters have been involved in the formation of secondary gypsum veins within the Dewey Lake, but that the Dewey Lake and Rustler hydrologic systems are largely separate.

The major near-surface units at the WIPP site are the Gatuna Formation and Mescalero caliche. The sandstones and stream-channel conglomerates within the Gatuna indicate that major changes in local climate have occurred over (at least) the last 600,000 years. The widespread preservation of the Mescalero caliche indicates not only the relative structural stability of the Livingston Ridge surface (on which the WIPP surface facilities are sited) over the last 400,000 years, but also that infiltration over this same time period has not been sufficient to dissolve a layer of carbonate 1 to 2 m thick.

## 5.2 Individual Conclusions and Discussions

This Section contains descriptions and discussions of more specific conclusions concerning geologic chracterization of the WIPP site and vicinity. In each case, the description of the conclusion is followed by a brief discussion.

### 5.2.1 Conclusions Concerning the Overall Geologic and Hydrologic Setting of the WIPP Site and Vicinity

1. Conclusion: The overall geologic behavior at the WIPP site has been transient since before the beginning of deposition of the Bell Canyon Formation approximately 250 million years ago. Radiometric age dating indicates that secondary polyhalites in the Salado Formation near the WIPP facility horizon crystallized approximately 200 million years ago, some 40 million years after deposition of the Salado. Fractures within MB139, which are now partially healed, probably formed in response to rapid unloading at the end of the Cretaceous or in the Tertiary, i.e., more than approximately 2 million years ago. The hydrologic setting of the WIPP site appears to be in transient response to the end of the last pluvial period.

Discussion: Not all of the secondary minerals in the Salado have been dated. The age of magnesite, which appears to play a large role in controlling the composition of fluid inclusions, has not been determined. The age of fracturing in MB139 has not been determined directly. However, given that estimated ages of secondary mineralization and fracturing within MB139 appear large relative to the regulatory time frame of 10,000 years, the present estimates are adequate. Understanding of the hydrology of the WIPP site, especially the Rustler Formation, has been a major focus of site-characterization activities (see below).

2. Conclusion: There is abundant evidence for climatic and hydrologic transients at the WIPP site over the time interval of approximately 600,000 to 300,000 years before the present, as well as for long-term structural stability of the Livingston Ridge surface, on which the WIPP surface facilities are sited. The Gatuna Formation indicates a much wetter climate approximately 600,000 years ago, resulting in the presence of relatively high-energy streams on what is now the Livingston Ridge surface. The formation of the Mescalero caliche and Berino soil indicate a relatively drier climate approximately 500,000 and 300,000 years ago. The widespread preservation of the Mescalero indicates structural stability of the Livingston Ridge surface for approximately 300,000 years. In addition to structural stability, the preservation of the Mescalero caliche indicates that the regional infiltration over approximately the last 500,000 years has been insufficient to dissolve the existing caliche.

Discussion: The available geologic data do not provide a continuous time-stratigraphic record over the last 600,000 years. For example, only the upper portion of the Gatuna Formation has been dated; the age of lower portions of the unit is unknown. No dated deposits younger than the Berino soil are present at the WIPP site. Regional preservation of the Mescalero caliche does not mean that there is no local infiltration of surficial waters, since local dissolution of caliche due to the action of plant roots is known; in some places, the resulting structures completely pierce the Mescalero.

3. Conclusion: There is localized evidence for climatic and hydrologic changes near the WIPP site on the time scale of 25,000 to 10,500 years ago. Gypsite springs along the east side of Nash Draw appear to have been inactive for approximately 25,000 years. Packrat middens northwest of Carlsbad indicate a climate approximately 10,000 years ago significantly cooler and wetter than that approximately 4,000 years ago.

Discussion: Neither gypsite springs nor packrat middens have been found at the WIPP site proper. The radiometric age-dating of the gypsite spring deposits is not internally consistent, although the faunal assemblage in the deposits is definitely Late Pleistocene in age. The gypsite springs and packrat middens provide only a qualitative indication of change in climate and precipitation. Therefore, they cannot be used as direct input for transient boundary conditions in numerical modeling of hydrology at the WIPP site. Little information is available concerning the climate and hydrology of the northern Delaware Basin between approximately 10,000 and 4,000 years ago.

4. Conclusion: There is abundant evidence that the natural fluid flow and geochemistry of the Rustler are dominated by confined flow within the Culebra dolomite at and near the WIPP site, and that flow within the Culebra is transient on a time scale of approximately 10,000 years or longer.

The hydrology and geochemistry of the Rustler, and therefore those of all other units as well, are recovering from the most recent pluvial interval in southeastern New Mexico. Factors indicating the overall transient setting of Rustler hydrology at and near the WIPP site include: a) the inconsistency between modern flow directions and present brine-density distribution within the Culebra dolomite if steady-state confined flow is assumed; b) the inconsistency between present hydrochemical facies within Culebra fluids and modern flow directions if steady-state confined flow is assumed; c) the inconsistency between the isotopic characteristics of Rustler fluids and both modern flow directions and surficial recharge to the Rustler at and near the WIPP site; and d) geologic, isotopic, and hydrologic studies indicating that vertical fluid movement into and out of the Rustler Formation is limited.

Because the transmissivities of non-carbonate units within the Rustler are not zero and different hydraulic heads are known in different Rustler members, there must be limited vertical fluid flow within the Rustler Formation. However, the transmissivities of Rustler anhydrites and the Tamarisk claystone at and near the WIPP site are too low to measure; therefore vertical fluid flow must be extremely limited.

Discussion: The present isotopic data bases are limited in size. Therefore, the presence of small structures inconsistent with regional interpretations is possible. In addition, because of the limited data base, directions of flow interpreted from uranium-disequilibrium studies include considerable uncertainty. The available results indicate that,

although stratabound flow within the Culebra dolomite dominates at and near the WIPP site, this is not necessarily true within Nash Draw. Because of the existence of small caves and sinkholes within Tamarisk and Forty-niner anhydrites in Nash Draw, there must be a qualitative increase in the transmissivity of these members somewhere between the WIPP site and Nash Draw. Avaliable evidence suggests that this change does not take place east of WIPP-33.

5. Conclusion: At least three types of man-induced transients at the WIPP site are known or can be expected. The transients include hydrologic, geochemical, and structural effects, independent of the emplacement of waste.

   The hydrology of the Rustler Formation at and near the WIPP has been and will continue to be affected by both hydrologic testing in the area and the construction and sealing of the WIPP shafts. The hydrologic behavior of the Salado Formation, both in the WIPP facility itself and adjacent to the access shafts, has been altered by construction of the WIPP facility and shafts. This alteration includes development of a local altered or disturbed rock zone, within which permeability is significantly increased and a zone of partial saturation has probably developed. The altered zone, however, is probably less extensive around lined shafts than at the facility horizon.

   In the Rustler Formation, the use of lost-circulation materials during the drilling of hydrocarbon-exploration holes and hydrologic test holes not drilled with air has resulted in development of at least local geochemical transients of unknown magnitude, lateral extent, and duration. Any far-field radionuclide migration outside the WIPP facility in the Rustler may be superimposed on these transients. Possible geochemical alteration within the Salado Formation due to the presence of the WIPP facility remains to be examined in detail, with the exception of effects due to emplacement of TRU wastes. For example, the long-term geochemical stability of grouting materials used in both the Rustler and Salado is not yet known.

   The construction of the WIPP facility imposes a transient near-field structural effect on at least nearby portions of the Salado Formation. At the facility horizon, this effect includes both local opening of preexisting fractures in MB139 and formation of fractures in halite. Transient structural behavior around the WIPP shafts will include the Rustler Formation and extend to the land surface. However, the limited information available to date suggests that structural effects around the WIPP shafts will be less than those at the facility horizon.

Discussion: The effective time scales of the man-induced transients in and near the WIPP facility are not well known. Transients directly resulting from the construction of the WIPP facility will last until reequilibration following the effective hydrologic and structural closure of the facility. The time scale of hydrologic transients within the Rustler induced by hydrologic testing is short, maybe decades. The time scale of induced geochemical transients within the Rustler is not known. Only those

transients which might affect the performance of the WIPP facility need be determined in any more detail than indicated here. Determination of which transients need be considered is part of the WIPP Performance Assessment activity.

### 5.2.2 Conclusions Concerning the Bell Canyon Formation

1. Conclusion: Calculations completed as part of the WIPP SPDV effort indicate that the Bell Canyon does not have sufficient brine-carrying capacity to dissolve halite rapidly enough for halite dissolution within the Castile and/or Salado Formations as a result of brine-density flow. Therefore, in regions of the Castile and Salado reasonably removed from concern regarding stratabound dissolution, such as the WIPP site, only halite dissolution as a result of diffusional processes need be considered. Such diffusion proceeds at a rate too slow to be of concern to the WIPP Project.

Discussion: The conclusions are dependent upon the assumed gradients within the Bell Canyon and range of Bell Canyon hydraulic properties, both of which are somewhat uncertain. The SPDV calculations did not result in total agreement that point-source dissolution was not a feasible mechanism at the WIPP site. However, the structure specifically proposed as a result of point-source dissolution was directly examined by drilling and testing of hole DOE-2, and was found to result from deformation within the Castile and Salado Formations, rather than from halite dissolution.

2. Conclusion: Investigations in holes Cabin Baby-1 and DOE-2 suggest indicate that the upper Bell Canyon Formation beneath the WIPP site is not significantly permeable. Therefore, regardless of the relative heads, the volumes of fluid flow between the Culebra dolomite and the upper Bell Canyon would be minor if the two units were interconnected as a result of drilling. These same studies indicate that the final direction of fluid flow would be downward into the Bell Canyon.

Discussion: Although Cabin Baby-1 and DOE-2 lie directly south and north of the WIPP site center, they provide only two data points. Given the regional trends of the Ramsey channel sands in the upper Bell Canyon, it is possible that a narrow sand crosses the center of the site from northeast to southwest, without having been intersected by either drill hole. The conclusion concerning directions of fluid flow pertains only to the final direction of flow, assuming halite saturation of both Bell Canyon and Culebra fluids as a result of dissolution of Salado halite. The conclusion does not describe either directions or rates of fluid flow prior to such saturation. In addition, the conclusion assumes that the fluid-carrying capacity of the Bell Canyon is sufficient to completely overwhelm any potential heads within the Salado Formation. This assumption appears reasonable, given the extremely small volumes of Salado flow intersected in hydrologic test holes at the WIPP site.

### 5.2.3 Conclusions Concerning the Castile and Salado Formations

1. Conclusion: Regional-scale deformation of the Castile and Salado Formations may well be ongoing at and near the WIPP site in response to gravity. However, estimation of the time required for formation of the WIPP-12 anticline indicates that such deformation probably occurs at a rate too slow to be of concern to the behavior of the WIPP facility. Fluids play a major role in regional-scale deformation of the Castile and Salado Formations, especially in deformation of halites and anhydrite stringers or laminae. Both estimated deformation rates and mechanistic considerations are consistent with pressure solution being a major deformation mechanism on the regional scale. This conclusion is consistent with greater deformation rates at lower differential stresses than would be the case for strictly anhydrous deformation. Inclusion of pressure solution as a deformation mechanism results in predicted strain rates at the WIPP site which are consistent with estimated rates elsewhere.

Discussion: Regional-scale deformation in response to gravity is not constrained to occur at a constant rate. Therefore, deformation rates averaged over long periods of time may be exceeded during shorter intervals. For pressure solution to be active, there must be a relatively continuous fluid film along grain boundaries. While textural evidence of pressure solution has been noted in core from the WIPP site, the presence of the required grain-boundary film has not been demonstrated directly. Although the role of pressure solution in regional-scale deformation is probable, it is not clear if or when the same mechanism will become dominant in near-field deformation around the WIPP facility. If it did become active, it would help accelerate mechanical closure of the facility by increasing deformation at relatively low differential stresses.

2. Conclusion: Much of the variability in both total and interval stratigraphic thicknesses of the Castile and Salado Formations at and near the WIPP site is due to syndepositional and postdepositional deformation, rather than to evaporite dissolution. Therefore, any interpretation of the thicknesses of these units must be done on a vertical scale involving as much of the Salado and Castile as possible, rather than on the scale of a single stratigraphic interval. Similarly, the interpretation must be done on as large a geographic scale as possible, since horizontal movement, especially of halites, is involved. Apparent one-hole anomalies are especially suspect.

Discussion: On the regional scale, especially in the western portion of the Delaware Basin, regional dissolution has apparently removed the halite from both the Castile and Salado Formations, and the original thickness of halite is unknown. At the local scale, as demonstrated in hole DOE-2, dissolution cannot be ruled out without interpretation on a broad stratigraphic and geographic scale.

3. Conclusion: The basinal structure in hole DOE-2, near the northern boundary of WIPP Zone 3, extends downwards from MB124 in the Salado to the top of Castile Anhydrite I. However, the DOE-2 structure resulted

from syndepositional and postdepositional deformation, rather than from halite dissolution. Deformation involved in formation of the DOE-2 structure resulted in displacement of all but 2 m of halite from the Castile Formation. However, both the Castile anhydrites and the entire Salado Formation (especially halites) are unusually thick in this hole. No evidence of dissolution was identified in DOE-2 core.

Discussion: The present understanding of the hydrology and structural behavior of the Castile and Salado Formations indicates that point-source dissolution of evaporites requires connection with a major source of unsaturated water, such as the Capitan limestone. This is not known to have occurrd within the body of the Delaware Basin, with the possible exception of the emplacement of Castile brines. While the present hydrologic and structural understanding does not allow prediction of where either point-source dissolution or a gravitational structure such as that at DOE-2 might form in the future, the drilling, coring, and hydrologic testing of DOE-2 demonstrates that no such structure presently exists within WIPP Zone 3. Calculations indicate that rates of gravitationally driven deformation are too slow to be of concern to the WIPP facility on the regulatory time scale.

4. Conclusion: The average far-field permeability of the Salado Formation, based on testing both from the surface and near the WIPP facility horizon, is 0.1 microdarcy or less, except where fractures locally contain small or large volumes of gas at elevated pressures. The stratigraphic variability of far-field permeability within the Salado is presently unknown, but appears negligible.

Discussion: It is not known for sure that the Salado is hydraulically saturated in the far-field. Known gas occurrences in drilling from the surface and within the WIPP facility indicate that partial saturation may be present in both the near-field and far-field, at relatively high confining pressures. The distribution of fracture systems, range of possible initial gas pressures, and effective fracture permeabilities in the far-field Salado remain unknown.

5. Conclusion: Where it has been possible to measure Salado fluid pressures, calculated heads indicate the potential for limited fluid flow upwards into the overlying Rustler Formation. Measurements to date indicate, however, that the amount of fluid available from the Salado is extremely limited. At least in the case of WIPP-12, the Salado fluid pressures and calculated heads exceed those in the underlying Castile brine reservoir. It has not been possible to determine any discrete source of fluid flow within the Salado Formation in testing from the surface.

Discussion: The measured Salado fluid pressures indicate only the possible directions of modern fluid flow. The measured pressures may be relict, developed under different geologic conditions than those at present, e.g., they may have been developed during the last pluvial period. The time scale on which such pressures or heads might change as part of the transient overall response of the WIPP hydrologic setting to the end of the

last pluvial period is not known, but must be long, given the low regional permeability of the Salado.

6. Conclusion: Water contents of Salado halites in the far-field appear to be as much as 2 weight percent, based on geophysical logging, greater than previously estimated. This does not have any direct impact on expected fluid flow into the WIPP facility, other than indicating that fluid volumes available to support long-term fluid flow may be greater than previously expected.

Discussion: To date, the interpretation of far-field water contents is based only on geophysical studies. Measurements on core are ongoing.

7. Conclusion: Consistent with assumptions maintained since brine was encountered in Castile Anhydrite III in WIPP-12, recent geophysical studies indicate that Castile brine may be present beneath a portion of the WIPP waste-emplacement panels. Brine is most likely present beneath the northern and northeastern portion of the waste-emplacement panels, and probably comes close to the southwestern and southeastern corners of the panels. However, the brines, if present, are 200 m or more below the WIPP facility horizon, and are not of concern except in the event of drilling-induced breach connecting a brine occurrence with the WIPP facility.

Discussion: Because of the dominant effect of the underlying Bell Canyon Formation, it is possible that the interpreted brine occurrences within the Castile are not real. Three-dimensional modeling of the results does not appear promising in defining the lateral distribution of Castile brines more accurately. Because of the vertical uncertainty inherent in the measurements, it is not possible to distinguish between brine occurrence within Anhydrite III and within Anhydrite II. However, where Castile brines have been encountered, it has always been present in the uppermost anhydrite.

8. Conclusion: Both uranium-disequilibrium studies and structural calculations appear consistent with emplacement of brines into fractured Castile anhydrites as a result of an episodic process. The process may involve either local brine movement during deformation and fracturing of anhydrite in low-pressure locations such as anticlinal crests, or long-distance fluid movement into preexisting fractures as a result of episodic hydrologic connection of the Capitan limestone and Castile Formation.

Discussion: It is not agreed that deformation or hydrologic connection of the Capitan limestone and Castile is the relevant episodic process involved in generation and/or emplacement of Castile brines. Structural studies indicate that deformation of the Castile Formation is episodic, with resultant episodic generation and emplacement of brines. Under these assumptions, generation of fractures and migration of brines into anhydrites may occur during the next 10,000 years, but probably at too low

a rate to be of concern to the WIPP Project. Isotopic studies are interpreted to indicate a residence time for Castile brines sampled at ERDA-6 and WIPP-12 of more than 100,000 years. While this interpretation indicates prior hydraulic connection of the Castile anhydrites and the Capitan limestone, it also indicates that this connection has not been operative for more than 100,000 years.

9. Conclusion: Both fluid-inclusion and grain-boundary fluids are present within the Salado Formation, in addition to loosely-held waters of hydration in hydrated minerals. The composition of Salado fluid inclusions is apparently controlled by the crystallization of polyhalite and magnesite. Radiometric age dating of polyhalites indicates that they are approximately 200 million years old. Therefore, the Salado fluid inclusions appear to be approximately 200 million years old. Fluids encountered within macroscopic flows into the WIPP facility appear to be dominantly grain-boundary fluids rather than fluids from fluid inclusions. The composition of grain boundary fluids within the Salado is apparently controlled by diagenetic reactions involving crystallization of Mg-rich layer silicates. Because the kinetics of these reactions are slow, it is concluded that the residence time of grain-boundary fluids within the Salado is at least several million years. The marked vertical variability of fluids near the WIPP facility horizon indicates very limited vertical fluid flow within the Salado.

Discussion: Crystallization of magnesite appears to have a major affect on fluid-inclusion compositions. However, magnesite from samples at the WIPP has not been dated. It has not been possible to estimate the residence time of Salado grain-boundary fluids directly. Radiometric measurements indicating ages for clay minerals greater than the Permian indicate that diagenetic or secondary reactions involving Mg have not involved complete recrystallization.

10. Conclusion: In the Salado Formation near the WIPP facility, there is strong coupling of deformation and hydraulic behavior. Within approximately 2 m of the underground rooms and entryways, fracturing and probable matrix dilation have led to a marked increase in permeability, and quite possibly to development of a zone of partial saturation. The increase in permeability appears to be both time-dependent and geometry-dependent. Within a few meters of the underground workings, however, the hydrologic properties of the Salado essentially become the same as regional properties.

The time scale on which the WIPP facility will affect the local hydrology of the Salado Formation, while undetermined at present, is likely to be extensive, continuing until reequilibration after effective mechanical closure of the facility. Within the facility, there is a three-stage generalized flow behavior. Holes are normally dry when first drilled. Fluid flow then normally rises rapidly to a maximum flow rate, after which it more slowly decreases to something approximating steady-state flow, though probably still decreasing. Porous-medium calculations based on the estimated far-field permeability indicate that steady-state fluid flow might not be

reached for more than 5000 years, because of the extremely low permeabilities; these calculations do not yet include consideration of facility closure. The observed "steady-state" flow is qualitatively consistent with measured far-field permeabilities. Both measurement and calculations to date indicate that effective pore pressures within the Salado have been affected by the presence of the WIPP facility only within a few meters of the facility.

Discussion: Within the altered zone around the WIPP facility, the porous-medium approximation may not be adequate for either flow or transport modeling. The distances from the underground workings at which this simplifying assumption becomes valid remain to be determined. At present, there is not an adequate characterization of the fracturing adjacent to the WIPP facility to allow realistic modeling of flow and transport behavior within the altered zone, nor do adequate models exist. The long-term extent of the altered (fractured) zone around both underground workings and shafts remains unknown. However, the zone should be larger around underground workings than around lined shafts. Both the total long-term brine seepage to be expected from the Salado and the total volume of the Salado affected by fluid flow depend on the available porosity as a function of time within the WIPP facility and any altered zone that may be present. The effects of stress relief around the WIPP facility on both near-field and far-field hydrology will be examined in detail during the WIPP operational-demonstration period.

11. Conclusion: Preliminary hydrologic testing adjacent to the WIPP waste-handling shaft indicates that all of the tested intervals, which include claystone and siltstone in the unnamed lower member of the Rustler and both halites and anhydrites within the Salado, are extremely low in permeability. While there was evidence of a hydraulic cone of depression around the shaft, there was no evidence of fracturing or alteration, except at the 850-ft level. At this level, pressurized fluids were encountered at the liner/rock interface and flowed into the test hole. Testing extended from approximately 2 m outside the shaft liner to a depth of some 10 m. The results are consistent with the interpretation that damage effects due to either blasting of the shaft or deformation around the shaft do not presently extend more than two meters into the surrounding rock mass.

Discussion: Due to scheduling constraints, only one or two holes was/were tested at each level. Therefore, these results do not indicate a complete absence of fracturing, merely that fractures were not intersected by the one or two holes at each level, except the 850-foot level. To better determine the presence or absence of fracturing by direct measurement, arrays of three or more holes would be needed at each level. The results do not indicate a potential altered zone within 2 m of the liner. Finally, the waste-handling shaft has been at its present diameter for approximately four years. The operational phase of the WIPP is expected to extend approximately 25 years, after which shaft seals must be emplaced successfully. The extrapolation of the present results to 25 years may not be reliable.

12. Conclusion: Anhydrite Marker Bed 139, approximately 1 to 2 m beneath the WIPP facility horizon, contains partially healed and filled fractures which predate construction of the WIPP facility and play a significant role in both mechanical deformation near the WIPP facility and the near-field enhancement in permeability. The estimated age of the fractures is at least two million years. However, the far-field permeability of MB139 is not significantly greater than that of the surrounding halites.

Discussion: Development of any altered zone around the WIPP facility will be time dependent. Therefore, the boundary between the hydrologic near-field and far-field regimes will also be time dependent. The rate and extent to which the fracture porosity and permeability of MB139 in the altered zone near the WIPP facility horizon will be reduced during closure of the WIPP facility has not yet been demonstrated.

### 5.2.4 Conclusions Concerning the Rustler Formation and Younger Units

1. Conclusion: The available transmissivity data base at and near the WIPP site suggests that: a) the Culebra dolomite is at least one order of magnitude more transmissive than other members of the Rustler at most locations; and b) except where it is fractured in or near Nash Draw, the transmissivity of the Magenta dolomite is the same order of magnitude as that of other members of the Rustler. Consequently, confined flow within the Culebra dominates the hydrology of the Rustler at and near the WIPP site, and Rustler karst is not present.

Discussion: The Magenta data base is significantly smaller than that of the Culebra. Transmissivities of Rustler claystone/siltstones are very low but measurable at the Site, except for the Tamarisk claystone, which has not been successfully tested due to its low transmissivity. The transmissivity of Rustler anhydrites at the Site are too low to measure successfully. Somewhere between the WIPP site and Nash Draw (including WIPP-33), there must be a marked increase in the local permeability of Rustler anhydrites/gypsums. Where they are exposed or relatively near the surface, i.e., in Nash Draw and at WIPP-33, Rustler anhydrites are capable of supporting open cavernous porosity. The character and location of this transition in behavior of the Rustler anhydrites are not known in detail, but apparently involve decreasing overburden pressure (allowing the gypsums to maintain open porosity) and specific structures at the locations of both recharge and discharge.

The WIPP-33 structure is unique at and near the WIPP site, since it includes the three components necessary but not sufficient for karstic geology within the Rustler: 1) a sufficiently large breach in the Mescalero caliche and relatively thin Dewey Lake Red Beds; 2) shallow enough depth to gypsums within the Forty-niner and Tamarisk Members to allow maintenance of open porosity in gypsums above and below the Magenta; and 3) a probable local base level at the time the structure was mainly active, namely the gypsite springs on the east side of Nash Draw. Both the deuterium/hydrogen ratios of secondary gypsum from WIPP-33 and approximate dating of the gypsite springs within Nash Draw suggest that the WIPP-33 structure is largely inactive at present.

2. Conclusion: Measurements of relative heads within the Rustler Formation at the WIPP site are not consistent with modern infiltration from the surface to the Magenta, let alone from the surface to the Culebra. Therefore, at least at the measured locations, there is no modern infiltration of surficial waters to Rustler carbonates.

Discussion: The holes on which this conclusion is based provide only limited geographic coverage, and do not include any locations at which the Dewey Lake Red Beds are known to be hydraulically saturated. Where tested, the Dewey Lake was too tight for hydraulic testing, and may be either completely or partially saturated. No head or transmissivity information is available from the Tamarisk Member of the Rustler, due to its exceedingly low transmissivity. These results do not rule out vertical movement of water from either the surface or the Dewey Lake into the Rustler in areas in which the Dewey Lake is saturated directly above the Rustler, or in any area in the past if heads in the Dewey Lake were higher at that time.

3. Conclusion: Culebra transmissivity varies by approximately six orders of magnitude in the region of the WIPP site and Nash Draw. Transmissivities generally decrease from west to east across the site area. For purposes of generalization, the distribution can be divided into broad areas of relatively low Culebra transmissivity ($\leq 10^{-6}$ $m^2/s$), in which the porous-medium assumption appears adequate to describe local hydraulic and transport behavior, and areas of relatively high transmissivity ($\geq 10^{-5}$ $m^2/s$), in which a dual-porosity formalism appears adequate to describe local hydraulic and transport behavior. Both of these zones are represented by several wells. Two wells (H-3 and H-18) penetrate an apparently thin transition zone, in which transmissivity varies between $10^{-6}$ and $10^{-5}$ $m^2/s$.

The central portion of the WIPP site, including all four WIPP shafts, lies within an apparently continuous area of low transmissivity. This area extends well east of the site, and includes the holes H-1, 2, 4, 5, 10, 12, 14, 15, 16, and 17; WIPP-12, 18, 19, 21, and 22; ERDA-9; Cabin Baby-1; P-15, 17, and 18, in addition to the WIPP shafts. North of the WIPP site, measurements at WIPP-30 indicate the presence of a northern zone of low transmissivity, which may or may not be continuous with the zone near the site center.

There is a zone of relatively high Culebra transmissivity southeast of the center of the Site, which is indicated both by point measurements at H-11 and DOE-1 and by the presence of very low hydraulic gradients south of WIPP Zone 3. Northwest of the site center, there is a relatively uniform high-transmissivity zone containing holes WIPP-13, DOE-2, and H-6. This zone is bounded by low-transmissivity domains to the north, east, and southeast, and by an even higher-transmissivity domain to the southwest and west. Within both Nash Draw and the valley south of the WIPP site containing H-7 and H-9, Culebra transmissivity is both high and variable.

Discussion: There are some exceptions to the generalizations listed above. WIPP-21, which has a low transmissivity, responds quite rapidly to activities in the WIPP shafts, indicating that the region containing WIPP-21 is connected to the shafts by a low-storativity structure, which may involve fractures. Tests at individual low-transmissivity wells examine only a very small area. Neither analytical nor numerical modeling is capable of identifying a small, discrete high-transmissivity structure embedded in a low-transmissivity domain, unless it is close to measured data points. No evidence for such a discrete structure is known at the WIPP site. On the other hand, the hydraulic behavior of the Engle well, which has a high transmissivity, shows no dual-porosity effects. Test results from the Culebra in Nash Draw have not been examined for dual-porosity behavior; fracturing may be extensive enough in Nash Draw to make a dual-porosity formalism unnecessary.

The boundaries of the low-transmissivity zone including WIPP-30 remain unknown. The interpretation based on the rapid and large response of this hole to the WIPP-13 pumping test suggests that the high-transmissivity domain including WIPP-13, DOE-2 and H-6 extends close to WIPP-30.

The boundaries of the high-transmissivity zone south of H-11 and DOE-1 and the connection of this zone with the larger high-transmissivity region containing H-7, H-8, and H-9 have not been determined directly, nor has the maximum transmissivity within the zone. The presence of the zone south of H-11 and DOE-1 is indicated by both analytical and numerical modeling of the H-3 multipad interference test, as well as by more recent calibration of Culebra transmissivities against calculated pre-shaft heads. This zone will be investigated during 1988 by a multipad interference test to be conducted at the H-11 pad. The reason for the relatively high transmissivities at H-11 and DOE-1 remains unknown.

4. Conclusion: The estimation error for Culebra transmissivities over most of the WIPP site (in terms of $m^2/s$) is less than one log unit at two standard deviations, including estimated uncertainties in field measurements. The estimation error is generally larger outside Zone 3.

Discussion: The statistical treatment of Culebra transmissivities should not be overinterpreted, since it does not include specific consideration of geologic processes. In addition, this treatment assumes vertical homogeneity within the Culebra. Testing at H-14 indicates that transmissivity may vary by a factor of about 2 across the Culebra at a given locality.

5. Conclusion: Groundwater flow rates within the Culebra vary greatly. Flow within Nash Draw is relatively rapid; flow in the central portion of the WIPP site and in regions further east is extremely slow. The estimated flow time from a position above the center of the WIPP waste-emplacement panels to the southern boundary of Zone 3, assuming steady-state distribution of the present heads and transmissivities within the Culebra, is approximately 13,000 years.

Discussion: Calculated particle-flow rates and integrated travel times are approximate. The head distribution and flow directions within the Culebra are not at steady state. The similar Culebra and Magenta heads within Nash Draw suggest that assumption of confined flow within the Culebra may not be realistic in this region. In addition, the calculations assume a uniform effective porosity of 16%. The effective Culebra porosity probably varies laterally, suggesting that both flow rates times and flow paths are more variable than calculated.

6. Conclusion: Single-pad interference testing at the H-3 and H-11 hydropads indicates a complex role of fracturing within the Culebra. At H-3, the system transmissivity is approximately 2 x $10^{-6}$ $m^2/s$, and no significant directional dependence of hydraulic response has been measured. However, the data from observation holes on the H-3 pad had to be interpreted as if the radius of the pumped well extended beyond the observation holes; i.e., the response of the observation holes to the beginning and end of pumping was practically instantaneous. At the H-11 pad, the transmissivity is 1.2 to 3.0 x $10^{-5}$ $m^2/s$. However, the observation holes on the H-11 pad responded more slowly during testing than those on the H-3 pad. The extent or effectiveness of fracturing is not a simple function of transmissivity.

Discussion: The available data are only sufficient for detailed interpretation of interference testing using a dual-porosity formalism, i.e., assuming uniform fracture spacing. This limitation is irreduceable, however, given the limited core recovery within the Culebra. Detailed interpretation of interference testing has been completed only for testing at the H-3 and H-11 hydropads. Interpretation of interference testing at the H-2, H-4, H-5, H-6, H-7, and H-9 hydropads will be completed in the next year.

7. Conclusion: Regional-scale simulations indicate that it is not necessary to incorporate a dual-porosity formalism into regional-scale modeling of Culebra head distributions. This is because the time scale for pressure equilibration between fracture and matrix for matrix-block sizes up to the thickness of the Culebra is very short relative to the time scale required for regional groundwater flow.

Discussion: The pressure effects of a discrete or narrow high-transmissivity structure embedded within a low-transmissivity domain remain to be determined in detail. It cannot be claimed that any reasonable amount of drilling or hydrologic testing will completely eliminate the possibility of a small high-transmissivity structure being present within the Culebra dolomite. However, no such structure is known to exist at or near the WIPP site.

8. Conclusion: Both fractures and matrix play a major role in pad-scale transport of contaminants within fractured portions of the Culebra dolomite. At the H-3 pad, the first detected arrival of conservative (non-reacting) tracers in a convergent-flow test was strongly

controlled by fracturing, while tracer behavior both at and after the time of peak concentration showed evidence of strong interaction between fractures and matrix. Storage within the matrix served to decrease peak concentrations, but also resulted in greater concentrations at longer times than expected for fracture transport alone. The results indicate that matrix storage should play a major role in regional-scale transport of even conservative contaminants, so long as these contaminants have a reasonable diffusion coefficient into the matrix.

In addition, the results of the conservative-tracer test at the H-3 pad indicate that the relationship between hydraulic properties and transport properties can be complex. At H-3, no directional dependence of hydraulic behavior has been measured. In contrast, the time interval before first detected arrivals of tracers along the two flow paths investigated differed by a factor of about four.

Discussion: Detailed interpretation of dual-porosity effects in contaminant transport within the Culebra is presently completed only for testing at the H-3 pad. An additional conservative-tracer test will be conducted during 1988 at the H-11 hydropad, along the apparent regional flow path from the center of the WIPP site to the southern boundary of Zone 3. Any significant role of the matrix in contaminant transport within fractured portions of the Culebra requires that conservative contaminants be able to diffuse into matrix blocks. Interpretation to date of the H-3 test involves superposition of two radial-flow solutions; calculations are ongoing to investigate the possible effects of matrix anisotropy on transport behavior.

9. Conclusion: Calculations indicate that regional-scale contaminant transport within the Culebra Dolomite can be modeled realistically using the porous-medium assumption, so long as the Culebra transport properties and flowpaths used in these calculations are representative, and at least so long as the existing distribution of head potentials within the Culebra is not significantly disturbed. Calculated times required for contaminants to break through to the southern boundary of WIPP Zone 3 following release at any point directly above the WIPP waste-emplacement panels are only approximately 10% lower if a dual-porosity formalism is used than if the same release is modeled using the porous-medium assumption. The completed regional-scale calculations assume a transmissivity distribution which probably assigns too high a transmissivity to the region including holes H-11 and DOE-1.

Discussion: Calculations are presently ongoing to investigate the utility validity of the porous-medium approximation in modeling transport within the Culebra in the event of a breach involving a Castile brine occurrence. The assumption that there is effective diffusion from fractures into the adjacent Culebra matrix is explicit in conclusions based on calculations completed to date. Results of interference testing support the conclusion that fluid flow is unrestricted between matrix blocks and fractures, i.e., that there are no significant or continuous low-permeability skins on

matrix blocks. This has been demonstrated in the conservative-tracer experiment at the H-3 pad. Effective matrix retardation within the Culebra has not yet been demonstrated for some radionuclides making up the WIPP inventory, but will be demonstrated experimentally in the laboratory during the WIPP operational-demonstration phase.

10. Conclusion: The variability in compositions of Culebra groundwaters allows their subdivision into four hydrochemical facies. Zone A, east of the WIPP site, contains saline Na-Cl brines. Zone B, south of the site, contains relatively fresh waters in which Ca and $SO_4$ are the main solutes. Zone C, which includes the WIPP site and the eastern part of Nash Draw, contains quite variable fluids. Zone D, within Nash Draw, shows evidence of contamination from potash refining operations. The modern distribution of hydrochemical facies within the Culebra is not consistent with steady-state confined flow within the Culebra. Therefore, the solute geochemistry of Culebra fluids is not at steady-state, nor is the overall hydrology of the Culebra.

Discussion: This conclusion assumes the dominance of confined flow within the Rustler in the vicinity of the WIPP site, consistent with both isotopic studies and measurements of the modern relative head potentials and transmissivities of the several members of the Rustler.

Interpretation of normative salts within Rustler fluids is partially consistent with steady-state flow, if extensive vertical mixing is allowed. The measured head relationships within the Rustler are inconsistent with infiltration from the surface. The composition of Culebra waters at P-18 and P-14 play a major role in normative interpretation Culebra waters. The representative character of groundwater samples from the Culebra from P-14 and P-18 is suspect.

11. Conclusion: Analyzed Culebra fluids are all undersaturated with respect to halite, but approximately saturated with respect to gypsum and carbonate (dolomite). All fluids except that from hole WIPP-29 are undersaturated with respect to anhydrite. Therefore, almost all Culebra waters are capable of converting into gypsum any anhydrite they may contact. Carbonates, sulfates, and clay minerals are ubiquitous in Culebra core. Halite not introduced during coring has not been identified reliably. With the exception of halite, all analyzed Culebra fluids appear to be in approximate equilibrium with the host rock. Studies to date have not identified any discrete variations in Culebra mineralogy that can be used to bound hydrochemical facies.

Discussion: The dominant reactions controlling the variability of Culebra fluids appear to be the dissolution of halite and reactions between fluids and a ubiquitous but variable clay-mineral phase. Both the compositions of clays and the detailed reactions between clays and Culebra remain to be determined in detail. It cannot be demonstrated that the mineralogy of intact core specimens is representative of portions of the Culebra that have been in significant contact with groundwater.

12. Conclusion: There appear to be significant lateral variations in the oxidation state of Culebra waters. Fluids from hydrochemical facies Zone B, south of the site, appear to be more oxidized than those within Zones A and C, which include the WIPP site. The available information from within Nash Draw indicates that the redox potential at WIPP-26 is similar to that within Zone B. Results at WIPP-25 appear to be problematical, due to evolution of $H_2S$ during sampling. The results indicate generally more oxidizing conditions south and southwest of the WIPP site than at the site itself.

Discussion: Oxidation states of Culebra fluids are not known in detail, and are generally bracketed by the occurrence of one member of a redox couple at too low a concentration for analysis. The possible effects of contamination have been evaluated only in hole WIPP-25.

13. Conclusion: Recent stable-isotope studies indicate that the bulk of the Rustler Formation and part of the Dewey Lake Red Beds at and near the WIPP site were last recharged under climatic conditions significantly different than those of today. This is consistent with the interpretations that the overall hydrology of the Rustler Formation is in transient response to the end of the last pluvial period in southeastern New Mexico, and that there is no modern meteoric recharge to the Rustler Formation at and near the WIPP.

Discussion: The data base on which the interpreted isotopic range of modern meteoric recharge is based includes measurements from several different rock types and locations, including the Capitan limestone in Carlsbad Caverns, alluvium at WIPP-15, the Ogallala Formation in both southeastern New Mexico and on the High Plains of Texas, and the Dewey Lake Red Beds near an active dune field. The Dewey Lake, however, appears to include both modern and older waters. The stable-isotopic signature of all analyzed waters from confined portions of the Culebra and Magenta dolomites are distinct from the defined meteoric field.

The stable-isotope results do not provide any direct information about the timing of recharge, only about different conditions of recharge. In addition, the results do not rule out modern recharge to the Rustler at some location removed from the WIPP site itself. However, the results do indicate that measurable amounts of recharge are not now occurring at the WIPP site.

14. Conclusion: Both stable-isotope and compositional characteristics of Rustler waters at Surprise Spring, in the southwestern portion of Nash Draw, are dominated by near-surface recharge and discharge, including partial evaporation. Major dilution would be required to derive the solute chemistry at Surprise Spring from Culebra waters at WIPP-29, which is nearby. In addition, Surprise Spring apparently discharges from the Tamarisk Member of the Rustler, rather than the Culebra. Therefore, Surprise Spring, does not appear to be a discharge point for Culebra or Magenta waters crossing the WIPP site.

Discussion: It is possible that some Rustler waters from the area of the WIPP site discharge in southern Nash Draw, including Surprise Spring. The results summarized here, however, suggest that the hydrology and solute chemistry at Surprise Spring are dominated by local processes and groundwaters, and that any input of waters from the area of the WIPP site would not be identifiable, even if present.

15. Conclusion: Use of lost-circulation materials in hydrocarbon-exploration hole and hydrologic test holes (except those drilled with air) and metabolism of these materials by introduced and/or natural organisms within the Rustler makes meaningful radiocarbon measurements on Rustler fluids difficult. All Rustler and Dewey Lake holes may be contaminated to some degree. Therefore, estimated periods for which Rustler or Dewey Lake waters have been isolated from atmospheric carbon should represent lower bounds.

16. Conclusion: Available radiocarbon measurements indicate isolation times of three Culebra and one Dewey Lake water from input of atmospherically generated nuclides for at least 12,000 years. This is consistent with paleoclimatic studies indicating a wetter climate in the northern Delaware basin approximately 10,000 years ago. The results are taken to imply that there has not been significant (i.e., detectable) vertical recharge to the Culebra and at least part of the Dewey Lake near the WIPP site in at least 12,000 years. The results also indicate, because of the relatively tight clustering of ages, that recharge may have been a pulse event rather than continuous. At any rate, the available radiocarbon results do not indicate any consistent age gradient for waters within the Culebra, and cannot be used to indicate paleoflow directions.

Discussion: The data base of successful radiocarbon measurements is extremely limited in size. Extrapolation of these results to the confined Culebra over the entire Site area may be tenuous, but is consistent with both the fact that the Culebra is regionally confined and the results of both stable-isotope uranium-disequilibrium studies. Additional radiocarbon measurements will be made over the next (approximately) two years.

17. Conclusion: Available uranium-disequilibrium results for Culebra rocks and groundwaters indicate that there must have been a significant distinct change in flow directions within the Culebra on the time scale of approximately 10,000 years. The paleoflow direction involved at least some component of easterly flow, in contrast to the modern flow directions within the Culebra, which are essentially north-south in the Site area. The change in flow directions has apparently occurred as a result of the end of Culebra recharge at or near the end of the last pluvial period. The estimated flow time to the vicinity of H-5 is at least several thousand years, and flow has occurred under reducing conditions, regardless of where recharge is interpreted to have taken place. Therefore, modern recharge is not occurring at H-5, regardless of the relatively high Culebra heads in the region. The

current distribution of total dissolved uranium in analyzed Culebra groundwaters is qualitatively consistent with regional variations in the oxidation potential within the unit, with more reducing conditions in the area at the WIPP site than south of the site and in at least part of Nash Draw. The interpretation based on uranium-disequilibrium studies is consistent with the distribution of Culebra hydrochemical facies, stable-isotope studies, and radiocarbon studies in indicating that the overall hydrologic and geochemical setting of the Rustler is transient on a time scale of approximately 10,000 years, and is recovering from the last pluvial period in southeastern New Mexico.

Discussion: The present uranium-disequilibrium data base is extremely limited in size, especially south of the WIPP site. Therefore, significant uncertainty remains concerning the constraints imposed by these studies on both paleo and modern flow directions. However, some change in flow directions within the Culebra is required by the data.

18. Conclusion: $^{87}Sr/^{86}Sr$ studies on both matrix minerals and coexisting mineral pairs from matrix and veins in the evaporitic units below the Dewey Lake Red Beds, and on veins and/or matrix materials from the Dewey Lake, Mescalero caliche, and gypsite springs in Nash Draw indicate distinct variations in the amounts of high-$^{87}Sr/^{86}Sr$ material derived from surficial weathering that are involved in the different units. The measured strontium-isotopic character of the gypsite springs and the Mescalero caliche indicate derivation from surficial components. The character of both matrix minerals and coexisting mineral pairs from matrix and veins in the Castile and Salado Formations, as well as in Rustler anhydrites and the Magenta dolomite indicate little or no input of surficial components. The isotopic compositions of coexisting mineral pairs from veins and matrices are statistically identical, indicating that the components of the veins were locally derived in all units but the Dewey Lake.

There is a broad range of strontium-isotopic character of vein minerals from the Dewey Lake, from surficial values to values similar to those from underlying anhydrites and the Magenta dolomite. Since sulfates and carbonates are very rare in the matrix of the Dewey Lake, the broad range in strontium-isotopic character of Dewey Lake vein gypsums is taken to indicate a mix of surface-type components and components from the underlying Rustler. Upward flow from the Rustler Formation is consistent with measured head relationship. The strontium-isotopic character of analyzed carbonate minerals from the Culebra shows more overlap with that of vein material from the Dewey Lake than does the character of either the intervening Rustler anhydrites or the Magenta dolomite. This is taken to imply that surficial components in the Culebra probably result from confined flow following recharge at some location removed from the WIPP site. If the Culebra near the WIPP site were presently receiving surficial components by vertical recharge, this recharge would be expected to have altered the isotopic character of Rustler zones above the Culebra.

Discussion: The isotopic data base for veins and host-rock minerals in the Rustler and Dewey Lake is limited in size. It has not yet been possible to date any of the secondary minerals directly. Therefore the strontium-isotopic results, while indicating the types of waters involved, do not provide any direct information concerning the ages of these waters.

19. Conclusion: The study of deuterium/hydrogen ratios in vein gypsums in the Dewey Lake and Rustler indicate that all of the gypsums, with the possible exception of vein gypsum from the Dewey Lake in WIPP-19, may have crystallized in the presence of varying amounts of Rustler-type water, rather than in the presence of water representing modern meteoric recharge in the region. The hydrogen-isotope character of secondary Rustler gypsums in hole WIPP-34 is consistently explained by Rustler-type fluids moving both upwards and downwards from the Magenta dolomite into surrounding members, with increasing rock/water ratios corresponding to increasing distance from the Magenta. This internal consistency is lost if crystallization of gypsums from WIPP-34 is assumed to have taken place in the presence of modern meteoric waters.

    In fact, it does not appear possible to have crystallized vein gypsums from either the Magenta and Tamarisk in WIPP-34 or from the Forty-niner in WIPP-33 in the presence of any amount of water representing modern meteoric recharge. Both WIPP-33 and WIPP-34 were drilled to investigate either geophysical anomalies or structures that might be the result of Rustler karst. There is no indication of anomalous structure at WIPP-34. The WIPP-33 structure is interpreted to be the result of karst hydrology, but is apparently unique at and near the WIPP site. The isotopic results suggest, consistent with geologic interpretations, that the WIPP-33 structure is no longer significantly active.

## 6.0 REFERENCES


Anderson, R.Y., 1978: Deep Dissolution of Salt, Northern Delaware Basin, New Mexico; unpubl. report to Sandia National Laboratories, January, 1978.

Anderson, R.Y., 1981: Deep-Seated Salt Dissolution in the Delaware Basin, Texas and New Mexico, NM Geol. Soc., Special Publ. No. 10, pp. 133-145.

Anderson, R.Y., Dean, W.E. Jr., Kirkland, D.W., and Snider, H.I., 1972: Permian Castile Varved Evaporite Sequence, West Texas and New Mexico; Geol. Soc. Am., Bull., v. 83, pp 59-86.

Bachman, G.O., 1973: Surficial Features and Late Cenozoic History in southeastern New Mexico; Open-File Report USGS-4339-8, U.S. Geol. Surv., Albuquerque, New Mexico.

Bachman, G.O., 1974: Geologic Processes and Cenozoic History Related to Salt Dissolution in Southeastern New Mexico; Open-File Report 74-194, U.S. Geol.Surv., Denver, Colorado.

Bachman, G.O., 1980: Regional Geology and Cenozoic History of the Pecos Region, Southeastern New Mexico; Open-File Report D-77-946, U.S. Geol. Surv., Albuquerque, New Mexico.

Bachman, G.O., 1985: Assessment of Near-Surface Dissolution At and Near the Waste Isolation Pilot Plant (WIPP), Southeastern New Mexico; SAND84-7178, Sandia National Laboratories, Albuquerque, New Mexico.

Bachman, G.O., 1987: Karst in Evaporites in Southeastern New Mexico; SAND86-7078, Sandia National Laboratories, Albuquerque, New Mexico.

Bard, S.T., 1982: Estimated Radiation Doses Resulting if an Exploratory Borehole Penetrates a Pressurized Brine Reservoir Assumed to Exist Below the WIPP Repository Horizon - A Single Borehole Scenario; Report EEG-15, New Mexico Environmental Evaluation Group, Santa Fe, New Mexico.

Barr, G.E., Lambert, S.J., and Carter, J.A., 1979: Uranium-Isotope Disequilibrium in Groundwaters of Southeastern New Mexico and Implications Regarding Age-Dating of Waters; in STI/PUB/403, Proceedings of the International Symposium on Isotope Hydrology, 1978; International Atomic Energy Agency, Vienna, Austria.

Barr, G.E., Miller, W.B., and Gonzalez, D.D., 1983: Interim Report on the Modeling of the Regional Hydraulics of the Rustler Formation; SAND83-0391, Sandia National Laboratories, Albuquerque, New Mexico.

Barrows, L.J., 1982: WIPP Geohydrology - The Implications of Karst; unpublished manuscript, discussed in Neill et al., 1983: Evaluation of the Suitability of the WIPP Site; EEG-23, New Mexico Environmental Evaluation Group, Santa Fe, New Mexico.

Barrows, L.J., Shaffer, S-E., Miller, W.B., and Fett, J.D., 1983: Waste Isolation Pilot Plant (WIPP) Site, Gravity Survey and Interpretation; SAND82-2922, Sandia National Laboratories, Albuquerque, New Mexico.

Beauheim, R.L., Black, S.R., Christensen, C.L., Hunter, T.O., Jarolimek, L., Kuhn, A.K., Lambert, S.J., McKinney, R.F., Meyer, D., Murray, J.B., Newton, R.S., Powers, D.W., Stein, C.L., Stephenson, D.E., Sullivan, B.R., Timmer, M.J., and Weart, W.D., 1983a: Results of Site Validation Experiments, Waste Isolation Pilot Plant (WIPP) Project, Southeastern New Mexico; TME3177, U.S. Dept. of Energy, Albuquerque, New Mexico (2 vols.).

Beauheim, R.L., Hassinger, B.W., and Klaiber, J.A., 1983b: Basic Data Report for Borehole Cabin Baby-1 Deepening and Hydrologic Testing, Waste Isolation Pilot Plant (WIPP) Project, Southeastern New Mexico; WTSD-TME-020, U.S. Dept. of Energy, Albuquerque, New Mexico.

Beauheim, R.L., 1986: Hydraulic-Test Results for Well DOE-2 at the Waste Isolation Pilot Plant (WIPP) Site; SAND86-1364, Sandia National Laboratories, Albuquerque, New Mexico 87185.

Beauheim, R.L., 1987a: Analysis of Pumping Tests of the Culebra Dolomite Conducted at the H-3 Hydropad at the Waste Isolation Pilot Plant (WIPP) Site; SAND86-2311, Sandia National Laboratories, Albuquerque, New Mexico.

Beauheim, R.L., 1987b: Interpretations of Single-Well Hydraulic Tests Conducted at and Near the Waste Isolation Pilot Plant (WIPP) Site, 1983-1987: SAND87-0039, Sandia National Laboratories, Albuquerque, New Mexico.

Beauheim, 1987c: Interpretation of the WIPP-13 Multipad Pumping Test of the Culebra Dolomite at the Waste Isolation Pilot Plant (WIPP) Site; SAND87-2456, Sandia National Laboratories, Albuquerque, New Mexico.

Bodine, M.W.Jr., 1978: Clay-Mineral Assemblages from Drill Core of Ochoan Evaporites, Eddy County; in Geology and Mineral Deposits of Ochoan Rocks in the Delaware Basin and Adjacent Areas, Circ. 159, New Mexico Bur. Mines and Resources, Socorro, New Mexico.

Bodine, M.W.Jr., and Jones, B.F., 1986: The Salt Norm: A Quantitative Chemical-Mineralogical Characterization of Natural Waters; Water-Resources Investigation Report 86-4086, U.S. Geol. Surv.

Bodine, M.W.Jr., and Jones, B.F., 1988: Normative Analyses of Groundwaters from the Rustler Formation, Associated with the Waste Isolation Pilot Plant (WIPP), Southeastern New Mexico, U.S. Geol. Surv., unpublished data.

Bodine, M.W.Jr., Jones, B.F., and Lambert, S.J., 1988: Normative Analysis of Groundwaters from the Rustler Formation; in Siegel, M.D., Lambert, S.J., and Robinson, K.L., eds., Hydrogeochemical Studies of the Rustler Formation and Related Rocks in the WIPP Area, Southeastern New Mexico; SAND88-0196, Sandia National Laboratories, Albuquerque, New Mexico.

Borns, D.J., 1983: Petrographic Study of Evaporite Deformation Near the Waste Isolation Pilot Plant (WIPP); SAND83-0166, Sandia National Laboratories, Albuquerque, New Mexico.

Borns, D.J., Barrows, L.J., Powers, D.W., and Snyder, R.P., 1983: Deformation of Evaporites Near the Waste Isolation Pilot Plant (WIPP) Site; SAND82-1069, Sandia National Laboratories, Albuquerque, New Mexico.

Borns, D.J., 1985: Marker Bed 139: A Study of Drillcore from a Systematic Array; SAND85-0023, Sandia National Laboratories, Albuquerque, New Mexico.

Borns, D.J., and Shaffer, S-E., 1985: Regional Well-Log Correlation in the New Mexico Portion of the Delaware Basin; SAND83-1798, Sandia National Laboratories, Albuquerque, New Mexico 87185.

Borns, D.J., 1987a: The Geologic Structures Observed in Drillhole DOE-2 and Their Possible Origins: Waste Isolation Pilot Plant; SAND86-1495, Sandia National Laboratories, Albuquerque, New Mexico 87185.

Borns, D.J., 1987b: Rates of Evaporite Deformation: the Role of Pressure Solution; SAND85-1599, Sandia National Laboratories, Albuquerque, New Mexico 87185.

Borns, D.J., and Stormont, J.C., 1987: Delineation of the Disturbed Rock Zone Around Excavations in Salt, Waste Isolation Pilot Plant (WIPP), SE New Mexico; Geol. Soc. Amer. Abstracts with Programs; v. 19, #6.

Brookins, D.G., and Lambert, S.J., 1987: Radiometric Dating of Ochoan (Permian) Evaporites, WIPP Site, Delaware Basin, New Mexico, USA; pp. 771-780 in Mat. Res. Soc. Symp. Proc., v. 84.

Brookins, D.G., and Lambert, S.J., 1988: WIPP Site Studies: Secondary Selenite Veins in the Rustler Formation and Dewey Lake Red Beds; in Mat. Res. Soc. Symp. Proc. for 1987 (in press).

Carter, N.L., and Heard, H.C., 1970: Temperature and Rate-Dependent Deformation of Halite; Amer. Jour. of Sci., v.269, pp. 193-249.

Carter, N.L., and Hansen, F.D., 1983: Creep of Rock-Salt; Tectono-Physics, v. 92, pp. 275-360.

Case, J.B., Dass, S.M., Franzone, J.G., and Kuhn, A.K., 1982: Analysis of Potential Impacts of Brine Flow Through Boreholes Penetrating the WIPP Storage Facility; TME 3155, U.S. Department of Energy, Albuquerque, New Mexico.

Channell, J.K., 1982: Calculated Radiation Doses from Radionuclides Brought to the Surface if Future Drilling Intercepts the WIPP Repository and Pressurized Brine; EEG-11, New Mexico Environmental Evaluation Group, Santa Fe, New Mexico.

Chapman, J.B., 1986: Stable Isotopes in Southeastern New Mexico Groundwater: Implications for Dating Recharge in the WIPP Area; EEG-35, New Mexico Environmental Evaluation Group, Santa Fe, New Mexico.

Chaturvedi, L., and Channell J.K., 1985: The Rustler Formation as a Transport Medium for Contaminated Groundwater; EEG-32, State of New Mexico, Environmental Evaluation Group, Santa Fe, New Mexico.

Craig, H., 1961: Isotopic Variations in Meteoric Waters; Science, v. 133, pp. 1702-1703.

Crawley, M.E., 1987: Second Data Release Report for the Pressure-Density Survey Program; IT Corporation/Westinghouse WID, Carlsbad, New Mexico.

Davies, P.B., 1983: Assessing the Potential for Deep-Seated Salt Dissolution and Subsidence at the Waste Isolation Pilot Plant (WIPP); unpbl. ms, presented at the State of New Mexico Environmental Evaluation Group Conference: "WIPP Site Suitability for Radioactive Waste Disposal," Carlsbad, New Mexico, May 12,13, 1983.

Deal, D.E., and Case, J.B., 1987: Brine Sampling and Evaluation Program, Phase I Report; DOE-WIPP-87-008, U.S. Dept. of Energy, Carlsbad, New Mexico.

Earth Technology Corp., 1987: Final Report for Time Domain Electromagnetic (TDEM) Surveys at the WIPP; SAND87-7144, Sandia National Laboratories, Albuquerque, New Mexico.

Epstein, S., Sharp, R.P., and Gow, A.J., 1965: Six-year Record of Oxygen and Hydrogen Isotope Variations in South Pole Firn; Jour. Geoph. Res., v. 70, pp. 1809-1814.

Epstein, S., Sharp, R.P., and Gow, A.J., 1970: Antarctic Ice Sheet: Stable-Isotope Analyses of Byrd Station Cores and Interhemispheric Climatic Implications: Science, v. 168, pp. 1570-1572.

Evans, G.V., Otlet, R.L., Downing, R.A., Monkhouse, R.A., and Rae, G., 1979: Some Problems in the Interpretation of Isotope Measurements in United Kingdom Aquifers; in Proceedings of the International Symposium on Isotope Hydrology, STI/PUB/493, Vol.2, International Atomic Energy Agency, Vienna, Austria.

Gonzalez, D.D., 1983a: Hydrogeochemical Parameters of Fluid-Bearing Zones in the Rustler and Bell Canyon Formations: Waste Isolation Pilot Plant (WIPP), Southeastern New Mexico (SENM); SAND 83-0210, Sandia National Laboratories, Albuquerque, New Mexico.

Gonzalez, D.D., 1983b: Groundwater Flow in the Rustler Formation, Waste Isolation Pilot Plant (WIPP), Southeast New Mexico (SENM): Interim Report; SAND82-1012, Sandia National Laboratories, Albuquerque, New Mexico.

Haug, A., Kelly, V.A., LaVenue, A.M., and Pickens, J.F., 1987: Modeling of Ground-Water Flow in the Culebra Dolomite at the Waste Isolation Pilot Plant (WIPP) Site: Interim Report; SAND86-7167, Sandia National Laboratories, Albuquerque, New Mexico.

Heard, H.C., 1972: Steady-State Flow in Polycrystalline Halite at Pressure of 2 Kilobars, in H.C. Heard, I.V. Borg, N.L. Carter, and C.B. Raleigh, eds.; Flow and Fracture of Rocks, (Geophys. Monogr. Series), Amer. Geophys. Union, v. 16, pp. 191-210.

Holt, R.M., and Powers, D.W., 1984: Geotechnical Activities in the Waste-Handling Shaft; WTSD-TME-038, U.S. Dept. of Energy, Carlsbad, New Mexico.

Holt, R.M., and Powers, D.W., 1987: Rustler Formation in the Waste-Handling and Exhaust Shafts, Waste Isolation Pilot Plant (WIPP) Site, Southeastern New Mexico, pp.26-35 in The Rustler Formation at the WIPP Site, Rept. EEG-34, State of New Mexico Environmental Evaluation Group, Santa Fe, New Mexico.

Hoy, R.N., and Gross, G.W., 1982: A Baseline Study of Oxygen 18 and Deuterium in the Roswell, New Mexico, Groundwater Basin; Report No. 144, New Mexico Water Resources Research Institute.

Hudson, T., 1987: Preliminary personal communication to J.S. Stormont (Sandia) on USGS moisture and density measurements in bedded rock salt at the WIPP site.

Hunter, R.L., 1985: A Regional Water Balance for the Waste Isolation Pilot Plant (WIPP) Site and Surrounding Area; SAND84-2233, Sandia National Laboratories, Albuquerque, New Mexico.

Hydro Geo Chem, Inc., 1985: WIPP Hydrology Program, Waste Isolation Pilot Plant, Southeastern New Mexico, Hydrologic Data Report #1; SAND85-7206, Sandia National Laboratories, Albuquerque, New Mexico.

INTERA Technologies, Inc., 1986: WIPP Hydrology Program, Waste Isolation Pilot Plant, Southeastern New Mexico, Hydrologic Data Report #3, SAND86-7109, Sandia National Laboratories, Albuquerque, New Mexico.

INTERA Technologies, Inc., and Hydro Geo Chem, Inc., 1985: WIPP Hydrology Program, Waste Isolation Pilot Plant, Southeastern New Mexico, Hydrologic Data Report #2; SAND85-7263, Sandia National Laboratories, Albuquerque, New Mexico.

Jarolimek, L., Timmer, M.J., and Powers, D.W., 1983: Correlation of Drillhole and Shaft Logs, Waste Isolation Pilot Plant (WIPP) Project, Southeastern New Mexico; Report TME 3179, U.S. DOE, Albuquerque, New Mexico.

Kelley, V.A., and Pickens, J.F., 1986: Interpretation of the Convergent-Flow Tracer Tests Conducted in the Culebra Dolomite at the H-3 and H-4 Hydropads at the Waste Isolation Pilot Plant (WIPP) Site; SAND86-7161, Sandia National Laboratories, Albuquerque, New Mexico.

Knauth, L.P., and Beeunas, M.A., 1986: Isotope Geochemistry of Fluid Inclusions in Permian Halite, with Implications for the Isotopic History of Ocean Water and the Origin of Saline Formation Waters; Geochim. et Cosmochim. Acta, v. 50, pp. 419-434.

LaVenue, A.M., Haug, A., and Kelley, V.A., 1988: Numerical Simulation of Ground-Water Flow in the Culebra Dolomite at the Waste Isolation Pilot Plant (WIPP) Site; Second Interim Report; SAND88-7002, Sandia National Laboratories, Albuquerque, New Mexico.

Lambert, S.J., 1983: Dissolution of Evaporities in and Around the Delaware Basin, Southeastern New Mexico and West Texas; SAND82-0461, Sandia National Laboratories, Albuquerque, New Mexico.

Lambert, S.J., and Carter, J.A., 1984: Uranium-Isotope Disequilibrium in Brine Reservoirs of the Castile Formation,Northern Delaware Basin, Southeastern New Mexico, I: Principles and Methods; SAND83-0144, Sandia National Laboratories, Albuquerque, New Mexico.

Lambert, S.J., and Robinson, K.L., 1984: Field Geochemical Studies of Groundwaters in Nash Draw, southeastern New Mexico; SAND83-1122, Sandia National Laboratories, Albuquerque, New Mexico.

Lambert, S.J., 1987a: Feasibility Study: Applicability of Geochronologic Methods Involving Radiocarbon and other Nuclides to the Groundwater Hydrology of the Rustler Formation; SAND86-1054, Sandia National Laboratories, Albuquerque, New Mexico.

Lambert, S.J., 1987b: Stable-Isotope Studies of Groundwaters in Southeastern New Mexico; SAND85-1978c, Sandia National Laboratories, Albuquerque, New Mexico, in Chaturvedi, L., ed.: The Rustler Formation at the WIPP Site; EEG-34, New Mexico Envir. Eval. Group, Santa Fe, New Mexico.

Lambert, S.J., and Carter, J.A., 1987: Uranium-Isotope Systematics in Groundwaters of the Rustler Formation, Northern Delaware Basin, Southeastern New Mexico; SAND87-0388, Sandia National Laboratories, Albuquerque, New Mexico.

Lambert, S.J., and Harvey, D.M., 1987: Stable-Isotope Geochemistry of Groundwaters in the Delaware Basin of Southeastern New Mexico; SAND87-0138, Sandia National Laboratories, Albuquerque, New Mexico.

Lambert, S.J., 1988: Isotopic Constraints on the Rustler and Dewey Lake Groundwater Systems; in Siegel, M.D., Lambert, S.J., and Robinson, K.L., eds., Hydrogeochemical Studies of the Rustler Formation and Related Rocks in the WIPP Area, Southeastern New Mexico; SAND88-0196, Sandia National Laboratories, Albuquerque, New Mexico.

Lowenstein, T.K., 1987: Post-Burial Alteration of the Permian Rustler-Formation Evaporites, WIPP Site, New Mexico; EEG-36, State of New Mexico, Environmental Evaluation Group, Santa Fe, New Mexico.

Mercer, J.W., 1983: Geohydrology of the Proposed Waste Isolation Pilot Plant Site, Los Medanos area, Southeastern New Mexico; U.S. Geological Survey, Water-Resources Investigations Report 83-4016, U.S. Geological Survey, Albuquerque, New Mexico.

Mercer, J.W., 1987: Compilation of Hydrologic Data from Drilling the Salado and Castile Fomations near the WIPP Site, Southeastern New Mexico; SAND86-0954, Sandia National Laboratories, Albuquerque, New Mexico 87185.

Mercer, J.W., and Orr, B.R., 1979: Interim Data Report on the Geohydrology of the Proposed Waste Isolation Pilot Plant Site, Southeast New Mexico; U.S. Geol. Surv., Water-Resources Investigations Rept. 79-98, U.S. Geol. Surv., Albuquerque, New Mexico.

Mercer, J.W., Beauheim, R.L., Snyder, R.P., and Fairer, G.M., 1987: Basic Data Report for Drilling and Hydrologic Testing of Drillhole DOE-2 at the Waste Isolation Pilot Plant (WIPP) Site; SAND86-0611, Sandia National Laboratories, Albuquerque, New Mexico 87185.

Mook, W.G., 1976: The Dissolution-exchange Model for Dating Groundwater with $^{14}C$; in Interpretation of Environmental Isotope and Hydrochemical Data in Groundwater Hydrology, International Atomic Energy Agency, Vienna, Austria.

Munson, D.E., 1979: Preliminary Deformation-Mechanism Map for Salt (with Application to WIPP); SAND79-0076, Sandia National Laboratories, Albuquerque, New Mexico 87185.

Myers, J., James, P., and Drez, P., 1988: The Redox State of the Culebra Member of the Rustler Formation; in Siegel, M.D., Lambert, S.J., and Robinson, K.L., eds., Hydrogeochemical Studies of the Rustler Formation and Related Rocks in the WIPP Area, Southeastern New Mexico; SAND88-0196, Sandia National Laboratories, Albuquerque, New Mexico.

Neill, R.H., Channell, J.K., Chaturvedi, L., Little, M.S., Rehfeldt, K., and Spiegler, P., 1983: Evaluation of the Suitability of the WIPP Site; EEG-23, New Mexico Environmental Evaluation Group, Santa Fe, New Mexico.

Nowak, E.J., 1986: Preliminary Results of Brine Migration Studies in the Waste Isolation Pilot Plant (WIPP); SAND86-0720, Sandia National Laboratories, Albuquerque, New Mexico.

Nowak, E.J., and McTigue, D.F., 1987: Interim Results of Brine Transport Studies in the Waste Isolation Pilot Plant (WIPP); SAND87-0880, Sandia National Laboratories, Albuquerque, New Mexico 87185.

O'Neil, J.R., Johnson, C.M., White, L.D., and Roedder, E., 1986: The Origin of Fluids in the Salt Beds of the Delaware Basin, New Mexico and Texas; Jour. App. Geoch., v.1.

Osmond, J.K., and Cowart, J.B., 1976: The Theory and Uses of Natural Uranium Isotopic Variations in Hydrology; Atomic Energy Review, v.14.

Pearson, F.J.Jr., and Swarzenki, W.W., 1974: $^{14}C$ Evidence for the Origin of Arid-Region Groundwater, Northeastern Province, Kenya; pp. 95-108 in Isotope Techniques in Groundwater Hydrology 1974, International Atomic Energy Agency, Vienna, Austria.

Peterson, E.W., Lagus, P.L., and Lie, K., 1987: WIPP Horizon Free Field Fluid Transport Characteristics; SAND87-7164, Sandia National Laboratories, Albuquerque, New Mexico 87185.

Pfeifer, M.C., 1987: Multicomponent Underground DC Resistivity Study at the Waste Isolation Pilot Plant, Southeast New Mexico; M.S. Thesis T-3372, Colorado School of Mines, Golden, Colorado.

Plummer, N.L., Parkhurst, D.L., Fleming, G.W., and Dunkle, S.A., 1988: PHRQPITZ - A Computer Program for Geochemical Calculations in Brines; U.S. Geol. Surv., unpublished data.

Popielak, R.S., Beauheim, R.L., Black, S.R., Coons, W.E., Ellingson, C.T., and Olsen, R.L., 1983: Brine Reservoirs in the Castile Formation, Waste Isolation Pilot Plant, Southeastern New Mexico; TME 3153, U.S. Dept. of Energy, Albuquerque, New Mexico.

Powers, D.W., Lambert, S.J., Shaffer, S-E., Hill, L.R., and Weart, W.D., eds., 1978: Geological Characterization Report, Waste Isolation Pilot Plant (WIPP) Site, Southeastern New Mexico; SAND78-1596, Sandia National Laboratories, Albuquerque, New Mexico.

Ramey, D.S., 1985: Chemistry of Rustler Fluids; EEG-31, New Mexico Environ. Eval. Group, Santa Fe, New Mexico.

Reeves, M., Ward, D.S., Johns, N.D., and Cranwell, R.M., 1986a: Theory and Implementation for SWIFT II, the Sandia Waste-Isolation Flow and Transport Model, Release 4.84; SAND83-1159, Sandia National Laboratories, Albuquerque, New Mexico (also NUREG/CR-3328).

Reeves, M., Ward, D.S., Johns, N.D., and Cranwell, R.M., 1986b: Data Input Guide for SWIFT II, the Sandia Waste-Isolation Flow and Transport Model for Fractured Media, Release 4.84; SAND84-1586, Sandia National Laboratories, Albuquerque, New Mexico (also NUREG/CR-3925).

Reeves, M., Kelley, V.A., and Pickens, J.F., 1987: Regional Double-Porosity Solute Transport in the Culebra Dolomite: An Analysis of Parameter Sensitivity and Importance at the Waste Isolation Pilot Plant (WIPP) Site; SAND87-7105, Sandia National Laboratories, Albuquerque, New Mexico.

Robinson, K.L., 1988: Analysis of Solutes in Groundwaters from the Rustler Formation at and Near the WIPP Site; SAND86-0917, Sandia National Laboratories, Albuquerque, New Mexico.

Sandia National Laboratories and United States Geological Survey, 1983: Basic Data Report for Drillhole ERDA-9 (Waste Isolation Pilot Plant - WIPP); SAND79-0270, Sandia National Laboratories, Albuquerque, New Mexico 87185.

Saulnier, G.J.Jr., Freeze, G.A., and Stensrud, W.A., 1987: WIPP Hydrology Program, Waste Isolation Pilot Plant, Southeastern New Mexico, Hydrologic Data Report #4, SAND86-7166, Sandia National Laboratories, Albuquerque, New Mexico.

Saulnier, G.J.Jr., 1987: Analysis of Pumping Tests of the Culebra Dolomite Conducted at the H-11 Hydropad at the Waste Isolation Pilot Plant (WIPP) Site; SAND87-7124, Sandia National Laboratories, Albuquerque, New Mexico.

Saulnier, G.J.Jr., and Avis, J.D., 1988: Interpretation of Hydraulic Tests Conducted in the Waste-Handling Shaft at the Waste Isolation Pilot Plant (WIPP) Site; SAND87-7001, Sandia National Laboratories, Albuquerque, New Mexico.

Sewards, T., Williams, M.L., Stein, C.L., and Keil, K., 1988: Mineralogy of the Culebra Dolomite; in Siegel, M.D., Lambert, S.J., and Robinson, K.L., eds., Hydrogeochemical Studies of the Rustler Formation and Related Rocks in the WIPP Area, Southeastern New Mexico; SAND88-0196, Sandia National Laboratories, Albuquerque, New Mexico.

Siegel, M.D., and Lambert, S.J., 1988: Summary of Hydrogeochemical Constraints on Groundwater Flow in the Rustler Formation; in Siegel, M.D., Lambert, S.J., and Robinson, K.L., eds., Hydrogeochemical Studies of the Rustler Formation and Related Rocks in the WIPP Area, Southeastern New Mexico; SAND88-0196, Sandia National Laboratories, Albuquerque, New Mexico.

Siegel, M.D., Lambert, S.J., and Robinson, K.L., eds., 1988a: Hydrogeochemical Studies of the Rustler Formation and Related Rocks in the WIPP Area, Southeastern New Mexico; SAND88-0196, Sandia National Laboratories, Albuquerque, New Mexico.

Siegel, M.D., Robinson, K.L., and Myers, J., 1988b: Solute Relationships in Groundwaters from the Culebra Member of the Rustler Formation near the WIPP site, southeastern New Mexico; in Siegel, M.D., Lambert, S.J., and Robinson, K.L., eds., Hydrogeochemical Studies of the Rustler Formation and Related Rocks in the WIPP Area, Southeastern New Mexico; SAND88-0196, Sandia National Laboratories, Albuquerque, New Mexico.

Snyder, R.P., 1985: Dissolution of Halite and Gypsum, and Hydration of Anhydrite to Gypsum, Rustler Formation, in the Vicinity of the Waste Isolation Pilot Plant, Southeastern New Mexico; Open-File Report 85-229, U.S. Geol. Survey, Denver, Colorado.

Snyder, R.P., and McIntyre, A.F., 1981: Basic Data Report for Drillhole WIPP-33; SAND80-2011, Sandia National Laboratories, Albuquerque, New Mexico.

Snyder, R.P., and Gard, L.M.Jr., 1982: Evaluation of Breccia Pipes in Southeastern New Mexico and Their Relation to the Waste Isolation Pilot Plant (WIPP) Site; Open-File Report 82-968, U.S. Geol. Surv., Denver, Colorado.

Stein, C.L., and Krumhansl, J.L., 1986: Chemistry of Brines in Salt from the Waste Isolation Pilot Plant (WIPP), Southeastern New Mexico: A Preliminary Investigation; SAND85-0897, Sandia National Laboratories, Albuquerque, New Mexico.

Stein, C.L., 1985: Mineralogy in the Waste Isolation Pilot Plant (WIPP) Facility Stratigraphic Horizon; SAND85-0321, Sandia National Laboratories, Albuquerque, New Mexico.

Stensrud, W.A., Bame, M.A., Lantz, K.D., LaVenue, A.M., Palmer, J.B., and Saulnier, G.J.Jr., 1987: WIPP Hydrology Program, Waste Isolation Pilot Plant, Southeastern New Mexico, Hydrologic Data Report #5, SAND87-7125, Sandia National Laboratories, Albuquerque, New Mexico.

Stensrud, W.A., Bame, M.A., Lantz, K.D., Cauffman, T.L., Palmer, J.B., and Saulnier, G.J.Jr., 1988: WIPP Hydrology Program, Waste Isolation Pilot Plant, Southeastern New Mexico, Hydrologic Data Report #6: SAND87-7166, Sandia National Laboratories, Albuquerque, New Mexico.

Stormont, J.C., Peterson, E.W., and Lagus, P.L., 1987: Summary of and Observations About WIPP Facility Horizon Flow Measurements Through 1986; SAND87-0176, Sandia National Laboratories, Albuquerque, New Mexico 87185.

Tamers, M.A., 1975: Validity of Radiocarbon Dates on Groundwater; Geophys. Surv., v.2., pp. 217-239.

Tomasko, D., and Jensen, A.L., 1987: A Linear-Flow Interpretation of the H-3 Multiwell Pumping Test Conducted at the Waste Isolation Pilot Plant (WIPP) Site; SAND87-0630, Sandia National Laboratories, Albuquerque, New Mexico.

U.S. Department of Energy, 1980: Final Environmental Impact Statement, Waste Isolation Pilot Plant; DOE/EIS-0026, U.S. Department of Energy, Washington, D.C.

U.S. Department of Energy and State of New Mexico, 1981: Agreement for Consultation and Cooperation Between [the U.S.] Department of Energy and the State of New Mexico on the Waste Isolation Pilot Plant, as amended 1985.

U.S. Environmental Protection Agency, 1985: Environmental Standards for the Management and Disposal of Spent Nuclear Fuel, High-Level and Transuranic Radioactive Waste; Final Rule; 40CFR191, pp. 38066-38089, Federal Register, Vol. 50, No. 182 (Sept. 19, 1985).

Uhland, D.W., Randall, W.S., and Carrascco, R.C., 1987: 1987 Annual Water-Quality Data Report for the Waste Isolation Pilot Plant; DOE WIPP 87-006, U.S. Dept. of Energy, Carlsbad, New Mexico.

Van Devender, T.R., 1980: Holocene Plant Remains from Rocky Arroyo and Last Chance Canyon, Eddy County, New Mexico; The Southwestern Naturalist, v. 25.

Weart, W.D., 1983: Summary of Evaluation of the Waste Isolation Pilot Plant (WIPP) Site Suitability; SAND83-0450, Sandia National Laboratories, Albuquerque, New Mexico 87185.

Williamson, C.R., 1979: Deep-sea Sedimentation and Stratigraphic Traps, Bell Canyon Formation (Permian), Delaware Basin; pp. 39-74 in Sullivan, N.M., ed., Guadalupian Delaware Mountain Group of West Texas and southeast New Mexico; Society of Economic Paleontologists and Mineralogists (Permian Basin Section), Publication 79-18.

Wood, B.J., Snow, R.E., Cosler, D.J., and Haji-Djafari, S., 1982: Delaware Mountain Group (DMG) Hydrology - Salt Removal Potential; TME 3166, U.S. Dept. of Energy, Albuquerque, New Mexico.

DISTRIBUTION:

U.S. Department of Energy, (5)
Office of Civilian Radioactive Waste
Management
Office of Geologic Repositories
Forrestal Building
Washington, DC 20585
Stephen H. Kale - RW-20
Associate Director
T. H. Isaacs - RW-20
Deputy Associate Director
James C. Bresee - RW-22
Director, Repository
Coordination Div.
Ralph Stein - RW-23
Director, Engineering &
Geotechnology
James P. Knight - RW-24
Director, Siting, Licensing
and Quality Assurance

U.S. Department of Energy (3)
Albuquerque Operations Office
P.O. Box 5400
Albuquerque, NM 87185
Bruce G. Twining
J. E. Bickel
D. G. Jackson, Director
Public Affairs Division

U.S. Department of Energy/AL
Attn: National Atomic Museum Librarian
P.O. Box 5400
Albuquerque, NM 87185

U.S. Department of Energy (9)
WIPP Project Office (Carlsbad)
P.O. Box 3090
Carlsbad, NM 88221
J. Tillman (4)
A. Hunt
T. Lukow (2)
V. Daub
B. Young

U.S. Department of Energy, SRPO (4)
Salt Repository Project Office
110 N. 25 Mile Avenue
Hereford, TX 79045
Jeff O. Neff
R. Wunderlich
G. Appel
R. Wu

U.S. Department of Energy
Research & Technical Support Division
P.O. Box E
Oak Ridge, TN 37830
D. E. Large

U.S. Department of Energy
Richland Operations Office
Nuclear Fuel Cycle & Production
Division
P.O. Box 500
Richland, WA 99352
R. E. Gerton

U.S. Department of Energy (5)
Office of Defense Waste and
Transportation Management
Washington, DC 20545
G. Daly ---------- DP-121
M. Duff --------- DP-121
A. Follett ------- DP-121
J. Mather -------- DP-121

U.S. Department of Energy (2)
Idaho Operations Office
Fuel Processing and Waste
Management Division
785 DOE Place
Idaho Falls, ID 83402

U.S. Department of Energy (4)
Savannah River Operations Office
Waste Management Project Office
P.O. Box A
Aiken, SC 29801
S. Cowan
W. J. Brumley
J. R. Covell
D. Fulmer

U.S. Nuclear Regulatory Commission (4)
Division of Waste Management
Mail Stop 623SS
Washington, DC 20555
Michael Bell
Hubart Miller
Jacob Philip
NRC Library

U.S. Geological Survey
Branch of Regional Geology
MS913, Box 25046
Denver Federal Center
Denver, CO 80225
    R. Snyder

U.S. Geological Survey (2)
Water Resources Division
Suite 200
4501 Indian School, NE
Albuquerque, NM 87110
    Cathy Peters (2)

State of New Mexico (3)
Environmental Evaluation Group
505 North Main Street
P.O. Box 3149
Carlsbad, NM 88221-3149
    Robert H. Neill, Director

NM Department of Energy & Minerals
P.O. Box 2770
Santa Fe, NM 87501
    Kasey LaPlante, Librarian

New Mexico Bureau of Mines
  and Mineral Resources (2)
Socorro, NM 87801
    F. E. Kottolowski, Director
    J. Hawley

Battelle Pacific Northwest Laboratories (6)
Battelle Boulevard
Richland, WA 99352
    D. J. Bradley
    J. Relyea
    R. E. Westerman
    S. Bates
    H. C. Burkholder
    L. Pederson

Battelle Memorial Institute (17)
Project Management Division
P.O. Box 2360
Hereford, TX 79045
    ONWI Library
    W. Carbiener, General Manager (3)
    V. Adams
    S. Basham
    P. Hoffman
    H. R. Hume
    H. N. Kalia
    J. Kirchner
    S. Matthews
    D. Moak
    J. Moody
    G. Raines
    J. Schornhorst
    O. Swanson
    J. Treadwell

Bechtel Inc. (2)
P.O. Box 3965
45-11-B34
San Francisco, CA 94119
    E. Weber
    H. Taylor

INTERA Technologies, Inc. (4)
6850 Austin Center Blvd., #300
Austin, TX 78731
    G. E. Grisak
    J. F. Pickens
    A. Haug
    A. M. LaVenue

INTERA Technologies, Inc.
P.O. Box 2123
Carlsbad, NM 88221
    Wayne Stensrud

IT Corporation (2)
P.O. Box 2078
Carlsbad, NM 88221
    R. McKinney

IT Corporation (3)
Suite 306
2340 Alamo, SE
Albuquerque, NM 87106
    W. E. Coons
    S. Niou
    J. Myers

RE/SPEC, Inc. (7)
P.O. Box 725
Rapid City, SD 57709
P. F. Gnirk
L. L. Van Sambeek
D. B. Blankenship
T. Brandshang
G. Callahan
T. Pfeifle
J. L. Ratigan

RE/SPEC, Inc.
P.O. Box 14984
Albuquerque NM 87191
S. W. Key

E. I. Dupont de Nemours Company (6)
Savannah River Laboratory
Aiken, SC 29801
N. Bibler
E. L. Albenisius
M. J. Plodinec
G. G. Wicks
C. Jantzen
J. A. Stone

Dupont Company
Building 704-S
Savannah River Plant
Aiken, SC 29808
Richard G. Baxter

George Dymmel
SAIC
101 Convention Center Dr.
Las Vegas, NV 89109

Systems, Science, and Software (2)
Box 1620
La Jolla, CA 92038
E. Peterson
P. Lagus

University of Arizona
Department of Nuclear Engineering
Tucson, AZ 85721
J. G. McCray

University of New Mexico (2)
Geology Department
Albuquerque, NM 87131
D. G. Brookins
Library

The Pennsylvania State University (1)
Materials Research Laboratory
University Park, PA 16802
Della Roy

Texas A&M University
Center of Tectonophysics
College Station, TX 77840

University of Texas at El Paso
Department of Geological Sciences
El Paso, TX 79968
D. W. Powers

Westinghouse Electric Corporation (7)
P.O. Box 2078
Carlsbad, NM 88221
Library
W. Moffitt
V. DeJong
W. Chiquelin
T. Dillon
V. Likar
R. Kehrman

National Academy of Sciences, WIPP Panel:

Dr. Konrad B. Krauskopf, Chairman
Department of Geology
Panama Street
Stanford University
Stanford, CA 94305

Dr. Frank L. Parker
Department of Environmental and
Water Resources Engineering
Vanderbilt University
Nashville, TN 37235

Dr. John O. Blomeke
Oak Ridge National Laboratory
P.O. Box X
Oak Ridge, TN 37830

Dr. John D. Bredehoeft
Western Region Hydrologist
Water Resources Division
U.S. Geological Survey
345 Middlefield Road
Menlo Park, CA 94025

Dr. Karl P. Cohen
928 N. California Avenue
Palo Alto, CA 94303

Dr. Fred M. Ernsberger
250 Old Mill Road
Pittsburgh, PA 15238

Dr. Rodney C. Ewing
Department of Geology
University of New Mexico
200 Yale, NE
Albuquerque, NM 87131

Dr. Charles Fairhurst
Department of Civil and
Mineral Engineering
University of Minnesota
500 Pillsbury Dr. SE
Minneapolis, MN 55455

Dr. William R. Muehlberger
Department of Geological Sciences
University of Texas at Austin
P.O. Box 7909
Austin, TX 78712

Dr. D'Arcy A. Shock
233 Virginia
Ponca City, OK 74601

Dr. Peter B. Myers, Staff
Director
National Academy of Sciences
Committee on Radioactive
Waste Management
2101 Constitution Avenue
Washington, D.C. 20418

Ms. Remi Langum
Staff Officer
Board on Radioactive Waste
Management
GF462
2101 Constitution Avenue
Washington, D.C. 20418

Hobbs Public Library
509 N. Ship Street
Hobbs, NM 88248
Ms. Marcia Lewis, Librarian

New Mexico Tech
Martin Speere Memorial Library
Campus Street
Socorro, NM 87810

New Mexico State Library
P.O. Box 1629
Santa Fe, NM 87503
Ms. Ingrid Vollenhofer

Zimmerman Library
University of New Mexico
Albuquerque, NM 87131
Zanier Vivian

WIPP Public Reading Room
Atomic Museum
Kirtland East AFB
Albuquerque, NM 87185
Ms. Gwynn Schreiner

WIPP Public Reading Room
Carlsbad Municipal Library
101 S. Halagueno St.
Carlsbad, NM 88220
Lee Hubbard, Head Librarian

Thomas Brannigan Library
106 W. Hadley St.
Las Cruces, NM 88001
Don Dresp, Head Librarian

Roswell Public Library
301 N. Pennsylvania Avenue
Roswell, NM 88201
Ms. Nancy Langston

Svensk Karnbransleforsorjning AB
Project KBS
Karnbranslesakerhet
Box 5864
10248 Stockholm, SWEDEN
Fred Karlsson

Institut fur Tieflagerung (4)
Theodor-Heuss-Strasse 4
D-3300 Braunschweig
FEDERAL REPUPLIC OF GERMANY
K. Kuhn

Bundesanstalt fur Geowissenschaften
und Rohstoffe
Postfach 510 153
3000 Hannover 51
FEDERAL REPUBLIC OF GERMANY
Michael Langer

Hahn-Mietner-Institut fur Kernforschung (1)
Glienicker Strasse 100
100 Berlin 39
FEDERAL REPUBLIC OF GERMANY
Werner Lutze

Bundesministerium fur Forschung und
Technologie
Postfach 200 706
5300 Bonn 2
FEDERAL REPUBLIC OF GERMANY
Rolf-Peter Rand

Physikalisch-Technische Bundesanstalt
Postfach 33 45
D-3300 Braunschweig
FEDERAL REPUBLIC OF GERMANY
Peter Brenneke

Kernforschug Karlsruhe (1)
Postfach 3640
7500 Karlsruhe
FEDERAL REPUBLIC OF GERMANY
K. D. Closs

Atomic Energy of Canada, Ltd. (2)
Whiteshell Research Estab.
Pinewa, Manitoba
CANADA ROE 1LO
Peter Haywood
John Tait

Studiecentrum Voor Kernenergie (1)
Centre D'Energie Nucleaire
SCK/CEN
Boeretang 200
B-2400 Mol
BELGIUM
Mr. A. Bonne

Dr. D. K. Mukerjee
Ontario Hydro Research Lab
800 Kipling Avenue
Toronto, Ontario
CANADA MBZ 554

Claude Sombret
Centre D'Etudes Nucleaires
De La Vallee Rhone
CEN/VALRHO
S.D.H.A. BP 171
30205 Bagnols-Sur-Ceze
FRANCE

Mr. Jean-Pierre Olivier
OECD Nuclear Energy Agency
Division of Radiation Protection
and Waste Management
38, Boulevard Suchet
75016 Paris
FRANCE

D. R. Knowles
British Nuclear Fuels, plc
Risley, Warrington, Cheshire WA3 6AS
1002607 GREAT BRITAIN

Shingo Tashiro
Japan Atomic Energy Research Institute
Tokai-Mura, Ibaraki-Ken
319-11 JAPAN

Netherlands Energy Research Foundation
ECN (2)
3 Westerduinweg
P.O. Box 1
1755 ZG Petten
THE NETHERLANDS
Tuen Deboer, Mgr.
L. H. Vons

Pannell Library
New Mexico Junior College
Lovington Highway
Hobbs, NM 88240
Ms. Ruth Hill

Argonne National Laboratory (1)
9700 South Cass Avenue
Argonne, IL 60439
D. Hambeley

Brookhaven National Laboratory (1)
Associated Universities, Inc.
Upton, NY 11973
Paul W. Levy, Senior Scientist

Los Alamos Scientific Laboratory
Los Alamos, NM 87545
B. Erdal, CNC-11

Oak Ridge National Laboratory (4)
Box Y
Oak Ridge, TN 37830
R. E. Blanko
E. Bondietti
C. Claiborne
G. H. Jenks

Oak Ridge National Laboratory
Bldg. 2001
Ecological Sciences Information Center
P.O. Box X
Oak Ridge, TN 37830
C. S. Fore

Rockwell International (1)
Rocky Flats Plant
Golden, CO 80401
C. E. Wickland

Rockwell International (3)
Atomics International Division
Rockwell Hanford Operations
P.O. Box 800
Richland, WA 99352
J. Nelson (HWVP)
P. Salter
W. W. Schultz

Sandia Internal:

| | |
|---|---|
| 1510 | J. W. Nunziato |
| 1520 | C. W. Peterson |
| 1521 | R. D. Krieg |
| 1521 | H. S. Morgan |
| 3141 | S. A. Landenberger (5) |
| 3151 | W. L. Garner (3) |
| 3154-1 | C. H. Dalin, For: DOE/OSTI (8) |
| 6000 | D. L. Hartley |
| 6230 | W. C. Luth |
| 6232 | W. R. Wawersik |
| 6233 | T. M. Gerlach |
| 6233 | J. L. Krumhansl |
| 6300 | R. W. Lynch |
| 6310 | T. O. Hunter |
| 6313 | T. Blejwas |
| 6330 | W. D. Weart |
| 6330 | G. R. Romero |
| 6331 | A. R. Lappin (15) |
| 6331 | R. L. Beauheim |
| 6331 | D. J. Borns |
| 6331 | P. B. Davies |
| 6331 | S. J. Lambert |
| 6331 | R. Z. Lawson |
| 6331 | K. L. Robinson |
| 6331 | M. D. Siegel |
| 6332 | L. D. Tyler |
| 6332 | J. G. Arguello |
| 6332 | R. Beraun |
| 6332 | B. M. Butcher |
| 6332 | R. V. Matalucci |
| 6332 | M. A. Molecke |
| 6332 | D. E. Munson |
| 6332 | E. J. Nowak |
| 6332 | R. J. Roginski |
| 6332 | J. C. Stormont |
| 6332 | T. M. Torres |
| 6332 | Sandia WIPP Central Files (2) (.410 WPP, .430 WPP/SDHLW) |
| 6333 | T. M. Schultheis |
| 6334 | D. R. Anderson |
| 6334 | S. Bertram-Howery |
| 6334 | K. Brinster |
| 6334 | L. Brush |
| 6334 | M. S. Y. Chu |
| 6334 | L. S. Gomez |
| 6334 | R. L. Hunter |
| 6334 | R. D. Klett |
| 6334 | M. G. Marietta |
| 6334 | R. R. Rechard |
| 6334 | A. Rutledge |
| 7100 | C. D. Broyles |

| | |
|---|---|
| 7110 | J. D. Plimpton |
| 7120 | M. J. Navratil |
| 7125 | R. L. Rutter |
| 7125 | J. T. McIlmoyle |
| 7130 | J. O. Kennedy |
| 7133 | O. Burchett |
| 7133 | J. W. Mercer |
| 7135 | P. D. Seward |
| 8524 | P. W. Dean (SNLL Library) |

☆ U.S. GOVERNMENT PRINTING OFFICE: 1988—573-049/81056

| Org. | Bldg. | Name | Rec'd by | Org. | Bldg. | Name | Rec'd by |
|---|---|---|---|---|---|---|---|
| | | | | | | | |
| | | | | | | | |
| | | | | | | | |
| | | | | | | | |
| | | | | | | | |
| | | | | | | | |
| | | | | | | | |
| | | | | | | | |
| | | | | | | | |
| | | | | | | | |
| | | | | | | | |
| | | | | | | | |
| | | | | | | | |
| | | | | | | | |
| | | | | | | | |
| | | | | | | | |

Sandia National Laboratories

# WIPP DESIGN VALIDATION FINAL REPORT
(U.S. Department of Energy)

THIS PAGE LEFT BLANK INTENTIONALLY

U.S. DEPARTMENT OF ENERGY

DOE-WIPP-86-010

DUPLICATE

WASTE ISOLATION PILOT PLANT

# DESIGN VALIDATION FINAL REPORT

JOB 12484

OCTOBER 1986

BECHTEL NATIONAL, INC.
SAN FRANCISCO, CALIFORNIA

# NOTICE

This report was prepared as an account of work sponsored by the United States Government. Neither the United States nor its Department of Energy, nor any of their employees, nor any of their contractors, subcontractors, or their employees, makes any warranty, expressed or implied, or assumes any legal liability or responsibility for the accuracy, completeness, or usefulness of any information, apparatus, product, or process disclosed, or represents that its use would not infringe privately owned rights.

## FOREWORD

The reference design for the underground facilities at the Waste Isolation Pilot Plant was developed using the best criteria available at initiation of the detailed design effort. These design criteria are contained in the U.S. Department of Energy document titled Design Criteria, Waste Isolation Pilot Plant (WIPP), Revised Mission Concept-IIA (RMC-IIA), Rev. 4, dated February 1984. The validation process described in the Design Validation Final Report has resulted in validation of the reference design of the underground openings based on these criteria. Future changes may necessitate modification of the Design Criteria document and/or the reference design. Validation of the reference design as presented in this report permits the consideration of future design or design criteria modifications necessitated by these changes or by experience gained at the WIPP. Any future modifications to the design criteria and/or the reference design will be governed by a DOE Standard Operation Procedure (SOP) covering underground design changes. This procedure will explain the process to be followed in describing, evaluating and approving the change.

The Department of Energy wishes to acknowledge the following for their contributions to the design validation program:

Bechtel National, Inc.
International Technology Corporation
Sandia National Laboratories
Peer Review Panel
  Neville G. W. Cook
  Francois E. Heuze
  Hamish D. S. Miller
  Robert L. Thoms

THIS PAGE LEFT BLANK INTENTIONALLY

CONTENTS


| | | Page |
|---|---|---|
| FOREWORD | | iii |
| CONTENTS | | v |
| TABLES | | xi |
| FIGURES | | xiv |
| EXECUTIVE SUMMARY | | 1 |
| CHAPTER 1 | INTRODUCTION | 1-1 |
| 1.1 | PURPOSE | 1-1 |
| 1.2 | SCOPE | 1-3 |
| 1.3 | HISTORICAL BACKGROUND | 1-5 |
| 1.4 | THE WIPP MISSION | 1-9 |
| 1.5 | DESIGN VALIDATION PROGRAM | 1-9 |
| | 1.5.1 Site and Preliminary Design Validation | 1-12 |
| | 1.5.2 Design Validation | 1-14 |
| CHAPTER 2 | BACKGROUND OF UNDERGROUND DESIGN | 2-1 |
| 2.1 | SITE CHARACTERIZATION AND EVALUATION | 2-1 |
| 2.2 | DESIGN CRITERIA | 2-5 |
| 2.3 | DESIGN BASES | 2-10 |
| 2.4 | DESIGN CONFIGURATIONS | 2-10 |
| 2.5 | DESIGN DEVELOPMENT | 2-10 |
| | 2.5.1 Conceptual Design | 2-11 |
| | 2.5.2 Preliminary Design | 2-11 |
| | 2.5.3 Detailed Design | 2-13 |
| 2.6 | DESIGN METHODS | 2-14 |
| | 2.6.1 Empirical Method | 2-14 |
| | 2.6.2 Closed Form Solutions | 2-15 |
| | 2.6.3 Model Simulation | 2-15 |
| CHAPTER 3 | UNDERGROUND FACILITIES | 3-1 |
| 3.1 | INTRODUCTION | 3-1 |

CONTENTS (continued)


| | | Page |
|---|---|---|
| 3.2 | SELECTION OF THE UNDERGROUND DEVELOPMENT LEVEL | 3-1 |
| 3.3 | DESCRIPTION OF UNDERGROUND FACILITIES | 3-8 |
| 3.3.1 | C & SH Shaft | 3-8 |
| 3.3.2 | Waste Shaft | 3-9 |
| 3.3.3 | Exhaust Shaft | 3-11 |
| 3.3.4 | Drifts | 3-12 |
| 3.3.5 | Test Rooms | 3-15 |
| 3.3.6 | Waste Storage Area | 3-15 |
| 3.4 | UNDERGROUND CONSTRUCTION | 3-16 |
| 3.4.1 | C & SH Shaft | 3-17 |
| 3.4.2 | Waste Shaft | 3-20 |
| 3.4.3 | Exhaust Shaft | 3-24 |
| 3.4.4 | Drifts | 3-27 |
| 3.4.5 | Test Rooms | 3-35 |
| CHAPTER 4 | SUPPORTING VALIDATION DOCUMENTS | 4-1 |
| 4.1 | INTRODUCTION | 4-1 |
| 4.2 | PRELIMINARY DESIGN VALIDATION REPORT | 4-1 |
| 4.2.1 | Purpose and Objectives | 4-1 |
| 4.2.2 | Data Acquisition Program | 4-2 |
| 4.2.3 | Geomechanical Instrumentation | 4-3 |
| 4.2.4 | Preliminary Conclusions | 4-4 |
| 4.3 | GEOTECHNICAL FIELD DATA REPORTS | 4-5 |
| 4.3.1 | Background | 4-5 |
| 4.3.2 | Objectives | 4-5 |
| 4.3.3 | Geomechanical Instrumentation | 4-6 |
| 4.3.4 | Geologic Data | 4-7 |
| 4.3.5 | Geomechanical/Structural Analyses | 4-8 |
| CHAPTER 5 | METHODOLOGY | 5-1 |
| 5.1 | INTRODUCTION | 5-1 |
| 5.2 | DATA COLLECTION | 5-1 |
| 5.2.1 | Geologic Mapping | 5-2 |
| 5.2.2 | Core Drilling and Logging | 5-2 |
| 5.2.3 | Laboratory Testing | 5-3 |
| 5.2.4 | Geomechanical Instrumentation | 5-3 |
| 5.2.5 | Field Observations | 5-12 |
| 5.3 | ANALYSIS AND EVALUATION | 5-12 |
| 5.3.1 | Observations | 5-13 |
| 5.3.2 | Laboratory Tests | 5-13 |
| 5.3.3 | In Situ Measurements | 5-13 |

CONTENTS (continued)


| | | Page |
|---|---|---|
| 5.4 | PREDICTION OF FUTURE BEHAVIOR | 5-13 |
| | 5.4.1 Extrapolation of In Situ Data | 5-14 |
| | 5.4.2 Closed Form Solutions | 5-15 |
| | 5.4.3 Model Simulations | 5-15 |
| CHAPTER 6 | GEOLOGIC CHARACTERIZATION | 6-1 |
| 6.1 | INTRODUCTION | 6-1 |
| 6.2 | DATA COLLECTION ACTIVITIES | 6-1 |
| | 6.2.1 Geologic Mapping | 6-1 |
| | 6.2.2 Core Drilling | 6-10 |
| | 6.2.3 Fluid Measurements | 6-19 |
| 6.3 | DESCRIPTION OF FACILITY GEOLOGY | 6-23 |
| | 6.3.1 Stratigraphy | 6-23 |
| | 6.3.2 Lithology | 6-34 |
| | 6.3.3 Structure | 6-42 |
| 6.4 | PROPERTIES OF HOST ROCKS | 6-42 |
| | 6.4.1 Laboratory Tests | 6-43 |
| | 6.4.2 In Situ Data | 6-47 |
| 6.5 | SURFACE SUBSIDENCE MONITORING | 6-49 |
| CHAPTER 7 | C & SH SHAFT | 7-1 |
| 7.1 | INTRODUCTION | 7-1 |
| 7.2 | DESIGN | 7-1 |
| | 7.2.1 Design Criteria | 7-1 |
| | 7.2.2 Design Bases | 7-2 |
| 7.3 | DESIGN VALIDATION PROCESS | 7-6 |
| | 7.3.1 Data Collection | 7-6 |
| | 7.3.2 Analysis and Evaluation | 7-20 |
| | 7.3.3 Prediction of Future Behavior | 7-47 |
| 7.4 | CONCLUSIONS AND RECOMMENDATIONS | 7-67 |
| | 7.4.1 Conclusions | 7-67 |
| | 7.4.2 Recommendations | 7-70 |

CONTENTS (continued)


| | | Page |
|---|---|---|
| CHAPTER 8 | WASTE SHAFT | 8-1 |
| 8.1 | INTRODUCTION | 8-1 |
| 8.2 | DESIGN | 8-1 |
| | 8.2.1 Design Criteria | 8-1 |
| | 8.2.2 Design Bases | 8-2 |
| 8.3 | DESIGN VALIDATION PROCESS | 8-5 |
| | 8.3.1 Data Collection | 8-5 |
| | 8.3.2 Analysis and Evaluation | 8-15 |
| | 8.3.3 Prediction of Future Behavior | 8-29 |
| 8.4 | CONCLUSIONS AND RECOMMENDATIONS | 8-38 |
| | 8.4.1 Conclusions | 8-38 |
| | 8.4.2 Recommendations | 8-41 |
| CHAPTER 9 | EXHAUST SHAFT | 9-1 |
| 9.1 | INTRODUCTION | 9-1 |
| 9.2 | DESIGN | 9-1 |
| | 9.2.1 Design Criteria | 9-1 |
| | 9.2.2 Design Bases | 9-1 |
| 9.3 | DESIGN VALIDATION PROCESS | 9-2 |
| | 9.3.1 Data Collection | 9-2 |
| | 9.3.2 Analysis and Evaluation | 9-6 |
| | 9.3.3 Prediction of Future Behavior | 9-13 |
| 9.4 | CONCLUSIONS AND RECOMMENDATIONS | 9-15 |
| | 9.4.1 Conclusions | 9-21 |
| | 9.4.2 Recommendations | 9-23 |
| CHAPTER 10 | DRIFTS | 10-1 |
| 10.1 | INTRODUCTION | 10-1 |
| 10.2 | DESIGN | 10-1 |
| | 10.2.1 Design Criteria | 10-2 |
| | 10.2.2 Design Bases | 10-2 |
| 10.3 | DESIGN VALIDATION PROCESS | 10-4 |
| | 10.3.1 Data Collection | 10-4 |
| | 10.3.2 Analysis and Evaluation | 10-19 |
| | 10.3.3 Prediction of Future Behavior | 10-52 |
| 10.4 | CONCLUSIONS AND RECOMMENDATIONS | 10-65 |
| | 10.4.1 Conclusions | 10-69 |
| | 10.4.2 Recommendations | 10-70 |

CONTENTS (continued)


| | | Page |
|---|---|---|
| CHAPTER 11 | TEST ROOMS | 11-1 |
| 11.1 | INTRODUCTION | 11-1 |
| 11.2 | DESIGN | 11-1 |
| 11.3 | DESIGN VALIDATION PROCESS | 11-2 |
| 11.3.1 | Data Collection | 11-2 |
| 11.3.2 | Analysis and Evaluation | 11-11 |
| 11.4 | CONCLUSIONS AND RECOMMENDATIONS | 11-82 |
| 11.4.1 | Conclusions | 11-82 |
| 11.4.2 | Recommendations | 11-84 |
| CHAPTER 12 | STORAGE AREA | 12-1 |
| 12.1 | INTRODUCTION | 12-1 |
| 12.2 | DESIGN | 12-1 |
| 12.2.1 | Design Criteria | 12-1 |
| 12.2.2 | Design Bases | 12-3 |
| 12.2.3 | Design Configuration | 12-8 |
| 12.3 | DESIGN VALIDATION PROCESS | 12-11 |
| 12.3.1 | Data Collection | 12-11 |
| 12.3.2 | Analysis and Evaluation | 12-11 |
| 12.3.3 | Prediction of Future Behavior | 12-14 |
| 12.4 | STORAGE AREA SEALS | 12-54 |
| 12.5 | STORAGE ROOM BACKFILL | 12-59 |
| 12.6 | CONCLUSIONS AND RECOMMENDATIONS | 12-60 |
| 12.6.1 | Conclusions | 12-60 |
| 12.6.2 | Recommendations | 12-62 |
| GLOSSARY | | |
| 6.1 | TERMINOLOGY | G-1 |
| 6.2 | ACRONYMS | G-5 |
| REFERENCES | | R-1 |

## APPENDICES

APPENDIX A DOE STIPULATED AGREEMENT WITH STATE OF NEW MEXICO (PARTIAL)
APPENDIX B GEOLOGIC CORRELATIONS
APPENDIX C MATHEMATICAL SIMULATION OF UNDERGROUND IN SITU BEHAVIOR
APPENDIX D C & SH SHAFT GEOLOGIC LOGS AND MAPS
APPENDIX E WASTE SHAFT GEOLOGIC LOGS AND MAPS
APPENDIX F EXHAUST SHAFT GEOLOGIC LOG
APPENDIX G TEST ROOMS GEOLOGIC MAPS AND SECTIONS
APPENDIX H DRIFT CROSS SECTIONS
APPENDIX I FACILITY LEVEL GEOLOGIC CORE HOLE LOGS
APPENDIX J GEOMECHANICAL INSTRUMENTATION DATA PLOTS
APPENDIX K ANALYTICAL DATA PLOTS

## TABLES


| | | Page |
|---|---|---|
| I | Evaluation Results for Abridged Design Criteria | 21 |
| II | Evaluation Results for C & SH Shaft Design Bases | 28 |
| III | Evaluation Results for Waste Shaft Design Bases | 29 |
| IV | Evaluation Results for Exhaust Shaft Design Bases | 30 |
| V | Evaluation Results for Storage Area Design Bases | 31 |
| VI | Evaluation Results for Design Configurations | 32 |
| 1-1 | Major Accomplishments of the WIPP Program | 1-8 |
| 1-2 | Design Validation Activity Schedule | 1-15 |
| 2-1 | Abridged WIPP Design Criteria | 2-6 |
| 3-1 | Facility Level Configurations - Nominal Excavated Dimensions of Major Drifts and Rooms | 3-13 |
| 3-2 | C & SH Shaft - Abridged Drilling History | 3-18 |
| 3-3 | Waste Shaft - Abridged Construction History | 3-21 |
| 3-4 | Exhaust Shaft - Abridged Construction History | 3-25 |
| 5-1 | C & SH Shaft-Instruments | 5-5 |
| 5-2 | Waste Shaft-Instruments | 5-6 |
| 5-3 | Exhaust Shaft-Instruments | 5-7 |
| 5-4 | Drifts-Instruments | 5-8 |
| 5-5 | Test Rooms-Instruments | 5-9 |
| 5-6 | Geomechanical Instrumentation Specification Summary | 5-11 |
| 6-1 | Summary of Core Hole Data | 6-12 |
| 6-2 | Insoluble Residues of Reference Core Samples | 6-18 |
| 6-3 | Description of Generalized Stratigraphy | 6-26 |
| 6-4 | Clay Seam Characteristics | 6-38 |
| 6-5 | Elastic Constants Determined from Laboratory Tests | 6-44 |
| 6-6 | Failure Constants Determined from Laboratory Tests | 6-44 |
| 6-7 | Creep Constants Determined from Laboratory Tests | 6-45 |
| 6-8 | Creep Parameters Determined from In Situ Data | 6-48 |

TABLES (continued)


| | | Page |
|---|---|---|
| 7-1 | Validation Elements of C & SH Shaft Design Bases | 7-4 |
| 7-2 | C & SH Shaft Liner and Key - Summary of Measured Water Pressures | 7-23 |
| 7-3 | C & SH Shaft Key - Summary of Strain Gauge Readings at Elevation 2554 Feet | 7-32 |
| 7-4 | C & SH Shaft Key - Performance History of Pressure Cells | 7-35 |
| 8-1 | Validation Elements of Waste Shaft Design Bases | 8-3 |
| 8-2 | Waste Shaft Liner and Key - Summary of Measured Water Pressures | 8-19 |
| 9-1 | Validation Elements of Exhaust Shaft Design Bases | 9-3 |
| 10-1 | Drifts - Results of Inspection of Vertical Boreholes in Roofs | 10-8 |
| 10-2 | Excavation Effects Program - Borehole Inspection Summary | 10-11 |
| 10-3 | Drifts - Results of Inspection of Vertical Boreholes in Floors | 10-14 |
| 10-4 | E140 Drift South of S1620 - Summary of Measured Closure | 10-34 |
| 10-5 | Comparisons of Closure in Drifts at S1150 | 10-35 |
| 11-1 | Test Rooms 1 Through 4 - Results of Inspection of Vertical Boreholes in Roofs | 11-5 |
| 11-2 | Excavation Effects Program - Borehole Inspection Summary | 11-6 |
| 11-3 | Test Rooms 1 Through 4 - Results of Inspection of Vertical Boreholes in Floor | 11-8 |
| 11-4 | Test Room 3 (Room T) - Summary of Drilling | 11-9 |
| 11-5 | Test Rooms - Assumed Excavation Dates for Data Analysis | 11-15 |
| 11-6 | Test Rooms - Roof-to-Floor Closure Comparisons | 11-28 |
| 11-7 | Test Rooms - Summary of Results of Regression Analyses for Roof-to-Floor Closure Rates | 11-41 |
| 11-8 | Test Rooms - Wall-to-Wall Closure Comparisons | 11-44 |

TABLES (continued)


| | | Page |
|---|---|---|
| 11-9 | Test Rooms - Summary of Results of Regression Analysis for Wall-to-Wall Closure Rates | 11-45 |
| 11-10 | Test Rooms - Wall Extensometer Collar Movements Versus Convergence Point Reading | 11-51 |
| 11-11 | Test Rooms - Closure Rate Comparisons | 11-52 |
| 11-12 | Test Room Creep Parameters Determined from Roof-to-Floor Closures | 11-66 |
| 11-13 | Test Room Creep Parameters Determined from Wall-to-Wall Closures | 11-71 |
| 12-1 | Validation Elements of Storage Area Design Bases | 12-6 |

## FIGURES


| | | Page |
|---|---|---|
| 1-1 | Location of the WIPP | 1-6 |
| 1-2 | Plan View of Underground Facility | 1-10 |
| 1-3 | The SPDV Underground Layout | 1-13 |
| 2-1 | General Site Stratigraphy | 2-2 |
| 2-2 | Perspective View of the WIPP | 2-12 |
| 3-1 | Functional Areas of the Underground Facility | 3-2 |
| 3-2 | SPDV Exploratory Shaft Station - Design Versus As-Built Configuration | 3-5 |
| 3-3 | Storage Room - Design Versus Revised Configuration | 3-6 |
| 3-4 | Excavation Summary | 3-29 |
| 3-5 | Test Room Excavation Sequence | 3-36 |
| 6-1 | Core Hole Locations | 6-14 |
| 6-2 | WIPP Generalized Stratigraphic Column | 6-25 |
| 6-3 | Clay Seams | 6-30 |
| 6-4 | Reference Stratigraphy | 6-33 |
| 7-1 | C & SH Shaft Liner - Instrumentation | 7-8 |
| 7-2 | C & SH Shaft Key - Instrumentation | 7-11 |
| 7-3 | C & SH Shaft Unlined Section - Instrumentation | 7-14 |
| 7-4 | C & SH Shaft Station - Instrumentation | 7-19 |
| 7-5 | C & SH Shaft Liner and Key - Water Pressure Distribution | 7-24 |
| 7-6 | C & SH Shaft Key - Stratigraphy | 7-28 |
| 7-7 | C & SH Shaft Key - Finite Element Model | 7-30 |
| 7-8 | C & SH Shaft Unlined Section - Average Diametric Closure | 7-36 |
| 7-9 | C & SH Shaft Unlined Section - Collar Movement Time History | 7-38 |
| 7-10 | C & SH Shaft Unlined Section - Rate of Collar Movement Versus Time | 7-39 |

FIGURES (continued)


| | | Page |
|---|---|---|
| 7-11 | C & SH Shaft Unlined Section - Finite Element Model | 7-41 |
| 7-12 | C & SH Shaft Station - Calculated Roof-to-Floor Closure Rates | 7-44 |
| 7-13 | C & SH Shaft Station - Typical Roof-to-Floor Closure History | 7-45 |
| 7-14 | C & SH Shaft Station - History of Collar Movements, Roof Extensometers | 7-46 |
| 7-15 | C & SH Shaft Station - Movement Distribution Along Roof Extensometer 51X-GE-00251 | 7-48 |
| 7-16 | C & SH Shaft Station - Movement Distribution Along Roof Extensometer 51X-GE-00227 | 7-49 |
| 7-17 | C & SH Shaft Liner - Lateral Pressure Comparison | 7-51 |
| 7-18 | C & SH Shaft Key - Radial Stress Distribution | 7-53 |
| 7-19 | C & SH Shaft Key - Tangential Stress Distribution | 7-54 |
| 7-20 | C & SH Shaft Key - Lateral Pressure Prediction | 7-55 |
| 7-21 | C & SH Shaft Key - Hoop Stress Prediction | 7-56 |
| 7-22 | C & SH Shaft Key - Diametric Closure | 7-58 |
| 7-23 | C & SH Shaft Key - Diametric Closure Prediction | 7-59 |
| 7-24 | C & SH Shaft Unlined Section - Radial Stress Distribution at Elevation 1353 Feet | 7-60 |
| 7-25 | C & SH Shaft Unlined Section - Tangential Stress Distribution at Elevation 1353 Feet | 7-61 |
| 7-26 | C & SH Shaft Unlined Section - Radial Displacement Distribution at Elevation 1353 Feet | 7-63 |
| 7-27 | C & SH Shaft Unlined Section - Effective Creep Strain Distribution at Elevation 1353 Feet | 7-64 |
| 7-28 | C & SH Shaft Unlined Section - Relative Diametric Closure | 7-65 |
| 7-29 | C & SH Shaft Unlined Section - Closure Prediction at Elevation 1353 Feet | 7-66 |
| 8-1 | Waste Shaft - Water Inflow Measurements | 8-8 |
| 8-2 | Waste Shaft - Instrumentation | 8-12 |
| 8-3 | Waste Shaft Key - Instrumentation | 8-13 |
| 8-4 | SPDV Ventilation Shaft Station - Instrumentation | 8-16 |

FIGURES (continued)


| | | Page |
|---|---|---|
| 8-5 | Waste Shaft Station - Instrumentation | 8-17 |
| 8-6 | Waste Shaft Liner - Water Pressure Measurements | 8-20 |
| 8-7 | Waste Shaft Liner - Lateral Pressure Comparison | 8-22 |
| 8-8 | Waste Shaft Key - Finite Element Model | 8-23 |
| 8-9 | Waste Shaft Unlined Section - Finite Element Model | 8-27 |
| 8-10 | Waste Shaft Key - Lateral Pressure Prediction | 8-31 |
| 8-11 | Waste Shaft Unlined Section - Radial Stress Distribution at Elevation 1350 Feet | 8-33 |
| 8-12 | Waste Shaft Unlined Section - Tangential Stress Distribution at Elevation 1350 Feet | 8-34 |
| 8-13 | Waste Shaft Unlined Section - Effective Stress Distribution at Elevation 1350 Feet | 8-35 |
| 8-14 | Waste Shaft Unlined Section - Effective Creep Strain Distribution at Elevation 1350 Feet | 8-36 |
| 8-15 | Waste Shaft Unlined Section - Closure Prediction at Elevation 1350 Feet | 8-37 |
| 9-1 | Exhaust Shaft Liner - Lateral Pressure Comparison | 9-8 |
| 9-2 | Exhaust Shaft Key - Finite Element Model | 9-10 |
| 9-3 | Exhaust Shaft Unlined Section - Finite Element Model | 9-12 |
| 9-4 | Exhaust Shaft Key - Lateral Pressure Prediction | 9-14 |
| 9-5 | Exhaust Shaft Unlined Section - Radial Stress Distribution at Elevation 1343 Feet | 9-16 |
| 9-6 | Exhaust Shaft Unlined Section - Tangential Stress Distribution at Elevation 1343 Feet | 9-17 |
| 9-7 | Exhaust Shaft Unlined Section - Effective Stress Distribution at Elevation 1343 Feet | 9-18 |
| 9-8 | Exhaust Shaft Unlined Section - Effective Creep Strain Distribution at Elevation 1343 Feet | 9-19 |
| 9-9 | Exhaust Shaft Unlined Section - Closure Prediction at Elevation 1343 Feet | 9-20 |
| 10-1 | Excavation Effects Program - Borehole Locations | 10-6 |
| 10-2 | Drifts - Instrumentation | 10-16 |
| 10-3 | Drifts - Geologic Log of Hole L2X-01 | 10-24 |

FIGURES (continued)


| | | Page |
|---|---|---|
| 10-4 | Drifts - Comparison of Measured Closure with Regression Curve at E140/S1879 | 10-27 |
| 10-5 | Drifts - Effect of Floor Lowering and Adjacent Excavations on Closure at E140/S1246 | 10-29 |
| 10-6 | Drifts - Comparison of Roof-to-Floor Closure in Drifts with Different Dimensions | 10-30 |
| 10-7 | Drifts - Comparison of Predicted and Observed Roof-to-Floor Closure | 10-32 |
| 10-8 | Drifts - Effect of Floor Lowering on Roof Behavior at E0/S1100 Intersection | 10-37 |
| 10-9 | Drifts - Effect of Floor Lowering on Closure at E0/N626 | 10-38 |
| 10-10 | Drifts - Effect of Floor Lowering on Closure at E140/N624 | 10-39 |
| 10-11 | Drifts - Rate of Floor Heave at E0/N1100 | 10-41 |
| 10-12 | Drifts - Finite Element Model, Before Floor Lowering | 10-43 |
| 10-13 | Drifts - Correlated Closure Histories | 10-46 |
| 10-14 | Drifts - Vertical Stress Distributions in Various Pillars | 10-51 |
| 10-15 | Drifts - Strain Versus Time Since Excavation, N1100/Test Room 2 Intersection | 10-53 |
| 10-16 | Drifts - Strain Rate Versus Time Since Excavation, N1100/Test Room 2 Intersection | 10-54 |
| 10-17 | Drifts - Effective Stress Distribution Immediately After Excavation | 10-56 |
| 10-18 | Drifts - Effective Stress Distribution Immediately Before Floor Lowering | 10-57 |
| 10-19 | Drifts - Principal Stresses Immediately After Excavation | 10-58 |
| 10-20 | Drifts - Principal Stresses Immediately Before Floor Lowering | 10-59 |
| 10-21 | Drifts - Deformed Shape Immediately Before Floor Lowering | 10-60 |
| 10-22 | Drifts - Comparison of Closure Component Responses | 10-62 |
| 10-23 | Drifts - Closure Effects Due to Pillar Width | 10-63 |
| 10-24 | Drifts - Numerical Modeling Versus In Situ Measurement Data from Roof Extensometer | 10-66 |
| 10-25 | Drifts - Numerical Modeling Versus In Situ Measurement Data from Floor Extensometer | 10-67 |

FIGURES (continued) .


| | | Page |
|---|---|---|
| 10-26 | Drifts - Numerical Modeling Versus Measured Wall-to-Wall Closure at E140/S1879 | 10-68 |
| 11-1 | Test Rooms - Instrumentation | 11-12 |
| 11-2 | Test Rooms - Excavation Sequence at Instrument Locations | 11-13 |
| 11-3 | Test Rooms - Measured Roof-to-Floor Closure Comparison | 11-27 |
| 11-4 | Test Rooms - Adjusted Roof-to-Floor Closure | 11-29 |
| 11-5 | Test Room 1 - Regression Analysis of Roof-to-Floor Closure | 11-33 |
| 11-6 | Test Room 1 - Predicted Roof-to-Floor Closure Rate | 11-35 |
| 11-7 | Test Room 1 - Roof-to-Floor Closure Rate, Results of Regression Analysis | 11-36 |
| 11-8 | Test Room 2 - Roof-to-Floor Closure Rate, Results of Regression Analysis | 11-37 |
| 11-9 | Test Room 3 - Roof-to-Floor Closure Rate, Results of Regression Analysis | 11-38 |
| 11-10 | Test Room 4 - Roof-to-Floor Closure Rate, Results of Regression Analysis | 11-39 |
| 11-11 | Test Room 1 - Predicted Additional Roof-to-Floor Closure | 11-40 |
| 11-12 | Test Rooms - Wall-to-Wall Closure Comparison | 11-43 |
| 11-13 | Test Room 1 - Wall-to-Wall Closure Rate, Results of Regression Analysis | 11-46 |
| 11-14 | Test Room 2 - Wall-to-Wall Closure Rate, Results of Regression Analysis | 11-47 |
| 11-15 | Test Room 3 - Wall-to-Wall Closure Rate, Results of Regression Analysis | 11-48 |
| 11-16 | Test Room 4 - Wall-to-Wall Closure Rate, Results of Regression Analysis | 11-49 |
| 11-17 | Test Room 3 - Wall Inclinometer Behavior | 11-53 |
| 11-18 | Test Room 4 - Wall Inclinometer Behavior | 11-55 |
| 11-19 | Test Room 1 - Roof Extensometers, Strain Versus Time Since Excavation | 11-56 |
| 11-20 | Test Room 1 - Roof Extensometers, Strain Rate Versus Time Since Excavation | 11-57 |
| 11-21 | Test Rooms - Finite Element Model | 11-60 |

FIGURES (continued)


| | | Page |
|---|---|---|
| 11-22 | Test Room 1 - Roof-to-Floor Closure History | 11-62 |
| 11-23 | Test Room 2 - Roof-to-Floor Closure History | 11-63 |
| 11-24 | Test Room 3 - Roof-to-Floor Closure History | 11-64 |
| 11-25 | Test Room 4 - Roof-to-Floor Closure History | 11-65 |
| 11-26 | Test Room 1 - Wall-to-Wall Closure History | 11-67 |
| 11-27 | Test Room 2 - Wall-to-Wall Closure History | 11-68 |
| 11-28 | Test Room 3 - Wall-to-Wall Closure History | 11-69 |
| 11-29 | Test Room 4 - Wall-to-Wall Closure History | 11-70 |
| 11-30 | Test Room 2 - Vertical Strain at Roof and Pillar Corner | 11-75 |
| 11-31 | Test Room 2 - Vertical Strain at Roof Center | 11-76 |
| 11-32 | Test Rooms 1 & 4 - Roof Extensometers, Numerical Modeling Versus In Situ Measurement Data | 11-78 |
| 11-33 | Test Rooms 2 & 3 - Roof Extensometers, Numerical Modeling Versus In Situ Measurement Data | 11-79 |
| 11-34 | Test Room 4 - Floor Extensometer, Numerical Modeling Versus In Situ Measurement Data | 11-80 |
| 11-35 | Test Rooms - Comparison of Laboratory Versus in Situ Data | 11-83 |
| 12-1 | Storage Area - Reference Design Plan | 12-2 |
| 12-2 | Storage Area - Drift Reference Design Dimensions | 12-4 |
| 12-3 | Storage Area - Room Reference Design Dimensions | 12-5 |
| 12-4 | Storage Area - Horizontal Emplacement of RH Waste | 12-10 |
| 12-5 | Storage Area - Room Finite Element Model | 12-13 |
| 12-6 | Storage Area - Drift Finite Element Model, After Floor Lowering | 12-15 |
| 12-7 | Storage Rooms - Horizontal Stress Distribution Immediately After Excavation | 12-17 |
| 12-8 | Storage Rooms - Horizontal Stress Distribution 1 Year After Excavation | 12-18 |
| 12-9 | Storage Rooms - Horizontal Stress Distribution 10 Years After Excavation | 12-19 |
| 12-10 | Storage Rooms - Vertical Stress Distribution Immediately After Excavation | 12-21 |

FIGURES (continued)


| | | Page |
|---|---|---|
| 12-11 | Storage Rooms - Vertical Stress Distribution 1 Year After Excavation | 12-22 |
| 12-12 | Storage Rooms - Vertical Stress Distribution 10 Years After Excavation | 12-23 |
| 12-13 | Storage Rooms - Effective Stress Distribution Immediately After Excavation | 12-24 |
| 12-14 | Storage Rooms - Effective Stress Distribution 1 Year After Excavation | 12-25 |
| 12-15 | Storage Rooms - Effective Stress Distribution 10 Years After Excavation | 12-26 |
| 12-16 | Storage Rooms - Effective Creep Strain Distribution 1 Year After Excavation | 12-28 |
| 12-17 | Storage Rooms - Effective Creep Strain Distribution 10 Years After Excavation | 12-29 |
| 12-18 | Storage Rooms - Principal Stresses and Deformed Shape Immediately After Excavation | 12-31 |
| 12-19 | Storage Rooms - Principal Stresses and Deformed Shape 1 Year After Excavation | 12-32 |
| 12-20 | Storage Rooms - Principal Stresses and Deformed Shape 10 Years After Excavation | 12-33 |
| 12-21 | Roof-to-Floor Closure - Geometry and Excavation Effects | 12-36 |
| 12-22 | Wall-to-Wall Closure - Geometry and Excavation Effects | 12-37 |
| 12-23 | Storage Area Drifts - Effective Stress Distribution Immediately After Floor Lowering | 12-45 |
| 12-24 | Storage Area Drifts - Effective Stress Distribution 5 Years After Excavation | 12-46 |
| 12-25 | Storage Area Drifts - Principal Stresses Immediately After Excavation | 12-48 |
| 12-26 | Storage Area Drifts - Principal Stresses 5 Years After Excavation | 12-49 |
| 12-27 | Storage Area Drifts - Deformed Shape 5 Years After Excavation | 12-50 |
| 12-28 | Storage Area Drifts - Roof-to-Floor Closure Prediction | 12-52 |

FIGURES (continued)


| | | Page |
|---|---|---|
| 12-29 | Storage Room Intersection - Roof-to-Floor Closure Prediction | 12-56 |
| 12-30 | Storage Area - Plug Locations | 12-57 |
| 12-31 | Storage Area - Proposed Panel Plug Reference Design | 12-58 |
| 12-32 | Storage Area - Modified Waste Stacking Configuration | 12-63 |

THIS PAGE LEFT BLANK INTENTIONALLY

# WASTE ISOLATION PILOT PLANT
# DESIGN VALIDATION
# EXECUTIVE SUMMARY

## INTRODUCTION

The Waste Isolation Pilot Plant (WIPP) is being developed by the U.S. Department of Energy (DOE) as a research and development facility to demonstrate the safe disposal of radioactive waste from U.S. defense programs. The facility is located in southeastern New Mexico, about 25 miles east of the city of Carlsbad. Underground development is at a depth of about 2,150 feet in thick deposits of bedded salt. The facility operation will include in situ experiments addressing technical issues for defense waste programs and storage of defense related contact-handled (CH) and remote-handled (RH) transuranic (TRU) waste.

In 1979, the DOE established a Site and Preliminary Design Validation (SPDV) Program to provide additional confidence in the siting and design of the WIPP facility. On July 1, 1981, the DOE entered into an agreement with the State of New Mexico whereby the DOE would perform certain work to validate the reference design of the WIPP underground openings. The results of the site validation portion of the program are presented in the report titled Results of Site Validation Experiments, Volumes I and II, TME document 3177, dated March 1983. The results of the preliminary design validation portion of the program are presented in the report titled Waste Isolation Pilot Plant Preliminary Design Validation Report, dated March 30, 1983.

Design validation of the WIPP is defined as the process by which the reference design of the underground openings is confirmed by determining the compatibility of the design criteria, design bases and reference design configurations using site specific information. The design validation process consists of an assessment of the condition and behavior of shafts, drifts and a full-sized, four-room test panel

excavated during the SPDV Program and full WIPP construction. Based on this assessment of these excavations, and on predictions of their future behavior, any modifications to the design criteria, design bases or design configurations required to achieve a validated reference design will be developed. In addition, the validated reference design may be modified in the future as still more data and experience are gained during a 5-year demonstration period (period during which all waste must be retrievable) and permanent storage operations.

The WIPP Preliminary Design Validation Report was an interim report prepared as part of the overall validation of the WIPP underground opening reference design. The WIPP Design Validation Final Report contains additional information gathered after completion of the SPDV Program. This information has been analyzed and evaluated to complete the design validation process for the WIPP.

Four types of information were gathered for the WIPP Design Validation Final Report:

(1) observations of the behavior of the underground openings;

(2) descriptions of the geologic conditions encountered during underground construction;

(3) descriptions of core samples from instrumentation and other holes in the roof and floor of the underground openings; and

(4) data from installed geomechanical instrumentation.

The design validation process provides for the collection, analysis and evaluation of in situ data. This process is designed to permit determination of the need to modify elements of the underground opening reference design so that construction and operation of the full facility can proceed in a timely, safe, environmentally acceptable and cost effective manner. Observation and instrumentation data have been

collected and evaluated for each of the underground design elements. Tables I through VI at the end of this summary present the evaluation results for the design criteria, design bases and design configurations of the shafts and horizontal openings.

## BACKGROUND OF UNDERGROUND DESIGN

Geologic characterization of the site began with a literature review and continued with the collection of field data. Special emphasis was placed on correlating data obtained from seismic reflection and resistivity surveys and borehole drilling. Design information regarding site stratigraphy from the ground surface to about 250 feet below the underground facility level was developed from geologic data obtained from drill holes ERDA-9, WIPP-12 and DOE-1, and from the SPDV exploratory and ventilation shafts.

The engineering designs for the WIPP surface and underground facilities began with the conceptual design, initiated in 1975 and completed in 1977. The conceptual design provided the basis for the development of the preliminary design of both the surface and underground facilities, which was completed in January 1980. The preliminary design incorporated the conventional room and pillar method for underground development.

Design of the WIPP provided for the access and storage openings to remain stable and provide minimum clearance for equipment during waste emplacement and the 5-year demonstration period, even though these openings will eventually close due to salt creep. Modeling techniques were used to estimate the geomechanical behavior and structural stability of the openings. The preliminary design included numerical modeling of the selected underground opening configurations. These models were used to predict opening closures and augmented other conventional mining industry methods of stability evaluation.

## UNDERGROUND FACILITIES

Seven stratigraphic horizons were identified in 1979 as potential locations for the facility level. These horizons were chosen from examinations of available geotechnical data and on horizon selection criteria established by the WIPP project participants. Selection of the final underground development level was made by the DOE following the recommendation of WIPP project participants.

The WIPP facility is composed of three shafts connected to a single underground facility level. The C & SH shaft provides the principal means of access and also serves as the primary air intake opening. The waste shaft is designed to permit the transport of radioactive waste between the surface waste-handling facilities and the underground storage area. The exhaust shaft is the primary opening for exhaust air from the underground facility. All three shafts have three principle constituents: a lined section penetrating the rock overburden; an unlined section penetrating the salt; and a key at the rock/salt contact to act as a transition from the lined section to the unlined section.

The storage level contains all of the underground facilities for waste handling, waste storage, operations and maintenance. All of the underground horizontal openings are rectangular in cross section. The drift configurations range from 8 feet to 12 feet high and 12 feet to 25 feet wide.

Underground construction was accomplished in two phases. The initial (SPDV) phase was conducted from May 1981 through March 1983. The second phase, full construction, was accomplished from October 1983 through February 1985. Both phases included the excavation and outfitting of shafts, drifts and rooms.

## SUPPORTING VALIDATION DOCUMENTS

The primary documents supporting design validation are the WIPP Preliminary Design Validation Report and quarterly geotechnical field data reports (GFDR).

The objective of preliminary design validation was to provide initial evaluation of the design criteria and design bases, and initial confirmation of the underground reference design. Geologic mapping, core drilling and logging, and geomechanical instrumentation data were assimilated to provide an early, short-term evaluation. The preliminary conclusions presented in the WIPP Preliminary Design Validation Report stated that the shafts and underground openings were performing as expected and were stable. In addition, gas had not been encountered in any significant quantity during excavation and no brine pockets had been encountered.

The GFDRs were initiated by the DOE to provide data from the SPDV Program and full construction in a timely manner. The GFDRs were intended to present in situ data on the geomechanical behavior of the strata surrounding the underground openings along with visual observations of opening behavior and analyses of selected underground design elements.

## METHODOLOGY

Design validation is accomplished by determining the compatibility of the design criteria, design bases and reference design using site specific information. The design validation process consists of three major steps: data collection; analysis and evaluation; and prediction of future behavior.

The data collection program was designed to provide information on the geologic conditions encountered throughout the underground facility and on the structural behavior of the underground openings. The program

included geologic mapping, core drilling and logging, laboratory testing, visual inspections, and geomechanical instrumentation measurements. The data collected from these activities were analyzed and evaluated to determine the behavior of the various components of the underground facility and predict their future behavior by projecting the results of both finite element model and regression analyses.

The geomechanical instrumentation measurements provided in situ data on the behavior of the underground openings. These data were then used in empirical equations relating time and closure. Laboratory test results were used to calculate the salt creep and elastic parameters. Salt creep parameters were also determined by the regression analysis of in situ data. Long-term behavior of the underground openings was predicted by extrapolation of the results of the regression analysis.

## GEOLOGIC CHARACTERIZATION

Geologic characterization of the WIPP underground openings began in June 1981. Data collection activities included geologic mapping, core drilling and logging, and fluid measurements. The SPDV exploratory shaft was mapped prior to selecting the storage horizon. The waste shaft was mapped, first as the SPDV ventilation shaft and again after it was enlarged to its final diameter. Geologic mapping was also conducted in the exhaust shaft.

Geologic mapping of the horizontal openings was conducted during design validation. This mapping was performed primarily to determine stratigraphic continuity. Mapping was conducted along one wall of the drifts to the northern extent of the facility and along the full length of the south exploratory drift. Geologic mapping was also conducted to the east and west facility boundaries in the experimental area and in the test rooms.

Geologic mapping confirmed the continuity of the stratigraphy within the horizontal openings to the facility boundaries. Core drilling and logging confirmed this stratigraphic continuity for a distance of 50 feet above and below the facility level. The geologic mapping and core logging did not detect any significant geologic structures. Data from the core holes were also used to establish the WIPP reference stratigraphy.

Fluid inflow measurements were obtained by various activities designed to characterize the two water-bearing dolomite members of the Rustler formation and the potential for the occurrence of gas and brine at the facility level. Measurements in the three shafts showed that water inflow from the Rustler formation is essentially negligible due to liner and seal performance.

Small amounts of pressurized gas have been encountered by some underground core holes. Brine has also been encountered in small quantities and is sometimes associated with gas occurrences. There has been no occurrence of gas or brine in quantities significant enough to jeopardize the stability or safety of the facility. Two programs, the brine testing program and the gas testing program, are being conducted to further characterize these occurrences. Neither program is associated with design validation.

Subsidence monuments have been installed on the surface over the shaft pillar area. The design criteria require that subsidence due to underground excavation not exceed 1 inch within a 500-foot radius of the waste shaft. It is not possible at this time to determine actual subsidence; this will occur over the next 25 years. Subsidence calculations used in the reference design indicate that the criteria limits will not be exceeded.

C & SH SHAFT

The C & SH shaft consists of a lined section, a shaft key, an unlined section and a shaft station. The shaft liner is made of structural steel that increases in thickness with depth to withstand increasing hydrostatic pressure. The reinforced concrete shaft key serves as a transition between the lined and unlined sections of the shaft. Chemical water seals behind the concrete key are designed to prevent ground water from flowing behind the key, into the unlined section of the shaft. The shaft station is excavated near the bottom of the unlined section.

Validation of the C & SH shaft reference design was accomplished by acquiring a variety of geotechnical data for analysis, evaluation and prediction of future behavior. The condition of the shaft liner and key are monitored by geomechanical instrumentation and visual inspections. Convergence points measure diametric closure; piezometers monitor ground-water pressures; strain gauges and pressure cells monitor the effect of salt creep on the concrete key. Telltale pipes in the shaft key provide information on the effectiveness of the chemical water seals. The unlined section of the shaft is monitored by extensometers and convergence points and is visually inspected for fracturing and rock slabbing. The shaft station has an extensive geomechanical instrumentation monitoring system and is inspected regularly.

The design basis hydrostatic pressure is suitable. Piezometer measurements indicate that the hydrostatic pressure is currently much less than the design pressure. Analysis of the shaft key indicates that lateral pressure on the key at the end of the operating period will be much less than the design basis lateral pressure requirement. Diametric closure of the key will be minimal. Computational analyses of stresses and strains indicate that the shaft will be stable and remain within the required safety limits during its operating life. Analysis of computed diametric closure near the bottom of the shaft

indicated that, while the closure will be within the design criteria and design basis limits, the lower buntons will be impacted.

The shaft design complies with the design criteria requirements for ground-water control. Regular inspections of shaft conditions show no signs of deterioration or instability.

The C & SH shaft station exhibits the highest degree of deterioration in the underground facility. The fracturing and separation observed has been stabilized, but will continue to develop. Closure during the 25-year operating life of the station will be on the order of 8 feet vertically and 5 feet horizontally. These conditions will require maintenance to ensure safety and to maintain the required minimum clearances for equipment and operations.

WASTE SHAFT

The waste shaft also consists of a lined section, a key, an unlined section and a shaft station. The shaft is lined with unreinforced concrete from the surface to the top of the Salado formation. The shaft liner terminates with a reinforced concrete key at the Rustler/Salado formation contact. The shaft is unlined, except for wire mesh, from the key to the bottom of the shaft.

Data collection activities in the waste shaft have consisted of geologic mapping, ground-water inflow measurements, geomechanical instrumentation measurements and periodic visual inspections. Except for convergence points, the geomechanical instruments are monitored remotely by the datalogger.

The waste shaft data was analyzed with respect to design parameters for each component of the shaft. As part of the engineering analysis, predictions of future behavior were made for each of the components.

Stability of the shaft liner has been confirmed. The water pressure exerted on it is significantly below the design hydrostatic pressure. If the pressure should reach the design hydrostatic pressure, the liner will still be stable. The shrinkage cracks in the liner do not present a structural problem.

The shaft key was designed to withstand a lateral pressure due to salt creep equivalent to 50 percent of the vertical overburden pressure. A numerical analysis was utilized to simulate the long-term effect of salt creep on the concrete key. It showed that the computed lateral pressure at the end of the operating period will be slightly higher than the design lateral pressure, but well below the total lateral pressure capacity of the key.

Observations of the waste shaft key have determined that only one minor seep occurs in the key and that no water seepage is occurring from the base of the key. This supports the conclusion that the water seals are functioning, that no water is seeping along the concrete/salt contact, and that salt dissolution is not occurring behind the key.

The design criteria require that no uncontrolled ground water reach the facility level through the shafts. Although minor amounts of fly water do reach the facility, this water has a negligible impact on operations and does not affect validation of this criterion.

The unlined section of the shaft was designed to be stable and maintain a diameter adequate for the operating life of the facility. The structural behavior of this section was analyzed using a finite element model and creep parameters determined from the C & SH shaft in situ data. The results indicate that the maximum stress occurred immediately after excavation and will decrease with time. Stress behavior will not cause a stability problem. Diametric closure due to salt creep will not exceed the design limits.

The design of the waste shaft station is based primarily on operational parameters. The closure and stability of the station was evaluated using in situ data from the C & SH shaft station. The estimated vertical closure rate will result in a total closure of over 7 feet during the 25 year operating life of the station. Actual closure may be less, but remedial work will still be required to maintain the proper clearances.

EXHAUST SHAFT

The exhaust shaft is constructed similarly to the waste shaft. It consists of a concrete lined section, a shaft key and an unlined section. The lined section is constructed of unreinforced concrete and the shaft key of reinforced concrete. The unlined section contains only rock bolts and wire mesh.

Data collection in the exhaust shaft has been on a much smaller scale than in the other two shafts. Geomechanical instrumentation was not required by the original shaft design because geologic and structural conditions were assumed to be similar to the other two nearby shafts. However, remotely monitored instrumentation has been installed to provide shaft-specific information for use in the sealing program. Geologic mapping and visual inspections have confirmed that the geologic and geohydrologic environment is similar to that of the other two shafts. Data from these two shafts have been used to predict the future performance of the exhaust shaft.

Geohydrologic and geomechanical data from the C & SH shaft and the waste shaft have been compared to model simulations for each section of the exhaust shaft. These models, field observations and instrumentation data confirm that the exhaust shaft reference design is suitable for its 25 year operating life.

The shaft liner is stable and has a water pressure against it that is less than the design basis hydrostatic pressure. If the pressure

increases, the liner will remain stable. Shrinkage cracks will not result in structural instability.

As with the waste shaft, an analysis of the exhaust shaft key indicates that the lateral pressure calculated for 25 years will slightly exceed the design lateral pressure, but will be well below the maximum allowable lateral pressure. Computational analyses of the stresses and strains indicate that the unlined section of the shaft will be stable and remain within safety limits during its operating life. The computed diametric closure will be within design criteria and design basis limits.

Water is entering the exhaust shaft through cracks and construction joints in the concrete liner. A small amount of water still reaches the shaft even after a remedial grouting program. When the exhaust fans are on, this water evaporates before reaching the facility. The water seals in the key appear to be functioning and there is no evidence of salt dissolution behind the key.

DRIFTS

The discussion of drifts contained in this section pertains to all horizontal underground openings except the shaft stations, test rooms, and storage area rooms and their associated drifts. The drifts were designed in accordance with the design criteria and design bases. The largest drifts were initially excavated 8 feet high and 25 feet wide. These drifts have been or will be enlarged to 12 feet high. This drift height is dictated by the minimum 11-foot operating clearance required for the waste storage equipment.

A variety of geotechnical activities were conducted to evaluate the behavior of the excavated drifts. These activities included geologic mapping, core drilling and logging, visual inspections, and geomechanical instrumentation measurements.

Visual inspections consisted of qualitative observations and documentation of various aspects of drift behavior. These observations are divided into four categories: roof and wall spalling; pillar fracturing; roof displacements and separations; and floor fracturing, displacements and separations.

Deformational behavior consisting of spalling from the roof and walls of the drifts and fracturing and spalling at pillar corners has occurred. Separations and lateral displacements have been detected in the halite above the roof, primarily at clay seams. These types of behavior are expected and will continue to occur, but can be controlled by scaling and rock bolting.

Fracturing has occurred in marker bed 139 (MB-139) and in the overlying halite beneath the floor of the drifts. The fracturing is not well developed and occurs primarily beneath large intersections. Based on experience in local potash mines, this fracturing is not expected to cause stability or operational problems.

The comparison of measured closure behavior in drifts with different dimensions indicates that the maximum closure and closure rate will occur in 12 x 25-foot drifts. The closure rates are affected by the presence of nearby parallel drifts and crosscuts as well as differences in salt properties. Based on available measurement data and the results of modeling analyses, the closure rate in the 13 x 25-foot storage area drifts may be 30 percent greater than that of a single, infinitely long drift with the same dimensions.

Analyses of salt behavior around the 25-foot wide drifts has determined both the redistribution of stresses due to creep and the locations of effective creep strain concentrations. The stresses which develop immediately after excavation relax with time due to creep behavior and will not cause future stability problems. The strain will remain within the limit required for structural stability with respect to catastrophic failure.

The evaluation of field observations and analytical results have shown that the design criteria were appropriate for design of the horizontal openings. The criteria identified as requiring specific evaluation were determined to be suitable. The reference design for the horizontal openings is therefore validated.

Based on the results of design validation of the drifts, it is recommended that all drifts be inspected frequently for operational clearance and safety. If the clearance is insufficient, the drifts must be trimmed to the required dimensions. Scaling and rock bolting should be performed where necessary for safety purposes.

TEST ROOMS

The test rooms comprise a panel of four rooms having a similar configuration as the planned storage rooms. They have been instrumented, observed and analyzed to evaluate the behavior of the future storage rooms. Data collection activities have consisted of geologic mapping, core drilling and logging, visual inspections and geomechanical instrumentation measurements. The instrumentation includes borehole extensometers, inclinometers, convergence points, convergence meters and rigid-inclusion, vibrating-wire stressmeters.

Room deterioration has been minimal and consists of spalling from the roof and walls, vertical fracturing in the pillars, minor displacements and separations above the roof and beneath the floor, and fracturing beneath the floor. Areas of drummy rock detected by roof and wall inspections immediately following excavation were scaled and rock bolted. These areas have not increased noticeably in size since the test rooms were excavated, over 3 years ago.

Subhorizontal fracturing has developed beneath the test room floors. Separations and fractures are on a small scale except for one isolated location beneath Test Room 3. Fracturing in this area is well developed and occurs in two distinct zones. Studies have not shown

fracturing of this magnitude to occur anywhere else within the underground WIPP facility.

The analysis of closure of the test rooms using creep constants derived from laboratory data underestimate actual closure. The design criteria closure of 12 inches in 5 years has been exceeded within 3 years. Strains measured in the test rooms compare well with strains computed by numerical modeling.

STORAGE AREA

The storage area rooms and drifts are designed to permit the permanent storage of defense-related CH and RH TRU waste. The storage area is composed of eight panels consisting of seven rooms each. Each room is 13 feet high, 33 feet wide and 300 feet long. The storage area, including all rooms and drifts, is designed to provide storage space for 6,330,000 cubic feet of CH TRU waste and 1,000 canisters of RH TRU waste.

Validation of the storage room reference design depends primarily on the analysis of data from the four test rooms. Evaluation of the storage rooms was based on the results of a finite element model analysis using creep parameters determined from the test room analyses. The results of this analysis provided determinations of horizontal and vertical stresses, effective stresses, effective creep strains, principal stresses, room deformation and closure, and intersection closure.

The analyses show that the stress arch around the opening migrates away with time. The maximum stress occurs immediately after excavation and is reduced as the opening deforms over time due to salt creep. These stresses will therefore not cause a stability problem in the future. However, MB-139, the anhydrite bed approximately 4 feet below the floor, is expected to be subjected to gradually increasing stress and may exhibit local failure.

Effective creep strains will intensify and concentrate at some locations around the opening. While minor spalls and failures are expected to occur on the excavation surfaces, the rooms will remain structurally stable.

The storage room reference design of 13 feet high and 33 feet wide was based on calculations using laboratory-derived average creep parameters. This design allowed for 12 inches of vertical closure and 9 inches of horizontal closure 5 years after excavation. This accommodates the design bases requirements for a minimum of 16 inches of ventilation space above the stored waste and a 12-foot minimum height for storage equipment. The current predicted vertical closure at 5 years is about 22 inches. For permanent storage, the additional 10 inches of closure can be accommodated by excavating the storage rooms to a height of 13 feet 10 inches.

If a decision is made to retrieve the stored waste, the design criteria assumed, using a one-shift-per-day basis, that a room may be as much as 15 years old before removal of all of the waste is completed. A 15-year old room has a predicted vertical closure of 54 inches. This closure is 14 inches greater than the maximum acceptable closure and would result in crushing and possible breaching of the waste containers. Because this is not in compliance with the design criteria, other alternatives must be considered.

A 10 year maximum for retrieval is conservative. If three shifts per day were utilized, no room would be older than 7 years by the time its waste was removed. A 7 year old room would have 28 inches of vertical closure. Additional closure benefits can be gained by excavating a room to is maximum dimensions and then trimming the room to those maximum dimensions after 1 year of closure. This will allow the room to close at the rate determined by secondary creep and will result in 21 inches of vertical closure 7 years after trimming. This will meet the design criteria requirements.

The design bases provide for 9 inches of horizontal closure in the first 5 years after room excavation. The current prediction, based on in situ data, is 15 inches of closure in the 33- to 34-foot wide rooms. If the rooms are excavated 34-feet wide and backfilled with loose salt, this closure will be suitable for permanent storage.

For retrieval, the horizontal closure 15 years after excavation will be approximately 36 inches. This closure will result in some crushing and possible breaching of the waste containers. Even if retrieval is effected within 7 years, some containers may still be crushed and breached.

The timing of retrieval operations and two-stage excavation can be used to reduce wall-to-wall closure. Using a three-shift-per-day basis, a 7 year old room would close approximately 20 inches. If a first in/first out storage and retrieval operations is utilized, and waste is removed before a room reaches an age of 6 years, horizontal closure will be reduced to 18 inches. Both these changes would decrease the possiblity of crushing or breaching the containers. If a 34-foot wide room is trimmed after 1 year to its initial full dimensions, the horizontal closure at 7 years will be about 14 inches. This will further minimize crushing or breaching of the containers. The extent to which crushing will be minimized is unknown. This is because the space between the waste canisters and the room wall will be filled with loose salt. The load transferring capabilities of the backfill is not known at the present time.

The reference design also provides for permanent waste storage in all of the storage area drifts. Fifteen years after excavation a 13 x 25-foot drift is predicted to have a vertical closure of about 25 inches and a horizontal closure of about 20 inches. This is suitable for waste storage but trimming will be required for equipment clearance.

The storage area entry drifts will contain plugs for the isolation of the storage panels. The final design of these plugs is not yet

complete. However, the conceptual design envisions a multiple-component plug approximately 100 feet long.

The reference design for the storage rooms will be considered to be validated when any of the following recommended alternative modifications, or combination of these modifications, are incorporated:

(1) Maintain the reference design storage room dimensions of 13 to 14 feet high and 33 to 34 feet wide and maintain the salt backfill, but reduce the volume of waste to be stored and modify the container stacking configuration for the 5-year demonstration period. Revise the design criteria to require that waste be retrieved before a room exceeds an age of 7 years. This will meet the criteria that the waste containers not be crushed or breached, but it will require a significant number of additional storage rooms.

(2) Maintain the reference design storage room dimensions and maintain the planned waste volume. Revise the design criteria to delete the requirement for salt backfill and to require that waste be retrieved before a room exceeds an age of 7 years. This will meet the criteria that the waste containers not be crushed or breached without requiring additional storage rooms.

(3) Maintain the reference design storage room dimensions, planned waste volume, and salt backfill requirement. Revise the storage operations so that the first-emplaced waste is the first-retrieved waste with retrieval effected before the room exceeds 6 years of age. Excavate the room to 14 x 34 feet, then, 1 year later, trim the room to its initial 14 X 34 foot dimensions. This will minimize container crushing and breaching. More storage rooms will be utilized during the 5-year demonstration period, but the total number of rooms will remain the same as provided by the reference

design. This modification will require changing the design criteria to allow crushing and breaching of the CH waste containers prior to retrieval and to require a demonstration of the retrieval and handling of crushed and breached containers.

(4) Reduce the reference design storage room width from 33 feet to 28 feet, maintain the room height at 13 to 14 feet, and reduce the pillar width to 84 feet. Maintain the first room for RH waste emplacement at the original reference design dimensions. Reduce the planned waste volume and maintain the salt backfill requirement. Excavate the rooms to 14 x 28 feet, then trim them to this dimension after 1 year. Use a first-in/first-out storage operation. This will reduce the creep to approximately that of a 13 x 25-foot drift. Stability will be enhanced and crushing and breaching will be minimized. The volume of excavation will be approximately the same as for the reference design storage rooms, but with the advantage of a lower creep rate. If this alternative is selected, additional engineering evaluation will be required.

(5) Maintain the reference design storage room dimensions, the planned waste volume, the salt backfill requirement, and the reference design optimized excavation and storage plan. Revise the design criteria, as in alternative number 3, to allow crushing and breaching of the CH waste containers prior to their retrieval. Require a demonstration of the retrieval and handling of crushed and breached containers prior to the receipt of waste. This will not only demonstrate the safe retrieval of waste during the 5-year demonstration period, but also during permanent storage.

In addition to these recommended alternative modifications, the following modifications are recommended:

(6) The drifts used for storage will require maintenance and trimming to accommodate the required equipment and storage clearances. Their closure rates are not critical for storage because they will be used only for permanent storage near the end of the permanent storage period.

(7) Add additional rooms to compensate for the space occupied by the plugs in the storage area entry drifts.

(8) Install instrumentation in the storage rooms to obtain in situ data to monitor storage room behavior.

## Table I

## EVALUATION RESULTS FOR ABRIDGED DESIGN CRITERIA



| ELEMENT | RESULT AND CHAPTER REFERENCE |
|---|---|
| (1) Facility design | |
| a. Designed for an operating life of 25 years. | * |
| b. Underground facilities and equipmentshall be designed to be compatible with retrieval operations for all contact-handled (CH) and remote-handled (RH) TRU waste, with a retrieval decision to be made within 5 years after the intial emplacement of each species. | Suitable 12.3.3 |
| c. The facility will be decommissioned after it has fulfilled its intended purposes. This will include backfilling the underground facilities, sealing the shafts and decommissioning the surface facilities. | * |
| (2) CH TRU waste ** | |
| a. Estimated annual volume is 500,000 cubic feet. | * |
| b. Estimated volume at the end of the 5 year retrieval decision period is 1,410,000 cubic feet. | * |
| c. Estimated total storage capacity is 6,330,000 cubic feet. | * |
| d. Heat generated from the waste is negligible; it will be less than 10 milliwatts for average drums, less than 20 milliwatts for average boxes, and 10 watts for few drums containing heat source plutonium. | * |

* Indicates element for which evaluation is not required.
** See Foreword.

Table I (continued)

EVALUATION RESULTS FOR ABRIDGED DESIGN CRITERIA



| ELEMENT | RESULT AND CHAPTER REFERENCE |
|---|---|
| e. Estimated annual quantities are 9,616 six-packs and 2,404 modular steel boxes. | * |
| f. Estimated total quantities are 121,700 six-packs and 30,430 modular steel boxes. | * |
| g. Underground facilities and equipment shall be designed to provide for a determination to effect retrieval of waste stored for a period up to 5 years after the initial emplacement and for a target of 5 to 10 years to reach the waste and retrieve it after the decision is made. | Suitable 12.6.1 12.6.2 |
| (3) RH TRU waste ** | |
| a. Assumed total receipt of 1,000 cansisters. | * |
| b. Assumed maximum receipt rate of two canisters per day and 250 canisters per year. | * |
| c. If assumed quantities are insufficient, additional RH waste storage will be accommodated within existing storage rooms. | * |
| d. Heat generated from the waste is on the order of 60 watts per canister. | * |
| e. Access shall be available to all emplacement positions throughout the retrievability period. | Suitable 12.3.3 |

Table I (continued)

EVALUATION RESULTS FOR ABRIDGED DESIGN CRITERIA



| ELEMENT | RESULT AND CHAPTER REFERENCE |
|---|---|
| f. When both CH and RH waste are scheduled for the same room, the RH waste shall be emplaced first. After the 5 year retrievability period has terminated, CH waste may be emplaced in that room. | * |
| (4) Shaft design | |
| a. Shafts shall be designed to be structurally stable throughout the operating life of the underground facility and the decommissioning period. | Suitable<br>7.4.1<br>8.4.1<br>9.4.1 |
| b. Time-dependent closure of shafts due to salt creep shall be considered. Shafts shall be designed so that minimum dimensions required for shaft functions are maintained during design life. | Suitable<br>7.4.1<br>8.4.1<br>9.4.1 |
| c. Ground-water flow into the shafts shall be controlled so that no uncontrolled ground water reaches the storage horizon via the shafts. | Suitable<br>7.4.1<br>8.4.1<br>9.4.1 |
| (5) Shaft liner design | |
| a. Help ensure that dimensions remain within limits required for shaft functions. | * |
| b. Prevent ground-water flow into the shaft. | Suitable<br>7.4.1<br>8.4.1<br>9.4.1 |
| c. Protect wall rock from deterioration. | * |

Table I (continued)

EVALUATION RESULTS FOR ABRIDGED DESIGN CRITERIA



| ELEMENT | RESULT AND CHAPTER REFERENCE |
|---|---|
| d. Preclude risk of rock fall from shaft wall. | * |
| (6) Mine design | |
| a. The underground openings shall be designed so that deformation of excavations and pillars will remain within limits required for structural function, ventilation and safety. | Suitable<br>7.4.1<br>8.4.1<br>10.4.1 |
| b. Rock bolts shall be used where necessary to provide positive support of roof and walls. | * |
| c. Surface subsidence resulting from underground excavation shall not exceed 1 inch within a 500-foot radius of the waste shaft. | Suitable<br>6.5 |
| d. Excavations and pillars shall be located and dimensioned to avoid geologic discontinuities. If discontinuities are encountered, remedial action shall be engineered to correct the problem. | Suitable<br>3.4<br>6.3.1.2<br>6.3.3 |
| e. Design shall be based on established mining procedures. | * |
| f. Predicted behavior of the salt shall be verified by in situ testing (SPDV) before proceeding with construction of the storage area. | * |
| g. Designed to accommodate creep closure and maintain the minimum dimensions required for the operating life of the opening. | Suitable<br>10.4.1<br>12.6.1 |

Table I (continued)

EVALUATION RESULTS FOR ABRIDGED DESIGN CRITERIA



| ELEMENT | RESULT AND CHAPTER REFERENCE |
|---|---|
| h. Creep closure rates used for design shall be confirmed by instrument observations in the excavations. | Suitable 11.3.2 12.3.2 |
| i. Excavation dimensions shall include allowance for creep closure sufficient to prevent container breaching by creep-induced stresses during the retrievability period. | Suitable 12.6.1 12.6.2 |
| j. Minimize the potential for repository rock fracturing. | Suitable 11.4.1 |
| k. Underground waste storage procedures shall include a designed backfill plan for fire protection. The backfill thickness shall be 1 to 2 feet. | Suitable 12.6.1 |
| l. Permit isolation of panels of rooms with plugs after storage and backfilling are completed. | Suitable 12.6.1 |
| m. Air locks, dampers, regulators and doors shall be designed and installed in such a manner that they can accommodate creep without impairment to their ability to maintain ventilation separation. | * |
| (7) Emplacement criteria | |
| a. The underground storage rooms and access drifts shall be designed to be compatible with the waste transport vehicle, with waste container sizes, shapes, weights and stacking configurations, and with waste emplacement equipment. | Suitable 12.6.1 |

Table I (continued)

EVALUATION RESULTS FOR ABRIDGED DESIGN CRITERIA



| ELEMENT | RESULT AND CHAPTER REFERENCE |
|---|---|
| b. Provisions shall be made to accommodate backfilling over and around CH waste containers. | Suitable<br>12.6.1 |
| c. Each storage panel shall have provisions for being isolated from other panels upon completion of storage operations in that panel. | Suitable<br>12.6.1 |
| (8) Retrievability | |
| a. All wastes placed into the WIPP are retrievable, with retrievability to be demonstrated, until such time as the pilot plant is converted to an operational repository for permanent disposal of wastes. | Suitable<br>12.6.1<br>12.6.2 |
| b. Each storage room shall allow for salt creep and shall be sized to minimize breaching of the CH waste containers for a period of 10 years. | Suitable<br>12.6.1<br>12.6.2 |
| (9) Underground excavation and haulage | |
| a. Mining shall be performed with continuous miners or equivalent machine type devices. Drill and blast-type mining shall be prohibited except where authorized. | * |
| b. Underground design shall provide maximum stability for excavated rooms and entries. | Suitable<br>7.4.1<br>8.4.1<br>10.4.1<br>11.4.1<br>12.6.1 |

Table I (continued)

EVALUATION RESULTS FOR ABRIDGED DESIGN CRITERIA



| ELEMENT | RESULT AND CHAPTER REFERENCE |
|---|---|
| c. Meet or exceed the intent of the applicable requirements of the MSHA in 30 CFR 57.9 and the New Mexico Mine Safety Code for All Mines. | * |

## Table II

### EVALUATION RESULTS FOR C & SH SHAFT DESIGN BASES

| ELEMENT | RESULT AND CHAPTER REFERENCE |
|---|---|
| (1) Shaft liner | |
| a. Hydrostatic pressure is considered to start 250 feet below the ground surface and extend to the top of the key. | Suitable 7.4.1 |
| b. Water shall be prevented from flowing down the unlined shaft from behind the liner. | Suitable 7.4.1 |
| (2) Shaft key | |
| a. Key shall be designed to resist the lateral pressure from the salt. (Assumed to be 75 percent of the overburden pressure.) | Suitable 7.4.1 |
| b. Key shall be designed to resist the hydrostatic pressure from above the salt. | Suitable 7.4.1 |
| (3) Unlined section | |
| Provide 11-foot 8-inch diameter to allow for future salt creep deformation. | Suitable 7.4.1 |

Table III

EVALUATION RESULTS FOR WASTE SHAFT DESIGN BASES

| ELEMENT | RESULT AND CHAPTER REFERENCE |
|---|---|
| (1) Shaft liner | |
| Hydrostatic pressure is considered to start 250 feet below the ground surface and extend to the top of the key. | Suitable 8.4.1 |
| (2) Shaft key | |
| Design lateral pressure shall be 50 percent of the vertical pressure due to soil, rock and salt overburden. | Suitable 8.4.1 |
| (3) Unlined section | |
| Provide 20-foot diameter to allow for future salt creep deformation. | Suitable 8.4.1 |

## Table IV

### EVALUATION RESULTS FOR EXHAUST SHAFT DESIGN BASES

| ELEMENT | RESULT AND CHAPTER REFERENCE |
|---|---|
| (1) Shaft liner | |
| Hydrostatic pressure is considered to start 250 feet below the ground surface and extend to the top of the key. | Suitable 9.4.1 |
| (2) Shaft key | |
| Design lateral pressure shall be 50 percent of the vertical pressure due to soil, rock and salt overburden. | Suitable 9.4.1 |
| (3) Unlined section | |
| Provide 15-foot diameter to allow for future salt creep deformation. | Suitable 9.4.1 |

## Table V

## EVALUATION RESULTS FOR STORAGE AREA DESIGN BASES

| ELEMENT | RESULT AND CHAPTER REFERENCE |
|---|---|
| (1) Operational requirements | |
| a. The storage area rooms, drifts and crosscuts shall be designed to allow for retrieval of all CH and RH waste stored for a period of up to 5 years after the initial emplacement of each waste species. | Suitable<br>12.6.1<br>12.6.2 |
| b. Excavation dimensions in the waste storage area shall be to a uniform height of 13 feet. | Suitable<br>12.6.1<br>12.6.2 |
| (2) Essential features | |
| Provide 1 foot vertical and 9 inches horizontal allowance for creep closure to maintain the minimum design dimensions up to 5 years after initial emplacement. | Suitable<br>12.6.1<br>12.6.2 |
| (3) Safety design requirements | |
| A minimum opening of 16 inches shall be left at the top of the rooms and drifts for air passage above the waste and backfill. | Suitable<br>12.6.1<br>12.6.2 |

## Table VI

### EVALUATION RESULTS FOR DESIGN CONFIGURATIONS



| ELEMENT | RESULT AND CHAPTER REFERENCE |
|---|---|
| (1) C & SH shaft | |
| a. Provide 5/8 to 1 1/2-inch thick and 10-foot I.D. stiffened steel liner in upper 846 feet. | Suitable<br>7.3.2.1<br>7.3.3.1 |
| b. Provide 30-inch thick, 10-foot I.D. and 39-foot long concrete key at rock/salt interface. | Suitable<br>7.3.2.2<br>7.3.3.2 |
| c. Provide 11-foot 10-inch diameter unlined shaft below the key. | Suitable<br>7.3.2.3<br>7.3.3.3 |
| d. Provide 17-foot high and 32-foot wide station. | Suitable<br>7.3.2.4<br>7.3.3.4 |
| (2) Waste shaft | |
| a. Provide 10 to 20-inch thick and 19-foot I.D. concrete liner in upper 837 feet. | Suitable<br>8.3.2.1<br>8.3.3.1 |
| b. Provide 51-inch thick, 19-foot I.D. and 63-foot long concrete key at rock/salt interface. | Suitable<br>8.3.2.2<br>8.3.3.2 |
| c. Provide 20-foot diameter unlined shaft below the key. | Suitable<br>8.3.2.3<br>8.3.3.3 |
| d. Provide 17-foot high and 30-foot wide station. | Suitable<br>8.3.2.4<br>8.3.3.4 |
| (3) Exhaust shaft | |
| a. Provide 10 to 16-inch thick and 14-foot I.D. concrete liner in upper 844 feet. | Suitable<br>9.3.2.1<br>9.3.3.1 |

Table VI (continued)

EVALUATION RESULTS FOR DESIGN CONFIGURATIONS



| ELEMENT | RESULT AND CHAPTER REFERENCE |
|---|---|
| b. Provide 42-inch thick, 14-foot I.D. and 63-foot long concrete key at rock/salt interface. | Suitable<br>9.3.2.2<br>9.3.3.2 |
| c. Provide 15-foot diameter unlined shaft below the key. | Suitable<br>9.3.2.3<br>9.3.3.3 |
| (4) Storage area | |
| a. Provide 13-foot high and 25-foot wide or smaller drifts. | Suitable<br>12.6.1<br>12.6.2 |
| b. Provide 13-foot high and 33-foot wide storage rooms. | Suitable<br>12.6.1<br>12.6.2 |

THIS PAGE LEFT BLANK INTENTIONALLY

# CHAPTER 1

# INTRODUCTION

## 1.1 PURPOSE

This report presents the results of validation of the underground opening reference design for the Waste Isolation Pilot Plant (WIPP). The basis for the report is defined in the Design Validation Plan (ref. 1-1) which, in part, includes certain data requirements defined in the Stipulated Agreement (ref. 1-2) reached between the U.S. Department of Energy (DOE) and the State of New Mexico on July 1, 1981.

Design validation of the WIPP is defined as the process by which the reference design of the underground openings is confirmed by determining the compatibility of the design criteria, design bases and reference design configurations using site specific information. The design validation process consists of an assessment of the condition and behavior of shafts, drifts and a full-sized, four-room test panel excavated during an initial stage known as the Site and Preliminary Design Validation (SPDV) Program and during full WIPP construction. Based on this assessment of these excavations, and on predictions of their future behavior, any modifications to the design criteria, design bases or design configurations required to achieve a validated reference design will be developed. In addition, the validated reference design may be modified in the future as still more data and experience are gained during a 5-year demonstration period (period during which all waste must be retrievable) and permanent storage operations.

In fulfilling the data requirements for design validation, this report provides documentation of actual underground conditions encountered as they relate to the design criteria, design bases and design configurations for the reference design of the underground openings. The contents of this report include all relevant data and field observations acquired for design validation. The underground openings excavated to date provide a firm basis for evaluation of the current and expected future behavior of the underground development.

The purpose of design validation is to:

- o validate the underground reference design, thus providing confidence in the safety and stability of the WIPP underground openings;

- o confirm the suitability of the design criteria, design bases and design configurations established specifically for the reference design of the underground openings;

- o re-confirm and expand upon the conclusions of the SPDV Program; and

- o comply with the DOE agreement with the State of New Mexico to validate the reference design of the WIPP underground openings.

This process was initially described in the WIPP Preliminary Design Validation Report (ref. 1-3) issued in March 1983. That report presented the results of a preliminary evaluation of the underground opening reference design based on activities conducted during the SPDV phase of underground development. That initial report was prepared in response to conditions contained in the Stipulated Agreement (Appendix A) between the DOE and the State of New Mexico which permitted a preliminary evaluation of design considerations at an early stage in underground development and allowed for any reference design modifications deemed necessary for full WIPP construction. The WIPP Design Validation Final Report (this report) is an extension of the preliminary report and presents further confirmation of the reference design based on additional data collected since completion of the SPDV Program in both old and new areas of underground excavation.

The WIPP Design Validation Final Report presents:

- o a summary of the background and development of the WIPP reference design;

- the design criteria and design bases used to develop the reference design for the underground openings;

- geologic characterizations of the shafts, drifts and test rooms;

- the methodology used for data collection, its analysis and evaluation, and the predictions of future behavior of the underground openings;

- the description of data collection activities in the shafts, drifts and test rooms;

- analyses and evaluations of the geologic behavior of the rock strata surrounding the shafts, drifts and test rooms based on visual inspections and geomechanical instrumentation measurements;

- predictions of expected future conditions of the underground openings based on model simulations using in situ data;

- an assessment of the suitability of the design criteria and design bases and validation of the reference design configurations, with recommendations for design modifications, if any;

- recommendations for operation and maintenance of the underground facility as they pertain to design validation; and

- all data and reference sources that support design validation.

## 1.2 SCOPE

Design validation of the WIPP underground openings has been accomplished through an assessment of their safety, stability and predicted future behavior. Observation and instrumentation data consistent with the Design Validation Plan objectives have been

collected and evaluated for each of the major design elements: shafts, drifts and test rooms.

Initial analyses and evaluations of the underground data obtained for design validation were provided in the WIPP Preliminary Design Validation Report. The WIPP Design Validation Final Report presents the results of activities whose objectives are outlined in the Design Validation Plan. These activities included field data collection and analyses of these data to determine the validity of the reference design.

Basically, four types of information were gathered for design validation. These are:

(1) observations of the behavior of the underground openings;

(2) descriptions of the geologic conditions encountered during underground construction;

(3) descriptions of core samples from instrumentation and other holes in the roof and floor of the underground openings; and

(4) data from installed geomechanical instrumentation.

Field tasks performed to gather this information included the following:

- establishment of survey control for underground excavations and reference points for geologic mapping;
- development of procedures and standards for activities such as geologic mapping/logging of underground excavations;
- geologic mapping in the shafts and horizontal openings;

- examination and logging of rock cores from boreholes to obtain geologic information;

- observation and measurement of ground-water flow into the shafts;

- measurement of hydrostatic and lateral pressures on the shaft liner and shaft key;

- monitoring the floor height of horizontal openings above the top of marker bed 139 (MB-139) and the height of clay seams above the roofs using core hole data;

- measurement of closure in the shafts and horizontal openings;

- determination of the presence of gases and fluids;

- survey of shaft verticality; and

- examination of all surfaces of underground openings for displacement of clay seams, fracturing, roof sagging, floor heaving, or other occurrences that may indicate unstable conditions.

## 1.3 HISTORICAL BACKGROUND

The WIPP is being developed by the DOE as a research and development (R & D) facility to demonstrate the safe disposal of radioactive waste from U.S. defense programs. The facility is located in southeastern New Mexico, about 25 miles east of the city of Carlsbad (Figure 1-1). The underground development level is at a depth of approximately 2,150 feet in thick deposits of bedded salt. The facility will include space for the permanent storage of defense related transuranic (TRU) waste and for in situ experiments addressing technical issues for high-level defense waste programs. The WIPP's phased design and construction resulted in initial confirmation of the underground opening reference design through the SPDV Program. Design

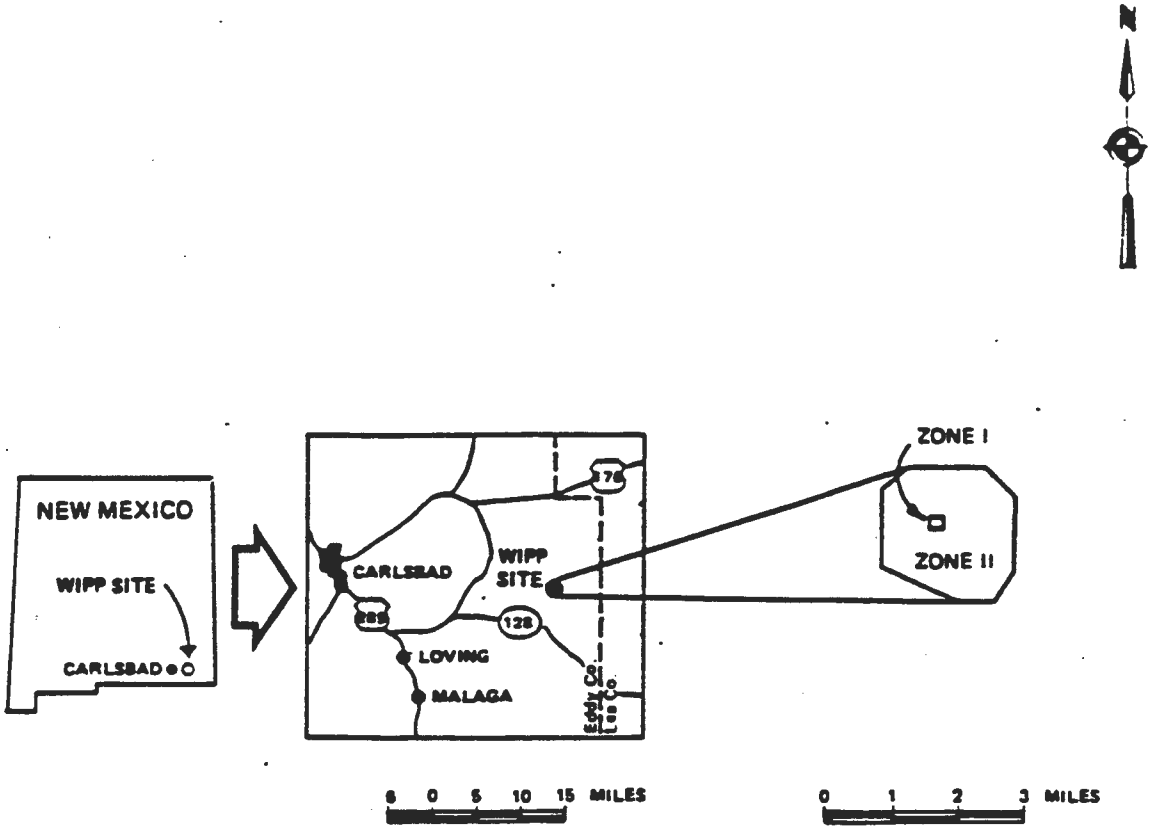


**ZONE DESCRIPTION**

ZONE I Surface Facilities Area
ZONE II Underground Storage Limits

Figure 1-1

LOCATION OF THE WIPP

validation will provide confirmation of the decision to continue facility construction with subsequent in situ experiments and defense TRU waste storage.

The WIPP project is the result of waste management program efforts that were started by the U.S. government as long ago as 1955 when the U.S. Atomic Energy Commission (AEC) requested that the National Academy of Sciences (NAS) evaluate methods for disposing of radioactive waste in geologic formations. The NAS recommended bedded salt as the geologic formation providing the highest confidence for long-term isolation of waste from the biosphere. As a result of these efforts, the DOE (formerly the AEC) initiated the WIPP program in 1975. The major accomplishments of the program are listed in Table 1-1.

Assessments that pertain to design of the WIPP include extensive analyses of the impact of the facility on present and future environments. A Final Environmental Impact Statement (FEIS) (ref. 1-4) was prepared which provides information about the environmental and safety consequences of the WIPP project. A Safety Analysis Report (SAR) (ref. 1-5) was also prepared to support construction and operation of the WIPP. The SAR addresses all aspects of industrial and nuclear safety of the project and is updated periodically.

The WIPP is being developed in phases. At the time this report was prepared, most of the site characterization, design and supporting technological development had been done. The engineering design of the underground openings began with a conceptual design followed by a preliminary design and finally a detailed reference design. Facility development at the site began with the SPDV Program which allowed direct observation of the underground facility geology through two shafts and associated underground drifts. This program provided data for preliminary evaluation and confirmation of the reference design of the proposed underground excavations. Design and construction of the surface facilities have proceeded virtually independent of the underground opening design validation and are not addressed in this report.

Table 1-1

MAJOR ACCOMPLISHMENTS OF THE WIPP PROGRAM

| ITEM | DATE STARTED | DATE COMPLETED |
|---|---|---|
| (1) National Academy of Sciences recommends salt as best geologic formation for disposal of nuclear waste. | - | 1957 |
| (2) Salt deposit studies conducted in New Mexico by U.S. Geological Survey and Sandia National Laboratories. | 1972 | 1975 |
| (3) Conceptual design of the WIPP. | 1975 | 1977 |
| (4) Characterization of the WIPP site. | 1975 | 1983 |
| (5) Public law authorizes capital funding for the WIPP. | - | 1977 |
| (6) Title I - Preliminary design of the WIPP. | 1/78 | 1/80 |
| (7) Safety Analysis Report issued for the WIPP. | - | 2/80 |
| (8) Final Environmental Impact Statement issued for the WIPP. | - | 10/80 |
| (9) SPDV Preliminary Design Validation Program. | 7/79 | 3/83 |
| (10) Detailed design for Site and Preliminary Design Validation (SPDV). | 7/79 | 10/80 |
| (11) SPDV Site Validation Experiments Program. | 8/80 | 3/83 |
| (12) Title II - Detailed design of the WIPP. | 2/81 | 2/84 |
| (13) Construction of SPDV shafts. | 5/81 | 3/82 |
| (14) Design validation. | 4/81 | 10/86 |
| (15) SPDV shaft outfitting and test room development. | 10/81 | 7/83 |
| (16) Authorization for full WIPP construction. | - | 7/83 |

## 1.4 THE WIPP MISSION

The authorized mission for the WIPP emphasizes its role as an R & D facility to demonstrate safe disposal of radioactive waste from U.S. defense programs. Its mission is also to provide information from site characterization, laboratory experiments, geomechanical instrumentation and in situ tests which can be used to develop performance-assessment models for technological applications. Figure 1-2 shows the underground layout of the three R & D areas at the WIPP.

The WIPP R & D Program consists of three major program areas:

(1) site characterization and evaluation;

(2) repository development and operation; and

(3) waste package interactions.

In addition to providing for the permanent storage of defense related TRU waste, these program areas include technology development in waste isolation, in situ tests without radioactive material, and in situ tests with radioactive material. The WIPP will also serve as a laboratory for experiments with high-level defense waste. All high-level wastes will be removed from the WIPP at the conclusion of the testing period. These in situ waste experiments and associated activities are not part of design validation and, therefore, are not discussed in this report. An initial description of the in situ testing plan for the WIPP R & D Program was provided in Sandia National Laboratories' (SNL) Report 2628 (ref. 1-6).

## 1.5 DESIGN VALIDATION PROGRAM

Validation of the WIPP facility underground reference design is based on a strategy consisting of a detailed plan and approach for validating major reference design elements. A description of this strategy is

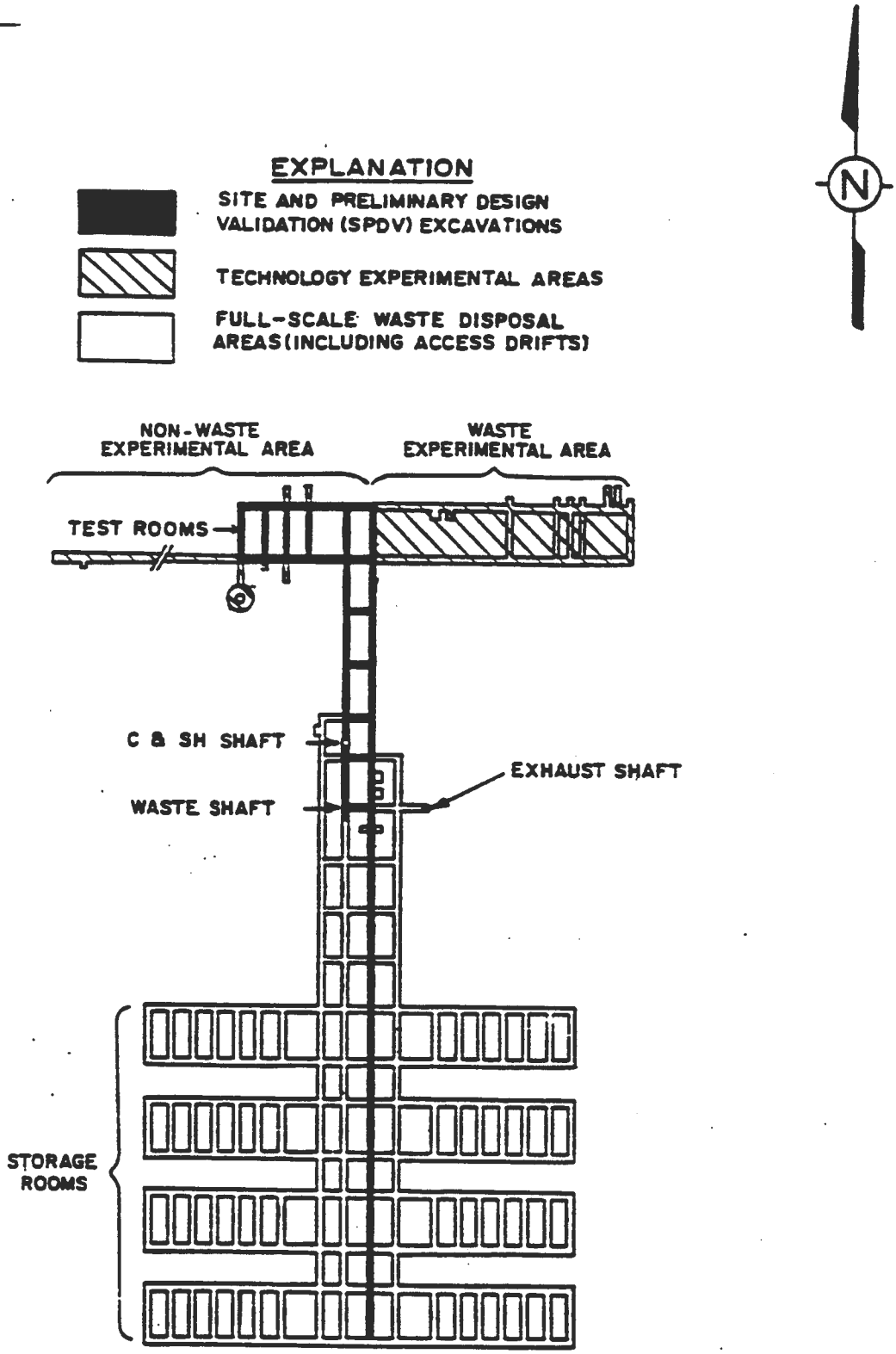


Figure 1-2

PLAN VIEW OF UNDERGROUND FACILITY

contained in the document titled Design Validation Strategy (ref. 1-7). The elements comprising the strategy for design validation are:

(1) Identify the design approaches and construction activities for the underground openings.

(2) Identify the design criteria, design bases and design configurations to be validated.

(3) Develop the methodology for validation.

(4) Acquire data on the underground development level from core samples, geologic mapping, laboratory tests, in situ tests, visual observations and mines in similar geologic formations.

(5) Synthesize the data obtained from the activities in element 4 to define the geologic environment of the facility level.

(6) Evaluate in situ geomechanical instrument measurements and visual observations to determine the response of the geologic materials to changes resulting from excavation or other disturbances.

(7) Predict the future behavior of the underground openings and salt surrounding the openings based on current in situ measurements, visual observations and computational analyses.

(8) Provide for comparisons of predicted and existing conditions at regular time intervals.

(9) Document design validation results and conclusions.

(10) Provide recommended design modifications as required.

(11) Provide data and reference sources to support the performance of the above activities.

Design validation efforts for the WIPP began with the SPDV Program. This program involved the excavation of underground openings, shafts, drifts and test rooms, representative of the full WIPP facility. These underground openings permitted the direct examination of geologic features and material behavior at the facility level. Additional observations and geomechanical instrumentation measurements were obtained following completion of the SPDV Program to complete the design validation program. A brief description of the design validation program is presented in the following subsections.

### 1.5.1 Site and Preliminary Design Validation (SPDV)

The SPDV Program was designed to further characterize and validate the WIPP site geology and provide preliminary validation of the underground opening reference design. The SPDV Program was composed of two integrated parts:

(1) site validation (ref. 1-8) to increase confidence in the process of site characterization and qualification; and

(2) preliminary design validation to assess the condition and behavior of excavated shafts, drifts and a full-sized, four-room test panel similar to those planned for the waste storage area.

The general SPDV underground layout is shown on Figure 1-3. The underground development level is located in Zone II, a WIPP site control zone that delineates the limits of underground storage. A preliminary design validation report was issued on March 30, 1983. This report presented the results of early observations and analyses of the condition and behavior of the SPDV excavations and is discussed in Chapter 4.

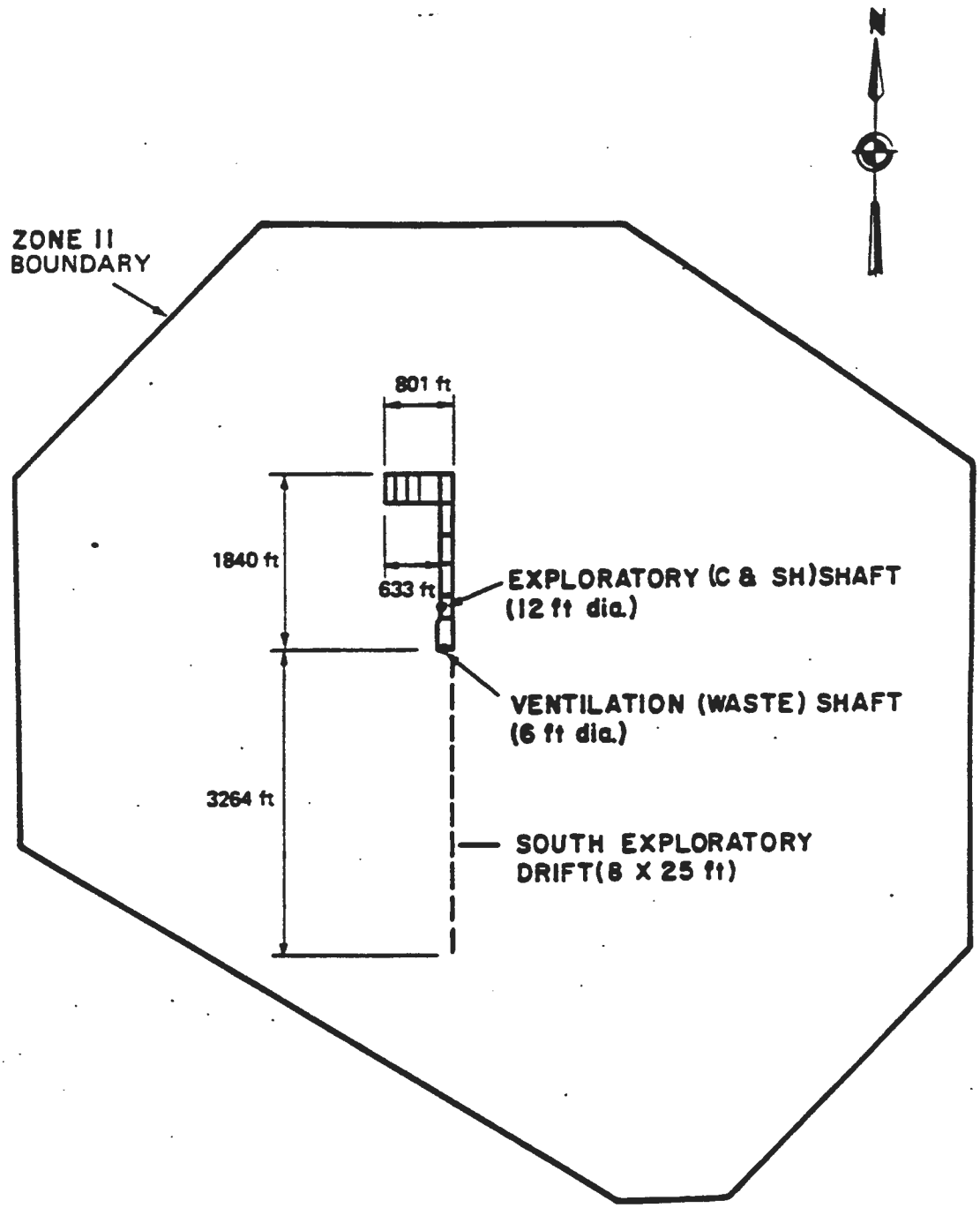


Figure 1-3

THE SPDV UNDERGROUND LAYOUT

### 1.5.2 Design Validation

Major activities related to design validation are cited in Table 1-2. As indicated by this table, field data collection activities that began with the SPDV Program were continued beyond the end of the program to provide additional data for design validation. The design validation process includes the evaluation and analysis of data obtained by these activities. The results of these evaluations and analyses have been presented in quarterly geotechnical field data reports (GFDR), each of which presents a discussion of different selected elements of the WIPP underground development. These reports provide supporting documentation for the WIPP Design Validation Final Report and are discussed in Chapter 4.

Some of the field data collection activities shown in Table 1-2 will continue after submittal of the WIPP Design Validation Final Report and beyond the completion of full WIPP construction. Collection of this data will provide additional information on the behavior of the underground openings through the 5-year demonstration period and through permanent storage operations. The data will also permit continuous monitoring of the safety of the openings. Underground facility reference design modifications will be made as required by an evaluation and analysis of these data. The data obtained will be periodically distributed to the project participants, the State of New Mexico, and will be placed in WIPP public reading rooms.

Table 1-2

DESIGN VALIDATION ACTIVITY SCHEDULE

| ACTIVITY | RESPONSIBILITY | SCHEDULE |
|---|---|---|
| (1) Prepare and issue Design Validation Plan | B/DOE | 7/82 - 1/83 |
| (2) Field data collection: | | |
| a. Geologic mapping of vertical and horizontal underground excavations | TSC/B | 3/82 - 3/83 |
| b. Geomechanical instrumentation measurements and visual observations in shafts, drifts, and test rooms | TSC/B | 4/82 - 3/83 |
| c. Log core from holes in horizontal underground openings | TSC/B | 10/82 - 3/83 |
| d. Fluid inflow measurements | TSC/B | 9/81 - 3/83 |
| e. Shaft verticality surveys | DOE/TSC | 1/82 - 3/83 |
| (3) Evaluate field data; prepare Preliminary Design Validation Report | B | 10/82 - 3/83 |
| (4) Issue Preliminary Design Validation Report | DOE | 3/83 |
| (5) Continue with (2a), (2b), (2c), and (2d) above | TSC/B | 3/83 - 7/86 |
| (6) Evaluate/analyze field data; prepare Design Validation Final Report | B | 3/83 - 5/86 |
| (7) Design Validation Final Report review by Peer Review Panel | B | 5/86 - 6/86 |
| (8) Issue Design Validation Final Report | DOE | 10/86 |

B = Bechtel National, Inc.; DOE = U.S. Department of Energy; TSC = Technical Support Contractor (Westinghouse Electric Corp.)

THIS PAGE LEFT BLANK INTENTIONALLY

# CHAPTER 2

## BACKGROUND OF UNDERGROUND DESIGN

### 2.1 SITE CHARACTERIZATION AND EVALUATION

WIPP site characterization programs have consisted of geologic and hydrologic studies as well as biologic, meteorologic and economic studies. Geologic and geohydrologic characterization of the site, which started with surveys of literature and existing data, continued with the collection of new data and had the greatest degree of influence on design of the underground facility. Special emphasis was placed on correlating data obtained by geophysical techniques and borehole drilling. The geophysical techniques most widely used were seismic reflection and resistivity. Borehole drilling programs included holes drilled primarily for stratigraphic information on or near the site and holes drilled at the edge of, or away from, the site to study salt dissolution. Three holes, WIPP-11, WIPP-12 and DOE-1, were drilled through the Salado formation to acquire geologic data on deeper strata outside the Zone II boundaries of the site (refs. 2-1, 2-2 and 2-3). Within Zone II, the drilling of deep exploratory holes, i.e., to the depth of the WIPP facility level, was restricted by siting criteria. Prior to the drilling of the SPDV exploratory and ventilation shafts (subsequently known as the C & SH and waste shafts, respectively), ERDA-9 was the only borehole within Zone II that extended below the facility level.

The generalized stratigraphic relationship of the geologic formations of interest beneath the WIPP site is shown on Figure 2-1. Siltstone and fine-grained sandstone are the main rock types forming the Dewey Lake red beds. The Rustler formation, composed primarily of anhydrite and fine-grained sandstone, siltstone and mudstone, contains two water-bearing dolomite beds. Saline water is found in these beds, the Magenta and Culebra members, and at the contact between the Rustler and Salado formations. The Salado formation consists largely of halite containing thin beds of anhydrite and polyhalite with occassional thin clay seams. The Castile is a thick anhydrite and halite formation

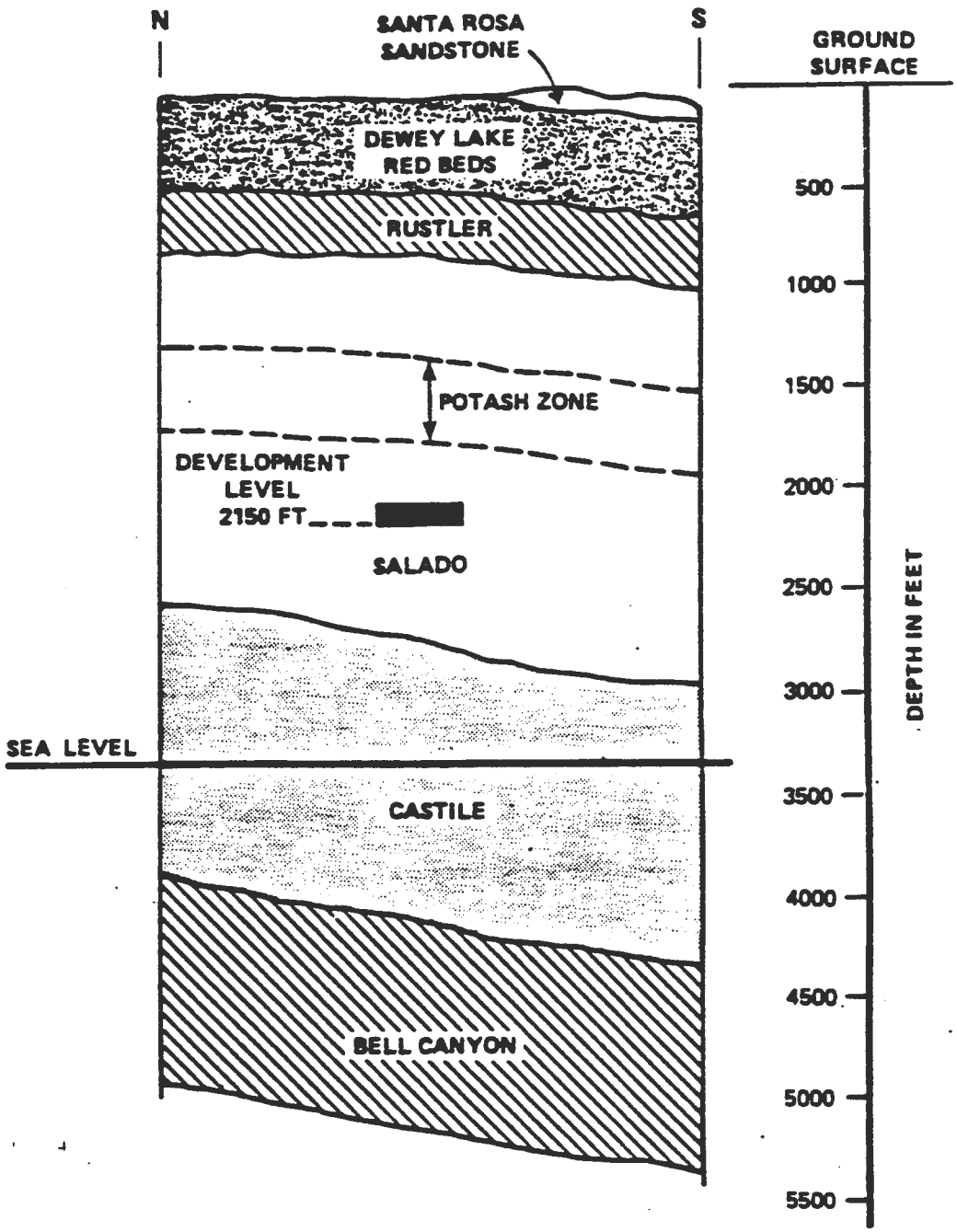


Figure 2-1

GENERAL SITE STRATIGRAPHY

underlying the Salado. The Bell Canyon formation consists primarily of sandstone, limestone and shale. No aquifers are present in the Salado or Castile formations beneath the site.

Site stratigraphy from the ground surface to about 250 feet below the underground facility level is presented in Appendix B, Figure B-1, Sheets 1 through 5. The stratigraphy shown is based on geologic data obtained from boreholes WIPP-12, ERDA-9 and DOE-1, and from the C & SH and waste shafts. An analysis of these data shows a strong correlation of the stratigraphy between the boreholes and shafts from the ground surface to below the underground facility level. This correlation is based primarily on the geophysical logs because core sample logging or "hands-on" mapping was not always carried out through the entire interval. Where possible, graphic lithologic descriptions based on logging or mapping of the rock strata have been included on Figure B-1 in Appendix B. This helps to more fully define the stratigraphic relationships shown by the geophysical logs.

The analysis between boreholes WIPP-12 to the north and DOE-1 to the south resulted in correlation of the major formation contacts and most marker beds in the Salado formation. Due to a lack of distinctive stratigraphic changes, the Dewey Lake red beds exhibit a relatively uniform profile in both the lithologic and geophysical logs. The Rustler formation, however, exhibits a much greater fluctuation in its geophysical profile as a result of the anhydrite, dolomite and fine-grained clastic beds it contains. Figure B-1 in Appendix B shows that the Rustler thickens slightly to the north with a slight rise in formation contacts occurring in the area of the WIPP facility.

Correlation of the Salado formation stratigraphy between WIPP-12 and DOE-1 verifies the consistency of most of the marker beds. The geophysical logs shows distinct breaks where polyhalite and anhydrite beds occur in the largely halitic rock strata. The major stratigraphic occurrence, in that portion of the Salado formation shown on Figure B-1 in Appendix B, is a thinning of strata to the north. This thinning

becomes apparent below marker bed 124 (MB-124) and is relatively well pronounced in the underground facility horizon. The effect of this thinning is to produce a reversal in the direction of dip of the strata above and below MB-124 between WIPP-12 and DOE-1. Above this marker bed the strata dip to the north, while below the marker bed the strata dip to the south. This thinning of strata controls the slope of the facility level excavation because the excavation must avoid encroachment on any stratigraphic horizons that could affect the stability or safety of the underground openings.

The figures in Appendix B show the continuity of rock strata across the WIPP site and in the area of underground excavation. These figures are intended to show that the major design assumptions which were made based on data from boreholes ERDA-9 and WIPP-12 remain valid, based on additional data obtained from geologic mapping of the underground openings and logging of underground core holes. Therefore, correlation of the site stratigraphy from the ground surface to below the underground facility level confirms the macroscopic continuity of stratigraphy beneath the WIPP site. Geologic characterization at the WIPP underground facility level is presented in Chapter 6.

Geohydrologic data pertaining to the site were obtained from conventional and special-purpose tests in many boreholes (ref. 1-5). Geophysical logging of these holes provided hydrogeologic information on the rock strata encountered. Pressure measurements, fluid samples and ranges of rock permeability were obtained for selected formations. Also, potentiometric surfaces of major aquifer systems were contoured by using measured water level elevations in boreholes.

Evaluation of data obtained from early site selection studies indicated that the current WIPP site was a suitable candidate for the establishment of a facility to demonstrate the safe disposal of radioactive waste. Additional studies have resulted in the issuance of numerous reports regarding the suitability of the WIPP site, including the Geological Characterization Report, Waste Isolation Pilot Plant

(WIPP) Site, Southeastern New Mexico (ref. 2-4), Final Environmental Impact Statement: Waste Isolation Pilot Plant (ref. 1-4), and the Waste Isolation Pilot Plant Safety Analysis Report (ref. 1-5). Final site validation was achieved in 1983 by an evaluation of the data contained in a report titled Results of Site Validation Experiments, Waste Isolation Pilot Plant (WIPP) Project, Southeastern New Mexico (ref. 2-5) which presented the results of studies performed to fully satisfy all site qualification criteria. This report was followed by a confirmation of overall site suitability in a report titled Summary Evaluation of the Waste Isolation Pilot Plant (WIPP) Site Suitability (ref. 2-6).

## 2.2 DESIGN CRITERIA

The Design Criteria, Waste Isolation Pilot Plant (WIPP), Site and Preliminary Design Validation (SPDV) (ref. 2-7), and the Design Criteria, Waste Isolation Pilot Plant (WIPP), Revised Mission Concept-IIA (RMC-IIA) (ref. 2-8) were used as guides by the Architect-Engineer (Bechtel National, Inc.) in developing the reference design for the WIPP underground openings. The documents contain general requirements which were addressed in the reference design. The Design Criteria, RMC-IIA, is the highest level design document for the project. All other design documents, such as design bases, drawings and specifications, were required to be in compliance with this document.

The design criteria also stipulate the type and estimated or assumed rate of waste to be received at the WIPP. The majority of the criteria presented in the RMC-IIA document are requirements which do not need evaluation as to their suitability and have no impact on validation considerations for the underground opening reference design. The major criteria that governed development of the reference design are presented in Table 2-1. Although some of the criteria in this table are elements which cannot be evaluated, they are included because of their influence on the reference design configurations. Those criteria that can be evaluated are discussed in later chapters of this report as

## Table 2-1

## ABRIDGED WIPP DESIGN CRITERIA



(1) Facility design

a. Designed for an operating life of 25 years.

b. Underground facilities and equipment shall be designed to be compatible with retrieval operations for all contact-handled (CH) and remote-handled (RH) TRU waste, with a retrieval decision to be made within 5 years after the initial emplacement of each species. (Chapter 12)

c. The facility will be decommissioned after it has fulfilled its intended purposes. This will include backfilling the underground facilities, sealing the shafts and decommissioning the surface facilities.

(2) CH TRU waste *

a. Estimated annual volume is 500,000 cubic feet.

b. Estimated volume at the end of the 5 year retrieval decision period is 1,410,000 cubic feet.

c. Estimated total storage capacity is 6,330,000 cubic feet.

d. Heat generated from the waste is negligible; it will be less than 10 milliwatts for average drums, less than 20 milliwatts for average boxes, and 10 watts for few drums containing heat source plutonium.

e. Estimated annual quantities are 9,616 six-packs and 2,404 modular steel boxes.

f. Estimated total quantities are 121,700 six-packs and 30,430 modular steel boxes.

g. Underground facilities and equipment shall be designed to provide for a determination to effect retrieval of waste stored for a period up to 5 years after the initial emplacement and for a target of 5 to 10 years to reach the waste and retrieve it after the decision is made. (Chapter 12)

(3) RH TRU waste *

a. Assumed total receipt of 1,000 canisters.

b. Assumed maximum receipt rate of two canisters per day and 250 canisters per year.

* See Foreword.

c. If assumed quantities are insufficient, additional RH waste storage will be accommodated within existing storage rooms.

d. Heat generated from the waste is on the order of 60 watts per canister.

e. Access shall be available to all emplacement positions throughout the retrievability period. (Chapter 12)

f. When both CH and RH waste are scheduled for the same room, the RH waste shall be emplaced first. After the 5 year retrievability period has terminated, CH waste may be emplaced in that room.

(4) Shaft design (Chapters 7, 8 and 9)

a. Shafts shall be designed to be structurally stable throughout the operating life of the underground facility and the decommissioning period.

b. Time-dependent closure of shafts due to salt creep shall be considered. Shafts shall be designed so that minimum dimensions required for shaft functions are maintained during design life.

c. Ground-water flow into the shafts shall be controlled so that no uncontrolled ground water reaches the storage horizon via the shafts.

(5) Shaft liner design

a. Help ensure that dimensions remain within limits required for shaft functions.

b. Prevent ground-water flow into the shaft. (Chapters 7, 8 and 9)

c. Protect wall rock from deterioration.

d. Preclude risk of rock fall from shaft wall.

(6) Mine design

a. The underground openings shall be designed so that deformation of excavations and pillars will remain within limits required for structural function, ventilation and safety. (Chapters 7, 8 and 10)

b. Rock bolts shall be used where necessary to provide positive support of roofs and walls.

c. Surface subsidence resulting from underground excavation shall not exceed 1 inch within a 500-foot radius of the waste shaft. (Chapter 6)

d. Excavations and pillars shall be located and dimensioned to avoid geologic discontinuities. If discontinuities are encountered, remedial action shall be engineered to correct the problem. (Chapters 3 and 6)

e. Design shall be based on established mining procedures.

f. Predicted behavior of the salt shall be verified by in situ testing (SPDV) before proceeding with construction of the storage area.

g. Designed to accommodate creep closure and maintain the minimum dimensions required for the operating life of the opening. (Chapters 10 and 12)

h. Creep closure rates used for design shall be confirmed by instrument observations in the excavations. (Chapters 11 and 12)

i. Excavation dimensions shall include allowance for creep closure sufficient to prevent container breaching by creep-induced stresses during the retrievability period. (Chapter 12)

j. Minimize the potential for repository rock fracturing. (Chapter 11)

k. Underground waste storage procedures shall include a designed backfill plan for fire protection. The backfill thickness shall be 1 to 2 feet. (Chapter 12)

l. Permit isolation of panels of rooms with plugs after storage and backfilling are completed. (Chapter 12)

m. Air locks, dampers, regulators and doors shall be designed and installed in such a manner that they can accommodate creep without impairment to their ability to maintain ventilation separation.

(7) Emplacement criteria

a. The underground storage rooms and access drifts shall be designed to be compatible with the waste transport vehicle, with waste container sizes, shapes, weights and stacking configurations, and with waste emplacement equipment. (Chapter 12)

b. Provisions shall be made to accommodate backfilling over and around CH waste containers. (Chapter 12)

c. Each storage panel shall have provisions for being isolated from other panels upon completion of storage operations in that panel. (Chapter 12)

(8) Retrievability

a. All wastes placed into the WIPP are retrievable, with retrievability to be demonstrated, until such time as the pilot plant is converted to an operational repository for permanent disposal of wastes. (Chapter 12)

b. Each storage room shall allow for salt creep and shall be sized to minimize breaching of the CH waste containers for a period of 10 years. (Chapter 12)

(9) Underground excavation and haulage

a. Mining shall be performed with continuous miners or equivalent machine type devices. Drill and blast-type mining shall be prohibited except where authorized.

b. Underground design shall provide maximum stability for excavated rooms and entries. (Chapters 7, 8, 10, 11 and 12)

c. Meet or exceed the intent of the applicable requirements of the MSHA in 30 CFR 57.9 and the New Mexico Mine Safety Code for All Mines.

indicated in the table.

## 2.3 DESIGN BASES

The design bases identify the detailed design requirements for the WIPP underground facilities. They are derived from the more general concepts presented in the design criteria. The design bases cover all aspects of the design and facility operations. Design bases applicable to design validation are listed in references 2-9 through 2-20. The essential elements of the design bases pertaining to design validation of the C & SH shaft, waste shaft, exhaust shaft, drifts and storage area are discussed in Chapters 7 through 10 and Chapter 12. The discussions cover only those bases that require evaluation. All other bases are requirements determined during design reviews and need not be evaluated for their suitability.

## 2.4 DESIGN CONFIGURATIONS

The reference design configurations are the engineered facilities designed to comply with the design criteria and design bases. They are described in various contract drawings and specifications. The essential elements of the design configurations are discussed in Chapters 3 and 12.

## 2.5 DESIGN DEVELOPMENT

Design of the WIPP surface and underground facilities consisted of three stages:

(1) the conceptual design;

(2) the preliminary design; and

(3) the detailed design, including the underground opening reference design.

At both the conceptual and preliminary design stages, an extensive, independent review of the underground layout and design was made by the

DOE and its consultants, SNL and Westinghouse Electric Corporation. The review included assessment of the underground design concept and consultation with Carlsbad area potash mine operators to obtain information from their experience. The preliminary design was also reviewed by other Federal agencies, the State of New Mexico and the NAS.

From these reviews and consultations, the DOE concluded that the detailed design, based on the current state of the art, was sound. However, for further confirmation, it was decided that the impact of site-specific geologic conditions on the underground opening reference design should be verified by direct observation. Consequently, the DOE initiated the SPDV Program described in Chapter 1. The SPDV Program provided in situ data on the local geology and on the geomechanical response of the strata to the underground openings.

### 2.5.1 Conceptual Design

Design of the WIPP surface and underground facilities began with the conceptual design, initiated in 1975 and completed in 1977 (ref. 2-21). The conceptual design provided the basis for development of the preliminary design of both the surface and underground facilities.

### 2.5.2 Preliminary Design

The WIPP preliminary design was begun in 1978 and completed in 1980 (ref. 2-22). The preliminary design (Figure 2-2) was based on empirical methods and local mining practices, incorporating the conventional room and pillar method for underground development. It included analytical evaluations of underground openings in bedded salt using the finite element method and laboratory test data (refs. 2-23 and 2-24). The roof and floor of the rooms and entries were checked for stability by methods described in the SME Mining Engineering Handbook (ref. 2-25). In addition to Bechtel, SNL performed confirming numerical analyses (refs. 2-26 and 2-27). These analyses predicted short- and long-term stress distributions around the selected openings as well as elastic and creep deformations.

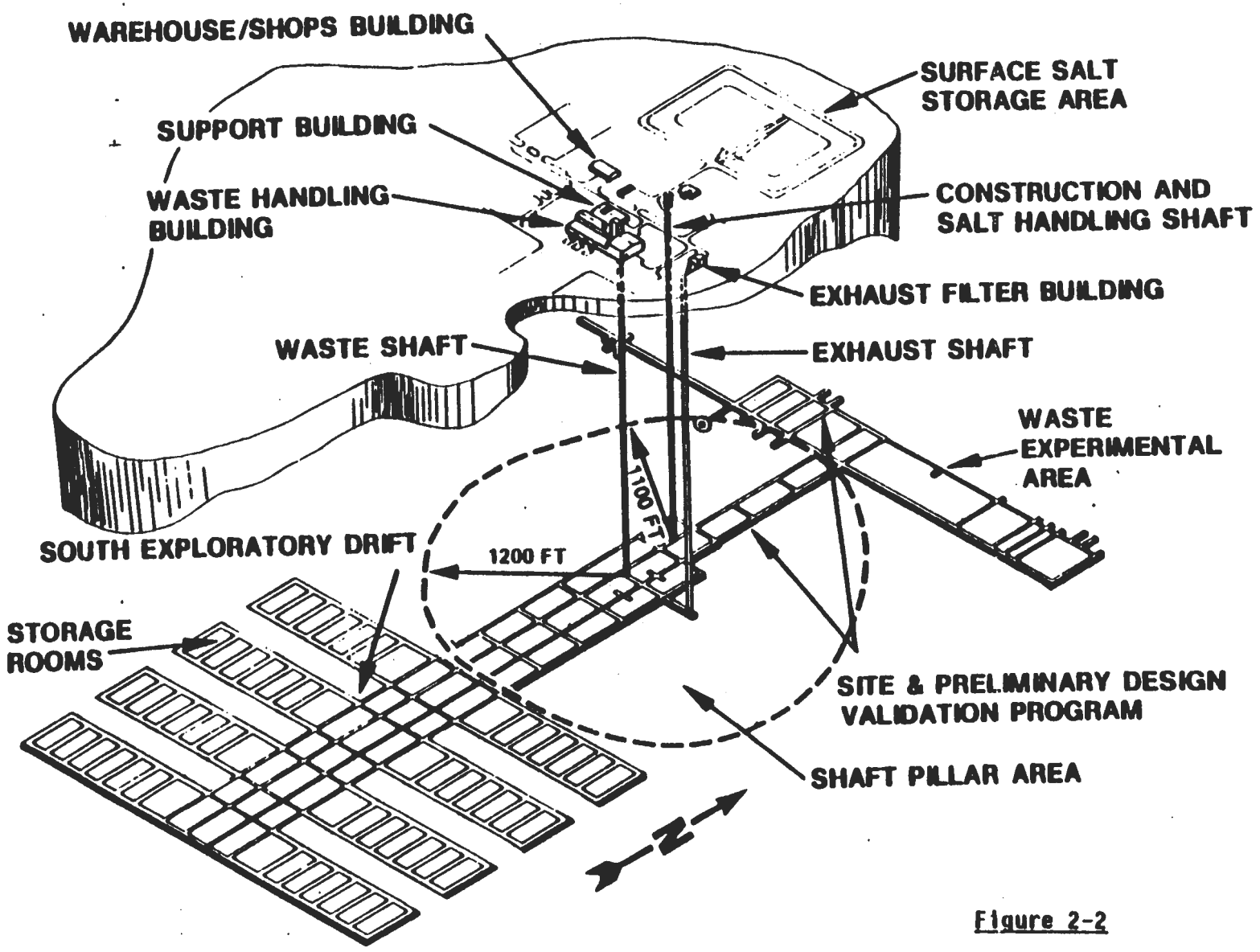


Figure 2-2

PERSPECTIVE VIEW OF THE WIPP

### 2.5.3 Detailed Design

Detailed design of the WIPP, begun in 1981 and completed in 1984, included design of the surface and underground facilities and the reference design for the underground openings. This was based on an extensive amount of data derived from the site characterization, including information from boreholes, surface geophysical measurements and laboratory tests. These data were used to establish the facility level and the design parameters. The number of holes drilled to the proposed facility level was restricted in order to retain its isolation from the surface. The layout and configuration of the underground openings were based mainly on empirical data which incorporates the room and pillar concept utilized in existing potash mines in Carlsbad and other mining areas, and on storage efficiency. The design was also based on mining and engineering standards universally applied to underground projects.

Analyses were performed to evaluate the stability of underground openings using material properties obtained from laboratory tests of core samples (ref. 2-28). Validation of the underground opening reference design with respect to the actual underground environment requires direct observation of geologic conditions at the facility level and the behavior of the underground openings. This interaction between observation of underground excavation and development of design is consistent with engineering practice for underground construction and with achieving the most cost-effective facility configuration.

Detailed design of the WIPP had sufficient flexibility to allow the incorporation of initial information obtained from excavation during the SPDV Program. This design flexibility was necessary for construction of the underground facilities. Calculations that applied material properties and analytical models developed from laboratory tests were performed to evaluate the behavior of the underground openings. Information obtained from the design validation program was used to confirm, refine, or alter the underground opening reference design as required to accommodate in situ conditions. The detailed

design included the development of construction details for the experimental areas and the full-scale waste storage area. It also included design of the surface facilities but this is not included in the design validation program.

## 2.6 DESIGN METHODS

Practical experience in the safe construction of salt and potash mines extends over many years. Empirical knowledge on the safe sizes of openings and pillars has been documented (ref. 2-29) and performance records of openings in salt are available. Different methods of analysis are required to determine the stability of openings in salt for different conditions of potential failure. The normal safety concepts of engineering, which relate a factor of safety to loads or stresses, cannot be transferred directly to the analysis of underground openings in salt. Therefore, postulated failure conditions were analyzed by other appropriate methods. In general, an opening in salt can be considered stable when the following two basic requirements are satisfied:

(1) the deformation of the opening conforms to the clearance envelope allowed for safe operation of the workings during design life; and

(2) the load bearing capacity of the salt around the opening is adequate to prevent sudden structural failure of the opening.

Subsections 2.6.1 through 2.6.3 discuss the empirical methods, closed form solutions and model simulations used for the reference design of the WIPP underground openings.

### 2.6.1 Empirical Method

Most of the seven potash mines in the Carlsbad area were visited by project participants on several occasions as the design evolved. The preliminary room and pillar configurations, including the width and

spacing of the rooms, drifts and pillars, were based primarily on experiences gained from general mining practices in those mines in areas with similar geology. The extraction ratio at the WIPP facility horizon is significantly less than that used in potash mines of similar depth in the Carlsbad area and in other parts of North America.

### 2.6.2 Closed Form Solutions

Closed form solutions in the SME Mining Engineering Handbook were used to check the design of the room-and-pillar system, including room dimensions, room spacing, pillar stresses and pillar width-to-height ratios. These types of solutions were also used to check room stability, including the stresses on the roof beams, and to estimate surface subsidence (ref. 2-30). Closed form solutions for steel and concrete structural design were used for design of the shaft liners and keys.

### 2.6.3 Model Simulation

To determine the geomechanical and structural behavior around the underground openings, mathematical models of the openings were generated and preliminary finite element analyses were performed to simulate this behavior. These analyses used material properties obtained from laboratory tests of drill core samples to estimate closure of the openings. In order to maintain the operational capability of the underground facility during its design life, allowances for roof, floor and wall closures were added to the operational clearance envelope of the underground openings. The design criteria require confirmation or modification of the estimated closure based on geomechanical instrument measurements obtained in the excavations.

Preliminary analyses were only considered parametric studies since important feedback from the design validation program observations and geomechanical instrument measurements was required to complete the understanding of the mechanism of creep deformation in the salt at the WIPP site.

THIS PAGE LEFT BLANK INTENTIONALLY

# CHAPTER 3

# UNDERGROUND FACILITIES

## 3.1 INTRODUCTION

This chapter presents a brief history of the underground development level selection process. It also describes the configurations of the WIPP shafts, drifts and rooms, and summarizes their excavation history. The discussion of excavation history includes those details pertaining to the "as-built" openings which are considered significant with respect to the reference design. The reference design of the underground openings was based on requirements contained in the Design Criteria (refs. 2-7 and 2-8) and Design Bases (refs. 2-9 through 2-20) documents.

The WIPP underground facility is divided into three general areas (Figure 3-1). The northern portion is the experimental area containing the design validation test rooms and technology experiments. The central area is the shaft pillar. The number of drifts in this area is restricted to minimize subsidence around the shafts. This portion of the facility will primarily contain shops and personnel areas. The southern portion of the facility is the waste storage area. Although some mining has been conducted in this area, it remains largely unexcavated at the time of publication of this report.

## 3.2 SELECTION OF THE UNDERGROUND DEVELOPMENT LEVEL

Selection of the WIPP underground development level evolved over several years and various facility design concepts. Seven stratigraphic horizons were identified in 1979 as potential locations for the facility level and ranked in order of their preference. These seven horizons were chosen based on an examination of available borehole data, primarily geologic and geophysical logs from borehole ERDA-9, and on horizon selection criteria established by the WIPP project participants. The selection criteria consisted of recommended distances between the underground opening surfaces and the nearest overlying or underlying clay seams or partings.

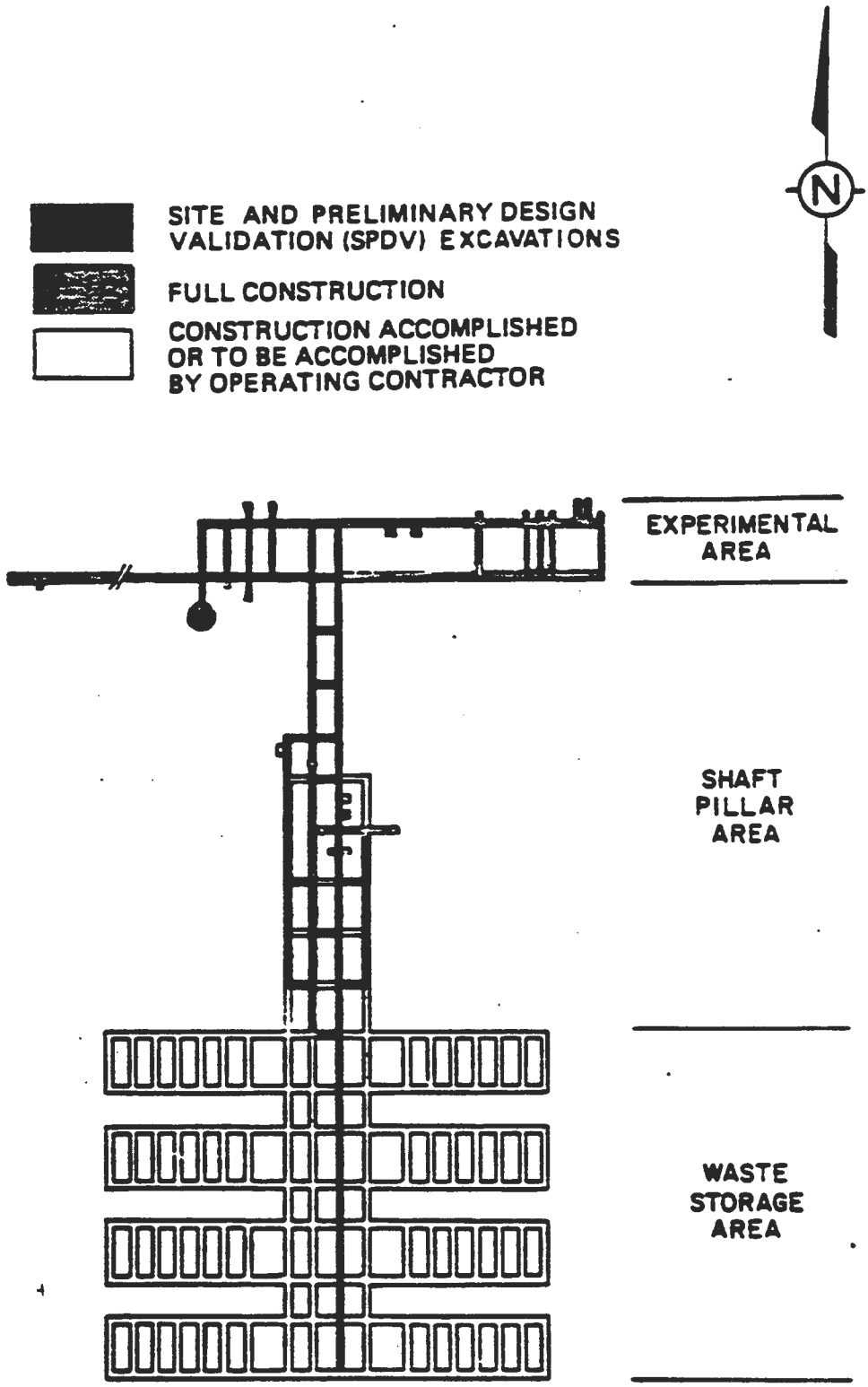


Figure 3-1

FUNCTIONAL AREAS OF THE UNDERGROUND FACILITY

Geologic mapping of the SPDV exploratory shaft in April and May 1982 permitted an assessment of the suitability of those intervals in the area of MB-139 preferred for the location of the facility level. This assessment included an evaluation of the intervals of interest against a modified version of the 1979 horizon selection criteria. These modified criteria were a result of changes to the initial WIPP facility concept, consisting of a reduction from two levels to one and alterations in the room size. The modified criteria were as follows:

(1) The rock comprising the underground facility horizon should contain no significant dissolution features, faults, or fractures. If any such features are noted, a detailed investigation must be conducted. (This element was not explicitly stated in the 1979 criteria.)

(2) There should be a minimum 4-foot thickness of halite between the top of MB-139 and the facility floor. The undulatory upper contact of MB-139 shall be considered in the selection of the facility floor level. (The 1979 criteria required a 5-foot thickness between the facility floor and the first underlying clay seam or parting.)

(3) There should be a minimum 14 1/2-foot section of halite for construction of nominal 13-foot high rooms. Minor impurities, such as argillaceous halite and polyhalite, may be acceptable. (The facility design in 1979 called for 12-foot high rooms.)

(4) There should be a minimum of 5 feet of halite between the facility roof and the first overlying clay seam (defined as 1/4 inch thick or greater) for purposes of roof stability. (This criterion was adjusted at the site to a 5- to 10-foot thickness at the verbal request of SNL personnel.)

(5) Horizons containing substantial amounts of polyhalite should be avoided. The minimum thickness of halite defined in the

third criterion listed above was increased from 14 1/2 feet to 17 feet or more to accommodate the 17-foot high SPDV exploratory shaft station.

Selection of the final underground development level was made following a series of meetings in which the interval ranked first was evaluated for its ability to satisfy these criteria. The selection was based primarily on the results of detailed geologic shaft mapping from a depth of 2,080 feet to 2,185 feet. A meeting, attended by representatives from the DOE, Westinghouse, SNL and Bechtel, was held on May 2, 1982, to discuss the results of the selection process and to present a recommendation for the facility level location to the DOE. The final level selected for the facility floor was at a preliminary depth of 2,149 feet (elev. 1258.4 feet). The recommendation was accepted by the DOE and later reviewed and concurred in by a representative of the New Mexico Environmental Evaluation Group (EEG).

Geologic mapping of the SPDV exploratory shaft and subsequent evaluation by the project participants showed that, as anticipated, the geology was similar to that encountered in borehole ERDA-9. One exception was the discovery of an additional anhydrite bed, anhydrite "b", and its underlying clay seam. Figures 3-2 and 3-3 show the preliminary design (pre-SPDV) of the shaft station and storage rooms. This preliminary design was based on the stratigraphy at the first-ranked alternative horizon. Figures 3-2 and 3-3 show that only one anhydrite layer and clay seam were expected above the facility level at this horizon, based on the interpretation of ERDA-9 core. This would have produced 12 feet of uninterrupted halite above the shaft station and 16 feet above the storage rooms. However, shaft mapping revealed an intermediate bed, anhydrite "b", approximately 7 feet below the known bed, anhydrite "a". This reduced the uninterrupted halite thickness above the facility level roof to 3.5 to 5 feet at the shaft station and 7 to 8.5 feet in the waste storage area. Despite this finding, the underground facility horizon chosen was judged to adequately meet all of the established criteria.

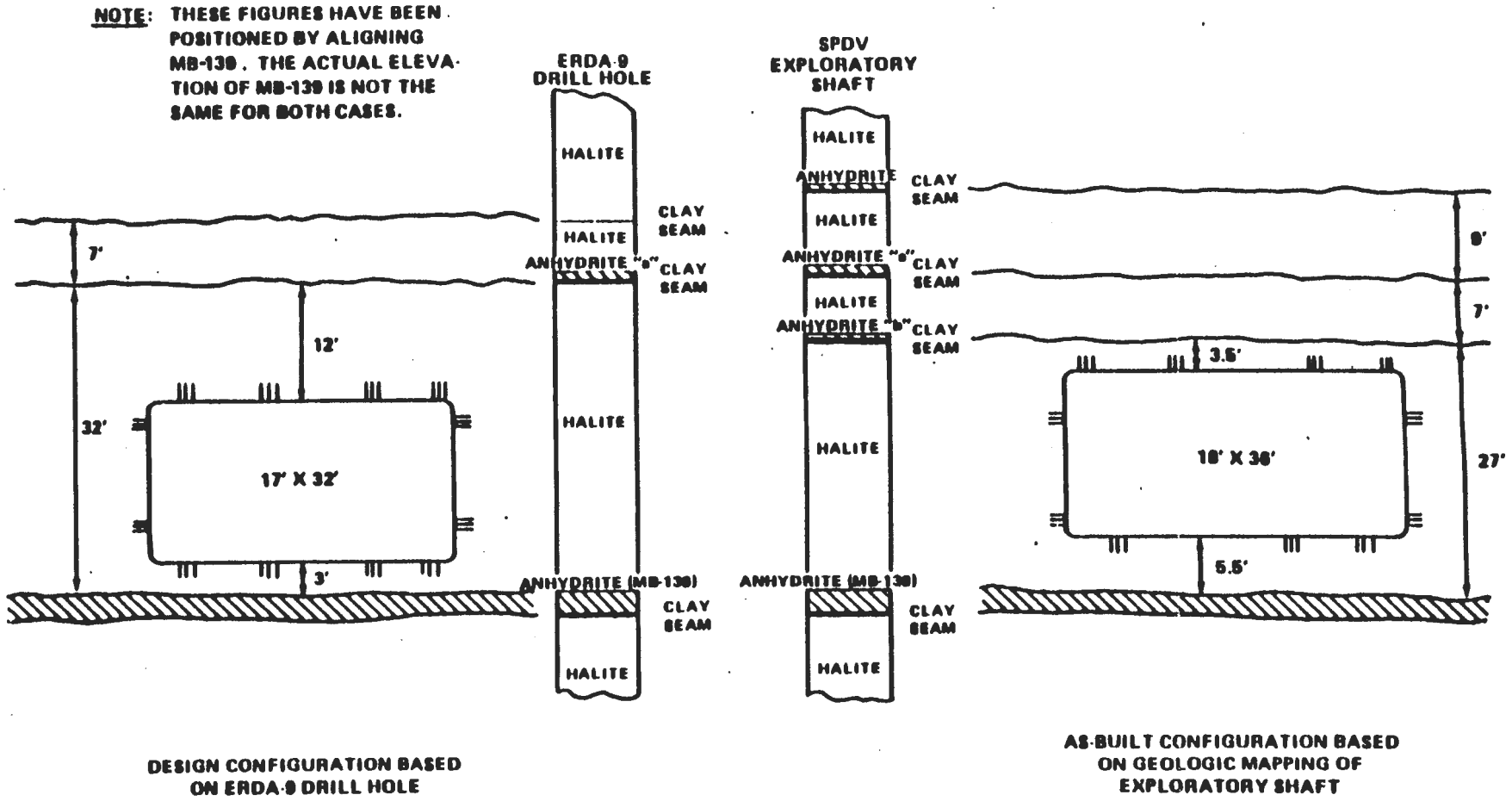


Figure 3-2

SPDV EXPLORATORY SHAFT STATION
DESIGN VERSUS AS-BUILT CONFIGURATION

**NOTE:** THESE FIGURES HAVE BEEN POSITIONED BY ALIGNING MB-139. THE ACTUAL ELEVATION OF MB-139 IS NOT THE SAME FOR BOTH CASES.

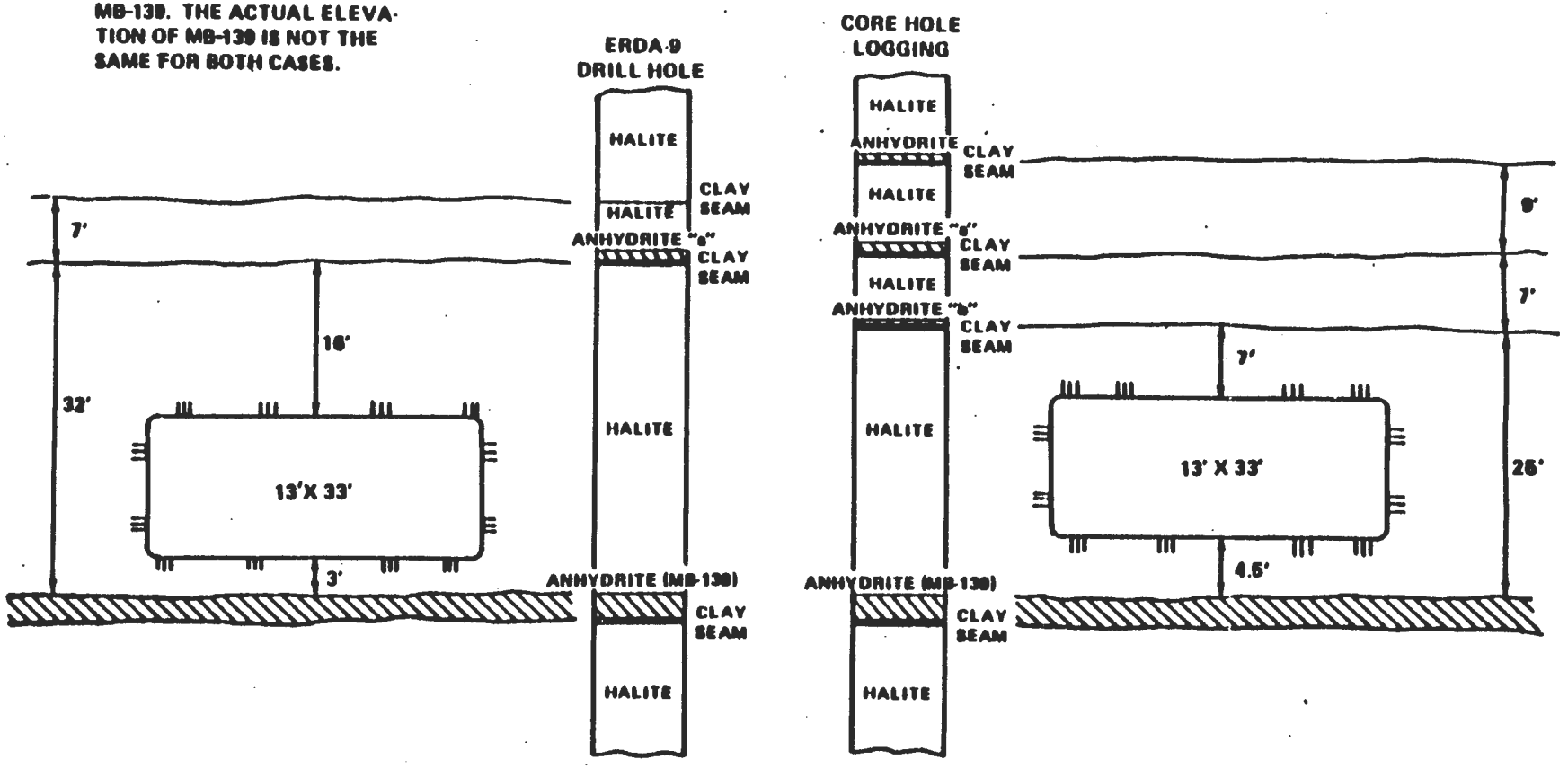


DESIGN CONFIGURATION BASED ON ERDA-9 DRILL HOLE

REVISED CONFIGURATION BASED ON CORE HOLE DATA

Figure 3-3

STORAGE ROOM
DESIGN VERSUS REVISED CONFIGURATION

At a meeting held on February 13, 1986, consideration was given to the desirability of relocating the facility level to a different stratigraphic horizon (ref. 3-2). The discussion was prompted by the following observations of the behavior of the underground openings:

(1) The effect of excavation on the strata surrounding the underground openings are being investigated by gas permeability testing. These tests indicate that zones of increased permeability due to fracturing, and proportional to the size of the opening, have developed between the floor of the openings and the base of MB-139 in the test rooms. These zones have also developed at intersections and other locations in the N1420 drift. Increased permeability has also been detected within anhydrite "b" above the roof of the test rooms. (Additional permeability testing is being conducted by SNL. The final results from this program are not yet available.)

(2) Fracturing has been encountered both within and above MB-139. It is especially well developed in the southern half of Test Room 3 (Room T). This fracturing is discussed in Chapter 10, subsection 10.3.2.1, and in Chapter 11, subsection 11.3.2.1.

(3) Both horizontal displacements and vertical separations have been observed above the roof of the underground openings. These occur primarily at anhydrite "b" and are associated with the underlying clay seam. This is discussed in Chapter 10, subsection 10.3.2.1, and in Chapter 11, subsection 11.3.2.1.

(4) In situ closure rates are almost three times greater than the rates originally predicted from laboratory test data. This is discussed in Chapters 10, 11 and 12.

The underground opening behavior occurring at the WIPP is similar to that of other openings excavated in areas with similar geologic formations. The conditions are understood and any problems encountered can be adequately mitigated using standard mining engineering procedures. The behavior experienced at the present facility level is likely to occur to some extent at any alternate horizon selected. These conclusions, and the fact that the behavioral characteristics and geologic environment at the existing level are known, resulted in a decision by the WIPP project participants to keep the facility level at its present location. Studies of the behavior of the rooms and drifts will continue beyond design validation as discussed in Chapter 1, subsection 1.5.2.

## 3.3 DESCRIPTION OF UNDERGROUND FACILITIES

### 3.3.1 C & SH Shaft

The construction and salt handling (C & SH) shaft is the principal means of access to the underground WIPP facility and is the primary fresh-air intake for the underground ventilation system. It was originally designated the exploratory shaft during the SPDV Program. The shaft provides a means of access for personnel and materials to and from the facility, and for the removal of excavated salt. Geomechanical instrumentation installed in the shaft provides important data for monitoring the behavior of the liner and key, the salt strata surrounding the shaft, and ground-water pressures.

The shaft is lined with steel casing having a 10-foot inside diameter from the ground surface to a depth of 846 feet. The 10-foot diameter extends through the concrete shaft key to a depth of 880 feet. From the key to the bottom of the shaft at 2,298 feet the shaft is a nominal 12 feet in diameter and is unlined.

The steel liner was designed to retain the rock formations above the salt and to prevent water seepage into the shaft. The liner was designed for both construction and permanent loads. The construction load was considered to be the hydrostatic pressure exerted on the liner

by the fluid used to "float" it into place for installation. The permanent load is the hydrostatic pressure exerted on the liner by ground water under artesian conditions in the water-bearing zones. Rock pressure was not used in design due to the controlling influence of the hydrostatic pressure. Since hydrostatic pressure increased with depth, the steel liner thickness was also increased. The liner is 5/8 inch thick at the top and increases to 1 1/2 inches thick at the bottom. The liner is held in place with cement grout.

The C & SH shaft key is a 37 1/2-foot long reinforced-concrete structure at the base of the steel liner. The key serves two important functions. First, it provides a transition from the lined to the unlined sections of the shaft. Second, as an integral part of the liner, it prevents ground water from the upper water-bearing members from dissolving the salt around and beneath the key. This water movement is obstructed primarily by two water seals installed behind the concrete. A third seal, installed at the interface of the steel liner and concrete key, prevents water from flowing out at the interface and down the inner surface of the key. A gravel-filled trench was constructed behind the concrete above the lower of the two seals to intercept water migration past the upper seal. This water is drained through four pipes, called "telltales", to the key surface and into a water collection ring at the base of the key.

The shaft is unlined below the concrete key. Excavation by the rotary drilling method has resulted in shaft walls that are smooth and undamaged. No support or protective wire mesh was required.

### 3.3.2 Waste Shaft

The waste shaft serves to connect the waste handling building on the ground surface with the WIPP underground facility. The shaft's primary function is to permit the transfer of radioactive waste from the surface to the underground storage area. It will also serve as an intake shaft for small volumes of air during storage operations and as an emergency escape route. The waste shaft was initially excavated as

a 6-foot diameter ventilation shaft, which was the primary exhaust route during the SPDV phase of construction. As in the C & SH shaft, geomechanical instruments installed in the waste shaft provide important geotechnical data with which to monitor the behavior of the shaft and its surrounding geologic environment.

The waste shaft is lined with unreinforced concrete from the ground surface to the top of the key at a depth of 837 feet. The purpose of the liner is to retain the surrounding rock and to prevent ground water from entering the shaft. The lined section of the shaft has a finished inside diameter of 19 feet. The liner thickness increases with depth from 10 inches at the surface to 20 inches at the key. A water collection ring was incorporated into the liner immediately beneath both the Magenta and Culebra water-bearing members. These rings are connected to another ring at the base of the key.

The waste shaft key is similar in construction to the C & SH shaft key. It serves as a transition from the concrete-lined section to the exposed salt section of the shaft and it prevents ground water from reaching the salt via the shaft opening. The key is 63 feet long, 4 1/4 feet thick and constructed of reinforced concrete. The bottom of the key is at a depth of 900 feet. In contrast to the C & SH shaft key, the waste shaft key has only two water seals.

A water collection ring at the base of the key collects water trickling down the surface of the key and conducts it, as well as water from the two upper rings, to the shaft station via a 2-inch diameter PVC pipe. Two guide pipes, consisting of 2-inch diameter polyvinyl chloride (PVC) pipe, were also installed in the concrete key at a depth of 843 feet at the request of SNL to serve as guides for drilling test holes across the contact of the Rustler formation with the Salado formation.

The section of the shaft below the key is 20 feet in diameter and consists of exposed salt lined with wire mesh anchored by rock bolts. The 20-foot diameter shaft enlarges to 23 feet just above the waste

shaft station. This 23-foot diameter extends to the bottom of the shaft, approximately 122 feet below the facility level.

### 3.3.3 Exhaust Shaft

The exhaust shaft is the primary ventilation exhaust for the underground facilities. It is designed as a duct to remove air from the underground areas up through the exhaust filter building at the ground surface. In addition, the exhaust shaft will serve as a backup escape route during emergencies. This shaft is also used to carry an auxiliary 15 kV power cable and signal cables underground. These redundant cables serve as emergency alternates should the primary cables in the C & SH shaft become inoperative. The exhaust shaft, like the C & SH and waste shafts, contains a suite of geomechanical instruments.

The exhaust shaft is lined with unreinforced concrete from the ground surface to the top of the shaft key at a depth of 844 feet. The purpose of the liner is the same as that in the other two shafts. The liner has an inside diameter of 14 feet. The liner thickness increases from 10 to 16 inches with depth.

The exhaust shaft key serves the same function as the keys in the other two shafts. It is a transition element between the concrete liner in the upper section of the shaft and the exposed salt in the lower section. It is also designed to prevent ground water in the upper water-bearing members from reaching the salt section of the shaft. The key is 63 feet long and 3 1/2 feet thick. The key contains eight telltale drains at a depth of 857 feet and nine drains each at 855 feet and 870 ft. The key also contains two water seals, a water collection ring, and two guide pipes for drilling test holes. The bottom of the key is at a depth of 907 feet.

The exhaust shaft below the key is 15 feet in diameter. It is lined with wire mesh anchored by rock bolts. The exhaust shaft terminates at the facility level; there is no shaft sump.

### 3.3.4 Drifts

The underground shaft stations and drifts have been designed to facilitate the handling and transport of radioactive waste. They also provide access for construction operations and experimental activities. The drifts are designed to provide adequate ventilation supply and exhaust for all areas of the underground facility.

All drifts are rectangular in cross section with typical dimensions that range from about 8 to 12 feet high and 14 to 25 feet wide. Access drifts serve as the main haulageways between the shafts and the experimental and waste storage areas. Cross-cut drifts (crosscuts) are designed to accommodate equipment, shops and traffic flow. The crosscuts are generally smaller in cross-sectional dimensions than the access drifts. The excavated dimensions of major drifts and rooms are presented in Table 3-1. The horizontal underground openings are oriented either north-south or east-west and are labeled based on a grid system having the centerline of the C & SH shaft as its origin. For example, the E0 drift runs north-south in line with the C & SH shaft and the N1100 drift is an east-west drift 1100 feet north of the C & SH shaft.

The northern part of the facility contains the experimental areas. Four test rooms were excavated west of the E0 drift as part of the SPDV Program. These rooms are discussed in subsection 3.3.5. The remaining experimental areas have been excavated for long-term experimental programs to be conducted under the direction of SNL. These experiments are not part of design validation and are addressed in this report only when necessary to clarify the discussion.

The shaft pillar area (Figure 3-1) is designed to protect the surface structures and shafts from settlement resulting from the natural closure of underground openings. The shaft pillar dimensions were derived in accordance with standard analyses developed by the U.S. Bureau of Mines (ref. 2-30). Excavation within the shaft pillar area was designed to maintain an extraction ratio of less than 15 percent.

Table 3-1

FACILITY LEVEL CONFIGURATIONS
NOMINAL EXCAVATED DIMENSIONS OF MAJOR DRIFTS AND ROOMS



| Drift or Room | | | | | Width (ft) | Height (ft) |
|---|---|---|---|---|---|---|
| E0 | From | N35 | To | N1420 | 25 | 12 |
| E140 | From | N140 | To | N1420 | 14 | 8 |
| E140 | From | N140 | To | S2210 | 25 | 12 |
| E140 | From | S2210 | To | S3264 (Exploratory Drift) | 25 | 8 |
| E300 | From | S90 | To | S1980 | 14 | 12 |
| W30 | From | S90 | To | S700 | 20 | 12 |
| W30 | From | S700 | To | S1950 | 14 | 12 |
| W170 | From | N140 | To | S1300 | 14 | 12 |
| N140 | From | E0 | To | E140 | 12 | 12/19 |
| N140 | From | E0 | To | W170 | 12 | 12/19 |
| N460 | From | E0 | To | E140 (Conference Room) | 20 | 8 |
| N780 | From | E0 | To | E140 | 12 | 12 |
| N1100 | From | E0 | To | E1546 | 14 | 9 |
| N1100 | From | E0 | To | W667 | 20 | 12 |
| N1100 | From | W667 | To | W1800 (Room G Entry Drift) | 20 | 9 |
| N1100 | From | W1800 | To | W2990 (Room G) | 20 | 10 |
| N1420 | From | E140 | To | E1546 | 14 | 12 |
| N1420 | From | E140 | To | W647 | 20 | 12 |
| S90 | From | E0 | To | E140 | 12 | 12 |
| S90 | From | E140 | To | E300 | 14 | 12 |
| S400 | From | E60 | To | E140 | 20 | 12 |
| S400 | From | E140 | To | E300 | 14/18 | 12/17 |
| S400 | From | E300 | To | E500 | 20 | 12 |
| S700 | From | W170 | To | W30 | 20/25 | 12 |
| S700 | From | W30 | To | E140 | 20 | 12 |
| S700 | From | E140 | To | E300 | 20/35 | 12 |
| S1000 | From | W170 | To | W30 | 20 | 12 |
| S1000 | From | W30 | To | E140 | 25 | 12 |
| S1000 | From | E140 | To | E300 | 20 | 12 |
| S1300 | From | W170 | To | W30 | 20 | 12 |
| S1300 | From | W30 | To | E140 | 20 | 12 |
| S1300 | From | E140 | To | E300 | 20 | 12 |
| S1600 | From | W170 | To | W30 | 20 | 12 |
| S1600 | From | W30 | To | E140 | 20 | 12 |
| S1600 | From | E140 | To | E300 | 20 | 12 |
| S1600 | From | E300 | To | E520 | 14 | 12 |
| S1950 | From | W30 | To | E140 | 14 | 12 |
| S1950 | From | E140 | To | E300 | 20 | 12 |
| S2180 | From | E140 | To | E300 | 14 | 12 |

Table 3-1 (continued)

FACILITY LEVEL CONFIGURATIONS
NOMINAL EXCAVATED DIMENSIONS OF MAJOR DRIFTS AND ROOMS



| Drift or Room | Width (ft) | Height (ft) |
|---|---|---|
| Test Rooms 1, 2, 3 & 4 (300 feet long) | 33 | 13 |
| Experimental Rooms A1, A2, A3, B & D (306 feet long) | 18 | 18 |
| Alcove I1 (43 feet long) | 24 | 12 |
| Alcoves I2, I3, I4, I5, I6 & I7 (33 feet long) | 33 | 12 |
| Rooms C1 & C2 (98 and 102 feet long) | 18 | 18 |
| Room J (98 feet long) | 33 | 12 |
| Rooms L1 & L2 (98 feet long) | 33 | 12 |
| Room H Entry | 12 | 10 |
| Room H (outside radius = 54 feet) | 36 | 10 |

A geomechanical instrumentation program was implemented to gather geotechnical data from the underground drifts. The program was designed to monitor the stability of the openings, to assess deformational characteristics of the salt, and to measure closure rates of typical drifts, rooms and intersections. In addition, an extensive program of geologic mapping, core drilling, laboratory testing and visual observations has been conducted. The methodology used and the results of these programs are discussed in other chapters of this report.

### 3.3.5 Test Rooms

Four test rooms were excavated in the northern section of the facility during the SPDV phase of construction. These rooms represent full-scale models of the future waste storage rooms and have the same dimensions, 13 feet high, 33 feet wide and 300 feet long, as the planned storage rooms.

The test rooms are designed to permit an assessment of deformation and closure rates due to salt creep as well as the stability of the future storage rooms. This has been accomplished by evaluations and analyses of geotechnical data gathered from geomechanical instruments installed in each room and the results of geologic mapping, core drilling, laboratory testing of samples from the surrounding strata, and qualitative visual observations by project geotechnical personnel. The results of these evaluations and analyses are presented in Chapters 11 and 12.

### 3.3.6 Waste Storage Area

The waste storage area will be developed in the southern portion of the facility (Figure 3-1). The reference design for this area includes a series of eight panels with seven storage rooms in each panel. The room dimensions are 13 feet high, 33 feet wide and 300 feet long. The width of the pillars between rooms is 100 feet. This configuration results in a storage area extraction ratio of less than 25 percent based on a line 100 feet beyond the storage area excavation neat line.

Full development of the waste storage area will eventually encompass about 140 acres. The reference design is based on the assumption that the storage rooms and panels will be excavated in stages coordinated with the scheduled arrival of waste. Waste storage is designed not only for the rooms but also for all drifts and crosscuts in the waste storage area (south of the S1600 drift).

## 3.4 UNDERGROUND CONSTRUCTION

The existing WIPP underground facility was constructed in two phases. The first phase, SPDV (Figure 3-1), was conducted from 1981 to 1983 and consisted of the excavation of the exploratory and ventilation shafts as well as several drifts and a panel of four test rooms. SPDV accomplished two objectives: (1) it permitted the completion of experiments and geotechnical activities required for the Site Validation Program (ref. 2-5); and (2) it provided for the initial in situ confirmation of the underground facility reference design. This allowed construction of the underground facility to proceed in a timely and cost-effective manner.

Excavation associated with the second phase of underground construction was accomplished from October 1983 through February 1985 and is designated as full construction on Figure 3-1. This excavation included enlarging the ventilation shaft for its conversion to the waste handling shaft, constructing the exhaust shaft, and mining additional underground drifts and test rooms for conducting R & D experiments. The operational name of the exploratory shaft changed to the C & SH shaft during this period. Design validation has been an integral part of this construction activity.

A third phase of underground construction is currently in progress. This is the initial operations phase during which excavation of the storage rooms will occur concurrently with waste emplacement. Mining for this phase started in June 1985 with the excavation of crosscuts for the installation of shops in the shaft piller area. Partial excavation of some storage rooms will follow. However, initial waste

emplacement is currently not scheduled to begin until late 1988. No discussion of the operations phase is presented in this report, although it will be strongly affected by the design validation results presented herein.

### 3.4.1 C & SH Shaft

C & SH shaft construction was performed during 1981 and 1982. Construction started in May 1981 with the excavation of a 98-foot deep pilot hole. The pilot hole was augered using a crane-mounted drilling unit. Steel surface casing with an interior diameter of 12 feet was grouted into place to a depth of 93.4 feet.

Shaft drilling started on July 4, 1981, and was completed 112 days later. The drilling was performed using a jacknife derrick with draw works capable of supporting a suspended load of 500 tons. The drilling method used consisted of air-lifted reverse circulation performed through double-walled drill pipe. The drilling fluid (brine) was maintained at a relatively constant level above the drill bit. The drill bit consisted of a 142-inch diameter full-face rolling cutter head. Shaft drilling was completed to a depth of 2,298 feet on October 24, 1981. Table 3-2 contains an abridged history of the C & SH shaft drilling program.

Liner installation began on November 12, 1981, and was completed on December 3, 1981. A steel liner was installed in 20- and 40-foot sections in the shaft above the salt formation. The steel sections were connected during installation using full-penetration bevel welds. Nondestructive radiographic examination was performed on each welded section. The liner was partially floated into place by filling the shaft with brine and adding brine to the inside of the liner to overcome the effect of buoyancy. Additional support for installation was provided by the drilling derrick and draw works. After the liner was in place, the annular space was grouted by the tremmie method. The grouting was completed on December 8, 1981.

## Table 3-2

## C & SH SHAFT - ABRIDGED DRILLING HISTORY



| | | |
|---|---|---|
| Location: | | Eddy County, New Mexico; New Mexico Grid Coordinates X 666894.89, Y 499687.23 |
| Elevation: | | Ground Surface = 3410.5 ft MSL |
| Drilling Contractors/Rig Types: | | Meredith Drilling Company/Auger (11.0 ft to 97.5 ft*); Challenger Drilling Company/ National 125 Jacknife Rotary (97.5 ft to 2,298 ft) |
| Drilling Data | Augered: | May 18 to June 17, 1981 |
| | Spudded: | July 4, 1981 |
| | Completed: | October 24, 1981 |
| | Casing: | 180-in. corrugated metal pipe, ground surface to 11 ft; 144-in. steel casing, ground surface to 93.4 ft; 120-in. steel liner, ground surface to 846 ft |
| | Drill Hole: | 142-in. (nominal) diameter uncased borehole to a total depth of 2,298 ft |
| | Drilling Fluid: | Brine |
| Directional Survey Contractor: | | Sperry-Sun (Gyroscopic Multishot Surveys) |
| Bottom Hole Coordinates: | | X 666893.45, Y 499686.56 at 2,276 ft |
| Horizontal Displacement: | | 1.59 ft S 65.03° W at 2,276 ft |

Table 3-2 (continued)

C & SH SHAFT - ABRIDGED DRILLING HISTORY



| | |
|---|---|
| Geophysical Logging Contractors: | Birdwell(B) and Dresser Atlas(D) |
| Geophysical Logs: | October 16 to December 17, 1981 |
| Fluid Density (D) | 1,200 ft to 550 ft |
| Fluid Density (B) | 750 ft to 20 ft |
| Density (B) | 2,294 ft to 50 ft |
| Caliper (3-diameter/aver.) (B) | 2,294 ft to 50 ft |
| Epithermal Neutron (B) | 2,294 ft to 50 ft |
| Gamma Ray (B) | 2,300 ft to 0 ft |
| Fluid Density (B) | 400 ft to 100 ft |
| Nuclear Cement Top Locator (NCTL) (B) | 827 ft to 0 ft |
| Nuclear Annulus Investigation Log (NAIL) (B) | 839 ft to 0 ft |
| Fluid Density (D) | 2,250 ft to 2,003 ft |

* All depths measured from ground surface.

A key was constructed at the base of the steel liner during March and April 1982. The key is 37 1/2 feet long and constructed of reinforced concrete. Key construction required additional excavation in the salt below the liner to enlarge the shaft diameter. After the installation of reinforcing steel, drains, geomechanical instruments, grout pipes and block-outs for the injection of chemical seals, concrete was placed in several lifts from the bottom of the key to the bottom of the liner. Finally, the chemical seals were placed by injection.

### 3.4.2 Waste Shaft

Drilling of the SPDV ventilation shaft started on December 24, 1981, and was completed to a depth of 2,196 feet on March 10, 1982. The drilling operation was performed with the same drill rig used to drill the C & SH shaft. The drill bit was a 72-inch diameter full-face rolling cutter head. An abridged history of the shaft drilling is presented in Table 3-3. Except for a 97-foot long surface casing, the ventilation shaft was unlined. The ventilation shaft, and later the waste shaft, served as the exhaust for the underground facility until excavation of the permanent exhaust shaft was completed.

Enlargement of the SPDV ventilation shaft to become the waste shaft began in October 1983 (Table 3-3). This enlargement was performed from the top to the bottom of the shaft using the smooth-wall drill and blast method. The blasting was accomplished in 10-foot rounds that permitted the muck to fall down the 6-foot diameter shaft to the facility level. The muck was removed from the waste shaft station and hauled to the surface via the salt-handling skip in the C & SH shaft.

Construction of the unreinforced concrete liner closely followed this excavation. Typically, the shaft crew would take out three rounds (30 feet) of rock before placing one 24-foot section of concrete. This arrangement normally left no more than 6 feet of unlined shaft below the concrete.

Table 3-3

WASTE SHAFT - ABRIDGED CONSTRUCTION HISTORY



| | | |
|---|---|---|
| Location: | | Eddy County, New Mexico; New Mexico Grid Coordinates X 666920.76, Y 499286.92 |
| Elevation: | | Ground Surface = 3407.5 ft MSL<br>Shaft Collar = 3407.9 ft MSL (ventilation shaft)<br>Shaft Collar = 3409.0 ft MSL (waste shaft) |
| **Ventilation Shaft** | | |
| Drilling Contractors/Rig Types: | | Meredith Drilling Company/Auger (8.0 ft to 98.2 ft*);<br>Challenger Drilling Company/ National 125 Jacknife Rotary (98.2 ft to 2,196 ft) |
| Drilling Data | Augered: | June 13 to 17, 1981 |
| | Spudded: | December 24, 1981 |
| | Completed: | March 10, 1982 |
| | Casing: | 108-in. corrugated metal pipe, ground surface to 8 ft;<br>74-in. steel casing, 0.5 ft above ground surface to 96.9 ft |
| | Drill Hole: | 72-in. (nominal) diameter uncased borehole to a total depth of 2,196 ft |
| | Drilling Fluid: | Brine |
| Directional Survey Contractor: | | Sperry-Sun (Gyroscopic Multishot Surveys) |
| | Bottom Hole Coordinates: | X 666918.81, Y 499285.81 at 2,177 ft |
| | Horizontal Displacement: | 2.25 ft S 60.2° W at 2,177 ft |

Table 3-3 (continued)

WASTE SHAFT - ABRIDGED CONSTRUCTION HISTORY



| | |
|---|---|
| Shaft Survey Contractor: | Cementation West, Inc. |
| Horizontal Displacement: | 1.37 ft SW at 2,150 ft |
| Geophysical Logging Contractor: | Birdwell |
| Geophysical Logs: | March 8 to 10, 1982 |
| Caliper (3-diameter/aver.) | 2,190 ft to 0 ft |
| Epithermal Neutron | 2,190 ft to 0 ft |
| Density | 2,190 ft to 0 ft |
| Gamma Ray | 2,100 ft to 0 ft |
| Fluid Density | 2,191 ft to 1,800 ft |
| **Waste Shaft** | |
| Excavation Contractor: | Ohbayashi Corporation |
| Excavation Method: | Smooth-wall drill and blast |
| Finished Shaft Diameter: | Lined = 19 ft<br>Unlined = 20 ft minimum |
| Shaft Collar Excavation Began: | October 11, 1983 |
| Liner Plate and Concrete Backfill Completed: | November 12, 1983 |
| Collar Pads and Sinking Headframe Foundations Poured: | November 14, 1983 |
| Concrete Liner Constructed: (including key) | November 30, 1983, to April 3, 1984 |
| Liner Plate at Magenta Dolomite Grouted: | March 8 to 10, 1984 |
| Liner Plate at Culebra Dolomite Grouted: | April 3 to 5, 1984 |
| Salt Section Excavated: | April 7 to June 11, 1984 |
| Sump Excavated: | June 20 to August 8, 1984 |
| Liner Grouted: | August 11 to 25, 1984 |

* All depths measured from ground surface.

As part of the shaft design, both the Magenta and Culebra dolomite members of the Rustler formation were overexcavated and covered with steel liner plate prior to concrete placement. The space between the liner plate and the rock provided room for water from these water-bearing zones to accumulate. This allowed the concrete liner to reach full strength without damage from hydrostatic pressure buildup. After the concrete liner had reached full strength, this annular space was grouted with Portland cement grout at a 1:1 cement-to-water ratio.

Construction of the waste shaft key was nearly identical with that of the C & SH shaft key. The key is 63-feet long and composed of reinforced concrete. The shaft was overexcavated and the reinforcing steel, drainpipes, geomechanical instruments and chemical seal blockouts were installed. Unlike in the C & SH shaft, the chemical seals were placed between lifts of concrete. Concrete was placed from the bottom of the key to the top in several lifts, with construction joints at the top of each lift and at each chemical seal blockout. At the chemical seal locations the seal material was placed into the blockout prior to placing the next lift of concrete. Construction of the shaft liner and key was completed on April 3, 1984.

Excavation of the shaft to its 20-foot finished diameter below the key began on April 7, 1984. This section of the shaft is lined with wire mesh anchored by 3-foot long rock bolts. Mesh installation, like liner installation, was accomplished concurrently with excavation. The shaft enlargement reached the facility level on June 11, 1984. The shaft sump was excavated between June 30 and August 8, 1984. The sump extends approximately 122 feet below the facility level.

The concrete liner and grouting at both water-bearing zones did not completely prevent water from entering the shaft. Water seeped through the liner at construction joints and some cracks from a depth of about 560 feet to 835 feet. A grouting program was undertaken to seal these leaks in August 1984. A total of 628 bags of Portland Type V cement, 103 bags of MC-500 microfine cement, and 76 gallons of Scotch-brand

5600 foam chemical grout were injected into 293 drilled holes (ref. 3-3). The grouting significantly reduced, but did not eliminate, water seepage through the concrete liner.

### 3.4.3 Exhaust Shaft

The exhaust shaft was constructed in two phases over a 16 month period. The first phase was the excavation of a 6-foot diameter pilot shaft using upreaming techniques. The second phase consisted of enlargement of this shaft by conventional drill and blast methods and lining of the upper 907 feet. The construction history is summarized in Table 3-4.

Shaft excavation began on September 22, 1983, with the drilling of a pilot hole. The pilot hole was a 7 7/8-inch diameter hole drilled from the ground surface to intersect with the S400 drift at a depth of about 2,150 feet. Therefore, directional control of the hole was critical. The upper 80 feet of the pilot hole was augered, then lined with a surface casing. Drilling progressed to a depth of 744 feet using a tri-cone roller bit and compressed air. A "Dynadrill" was then used to correct hole alignment from 735 to 1,183 feet based on the results of gyroscopic hole surveys. The circulating medium was also changed at this time from air to brine. The tri-cone bit was used to complete the pilot hole. The hole diameter was then reamed to 11 inches from the surface to the facility level, again using a tri-cone roller bit. Pilot hole drilling was completed on December 16, 1983.

Excavation of the pilot shaft was performed by reaming the 11-inch diameter pilot hole to a diameter of 6 feet. This was accomplished by the raise-bore method. Reaming was performed from the facility level to the ground surface. The raise-boring operation was conducted from December 31, 1983, to February 10, 1984, using a Robbins series 61R1131 raise-bore machine. This machine utilizes a full-face rolling cutter head pulled to the surface with hydraulic jacks. Drill cuttings fell to the facility level and were hauled to the surface via the C & SH shaft.

Table 3-4

EXHAUST SHAFT - ABRIDGED CONSTRUCTION HISTORY

| | |
|---|---|
| Location: | Eddy County, New Mexico; New Mexico Grid Coordinates X 667370.39, Y 499287.23 |
| Elevation: | Shaft Collar = 3411.5 ft MSL<br>Shaft Reference = 3409.0 ft MSL |
| Excavation Contractor: | Ohbayashi Corporation |
| Excavation Method: | Raise-bore 6-ft diameter pilot shaft; smooth-wall drill and blast to final dimensions |
| Subcontractors for Raise-Bore Excavation: | Raisebore, Inc., and J. S. Redpath Co. |
| Finished Shaft Diameter: | Lined = 14 ft<br>Unlined = 15 ft |
| Pilot Hole Drilled: | September 22 to December 16, 1983 |
| Raise-Bore Excavation: | December 31, 1983, to February 10, 1984 |
| Shaft Collar Excavation Began: | July 15, 1984 |
| Liner Plate and Concrete Backfill Completed: | July 17, 1984 |
| Concrete Liner Constructed: (including key) | July 18 to November 29, 1984 |
| Liner Plate at Culebra Dolomite Grouted: | December 2 to 4, 1984 |
| Liner Plate at Magenta Dolomite Grouted: | December 4 to 5, 1984 |
| Salt Section Excavated: | December 7, 1984, to January 17, 1985 |
| Liner Grouted: | June 1 to July 31, 1985 |

Enlargement of the pilot shaft from 6 feet to the final exhaust shaft diameter of 15 feet began on July 15, 1984, and was accomplished by drilling and blasting in 10-foot rounds. Excavation was performed from the ground surface to the facility level. The rock was blasted into the open pilot shaft so that it fell to the facility level where it could be removed and hauled to the surface via the C & SH shaft.

The upper 844 feet of the exhaust shaft is lined with unreinforced concrete. As in the waste shaft, construction of the exhaust shaft liner occurred concurrent with the drill and blast excavation. Concrete placement for the liner was completed on November 29, 1984. The two water-bearing zones in the Rustler formation, the Magenta and Culebra dolomites, received the same special treatment that was performed in the waste shaft. Each zone was overexcavated and covered with steel liner plate prior to placing the concrete liner. After the liner had cured, grout was injected behind the liner plates.

Exhaust shaft key construction, similar to that in the waste shaft, was performed in November 1984. The key consists of reinforced concrete and extends from a depth of 844 to 907 feet. It initially contained 2 chemical seals, 8 telltale drains, 2 guide pipes for test hole drilling, and geomechanical instrumentation. Placement of the concrete and chemical seal material was identical to that performed in the waste shaft. Two additional sets of telltale drains were installed in the key by drilling after its construction. Each set contains nine drains. One set was installed above and one set below the initial eight-drain set.

The exhaust shaft is 15 feet in diameter from the bottom of the key to the facility level. For safety, the walls are covered with wire mesh anchored by rock bolts. Excavation of the shaft to its final dimensions was completed on January 17, 1985.

As in the waste shaft, water began seeping through the exhaust shaft liner at construction joints and small cracks. Total water inflow

through the liner was measured at 0.35 gallons per minute in January 1985. A grouting program, using Portland cement and chemical grout, was conducted from June 1 through July 31, 1985, to seal these leaks and to ensure that the integrity of the shaft key was maintained. A total of 164 bags of Class C cement and 826.9 gallons of Terragel 5531 chemical grout were used. The total water inflow was reduced by this grouting to an essentially non-measureable quantity.

### 3.4.4 Drifts

The exploratory (C & SH) shaft station was the first underground horizontal opening excavated after completion of the SPDV exploratory and ventilation shafts. The initial shaft station excavation was performed from May 2 to June 3, 1982, using the drill and blast method. The station was trimmed to its final dimensions using the Dosco continuous mining machine discussed later in this subsection. The station area north of the shaft is 32 feet long, 32 to 35 feet wide and 12 feet high. South of the shaft, the station is 90 feet long and 32 to 38 feet wide. The height of the station south of the shaft is 18 feet for a distance of 54 feet and 14 feet for the remaining 36 feet. Cartridge water-gel explosives detonated by electric detonators were used for the drill and blast excavation. A detailed description of the SPDV exploratory shaft station excavation is presented in the WIPP Preliminary Design Validation Report (ref. 1-3).

Following the initial excavation of this station, the drill and blast method was used to excavate a drift southward to provide a connection between the two shafts so ventilation could be established. This drift was approximately 310 feet long, 18 feet wide and 9 feet high. Excavation of the drift was accomplished from June 3 to June 13, 1982.

The only other major use of the drill and blast method at the facility level was for construction of the loading pocket in the SPDV exploratory shaft. This pocket was constructed from June 1 through 30, 1982, on the north side of the shaft below the facility floor level.

It was later outfitted with a steel hopper and other equipment associated with the salt handling system.

The initial (SPDV) underground construction phase was conducted by Cementation West, Inc., of Tucson, Arizona. A British-made Dosco LH 1300, boom-type continuous mining machine was mobilized underground to the SPDV exploratory shaft station during late summer of 1982. This machine was used to excavate the remaining horizontal underground openings during the SPDV Program. The Dosco was capable of excavation rates of 1,000 to 1,200 tons per 24 hours (excavation was conducted on a three-shifts-per-day, seven-days-per-week basis). However, the excavation rate was often much less due to numerous construction and engineering related constraints. The mining machine was demobilized in May 1983 at the completion of the SPDV Program.

A second underground construction contract for full WIPP construction was awarded to Ohbayashi Corporation of South San Franicsco, California. During this phase of construction, two Japanese Mitsui Miike, boom-type continuous mining machines were used for excavation of the underground horizontal openings. Each of these machines excavated at a rate of 300 to 400 tons per 24 hours. These machines were mobilized to the underground facility in October 1983 and demobilized in April 1985.

A summary of the excavation sequence for the underground horizontal openings is presented on Figure 3-4. This figure shows the mining progress on a daily basis from October 14, 1982, through March 31, 1986. The underground mining operation was performed in the same manner during both construction phases regardless of the type of mining machine being used. The rotating head on the boom of the mining machine cut the salt away from the working face. The "muck" was pulled through the machine on a conveyor and deposited in one of several types of haul vehicles. Typically, the haul vehicles were underground trucks capable of carrying about 5 tons of muck. Other vehicles used included LHDs (Load-Haul-Dump, a type of front-end loader) and a telescoping-bed haul truck. The trucks carried the muck to the C & SH shaft station

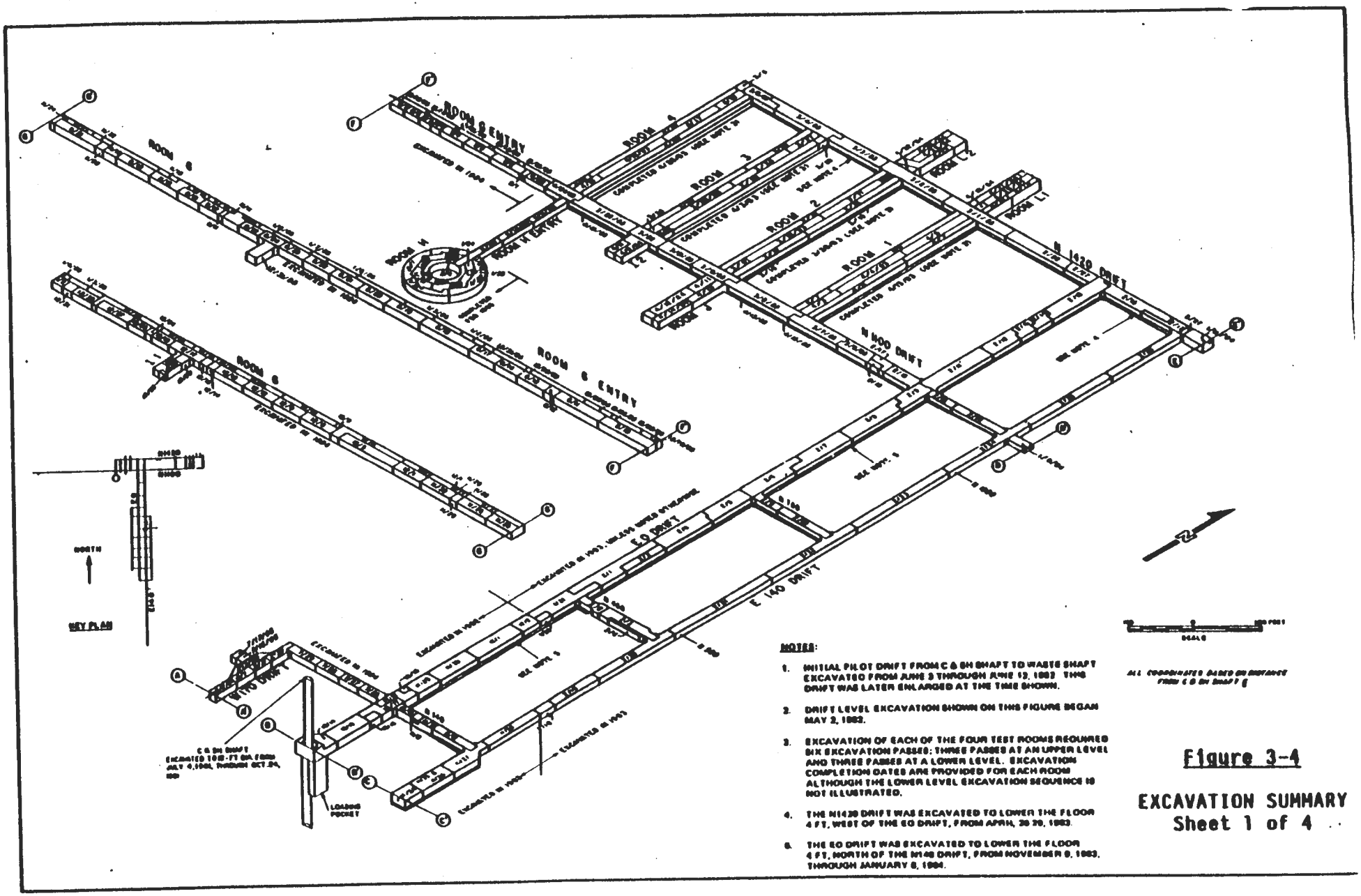


Figure 3-4

EXCAVATION SUMMARY
Sheet 1 of 4

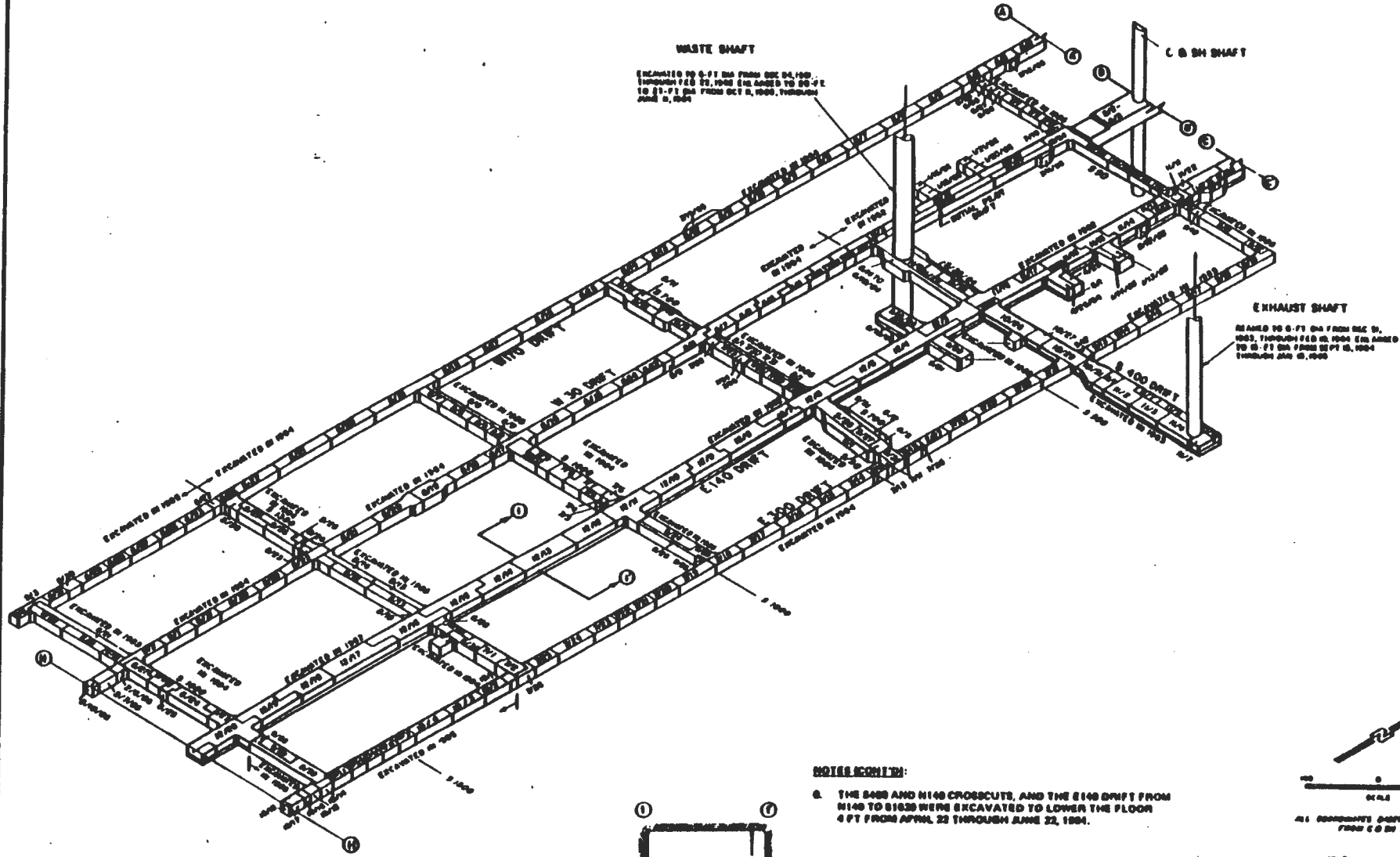

SOUTH EXPLORATORY DRIFT
SECTION 1-1'

NOTES CONT'D:

6. THE S400 AND N140 CROSSCUTS, AND THE E140 DRIFT FROM N140 TO S1630 WERE EXCAVATED TO LOWER THE FLOOR 4 FT FROM APRIL 22 THROUGH JUNE 22, 1994.

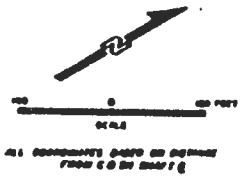


ALL COORDINATES BASED ON DISTANCE FROM C & SH SHAFT ℄

**Figure 3-4**

**EXCAVATION SUMMARY**
**Sheet 2 of 4**

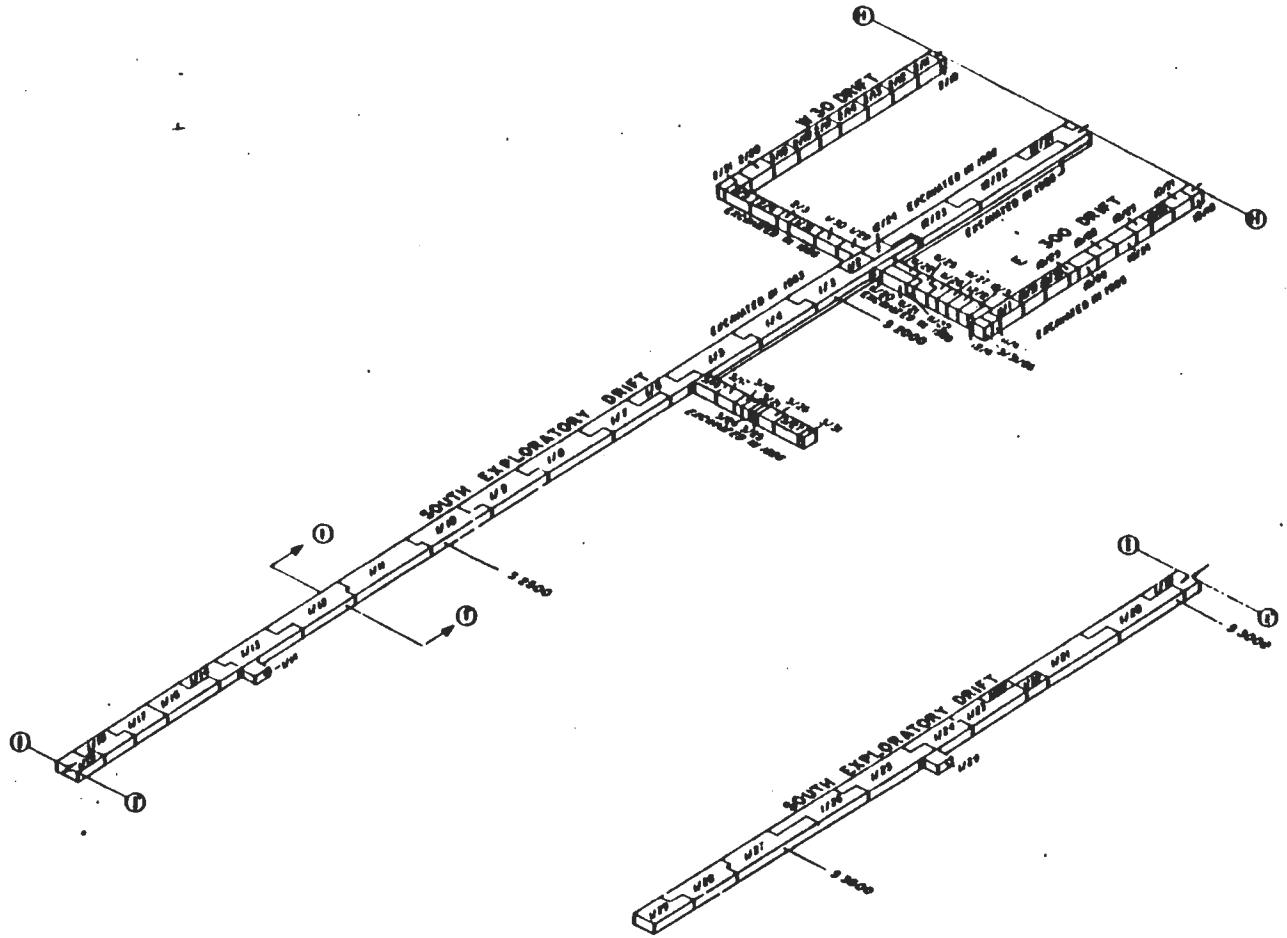


**Figure 3-4**

**EXCAVATION SUMMARY**
**Sheet 3 of 4**

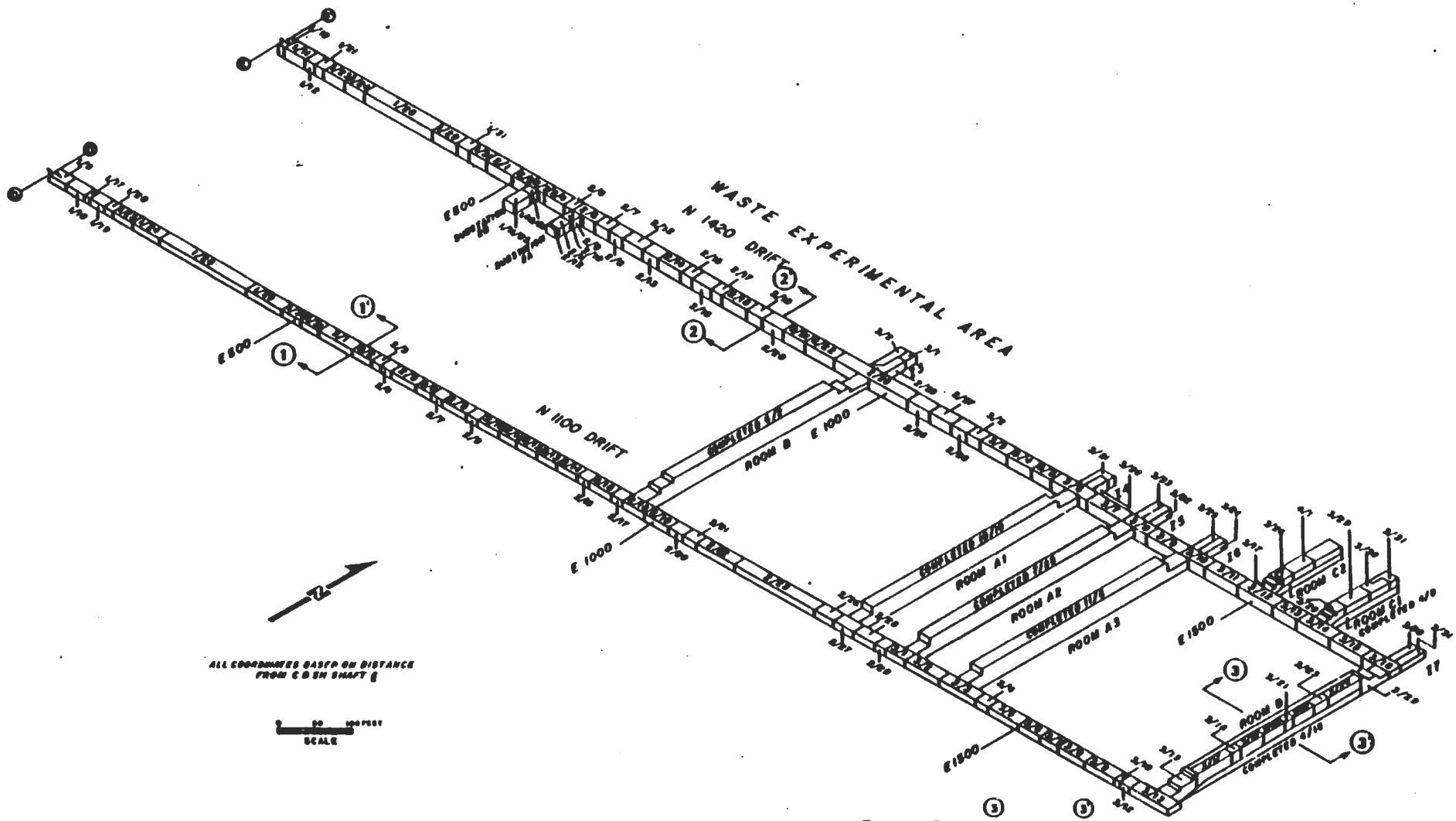


NOTES:

1. EXCAVATION SUMMARY FOR ROOMS A1, A2, A3, AND B ARE NOT PRESENTED.
2. ALL EXCAVATIONS SHOWN ON THIS SHEET WERE MADE IN 1984, EXCEPT FOR SUBSTATION 28

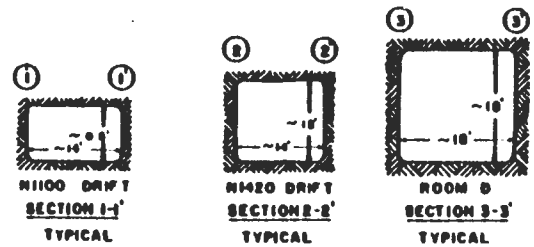


**Figure 3-4**

**EXCAVATION SUMMARY**
**Sheet 4 of 4**

and dumped it into the loading pocket. From there, the muck was carried to the surface in 7- to 8-ton loads in the skip. The skip dumped the muck at the surface into 50-ton Caterpillar or Euclid haul trucks which then carried the muck to the surface salt storage area.

During and immediately after excavation, a sounding survey of the roofs in the horizontal openings was made using a scaling bar to identify areas of drummy or slabby rock which could pose safety or stability problems. Remedial work was performed immediately after sounding in any areas identified as potentially unstable. This work consisted of hand-scaling thin drummy areas, removing larger drummy areas up to 18 inches thick with the mining machine, or rock bolting. In addition, two follow-up surveys were made of the roofs in all of the horizontal openings excavated at the time of the survey. The first survey was completed in July 1983 and the second in November 1984. Remedial work was performed on problem areas identified during these surveys. This work consisted of scaling, excavation, or rock bolting. It should be noted that the drummy areas identified during the July 1983 survey were sounded again in the November 1984 survey and did not show any noticeable enlargement.

Rock bolts are used selectively throughout the underground drifts for both remedial work and safety. The roofs of many high-traffic personnel areas are pattern bolted and covered with wire mesh as an additional safety precaution.

The C & SH shaft station has presented the majority of problems associated with roof stability. Due to its initial excavation by the drill and blast method, and the proximity of overlying clay seams, the roof in the station has required support by a large number of rock bolts. The method of rock bolting has evolved through several phases due to the effect of salt creep on roof separation along the clay seams.

Rock bolts were initially installed in the C & SH shaft station roof

from May 9 to June 20, 1982. These bolts were 1 inch in diameter, 8, 10 or 12 feet in length, and made of grade 60 steel. They were anchored using resin cartridges.

These resin-anchor bolts began failing at the head assemblies shortly after their installation was completed. The failed bolts were replaced with 8-foot long, 5/8-inch diameter mechanical-anchor bolts with 2 x 12 x 12-inch wooden blocks installed between the steel head assembly plate and the salt. A total of over 400 resin-anchor and mechanical-anchor bolts were installed in the shaft station roof through April 1983.

During December 1983 and January 1984, 146 additional mechanical-anchor bolts, 5/8 inch in diameter and 8 feet long, were installed in the C & SH shaft station roof. In May 1984, another 91 similar anchor bolts were installed. After the mechanical-anchor bolts were installed, the nut and head assembly plate were cut off those older resin-anchor bolts showing evidence of excessive deformation. This was to prevent injury to personnel from falling nuts and plates should these resin-anchor bolts fail.

From mid-April through early August 1985, approximately 133 3/4-inch diameter mechanical-anchor bolts, 6 and 8 feet long, were installed in the station roof on approximately 3 1/2-foot centers. In addition, 245 resin-anchor bolts, 1 inch in diameter, were anchored above anhydrite "b" and across anhydrite "a". These bolts were 12 and 14 feet in length. The entire station roof was covered at this time with wire mesh secured with 2-foot long, 5/8-inch diameter mechanical-anchor bolts. Approximately 750 of the 2-foot long bolts were installed.

Although some resin-anchor bolts were used in the SPDV drifts and test rooms excavated in 1982 and 1983, mechanical-anchor bolts have been used in all subsequently excavated areas. Bolt lengths vary from 2 to 8 feet in the drifts and rooms. Wire mesh secured by 2-foot long mechanical-anchor bolts has been installed on the roofs of all high-traffic personnel areas. This includes instrument-shed and

electrical alcoves, many of the shop areas, and some of the brows above the entries to the waste experimental rooms. Rock bolts and wire mesh have also been installed in the roof of the N140 crosscut.

Rock bolts and wire mesh have been installed for roof support in the waste shaft station waste transfer area. The bolts, 3/4 inch in diameter and 12 feet long, are mechanical-anchor steel bolts set on nominal 4-foot centers.

### 3.4.5 Test Rooms

As part of the SPDV Program, four test rooms were excavated at the north end of the underground facility (Figure 3-4) by Cementation West, Inc., using the Dosco mining machine. The test room excavation was conducted from March 9 to April 25, 1983. Test Room 2 was excavated first, followed by Test Rooms 3, 1 and 4, in that order. Each room was excavated in a series of six passes along its longitudual axis (Figure 3-5). The first pass was the largest in cross section and was conducted down the center of the planned room along its roof. This pass was approximately 15 feet wide and 8 feet high. The second and third passes were conducted on either side of the first pass. Each of these passes were about 9 feet wide and 8 feet high. The last three passes lowered the floor 5 feet to complete the room excavation to its design height and width of 13 x 33 feet.

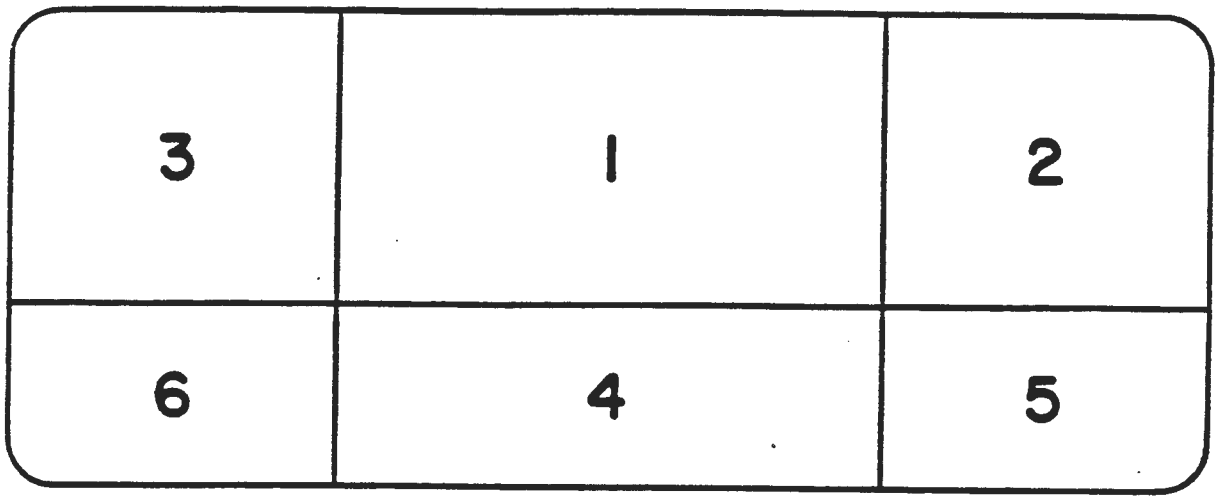


Figure 3-5

TEST ROOM EXCAVATION SEQUENCE

# CHAPTER 4

# SUPPORTING VALIDATION DOCUMENTS

## 4.1 INTRODUCTION

This chapter discusses the principle documents containing information used to support design validation. These documents are the Waste Isolation Pilot Plant Preliminary Design Validation Report (ref. 1-3) and geotechnical field data reports (refs. 4-1 thru 4-19). These documents contain all of the data which has been collected, analyzed and evaluated for design validation since site construction activities began in July 1981. Other documents pertaining to design and site characterization are referenced throughout this report. However, they are considered peripheral documents not directly related to the design validation process and, therefore, are not described in this report. Because these other reports are public documents, they are available to anyone interested in obtaining additional background information or detailed data on the WIPP project.

## 4.2 PRELIMINARY DESIGN VALIDATION REPORT

The following subsections present a summary of the WIPP Preliminary Design Validation Report produced for the SPDV Program described in Chapter 1.

### 4.2.1 Purpose and Objectives

The purpose of the WIPP Preliminary Design Validation Report was to provide documentation on the behavior of the initial underground openings. Four types of information were gathered for this purpose:

(1) observations of the behavior of the underground openings;

(2) descriptions of the geologic conditions encountered during SPDV underground construction;

(3) descriptions of core samples from instrumentation and exploratory holes in the roof and floor of the underground openings; and

(4) data from installed geomechanical instrumentation.

The objective of the report was to provide initial evaluations of the suitability of the design criteria and design bases and initial confirmation of the underground opening reference design in order to permit full facility construction. This initial confirmation was based on data obtained from geologic field activities and geomechanical instrumentation which were subjected to preliminary analysis and evaluation.

### 4.2.2 Data Acquisition Program

The preliminary design validation data acquisition program consisted of geologic field activities which provided information for initial validation of the WIPP underground opening reference design. Data was obtained from three principal activities:

(1) geologic mapping;

(2) vertical core hole logging; and

(3) geomechanical instrument measurements.

All of the data collected was verified at the site field office, then sent to the DOE/Technical Support Contractor (TSC) offices in Albuquerque, New Mexico, for preparation and inclusion into the GFDRs and other reports. Due to the qualitative nature of the geologic mapping and core hole data, efforts for preparation of this material generally required only limited evaluation, editing and drafting. The geomechanical instrumentation data, however, required more extensive preparation and analysis due to its applications to various aspects of underground opening behavior and the calculation of in situ salt properties.

### 4.2.3 Geomechanical Instrumentation

The SPDV geomechanical instrumentation program for the WIPP was designed to provide empirical data on the behavior of the salt around the underground openings and on the pressure developed behind the exploratory shaft liner and key by ground water and salt creep. The objective of the geomechanical instrumentation program for SPDV was to provide:

(1) short-term in situ measurements for assessment of the preliminary design performance of the underground openings;

(2) early detection of conditions that could affect the safety of personnel during construction; and

(3) data on adverse ground conditions that may be developing, in order to identify potential problems and plan and implement remedial measures.

Instruments were initially installed in the SPDV exploratory shaft, exploratory shaft station, ventilation shaft station, the E0, E140 and N1100 drifts, and the S90 crosscut to provide data input for the WIPP Preliminary Design Validation Report. The exploratory drift extending south of the ventilation shaft was added to the SPDV Program to provide additional information on the geology in the area proposed for excavation of the waste storage rooms. Geomechanical instruments were installed at several locations in this drift.

For the WIPP Preliminary Design Validation Report, borehole extensometer and convergence point data from the SPDV exploratory shaft, as well as data from the ventilation shaft station and drifts, were insufficient to estimate long-term closure rates. Most drift extensometers and convergence points had been installed only a relatively short time before the report was prepared. A period of 1 year or more was thought to be required before a relatively steady closure rate could be established. The data were useful in

demonstrating short-term stability of the excavations and for developing cumulative closure amounts. Instruments with the most extensive data typically showed a maximum of only 3 or 4 months of regular monitoring since installation.

### 4.2.4 Preliminary Conclusions

Preliminary conclusions presented in the WIPP Preliminary Design Validation Report were:

(1) The walls of the finished shafts are stable, both in the overburden and salt formations. The mapped shaft stratigraphy is generally comparable to the stratigraphy used in the design. Ground-water control is satisfactory. The shaft liner and shaft key are performing as expected. No major revision of design elements or parameters is foreseen for future WIPP shafts as a result of the findings of preliminary design validation.

(2) The underground horizontal openings are also stable. After excavation, repeated inspections of the exploratory and ventilation shaft stations, entry drifts, crosscuts and the south exploratory drift revealed essentially no deterioration in rock stability. The underground drifts and shaft stations are stable and provide safe working conditions.

(3) Encounters of gas were expected and are typical of nearby potash mines. The small amount of gas encountered is well below the limit permitted in the underground facility by MSHA regulations. No brine pockets have been encountered or detected during excavation of the shafts and underground openings.

## 4.3 GEOTECHNICAL FIELD DATA REPORTS

### 4.3.1 Background

The compilation of GFDRs was initiated by the DOE to provide geotechnical and related information from the WIPP underground activities to interested persons or groups in a timely manner. These reports provided data from the two major phases of WIPP development: SPDV and full construction. As discussed previously, SPDV was established as an early construction phase to permit validation of the WIPP site and preliminary validation of the reference design of the underground openings. The full construction phase following SPDV was utilized to continue visual inspections of the underground openings, monitoring and interpretation of data from geomechanical instruments, and evaluations and computational analyses of the behavior of the underground openings for design validation.

The GFDRs were eventually produced on a quarterly basis. These quarterly reports contain an evaluation of selected aspects of the WIPP underground environment based on preliminary interpretation and analyses of data collected from the above activities. The analyses and evaluations contained in the GFDRs provide the supporting documentation required for design validation.

### 4.3.2 Objectives

As stated in the GFDRs, the geomechanical instrumentation program for SPDV and design validation was designed and implemented to provide in situ data on the behavior of the rock (primarily salt) around the shafts and horizontal underground openings. More specifically, the instrumentation program was designed to provide:

(1) early detection of conditions that could affect operational safety;

(2) monitoring of closure rates to allow evaluation of waste storage and retrievability;

(3) a greater understanding of the in situ behavior of bedded salt by comparison of observed response with current facility reference design calculations; and

(4) measurements of salt deformation and stresses to confirm or indicate the necessity for revisions to the opening configuration and the parameters used in underground facility design based on clearance requirements.

### 4.3.3 Geomechanical Instrumentation

An extensive geomechanical instrumentation program was implemented to provide in situ data on the shafts and horizontal underground openings as part of the investigations performed at the WIPP site. These instruments have been providing data on deformation, pressure, loads and stress on a regular basis for analysis and evaluation. Instruments for measuring the geomechanical response of the shafts and horizontal underground openings include convergence points, convergence meters, multiple-point and single-point borehole extensometers, load cells, pressure cells, stressmeters, strain gauges, inclinometers, piezometers and lateral movement gauges.

Data from these geomechanical instruments are read remotely by an automatic datalogger system and/or collected manually. All data obtained are entered on magnetic tape for data reduction, tabulation, analysis and archiving. Data collected from the geomechanical instruments have been documented in the GFDRs. These data are the basis for analysis and evaluation by the project participants and other interested groups. The geomechanical instruments provide data for the analysis and evaluation of several phenomena at various locations, including strain in the C & SH shaft key, water pressure behind the C & SH and waste shaft liners, radial closure of shafts, pressures between shaft keys and wall rock, roof-to-floor and wall-to-wall closure in the shaft stations, drifts and rooms, and displacements at depth into the walls, roof and floor of shaft stations, drifts and rooms.

The frequency of data collection is determined on a per instrument basis and is dependent upon instrument location, method of instrument reading (manual or datalogger), and the number of days elapsed since excavation at the instrument location. After installation, the instrument is read frequently, but with time this reading frequency is decreased since the rate at which the salt mass responds following excavation also decreases with time.

The geomechanical instrumentation data are presented graphically in the GFDRs and represent readings collected from the WIPP site since April 1982. The data plots in the reports are grouped by areas within the underground facility and also by instrument type. The data plots are updated as new data become available. Summary tables of the instruments, with the latest readings and the operating histories, are also presented in the reports.

### 4.3.4 Geologic Data

Geologic data presented in the GFDRs have included the results of geologic mapping activities, core hole logging, and observations of the condition and behavior of underground opening surfaces. Geologic maps of the shafts and representative horizontal opening surfaces have been presented periodically in the GFDRs or in topical reports issued separately. Geologic logs containing descriptions of core samples obtained from core holes in the underground openings were presented in the GFDRs as they became available.

Frequent observations by project geotechnical personnel have provided qualitative determinations of the condition of the underground openings. These assessments were presented in the GFDRs to document changes in the condition of the underground openings and in salt behavior on a regular basis. Observations such as the condition of the roof and rock bolts in shaft stations, fractures in pillar corners at drift intersections and in the salt surrounding the drifts and rooms, behavior of the roof and walls of the drifts and rooms, and horizontal displacements, vertical separations and fracturing detected in open

boreholes were documented. This information has provided important input for design evaluation and safety assessments.

### 4.3.5 Geomechanical/Structural Analyses

The quarterly GFDRs contain sections on both geotechnical and computational analyses. These sections present analyses of various elements of the underground excavations. The analyses are updated periodically to include the most current data available at the time the reports are published. They have provided a significant amount of information related to the geomechanical and structural behavior of the underground openings.

# CHAPTER 5
# METHODOLOGY

## 5.1 INTRODUCTION

Design validation of the WIPP underground openings is accomplished by determining the compatibility of the design criteria, design bases and reference design configurations using site specific information. Design validation also allows for the development of recommendations to improve or optimize the reference design. The methods used to validate the reference design may also be used to validate any recommended design modifications. Mathematical models containing the modifications can be generated and analyses performed to predict the future behavior of the modified reference design.

The design validation process consists of three major steps:

(1) data collection;

(2) analysis and evaluation; and

(3) prediction of future behavior.

Sections 5.2 through 5.4 present the methods used for data collection, analysis and evaluation, and prediction of future behavior.

## 5.2 DATA COLLECTION

One of the principal areas of effort in support of design validation was the compilation of geotechnical data. This data formed the basis for later analysis and evaluation and for predictive modeling. Data collected from geologic mapping, core drilling and logging, laboratory testing, geomechanical instrumentation and field observations have provided information for validation of the underground opening reference design. These data can be categorized based on their relationship to observations of geologic conditions or to structural behavior. Geologic observations include an assessment of the rock

characteristics; stability of the openings in rock; reaction of the rock to excavation; and movements along clay seams. Structural behavior is the development or modification of stresses and strains in the salt created by excavation of the underground openings, and the pressures occurring at rock/structure interfaces.

### 5.2.1 Geologic Mapping

Geologic mapping of the shafts, drifts and test rooms was conducted by site geologists. The objectives of the mapping were:

(1) provide confirmation and documentation of the continuity of the stratigraphy, lithology and structure above and below the facility horizon;

(2) evaluate any geologic conditions which may affect the excavation, stability, or safety of the horizontal openings;

(3) support field adjustments and modifications to the reference design based on the geologic conditions encountered; and

(4) finalize geomechanical instrument locations.

### 5.2.2 Core Drilling and Logging

Information on stratigraphy and lithology was obtained from core holes drilled into the floor and roof of the underground openings. The objectives of the core drilling program were:

(1) confirm the thickness, lateral extent, mineralogy and stratigraphic continuity of the host rock beyond the limits of the excavations;

(2) confirm the continuity of the geologic structure and the absence of any unusual features within the immediate zone of influence of the excavations; and

(3) obtain stratigraphic information in order to determine extensometer anchor depths.

Details of the core drilling program are discussed in Chapter 6.

### 5.2.3 Laboratory Testing

Initial laboratory tests were performed on core samples of evaporite minerals and clay from exploratory boreholes AEC-7 and ERDA-9. These tests were performed by RE/SPEC, Inc., of Rapid City, South Dakota, and by SNL (refs. 5-1 and 5-2). The evaporite samples were tested in triaxial vessels at both room and elevated temperatures. Quasi-static compression tests were performed under different constant confining pressures and variable axial loads in steps, each load step being maintained for about 10 minutes. Quasi-static compression tests were considered as constant stress-rate tests for all practical purposes. Direct shear tests were performed on samples of clay to determine the coefficient of sliding friction.

### 5.2.4 Geomechanical Instrumentation

Geomechanical instruments in the WIPP underground facility provide data on deformation, pressure, loads and stress. Instruments for measuring the geomechanical response of the shafts and other underground openings include convergence points, convergence meters, multiple-point and single-point borehole extensometers, load cells, pressure cells, stressmeters, strain gauges, inclinometers, piezometers and lateral movement gauges. Data from the geomechanical instruments are collected manually as well as read remotely by an automatic datalogger system at the surface. All data are entered on magnetic tape for data reduction, tabulation, analysis and archiving. These data are a basis for the analysis and evaluation of underground opening behavior.

The geomechanical instrumentation program for design validation was designed and implemented to provide in situ data on the behavior of the

rock (primarily salt) around the shafts and underground openings. More specifically, the instrumentation program was designed to provide:

(1) early detection of conditions that could affect construction and operational safety;

(2) closure monitoring for evaluation of the ability of the underground openings to permit waste storage and retrieval;

(3) a greater understanding of the in situ behavior of bedded salt by a comparison of the observed responses with underground opening reference design calculations; and

(4) measurements of salt deformation to permit confirmation or revision of the opening configurations and the parameters used in the underground opening reference design based on clearance requirements.

Tables 5-1 through 5-5 present information on the distribution of geomechanical instruments installed at the WIPP. The instruments provide data for the evaluation and analyses of several phenomena at various locations, including strain in the C & SH shaft key, water pressure behind the C & SH and waste shaft liners, radial closure of the shafts, pressures between the concrete shaft keys and wall rock, roof-to-floor and wall-to-wall closure in the shaft stations, drifts and rooms, and displacements at depth into the walls, roof and floor of shaft stations, drifts and rooms.

Data from the geomechanical instruments are collected manually or read remotely by an automatic datalogger system. The datalogger is a computer system that automatically collects and records output from instruments at specified polling times. The signals from the instruments are first sent to local termination cabinets (LTC) where the signal is digitized and then transmitted to the datalogger for disk storage. Manual readings are manually entered into the computer system. Changes from initial readings and rates of change are

Table 5-1

C & SH SHAFT
INSTRUMENTS

| Location and Type | Purpose |
|---|---|
| **Lined Section** | |
| Convergence points | Measure wall-to-wall closure of shaft |
| Piezometer | Measures fluid pressure buildup behind liner due to water accumulation |
| **Key** | |
| Piezometer | Measures fluid pressure buildup behind key due to water accumulation |
| Pressure cell | Measures contact pressure buildup between concrete key and wall rock |
| Welded strain gauge | Measures strain in reinforcing steel of shaft key |
| Embedment strain gauge | Measures strain in concrete of shaft key |
| **Unlined Section** | |
| Multiple-point extensometer | Measures salt creep deformation |
| Convergence points | Measure wall-to-wall closure of shaft |
| **Station** | |
| Convergence points (includes permanent and temporary convergence points and wall shortening points) | Measure roof-to-floor and wall-to-wall closure of openings and pillar shortening |
| Extensometer (single-point and multiple-point) | Measures salt creep deformation in roof, floor and walls |
| Rock bolt load cell | Measures tensile loads on rock bolts |
| Lateral movement gauge | Measures lateral movement in roof |

Table 5-2

WASTE SHAFT
INSTRUMENTS

| Location and Type | Purpose |
|---|---|
| **Lined Section** | |
| Piezometer | Measures fluid pressure buildup behind liner due to water accumulation |
| **Key** | |
| Piezometer | Measures fluid pressure buildup behind key due to water accumulation |
| Pressure cell | Measures contact pressure buildup between concrete key and wall rock |
| **Unlined Section** | |
| Convergence points | Measure wall-to-wall closure of shaft |
| Multiple-point extensometer | Measures salt creep deformation |
| **Station** | |
| Convergence points (includes permanent and temporary points) | Measure roof-to-floor and wall-to-wall closure of openings |
| Multiple-point extensometer | Measures salt creep deformation in roof, floor and walls |

Table 5-3

EXHAUST SHAFT
INSTRUMENTS

| Location and Type | Purpose |
|---|---|
| Lined Section | |
| Piezometer | Measures fluid pressure buildup behind liner due to water accumulation |
| Key | |
| Piezometer | Measures fluid pressure buildup behind key due to water accumulation |
| Pressure cell | Measures contact pressure buildup between concrete key and wall rock |
| Unlined Section | |
| Multiple-point extensometer | Measures salt creep deformation |

Table 5-4

DRIFTS
INSTRUMENTS

| Location and Type | Purpose |
|---|---|
| Convergence points (includes permanent and temporary convergence points and wall shortening points) | Measure roof-to-floor and wall-to-wall closure of openings and pillar shortening |
| Extensometer (single- and multiple-point) | Measures salt creep deformation in roof, floor and walls of openings |

Table 5-5

TEST ROOMS
INSTRUMENTS

| Location and Type | Purpose |
|---|---|
| Convergence points | Measure roof-to-floor and wall-to-wall closure |
| Multiple-point extensometer | Measures salt creep deformation in roof, floor and walls |
| Inclinometer | Measures direction and amount of salt movement above the roof, below the floor, and in the walls |
| Rigid-inclusion stressmeter | Monitors changes in stress within anhydrite |
| Convergence meter | Measures vertical closure |

calculated and stored in the computer. The data is transferred monthly to magnetic tapes which are made available to project participants.

Instruments connected to the datalogger include extensometers, piezometers, strain gauges, pressure cells, convergence meters and stressmeters. All convergence points, inclinometers, rock bolt load cells, lateral movement gauges and some extensometers must be read manually. Strain gauges, piezometers and pressure cells have been read manually at times.

The frequency of data collection is determined on a per instrument basis and is dependent upon instrument location, method of instrument reading (manual or datalogger). and the number of days elapsed since excavation at the instrument location. After installation the instrument is read frequently, but with time this reading frequency is decreased since the rate at which the salt mass responds following excavation also decreases with time.

The frequency of readings has been influenced by access limitations caused by construction operations and by the volume of data to be collected. At a few convergence point stations in newly excavated areas, readings were taken frequently to record the early rock response. Monitoring periods in these instances were typically every 4 to 12 hours for 24 hours, then once daily. Most manually read instruments were initially read weekly, then once every 2 weeks, and then once every month. Instruments connected to the datalogger were initially read at 24-hour intervals, then several times per week, and then once every 2 weeks. The current schedule for obtaining readings is shown in Table 5-6. Each instrument's range, sensitivity, resolution and precision are also presented in this table. These parameters are important when interpreting and evaluating the data, especially those readings which reflect changes that are close to the resolution, sensitivity, or precision limits of the instrument.

Table 5-6

GEOMECHANICAL INSTRUMENTATION SPECIFICATION SUMMARY

| Location | Instrument Type | Phenomenon Monitored | Parameters to be Evaluated | Scheduled Frequency of Readings as of this Report | Instrument Specifications: Range (R), Sensitivity (S) Resolution (E), Precision (P) |
|---|---|---|---|---|---|
| C&SN shaft | Borehole extensometers | Deformation | $\Sigma\delta^{*}$, $\frac{\Delta L^{**}}{\Delta t}$ | Weekly (B) | (R): 0-2 in. (P): 0.001 in.<br>(E): 0.001 in. |
| C&SN shaft key | Strain gauges | Strain | $\Sigma$ Strain* | As accessible (M) | (R): 0-3000 μin./in.-embedded<br>(R): 0-2500 μin./in.-spot welded<br>(S): 1 μin./in. |
| C&SN shaft key | Pressure cells | Pressure | $\Sigma$ Pressure* | As accessible (M) | (R): 0-1000 psi<br>(S): 1 psi |
| C&SN shaft liner & key | Piezometers | Water pressure | $\Sigma$ Pressure* | Monthly (M) | (R): 0-500 psig<br>(E): ±0.5 psi |
| C&SN shaft | Convergence points | Deformation | $\Sigma\delta^{*}$, $\frac{\Delta L^{**}}{\Delta t}$ | As accessible (M) | (R): 2-50 ft<br>(P): ±0.005 in. |
| Waste shaft | Borehole extensometers | Deformation | $\Sigma\delta^{*}$, $\frac{\Delta L^{**}}{\Delta t}$ | As accessible (B) | (R): 0-2 in. (P): 0.001 in.<br>(E): 0.001 in. |
| Waste shaft Key | Pressure cells | Pressure | $\Sigma$ Pressure* | Weekly (B) | (R): 0-1000 psi<br>(S): 1 psi |
| Waste shaft liner & key | Piezometers | Water Pressure | $\Sigma$ Pressure* | Weekly (B) | (R): 0-500 psig<br>(E): ±0.5 psi |
| Waste shaft | Convergence points | Deformation | $\Sigma\delta^{*}$, $\frac{\Delta L^{**}}{\Delta t}$ | As accessible (M) | (R): 2-50 ft<br>(P): ±0.005 in. |
| Exhaust shaft | Borehole extensometers | Deformation | $\Sigma\delta^{*}$, $\frac{\Delta L^{**}}{\Delta t}$ | Weekly (B) | (R): 0-2 in. (P): 0.001 in.<br>(E): 0.001 in. |
| Exhaust shaft liner & key | Piezometers | Water pressure | $\Sigma$ Pressure* | Monthly (M) | (R): 0-500 psig<br>(E): ±0.5 psi |
| Exhaust shaft key | Pressure cells | Pressure | $\Sigma$ Pressure* | As accessible (M) | (R): 0-1000 psi<br>(S): 1 psi |
| Drifts | Rockbolt load cells | Load | $\Sigma$ Load*, $\frac{\Delta\sigma^{**}}{\Delta t}$ | Monthly (M) | (R): 0-300 kips<br>(S): 16 lb |
| Drifts | Borehole extensometers | Deformation | $\Sigma\delta^{*}$, $\frac{\Delta L^{**}}{\Delta t}$ | Weekly (B)/ Monthly (M) | (R): 0-2 in. (P): 0.001 in.<br>(E): 0.001 in. |
| Drifts | Convergence points | Deformation | $\Sigma\delta^{*}$, $\frac{\Delta L^{**}}{\Delta t}$ | Monthly to every 2 months (M)(1) | (R): 2-50 ft<br>(P): ±0.005 in. |
| Drifts | Lateral movement gauges | Deformation | $\Sigma\delta$ | No longer read | (R): 0-5 in. (E): 1/64 in.<br>(P): ±1/64 in. |
| Test rooms | Vertical inclinometers | $\theta_x$, $\theta_y$ | $\Sigma\delta_x^{*}$, $\Sigma\delta_y^{*}$, $\Sigma\delta_{xy}^{*}$, Azimuth*, $\frac{\Delta\Sigma w_x}{\Delta t}$, $\frac{\Delta\Sigma w_y}{\Delta t}$, $\frac{\Delta\Sigma\delta_{xy}}{\Delta t}$ | Every 2 months (M) | (R): 0-30°<br>(P): ±0.3 in./100 ft of casing<br>(E): ±0.001 in./2 ft of casing<br>(S): ±0.001 ft/2 ft of casing |
| Test rooms | Horizontal inclinometers | $\theta_z$ | $\Sigma w_z^{*}$, $\frac{\Delta\Sigma w_z}{\Delta t}$ | Every 2 months (M) | (R): 0-30°<br>(P): ±0.3 in./100 ft of casing<br>(E): ±0.001 in./2 ft of casing<br>(S): ±0.001 ft/2 ft of casing |
| Test rooms | Vibrating wire stressmeters | Stress | $\Sigma S^{*}$, $\frac{\Delta S^{*}}{\Delta t}$ | Weekly (B, M) | (R): 12,000-44,000 psi wire stress |
| Test rooms | Convergence meters | Deformation | $\Sigma\delta^{*}$, $\frac{\Delta L^{**}}{\Delta t}$ | Weekly (B) | (R): Approximately 2.5 ft<br>(S): ±0.001 in. |
| Test rooms | Convergence points | Deformation | $\Sigma\delta^{*}$, $\frac{\Delta L^{**}}{\Delta t}$ | Monthly (M) | (R): 2-50 ft<br>(P): 0.005 in. |
| Test rooms | Borehole extensometers | Deformation | $\Sigma\delta^{*}$, $\frac{\Delta L^{*}}{\Delta t}$ | Weekly (B) | (R): 0-2 in. (P): 0.001 in.<br>(E): 0.001 in. |

Notes:

(B) = read through datalogger
(M) = read manually
$\Sigma\Delta$ = total change from t = 0
$\theta$ = angle
$\Delta L$ = change from last reading
$\Delta t$ = elapsed time since last reading

(1) Now convergence points are read weekly for the first month after installation.
*Design/validation parameter
**Safety/operational parameter

### 5.2.5 Field Observations

The determination of underground conditions includes a qualitative assessment based on frequent observations by WIPP site geotechnical personnel. Changes in rock conditions and in the behavior of the underground openings have been observed and documented on a regular basis in the GFDRs. In addition, quarterly inspections have been made by Bechtel home office design engineering personnel. These inspections augmented the site geologists' observations and helped highlight those changes which occurred so slowly that they were difficult to detect on a daily basis.

Periodic inspections of the C & SH shaft have been made since the shaft was completed. Conditions of the shaft walls, liner and key have been observed in addition to any water flow into the shaft. Similar inspections of the waste and exhaust shafts have also been made but less frequently due to limited accessibility.

Observations of the horizontal openings include such items as the condition of their roofs and walls; fracturing in pillar corners at drift and room intersections and in roofs and floors; and horizontal displacements and vertical separations measured in open boreholes. This information has provided important input for design and safety evaluations.

## 5.3 ANALYSIS AND EVALUATION

Data collected at the WIPP site have been analyzed and evaluated by qualified engineers and scientists. Engineering experience and judgement were used in the evaluation of field observed conditions. Laboratory tests were performed on core samples to determine the constitutive equations for the host rocks. Theoretical and applied aspects of measurements, statistics and physics were utilized to analyze and evaluate geomechanical instrument data.

### 5.3.1 Observations

The observations of geologic conditions documented during visual inspections are used to evaluate the performance of the underground openings. These evaluations are made in conjunction with the analytical techniques. The evaluations are qualitative, however, and are subjective assessments of the behavior of the salt surrounding the excavations.

### 5.3.2 Laboratory Tests

The results of the laboratory testing described in subsection 5.2.3 on samples of halite, argillaceous halite, anhydrite, polyhalite and clay from the facility level were evaluated and statistically analyzed to determine elastic and creep constants. Constitutive equations for each of these materials were established and their material property constants were determined (ref. 5-3). The material property constants based on the laboratory test results are presented in Chapter 6.

### 5.3.3 In Situ Measurements

Statistical and numerical methods were used to analyze in situ data and to evaluate the physical behavior of salt. Numerical models were used to compute creep parameters from the in situ data.

In situ measurement data from selected geomechanical instruments in the drifts and test rooms were fitted with analytical equations using regression procedures. Since early data are lacking for most of the instruments, one approach was to calculate the closure rates and fit an equation to the closure rate versus elapsed time relationship. An estimate of the early closure not measured by the instruments was independently derived.

## 5.4 PREDICTION OF FUTURE BEHAVIOR

Validation of the underground opening reference design requires predicting the future behavior of the openings. This was achieved by collecting in situ data consisting of field observations and

geomechanical instrument measurements. Statistical methods were then used to extrapolate the data obtained from the geomechanical instruments. Selected in situ data were fitted to analytical curves and predictions were made based on the extrapolated results. Closed form solutions and engineering experience were also utilized to substantiate the adequacy of the facility. A model simulation method was used to verify the creep model of salt based on creep constants derived from data obtained from laboratory material tests. After the determination of creep parameters using a statistical technique, the numerical model for simulating the facility was also utilized to predict and evaluate future behavior. This includes the closures, strain distributions and stress distributions over the operating life of the facility.

Design reviews were performed as required during design of the WIPP underground facility. Experience and judgment were an important adjunct in predicting the future behavior of the underground openings. More than 3 years of continuous data collection and analysis and evaluation have provided an adequate data base for predicting future behavior.

Subsections 5.4.1 through 5.4.3 describe the methods used for predicting the future behavior of the underground openings.

### 5.4.1 Extrapolation of In Situ Data

Selected in situ closure data were analyzed and fitted by analytical curves for extrapolation of future responses. Regression analyses by the Gauss-Newton or Marquardt compromise techniques were performed to determine the regression parameters. These regression parameters were assumed to be valid for the future behavior of the opening, and the equations were used to predict the future closure rate. To estimate the additional closure that could occur, the equation was integrated over the required time interval.

### 5.4.2 Closed Form Solutions

Closed form solutions provided in the SME Mining Engineering Handbook (ref. 2-25) were used to evaluate the selected room and pillar sizes and their stability. Closed form solutions for steel and concrete structural design were also used to substantiate the adequacy of the shaft liners and keys (refs. 5-4 thru 5-7).

### 5.4.3 Model Simulations

Numerical analyses were performed to compute the predicted responses of the underground openings. The constitutive laws discussed in Appendix C were used in these analyses. However, yield or failure criteria developed for halite and non-halitic materials based on the results of laboratory tests were not incorporated in the numerical modeling. Due to the idealization of the real system in a mathematical model, the uncertainty of in situ auxiliary conditions corresponding to the mathematical model, and deviations in the material properties obtained from the laboratory tests, analyses using laboratory test data did not provide suitable results for design validation. Therefore, an engineering approach using curve fitting methods was employed. Creep parameters computed by the following procedure were used for the analyses. Additional information pertaining to material property deviations based on laboratory tests is presented in Chapter 6.

Numerical models were generated for the locations of specific instruments to simulate the instrument response and compute the creep parameters.

After generating the numerical models for these locations, their creep parameters were computed and the structural behavior was simulated by performing an analysis using the statistical method presented in Appendix C and the following procedures:

(1) At the initial stage, the surface of the openings were restrained to simulate the unexcavated condition.

(2) An internal stress was applied at each element to represent the initial lithostatic stress state, which is defined as:

$$\delta_{xx} = \delta_{yy} = \delta_{zz} = -\int_0^y pgdy \qquad (5\text{-}1)$$

where: p is the rock mass per unit volume;
g is the gravitational constant; and
y is the depth.

(3) The overburden and support pressures at the boundaries and the weight of the rock were applied to compute the static solution.

(4) The restraints at the surface of the openings were then removed to simulate the excavation.

(5) The structural responses were computed using a time step integration scheme. Normalized time steps were used throughout the analysis. At the first time step, the time increment was calculated by an iterative scheme using a predetermined initial time increment.

(6) In subsequent time steps, the time increment for each time step was calculated based upon the previous time steps and the specified maximum tolerances of stress and strain increments at the previous and current time steps. The structural responses were computed at each normalized time step.

# CHAPTER 6

# GEOLOGIC CHARACTERIZATION

## 6.1 INTRODUCTION

Geologic characterization of the underground excavations for design validation of the WIPP began in June 1981. Initial characterization activities consisted of monitoring the drilling and geophysical logging of the SPDV exploratory shaft. As shaft outfitting and underground excavation progressed, the geologic work evolved into mapping of the shafts and underground horizontal openings, performing ground-water inflow tests, monitoring geomechanical instrumentation installations and taking subsequent readings or measurements, logging underground core hole samples, and performing other tasks related to defining the geologic integrity of the WIPP site. Data from these activities were evaluated in conjunction with information from previous site studies to more accurately define site geologic conditions as they related to design validation of the WIPP underground facility.

## 6.2 DATA COLLECTION ACTIVITIES

### 6.2.1 Geologic Mapping

An important aspect of validating the WIPP underground opening reference design included geologic mapping of the shafts and drifts. The objectives of this mapping were discussed in Chapter 5.

#### 6.2.1.1 C & SH Shaft

Geologic characterization of the C & SH shaft began in late June 1981 with the drilling of the SPDV exploratory shaft (see Chapter 3, subsection 3.3.1, for an explanation of the two shaft names). The initial activity conducted to develop this characterization consisted of logging the drill cuttings at periodic intervals to permit a determination of rock types and to provide a description of the geologic formations penetrated (Appendix D, Figure D-1). These formations included, in descending order, the Dewey Lake red beds, the Rustler formation and the Salado formation.

After completion of the drilling operation, geophysical logging was performed in the shaft to determine the condition of the shaft wall and to more accurately define the stratigraphy penetrated. These logs were the caliper, gamma ray, density and epithermal neutron. The logs were analyzed to better determine the depths to various stratigraphic horizons and correlate them with those found in holes drilled during previous site investigation phases (Appendix B, Figure B-1).

Reconnaissance and detailed geologic mapping of the C & SH shaft was performed between March 31, 1982, and May 2, 1982, from a depth of about 846 feet (elev. 2564 feet) near the Rustler/Salado formation contact to a depth of 2,193 feet (elev. 1217 feet). Mapping above the 846-foot depth could not be performed due to the presence of the permanent steel liner, while drilling fluid and muck prevented mapping below the 2,193-foot depth. The results of this mapping, combined with criteria established as a result of previous site investigations, were used to select the final depth for the underground development level (Chapter 3, Section 3.2). The mapping results are shown in Appendix D, Figures D-2 through D-4. A detailed discussion of the mapping is contained in reference 3-1.

Vertical control for the shaft mapping was established by tape measure from a known elevation provided by the SPDV underground excavation contractor at the shaft collar. The scope of work and methodology for the shaft geotechnical activities are contained in reference 6-1.

Reconnaissance geologic mapping of the shaft from a depth of about 920 feet (elev. 2490 feet) to 2,083 feet (elev. 1327 feet) was accomplished after construction of the shaft key. The mapped area was limited to a strip 1 to 5 feet wide along the south side of the shaft. One interval from about 1,832 feet (elev. 1578 feet) to 1,892 feet (elev. 1518 feet) was not mapped due to the interference of shaft outfitting activities.

Detailed circumferential geologic mapping was performed in the key area from the base of the steel liner to a depth of about 920 feet.

Detailed mapping was also performed from a depth of about 2,083 feet to about 2,193 feet. Detailed mapping was carried out through this interval to obtain sufficient geologic information for use in making the final facility level selection. The facility level selection mapping was performed by several teams of geologists working over a 3-day period from April 30 to May 2, 1982. The detailed mapping was generally performed independently of shaft outfitting activities to permit better observation and interpretation of the shaft geologic characteristics.

Representative samples of the geologic strata surrounding the shaft were obtained during mapping for later, more detailed classification. Photographs were taken at various locations along the shaft wall for verification of the mapping results and record-keeping purposes. As mapping progressed, observations of the shaft wall were also made to determine the condition of the salt as a result of its behavior following excavation.

Based on the data obtained from the above activities, characterizations were made of the geologic formations penetrated by the C & SH shaft. The characterizations consisted primarily of descriptions of the stratigraphy, lithology and structure of the formations. Other detailed data were included, where relevant, to more accurately characterize the salt strata in areas of primary concern to the design of the WIPP underground facility.

The C & SH shaft geologic activities served to further refine and confirm the data obtained from previous site investigations. The geologic conditions observed in the C & SH shaft within the mapped interval corresponded to the conditions expected from previous investigations. Borehole ERDA-9, in particular, showed conditions similar to the C & SH shaft. Although some variation was observed, it was attributed to core loss in ERDA-9 which prevented the early detection of these conditions.

Only minor modifications to the reference design of the C & SH shaft key structure and the geomechanical instrumentation levels were made to accommodate the observed geology.

6.2.1.2 Waste Shaft

Drilling of the initial 6-foot diameter SPDV ventilation shaft (later to be enlarged to the waste shaft) was conducted from December 1981 to February 1982. Samples of the drill cuttings were obtained at periodic intervals from the drilling fluid to permit monitoring of the stratigraphy being penetrated. After the drilling was completed, a set of geophysical logs was run to determine the shaft wall conditions and to further define the boundaries of the rock strata penetrated.

Geologic mapping of the 6-foot diameter shaft began in July 1982 in conjunction with the initiation of shaft outfitting. Initially, five areas of weaker rock which had been washed out by the drilling operation were mapped between July and September 1982 before steel liner plate was placed over these areas for safety purposes. Geologic mapping of the SPDV ventilation shaft from the bottom of the steel surface casing at 97 feet (elev. 3312 feet) to the bottom of MB-139 was conducted during September and October 1982.

Both reconnaissance and detailed geologic mapping were performed in the 6-foot diameter shaft. The mapping extended from a depth of 97 feet below the ground surface to a depth of about 2,170 feet (elev. 1239 feet). The results of this mapping are shown in Appendix E, Figures E-1 through E-6. In addition, a lithologic log, based on the geologic mapping, and a geophysical density log are shown in Appendix B, Figure B-1, for correlation with the C & SH shaft and boreholes WIPP-12, ERDA-9 and DOE-1. A detailed description of the SPDV ventilation shaft geotechnical activities is contained in reference 4-3.

Mapping of the SPDV ventilation shaft was generally performed by a team of two geologists. Depth control was maintained by hanging a tape down the shaft wall at 100- to 200-foot intervals from the top of the

surface casing. Orientation in the shaft was maintained by following a steel guide installed on the southwest wall to control movement of the work platform used in the shaft. Most of the shaft was mapped in a strip about 2 to 3 feet wide along the steel guide. Although only a portion of the shaft wall was mapped, visual examination was made of the entire wall to determine if any geologic abnormalities existed. Below a depth of about 1,180 feet (elev. 2229 feet), mapping was performed on a limited basis due to salt incrustation on the shaft wall. This crust was apparently the result of dust from the facility level that was exhausting through the shaft and depositing on the wet shaft wall. Representative samples of the rock strata were collected to permit a more detailed description. Photographs were taken at various locations along the shaft wall for verification of the mapping results and record-keeping purposes. In addition to providing a description of the rock strata, observations of the shaft wall were made to determine, where possible, the reaction of the rock to excavation.

Detailed mapping around the full circumference of the 6-foot diameter shaft was performed at the following five intervals:

(1) Magenta dolomite member,
(2) Culebra dolomite member,
(3) Rustler formation fracture zone;
(4) Rustler/Salado formation contact; and
(5) MB-139.

Because of salt incrustation on the shaft wall immediately above the facility level, detailed circumferential mapping could not be performed in this area. However, two opposing strips about 1 foot wide were cut through the crust to permit mapping of the shaft wall for a distance of about 50 feet above the facility level. Depths in the facility level area were verified by a separate survey utilizing elevation points established in the C & SH shaft station.

The enlargement of the SPDV ventilation shaft into the waste shaft began in October 1983 and was completed in August 1984. Additional geologic mapping and visual inspections were conducted concurrently with this excavation. Mapping was conducted from December 9, 1983, to August 10, 1984. Visual inspections of the shaft surface were performed throughout the shaft enlargement operations. The lithology of the exposed shaft stratigraphy was described and compared with the description of the same stratigraphic interval mapped in the SPDV ventilation shaft. Any differences or additional detail were noted and the SPDV ventilation shaft geologic map was modified accordingly.

In the lined section of the waste shaft, the depth to the base of each successive concrete segment was provided by the shaft excavation contractor. Vertical control for mapping was then established from the base of the previous segment. During enlargement of the unlined section of the shaft, vertical control was established from occasional survey control points installed by the contractor and from the previously mapped SPDV ventilation shaft geology. In the shaft sump, vertical control was based on a contractor survey point installed at a depth of 2,167 feet (elev. 1242 feet).

Detailed, full circumference geologic mapping was performed in areas of specific geologic interest. These areas were selected because of their poor exposure in the SPDV ventilation shaft, the possible occurrence of dissolutioning, or their hydrologic significance. These areas of detailed mapping were:

(1) the Forty-niner member claystone;
(2) the Magenta dolomite member;
(3) the Tamarisk member claystone;
(4) the Culebra dolomite member;
(5) the upper portion of the unnamed lower member of the Rustler formation; and
(6) the Rustler/Salado formation contact and key area.

The detailed mapping in the waste shaft was generally conducted as outlined in reference 6-1. Mapping was conducted by teams of four to six people. Once vertical control was established by the contractor from the base of the previous concrete segment, a 5 x 5-foot grid was painted on the shaft surface around its circumference to permit the accurate location of any lithologic contacts and geologic features.

Reconnaissance geologic mapping was performed in the waste shaft sump. A vertical strip, approximately 5 feet wide, was cleaned and mapped along the entire length of the sump.

A detailed description of the geotechnical activities conducted in the waste shaft is contained in reference 6-2. The results of the mapping are shown in Appendix E, Figure E-1.

The geologic mapping and visual inspections of the SPDV ventilation/waste shaft has provided additional documentation of the strata above and below the WIPP underground development level. Based on the data obtained from the shaft mapping activities, a general characterization of the stratigraphy, lithology and structure of the geologic formations penetrated by the waste shaft was made.

The waste shaft penetrates five formations. In descending order, they are the Gatuna formation of Quaternary age, the Santa Rosa sandstone of Triassic age, and the Dewey Lake redbeds, Rustler formation and Salado formation, all of Permian age. In addition, the waste shaft also penetrates thin surficial Quaternary dune sands and the Mescalero caliche. In the WIPP site area, the Santa Rosa sandstone and the Gatuna formation are represented by thin layers of sandstone (ref. 6-3). They were not mapped in the waste shaft due to installation of the shaft collar facilities.

The results of the geologic mapping of the waste shaft correlate well with the SPDV ventilation shaft mapping results. The stratigraphic units penetrated by the waste shaft are the same as those encountered by the C & SH shaft.

Post-depositional dissolution features were not observed in any stratigraphic horizons in the waste shaft. Several zones previously identified as containing dissolution residues in borehole ERDA-9 are now considered to contain pronounced primary sedimentary features.

6.2.1.3 Exhaust Shaft

The exhaust shaft was enlarged from a 6-foot diameter raise-bored shaft to its finished 14- to 15-foot diameter using conventional drill and blast methods from July 1984 to January 1985. Geologic mapping of the shaft wall was conducted concurrently with excavation and construction activities.

Reconnaissance geologic mapping was performed along the entire length of the shaft with the exception of selected areas where detailed mapping was performed. A vertical strip, approximately 5 feet wide, was cleaned and mapped. The procedures used for the reconnaissance mapping are contained in reference 6-1.

Detailed circumferential mapping of specific areas of geologic interest was also performed. These areas included those previously described in the C & SH and waste shafts and four additional areas within the Dewey Lake redbeds, three of which contain gypsum filled fractures. The areas of detailed mapping in the exhaust shaft were:

(1) gypsum-filled fractures at a depth of 195.0 to 210.0 feet;
(2) gypsum-filled fractures at a depth of 269.0 to 280.5 feet;
(3) gypsum-filled fractures at a depth of 353.5 to 375.0 feet;
(4) the Dewey Lake/Rustler formation contact (546.4 feet);
(5) the Forty-niner member claystone (575.5 to 586.5 feet);
(6) the Magenta dolomite member (602.5 to 627.0 feet);
(7) the Tamarisk member claystone (689.0 to 695.5 feet);
(8) the Culebra dolomite member (713.5 to 736.0 feet);
(9) the upper portion of the unnamed lower member (736.0 to 800.0 feet); and
(10) the Rustler/Salado formation contact and key (845.0 to 912.0 feet).

The detailed geologic mapping was performed in a manner similar to that in the waste shaft, using a 5 x 5-foot grid. Vertical survey control was provided by the shaft excavation contractor. As the shaft liner was constructed, the depth to the base of each successive concrete segment was provided by the contractor. Vertical control for mapping was then established from the base of the previous segment. During excavation of the unlined section of the shaft, vertical control was established with survey chains suspended from contractor-installed survey control points.

The results of the exhaust shaft mapping are shown in Appendix F, Figure F-1. A detailed description of the geotechnical activities in the exhaust shaft are included in the report titled Geotechnical Activities in the Exhaust Shaft (ref. 6-4).

In general, the exhaust shaft mapping results correlate well with the results from the waste shaft. Slight lateral variations in the geology produce minor exceptions. The exhaust shaft geologic mapping activities have produced additional confirmation of data obtained from previous site investigations. This mapping confirms the suitability of the shaft reference design, with some minor modifications, based on the original design parameters.

#### 6.2.1.4 Drifts and Test Rooms

Geologic mapping of the drifts and test rooms was performed to characterize the facility level geology, demonstrate its continuity, and provide permanent documentation of the geology exposed in the underground excavations. Those drifts and rooms that were not mapped were visually inspected by site geologists to verify that the stratigraphy is laterally continuous and similar to that exposed in the mapped areas of the facility. No unusual geologic features were observed.

Geologic mapping was conducted in accordance with the procedures established in reference 6-1. A horizontal level-line referenced to

the C & SH shaft station floor elevation was established in the drifts and rooms using an engineer's tripod level. All stratigraphic contacts and geologic features were referenced to this level-line datum. Horizontal distances were measured with an engineer's tape using the C & SH shaft centerline as the zero reference point. Detailed mapping was performed at 10-foot intervals along one wall of the drifts. Between these intervals, the continuity of the stratigraphic contacts and the nature of the individual units were observed and noted on the map. The mapped drifts were the E140 drift, the E0 drift, the N1100 drift and the N1420 drift. Selected figures showing the megascopic results of this mapping are contained in Appendix B.

Geologic Mapping in the test rooms consisted of describing a 6- to 10-foot wide strip surrounding the instrument array in the center of each room. Both walls and the roof in each room were mapped. The remainder of the room was carefully inspected to confirm lateral continuity of the stratigraphic units. The strip maps from the test rooms are presented in Appendix G, Figures G-1 through G-4.

### 6.2.2 Core Drilling

#### 6.2.2.1 Purpose

Vertical core holes were drilled into the floor and roof of the underground openings to provide geologic information for design validation. The objectives of the vertical core holes are described in Supporting Document 3 of reference 2-5. The purpose of the program was discussed in Chapter 5 of this report.

#### 6.2.2.2 Summary of Drilling

A total of 124 vertical core holes have been drilled and logged in the underground drifts and in the SPDV test rooms, excluding those drilled as part of SNL's in situ tests. This number includes 16 holes drilled to replace holes that had poor core recovery and four holes drilled to obtain information on non-cored sections in the original holes. The

holes were generally drilled in pairs, one hole drilled vertically into the roof and one hole drilled vertically into the floor. Core was obtained in each hole to a nominal depth of 50 feet. Table 6-1 presents a summary of the core hole data. A map showing the core hole locations is presented on Figure 6-1. Geologic cross sections at selected core hole locations in the drifts are contained in Appendix H. Geologic drill logs of all of the core holes are contained in Appendix I.

Drilling was performed by the underground excavation contractor. The drill rig was set up by the driller and the attitude of the core hole was checked by site geotechnical personnel. Logging and handling of the core were performed by geotechnical personnel in conformance with the procedures outlined in Supporting Document 3 of reference 2-5.

All core holes were drilled using rotary equipment and compressed air or saturated brine as the circulating medium. The holes were drilled with a diamond impregnated bit which produced 2-inch or 2 3/8-inch diameter core. A 5-foot long double-tube or split double-tube core barrel was used to retain the core.

The core was logged underground as it was removed from the core barrel or after the drilling of the hole was completed. Logging was generally performed by the same geologist to maintain consistency in the descriptions of the geologic materials. The following data are recorded on each log:

(1) location of core hole and direction of drilling (up or down);
(2) beginning and completion dates of drilling;
(3) length and number of core run;
(4) amount and percentage of core recovery;
(5) stratigraphic and lithologic descriptions (color descriptions are based on the Geological Society of America (GSA) Rock-Color Chart);
(6) graphic lithologic profile; and

Table 6-1

SUMMARY OF CORE HOLE DATA



| Core Hole No. | Direction | Collar Elevation (ft-MSL) | Approximate Station (ft) | | Facility Coordinates (ft) | | Depth/ Penetration (ft) | Instrument Designation |
|---|---|---|---|---|---|---|---|---|
| MB-139-1 | Down | 1264.1 | N79 | W6 | N9766 | E6888 | 10.0 | None |
| MB-139-2 | Down | 1251.2 | S410 | E150 | N9277 | E7044 | 15.7 | None |
| MB-139-3 | Down | 1260.5 | S101 | E157 | N9586 | E7051 | 16.0 | None |
| MB-139-4 | Down | 1258.7 | S99 | W17 | N9588 | E6877 | 16.2 | None |
| DH-01 | Up | 1318.2 | N1424 | E439.5 | N11110.9 | E7335.5 | 50.8 | None |
| DH-02(1) | Down | | N1424 | E440 | N11110.9 | E7336.06 | 50.2 | None |
| DH-02A(1) | Down | | N1424 | E435 | N11110.9 | E7331.29 | 49.2 | None |
| DH-02B | Down | 1306.3 | N1424 | E442 | N11110.9 | E7331.29 | 53.0 | None |
| DH-03 | Up | 1318.1 | N1112 | E444 | N10799.2 | E7335.4 | 48.8 | None |
| DH-03A | Up | 1317.4 | N1112 | E450.5 | N10779.2 | E7341.92 | 49.9 | None |
| DH-04 | Down | 1309.6 | N1112.5 | E444 | N10799.2 | E7335.4 | 45.8 | None |
| DH-04A(1) | Down | 1309.6 | N1113 | E446 | | | 11.2 | None |
| DH-04B | Down | 1309.7 | N1112 | E450.5 | N10799.70 | E7341.85 | 51.4 | None |
| DH-05 | Up | 1329.9 | N1463 | E972 | N11149.6 | E7865.0 | 51.0 | None |
| DH-06 | Down | 1317.9 | N1463 | E972 | N11149.7 | E7864.9 | 49.75 | None |
| DH-07 | Up | 1326.7 | N1112 | E976.5 | N10799.3 | E7870.8 | 49.8 | None |
| DH-08 | Down | 1318.8 | N1112 | E976.5 | N10795.4 | E7870.9 | 36.3 | None |
| DH-08A(1) | Down | 1318.7 | N1112 | E975 | | | 50.7 | None |
| DH-08B | Down | 1318.0 | N1112 | E979.5 | N10799.47 | E7866.66 | 51.4 | None |
| DH-09 | Up | 1324.5 | N1432 | E1332.5 | N11108.71 | E8227.11 | 51.1 | None |
| DH-10 | Down | 1312.1 | N1432 | E1332.5 | N11106.70 | E8227.09 | 52.0 | None |
| DH-11 | Up | 1320.5 | N1112 | E1332.5 | N10799.8 | E8227.3 | 50.9 | None |
| DH-12 | Down | 1311.1 | N1112 | E1332.5 | N10799.4 | E8227.2 | 51.3 | None |
| DH-13 | Up | 1311.4 | N1424 | E1690 | N11112 | E8585 | 13.8 | None |
| DH-13A | Up | 1311.5 | N1424.5 | E1691 | N11112 | E8586 | 49.0 | None |
| DH-13B | Up | 1311.4 | N1425 | E1695 | N11112.6 | E8590.1 | 21.0 | None |
| DH-14 | Down | 1299.5 | N1425 | E1695 | N11112.6 | E8590.1 | 49.1 | None |
| DH-15 | Up | 1308.9 | N1104 | E1688.5 | N10793.26 | E8589.96 | 51.0 | None |
| DH-16 | Down | 1300.3 | N1104 | E1688 | N10792.89 | E8589.39 | 51.0 | None |
| DH-17 | Up | 1316.5 | N1427 | E178 | N11114.2 | E7071.8 | 52.0 | None |
| DH-18 | Down | 1305.1 | N1429 | E181 | N11114.2 | E7071.8 | 50.8 | None |
| DH-19 | Up | 1314.7 | N1107 | E206.5 | N10794.2 | E7101.7 | 51.6 | None |
| DH-20 | Down | 1306.2 | N1109 | E206 | N10794.2 | E7101.7 | 51.1 | None |
| DH-21 | Up | 1331.0 | N1421 | E786 | N11109.1 | E7680.9 | 50.4 | None |
| DH-22 | Down | 1318.8 | N1421.5 | E785.5 | N11109.2 | E7680.9 | 51.0 | None |
| DH-23 | Up | 1328.0 | N1112 | E781 | N10799.2 | E7679.9 | 51.0 | None |
| DH-24 | Down | 1319.5 | N1112 | E781 | N10799.2 | E7679.8 | 49.4 | None |
| DH-24A | Down | 1319.5 | N1112 | E780 | N10799.06 | E7678.59 | 50.4 | None |
| DH-25 | Up | 1318.8 | N1422 | E1510 | N11109.7 | E8403.8 | 51.8 | None |
| DH-26 | Down | 1307.2 | N1427 | E1510 | N11114.3 | E8403.8 | 53.0 | None |
| DH-27 | Up | 1300.8 | N1107 | W682 | N10793.7 | E6218.4 | 50.5 | None |
| DH-28 | Down | 1289.9 | N1107 | W682 | N10793.8 | E6218.3 | 50.5 | None |
| DH-29 | Up | 1298.3 | N1099 | W982 | N10785.4 | E5932.4 | 50.4 | None |
| DH-29A | Up | 1298.1 | N1099 | W987 | N10786.1 | E5927.3 | 35.0 | None |
| DH-30 | Down | 1289.2 | N1099 | W982 | N10785.5 | E5932.2 | 50.1 | None |
| DH-31 | Up | 1298.5 | N1099 | W1282 | N10784.9 | E5632.3 | 50.5 | None |
| DH-31A | Up | 1298.5 | N1099 | W1280 | N10784.8 | E5630.5 | 49.2 | None |
| DH-31B | Up | 1298.5± | N1099 | W1261 | N10786.7 | E5652.2 | 4.9 | None |
| DH-32 | Down | 1289.6 | N1099 | W1282 | N10784.9 | E5632.2 | 50.0 | None |
| DH-32A | Down | 1289.5 | N1099 | W1261 | N10786.7 | E5652.2 | 5.5 | None |
| DH-33 | Up | 1298.6 | N1099 | W1582 | N10786.0 | E5331.1 | 50.5 | None |
| DH-33A | Up | 1297.4 | N1099 | W1570 | N10786.8 | E5342.0 | 4.1 | None |
| DH-34 | Down | 1289.4 | N1099 | W1582 | N10786.5 | E5331.7 | 51.5 | None |
| DH-34A | Down | 1289.2 | N1099 | W1570 | N10786.8 | E5341.9 | 3.6 | None |
| DH-35 | Up | 1294.4 | N1102 | W1882 | N10789.4 | E5032.2 | 52.0 | None |
| DH-36 | Down | 1284.6 | N1102 | W1882 | N10789.4 | E5032.2 | 51.5 | None |
| DH-37 | Up | 1297.4 | N1101 | W2182 | N10788.9 | E4732.0 | 51.5 | None |
| DH-38 | Down | 1287.0 | N1101 | W2182 | N10788.8 | E4731.9 | 47.5 | None |
| DH-39 | Up | 1296.0 | N1101 | W2482 | N10789.2 | E4430.7 | 50.7 | None |
| DH-40 | Down | 1286.1 | N1101 | W2482 | N10789.2 | E4431.0 | 51.0 | None |
| DH-41 | Up | 1295.8 | N1101 | W2782 | N10789.0 | E4132.6 | 49.9 | None |
| DH-42 | Down | 1285.9 | N1101 | W2782 | N10789.0 | E4132.4 | 51.2 | None |
| DH-42A | Down | 1285.7 | N1101 | W2789 | N10789.2 | E4125.5 | 40.5 | None |

(1) Survey data not available.

Table 6-1 (continued)

SUMMARY OF CORE HOLE DATA



| Core Hole No. | Direction | Collar Elevation (ft-MSL) | Approximate Station (ft) | | Facility Coordinates (ft) | | Depth/ Penetration (ft) | Instrument Designation |
|---|---|---|---|---|---|---|---|---|
| DH-207 | Up | 1259.8 | S697 | E155 | N8989.7 | E7049.1 | 53.0 | GE-246 |
| DH-208 | Down | 1251.6 | S698 | E150 | N8968.8 | E7044.0 | 49.2 | None |
| DH-211 | Up | 1270.5 | S1320 | E163 | N8366.5 | E7057.1 | 50.0 | None |
| DH-212 | Down | 1261.7 | S1320 | E163 | N8366.5 | E7057.1 | 52.1 | None |
| DH-215 | Up | 1272.0 | S1960 | E153 | N7727.2 | E7046.9 | 52.0 | GE-247 |
| DH-216 | Down | 1262.6 | S1960 | E153 | N7727.2 | E7046.9 | 54.2 | GE-248 |
| DH-219 | Up | 1266.3 | S2422 | E162 | N7264.9 | E7056.6 | 51.0 | None |
| DH-219A | Up | 1266.1 | S2418 | E162 | N7268.5 | E7056.2 | 11.3 | None |
| DH-220 | Down | 1257.4 | S2421 | E162 | N7255.5 | E7055.9 | 51.8 | None |
| DH-223 | Up | 1255.1 | S3079 | E154 | N6607.2 | E7048.5 | 52.6 | GE-249 |
| DH-224 | Down | 1246.6 | S3079 | E154 | N6607.5 | E7048.5 | 52.5 | None |
| DH-227 | Up | 1247.0 | S3656 | E147 | N6030.7 | E7041.2 | 51.7 | None |
| DH-228 | Down | 1237.8 | S3656 | E147 | N6030.7 | E7041.2 | 50.4 | None |
| DH-301 | Up | 1276.9 | N150 | W170 | N9830.5 | E6724.5 | 50.75 | None |
| DH-302 | Down | 1264.9 | N150 | W170 | N9830.5 | E6724.5 | 50.6 | None |
| DH-303 | Up | 1267.2 | S400 | W170 | N9282.3 | E6726.1 | 51.4 | None |
| DH-304 | Down | 1254.3 | S400 | W170 | N9282.5 | E6726.1 | 50.5 | None |
| DH-306 | Down | 1244.1 | S400 | E140 | N9287.3 | E7049.9 | 52.0 | None |
| DH-306A | Down | 1244.0 | S400 | E125 | N9287.9 | E7034.6 | 6.5 | None |
| DH-307 | Up | 1262.6 | S400 | E300 | N9286.7 | E7194.2 | 52.0 | GE-263 |
| DH-309 | Up | 1259.8 | S700 | E220 | N8987.1 | E7123.0 | 52.3 | GE-265 |
| DH-311 | Up | 1264.4 | S1000 | E300 | N8686.3 | E7194.9 | 52.0 | GE-264 |
| DH-313 | Up | 1270.6 | S1300 | E300 | N8385.9 | E7190.6 | 19.6 | None |
| DH-313A | Up | 1270.9 | S1300 | E299 | N8386.6 | E7189.5 | 50.2 | None |
| DH-314 | Down | 1258.3 | S1300 | E300 | N8386.5 | E7189.5 | 50.75 | None |
| DH-315 | Up | 1272.1 | S1300 | W170 | N8387.3 | E6725.5 | 50.3 | None |
| DH-316 | Down | 1259.9 | S1300 | W170 | N8387.2 | E6725.3 | 50.1 | None |
| DH-317 | Up | 1271.3 | S1600 | W33 | N8077.4 | E6875.9 | 50.1 | None |
| DH-317A | Up | 1271.2 | S1600 | W30 | N8077.5 | E6879.5 | 5.0 | None |
| DH-317B | Up | 1271.2 | S1597 | W30 | N8080.3 | E6881.0 | 51.0 | None |
| DH-318 | Down | 1258.5 | S1600 | W30 | N8077.3 | E6876.1 | 50.0 | None |
| DH-319 | Up | 1260.0 | S700 | E300 | N8988.1 | E7191.6 | 51.05 | None |
| DH-321 | Up | 1261.4 | S400 | E0 | N9792.0 | E6891.8 | 52.0 | GE-268 |
| DH-323 | Up | 1261.2 | S400 | E55 | N9291.7 | E6952.5 | 52.5 | GE-267 |
| DO-45 | Up | 1285.5 | N254 | E147 | N9941.0 | E7041.3 | 52.4 | GE-230 |
| DO-46 | Down | 1276.5* | N254 | E147 | N9941.0 | E7041.3 | 51.5 | None |
| DO-52 | Up | 1280.4 | N146 | W4 | N9832.5 | E6890.5 | 51.6 | GE-226 |
| DO-53 | Down | 1266.6 | N146 | W4 | N9832.5 | E6890.5 | 49.2 | None |
| DO-56 | Up | 1296.8 | N621 | E0 | N10311.8 | E6892.3 | 52.1 | GE-234 |
| DO-57 | Down | 1288.1 | N621 | E0 | N10311.8 | E6892.4 | 52.1 | None |
| DO-63 | Up | 1310.6 | N1110 | E0 | N10796.0 | E6891.9 | 52.8 | GE-243 |
| DO-64 | Down | 1301.5 | N1110 | E0 | N10796.0 | E6891.6 | 52.8 | GE-221 |
| DO-67 | Down | 1296.8 | N1265 | W231.5 | N10952.1 | E6662.9 | 51.7 | GE-220 |
| DO-69 | Up | 1310.1 | N1265 | W231.5 | N10951.9 | E6662.5 | 51.4 | GE-218 |
| DO-77 | Down | 1294.6 | N1270 | W364.5 | N10962.5 | E6529.6 | 53.4 | GE-216 |
| DO-79 | Up | 1307.7 | N1270 | W364.5 | N10962.6 | E6529.5 | 51.8 | GE-214 |
| DO-88 | Up | 1305.9 | N1265 | W497.5 | N10952.8 | E6396.5 | 52.7 | GE-212 |
| DO-90 | Down | 1292.1 | N1265 | W497.5 | N10952.6 | E6396.4 | 53.6 | GE-210 |
| DO-91 | Down | 1292.1 | N1275 | W630.5 | N10961.5 | E6263.9 | 51.8 | GE-209 |
| DO-93 | Up | 1304.9 | N1275 | W630.5 | N10961.1 | E6263.9 | 52.0 | GE-207 |
| DO-201 | Up | 1262.2 | S406 | W19 | N9280.6 | E6874.9 | 51.7 | None |
| DO-202 | Down | 1248.6 | S406 | W19 | N9280.6 | E6874.9 | 51.4 | None |
| DO-203 | Up | 1298.2 | N624 | E140 | N10308.6 | E7041.7 | 52.0 | GE-235 |
| DO-204 | Down | 1290.5 | N640 | E140 | N10308.5 | E7041.5 | 51.6 | None |
| DO-205 | Up | 1316.5 | N1410 | E0 | N11095 | E6892 | 50.7 | None |
| DO-206 | Down | 1306.0 | N1410 | E0 | N11095 | E6892 | 50.6 | None |
| DO-229 | Up | 1259.8 | S401 | E153 | N9287 | E7049 | 50.6 | None |
| OH-9 | Up | 1310 | N1433 | W231.5 | N11125.6 | E6662.9 | 15.4 | None |
| OH-11 | Up | 1308 | N1433 | W364.5 | N11125.6 | E6529.6 | 19.7 | None |
| OH-13 | Down | 1298 | N1433 | W231.5 | N11125.6 | E6662.9 | 9.5 | None |
| OH-14 | Down | 1296 | N1433 | W364.5 | N11125.6 | E6529.6 | 9.7 | None |

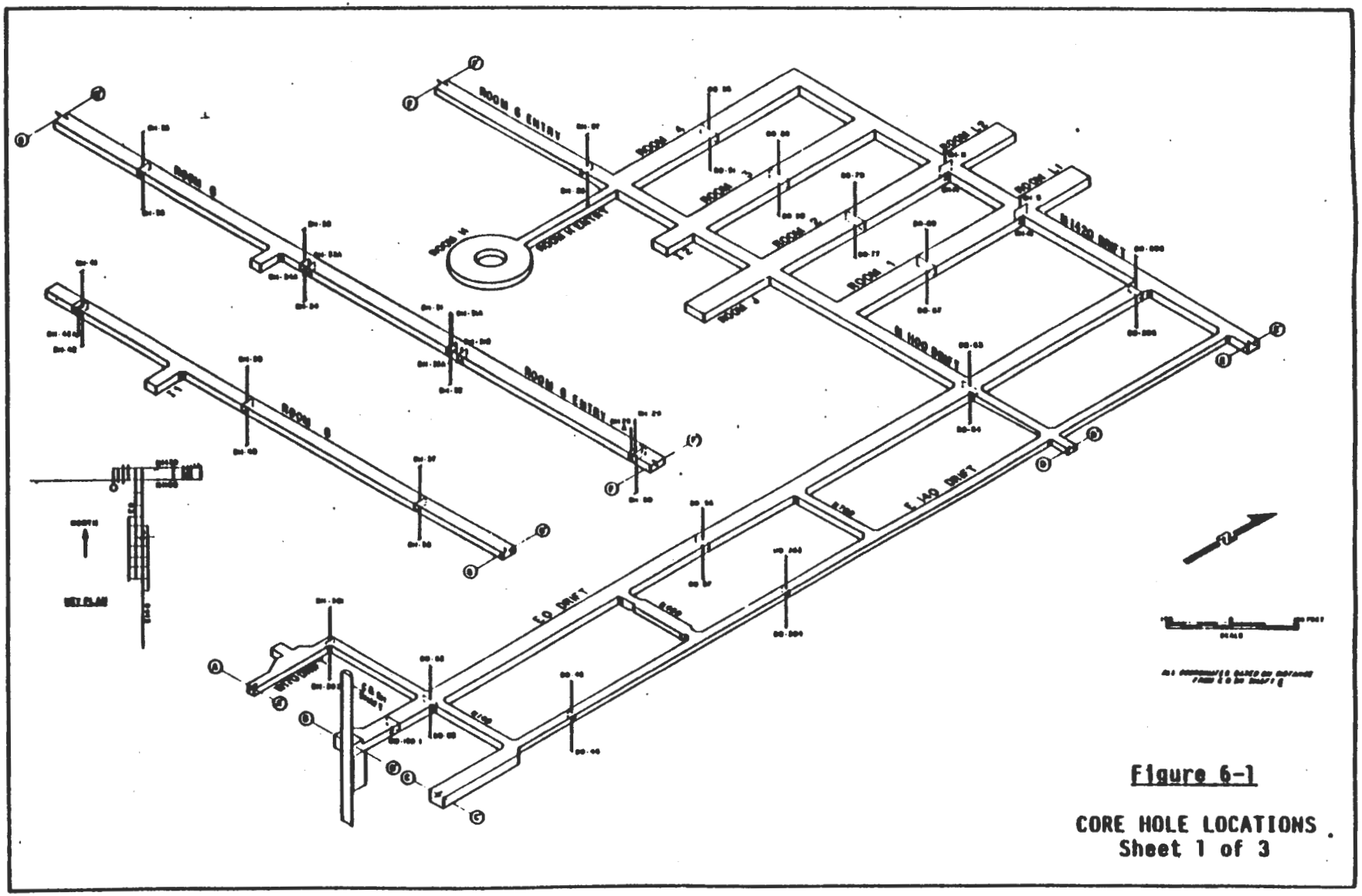


Figure 6-1

CORE HOLE LOCATIONS
Sheet 1 of 3

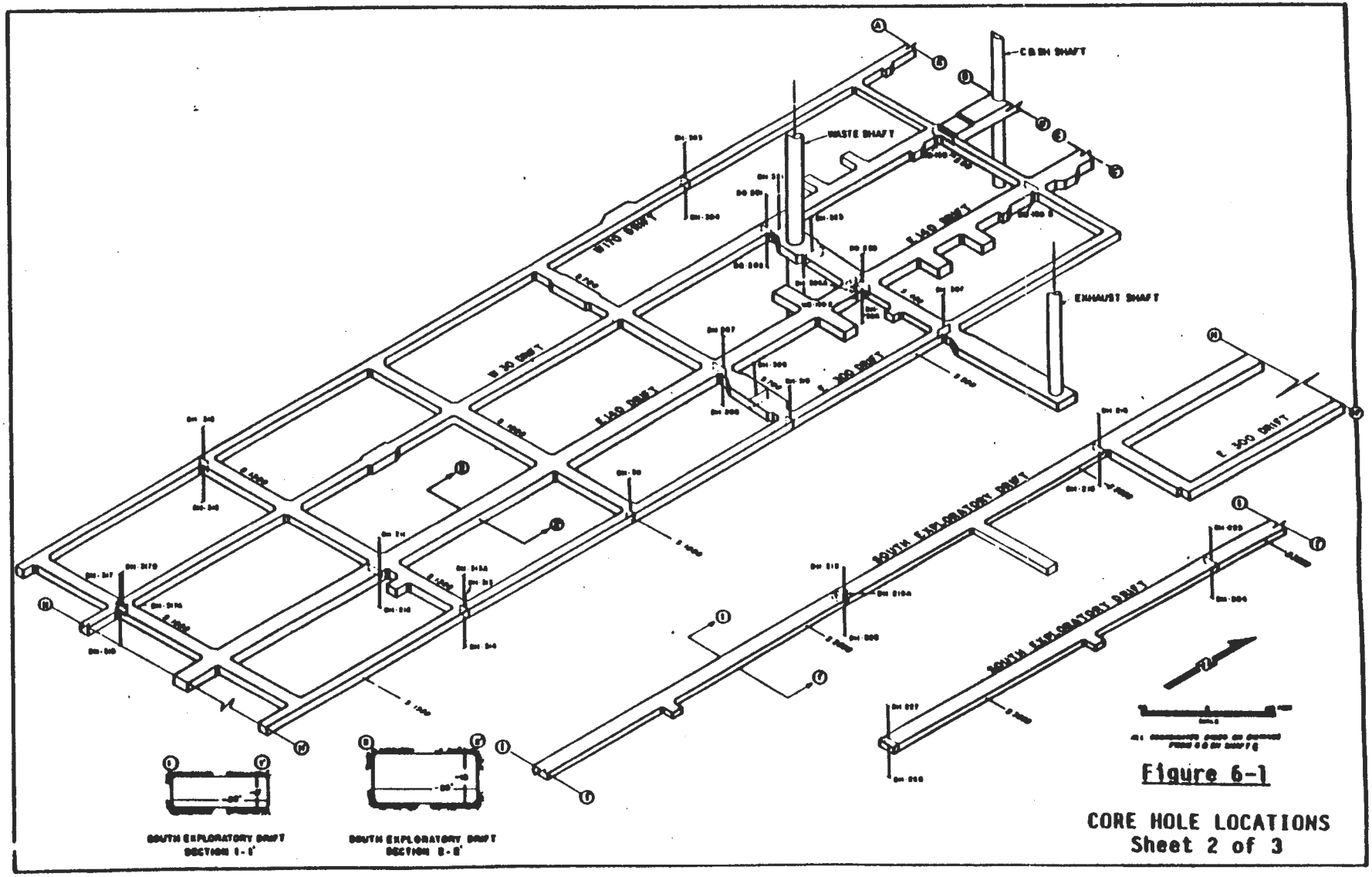


Figure 6-1

CORE HOLE LOCATIONS
Sheet 2 of 3

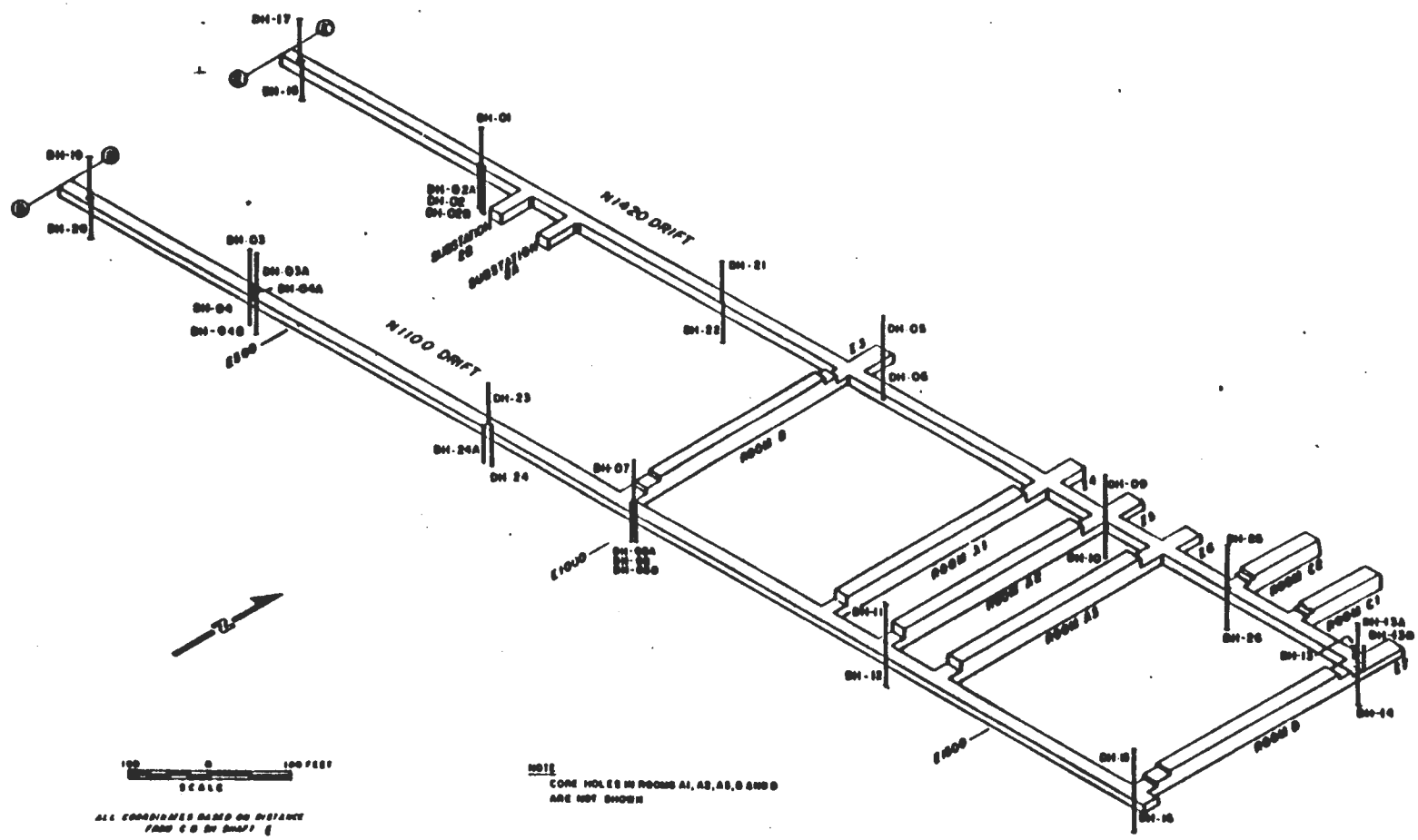
N1100 DRIFT
N1200 DRIFT
SUBSTATION 20
SUBSTATION 21
ROOM B
ROOM A1
ROOM A2
ROOM A3
ROOM C2
ROOM C1
ROOM D
DH-17
DH-18
DH-19
DH-20
DH-01
DH-02A
DH-02
DH-02B
DH-03
DH-03A
DH-04A
DH-04
DH-04B
DH-21
DH-22
DH-05
DH-06
DH-23
DH-24A
DH 24
DH-07
DH-08A
DH-08
DH-08B
DH-09
DH-10
DH-11
DH-12
DH-25
DH-26
DH-13
DH-13A
DH-13B
DH-14
DH-15
E5
E6
E7
E8
E9
E10
E11
E12
E13
E14
E15
E16
E17
E18
E19
E20
E21
E22
E23
E24
E25
E26
E27
E28
E29
E30
E31
E32
E33
E34
E35
E36
E37
E38
E39
E40
E41
E42
E43
E44

(7) other pertinent information related to core conditions and observations made during drilling.

Included on the logs of many of the core holes is a core sample reference number for each distinguishable stratigraphic unit (except anhydrite). This number (in some cases several numbers) is shown in brackets at the end of the unit description. The number identifies a specific core sample that has undergone a laboratory analysis to determine its percentage of insolubles (clay/polyhalite). A listing of the reference core samples and their laboratory test results for insoluble residues are presented in Table 6-2. The reference sample system was used to provide uniformity in the logging of the core and to facilitate the comparison of unit descriptions with samples having a known insoluble content. The sample number or numbers which appear on the log are those which are visually most similar to the overall unit. The crystal size in the reference samples may not be the same as in the units with which they are correlated.

Each box of core was photographed and then stored in the WIPP core library. After data from several of the core holes was collected, correlations between the holes were developed.

6.2.2.3 Summary of Results

The underground core drilling program has demonstrated the lateral continuity of stratigraphy throughout the underground facility horizon. Three anhydrite units were identified in the upholes and two anhydrite units were identified in the downholes. These units are consistently underlain by clay seams. In addition, a clay seam designated clay I was found in most of the upholes and a clay seam designated clay D was found in many of the downholes. Anhydrite is commonly associated with these two seams. The remaining units consist of halite with varying amounts of argillaceous material and polyhalite. Individual units vary slightly from hole to hole in thickness, crystal size, and the percentage of accessory constituents such as argillaceous material and polyhalite. The stratigraphy

Table 6-2

INSOLUBLE RESIDUES OF REFERENCE CORE SAMPLES
SANDIA NATIONAL LABORATORIES

| Reference Sample Number | Hole Number | Depth Interval (feet) | Water-Insoluble | | | EDTA-Insoluble (1) | | |
|---|---|---|---|---|---|---|---|---|
| | | | Sample Weight (grams) | Residue Weight (grams) | Percent Weight | Sample Weight (grams) | Residue Weight (grams) | Percent Weight |
| 1 | DO-52 | 9.0 - 9.7 | 451.09 | 0.03 | 0.01 | | | |
| 2 | DO-52 | 39.4 - 40.0 | 336.10 | 0.11 | 0.03 | | | |
| 3 | DO-52 | 14.3 - 15.0 | 415.57 | 2.15 | 0.52 | 1.61 | 0.72 | 44.72 |
| 4 | DO-53 | 14.1 - 14.5 | 251.72 | 0.40 | 0.16 | 0.36 | 0.14 | 38.89(2) |
| 5 | DO-53 | 4.0 - 4.3 | 206.53 | 1.28 | 0.62 | 0.80 | 0.28 | 35.00(2) |
| 6 | DO-53 | 23.7 - 24.1 | 155.36 | 1.26 | 0.81 | 0.96 | 0.59 | 61.46 |
| 7(3) | DH-48 | 18.0 - 18.35 | | | 0.22 | | | |
| 8 | DO-52 | 2.0 - 2.75 | 436.67 | 2.16 | 0.49 | 1.32 | 0.91 | 68.94 |
| 9(3) | DH-12 | 28.15- 28.6 | | | 0.75 | | | 57.1 |
| 10(3) | DH-11 | 46.5 - 46.9 | | | 3.85 | | | 39.2 |
| 11(3) | DH-12 | 50.05- 50.4 | | | | | | |
| 12(3) | DH-11 | 32.8 - 33.35 | | | 2.36 | | | 50.0 |
| 13 | DO-53 | 36.1 - 36.7 | 364.13 | 1.89 | 0.52 | 1.47 | 1.17 | 79.59 |
| 14 | DO-52 | 42.6 - 43.5 | 543.62 | 17.97 | 3.31 | 5.13 | 4.58 | 89.28 |
| 15 | DO-52 | 33.8 - 34.7 | 538.73 | 20.28 | 3.76 | 5.05 | 3.98 | 78.81 |
| 16 | DO-52 | 48.7 - 49.2 | 315.06 | 16.59 | 5.27 | 5.31 | 4.33 | 81.54 |
| 17(3) | DH-10 | 43.3 - 43.6 | | | 0.52 | | | 49.2 |

Notes:

(1) For description of sample preparation see Results of Site Validation Experiments, Waste Isolation Pilot Plant (WIPP) Project, Southeastern New Mexico, Section 5.4 (ref. 2-5).

(2) Small sample volume may have produced inaccurate result.

(3) Reference sample used for visual comparison is identical to the sample tested in the laboratory, but is from different interval within the same unit.

encountered in the core holes was used to prepare the reference stratigraphic column discussed in subsection 6.3.1.3.

The presence of any gas or brine detected during drilling is recorded on the drill logs. Usually within 2 weeks of completing an air-drilled uphole, brine weeps or moisture halos appear at the collar of the hole. Brine has also collected in some downholes which were dry during drilling. Observations of gas and brine occurrences are discussed in the following subsection.

### 6.2.3 Fluid Measurements

#### 6.2.3.1 General Description

Ground-water inflow measurements were taken in both the SPDV exploratory and ventilation shafts as part of the geologic field activities for the SPDV Program. In addition, measurements in the waste shaft and exhaust shaft were taken as part of design validation. Gas and brine have been encountered in boreholes and at excavation faces in the facility level drifts and rooms. Studies are being performed by other WIPP project participants to further investigate and evaluate these occurrences.

#### 6.2.3.2 C & SH Shaft

Measurements of fluid inflow were taken during the SPDV exploratory shaft drilling operation when the drill tools were out of the hole for a bit change. The measurements were taken by monitoring changes in the drilling fluid level over a period of several hours. These data were then used to estimate approximate ground-water flow rates into the shaft.

#### 6.2.3.3 Waste Shaft

Ground-water inflow measurements were taken in the 6-foot diameter SPDV ventilation shaft during shaft outfitting. These measurements were taken in the shaft sump and at the base of the Rustler formation. The measurements in the shaft sump were used to determine total flow into

the shaft from all ground-water sources penetrated. Periodic measurements to determine water level rise with respect to a known point at the top of the sump were obtained during test intervals ranging from about 1.5 to 90 hours. The data obtained from these measurements were used to calculate approximate ground-water flow rates into the shaft ranging from 0.3 to 0.9 gallons per minute (gpm). The average flow rate was determined to be about 0.6 gpm.

An attempt to measure ground-water inflow from the rock strata above the Salado formation was only partially successful. A collection system to retain ground-water inflow was constructed at the base of the Rustler formation by placing plastic sheeting across the shaft and attaching it to the wall. The quantity of water collected in the sheeting and drained into a graduated container was calculated to accumulate at a rate of approximately 0.3 to 0.4 gpm from all sources above the Salado formation.

No direct inflow from the Magenta or Culebra dolomite members or at the Rustler/Salado formation contact was measured. The Magenta dolomite did not exhibit measurable flow. Ground water from this member resulted in the wetting of the wall below the dolomite for a distance of about 20 feet. Below this distance the shaft wall was essentially dry. Therefore, it was concluded that the Magenta was making no contribution to the collection system at the base of the Rustler formation. Visual inspection of the Rustler/Salado formation contact, and shaft wall conditions immediately above and below this contact, suggested that the zone was making little, if any, contribution to the water accumulating in the sump. Based on these results, it was concluded that the Culebra dolomite member was contributing the majority of ground water reaching the SPDV ventilation shaft sump.

The 6-foot diameter SPDV ventilation shaft was later enlarged to become the waste shaft for the WIPP facility. Of the three formations observed during geologic mapping activities in the enlarged shaft, only the Magenta and Culebra dolomite members of the Rustler formation were

obvious fluid-bearing zones. The Magenta exhibited only a few weeps and generally produced very little water. The entire Culebra section, however, was wet, but no obvious local concentrations of water inflow were observed. Wherever a ledge was present, a steady dripping of water occurred. The Rustler/Salado formation contact, often considered a fluid-producing zone, did not contain any observable fluid except for some dampness around rock bolts.

After the waste shaft liner was constructed, ground water was observed seeping through cracks and construction joints in it. These observations are discussed in Chapter 8, subsection 8.3.1.1.

#### 6.2.3.4 Exhaust Shaft

A water inflow measurement of approximately 0.4 gpm into the 7 7/8-inch diameter pilot hole for the exhaust shaft was taken on December 1, 1983. On December 21, 1983, a water inflow of 0.47 gpm was measured after the pilot hole was enlarged to 11 inches in diameter.

After the shaft was excavated to its finished dimensions, water inflow through cracks and construction joints in the liner was measured. Measurement was made from the 2-inch drainpipe that connects the three water collection rings in the shaft. The measured flow was 0.35 gpm in January 1985. A grouting program, conducted in June and July 1985 within the lined section of the shaft, reduced this inflow to a non-measurable quantity.

#### 6.2.3.5 Drifts and Test Rooms

Small amounts of gas under pressure have been encountered by some underground boreholes and at the working face of underground horizontal excavations. Brine is observed to weep locally from walls and into some boreholes. The brine occurrences are visible during or immediately after excavation or drilling and remain moist or produce fluid for a period of from several weeks to more than 3 years. The formation of salt blisters on walls and salt straws and precipitate at

hole collars are common. Salt incrustations forming on the roof are being monitored at three locations: W30/S1600, E140/S2190 and E140/S2740.

The gas occurrences encounterd by boreholes are indicated on the geologic drill logs. Pressure transient testing and gas sampling were performed in several holes in the roof and floor of the facility as reported in reference 4-11. Only two occurrences of gas at the working face were documented prior to the end of December 1985. In both cases, degassing could be heard at the face for short periods of time.

The locations of major weeps occurring on walls that were geologically mapped are indicated on the maps and a discussion of their occurrence and structure is presented in reference 4-10. Sampling of brine from weeps for chemical analysis is currently being conducted. A preliminary inventory of brine occurrences at accessible locations is presented in reference 4-15.

The flow of gas from monitored holes has been low and erratic. It appears to be associated with clay seams or a result of fracture permeability in anhydrite beds. The spatial distribution of brine occurrences is also undefined. Although very few weeps have been observed on the roof surface, boreholes in the roof sometimes weep brine. The amount and duration of flow from boreholes and wall areas varies considerably. Based on observations made during preliminary gas testing, the brine appears to be associated primarily with anhydrite beds and their underlying clay seams. However, brine can also weep directly from halitic units, as observed on the walls and roof of drifts and in the drum durability test pit in Room J.

Two program plans have been developed to investigate gas and brine occurrences in the WIPP underground facility. The programs will investigate the origin, migration, volume and composition of the occurrences. Work on the Brine Testing Program (BTP) is presently

being conducted and will continue through 1987. The Gas Testing Program (GTP) is also currently in progress.

As part of the BTP, 36 accessible boreholes containing brine have been monitored. These holes include the shallow holes for the Material Interface-Interactions Test (MIIT) in Room J, inclinometer holes in Test Rooms 1 and 2 (51X-IG-00201 and 51X-IG-00202), an abandoned stressmeter hole (51X-NG-00252) in Test Room 2, hole L1-X00 in Room L1, nine stratigraphic core holes in Room G (DH-35 through DH-42A), and eight stratigraphic core holes in experimental Rooms A1, A2, A3 and B (A1X01, A1X02, A2X01, A2X02, A3X01, A3X02, BX01 and BX02). The static level of any brine in the holes is measured and recorded on a regular basis. The brine is then evacuated from the hole and its volume measured.

The BTP monitoring of brine occurrences in the MIIT holes in Room J was suspended at the end of April 1985 due to interference with experimental activities in the room. Monitoring of the remainder of the boreholes listed above continues. As new monitoring locations for the BTP are identified, they will be added to the program.

An inventory of all boreholes drilled in the underground facility has been assembled. Data contained in the inventory include hole location, diameter, depth, present status, drilling fluid used, and any observations on the occurrence of gas or brine. Over 1400 holes are presently listed, most of which contain geomechanical instruments or are otherwise inaccessible. The list will be used to locate accessible boreholes that may be suitable for use in the gas and brine testing programs.

## 6.3 DESCRIPTION OF FACILITY GEOLOGY

### 6.3.1 Stratigraphy

The stratigraphy within the WIPP underground facility horizon has been determined through vertical core hole drilling and geologic mapping of

the excavation walls. A description of the generalized stratigraphy and evidence for stratigraphic continuity is presented in the following subsections. Figures showing the stratigraphy within the WIPP underground facility horizon are presented in Appendix B.

#### 6.3.1.1 Generalized Stratigraphy

The WIPP underground facility horizon consists primarily of halite containing varying amounts of polyhalite and clay. This halite is interrupted by 5 anhydrite beds, 12 clay seams and 6 argillaceous layers. Figure 6-2 contains a generalized stratigraphic column showing the relationship of these materials. Detailed descriptions of the individual units (except clay seams) are presented in Table 6-3. Figure 6-3 shows the individual clay seams and their descriptions.

Because of the difference in the behavior of halite and anhydrite, the five anhydrite beds represent significant boundaries above and below the horizontal underground openings. Three of the beds, abouth 1 1/2 to 12 inches thick, occur approximately 7, 14 and 35 feet above the roof of the storage level drifts and rooms. The remaining two beds occur beneath the floor of the drifts and rooms. The most significant of these two beds is MB-139 which occurs approximately 3 1/2 to 4 1/2 feet below the floor of the storage level and varies from 2.5 to 4 feet in thickness. The remaining bed occurs about 32 feet below the storage level and is approximately 4 inches thick. Thin clay seams underlie all of the anhydrite beds.

Fifteen lithologic units have been identified during geologic mapping within the facility level drifts, rooms and waste experimental area. The majority of these units are halite containing varying amounts of polyhalite and argillaceous material, usually less than 2 percent. The remaining units consist of 2 anhydrite beds, 2 argillaceious halite units and 1 polyhalitic halite unit. Each of the 15 mapped units has been assigned a numerical designation as shown on Figure 6-2 and contained in Table 6-3.

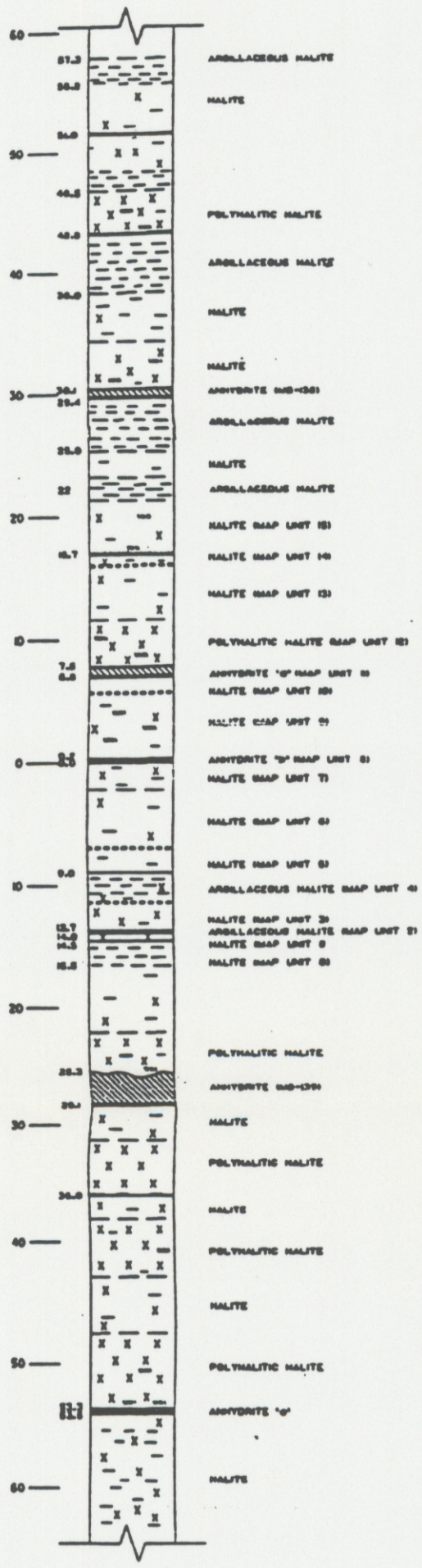


(SEE TABLE 6-3 FOR DETAILED DESCRIPTIONS OF UNITS)

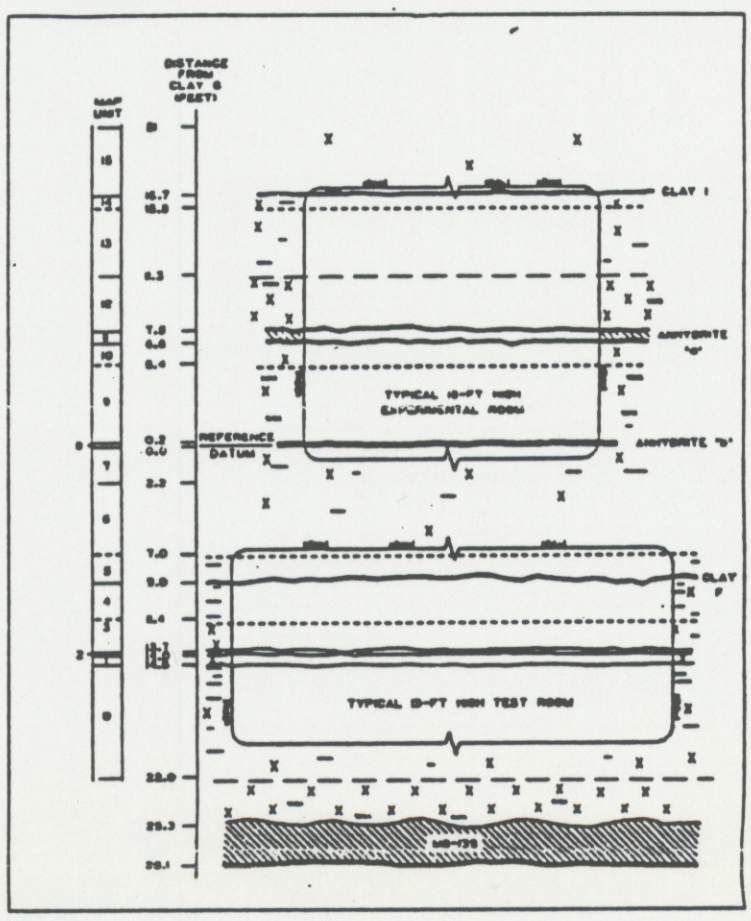


## EXPLANATION

ROCK TYPE

HALITE — ANHYDRITE — POLYHALITIC HALITE — ARGILLACEOUS HALITE

ACCESSORY CONSTITUENTS

POLYHALITE — LAMINAR FEATURES: CLAY SEAM (MM OR CM THICK) — ARGILLACEOUS MATERIAL — ANHYDRITE STRINGERS

LITHOLOGIC CONTACTS

SHARP (IDENTIFIABLE WITHIN 0.05 FT.) — GRADATIONAL (IDENTIFIABLE WITHIN 0.05 TO 0.5 FT.) — DIFFUSE (IDENTIFIABLE WITHIN 0.5 TO 5.0 FT.)

**NOTES:**

1. DISTANCES ARE MEASURED FROM THE BASE OF ANHYDRITE "B" (CLAY G) AND ARE AVERAGED FROM REPRESENTATIVE CORE HOLE LOGS, SHAFT AND TEST ROOM MAPPING. ACTUAL DISTANCES AND UNIT THICKNESSES MAY VARY LOCALLY FROM THOSE SHOWN.
2. DESCRIPTIONS OF UNITS ARE BASED ON CORE HOLE DATA, SHAFT MAPPING AND VISUAL INSPECTION OF EXPOSURES IN UNDERGROUND DRIFTS AND ROOMS.
3. DETAILED DESCRIPTIONS OF CLAY SEAMS ARE PRESENTED ON FIGURE 6-4.
4. PERCENTAGES OF ARGILLACEOUS MATERIAL AND POLYHALITE ARE BASED ON VISUAL ESTIMATES FROM EXAMINATION OF DRILL CORE AND EXPOSURES IN THE UNDERGROUND EXCAVATIONS. SANDIA NATIONAL LABORATORIES' MEASUREMENTS OF INSOLUBLES FROM SELECTED CORE WERE USED AS A POINT OF REFERENCE.

**Figure 6-2**

**WIPP GENERALIZED STRATIGRAPHIC COLUMN**

Table 6-3

DESCRIPTION OF GENERALIZED STRATIGRAPHY



| Approximate Distance From Clay G (Ft) | Stratigraphic Unit | Description* |
|---|---|---|
| 55.2 to 57.3 | Argillaceous halite | Clear to moderate brown, medium to coarsely crystalline. <1 to 3% brown clay. Intercrystalline and discontinuous breaks. In one core hole, consists of a 1 in. thick clay seam. Unit can vary up to 4 ft thickness. Contact with lower unit is gradational. |
| 46.5 to 55.2 | Halite | Clear to moderate reddish orange and moderate brown, coarsely crystalline, some medium. ≤1% brown clay, locally argillaceous (clays M-1 and M-2). Scattered anhydrite stringers locally. |
| 42.8 to 46.5 | Polyhalitic halite | Clear to moderate reddish orange, some moderate brown, coarsely crystalline. <1 to 3% polyhalite. None to 1% brown and some gray clay. Scattered anhydrite locally. Contact with unit below is fairly sharp. |
| 38.0 to 42.8 | Argillaceous halite | Clear to moderate brown, medium to coarsely crystalline, some fine. <1 to 5% brown clay. Locally contains 10% clay. Intercrystalline and scattered breaks. Locally contains partings and seams. Contact with lower unit is gradational based on increased clay content. Average range of unit is 38.0 to 42.8 ft above clay G but does vary from 33.8 to 46 ft. |
| 34.0 to 38.0 | Halite | Clear to moderate brown, some moderate reddish brown, coarsely crystalline, some fine and medium. ≤1% brown clay, trace gray clay locally. Scattered breaks. Locally argillaceous. <1% polyhalite. Contact with unit below is gradational based on clay and polyhalite content. |
| 30.1 to 34.0 | Halite | Clear to moderate reddish orange, coarsely crystalline. <1 to 3% polyhalite. Commonly polyhalitic. Scattered anhydrite stringers with anhydrite layers up to 1/2 in. thick locally. Scattered brown clay locally. Contact with MB-138 below is sharp. |
| 29.4 to 30.1 | Anhydrite (MB-138) | Light to medium gray, microcrystalline. Partly laminated. Scattered halite growths. Clays seam K found at base of unit. |
| 25.0 to 29.4 | Argillaceous halite | Clear to moderate brown, some light moderate reddish orange. Medium to coarsely crystalline. <1 to 3% brown clay, some gray. Locally up to 5% clay. Clay is intercrystalline with scattered breaks and partings present. < 1/2% dispersed polyhalite. Contact with lower unit is gradational based on clay content. Upper contact is sharp with clay K. |
| 23.0 to 25.0 | Halite | Clear, some light moderate brown, coarsely crystalline. <1/2% brown clay. Contact with clay J below varies from sharp to gradational depending if clay J is a distinct seam or merely an argillaceous zone. |
| 21.0 to 23.0 | Argillaceous halite | Usually consists of scattered breaks or argillaceous zone containing <1 to 3% brown clay. In C & SH shaft, it is a 1/2 in. thick brown clay seam. |
| 16.7 to 21.0 | Halite (Map Unit 15) | Clear, coarsely crystalline, scattered medium. None to <1% dispersed polyhalite and brown clay. Scattered anhydrite. Lower contact is sharp with clay I. |
| 15.8 to 16.7 | Halite (Map Unit 14) | Clear to grayish orange-pink, coarsely crystalline, some medium. <1/2% dispersed polyhalite. Scattered discontinuous gray clay stringers. Clay I is along upper contact. Contact with lower unit is diffuse. |
| 11.5 to 15.8 | Halite (Map Unit 13) | Clear to moderate reddish orange and moderate brown, medium to coarsely crystalline, some fine. ≤1% brown clay, locally up to 3%. Trace of gray clay. Scattered discontinuous breaks. <1% dispersed polyhalite and polyhalite blebs. Contact with unit below is gradational based on clay and polyhalite content. |

Table 6-3 (continued)

DESCRIPTION OF GENERALIZED STRATIGRAPHY



| Approximate Distance From Clay G (Ft) | Stratigraphic Unit | Description* |
|---|---|---|
| 7.5 to 11.5 | Polyhalitic halite (Map Unit 12) | Clear to moderate reddish orange, coarsely crystalline. <1 to 3% dispersed polyhalite and polyhalite blebs. Scattered anhydrite stringers. Contact is sharp with unit below. |
| 6.8 to 7.5 | Anhydrite "a" (Map Unit 11) | Light to medium gray, light brownish gray and sometimes light moderate reddish orange. Microcrystalline. Halite growths within. Partly laminated. Clear, coarsely crystalline halite layer, up to 2 in. wide, found within exposures in waste experimental area. Thin gray clay seam H at base of unit. |
| 5.5 to 6.8 | Halite (Map Unit 10) | Clear to moderate reddish orange/brown, fine to coarsely crystalline. <1% brown and/or gray clay and dispersed polyhalite. Discontinuous clay stringers locally. Contact with lower unit is diffuse based on crystal size and varying amounts of clay and polyhalite. |
| 0.2 to 5.5 | Halite (Map Unit 9) | Clear to light moderately reddish orange, coarsely crystalline, some medium. None to <1% polyhalite. Trace of gray clay locally. Scattered anhydrite stringers. Contact with unit below is sharp. |
| 0.0 to 0.2 | Anhydrite "b" (Map Unit 8) | Light to medium gray, microcrystalline anhydrite. Scattered halite growths. Thin gray clay seam G at base of unit. |
| 0.0 to -2.2 | Halite (Map Unit 7) | Clean to light/medium gray, some moderate reddish orange/brown. Coarsely crystalline, some fine and medium. <1 brown and gray clay. Locally up to 2% clay. <1% dispersed polyhalite. Upper contact is sharp with clay G. Contact with lower unit is gradational. |
| -2.2 to -7.0 | Halite (Map Unit 6) | Clear, some moderate reddish orange, coarsely crystalline, some fine to medium locally. <1/2% gray clay and polyhalite. Contact with lower unit gradational and/or diffuse. |
| -7.0 to -9.0 | Halite (Map Unit 5) | Clear coarsely crystalline. <1/2% gray clay. Contact with lower unit is usually sharp with clay F. |
| -9.0 to -11 4 | Argillaceous halite (Map Unit 4) | Clear to moderate brown and moderate reddish brown, coarsely crystalline. <1% polyhalite. <1 to 5% argillaceous material; predominantly brown, some gray, locally. Intercrystalline and discontinuous breaks and partings common in upper part of unit. Decreasing argillaceous content downward. Contact with lower unit is gradational. |
| -11.4 to -13.7 | Halite (Map Unit 3) | Clear to moderate reddish orange, coarsely crystalline. <1% dispersed polyhalite and polyhalite blebs. Locally polyhalitic. Scattered gray clay locally. Contact with lower unit is sharp. |
| -13.7 to -14.0 | Argillaceous halite (Map Unit 2) | Moderate reddish brown to medium gray, medium to coarsely crystalline. <1 to 3% argillaceous material. Contact with lower unit is usually sharp. |
| -14.0 to -14.5 | Halite (Map Unit 1) | Light reddish orange to moderate reddish orange, medium to coarsely crystalline. <1% dispersed polyhalite. Contact with lower unit is sharp. |
| -14.5 to -22.0 | Halite (Map Unit 0) | Clear to moderate reddish orange/brown, moderate brown and grayish brown. Medium to coarsely crystalline. <1 to 5% argillaceous material. Predominantly brown, some gray, intercrystalline argillaceous material and discontinuous breaks and partings. Upper two feet of unit is argillaceous halite decreasing in argillaceous material content downward. None to <1% polyhalite. Contact with lower unit is gradational based on polyhalite content. |

Table 6-3 (continued)

DESCRIPTION OF GENERALIZED STRATIGRAPHY



| Approximate Distance From Clay G (Ft) | Stratigraphic Unit | Description* |
|---|---|---|
| -22.0 to -25.3 | Polyhalitic halite | Clear to moderate reddish orange. Coarsely crystalline, some medium locally. <1 to 3% polyhalite. Scattered anhydrite. Scattered gray clay locally. Contact with lower unit (MB-139) is sharp, but commonly irregular and undulating. Trace of gray locally present along this contact. |
| -25.3 to -28.1 | Anhydrite (MB-139) | Moderate reddish orange/brown to light and medium gray, microcrystalline anhydrite. "Swallowtail" pattern, consisting of halite growths within anhydrite, common in upper part of unit. Locally, hairline, clay-filled, low-angle fractures found in lower part of unit. Thin halite layer common close to lower contact. Clay seam E found at base of unit. Upper contact is irregular, undulating and sometimes contains <1/16 in. gray clay. |
| -28.1 to -31.2 | Halite | Clear to moderate reddish orange, and light gray. Coarsely crystalline, some fine and medium. ≤1% polyhalite and intercrystalline gray clay. Contact with lower unit is gradational based on increased polyhalite content. |
| -31.2 to -36.0 | Polyhalitic halite | Clear to moderate reddish orange, coarsely crystalline. <1 to 3% polyhalite. Contact with lower unit is usually sharp along clay D. |
| -36.0 to -37.8 | Halite | Clear to moderate reddish orange, some light gray. Medium to coarsely crystalline. ≤1% polyhalite and gray clay. Contact with lower unit is gradational based on increased polyhalite content. |
| -37.8 to -42.7 | Polyhalitic halite | Clear to moderate reddish orange/brown, coarsely crystalline. <1 to 3% polyhalite. Trace of clay locally. Scattered anhydrite locally. Contact with lower unit is gradational, based on decreased polyhalite content. |
| -42.7 to -47.3 | Halite | Clear to moderate reddish orange, medium to coarsely crystalline. <1% dispersed polyhalite. <1% brown and/or gray clay. Contact with lower init is gradational and/or diffuse. |
| -47.3 to -53.3 | Polyhalitic halite | Clear to moderate reddish orange. Coarsely crystalline with some medium sometimes present close to lower contact. <1 to 3% polyhalite. Scattered anhydrite especially common close to anhydrite "c". Lower contact is sharp with anhydrite "c". |
| -53.3 to -53.5 | Anhydrite "c" | Light to medium gray, microcrystalline anhydrite. Scattered halite growths. Faintly laminated locally. Clay seam B found at base of unit. |
| -53.5 to -65.7 | Halite | Clear to medium gray and moderate brown. Medium to coarsely crystalline, some fine locally. ≤1% polyhalite, locally polyhalitic. <1 to 3% clay, both brown and gray. Intercrystalline clay with discontinuous breaks and partings. Zones of argillaceous halite found within unit. Seams of clay mixed with halite crystals present locally. Upper contact of this unit is sharp with clay B. |

* Descriptions are based on examination of drill core and exposures of units in shafts and other underground openings.

Map units 1 through 6 occur within the storage level drifts and rooms. Unit 1 is a distinct, relatively thin, orange-colored unit commonly referred to as the "orange marker bed". This unit is continuous throughout the facility level excavations. During excavation, it was used as a marker to help keep the underground openings within the proper stratigraphy. The descriptions for map units 7 through 15 represent the lithology most frequently encountered in the drifts and rooms in the waste experimental area. Minor variations in these lithologies occur at various locations but they are not of sufficient difference to justify their inclusion in the generalized descriptions.

#### 6.3.1.2 Stratigraphic Continuity

The results of geologic mapping and core hole drilling in the underground facility have confirmed the lateral extent and stratigraphic continuity of the geologic units within the underground facility horizon. Strata exposed in the drifts have been traced continuously for 4,500 feet in an east-west direction and more than 5,000 feet in a north-south direction. North-south and east-west correlations between the vertical core holes have also demonstrated the continuity of the stratigraphic units above and below the facility level. Figures B-4 through B-9 in Appendix B show the correlations of stratigraphic horizons that have been made based on core hole data. These figures also demonstrate the slight southern dip of the units. Figure B-5 shows a slight thinning of units to the south by about 5 percent. Figures B-1 and B-2 show a larger correlation of stratigraphic horizons between boreholes WIPP-12 to the north and DOE-1 to the south. The five anhydrite beds shown on Figure 6-2 are laterally continuous across the WIPP site.

Although the general character of each stratigraphic unit remains constant throughout the underground facility horizon, minor variations occur. Some thin clay seams are discontinuous and some halite units thin locally or pinch out. The disruptions of some of these units are localized phenomena thought to result from syndepositional processes. Both lateral and vertical variations in the argillaceous and polyhalite

content of the halite units are common. The size of halite crystals varies from fine to coarse both laterally and vertically within inidvidual units. Although the anhydrite is microcrystalline, the beds vary laterally in color, thickness and polyhalite or halite content. The upper surface of MB-139 is undulatory with amplitudes of up to 12 inches.

The halite around the underground openings exhibits slightly varied behavior in response to excavation at different locations. This may be due to minor variations in crystal size or clay content. The clear halite in the roof of the E140 drift south of the waste shaft exhibits more spalling than is apparent in similar halite in other areas of the underground openings. Spalling along the upper portion of map unit 4 occurs in many of the facility level drifts and rooms. In the locations where this unit contains abundant argillaceous material, the spalling appears to be more pronounced. This behavior is discussed in Chapters 10 and 11.

#### 6.3.1.3 Reference Stratigraphy

A meeting was held on November 15, 1979, to determine a reference stratigraphy for the WIPP site. This was titled the "November '79 Reference Stratigraphy" and was based on data obtained from exploratory boreholes. The purpose of the reference stratigraphy was to provide input data for thermal/structural analyses of shafts, drifts and rooms at the WIPP that could be referenced by all structural analysts and updated as more data became available.

The "November '79 Reference Stratigraphy" was revised in July 1981 and again in September 1983 as more data were collected from construction activities and underground core holes. The 1983 revision was titled "September '83 Reference Stratigraphy". This revision was based on the evaluation of 39 core hole logs and the geologic mapping performed in the SPDV exploratory and ventilation shafts.

The evaluation determined that the strata are fairly horizontal but dip slightly to the south. Based on a statistical analysis, the entire stratigraphic section was found to vary in elevation in a regular manner, but individual unit thicknesses and the relative separation between units were found to have no statistically significant variation between the northern and southern limits of the underground facility horizon (ref. 5-3).

Figure 6-4 shows the reference stratigraphy developed by this statistical analysis. This stratigraphy consists of 1 polyhalite bed, 2 argillaceous halite units, 7 anhydrite beds, 12 clay seams, and halite as the remaining constituent. This reference stratigraphy extends approximately 165 feet above and below the facility level. The location and thickness of the various units were adjusted by averaging values determined from the core holes. Geologic maps of the SPDV exploratory and ventilation shafts and the log of borehole ERDA-9 were used for units outside the WIPP underground facility horizon. The uniformity of the rock in the core holes and shafts, the lack of a statistically significant variation in unit thicknesses and elevation, and the expected small influence of any differences on structural behavior resulted in a decision to use the same reference stratigraphy throughout the site.

Subsequent to the development of the September 1983 reference stratigraphy, additional core holes were drilled and logged, the ventilation shaft was enlarged to the waste shaft, the exhaust shaft was completed, and both of these shafts were geologically mapped. Based on additional data from these activities, a generalized stratigraphic column of the underground facility horizon was developed (Figure 6-2 and Table 6-3). This stratigraphic column does not vary significantly from the earlier 1983 reference stratigraphy. Therefore, the 1983 reference stratigraphy continued to be used for model calculations.

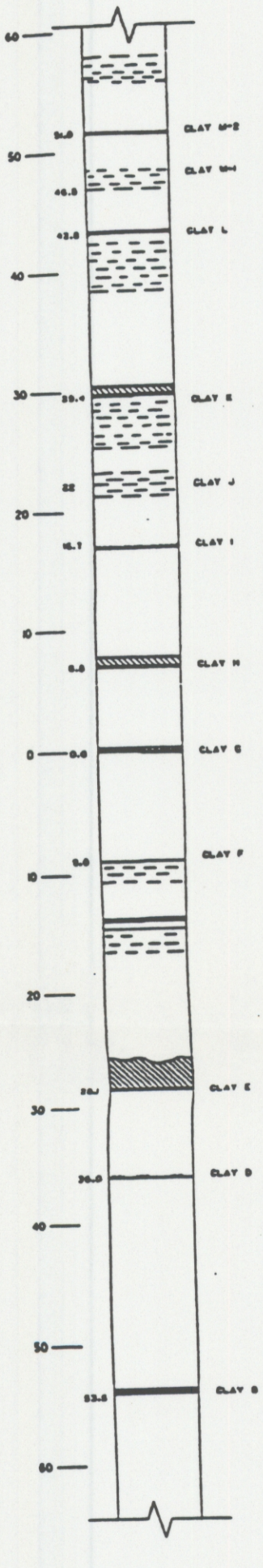


VARIES FROM AN ARGILLACEOUS HALITE ZONE CONTAINING <1 TO 3% BROWN CLAY TO A CLAY/HALITE SEAM UP TO 3 1/2 INCHES THICK.

COMMONLY FOUND AS AN ARGILLACEOUS HALITE ZONE CONTAINING <1 TO 3% BROWN CLAY OR MERELY A BROWN, SOMETIMES GRAY, CLAY PARTING. LOCALLY FOUND AS A SEAM UP TO 1/2-INCH THICK.

IN C & SH SHAFT, IT IS A 2-INCH THICK BROWN CLAY SEAM. MOST COMMONLY IT IS FOUND AS THE UPPER CONTACT OF THE ARGILLACEOUS ZONE BELOW.

USUALLY BROWN CLAY BUT SOMETIMES GRAY TO GRAY-BROWN IN CORE. MOST COMMONLY FOUND AS 3/4 TO 1 1/4-INCH HARD, BROWN CLAY SEAM. IN THE C & SH SHAFT, IT IS UP TO 1 1/2 INCHES THICK. USUALLY IT IS A LOW ANGLE CONTACT.

IN C & SH SHAFT, CONSISTS OF A REDDISH BROWN CLAY SEAM UP TO 1/2-INCH THICK. IN CORE HOLES, FOUND AS SCATTERED BREAKS OR ARGILLACEOUS HALITE CONTAINING <1 TO 3% CLAY.

1/4 TO 5/8-INCH THICK CLAY. COMMONLY BROWN OR BROWNISH GRAY IN CORE BUT GRAY WHERE EXPOSED IN EXPERIMENTAL TEST ROOMS. COMMONLY ASSOCIATED WITH THIN ANHYDRITE ABOVE. EXPOSURES IN EXPERIMENTAL TEST ROOMS SHOW IT TO BE FAIRLY REGULAR WITH UNDULATIONS USUALLY LESS THAN 1INCH AMPLITUDE. SOME SCATTERED HALITE GROWTHS LOCALLY WITHIN CLAY.

AVERAGES 1/4-INCH THICK CLAY BUT VARIES FROM TRACE UP TO 1/2 INCH. USUALLY GRAY COLOR BUT BROWN IN SEVERAL CORE HOLES. CLAY H IS EXPOSED IN THE WASTE EXPERIMENTAL AREA. HERE IT IS A GRAY, IRREGULAR SEAM WITH UNDULATIONS OF 1 TO 3 INCHES AMPLITUDE.

TRACE UP TO 3/8-INCH THICK GRAY CLAY. USUALLY A LOW ANGLE CONTACT IN CORE. EXPOSED IN WASTE EXPERIMENTAL AREA WHERE IT IS A GRAY, FAIRLY REGULAR SEAM WITH UNDULATIONS AVERAGING <2 INCHES AMPLITUDE. LOCALLY, MOISTURE IS NOTED ALONG THIS SEAM. EXPOSED ALONG THE WALLS OF MANY OF THE FACILITY LEVEL DRIFTS AND ROOMS ALONG THE UPPER CONTACT OF MAPPING UNIT 4, VERY IRREGULAR.

GRAY TO BROWN SEAM 1/8 TO 1/2-INCH THICK. HALITE IS COMMONLY MIXED WITH CLAY AND SILT. SOMETIMES BIFURCATES INTO TWO SEAMS. LOCALLY DISCONTINUOUS. UNDULATIONS OF 2 TO 8 INCHES AMPLITUDE.

1/4 TO 1 1/2-INCH GRAY CLAY SEAM. MOISTURE PRESENT IN SOME LOCATIONS. LOCALLY IRREGULAR WITH UNDULATIONS UP TO 4 INCHES AMPLITUDE.

VARIES FROM A ZONE OF CLAY BREAKS UP TO A 3/4-INCH GRAY CLAY SEAM. SOMETIMES THIN ANHYDRITE IS ASSOCIATED ABOVE. NEAR HORIZONTAL IN CORE.

GENERALLY 1/8 TO 1/4-INCH GRAY CLAY SEAM BUT LOCALLY UP TO 1 1/4 INCHES. USUALLY LOW ANGLE AND SLIGHTLY IRREGULAR IN CORE.

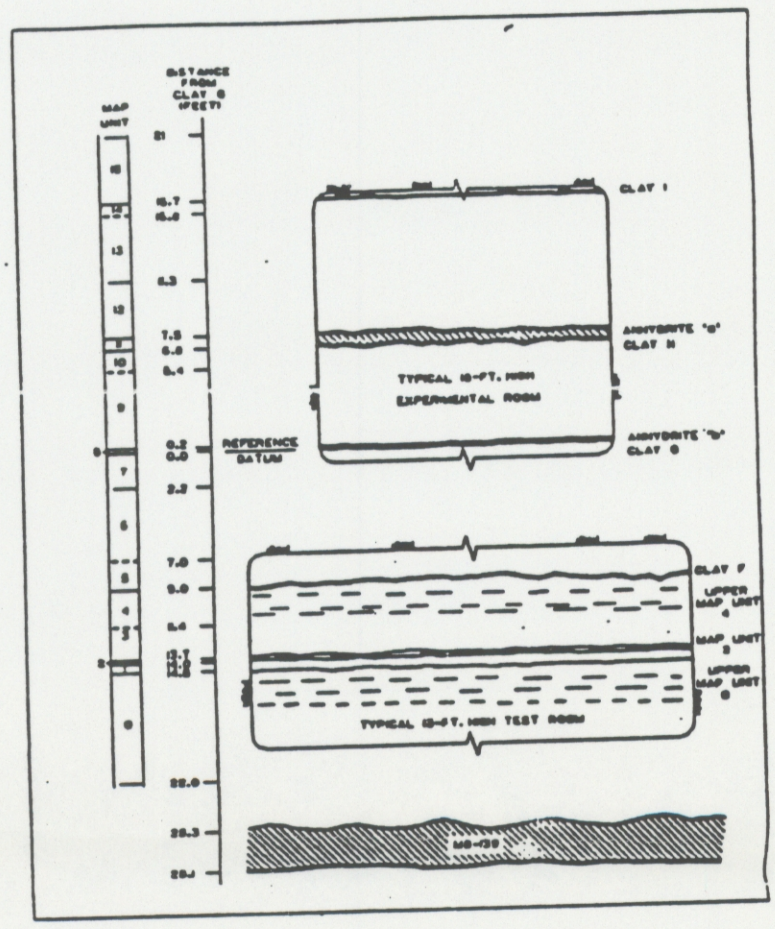


## EXPLANATION

### ROCK TYPE

ANHYDRITE

ARGILLACEOUS HALITE

### ACCESSORY CONSTITUENTS

ANHYDRITE STRINGERS

LAMINAR FEATURES

CLAY SEAM 1/4 IN. THICK

### LITHOLOGIC CONTACTS

SHARP

GRADATIONAL WITHIN 0.25 FT.

**NOTES:**

1. DISTANCES ARE MEASURED FROM CLAY G AND ARE AVERAGED FROM REPRESENTATIVE CORE HOLE LOGS AND SHAFT MAPPING.
2. DESCRIPTIONS OF CLAY SEAMS ARE BASED ON CORE HOLE DATA, SHAFT MAPPING AND VISUAL INSPECTION OF EXPOSURES IN UNDERGROUND DRIFTS AND ROOMS.
3. ONLY CLAY SEAMS ARE SHOWN ON THIS FIGURE. ALL OTHER UNITS ARE SHOWN ON FIGURE 6-2 AND DESCRIBED IN TABLE 6-3.

**Figure 6-3**

**CLAY SEAMS**

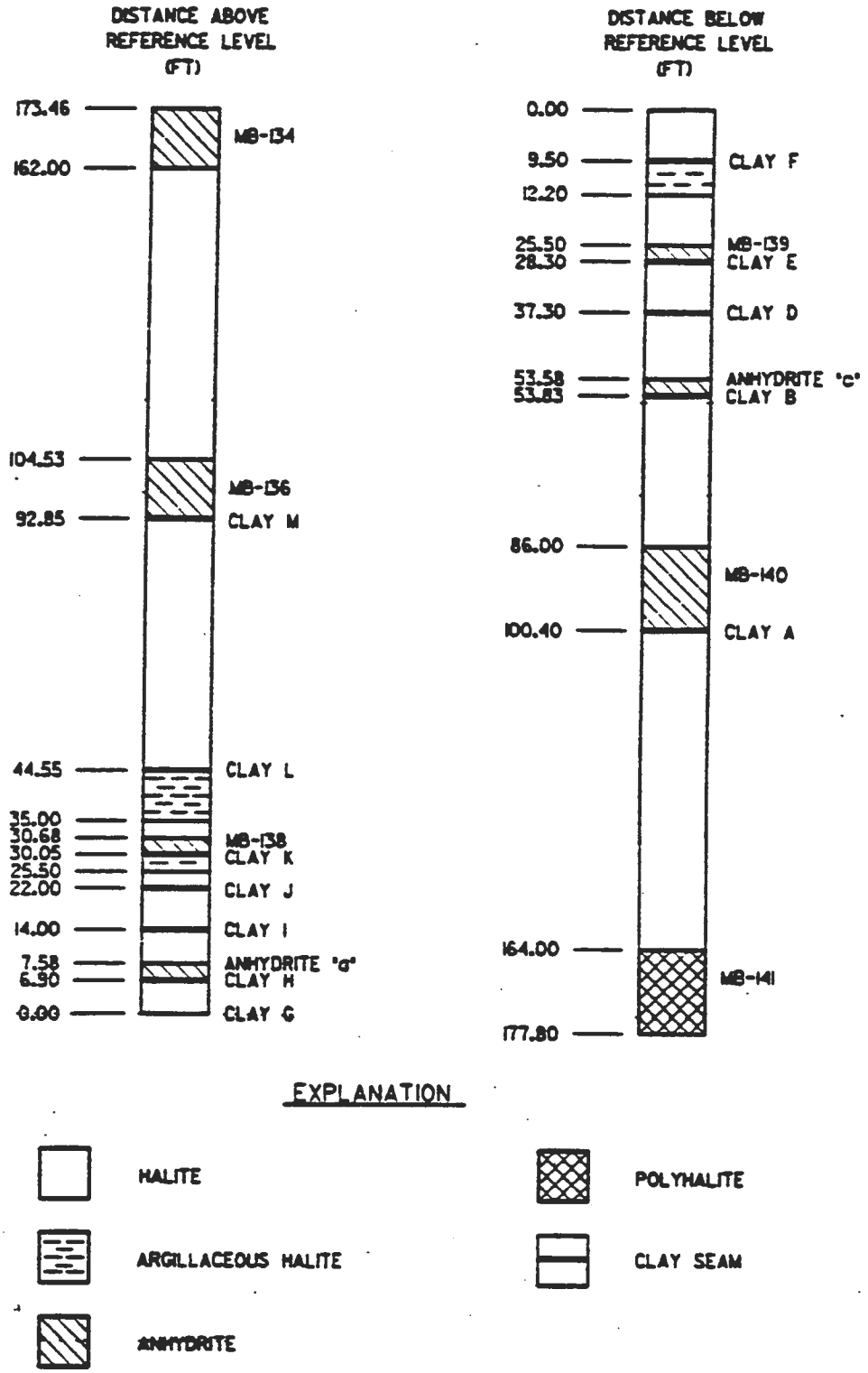


Figure 6-4

REFERENCE STRATIGRAPHY

### 6.3.2 Lithology

The Salado formation is predominantly halite, but other evaporite minerals and argillaceous materials are present that may locally compose up to 50 percent of the salt. Anhydrite, an early-precipitated evaporite mineral, is found in beds (usually less than 5 feet thick) which are typically underlain by a clay seam (1/16 to 3/4 inch thick). Polyhalite, a late-forming evaporite mineral, is commonly found as an accessory mineral in the Salado formation. Clay and silt may be found disseminated through the halite or in thin seams, partings, or breaks. Following is a description of the major lithologies occurring within the underground facility horizon.

Clear Halite. These units consist of halite with only trace amounts of impurities. The halite is predominantly medium to coarsely crystalline and clear to very light gray or moderate reddish orange. Less commonly, it occurs as finely crystalline, opaque, very light gray halite with a sucrose texture. Trace impurities of clay and/or polyhalite are generally dispersed in the halite. Scattered very light gray to white anhydrite or magnesite stringers may be present.

Polyhalitic Halite. These units are composed mainly of medium to coarsely crystalline halite with accessory amounts of polyhalite. As the polyhalite content increases, the color of the rock changes from transparent light orange-pink to translucent moderately reddish orange/brown or dark reddish brown. The polyhalite occurs primarily as interstitial blebs or patches and, less commonly, in stringers about 1/4 to 3/4 inch thick.

Argillaceous Halite. Six argillaceous halite units, three above and three below clay G, occur within the underground facility horizon. Generally, these units consist of medium to coarsely crystalline and some finely crystalline halite with from less than 1 to as much as 5 percent silty clay. The clay is predominantly brown in color with some gray. It is commonly intercrystalline or forms scattered breaks or partings. Discontinuous clay seams are present locally. The percent

of clay is a visual estimate; laboratory measurements of insolubles (ref. 6-5) were used as a reference.

The contacts between these units and the surrounding materials vary from gradational to distinct. Clays F, K and L occur at the upper contact of three of these argillaceous units. The three units below clay G are exposed in the underground drifts and rooms. These are geologic map units 2 and 4 and the upper portion of map unit O (Figure 6-2). They are exposed continuously throughout the openings except in the waste experimental area which is stratigraphically higher. Map unit 2 is very thin and absent in places.

No significant moisture is associated with these argillaceous halite layers. Commonly, they are slightly moist immediately after excavation and locally develop brine blisters on the walls of the underground openings.

Anhydrite. These beds range in thickness from a few inches to a few feet. Because they are readily identified, the anhydrite beds in the vicinity of the facility level have served as reference units.

Three anhydrite beds, 0.15 to 1.05 feet thick, are present above and two beds, 0.3 and 2.5 to 4 feet thick, are present below the facility level (Figure 6-2). All of the beds are laterally continuous and each is underlain by a thin clay seam. Locally, very thin anhydrite seams are associated with identified clay seams and scattered anhydrite stringers are common in several of the halite units. The anhydrite is microcrystalline and commonly ranges from a very light gray to medium gray-green color, although it is sometimes a moderate reddish to pinkish color. Halite growths are common, especially within MB-139. Anhydrite "a" commonly contains a clear halite seam up to 1 1/2 inches thick.

MB-139 is the thickest anhydrite unit within the underground facility horizon and is the most variable in color and composition. It is

described here in detail because of its importance in the deformational behavior of the underground openings, particularly the test rooms (Chapter 11).

MB-139 ranges from 2.5 to 4 feet thick. For mapping purposes, it has been divided into two subunits (Appendix G, Figures G-10 through G-34). Subunit A corresponds to Zones I, II and III described in reference 6-6. This subunit consists predominantly of reddish polyhalitic anhydrite and anhydrite mixed with light to medium gray anhydrite. Pods, lenses and seams of light to very light gray anhydrite are commonly scattered throughout the subunit. Irregular halite growths, ranging from less than 1/16 to more than 25 square inches, are common, especially in the upper half of subunit A. Commonly, a 1- to 2-inch thick seam of moderately reddish-orange to gray polyhalitic anhydrite with scattered halite and polyhalitic halite growths occurs along the upper contact. This corresponds to Zone I described in reference 6-6. Swallowtail growth patterns and hopper crystals are occasionally present in the upper 12 inches of subunit A, commonly within an upward undulation of the marker bed. Halite-filled fractures are found in places within the undulations. Scattered within the reddish polyhalitic anhydrite is an irregular and sometimes discontinuous layering of light gray anhydrite, which varies from less than 1/8 inch to 1/2 inch thick. Pods and lenses of gray anhydrite are often faintly aligned, although discontinuously, with the general trend of the layering. These pods and lenses are most prevalent in the lower half of subunit A.

Subunit B corresponds to Zones IV and V in reference 6-6. Its contact with subunit A is diffuse and based mainly on a change in color. Subunit B consists of light to medium gray anhydrite. Some core samples exhibit layering which faintly follows the general trend of the layering in subunit A. Halite growths are present, but to a much lesser degree than in subunit A. Usually the lower 4 to 8 inches of the subunit is faintly laminated and contains a few halite growths. A subhorizontal halite layer, usually less than 1/8 inch thick, is occassionally present close to the lower contact.

The upper contact of MB-139 is undulatory. The lower contact is underlain by clay E. This clay ranges from 1/4 inch to 1 1/2 inches thick. It is often slightly moist and sometimes wet.

Clay Seams. Characteristics of the clay seams within the underground facility horizon are shown on Figure 6-3 and summarized in Table 6-4. These include qualitative and/or quantitative characterizations and descriptions of the clay seams in terms of the following:

(1) color;
(2) thickness;
(3) moisture;
(4) grain size;
(5) consistency/plasticity;
(6) planar trend; and
(7) continuity/uniformity.

This information has been gathered through a review of core hole logs, geologic mapping and inspection of existing exposures.

The clay seams underlying anhydrite beds usually vary from less than 1/8 inch to 3/4 inch in thickness but may range up to 1 1/2 inches thick, as is common for clay E. The other, less continuous seams are usually less than 3/4 inch thick but may be as much as 2 inches thick, as is clay L in the C & SH shaft. Clay M-1 was as much as 3 1/2 inches thick in one hole but it consisted of a mixture of clay and halite crystals at this location.

Generally, the seams consist of clay with some silt. The clay varies from gray to brown in color. Only field classifications of the clay in core and underground exposures have been performed. These classifications indicate that the seams generally consist of soft to hard, medium plastic material. Locally, fine to coarse halite crystals are present in some of the seams. Clays F and M-1 commonly contain

Table 6-4

CLAY SEAM CHARACTERISTICS



| Seam | Rating[1] | Color | Thickness | Moisture | Grain Size | Consistency/ Plasticity | Planar Trend | Continuity/ Uniformity | Occurrence |
|---|---|---|---|---|---|---|---|---|---|
| B | 1 | Gray | <1/8 to 1/4 in. average; locally up to 1 1/4 in. | Dry to slightly moist. | Passes #200 sieve. | Generally hard. | Slightly irregular; generally low angle in core but locally up to 35°. | Continuous. | Present in core holes and C & SH and waste shaft mapping. |
| D | 2 | Gray | ≤3/4 in. | Dry except hole DD-57 where clay is moist; hole drilled with fluid. | Passes #200 sieve. | Hard to medium soft; medium to highly plastic. | Near horizontal in core. | Varies from zone of breaks to seam with associated anhydrite. | Present in many core holes and in C & SH shaft mapping |
| E | 1 | Gray | 1/4 to 1 1/2 in. | Locally moist to wet. | Passes #200 sieve. | Soft to hard; medium plastic | --- | Continuous. | Present in many core holes and in C & SH and waste shaft mapping. |
| F | 2 | Gray, sometimes brown. | <1/8 to 1/2 in. | Slight. | Passes #200 sieve. Commonly mixed with halite crystals. | Slightly plastic. | Very irregular; undulations of 2-in. to 4-in. amplitude. | This is at the upper contact of map unit 4; locally discontinuous; sometimes bifurcates into two seams. | Exposed along walls of many of the facility level drifts and rooms. |
| G | 1 | Gray | Trace up to 3/8 in. | Slightly to moderately moist; weeps along exposures in underground excavations. | Passes #200 sieve. | Soft to hard; medium plastic. | Fairly regular; undulations average <2-in. amplitude. | Continuous. | Found in most core holes, shaft mapping and underground waste experimental area excavation. |
| H | 1 | Gray; brown in several core holes. | Average ≤1/4 in. but ranges from trace up to 1/2 in. | Slightly to moderately moist. | Passes #200 sieve. | Medium plastic. | Fairly irregular; undulations of 1-in. to 3-in. amplitude. | Continuous. | Found in most core holes, shaft mapping and underground waste experimental area excavation. |

Table 6-4 (continued)

CLAY SEAM CHARACTERISTICS



| Seam | Rating (1) | Color | Thickness | Moisture | Grain Size | Consistency/ Plasticity | Planar Trend | Continuity/ Uniformity | Occurrence |
|---|---|---|---|---|---|---|---|---|---|
| I | 1 | Brown-brownish gray in core; gray where exposed in waste experimental rooms. | <1/4 to 5/8 in. | Slightly moist. | Passes #200 sieve; some scattered halite crystals locally. | Hard in some core holes; medium plastic. | Regular; undulations generally <1-in. amplitude. | Fairly continuous. | Commonly found in core holes, C & SH and exhaust shafts; also exposed in waste experimental room excavation. |
| J | 3 | Reddish-brown | 1/2 in. in C & SH Shaft only. | --- | Passes #200 sieve; trace silt, trace to some halite crystals. | --- | --- | Generally found as scattered breaks or localized argillaceous zone. | Found in C & SH shaft as 1/2 in. seam; not found in other shafts; in core holes, found as scattered breaks or localized argillaceous zone; absent in many core holes. |
| K | 1 | Brown, sometimes gray to gray-brown. | 3/4 to 1 1/2 in. | Dry to moist; locally wet. | Passes #200 sieve; claystone in exhaust shaft. | Hard to medium hard; medium plastic. | Generally low angle contact in core; fairly regular. | Continuous. | Present in many core holes and shafts. |
| L | 3 | Brown | Up to 2 in. in C & SH shaft; usually found only as top of argillaceous unit. | --- | Passes #200 sieve; some halite crystals. | --- | --- | Not a continuous seam; it is found generally as the top of argillaceous zone throughout core holes and shafts. | Exposed in C & SH shaft as seam; otherwise only noted as top of argillaceous unit. |

Table 6-4 (continued)

CLAY SEAM CHARACTERISTICS



| Seam | Rating (1) | Color | Thickness | Moisture | Grain Size | Consistency/ Plasticity | Planar Trend | Continuity/ Uniformity | Occurrence |
|---|---|---|---|---|---|---|---|---|---|
| M-1 | 4 | Brown | <1/16 to 1/2 in. | Dry | Passes #200 sieve. | --- | --- | Unknown. | These two layers found in core holes in waste experimental area; not noted in shaft mapping. |
| M-2 | 4 | Brown | Up to 3 1/2 in. | Dry | Clay mixed with halite crystals. | --- | --- | Unknown. | |

Notes:

(1) Key to "Rating": 1 - continuous throughout facility level;
2 - generally continuous, but varies in character and regularity;
3 - discontinuous and not always well developed;
4 - continuity unknown.

(2) Clays B, E, G, H and K are sometimes noted as only a trace or not at all on core logs. This is usually because core grinding or washing during drilling removed evidence of clay.

(3) Some core logs note clay layers are moist. In holes drilled with brine, this may be due to drilling fluid. Many layers are dry in holes drilled with air. These may actually be slightly moist in the in situ state, but dried out by the drilling process.

(4) Clays B, E, G, H and K always underly continuous anhydrite layers. Clays I and U are commonly associated with thin anhydrite layers.

(5) Plasticity and consistency based on evaluation of in situ condition.

more halite mixed with the clay/silt fraction. Clay F also appears to be more silty and less plastic than the other seams.

Generally, the clay seams are slightly moist in their in situ state. However, some of the seams are wet and exhibit some brine weeping in places. This was observed for clays E, G, H and K in some core holes. The clay seams in some of the holes where brine was used as a drilling fluid were observed to be moist. This was probably due in part to the drilling fluid. In contrast, clay seams were observed to be dry in many of the core holes drilled using air circulation. It is expected that, in the in situ state, these seams contain a slight amount of moisture which was evaporated as a result of the drilling method. Some moisture can be seen along exposures of clay H and clay G in the waste experimental area. More moisture is evident along clay G and some salt blisters have accumulated locally along this seam. The clay seams exposed in the underground openings are generally slightly moist during and immediately after excavation. Some seams have continued to expel moisture long after excavation. Often, however, they dry out at the surface within a few days after their exposure.

Clays G, H and I, exposed in the waste experimental area, commonly contain white specks which may be salt resulting from the air drying of the clay. The clay usually has a slightly salty taste. These white specks are soft, can be easily crushed between the fingers, and have a slightly bitter taste.

The consistency of the clay encountered in the core holes and excavations is related to its moisture content. When wet or moist, the clay is generally soft to medium stiff and can be picked out with the fingers and molded into a ball in the hand. When the clay is only slightly moist or dry, it is stiff to hard and is difficult to work in the hand.

### 6.3.3 Structure

Geologic mapping of the underground openings has not identified any faults, joints, significant folds, or other structural disruptions that could affect the suitability of the WIPP facility for storing radioactive waste. Very small scale (approximately 1 foot), localized disruptions of the bedding have been encountered. These are attributed to penecontemporaneous processes.

Detailed correlations between vertical core holes, combined with the results of geologic mapping in the drifts and test rooms, indicate that the strata within the underground facility horizon are deformed slightly into a sinusoidal shape. Figure B-4 in Appendix B depicts this shape, but greatly exaggerates the amplitude of the deformation. The amplitude of the fold is approximately 10 to 15 feet and its wavelength is approximately 2,000 to 3,000 feet. The fold is superimposed on a gentle southward dip.

The deformation of the strata is post-depositional in origin. While undulations of depositional surfaces are common, all of the strata in the interval from 50 feet above to 50 feet below the facility level exhibit parallel undulations. This consistency in folding over a relatively large interval containing numerous depositional sequences suggests that the beds were deformed after deposition. The folding is a minor feature which does not adversely affect the suitability of the facility for waste storage.

## 6.4 PROPERTIES OF HOST ROCKS

As discussed in subsection 6.3.2, the underground facility horizon is composed of halite containing beds of argillaceous halite, anhydrite, polyhalite and thin clay seams. Laboratory tests were performed to determine the constitutive equations and material property constants for these host rocks (ref. 5-3). Subsections 6.4.1 and 6.4.2 present the properties of the host rocks based on laboratory and in situ data. In situ closure measurements were also used to "back calculate" the creep parameters for halite.

### 6.4.1 Laboratory Tests

Laboratory tests were performed on core samples from surface boreholes at the WIPP site prior to the initiation of underground excavation (ref. 5-3). Material property constants determined from the laboratory tests are presented in Tables 6-5 through 6-7. Table 6-5 shows the elastic constants for halite, argillaceous halite, anhydrite and polyhalite.

The failure criteria for both anhydrite and polyhalite were defined based on the results of the laboratory tests. One such criterion is Mohr-Coulomb, which defines failure in terms of friction and cohesion. Failure means that the material is unable to hold a deviatoric stress beyond a certain value. Once this value is reached, the material starts yielding. However, the Mohr-Coulomb criterion ignores the effect of intermediate principal stress on failure. In terms of principal stresses at failure,

$$(\sigma_3 - \sigma_1) = 2\Theta_0 \cos\beta - (\sigma_3 + \sigma_1) \sin\beta \qquad (6\text{-}1)$$

where: $\Theta_0$ and $\beta$ are Mohr-Coulomb parameters; and

$\sigma_1$ and $\sigma_3$ are principal stresses that are positive in tension.

Because the process of yield must be independent of the choice of axes, the failure criterion must be independent of the choice of axes and should be expressed in terms of stress invariants. The Drucker-Prager yield criterion is expressed as follows:

$$\sqrt{J_2'} = c - aJ_1 \qquad (6\text{-}2)$$

where: $\sqrt{J_2'}$ is the second stress invariant and is equal to $\bar{\sigma}/\sqrt{3}$; and

$J_1$ is the first stress invariant:

$$J_1 = \sigma_1 + \sigma_2 + \sigma_3 \qquad (6\text{-}3)$$

$$\bar{\sigma} = \frac{1}{\sqrt{2}} [(\sigma_1 - \sigma_2)^2 + (\sigma_2 - \sigma_3)^2 + (\sigma_3 - \sigma_1)^2]^{1/2} \qquad (6\text{-}4)$$

## Table 6-5

ELASTIC CONSTANTS DETERMINED FROM LABORATORY TESTS

| MATERIAL | E (ksf) | $\nu$ |
|---|---|---|
| Halite | 647,450. | 0.25 |
| Argillaceous halite | 647,450. | 0.25 |
| Anhydrite | 1,568,500. | 0.35 |
| Polyhalite | 1,155,000. | 0.36 |

Note:

E = elastic modulus

$\nu$ = Poisson's ratio

## Table 6-6

FAILURE CONSTANTS DETERMINED FROM LABORATORY TESTS

| | ULTIMATE | | | | YIELD | | | |
|---|---|---|---|---|---|---|---|---|
| MATERIAL | $\Theta_o$ (ksf) | $\beta$ (°) | a | c (ksf) | $\Theta_o$ (ksf) | $\beta$ (°) | a | c (ksf) |
| Anhydrite | 627. | 37.0 | 0.279 | 752. | 564. | 29.0 | 0.226 | 689. |
| Polyhalite | 395. | 51.0 | 0.395 | 414. | 359. | 46.5 | 0.361 | 403. |

Table 6-7

CREEP CONSTANTS DETERMINED FROM LABORATORY TESTS

| | PRIMARY CONSTANTS | | | SECONDARY CONSTANTS | | |
|---|---|---|---|---|---|---|
| MATERIAL | A | B | $\dot{\varepsilon}^*$ ($sec^{-1}$) | D ($ksf^{-4.9}$ $sec^{-1}$) | n | Q (kcal/mole) |
| Halite | 4.56 | 127 | $5.39 \times 10^{-8}$ | $4.96 \times 10^{-13}$ | 4.9 | 12.0 |
| Standard Error | | | | $1.05 \times 10^{-13}$ | 0.27 | 0.65 |
| Argillaceous Halite | 4.56 | 127 | $5.39 \times 10^{-8}$ | $1.49 \times 10^{-12}$ | 4.9 | 12.0 |

For anhydrite, however, the ultimate strength decreases somewhat with the change in strain rate. That is, a 10 percent decrease occurs as the strain rate is decreased from $10^{-4}$ $sec^{-1}$ to $10^{-6}$ $sec^{-1}$. For polyhalite, the ultimate strength is assumed to be independent of the strain rate. Table 6-6 shows the failure constants for anhydrite and polyhalite.

Table 6-7 shows the creep constants for halite and argillaceous halite. Although the data for most individual creep tests are internally consistent, steady-state creep rates obtained from different specimens tested under the nominally same conditions may scatter by an order of magnitude. Nevertheless, statistical analysis has resulted in a "best fit" to the data. Table 6-7 also shows the deviation of the secondary creep constants for halite. It was concluded that when such large deviations or uncertainty exist, calculations using mean values are apt to be meaningless and the design process requires considerable judgement (ref. 6-7).

Based on laboratory tests, the failure criterion of halite can be described using a failure function $\phi$, such that when $\phi$ becomes positive, halite no longer supports any deviatoric stress. The function $\phi$ is assumed to be:

$$\phi = \bar{\varepsilon} - 0.023 - f(p) \qquad (6\text{-}5)$$

where: $\bar{\varepsilon}$ is the effective creep strain (see Appendix C) and the function f(p) is expressed as:

$$f(p) = \begin{cases} 0.132 & \text{for } p \geq 125.26 \text{ ksf} \\ p(a - bp) & \text{for } p \leq 125.26 \text{ ksf} \end{cases} \qquad (6\text{-}6)$$

where: p, the pressure in ksf, is expressed as

$$p = -\frac{\sigma_1 + \sigma_2 + \sigma_3}{3} \qquad (6\text{-}7)$$

and is positive in compression; and

a and b are equal to $2.122 \times 10^{-3}$ $ksf^{-1}$ and $8.487 \times 10^{-6}$ $ksf^{-2}$, respectively (ref. 5-3).

Equation 6-5 indicates that if $\bar{\varepsilon} \geq 0.023 + f(p)$ at any point in the halite, yielding will be initiated at that point. For p greater than 120 ksf, the failure effective strain is about 0.16.

Laboratory test results have also shown that a clay seam will be active for a frictional coefficient of 0.4, and that clay seam separation is unlikely unless the seam is very near the opening.

The average unit weight of the salt within the reference stratigraphy interval was determined to be 143.6 pounds per cubic foot (pcf) (ref. 5-3).

### 6.4.2 In Situ Data

In situ data was gathered from geomechanical instruments at various underground locations. The creep law shown by equation C.4-1 in Appendix C was used to fit the in situ data and to determine the creep parameters. The MARC General Purpose Finite Element Program (ref. 6-8) was used for the numerical computation based on the theory discussed in Appendix C. Table 6-8 shows the primary and secondary creep parameters determined from test room in situ data. Chapter 11 presents a more detailed discussion of the procedures used for computing these parameters.

Secondary creep parameters were also computed using in situ data from the C & SH shaft. The secondary creep parameters computed from horizontal deformations in the C & SH shaft and in the test rooms are reasonably close. The parameter based on test room wall-to-wall

Table 6-8

CREEP PARAMETERS DETERMINED FROM IN SITU DATA

| MATERIAL | PRIMARY PARAMETERS A | PRIMARY PARAMETERS z ($sec^{-1}$) | SECONDARY PARAMETER C ($ksf^{-4.9}$ $sec^{-1}$) |
|---|---|---|---|
| Halite | | | |
| Roof-to-Floor | 1.774 | $5.573 \times 10^{-8}$ | $2.588 \times 10^{-21}$ |
| Wall-to-Wall | 1.618 | $4.757 \times 10^{-8}$ | $1.361 \times 10^{-21}$ |

closure is $1.36 \times 10^{-21}$ $ksf^{-4.9}$ $sec^{-1}$ while the parameter based on extensometer measurements in the C & SH shaft is $1.30 \times 10^{-21}$ $ksf^{-4.9}$ $sec^{-1}$.

## 6.5 SURFACE SUBSIDENCE MONITORING

The design criteria state that subsidence due to underground excavation shall not exceed 1 inch within a 500-foot radius of the waste shaft. The layout of the underground excavation and the extraction ratio requirements were established to comply with this criteria. Subsidence monuments have been installed on the ground surface above the shaft pillar area (Chapter 2, Figure 2-2). Additional subsidence monuments are scheduled to be installed above the storage area in mid-1986. These monuments will be used to determine surface subsidence during the 25-year facility operating life.

Because the storage area has not yet been excavated, actual subsidence cannot be measured. This subsidence will occur over the next 25 years. The calculations used for the reference design indicate that subsidence is not likely to exceed the criteria limit. Therefore, the reference design subsidence criteria is considered validated on a computational basis rather than on actual measurement data. A review of this conclusion may be required later when a history of actual subsidence is available.

THIS PAGE LEFT BLANK INTENTIONALLY

# CHAPTER 7

# C & SH SHAFT

## 7.1 INTRODUCTION

This chapter presents the results of the design validation program for the C & SH shaft. Included are discussions of the design criteria, design bases and design configurations pertaining to the C & SH shaft. This is followed by information and data from the design validation process including the data collected, its analysis and evaluation, and predictions regarding future behavior of the shaft liner and key and the rock strata surrounding the shaft. Conclusions and recommendations are presented based on a comparison of the results of the design validation process with the reference design.

## 7.2 DESIGN

This section presents the design criteria and design bases used to develop the reference design for the C & SH shaft. The configuration of the shaft is discussed in Chapter 3, subsection 3.3.1.

### 7.2.1 Design Criteria

The Design Criteria document (ref. 2-8) contains the general concepts that were used as a guide for design of the WIPP underground openings. Table 2-1 summarizes those design criteria elements that are to be evaluated by the design validation process. The following discussion provides a summary of the elements that pertain to validation of the C & SH shaft reference design.

The design criteria specify that all shafts shall be designed for structural stability over an operating life of 25 years. The design shall also consider the requirements for shaft decommissioning and sealing. Shaft design shall prevent wall deformations which would interfere with shaft functions or affect the safety of operations within the shafts. Rock support shall be used as required to limit rock deformations and to prevent loosening and fallout of wall rock.

The time-dependent diametric closure of the shafts due to creep shall be considered in their design. The shafts shall be designed so that the minimum dimensions required for shaft functions are maintained throughout the operating life of the facility. Provisions for instruments to measure closure shall be included in the design.

Ground-water flow into the shafts shall be controlled so that no uncontrolled ground water reaches the facility level via the shafts. Ground-water pressures and inflows shall be measured throughout the construction period and operating life of the shaft.

Shaft design shall consider the requirements of decommissioning and backfilling upon termination of operations. The design shall accommodate the need to ultimately seal potential pathways between the storage facility and the biosphere.

The shaft liner shall be designed to help ensure that the shaft dimensions remain within the limits required for shaft functions, prevent ground-water flow into the shaft, protect wall rock from deterioration, and preclude the risk of rockfall from the shaft walls.

The shaft stations shall be designed to provide structurally stable excavations and pillars. Deformations of excavations and pillars shall remain within the limits required for structural functions, ventilation and safety. The excavation design shall maintain the minimum dimensions required for the operating life of the opening by accommodating closure. Closure rates used for design shall be confirmed or modified by instrument observations in the excavations. Rock bolts shall be used where necessary to provide support of the roof and walls.

### 7.2.2 Design Bases

The Design Basis, Exploratory Shaft (ref. 2-10) and the Design Basis, Exploratory Shaft Geomechanical Instrumentation (ref. 2-12) were the primary documents used as a basis for design of the C & SH shaft. These documents, described in Chapter 2, provided the detailed design

requirements for the C & SH shaft. Table 7-1 summarizes those design basis elements which are to be evaluated by the design validation process. The following discussion provides a summary of the major design bases for the C & SH shaft. Not all of these bases require evaluation as seen by comparing the discussion with Table 7-1.

The design bases specify that the C & SH shaft shall be designed to provide access for personnel and equipment to excavate and operate the underground facility and to provide a means by which the excavated salt can be transported to the surface. It shall also serve as the ventilation intake shaft.

The shaft liner shall be made of structural steel and have an inside diameter of 10 feet. The remainder of the shaft shall be unlined and have an approximate diameter of 11 feet 8 inches. The steel liner shall extend from 1 foot above the ground surface to the top of the salt formation at a depth of approximately 850 feet. The primary materials used to line the shaft shall be cement grout, steel casing, corrugated metal pipe, structural steel and reinforced concrete.

The liner shall protect against sloughing, fallout and deterioration of the rock formations and shall prevent water seepage into the shaft. It shall have a smooth inner surface to reduce air friction. The liner shall be designed for temporary installation loads and permanent loads. The permanent load shall consist of a hydrostatic lateral pressure starting 250 feet below the ground surface and extending to approximately 837 feet below the surface. Rock pressure shall not be used as a factor in the design analysis. Installation loads to be considered shall be the compressive and tensile forces resulting from lateral pressure due to unequal heights of drilling fluid during the various stages of installation.

During shaft drilling, ground-water flow into the shaft shall be determined. If the amount of ground water entering the shaft is determined to be unacceptable by the DOE Contracting Officer, approved

## Table 7-1

### VALIDATION ELEMENTS OF C & SH SHAFT DESIGN BASES

(1) Shaft Liner

a. Hydrostatic pressure is considered to start 250 feet below the ground surface and extend to the top of the key.

b. Water shall be prevented from flowing down the unlined shaft from behind the liner.

(2) Shaft Key

a. Key shall be designed to resist the lateral pressure from the salt. (Assumed to be 75 percent of the overburden pressure.)

b. Key shall be designed to resist the hydrostatic pressure from above the salt.

(3) Unlined Section

Provide 11-foot 8-inch diameter to allow for future salt creep deformation.

corrective action shall be taken to control the water inflow. The basis for determining if the amount of ground water flowing into the shaft is unacceptable shall be if the inflow exceeds an amount which can be tolerated without appreciably altering the drilling fluid characteristics as approved by the DOE Contracting Officer.

The shaft key shall be constructed using reinforced concrete and will serve as the transition element between the lined and the unlined sections of the shaft. It shall retain the rock formation and shall be provided with chemical water seals and a water collection ring with drains to prevent water from flowing from behind the liner down the unlined shaft. The key shall be designed to resist lateral pressure generated by salt creep, rock and soil overburden, and by hydrostatic pressure from above the salt. The design lateral pressure was selected as 75 percent of the overburden pressure based on the configuration of mine shafts in the vicinity of the WIPP. These shafts generally have a concrete liner that is thinner and that extends to a greater depth than the shaft key at the WIPP. Most of these shafts are at least 25 years old and show no significant deterioration or structural instability.

No liner or wire mesh is planned for the section of the shaft in the Salado formation. However, if field conditions require, rock bolts and wire mesh may be installed in zones of fractured salt.

The shaft station excavation shall be the minimum required to meet the operational and safety requirements in the shaft pillar area of the waste storage level. Supports of underground workings shall comply with Federal and New Mexico codes. The use of rock bolts and wire mesh in specific areas shall be determined by excavation conditions and code requirements. The roof, walls and floor shall be checked periodically for loose salt in accordance with applicable codes.

The bottom of the shaft shall extend below the facility level to accommodate the salt handling equipment and a sump to collect water that might enter the shaft. Should the stratigraphy of the facility

level be unsuitable for waste storage, the shaft bottom may be lowered to reach a more suitable stratigraphy.

Geomechanical instruments shall be provided to measure radial convergence (closure) of the shaft, water pressure behind the liner, salt creep, forces on the concrete key, and the variation of load on rock bolts. The type of instruments installed shall be strain gauges, pressure cells, piezometers, stressmeters, extensometers, load cells and radial convergence points.

The shaft liner, key, unlined section and furnishings shall be inspected at approximately 1 month intervals, or lesser intervals as required, to detect cracking, corrosion, deterioration and water intrusion.

## 7.3 DESIGN VALIDATION PROCESS

The design validation process for the C & SH shaft consists of data collection, analysis and evaluation, and predictions of future behavior. The following discussions of each of these activities have been divided into four sections: the lined section of the shaft; the shaft key; the unlined section; and the shaft station. This division is based on the different in situ and design conditions in each of these areas.

### 7.3.1 Data Collection

Data collection in the C & SH shaft has consisted of geologic mapping, visual inspections and geomechanical instrument measurements. The results of shaft mapping have been discussed in Chapter 6. Field observations and the geomechanical instrumentation program are discussed in the following subsections.

#### 7.3.1.1 Lined Section

Field Observations. The C & SH shaft has been inspected on a regular basis since its construction. During the facility level construction

phase, the mining contractors conducted weekly shaft inspections for safety and shaft maintenance. These weekly inspections are being continued by the facility operator.

Site geologists inspect the shaft at approximately 6-month intervals. These inspections provide geotechnical evaluations of the condition of the shaft, and of instrument conditions and their performance. Shaft inspections were performed on the following dates: August 29, October 1, October 5, October 22, November 19 and December 3, 1983; June 2, June 21, October 13 and November 12, 1984; and April 9 and December 9, 1985. The results of these inspections are presented in the GFDRs.

Geomechanical Instrumentation. Nine sets of radial convergence points were installed in the C & SH shaft between July 7 and 17, 1982. Two additional sets were installed on October 8, 1982. Five of these 11 sets were installed in the lined section of the shaft (Figure 7-1). Plots of the convergence point data from the lined section are presented in Appendix J, Figures J-205 through J-209.

Ten piezometers were installed in the lined section of the C & SH shaft above the shaft key between July 10 and 17, 1982 (Figure 7-1). Two piezometers each are at elevations of 2830, 2790, 2719, 2684 and 2608 feet. All of these piezometers are in the Rustler formation. The piezometers at elevations of 2790 and 2684 feet are in the water-bearing dolomite members, the Magenta and Culebra, respectively. Graphic plots of piezometer data are presented in Appendix J, Figures J-34 through J-44. The piezometers are dual-component instruments containing a vibrating-wire gauge and a pneumatic gauge. The vibrating-wire gauge is the principal instrument used to measure water pressure. The pneumatic gauge is used for initial calibration and periodic performance checks on the vibrating-wire units. The vibrating-wire piezometers were connected to the datalogger on October 30, 1982. The pneumatic units can only be read manually at the instrument location; however, most of the pneumatic units are no longer functioning.

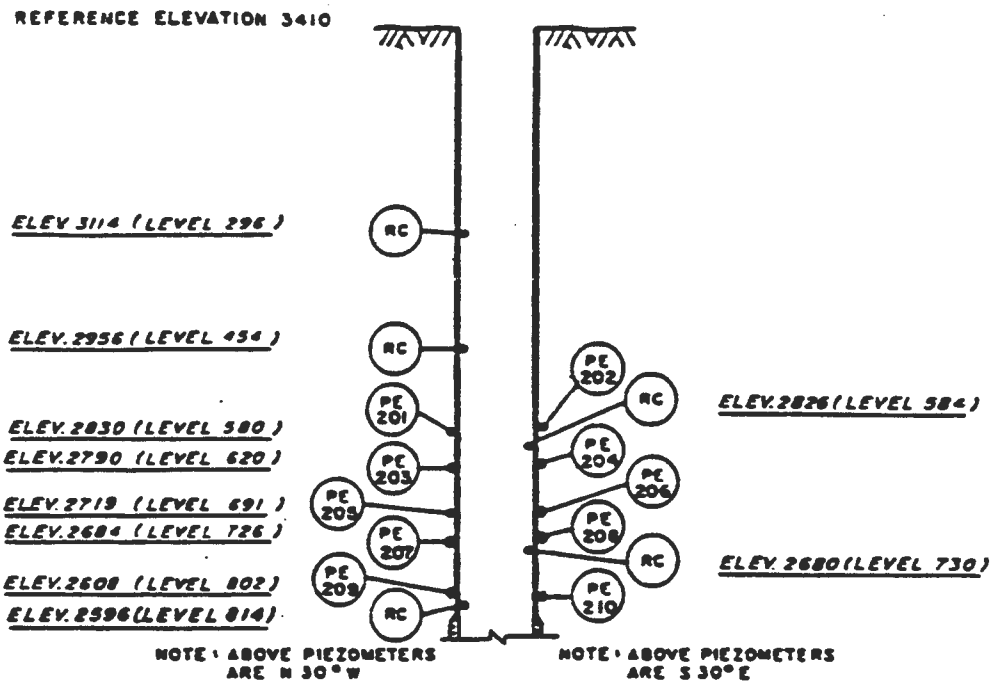


## LEGEND

- (PE) PIEZOMETER
- (RC) RADIAL CONVERGENCE POINTS
- (GE) EXTENSOMETER

*NOT TO SCALE*

## NOTES

1. RC'S AT EACH LEVEL CONSIST OF FOUR POINTS.
2. THE TERM "LEVEL" IS AN APPROXIMATE DEPTH IN FEET FROM THE TOP OF THE SHAFT BUNTON AT ELEVATION OF 3410.0 FT MSL. ELEVATIONS ARE FROM CEMENTATION WEST, INC., 1983, WIPP SHAFT AND STATION SURVEY.

**Figure 7-1**

**C & SH SHAFT LINER INSTRUMENTATION**

The shaft instrumentation has had a history of damage. Convergence points and especially piezometers are susceptible to damage from falling objects and construction activities. Damage in the lined section of the shaft has generally consisted of sheared data cables, sheared or bent convergence points, broken junction boxes and water damage.

Water intrusion has been a major problem with most of the shaft instruments and control systems. One water source has been the holes drilled into the steel liner for piezometer installation. The bushing in the liner through which the piezometer was installed did not have tapered threads, making it difficult to seal the hole in the liner. Leakage through these holes has generally occurred at some time in their history. It was especially difficult to effect a seal when a piezometer was reinstalled after being repaired due to other damage.

Water trickling down the liner from around these bushings has sometimes entered damaged fiberglass junction boxes and terminal boxes through cracks. Water has also seeped into the conduit connecting piezometers with the nearest junction box. This water has corroded terminal blocks and seeped down cables connecting lower terminal boxes.

A second water source has been rainfall. During periods of heavy rain, water runs down the shaft along the surface of the liner. This water can enter terminal boxes broken by impact or construction activities. Once in the boxes, it causes corrosion and cable damage.

A great deal of effort has been exerted correcting these problems. Shields were placed over boxes, cables were replaced and rerouted, and piezometers were repaired and sealed as well as possible. These measures improved performance somewhat, but problems still exist. The data acquired from the instruments is considered valid, but must be interpreted in light of the various interruptions in data monitoring. The specific details of instrument damage are updated in every GFDR, particularly in the tables of operating histories.

7.3.1.2 Shaft Key

Field Observations. The shaft inspections conducted on October 1 and November 19, 1983, June 2 and October 13, 1984, and April 3 and December 9, 1985, paid particular attention to the shaft key. The design of the key provides a means to determine if any water from the water-bearing zones in the Rustler formation is flowing behind the key. This situation, if it existed, could cause dissolution of the salt around the key resulting in eventual structural instability.

During inspection of the shaft key, the condition of four telltale drains that connect to a French drain behind the key is observed. Any moisture in the drains is noted. Similarly, other capped pipes (those for possible future injection of grout and those originally used for chemical seal injection) are checked for accumulated water. The interface between the salt and the bottom of the key receives particular attention.

The latest geotechnical inspection of the shaft key was made on December 9, 1985. The four telltale drains at the key were inspected and cleaned. Only the hole on the northwest side of the shaft was weeping, resulting in salt accumulation on the terminal box below. After chipping off this salt, a small amount of liquified chemical seal material began oozing out of the telltale. Inspection of the bottom of the key showed no evidence of seepage below the concrete.

Geomechanical Instrumentation. Twenty-four embedment strain gauges, 16 spot-welded strain gauges, and 4 pressure cells were installed in the C & SH shaft key from April 11 to 17, 1982. Two piezometers were installed in the shaft key on July 10, 1982. The locations of these instruments are shown on Figure 7-2. All instruments were read manually until they were connected to the datalogger system on October 30, 1982. Appendix J contains plots of the data from these instruments. Piezometer data are presented on Figures J-44 and J-45. Figures J-54 through J-57 present pressure cell data. The strain gauge data are presented on Figures J-58 through J-97.

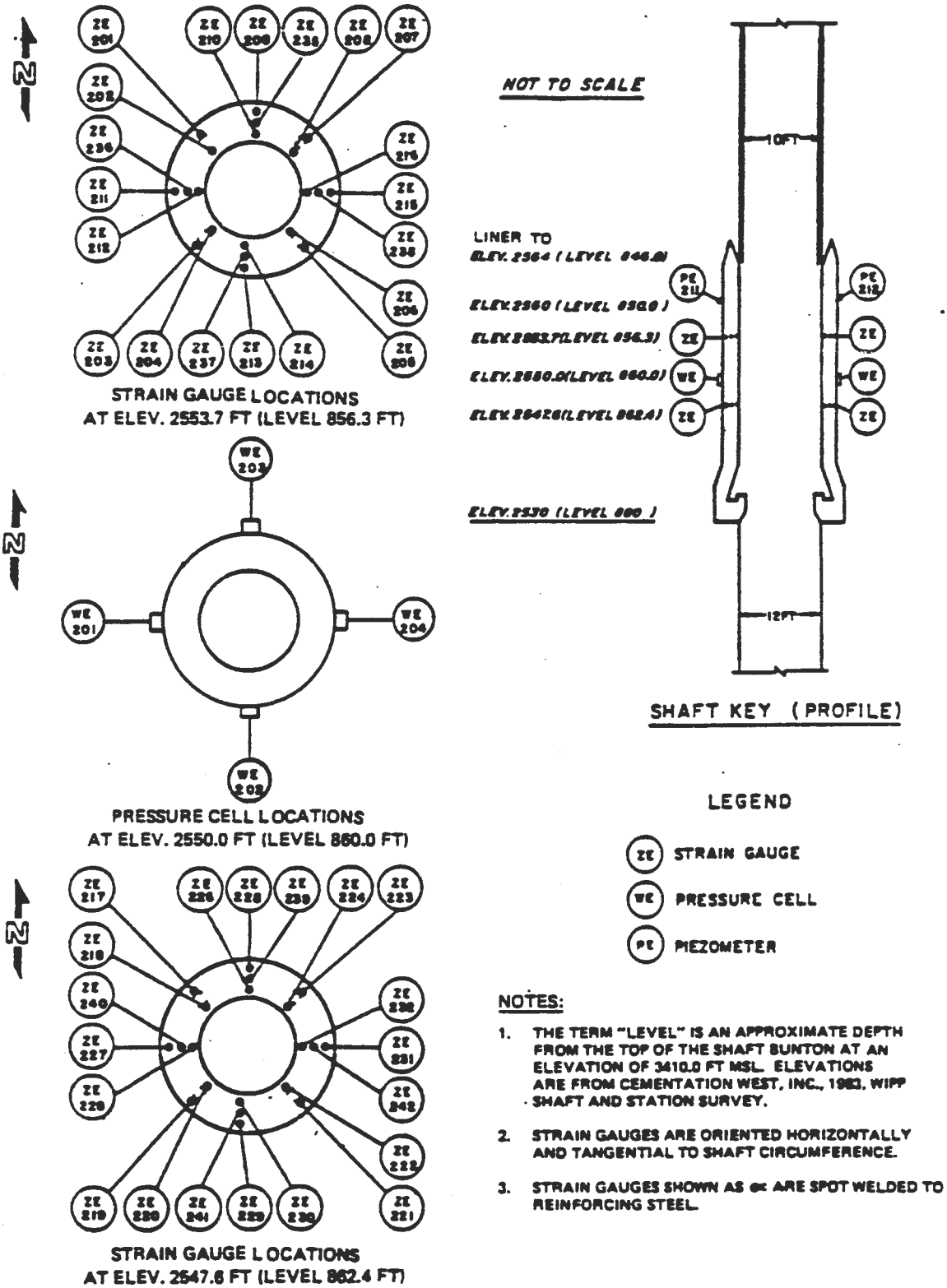


NOTES:

1. THE TERM "LEVEL" IS AN APPROXIMATE DEPTH FROM THE TOP OF THE SHAFT BUNTON AT AN ELEVATION OF 3410.0 FT MSL. ELEVATIONS ARE FROM CEMENTATION WEST, INC., 1983, WIPP SHAFT AND STATION SURVEY.
2. STRAIN GAUGES ARE ORIENTED HORIZONTALLY AND TANGENTIAL TO SHAFT CIRCUMFERENCE.
3. STRAIN GAUGES SHOWN AS ⊗ ARE SPOT WELDED TO REINFORCING STEEL.

Figure 7-2

C & SH SHAFT KEY
INSTRUMENTATION

The instruments for monitoring the shaft key, and especially their electrical boxes and cables, have had the same performance problems as the piezometers and convergence points in the lined section above. The two key piezometers have been damaged and repaired repeatedly.

The major problem in the key has been water damage inside the various electrical boxes. The worst damage was in termination cabinet LTC-1. Water seeping down inside cables connected to water-damaged boxes in the lined section of the shaft corroded the terminals in the LTC. LTC-1 links the piezometers, strain gauges and pressure cells to the surface datalogger. Several attempts were made to repair the LTC components. The components were permanently removed in October 1984 in order to avoid further damage. The shaft instrumentation system is scheduled for an overhaul during a future construction contract. Meanwhile, all LTC-1-controlled instruments are read manually during shaft inspections.

The terminal boxes for the pressure cells and strain gauges have also been damaged. Initial damage was to the fiberglass boxes and data cables as they were struck by falling objects and construction materials traveling on the shaft conveyance. Subsequent damage was by water seeping into the boxes. The boxes and cables have been repaired numerous times.

Detailed accounts of instrument damage are presented in the GFDRs, particularly in the tables of operating histories. The GFDRs also discuss data collection, data plots and interpretative problems with the C & SH shaft key instruments.

7.3.1.3 Unlined Section

Field Observations. Shaft inspections include observations of the unlined section of the C & SH shaft. This section of the shaft consists of exposed salt forming a smooth wall. The inspections consist primarily of determining if any spalling or fracturing of the salt is occurring.

The unlined section was inspected to a depth of 2,057 feet (elev. 1353 feet) on December 9, 1985. One near-vertical fracture was observed on the west side of the shaft between a depth of 1,021 feet and 1,043 feet (elev. 2389 feet and 2367 feet). It ranged from closed to less than 1/4-inch wide at the wall surface and extended about 10 feet in length. It did not appear on the east side of the shaft. Previous shaft mapping showed the presence of halite-filled vertical fractures in anhydrite from a depth of approximately 1,023 feet to 1,038 feet (elev. 2387 feet to 2372 feet). The fracture observed appears to be one of those previously mapped. Salt blisters and precipitate were noted in various areas commonly associated with clay layers. The most notable area was a 4-foot zone around the entire shaft circumference from a depth of approximately 1,038 feet to 1,042 feet (elev. 2372 feet to 2368 feet).

Geomechanical Instrumentation. Nine borehole extensometers were installed in the unlined section of the C & SH shaft between July 6 and 8, 1982. These extensometers are arranged in three-instrument arrays at elevations of 2337 feet, 1846 feet and 1353 feet (Figure 7-3). Readings were taken manually until the extensometers were connected to the datalogger system in October 1982.

The extensometers are the multiple-point, sonic-probe type consisting of four anchors. The anchors for each extensometer were set at depths of 4, 9, 18 and 36 feet. The collar of the extensometers was recessed 1 foot into the salt. Data plots for the extensometers are presented in Appendix J, Figures J-116 through J-124.

The extensometers have not been damaged as much as the other instruments in the shaft. Their operating histories rarely show any interruption in the data. This lack of damage is a result of several factors. The diameter of the unlined shaft is 2 feet greater than that of the key or lined section. The instruments are recessed and therefore not susceptible to damage from falling objects. The extensometers are connected to LTC-2 and LTC-3, which are not directly

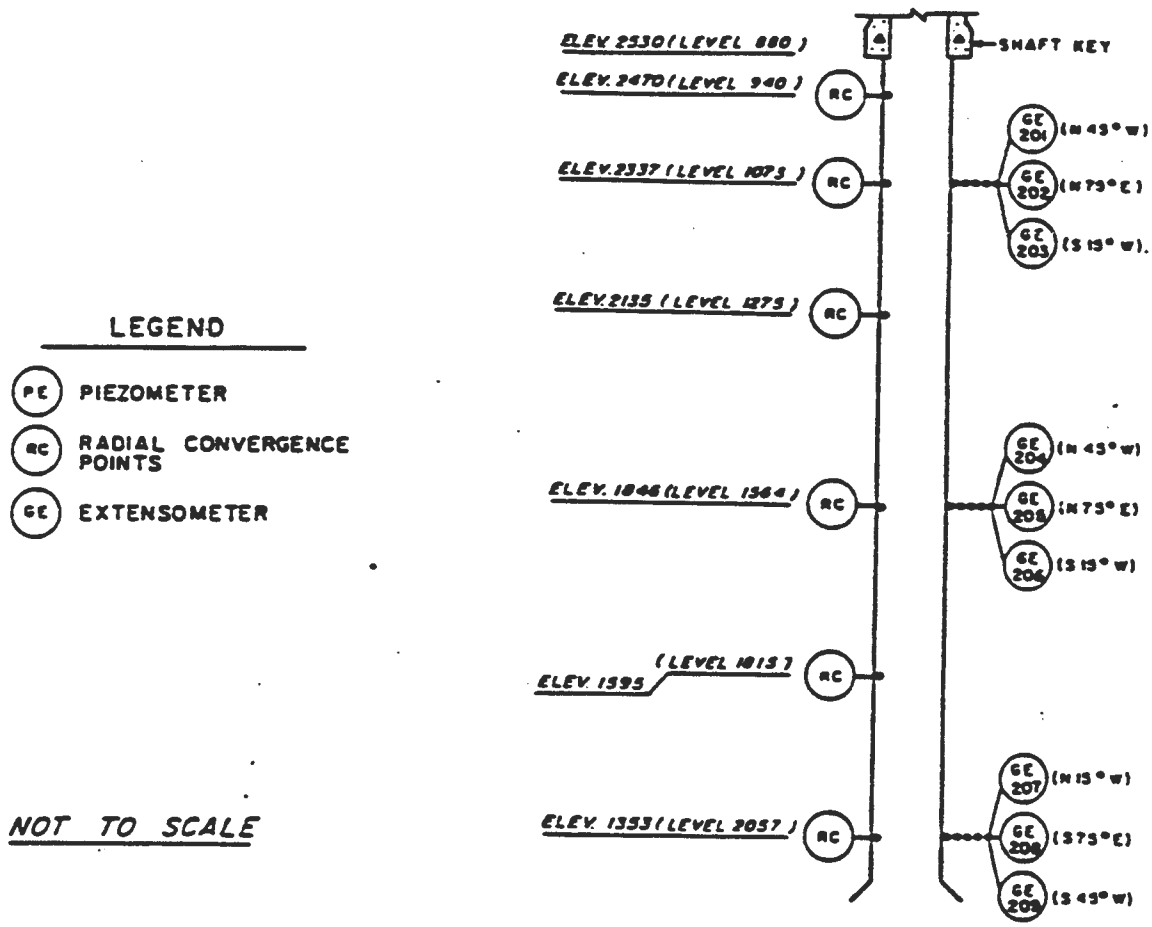


## NOTES

1. RC'S AT EACH LEVEL CONSIST OF FOUR POINTS.
2. THE TERM "LEVEL" IS AN APPROXIMATE DEPTH IN FEET FROM THE TOP OF THE SHAFT BUNTON AT ELEVATION OF 3410.0 FT MSL. ELEVATIONS ARE FROM CEMENTATION WEST, INC., 1983, WIPP SHAFT AND STATION SURVEY.

**Figure 7-3**

**C & SH SHAFT UNLINED SECTION INSTRUMENTATION**

linked to LTC-1 and the piezometers. Thus, water damage has not been a problem.

Six sets of radial convergence points are located in the unlined section of the shaft. These points have a history of damage and replacement similar to that of the other convergence points. This history is discussed in the GFDRs. Plots of the convergence point data from the unlined section are presented in Appendix J, Figures J-210 through J-214. Only five plots are presented since damage to the set of points at elevation 1595 feet prevented the obtaining of reliable readings.

7.3.1.4 Shaft Station

Field Observations. Site geologists monitor the deformational behavior of the C & SH shaft station on a regular basis. Particular attention is given to four aspects of movement or failure: roof and wall spalling; fracturing at pillar corners; roof displacements and separations; and floor displacements, separations and fracturing. The observations are recorded at least every 3 months and have been published in each GFDR since the February 1984 issue.

A description of the C & SH shaft station excavation and roof support methods were presented in Chapter 3. The failure of resin-anchored rock bolts installed initially in the shaft station roof has been attributed to a combination of the following factors:

(1) the resin firmly held the bolt shank in place and salt creep caused failure at the first weak point;

(2) improper bolt installation resulted in damage to the threaded section of the bolt (improper torque and lack of beveled or spherical washers); and

(3) contributing factors such as corrosion and hydrogen embrittlement.

Rock bolts installed to replace the failed bolts, and subsequent bolt installations, used mechanical anchors. As the load on these bolts increases due to salt creep, the anchor yields by slipping in the hole. Although this slipping is not desirable for the roof support of underground openings in hard rock, it provides more control than rigid anchors that do not yield but instead produce sudden bolt failure as a result of the stress created by creeping salt. The slipping reduces the load on the bolt, thus reducing the potential for bolt failure, but allows continued roof support and prevents sudden roof falls. Each mechanical-anchor rock bolt supports a load that is less than its capacity, but the aggregate support provided by all of the rock bolts in a pattern is more than adequate for positive ground control. The experience at WIPP shows that the mechanical-anchor rock bolts perform well in creeping salt if periodically inspected and maintained.

The station roof and walls have exhibited continual slabbing and spalling which has required periodic scaling. Wire mesh has been installed over the entire station roof to contain any small, loose salt fragments.

Vertical fractures have developed in the pillar corners at the S90 crosscut. The condition of these fractures has been monitored and the results reported on a regular basis in the GFDRs. A discussion of fracturing at pillar corners is presented in Chapters 10 and 11.

Displacements, separations and fractures have been detected in boreholes drilled into the station roof and minor separations have been detected in some holes drilled into the station floor. Separations and fracturing at clay G and in the underlying halite were detected shortly after the initial station excavation. Horizontal displacements have been observed in various boreholes during the past 2 years.

In May and June 1986, 20 boreholes were drilled in four arrays in the shaft station to further investigate the extent of separations and fracturing in the roof and floor. This drilling was conducted as part

of a program to characterize excavation effects in the salt surrounding the openings and particularly in MB-139. This program is discussed more fully in Chapters 10 and 11.

The new boreholes were inspected for the existence of separations and fractures. Existing holes were inspected for horizontal displacements. The probe used for this inspection consisted of an aluminum rod with a 1/16-inch thick nail attached perpendicular to one end. When applying moderate pressure, the nail snags on the borehole wall if a separation, fracture, or clay seam is encountered. The separation is considered to be less than 1/16 inch wide if the nail catches on, but does not penetrate the hole wall. If the separation at the wall surface is at least the nail width (approximately 1/16 inch) there will be a slight penetration. If the separation is larger, the nail penetrates its entire 1/2-inch length into the wall. When the probe catches on the hole wall, the feature is probed on all sides of the hole. This ensures that it is a continuous feature and not a clay pocket or an imperfection caused by the drilling.

Fracture zones, anhydrite beds, or clay seams were sometimes identified by picking out pieces of the material with the probe nail. An estimate of their vertical dimension was made by moving the probe rod up and down within the limits of the feature. Occassionally a slight penetration occurred at the clay seams due to a very small separation or penetration into the softer clay.

In the array of holes drilled north of the shaft, no separations or fractures were detected in the roof. In the two arrays drilled south of the shaft, multiple separations and fractures, ranging from approximately 1/16 inch to 4 inches wide, were found in most of the roof holes within the halite below clay G. Many of the fractures occur within 3 feet of the roof. Some separation and fracturing appears to be associated with clay G based on data from other holes in the station area and from the central roof holes in the two arrays, but no significant occurrence appears to have developed in the holes closest

to the station walls. A separation, less than 1/16 inch wide was detected in only one roof hole beyond a depth of 4 feet.

Only a few separations or fractures, less than 1/8 inch wide, were detected in the central floor hole of the hole array drilled north of the shaft. Some separations and fractures, less than 1/16 inch to 1 inch wide, were detected in the two floor hole arrays drilled south of the shaft. These occurrences were in MB-139 and the overlying halite. Essentially no separation was encountered at clay E at the base of MB-139. Holes drilled around the edge of the electrical substation concrete base slab foundation to investigate a potential source of its tilting encountered only small scattered separations. The total accumulated vertical separation is estimated to be less than 1/2 inch.

Geomechanical Instrumentation. As in other areas of the underground facility, a suite of geomechanical instruments was installed in the C & SH shaft station (Figure 7-4). The original instrumentation design consisted of 6 rock bolt load cells, 3 borehole extensometers, and 2 sets of convergence points. These instruments were installed between June 30 and November 16, 1982. Subsequently, 4 extensometers, 4 lateral movement gauges, 3 convergence point sets, and 1 set of wall shortening points were installed between January 8 and February 3, 1983. The purpose of this second suite of instruments was primarily to monitor any vertical or lateral movement of the immediate roof in the C & SH shaft station. The immediate station roof consists of a "beam" of salt resulting from separation along the thin clay seam beneath anhydrite "a". South of the shaft this beam is about 3 to 4 1/2 feet thick, while north of the shaft it is about 7 feet thick. Chapter 3, Section 3.2, presents a brief discussion of the underground facility horizon selection and the resulting location of the station with respect to overlying and underlying clay seams and anhydrite layers.

The data plots for the C & SH shaft station are presented in Appendix J. Figures J-146, J-147, J-163, and J-170 through J-173 show

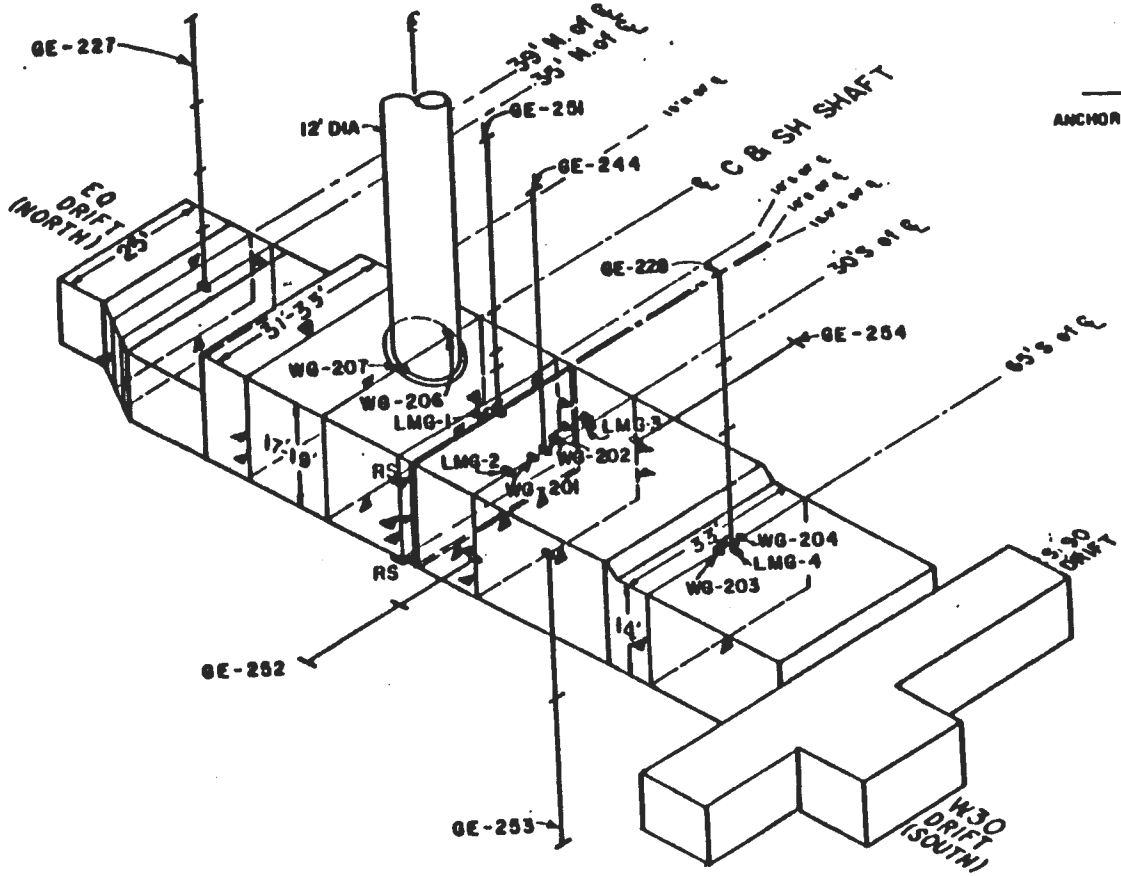


## LEGEND

ANCHOR COLLAR

- GE EXTENSOMETER
- RC CONVERGENCE POINT
- RS WALL SHORTENING POINT
- WG ROCKBOLT LOAD CELL
- LMG LATERAL MOVEMENT GAUGE

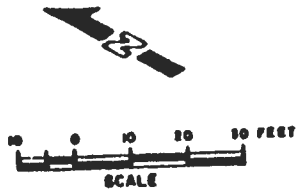


Figure 7-4

C & SH SHAFT STATION INSTRUMENTATION

the extensometer data. Convergence point data are presented on Figures J-188 through J-194 and rock bolt load cell data are shown on Figures J-192 through J-197.

Four lateral movement gauges were installed in the roof of the station. These were intended to measure lateral displacement of the salt above anhydrite "b". However, the lateral movement measurements were distorted by the vertical movement of the roof and a meaningful trend or pattern in the relative direction of horizontal movement did not develop. Therefore, reading of the lateral movement gauges was discontinued and the data are not presented in this report.

### 7.3.2 Analysis and Evaluation

The data collected from the C & SH shaft have been reviewed and subjected to statistical analysis, closed form solution and model simulation techniques for evaluation against the reference design parameters. The following subsections present discussions of these analyses and evaluations for the four sections of the shaft.

#### 7.3.2.1 Lined Section

Observed Conditions. Observations of the steel liner during shaft inspections have detected no signs of deterioration. There is no indication of any liner instability due to shaft deformation. Water seepage has occurred only through the previously discussed piezometer bushings.

Structural Analysis. As a result of increasing hydrostatic pressure with depth, the thickness of the C & SH shaft steel liner and the size and spacing of its stiffener rings vary accordingly. The stiffener rings are 3-inch thick steel rings welded to the outer face of the liner. The thickness of the liner and the width and spacing of the stiffener rings for various depths are:

| Depth (feet) | Plate Thickness (inches) | Stiffener Width (inches) | Stiffener Spacing (feet) |
|---|---|---|---|
| 0.00 to 182.45 | 5/8 | 7-1/2 | 10 |
| 182.45 to 362.45 | 1 | 12 | 10 |
| 362.45 to 542.45 | 1 | 11 | 5 |
| 542.45 to 642.45 | 1-1/4 | 10-1/2 | 5 |
| 642.45 to 742.45 | 1-3/8 | 9 | 4 |
| 742.45 to 842.45 | 1-1/2 | 10-1/2 | 4 |

A structural analysis was performed for the shaft liner based on these depths and dimensions. The liner and stiffeners were made of A-441 steel fabricated into 20-foot sections by full penetration bevel welds between the liner sections and by fillet welds between the liner and the stiffeners. Radiographic acceptance examinations were performed on all welds in accordance with the American Welding Society (AWS) (ref. 7-1) and the ASME Boiler and Pressure Vessel Code, Sections VIII and IX (ref. 7-2).

A computer program was used to design the steel liner against elastic buckling between the stiffeners, elastic buckling of the combined liner and stiffener, and the yielding of the liner. This program was developed jointly by Fenix & Scisson and Southwest Research Institute and was based on Theory of Plates and Shells by S. P. Timoshenko and S. Woinowsky-Krieger (ref. 7-3).

The computational results of the analysis of the liner, based on the depths and dimensions presented above, show that the external pressure capacities and corresponding closure limits (maximum diametric changes) at the midpoint of a stiffener and at the midpoint between stiffeners are:

| Depth (feet) | Pressure Capacity (psi) | Closure Limit at Stiffener (inches) | Closure Limit Between Stiffeners (inches) |
|---|---|---|---|
| 0.00 to 182.45 | 139 | 0.007 | 0.054 |
| 182.45 to 362.45 | 281 | 0.010 | 0.069 |
| 362.45 to 542.45 | 434 | 0.019 | 0.108 |
| 542.45 to 642.45 | 518 | 0.030 | 0.104 |
| 642.45 to 742.45 | 595 | 0.043 | 0.112 |
| 742.45 to 842.45 | 684 | 0.043 | 0.118 |

In situ hydrostatic pressures determined from piezometer readings at elevations of 2830, 2790, 2719, 2684 and 2608 feet (Figure 7-1) were compared with design pressures and the pressure capacity of the liner as discussed below.

Measured Water Pressure. Piezometers are used to monitor the hydrostatic pressure exerted on the steel liner by water from the two water-bearing zones in the Rustler formation. Selected water pressure measurements are presented in Table 7-2. Because of the piezometer history of damage and leakage, the data must be used with caution. However, as expected, the data show a general trend of increasing pressure (Figure 7-5). The exceptions, 37X-PE-00211 and 37X-PE-00212, are discussed in the next subsection.

As indicated in Table 7-1, the design basis hydrostatic pressure is assumed to begin at a depth of 250 feet below ground level. This corresponds to the potentiometric surface of the water-bearing members in the Rustler formation. The hydrostatic design pressure gradient of the liner in the Rustler formation is shown on Figure 7-5. Piezometer reading data from June 1986 indicate pressures significantly less than the design hydrostatic pressure. This can be explained by a combination of the following conditions:

(1) drawdown of the potentiometric surface in the vicinity of the shafts;

Table 7-2

C & SH SHAFT LINER AND KEY
SUMMARY OF MEASURED WATER PRESSURES (psi)

| Date of Reading | PIEZOMETER NO. 37X-PE-00 | | | | | | | | | | | |
|---|---|---|---|---|---|---|---|---|---|---|---|---|
| | 201 | 202 | 203 | 204 | 205 | 206 | 207 | 208 | 209 | 210 | 211 | 212 |
| | Elev. 2830 | | Elev. 2790 | | Elev. 2719 | | Elev. 2684 | | Elev. 2608 | | Elev. 2560 | |
| Pressure capacity of liner | 518 | | 518 | | 595 | | 595 | | 684 | | | |
| Jun. 20,'83 | 112 | 111 | 108 | 108 | 86 | 86 | 110 | 104 | 140 | 142 | 6 | 12 |
| Dec. 3,'83 | 96 | 96 | 100 | 101 | 84 | 84 | 98 | 100 | 137 | 139 | 13 | 9 |
| Jun. 5,'84 | 90 | 93 | - | - | 79 | - | 90 | 96 | 127 | 129 | 5 | 1 |
| Dec. 27,'84 | 93 | 95 | 119 | 119 | 102 | 100 | 105 | 116 | - | 152 | 3 | 0 |
| Feb. 8,'85 | 98 | 100 | 131 | 130 | 109 | 105 | 107 | 117 | - | 157 | 10 | 7 |
| May 21,'85 | 90 | 93 | 84 | 81 | 61 | 44* | 105 | -** | 146* | 137* | 5 | 6 |
| Jun. 29,'85 | 89 | 92 | 91 | -** | 97 | -** | 104 | -** | -** | -** | 4 | 7 |
| Dec. 9,'85 | 90 | 91 | 108 | 104 | 100 | -** | 108 | -** | -** | -** | -1 | -1 |
| Mar. 24, '86 | 101 | 102 | - | 134 | 107 | -** | 104 | -** | -** | -** | -2 | -4 |
| Jun. 02, '86 | 89 | 91 | 104 | - | 100 | -** | 108 | -** | -** | -** | - | -2 |

NOTE: All piezometers have leaked or suffered damage at one time or another.

* Piezometer leaking.

** Piezometer removed for repair.

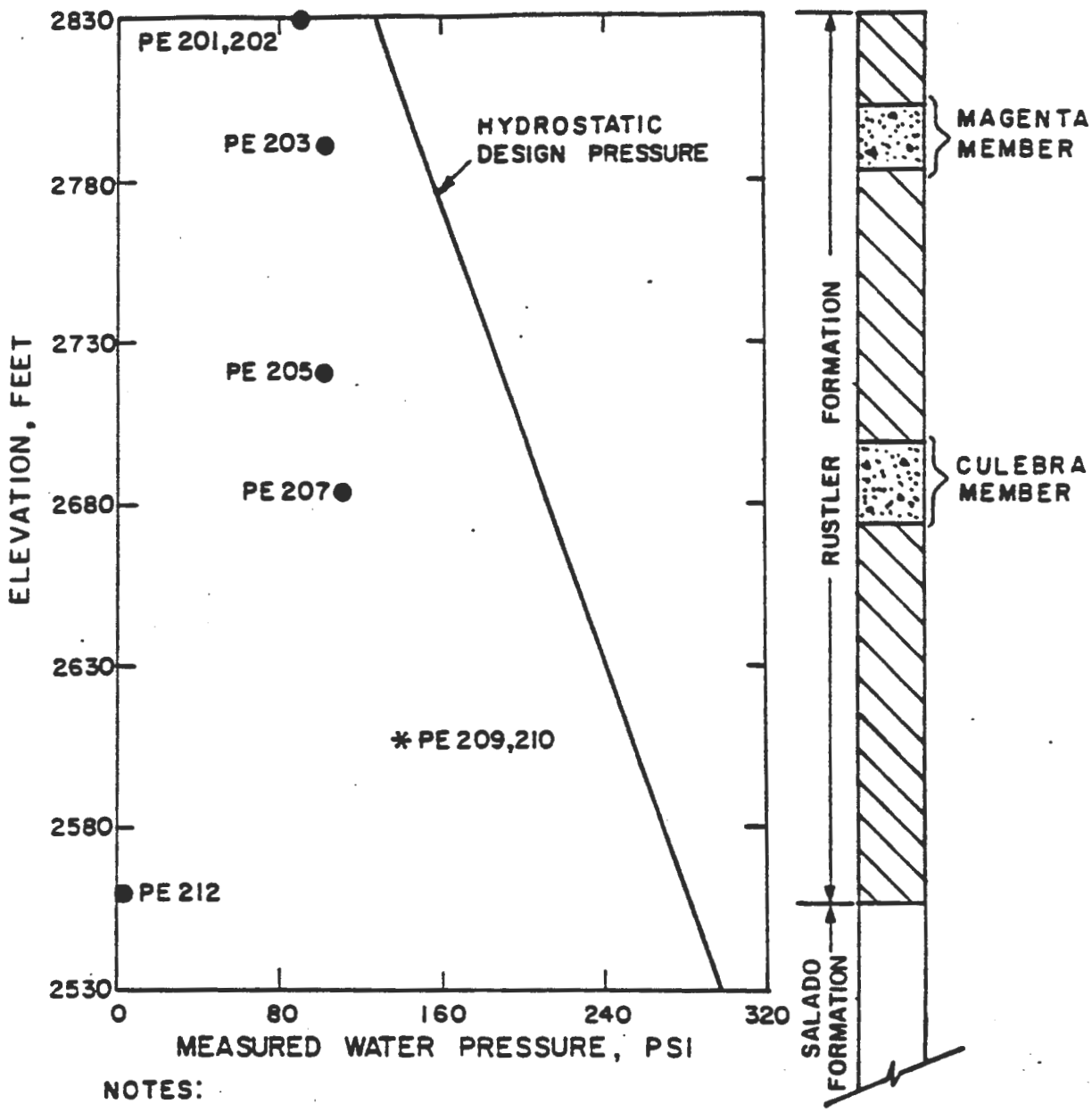


NOTES:

● READINGS TAKEN ON JUNE 2, 1986

* READING TAKEN ON MAY 21, 1985

Figure 7-5

C & SH SHAFT LINER AND KEY
WATER PRESSURE DISTRIBUTION

(2) incomplete hydraulic continuity behind the liner;

(3) water leakage through the piezometer bushings and telltales; and

(4) partial plugging of the piezometer filters.

Lowering of the potentiometric surface is primarily the result of water flowing into the unlined SPDV ventilation shaft and later through cracks in both the waste and exhaust shaft liners. Hydrologic testing at the site by SNL has also contributed to lowering the potentiometric surface.

The annular space between the steel liner and the rock was filled with grout during liner installation (Chapter 3). In addition to supporting the liner, the grout was intended to help prevent water in the water-bearing zones from contacting the salt in the key area. The variations in water pressure at the different piezometer elevations, and especially the lack of a linear increase with depth, suggests that this objective has been at least partially achieved. The absence of hydraulic continuity along the rock/liner interface could prevent the water at individual piezometer elevations from achieving the anticipated pressures.

Most of the piezometers have developed leaks at some time in their history. This leakage would result in a drop in water pressure at the affected piezometer. The piezometer would then measure a water pressure that is lower than anticipated. The influence of the leaks on piezometer readings is considered to be minor because, as individual piezometers are repaired or bushings are sealed, the data plots do not show a significant change from the normal variation within the data.

The fourth cause of variation in the pressure readings could be a result of partially-plugged filters. Each piezometer contains a stainless steel, porous stone filter. It has been noted during their

repair that some filters are partially covered with salt deposits and corrosion. It is not clear how much of an effect this may have on the piezometer readings. It is possible that there is no effect if the corrosion and salt deposition occurred after the filter was exposed to the atmosphere during piezometer removal.

Closure. Closure data show the in situ diametric changes in the liner based on radial convergence point measurements at elevations of 3114, 2956, 2826 and 2680 feet (Figure 7-1). These data are considered a lower bound because the in situ readings represent only relative closures since the first readings were taken 329 days after excavation. In addition to the effect of hydrostatic pressure, the closure data are also affected by variables such as temperature and lithostatic pressure.

Radial convergence point measurements in the lined section of the shaft indicate that the maximum diametric closure is less than 0.10 inch. Since the shaft is used for ventilation purposes and is open to the atmosphere, changes in ambient temperature from around 0°F in the winter to over 100°F in the summer may affect the diametric closure by approximately 0.075 inch. Consequently, only closure data recorded at approximately the same temperature should be used for analysis.

7.3.2.2 Shaft Key

Observed Conditions. Shaft key inspections indicate that the key is stable. Certain observations, however, dictate that continuous monitoring of the key will be required. The telltale drains, connected to a French drain behind the key, drip intermittently. Several other capped pipes typically produce small amounts of water when opened after being closed for several weeks.

No water has been observed bypassing the lower chemical water seal. During the June 2, 1984, inspection, liquified chemical seal material was observed in two chemical seal injection pipes. It is likely that chemical seal material is migrating behind the key since small amounts

were observed dripping from the northwest telltale drain and from piezometer 37X-PE-00211. These fluid observations do not present any immediate cause for concern. However, the key should be monitored on a regular basis and appropriate actions taken if required to mitigate any significant increase in fluid discharge.

Inspection of the bottom of the key has revealed no evidence of seepage below the concrete. Some salt stalactites have been observed hanging from the concrete but these originate from brine dripping from the leaking piezometers or telltale drains above.

Model Simulation. The long-term impact of C & SH shaft salt creep on the concrete key was evaluated by a nonlinear computational analysis using the finite element method (ref. 7-4). The objective of the analysis was to determine the structural adequacy of the shaft key based on the appropriate ACI Codes (ref. 7-5). Site stratigraphy was considered in the analysis. The creep behavior of the salt was incorporated into the material properties used in the finite element model. The shrinkage of the concrete during initial curing was also simulated in the computation (ref. 7-6).

From the shaft geologic mapping, it was determined that the stratigraphy in the shaft key area consists of horizontal layers of halite, argillaceous halite, anhydrite and siltstone, with clay seams between some of these layers (Figure 7-6). This stratigraphy was used as the basis in modeling.

The properties for the host rock are based on laboratory test results (refs. 5-3 and 7-7) as described in Appendix C. Because the analysis was performed early in design validation, before the methods of computing primary creep and using in situ material properties were developed (ref. 5-1), the analysis included only the secondary creep of salt based on laboratory test data.

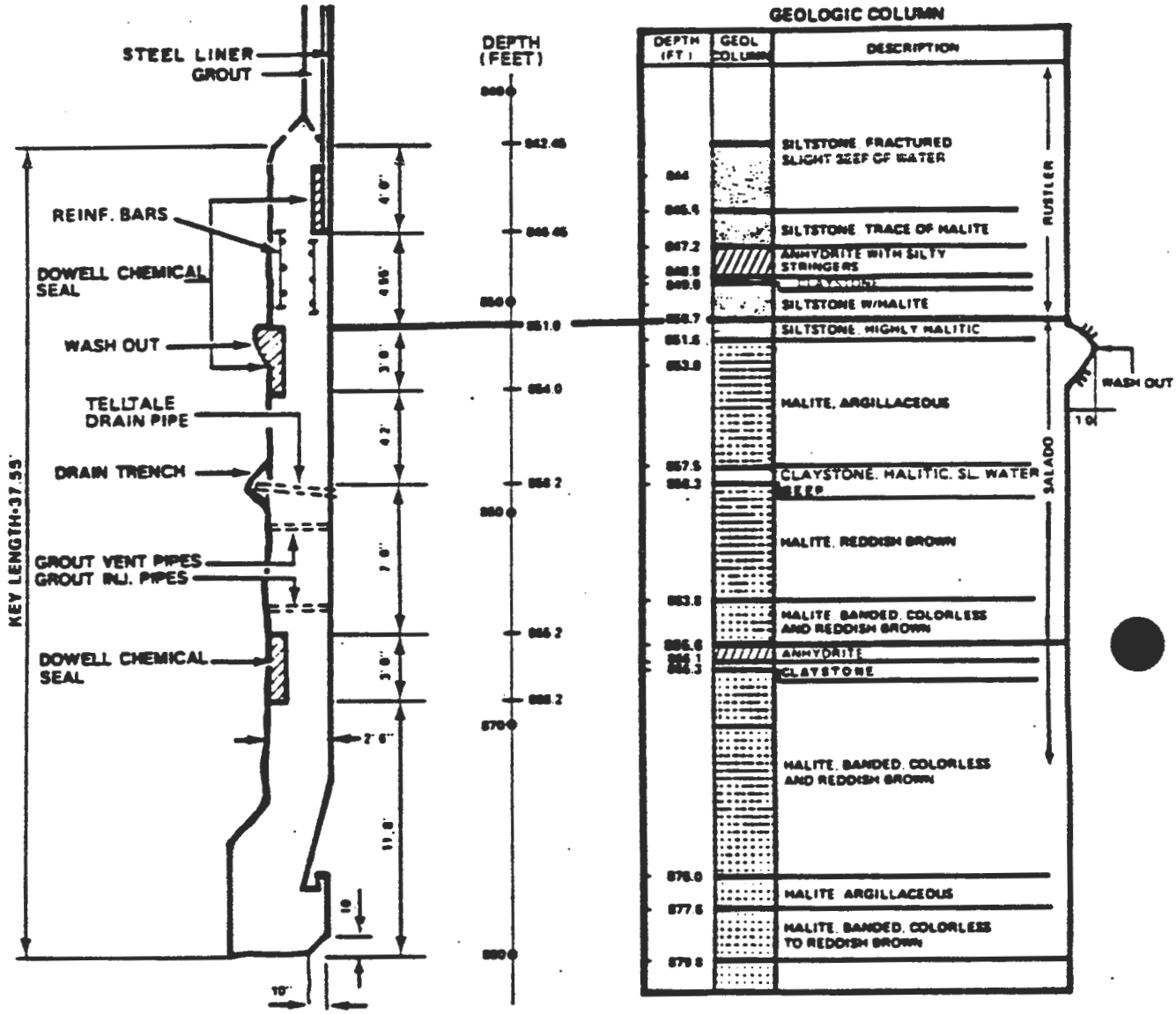


Figure 7-6

C & SH SHAFT KEY
STRATIGRAPHY

The relationship for concrete shrinkage (ref. 7-8) can be expressed as:

$$\varepsilon_{sh} = \frac{t}{35 + t} \varepsilon_{shu} C_{the} C_h C_s C_{cem} C_{fa} \qquad (7\text{-}1)$$

for t in days, or:

$$\varepsilon_{sh} = \frac{t}{3{,}024{,}000 + t} \varepsilon_{shu} C_{the} C_h C_s C_{cem} C_{fa} \qquad (7\text{-}2)$$

where: t is the shrinkage time in seconds;

$\varepsilon_{shu}$ is the ultimate shrinkage strain, taken to be 0.0008;

$C_{the}$ is the correction factor for thickness (1.17 - 0.029T);

$C_h$ is the correction factor for humidity (1.40 - 0.010H);

$C_s$ is the correction factor for slump (0.89 + 0.041S);

$C_{cem}$ is the correction factor for cement content (0.75 + 0.034B); and

$C_{fa}$ is the correction factor for percent fines and air content, taken to be 1.0.

The thickness T of the key wall is 30 inches; the humidity H is very low in the region of the key and is assumed to be 50 percent; the slump S of 4 inches is taken as the average value for 5,000 psi concrete; and B is the number of sacks of cement per cubic yard of concrete, considered to be equal to seven. The values of the correction factors $C_{the}$, $C_h$, $C_s$ and $C_{cem}$, as calculated from the equations above, are 0.3, 0.90, 1.05 and 0.99, respectively.

Figure 7-7 shows the finite element model for the creep analysis. Since the structure is symmetrical about the centerline of the shaft, the shaft key and the area around it were modeled using 196 quadrilateral ring finite elements representing 18 distinct geologic layers. The MARC General Purpose Finite Element Analysis Program (ref. 6-8) was used for the analysis. To reduce the computation time, the stress and strain were computed at the centroid of each element. Four clay seams, at depths of 848.9, 857.9, 866.2 and 900.9 feet, were considered as active slip planes, represented by 25 friction and gap link elements with a coefficient of friction equal to 0.4. The outside

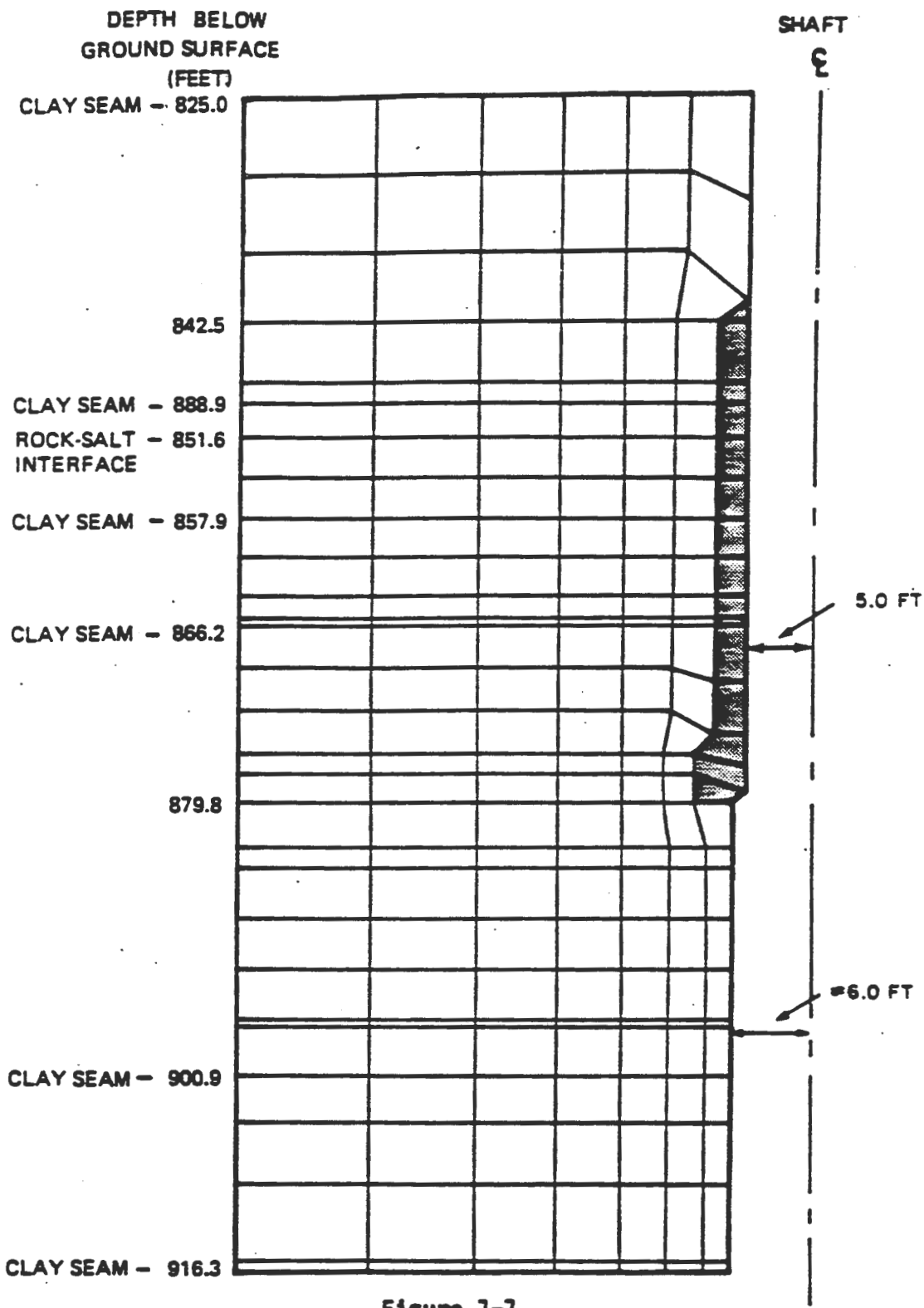


Figure 7-7

C & SH SHAFT KEY
FINITE ELEMENT MODEL

vertical boundary had zero horizontal displacement and the bottom boundary had zero vertical displacement. The boundary conditions at the top of the model were uniform calculated pressures based on the mass density of the geologic formation from the ground surface to the elevation of the boundaries. The lithostatic stress state was defined as described in Chapter 5, equation 5-1.

Creep analysis was performed on the mathematical model by using the procedures described in Chapter 5. The analysis was carried out for a 5-year interval without the key and a comparison was made of the corresponding radial deformations to determine the time when creeping salt would come into contact with the shrinking concrete key. The times computed for various layers behind the key were between 1.6 and 3.9 years with an average value of 2.7 years after excavation of the shaft (or 2 years after construction of the shaft key). To simulate contact of the shaft wall with the concrete key, the elements of the key were tied to the proper locations on the shaft wall and the analysis was continued for a total of 27 years (refs. 7-4 and 7-6).

Deformation. Readings from the strain gauges embedded in the concrete key show a range of strains from approximately 0.00014 in compression to 0.00021 in tension with an average compressive strain of 0.00004 through December 9, 1985. The readings from the strain gauges welded to the reinforcing steel show a range of approximately 0.00031 in compression to 0.00054 in tension with an average tensile strain of 0.00006.

Table 7-3 summarizes the changes in readings of the embedment and welded gauges at a depth of 856 feet (elev. 2554 feet) since April 22, 1982, immediately after concrete was placed for the shaft key. The trend of the change in strain readings indicates that the salt had not made contact with the key by June 1985.

Water Pressure. Figure 7-5 shows water pressure readings from piezometers 37X-PE-00211 and 37X-PE-00212. These piezometers have

## Table 7-3

C & SH SHAFT KEY
SUMMARY OF STRAIN GAUGE READINGS AT ELEVATION 2554 FEET

| Strain Gauge No. | Change in strain x $10^{-6}$ since April 22, 1982 | | | | Remarks |
|---|---|---|---|---|---|
| | Jun. 5, 1984 | Feb. 8, 1985 | Jun. 29, 1985 | Dec. 9, 1985 | |
| 37X-ZE-209 | -63 | -59 | -81 | -9.5 | Embedment |
| 211 | -23 | -16 | -34 | -51 | strain gauges |
| 213 | -133 | -104 | -139 | -144 | 14.5 inches |
| 215 | -82 | -67 | -99 | -111 | from inner surface |
| 235 | -12 | 16 | -23 | -47 | Embedment |
| 236 | 56 | 88 | 37 | 16 | strain gauges |
| 237 | -18 | 35 | -23 | -8 | 9 inches from |
| 238 | -63 | -23 | -81 | -99 | inner surface |
| 210 | -110 | -71 | -123 | -154 | Embedment |
| 212 | 178 | 272 | 201 | 215 | strain gauges |
| 214 | 58 | 128 | 65 | 79 | 3.5 inches |
| 216 | -53* | -7 | -61 | -76 | from inner surface |
| 201 | -93 | -100 | -102 | -138 | Strain gauges |
| 203 | - | - | 444* | - | welded to the |
| 205 | -235 | -286 | -352 | -371 | outer rein- |
| 207 | -102 | -127 | -142 | -95 | forcing bar |
| 202 | -43 | - | -61 | -58 | Strain gauges |
| 204 | 443 | 2066 | 1056 | 541 | welded to the |
| 206 | -193 | -147 | -230 | -246 | inner rein- |
| 208 | - | - | -1659** | - | forcing bar |

NOTE: Negative strain change indicates compression.

* Reading taken on May 3, 1984.
** Reading taken on Dec 30, 1982.

shown a range of readings from a maximum of 30 psi in 1982 to a current reading of 2 psi. As shown on the figure and in Table 7-2, the readings of these two piezometers are consistently lower than the readings from the upper piezometers. These lower piezometers are at a depth of 850 feet (elev. of 2560 feet), just above the chemical water seal at a depth of 851 feet (elev. 2559 feet). It appears that this seal may be breached and that water is able to bypass it and exit through the French drain and telltales. Piezometers 37X-PE-00211 and 37X-PE-00212 may also be isolated from the upper piezometers by the grout that was injected behind the steel liner at a depth of 843 feet (elev. 2567 feet).

The assumption that the chemical water seal just below the piezometers may be breached is based on observations of piezometer behavior during the October 1983 inspection. As discussed in subsection 7.3.1.2, several capped pipes in the key were found to contain small amounts of water during this inspection and were drained. Prior to this, piezometers 37X-PE-00211 and 37X-PE-00212 indicated pressures of around 6 to 8 psi. After draining the pipes, both piezometers showed a drop to 2 psi within 2 days. This indicates a hydraulic connection across the water seal.

It is unlikely that water in the key originates from higher in the shaft. Detailed mapping in the shaft key noted weeps from claystone and siltstone beds at depths of 842. 846 and 858 feet. This is probably the source of the water seen in the French drain telltales and other pipes in the key. The fact that the key piezometers have had consistently lower readings than the upper piezometers indicates that there is probably no hydraulic connection with the water-bearing members higher in the shaft. The draining of water from the grout pipes influenced only those piezometers in the key; none of the upper piezometers showed any pressure drop. The existence of a source of water in the key area provides a better explanation of the dripping from the telltales and the performance of the key piezometers than does the migration of water from the water-bearing members higher in the shaft.

Salt Pressure. The four earth pressure cells installed between the concrete of the shaft key and the salt have a combined average reading of less than 10 psi in compression. These four cells, located 90 degrees apart at elevation 2550 feet (Figure 7-2), are intended to register changes in lateral pressures on the shaft key exerted by the creeping salt. Table 7-4 shows that the pressure cells have not registered any significant change in readings for a period of over 3 years since construction of the concrete key.

If we assume that the pressure cells are functioning properly, then the halite between a depth of 858 feet and 863 feet (elev. 2552 feet and 2547 feet) had not made contact with the pressure cell diaphragms as of December 9, 1985. According to the results of computational analyses, the contact between the salt and concrete will be reestablished at different elevations at different times between 1984 and 1986.

7.3.2.3 Unlined Section

Observed Conditions. The unlined section of the shaft appears to be stable with no evidence of rock spalling, wall deterioration, or dissolution by water.

Closure. Figure 7-8 compares average diametric closure readings at six elevations on December 9, 1985. The readings reflect only relative closure since the initial readings were taken nearly 1 year after completion of shaft excavation. Thus, the maximum diametric closure at a depth of 2,057 feet (elev. 1353 feet), near the bottom of the shaft, will be more than 1.0 inch. At higher elevations in the shaft, the actual diametric closure over the same period will, likewise, be higher than those shown on the figure.

Deformation. The radial deformation of salt behind an opening can be determined from the measurements of movements of borehole extensometers with multiple anchor points.

Table 7-4

C & SH SHAFT KEY
PERFORMANCE HISTORY OF PRESSURE CELLS

| Description | Pressure Cell Reading (psi) WE-201 | WE-202 | WE-203 | WE-204 | Date of Reading |
|---|---|---|---|---|---|
| Initial Irad Gage Co calibration | +1 | +2 | +6 | +13 | Feb. 3,'82 |
| Initial SRI calibration | +8 | +7 | +8 | +8 | Feb. 16,'82 |
| Site received, inspection | -1 | +1 | 0 | -2 | Mar. 30,'82 |
| Pre-installation, surface | -1 | +1 | -5 | -2 | Apr. 4,'82 |
| Pre-installation, in shaft | 0 | -1 | -2 | -2 | Apr. 15,'82 |
| After plaster of paris | -2 | -2 | 0 | -2 | Apr. 15,'82 |
| After concrete placement | 0 | 0 | 0 | 0 | Apr. 15,'82 |
| Initial installed reading | 0 | 0 | 0 | 0 | Apr. 16,'82 |
| Time after installation: | | | | | |
| 7 days | +2 | -1 | +2 | +17 | Apr. 22,'82 |
| 107 days | -1 | -3 | -2 | 0 | Jul. 31,'82 |
| 529 days | -2 | -5 | -31 | +1 | Sep. 26,'83 |
| 530 days | +1 | -3 | 0 | -2 | Sep. 27,'83 |
| 544 days | -4 | -8 | -32 | -3 | Oct. 11,'83 |
| 597 days | -4 | -7 | - | 0 | Dec. 3,'83 |
| 797 days | -1 | -7 | -38 | 0 | Jun. 20,'84 |
| 938 days | -12 | -11 | -27 | 0 | Nov. 8,'84 |
| 1030 days | -12 | -30 | - | -2 | Feb. 8,'85 |
| 1140 days | -6 | -10 | -25 | +3 | May 21,'85 |
| 1179 days | -6 | -11 | -25 | +5 | Jun. 29,'85 |
| 1342 days | -14 | -10 | -25 | -2 | Dec. 9,'85 |

NOTE: Negative sign indicates tension.

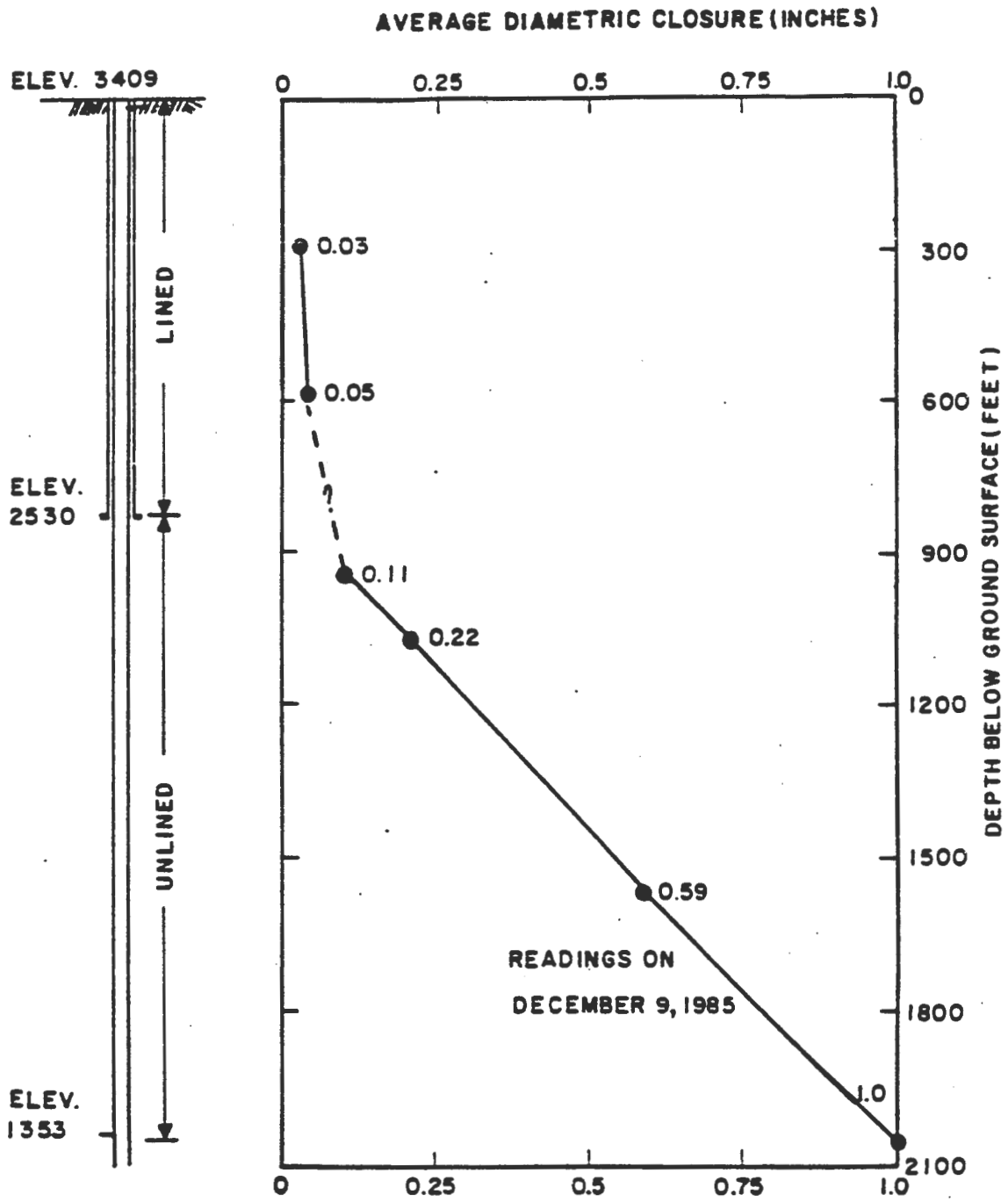


NOTES:

1. SHAFT WAS EXCAVATED FROM JULY THROUGH OCTOBER 1981
2. CONVERGENCE POINTS WERE INSTALLED FROM JULY THROUGH OCTOBER 1982.

Figure 7-8

C & SH SHAFT UNLINED SECTION
AVERAGE DIAMETRIC CLOSURE

According to extensometer readings on September 16, 1985, the total average collar displacements at elevations 1846 feet and 1353 feet (Figure 7-3) were 0.19 inches and 0.235 inches, respectively. However, the extensometers were installed nearly 7 1/2 months after the completion of shaft excavation.

Figure 7-9 shows the collar movement time histories for multiple-point borehole extensometers 37X-GE-00202, 37X-GE-00205 and 37X-GE-00208 relative to their deepest anchor. The undulating shape of the curves appears to reflect the influence of seasonal temperature changes on the extensometers. The effect of temperature changes is more pronounced on the instrument behavior than on the salt surrounding the instrument. Figure 7-10 shows the change in calculated rates of collar movement with time for the extensometer time histories on Figure 7-9. The maximum rates coincide with the hottest months while during mid-winter the rates are close to, or slightly less than, zero. Because the time interval chosen for calculating the rate of collar movement is much less than the total observation period of 2 years, these rates are probably very close to the actual rates.

Comparison of the extensometer collar movements with convergence point readings suggests that the salt in the vicinity of the deepest anchor may also be moving. Thus collar movement does not reflect the true radial closure of the shaft. The amount of movement of the deepest anchor for any extensometer of given length can be estimated so that the collar displacement provides absolute radial closure. The diametric closure can be computed by model simulation as described below, by curve fitting as described in reference 4-19, or by closed form solution, also described in reference 4-19. Based on this analysis, the absolute movements of the collar and intermediate anchors for the 36-foot long shaft extensometers will deviate from the measured values by only 0.03 inch.

<u>Model Simulation</u>. The structural behavior of the unlined section of the C & SH shaft was analyzed by a nonlinear creep analysis using the

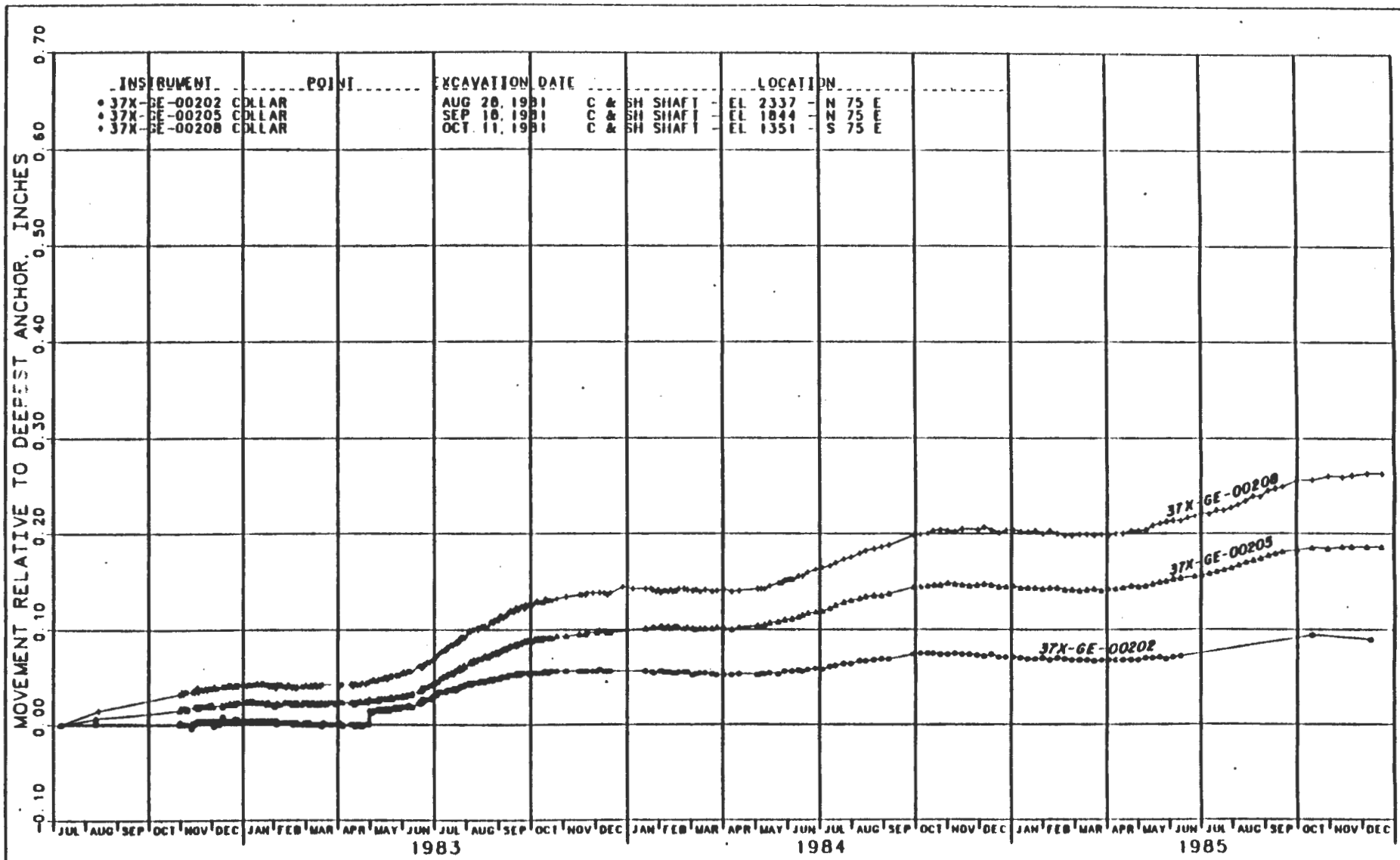


**Figure 7-9**

C & SH SHAFT UNLINED SECTION
COLLAR MOVEMENT TIME HISTORY

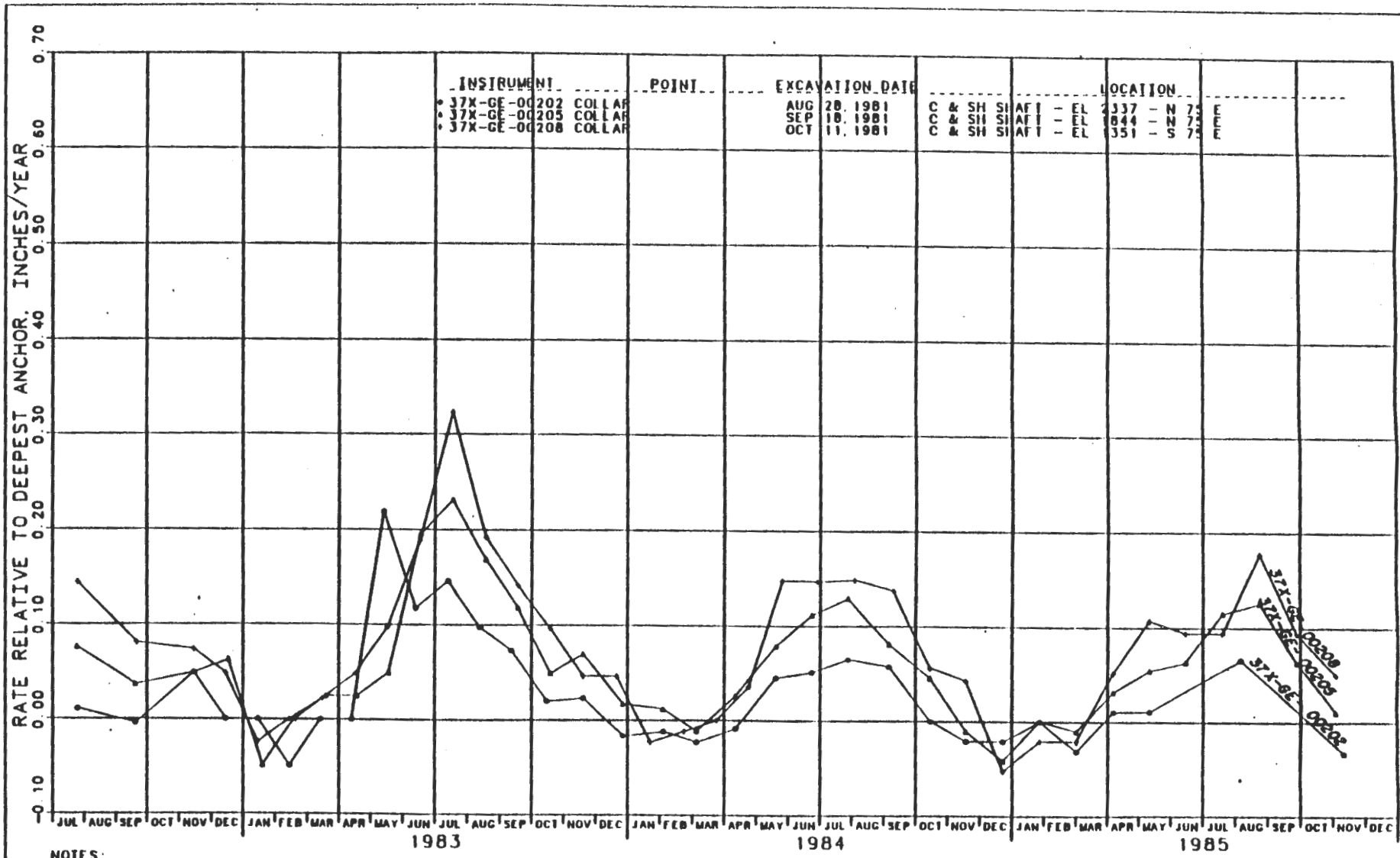


NOTES:

1. RATE CALCULATED FOR MINIMUM INTERVALS OF 30 DAYS

**Figure 7-10**

C & SH SHAFT UNLINED SECTION
RATE OF COLLAR MOVEMENT VERSUS TIME

MARC General Purpose Finite Element Program (ref. 6-8). The objective of the analysis was to compute actual structural behavior by utilizing available in situ data, thereby verifying the design adequacy of the unlined section of the shaft.

The finite element model used for the analysis utilizes a single horizontal plane of quadrilateral ring elements with the upper and lower horizontal boundaries restrained against vertical displacement. This model is shown on Figure 7-11. The outside vertical boundary was given a constant uniform pressure based upon the lithostatic stress state defined in Chapter 5, equation 5-1. The inside boundary was also given a uniform pressure based upon the same lithostatic stress assumption; however, the pressure was removed in a step-wise fashion over a period of approximately 1 day. This was done to simulate the excavation of the drilled shaft, which results in a gradual relief of overburden pressure on the shaft interior and affects structural behavior in the early stage of excavation.

The secondary creep parameter C in Chapter 6, Table 6-8, was determined based on extensometer data at a depth of 2,057 feet (elev. 1353 feet). The value of C can be computed for each extensometer location using the analytical results and in situ data from the extensometer. Because C, determined from each extensometer, may vary, predicted diametric closures along each extensometer will vary accordingly. Using the diametric closures predicted at different directions on the horizontal plane, the principal directions of the strain on the horizontal plane can be determined. Consequently, closure along two horizontal principal directions can be predicted. Based on the predicted diametric closures at a depth of 2,057 feet in the N15°W, S75°E and S45°W directions, the major axis was found to be N17°40'W and the minor axis N72°20'E.

Closure predictions were made for two principal directions on the horizontal plane. Because the stress and strain distributions are not sensitive to the value of the secondary creep parameter, except during

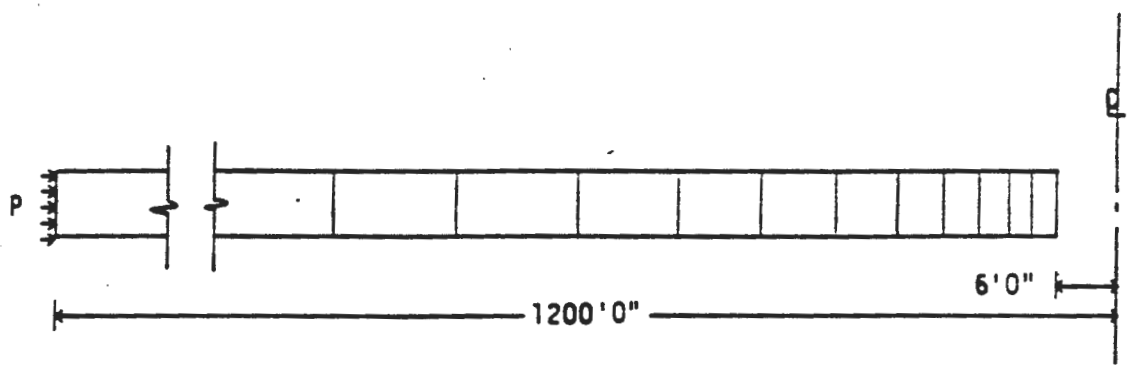


Figure 7-11

C & SH SHAFT UNLINED SECTION
FINITE ELEMENT MODEL

the initial stages of creep, the stress and strain distributions were computed based on the average values of the creep parameter C determined from three different directions.

7.3.2.4 Shaft Station

Observed Conditions. The C & SH shaft station exhibits spalling from both the roof and wall surfaces that requires continual routine maintenance. Displacements, separations and fracturing occuring above the roof at clay G and in the underlying halite were expected.

Data from the Excavation Effects Program indicate that the halite from 4 to 10 feet above the roof contains essentially no separations or fracturing. Floor heave is evident at the electrical substation where the concrete base slab has tilted several degrees, but holes drilled into the station floor encountered only minor separations and fracturing. Extensometer 51X-GE-00253, in the station floor, does not show any significant increase in collar movement that would be expected if floor heave and fracturing is occurring. Although the C & SH shaft station is the oldest and largest horizontal opening, the extent of separations and fracturing beneath the floor is very small relative to the fracturing found in the floor beneath Test Room 3 (Chapter 11).

The observed behavior in the station is apparently due in large part to its initial excavation by blasting. No other underground area has exhibited the degree of spalling that has occurred in the station. The blasting is thought to have accelerated separations at clay G and in the underlying halite in the main station area south of the shaft. However, the extensive rock bolting in the roof appears to have effectively controlled these separations.

Fracturing in the pillar corners at the S90 crosscut has continued to evolve as the salt responds to stresses produced by the station excavation. Changes in the fracturing are exhibited primarily by the appearance of new vertical fractures and by the elongation and widening of existing fractures. Minor spalling has also occurred, particularly

at the roof and wall intersection in the upper portion of geologic map unit 4.

Closure. Figure 7-12 shows closure rates calculated from the readings of roof-to-floor convergence points. The maximum rate appears to have occurred during the early part of August 1984.

The closure rates shown on Figure 7-12 cannot be directly compared without considering the differences in dimensions at the locations shown, as well as differences in the thickness of the roof beam below clay G, and the number of rock bolts in the vicinity of the respective convergence measurement stations.

Figure 7-13 compares the central vertical closure readings at stations S18.5 and N39. Although the closure measurements are very close at both stations, actual total closure at the S18.5 station will be greater since the initial reading at this station was taken nearly 261 days after the completion of excavation, compared to only 35 days at the N39 station. In addition, the larger opening dimensions at the S18.5 station will also result in more rapid closure. Even though the density of rock bolts is greater south of the C & SH shaft than north of it, the roof-to-floor closure is greater to the south. This is probably because the roof beam below clay G is thinner and longer to the south.

Figure 7-14 shows the collar movements of multiple-point borehole extensometers 51X-GE-00227 and 51X-GE-00228 in the station roof, 35 feet north and 65 feet south of the C & SH shaft, respectively. The average collar movement rate of 51X-GE-00228 is higher than that of 51X-GE-00227, as determined from Figure 7-14. The roof closure rate south of the shaft is currently more than the rate north of the shaft.

A double-point borehole extensometer (51X-GE-00253) was installed in the floor of the C & SH shaft station. The initial reading from this extensometer was taken nearly 238 days after the completion of

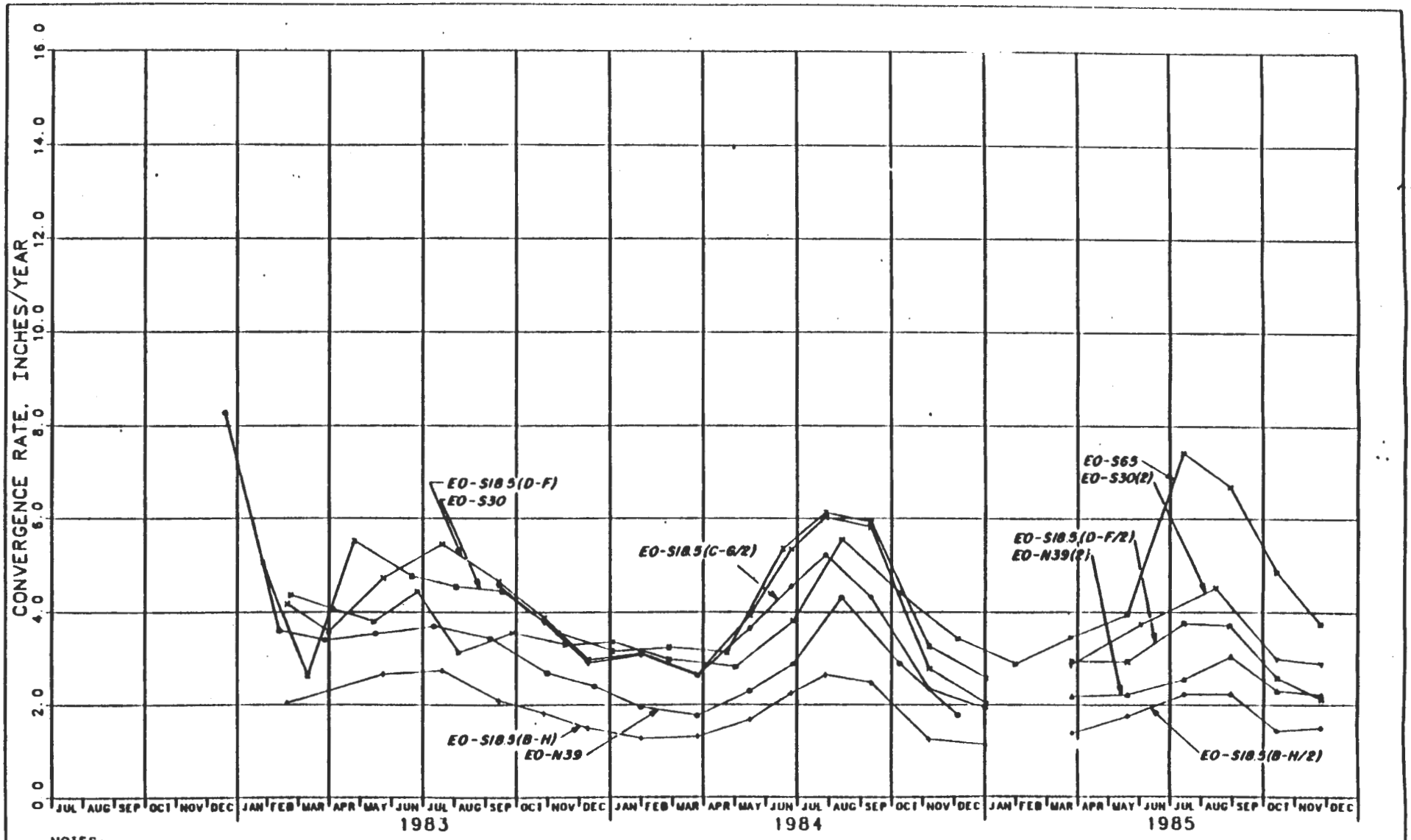


NOTES

1. RATE CALCULATED FOR MINIMUM INTERVALS OF 30 DAYS

**Figure 7-12**

C & SH SHAFT STATION
CALCULATED ROOF-TO-FLOOR CLOSURE RATES

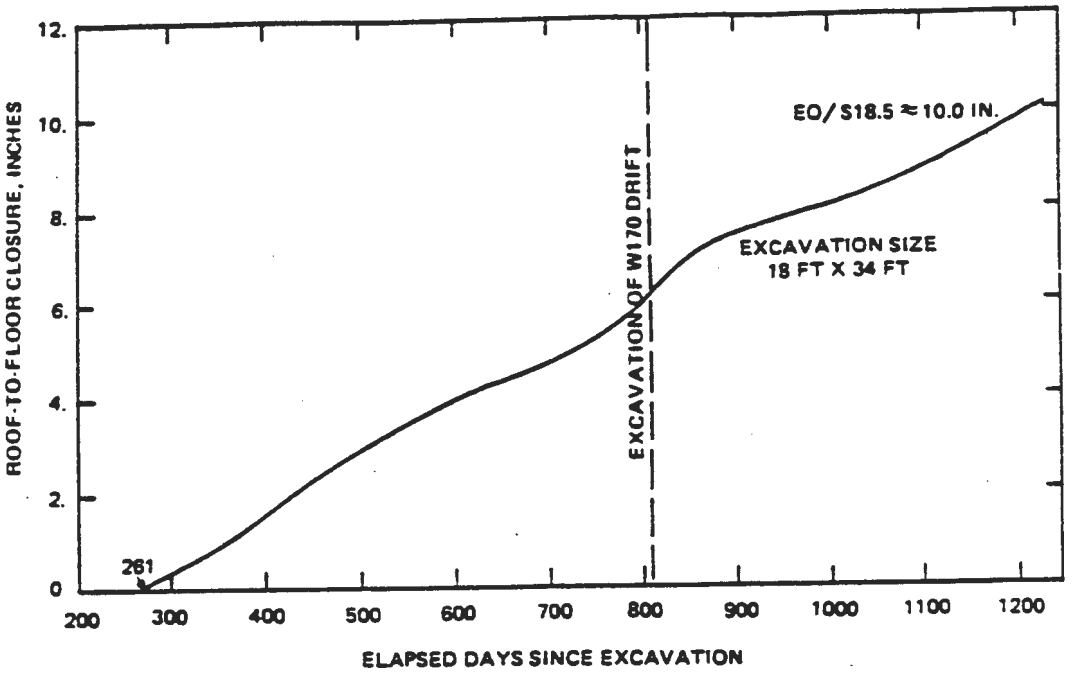


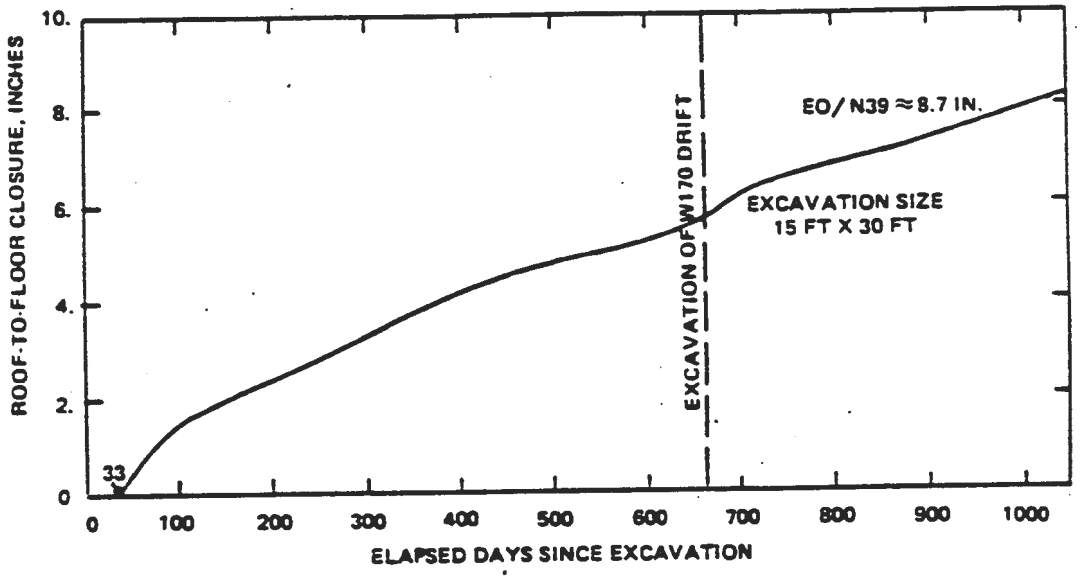


Figure 7-13

C & SH SHAFT STATION
TYPICAL ROOF-TO-FLOOR CLOSURE HISTORY

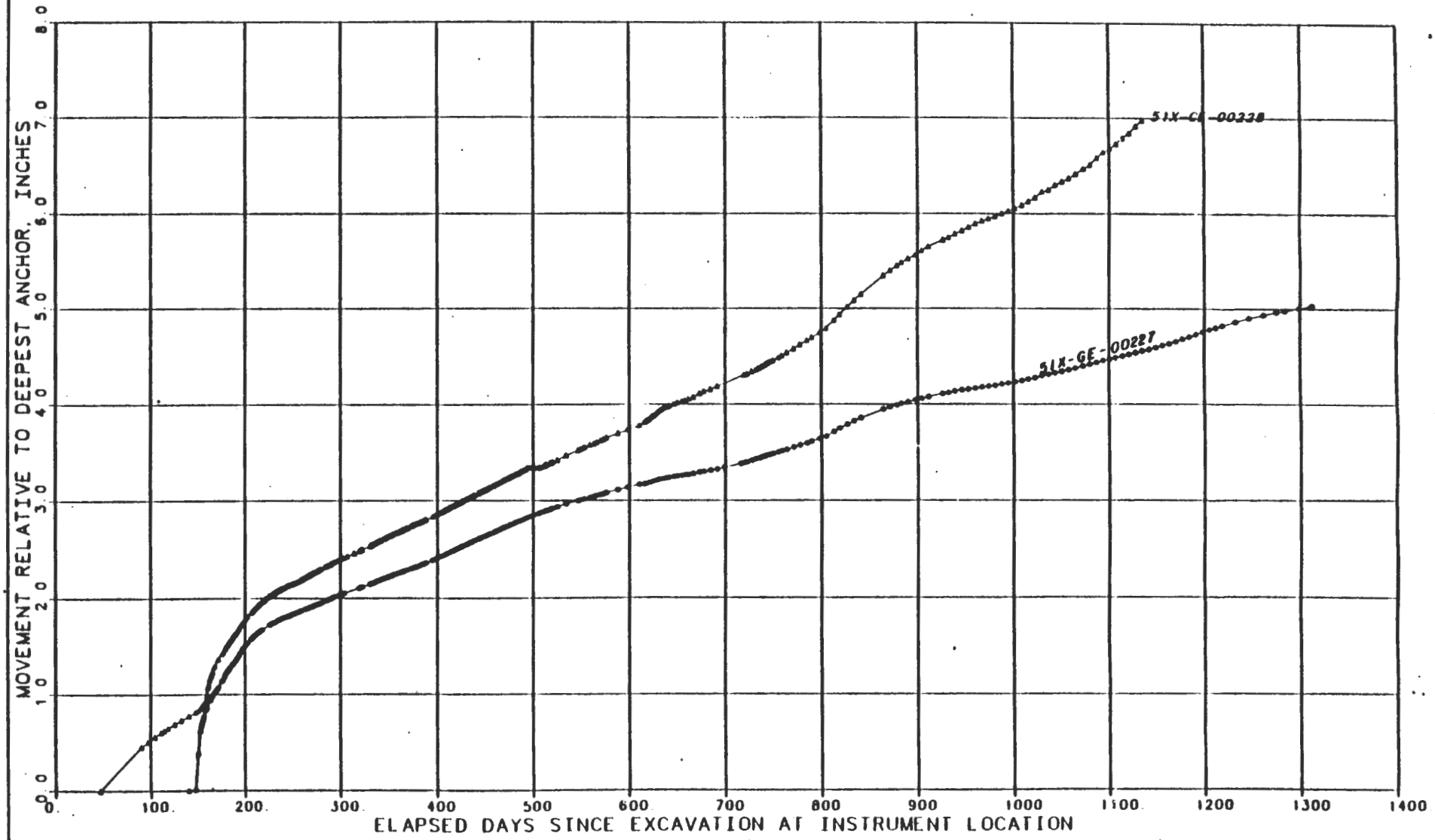


**Figure 7-14**

C & SH SHAFT STATION
HISTORY OF COLLAR MOVEMENTS - ROOF EXTENSOMETERS

excavation at the instrument location (Appendix J, Figure J-172). The measured collar movement relative to the deepest anchor was 3.26 inches on December 20, 1985. Actual floor heave will be higher as a result of the time-lag between the end of excavation and the initial reading date. There was a slight increase in the collar movement rate due to excavation of the nearby W170 drift, but the rate has since become steady.

Roof Stability. Figure 7-15 shows the distribution of measured movements along roof extensometer 51X-GE-00251, 18 1/2 feet south of the C & SH shaft, for the readings taken on September 18, 1985. The magnitudes shown are cumulative between the initial reading date of January 11, 1983, and September 18, 1985. The movements are also expressed as percentages of the collar reading. Sixty-one percent of the relative movement has taken place between the collar and anchor A. This has remained practically constant since December 1983 and is an indirect indication that there is no accelerating trend in the rate of opening at clay G in the vicinity of this extensometer. For comparison, the distribution of measured movement along roof extensometer 51X-GE-00227, 35 feet north of the C & SH shaft, is shown on Figure 7-16. The relative movement between the collar and anchor A has remained constant at 52 percent through December 1985. Based on these measurements, there is no indication that clay G is parting at an accelerating rate either north or south of the shaft.

### 7.3.3 Prediction of Future Behavior

This subsection presents the results of the analysis and evaluation of the finite element modeling and the data collected in the C & SH shaft. These results are presented in the form of predictions for future behavior of the constructed shaft elements (liner and key) and of the salt surrounding the unlined section of the shaft and the shaft station.

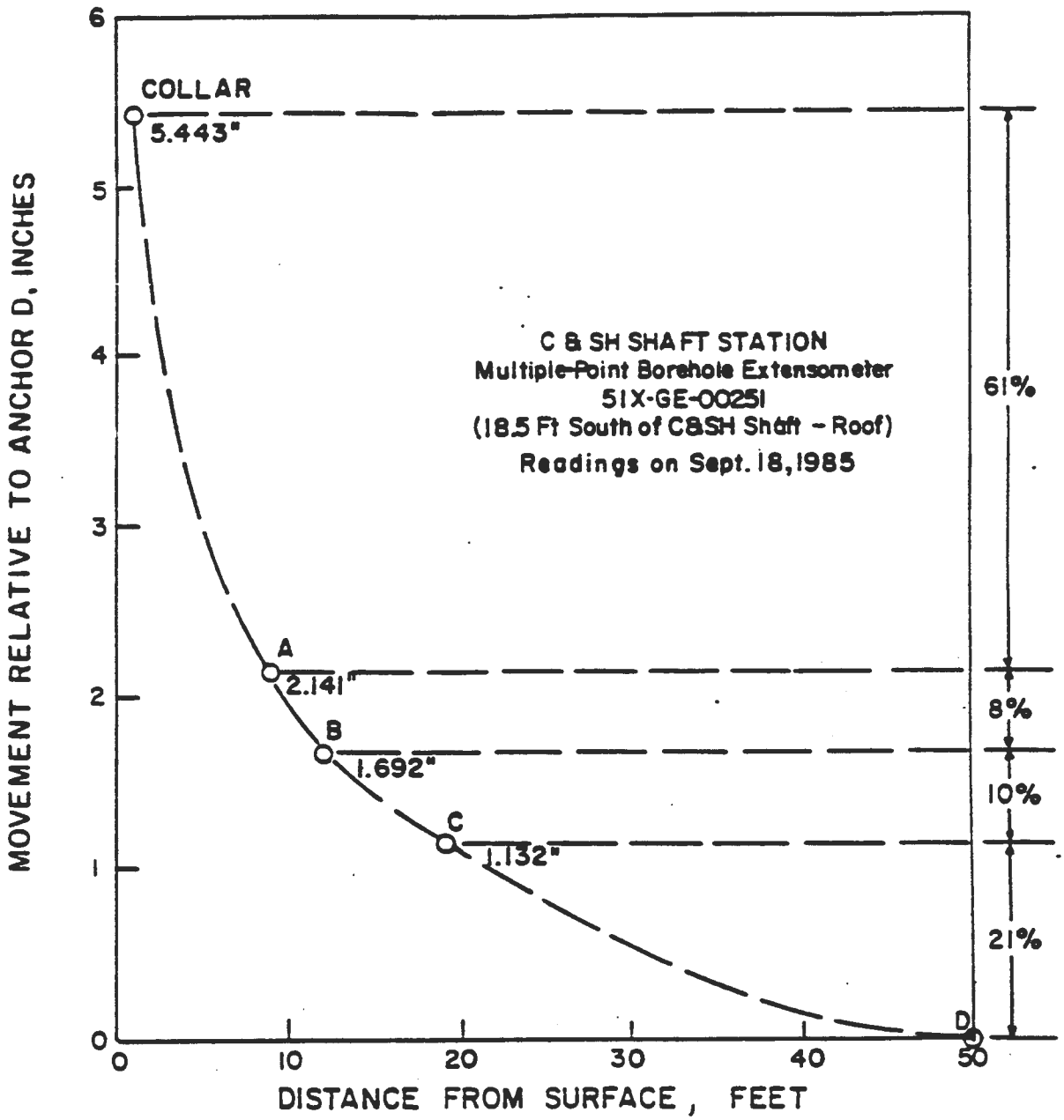


Figure 7-15

C & SH SHAFT STATION
MOVEMENT DISTRIBUTION ALONG ROOF EXTENSOMETER 51X-GE-00251

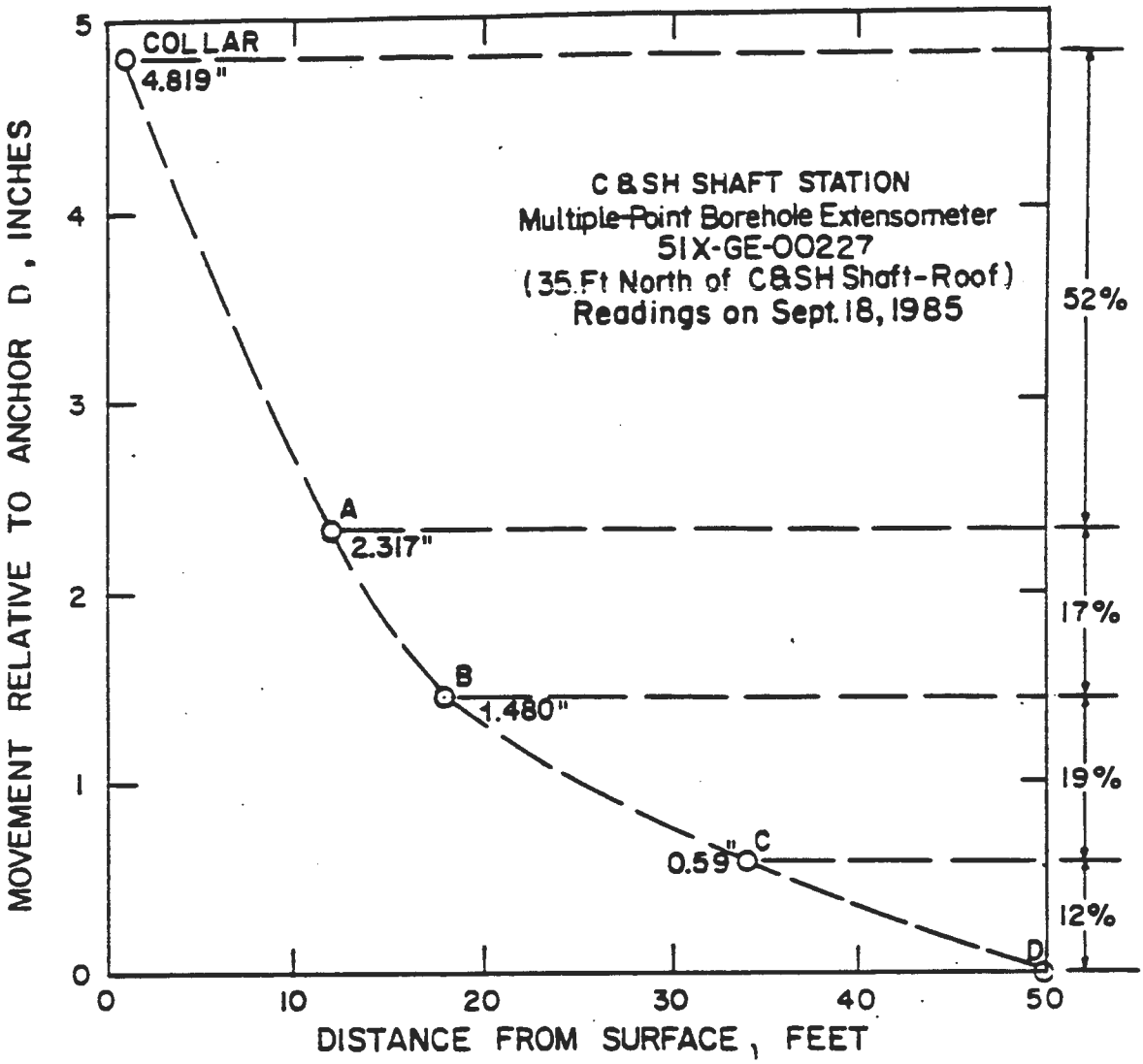


Figure 7-16

C & SH SHAFT STATION
MOVEMENT DISTRIBUTION ALONG ROOF EXTENSOMETER 51X-GE-00227

#### 7.3.3.1 Lined Section

The water pressure on the shaft liner to date has been less than the hydrostatic design pressure. The prediction of future water pressures behind the liner is difficult due to the reasons discussed in subsection 7.3.2.1. The lower potentiometric surface and lack of hydraulic continuity along the rock/liner interface may prevent the ground water from reaching the design hydrostatic head. In addition, leaks around the piezometers and possibly obstructed filters may cause the measurements to be somewhat less than the actual pressure conditions.

Figure 7-17 shows that if the water pressure does reach the design hydrostatic pressure, the liner will remain stable based on its design factor of safety. The figure shows that the pressure capacity of the liner far exceeds the design hydrostatic pressure. This pressure was determined based on water level data obtained at the site during preliminary design activities. The data indicated that the highest potentiometric surface in the Rustler formation beneath the site occurred at a depth of approximately 250 feet below the ground surface. This data was later confirmed by investigations conducted in the site vicinity by the U.S. Geological Survey (USGS) (ref. 7-9). It is not expected that this potentiometric surface will be exceeded during the 25-year operating life of the facility. If any external water were to infiltrate along the rock/liner interface to form a column of water that would exceed the hydrostatic head contained in the design bases, the stability and safety of the steel liner would still not be compromised based on the design factor of safety.

#### 7.3.3.2 Shaft Key

The results of the shaft key analysis indicate that after concrete is placed against the shaft wall it shrinks away from the wall at a rate greater than the rate of salt creep, resulting in a separation between the concrete and the salt. The rate of concrete shrinkage decreases with time and continuous salt creep eventually results in the salt

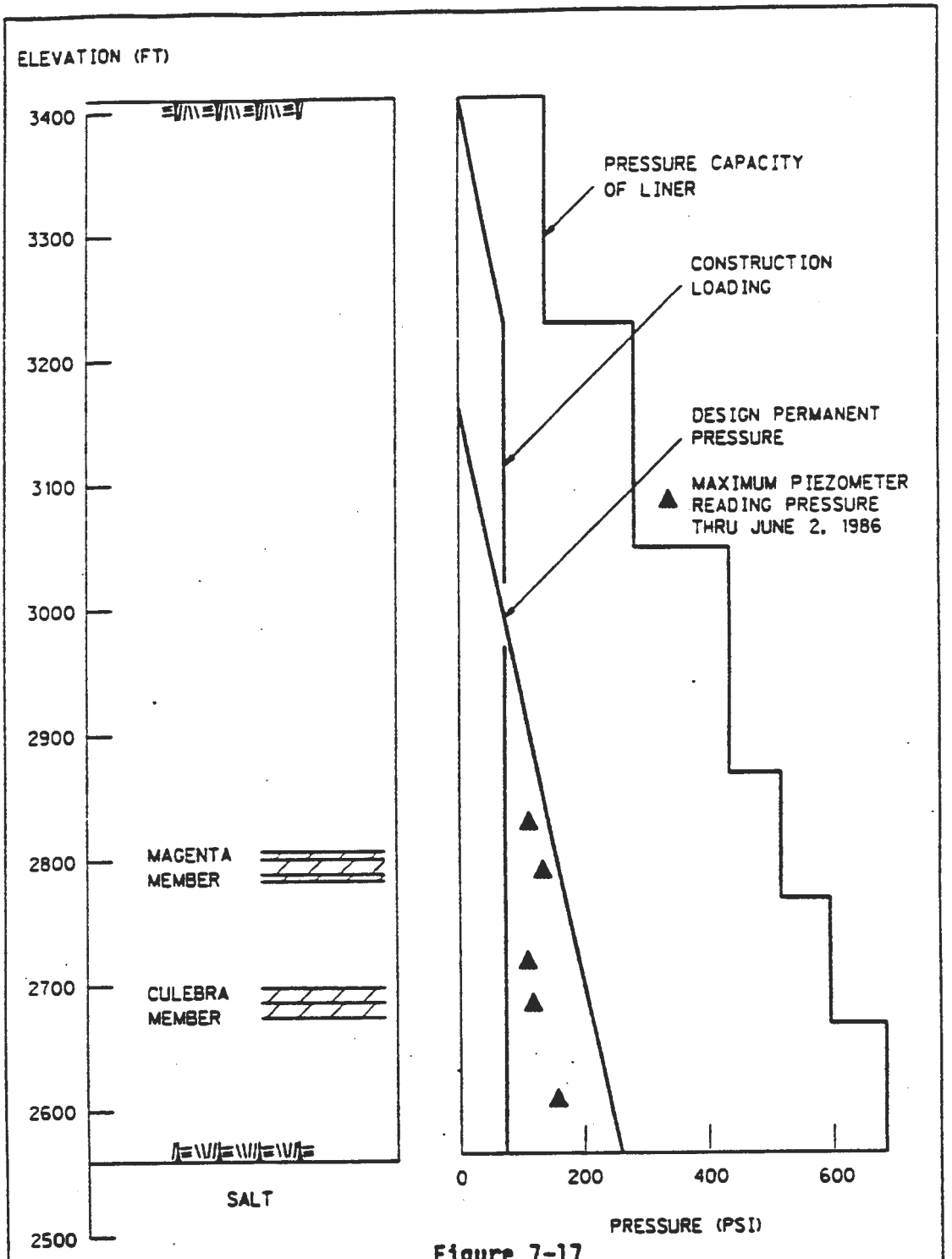


**Figure 7-17**

**C & SH SHAFT LINER**
**LATERAL PRESSURE COMPARISON**

contacting the concrete again. The interactive pressure between the concrete and the salt will then gradually increase due to continuous salt creep.

In the key area, the shaft wall radial and tangential stresses (Figures 7-18 and 7-19, respectively) were plotted as a function of distance from the centerline of the shaft for a typical section immediately after excavation of the shaft and for 1 year and 25 years after concrete placement. As expected, the radial stresses in the salt are initially relieved near the opening but begin increasing after the salt comes in contact with the concrete. Further away from the opening, the stresses trend toward the overburden pressure.

The tangential stresses in the salt 3 days after excavation show an elastic response which gives very high values near the opening. The stresses are relieved near the opening from the time the salt starts to creep until it contacts the concrete. After contact is made, and for the remainder of the 25 year analysis period, the stresses in the salt and concrete key increase. There exists a discontinuity of stress at the concrete/salt interface which is primarily due to differences in their material properties. Like the radial stresses, the tangential stresses approach the overburden pressure with increasing distance from the opening.

At 25 years, the radial stresses, which are equal to the lateral pressures on the salt face of the key, will increase to an average value of 275 psi. At the same time, the maximum hoop stress at the inside face of the concrete key has an approximate value of 1,000 psi, with an average value across the key of about 825 psi. Figures 7-20 and 7-21 show the predictions for average lateral pressures and average hoop stresses, respectively. A lateral pressure capacity in the key of 833 psi, based on an allowable hoop stress controlled by a concrete compression of 3,000 psi, results in a factor of safety of approximately three.

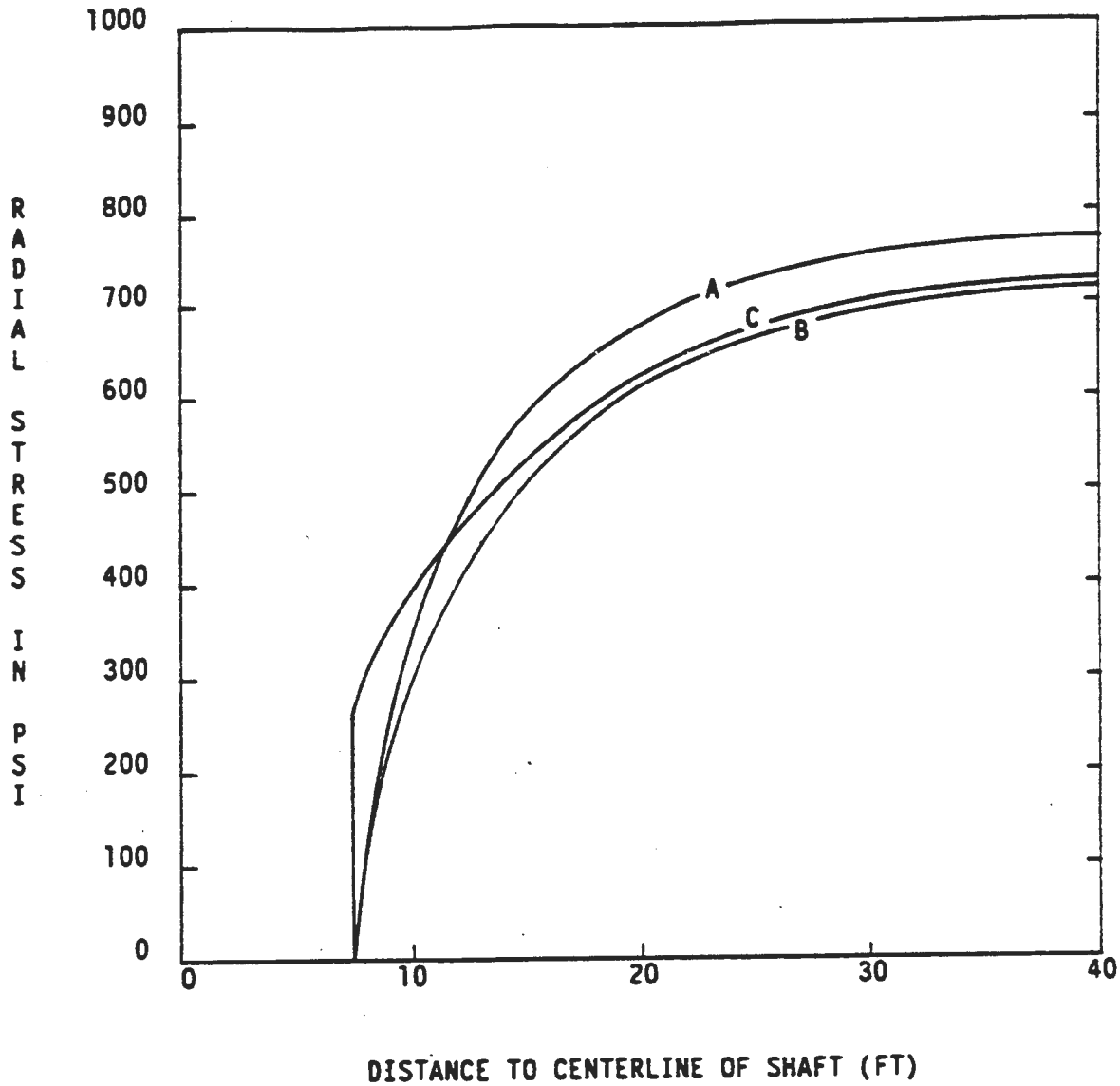


A – IMMEDIATELY AFTER EXCAVATION
B – ONE YEAR AFTER CONCRETE PLACEMENT
C – 25 YEARS AFTER CONCRETE PLACEMENT

Figure 7-18

C & SH SHAFT KEY
RADIAL STRESS DISTRIBUTION

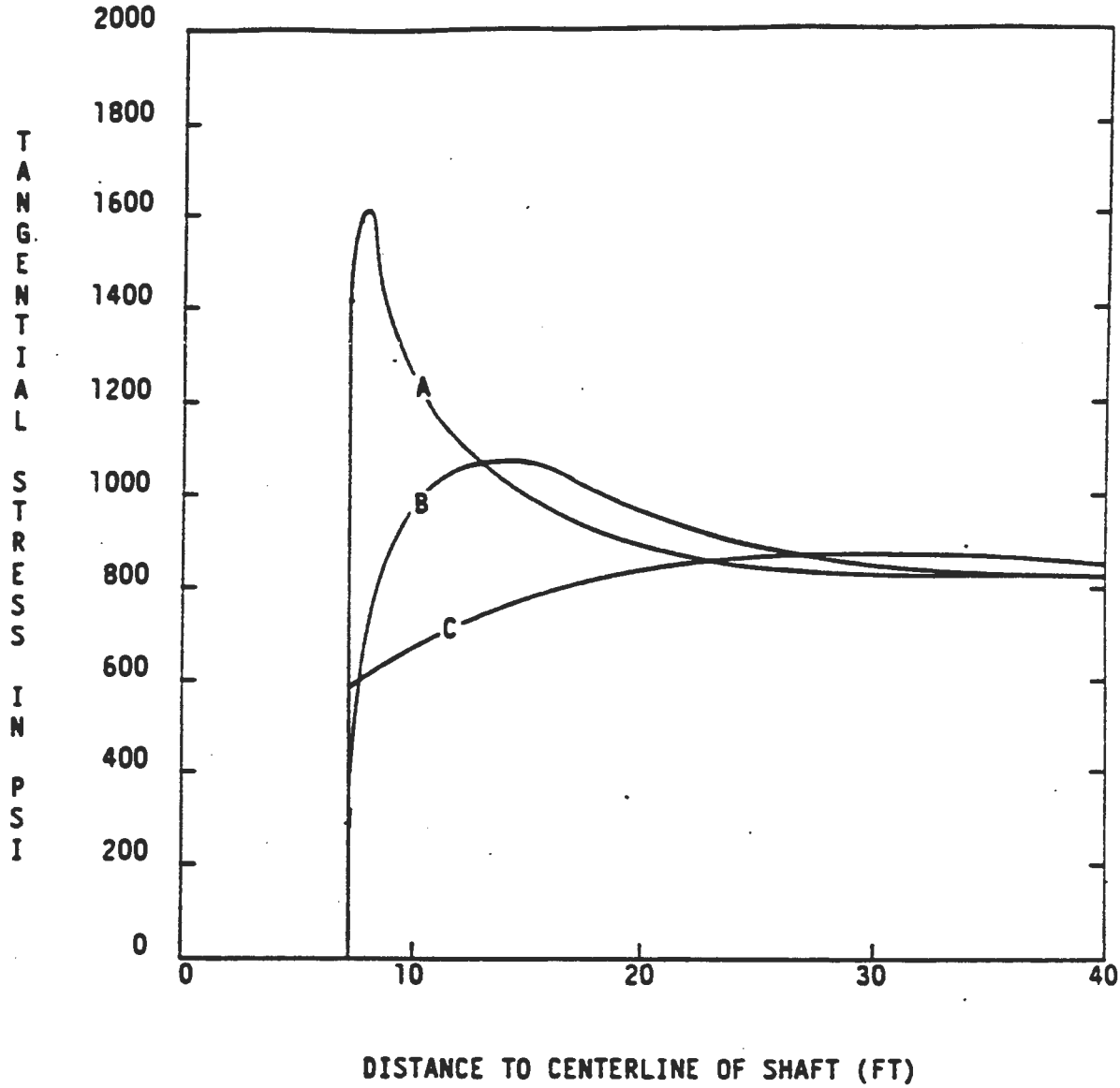


A – IMMEDIATELY AFTER EXCAVATION
B – ONE YEAR AFTER CONCRETE PLACEMENT
C – 25 YEARS AFTER CONCRETE PLACEMENT

Figure 7-19

C & SH SHAFT KEY
TANGENTIAL STRESS DISTRIBUTION

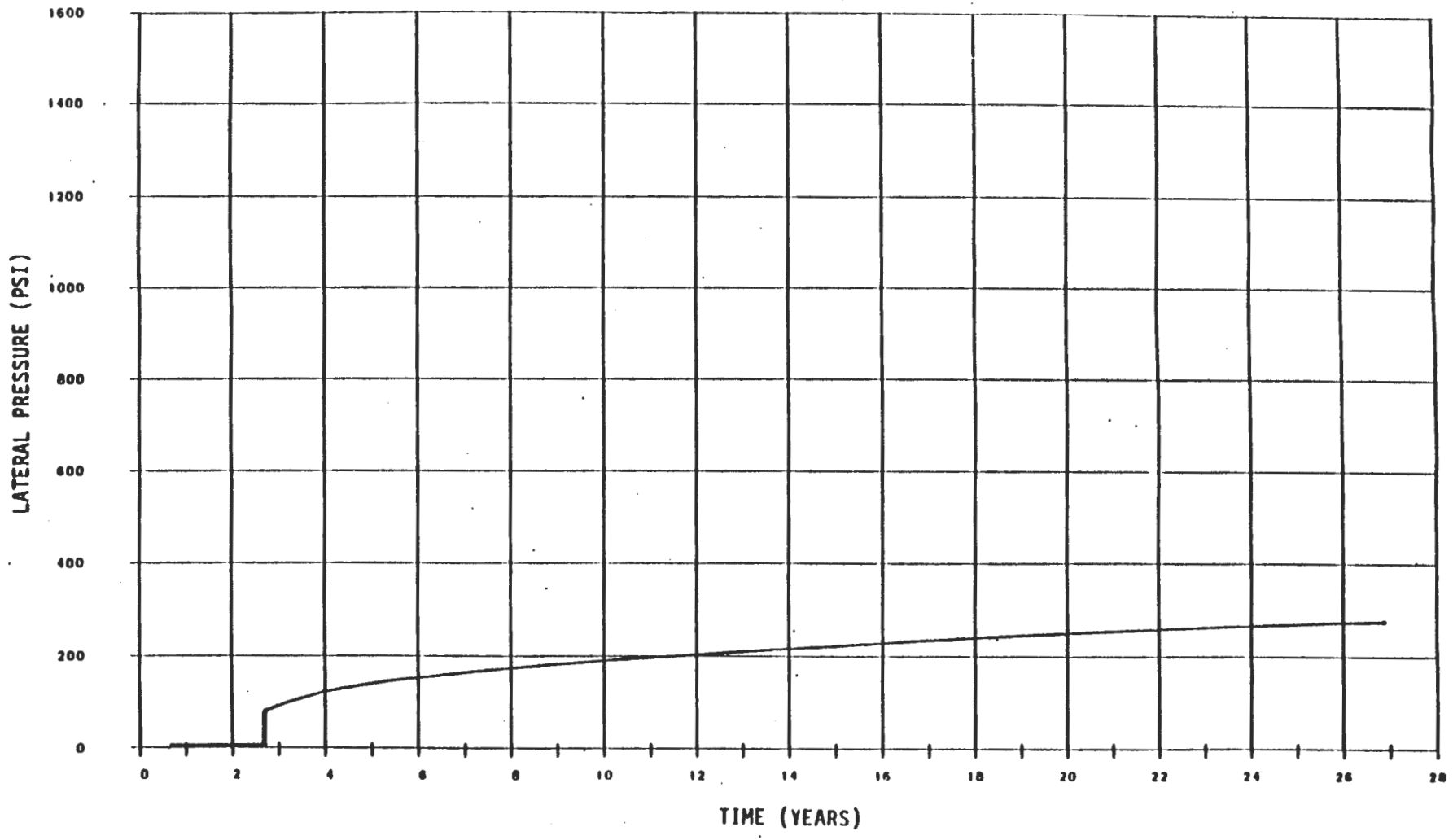


Figure 7-20

C & SH SHAFT KEY
LATERAL PRESSURE PREDICTION

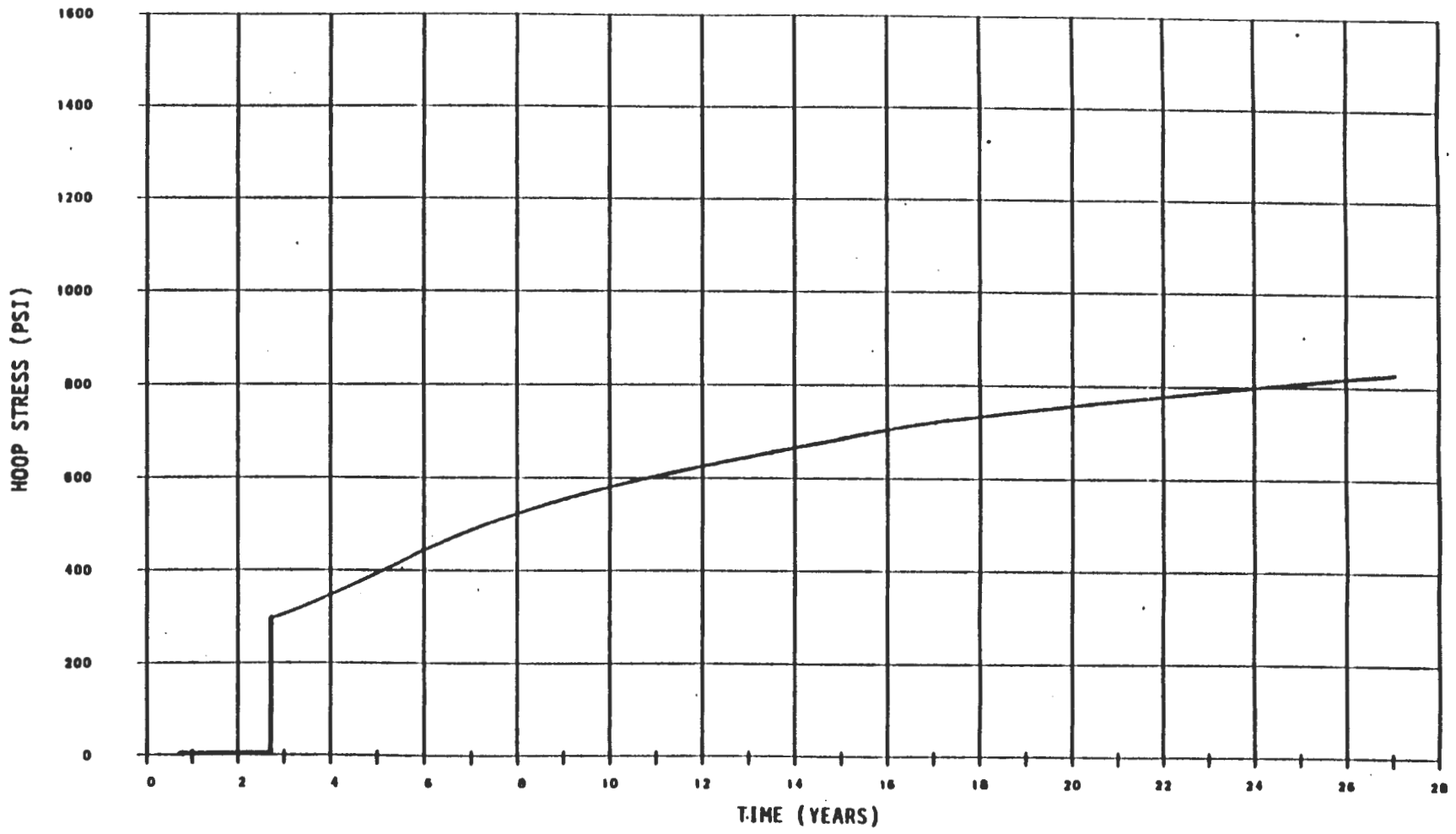


Figure 7-21

C & SH SHAFT KEY
HOOP STRESS PREDICTION

The average diametric closure of the key at 27 years is expected to be about 0.1 inch with a maximum value of 0.175 inch, or about half the predicted value for the salt in the unlined section immediately below the key (Figure 7-22). The average diametric closure of the unlined section immediately below the key at 27 years varies from 0.03 inch for the anhydrite bed to 0.38 inch for the argillaceous halite layer. Figure 7-23 shows the diametric closure predictions for both the concrete key and the salt in the adjacent shaft wall.

7.3.3.3 Unlined Section

Extrapolation of In Situ Responses. Convergence point measurements are too few to be used for the extrapolation of future in situ responses in the unlined section of the shaft. Thus, the readings of collar movements of multiple-point borehole extensometers must be used for this extrapolation. Because the extensometer collars are recessed 1 foot into the wall, and the readings are referenced to the deepest anchor which is also moving, extrapolation of collar movement will not produce an exact estimate of the movement of the shaft surface.

The maximum collar movement occurs at multiple-point borehole extensometer 37X-GE-00208 at a depth of 2,057 feet (elev. 1353 feet) (Figure 7-3). As discussed earlier, and as shown on Figure 7-9, the collar movement is affected by seasonal temperature fluctuations. However, if we consider only the later portion of the curve, its slope is approximately 0.125 inch/year between June 1984 and June 1985. Assuming this rate to be constant for another 22 years, the additional radial movement of the collar will be nearly 3 inches. Thus, the effective diameter of the unlined shaft will be reduced by nearly 6 inches.

Replication of In Situ Responses. Figures 7-24 and 7-25 show the radial and tangential stress distributions relative to the overburden stress at different times. Figure 7-24 indicates that the zone where radial stresses are affected increases in size with time while Figure 7-25 indicates that tangential stresses are only affected within an approximately constant radius of 60 feet.

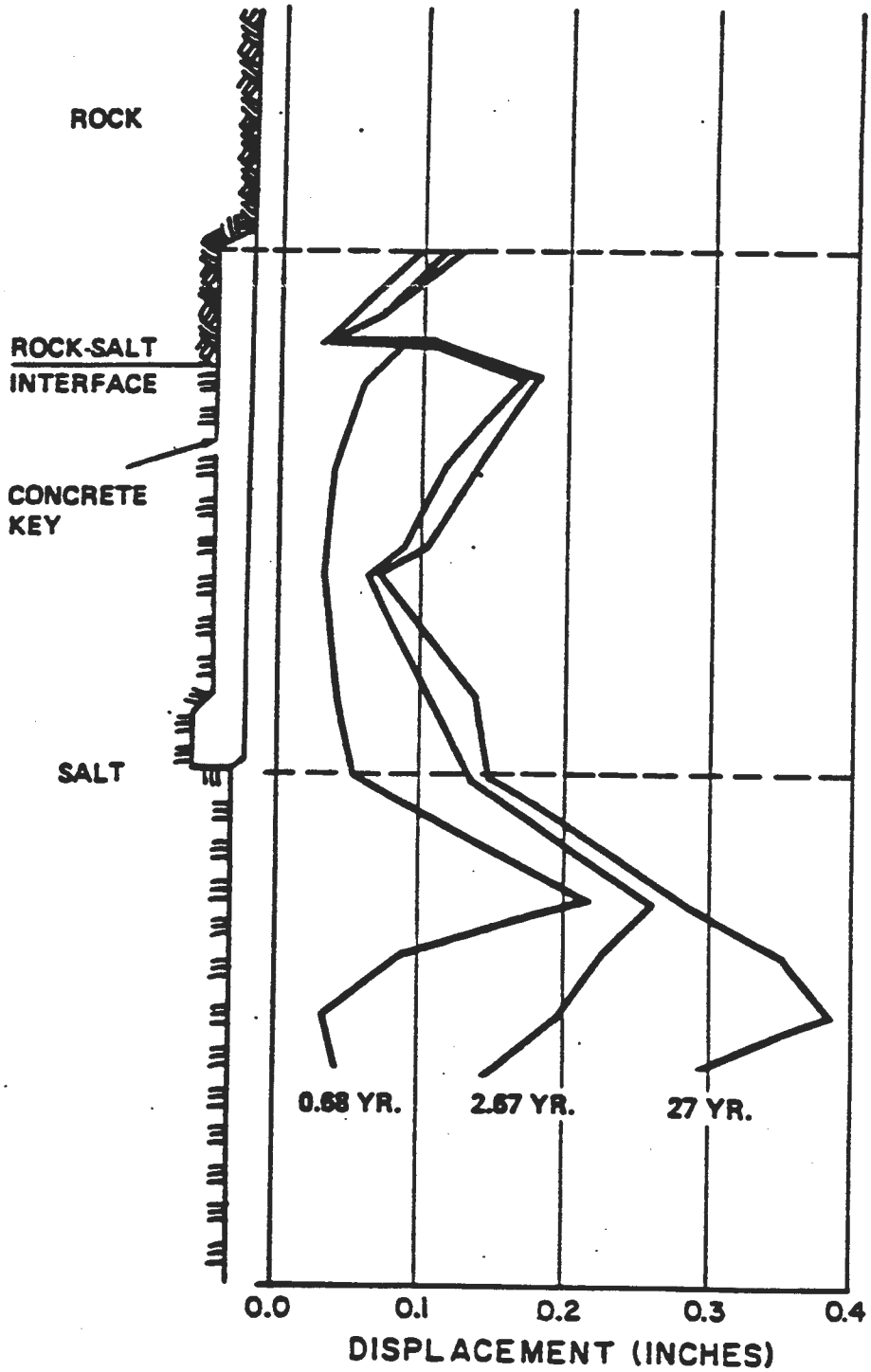


Figure 7-22

C & SH SHAFT KEY
DIAMETRIC CLOSURE

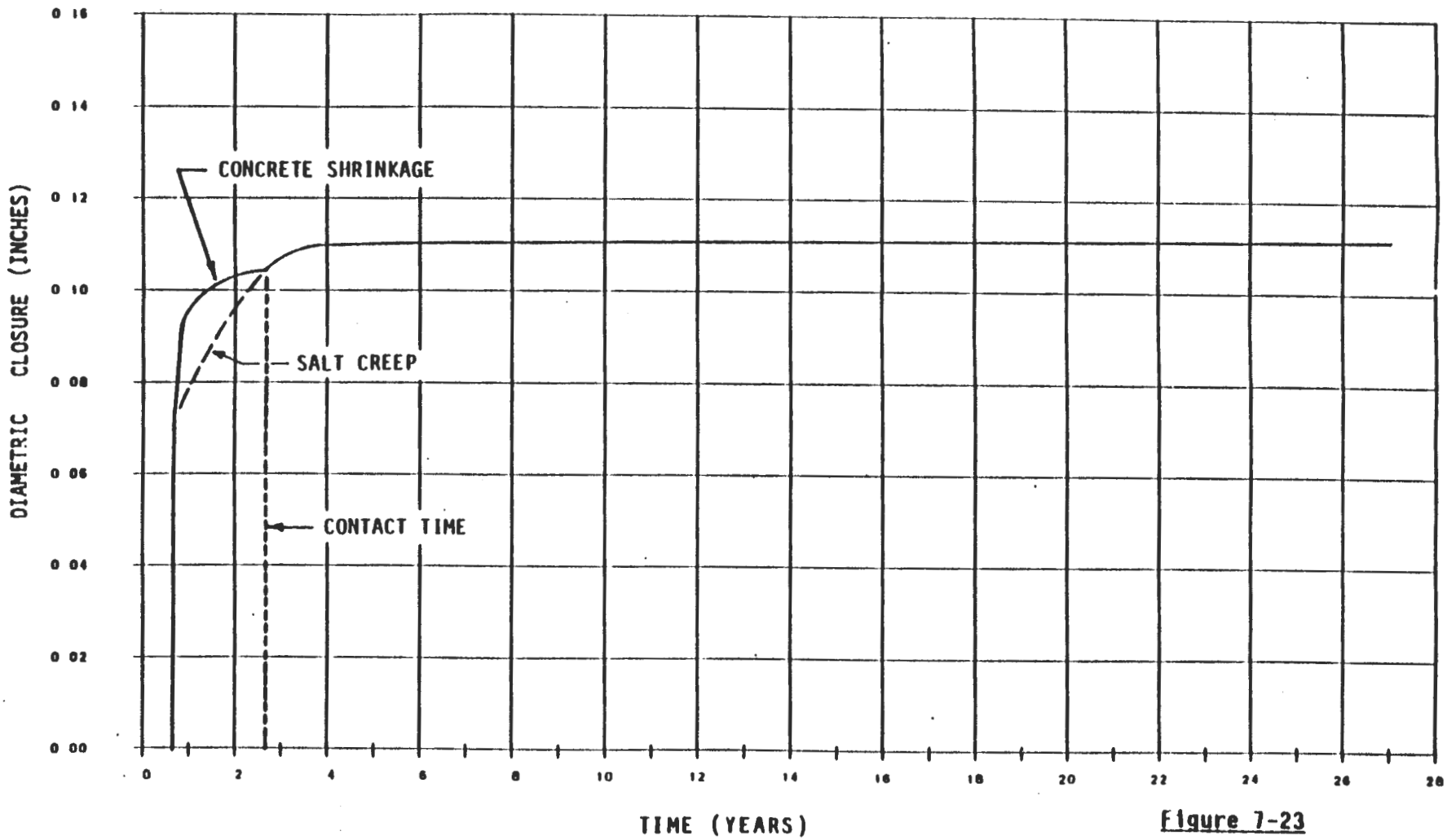


Figure 7-23

C & SH SHAFT KEY
DIAMETRIC CLOSURE PREDICTION

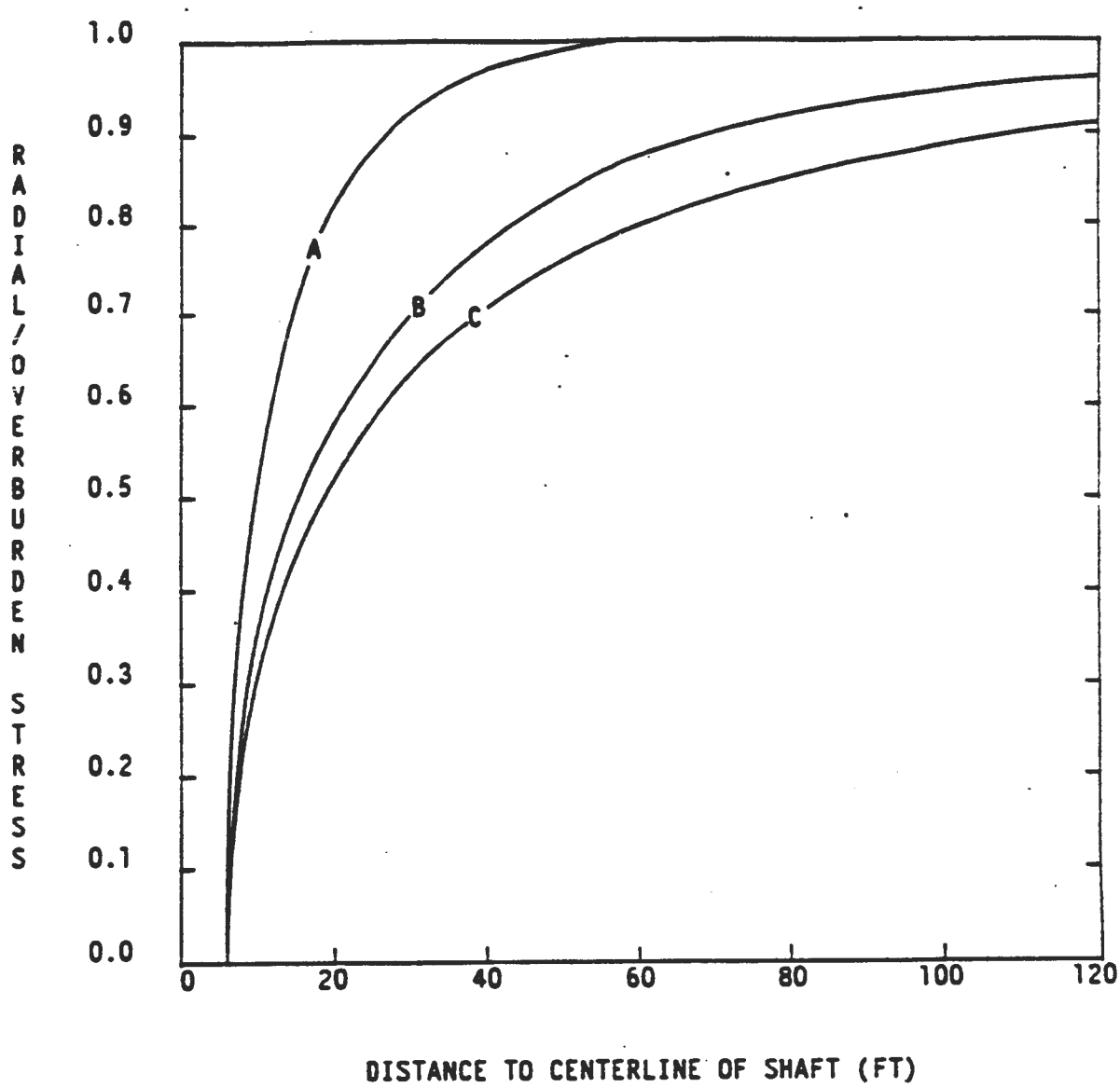


A – IMMEDIATELY AFTER EXCAVATION
B – ONE YEAR AFTER EXCAVATION
C – 15 YEARS AFTER EXCAVATION

Figure 7-24

C & SH SHAFT UNLINED SECTION
RADIAL STRESS DISTRIBUTION AT ELEVATION 1353

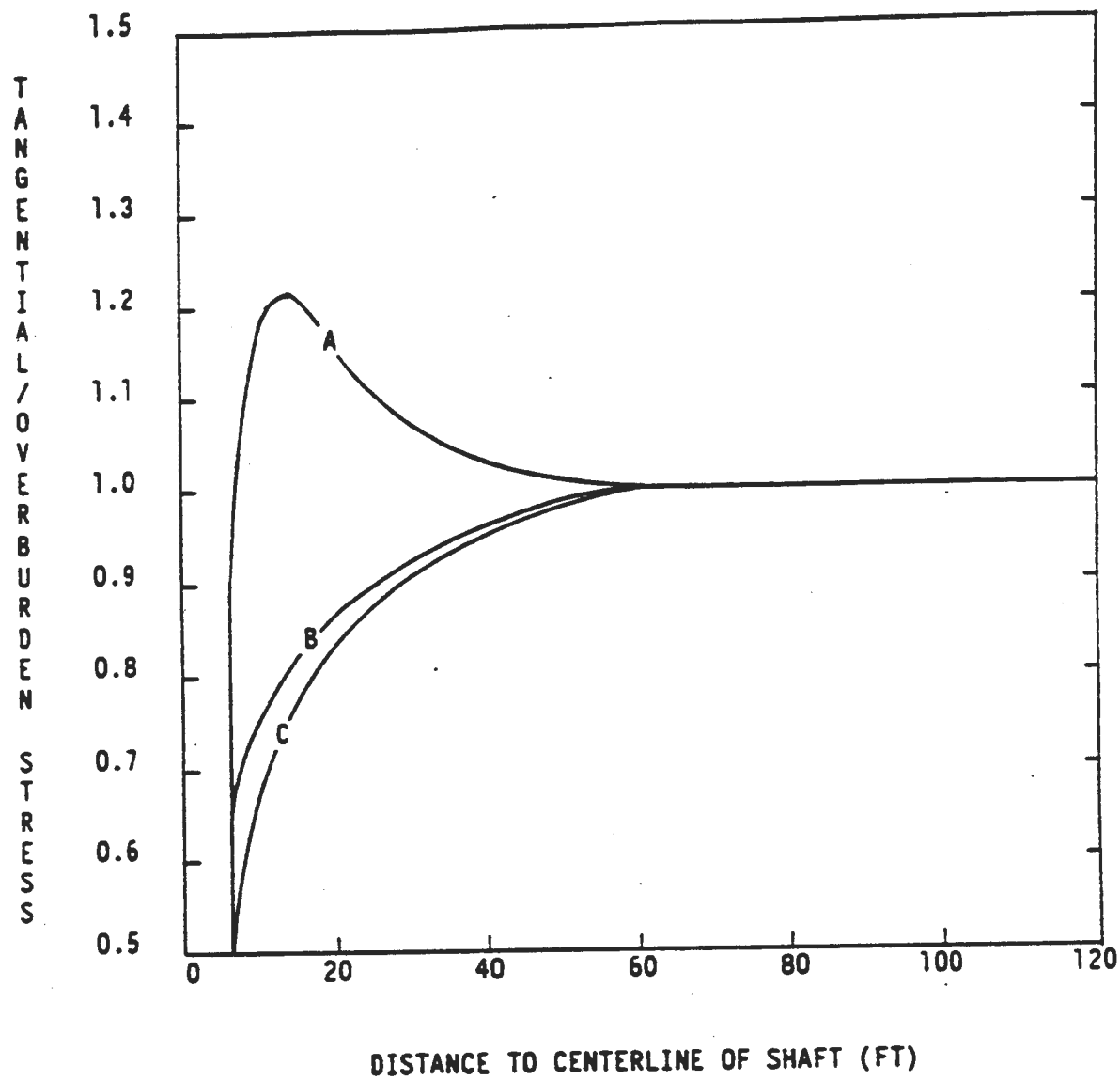


A – IMMEDIATELY AFTER EXCAVATION
B – ONE YEAR AFTER EXCAVATION
C – 15 YEARS AFTER EXCAVATION

Figure 7-25

C & SH SHAFT UNLINED SECTION
TANGENTIAL STRESS DISTRIBUTION AT ELEVATION 1353

Figure 7-26 shows the ratio of radial displacements at various distances from the shaft centerline relative to the radial displacement of the shaft wall at different times. Based on this figure, the ratio of the displacements between each extensometer anchor point and the shaft wall can be determined. This figure indicates that the extensometer collar readings relative to the deepest anchor will reach about 84 percent of the actual radial displacement of the shaft wall 15 years after excavation.

Figure 7-27 illustrates the effective creep strain distribution in the shaft at a depth of 2,057 feet (elev. 1353 feet) at selected times after excavation. The magnitude of effective strain at the shaft wall at 15 years approaches a value of approximately 0.03.

Figure 7-28 shows diametric closure versus depth at different times. The response curves are drawn relative to the time the initial instrument readings were made. The response indicated by the curve to the left of the vertical axis corresponds to the computed response which took place between excavation and the initial instrument reading. The relative response between October 1982 and June 1984 is correct regardless of the time offset. Varying the time offset in effect shifts the position of all other response curves relative to the vertical axis. The diametric closure prediction at a depth of 2,057 feet is shown on Figure 7-29.

7.3.3.4 Shaft Station

Figure 7-15 shows that, for roof extensometer 51X-GE-00251 in the C & SH shaft station, the relative movement between the collar and anchor A, expressed as a percentage of the collar reading, has remained practically constant for the last 2 years. Thus, provided that no failure of the mechanical-anchor rock bolts occurs, the closure rate of the roof is expected to stabilize. It is assumed that no new excavation will occur close to the station. If additional excavation is performed, the rate of closure between the roof and floor and between the walls may be accelerated.

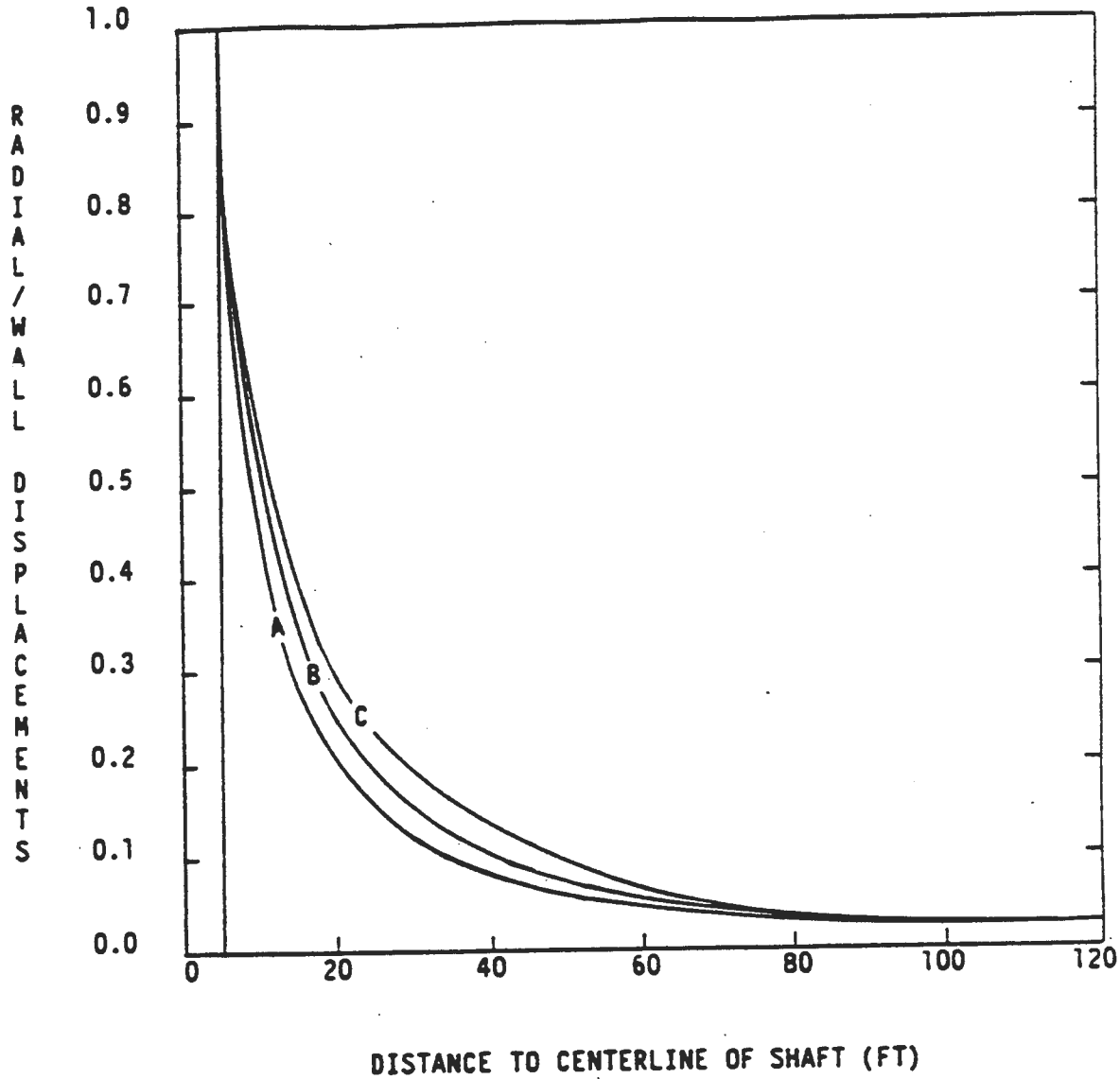


A – IMMEDIATELY AFTER EXCAVATION
B – ONE YEAR AFTER EXCAVATION
C – 15 YEARS AFTER EXCAVATION

Figure 7-26

C & SH SHAFT UNLINED SECTION
RADIAL DISPLACEMENT DISTRIBUTION AT ELEVATION 1353

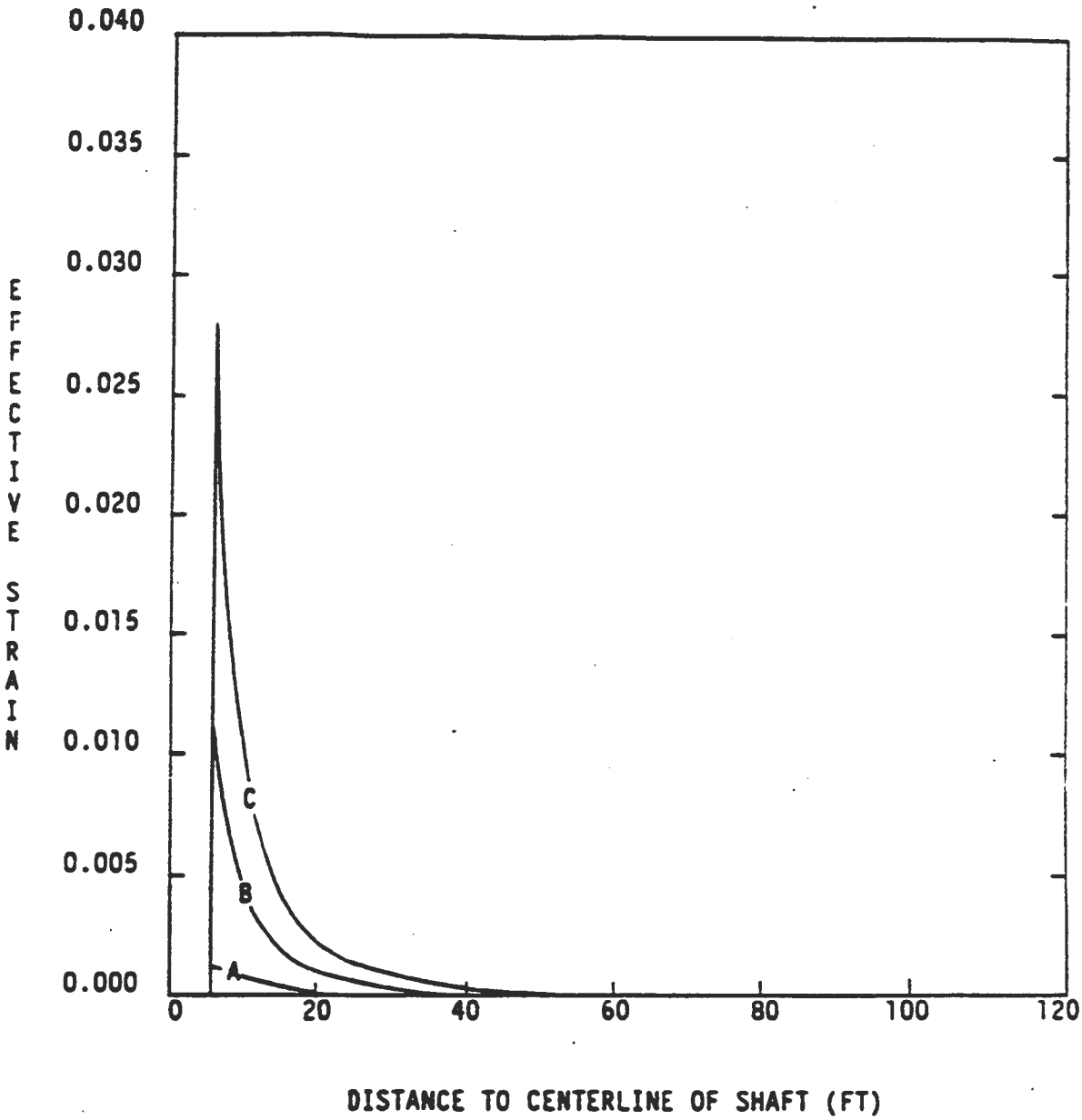


A – IMMEDIATELY AFTER EXCAVATION
B – ONE YEAR AFTER EXCAVATION
C – 15 YEARS AFTER EXCAVATION

Figure 7-27

C & SH SHAFT UNLINED SECTION
EFFECTIVE CREEP STRAIN DISTRIBUTION AT ELEVATION 1353

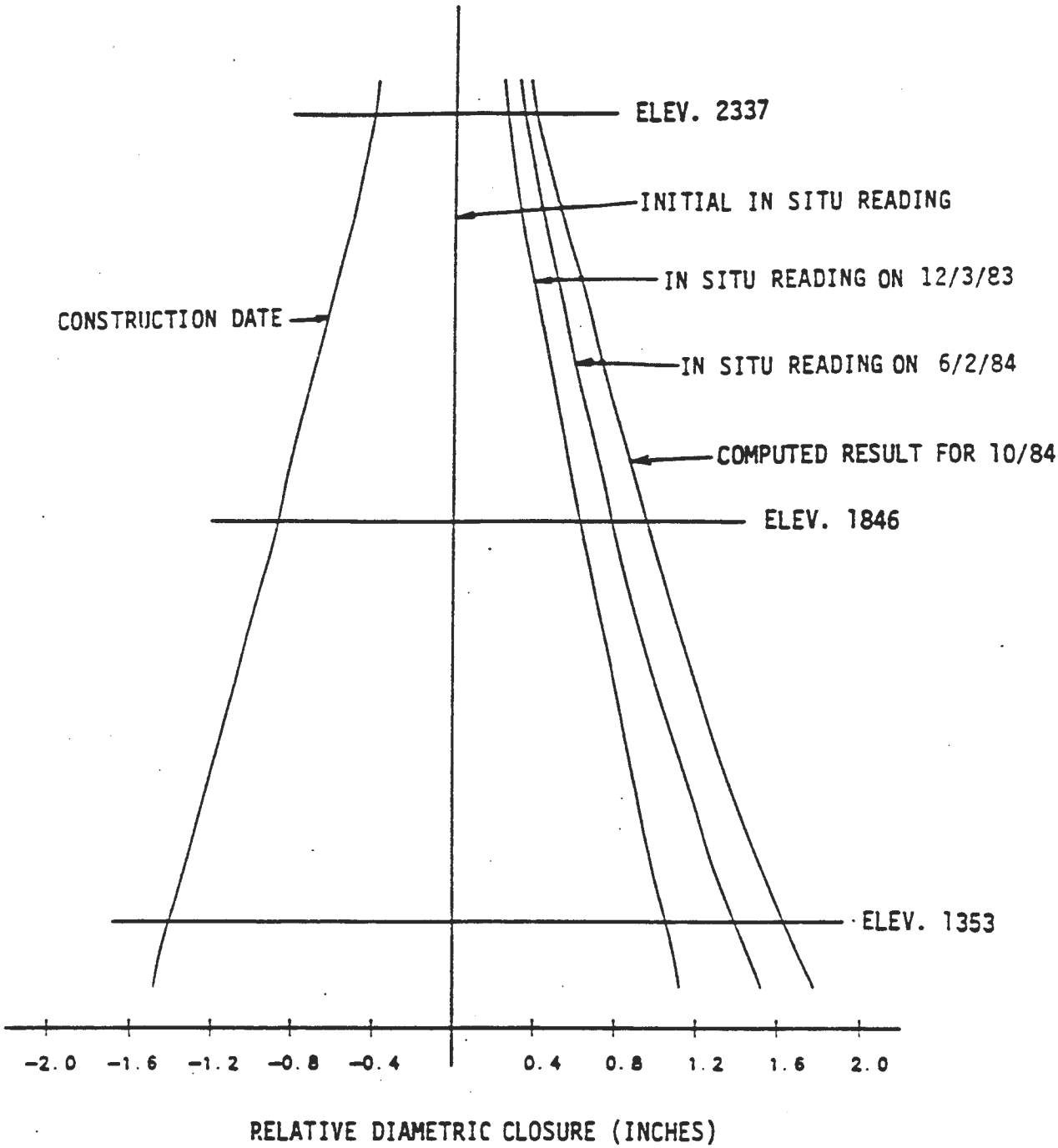


Figure 7-28

C & SH SHAFT UNLINED SECTION
RELATIVE DIAMETRIC CLOSURE

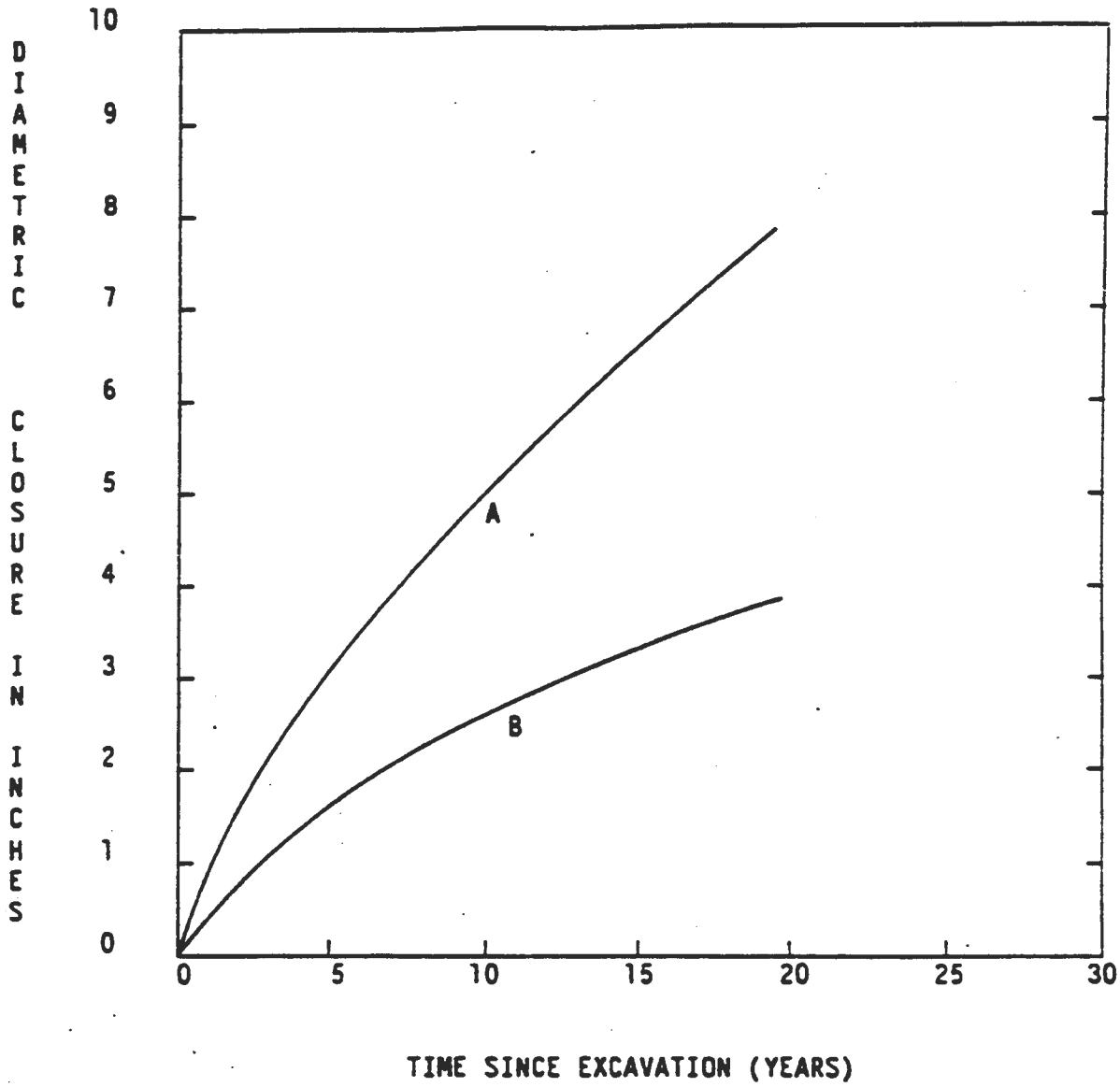


A – NORTH 17°40' WEST- MAJOR AXIS
B – NORTH 72°20' EAST- MINOR AXIS

Figure 7-29

C & SH SHAFT UNLINED SECTION
CLOSURE PREDICTION AT ELEVATION 1353

The rock bolts and wire mesh in the station roof will control spalling and stabilize the roof to provide a safe working environment but will not control salt creep. Although separations and fracturing have developed in the salt surrounding the shaft station, they exist on a much smaller scale than those observed in Test Room 3. They are expected to continue to develop throughout the operating life of the facility.

The total measured roof-to-floor closure in the C & SH shaft station was approximately 10 inches on September 16, 1985, nearly 3 1/4 years after the completion of excavation. The measured wall-to-wall closure over the same period was about 6 inches. Actual closure values are higher because the initial readings were taken nearly 260 days after the station was excavated. The average rate of roof-to-floor closure over the measurement period is approximately 3.89 inches/year. Assuming this rate will be constant throughout the operating life of 25 years, an additional roof-to-floor closure of about 8 feet is expected. Since the wall-to-wall closure is approximately 60 percent of the roof-to-floor closure, the additional wall-to-wall closure is expected to be nearly 5 feet.

## 7.4 CONCLUSIONS AND RECOMMENDATIONS

Design validation requires a determination of the compatibility of the design criteria, design bases and design configurations used in the reference design. Therefore, the following conclusions and recommendations address those criteria identified as applicable to the C & SH shaft in Chapter 2, Table 2-1, and the design basis elements presented in this chapter, Table 7-1. Other conclusions and recommendations that are a product of the design validation process are also presented.

### 7.4.1 Conclusions

Validation of the C & SH shaft reference design is based on a comparison of the applicable elements contained in the Design Criteria

and Design Bases documents with in situ conditions. These documents contain the requirements that the C & SH shaft must meet in terms of shaft stability, deformation, water pressure, water control, and shaft station stability and deformation.

Observations made during shaft inspections have not detected any signs of deterioration or instability. Due to its design pressure capacity, the liner is expected to remain stable even if the water pressure exceeds the design hydrostatic pressure.

The design basis assumption that the hydrostatic pressure begins 250 feet below the ground surface is suitable. Piezometer measurements indicate that the hydrostatic pressure is currently much less than the design basis pressure. These measurements are of sufficient accuracy to indicate that an anomalously high hydrostatic condition does not exist.

The design basis requirement that the key be designed to resist lateral pressure from the salt equal to 75 percent of the overburden pressure, approximately 640 psi, is suitable. The shaft key analysis indicates that the lateral pressure on the key at the end of 25 years will be approximately 275 psi. The lateral pressure capacity of the key is 833 psi. This provides for a factor of safety of about three. The analysis further shows that the maximum diametric closure expected for the key at the end of the operating period is only 0.175 inch. If the plastic flow or creep properties of the concrete were included in the analysis, the results would indicate that the design pressure would not be reached until after the 25-year operating life of the facility.

Based on the computed vertical, horizontal and effective stresses in the unlined section, the magnitude of stresses immediately adjacent to the opening decreases with time as the stress arch around the opening migrates away. The maximum stress occurs immediately after excavation and is followed by relaxation due to creep behavior. The stresses will, therefore, not cause a future stability problem in the unlined section of the C & SH shaft.

The analyses show the locations of effective creep strain concentrations in the unlined section of the shaft at different times. It is predicted that the maximum effective creep strain will not exceed 0.05 at the end of the operating life of the shaft. Based on the effective creep strain limit discussed in Chapter 6, the structural stability of the C & SH shaft will remain within required safety limits during its operating life.

The analyses also predict that the diametric closure near the bottom of the shaft at the end of its operating life will be approximately 10 inches along the major axis of principal strain, approximately 18 degrees from the longitudinal direction of the shaft tubular steel supports (buntons). Based on the predicted deformations and closures, the unlined section of the shaft will meet the requirements stated in the design criteria. The diameter of approximately 12 feet in the unlined section will allow for salt creep over the operating life, as required by the design bases. However, based on the design configuration of the C & SH shaft, the connections at both ends of some buntons do not provide sufficient allowance for longitudinal adjustment.

The C & SH shaft reference design complies with the criteria that require control of ground-water flow. This conclusion is made despite the fact that considerable instrumentation damage has been caused by water flow. This water has seeped into the shaft through holes cut in the liner for piezometer installation or is a result of direct rainfall. The piezometer leakage problem has been addressed and will receive additional corrective attention during a future shaft renovation. The rainwater does not reach the facility level in any significant or measureable quantity.

The chemical water seal just below the key piezometers is probably breached. The lowest water seal in the key is functioning properly. The water draining from the telltale drains has a local source. Therefore, it is concluded that there is no solutioning of the salt behind the key.

The C & SH shaft station exhibits the highest degree of deterioration in the underground facility. This is considered to be the result of the effects of blasting for initial excavation of the station. The station roof has been stabilized by rock bolting and no further significant deterioration is expected. However, removal of the 3-foot thick salt beam between the roof and clay G may be required for safety reasons in the future. Closure will continue at a rate of 3.89 inches/year vertically and 2.33 inches/year horizontally. Total closure after 25 years will be on the order of 8 feet vertically and 5 feet horizontally. This closure will require that the station roof or floor, and walls be trimmed periodically to maintain the design dimensions.

Separation and fracturing in the salt is expected to continue in the station roof and beneath the floor. Both closure and fracturing in the station will necessitate periodic maintenance during its operating life in order to maintain safety as well as the required clearances for equipment and operations.

The reference design for the C & SH shaft is validated based on the preceding discussions. The reference design complies with the design criteria and design bases. Except for instrument repair and maintenance, no modifications are required to the shaft reference design. The C & SH shaft will perform its functions as required during the operating life of the facility.

### 7.4.2 Recommendations

Based on the results of design validation, the following recommendations are made with respect to the C & SH shaft:

(1) Water behind the shaft key is undesirable and should be monitored carefully. If the volume of water behind the key increases, or if water starts flowing from beneath the key, past the lower water seal, it may become necessary to inject grout above the top water seal in the key. Grout should not

be placed behind the key (below the top seal) unless absolutely necessary. If this cannot be avoided, the grout must be a chemical gel (or other non-rigid grout) and must be compatible with both the existing water seal material and with the Plugging and Sealing Program requirements.

(2) Based on the results of design validation of the C & SH shaft, it is recommended that, during inspection of the shaft furnishings, the bunton connections should be inspected for closure allowance. If the allowance is insufficient, corrective action should be taken to provide for additional closure.

(3) The observation holes drilled in the roof of the shaft station to monitor displacements and separations, and in the floor to monitor fracturing, should be maintained. Continued observations of conditions in these holes will be valuable in assessing the safety and stability of the station.

THIS PAGE LEFT BLANK INTENTIONALLY

# CHAPTER 8

# WASTE SHAFT

## 8.1 INTRODUCTION

The waste shaft provides the connection between the surface waste handling facilities and the underground storage level. A discussion of shaft construction was presented in Chapter 3 and geologic characterization of the shaft stratigraphy was presented in Chapter 6. This chapter presents discussions of the design criteria and design bases pertaining to the waste shaft. It documents the collection of waste shaft geotechnical data, its analysis and evaluation, and presents predictions of future shaft behavior. Conclusions and recommendations are presented based on a comparison of the results of the design validation process with the shaft reference design.

## 8.2 DESIGN

This section presents the design criteria and design bases used to develop the reference design for the waste shaft. The design configuration of the shaft is discussed in Chapter 3, subsection 3.3.2.

### 8.2.1 Design Criteria

The design criteria for the waste shaft are the same as those for the C & SH shaft. The criteria requiring validation are indicated in the listing of abridged criteria presented in Chapter 2, Table 2-1, and are discussed in Chapter 7.

The design criteria requiring evaluation for design validation of the waste shaft are:

(1) shaft shall be designed to be structurally stable;

(2) shaft shall be designed to accommodate salt creep;

(3) ground-water flow into the shaft shall be controlled;

(4) underground openings (i.e. waste shaft station) shall be designed to accommodate deformation; and

(5) underground openings shall be stable.

### 8.2.2 Design Bases

The Design Basis, Waste Shaft (ref. 2-15) was the primary document used as a guide for waste shaft design. The major elements of this basis are summarized in this subsection. Only a few of these elements must be evaluated or have a direct impact on design validation. These particular elements are presented in Table 8-1.

The design bases specify that the waste shaft shall be designed to transport personnel, materials and radioactive waste. It shall also serve as an intake shaft for a small volume of air during normal operations and as an escape route during emergency operations.

The shaft shall be lined with unreinforced concrete from the bottom of its collar in the waste handling building to the top of the shaft key at the rock/salt interface. The liner shall be permanent and shall protect against spalling, fallout and deterioration of the rock in the shaft wall. It shall also prevent water seepage into the shaft.

The shaft liner shall be designed in compliance with applicable ACI Codes. A load factor of 1.4 shall be used for designing the concrete liner. The specified concrete compressive strength shall be 5,000 psi. No lateral rock pressure shall be assumed for design of the shaft liner. Hydrostatic pressure shall be considered to start at 250 feet below the ground surface and extend to the rock/salt interface at the top of the key. The water pressure shall be considered to increase 0.437 pounds per square inch (psi) for each foot of depth.

At water-bearing zones, the shaft shall be enlarged and liner plate installed to provide pressure relief and drainage space behind the liner during concrete placement and curing. Drainage pipes and

Table 8-1

VALIDATION ELEMENTS OF WASTE SHAFT DESIGN BASES

(1) Shaft liner

Hydrostatic pressure is considered to start at 250 feet below the ground surface and extend to the top of the key.

(2) Shaft key

Design lateral pressure shall be 50 percent of the vertical pressure due to soil, rock and salt overburden.

(3) Unlined section

Provide 20-foot diameter to allow for future salt creep deformation.

temporary hoses shall be installed to control water inflow prior to placement of the concrete liner. When the concrete liner has attained adequate strength, the area behind the liner plate shall be grouted to preclude deterioration of the dolomite and mudstone in the water-bearing zones.

The shaft key at the bottom of the concrete liner shall be constructed of reinforced concrete keyed into the rock and salt strata. A chemical water seal shall be placed behind the top and bottom of the key to prevent the migration of water. After the completion of shaft excavation and construction of the concrete liner and key, permanent piping from water collection rings to the shaft station shall be installed. Water from the collection rings shall be piped to a tank in the shaft station and then transported to the surface. The piping shall include inspection and clean-out fittings. Inspection and cleaning of the water collection rings and drainage piping shall be performed as necessary.

A load factor of 1.7 shall be applied to the design loading used for the concrete in the shaft key. The key shall be designed to resist lateral pressure generated by salt creep. The design lateral pressure shall be 50 percent of the total vertical pressure due to the soil, rock and salt overburden.

Below the key, the shaft shall be excavated 20 feet in diameter to allow for future salt creep deformation. Rock bolts and wire mesh shall be installed in this unlined section of the shaft in order to provide a structurally stable salt surface.

A shaft station shall be excavated at the storage level. The shaft shall extend below the storage level to such a depth as required by the hoisting equipment and sump. The use of rock bolts and wire mesh shall be dictated by the condition of excavated surfaces as well as code requirements. The roof, walls and floor shall be checked periodically for loose salt in accordance with applicable codes. The tolerance for

excavation of roof, floor and wall surfaces shall be no greater than plus 6 inches. In no case shall the finished cross section dimensions be less than the design dimensions.

Geomechanical instruments shall be installed to measure water pressure behind the shaft liner, salt creep pressure behind the key, and radial convergence in the unlined section of the shaft. The types of instruments installed shall be piezometers, pressure cells, radial convergence points and extensometers.

The shaft, including the liner, key, unlined section, station and furnishings, shall be inspected at 1 month intervals, or as required by applicable codes, to detect cracking, corrosion, deterioration and water intrusion.

## 8.3 DESIGN VALIDATION PROCESS

The design validation process for the waste shaft consists of analytical calculations, finite element modeling, and the analysis of data collected from geomechanical instruments installed in the C & SH and waste shafts. The in situ material parameters of salt determined from C & SH shaft instrumentation data were used to analyze the closure behavior of the waste shaft. For the shaft station, the in situ measurement data obtained from the C & SH shaft station were used to predict future closure behavior. The following subsections present information pertaining to validation of the waste shaft reference design.

### 8.3.1 Data Collection

Data collection in the waste shaft has consisted of geologic mapping, visual observations and geomechanical instrumentation measurements. Data obtained from the geologic mapping were presented in Chapter 6. The following subsections discuss the field observations and the geomechanical instrumentation in the shaft.

#### 8.3.1.1 Field Observations

Waste shaft inspections have been concerned primarily with water seepage through the concrete liner, salt incrustation on the surface of the liner, dissolution in the shaft sump and the results of the liner grouting program.

Water seepage through the waste shaft liner has occurred since construction. As discussed in Chapter 3, subsection 3.4.2, grouting during construction behind the steel liner plate at both the Magenta and Culebra members did not completely prevent water from entering the shaft. It was estimated that the total water seepage through the liner was approximately 0.5 gallons per minute (gpm). A remedial grouting program (ref. 3-3), conducted from August 11 through August 25, 1984, reduced the seepage to about 0.015 gpm as measured in October 1984. Subsequent inspections in February and June 1985 determined that fresh water had begun seeping through cracks and construction joints in the liner from zones within and above the grouted area. The highest level of water seepage was occurring at a depth of only 60 feet below the shaft collar. Because this is higher than the potentiometric surface of ground water in the Magenta and Culebra members, the source of the seepage was probably rainwater and construction water contained in the backfill around the shaft collar and in the underlying Gatuna sandstone. This is based on the fact that heavy rains in the late summer of 1984 left substantial quantities of water ponded in the waste-handling building excavations and in the remnant of the SPDV ventilation shaft drilling fluid reserve pit.

The initial rate of this renewed seepage could not be measured because the PVC drainpipe had been broken in several places. Subsequent repair of the drainpipe has permitted the rate of water inflow to be measured on a regular basis. The measurements are obtained by timing the flow of water from the drainpipe into a calibrated bucket. These measurements do not consider the small amount of uncontrolled "fly water" that falls down the inside of the shaft. The initial measurement, in January 1986, was 0.47 gpm. The measurements, are

plotted on Figure 8-1 and show a generally decreasing trend in the flow rate. This trend may be influenced by three factors. First, the water contained in the backfill and sandstone has slowly drained into the shaft. Second, the rate of evaporation increases as the outside air temperature increases, thus reducing the amount of water reaching the drains. Both of these conditions are temporary. A series of rainstorms could recharge the backfill and sandstone, and evaporation will decrease with cooler winter temperatures. Heavy rains in June 1986 may have been responsible for the increased flow detected by the late June reading. The third factor influencing the flow trend is the possibility that the water collection rings and the drainpipe may be partially blocked by debris. This would result in reduced water flow through the drainpipe and an increase in the amount of unmeasureable fly water.

Although there has been limited access to the waste shaft since August 1984, several inspections of the shaft and sump have been made. One inspection was made on February 21, 1985, at which time some instrumentation damage was observed. In addition, the PVC drainpipe was observed to have been broken in several locations. Appreciable salt incrustation was noted on the surface of the concrete liner and on many of the instrumentation boxes and cables. This incrustation was primarily attributed to salt dust from the underground excavation adhering to the damp shaft walls during the period since September 1984 when the waste shaft was used as an exhaust shaft. A small percentage of this salt incrustation was also attributed to water seepage through the liner.

On June 16, 1985, another inspection of the waste shaft was made to within 60 feet of the shaft station. The shaft ventilation had been changed from upcast to downcast after the February inspection. Very little salt incrustation was present on the concrete liner and only a small amount was present in places on the wire mesh. Fresh water entering the shaft through the liner, from approximately 60 feet below the collar, was running down the liner. Although much of the liner was

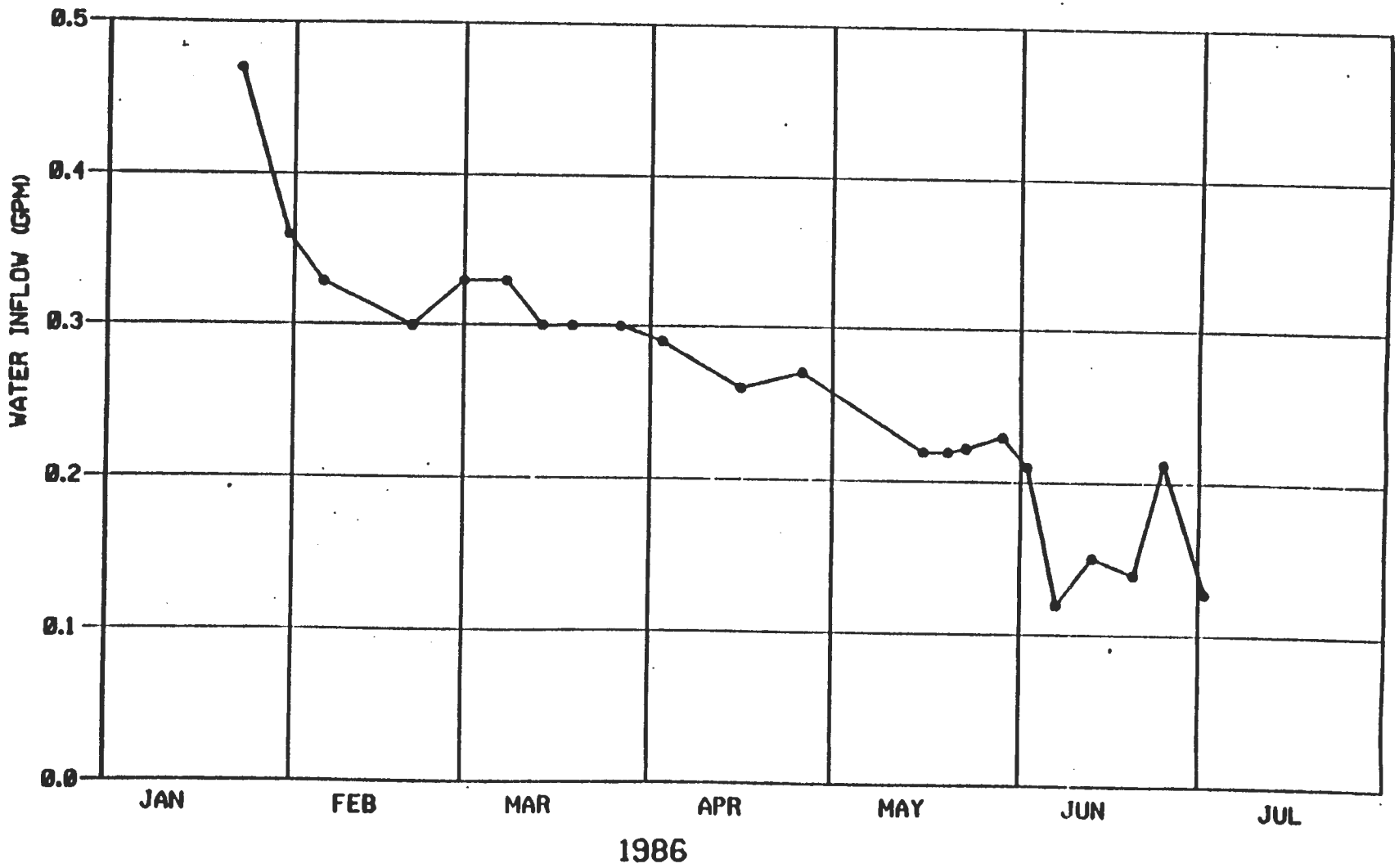


Figure 8-1

WASTE SHAFT
WATER INFLOW MEASUREMENTS

observed to be wet, the water rings were not full. This water appeared to have dissolved the salt incrustation observed in the February 1985 inspection. Cracks were common in the liner to within 60 feet of the collar. The PVC drainpipe damage had not been repaired. No water was seen draining from below the concrete key. The shaft sump contained water to within 60 feet of the shaft station floor. This water was a combination of rainwater, construction water and ground water. It was pumped out in September 1985.

On December 1, 1985, another inspection of the waste shaft was made. The PVC drainpipe was still broken or disconnected at several levels. The water rings were plugged and overflowing. There appeared to be an increase in water flow into the shaft, most noticeably at the Culebra member. An approximately 1/8- to 1/4-inch thickness of salt had been deposited on the liner below the Culebra.

On December 11, 1985, an inspection of the waste shaft sump was made. During this inspection, and a subsequent inspection on December 12, 1985, MB-139 was observed closely. The clay along the lower contact was distinct and no separations were noted. Although the upper contact could not be distinguished behind a covering of wire mesh, MB-139 could be seen quite well and appeared to be intact and undisturbed. One small fracture, approximately 2 feet long and 1/2 inch wide was observed on the west side of the shaft approximately 1 foot above the lower contact.

An anhydrite bed 61 to 66 feet below the station floor was also observed during this inspection. A zone of dissolution was present along the upper contact of this layer in the northwest to southeast half of the shaft. The dissolution occurred partially within the anhydrite bed. The maximum void width of approximately 0.7 foot occurred on the south-southwest side of the shaft and extended approximately 18 feet south into the salt. The zone of dissolution pinched out going around the shaft in either direction away from the area of maximum opening. There did not appear to be any disturbance of

the strata overlying or underlying this zone anywhere around the shaft and no voids or disturbance of the anhydrite existed on the opposite side of the shaft. The upper contact of the anhydrite with the overlying halite did not exhibit any irregularities. From the physical evidence available, it appeared that this feature was the result of localized dissolution. No dissolution of the anhydrite was observed. The dissolved material was probably a soluble evaporite mineral representing a facies change within the Salado formation. The dissolution appeared to have resulted from the previously discussed water which had been standing in the sump. The level of this water was measured at 60 feet from the shaft station floor prior to its being pumped out in September 1985. The shaft wall below the water line exhibited no significant deterioration due to the standing water. However, some sloughing of an anhydrite layer 71 to 75 feet below the shaft station floor and widening of the shaft near the bottom of the sump was evident. The shaft wall exhibited a glazed surface which probably resulted from minor dissolution of the salt surface.

A shaft inspection was conducted on July 24, 1986. The inspection team mapped the location of cracks in the concrete liner and any associated seepage. They also mapped the location of leaking construction joints. This mapping indicates that additional cracks have developed in the liner since mapping was conducted prior to the August 1984 grouting program. The shaft was found to be considerably drier than during the 1984 mapping program. Many of the new cracks mapped may have existed in 1984 but were masked by the water on the shaft walls. Also, salt precipitates now enhance the outline of the cracks. The inspection also revealed that recent construction work inside the shaft has resulted in some instrument cable and junction box damage and in breakage of the previously repaired PVC drainpipe.

The waste shaft station has shown little deterioration since it was enlarged from the SPDV ventilation shaft station dimensions. Visual surveys are performed approximately every 3 months by site geologists. The results of these inspections are documented in the GFDRs. Only

minor spalling along the station walls has occurred. Vertical fractures similar to those found in the drifts and test rooms have developed at intersection corners. The roof, although showing no visible evidence of deterioration, has been covered by wire mesh and rock bolts for safety purposes. During the July 1986 shaft inspection, some separation at clay G was observed on the east and west sides of the shaft. The separation was a maximum of 3/4 inch wide at the shaft surface and decreased away from the shaft. No separation was observed at clay H.

Minor separations and fracturing in MB-139 and in the overlying halite have been observed in the station floor. A dish-like fracture zone similar to that found in Test Room 2 is present, but has developed on a much smaller scale. Inspection of MB-139 in the shaft sump, and evidence from boreholes drilled in the station floor, show that the marker bed and the overlying halite are, for the most part, intact.

8.3.1.2 Geomechanical Instrumentation

The waste shaft geomechanical instrumentation is similar in design to that of the C & SH shaft. The shaft contains 12 vibrating-wire piezometers, 4 pressure cells, 9 multiple-point borehole extensometers, and 3 sets of radial convergence points. Figure 8-2 shows the instrument locations in the waste shaft and Figure 8-3 shows details of the key instrumentation.

As in the C & SH shaft, all of the geomechanical instruments, except the convergence points, are monitored remotely. The instruments are connected to the surface datalogger that polls all of the remotely-read underground instruments on a scheduled basis.

The 12 piezometers were installed on September 7 and 8, 1984, after the 6-foot diameter SPDV ventilation shaft had been enlarged to become the 20-foot to 23-foot diameter waste shaft. The water that could exert pressure on the liner is expected to come from the two water-bearing members in the Rustler formation. The Magenta dolomite member occurs

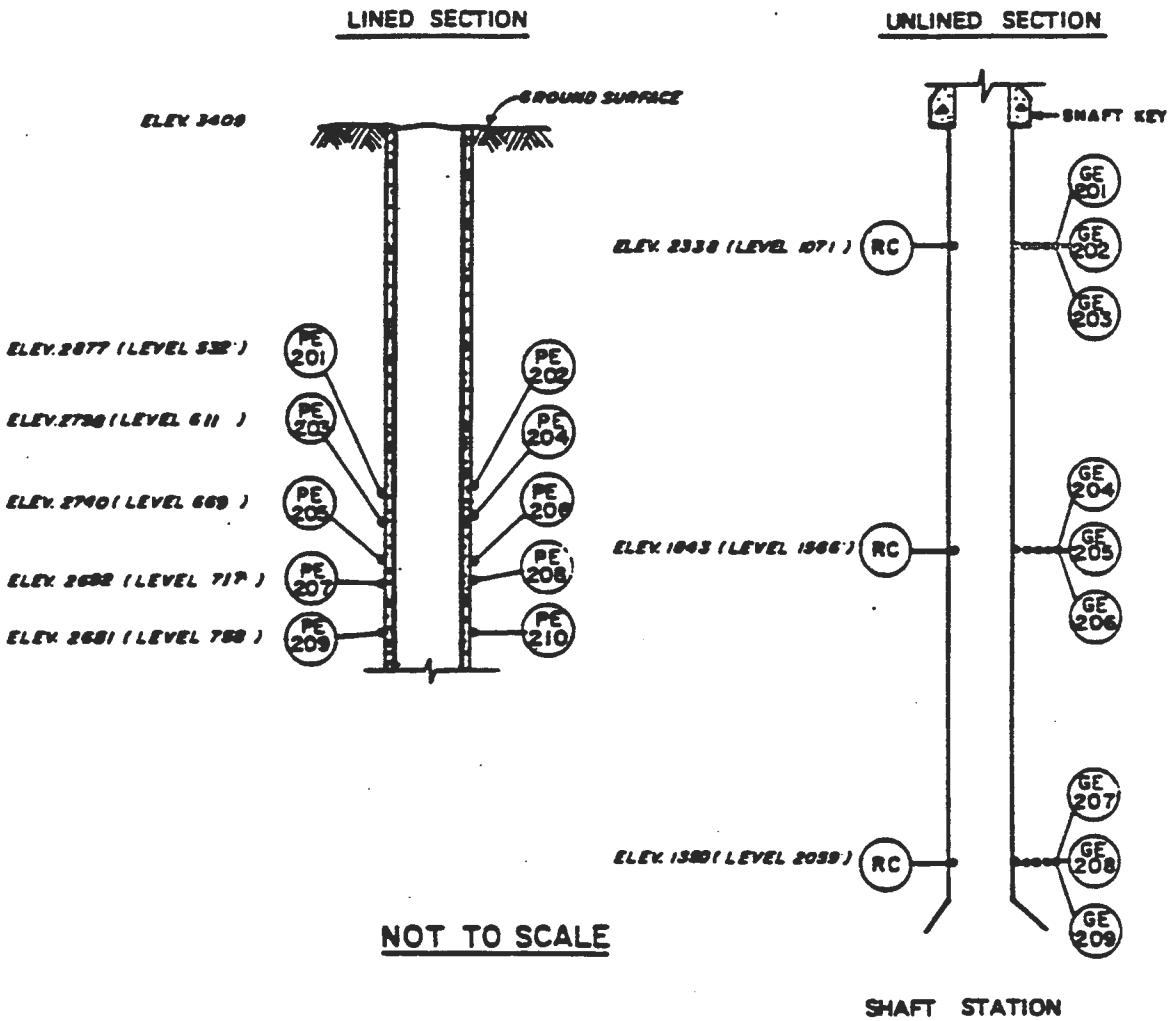


**LEGEND**

- (PE) PIEZOMETER
- (RC) CONVERGENCE POINTS
- (GE) EXTENSOMETER

NOTES:

1. PC'S AT EACH LEVEL CONSIST OF FOUR POINTS.
2. THE TERM "LEVEL" IS AN APPROXIMATE DEPTH IN FEET FROM THE SHAFT COLLAR AT ELEVATION 3409 FT MSL
3. SEE FIGURE 8-2 FOR DETAILS OF SHAFT KEY INSTRUMENTATION

**Figure 8-2**

**WASTE SHAFT INSTRUMENTATION**

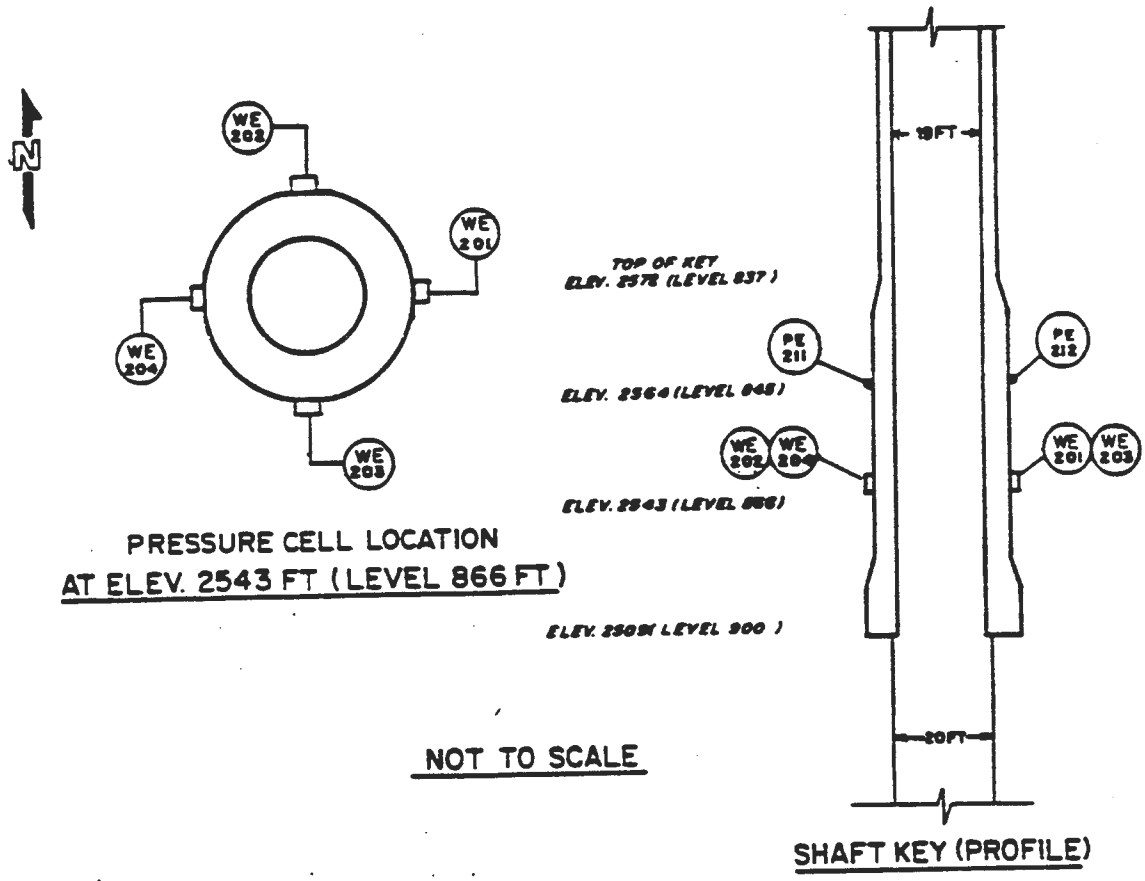


LEGEND

WE - PRESSURE CELL

PE - PIEZOMETER

NOTES:

1. THE TERM "LEVEL" IS AN APPROXIMATE DEPTH IN FEET FROM THE SHAFT COLLAR AT ELEVATION 3409 FT MSL
2. PRESSURE CELLS LOCATED AT CONCRETE-ROCK INTERFACE.

**Figure 8-3**

**WASTE SHAFT KEY INSTRUMENTATION**

from a depth of 596 feet to 621 feet (elev. 2813 to 2788 feet) and the Culebra dolomite member from a depth of 706.5 feet to 728.5 feet (elev. 2702.5 to 2680.5 feet). Two piezometers are at each of the following elevations: 2877, 2798, 2740, 2692, 2651 and 2564 feet (Figures 8-2 and 8-3). The piezometers are located on opposite sides of the shaft, one at N60°E and the other at S60°W. Piezometer readings are shown on the data plots in Appendix J.

The four pressure cells are located in the waste shaft key between the salt of the shaft wall and the concrete comprising the key. The pressure cells were installed at a depth of 866 feet (elev. 2543 feet). The four cells are spaced 90 degrees apart around the shaft at the north, east, south, and west positions (Figure 8-3). Initial pressure cell readings were taken on April 6, 1984. The waste shaft key concrete was placed between March 23 and April 3, 1984. Pressure cell data plots are also presented in Appendix J.

The extensometers and convergence points were installed only in the unlined section of the shaft below the key. These instruments, whose locations are shown on Figure 8-2, were installed after enlargement of the shaft to its final dimensions.

The nine multiple-point borehole extensometers were installed between August 31 and September 5, 1984, 3 to 5 months after the completion of shaft enlargement. Three extensometers each are located at three elevations in the unlined section of the shaft: 2338, 1843 and 1350 feet (Figure 8-2). The extensometers are spaced 120 degrees apart around the shaft. Plots of the readings are presented in Appendix J.

A set of radial convergence points, consisting of four points each, is located at each of the same elevations as the extensometers. The convergence points were installed immediately after enlargement of the shaft. Due to interference by shaft furnishings, it was not possible to set the convergence points at 90 degrees from each other. The set of convergence points at a depth of 1,071 feet consists of two points

on each side of the shaft conveyance furnishings. The two points were set 44 degrees apart. At the other two depths the two points on each side of the shaft are set 53 degrees apart. Convergence point readings were obtained from April through June 1984 and are plotted in Appendix J. However, their performance is considered poor and erratic. The readings have been affected by salt incrustation on the convergence point eyebolts and extensions. Convergence point readings were discontinued when the temporary waste shaft hoist was decommissioned on September 12, 1984. The convergence points will be inaccessible until approximately December 1986, when the permanent waste shaft hoist is installed.

Geomechanical instruments were installed in the SPDV ventilation shaft station in late 1982. The instrumentation consisted of three multiple-point borehole extensometers and two sets of convergence points as shown on Figure 8-4. When the shaft was enlarged to become the waste shaft, the station was also enlarged and the original instruments were destroyed. Two extensometers were then installed in the enlarged shaft station. Both of these extensometers are in the roof, one on either side of the waste shaft (Figure 8-5).

### 8.3.2 Analysis and Evaluation

Analysis of the waste shaft data and its evaluation against reference design parameters has been divided into four elements: the concrete-lined section of the shaft; the shaft key; the unlined section; and the shaft station. This division is based on the different in situ and design conditions in each of these areas.

#### 8.3.2.1 Lined Section

Engineering mechanics principles were used to design the concrete liner against elastic buckling. Both axial and flexural stresses were considered in the design. Permissible stress values were those used for structural plain concrete (ref. 8-1) utilizing the ultimate strength design method. Since there are no significant salt strata in

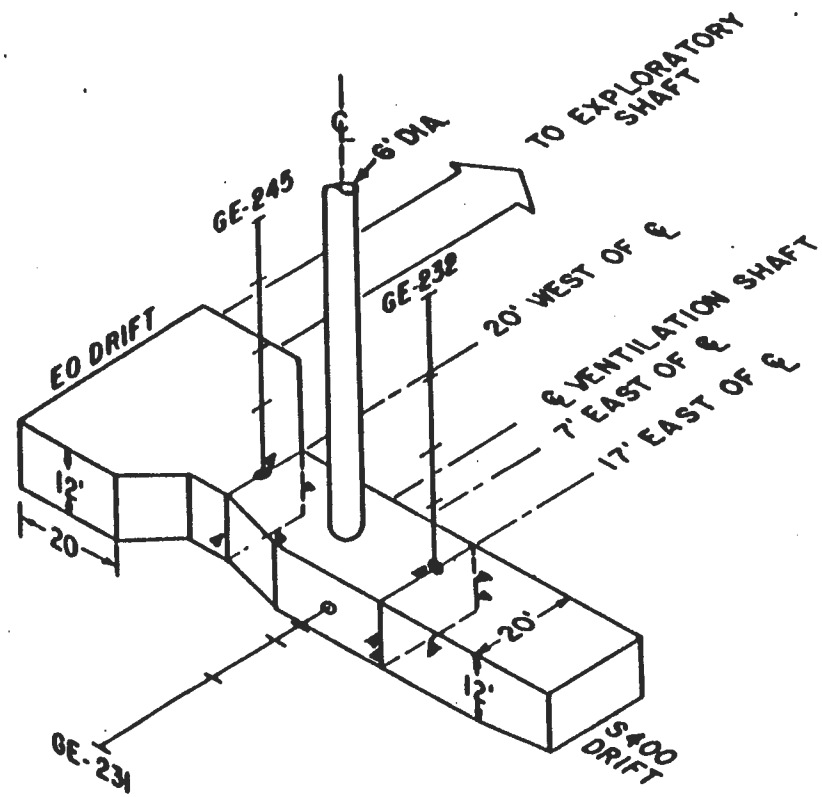


**EXPLANATION**

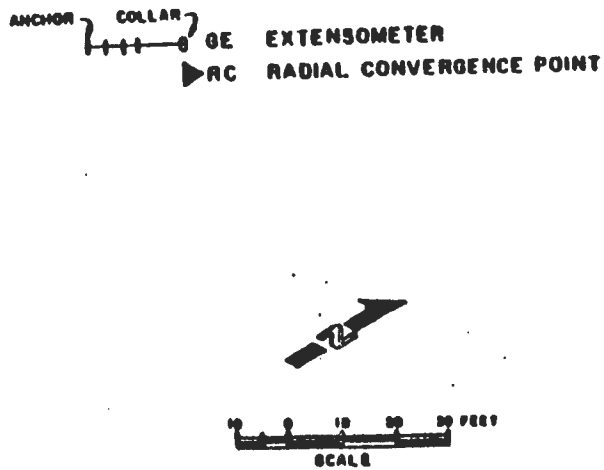


Figure 8-4

SPDV VENTILATION SHAFT STATION INSTRUMENTATION

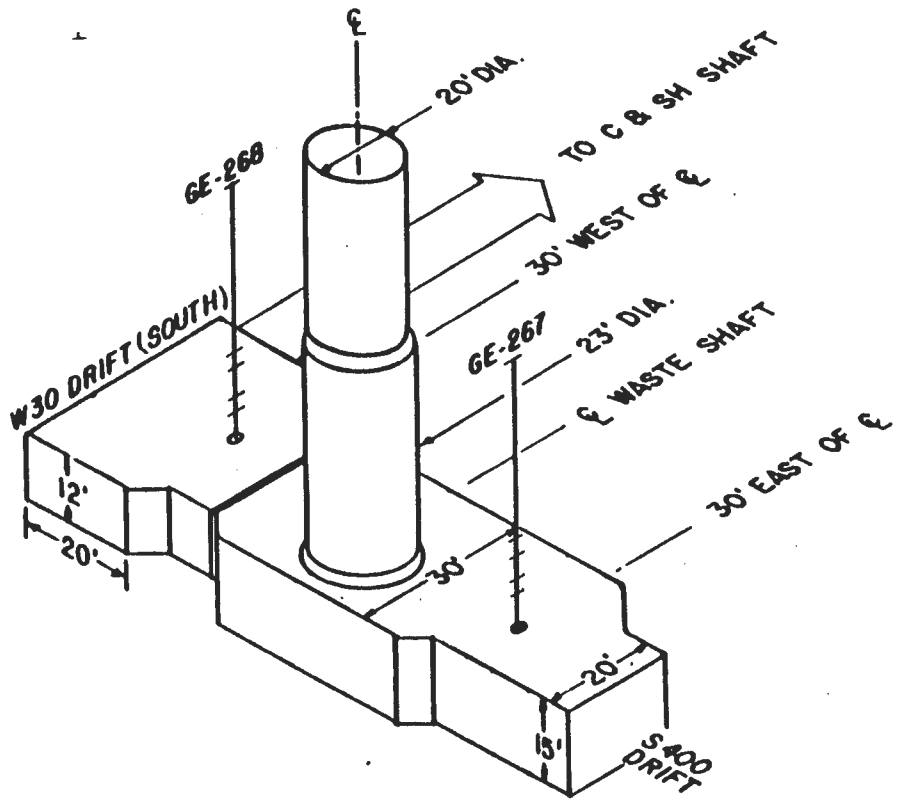


**EXPLANATION**

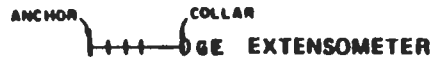


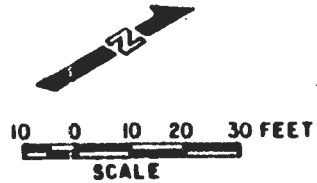


**NOTES:**

1. PREVIOUSLY IDENTIFIED AS THE SPDV VENTILATION SHAFT STATION.
2. INITIAL INSTRUMENTATION WAS DESTROYED IN JUNE 1984. EXTENSOMETERS GE-267 AND GE-268 WERE INSTALLED AFTER STATION ENLARGEMENT.

**Figure 8-5**

**WASTE SHAFT STATION INSTRUMENTATION**

the rock surrounding the liner, rock creep and the resulting rock pressure against the liner were assumed to be negligible. Hydrostatic pressure acting from a depth of 250 to 844 feet was used in the design based on the applicable design basis element (Table 8-1).

Additional stresses in the liner due to initial imperfections in roundness and grouting pressures were also considered. For stress calculations, an initial imperfection of 1 inch was assumed in the roundness of the liner. In place of the local water pressures, grouting pressures 1.3 times the ground-water pressure were assumed to act over one-sixth of the circumference of the liner. Due to localized effects, a 20 percent increase in the allowable concrete stress was assumed due to the short-term loading of the grouting pressure.

The external pressure capacities and corresponding closure limits (maximum diametric changes) for different thicknesses of the liner are:

| Depth (feet) | Liner Thickness (inches) | Pressure Capacity (psi) | Closure Limit (inches) |
|---|---|---|---|
| 27 to 462 | 10 | 216 | 0.165 |
| 462 to 580 | 14 | 370 | 0.215 |
| 580 to 762 | 18 | 523 | 0.251 |
| 762 to 837 | 20 | 598 | 0.266 |

The intent of the shaft piezometers is to monitor the pressure exerted on the liner by water from the Rustler formation. These data would indicate if the design hydrostatic pressure from the design basis was suitable.

Table 8-2 summarizes the variation in measured water pressures behind the liner at different times. Figure 8-6 shows the average reading on September 18, 1985, for each piezometer pair plotted against shaft depth. For comparison, the hydrostatic design pressure for the liner through this interval is also shown.

The measured pressures at this time are lower than the design pressure for two apparent reasons. First, water seepage through cracks and

Table 8-2

WASTE SHAFT LINER AND KEY
SUMMARY OF MEASURED WATER PRESSURES (psi)

PIEZOMETER NO. 31X-PE-00

| Date of Reading | 201 | 202 | 203 | 204 | 205 | 206 | 207 | 208 | 209 | 210 | 211 | 212 |
|---|---|---|---|---|---|---|---|---|---|---|---|---|
| | Elev. 2879 | | Elev. 2798 | | Elev. 2740 | | Elev. 2692 | | Elev. 2651 | | Elev. 2564 | |
| Dec. 26, 1984 | -1 | 0 | 16 | 20 | -7 | -8 | 77 | 93 | 65 | 76 | 13 | 11 |
| May 16, 1985 | -2 | 0 | 11 | 16 | 12 | -15 | 79 | 95 | 58 | 84 | 8 | 10 |
| June 27, 1985 | * | 0 | 13 | 19 | * | -16 | 78 | 95 | * | 91 | 11 | 12 |
| Sep. 18, 1985 | * | 1 | 17 | 26 | * | -14 | 99 | 115 | * | 107 | 19 | 22 |
| Dec. 18, 1985 | * | -3 | -3 | -2 | * | -3 | 47 | 51 | * | 27 | 4 | 8 |
| Mar. 16, 1986 | * | -3 | 2 | 6 | * | -13 | * | 63 | * | 47 | 5 | 12 |
| June 13, 1986 | * | 0 | 10 | 15 | * | -20 | * | 85 | * | 74 | 18 | 19 |

* Piezometer not functioning.

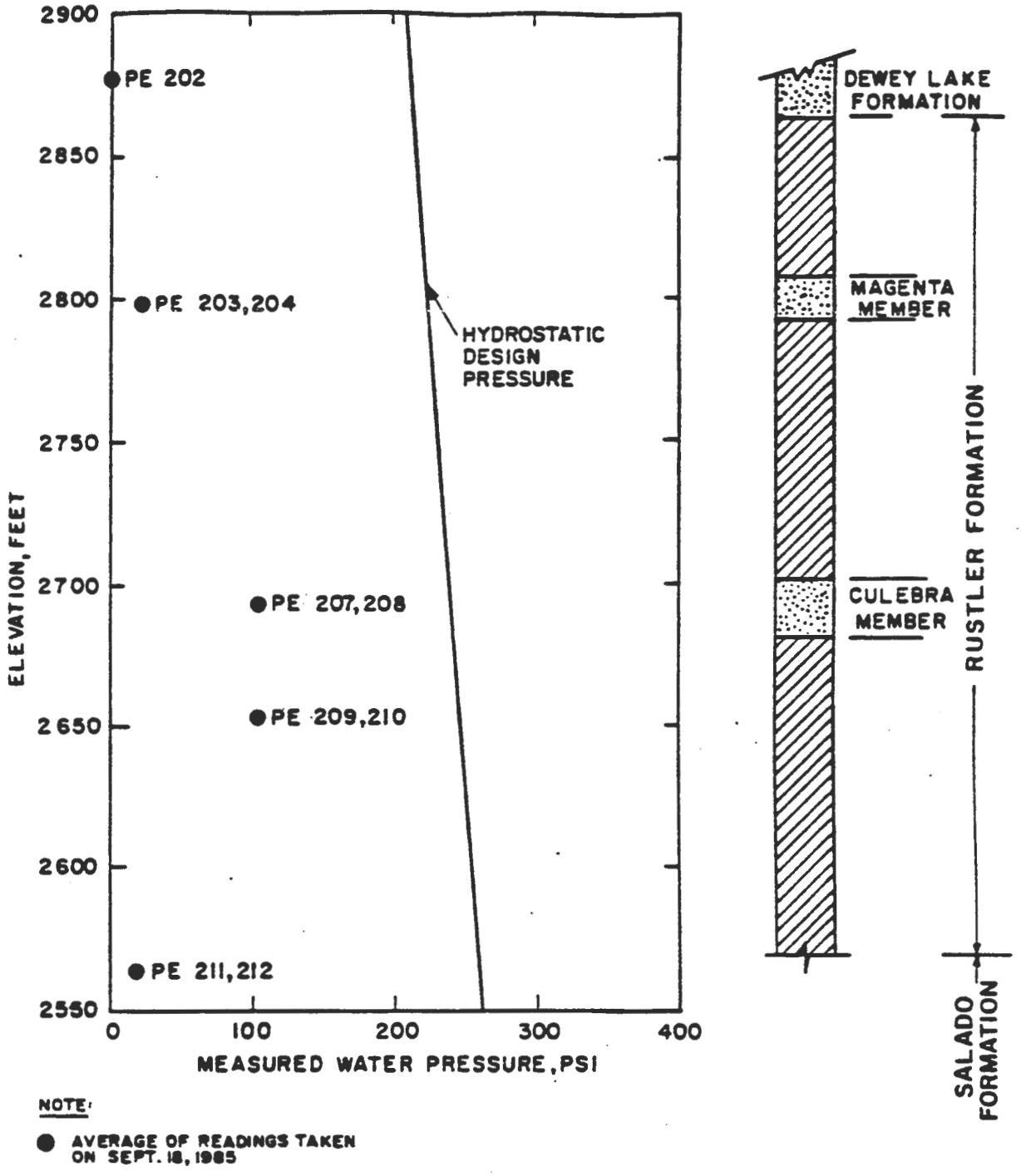


Figure 8-6

WASTE SHAFT LINER
WATER PRESSURE MEASUREMENTS

construction joints in the liner has not allowed the water to build up to its full hydrostatic head. This means that the piezometers are not measuring the full pressure that might be expected against the liner if the leaks were sealed. Second, the low pressure readings, and especially the variation in readings, suggest that hydraulic continuity is incomplete along the rock/liner interface. It is possible that water from the Culebra has been isolated, or at least restricted, in its vertical extent. This is suggested by the distribution of pressures shown on Figure 8-6.

The pressure distribution of the piezometers is also shown on Figure 8-7. These readings, however, are the maximum pressure values measured for each piezometer elevation. The figure also shows the design hydrostatie pressure distribution for the entire liner and its pressure capacity. The pressure capacity provides a significant factor of safety over the design hydrostatic pressure.

8.3.2.2 Shaft Key

Due to lithostatic pressure, the salt formation behind the shaft key tends to creep over time. The result is a buildup of inward pressure against the concrete key. The concrete key was designed to withstand a lateral pressure equal to 50 percent of the vertical overburden pressure (approximately 60 ksf) for at least 25 years after its construction. This reduction in lateral pressure from 75 percent of the overburden pressure for the C & SH shaft to 50 percent for the waste shaft was based on the results of the analysis of data obtained from the C & SH shaft (Chapter 7).

A nonlinear finite element analysis was utilized to simulate the long-term creep interaction of the salt and the concrete key. The analysis was performed using the MARC Finite Element Program discussed in Chapter 6. The material properties of the finite element model simulated the creep behavior of the salt via a power law (equation C.4-6 in Appendix C) provided in the analysis.

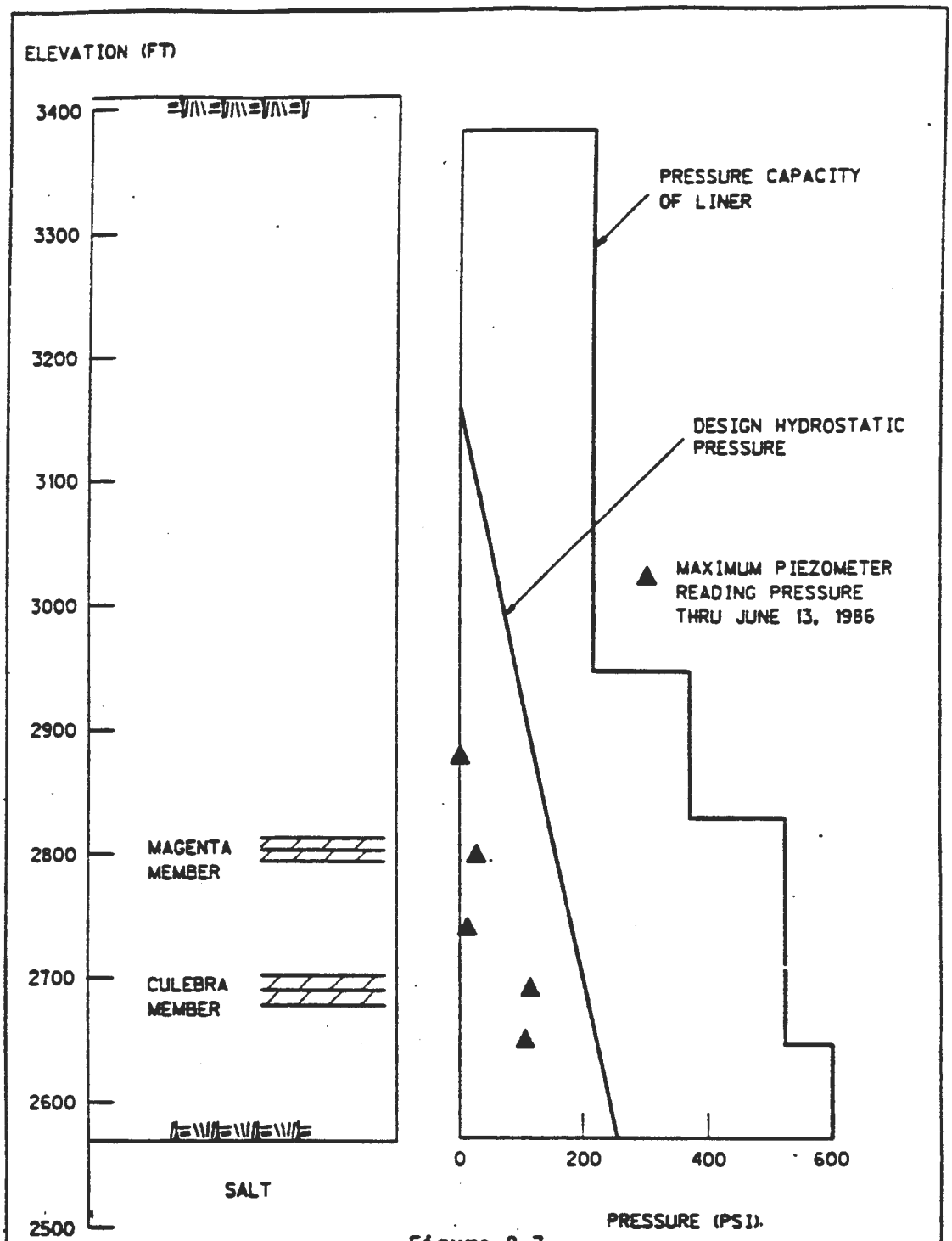


Figure 8-7

WASTE SHAFT LINER
LATERAL PRESSURE COMPARISON

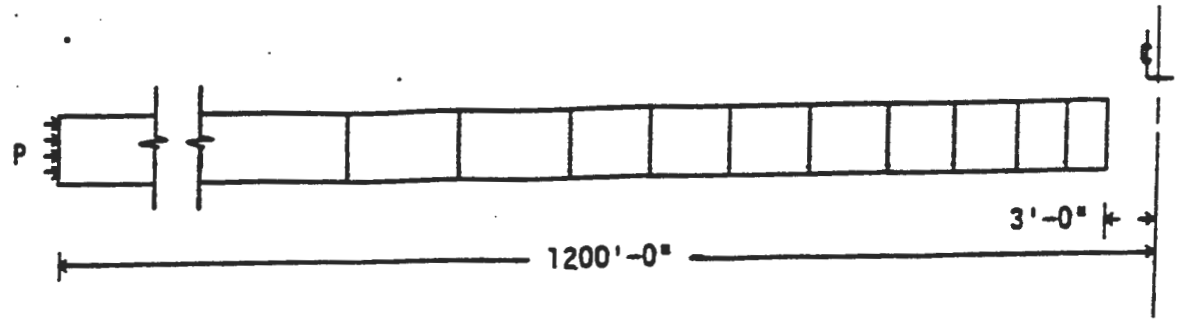


(A) BEFORE ENLARGEMENT

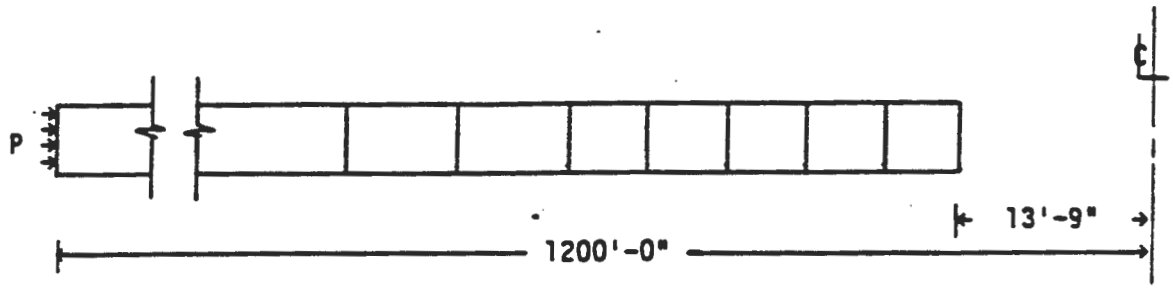


(B) AFTER ENLARGEMENT

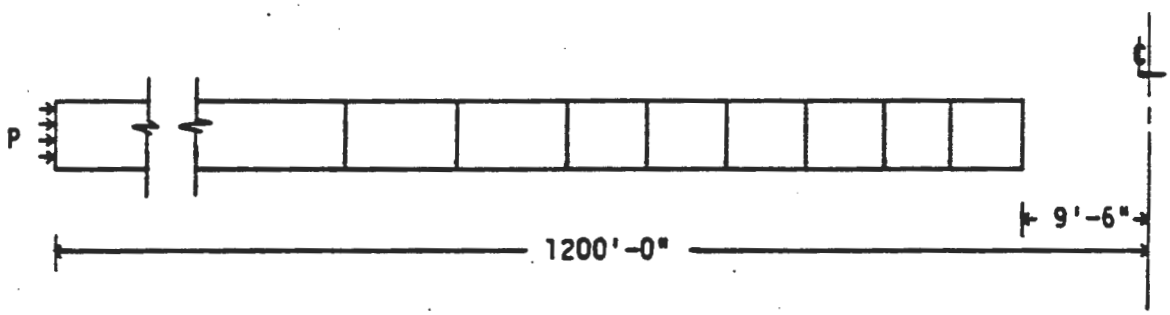


(C) AFTER CONCRETE CONSTRUCTION

Figure 8-8

WASTE SHAFT KEY
FINITE ELEMENT MODEL

Model Simulation. Unlike the more sophisticated analysis of the C & SH shaft key (which employed a multi-layered, axisymmetric finite element model), the finite element model for the waste shaft key and surrounding salt consists of a single layer of quadrilateral, axisymmetric ring elements as shown on Figure 8-8. Because only the lateral flexural stiffness of the shaft key was considered in the finite element model, and not its longitudinal flexural stiffness, the analysis provides conservative results. Also for conservatism, the shrinkage effect of the concrete was not taken into account in this analysis.

An inner element of the model, shown on Figure 8-8, represents a segment of the concrete key. In order to simulate the time interval between shaft excavation and concrete placement for the key, this element was not tied to the surrounding salt deposits. All depth-dependent input values, such as overburden stresses, were computed for a depth of 892 feet, low in the key, where such values are at a maximum. Because halite is the most dominant material in the rock around the shaft key, its properties were used for the model elements. Halite is also the material at the base of the shaft key where lateral pressure is at a maximum.

The following analytical procedure was used to perform a creep analysis of the waste shaft key:

(1) Initially, lateral forces were applied outwardly against the inside surface of the shaft. This simulates the condition prior to excavation of the original 6-foot diameter shaft.

(2) Lateral forces were applied inwardly against the outer vertical boundary of the model. The magnitude of these forces were based on the lateral earth pressure, equal to 892 feet of overburden, computed for the key elevation of 2517 feet.

(3) Internal stresses were applied in each element to represent the initial lithostatic stress state.

(4) All nodes of the model were restrained against vertical displacement.

(5) Subsequently, outward lateral forces against the inside surface of the shaft were removed to simulate excavation of the original 6-foot diameter shaft.

(6) A creep analysis was performed on the salt deposits surrounding the 6-foot diameter shaft until that time when the shaft diameter was enlarged and the concrete for the key was placed (795 days).

(7) The three innermost ring elements were detached (tie constraints removed) from the model to represent the enlargement of the shaft. A concrete ring element (tie constraints added to the model) then replaced the three salt elements just removed to model the concrete key.

(8) A second creep analysis was performed using this new model and a creep time representing 28 years after placement of the concrete key.

The stratigraphy in the upper section of the waste shaft is similar to that in the C & SH shaft. The creep parameters determined from in situ salt behavior in the C & SH shaft were, therefore, assumed to be valid for correlating analytical results of the waste shaft from normalized time to real time. The secondary creep parameter C was found to equal $5.70 \times 10^{-21}$ $ksf^{-4.9}$ $sec^{-1}$. Because early in situ measurements were not available for the C & SH shaft, the primary creep parameters A and z were determined from in situ data from the horizontal drifts and were found to be 3.2 and $1.1 \times 10^{-7}$ $sec^{-1}$, respectively.

Seepage Evaluation. The structural integrity of the shaft key is not totally dependent upon salt creep. The stability of the key, and consequently the shaft liner, can be compromised by water dissolving the salt surrounding the key. Water is prevented from seeping from the upper water-bearing zones down into the salt around the key primarily by two chemical water seals. The key configuration, including the seals, is described in Chapter 3.

The number of piezometers in the key are not sufficient to conclusively support an evaluation of seepage. However, the distribution of water pressure behind the liner and key provides an indication that there is probably no hydraulic continuity along the rock/liner interface. This is especially evident at the lowermost water-bearing zone at a depth of 717 feet (elev. 2692 feet). Here, water pressures are over 100 psi. The next lower level of piezometers, at a depth of 758 feet (elev. 2651 feet), also indicate pressures of about 100 psi. However, the lowest level of piezometers, in the shaft key, reflect pressures of less than 25 psi.

The telltale drains in the waste shaft key could not be located during the July 1986 inspection. Assuming they were constructed as designed, they may be covered by a thin veneer of concrete formed during concrete placement. A seep was noted on one side of the shaft at the approximate design level of the telltales. Inspection of the base of the key determined that no water was seeping from behind the key. This indicates that ground water is not bypassing the lower water seal between the key and the surrounding halite.

#### 8.3.2.3 Unlined Section

The structural behavior of the unlined section of the waste shaft was also computed by a nonlinear creep analysis using the MARC Finite Element Program (ref. 6-8). The objective of the analysis was to compute the actual structural behavior by utilizing applicable in situ data from the C & SH shaft and the horizontal drifts, and to verify the design adequacy of the unlined section of the shaft.

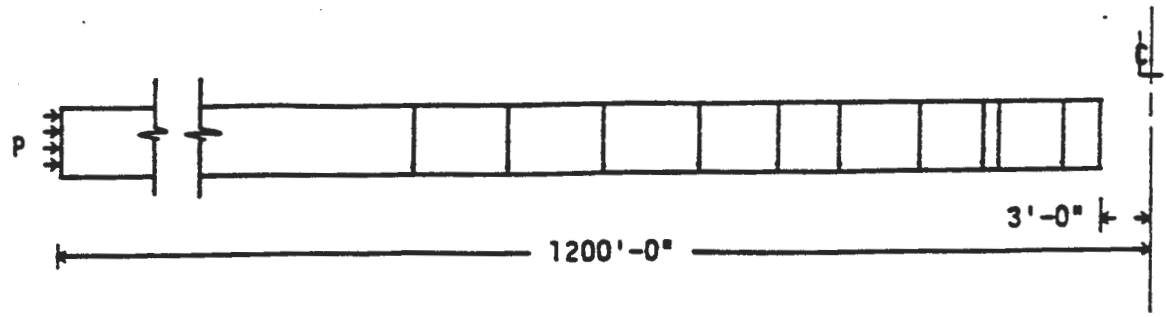


(A) BEFORE ENLARGEMENT

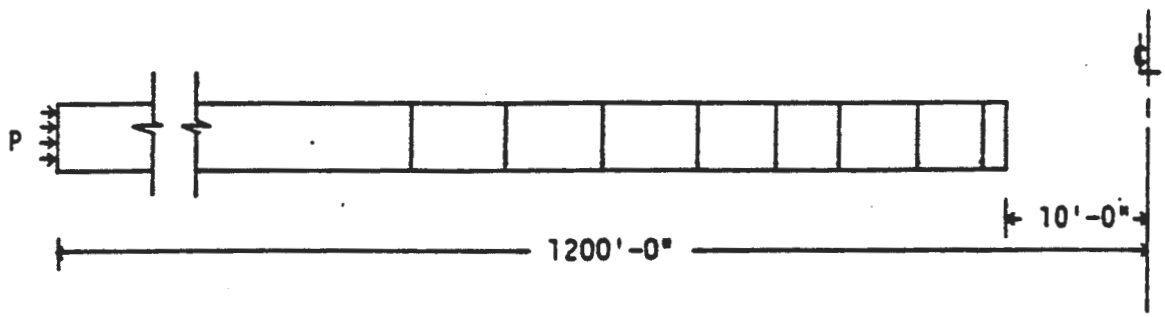


(B) AFTER ENLARGEMENT

Figure 8-9

WASTE SHAFT UNLINED SECTION
FINITE ELEMENT MODEL

Model Simulation. The finite element model used for the unlined section of the waste shaft utilizes a single horizontal row of 70 quadrilateral axisymmetric ring elements. The model, shown on Figure 8-9, has its upper and lower horizontal boundaries restrained against vertical movement and a constant uniform lithostatic pressure, equal to 2,059 feet of overburden, applied to its outside vertical boundary. The same lithostatic pressure was initially applied to the inside vertical boundary as well; however, that pressure was later removed from the inside boundary to simulate the drilling of the original 6-foot diameter shaft.

The analysis simulates the salt creep until that time when the 6-foot diameter shaft was enlarged to its present 20-foot diameter. The shaft enlargement was simulated in the model by removing those ring elements that were located within the 20-foot diameter shaft opening. With the enlarged shaft configuration, simulated salt creep for another 28 years was analyzed.

Determination of Creep Parameters. Because the stratigraphy beneath the WIPP site is fairly uniform, the values of the creep parameters for the unlined section of the waste shaft were assumed to be identical to those values calculated at the corresponding elevations of the C & SH shaft. In addition, the C & SH shaft was drilled at a much earlier date than was the waste shaft; therefore, more in situ geomechanical instrument measurements were available for the C & SH shaft. The values of the creep parameters for the C & SH shaft were determined by correlating analytical results with extensometer readings obtained from a depth of 2,057 feet (elev. 1353 feet) in the shaft. The creep parameters C, A and z for the C & SH shaft were found to be $1.30 \times 10^{-21}$ $ksf^{-4.9}$ $sec^{-1}$, 3.2 and $1.1 \times 10^{-7}$ $sec^{-1}$, respectively. Chapter 7 presents specific details on how the creep parameters were evaluated for the C & SH shaft.

#### 8.3.2.4 Shaft Station

The analysis of closure and stability of the waste shaft station is based upon closure measurements in the C & SH shaft station. This is due to the limited amount of geomechanical instrumentation data available from the waste shaft station for the reasons discussed in subsection 8.3.1. The following discussion presents a brief comparison of the two shaft stations.

The waste shaft station cross-section dimensions are 15 feet high and 30 feet wide. These dimensions are comparable to those of the C & SH shaft station. However, the C & SH shaft station was excavated by drilling and blasting while the waste shaft station was excavated using a mining machine. The density of rock bolts in the roof of the C & SH shaft station is much greater than that in the waste shaft station. Also, the roof of the C & SH shaft station close to the shaft is approximately 3 feet below clay G, while clay G at the waste shaft station is nearly 8 feet above the roof. Thus, closure analysis of the waste shaft station using measurement data from the C & SH shaft station will be conservative.

The dimensions of the waste shaft station are also comparable to those of the test rooms and storage rooms. Computational analysis of the storage rooms (Chapter 12) predicts that failure will occur in MB-139, below the floor, due to gradual stress buildup. Similar behavior is expected to occur in MB-139 beneath the waste shaft station.

### 8.3.3 Prediction of Future Behavior

This subsection presents predictions of future behavior for the various elements of the waste shaft including the lined section, the shaft key, the unlined section and the shaft station.

#### 8.3.3.1 Lined Section

The cracks in the concrete-lined section of the shaft are primarily the result of normal tension cracking occurring during the restrained

shrinkage of plain concrete. The cracks are not detrimental to the liner's structural integrity but sealing by grouting will be required to meet the design criteria regarding ground-water control.

Although the rate of water flowing into the waste shaft has been minor, the total volume of flow has resulted in the lowering of the potentiometric surface around the shaft. Other activities have also affected the potentiometric level in the vicinity of the shafts. Most notably, SNL pumping tests in borehole H-3 in late 1985 lowered the potentiometric surface approximately 40 feet (A.R. Lappin, SNL, personal communication). Due to the unknown effect of current and future hydrologic studies at the WIPP, it is difficult to predict the magnitude of future water pressure on the liner. However, two statements can be made concerning this water pressure:

(1) The piezometer data present a valid indication of water pressures behind the liner. Although this data cannot be used for predicting future pressures, continuous monitoring of these instruments will reflect current pressures and indicate short-term trends. This information can be compared with the design basis pressure distribution (Figures 8-6 and 8-7) to evaluate liner stability.

(2) Following the next grouting program in the waste shaft, if all water seepage through the liner has been stopped, it is possible that the potentiometric surface could return to its highest level determined during preliminary design activities. Assuming complete hydraulic continuity behind the liner, this condition would result in a pressure distribution equal to that of the hydrostatic pressure used for liner design. This condition would be within the design limits.

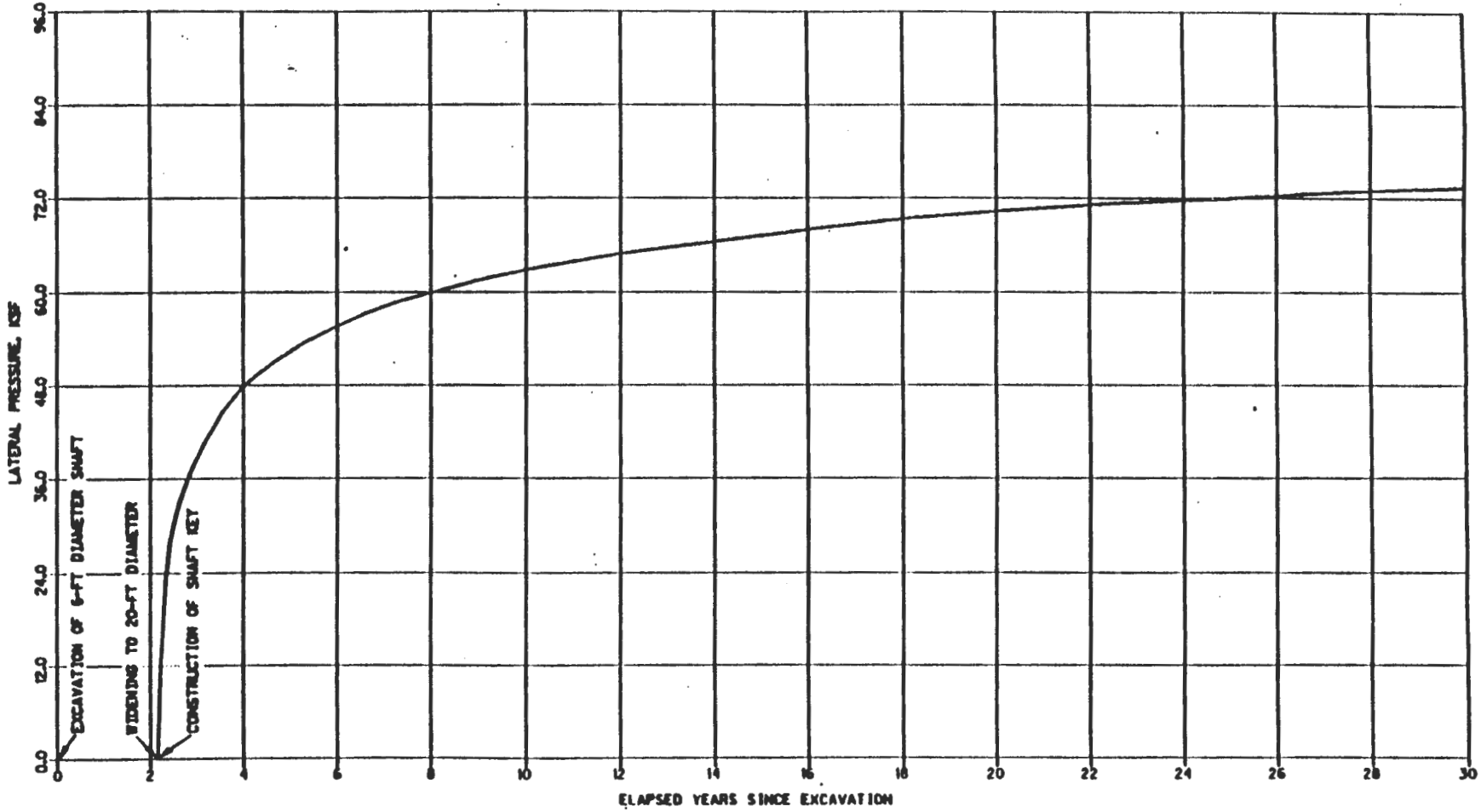


Figure 8-10

WASTE SHAFT KEY
LATERAL PRESSURE PREDICTION

8.3.3.2 Shaft Key

Figure 8-10 shows the predicted lateral pressure curve for the concrete key based on the finite element analysis. The key was designed as a compression cylinder in accordance with the strength design method for reinforced concrete (ref. 7-5) using an ultimate hoop stress of 4.25 ksi (0.85 $f'_c$). Using the design basis load factor of 1.7 for lateral loads, the maximum allowable hoop stress in the concrete key is 2.50 ksi, which results in an allowable lateral rock pressure of 148 ksf based on the diameter of the key. The design basis lateral pressure design requirement is approximately 60 ksf. Figure 8-10 shows a lateral pressure on the shaft key of approximately 72 ksf at the end of the 25-year shaft operating life. If the shrinkage and creep properties of the concrete were taken into account in the finite element analysis, the lateral pressure would actually be less than 72 ksf at 25 years.

The reinforced concrete of the shaft key is expected to exhibit cracks due to shrinkage. These are tensile cracks due to the reinforcement restraining the concrete from shrinking. The cracks are not considered significant because they are common to most reinforced concrete structures.

8.3.3.3 Unlined Section

Figures 8-11 and 8-12 show the radial and tangential (hoop) stress distributions relative to the overburden stress for different times in the unlined section of the waste shaft. Figure 8-11 shows the zone around the shaft opening where radial stresses are affected and indicates a decrease in magnitude over time. The computational results depicted on Figure 8-12 indicate that tangential stresses are only affected within a radius of approximately 120 feet.

Figures 8-13 and 8-14 show the effective stress and effective creep strain distributions in the unlined section of the waste shaft. The effective stress in the shaft wall at 25 years is approximately 140 ksf

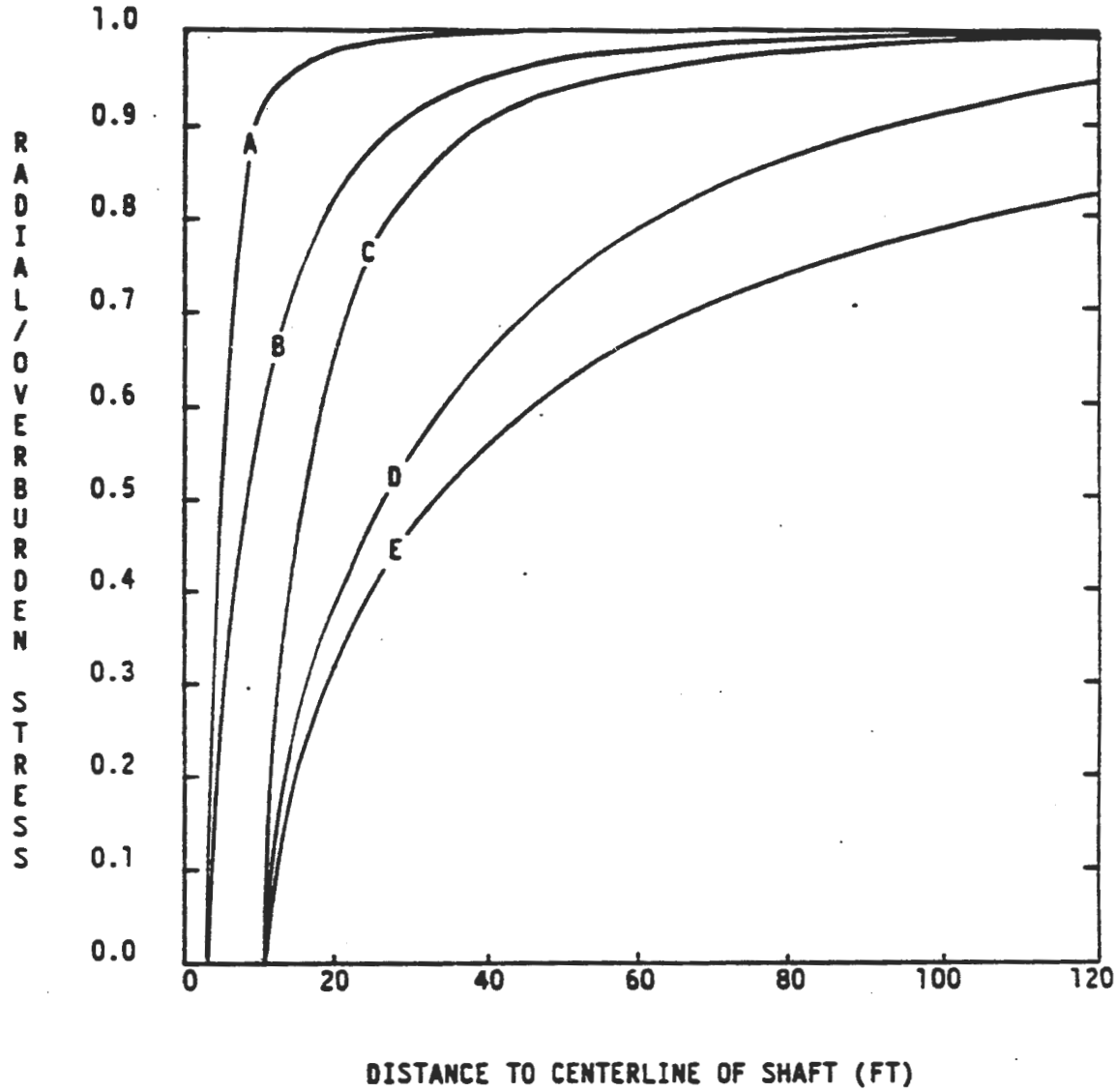


A - IMMEDIATELY AFTER EXCAVATION OF 6-FT DIAMETER SHAFT
B - IMMEDIATELY BEFORE WIDENING TO 20-FT DIAMETER
C - IMMEDIATELY AFTER WIDENING TO 20-FT DIAMETER
D - ONE YEAR AFTER WIDENING OF SHAFT
E - 25 YEARS AFTER WIDENING OF SHAFT

Figure 8-11

WASTE SHAFT UNLINED SECTION
RADIAL STRESS DISTRIBUTION AT ELEVATION 1350 FEET

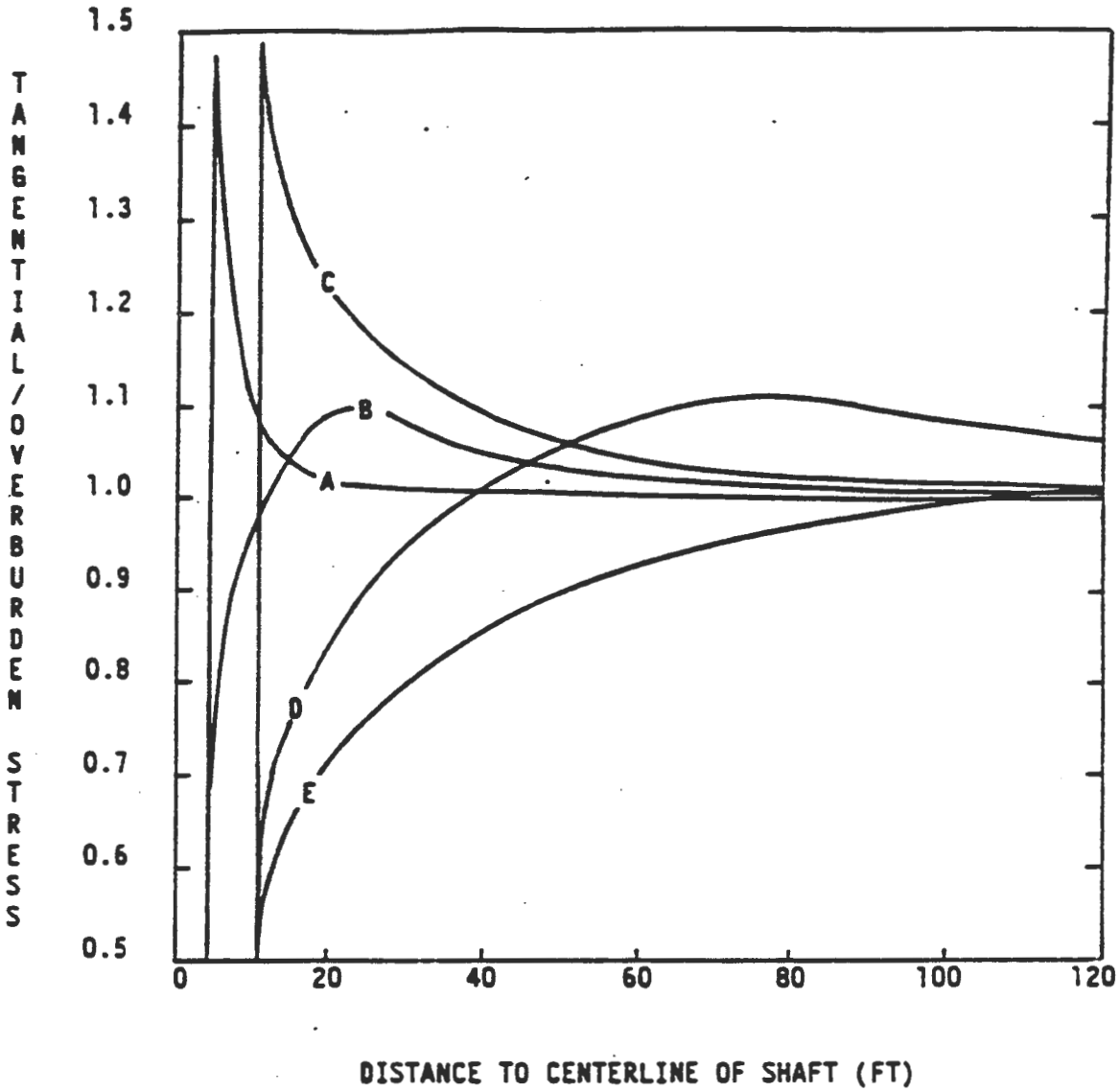


A - IMMEDIATELY AFTER EXCAVATION OF 6 FT-DIAMETER SHAFT
B - IMMEDIATELY BEFORE WIDENING TO 20 FT-DIAMETER
C - IMMEDIATELY AFTER WIDENING TO 20 FT-DIAMETER
D - ONE YEAR AFTER WIDENING OF SHAFT
E - 25 YEARS AFTER WIDENING OF SHAFT

Figure 8-12

WASTE SHAFT UNLINED SECTION
TANGENTIAL STRESS DISTRIBUTION AT ELEVATION 1350 FEET

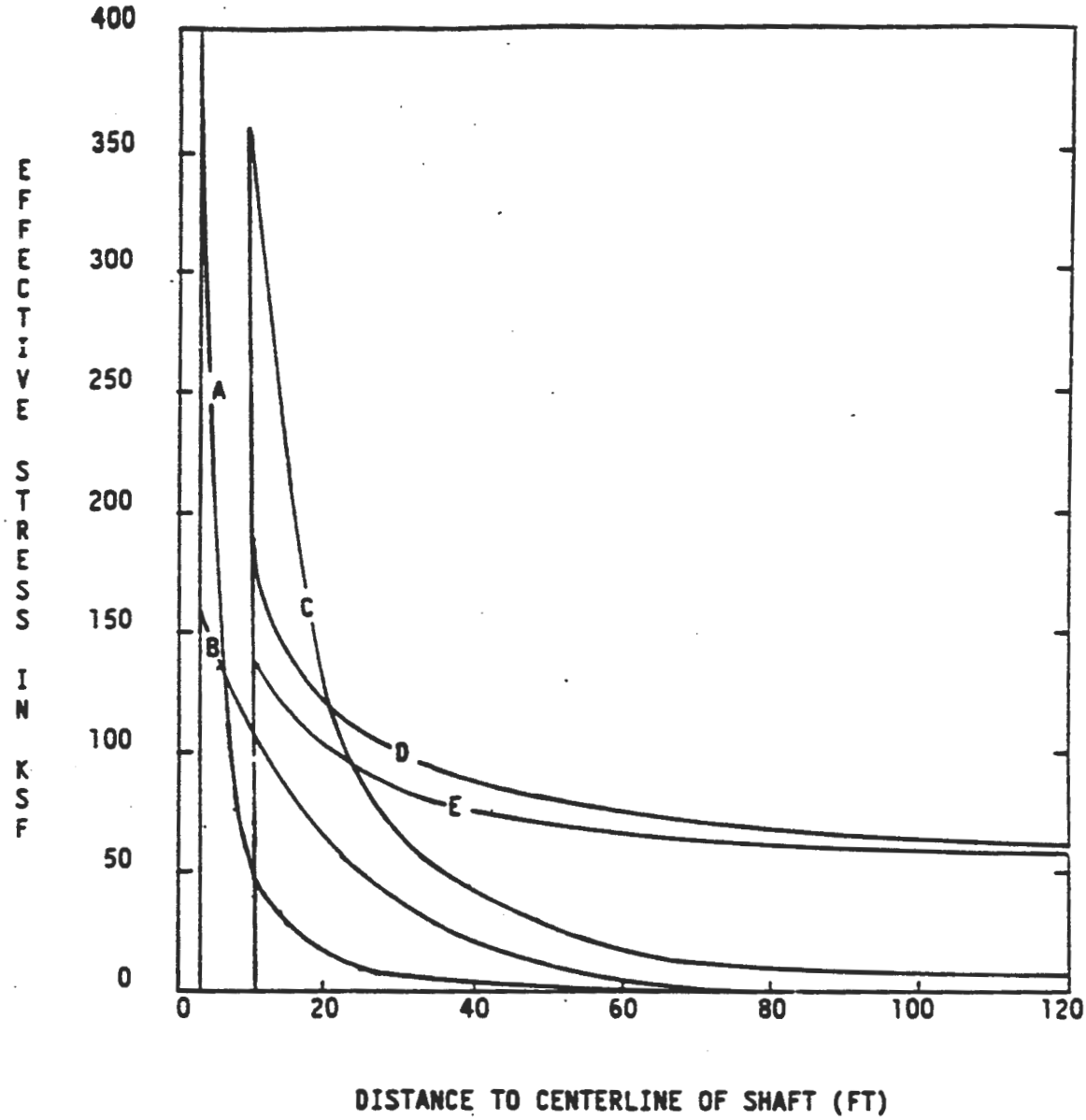


A - IMMEDIATELY AFTER EXCAVATION OF 6-FT DIAMETER SHAFT
B - IMMEDIATELY BEFORE WIDENING TO 20-FT DIAMETER
C - IMMEDIATELY AFTER WIDENING TO 20-FT DIAMETER
D - ONE YEAR AFTER WIDENING OF SHAFT
E - 25 YEARS AFTER WIDENING OF SHAFT

Figure 8-13

WASTE SHAFT UNLINED SECTION
EFFECTIVE STRESS DISTRIBUTION AT ELEVATION 1350 FEET

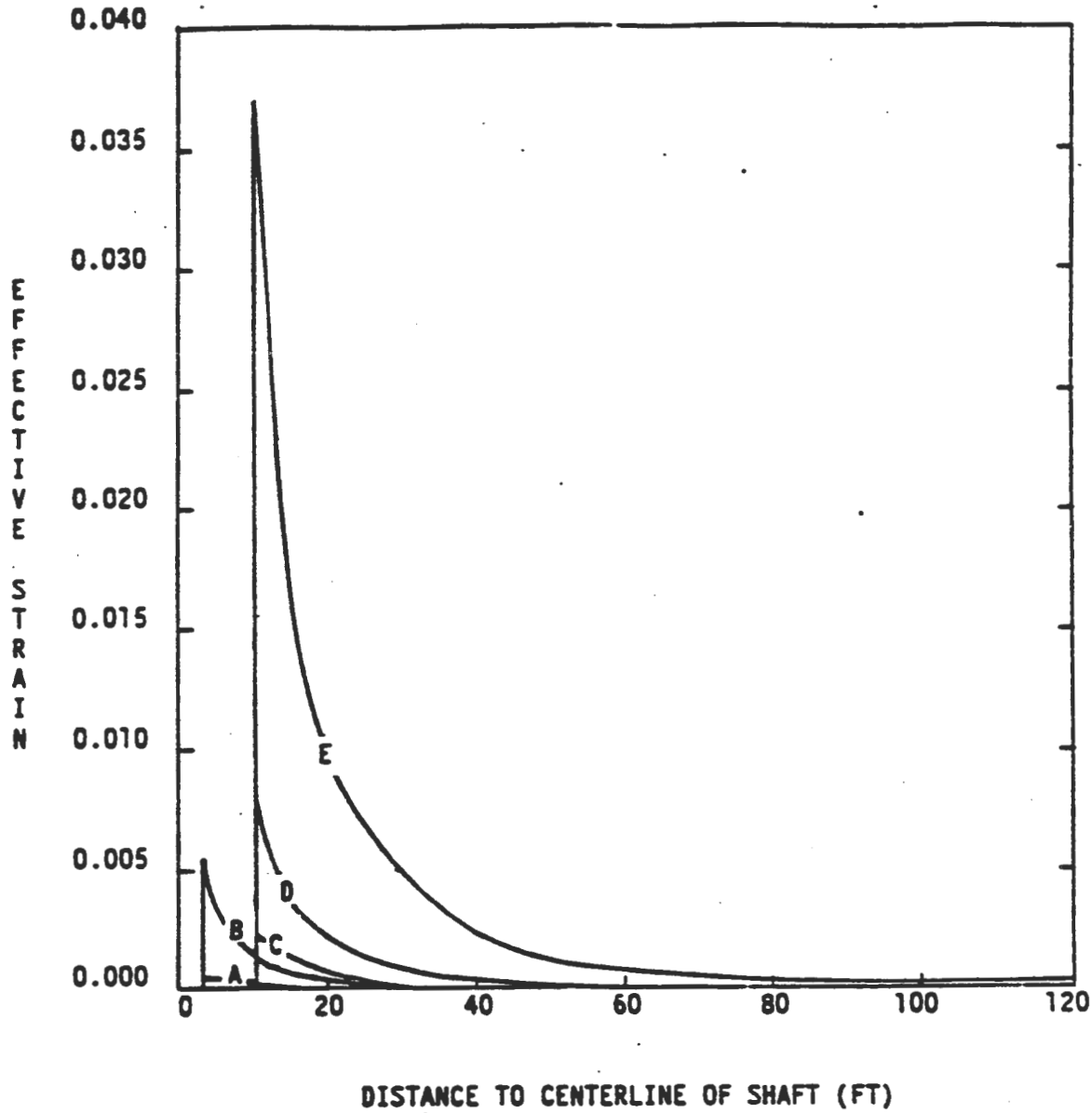


A - IMMEDIATELY AFTER EXCAVATION OF 6-FT DIAMETER SHAFT
B - IMMEDIATELY BEFORE WIDENING TO 20-FT DIAMETER
C - IMMEDIATELY AFTER WIDENING TO 20-FT DIAMETER
D - ONE YEAR AFTER WIDENING OF SHAFT
E - 25 YEARS AFTER WIDENING OF SHAFT

Figure 8-14

WASTE SHAFT UNLINED SECTION
EFFECTIVE CREEP STRAIN DISTRIBUTION AT ELEVATION 1350 FEET

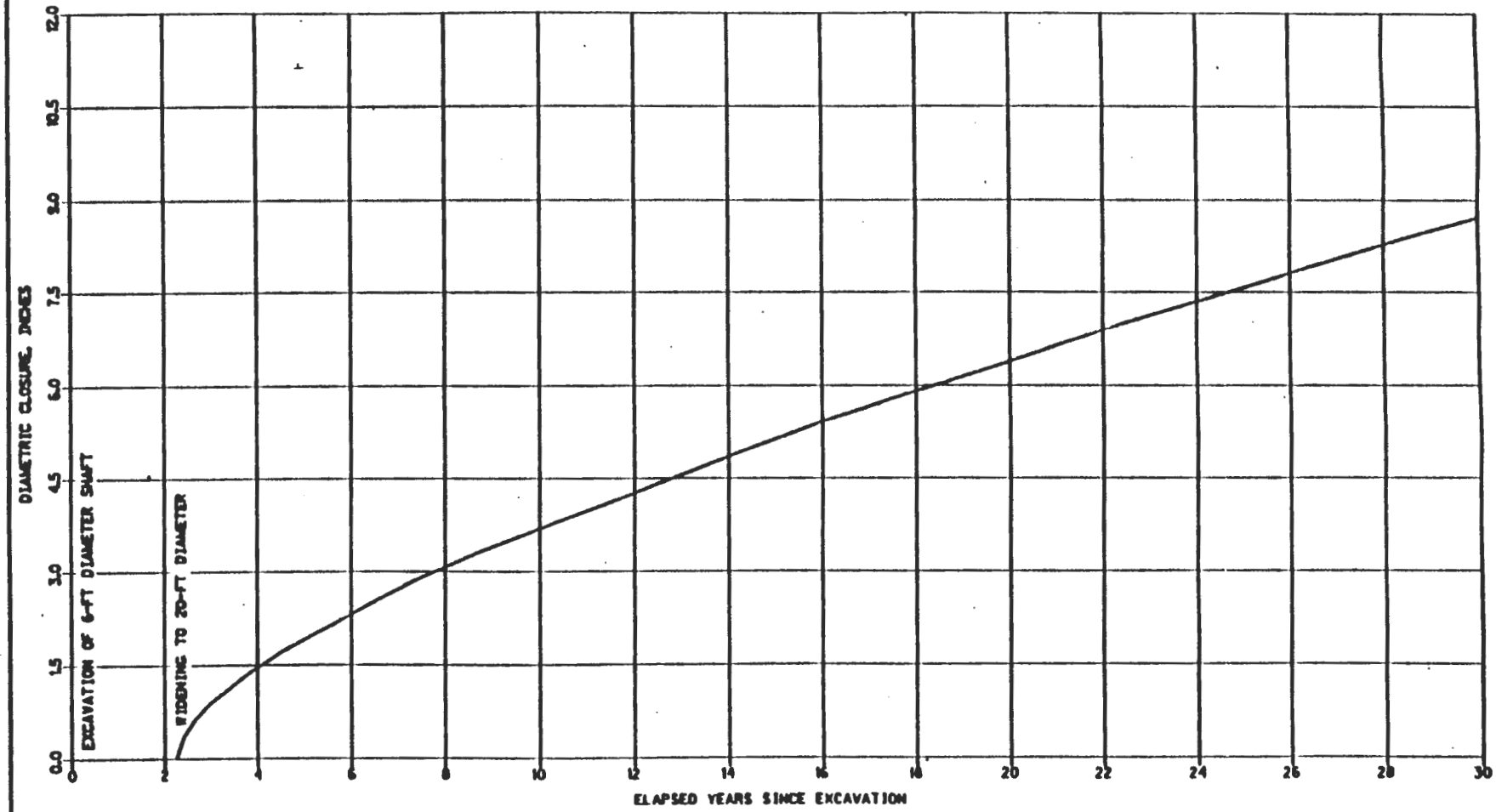


Figure 8-15

WASTE SHAFT UNLINED SECTION
CLOSURE PREDICTION AT ELEVATION 1350 FEET

while the effective creep strain in the shaft wall at 25 years reaches a value of approximately 0.037.

Figure 8-15 contains the prediction of diametric closure for the unlined section of the waste shaft at a depth of 2,059 feet (elev. 1350 feet). This figure shows a diametric closure of approximately 7 1/2 inches over the 25-year operating life of the shaft.

#### 8.3.3.4 Shaft Station

Closure in the waste shaft station is predicted using measurement data from the C & SH shaft station. The measured roof-to-floor closure in the C & SH shaft station was approximately 10 inches on September 16, 1985, over 3 years after the completion of excavation. The measured wall-to-wall closure is greater than 6 inches over the same time period. However, the initial readings were taken nearly 260 days after the station was excavated; therefore, the actual closure magnitudes will be higher. The average rate of roof-to-floor closure over the measurement period was approximately 3.89 inches/year. Using this value as a constant closure rate over the plant operating life of 25 years, an additional roof-to-floor closure of about 8 feet is expected to occur. The wall-to-wall closure over the same period is expected to be approximately 60 percent of the roof-to-floor closure, or about 5 feet. Actual closure may be lower as discussed in subsection 8.3.2.4.

## 8.4 CONCLUSIONS AND RECOMMENDATIONS

Design validation requires an assessment of the compatibility of the design criteria, design bases and design configurations used for the reference design. The following conclusions and recommendations address those design elements identified in Section 8.2. Other conclusions and recommendations resulting from the design validation process are also presented.

### 8.4.1 Conclusions

The design criteria require that all of the shafts are to be stable. Shaft stability has been evaluated using analytical calculations,

finite element modeling and in situ data analysis. The shaft liner is considered stable because the water pressure exerted on it has remained significantly below the design hydrostatic pressure. If the water pressure increases to the design hydrostatic pressure, as may be expected if the leaks are sealed by additional grouting, liner stability will not be compromised. The pressure capacity of the liner sufficiently exceeds the design hydrostatic pressure.

Based on existing evidence, the cracks in the liner and key do not present a structural problem. The unreinforced concrete liner is expected to function as intended, provided that the existing cracks and construction joints are grouted and contact grouting is performed at the rock/liner interface. Consolidation grouting of the surrounding rock may also be necessary to achieve a dry shaft.

The shaft key was designed to withstand a design basis lateral pressure equal to 50 percent of the overburden pressure (approximately 60 ksf). The finite element analysis determined that the lateral pressure on the key at the end of the facility operating life will be approximately 72 ksf. Although this value is higher than the design lateral pressure, the key is expected to remain stable throughout its operating life because the allowable lateral rock pressure is 148 ksf. This is twice the lateral pressure predicted and provides a sufficient margin of safety. Furthermore, if the shrinkage and creep properties of the concrete were taken into account in the analysis, the lateral pressure would be less than 72 ksf.

The analytical results for the waste shaft, presented in Section 8.3, show the calculated redistribution of stresses around the shaft due to the effetts of creep. Based on the computed vertical, horizontal and effective stresses in the unlined section, the magnitude of stresses immediately adjacent to the opening decreases with time as the stress arch around the opening migrates away. The maximum stress occurs immediately after excavation and is followed by relaxation due to creep behavior. Therefore, the stresses will not cause a future stability

problem in the waste shaft except in the anhydrite bed (MB-139) below the floor of the shaft station. Gradual buildup of stress in this bed may result in floor heave and fracturing.

The analysis shows the locations of effective creep strain concentrations for selected times in the unlined section. Based on these predicted values of effective creep strain and the strain limit discussed in Chapter 6, the waste shaft will remain structurally stable over its planned 25-year operating life.

The analysis predicts that diametric closure in the unlined section of the waste shaft will be approximately 7 1/2 inches over its 25-year operating life. Based on the predicted deformations and closures, the waste shaft will meet the requirements stated in the design criteria and the 20-foot diameter unlined section will provide sufficient operating clearance to allow for salt creep.

The design criteria requires that no uncontrolled ground water reach the facility level via the shafts. The majority of water seeping through cracks and construction joints in the liner is collected in three water-collection rings and directed to the underground facility where it is disposed. Only minor amounts of uncontrolled fly water reach the facility level. This water has a negligible impact and does not affect validation of the criterion regarding ground water reaching the facility level.

Shaft inspections have determined that only one minor seep occurs in the key and that no water seepage occurrs from the base of the key. This supports the conclusion that the water seals are functioning, that no water is seeping along the concrete/salt interface, and that no salt dissolution is occurring behind the concrete key. The installation technique for the waste shaft water seals was improved over that used for the C & SH shaft water seals (Chapter 3).

The zone of dissolution observed in the shaft sump wall is not considered to be detrimental to the operation of the facility. The

material was dissolved differentially by standing water in the sump resulting from construction activities. It is not the result of any geologic discontinuity or process. This zone will not produce any structural problems in construction of the waste shaft facilities.

The waste shaft station is expected to undergo roof-to-floor closure at a rate of 3.89 inches/year. However, this rate has been obtained by using the C & SH shaft station instrument data. The actual closure rate may be lower. Additional heave and fracturing in the salt beneath the floor, as well as in MB-139, is expected to occur. Some remedial work will be required to maintain the required roof-to-floor clearance for operational equipment and activities.

The reference design for the waste shaft is considered to be validated in accordance with the objectives of the design validation program based on the analyses, evaluations and predictions of future behavior presented in this chapter. With one exception, the waste shaft reference design complies with the design criteria and the design bases. The criterion that stipulates that shaft liner design shall prevent ground-water flow into the shaft has not been met. The rate of water currently seeping into the waste shaft is not considered to be detrimental to the stability of the shaft or to its functional purpose. However, the criteria will be satisfied when additional remedial grouting has been performed. No modifications to the shaft reference design will be required.

### 8.4.2 Recommendations

Based on the results of design validation, the following recommendations with respect to the waste shaft are made:

(1) Due to the limited in situ data base, validation of the waste shaft key and unlined section relies on numerical modeling utilizing creep parameters derived from the C & SH shaft in situ data. It is recommended that the modeling be repeated, prior to the first receipt of waste, using the latest in situ

data from the waste shaft. This analysis should be repeated periodically for comparison and verification of in situ data against design parameters.

(2) Grouting should be performed to completely seal the waste shaft liner. This should include contact grouting behind the liner and grouting of shrinkage cracks and construction joints. Consolidation grouting may also be required. Qualified personnel should inspect the shaft at regularly scheduled intervals. The liner should be checked for leaks after grouting has been completed. The key should be checked for water seeping from behind the key at its base. If any seepage is detected it may become necessary to grout the area above the upper water seal. If possible, grout should not be placed behind the key below the upper seal. However, should grouting behind the key become necessary, the grout must be a chemical gel (or other non-rigid grout) and must be compatible with both the existing water seal material and with the requirements of the Plugging and Sealing Program.

(3) The dissolution zone in the waste shaft sump should be filled with a salt-compatible cement mortar.

(4) Because waste shaft station closure is based on C & SH shaft station data, and because of the importance of the waste shaft station in general, vertical convergence points or meters should be installed at selected locations and measurements taken periodically. These data should then be analyzed to obtain better estimates of station closure.

# CHAPTER 9

# EXHAUST SHAFT

## 9.1 INTRODUCTION

This chapter presents information on design validation of the exhaust shaft. Included are discussions of its design, the design validation process, and conclusions and recommendations pertaining to validation of the reference design.

## 9.2 DESIGN

This section presents the design criteria and design bases used to develop the reference design for the exhaust shaft. The design configuration of the shaft is discussed in Chapter 3, subsection 3.3.3.

### 9.2.1 Design Criteria

The design criteria for the exhaust shaft are identical to those for the other two shafts. The criteria requiring validation are indicated in the listing of abridged criteria presented in Chapter 2, Table 2-1, and are discussed in Chapter 7.

The design criteria requiring evaluation for design validation of the exhaust shaft are:

(1) shaft shall be designed to be structurally stable;

(2) shaft shall be designed to accommodate salt creep; and

(3) ground-water flow into the shaft shall be controlled.

### 9.2.2 Design Bases

The design bases are the detailed design requirements developed from the design criteria. The primary design basis document for the exhaust shaft is the Design Basis, Exhaust Shaft (ref. 2-16). The major elements of the design bases are the same as those for the waste shaft,

except for the items discussed in the next paragraph. The elements that require evaluation or that have a direct impact on design validation are presented in Table 9-1.

In addition to adhering to the design basis elements discussed previously for the waste shaft, the exhaust shaft shall be designed to connect the facility level with the exhaust filter building at the ground surface. The exhaust shaft shall be used to remove air from the underground development level during construction and storage operations. The entire shaft shall be inspected utilizing a closed-circuit television camera that shall be lowered from the top of the shaft. Unlike the design bases for the other two shafts, the exhaust shaft design basis does not require the installation of geomechanical instrumentation.

## 9.3 DESIGN VALIDATION PROCESS

As discussed in Chapter 5, design validation of the exhaust shaft has been achieved by data collection, its analysis and evaluation, and the prediction of future behavior. Data collection activities have included geologic mapping and visual observations of the exhaust shaft wall. Although geomechanical instruments have been installed in the shaft, no data was available for design validation due to the late date of installation.

Computational analyses for the exhaust shaft were performed in the same manner as those for the waste shaft. The finite element analyses of the shaft key and unlined section used the material parameters for salt obtained from the C & SH shaft and horizontal drift analyses. The results of the analyses were then used to predict future behavior.

### 9.3.1 Data Collection

Data collection in the exhaust shaft was on a much smaller scale than in the other two shafts. Geologic mapping was conducted in the shaft to verify the stratigraphy. This mapping is discussed in detail in Chapter 6. Visual inspections and observations in the shaft were

Table 9-1

VALIDATION ELEMENTS OF EXHAUST SHAFT DESIGN BASES

(1) Shaft liner

Hydrostatic pressure should be considered to start at 250 feet below the ground surface and extend to the top of the key.

(2) Shaft key

Design lateral pressure shall be 50 percent of the vertical pressure due to soil, rock and salt overburden.

(3) Unlined section

Provide 15-foot diameter to allow for future salt creep deformation.

sporadic due to limited access. The following discussion presents those observations which affect design validation.

9.3.1.1 Field Observations

Exhaust shaft construction was completed on January 15, 1985. Initial of the lined section of the shaft was performed on January 30, 1985. At that time water seepage through cracks and construction joints in the liner was observed. Seepage into the shaft was measured at 0.35 gallons per minute (gpm).

Subsequent inspections of the exhaust shaft liner were made in February and May 1985 to observe its condition and to evaluate the need for grouting to reduce water seepage. The first occurrence of moisture on the liner was observed 25 feet below the shaft collar. The majority of water seepage was occurring between approximate depths of 569 feet and 759 feet (elev. 2840 feet and 2650 feet). Below a depth of 759 feet the entire shaft liner was wet, making it difficult to determine the exact source of seepage. Some salt accumulation was observed on the liner below the Culebra water-bearing member. The May 1985 inspection generally revealed a 1/4- to 3/8-inch thickness of salt incrustation in this area with some local accumulation up to 4 inches in thickness.

Salt accumulation at two telltale drain holes, at a depth of 857 feet (elev. 2552 feet) on the northeast and east sides of the shaft key, had resulted in the almost complete plugging of these holes. The six other drain holes had minor salt accumulation. The bottom of the key had salt stalactites hanging from the concrete but no flow of water under the concrete was observed. There was no evidence of any dissolution of salt at the concrete/salt contact.

A cement/chemical grouting program was conducted in the exhaust shaft from June 1 through July 31, 1985. An inspection of the exhaust shaft liner was made on July 30, 1985. The liner was appreciably drier than it had been prior to grouting, especially below the Culebra member. One collar pipe, for future piezometer installation at a depth of 616

feet (elev. 2793 feet), was weeping and one pipe, at a depth of 722 feet (elev. 2687 feet), was dripping. This water constituted the majority of the total seepage into the shaft. Weeping from random cracks above a depth of 617 feet appeared to be of the same magnitude as before grouting. The water ring at the base of the shaft key was relatively dry. New telltale drain holes at a depth of 870 feet (elev. 2539 feet) were all dry. Several of the original drain holes, at 857 feet, and several new holes, at a depth of 855 feet (elev. 2554 feet), were weeping slightly. No evidence of seepage at the concrete key/salt contact was observed. The grouting program reduced water seepage into the exhaust shaft to an essentially non-measurable quantity.

Cursory inspections of the exhaust shaft made during the installation of geomechanical instruments in November and December 1985 indicated no appreciable change in the condition of the shaft liner since the July 1985 inspection.

A second grouting program was conducted in the exhaust shaft during August, September and October, 1986. The program was performed at this time to reduce the possible need for grouting in the future when shaft access will be limited. The grouting was conducted on a smaller scale than in the earlier program. It consisted of injecting grout through existing sleeves from the top of the salt in the key are to the top of the Magenta member. Grouting was also performed, as required, above the Magenta through sleeves in the liner. The results of the grouting were not available at the time of publication of this report.

#### 9.3.1.2 Geomechanical Instrumentation

The original exhaust shaft design contained no provision for the installation of geomechanical instrumentation based on the assumption that rock behavior would be similar to that in the waste shaft. However, it was subsequently decided that geomechanical instrumentation should be installed to obtain shaft-specific behavior information for later use in the shaft sealing program.

Instrument locations in the exhaust shaft were based on waste shaft instrument locations. Twenty-one piezometers, 4 pressure cells and 9 extensometers have been installed in the exhaust shaft. The instrument installation was completed on December 27, 1985, 385 days after the completion of shaft excavation. All exhaust shaft instruments are monitored remotely by the datalogger.

### 9.3.2 Analysis and Evaluation

The analysis and evaluation of the constructed exhaust shaft has been performed using direct observation data and geomechanical instrumentation readings from the C & SH and waste shafts. This analysis and its evaluation against reference design parameters was performed for the three major sections of the shaft: the lined section; the shaft key; and the unlined section.

The adequacy of the exhaust shaft reference design was evaluated based on a complete spectrum of geomechanical behavior including stress, strain and deformation over the planned operating life of 25 years. The analyses used creep parameters computed from the C & SH shaft and the 8 x 25-foot drifts as well as hydrostatic pressures from the waste shaft.

#### 9.3.2.1 Lined Section

Analyses were performed for the unreinforced concrete liner in the exhaust shaft. However, because no instrumentation data from this shaft were available, the analyses were based on data obtained from the C & SH and waste shafts.

The structural analysis and design of the exhaust shaft were performed using engineering mechanics principles and design bases similar to those used for the waste shaft as described in Chapter 8. For example, both axial and flexural stresses were considered in the design of the concrete liner, with permissible stress values taken as those used for structural unreinforced concrete (ref. 8-1) utilizing the ultimate

strength design method. Loads considered in the design of the concrete liner included a hydrostatic pressure assumed to act from a depth of 250 to 844 feet; a grouting pressure equal to 1.3 times the ground-water pressure acting over one-sixth of the circumference of the liner; and stresses due to an initial imperfection of 1 inch in the roundness of the liner. Since there is no major salt strata surrounding the liner, no significant creep will occur and rock pressures against the liner were assumed to be negligible.

Based on its finished dimensions, the computational results show that the external pressure capacities and corresponding closure limits (maximum diametric changes) for different thicknesses of the exhaust shaft liner are:

| Depth (feet) | Liner Thickness (inches) | Pressure Capacity (psi) | Closure Limit (inches) |
|---|---|---|---|
| 15 to 500 | 10 | 320 | 0.140 |
| 500 to 740 | 14 | 513 | 0.175 |
| 740 to 844 | 16 | 611 | 0.190 |

Since no measurements of the finished liner diameter were taken during construction, the actual closure is not available for comparison.

Figure 9-1 shows the relationship between the hydrostatic design pressure and the pressure capacity of the liner. The hydrostatic pressure is identical to that used for design of the waste shaft. Because the exhaust shaft liner also has water seeping through cracks and construction joints, the hydrostatic pressure is expected to behave in the same manner as discussed for the waste shaft in Chapter 8. That is, the design hydrostatic pressure is not expected to be reached until the shaft liner is completely sealed. When the design hydrostatic pressure is reached, the liner will have a factor of safety greater than two, based on the liner pressure capacity.

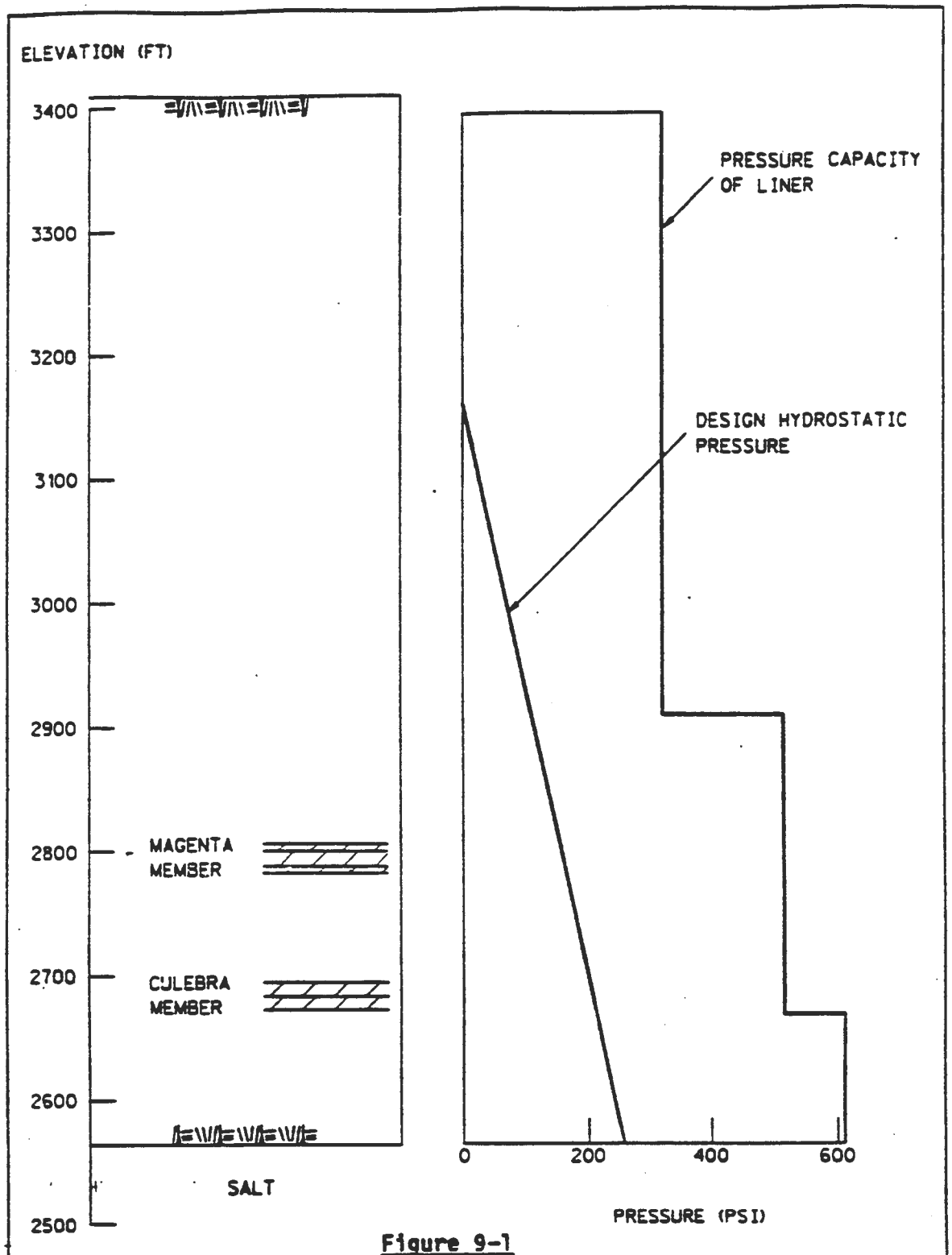


Figure 9-1

EXHAUST SHAFT LINER
LATERAL PRESSURE COMPARISON

#### 9.3.2.2 Shaft Key

The exhaust shaft key was designed to withstand a lateral pressure equal to 50 percent of the vertical overburden pressure or about 60 ksf. A nonlinear finite element analysis, similar to that performed for the waste shaft key described in Chapter 8, was used to simulate the long-term creep interaction of the salt and the concrete key. The creep behavior of the salt was simulated using a power law (equation C.4-6 in Appendix C). For conservatism, the shrinkage effects and creep of the concrete were not taken into account in the analysis.

Model Simulation. The finite element model for the exhaust shaft key and surrounding salt consists of a single layer of quadrilateral axisymmetric ring elements as shown on Figure 9-2. An inner element of the model represents a segment of the concrete key; however, this element is not tied to the surrounding salt deposits until that time when the concrete for the shaft key is actually placed. All depth dependent input values, such as overburden stresses, initial lithostatic state, etc., were computed based on a depth of 891.5 feet, low in the key, where such values are at a maximum. Halite is the prevalent material present at the base of the shaft key and its properties were used for the parameters modeling the salt deposits surrounding the key.

The analytical procedure used to perform the creep analysis for the exhaust shaft key was similar to that used for the waste shaft key analysis described in Chapter 8. However, in the finite element model for the exhaust shaft, the key diameter was enlarged to 21 feet with a finished inside diameter of 14 feet.

#### 9.3.2.3 Unlined Section

The structural behavior of the unlined section of the exhaust shaft was also computed using the MARC Finite Element Program discussed in Chapter 6. The analysis computed the actual structural behavior by utilizing applicable in situ data from the C & SH shaft and the horizontal drifts.

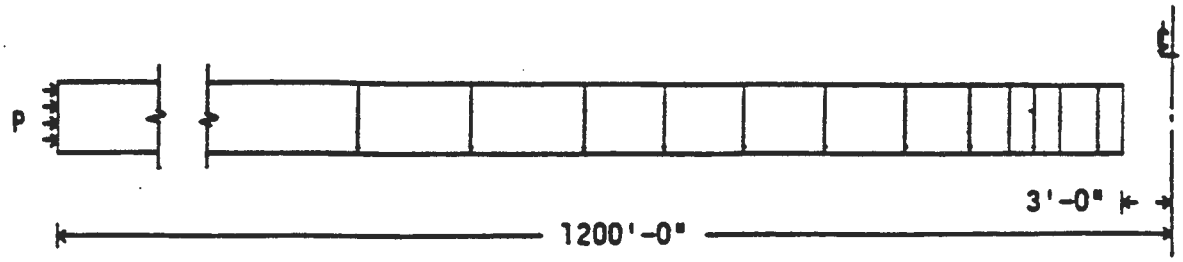


(A) BEFORE ENLARGEMENT

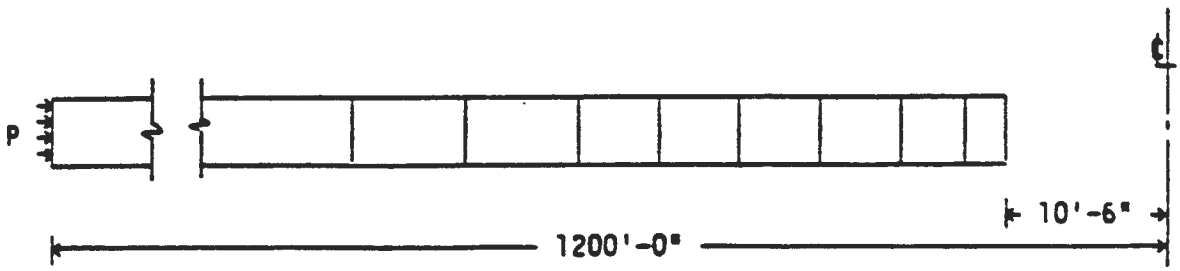


(B) AFTER ENLARGEMENT

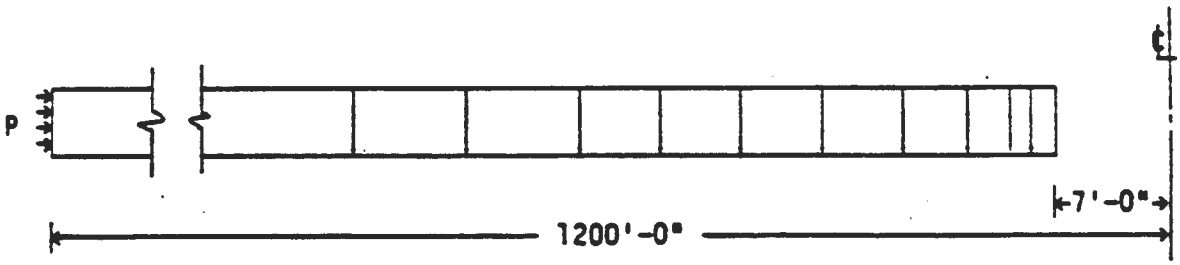


(C) AFTER KEY PLACEMENT

Figure 9-2

EXHAUST SHAFT KEY
FINITE ELEMENT MODEL

Model Simulation. The finite element model used for the unlined section of the exhaust shaft utilizes a single horizontal row of 70 quadrilateral axisymmetric ring elements. The model, shown on Figure 9-3, has its upper and lower horizontal boundaries restrained against vertical movement and has a constant lithostatic uniform pressure, equal to 2,066 feet of overburden, applied to its outside vertical boundary. The same lithostatic pressure was initially applied to the inside vertical boundary; however, that pressure was later removed from the inside boundary to simulate the drilling of the 6-foot diameter pilot bore.

The analysis simulates the salt creep until that time when the 6-foot diameter hole was enlarged to its present 15-foot diameter. The shaft enlargement is simulated in the model by removing those ring elements which are located within the newly-excavated 15-foot diameter. With the enlarged shaft configuration, simulated salt creep for another 25 years was analyzed.

Determination of Creep Parameters. Since the stratigraphy surrounding the C & SH shaft is similar to that surrounding the exhaust shaft, the creep parameters determined from the in situ salt behavior in the C & SH shaft were assumed to be valid for correlating analytical results for the exhaust shaft from normalized time to real time. The secondary creep parameter C for the C & SH shaft was found to equal $5.70 \times 10^{-21}$ $ksf^{-4.9}$ $sec^{-1}$. Since early in situ measurements were not available for the C & SH shaft, the primary creep parameters A and z were determined from in situ data from the horizontal drifts and were found to be 3.2 and $1.1 \times 10^{-7}$ $sec^{-1}$, respectively.

Chapter 7 presents specific details on the computation of the secondary creep parameter C from the C & SH shaft. Chapter 10 presents the computation of the primary creep parameters A and z from the drifts.

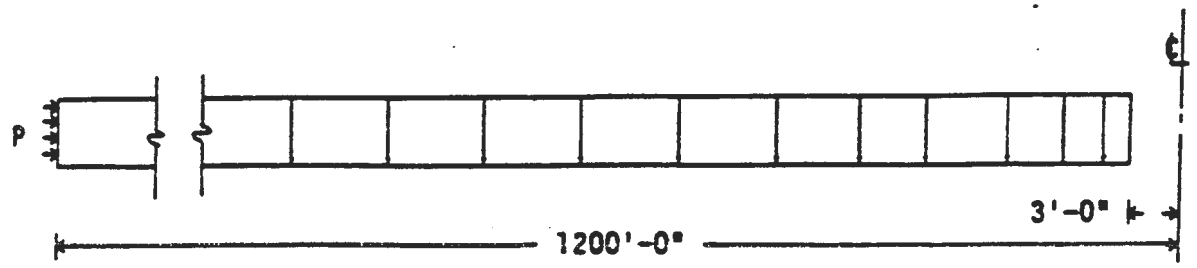


(A) BEFORE ENLARGEMENT

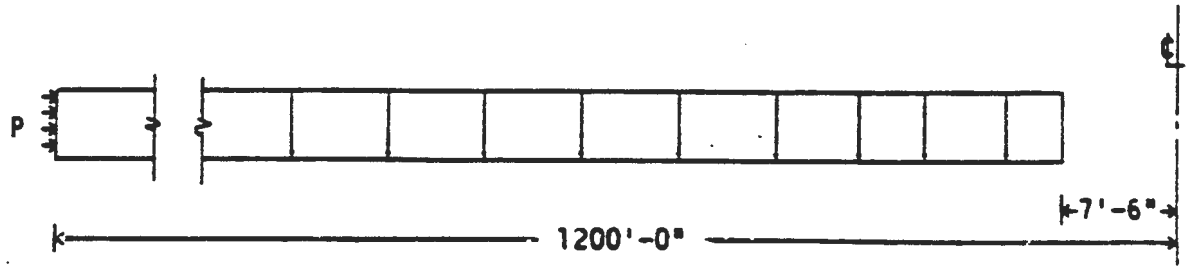


(B) AFTER ENLARGEMENT

**Figure 9-3**

EXHAUST SHAFT UNLINED SECTION
FINITE ELEMENT MODEL

### 9.3.3 Prediction of Future Behavior

This subsection presents the results of the analysis and evaluation of the exhaust shaft. Predictions of future behavior for the lined section, key and unlined section are discussed.

#### 9.3.3.1 Lined Section

The cracks in the concrete liner of the exhaust shaft are primarily tension cracks formed during restrained shrinkage we described in Chapter 8 with respect to the waste shift liner. These are neither unusual nor unexpected. Grouting of the cracks, as well as the leaking construction joints, will be required to meet the design criteria regarding ground-water control.

As discussed in Chapter 7, subsection 7.3.3.1, there is no reason to expect that the potentiometric surface at the WIPP site will exceed the design basis depth of 250 feet below the ground surface over the operating life of the facility. In the future, the recently installed piezometers will permit monitoring of the actual water pressure on the liner. Even if the water pressure rises to the design pressure, the pressure capacity of the liner will provide a sufficient margin of safety.

#### 9.3.3.2 Shaft Key

The elapsed time from the drilling of the 6-foot diameter pilot bore to its widening to 21 feet in the key area and construction of the concrete key was approximately 316 days. Figure 9-4 shows the predicted lateral pressure curve for the concrete key based on the finite element analysis. The key was designed as a compression cylinder in accordance with the strength design method for reinforced concrete (ref. 7-5) using an ultimate hoop stress of 4.25 ksi. Using a load factor of 1.7 for lateral loads, the maximum allowable hoop stress in the key is 2.50 ksi. This hoop stress results in an allowable lateral rock pressure of 154 ksf based on the diameter of the key. Figure 9-4 shows a lateral pressure on the key of approximately 72 ksf

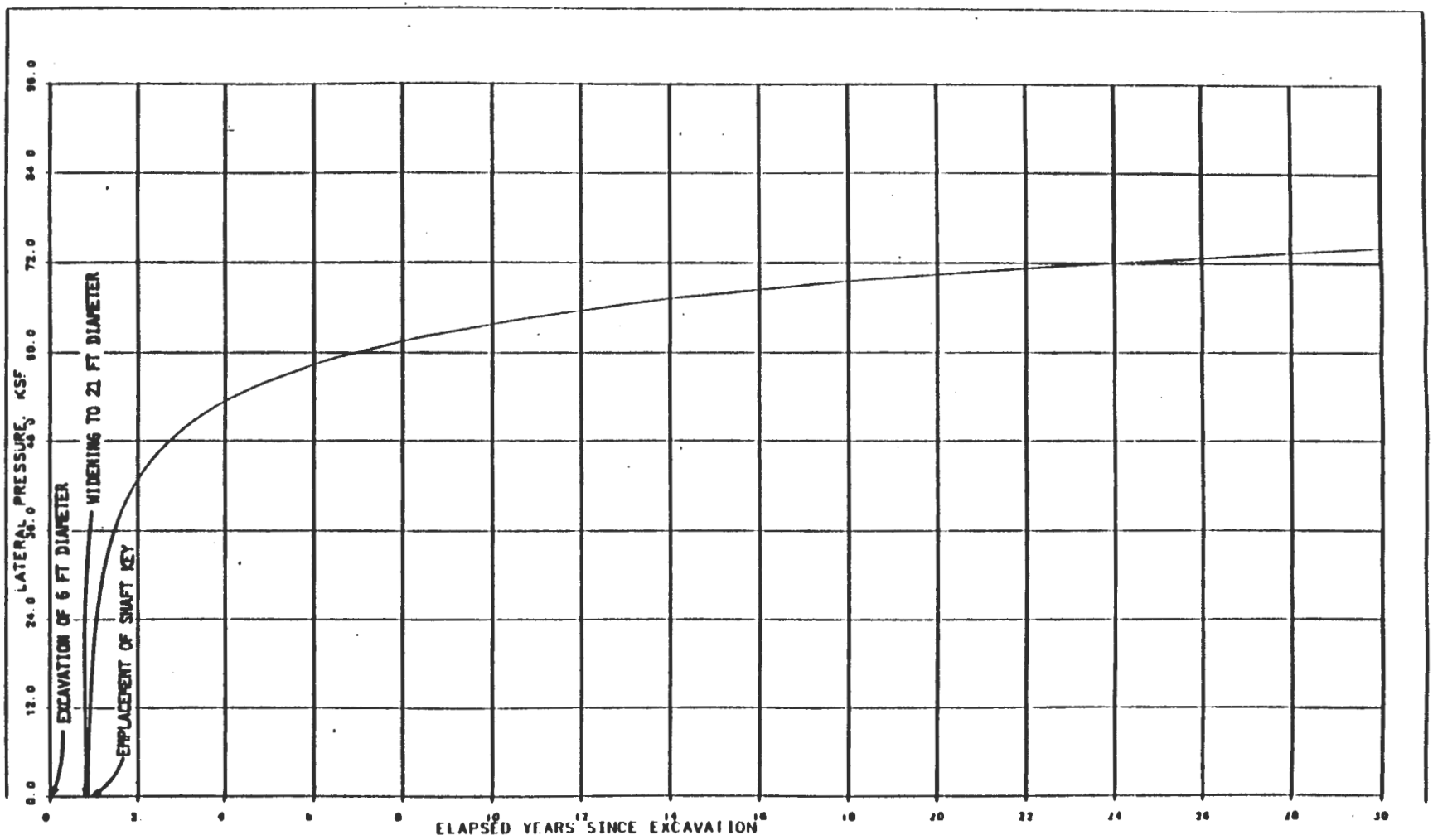


**Figure 9-4**

**EXHAUST SHAFT KEY**
**LATERAL PRESSURE PREDICTION**

at 25 years. Although higher than the design basis lateral pressure of 60 ksf, this value is about 50 percent of the allowable lateral pressure. In addition, the lateral pressure would actually be less than 72 ksf if concrete shrinkage and creep were taken into account in the finite element analysis.

Although no shrinkage cracks have been found in the reinforced concrete in the key, their presence would not be unexpected. They are common to most reinforced concrete structures and should not be of major concern.

#### 9.3.3.3 Unlined Section

Figures 9-5 and 9-6 show predictions for radial and tangential (hoop) stress distributions relative to the overburden stress at different times for the unlined section of the exhaust shaft. Figure 9-5 shows the zone around the shaft opening where radial stresses are affected and their decrease in magnitude over time. The computational results indicate that tangential stresses are affected only within a radius of approximately 120 feet.

Figures 9-7 and 9-8 show predictions of the effective stress and effective creep strain distributions in the unlined section of the exhaust shaft. The magnitude of the effective stress in the shaft wall at 25 years approaches 140 ksf while the effective creep strain reaches a value of approximately 0.037.

Figure 9-9 shows approximately 6 inches of diametric closure in the unlined section of the exhaust shaft at a depth of 2,066 feet (elev. 1343 feet) over the 25-year operating life of the shaft.

## 9.4 CONCLUSIONS AND RECOMMENDATIONS

Design validation of the exhaust shaft requires an assessment of the compatibility of the design criteria, design bases and design configurations used for the reference design. The following discussion presents conclusions and recommendations regarding validation of the

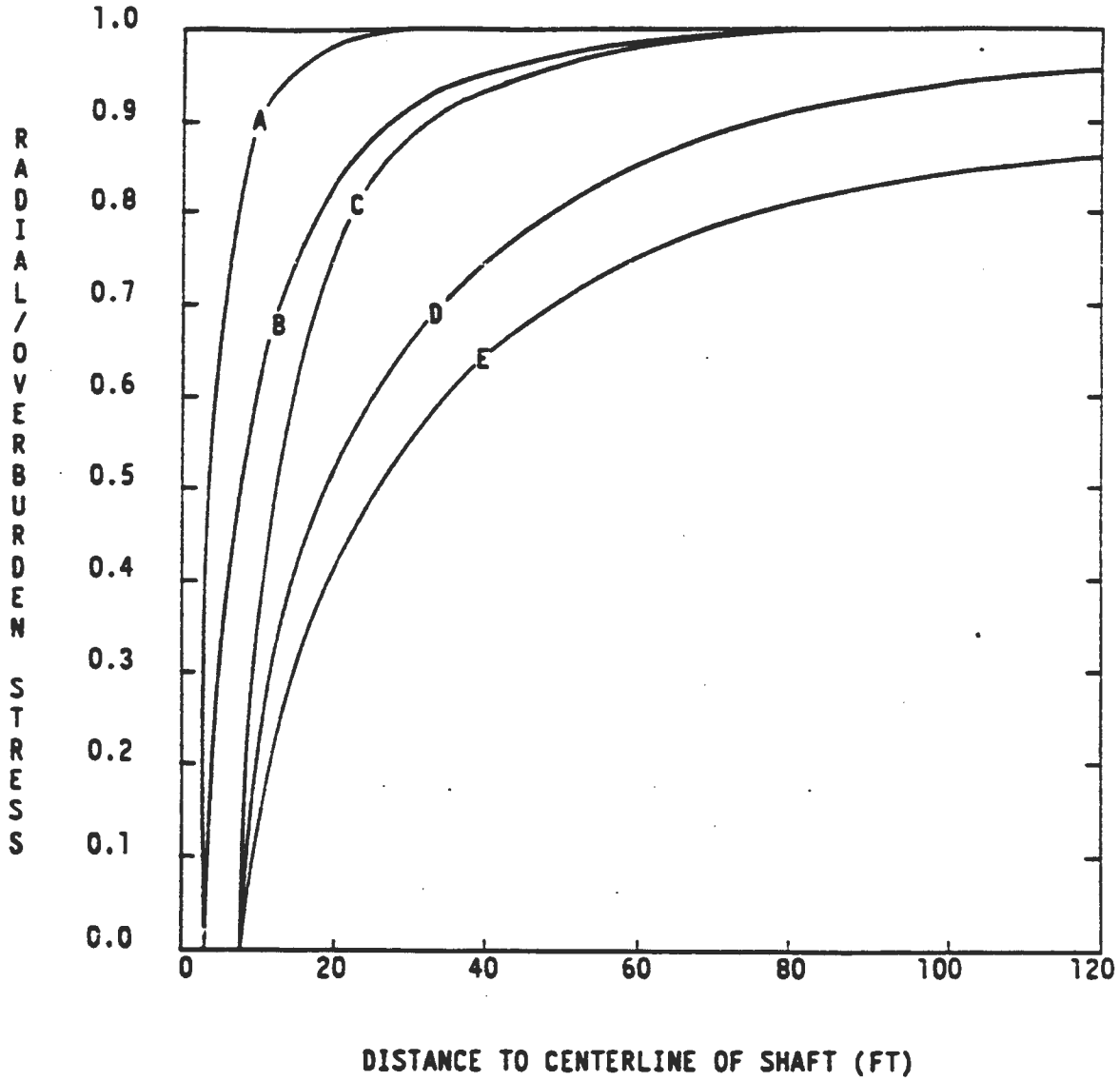


A - IMMEDIATELY AFTER EXCAVATION OF 6-FT DIAMETER SHAFT
B - IMMEDIATELY BEFORE WIDENING TO 15-FT DIAMETER
C - IMMEDIATELY AFTER WIDENING TO 15-FT DIAMETER
D - ONE YEAR AFTER WIDENING OF SHAFT
E - 25 YEARS AFTER WIDENING OF SHAFT

Figure 9-5

EXHAUST SHAFT UNLINED SECTION
RADIAL STRESS DISTRIBUTION AT ELEVATION 1343 FEET

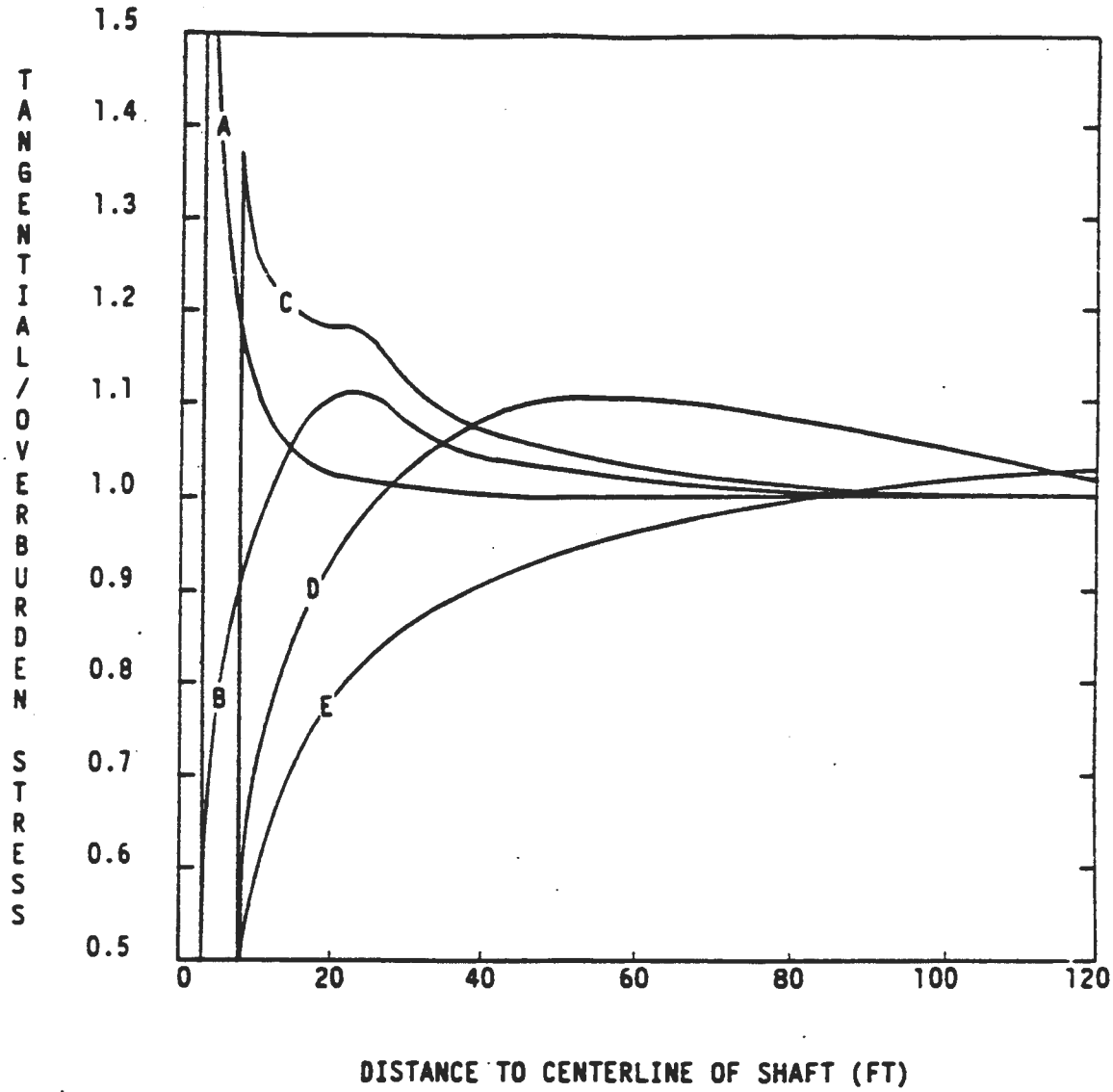


A - IMMEDIATELY AFTER EXCAVATION OF 6-FT DIAMETER SHAFT
B - IMMEDIATELY BEFORE WIDENING TO 15-FT DIAMETER
C - IMMEDIATELY AFTER WIDENING TO 15-FT DIAMETER
D - ONE YEAR AFTER WIDENING OF SHAFT
E - 25 YEARS AFTER WIDENING OF SHAFT

**Figure 9-6**

EXHAUST SHAFT UNLINED SECTION
TANGENTIAL STRESS DISTRIBUTION AT ELEVATION 1343 FEET

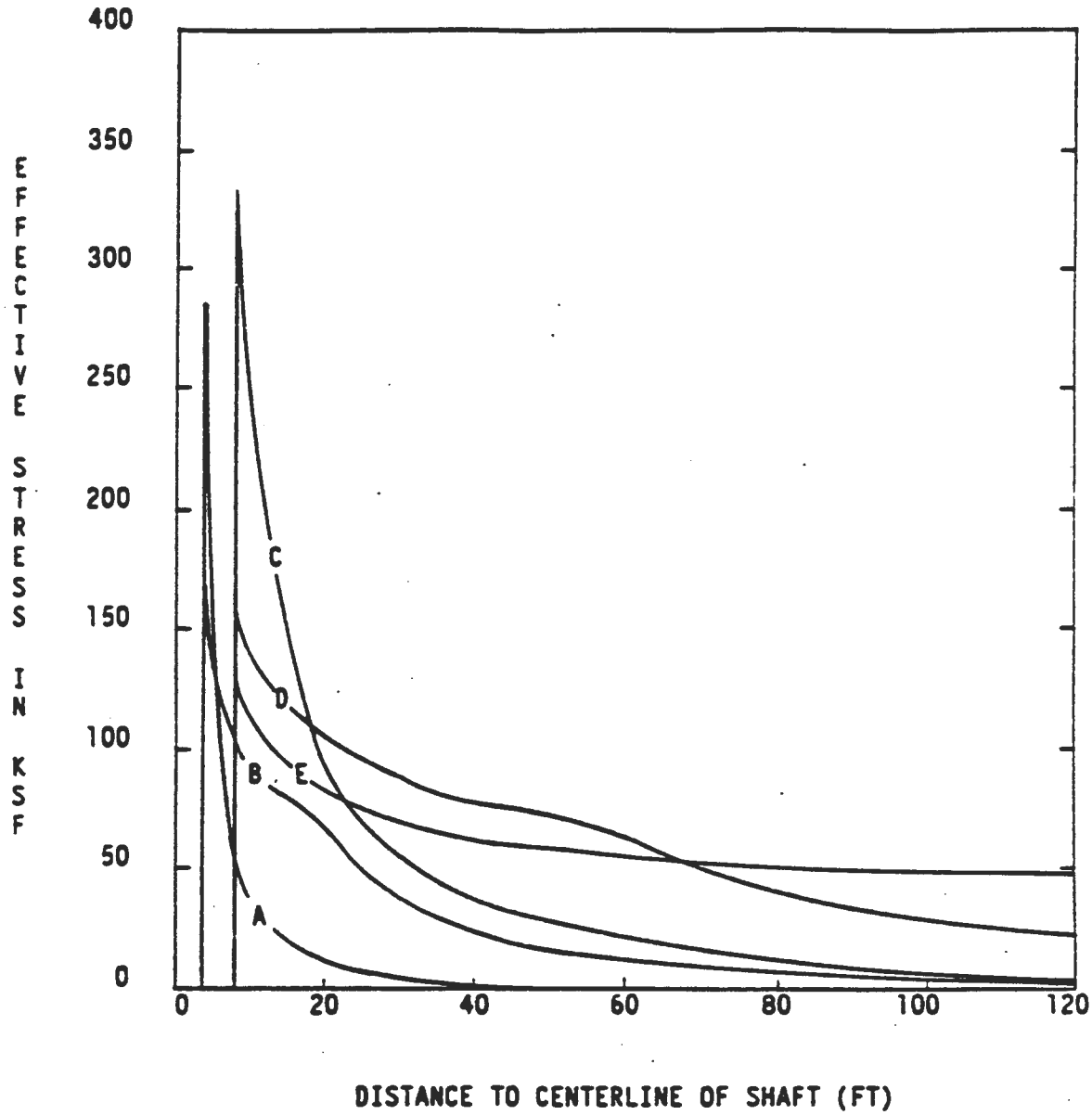


A - IMMEDIATELY AFTER EXCAVATION OF 6-FT DIAMETER SHAFT
B - IMMEDIATELY BEFORE WIDENING TO 15-FT DIAMETER
C - IMMEDIATELY AFTER WIDENING TO 15-FT DIAMETER
D - ONE YEAR AFTER WIDENING OF SHAFT
E - 25 YEARS AFTER WIDENING OF SHAFT

Figure 9-7

EXHAUST SHAFT UNLINED SECTION
EFFECTIVE STRESS DISTRIBUTION AT ELEVATION 1343 FEET

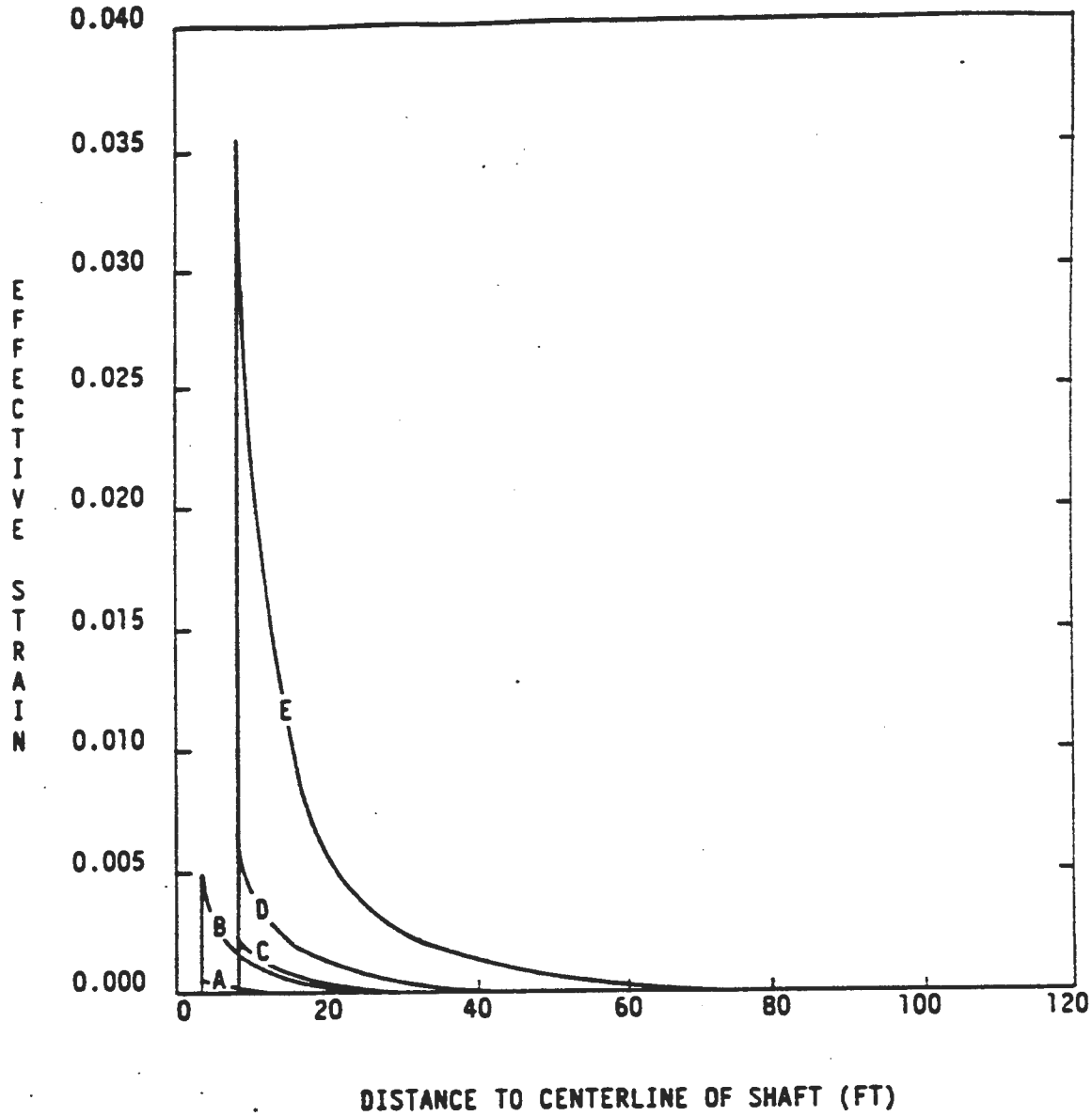


A - IMMEDIATELY AFTER EXCAVATION OF 6-FT DIAMETER SHAFT
B - IMMEDIATELY BEFORE WIDENING TO 15-FT DIAMETER
C - IMMEDIATELY AFTER WIDENING TO 15-FT DIAMETER
D - ONE YEAR AFTER WIDENING OF SHAFT
E - 25 YEARS AFTER WIDENING OF SHAFT

**Figure 9-8**

EXHAUST SHAFT UNLINED SECTION
EFFECTIVE CREEP STRAIN DISTRIBUTION AT ELEVATION 1343 FEET

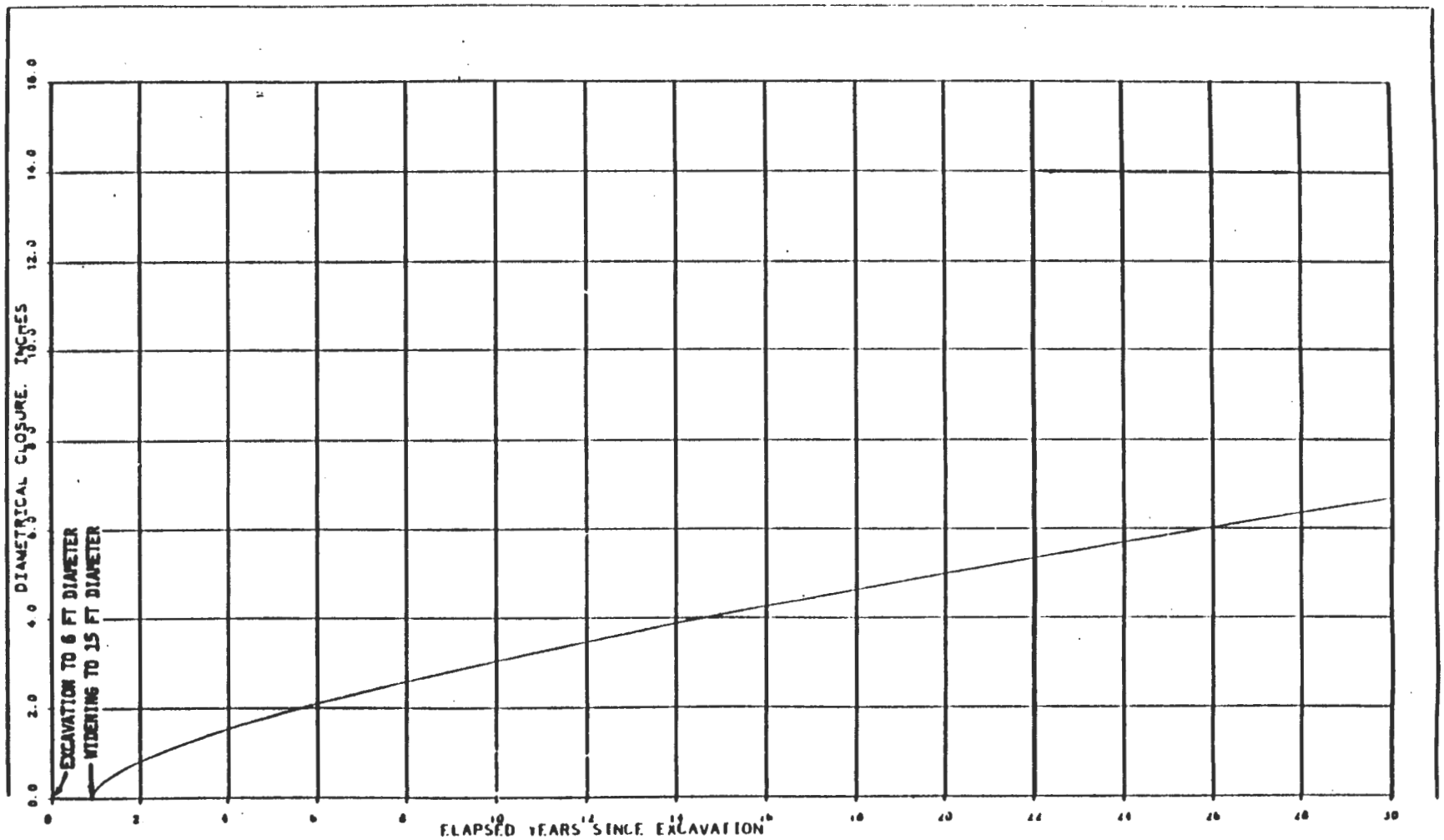


**Figure 9-9**

**EXHAUST SHAFT UNLINED SECTION**
**CLOSURE PREDICTION AT ELEVATION 1343 FEET**

exhaust shaft design as they pertain to the design elements identified in Section 9.2. These design elements stipulate the requirements that the exhaust shaft must meet in terms of shaft stability, deformation, water pressure and water control. Other conclusions and recommendations that are a product of the design validation process are also presented.

### 9.4.1 Conclusions

The stability of the exhaust shaft has been evaluated using analytical calculations, finite element modeling and analysis of data from the C & SH and waste shafts. The conclusions regarding shaft stability are the same as those for the waste shaft. The water pressure exerted on the shaft liner is currently less than the design hydrostatic pressure. If the hydrostatic pressure increases to its design limit, the liner will remain stable because its pressure capacity exceeds the design hydrostatic pressure by a factor greater than two. The cracks in the liner are not expected to result in any structural instability.

Analytical results show that the lateral pressure on the shaft key at the end of the 25-year operating life will be approximately 72 ksf. Although this pressure exceeds the design basis lateral pressure of 60 ksf, the allowable lateral pressure on the key is 154 ksf, or more than twice the predicted lateral pressure at 25 years. This provides a sufficient margin of safety against failure. If concrete shrinkage and creep were taken into account in the analysis, the margin of safety would be even greater.

The analytical results also show the redistribution of stresses around the unlined section of the shaft due to the effects of salt creep. Based on the computed vertical, horizontal and effective stresses in the unlined section, the magnitude of stresses immediately adjacent to the opening decreases and the stress arch around the opening migrates away with time. The maximum stress occurs immediately after excavation and is followed by relaxation due to creep behavior. Therefore, the stresses will not cause a future stability problem in the unlined

section of the shaft. The analysis shows the locations of effective creep strain concentrations at different times around the opening in the unlined section. Based on the predicted values of effective creep strain and the strain limit discussed in Chapter 6, the exhaust shaft will remain structurally stable within the limits required for safety during its operating life.

The analysis also predicts that the maximum diametric closure in the unlined section at the end of the operating period will be approximately 6 inches. Based on the predicted deformations and closures, the exhaust shaft will meet the requirements stated in the design criteria. The design basis requirement that the 15-foot diameter unlined section allow for salt creep over its operating life will be met.

As in the waste shaft, water is entering the exhaust shaft through cracks and construction joints in the concrete liner. The amount of water seepage was greatly reduced by grouting conducted after construction. The small amount of water still reaching the open shaft quickly evaporates in the upcast flow of exhaust air. While the exhaust fans are operating, no water reaches the underground facility level. The water seals behind the shaft concrete key appear to be functioning as intended at the bottom of the key. No water is seeping from the concrete/salt interface. There is no evidence of salt dissolution behind the key.

The reference design for the exhaust shaft has been validated in accordance with the objectives of the design validation program, based on the analyses, evaluations and predictions of future behavior presented in this chapter. With one exception, the exhaust shaft reference design complies with the design criteria and the design bases. The criterion that the liner shall prevent ground-water flow into the shaft has not been met. However, the water currently seeping into the shaft is not considered to be detrimental to shaft stability or function. No modifications to the exhaust shaft reference design are required.

### 9.4.2 Recommendations

Based on the results of design validation, recommendations similar to those for the waste shaft are made for the exhaust shaft:

(1) Validation of the exhaust shaft key and unlined section relied on analysis and modeling using in situ data from the C & SH and waste shafts. It is recommended that the numerical modeling be repeated, prior to the first receipt of waste, using in situ data from the exhaust shaft instruments. This analysis should be repeated periodically for the comparison of in situ data against design parameters.

(2) The exhaust shaft should be inspected by qualified personnel at regularly scheduled intervals. The liner should be inspected for renewed seepage and grouting performed if an amount of water considered sufficient to affect the liner's stability or functional purpose is observed. The key should be inspected for water seeping from behind the key at its base. If any is detected, grout should be injected above the top water seal. Grout should not be placed behind the key below the top seal. If this cannot be avoided, the grout must be a chemical gel (or other non-rigid grout) and must be compatible with both the existing water seal material and with the requirements of the Plugging and Sealing Program.

THIS PAGE LEFT BLANK INTENTIONALLY

# CHAPTER 10

# DRIFTS

## 10.1 INTRODUCTION

This chapter presents the results of validation of the reference design for the underground drifts. Discussions are presented on the reference design, data collected from the openings, its analysis and evaluation, and predictions of future behavior. Conclusions and recommendations pertaining to the reference design are presented based on the results of the validation process.

The term drifts includes all horizontal underground openings except the shaft stations, test rooms, and storage area rooms and their associated drifts. Discussions of the shaft stations are presented in Chapters 7 and 8. Discussions of the test rooms, storage rooms and storage area drifts are presented in Chapters 11 and 12.

The largest drifts planned for the underground facility were initially excavated 8 feet high and 25 feet wide. These drifts have been or will be enlarged to 12 feet high. The present 12-foot high, 25-foot wide drifts were excavated earlier than most of the smaller drifts and, therefore, have the longest history of in situ data collection. Because these 12 x 25-foot drifts are the largest to be excavated, they also have the most critical dimensions. Consequently, the analyses, evaluations and predictions are based primarily on these larger drifts. The smaller drifts and rooms are, therefore, considered to be validated as a result of the validation of the larger 12 x 25-foot drift reference design.

## 10.2 DESIGN

This section presents the design criteria and design bases used to develop the reference design of the drifts.

### 10.2.1 Design Criteria

The design criteria established for the design of the WIPP underground facility are discussed in Chapter 2 and summarized in Table 2-1. Table 2-1 presents the major criteria affecting underground design, including such items as waste receipt rate, type of waste, backfill requirement, etc. Those criteria requiring evaluation of their suitability for design validation are indicated in Table 2-1. The remaining criteria contained in the Design Criteria document (ref. 2-7) do not require evaluation.

Three of the indicated criteria pertain directly to the drift reference design. The first criterion states that the underground openings shall be designed to provide structurally stable excavations and pillars. "Stable" is defined in the criteria document to mean that deformations of excavations and pillars are to remain within the limits required for structural function, ventilation and safety. The second criterion states that the underground opening reference design shall provide maximum stability for the excavated rooms and drifts. The third criterion stipulates that the underground excavation shall be designed to accommodate creep closure and maintain the minimum dimensions required for the operating life of the opening. Not only are these criteria to be evaluated for their suitability, but the reference design configurations based on them must also be evaluated. These reference design configurations were discussed in Chapter 3.

### 10.2.2 Design Bases

The design bases comprise the second level of the design documents. They outline specific design requirements that were followed in designing the final drift configurations. Only those design bases that apply directly to the underground drift configurations are discussed in this subsection. The Design Basis, Underground Excavations (refs. 2-9 and 2-18), Design Basis, Underground Shops and Facilities (ref. 2-20), and Design Basis, Geomechanical Instrumentation (ref. 2-17) should be referred to for details of the appropriate design bases used for the underground drifts. None of these design bases contained elements

pertaining specifically to the drifts that required evaluation during the validation program. Those bases that required evaluation for validation pertain only to the storage area drifts and are discussed in Chapter 12.

The design bases specify that excavation within the shaft pillar area shall be the minimum required to meet the operational and safety requirements of the waste storage level. The area extraction ratio was, therefore, kept below 15 percent in this area.

The maximum tolerance for excavation of the roof, floor and walls shall be plus six inches. In no case shall the finished dimensions be less than those specified by the design. The minimum vertical dimension for equipment clearances used to meet this basis was 11 feet.

Supports for underground workings shall comply with Federal and New Mexico codes. The use of rock bolts and wire mesh in specific areas shall be determined by mine conditions and code requirements. Entry roofs, walls and floors shall be checked periodically for loose salt in accordance with applicable codes. Methods of locating gas or brine accumulations shall be implemented, such as drilling holes ahead of the excavation and testing for the presence of gas.

A geomechanical instrumentation system shall be installed to provide in situ measurement data for design verification or modification and for subsequent operational planning. In addition, the instrumentation system shall monitor stress change, closure and creep to provide a record of the structural stability of the drifts and to provide early warning of abnormal conditions for operational safety.

Deformation measurements in the drifts shall be measured as a function of horizontal and vertical closure. Salt creep and stress distributions around the drifts and at intersections shall also be measured.

The instrumentation shall provide the primary detection of changes in structural behavior. Visual observations shall follow any detected abnormal strain, pressure or deformation for evaluation of the safety of the underground working places. In addition, a program shall be provided for periodic visual inspection of all underground working places.

## 10.3 DESIGN VALIDATION PROCESS

Validation of the reference design of the underground drifts includes the collection of data and the presentation of results based on its analysis and evaluation. The results of the design validation process are used to present conclusions regarding the compatibility of the design criteria, design bases and design configurations, and recommendations for modifications, if any. This section presents the data collected and predictions of future drift behavior based on analysis and evaluation of the data.

### 10.3.1 Data Collection

Data pertaining to the underground drifts was collected from various sources. Geologic data was acquired from geologic mapping and core drilling. These data verified the stratigraphic continuity at the facility level and are discussed in detail in Chapter 6. Data were also acquired from periodic visual inspections and from geomechanical instrumentation. Collection of these data are described in the following subsections.

#### 10.3.1.1 Field Observations

Various aspects of underground behavior are evaluated by qualitative observations and documentation. Visual inspections of the drifts include observations of their general surface conditions in response to stress redistribution and creep. These conditions include shallow spalls from the roof and walls, especially at their intersection; and vertical fracturing in the pillars, both at corners and parallel to the walls. In addition to visual inspections, other techniques are used. Boreholes are surveyed using video cameras and displacements,

separations and fracturing of geologic strata surrounding the boreholes are detected using a simple probe. Surveys of underground conditions have been performed at least once every 3 months. Each survey is documented in a GFDR beginning with the February 1984 edition (refs. 4-12 through 4-19).

Recently, a special program was conducted to determine the effect of excavation induced deformation on the salt strata surrounding the facility level. An array of boreholes was drilled into the roof and floor at 30 locations in the drifts and test rooms during May through July 1986. These arrays are shown on Figure 10-1. These boreholes were used to locate separations and fractures in the halite and anhydrite near the horizontal underground openings. This Excavation Effects Program was instigated after the discovery of significant fracturing beneath the southern half of Test Room 3 (Room T). The objectives of this excavation effects study were to determine if fracturing of this magnitude has occurred anywhere else and to investigate existing conditions at selected localities throughout the facility.

The documented field observations can be separated into four categories: roof and wall spalling; pillar fracturing; roof displacements and separations; and floor displacements, separations and fracturing.

Roof and Wall Spalling. During and immediately after excavation, a sounding survey of the roofs of all drifts was performed. Each survey identified areas of potential instability, such as drummy or slabby salt. Remedial work was accomplished immediately and included scaling, additional excavation, or rock bolting. Comprehensive sounding surveys were also performed in every underground opening in July 1983 and November 1984. The behavior of the roof and walls is documented in the table entitled "Condition of Roof and Walls" in each GFDR.

THIS PAGE LEFT BLANK INTENTIONALLY

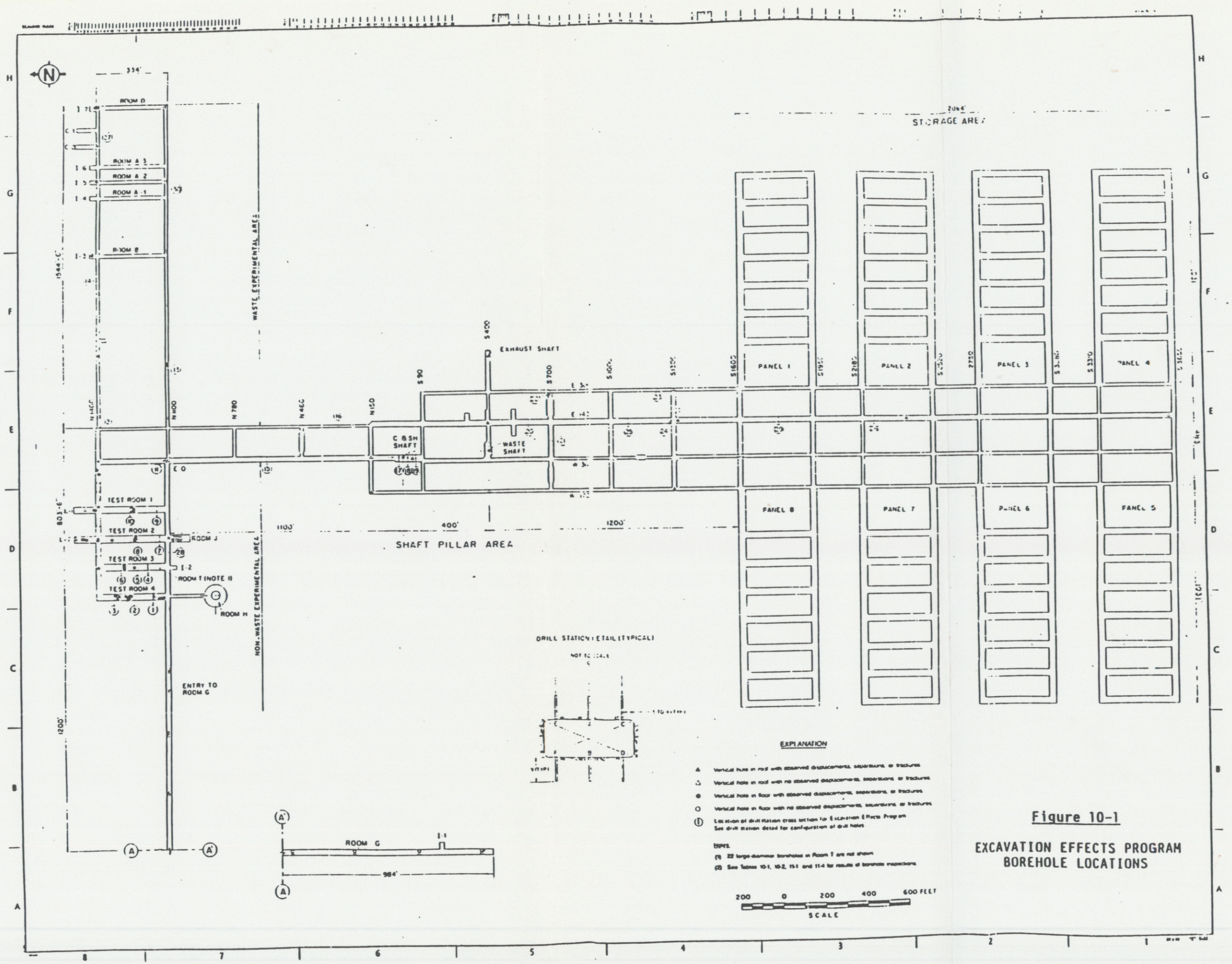


Figure 10-1

EXCAVATION EFFECTS PROGRAM
BOREHOLE LOCATIONS

Pillar Fracturing. Vertical fractures have developed in the corners formed by drift intersections. These fractures began appearing about 3 to 6 months after excavation. Site geologists have monitored the growth of these fractures and have included their observations in the GFDRs.

Vertical fractures parallel to the drift walls have been detected in several horizontal boreholes. These fractures were not present at the time of drilling. They were first observed in May 1986 and occur within 1 to 2 feet of the wall surface.

Roof Displacements and Separations. Horizontal displacements and vertical separations have been detected in some open boreholes in the drifts during the past 2 years. Periodic inspections of all accessible boreholes in the drifts have been made since September 1985. The results of these inspections in the roof holes are presented in Table 10-1.

Visual inspections were conducted directly or remotely using a video camera and/or probe. The probe used was described in Chapter 7, subsection 7.3.1.4. Depths to displacements and separations were measured with a tape measure. Relative horizontal displacements were measured where possible or estimated.

The recently conducted Excavation Effects Program consisted of drilling numerous arrays of 1 7/8-inch and 3-inch diameter holes at selected locations along the drifts (Figure 10-1). The holes were drilled approximately 9 feet into the roof and floor and inspected using a probe. The results of the inspection of these holes are presented in Table 10-2.

The N1100 and N1420 drifts were excavated eastward to E1680 in early 1984. These drifts incline upward to the experimental area. The roofs of both drifts intersect anhydrite beds "a" and "b". Slabby rock at the intersection was removed by the mining machine and rock bolts

Table 10-1

DRIFTS
RESULTS OF INSPECTION OF VERTICAL BOREHOLE IN ROOFS



| Hole | Date Completed | Hole Size (in.) | Depth (ft) | Approximate Location | Observed Condition* |
|---|---|---|---|---|---|
| DH-01 | 2-10-84 | 3 | 50.8 | N1424/E439.5 | None |
| DH-03 | 2-7-84 | 3 | 48.8 | N1112/E444 | D |
| DH-03A | 3-12-84 | 3 | 49.9 | N1112/E450.5 | D |
| DH-05 | 3-9-84 | 3 | 51.0 | N1463/E972 | D |
| DH-07 | 2-22-84 | 3 | 49.8 | N1112/E976.5 | None |
| DH-09 | 3-14-84 | 3 | 51.1 | N1432/E1332.5 | None |
| DH-11 | 3-6-84 | 3 | 50.9 | N1112/E1332.5 | None |
| DH-13 | 3-28-84 | 3 | 13.8 | N1424/E1690 | D, S |
| DH-13A | 3-29-84 | 3 | 49.0 | N1425/E1691 | D, S |
| DH-13B | 4-5-84 | 3 | 21.0 | N1425/E1695 | D, S |
| DH-15 | 3-21-84 | 3 | 51.0 | N1104/E1688.5 | None |
| DH-17 | 1-19-84 | 3 | 52.0 | N1104/E1688 | None |
| DH-19 | 1-21-84 | 3 | 51.6 | N1107/E206.5 | None |
| DH-21 | 2-27-84 | 3 | 50.4 | N1421/E786 | None |
| DH-23 | 2-15-84 | 3 | 51.0 | N1112/E781 | None |
| DH-25 | 3-30-84 | 3 | 51.8 | N1422/E1510 | D, S |
| DH-27 | 7-27-84 | 3.5 | 50.5 | N1107/W682 | None |
| DH-29 | 7-25-84 | 3.5 | 50.4 | N1099/W982 | None |
| DH-29A | 9-12-84 | 3.5 | 35.0 | N1099/W987 | None |
| DH-31 | 7-19-84 | 3.5 | 50.5 | N1099/W1282 | None |

* D = displacement; S = separation; F = fracturing

Table 10-1 (continued)

DRIFTS
RESULTS OF INSPECTION OF VERTICAL BOREHOLES IN ROOFS



| Hole | Date Completed | Hole Size (in.) | Depth (ft) | Approximate Location | Observed Condition* |
|---|---|---|---|---|---|
| DH-31A | 7-24-84 | 3.5 | 49.2 | N1099/W1280 | None |
| DH-31B | 9-12-84 | 3.5 | 4.9 | N1099/W1261 | None |
| DH-33 | 7-18-84 | 3.5 | 50.5 | N1099/W1582 | None |
| DH-33A | 9-13-84 | 3.5 | 4.1 | N1099/W1570 | None |
| DH-35 | 1-27-85 | 3.5 | 52.0 | N1102/W1882 | None |
| DH-37 | 1-26-85 | 3.5 | 51.5 | N1101/W2182 | None |
| DH-39 | 1-24-85 | 3.5 | 50.7 | N1101/W2482 | None |
| DH-41 | 1-24-85 | 3.5 | 49.9 | N1101/W2782 | None |
| DH-205 | 2-18-83 | 3 | 50.7 | N1410/E0 | None |
| DH-211 | 12-19-82 | 3 | 50.0 | S1320/E163 | None |
| DH-219 | 1-14-83 | 3 | 51.0 | S2422/E162 | None |
| DH-227 | 1-28-83 | 3 | 51.7 | S3656/E147 | None |
| DH-301 | 8-30-84 | 3.5 | 50.8 | N150/W170 | D |
| DH-303 | 9-4-84 | 3.5 | 51.4 | S400/W170 | None |
| DH-313 | 7-10-84 | 3 | 19.6 | S1300/E300 | None |
| DH-313A | 7-12-84 | 3 | 50.2 | S1300/E299 | None |
| DH-315 | 9-6-84 | 3.5 | 50.3 | S1300/W170 | D |
| DH-317 | 7-6-84 | 3 | 50.1 | S1600/W33 | None |
| DH-317A | 7-6-84 | 3 | 5.0 | S1600/W30 | None |
| DH-317B | 9-7-84 | 3.5 | 51.0 | S1597/W30 | None |
| DH-319 | 9-10-85 | 3.5 | 51.1 | S700/E300 | None |

Table 10-1 (continued)

DRIFTS
RESULTS OF INSPECTION OF VERTICAL BOREHOLES IN ROOFS



| Hole | Date Completed | Hole Size (in.) | Depth (ft) | Approximate Location | Observed Condition* |
|---|---|---|---|---|---|
| OH-2 | 8-83 | 4 | 20 | S410/E147 | None |
| OH-3 | 8-83 | 4 | 20 | Room 2 centerline | S, F |
| OH-4 | 8-83 | 4 | 20 | N1110/W365 | S |
| OH-6 | 8-83 | 4 | 20 | N1110/W5 | None |
| OH-7 | 8-83 | 4 | 20 | S70/E0 | D, S, F |
| OH-8 | 8-83 | 4 | 20 | N140/E0 | None |
| OH-9 | 2-84 | 4 | 15.4 | N1433/W232 | S, F |
| OH-10 | 2-84 | 4 | 21.0 | N1420/W218 | D |
| OH-11 | 2-84 | 4 | 19.7 | N1433/W365 | None |
| - | - | 5 | 10 | Room L1 centerline | None |
| L2PU-02 | - | 5 | 9.2 | Room L2 centerline | None |

Table 10-2

EXCAVATION EFFECTS PROGRAM

BOREHOLE INSPECTION SUMMARY



| SECTION | OPENING DIMENSIONS (HxW-FT) | EXCAVATION DATE | LOCATION | DATE DRILLED | DATE INSPECTED | OBSERVED CONDITIONS | | | | | |
|---|---|---|---|---|---|---|---|---|---|---|---|
| | | | | | | ROOF HOLES | | | FLOOR HOLES | | |
| | | | | | | E | A | C | F | B | D |
| 8 | 12x25 | 2/83 (FLOOR LOWERED 4 FT 12/83) | N110, W02 | 5/30/86 | 6/02/86 | C | NONE | C (POSSIBLY CLAY (3) | C | S, C | C |
| 12 | 12x44 | 2/83 | N430, E140 | 6/05/86 | 6/10/86 | S, C | C | C | S, C | S | S(?), C |
| 13 | 8x14 | 1/84 | N110, E439 | 6/20/86 | 6/30/86 | D * | NONE | NONE | NONE | NONE | NONE |
| 14 | 12x44 | 2/84 | N430, E875 | 6/05/86 | 6/10/86 | S | S(?) | S | S(?) | C | S(?) |
| 15 | 12x25 | 2/83 (FLOOR LOWERED 4 FT 12/83) | N626, W02 | 6/20/86 | 6/30/86 | NONE | C | S, C | C | S, C | C |
| 16 | 8x14 | 2/83 | N305, E141 | 7/15/86 | 7/18/86 | NO ROOF HOLES | | | NONE | C | C |
| 17 | 12x32 | 10/82 | CASH SHAFT STATION - N028 | 5/30/86 | 6/02/86 | C | NONE | F | NONE | S, F | NONE |
| 18 | 17x35 | 6/82 | CASH SHAFT STATION - S024 | 6/04/86 | 6/04/86 | C | S, F | F | S | NONE | S |
| 19 | 15x35 | 6/82 | CASH SHAFT STATION - S056 | 6/03/86 | 6/04/86 | F, C | F | F | F, C | C | C |
| 20 | 14x25 | 12/82 (FLOOR LOWERED 5/84) | S592, E155 | 7/10/86 | 7/11/86 | NONE | NONE | NONE | S, C | NONE | NONE |
| -- | 15x35 | 6/82 | CASH SHAFT STATION - ELECTRICAL SUBSTATION | 6/05/86 | 6/06/86 | | | | | X<br>S, C | Y<br>S, C |
| 21 | 12x20 | 7/85 | S100, E66 | 7/08/86 | 7/09/86 | NONE | NONE | NONE | NONE | S | C (POSSIBLY CLAY E) |
| 22 | 12x14 | 5/84, 7/84 | S100, E300 | 7/08/86 | 7/09/86 | NONE | NONE | NONE | C | NONE | NONE |
| 23 | 12x44 | 7/84 | S890, E229 | 7/09/86 | 7/10/86 | NONE | NONE | C | NONE | C | C |
| 24 | 12x20 | 12/82, 8/85, 6/84 | S1300, E55 | 7/09/86 | 7/10/86 | NONE | NONE | NONE | NONE | NONE | NONE |

## Table 10-2 (continued)

### EXCAVATION EFFECTS PROGRAM
### BOREHOLE INSPECTION SUMMARY



| SECTION | OPENING DIMENSIONS (W×H-FT) | EXCAVATION DATE | LOCATION | DATE DRILLED | DATE INSPECTED | OBSERVED CONDITIONS | | | | | |
|---|---|---|---|---|---|---|---|---|---|---|---|
| | | | | | | ROOF HOLES | | | FLOOR HOLES | | |
| | | | | | | E | A | C | F | B | D |
| 25 | 12×25 | 12/82 FLOOR LOWERED 5/84 | S828, E55 | 7/9/86 | 7/10/86 | NONE | NONE | NONE | C | C | C |
| 26 | 8×25 | 1/83 | ●● S2205, E54 | 7/15/86 | 7/18/86 | NO ROOF HOLES | | | NONE | NONE | C |
| 27 | 12×44 | 3/84 | ●● N430, E555 | 7/11/86 | 7/18/86 | NO ROOF HOLES | | | NONE | NONE | C |
| 28 | 12×20 | 3/83 FLOOR LOWERED 4/83 | ●● N80, W432 | 7/15/86 | 7/18/86 | NONE | NO HOLE | NONE | NONE | NO HOLE | C |
| 29 | 12×25 | 12/82 FLOOR LOWERED 8/83 | ●● S1700, E55 | 7/10/86 | 7/11/86 | C | NONE | NONE | NO FLOOR HOLES | | |
| 30 | 8×44 | 2/84 | ●● N80, E1303 | 7/11/86 | 7/18/86 | C | NO HOLE | NONE | C | NO HOLE | NONE |

● EXISTING HOLE.
●● LOCATION APPROXIMATE. NOT SURVEYED.

**EXPLANATION**

D = HORIZONTAL DISPLACEMENT. FOUND ONLY IN PREVIOUSLY DRILLED HOLES. DISPLACEMENT APPEARS TO DEVELOP WITH TIME FOLLOWING HOLE DRILLING.

S = VERTICAL SEPARATION. PROBE NAIL PENETRATES HOLE WALL SURFACE. VERTICAL SEPARATIONS RANGE FROM APPROXIMATELY 1/16 INCH TO 6 INCHES.

F = FRACTURE ZONE. PIECES OF HALITE COMMONLY PICKED OUT OF ZONE BY PROBE NAIL.

C = PROBE NAIL CATCHES ON HOLE WALL SURFACE BUT DOES NOT PENETRATE. INDICATES POSSIBLE SEPARATION OF LESS THAN 1/16 INCH. OCCURENCES AT KNOWN CLAY LAYERS ARE NOT INDICATIVE OF SEPARATION AND ARE NOT INCLUDED IN THIS TABLE.

**NOTES:**

1. SECTION LOCATIONS AND HOLE CONFIGURATIONS ARE SHOWN ON FIGURE 10-1.
2. HOLES WERE DRILLED VERTICALLY USING A JACK-LEG DRILL.
3. NOMINAL HOLE DEPTH IS 9 FEET BUT SOME HOLES ARE SHORTER DUE TO LOW DRIFT ROOF OR DRILLING DIFFICULTIES.
4. ONE ROOF AND ONE FLOOR HOLE OF EACH ARRAY WERE GENERALLY DRILLED 3 INCHES IN DIAMETER TO ACCOMODATE USE OF BOREHOLE CAMERA IF DESIRED. OTHER HOLES WERE DRILLED 1-7/8 INCHES IN DIAMETER. EXISTING HOLES WERE USED WHERE POSSIBLE.
5. OBSERVATIONS WERE MADE USING A PROBE CONSISTING OF A NAIL ATTACHED PERPENDICULAR TO THE END OF A ROD.
6. HOLES AT SECTION 13 WERE DRILLED TO ONLY 6- OR 6.5-FT DEPTH DUE TO LOW DRIFT ROOF. NO ROOF HOLES WERE DRILLED AT SECTIONS 16 OR 26 DUE TO LOW DRIFT ROOF.
7. POSSIBLE SEPARATIONS IN FLOOR HOLES AT SECTION 25 ARE PROBABLY AT CLAY E.

and wire mesh were installed. Several fractures in the roof brow at these anhydrites have been observed.

A portion of the N140 crosscut between W170 and E140 has been excavated above clay G. An inspection of this area in June 1986 showed some minor vertical separation, on the order of 1/8 inch, as well as some squeezing out of clay G. No fractures in the underlying halite were observed.

Floor Displacements, Separations and Fracturing. Fracturing has developed beneath the floor in some locations. These fractures occur in the halite above MB-139 and sometimes extend into MB-139. The most prominent fracturing at present is beneath Test Room 3, as discussed in Chapter 11.

As with the roof boreholes, observations were accomplished using both video equipment and a probe. The results of floor hole inspections conducted through July 1986 in accessible boreholes are presented in Table 10-3. Results of the Excavation Effects Program are included in Table 10-2.

10.3.1.2 Geomechanical Instrumentation

An extensive system of geomechanical instruments has been installed in the underground drifts (Figure 10-2) to provide in situ data on the deformational behavior of these openings. The majority of the instruments were installed during the SPDV Program and therefore have been monitored for over three years. Additional instrumentation was installed after the SPDV program was completed.

Instrumentation in the drifts consists of radial convergence points and multiple-point borehole extensometers. The convergence points consist of pairs of eyebolts anchored in the salt of the roof, floor and walls of the drifts as well as at corners of intersections. The closure of the opening is measured between a pair of convergence points using a tape extensometer. The borehole extensometers are the sonic-probe type

Table 10-3

DRIFTS
RESULTS OF INSPECTION OF VERTICAL BOREHOLES IN FLOORS



| Hole | Date Completed | Hole Size (in.) | Depth (ft) | Approximate Location | Observed Condition* |
|---|---|---|---|---|---|
| DH-36 | 1-26-85 | 3.5 | 51.5 | N1102/W1882 | None |
| DH-38 | 1-26-85 | 3.5 | 47.5 | N1101/W2182 | None |
| DH-40 | 1-25-85 | 3.5 | 51.0 | N1101/W2482 | None |
| DH-42 | 1-23-85 | 3.5 | 51.2 | N1101/W2782 | None |
| DH-42A | 1-25-85 | 3.5 | 40.5 | N1101/W2789 | None |
| DH-228 | 1-28-83 | 3 | 50.4 | S3656/E147 | None |
| OH-13 | 2-84 | 4 | 9.5 | N1433/W232 | S, F |
| OH-14 | 2-84 | 4 | 9.7 | N1433/W365 | D, S, F |
| JV-01 | 9-85 | 36 | 8 | Room J | None |
| JV-02 | 9-85 | 36 | 8 | Room J | None |
| JV-03 | 9-85 | 36 | 8 | Room J | None |
| JV-04 | 9-85 | 36 | 8 | Room J | None |
| JV-05 | 9-85 | 36 | 8 | Room J | None |
| JV-06 | 9-85 | 36 | 8 | Room J | None |
| JV-07 | 9-85 | 36 | 8 | Room J | None |
| JV-08 | 9-85 | 36 | 8 | Room J | F |
| JV-09 | 9-85 | 36 | 8 | Room J | None |
| L2X-01 | 1-85 | 30 | 12 | Room L2 | None |
| L2PD-01 | - | 5 | 13.0 | Room L2 centerline | D, S, F |
| - | - | 5 | 11.3 | Room L2 centerline | S, F |

* D = displacement; S = separation; F = fracturing

Table 10-3 (continued)

DRIFTS
RESULTS OF INSPECTION OF VERTICAL BOREHOLES IN FLOORS



| Hole | Date Completed | Hole Size (in.) | Depth (ft) | Approximate Location | Observed Condition* |
|---|---|---|---|---|---|
| - | - | 16 | 10.3 | Room L2 centerline | D, S |
| NPD-03 | 1-86 | 5 | 9.3 | N1420, east of Test Room 1 | None |
| NPD-04 | 1-86 | 5 | 9.5 | N1420, east of Test Room 1 | None |
| NPD-05 | 1-86 | 5 | 9.6 | N1420/Room L1 | None |
| NPD-06 | 1-86 | 5 | 9.5 | N1420/Room L1 | None |
| NPD-07 | 1-86 | 5 | 9.0 | N1420/Room L2 | S, F |
| NPD-08 | 1-86 | 5 | 12.0 | N1420, east of Test Room 1 | S |
| NPD-11 | 1-86 | 5 | 8.9 | N1420, between Test Rooms 2 and 3 | None |
| NPD-12 | 1-86 | 5 | 9.0 | N1420, between Rooms L1 and L2 | None |

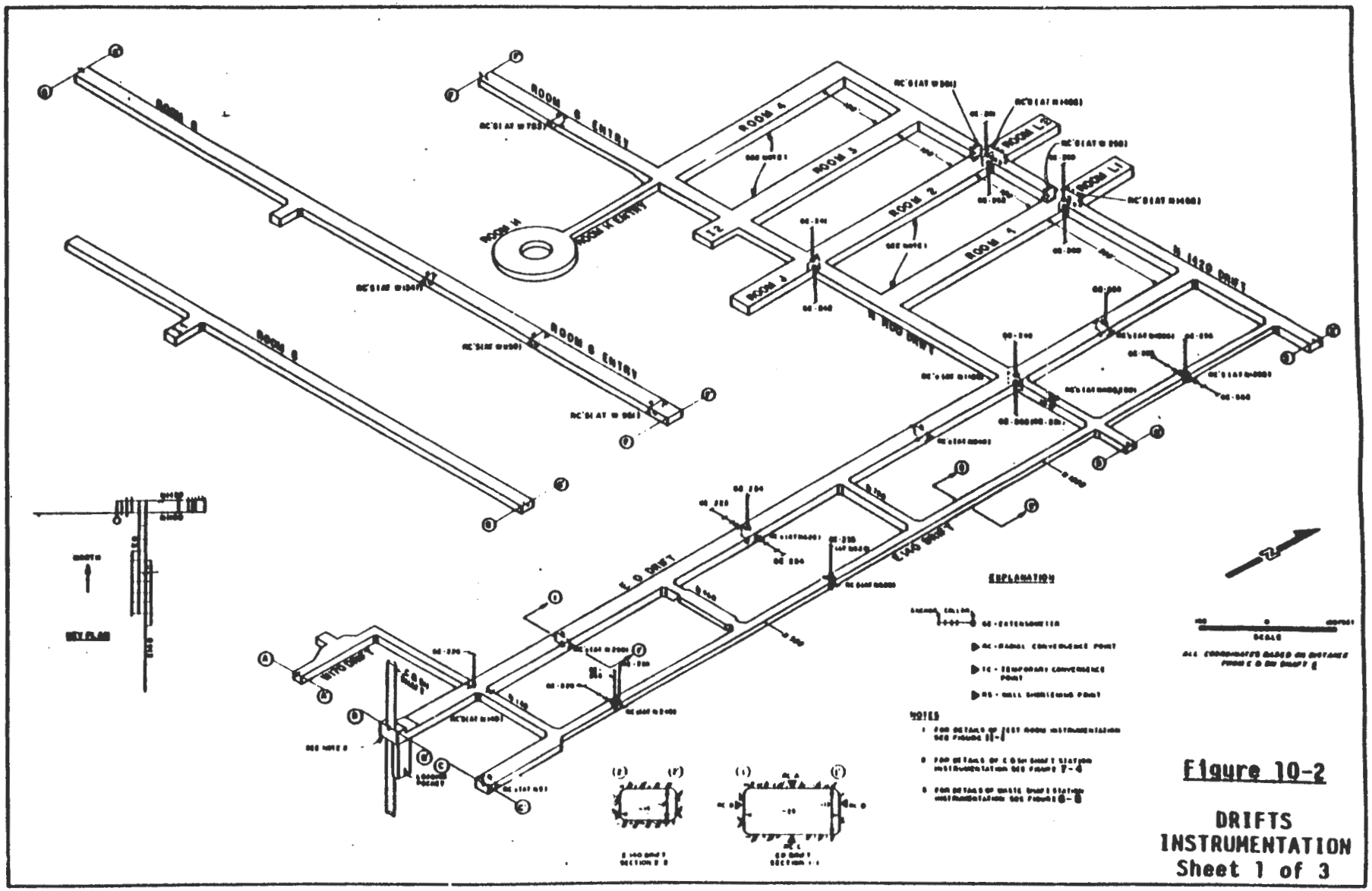


Figure 10-2

DRIFTS INSTRUMENTATION
Sheet 1 of 3

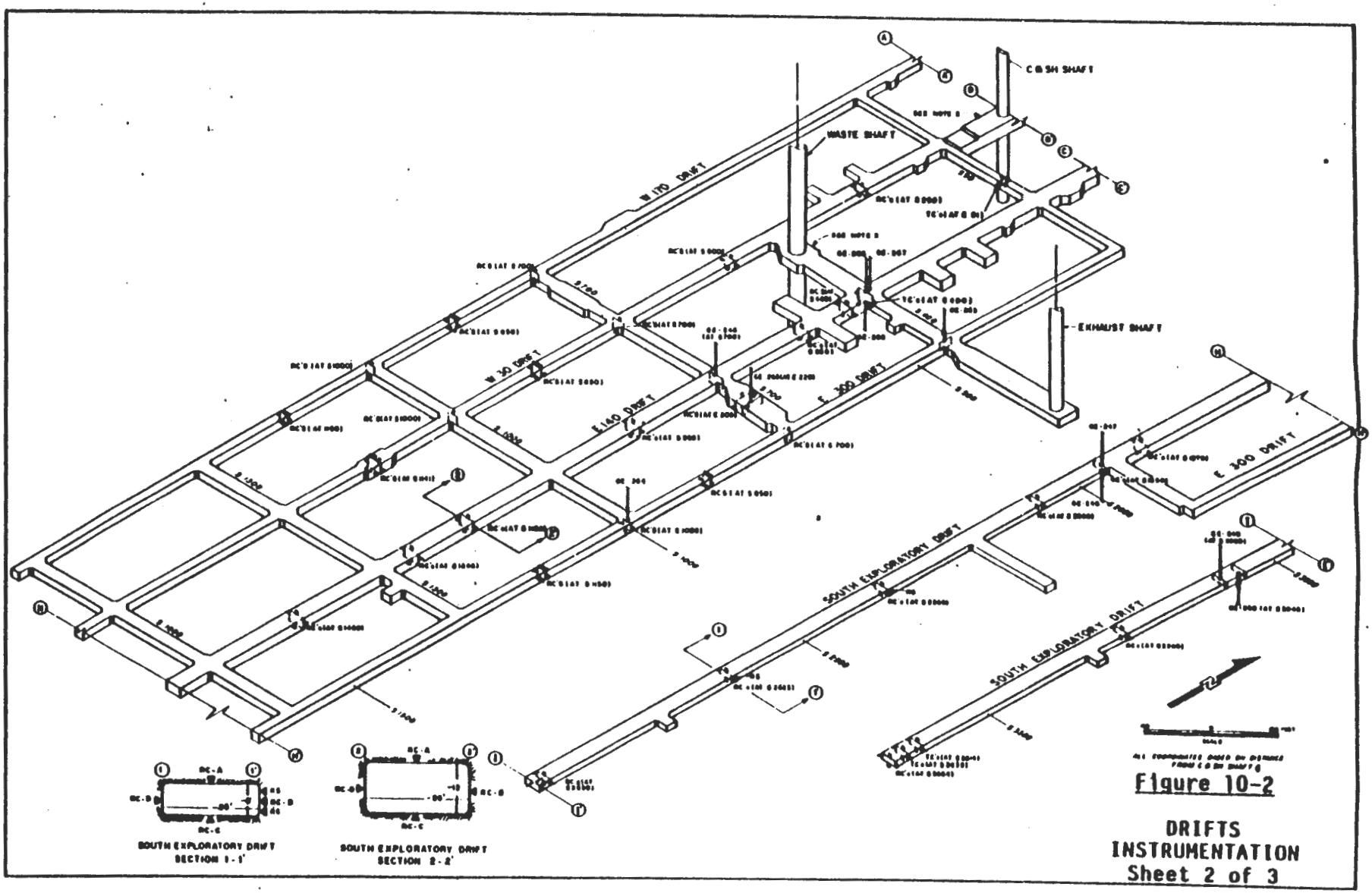


Figure 10-2

DRIFTS
INSTRUMENTATION
Sheet 2 of 3

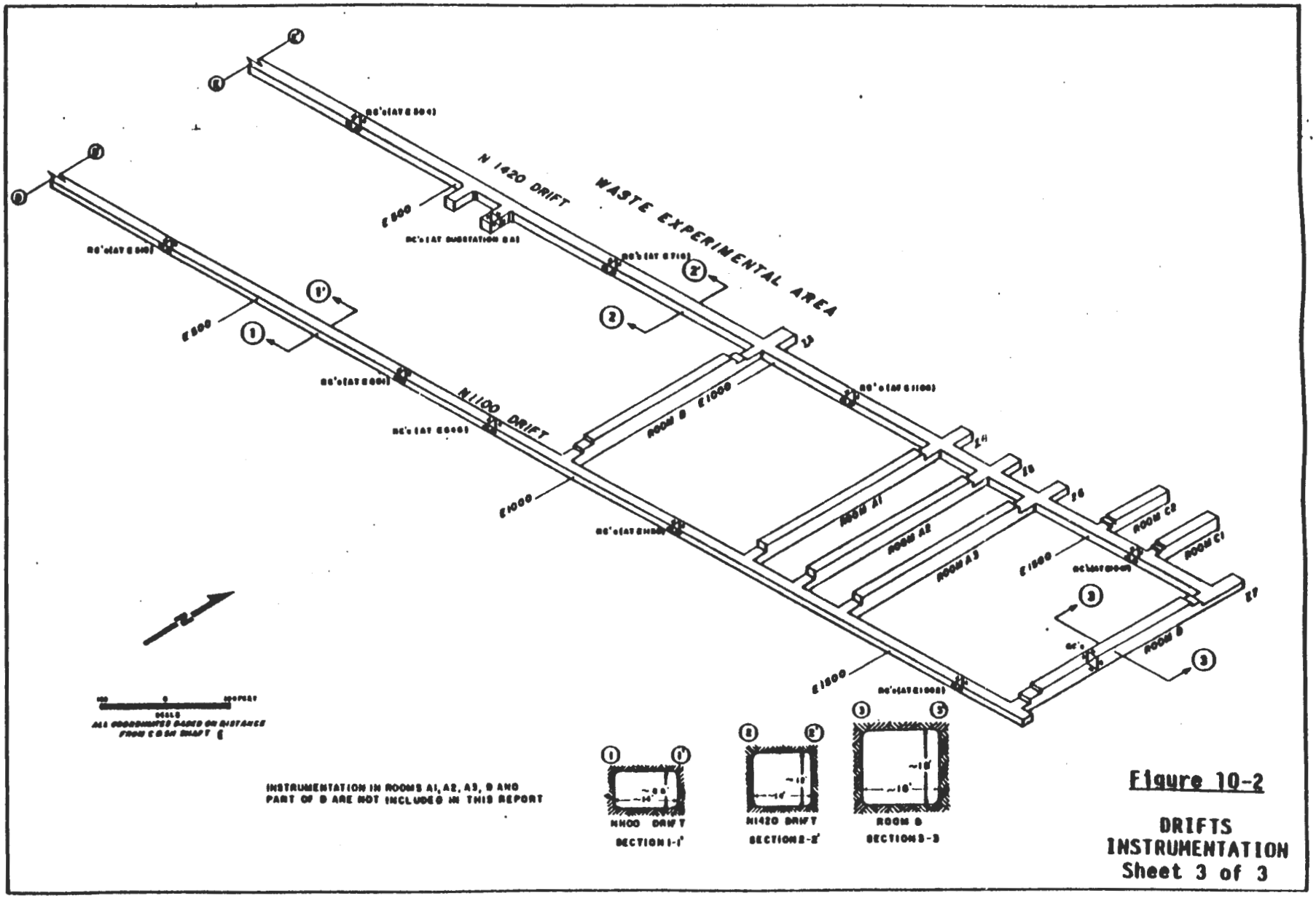


Figure 10-2

DRIFTS INSTRUMENTATION Sheet 3 of 3

with stainless steel anchor rods and expansion-ring anchors. Two-anchor, four-anchor and five-anchor extensometers have been installed. Anchor depths vary with locality and site-specific stratigraphy. Recent data plots for the drift instruments are presented in Appendix J.

No stressmeters were installed in either the halite or anhydrite surrounding the drift openings. A program to develop reliable stressmeters for use in halite was begun but abandoned when other WIPP participants initiated similar programs. The results of their programs indicate that measurements using modified stressmeters are not yet sufficiently reliable to be considered for design validation. Therefore, numerical modeling was relied upon to analyze stress changes with time in the halite and anhydrite around the openings. The reliability of the readings from the two stressmeters installed in MB-139 beneath Test Room 2 is discussed in Chapter 11.

The underground instrumentation system has had a complex history. All extensometers have been reset at least once because salt creep moved the anchor-rod magnets beyond the initial 2-inch measurement limit. Convergence points were frequently damaged by construction activities and were regularly replaced. Extensometers were also damaged during construction; some were replaced and others were abandoned. The operational history of the instruments is presented in each issue of the GFDRs.

### 10.3.2 Analysis and Evaluation

The in situ data collected and observations made during the design validation process were analyzed and evaluated to determine the effects of salt behavior on the drift excavations. Closure data were analyzed and a model simulation was performed for a typical 8 x 25-foot wide drift. An option for lowering the floor 5 feet was incorporated into the model for subsequent analysis of the drifts in the storage area. The results of the analysis of the larger drifts are presented in Chapter 12.

### 10.3.2.1 Observed Conditions

Evaluation of observed conditions is a qualitative process. It represents the assessment of qualified geologists and engineers and is an important component of the analysis and evaluation of measured responses and structural calculations.

Roof and Wall Spalling. Changes in roof and wall conditions occur slowly. Drummy areas detected during the original soundings have not enlarged significantly. These drummy areas occur in clear halite and are not associated with any noticeable clay deposits. Separations occur along planes of weakness, probably created by the orientation of crystal faces. Few new slabby areas have developed. For an unknown reason, more slabby areas developed in the roof of the E140 drift south of the waste shaft during excavation than in any other underground area. These areas have shown little, if any, growth.

Wall spalling is even more subdued. The most noticeable spalling occurs in the argillaceous halite unit and associated clay seam (geologic map unit 4 and clay F) near the intersection of the wall and roof. This area has exhibited slowly deteriorating conditions and requires occasional scaling. This spalling of map unit 4 and the squeezing out of associated clay F is most noticeable in the N1420 drift north of the test rooms and along the E140 drift south of the waste shaft. Spalling results from room closure and is related to the percentage of argillaceous material in the halite and to the proximity of the roof intersection. Similar behavior associated with anhydrite "b", anhydrite "a" and clay I has been observed in the walls of the drifts and test rooms in the waste experimental area. Some minor squeezing of clay G, clay H and clay I has occurred where these clays are exposed along drift walls. Relative motion along these clays similar to clay F is exhibited by the lower section of the wall moving into the excavation relative to the upper section. Some spalling of map unit 0 has also been noted along the E140 drift south of approximately S2500.

Pillar Fracturing. The vertical fractures that have developed in the pillar corners occur throughout the underground facility. They are particularly prominent in corners that were not beveled during excavation. The fractures range in width from closed to about 2 inches and extend into the salt essentially perpendicular to the surface.

The fractures grow steadily with time as the halite responds to deformation around the opening. Pillar corner fractures are the most obvious manifestation of pillar shortening in the drifts and rooms. These fractures will continue to grow and the corners will continue to deteriorate, with increasing spalling as a result. This behavior is expected and poses no stability problems, but it will require monitoring and maintenance throughout the operating life of the facility.

Vertical fractures have developed in the walls of the drifts parallel to the longitudinal drift axis. The fracture openings range from closed to 1/16 inch in width. The fractures have been detected in some boreholes where they occur within 2 feet of the wall surface. This type of fracturing is typical of underground excavations and probably represents tension fractures developed due to stress relief.

Roof Displacements and Separations. Clay G and clay H, above the roof of the facility level drifts, and clay I, above the roof of the drifts in the experimental area, have exhibited displacements and separations. Table 10-1 presents the results of observations made through July 1986 in 58 open boreholes. Twenty of these holes exhibited positive evidence of the occurrence of displacements and/or separations. Sixteen of these holes are at intersections. The vertical separations range from closed to 1/4 inch in width, and the horizontal displacements are up to 1 inch wide.

An additional 32 holes in 11 arrays were drilled in the roof at various facility level drift locations during the Excavation Effects Program (Figure 10-1). Of these, four arrays were drilled at intersections. Three additional arrays were drilled in the roof of drifts in the waste experimental area.

Inspection of the recently drilled holes using a probe indicate that minimal separation has occurred at the intersections and along the drifts. The size of the opening as well as the elapsed time since its excavation do not appear to have a significant effect on this phenomenon. Although the E140 drift south of the waste shaft was excavated early in construction and has the largest opening dimensions (12 x 25 feet), only minimal separations, less than 1/16 inch wide, were detected.

No separations were detected at clay G in the drift hole arrays, and the separations in the halite were usually less than 1/16 inch. There appears to be about 1/8 inch of separation at clay I in the array at E875 in the N1420 drift. This is consistent with observations made in previously drilled holes in the waste experimental area.

The observed displacements and separations immediately above the facility drifts appear to be normal deformational behavior. As the deviatoric stress around the underground openings increases following excavation, the surrounding salt will deform. The clay seams are zones of weakness that provide slip planes for salt movement during lateral loading. Movement is generally represented by the halite section below the clay seams moving into the excavation relative to the section above.

<u>Floor Displacements, Separations and Fracturing.</u> Minor displacements, separations and fracturing have occurred beneath the floor of the drifts. Table 10-3 presents the results of observations made in 34 open boreholes through July 1986. Ten of these holes exhibited displacements, separations or fracturing. Displacements up to 3/4 inch wide and separations up to 1/2 inch wide have been observed in boreholes at the intersection of Test Room 1 and Room L1, as well as at the intersection of Test Room 2 and Room L2. These are large, four-way intersections with 20 x 33-foot dimensions. Some displacements, separations and fracturing were also detected in three open boreholes in Room L2. Only two holes in the N1420 drift east of Test Room 1 exhibited separations, less than 1/8 inch wide. No other separations

have been detected in any other open boreholes in the N1420 drift or Room G. Only closed fractures were observed in the 30-inch diameter hole (L2X-01) in Room L2 (Figure 10-3). These fractures, many coated with clay, appeared to have originated prior to room excavation.

Nine small-diameter holes were drilled in the floor of the 35-foot wide S700 crosscut and inspected using a probe. These holes were drilled to determine the depth to MB-139 as well as to determine if any fractures were present. Fracture zones up to 1 inch wide were encountered in two locations in the halite above MB-139. Only one borehole contained a hairline fracture within MB-139.

During September 1985, nine 36-inch diameter holes were drilled in the floor of Room J, a 33-foot wide room, to accommodate structural steel columns. Only one near-horizontal fracture, less than 1/32 inch wide, was encountered in the halite above MB-139 in hole JV-8. No fractures were found in the other holes in Room J.

One fracture has been detected in the floor of the E140 drift south of the waste shaft. This fracture was observed while the drift was being enlarged from 8 feet to 12 feet high from April through June 1984. The fracture was about 18 inches below the original floor in halite and extended from approximately S1859 to S1871. Separation ranged from 1/16 inch to 1/2 inch and was associated with some clay. It curved upwards toward the floor at its northern and southern limits.

The results of the Excavation Effects Program indicate that minimal separations occur beneath the floor of the drifts and intersections. As determined from the roof holes, the size of the opening and elapsed time since excavation do not appear to have any effect on the occurrence of separations in the salt beneath the floor. No fracture zones were detected in any of the holes and separations where encountered, ranged from less than 1/16 inch to 1/8 inch wide. As with the older open boreholes, the Excavation Effects Program holes show evidence of separations within MB-139, at clay E and in the overlying halite.

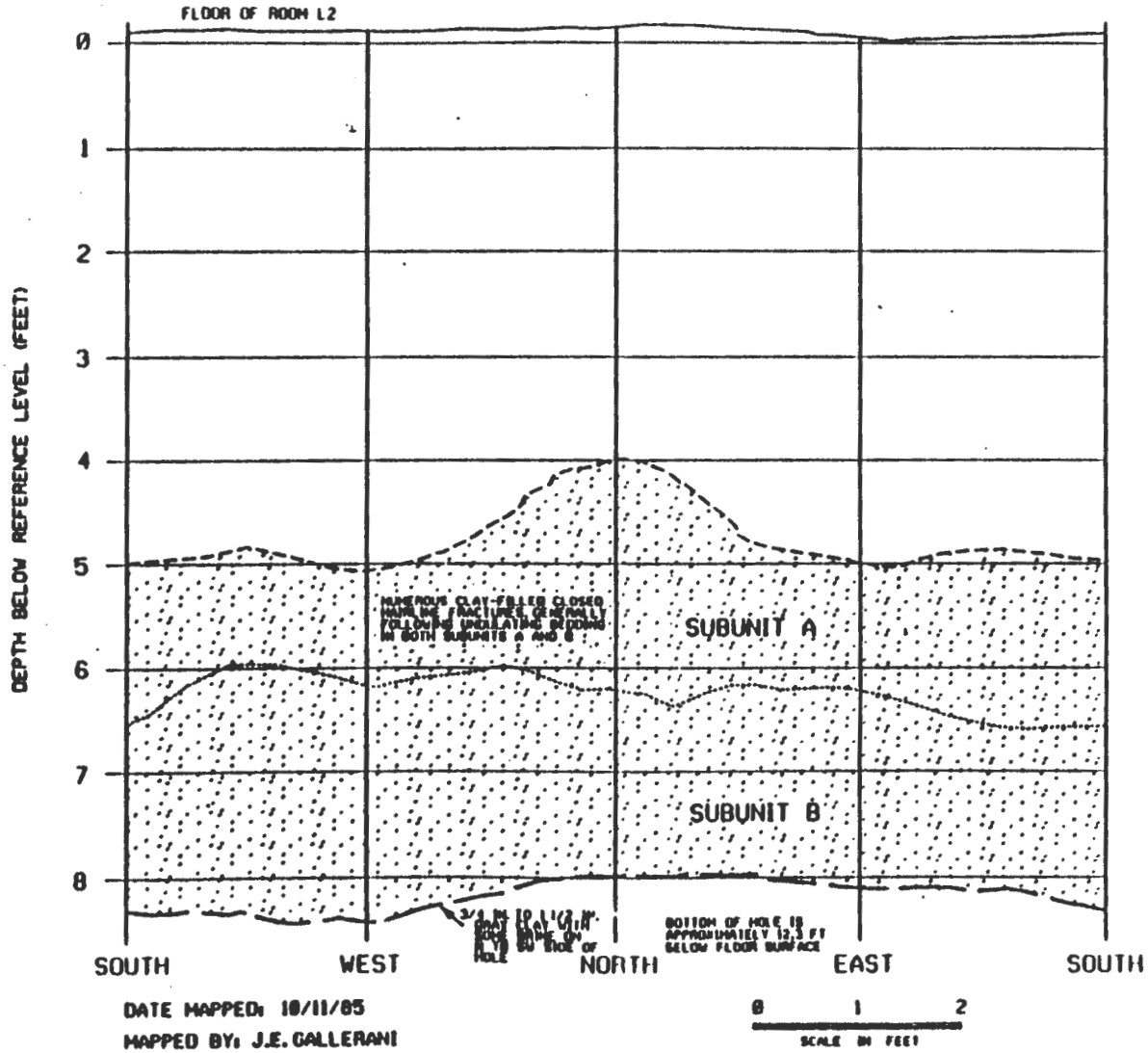


DATE MAPPED: 10/11/85

MAPPED BY: J.E. GALLERANI

## EXPLANATION

- HALITE
- MARKER BED 139
- UPPER CONTACT OF MB-139
- UPPER CONTACT OF SUBUNIT B
- CLAY E (LOWER CONTACT OF MB-139)
- FRACTURE TRACE
  DISTINCT FRACTURES, USUALLY CLOSED WITHIN A FEW INCHES OF THE BOREHOLE WALL.
- FRACTURE ZONE
  ZONE OF FRACTURED SALT BOUNDED BY DISTINCT FRACTURES.
- SMALL FRACTURE
  CLOSED HAIRLINE FRACTURES, USUALLY FORMING FRACTURE ZONES LESS THAN ONE INCH WIDE.
- (1/2) APPROXIMATE WIDTH OF SEPARATION, IN INCHES. SEPARATIONS ARE MEASURED WITHIN THE OPENING, 12 INCHES FROM BOREHOLE WALL.

NOTES:

1. BOREHOLE IS 30 INCHES IN DIAMETER.
2. MAPPING WAS PERFORMED FROM INSIDE THE HOLE. ALL FEATURES WERE MEASURED FROM AN UNSURVEYED REFERENCE LINE.
3. MAPPING WAS PERFORMED AT A SCALE OF 1 INCH EQUALS 1 FOOT.

**Figure 10-3**

**DRIFTS**
**GEOLOGIC LOG OF HOLE L2X-01**

The floor hole array in the N1420 drift at E875 encountered a slight separation of approximately 1/16 inch, coincident with a clay seam at a depth of about 8 1/2 feet. MB-139 at this location is about 22 feet below the floor.

Brine was encountered during the drilling of the central hole in the array at S700/E66 and continued to flow from the hole for several days after the completion of drilling. The hole encountered several separations up to 1/16 inch wide between a depth of 7.4 and 7.7 feet. No separations were detected in the other holes of this array. Brine has been encountered at several other hole array locations but no significant separations were detected in the holes.

The observations made to date indicate that fracturing in the drift floors is minimal. This includes observations of the E140 drift, which was one of the earliest excavations made during the SPDV Program. No fractures of the magnitude found in Test Room 3 (Chapter 11) have been detected in any of the drifts. Displacements, separations and fracturing beneath the floor is expected to continue in the future.

10.3.2.2 Closure Behavior at Selected Stations

Analyses were performed at selected stations to study roof-to-floor and wall-to-wall closure. Analysis was also performed to study the effect of floor lowering on closure.

Roof-to-Floor Closure. Until May 1984, the E140 drift south of the waste shaft was unique in that there were neither crosscuts nor nearby parallel drifts. However, in May and June 1984 the floor of the drift was lowered by 4 feet and new drifts and crosscuts were added between stations N140 and S1620. These two operations have resulted in an increase in closure rates for this portion of the drift. Since both operations occurred concurrently, it is difficult to isolate their effects on closure. However, it has generally been observed that any far field disturbance has only a short-term effect on the closure, and

that the closure rate, after a momentary increase, decays to its pre-perturbation rate pattern.

If we assume that the closure at station E140/S1879 is not measurably affected by the additional excavations performed north of station S1620, this station can then represent the closure of an infinitely long opening in a geologically uniform formation. However, because the convergence points were installed nearly 4 days after the completion of excavation, the roof-to-floor closure versus elapsed time curve was extrapolated backwards by fitting an equation in the form of

$$t = t_1 \, (1 + R(t)/R_1)^3 \qquad (10\text{-}1)$$

where: $R(t)$ is the instrument reading at elapsed time $t$ since the end of excavation; and

$R_1$ is the regression parameter, equal to total closure at elapsed time $t_1$ since the end of excavation.

This equation indicates that at $t$ equal to 0, the slope of the closure curve is infinite. This is not true because the slope at $t$ equal to 0 is finite but large.

Based on the results of the regression analysis, the value of $R_1$ was determined to be 1.97 inches. However, the curve-fitting was not very good, probably because excavation at the instrument location was done in two stages making it difficult to assign the value for $t_1$. Because the shape of the early part of the closure versus time curve is not smooth, the estimated value of $t_1$ is approximate.

Figure 10-4 compares the measured closure with the adjusted curve at station E140/S1879 using the results of the regression analysis. The reading of roof-to-floor closure on August 26, 1985, was 5.84 inches and the adjusted value is 7.81 inches. Note that this station is nearly 230 feet from the boundary location north of which the floor was lowered 4 feet. It is likely that the excavation had some effect on

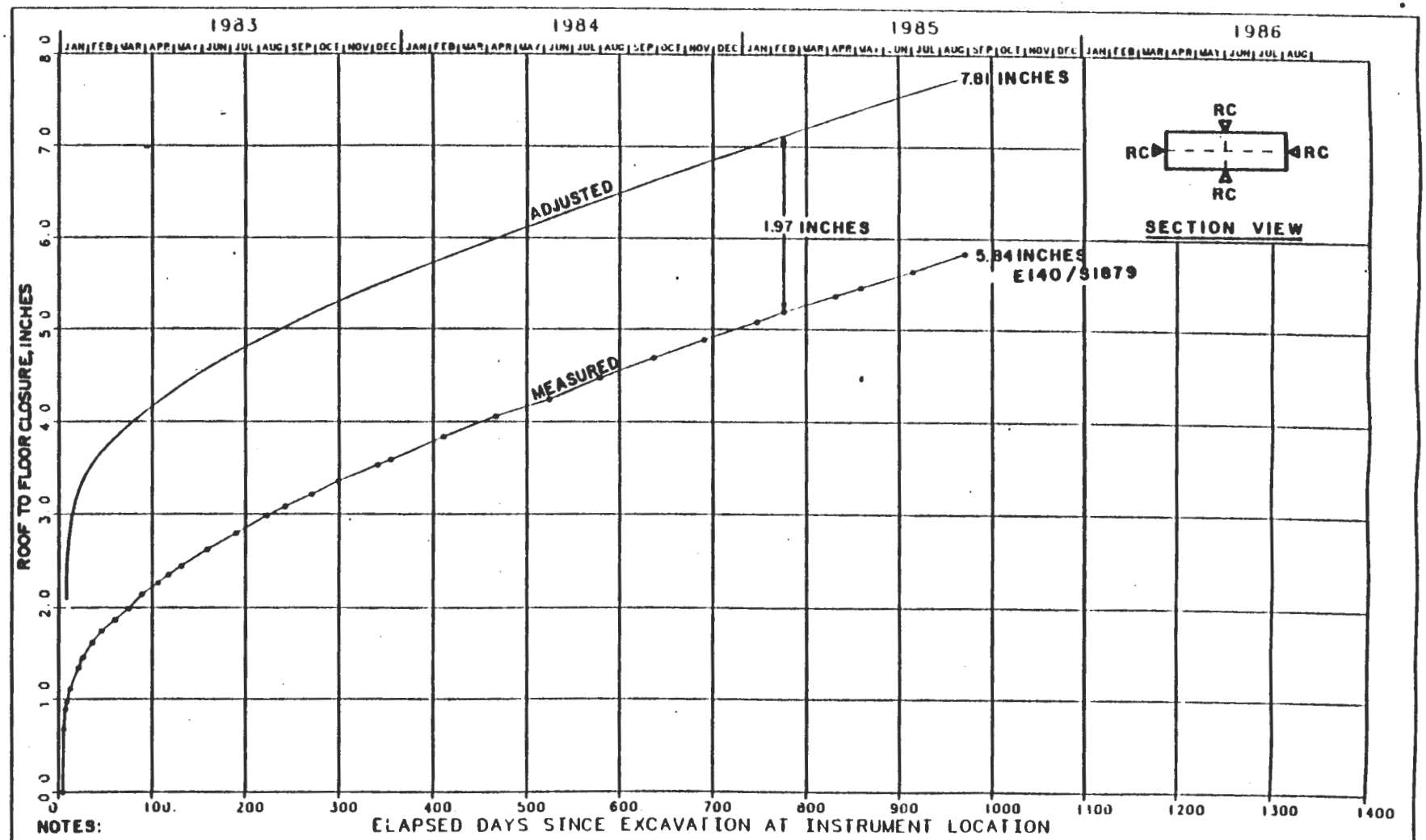


NOTES:

1. EXCAVATION DIMENSIONS = 8FT X 25FT
2. ADJUSTED CURVE OBTAINED USING THE RESULTS OF REGRESSION ANALYSIS

**Figure 10-4**

**DRIFTS**
**COMPARISON OF MEASURED CLOSURE WITH REGRESSION CURVE AT E140/S1879**

the closure at this station, although Figure 10-4 does not clearly show such an effect. The convergence points at this location have since been destroyed.

Figure 10-5 shows the central roof-to-floor closure at E140/S1246. The roof-to-floor convergence points were installed nearly 14 days after excavation at this location. This figure shows the effect that lowering the floor 4 feet has on the closure. In addition, the E300 drift excavation passed this location on August 21 and 22, 1984. The effect of lowering the floor, though, masks the effects of the adjacent excavation. As of August 26, 1985, the roof-to-floor closure of the 12 x 25-foot drift was 4.18 inches. The initial reading was taken on July 11, 1985, 1 day after the floor was lowered. Because the closure rate is very high at the early stages, actual roof-to-floor closure is greater than 4.18 inches.

Relationship Between Roof-to-Floor Closure and Drift Dimensions. Convergence points have been installed at various stations in underground drifts having different cross section dimensions. Some of the drifts, especially the E140 drift south of S1600, are isolated, while most of the other drifts have nearby parallel drifts and crosscuts. The closure behavior of these drifts is affected not only by the opening dimensions but also by the presence of adjacent openings. Differences in creep properties of the salt may also be responsible for differences in creep behavior. In addition, the closure behavior is affected by the 4- to 5-foot lowering of the drift floor.

Figure 10-6 shows measured roof-to-floor closure at selected stations in drifts with different cross section dimensions. Because measurements were not made immediately after the opening was excavated, the closure values were normalized to the values at approximately 10 days after the completion of excavation at the respective instrument station. As shown on this figure, the maximum closure and closure rate occur in drifts with opening dimensions of 12 x 25-feet. Because the

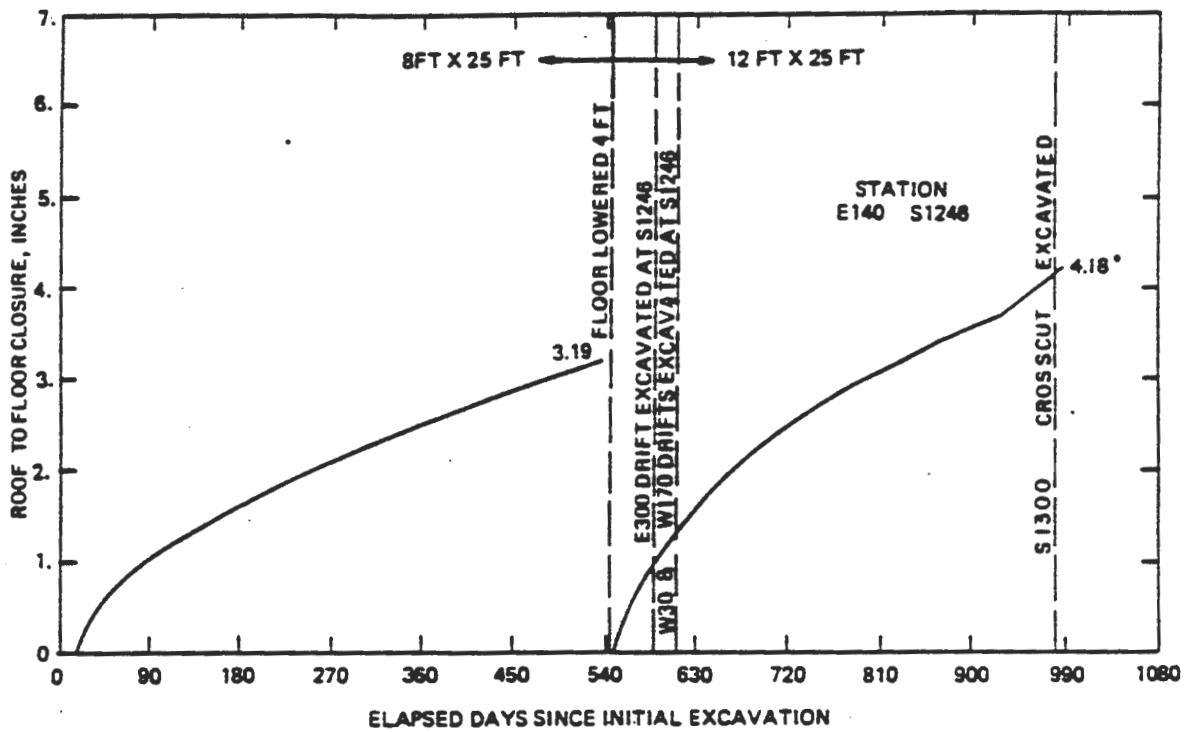


*MEASUREMENT ON AUGUST 26, 1985.

Figure 10-5

DRIFTS
EFFECT OF FLOOR LOWERING AND ADJACENT EXCAVATIONS
ON CLOSURE AT E140/S1246

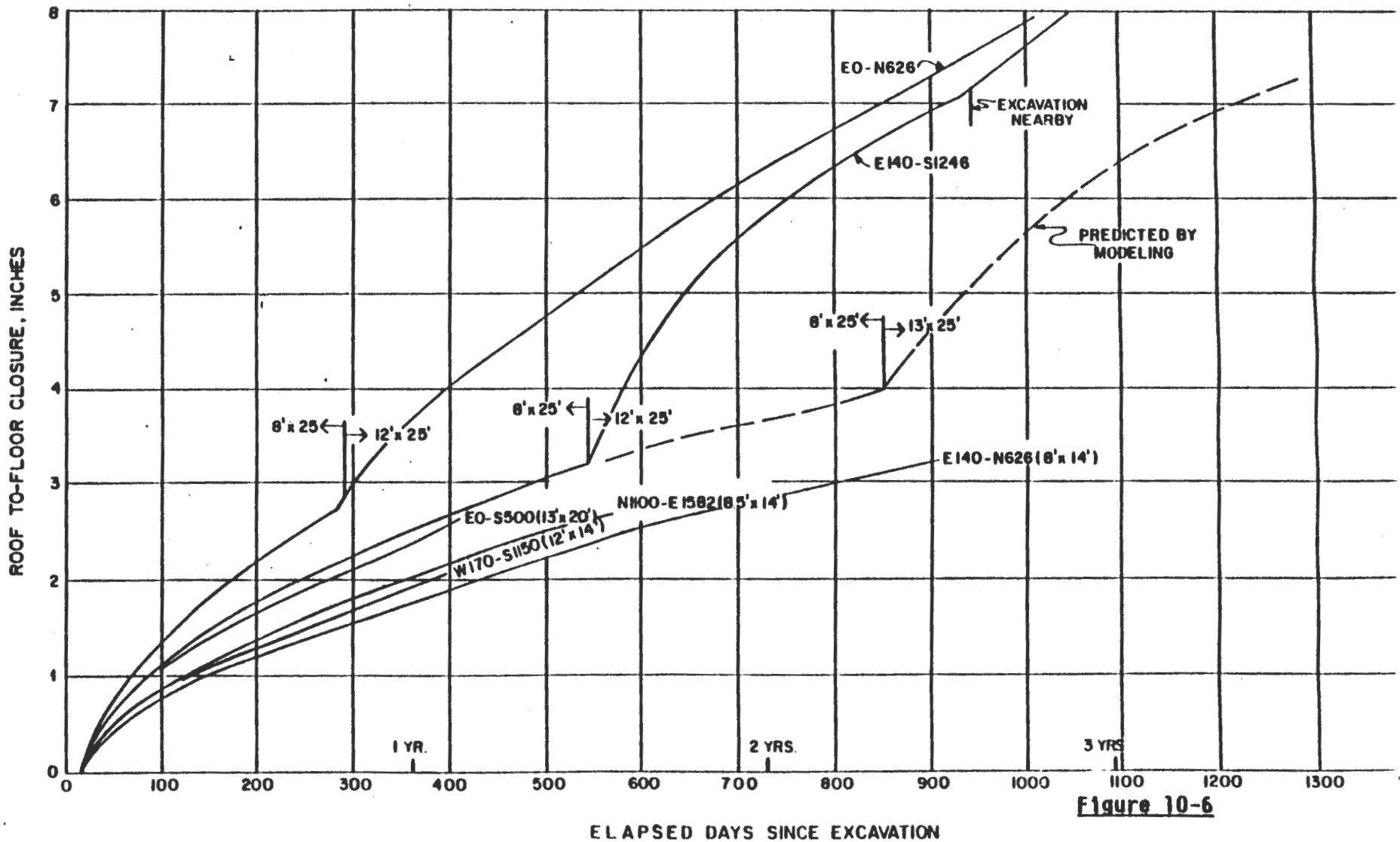


Figure 10-6

DRIFTS
COMPARISON OF ROOF-TO-FLOOR CLOSURE IN DRIFTS
DIFFERENT DIMENSIONS

drifts in the storage area will have cross section dimensions of 13 x 25 feet, the modeling analysis discussed in this chapter and in Chapter 12 focuses on predicting the behavior of the 13 x 25-foot drift opening for the operating life of 25 years.

The effect of lowering the floor 4 feet at instrument stations E0/N626 and E140/S1246 is to increase the closure rate permanently. Although the floor lowering was performed at different times at these stations, the steady state rate after excavation appears to be nearly the same. However, if the floor lowering is performed at a much later date following the initial excavation, it is likely that the total closure may be somewhat decreased. The closure behavior at these two stations is influenced by the presence of nearby parallel drifts and crosscuts, as well as likely differences in the creep properties of the salt.

Figure 10-6 also shows the predicted roof-to-floor closure of an infinitely long, single drift with cross section dimensions of 13 x 25 feet. This closure was obtained by modeling and is discussed in Chapter 12. The approximate steady state closure rate at E0/N626 and E140/S1246 is 2.00 inches/year. The steady state closure rate predicted for the infinitely long, single drift is 1.60 inches/year. The nearly 25 percent difference in these rates is probably due to the presence of adjacent drifts and crosscuts. This value compares well with the value of 30 percent obtained from modeling as discussed in subsection 10.3.3.3.

Figure 10-7 presents a comparison of the predicted closure of a 13 x 25-foot drift with the observed behavior of a 12 x 25-foot drift at E0/N626. The closure for the 13 x 25-foot drift was obtained by increasing the closure rate obtained from modeling the infinitely long, single drift by 30 percent. The roof-to-floor closure at E0/N626 does not include the values before the floor was lowered by 4 feet. This comparison indicates that it is reasonable to increase the closure rate of a single, infinitely long, 13 x 25-foot drift by 30 percent to account for the presence of adjacent parallel drifts and crosscuts.

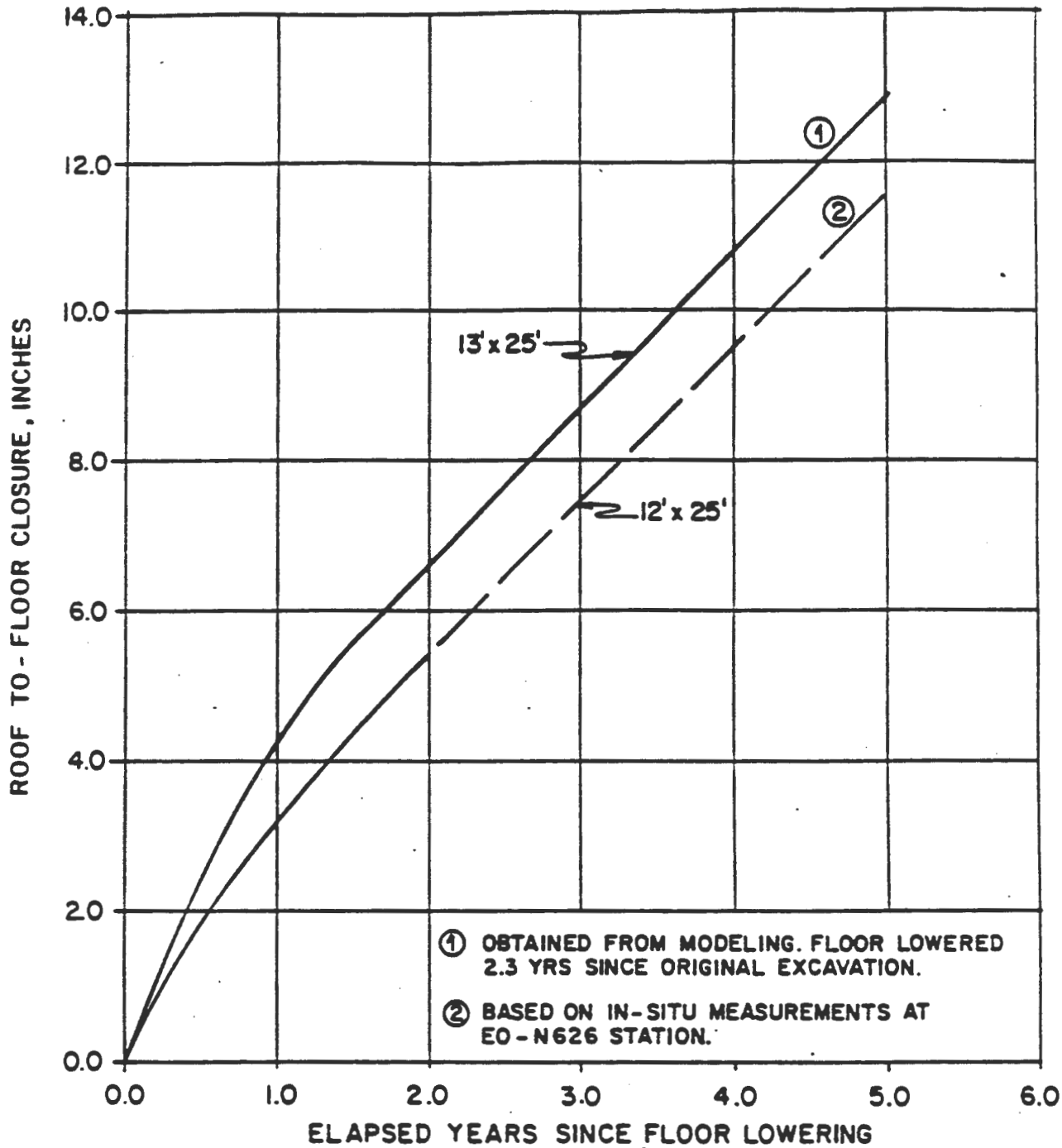


Figure 10-7

DRIFTS
COMPARISON OF PREDICTED AND OBSERVED
ROOF-TO-FLOOR CLOSURE

Wall-to-Wall Closure. The wall-to-wall convergence points at the S1246 station were installed immediately after the original excavation at this location was completed. When the cross section dimensions were 8 x 25 feet, the measurements were close to the true wall-to-wall closure at midheight of the instrument location. On June 30, 1984, the wall-to-wall closure was 5 inches for an elapsed time period of 564 days. After the floor was lowered, a new set of wall-to-wall convergence points was installed. The additional wall-to-wall closure was 3.31 inches through August 26, 1985.

Comparison of Roof-to-Floor to Wall-to-Wall Closures. Table 10-4 summarizes the closure of the E140 drift for locations south of S1620. Until August 1985, these locations were unique in that there were no crosscuts and no nearby parallel drifts at the time of the analysis. The cross section dimension was 8 x 25 feet. The maximum measured roof-to-floor closure of 5.19 inches was at station S1879. Stations S3614, S3639 and S3664 are influenced by the end constraints of the drift which terminates at about S3664.

Effect of Adjacent Drifts. Table 10-5 compares closure in the drifts at S1150. Because the initial readings were not taken immediately after the station location was excavated, the comparison is approximate. Note that, for the E140/S1150 station, the original cross section dimensions were 8 x 25 feet until June 8, 1984, and that no convergence points existed at this location prior to lowering the floor. The closure values at E140/S1150 are the maximum, not only because the opening dimensions are the largest, but also because the opening had already existed for nearly 550 days before the floor was lowered 4 feet. It is also likely that there is mutual influence between the openings.

Effect of Floor Lowering. The E0 drift between N140 and N1420 was increased in height from 8 feet to 12 feet (by lowering the floor) from November 9, 1983, through January 9, 1984. The closure readings increased rapidly as excavation approached the measurement stations but

Table 10-4

E140 DRIFT SOUTH OF S1620
SUMMARY OF MEASURED CLOSURE
(CROSS SECTION DIMENSIONS = 8 x 25 feet)

| Instrument Location | Time-lag between end of excavation and initial reading (days) | | Convergence point reading (inches) Feb. 12, 1985 | |
|---|---|---|---|---|
| | R-T-F* | W-T-W* | R-T-F* | W-T-W* |
| E140/S3664 | 14 | 0 | 1.70 | 1.48 |
| E140/S3639 | 0 | 0 | 4.07 | 3.24 |
| E140/S3614 | 0 | 0 | 4.49 | 3.72 |
| E140/S3250 | 11 | 11 | 4.13 | 2.97 |
| E140/S2950 | 10 | 10 | 4.19 | 3.18 |
| E140/S2625 | 6 | 6 | 4.43 | 3.59 |
| E140/S2350 | 9 | 9 | 4.33 | 3.44 |
| E140/S2066 | 8 | 8 | 4.32 | 3.40 |
| E140/S1879 | 4 | 2 | 5.46 | 4.00 |

* R-T-F = roof-to-floor
W-T-W = wall-to-wall

## Table 10-5

## COMPARISONS OF CLOSURE IN DRIFTS AT S1150

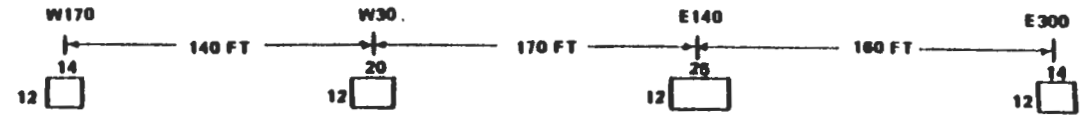


| | W170 | W30 | E140 | E300 |
|---|---|---|---|---|
| INSTRUMENT LOCATION | W170/S1150 | W30/S1141 | E140/S1150 | E300/S1150 |
| DATE OF EXCAVATION | AUGUST 21, 1984 | AUGUST 21, 1984 | JUNE 8, 1984* | JULY 23, 1984 |
| DATE OF INITIAL READING | | | | |
| CENTRAL ROOF-TO-FLOOR | AUGUST 23, 1984 | AUGUST 22, 1984 | JUNE 14, 1984 | JULY 26, 1984 |
| CENTRAL WALL-TO-WALL | AUGUST 23, 1984 | AUGUST 22, 1984 | JUNE 14, 1984 | JULY 26, 1984 |
| DATE OF LATEST READING FOR BOTH ROOF-TO-FLOOR AND WALL-TO-WALL CONVERGENCE POINTS | SEP. 16,1985 | SEP. 16, 1985 | AUG. 26, 1985 | SEP. 30, 1985 |
| CLOSURE (IN) | | | | |
| CENTRAL ROOF-TO-FLOOR | 2.46 | 3.10 | 3.61 | 2.18 |
| CENTRAL WALL-TO-WALL | 2.62 | 2.76 | 3.03 | 2.36 |

* FLOOR LOWERED BY 4 FT ON JUNE 8, 1984. DIMENSIONS WERE 8 FT X 25 FT BEFORE JUNE 8, 1984. CROSS DRIFTS S1100 AND S1300 EXCAVATED IN AUGUST, 1985.

dropped rapidly to, or slightly above, the pre-excavation rate. The floor lowering has affected the salt material above the roof of the openings to distances of at least 30 feet.

Figure 10-8 shows the relationship of the movement rates for the collar and two intermediate anchors of roof extensometer 51X-GE-00243 at the E0/N1100 intersection. The figure shows that the movement rate of the collar and these anchors increased due to floor lowering but then began decreasing until March 1984 (about 400 days after the initial excavation). The rate then began increasing again from March until August 1984 (about 550 days after the initial excavation). Because excavation activities were performed in the area of this instrument at this time, it is possible that parting at the clay seams above the roof was occurring at an increasing rate.

Figure 10-9 shows the movement rates of the collar and anchors of roof and wall extensometers at E0/N626. The collar movement rate of the east wall extensometer appears to be somewhat less than that of the west wall extensometer. It was also observed that floor lowering has affected the closure behavior of pillars as far as 25 feet from the opening. Similarly, roof behavior has been affected, probably up to at least 30 feet above the roof.

The height of the E140 drift remained at 8 feet during floor lowering in the E0 drift between N140 and N1420. However, excavation performed in the E0 drift appears to have affected the closure behavior of the E140 drift. Figure 10-10 shows the movement rates of the collar and anchor A for roof extensometer 51X-GE-00235 at E140/N624. The collar movement rate was decreasing monotonically until late December 1983. However, it appears to have increased around January 1984. Assuming the instrument was functioning properly and there was no anomalous behavior of clay seams in the roof of the E140 drift, excavation in the E0 drift may have influenced salt behavior as much as 150 feet from the E0 drift.

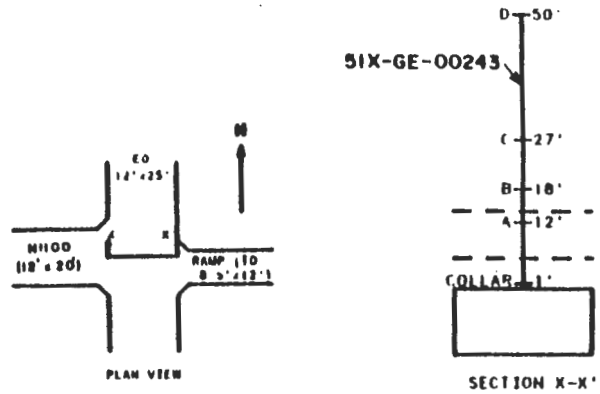


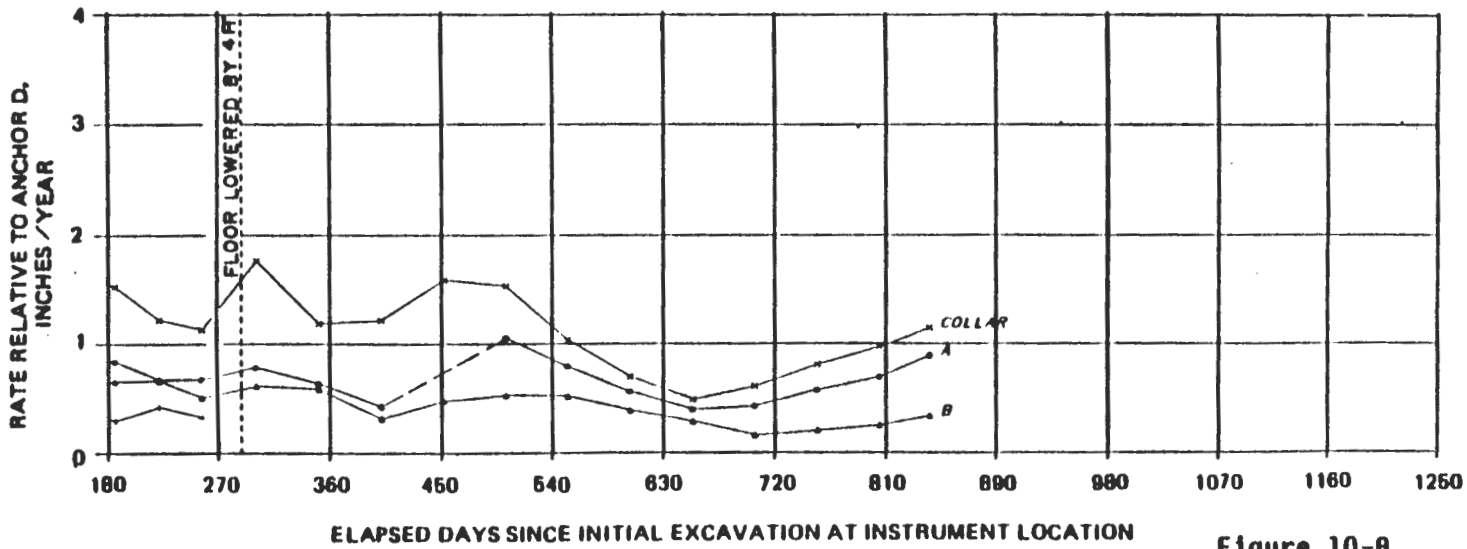


**Figure 10-8**

DRIFTS
EFFECT OF FLOOR LOWERING ON ROOF BEHAVIOR
AT EO/N1100 INTERSECTION

NOTE: RATE CALCULATED FOR MINIMUM INTERVALS OF 30 DAYS.

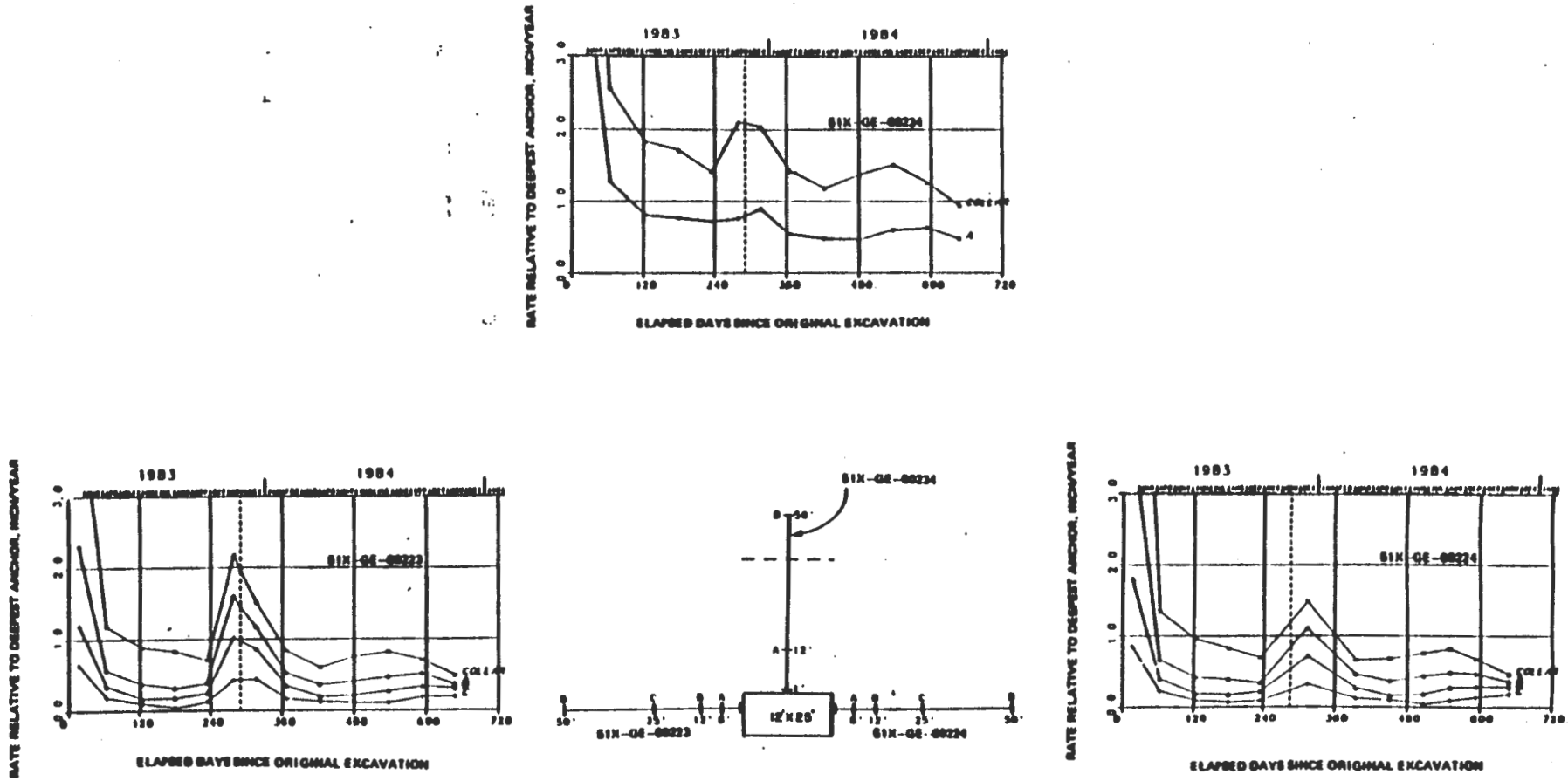


NOTE:
VERTICAL DASHED LINE INDICATES TIME WHEN THE FLOOR WAS EXCAVATED FOUR FEET.

**Figure 10-9**

**DRIFTS**
**EFFECT OF FLOOR LOWERING ON CLOSURE AT EO/N626**

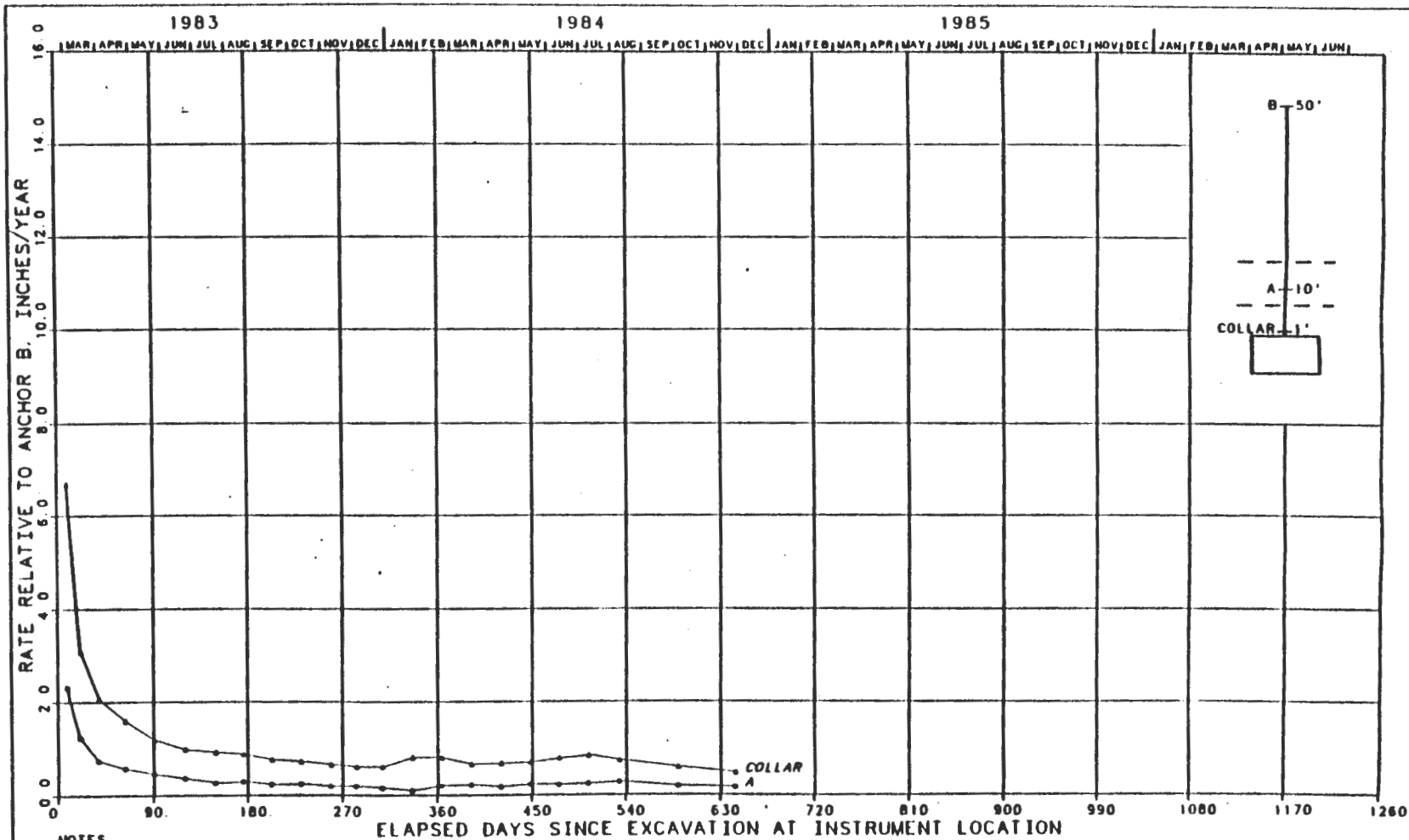


NOTES
1 RATE CALCULATED FOR MINIMUM INTERVALS OF 7 DAYS
2 SIZE OF EXCAVATION 8 FT X 14 FT

**Figure 10-10**

**DRIFTS**
**EFFECT OF FLOOR LOWERING ON CLOSURE AT E140/N624**

Observations of the effect of floor lowering on closure behavior are summarized below:

(1) The closure reading at an instrument station increases rapidly as floor excavation approaches the station and decreases rapidly to, or slightly above, the pre-excavation closure rate as excavation passes the instrument station.

(2) Floor lowering affects creep behavior of the salt above the roof of the openings to depths of at least 30 feet. This effect is short-lived, however, extending over a period of only a few months.

(3) Although the floor of the E140 drift north of the C & SH shaft was not lowered for most of its length, excavation performed in the E0 drift appears to have affected the E140 drift closure.

The movement rates of the anchors of extensometer 51X-GE-00243 at the E0/N1100 intersection increased and then decreased between March and August 1984. Because no excavation activity took place at this time in the vicinity of the instrument station, it was assumed that the clay seams above the roof may have been parting at an increasing rate. Figure 10-8 shows the variation in closure rates for the collar and anchor points with time. The rates of the collar and anchor movements have subsided and are probably returning to their pre-perturbation values. For comparison, the rates of collar and anchor movements of floor extensometer 51X-GE-00258 are shown on Figure 10-11. The rates of movements of the collar and intermediate anchors have a similar trend as the roof extensometer over the same time period. However, this extensometer was damaged due to mining operations on February 8, 1985. Since then, the readings have remained anomalous.

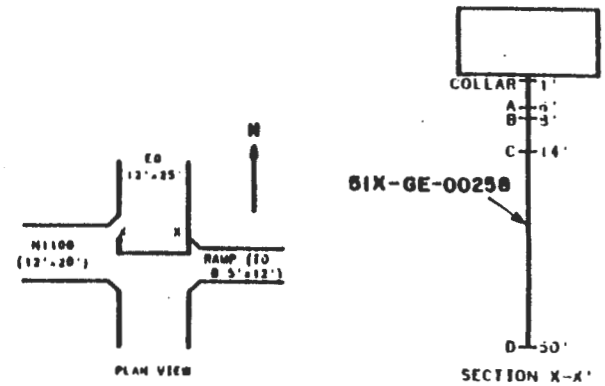


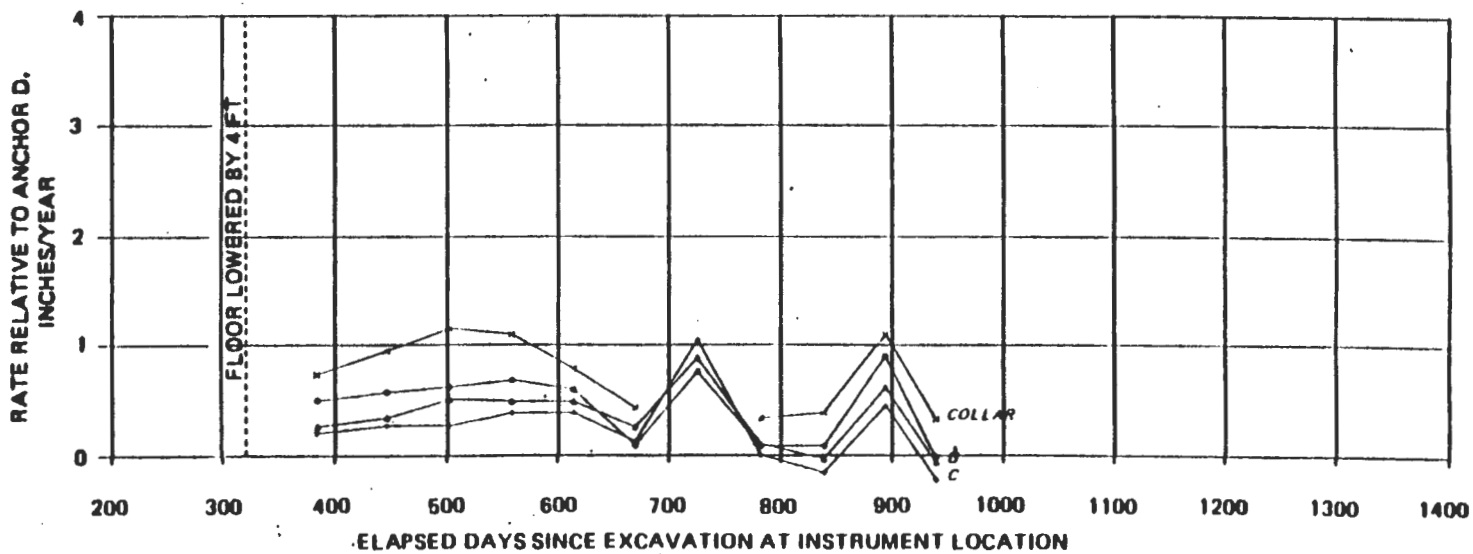


NOTE: RATE CALCULATED FOR MINIMUM INTERVALS OF 30 DAYS.

Figure 10-11

DRIFTS
RATE OF FLOOR HEAVE AT EO/N1100

### 10.3.2.3 Model Simulation

A finite element model utilizing an engineering approach was used to simulate the behavior of an 8 x 25-foot drift. The method described in Appendix C was used to mathematically simulate the in situ behavior of the drifts by determining the creep parameters C, A, and z. The following discussion describes the numerical modeling and the utilization of in situ data for the drifts. Also discussed are simulations of the effect of adjacent parallel and perpendicular drifts.

Utilization of Reference Stratigraphy. The reference stratigraphy described in Chapter 6 was used in the analysis. The reference level representing the elevation of clay G is 2,129.40 feet below the ground surface, based on the core hole log at station E140/S1960. Because the finite element method lends itself well to multiple layer analysis in which distinct material properties can be accounted for, the MARC General Purpose Finite Element Program (ref. 6-8) was used.

Structural Characterization. Figure 10-12 shows the finite element model used to predict closures, stresses and deformed shapes as a function of time for an 8 x 25-foot opening. The model consists of 122 plane strain elements with 21 gap/friction link elements modeling the clay seams and an option for lowering the floor 5 feet. The top and bottom boundaries of the model are at depths of 2,045.00 feet and 2,245.00 feet, respectively, below the ground surface. The drift roof, drift floor before lowering, and drift floor after lowering are at depths of 2,128.70, 2,136.70, and 2,141.70 feet, respectively, below the ground surface. The roof beam is 8.10 feet thick and the final floor level is 4.39 feet above MB-139.

Only anhydrite layers with thicknesses greater than 1 foot were included in the model. Calculations showed that most anhydrite layers less than 1 foot thick failed at vertical stresses less than 1 percent of the overburden pressure. Therefore, because their contribution to the stiffness of the model would be insignificant, they were not included.

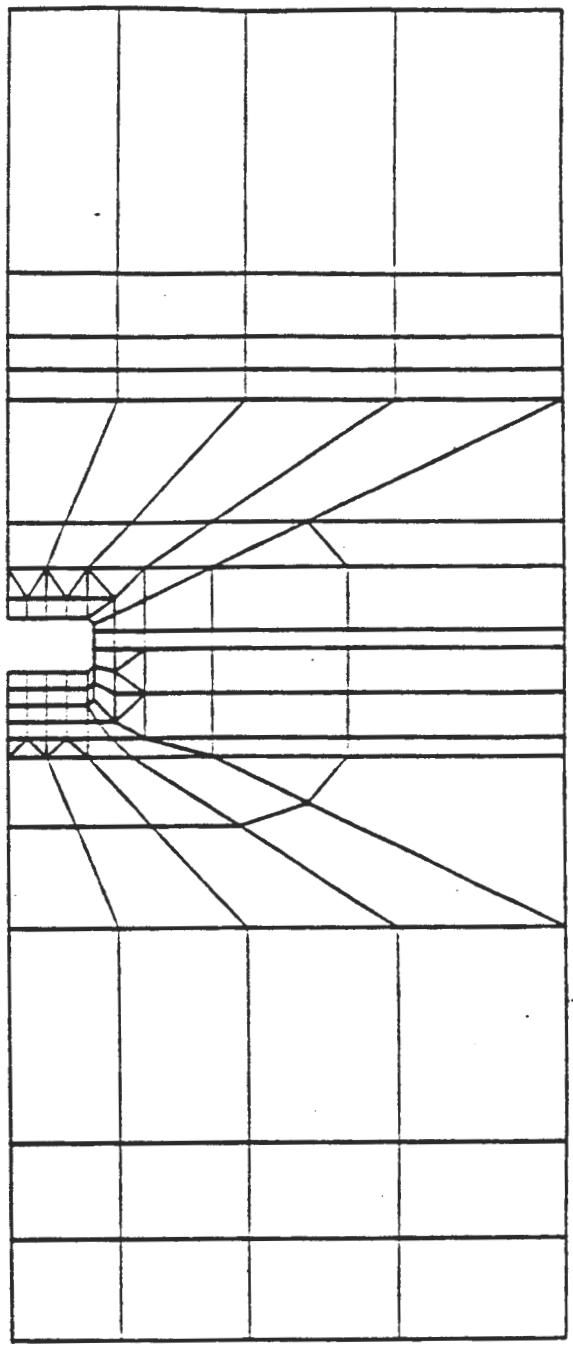

Figure 10-12

DRIFTS
FINITE ELEMENT MODEL - BEFORE FLOOR LOWERING

Clay seams in the model were limited to two above and two below the drift opening. The justification for this is twofold: first, reference 5-4 states that "90 percent of the drift closure measured with ten active slidelines could be captured with four slidelines, two directly above and two directly below the drift"; second, previous analyses have shown that, at locations representative of the more distant clay seams, the shear force is considerably less than the normal force; therefore, any slippage along these clay seams would be negligible compared to that along seams closer to the opening and they need not be included in the model. To simplify the analysis of this model, a coefficient of friction equal to 0.0 was assumed for the gap/friction elements modeling the clay seams.

The lateral boundaries of the model are 82 feet apart and were established based upon vertical axes of symmetry with regard to adjacent drifts. The upper and lower boundaries of the model were based upon experience from previous analyses and were extended far enough in both directions so that the difference between vertical and horizontal stresses at each point of the boundaries would be within 10 percent of the vertical stresses. Horizontal restraints were assumed for the lateral boundaries while vertical restraints were assumed for the lower boundary of the model. Stress boundary conditions were utilized for the upper boundary.

Element sizes were established to make them proportional in size to the estimated stress gradient across each element. In addition, the orientations of the elements were established in order to have the radiating mesh coincide with the assumed principal stress axes. These aspects of the model were designed to enhance the overall efficiency of the analysis.

<u>Consideration of Drift Opening</u>. The drift openings were originally excavated to 8 x 25 feet. Further development trimmed an additional 4 feet from the floor to provide a 12 x 25-foot opening in the shaft pillar area. To provide continuous response histories from initial

excavation through the floor lowering period, special considerations were provided for modeling the opening.

Determination of Creep Parameters. Data from ten different locations along the E140 drift from S550 to S3250 were reviewed and one representative location was selected to calculate creep parameters for the drifts and for use in predicting closures and stress distributions.

Figure 10-13 shows the correlated roof-to-floor and wall-to-wall in situ data curves from the selected location, as well as the predicted closure based on the calculated creep parameters.

Transformation of Time Domains. Having determined the values of C, A and z to be $1.40 \times 10^{-21}$ $ksf^{-4.9}$ $sec^{-1}$, 3.2 and $1.1 \times 10^{-7}$ $sec^{-1}$, respectively, the normalized time at which the floor lowering was scheduled to take place was determined by transforming $7.25 \times 10^{7}$ sec (or 2.3 years) to normalized time using equation C.4-17 in Appendix C.

The normalized time which corresponds to the scheduled real time for drift floor lowering was determined to be $1.4205 \times 10^{-13}$ $ksf^{-4.9}$ or 418 time increments from the start of the program. Accordingly, the drift height was changed at the end of increment 418, and the analysis continued until a total real time of approximately 5 years was reached.

Effect of Parallel Drifts. The extraction ratio at a particular location is dependent upon the arrangement of the drifts and pillars. Therefore, the effect that the extraction ratio has on structural responses can be determined by considering the effect of adjacent drifts. Two different cases were considered in the analysis. One case assumes the adjacent drifts are parallel to the drift being analyzed while the other case assumes adjacent drifts are perpendicular to the drift being analyzed.

To simplify and minimize the computational effort, a multiple drift model was used for the analysis of the 8 x 25-foot drift. For this

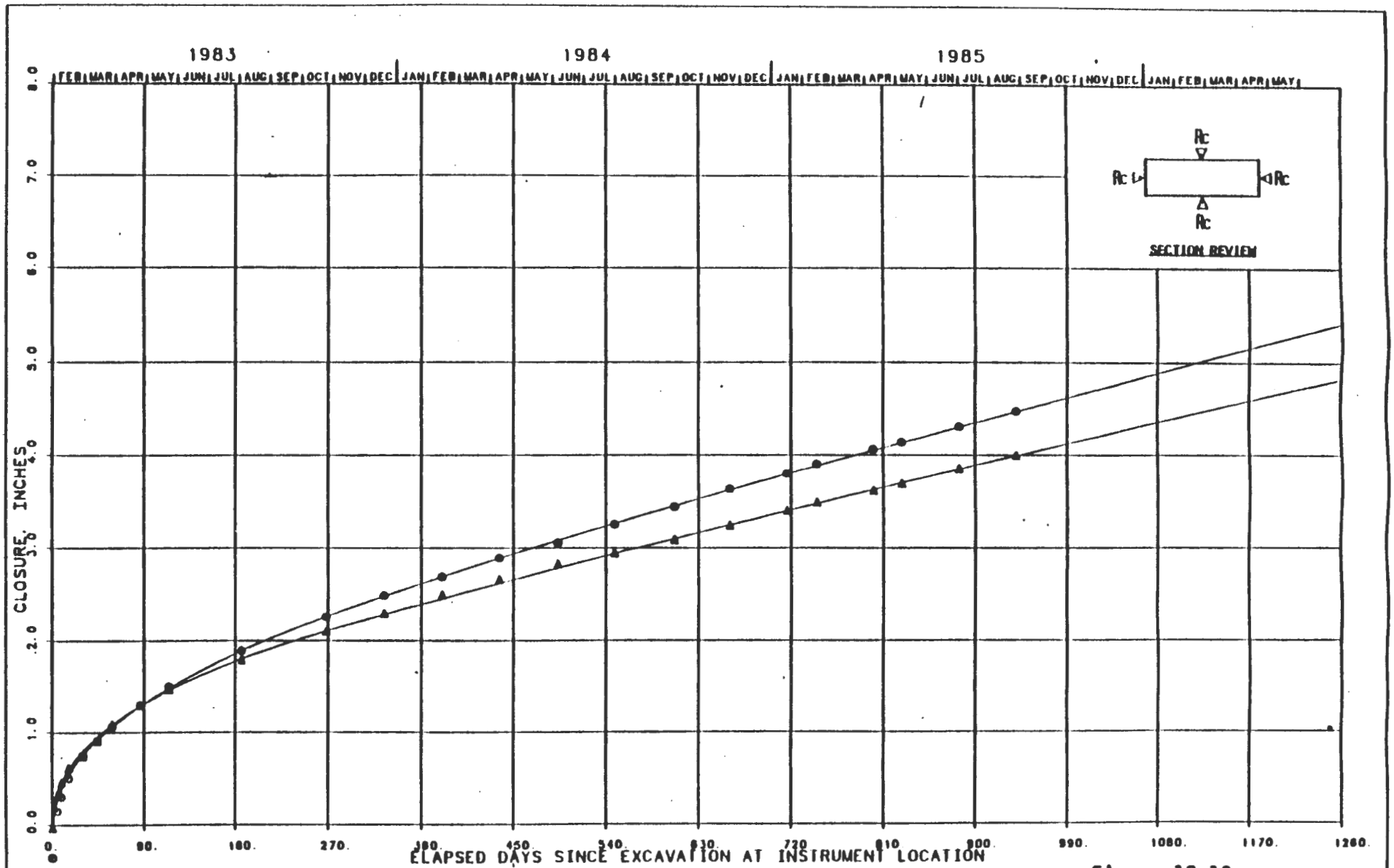


Figure 10-13

DRIFTS
CORRELATED CLOSURE HISTORIES

model, the drift was assumed to be located between an infinite number of parallel drifts, with each having identical cross sections and pillar widths. Two-dimensional analyses using this model were performed assuming a state of plane strain. The boundary displacement conditions at the centerline of the pillar were assumed to be restrained in the horizontal direction but free in the vertical direction. Under these assumptions, this mathematical model can more accurately simulate the geologic conditions in the future when adjacent drifts will exist rather than at the present time when only a single drift exists. Computational results for the parallel drifts are presented in subsection 10.3.3. Parallel drifts with different dimensions and spacings can be incorporated into the present mathematical model and corresponding structural responses can be computed.

Effect of Perpendicular Drifts. Ideally, a three-dimensional analysis is required for the case when the drifts are not parallel to each other. However, the structural responses can be approximated based on the two-dimensional analysis described in this section.

Additional drifts which intersect perpendicular to the drift in question increase the average overburden pressure in the pillar. The two-dimensional analysis of parallel drifts has indicated that the vertical stresses initially increase sharply in the pillar area adjacent to the opening. Over time, salt creep reduces this stress peak as the stresses are redistributed over the width of the pillar. Eventually, the vertical stress level becomes nearly uniform over most of the pillar width.

The total overburden load in the pillar is equal to the average vertical stress multiplied by the pillar support area. Because this total overburden load remains constant before and after the excavation of perpendicular drifts, the average vertical pressure is inversely

proportional to the support area. This increased average vertical stress can, therefore, be expressed as:

$$\bar{\sigma}_r = \bar{\sigma}_i \, W_t/W_2 \qquad (10\text{-}2)$$

where: $\bar{\sigma}_r$ is the average vertical stress of a rectangular pillar, i.e., pillar within a gridwork of intersecting drifts;

$\bar{\sigma}_i$ is the average vertical stress of an infinitely long pillar, i.e., pillar without the perpendicular drifts;

$W_t$ is the distance between the center lines of the perpendicular drifts; and

$W_2$ is the pillar width in the perpendicular direction, i.e., $W_t$ minus the width of the perpendicular drift.

After the excavation of additional drifts in the perpendicular direction, the restraints at the new wall boundaries are released. Consequently, the distribution of effective stress in the pillar changes. Actual distribution of the effective stresses can be obtained through a three-dimensional computational analysis. However, a two-dimensional analysis can be used to estimate the stress distribution.

A two-dimensional analysis can neither model the restraint conditions nor predict out-of-plane displacements that occur at the boundary of the perpendicular drifts. As a result, the vertical stress distribution from the two-dimensional analysis is assumed to represent a plane some distance from the perpendicular drifts where the actual behavior more closely represents the plane strain condition. The accuracy of this assumption depends upon the distance between the plane being analyzed and the perpendicular drift. In all cases, the results of a two-dimensional analysis represent a lower bound on the effects of perpendicular drifts.

The pillar dimensions are identified as $W_1$ for the width of the pillar between parallel drifts and $W_2$ for the width of the pillar

between perpendicular drifts. For an infinitely long pillar, which can be considered as a rectangular pillar with $W_1/W_2$ equal to zero, the vertical stress distribution of the drift to the center of the pillar can be determined from a two-dimensional analysis. The distribution of the vertical stress $\sigma_i(y)$, shown at the top of Figure 10-14, is symmetrical with respect to the centerline of the pillar and stabilizes within several months after excavation.

For a square pillar, which can be considered as a special case of the rectangular pillar with $W_1/W_2$ equal to one, the vertical stress distribution should be symmetrical with respect to the two centerlines and two diagonals of the pillar. This is shown graphically in the middle of Figure 10-14, where the x-axis is assumed to be along the drift axis. Assuming the vertical stress distribution $\sigma_s(x,y)$ from the center of the pillar to any of the four walls is the same as the stress distribution $\sigma_i(y)$ across the width of the infinite pillar, the ratio of the average vertical stresses between the square and the infinite pillars can then be estimated from equation 10-3:

$$\frac{\bar{\sigma}_s}{\bar{\sigma}_i} = \frac{\int_0^{W/2} \int_{-x}^{+x} \sigma_s(x,y)\ dydx}{\int_0^{W/2} \int_0^{W/2} \sigma_i(y)\ dydx} \qquad (10\text{-}3)$$

where: $\bar{\sigma}_i$ is the average vertical stress for the infinitely long pillar;

$\bar{\sigma}_s$ is the average vertical stress for the square pillar;

$\sigma_i(y)$ is the vertical stress distribution for the infinitely long pillar; and

$\sigma_s(x,y)$ is the vertical stress distribution for the square pillar.

Based on the computational results from the previous analyses, the average vertical stress of a square pillar is estimated to be 15 percent higher than that for the infinitely long pillar. At the WIPP

facility level, most of the pillars have a rectangular shape. As shown at the bottom of Figure 10-14, a rectangular pillar can be separated into regions which are assumed to act either as an infinite or square pillar. By using a weighted area method, the following equation expresses the effect of varying the pillar's aspect ratio on the average vertical stress:

$$\bar{\sigma}_r = (1 + 0.15 \cdot \frac{W_1}{W_2})\ \bar{\sigma}_i \qquad (10\text{-}4)$$

where: $\bar{\sigma}_r$ is the average vertical stress for the rectangular pillar.

The corresponding change in pillar shortening is proportional to the ratio of $\bar{\sigma}_r$ to $\bar{\sigma}_i$, raised to some power, with an exponent not exceeding n, where n is the exponent in the power law expression for the creep behavior. Subsection 10.3.3.3 presents the results using equation 10-4.

10.3.2.4 Bay Strains

Strains around an opening in salt vary with space and time. Although, it is difficult to measure these strains directly, they can be inferred from the measurements of anchor displacements of multiple-point borehole extensometers. Relative movements between anchors will provide an approximate distribution of strain along the axis of the extensometer. If these relative displacements are normalized over the spacing between the anchors, then these normalized relative displacements are termed "bay strains". The bay strain will be closer to the true strain provided that the spacing between anchors is small and that the deformation varies linearly with spacing between anchors. Bay strains are useful in detecting any anomalous behavior in salt around an opening such as that influenced by discontinuities, clay seams, or the effect of local stress concentrations.

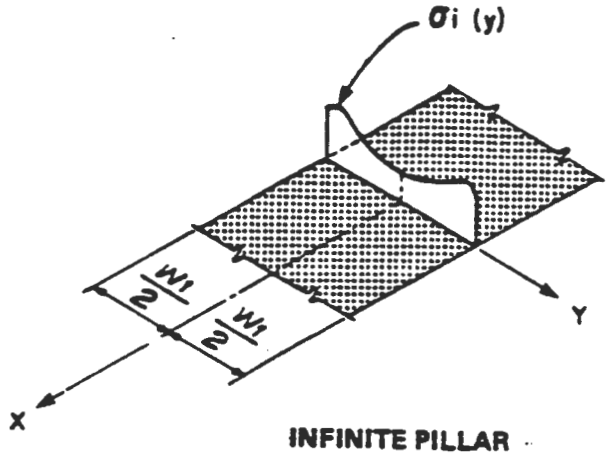


INFINITE PILLAR

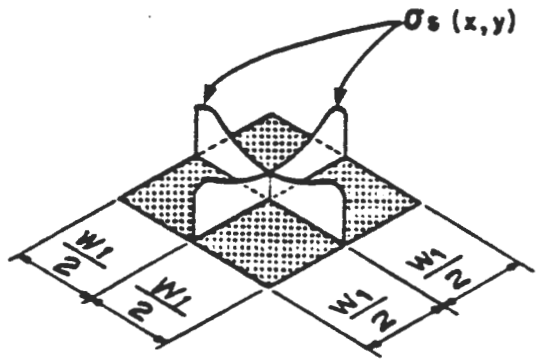


SQUARE PILLAR

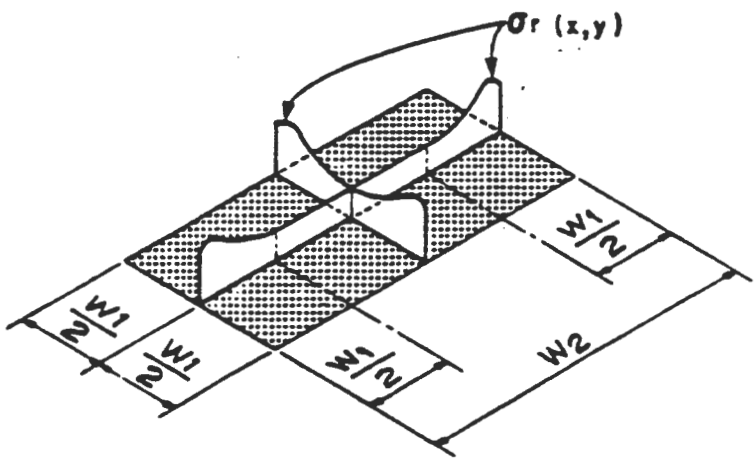


RECTANGULAR PILLAR

Figure 10-14

DRIFTS
VERTICAL STRESS DISTRIBUTIONS IN VARIOUS PILLARS

Figure 10-15 shows the variation of bay strains with elapsed time since completion of excavation for floor extensometer 51X-GE-00242. This extensometer is located at the intersection of Test Room 2 and the N1100 drift. The sudden increase in the bay strains may not be related to salt behavior and is apparently related to system measurement. Thus, it is likely that the maximum average bay strain in the first 6 feet of salt in the floor is no more than 1 percent. The analysis of bay strains in the floor of the drifts in other locations indicates that the maximum average bay strain generally occurs in the first 6 feet (collar to anchor A) in either the roof or the floor. Figures K-36 to K-45 in Appendix K show the variation of bay strains with elapsed time since excavation.

Figure 10-16 shows the rate of bay strains for extensometer 51X-GE-00242. The overall trend is that the rates decrease with time and are currently less than 0.5 percent/year. Figures K-46 to K-55 in Appendix K summarize the variation of strain rates with time.

The decreasing trend in the rates of bay strain with time is an indication that the salt in the roof and floor of the drifts is currently stable.

### 10.3.3 Prediction of Future Behavior

The results of the analysis of the 8 x 25-foot drift have been categorized as follows:

(1) Effective stresses and effective creep strains immediately after initial excavation; immediately before and after floor lowering; and 5 years after initial excavation.

(2) Principal stresses immediately after initial excavation; immediately before and after floor lowering; and 5 years after initial excavations.

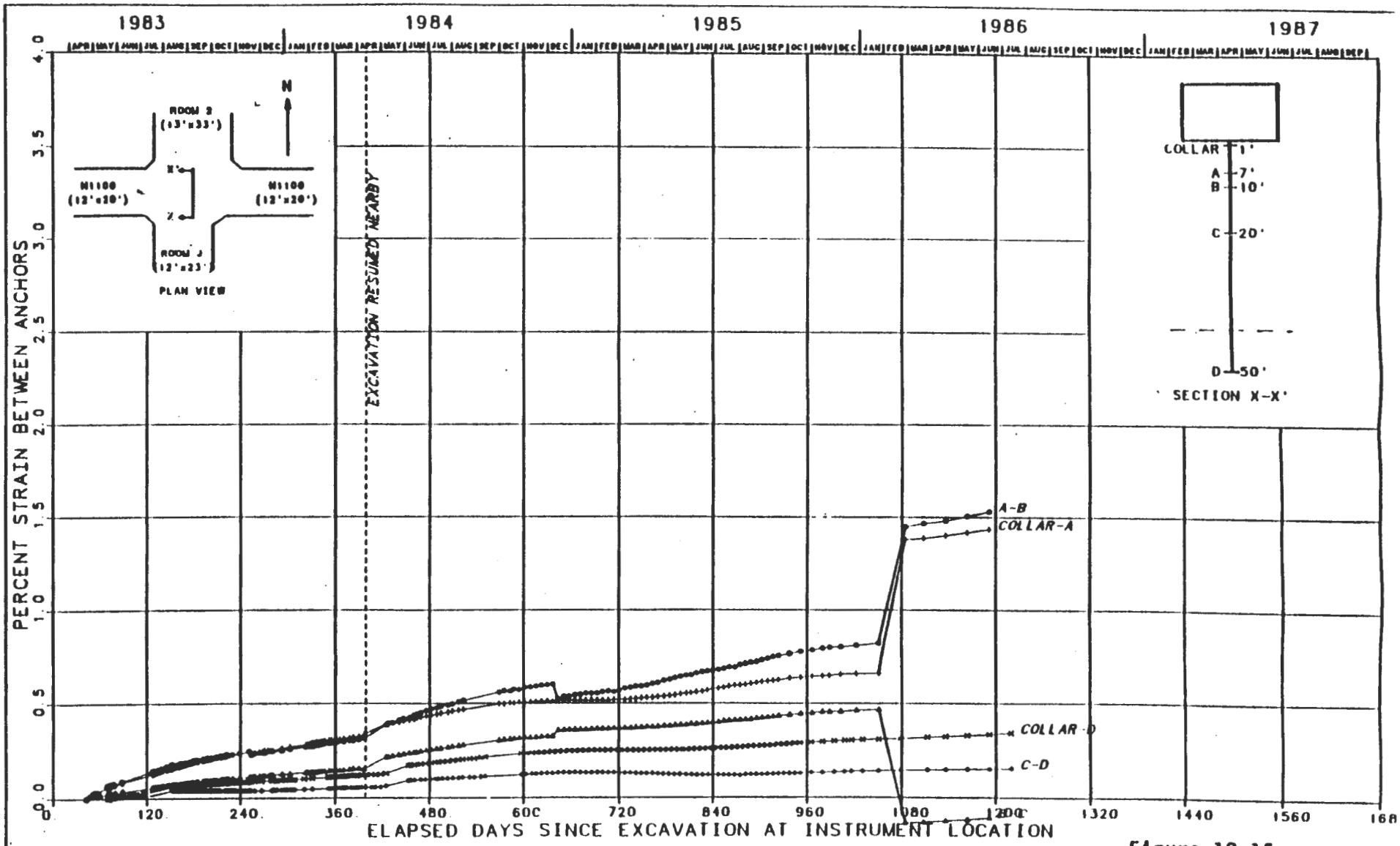


Figure 10-15

DRIFTS
STRAIN VERSUS TIME SINCE EXCAVATI(
N1100/TEST ROOM 2 INTERSECTION

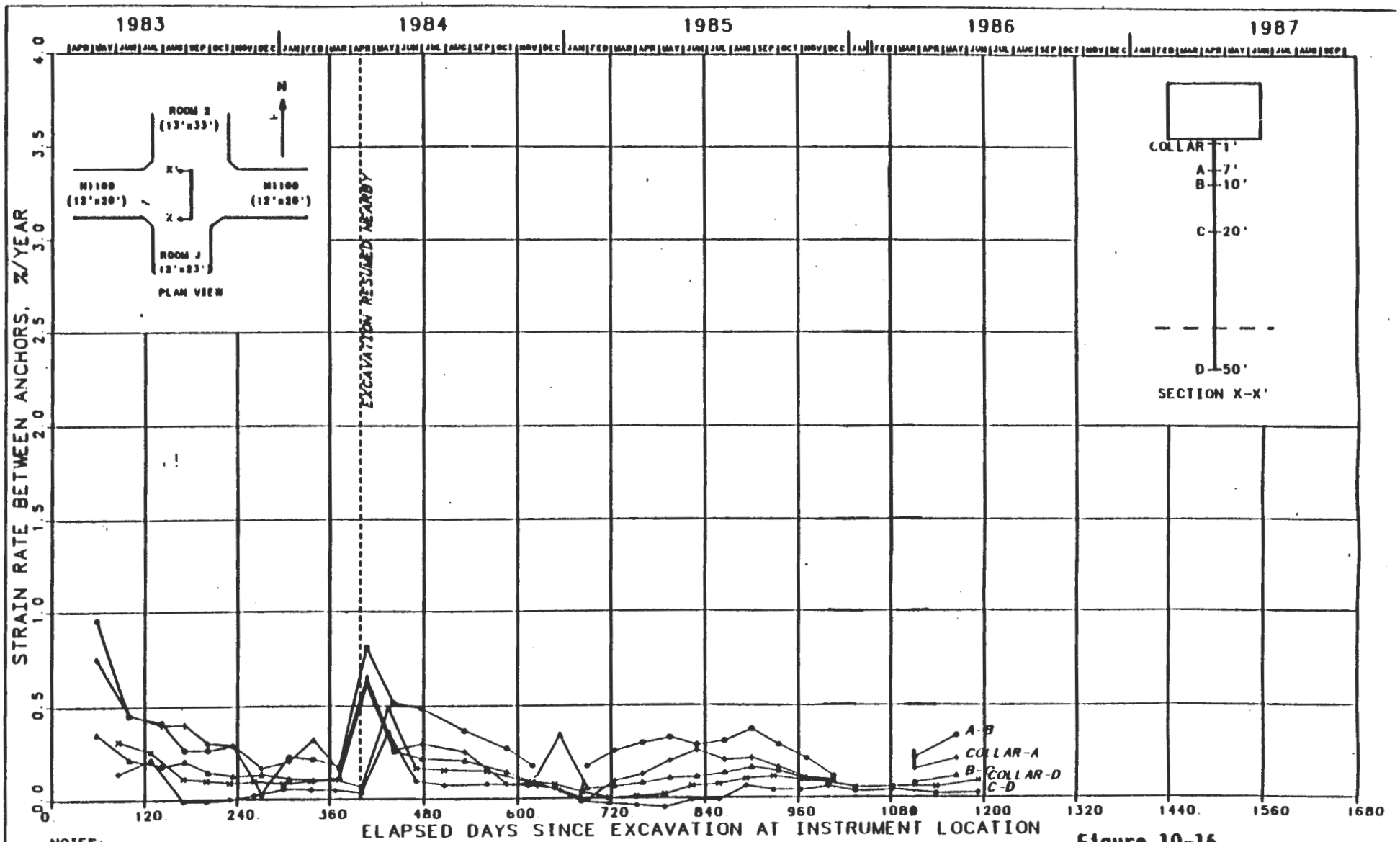


NOTES:
1. RATE CALCULATED FOR MINIMUM INTERVALS OF 30 DAYS

Figure 10-16

DRIFTS
STRAIN RATE VERSUS TIME SINCE EXCAVATION
N1100/TEST ROOM 2 INTERSECTION

(3) Deformed drift shapes immediately before floor lowering and 5 years after initial excavation.

10.3.3.1 Effective Stresses

Figures 10-17 and 10-18 show the distribution of effective stresses in each of the elements of the mesh located near the midheight of the finite element model. The contours are numbered with integers from 1 to 10 with each contour interval representing an effective stress increment of 100 ksf. As time passes, the plots show the effective stresses becoming more concentrated in the anhydrite layer. That is, more energy in the form of strain energy is transferred from the creeping halite and argillaceous halite layers to the anhydrite.

10.3.3.2 Principal Stresses

The principal stress plots (Figures 10-19 and 10-20) show that, immediately after excavation, the magnitudes of the predicted principal stresses are relatively large in the corners of the drift and in the anhydrite layer. As the salt creeps, the principal stresses concentrate in the anhydrite layer near the centerline of the drift.

10.3.3.3 Deformation and Closure

A mesh showing the deformed drift shape is presented on Figure 10-21. This mesh shows the outline of the original, undeformed drift in dashed lines while the deformed shape at the corresponding creep time is shown in solid lines.

The deformed shape immediately before floor lowering shows significant vertical deflection (downward) in the roof area of the drift. The drift floor has heaved upward only slightly and the walls have begun to creep inward.

Effects Due to Extraction Ratio. An analysis was performed to simulate the effect on the response of the drift due to a change in the extraction ratio. A change in the extraction ratio is caused by

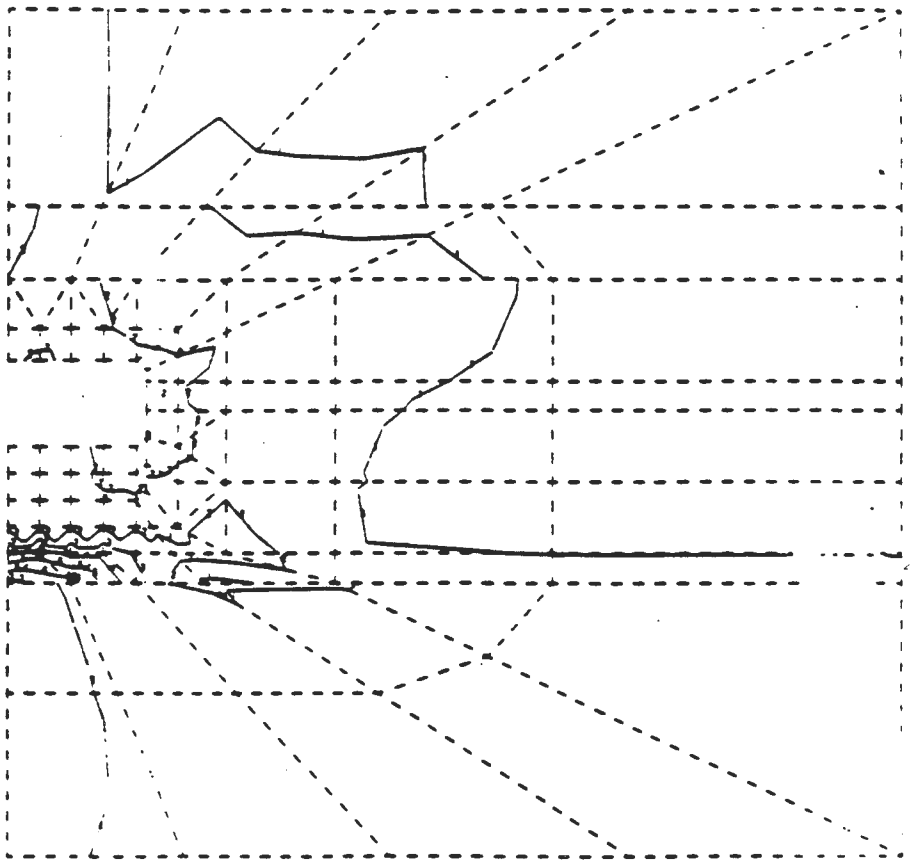

EXPLANATION OF CONTOUR LINES

1 = 100 KSF
2 = 200 KSF
3 = 300 KSF
4 = 400 KSF
5 = 500 KSF
6 = 600 KSF
7 = 700 KSF
8 = 800 KSF
9 = 900 KSF
10 = 1000 KSF

NOTE:
KSF = Kips per square foot.

Figure 10-17

DRIFTS
EFFECTIVE STRESS DISTRIBUTION IMMEDIATELY AFTER EXCAVATION

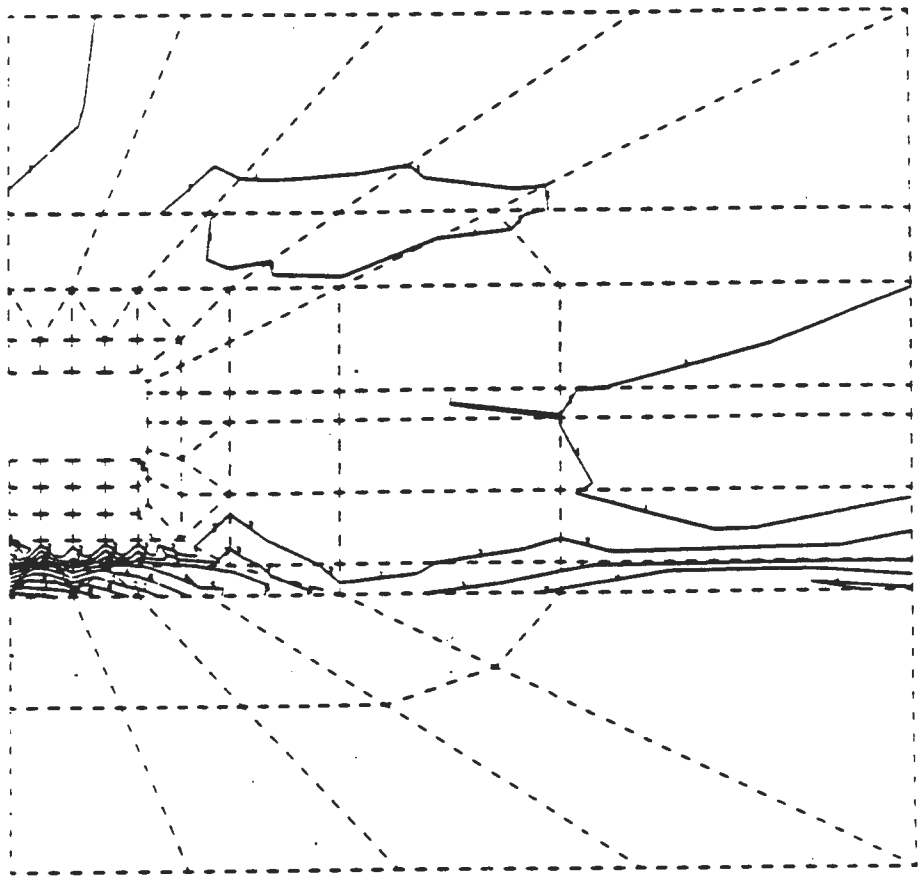

EXPLANATION OF CONTOUR LINES

1 = 100 KSF
2 = 200 KSF
3 = 300 KSF
4 = 400 KSF
5 = 500 KSF
6 = 600 KSF
7 = 700 KSF
8 = 800 KSF
9 = 900 KSF
10 = 1000 KSF

NOTE:
KSF = Kips per square foot.

Figure 10-18

DRIFTS
EFFECTIVE STRESS DISTRIBUTION IMMEDIATELY BEFORE FLOOR LOWERING

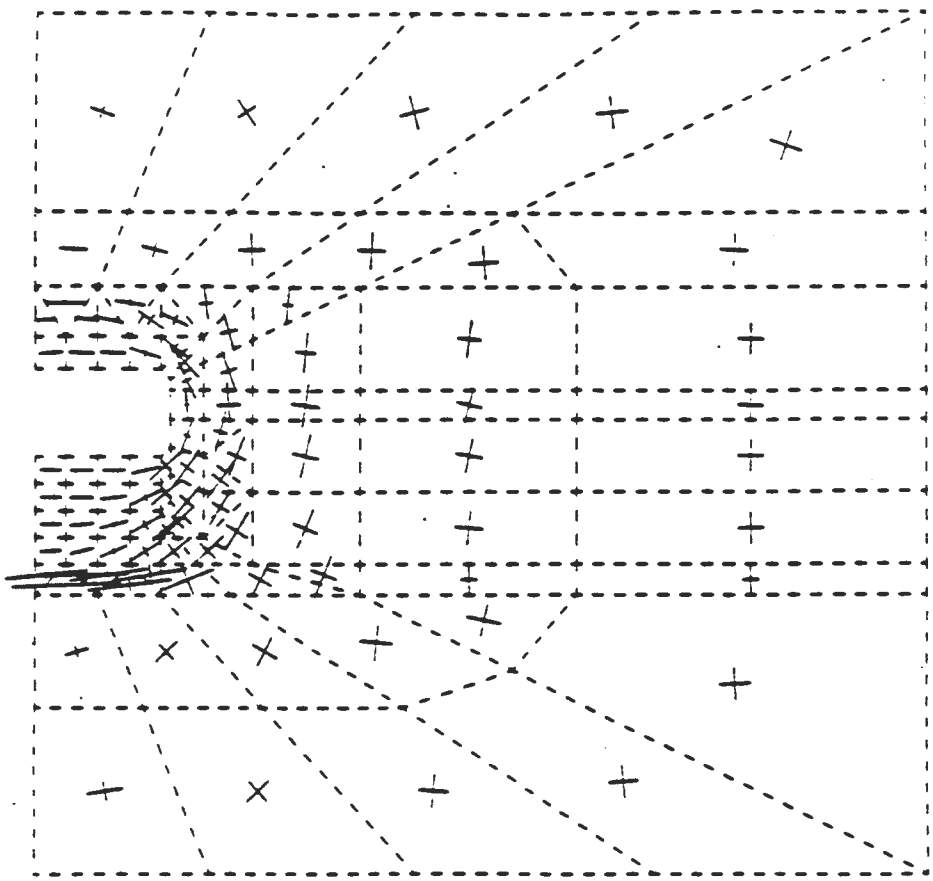

Figure 10-19

DRIFTS
PRINCIPAL STRESSES IMMEDIATELY AFTER EXCAVATION

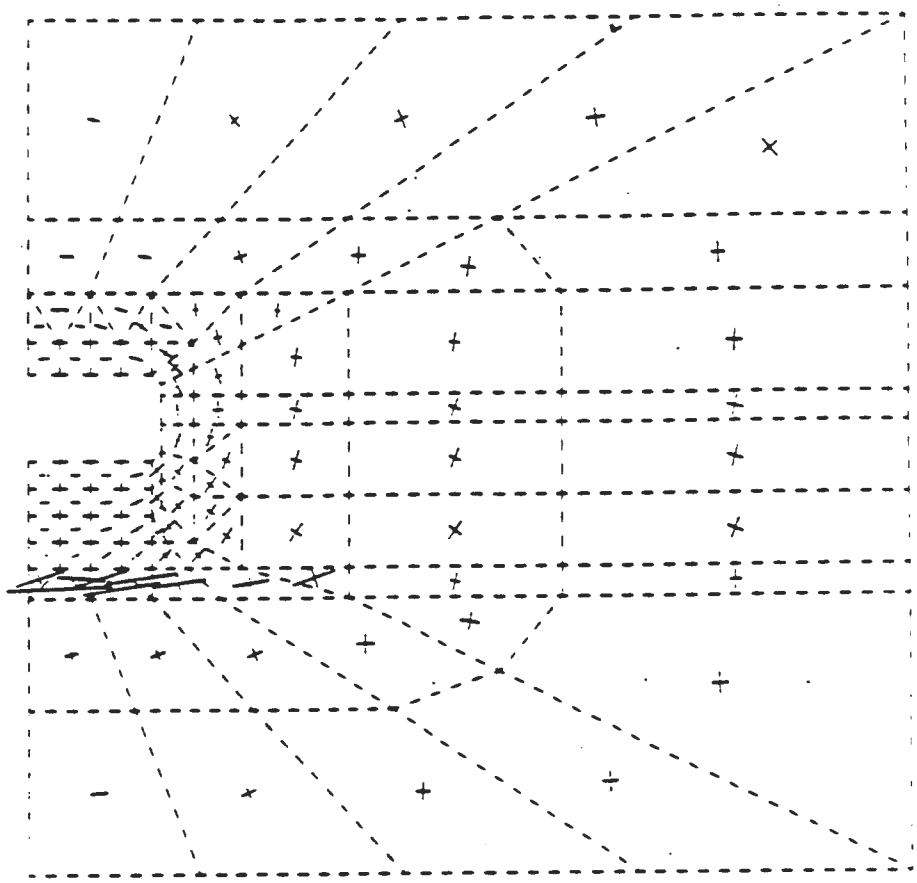

Figure 10-20

DRIFTS
PRINCIPAL STRESSES IMMEDIATELY BEFORE FLOOR LOWERING

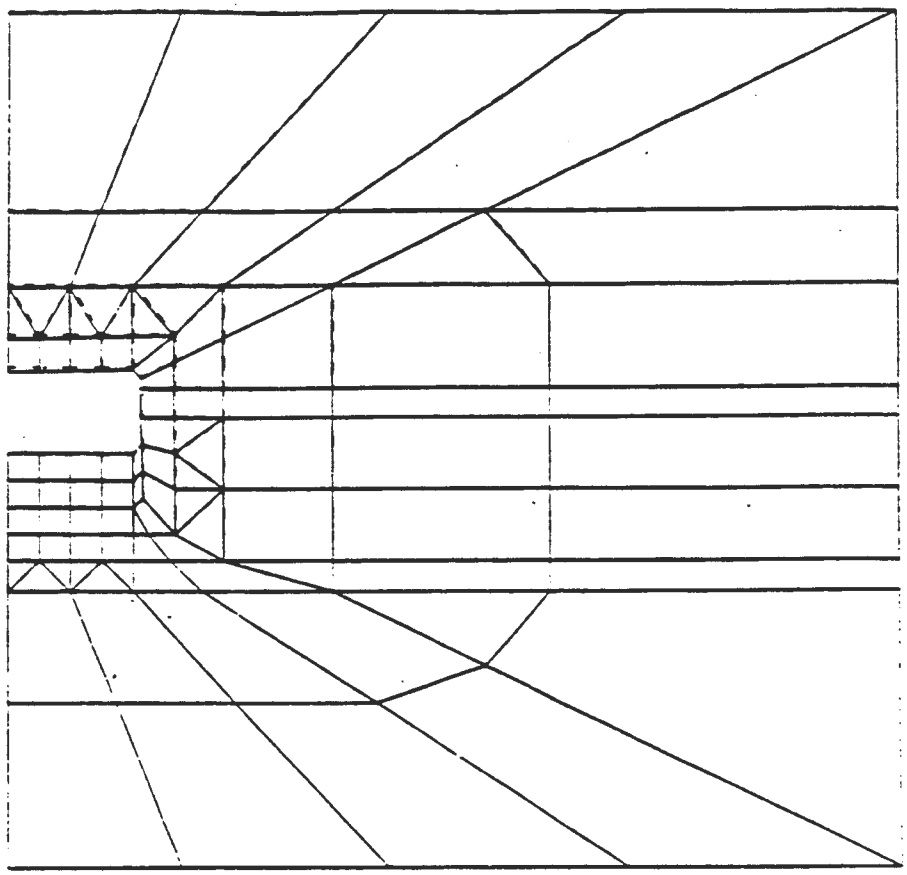

Figure 10-21

DRIFTS
DEFORMED SHAPE IMMEDIATELY BEFORE FLOOR LOWERING

excavation in adjacent or remote areas. The effect due to excavation in adjacent areas was simulated by modifying the finite element model used in the analysis. The difference is essentially a comparison of a single drift to a set of intersecting multiple drifts. Developing a single drift model which accurately represents the behavior of the infinite pillar requires assuming a width for the model. Therefore, to examine the effect of pillar width on analytical results, a 139-foot wide model similar to the one shown on Figure 10-12 was used as a base case and was later widened to 278 feet. Each model consists of an 8 x 25-foot drift.

Figures 10-22 and 10-23 show comparisons of the closure behavior for the two different pillar widths. Because the width of the model is expected to affect the vertical stresses, both the pillar shortening and roof sag components of closure are included. The top graph in both figures indicates that by halving the pillar width to that of the northern area spacing the roof-to-floor closure increases by about 15 percent.

The effects on pillar shortening due to increased overburden stress from the perpendicular drifts can be seen on the middle graph in Figure 10-22. Comparison of the infinite pillar with and without perpendicular drifts indicates a 15 percent increase in pillar shortening due to the presence of the intersecting drifts. Comparing the curves for the narrow pillar in the top two graphs indicates that pillar shortening contributes approximately half of the total closure response. The 15 percent increase in the pillar shortening then corresponds to a 7 1/2 percent contribution in total closure. This is also true for the total closure rate. The combined effects of single versus multiple drifts and multiple parallel drifts versus an intersecting gridwork account for about a 24 percent difference in the total closure rate.

The effects of releasing the boundary constraints at the perpendicular drift wall can be estimated by the use of equation 10-4. For the

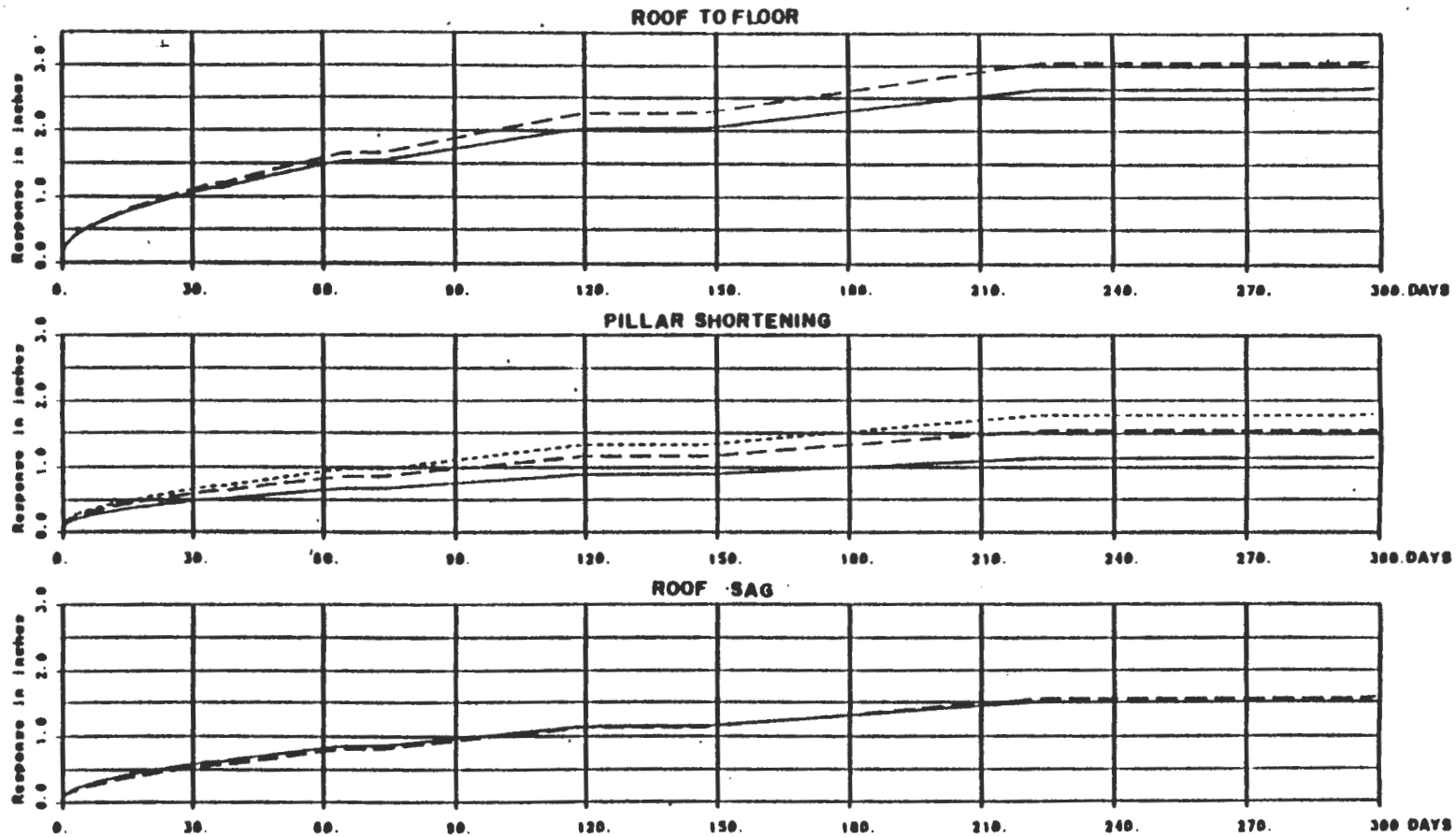


Wide Pillar
Narrow Pillar
Narrow Pillar with Perpendicular Drift

Figure 10-22

DRIFTS
COMPARISON OF CLOSURE COMPONENT RESPONSES

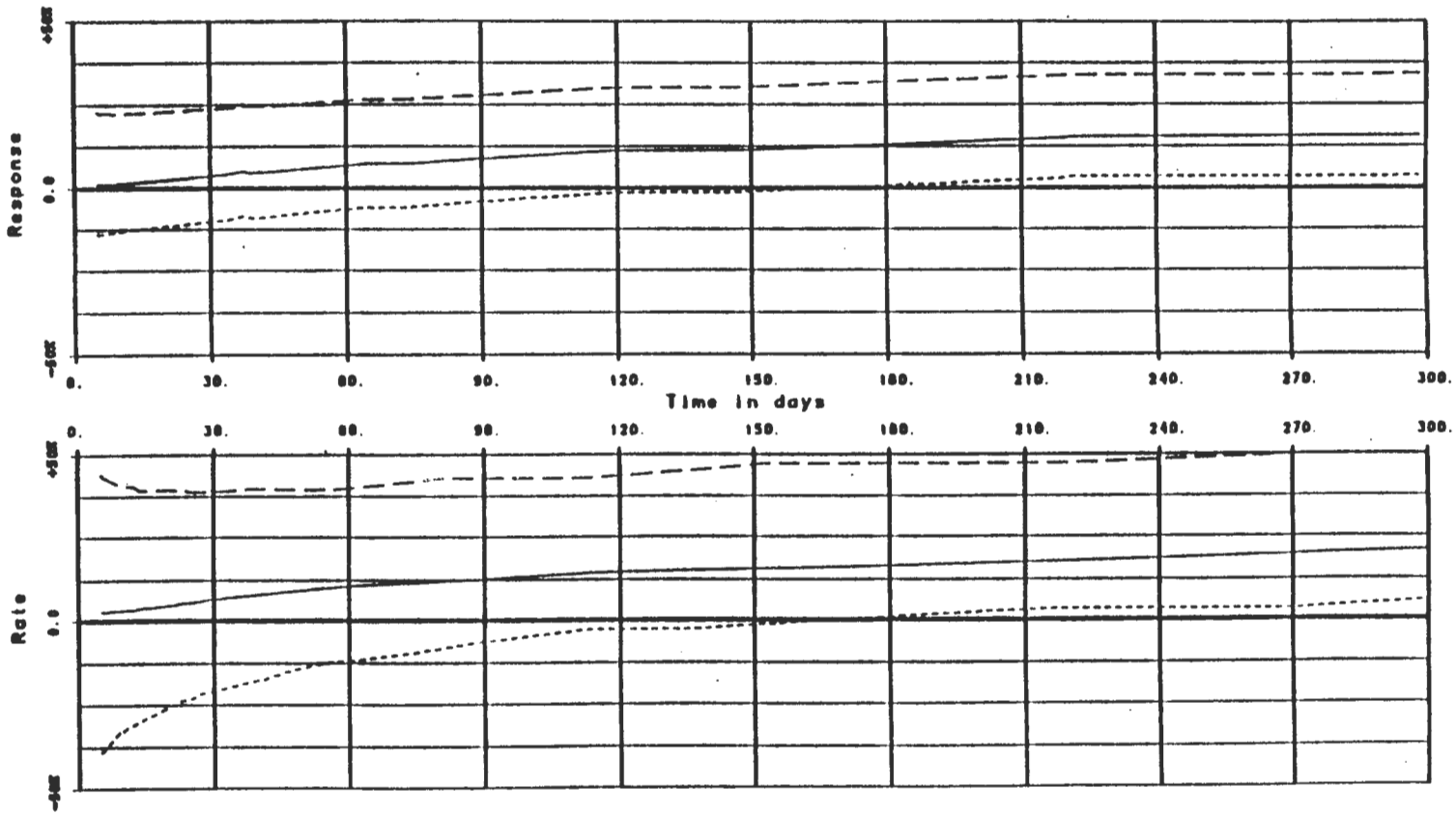


Roof-to-floor
Pillar Shortening
Roof Sag

**Figure 10-23**

DRIFTS
CLOSURE EFFECTS DUE TO PILLAR WIDTH

northern area where the $W_1/W_2$ ratio is approximately 0.4, the average effective stress is increased by about 6 percent. If the pillar shortening rate is proportional to the square of the increase in average effective stress in the pillar, the boundary release accounts for a 12 percent increase in pillar shortening. As described in the previous paragraph, this 12 percent increase in pillar shortening rate corresponds to about a 6 percent increase in the total closure rate. This factor, combined with the previously described effects, yields about a 30 percent difference in the total closure rate. This compares well with the value presented in subsection 10.3.2.2.

The roof sag component of closure is shown in the bottom graph of Figure 10-23. Figure 10-22 shows the comparison of the closure components of the narrow model relative to the wide model which is equivalent to comparing multiple parallel drifts to a single drift. As this figure indicates, the behavior differences appear to stabilize after about 200 days.

10.3.3.4 Effectiveness of Numerical Modeling

The creep parameters C, A and z were determined using roof-to-floor and wall-to-wall closure data. The effectiveness of the numerical modeling which uses one set of measured data to predict with reasonable accuracy other variables such as stress and strain needs to be verified to infuse confidence in the numerical modeling procedure. Besides, such a comparison will enable testing the adequacy of the basic creep level as well as assumptions regarding the statigraphy assumed for the model.

The 8 x 25-foot drift south of S2180 was isolated until July 1986 and different sets of creep parameters were determined by numerical modeling using roof-to-floor closure data from various convergence point measurements. In situ roof-to-floor closure data for stations south of S2180 indicate that the drift behaves essentially like an infinitely long isolated opening except at the very end of the E140 drift. This affords an opportunity to compare the measured relative displacements in the roof as well as in the floor at one instrument

location with the values obtained from numerical modeling which used roof-to-floor closure data from measurements at some other instrument location to "back calculate" the creep parameters.

Figure 10-24 compares the measured relative displacement between the collar and anchor D of extensometer 51X-GE-00247, in the roof at E140/S1950, with the values obtained from the numerical modeling. The calculated value is the relative vertical displacement of two nodes comparable to the positions of the collar and anchor D of the extensometer. The parameters C, A and z were obtained using roof-to-floor closure data from the instrument location at E140/S1879. The agreement is reasonable because the slopes of both the measured and calculated relative displacements are nearly identical. Figure 10-25 similarly compares the measured relative displacement in floor extensometer 51X-GE-00248 at E140/S1950 with the calculated values from the same numerical modeling. The slope of the in situ curve is 28 percent steeper than the calculated value. This is probably because the numerical model assumes that the anhydrite layer in the floor of the drift as linearly elastic with infinite strength. This may not be true if the anhydrite has pre-existing fractures, and thus may not be able to absorb the heave from the salt below.

Figure 10-26 compares the measured wall-to-wall closure at E140/S1879 with the calculated wall-to-wall closure from the results of the same numerical modeling. The average slope of the curve from numerical modeling is nearly 43 percent steeper than the slope of the curve from measurement data.

## 10.4 CONCLUSIONS AND RECOMMENDATIONS

The following subsections present conclusions pertaining to validation of the drift reference design and recommendations for design modifications. These are based on a comparison of the design criteria, design bases and reference design configurations with the results of the analysis and evaluation of data collected during the design validation process.

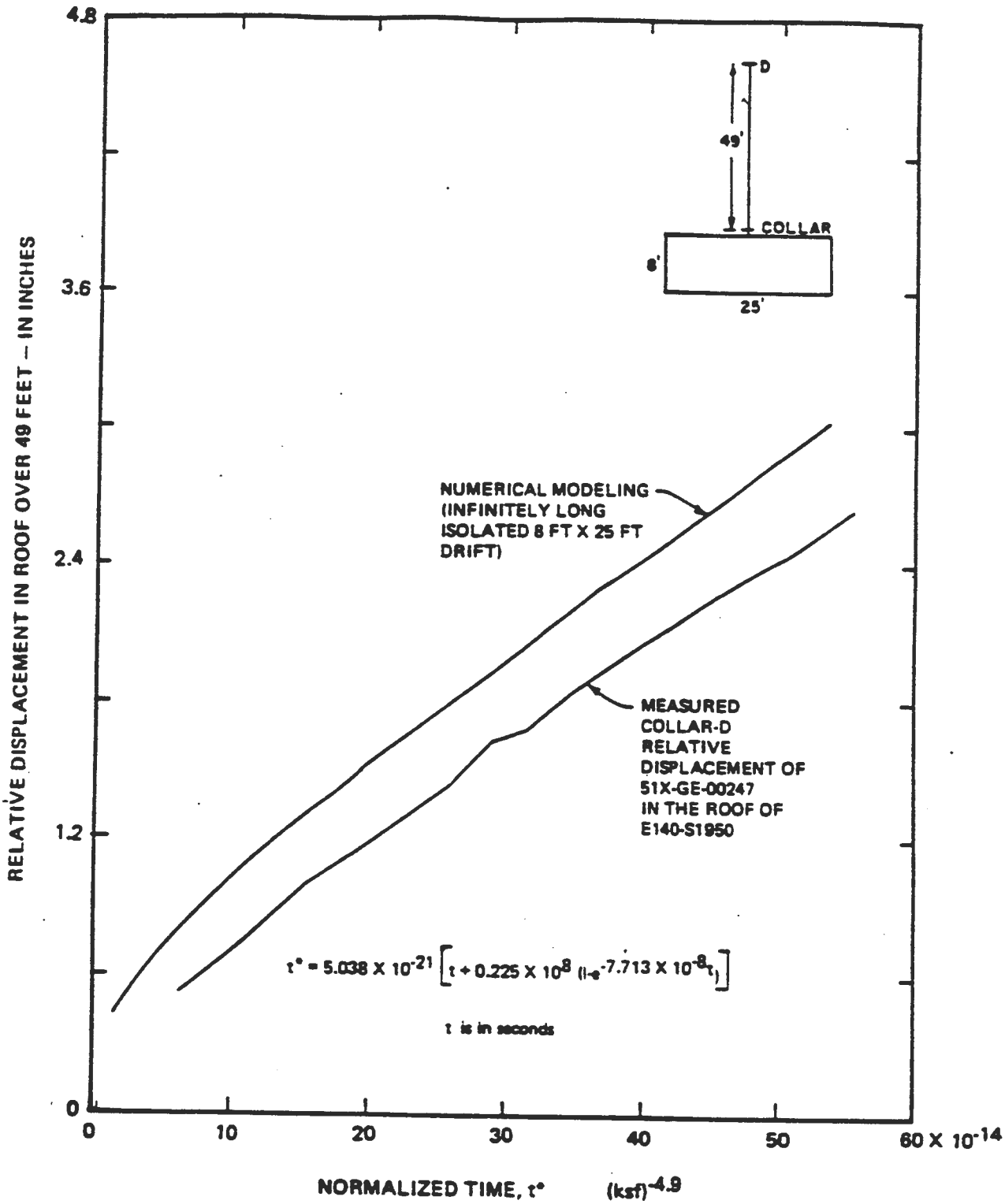


Figure 10-24

DRIFTS
NUMERICAL MODELING VERSUS IN SITU MEASUREMENT
DATA FROM ROOF EXTENSOMETER

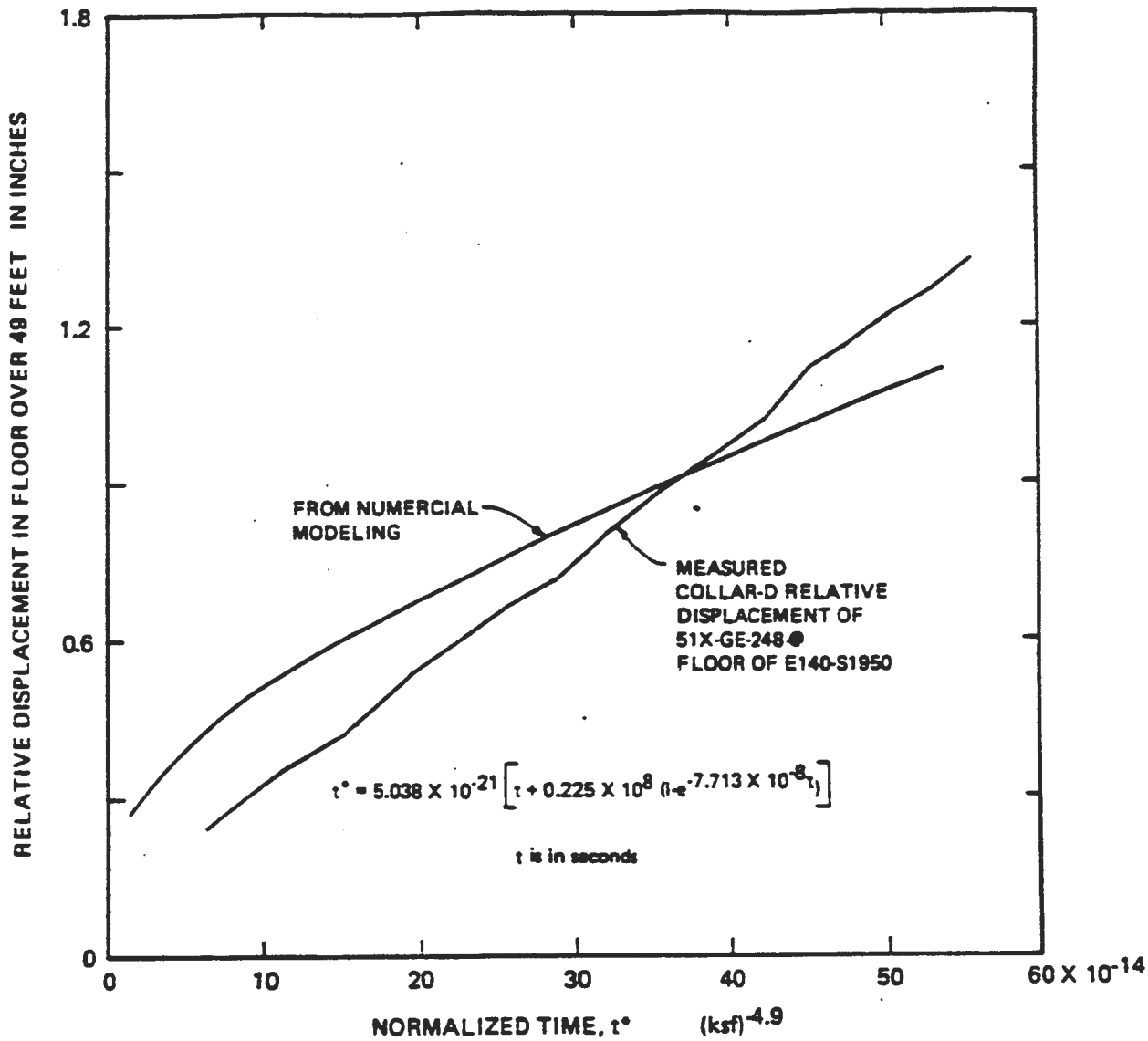


Figure 10-25

DRIFTS
NUMERICAL MODELING VERSUS IN SITU MEASUREMENT
DATA FROM FLOOR EXTENSOMETER

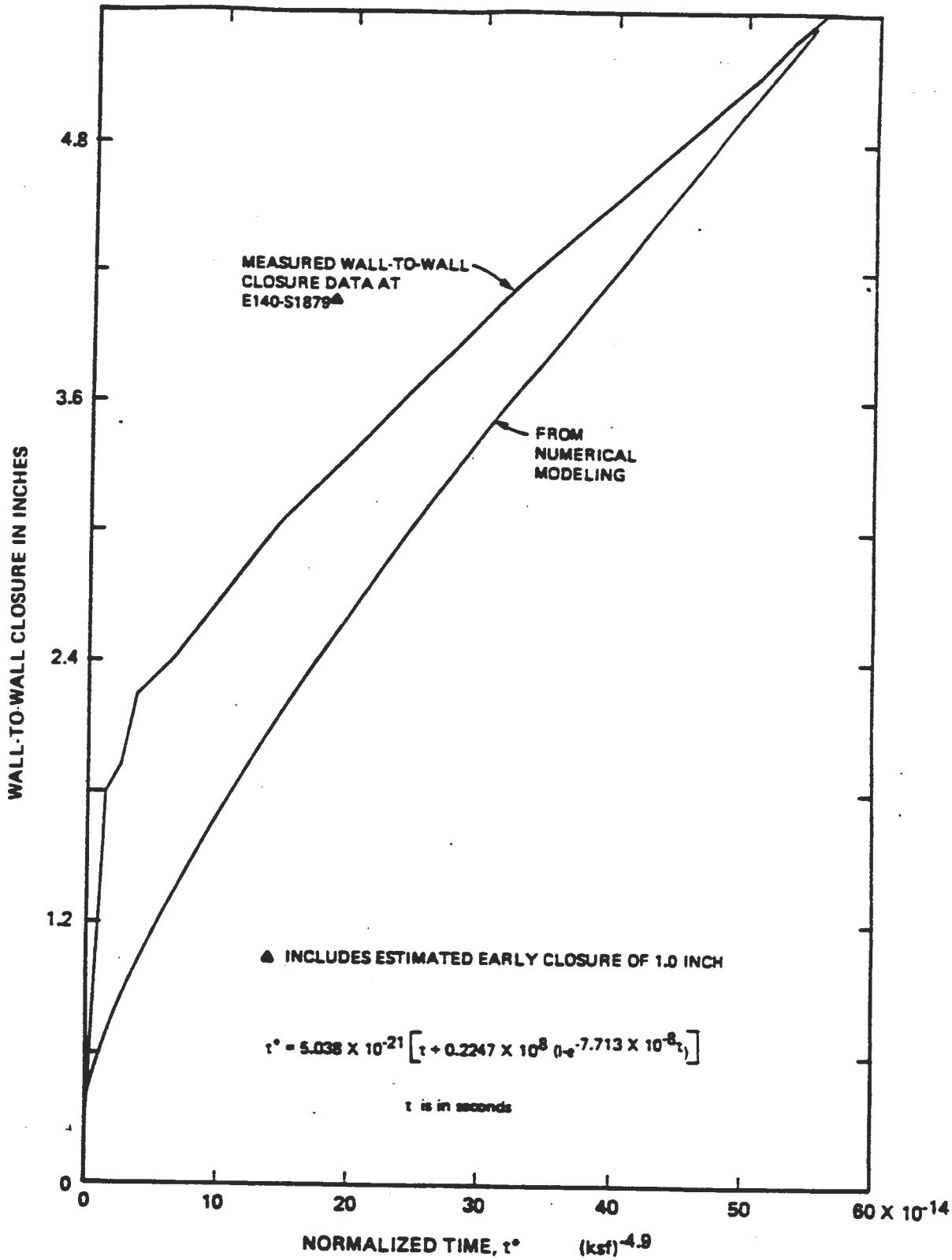


Figure 10-26

DRIFTS
NUMERICAL MODELING VERSUS MEASURED WALL-TO-WALL CLOSURE
AT E140/S1879

### 10.4.1 Conclusions

The evaluation of field observations and analytical results shows that the design criteria were appropriate for design of the horizontal openings. The three criteria identified as requiring specific evaluation, that the drifts remain within the required structural limits, provide maximum stability, and maintain the minimum required dimensions, were determined to be suitable. The reference design for the horizontal openings is therefore validated.

Spalling from the roof and walls of the drifts and fracturing and spalling at pillar corners will continue. Displacements and separations at clay seams above the roof may slowly increase. This deformational behavior is expected and can be controlled by scaling and rock bolting as necessary.

The average bay strains determined from the relative displacements of extensometer anchors 3 years after drift excavation are within 1 percent. The strain rates as well as the closure rates decrease with time indicating that the drifts are stable. Based on the projections of closure rates, the drifts will continue to be stable.

Fracturing beneath the floor of the drifts is minor and has nowhere developed to near the degree as that beneath the floor of Test Room 3. If additional fracturing develops in the future beneath the drifts, it is also expected to be minor. Based on experience in local potash mines, this type of fracturing is not expected to cause stability or operational problems.

The comparison of measured closure behavior in drifts with different dimensions indicates that the maximum closure and closure rate will occur in 12 x 25-foot drifts. The closure rates are affected by the presence of nearby parallel drifts and crosscuts as well as differences in salt properties. Based on available measurement data and the results of modeling analyses, the closure rate in the 13 x 25-foot

storage area drifts may be 30 percent greater than that of a single, infinitely long drift with the same dimensions (Chapter 12).

Analyses of salt behavior around the 25-foot wide drifts has determined the redistribution of stresses due to the effect of creep. Based on the computed vertical, horizontal and effective stresses, the stress which develops immediately after excavation is followed by relaxation due to creep behavior. According to the analyses, stress should not cause future stability problems in the drifts.

The analyses have also determined the locations of effective creep strain concentrations around the drifts at different times. Based on the predicted values of effective creep strain and the strain limit discussed in Chapter 6, the drifts will remain within the structural stability limits required, with respect to catastrophic failure, during the facility operating life. Minor spalls from the roof and wall surfaces are expected to occur. Analysis of observations in mines and discussion with mine personnel indicates that the surfaces of the drifts may start to deteriorate more rapidly after about 15 years. Increased maintenance will then be required.

### 10.4.2 Recommendations

Based on the results of design validation of the drifts, it is recommended that all drifts be inspected frequently for operational clearance and safety. If the clearance is insufficient, the drifts must be trimmed to the required dimensions. Trimming the floor to increase drift height is preferred over trimming the roof. Over the 25 year operating life, the roof should not be trimmed more than 12 inches for drifts 25 feet wide or less. Trimming the roof more than 12 inches would make the beam of salt too thin and increase the possiblity of a roof fall. Further trimming must be accomplished from the floor even though this will decrease the thickness of the salt above MB-139. Scaling and rock bolting should be performed where

necessary for safety purposes. Periodic inspection of accessible open boreholes should be performed to monitor the occurrence and behavior of displacements, separations and fracturing in the salt above the roof and beneath the floor of the drifts.

THIS PAGE LEFT BLANK INTENTIONALLY

# CHAPTER 11

# TEST ROOMS

## 11.1 INTRODUCTION

The four test rooms comprise a panel with a configuration similar to that designed for the waste storage area. The test rooms were instrumented, observed and analyzed in order to evaluate the potential behavior of the storage rooms. This chapter presents the results of data collection activities in the test rooms and the analysis and evaluation of the data with respect to the behavior of the excavated rooms. The information presented here will be used in Chapter 12 to predict the future behavior of the storage rooms and to validate their reference design.

## 11.2 DESIGN

The test rooms represent a portion of the storage room reference design configuration. The purpose of the test rooms is to provide geotechnical information that can be used to predict the potential behavior of the storage rooms. Because they were excavated to permit validation of the storage room reference design, and will not be used for permanent storage, the test rooms were not specifically addressed in the Design Criteria document. The design criteria apply to the configuration of the storage rooms and, therefore, only indirectly to the configuration of the four-room test panel.

No Design Basis documents were developed specifically for the test rooms. Only two Design Basis documents (refs. 2-9 and 2-18) contain elements pertaining to the test rooms. These elements specify that test rooms shall be provided to verify underground conditions as required by the SPDV Program and that their dimensions shall be 33 feet wide, 13 feet high and 300 feet long. All other design bases that require evaluation are applicable to the storage rooms rather than to the test rooms.

## 11.3 DESIGN VALIDATION PROCESS

The test room panel is the experimental model for the storage rooms. Validation of the test panel reference design configuration is not required. The test room data and analyses presented in this chapter are the bases for validation of the storage rooms. Predictions of the future behavior of the storage rooms based on these data analyses are presented in Chapter 12.

### 11.3.1 Data Collection

Data collection in the test rooms consisted of the accumulation of geotechnical data from geologic mapping, core drilling, observations of deformational behavior and geomechanical instrument measurements. Geologic mapping and core drilling were performed in the four test rooms. The stratigraphy defined by the mapping and core logging is discussed in Chapter 6. Observations of in situ behavior and data from the geomechanical instrumentation program are presented in the following subsections.

#### 11.3.1.1 Field Observations

Some aspects of test room behavior can only be evaluated by visual observation. Visual inspections of the rooms include observations of their general surface conditions in response to stress redistribution and salt creep. These conditions include small spalls from the roof and walls, especially at their intersection, and vertical fracturing at pillar corners and along the walls in response to pillar shortening.

Field observations include other qualitative and quantitative techniques in addition to visual inspections of excavation surfaces. Boreholes are surveyed using video cameras. Horizontal displacements and vertical separations of the geologic strata surrounding boreholes are determined using a probe, as described in Chapter 7, subsection 7.3.1.4. Wall surfaces of large diameter holes are mapped by a geologist.

A qualitative determination of the conditions of the test rooms is made

by site geologists during an inspection of the rooms at least once every 3 months. These inspections have been documented in each GFDR starting with the February 1984 edition (refs. 4-12 through 4-19). Detailed descriptions of observed test room behavior are contained in each of these reports.

As discussed in Chapter 10, an Excavation Effects Program was conducted throughout the underground facility during May through July 1986. This program was conducted to further characterize near-field deformation above and below the facility level. Ten arrays of boreholes were drilled in the roof and floor of the test rooms. The locations of the arrays are shown on Figure 10-1 in Chapter 10.

The results of some of these observations are used in conjunction with the results of numerical analysis and in situ measurement data to quantify the structural behavior of the test rooms. The documented field observations can be separated into four categories: roof and wall spalling; pillar fracturing; roof displacements and separations; and floor displacements, separations and fracturing.

Roof and Wall Spalling. A sounding survey of the roof of each test room was conducted during and immediately after excavation. Only a few areas of drummy rock were discovered and these were either removed or rock bolted.

The rooms have exhibited only minimal spalling over a period of 3 years since their excavation. The drummy areas originally found in the roofs have not grown noticeably, but some additional areas have been discovered by subsequent roof soundings. Additional scaling and rock bolting have been performed in most of these areas. The most noticeable spalling is associated with the argillaceous halite unit (geologic map unit 4, Appendix G, Figures G-1 through G-4) high on the test room walls. This spalling is generally continuous but shallow. Some spalling from the roof close to the walls has also been observed within the past year that has required support by rock bolts in selected areas.

Pillar Fracturing. Vertical fracturing has occurred in the corners formed by the intersection of drifts with the test rooms. The fractures have separations that range from essentially closed to about 2 inches wide. They generally extend into the rock perpendicular to the rock surface for an unknown distance. All corners of the test rooms show fracturing and consequent spalling. The fractures first appeared in the pillar corners about 3 to 6 months after excavation. They started as thin, hairline fractures and have steadily grown in length, width and presumably depth. Each of the GFDRs document this gradual development of the fractures. Scaling of these corners has been performed periodically.

Vertical fracturing has developed in the pillars parallel to the room walls. This fracturing is relatively minor and, to date, has been observed only in Test Rooms 3 and 4. The fracturing has been detected in horizontal boreholes drilled into the walls and occurs within approximately 2 feet of the wall surface. The fractures range from closed to about 1/32 inch wide.

Roof Displacements and Separations. Inspections of open boreholes in the test room roofs were conducted using a video camera and/or probe. The video camera produces high-resolution, color videotapes that are useful in identifying horizontal displacements and vertical separations. The probe is used in conjunction with a tape measure to determine the location and amount of movement in the boreholes. As in other areas of the underground facility, expected horizontal and vertical movements of the geologic strata surrounding the boreholes have been observed or measured in the test rooms. These observations are summarized in Table 11-1.

Ten arrays of boreholes were drilled in the test rooms in May 1986 as part of the Excavation Effects Program. These holes were used for additional investigation of test room roof displacements and separations. Each hole was inspected using a probe. Table 11-2 presents a summary of the results of this study.

Table 11-1

TEST ROOMS 1 THROUGH 4
RESULTS OF INSPECTION OF VERTICAL BOREHOLES IN ROOFS

| Hole | Date Completed | Hole Size (in.) | Depth (ft) | Approximate Location | Observed Condition* |
|---|---|---|---|---|---|
| IG-205 | 4-17-83 | 3 | 56 | Room 1; 1 ft from west wall | D |
| IG-206 | 4-15-83 | 3 | 52 | Room 1; 1 ft from east wall | D |
| IG-203 | 3-26-83 | 3 | 52 | Room 2; 1 ft from west wall | D |
| IG-204 | 3-83 | 3 | 52 | Room 2; 1 ft from east wall | D |
| OH-3 | 8-83 | 4 | 20 | Room 2 centerline | S, F |
| P4X-26 | 10-83 | 5 | 52.1 | Room 4; N1360/W630 | None |
| P4X-30 | 12-83 | 4 | 50.9 | Room 4; N1360/W630 | S |
| - | - | 6 | 8 | Room 4; N1360/W639 | D, F |
| - | - | 5 | 9± | Room 4 center; N1176 | S(?) |

* D = Displacement; S = Separation; F = Fracturing

## Table II-2

### EXCAVATION EFFECTS PROGRAM
### BOREHOLE INSPECTION SUMMARY

| SECTION | OPENING DIMENSIONS (Hx(W-FT) | EXCAVATION DATE | LOCATION | DATE DRILLED | DATE INSPECTED | OBSERVED CONDITIONS | | | | | |
|---|---|---|---|---|---|---|---|---|---|---|---|
| | | | | | | ROOF HOLES | | | FLOOR HOLES | | |
| | | | | | | E | A | C | F | B | D |
| 1 | 13x33 | 4/83 | ROOM 4, N175 | 5/15/86 | 5/15/86 | C | S(?) * | C(?) | D, S * | C | S, C |
| 2 | 13x33 | 4/83 | ROOM 4, N264 | 5/16/86 | 5/16/86 | C(?) | NONE | C | NONE | C | S |
| 3 | 13x33 | 4/83 | ROOM 4, N361 | 5/16/86 | 5/16/86 | NONE | D * | NONE | NONE | D, S, F * | S |
| 4 | 13x33 | 4/83 | ROOM 3, N198 | 5/15/86 | 5/15/86 | NONE | NONE | S | NONE | S | S |
| 5 | 13x33 | 4/83 | ROOM 3, N243 | 5/15/86 | 5/15/86 | NONE | NONE | NONE | S, F (USED ROOM 3 LARGE DIAMETER HOLES) | | |
| 6 | 13x33 | 4/83 | ROOM 3, N302 | 5/15/86 | 5/15/86 | S | C | NONE | D, S, F (USED PREVIOUSLY DRILLED HOLES MB-F1-01 THROUGH 03) | | |
| 7 | 13x33 | 3/83 | ROOM 2, N147 | 5/21/86 | 5/22/86 | NONE | NONE | C | C | F, C | NONE |
| 8 | 13x33 | 3/83 | ROOM 2, N231 | 5/21/86 | 5/22/86 | F | F | NONE | S | S, F, C | F |
| 9 | 13x33 | 4/83 | ROOM 1, N159 | 5/21/86 | 5/22/86 | C | F | NONE | C | S, C | NONE |
| 10 | 13x33 | 4/83 | ROOM 1, N275 | 5/21/86 | 5/22/86 | F | S, F, C | NONE | C | S | S, C |

* EXISTING HOLE.

**EXPLANATION**

D = HORIZONTAL DISPLACEMENT, FOUND ONLY IN PREVIOUSLY DRILLED HOLES. DISPLACEMENT APPEARS TO DEVELOP WITH TIME FOLLOWING HOLE DRILLING.

S = VERTICAL SEPARATION. PROBE NAIL PENETRATES HOLE WALL SURFACE. VERTICAL SEPARATIONS RANGE FROM APPROXIMATELY 1/16 INCH TO 6 INCHES.

F = FRACTURE ZONE. PIECES OF HALITE COMMONLY PICKED OUT OF ZONE BY PROBE NAIL.

C = PROBE NAIL CATCHES ON HOLE WALL SURFACE BUT DOES NOT PENETRATE. INDICATES POSSIBLE SEPARATION OF LESS THAN 1/16 INCH. OCCURENCES AT KNOWN CLAY LAYERS ARE NOT INDICATIVE OF SEPARATION AND ARE NOT INCLUDED IN THIS TABLE.

**NOTES:**

1. SECTION LOCATIONS AND HOLE CONFIGURATIONS ARE SHOWN IN CHAPTER 10, FIGURE 10-1.
2. HOLES WERE DRILLED VERTICALLY USING A JACK-LEG DRILL.
3. NOMINAL HOLE DEPTH IS 9 FEET BUT SOME HOLES ARE SHORTER DUE TO LOW DRIFT ROOF OR DRILLING DIFFICULTIES.
4. ONE ROOF AND ONE FLOOR HOLE OF EACH ARRAY WERE GENERALLY DRILLED 3 INCHES IN DIAMETER TO ACCOMODATE USE OF BOREHOLE CAMERA IF DESIRED. OTHER HOLES WERE DRILLED 1-7/8 INCHES IN DIAMETER. EXISTING HOLES WERE USED WHERE POSSIBLE.
5. OBSERVATIONS WERE MADE USING A PROBE CONSISTING OF A NAIL ATTACHED PERPENDICULAR TO THE END OF A ROD.

Floor Displacements, Separations and Fracturing. Horizontal displacements, vertical separations and fracturing have been observed beneath the floor of the test rooms in boreholes. They have been observed to occur in MB-139 and in the overlying halite. Geologic maps of Test Room 3 (Room T) boreholes are presented in Appendix G, Figures G-10 through G-31. A summary of the results of the inspection of all small-diameter boreholes drilled in the floor of the test rooms is presented in Table 11-3. The inspections were accomplished using video equipment and/or a probe.

The only prominent exposure of floor fracturing is in the 36-inch diameter boreholes drilled in the floor of the south half of Test Room 3 (Room T). A total of 22 holes were drilled in this area during September and November 1985 for the erection of structural steel columns. A drilling summary is presented in Table 11-4. The holes are approximately 7.2 feet deep. The bottom of many of the holes coincides with the occurence of clay E at the base of MB-139. The remaining holes were terminated above the base of the marker bed.

The holes were logged on a 360 degree foldout at a scale of 1 inch to 1 foot. All features were measured from a level reference line which was later surveyed to determine elevations. Fracture traces, fracture zones and hairline fractures, in addition to lithologic contacts, were logged. A fracture trace is a distinct fracture surface exposed on the wall of the borehole. Fracture traces shown on the logs, unless otherwise noted, are closed within a few inches of the wall surface. A fracture zone is an area on the wall bounded by distinct fractures. Rock within the zone is broken by numerous smaller fractures spaced less than 1 inch apart. The fractured rock is commonly broken out very close to the wall surface of the borehole due to drilling, but becomes closed within 1/2 to 2 inches of the wall surface. Locally, the zone is open or partially filled with drill cuttings. At a distance of 12 inches from the borehole, the cumulative vertical separation measured over the length of the hole varies from less than 1/4 inch to 6 inches. The hairline fractures are closed fractures usually found

Table 11-3

TEST ROOMS 1 THROUGH 4
RESULTS OF INSPECTION OF VERTICAL BOREHOLES IN FLOOR

| Hole | Date Completed | Hole Size (in.) | Depth (ft) | Approximate Location | Observed Condition* |
|---|---|---|---|---|---|
| IG-202 | 4-18-83 | 3 | 52 | Room 1; 1 ft from west wall | D |
| GE-269 | 1-86 | 3 | 55 | Room 1 centerline | S, F |
| IG-201 | 3-26-83 | 3 | 52 | Room 2; 1 ft from west wall | D |
| NG-254 | 3-84 | 6 | 7 | Room 2 centerline | None |
| GE-270 | 1-86 | 3 | 55 | Room 2 centerline | S, F |
| 2NPD-01 | 2-86 | 5 | 8.9 | Room 2; N1370 | S, F |
| MB-FI-01 | 12-85 | 4 | 12.0 | Room 3; N1309 | D, S, F |
| MB-FI-02 | 12-85 | 4 | 12.0 | Room 3; N1309 | D, S, F |
| MB-FI-03 | 12-85 | 4 | 12.0 | Room 3; N1309 | D, S, F |
| GE-271 | 1-86 | 3 | 55 | Room 3 centerline | S, F |
| P4X-06 | 1983 | 5 | 9.0 | Room 4; N1369/W625 | D, S, F |
| P4X-25 | 10-83 | 5 | 50.2 | Room 4; N1360/W630 | D, S, F |
| P4X-27 | 10-83 | 5 | 51.1 | Room 4; N1360/W630 | D, S, F |
| P4X-29 | 10-83 | 5 | 49.5 | Room 4; N1360/W630 | D, S, F |
| P4X-31 | 11-83 | 5 | 50.4 | Room 4; N1360/W630 | D, S, F |
| P4X-81 | 11-83 | 16 | - | Room 4 | D, S, F |
| P4X-83 | 12-83 | 16 | 6.1 | Room 4 | S, F |
| P4X-84 | 1-84 | 36 | 9.5 | Room 4 | D, S, F |

* D = Displacement; S = Separation; F = Fracturing

Table 11-4

TEST ROOM 3 (ROOM T)
SUMMARY OF DRILLING



| Hole | Date Completed | Drilling Fluid | Communication During Drilling* |
|---|---|---|---|
| TV-01 | 10-25-85 | Brine** | --- |
| TV-02 | 10-28-85 | Air | --- |
| TV-03 | 11-05-85 | Air | TV-07, TV-14 through 75° dipping fracture. TV-15 through fractures in halite close to surface on east side. Surface fracture close to east wall 25 feet south of TV-03. No communication to TV-13. TV-17, TV-12. |
| TV-04 | 11-08-85 | Air | --- |
| TV-05 | 11-20-85 | Air | --- |
| TV-06 | 11-13-85 | Air | --- |
| TV-07 | 10-29-85 | Air | TV-12 |
| TV-08 | 11-19-85 | Air | --- |
| TV-09 | 11-21-85 | Air | --- |
| TV-10 | 11-14-85 | Air | TV-13, TV-14, TV-17, TV-15, TV-06, TV-11 |
| TV-11 | 11-11-85 | Air | --- |
| TV-12 | 9-17-85 | Air | --- |
| TV-13 | 10-09-85 | Air | TV-12, TV-15 |
| TV-14 | 10-11-85 | Air | TV-15 |
| TV-15 | 9-23-85 | Air | TV-19 |
| TV-16 | 9-30-85 | Air | TV-19, TV-20 |

Table 11-4 (continued)

TEST ROOM 3 (ROOM T)
SUMMARY OF DRILLING



| Hole | Date Completed | Drilling Fluid | Communication During Drilling* |
|---|---|---|---|
| TV-17 | 10-15-85 | Air | --- |
| TV-18 | 10-02-85 | Air | --- |
| TV-19 | 9-20-85 | Air | --- |
| TV-20 | 9-25-85 | Air | TV-19 along main fracture zone on north-northeast side. |
| TV-21 | 10-18-85 | Air | --- |
| TV-22 | 10-19-85 | Air | TV-19 along main fracture zone on north-northeast side. TV-20 along main fracture zone on west side. |

* Communication is indicated by drilling dust emanating from connected holes and detected by driller or geologist.

** Source of brine encountered in TV-01 is clay E at base of MB-139. Driller noted that this clay and about 4 inches of the overlying anhydrite were moist in many holes.

within fracture zones less than 1 inch wide. Some of these appear to be pre-excavation features within MB-139.

Additional small-diameter boreholes were drilled into the test room floors as part of the Excavation Effects Program. The 10 arrays summarized in Table 11-2 include three floor holes at each array. These holes were drilled primarily to determine if the fracturing observed in the 22 large-diameter holes in Test Room 3 extends to other areas beneath the test rooms.

#### 11.3.1.2 Geomechanical Instrumentation

Geomechanical instrumentation in Test Rooms 1 through 4 initially consisted of 19 borehole extensometers, 16 horizontal inclinometers, 6 vertical inclinometers, 4 sets of convergence points, 2 convergence meters, and 2 rigid-inclusion vibrating-wire stressmeters (Figure 11-1). These instruments, with the exception of the inclinometers and convergence points, were connected to the datalogger system on May 13, 1983.

Due to failure for various reasons, some instruments in the test rooms had to be replaced. Those instruments replaced include both stressmeters in Test Room 2 and the extensometers in the floor of Test Rooms 1, 2 and 3. The history of instrument performance and maintenance is discussed in the GFDRs.

Figure 11-2 shows the instruments in each test room and the excavation dates at the instrument locations. Because the excavation of each test room required about 10 days to complete, it was difficult to assign a single date of excavation for some instrument locations. Table 11-5 presents the dates of excavation used for plotting and analysis of the test room data.

### 11.3.2 Analysis and Evaluation

This section discusses the analysis and evaluation of the results of

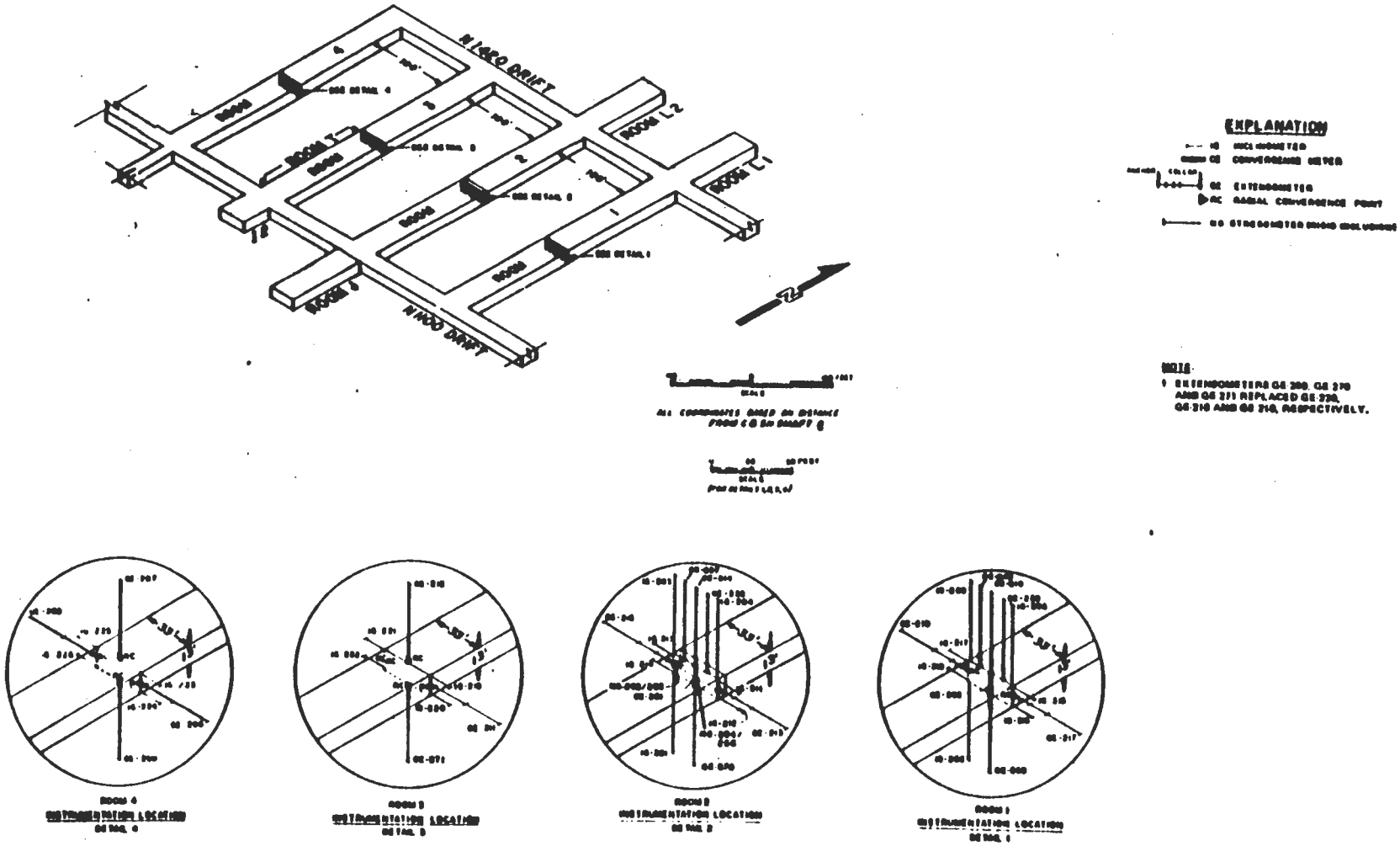


Figure 11-1

TEST ROOMS
INSTRUMENTATION

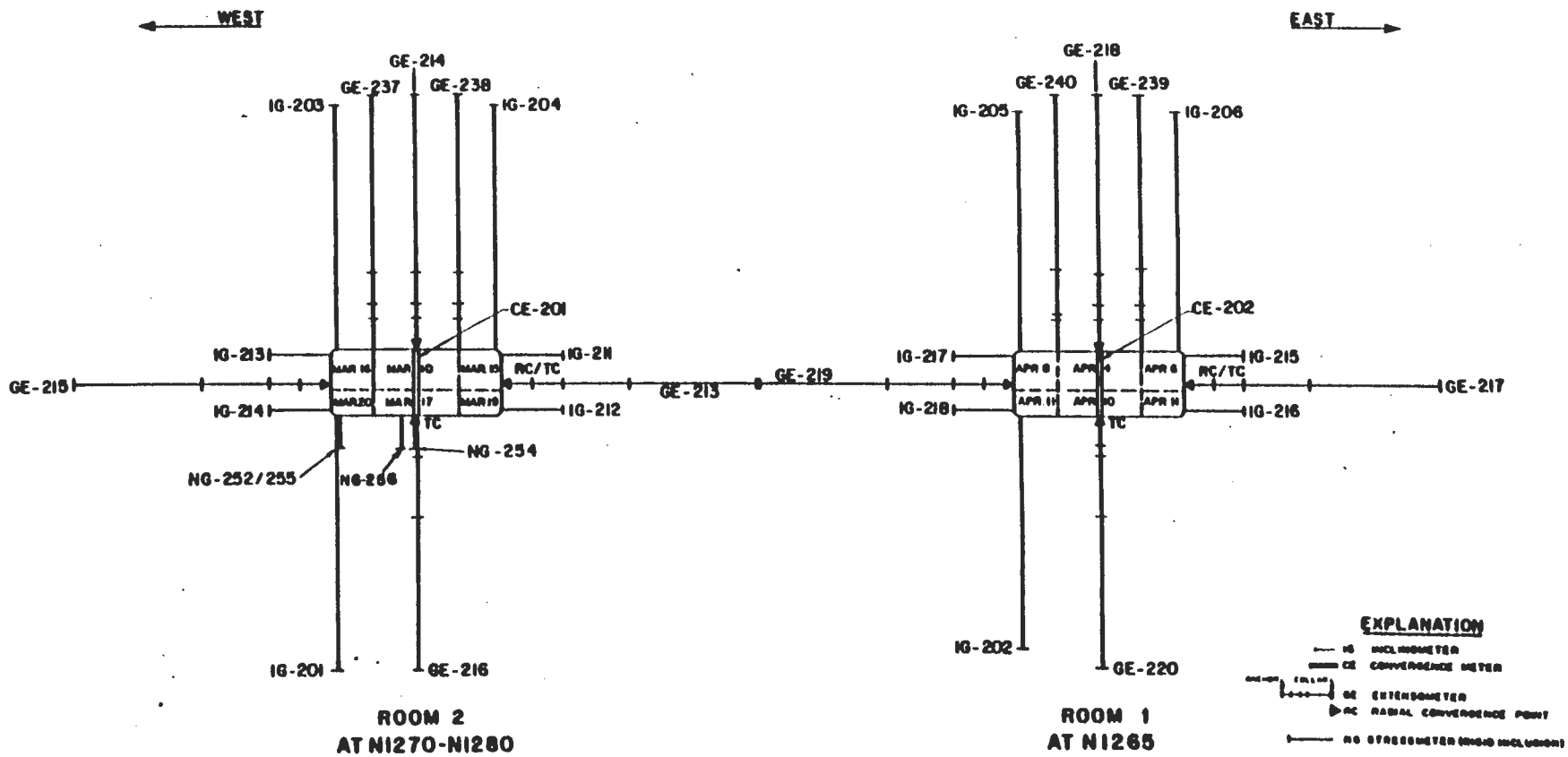


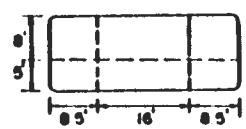


DIMENSIONS OF PASSES

NOTE: EXCAVATION OF THE TEST ROOMS WAS PERFORMED IN 1983.

Figure 11-2

TEST ROOMS
EXCAVATION SEQUENCE AT INSTRUMENT LOCATIONS
Sheet 1 of 2

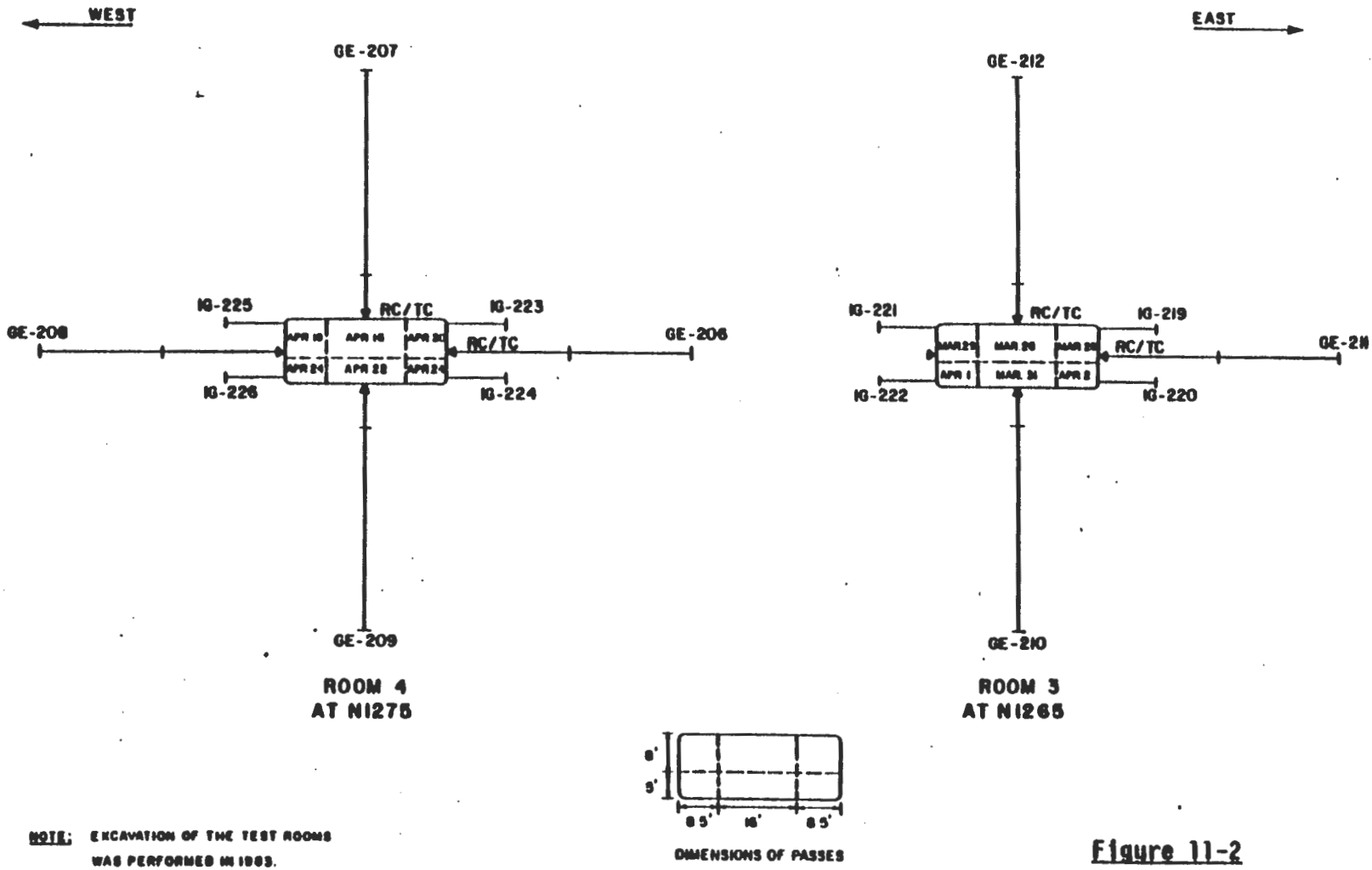


NOTE: EXCAVATION OF THE TEST ROOMS WAS PERFORMED IN 1983.

Figure 11-2

TEST ROOMS
EXCAVATION SEQUENCE AT INSTRUMENT LOCATIONS
Sheet 2 of 2

Table 11-5

TEST ROOMS
ASSUMED EXCAVATION DATES FOR DATA ANALYSIS



| Type of Instrument/Location | Instrument Designation | Assumed Date of Excavation Room 1 | Room 2 | Room 3 | Room 4 | Basis for Selection |
|---|---|---|---|---|---|---|
| Convergence meters | SIX-CE-00202<br>SIX-CE-00201 | Apr. 7, 1983 | Mar. 13, 1983 | | | Average of dates for upper and lower center passes. |
| Roof extensometers - center | SIX-GE-00218<br>SIX-GE-00214<br>SIX-GE-00212<br>SIX-GE-00207 | Apr. 4, 1983 | Mar. 10, 1983 | Mar. 26, 1983 | Apr. 16, 1983 | Date for upper center pass. |
| Floor extensometers - center | SIX-GE-00220<br>SIX-GE-00216<br>SIX-GE-00210<br>SIX-GE-00209 | Apr. 10, 1983 | Mar. 17, 1983 | Mar. 31, 1983 | Apr. 22, 1983 | Date for lower center pass. |
| Roof extensometers - east side | SIX-GE-00239<br>SIX-GE-00238 | Apr. 5, 1983 | Mar. 13, 1983 | | | Average of dates for upper center and upper east passes. |
| Roof extensometers - west side | SIX-GE-00240<br>SIX-GE-00237 | Apr. 6, 1983 | Mar. 13, 1983 | | | Average of dates for upper center and upper west passes. |
| Wall extensometers - east side | SIX-GE-00217<br>SIX-GE-00213<br>SIX-GE-00211<br>SIX-GE-00206 | Apr. 6, 1983 | Mar. 15, 1983 | Mar. 28, 1983 | Apr. 20, 1983 | Date for upper east pass. |
| Wall extensometers - west side | SIX-GE-00219<br>SIX-GE-00215<br>SIX-GE-00208 | Apr. 8, 1983 | Mar. 16, 1983 | | Apr. 19, 1983 | Date for upper west pass. |

Table 11-5 (continued)

TEST ROOMS
ASSUMED EXCAVATION DATES FOR DATA ANALYSIS



| Type of Instrument/Location | Instrument Designation | Assumed Date of Excavation: Room 1 | Room 2 | Room 3 | Room 4 | Basis for Selection |
|---|---|---|---|---|---|---|
| Wall shortening points - east side | IG 215-216 RS<br>IG 211-212 RS<br>IG 219-220 RS<br>IG 223-224 RS | Apr. 8, 1983 | Mar. 17, 1983 | Mar. 30, 1983 | Apr. 22, 1983 | Average of dates for upper and lower east passes. |
| Wall shortening points - west side | IG 217-218 RS<br>IG 213-214 RS<br>IG 221-222 RS<br>IG 225-226 RS | Apr. 9, 1983 | Mar. 18, 1983 | Mar. 30, 1983 | Apr. 21, 1983 | Average of dates for upper and lower west passes. |
| Wall-to-Wall convergence points - near roof | IG 211-213 TC<br>IG 219-221 TC | | Mar. 15, 1983 | Mar. 28, 1983 | | Average of dates for upper east and west passes. |
| Wall-to-Wall convergence points - near floor | IG 212-214 TC<br>IG 220-222 TC | | Mar. 19, 1983 | Apr. 1, 1983. | | Average of dates for lower east and west passes. |
| Wall-to-Wall permanent convergence points - center | Room 1 RC<br>Room 2 RC<br>Room 3 RC<br>Room 4 RC | Apr. 7, 1983 | Mar. 15, 1983 | Mar. 29, 1983 | Apr. 19, 1983 | Average of dates for upper east and west passes. |
| Roof-to-Floor permanent convergence points - center | Room 3 RC<br>Room 4 RC | | | Mar. 28,1983 | Apr. 19, 1983 | Average of dates for upper and lower center passes. |

Table 11-5 (continued)

TEST ROOMS
ASSUMED EXCAVATION DATES FOR DATA ANALYSIS



| Type of Instrument/Location | Instrument Designation | Assumed Date of Excavation Room 1 | Room 2 | Room 3 | Room 4 | Basis for Selection |
|---|---|---|---|---|---|---|
| Wall-to-Wall temporary convergence points - center | Room 1 TC<br>Room 2 TC<br>Room 3 TC<br>Room 4 TC | Apr. 7, 1983 | Mar. 15 1983 | Mar. 29, 1983 | Apr. 19, 1983 | Average of dates for upper east and west passes. |
| Roof-to-Floor temporary convergence points - center | Room 1 TC<br>Room 2 TC<br>Room 3 TC<br>Room 4 TC | Apr. 7, 1983 | Mar. 13, 1983 | Mar. 28, 1983 | Apr. 19, 1983 | Average of dates for upper and lower center passes. |
| Floor stressmeters - west corner | SIX-MG-00252<br>SIX-MG-00255 | | Mar. 20, 1983<br>Mar. 20, 1983 | | | Date for lower west pass.<br>Date for lower west pass. |
| Floor stressmeters - center | SIX-MG-00254<br>SIX-MG-00256 | | Mar. 17, 1983<br>Mar. 17, 1983 | | | Date for lower center pass.<br>Date for lower center pass. |

Notes:

(1) The "Elapsed Days Since Excavation" shown on the data plots in Appendix J were calculated using this "Assumed Date of Excavation".

(2) See Figure 11-2 for the excavation sequence at the center of the test rooms.

(3) The dates of excavation for individual inclinometers were not used for plotting.

field observations and in situ measurement data. The results of numerical modeling of the test rooms using in situ measurement data are also presented. In addition, regression analyses of the closure rate obtained from the closure measurements were also performed. The fitted equations were used to supplement the prediction of closure behavior in the storage rooms and are discussed in Chapter 12.

11.3.2.1 Observed Conditions

Roof and Wall Spalling. Minor spalling from the roof in the test rooms, resulting in shallow drummy areas, has occurred as expected. Drummy areas usually occur within 3 to 6 inches of the roof in areas of clear halite not associated with any noticeable clay. Separations occur along local planes of weakness in the halite, probably created by the orientation of crystal surfaces. This same phenomenon occurs in the drifts. Drummy areas have been identified immediately after excavation and additional areas have developed since that time. These later-occurring drummy areas appear to develop primarily along the roof within several feet of the walls.

Spalling along the walls of the test rooms is a result of local stress concentrations and the low tensile properties of salt. It is also related to the percentage of argillaceous material in the halite and to the proximity of floor and roof intersections. The squeezing of clay F at the upper contact of geologic map unit 4 is associated with the spalling phenomenon. Minor spalling is also associated with map unit O, near the floor.

Pillar Fracturing. Vertical fracturing in the pillars is the expected result of room deformation and stress concentrations. The fractures that have developed in the walls of the test rooms, parallel to the rooms, are considered to be tension fractures resulting from stress relief. Fractures detected in boreholes drilled in the upper portion of geologic map unit 4 are related to the spalling occurring in this unit.

Horizontal inclinometers in the test room walls show both upward and downward vertical movement toward the center of the wall (Appendix J, Figures J-320 through J-335). Although no displacements have been observed, the inclinometer data indicate that the salt has moved toward the central horizontal axis of the room. This movement, due to vertical compressive stress and salt creep, is discussed further in subsection 11.3.2.2. Tensile stresses resulting from this salt creep and pillar shortening have caused fractures to lengthen and widen and new fractures to develop. Fracturing is more prominent at pillar corners that were not beveled to the 4 x 4-foot design.

Fracturing parallel to the room walls will continue to occur. Spalling and local failure will also continue at pillar corners and will require periodic maintenance.

Roof Displacements and Separations. The displacements observed in various open boreholes in the test room roofs are the result of deformation around the openings. The halite at the storage horizon is interrupted by anhydrite beds and thin clay layers. These layers, particularly anhydrite "b" and the underlying clay G, are directly associated with the displacements observed in the test room roofs.

Lateral displacement in the salt above the test rooms is similar to that detected above the drifts. The halite bounded by the roof and clay G moves toward the room center relative to the upper layers of salt. The movement is, however, not exactly symmetrical about the room centerline. This is confirmed by inclinometer readings in the roof of Test Rooms 1 and 2 which show that the lateral movement of the salt close to the roof is greater to the west than to the east (Appendix J, Figures J-316 through J-319). However, this trend is reversed at about 32 feet above the roof of the test rooms. The halite comprising the lower roof beam is subjected to horizontal compressive stresses resulting in shear along clay G and possible vertical separation as the beam moves downward. Some casing deformations have also been observed within 1 foot of the hole collar of the roof inclinometers. The

relative movement here is opposite to that observed above and is probably due to the near surface halite resisting the shear movement along clay G.

Movement within the halite below clay G, opposite to that found elsewhere, has been observed in one borehole in Test Room 4. This may be the result of movement along existing planes of weakness in the halite or of the resistance of the halite to shear movement along clay G.

The current results of the Excavation Effects Program indicate that minimal separation or fracturing has occurred at clay G or in the underlying halite above the test room roofs. In Test Rooms 3 and 4, separations less than 1/16 inch wide have been observed. No separation has been observed at clay G. In the array of holes comprising Section 5 in Table 11-2, above the 36-inch diameter holes in the floor of Test Room 3 (Room T), no separations or fracturing were detected. In hole C of Section 4 in Test Room 3, two 1/4-inch vertical separations were found within 1 foot of the roof. These fractures resulted from roof spalling.

Similar small separations were observed in the roof of Test Rooms 1 and 2. Also, fracture zones (in one case 2.4 inches wide) were detected in the halite below clay G in the center hole of three of the four arrays.

<u>Floor Displacements, Separations and Fracturing</u>. The only prominant display of fracturing observed throughout the entire WIPP undergrounc facility during design validation has been in the area of the 36-inch diameter holes drilled in the floor in the south half of Test Room 3 (Room T). Cross sections of the room floor through these holes are presented in Appendix G, Figures G-33 and G-34. Two distinct fracture zones are evident. The first is a dish-shaped zone that angles 10 to 20 degrees downward from near the room walls, intersects MB-139, and flattens near the room center. This zone is most pronounced along the series of holes shown on Figure G-34. In the

northern cross section (Figure 6-33), this fracture zone is evident in the holes west of the room centerline but is not present in the holes east of the centerline. In both sections, this upper fracture zone "daylights" at the floor surface or pinches out before reaching the room pillars.

A second fracture zone, dipping approximately 50 to 60 degrees from horizontal and exposed in the holes closest to the room walls, occurs below the upper fracture zone. This lower zone is more regular and planar than the upper zone. With the exception of one hole, this lower zone occurs entirely within MB-139 and is more developed on the west side of the room.

In addition to the two major fracture zones, some subhorizontal fracturing is present just above clay E at the base of MB-139. This fracturing is most evident in the holes closest to the room centerline. No separations along clay E were observed in any of the holes.

Communication between holes during drilling was observed and is described in Table 11-3. During the drilling of hole TV-03, drilling dust was observed coming up through a surface fracture close to the east wall, 25 feet south of the hole location.

A series of measuring pins were installed in two open holes, TV-03 and TV-19, in late January 1986 to monitor movements within the holes. The pins were installed in MB-139 and in the overlying halite and straddle the fracture zones. Measurements taken until the holes became inaccessible in June 1986 indicated that some small-scale dilation was occurring in both of the holes.

The fractures observed beneath the floor of Test Room 3 are directly related to the excavation geometry and the stratigraphy. Some fractures within MB-139 may have been pre-existing but have opened since room excavation.

Three 4-inch diameter holes were drilled in the north half of Test Room 3 to determine if fracturing is occuring there. These holes were drilled to a nominal depth of 12 feet below the floor. A thin fracture zone was detected within 1 1/2 feet of the floor in two of the holes and minor fracturing was detected in MB-139 in all of the holes. This fracturing is significantly less developed than that observed in the south half of Test Room 3.

The 22 large-diameter holes in Test Room 3 were drilled late in 1985. They are, therefore, too recent to document any lateral displacements along the observed fractures. However, other older floor boreholes do indicate relative displacement. In Test Room 4, boreholes P4X-06, P4X-25, P4X-27, P4X-29 and P4X-31 all show multiple displacements and vertical separations (Table 11-2). These are primarily within MB-139 and exhibit up to 2 inches of lateral displacement and up to 1/2 inch of vertical separation. These five holes are near the room centerline. The relative movement of the multiple displacements observed is complicated and does not follow the simpler interpretation of the roof displacements. The most significant displacements in all of the holes have taken place closest to the floor surface and, in all cases, the salt above the fracture has moved east relative to the underlying salt. Inclinometers IG-202 and IG-201, in Test Rooms 1 and 2, also exhibit similar relative displacement. Both of these inclinometers are on the west side of their respective test rooms. The marker bed and the overlying salt have moved east towards the room centerline relative to the underlying salt. Movement is apparently along clay E and is approximately 3/4 inch.

Although no detailed investigation of the salt beneath the test room pillars has been performed, the Test Room 3 fracture mapping indicates that it is unlikely that fractures extend beneath them to any significant extent. Neither of the two fracture zones identified can be traced into the pillars. The upper fracture zone pinches out prior to reaching the walls or daylights at the floor surface. The lower fracture zone cannot be traced beyond the hole walls, but it is not

suspected of continuing beneath the pillars. One small diameter hole was drilled at an angle into each of the walls of Test Room 3 in May 1986. Except for a localized clay break at a depth of 3.2 feet, there was no evidence of separation.

Fractures and separations have been observed in four large-diameter holes drilled in the floor in the south end of Test Room 4. Fractures were observed in these holes during drilling in November 1983 and January 1984. The fracturing was minor, however, with no separations observed. One hole became inaccessible soon thereafter. Fractures in the other holes have been observed to increase in number and to exhibit separation (Table 11-2). Fractures occur in the marker bed and in the overlying halite. Because two of the holes have restricted access, monitoring of the fractures is difficult. Borehole P4X-84, in the southwest corner of Test Room 4, was mapped in February 1986 and the results are shown in Appendix G, Figure G-32. The separations and displacements in P4X-84 over the 2 year period since excavation are small in comparison to those in the floor holes in the south half of Test Room 3.

A low-angle fracture in the floor of Test Room 2 was observed in August 1985. An inspection in June 1986 showed that it extended from approximately N1242 to N1208. This fracture daylights at the floor surface, 1.5 feet to 6 feet from the west wall, and extends 2 feet below the floor surface toward the east. Approximately 8 to 10 inches of separation is present along this fracture, and approximately 25 square feet of floor in the vicinity of this fracture sounds drummy.

As part of the Excavation Effects Program, a series of holes were drilled in each of the test rooms to determine the extent of floor fracturing and for future monitoring of this phenomenon. Existing boreholes, such as those in Test Rooms 3 and 4, were utilized where possible. The locations of the holes are shown on Figure 10-1 in Chapter 10. These holes were inspected using a probe and the results are summarized in Table 11-2. The holes exhibited some fractures and

separations. The dish-shaped fracture profile observed in the holes Test Room 3 was also found in some of the hole arrays, although on a much smaller scale. It was most pronounced in several of the holes close to the room walls where separations were estimated to be a maximum of 6 inches. In other locations, the separation ranged from 1/8 inch to 3 inches. Within MB-139, fractures and separations found in the central holes of the Test Room 1 array ranged from approximately 1/8 inch to 3 inches. For other hole arrays, the maximum separations were 1/2 inch and, again, these were found in the central holes.

Horizontal displacements and vertical separations have been observed in various small-diameter boreholes in the test room floors. Horizontal displacements up to 2 1/2 inches and vertical separations estimated to be up to 1/2 inch wide were present in some of these holes. Multiple displacements in single boreholes were also present. The horizontal displacements and vertical separations found in many of the holes are within MB-139 or coincide with the lower contact of this unit. These displacements and separations have developed since room excavation, although some of them may have developed along pre-existing planes of weakness in the marker bed.

In addition to observations made in open boreholes, ground-penetrating radar and gas permeability testing have been conducted in some of the test rooms. A radar survey was conducted in Test Rooms 2 and 3. The radar method has some limitations. It appears to be effective in locating the first reflector such as a fracture or clay seam beneath the floor, but the structure below this is not easily distinguished. MB-139 is readily defined on the records but fractures within it cannot be discerned.

Zones of relatively high permeability have been found to develop immediately beneath the floor of the test rooms and beneath the intersections of Test Rooms 1 and 2 with the N1420 drift. There also appears to be a slight increase in permeability, relative to background values, within MB-139 and immediately beneath the floor of the N1420

drift between Test Rooms 1 and 2. Some increase in permeability also appears to occur in MB-139 near the center of the pillar between Test Rooms 2 and 3. This data is only preliminary, however, because only one hole intersecting MB-139 beneath the pillar has been drilled and tested for permeability.

Gas tr er measurements performed along the centerline in the north half of Test Room 2 and across the N1420 drift to Room L2 indicate the existence of fracturing beneath the floor. A video survey of the boreholes used for the tracer tests shows the presence of fracture zones and separations mainly within MB-139. Holes tested along the N1420 drift, except at intersections, show little increase in background permeability. A video survey of these holes did not show any separations or fracturing.

In summary, subhorizontal fracturing has developed beneath the test room floors. The majority of this fracturing occurs as single fractures or thin fracture zones within MB-139 and the overlying halite. Horizontal displacements ranging up to 2 inches and separations generally ranging up to 1/2 inch have been measured in small diameter boreholes. Separations up to 6 inches have been observed locally. Only the south half of Test Room 3 (Room T) in the WIPP underground facility has exhibited extensive fracturing beneath the floor.

The Excavation Effects Program was designed in part to determine if fracturing similar to that occurring beneath the floor of Test Room 3 has developed in other areas of the facility. The results of this program show that, although small-scale fracturing is occurring beneath all of the test rooms, no other areas of fracturing have developed on the same order of magnitude as that in Test Room 3. The fracturing occurring beneath the floor of Test Room 3 appears to have existed prior to drilling. The stress changes induced by the size and number of holes drilled in this area probably exacerbated the existing fractures.

11.3.2.2 Closure

Roof-to-Floor Closure. Figure 11-3 shows the relationship between measured roof-to-floor closure and the elapsed time since excavation of the four test rooms, as determined from convergence meter and convergence point data. Because of differences in time-lag between the end of excavation and the time of the initial readings, the relative positions of these curves are deceptive. For analysis purposes, the roof-to-floor closure that occurred before installation of the convergence instruments was determined using equation 10-1 in Chapter 10.

In addition, part of the measurement data from the temporary convergence points were added to the permanent convergence instrument data to obtain approximate values of the actual roof-to-floor closure. Table 11-6 shows roof-to-floor convergence point readings and adjusted closure magnitudes for the test rooms. Item 7 in this table shows the approximate roof-to-floor closure obtained by adding suitable portions of the temporary convergence point readings to the readings of the permanent convergence instruments.

It is apparent that the fracturing observed in the floor of the test rooms, and vertical separations in the roof, have contributed to the total roof-to-floor closure. However, based on measured cumulative vertical separations in September 1985, the contribution of floor fracturing to the total roof-to-floor closure is not more than 1 inch.

The total estimated closure (item 9 in Table 11-6) includes the values of early closure estimated by using equation 10-1 in Chapter 10. Based on the indicated additive values, the maximum roof-to-floor closure of approximately 16 1/2 inches through June 1986 occurs in Test Rooms 2 and 3. Test Room 4 has undergone the least roof-to-floor closure. Figure 11-4 shows the adjusted roof-to-floor closure values as a function of time.

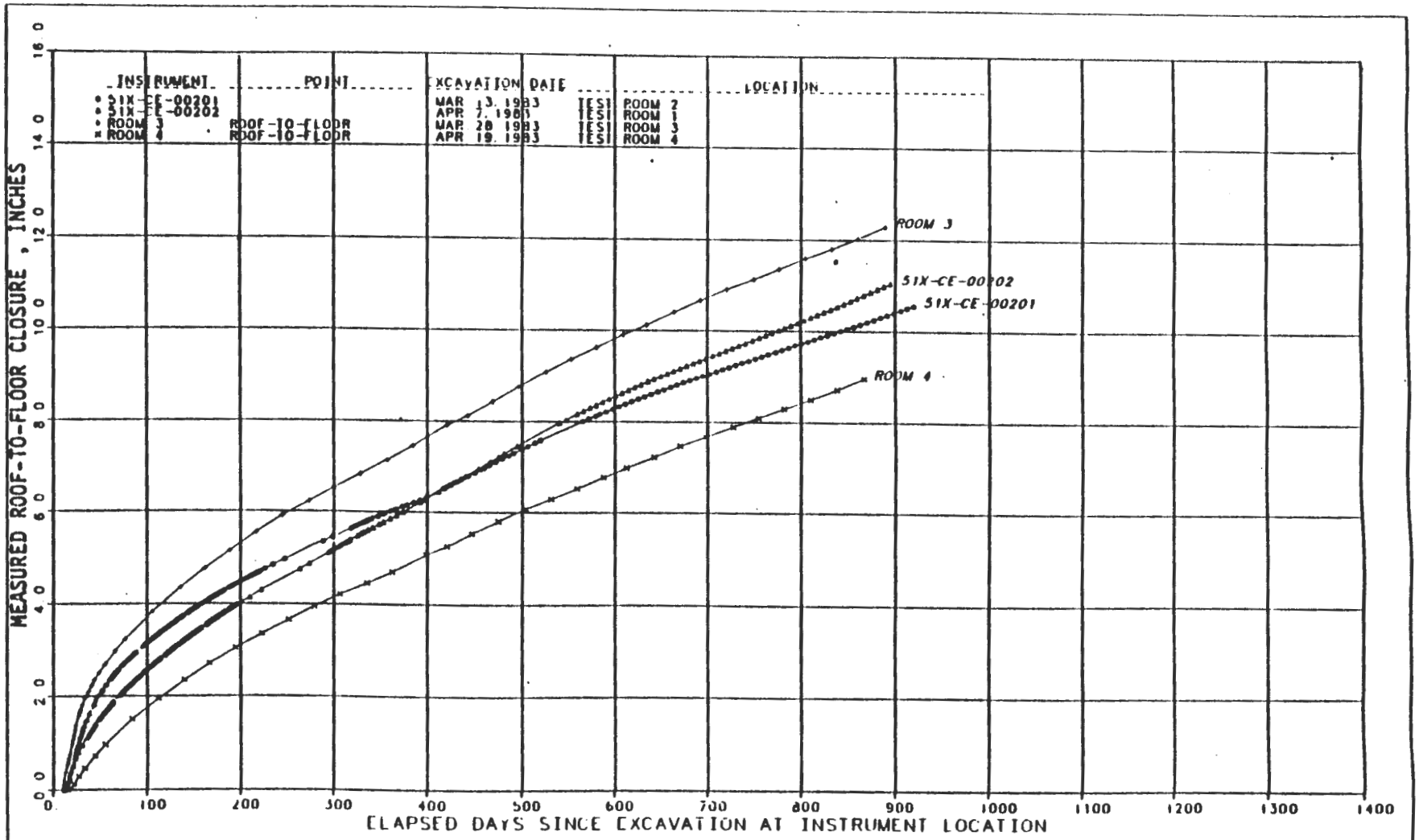


**Figure 11-3**

**TEST ROOMS**
**MEASURED ROOF-TO-FLOOR CLOSURE COMPARISON**

Table 11-6

TEST ROOMS
ROOF-TO-FLOOR CLOSURE COMPARISONS

| Description | Test Room 1 | 2 | 3 | 4 |
|---|---|---|---|---|
| (1) Excavation period | April 3-13 1983 | March 9-20 1983 | March 24-April 3 1983 | April 15-25 1983 |
| (2) Date of first reading of temporary convergence (TC) points | April 12, 1983 | March 21, 1983 | April 4, 1983 | April 26, 1983 |
| (3) Date of first reading of permanent convergence (RC and CE) instruments | April 20, 1983 | March 29, 1983 | April 7, 1983 | May 6, 1983 |
| (4) Reading of TC points (inches) on date indicated | 0.84 April 20, 1983 | 0.88 March 28, 1983 | 0.40 April 7, 1983 | 0.45 May 5, 1983 |
| (5) Reading of RC and CE instruments (inches) on date indicated | 13.11 June 13, 1986 | 12.20 June 13, 1986 | 13.83 April 28, 1986 | 10.62 April 28, 1985 |
| (6) Total elapsed days of combined TC and RC measurements [Date for (5) - Date for (2)] | 1157 | 1179 | 1120 | 1098 |
| (7) Total measured closure (inches) [(4) + (5)] | 13.95 | 13.08 | 14.23 | 11.07 |
| (8) Estimated closure (inches) by regression analysis for the period of (2) - (1) | 2.39 | 3.72 | 2.17 | 1.32 |
| (9) Total estimated closure (inches) [(7) + (8)] | 16.34 | 16.80 | 16.40 | 12.39 |

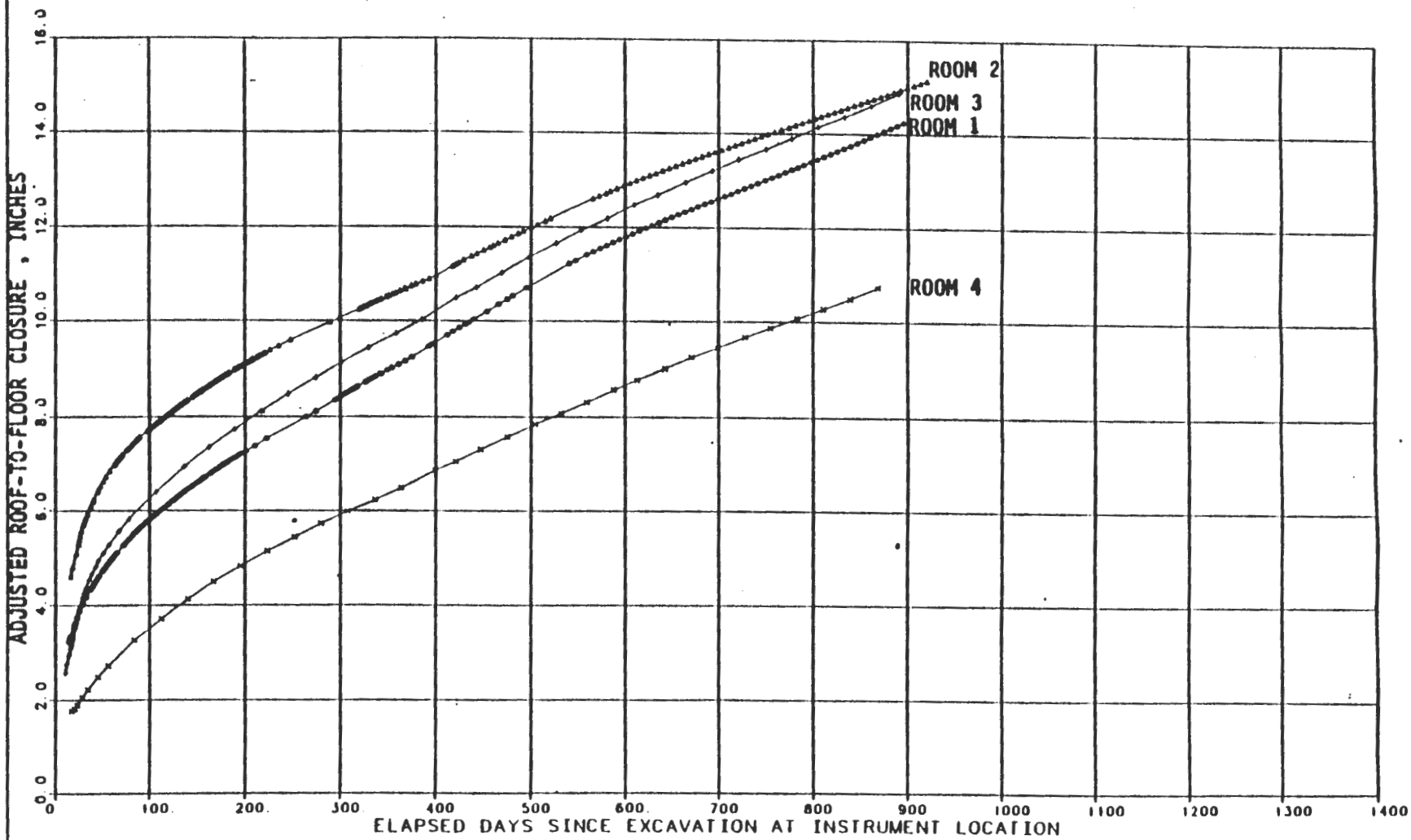


**Figure 11-4**

**TEST ROOMS**
**ADJUSTED ROOF-TO-FLOOR CLOSURE**

Figure 11-4 shows that the closure rate generally decreases with time, except for occasional increases due to disturbances from nearby excavations. Provided there are no additional perturbations in and around the test rooms, it is likely that the rate of closure will reach a steady state value. It is possible to get an estimate of the rate of closure using either a phenomenological rheological model or an empirical model that is essentially a curve-fitting procedure. Both methods have been attempted. Numerical methods using the phenomenological approach are discussed in Chapter 5.

Closure rates rather than measured closure are used in the empirical approach because measured closure is not absolute. Early closure measurements are not available because the instruments could not be installed immediately after excavation. However, the calculation of closure rates is not affected by the lack of early measurements. The closure rates are calculated by assuming a linear relationship between closure and elapsed time over a short interval. This time interval has been arbitrarily chosen as a minimum of 7 days.

Because it is expected that the closure rate will initially be relatively high and then decrease to a steady rate, the following equation was used:

$$C(t) = \frac{A}{t^n} + C_c(1 - e^{-at}) \qquad (11\text{-}1)$$

where: $C(t)$ is the closure rate at elapsed time t after excavation;
A, a and n are constants which depend upon the deformation characteristics of the salt, initial stress regime and dimensions of the opening; and
$C_c$ is the steady state closure rate.

The value of C(t) is obtained by arbitrarily choosing a time interval of not less than 7 days. If $R_i$ is the closure reading at calendar time $t_i$ and $R_{i+1}$ is the closure reading at $t_{i+1}$, then

$$C(t) = \frac{R_{i+1} - R_i}{\Delta t} \tag{11-2}$$

where: $\Delta t = (t_{i+1} - t_i) \quad \geq 7$ days (11-3)

The value of t is defined as:

$$t = \frac{t_i + t_{i+1}}{2} \tag{11-4}$$

A regression analysis, which is the fitting of an equation like 11-1 to the set of [C(t),t] data points, was performed using NLIN, a commercially available statistical software package (ref. 11-1). The general method used to estimate the constants, herein called the regression parameters, was to minimize the sum of the squares of the differences between the actual measured values and the values predicted by the proposed equation.

Equation 11-1, a nonlinear equation, cannot be converted into linear form. The statistical software NLIN employs iterative methods that attempt to find least-square estimates for nonlinear models. The methods commonly employed are the Gauss-Newton technique and the Marquardt compromise technique (ref. 11-2). However, the requisite partial derivatives of the equation with respect to the parameters must be specified. In many cases, the Marquardt compromise, which is considered to work well in many circumstances, gives a better estimate and provides quicker convergence of the values of the regression parameters. However, nonlinear regression analyses may not always result in good estimates of the regression parameters. In addition, the analysis tacitly assumes that the regressor variables are measured without error. Thus, the observations, which in this case are the values of C(t), were not weighted.

Figure 11-5 compares the roof-to-floor closure rates for Test Room 1 calculated by equation 11-1 to the values calculated using the fitted equation 11-2. The data used was obtained during the first year following the completion of excavation. The regression analysis showed that, for all practical purposes, equation 11-1 could be simplified as

$$C(t) = \frac{A}{t^n} + C_c \qquad (11\text{-}5)$$

because the value of 'a' obtained from the regression analysis was large enough to make the term $e^{-at}$ comparatively negligible. The fitted equation for the roof-to-floor closure data in Test Room 1 has the form

$$C(t) = \frac{206.58}{t^{0.84}} + 2.24(1-e^{-5.27t}) \text{ inches/year} \qquad (11\text{-}6)$$

where: t is the elapsed time in days since excavation.

However, as shown by equation 11-5, equation 11-6 can be approximated as

$$C(t) = \frac{206.58}{t^{0.84}} + 2.24 \text{ inches/year} \qquad (11\text{-}7)$$

The method used was the Marquardt compromise technique. The coefficient of determination is 0.99.

The analysis was repeated later using roof-to-floor closure data at 980 days (2.68 years) after the completion of excavation. The regression equation was

$$C(t) = \frac{211.16}{t^{0.85}} + 2.44 \text{ inches/year} \qquad (11\text{-}8)$$

The steady state closure rate determined using the first year of data only is 9 percent less than the rate determined by using 2.68 years of

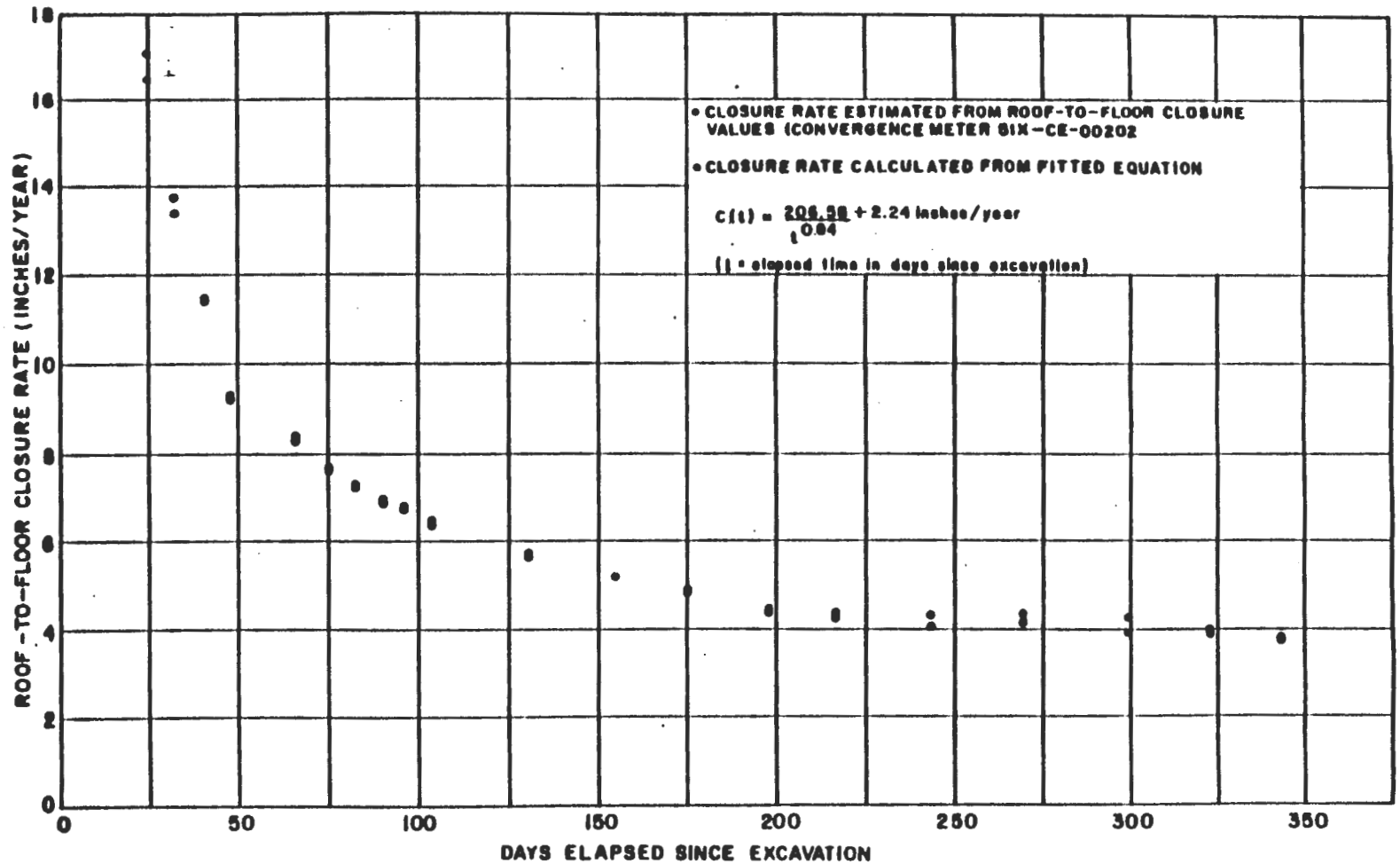


Figure 11-5

TEST ROOM 1
REGRESSION ANALYSIS OF ROOF-TO-FLOOR CLOSURE

data. A third analysis, using 3 years of measurement data, up to June 1986, gave

$$C(t) = \frac{208}{t^{0.85}} + 2.40 \text{ inches/year} \qquad (11\text{-}9)$$

Equations 11-7, 11-8 and 11-9 show the consistency of the regression parameters for different input data sets.

Figure 11-6 shows the predicted roof-to-floor closure rate for Test Room 1 as a function of elapsed time in years using equation 11-9. Based on equation 11-7, the roof-to-floor closure rate at the end of 25 years is expected to be approximately 2.34 inches/year. Using equation 11-8, it will be 2.53 inches/year or 2.49 inches/year using equation 11-9.

Figures 11-7 through 11-10 show the fitted curves based on roof-to-floor closure rates calculated from equation 11-2, using data up to June 1986. To get an approximate idea of the roof-to-floor closure for periods of time greater than 1 year since the completion of excavation, equation 11-7 was integrated with respect to time between the limits of 1 year and time $t_2$ (in years) to yield

$$R(t) = 0.78(t_2^{0.147} - 1) + 0.20(t_2 - 1) \qquad (11\text{-}10)$$

Figure 11-11 shows the predicted roof-to-floor closure in feet for Test Room 1 (excluding that which has occurred in the first year after excavation) as a function of time in years. According to this prediction, 25 years after excavation this value will be 5.34 feet. A similar analysis using equation 11-9 gave a value of 5.3 feet.

Table 11-7 is a summary of the results of the nonlinear regression analyses for the roof-to-floor closure rates in the test rooms using 3 years of measurement data. The parameters contained in this table are applicable for an elapsed time expressed in years. For Test Room 4, the regression analysis using only the permanent convergence point data did not produce satisfactory results. The analysis was

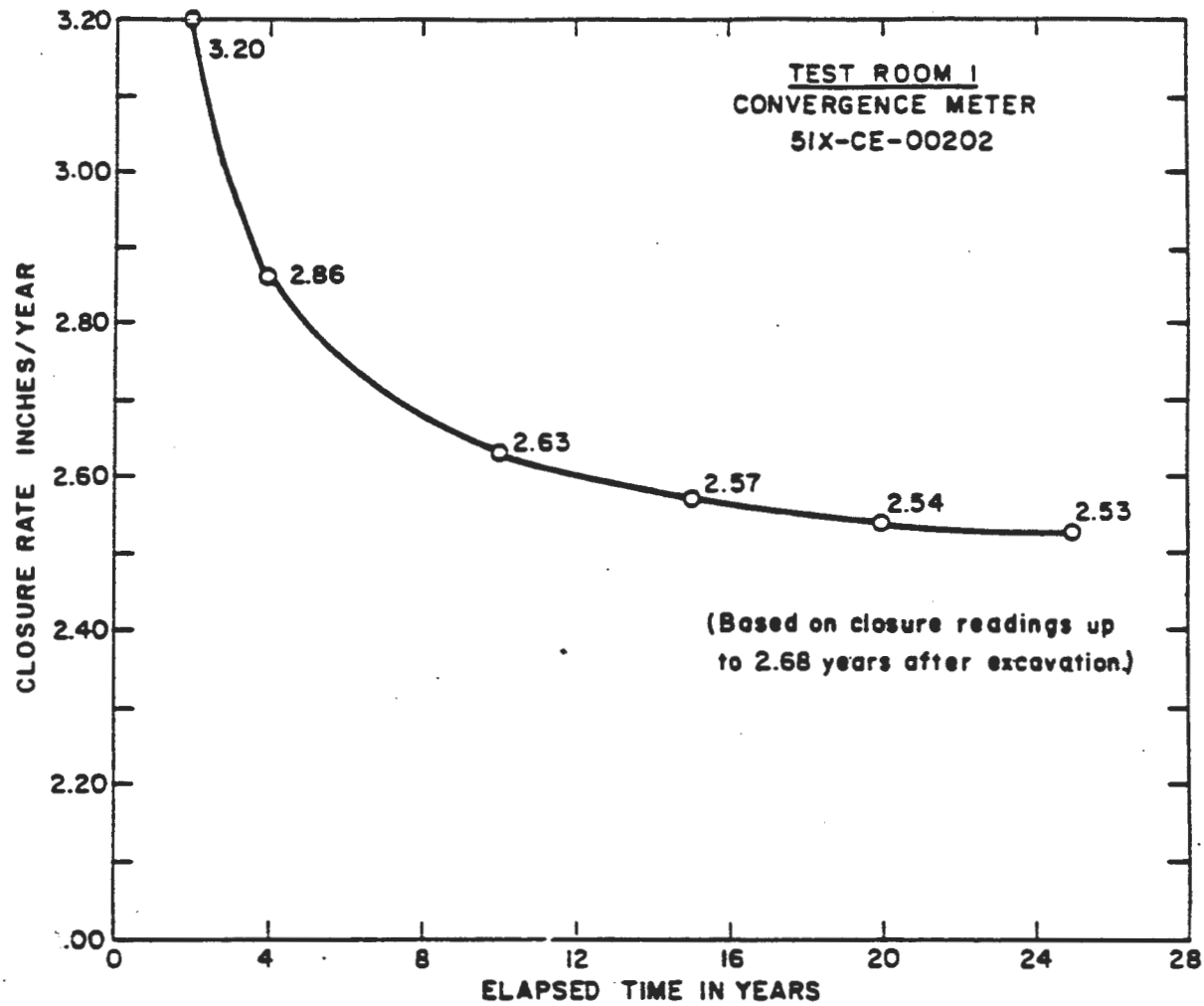


Figure 11-6

TEST ROOM 1
PREDICTED ROOF-TO-FLOOR CLOSURE RATE

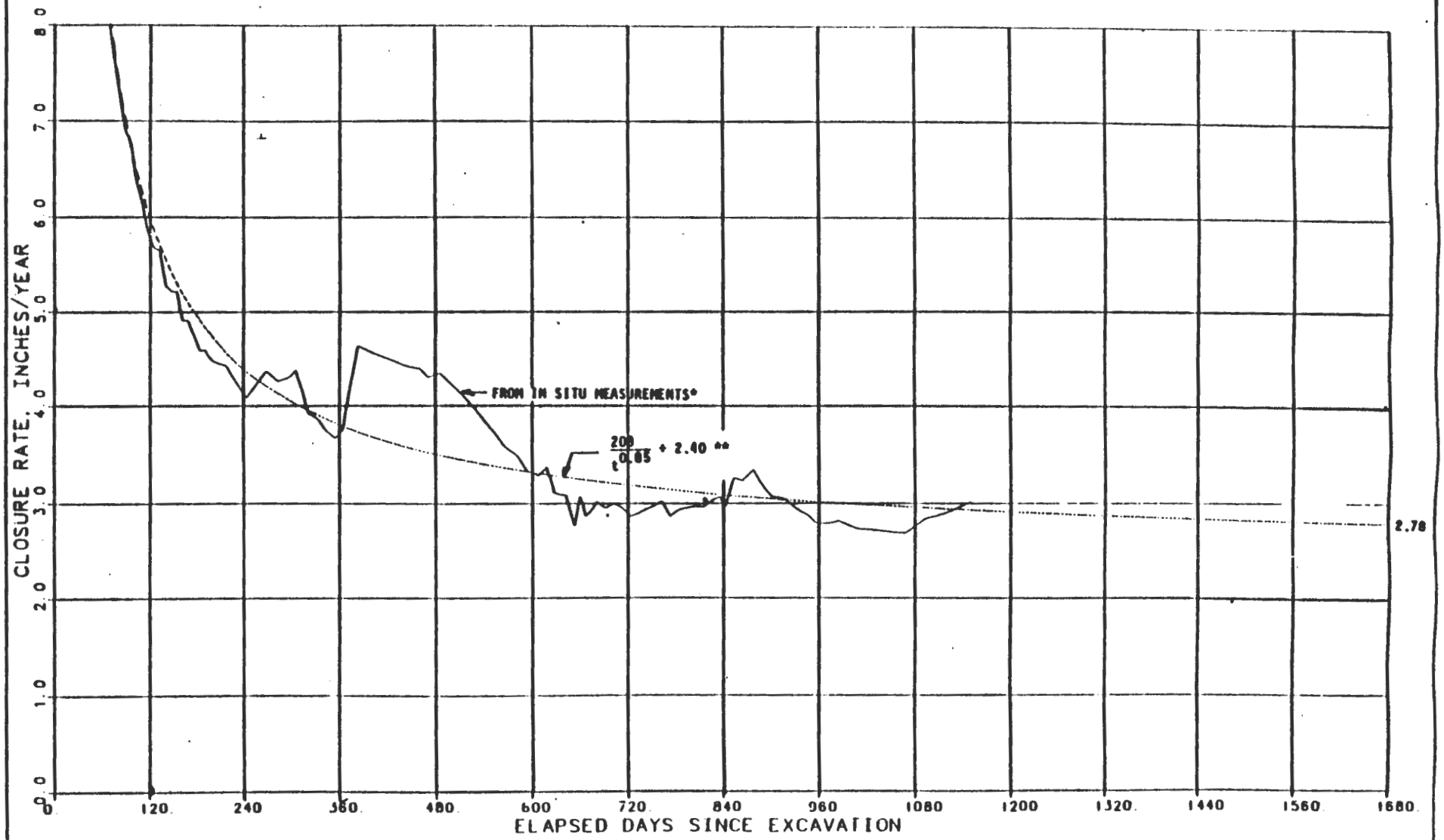


* RATE CALCULATED FOR TIME INTERVAL ≥7 DAYS.

** REGRESSION ANALYSIS OF IN SITU DATA UP TO JUNE 1986.

**Figure 11-7**

**TEST ROOM 1 ROOF-TO-FLOOR CLOSURE RATE RESULTS OF REGRESSION ANALYSIS**

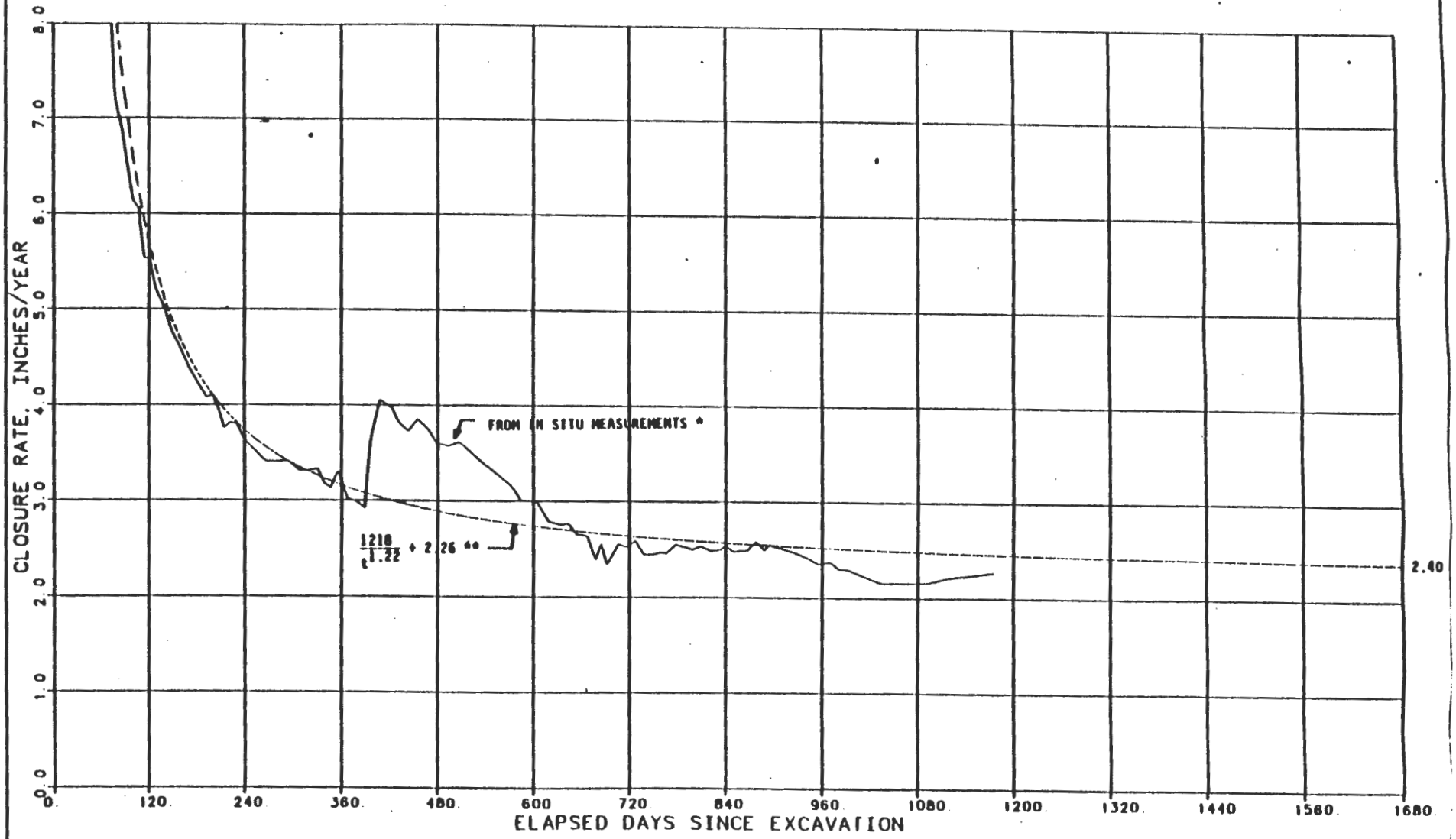


* RATE CALCULATED FOR TIME INTERVAL ≥7 DAYS.

** REGRESSION ANALYSIS OF IN SITU DATA UP TO JUNE 1986.

**Figure 11-8**

TEST ROOM 2 ROOF-TO-FLOOR CLOSURE RATE
RESULTS OF REGRESSION ANALYSIS

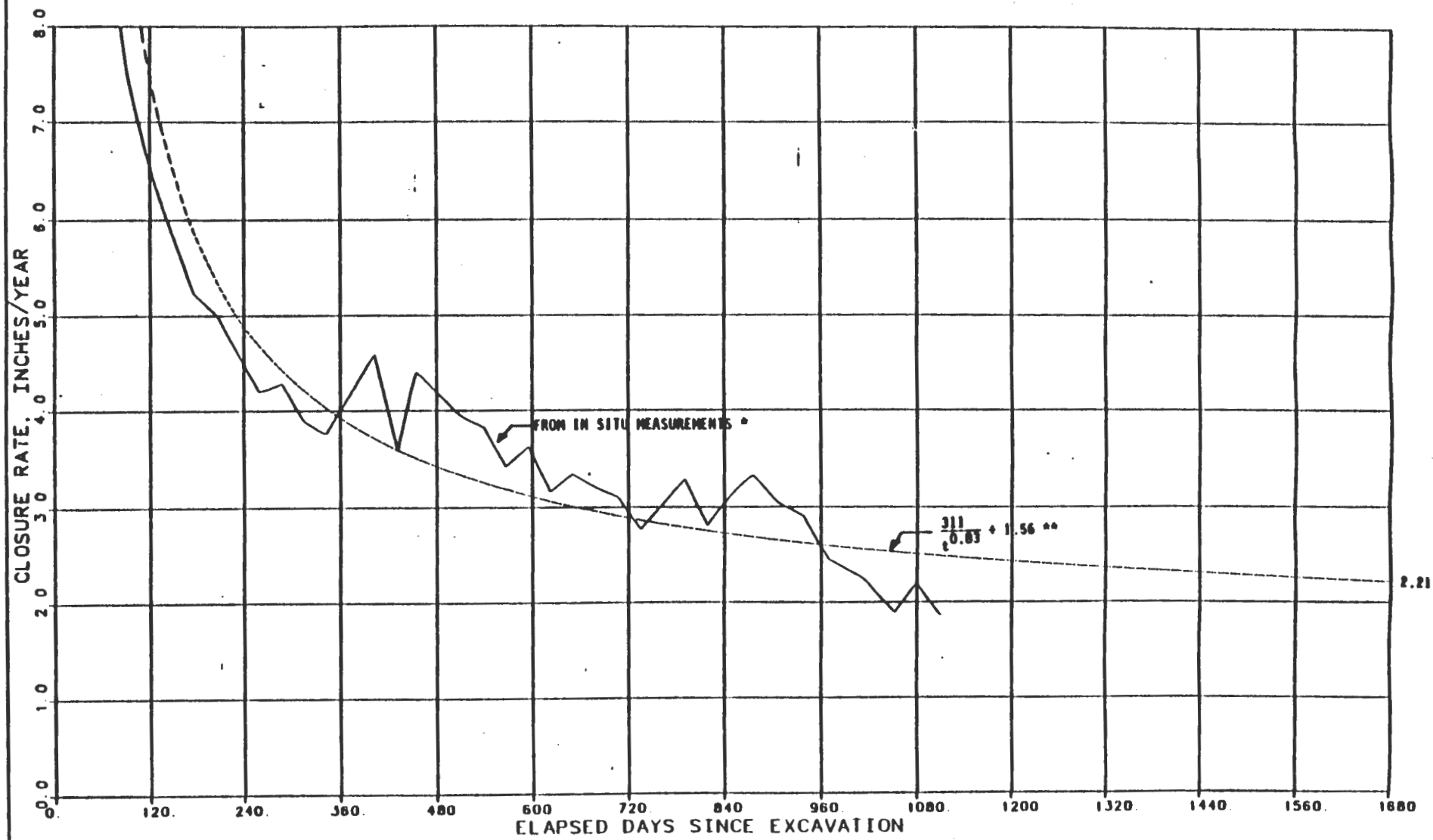


* RATE CALCULATED FOR TIME INTERVAL ≥7 DAYS.

** REGRESSION ANALYSIS OF IN SITU DATA UP TO JUNE 1986.

**Figure 11-9**

**TEST ROOM 3 ROOF-TO-FLOOR CLOSURE RATE RESULTS OF REGRESSION ANALYSIS**

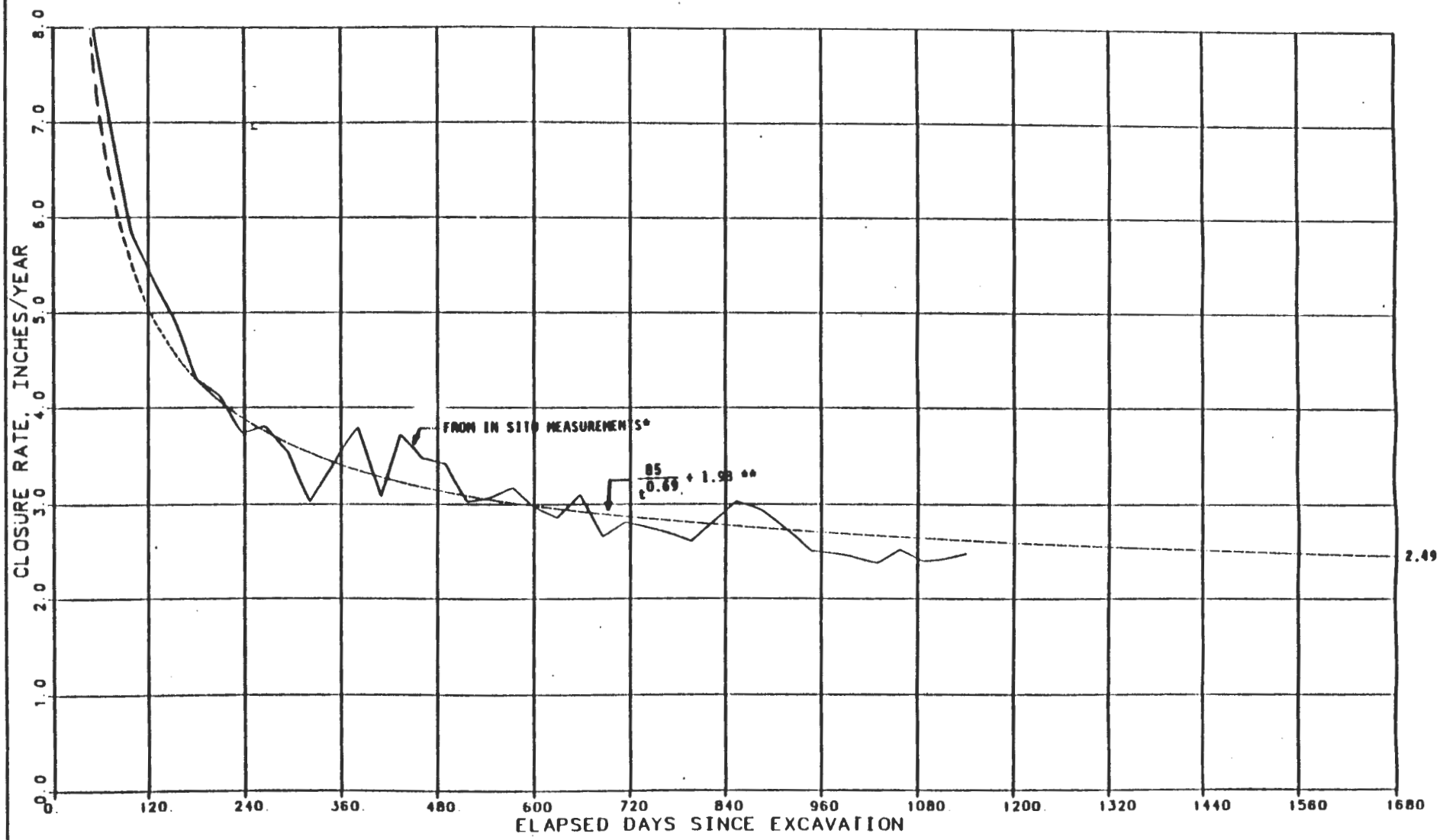


* RATE CALCULATED FOR TIME INTERVAL ≥7 DAYS.

** REGRESSION ANALYSIS OF IN SITU DATA UP TO JUNE 1986.

**Figure 11-10**

**TEST ROOM 4 ROOF-TO-FLOOR CLOSURE RATE RESULTS OF REGRESSION ANALYSIS**

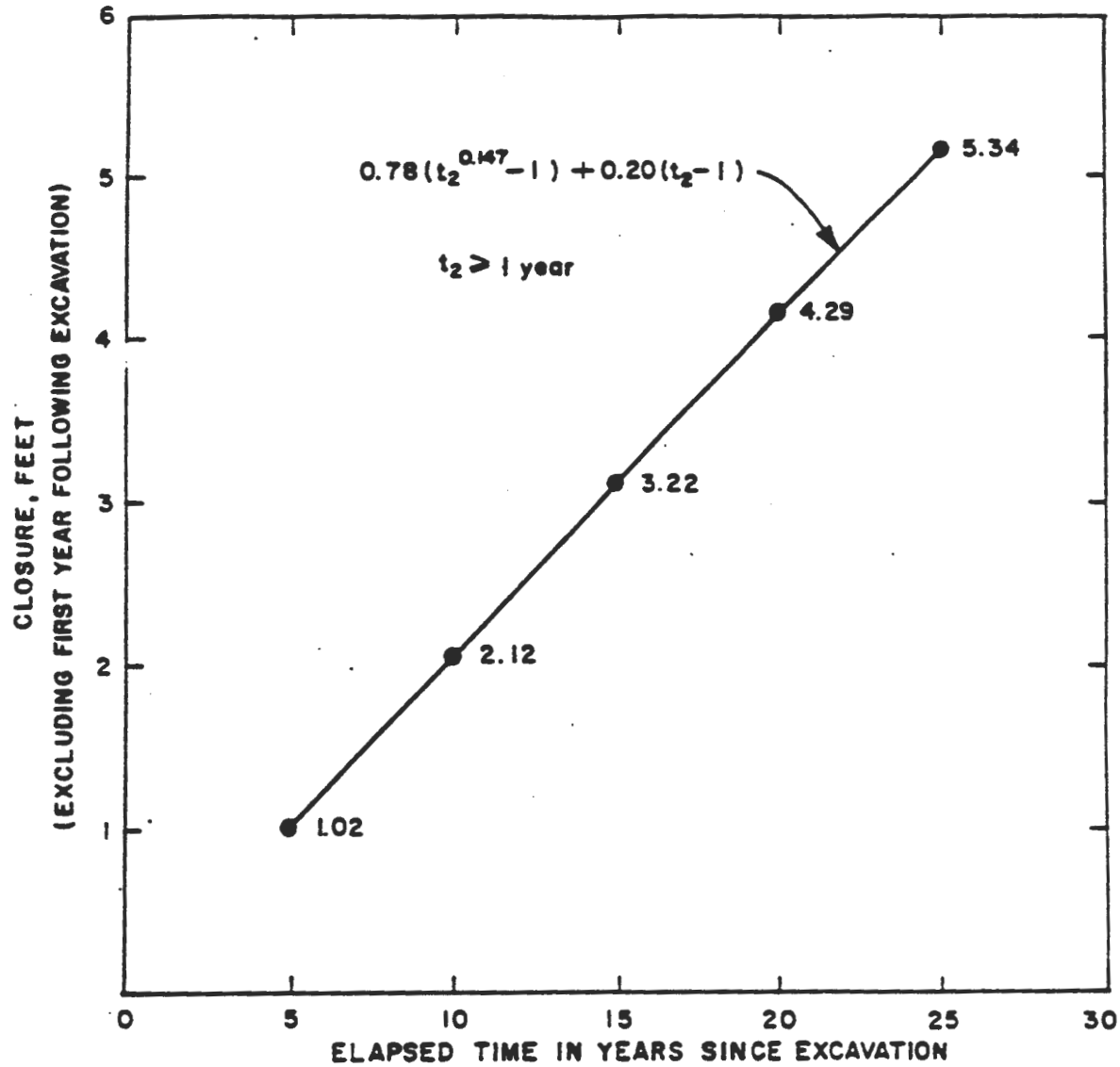


Figure 11-11

TEST ROOM 1
PREDICTED ADDITIONAL ROOF-TO-FLOOR CLOSURE

Table 11-7

TEST ROOMS
SUMMARY OF RESULTS OF REGRESSION ANALYSES
FOR ROOF-TO-FLOOR CLOSURE RATES

| Description | Test Room 1 | 2 | 3 | 4* |
|---|---|---|---|---|
| Regression Parameters** | | | | |
| A | 208 | 1218 | 311 | 85 |
| n | 0.85 | 1.22 | 0.83 | 0.69 |
| $C_c$ | 2.40 | 2.26 | 1.56 | 1.98 |
| $r^2$ | 0.99 | 0.98 | 0.94 | 0.97 |

Note: Analyses based on data obtained through June 1986.

* Data used for regression analysis includes data from temporary convergence points.

** Equation is: $C(t) = \frac{A}{t^n} + C_c$

where: C(t) is closure rate in inches/year;
A and n are constants;
t is elapsed time in days; and
$C_c$ is steady state closure rate.

$r^2$ is the coefficient of determination.

repeated with the inclusion of temporary convergence point data, and produced good results. The results of the regression analysis of roof-to-floor closure rates discussed in this subsection are used in Chapter 12 to define the bounds on the roof-to-floor closure rates for the storage rooms.

Wall-to-Wall Closure. Figure 11-12 summarizes the measured wall-to-wall closure magnitudes for the test rooms. Because of the lack of early measurements, the relative positions of the individual curves are not absolute. Table 11-8 presents an estimate of the actual wall-to-wall closure for the four test rooms. The approach is similar to the one used for estimating the actual roof-to-floor closure values. The maximum wall-to-wall closure occurs in Test Room 3 and is about 13 inches. The minimum wall-to-wall closure is about 9 inches in Test Room 4.

The regression analysis of wall-to-wall closure rates for Test Room 1, using measurement data up to June 1986, shows that the equation has the form

$$C(t) = \frac{202}{t^{0.94}} + 1.75 \text{ inches/year} \qquad (11\text{-}11)$$

where: t = elapsed time in days since excavation.

Comparing equation 11-11 with equation 11-9, the long-term wall-to-wall closure rate will be 73 percent of the roof-to-floor closure rate.

Table 11-9 is a summary of the results of the regression analyses for the wall-to-wall closure rates in Test Rooms 1 through 4. The closure rate values determined from temporary convergence point readings were included in the analysis of Test Room 2. The fitted curves for Test Rooms 2 and 3 are relatively poor. Figures 11-13 through 11-16 show the fitted equations for the wall-to-wall closure rate versus elapsed time curves for Test Rooms 1 through 4.

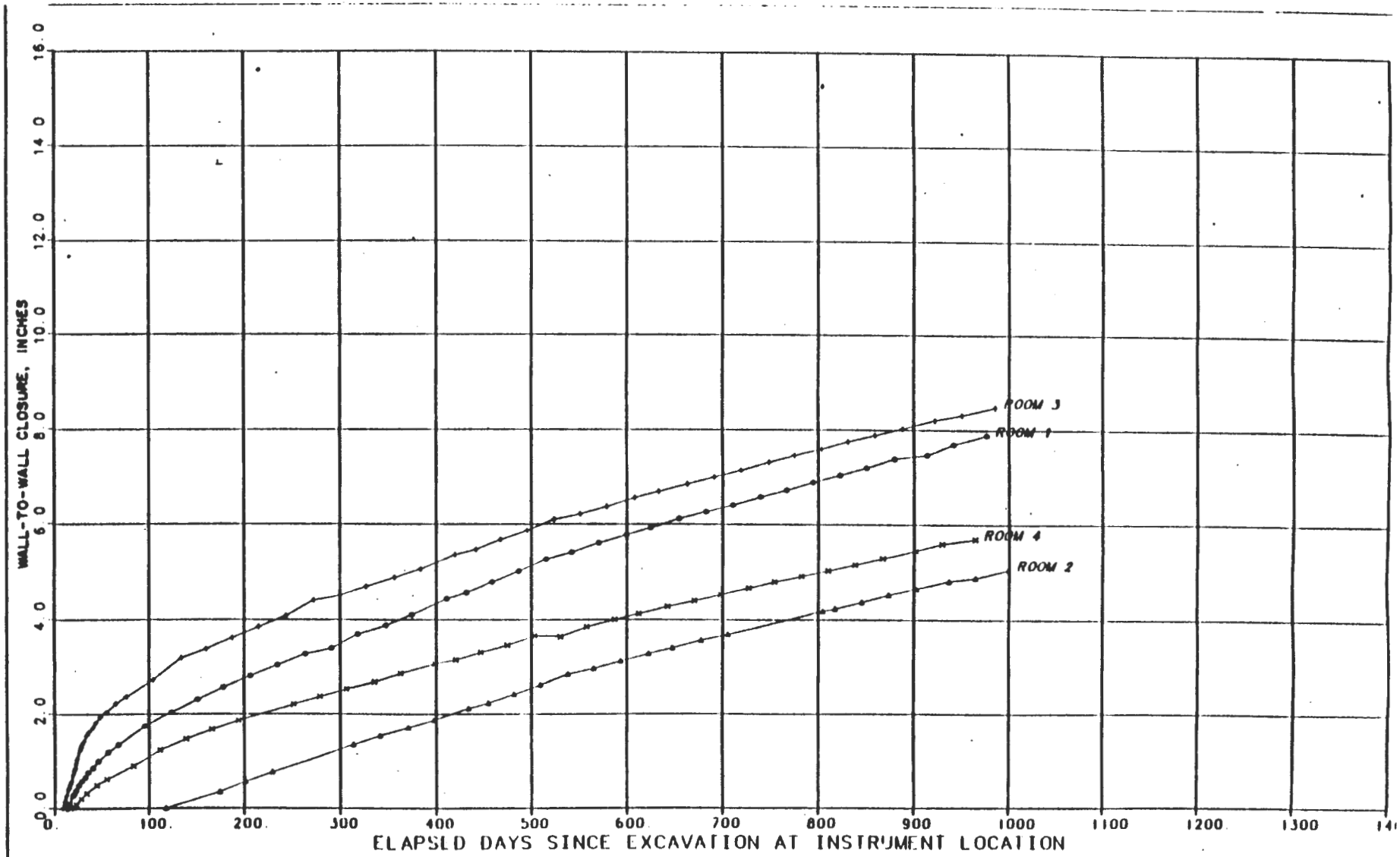


**Figure 11-12**

**TEST ROOMS**
**WALL-TO-WALL CLOSURE COMPARISON**

Table 11-8

TEST ROOMS
WALL-TO-WALL CLOSURE COMPARISONS

| Description | Test Room 1 | Test Room 2 | Test Room 3 | Test Room 4 |
|---|---|---|---|---|
| (1) Excavation period | April 3-13 1983 | March 9-20 1983 | March 24-April 3 1983 | April 15-25 1983 |
| (2) Date of first reading of temporary convergence (TC) points | April 9, 1983 | March 21, 1983 | March 31, 1983 | April 21, 1983 |
| (3) Date of first reading of permanent convergence (RC) points | April 20, 1983 | July 12, 1983 | April 7, 1983 | May 6, 1983 |
| (4) Reading of TC points (inches) on date indicated | 1.58 April 20, 1983 | 3.36 July 12, 1983 | 1.42 April 7, 1983 | 1.48 May 5, 1983 |
| (5) Reading of RC points (inches) on date indicated | 8.82 June 16, 1986 | 5.82 June 16, 1986 | 9.24 June 16, 1986 | 6.39 June 16, 1986 |
| (6) Total elapsed days of combined TC and RC measurements [Date for (5) - Date for (2)] | 1166 | 1151 | 1176 | 1151 |
| (7) Total measured closure (inches) [(4) + (5)] | 10.40 | 9.18 | 10.66 | 7.87 |
| (8) Estimated closure (inches) by regression analysis for the period of (2) - (1) | 1.79 | 2.51 | 2.16 | 1.42 |
| (9) Total estimated closure (inches) [(7) + (8)] | 12.19 | 11.69 | 12.82 | 9.29 |

Table 11-9

TEST ROOMS
SUMMARY OF RESULTS OF REGRESSION ANALYSES
FOR WALL-TO-WALL CLOSURE RATES

| Description | Test Room 1 | 2* | 3 | 4 |
|---|---|---|---|---|
| Regression Constants** | | | | |
| A | 202 | 222 | 231 | 1766 |
| n | 0.94 | 0.79 | 0.83 | 1.81 |
| $C_c$ | 1.75 | 0.30 | 0.74 | 1.88 |
| $r^2$ | 0.96 | 0.95 | 0.92 | 0.99 |

Note: Analyses based on data obtained through June 1986.

* Data used for regression analysis includes data from temporary convergence points.

** Equation is: $C(t) = \frac{A}{t^n} + C_c$

where: C(t) is closure rate in inches/year;
A and n are constants;
t is elapsed time in days; and
$C_c$ is steady state closure rate.

$r^2$ is the coefficient of determination.

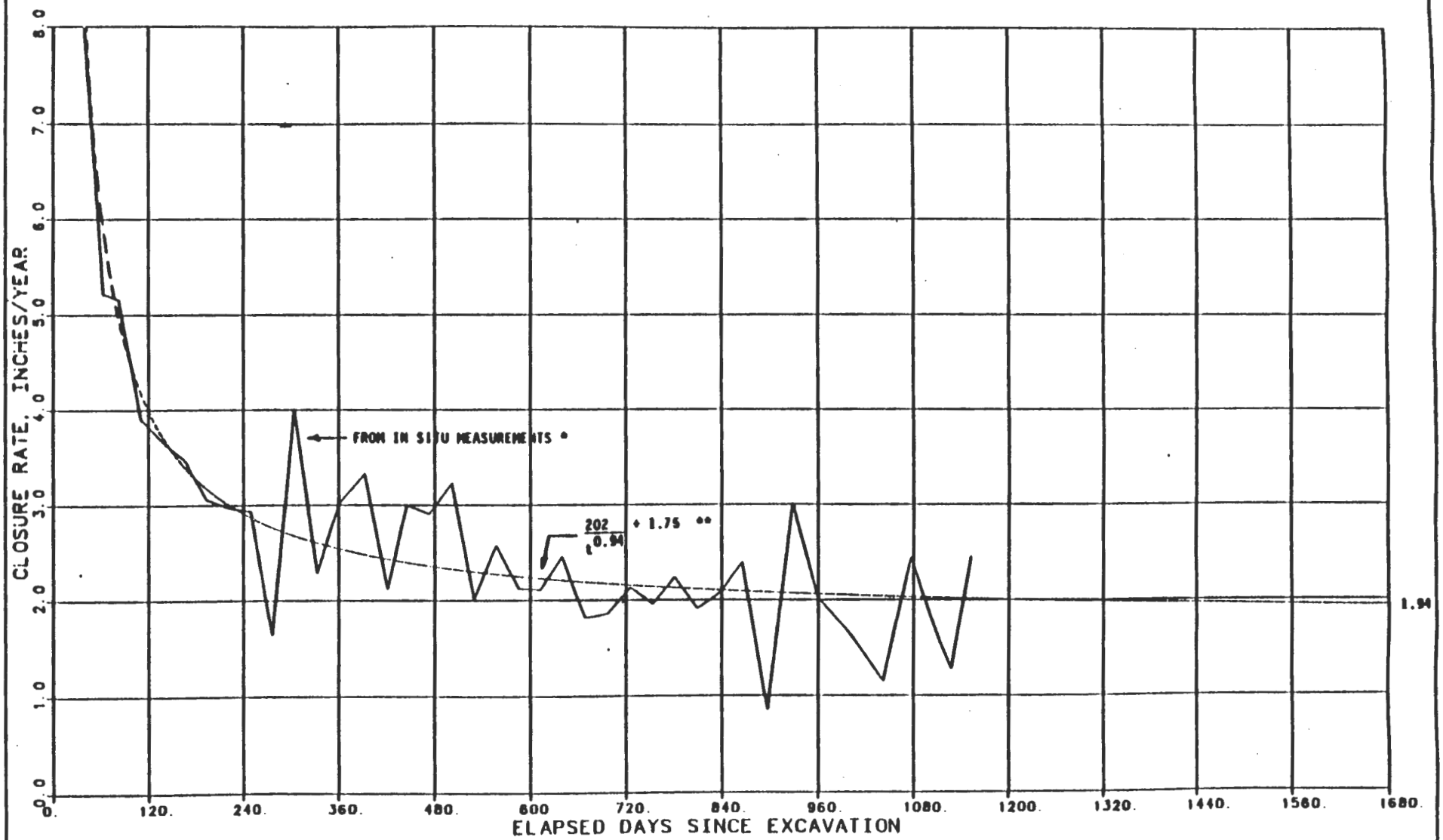


* RATE CALCULATED FOR TIME INTERVAL ≥7 DAYS.

** REGRESSION ANALYSIS OF IN SITU DATA UP TO JUNE 1986.

**Figure 11-13**

**TEST ROOM 1 WALL-TO-WALL CLOSURE RATE RESULTS OF REGRESSION ANALYSIS**

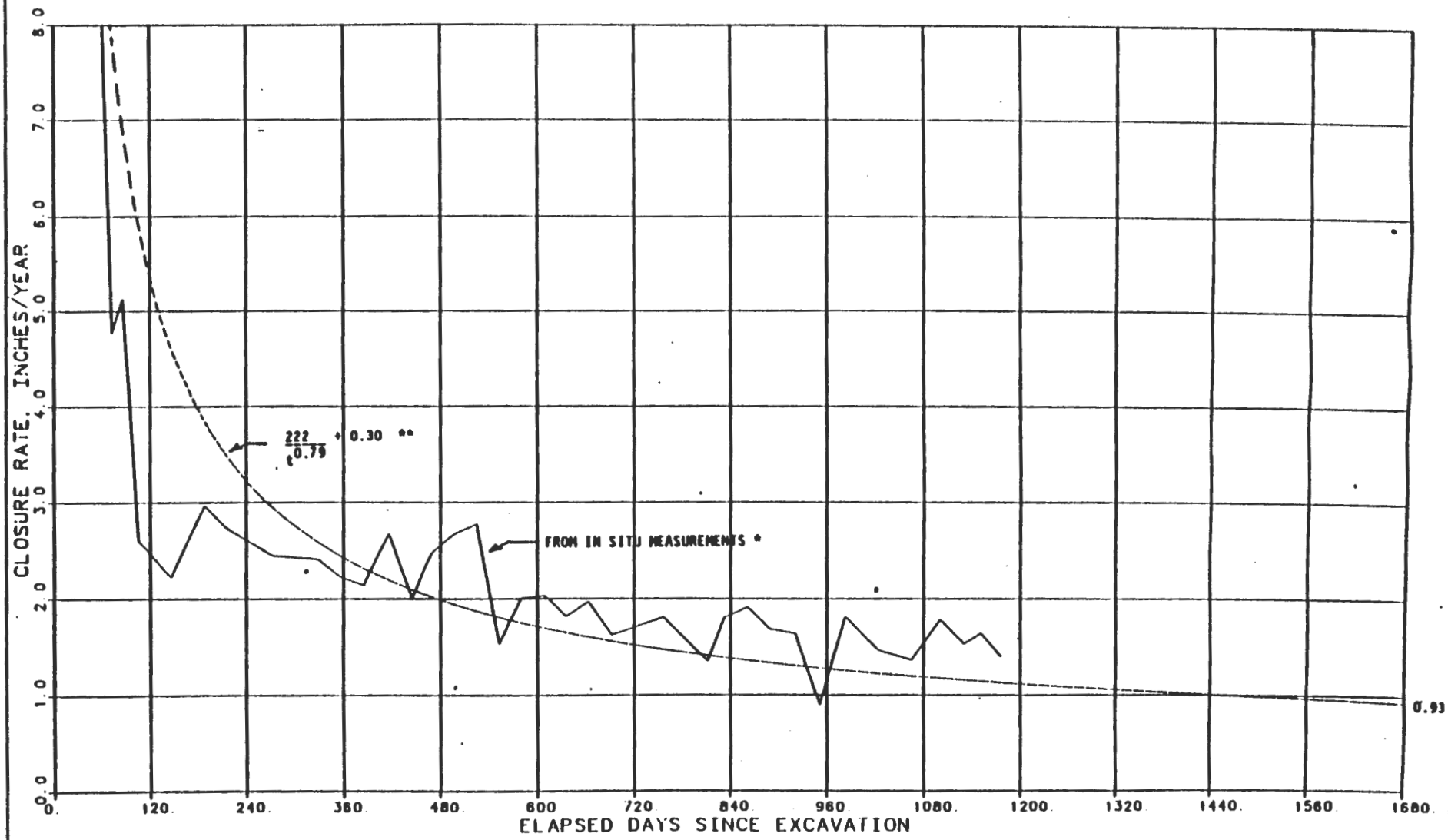


* RATE CALCULATED FOR TIME INTERVAL ≥7 DAYS.

** REGRESSION ANALYSIS OF IN SITU DATA UP TO JUNE 1986.

**Figure 11-14**

**TEST ROOM 2 WALL-TO-WALL CLOSURE RATE RESULTS OF REGRESSION ANALYSIS**

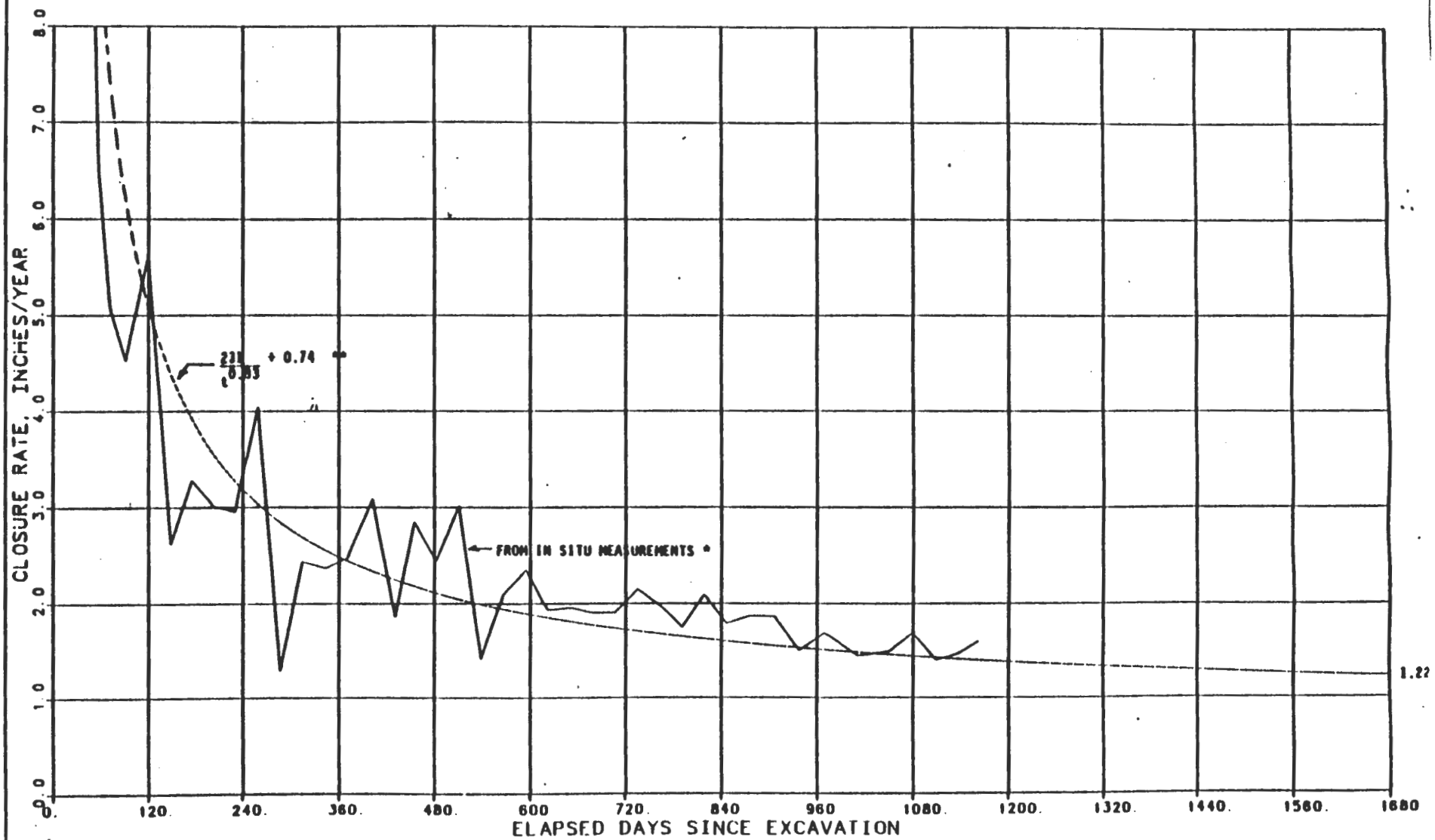


* RATE CALCULATED FOR TIME INTERVAL ≥7 DAYS.

** REGRESSION ANALYSIS OF IN SITU DATA UP TO JUNE 1986.

**Figure 11-15**

TEST ROOM 3 WALL-TO-WALL CLOSURE RATE
RESULTS OF REGRESSION ANALYSIS

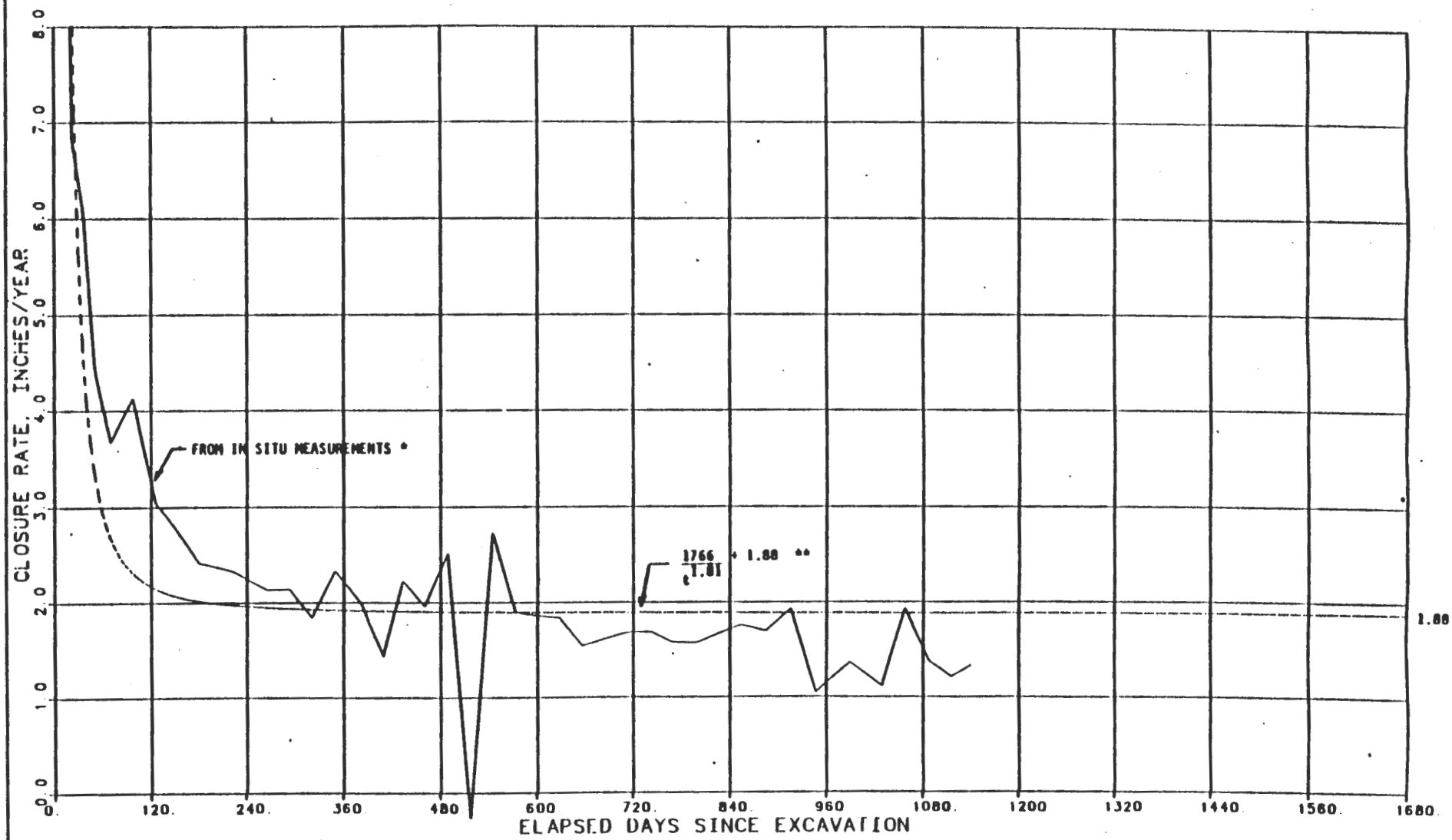


* RATE CALCULATED FOR TIME INTERVAL ≥7 DAYS.

** REGRESSION ANALYSIS OF IN SITU DATA UP TO JUNE 1986.

**Figure 11-16**

**TEST ROOM 4 WALL-TO-WALL CLOSURE RATE RESULTS OF REGRESSION ANALYSIS**

Table 11-10 is a summary of the collar readings from the wall multiple-point borehole extensometers in the test rooms. Because the extensometers could not be installed as soon as the excavation was completed, the collar readings do not reflect absolute closure. The table also shows the sum of the collar movements from both the east and west walls in each of the rooms except Test Room 3, which has no extensometer in the west wall. The last two columns of this table permit a comparison of the sum of the collar movements with wall-to-wall convergence point readings. Ideally, providing the salt is homogeneous, the central vertical lines of the pillars between Test Rooms 1 and 2 and Test Rooms 2 and 3 should be lines of symmetry with zero lateral strain. The deepest anchor at 50 feet for extensometers 51X-GE-00213 and 51X-GE-00215 should be expected to undergo negligible displacement. Therefore, the sum of the collar movements for Test Rooms 2 and 3 should be approximately the same as the wall-to-wall convergence point readings. As shown in Table 11-10, this is the case for Test Room 2. Exact equivalence is difficult to obtain because the collars of the extensometers are recessed into the wall by variable amounts and the time-lag between the end of excavation and the date of initial reading is not the same for the extensometers and the convergence points.

Comparison of Roof-to-Floor to Wall-to-Wall Closure Rates. Table 11-11 presents recent roof-to-floor and wall-to-wall closure rates for the test rooms. The rates were calculated using convergence point readings with a time interval of approximately 1 month. Based on these readings, the average wall-to-wall closure rate is approximately 68 percent of the roof-to-floor closure rate.

### 11.3.2.3 Deformation

An indication of the deformation of the salt around the test rooms may be obtained by comparing inclinometer measurements around a room. Figure 11-17 shows the cumulative measurements from the four wall inclinometers located around Test Room 3 through March 6, 1985. The inclinations are measured along the plane of the cross section.

Table 11-10

TEST ROOMS
WALL EXTENSOMETER COLLAR MOVEMENTS VERSUS CONVERGENCE POINT READINGS

| Test Room | Extensometer | Location | Readings on June 13, 1986 (inches) | Sum of East & West Readings (inches) | Wall-to-Wall Convergence Point Readings on June 16, 1986 (inches) |
|---|---|---|---|---|---|
| 1 | 51X-GE-00217 | East wall | 3.16 | 7.36 | 8.82* |
| | 51X-GE-00219 | West wall | 4.20 | | |
| 2 | 51X-GE-00213 | East wall | 4.95 | 9.52 | 9.18** |
| | 51X-GE-00215 | West wall | 4.57 | | |
| 3 | 51X-GE-00211 | East wall | 4.17 | - | 9.24* |
| | - | West wall | - | | |
| 4 | 51X-GE-00206 | East wall | 3.26 | 5.95 | 6.39* |
| | 51X-GE-00208 | West wall | 2.69 | | |

* From (5) in Table 11-8.
** From (7) in Table 11-8.

Table 11-11

TEST ROOMS
CLOSURE RATE COMPARISONS

| Description of Closure Location | Test Room 1 | Test Room 2 | Test Room 3 | Test Room 4 |
|---|---|---|---|---|
| **Roof-to-Floor** | | | | |
| Reading/Date | 12.88/May 16, 1986 | 12.03/May 16, 1986 | 13.65/Mar. 24, 1986 | 10.39/Mar. 24, 1986 |
| Reading/Date | 13.11/June 13, 1986 | 12.20/June 13, 1986 | 13.83/Apr. 28, 1986 | 10.62/Apr. 28, 1986 |
| Difference in readings | 0.23 inch | 0.17 inch | 0.18 inch | 0.23 inch |
| Time interval | 28 days | 28 days | 27 days | 27 days |
| Rate ($\dot{V}$) | 3.00 inch/yr | 2.22 inch/yr | 2.43 inch/yr | 3.10 inch/yr |
| **Wall-to-Wall** | | | | |
| Reading/Date | 8.63/May 19, 1986 | 5.72/May 19, 1986 | 8.90/Mar. 24, 1986 | 6.09/Mar. 24, 1986 |
| Reading/Date | 8.82/June 16, 1986 | 5.82/June 16, 1986 | 9.03/Apr. 28, 1986 | 6.22/Apr. 28, 1986 |
| Difference in | 0.19 inch | 0.10 inch | 0.13 inch | 0.13 inch |

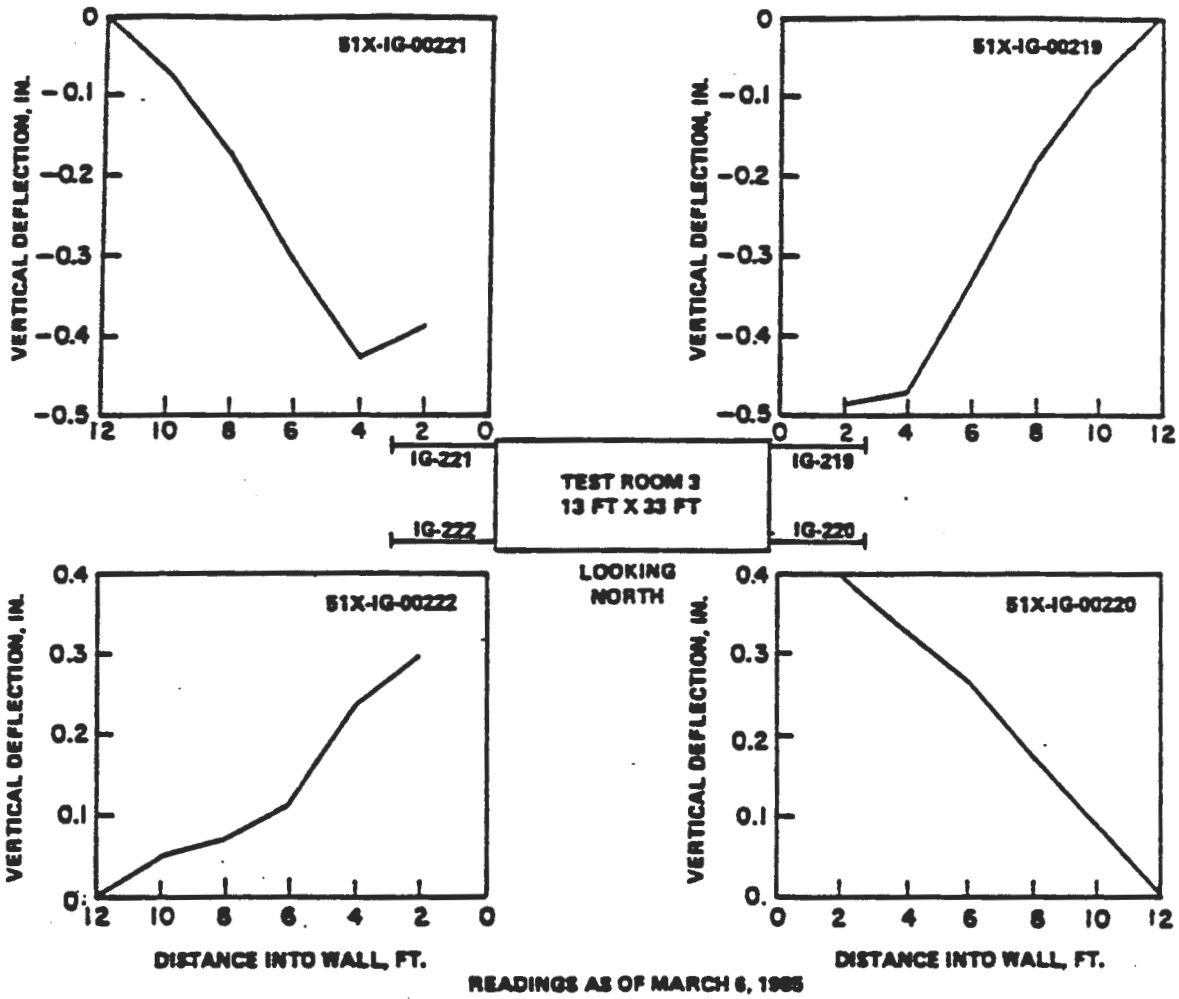


Figure 11-17

TEST ROOM 3
WALL INCLINOMETER BEHAVIOR

Figure 11-18 shows the inclinometer behavior around Test Room 4 through March 6, 198 . The initial readings from these inclinometers were taken 9 to 15 days after the completion of excavation in the test room. The current readings indicate that the maximum relative vertical deflection is on the order of 1 inch over a length of 12 feet.

The inclinometers near the roof show vertical downward deflection while those near the floor indicate upward deflection. This indicates that the central multiple-point borehole extensometers located in the walls of the test rooms probably undergo negligible vertical deflection.

11.3.2.4 Bay Strains

Relative movements between anchors of the multiple-point borehole extensometers will provide an approximate distribution of salt deformation around the excavated openings. The relative displacements are normalized over the spacing between anchors and are termed "bay strains". The bay strain is approximately the average axial strain between any two anchor points and will be closer to the true strain provided that the spacing between the anchors is small and that the deformation varies linearly with the spacing between the anchors. Bay strains are useful in detecting any anomalous behavior in the salt around an opening, such as that influenced by discontinuities, clay seams, or the effect of local stress concentrations.

Figure 11-19 shows the strain between the collar and anchor A for the roof extensometers in Test Room 1. The distance between the collar and anchor A is 5 feet. The maximum strain occurs at the east and west sides of the roof of the test room and is equal to approximately 4 percent through June 1986. Although the roof sag, as depicted by collar movement, is higher at the center of the rooms than at the sides, the bay strain is higher at the sides than at the center. As discussed in subsection 11.3.2.5, the numerical modeling also indicates higher strain at the roof and wall intersections. Figure 11-20 shows the vertical strain rates for these same extensometers. The rates are

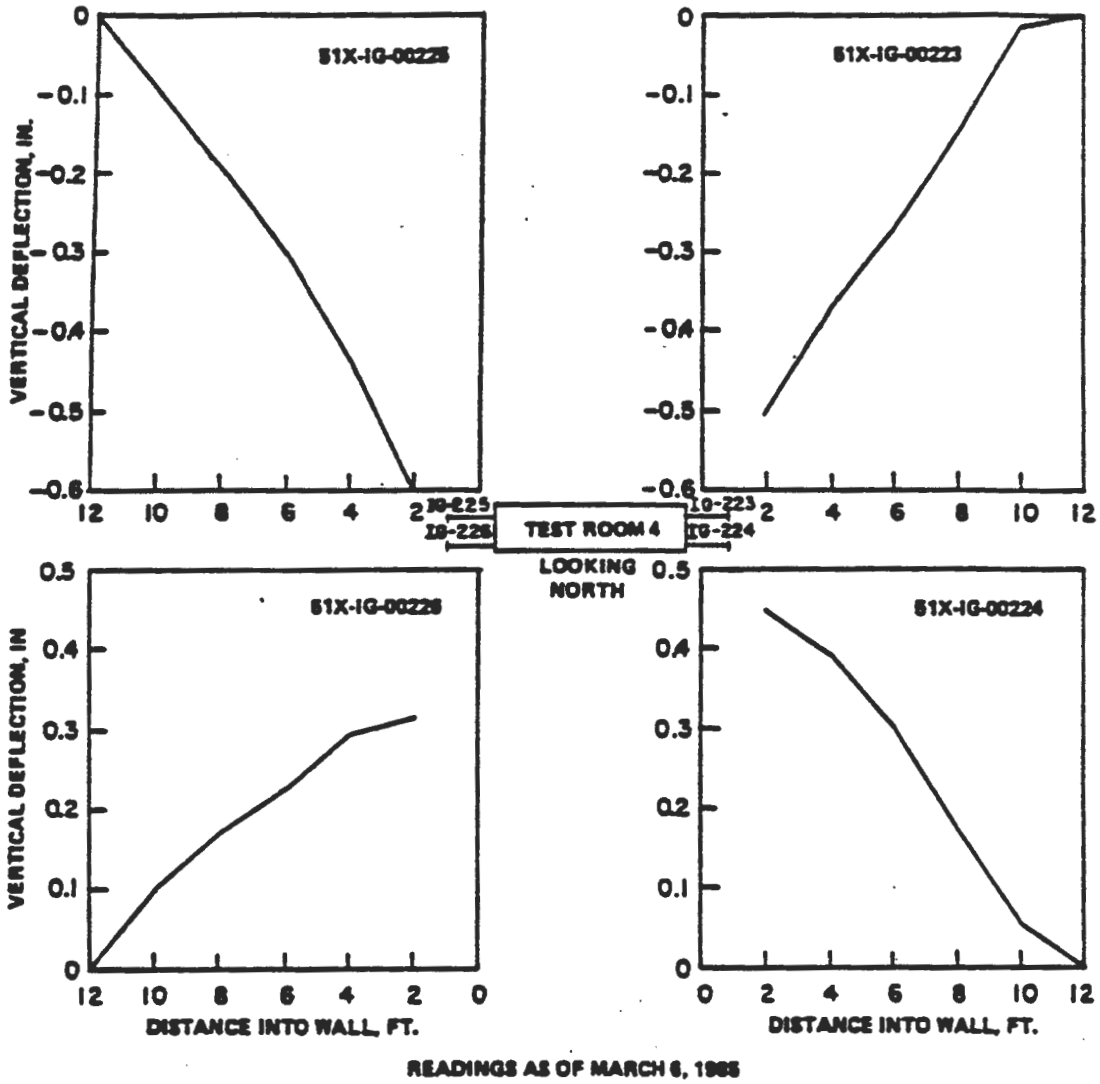


Figure 11-18

TEST ROOM 4
WALL INCLINOMETER BEHAVIOR

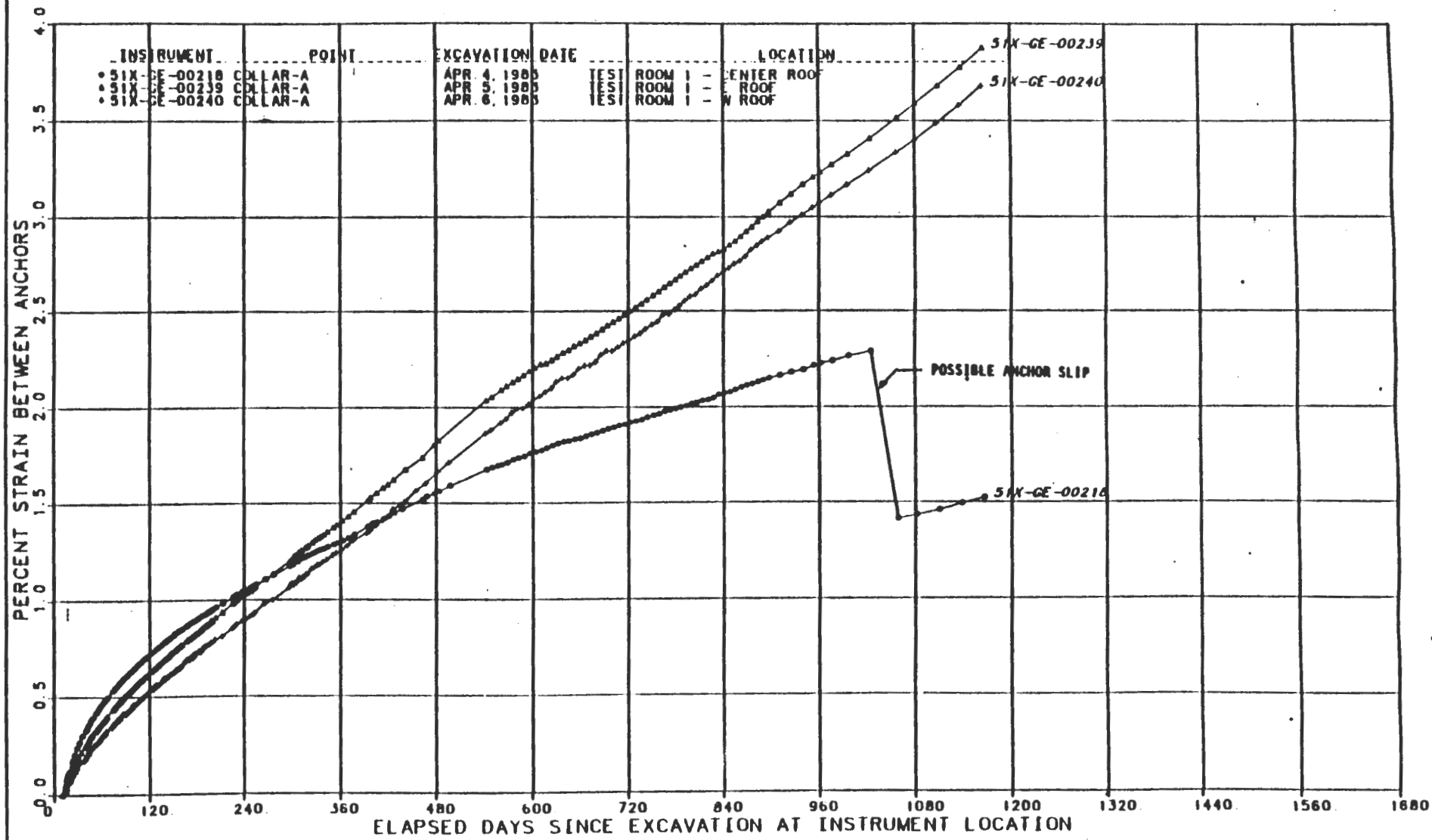


**Figure 11-19**

**TEST ROOM 1 ROOF EXTENSOMETERS**
**STRAIN VERSUS TIME SINCE EXCAVATION**

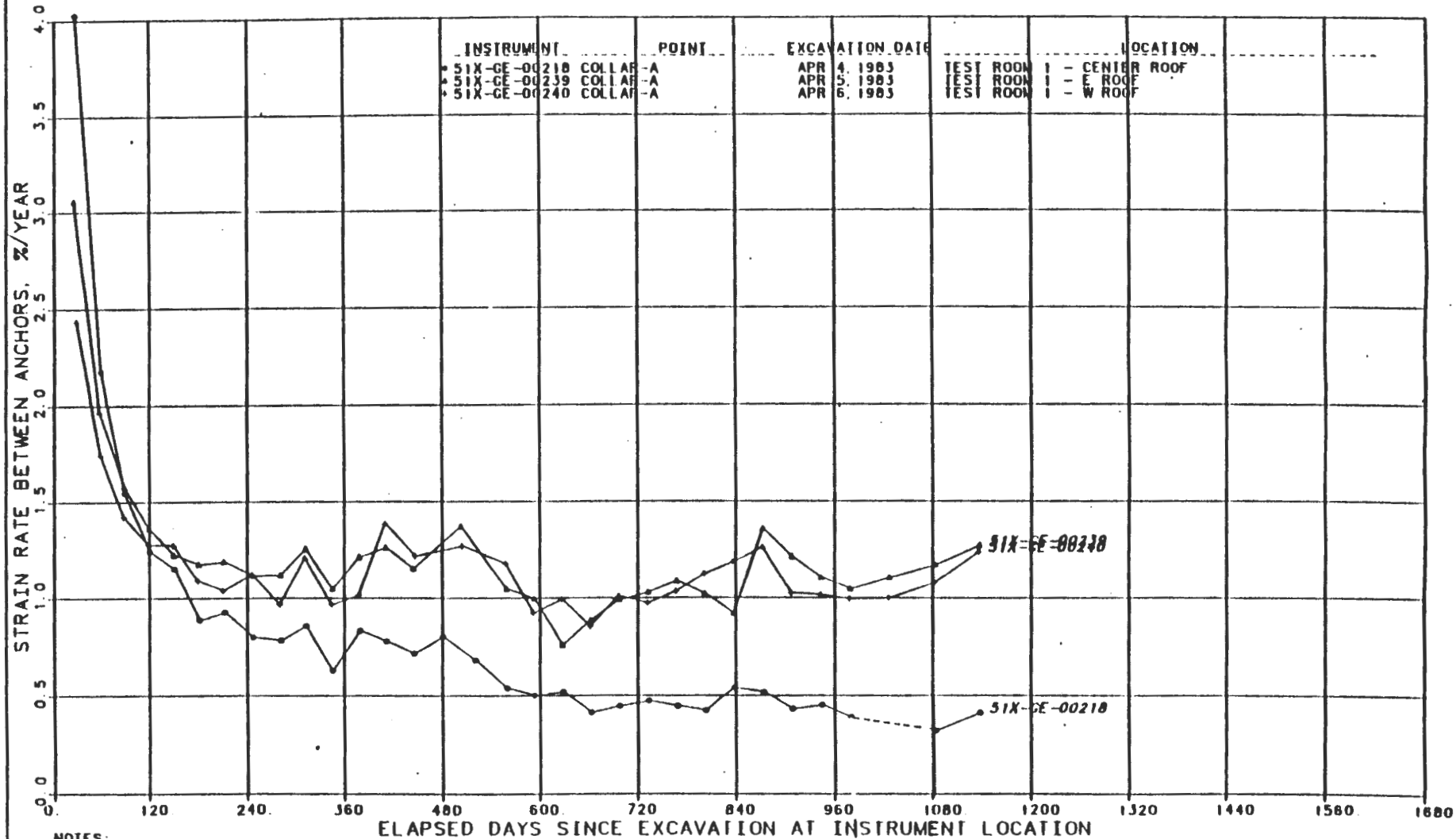


NOTES:

1. RATE CALCULATED FOR MINIMUM INTERVALS OF 30 DAYS

**Figure 11-20**

**TEST ROOM 1 ROOF EXTENSOMETERS**
**STRAIN RATE VERSUS TIME SINCE EXCAVATION**

generally decreasing with time. As with the strains, the strain rates are higher close to the pillars.

Figures K-37 through K-46 in Appendix K show the bay strains in percent as a function of elapsed time since excavation for all of the test rooms. To monitor more closely the separation across the clay seam at the base of anhydrite "b", the spacing between anchors A and B in Test Rooms 1 and 2 is 1 foot. Currently, the maximum strain occurs between anchors A and B on the west side and central part of the roof in Test Room 1, and is on the order of 5 percent. Because the anchors are not equally spaced, and the deformation varies nonlinearly with the distance along the anchor, a comparison of bay strain between successive anchors may be misleading.

Figures K-47 through K-56 in Appendix K show the strain rate plots for all of the roof and floor extensometers. In general, the strain rate is decreasing with time, except for floor extensometer 51X-GE-00210 in Test Room 3 where, for anchor A, the strain rate increased with time until the extensometer failed (Figure K-42). The decreasing trend in the strain rates is an indication that the salt above the roof and below the floor is currenty stable and will remain stable based on the projected decreasing rate.

11.3.2.5 Model Simulation

As discussed in Chapter 5, Section 5.3, numerical analyses using creep constants obtained from laboratory tests did not provide a good correlation with in situ measured closure. Therefore, an engineering approach using curve fitting methods was employed. The finite element method was used to simulate the behavior of the test rooms and to determine stress distributions. The effects of material properties and the proximity to other rooms were considered for incorporation into the model. The reference stratigraphy used in the model and the material properties of the geologic layers are described in Chapter 6. The constitutive equations used in the analyses, particularly the governing creep equations, are presented in Appendix C. Using the procedures

described in Chapter 5, Section 5.4, in situ roof-to-floor closure data through June 30, 1985, were correlated with the finite element responses to determine the values of creep parameters C, A and z for each test room. In order to eliminate the effect of excavation sequence on computation of the creep parameters, only in situ data taken after the completion of all test room excavation activities were utilized. The average values of these parameters for the four test rooms were then used to predict the responses of the future storage rooms as described in Chapter 12.

Figure 11-21 shows the finite element model for the test room panel based on the reference stratigraphy. The model has 363 nodes and consists of 270 plane strain elements, with gap/friction link elements modeling a clay seam at a depth of 2,104.87 feet. A friction coefficient of 0.4 was used for a member property of the gap/friction link elements. MB-139 was modeled as an elastic layer from a depth of 2,130.36 to 2,133.18 feet. The top and bottom boundaries of the model are at depths of 1,978.5 feet and 2,250.0 feet, respectively. The roof and floor of the room are at depths of 2,112.56 feet and 2,125.56 feet, respectively.

Two openings were incorporated in the finite element model to simulate differences resulting from the proximity of inner and outer rooms. These openings were modeled using height and width dimensions of 13 feet and 33 feet respectively. The boundary on one side of the model was taken as the vertical axis of symmetry for the center pillar and consists of horizontal restraints. The boundary on the other side of the model also utilized horizontal restraints. These boundaries were established based on experience from previous analyses and were extended far enough so that the effects of the boundaries on the structural responses were minimal. Stress boundary conditions were used at the top and bottom of the finite element model. A single vertical restraint at the lower left corner of the model was used to eliminate any rigid body modes in the model.

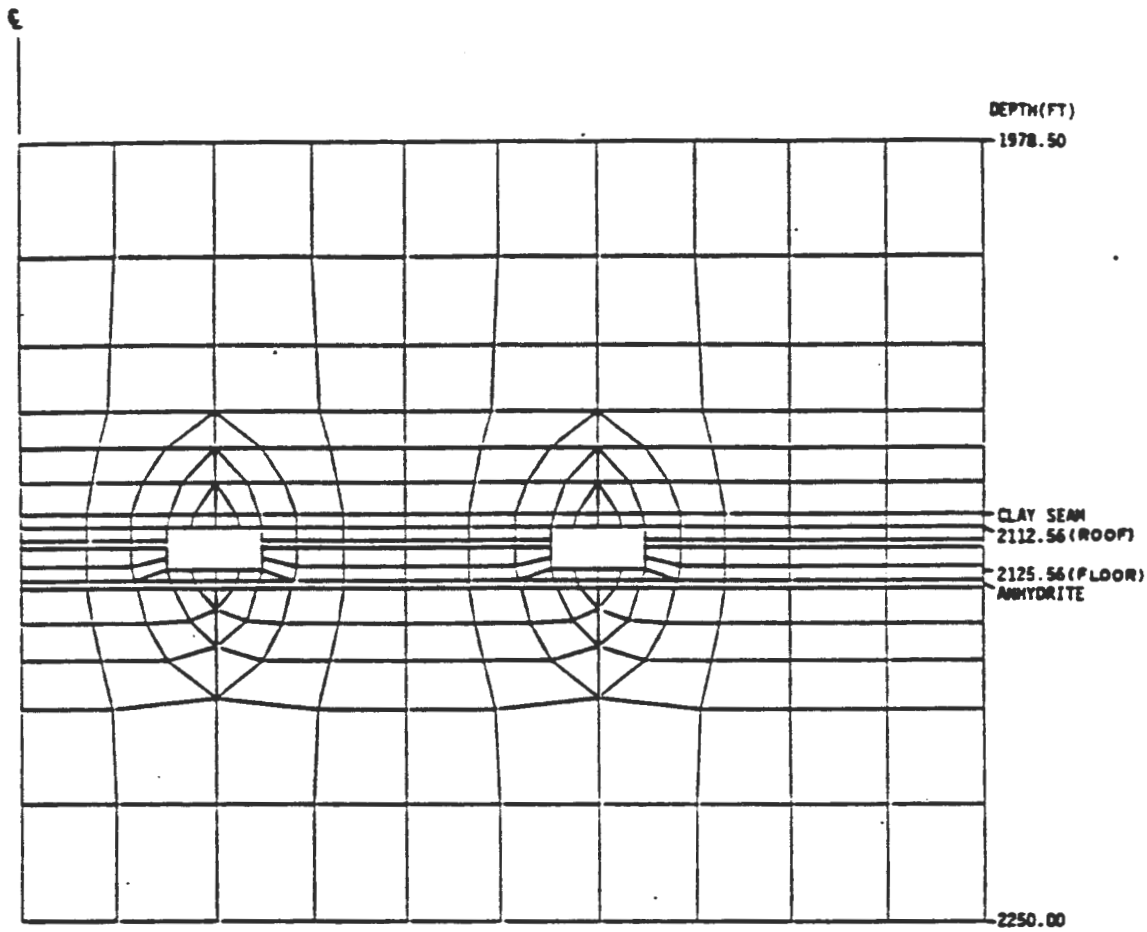


Figure 11-21

TEST ROOMS
FINITE ELEMENT MODEL

Element sizes were proportioned to minimize the stress gradients across each element. In addition, elements were oriented to have the mesh radiating from the opening of the model to be commensurate with estimated orientations of the principal stress axes. These aspects of the model were designed to increase the overall efficiency of the analyses.

Computation of In Situ Responses and Creep Parameters. The test room analyses were performed using the procedures described in Chapter 6 and the MARC General Purpose Finite Element Program (ref. 6-8). Time steps used in the analyses were within the specified tolerances recommended by the MARC Program. The analysis was performed in several stages with each stage containing between 50 and 100 integration steps. After completing each stage, the corresponding real time was computed to determine the required number of integration steps for the subsequent runs.

Figures 11-22 through 11-25 show the correlations of in situ and analytical roof-to-floor closures for Test Rooms 1 through 4. The in situ roof-to-floor closure data for Test Rooms 1 and 2 are from convergence meter readings while the measurements for Test Rooms 3 and 4 are from convergence points. Table 11-12 shows the individual creep parameters C, A and z for all four test rooms determined by numerically correlating the in situ roof-to-floor closure data. The table also shows the mean values of the creep parameters for three test room combinations.

Similarly, Figures 11-26 through 11-29 show the correlations of in situ and finite element wall-to-wall closures for Test Rooms 1 through 4. The in situ wall-to-wall closure data for Test Rooms 1, 3 and 4 are from permanent convergence points while the data from Test Room 2 consists of both temporary and permanent convergence point measurements. Table 11-13 shows the individual creep parameters C, A and z for all four test rooms determined by numerically correlating the in situ wall-to-wall closure data. The table also shows the mean values of the creep parameters for three test room combinations.

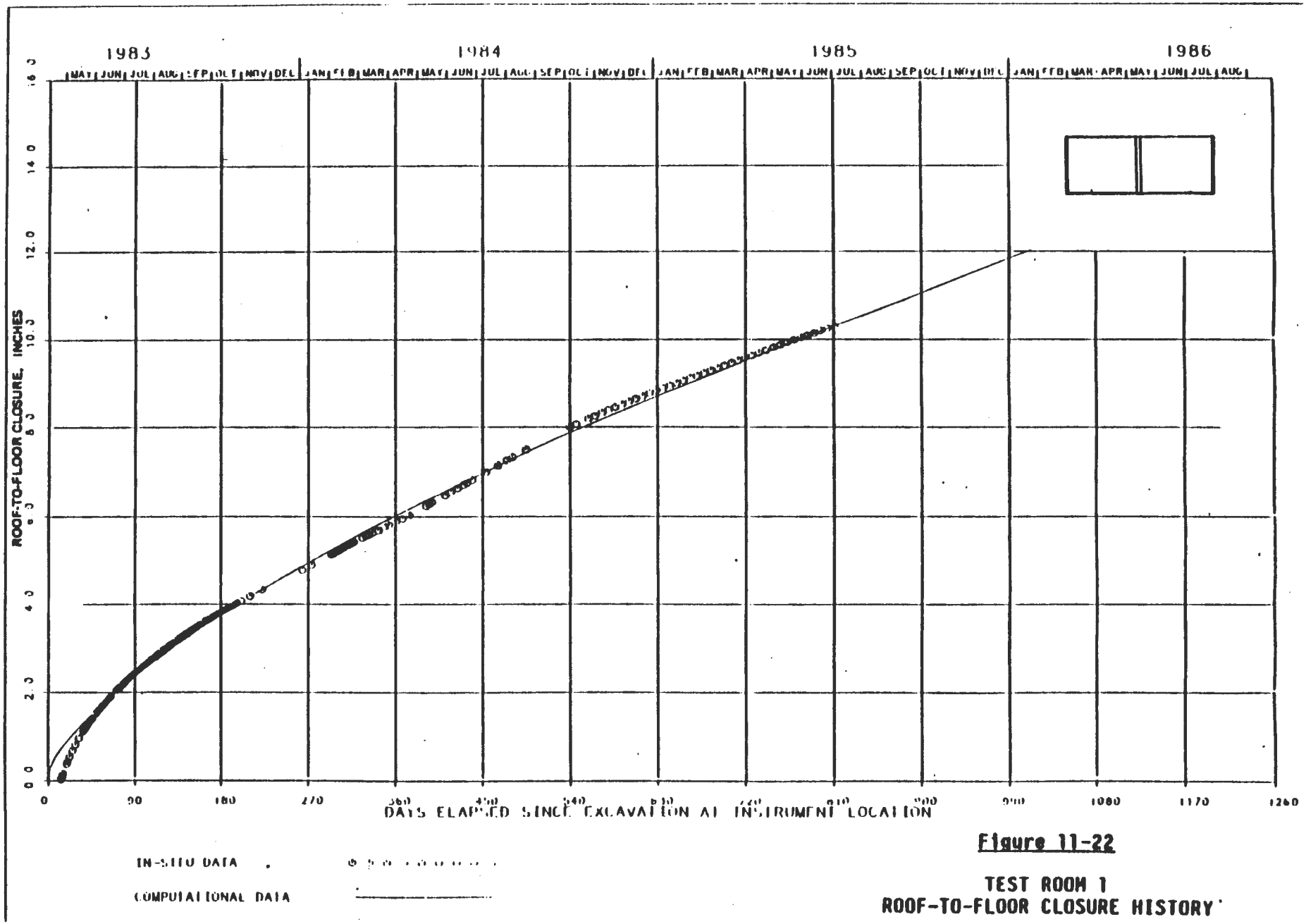


**Figure 11-22**

**TEST ROOM 1**
**ROOF-TO-FLOOR CLOSURE HISTORY**

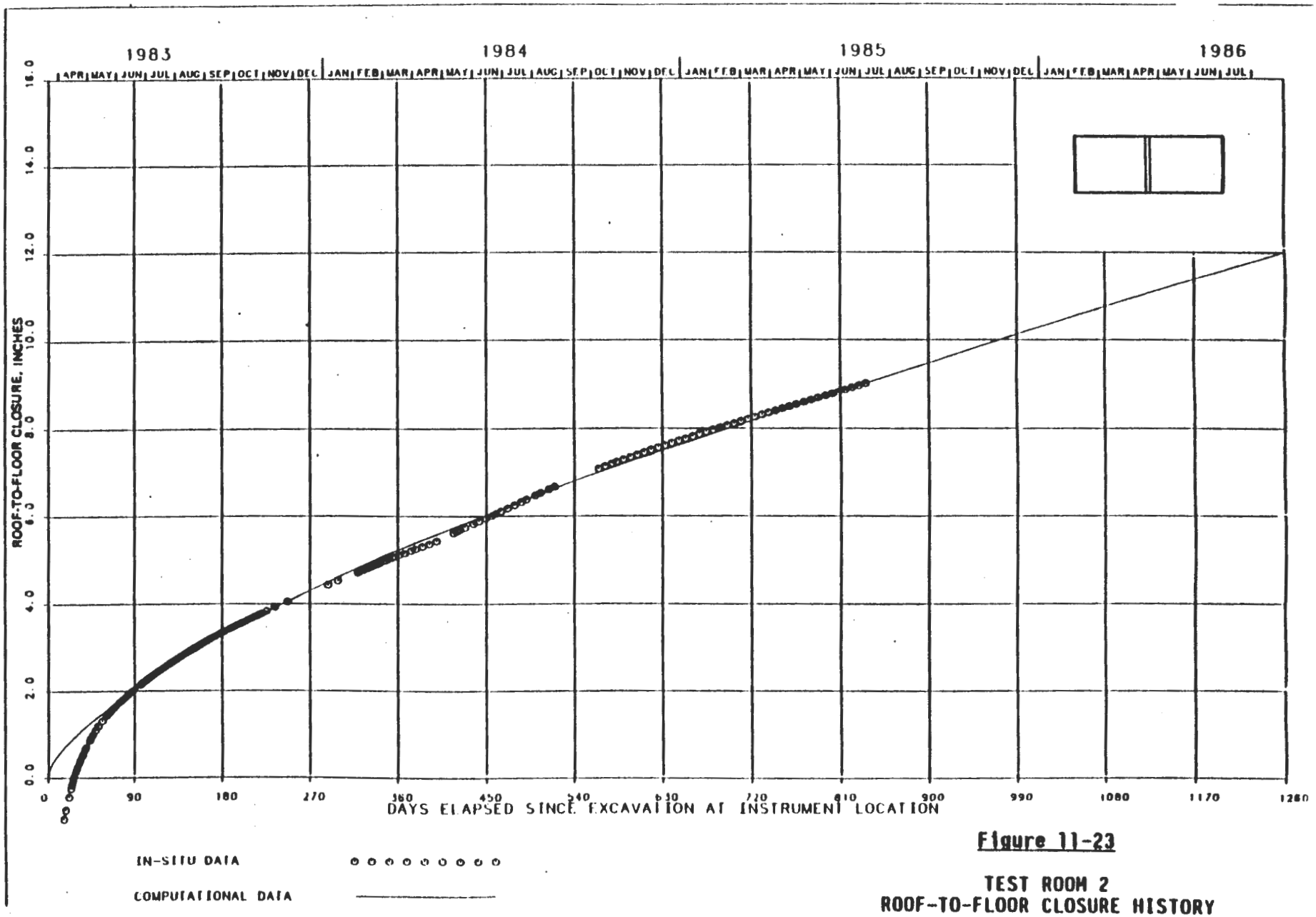


**Figure 11-23**

**TEST ROOM 2**
**ROOF-TO-FLOOR CLOSURE HISTORY**

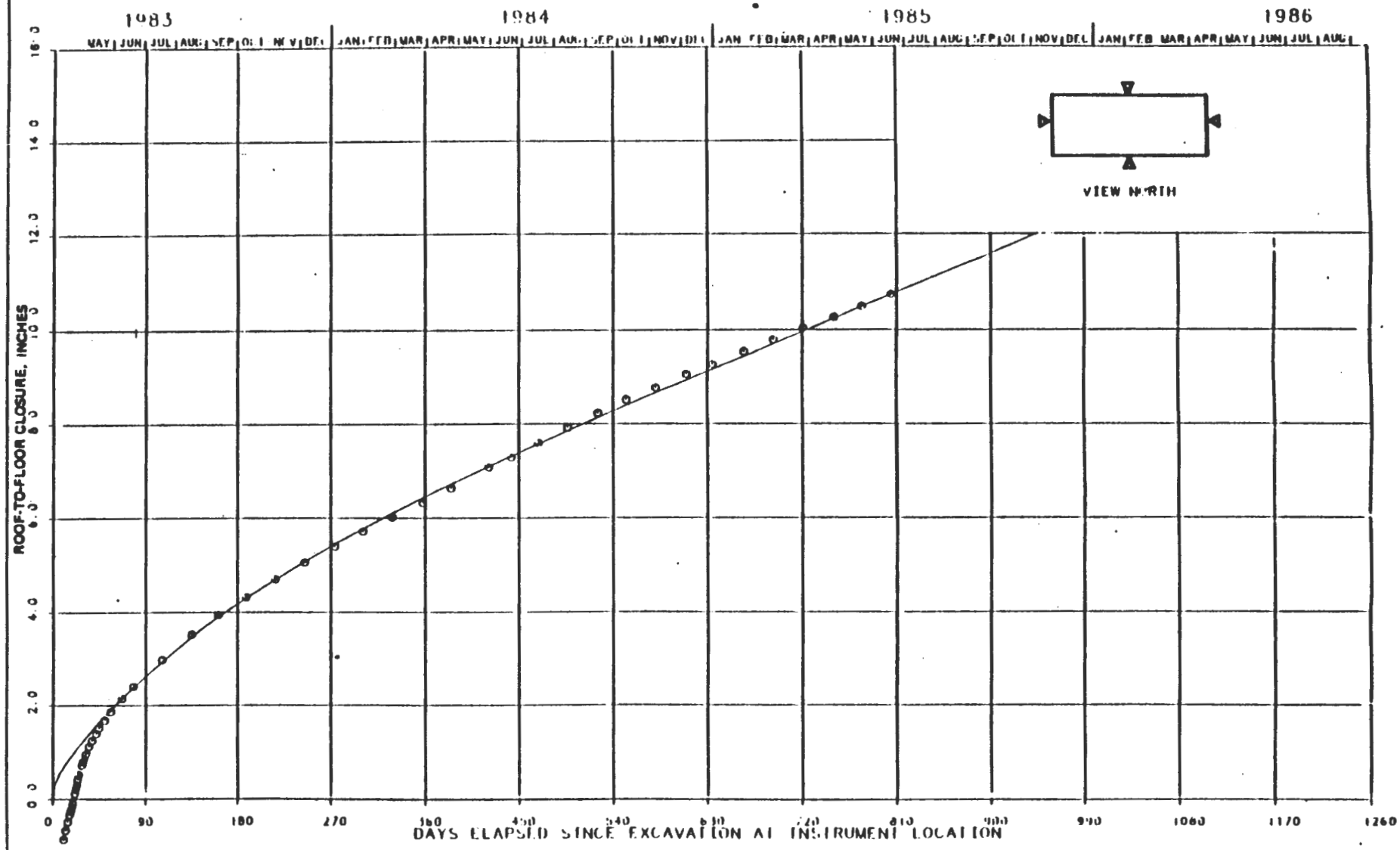


**Figure 11-24**

**TEST ROOM 3**
**ROOF-TO-FLOOR CLOSURE HISTORY**

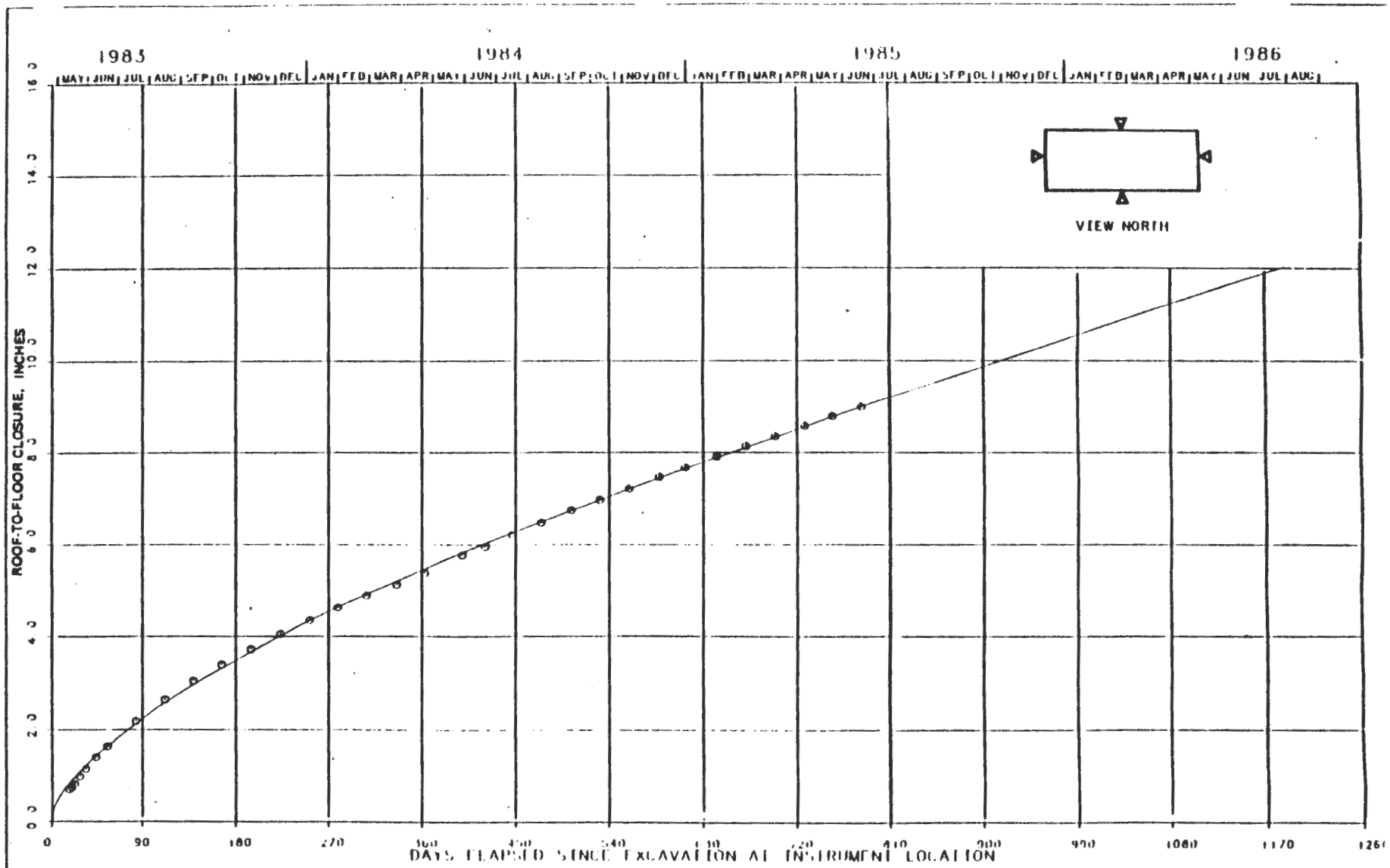


**Figure 11-25**

**TEST ROOM 4**
**ROOF-TO-FLOOR CLOSURE HISTORY**

Table 11-12

TEST ROOM CREEP PARAMETERS
DETERMINED FROM ROOF-TO-FLOOR CLOSURES

| Test Room | C ($ksf^{-4.9} sec^{-1}$) | A | z ($sec^{-1}$) |
|---|---|---|---|
| 1 | $3.103 \times 10^{-21}$ | 1.593 | $4.670 \times 10^{-8}$ |
| 2 | $1.919 \times 10^{-21}$ | 1.712 | $4.782 \times 10^{-8}$ |
| 3 | $2.516 \times 10^{-21}$ | 2.077 | $7.268 \times 10^{-8}$ |
| 4 | $2.813 \times 10^{-21}$ | 1.712 | $5.572 \times 10^{-8}$ |
| Mean $\bar{X}$ (Rooms 1 thru 4) | $2.588 \times 10^{-21}$ | 1.774 | $5.573 \times 10^{-8}$ |
| Mean $\bar{X}$ (Rooms 1 & 4) | $2.958 \times 10^{-21}$ | 1.653 | $5.121 \times 10^{-8}$ |
| Mean $\bar{X}$ (Rooms 2 & 3) | $2.218 \times 10^{-21}$ | 1.895 | $6.025 \times 10^{-8}$ |

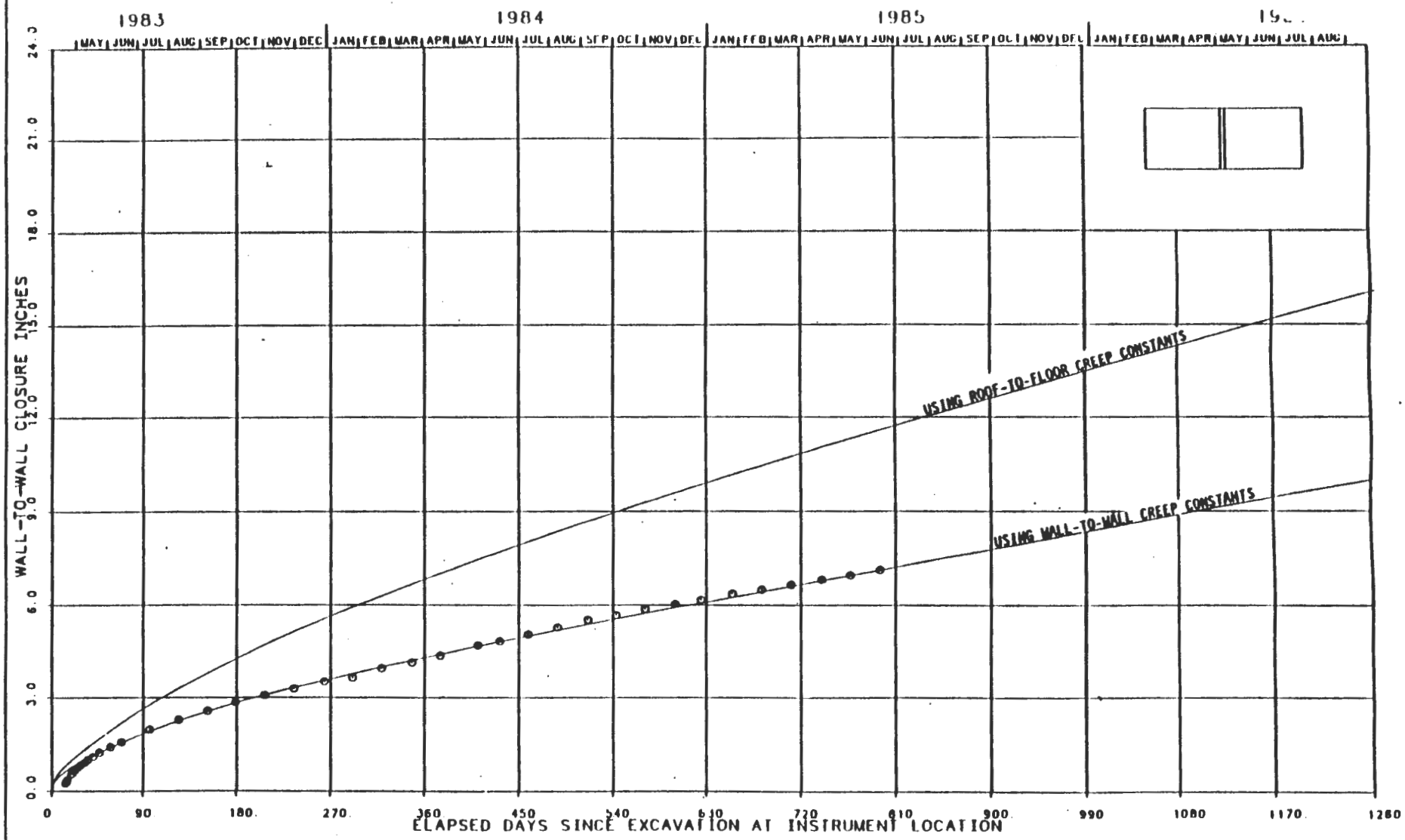


IN-SITU DATA o o o o o o o o o

COMPUTATIONAL DATA ————————

**Figure 11-26**

**TEST ROOM 1**
**WALL-TO-WALL CLOSURE HISTORY**

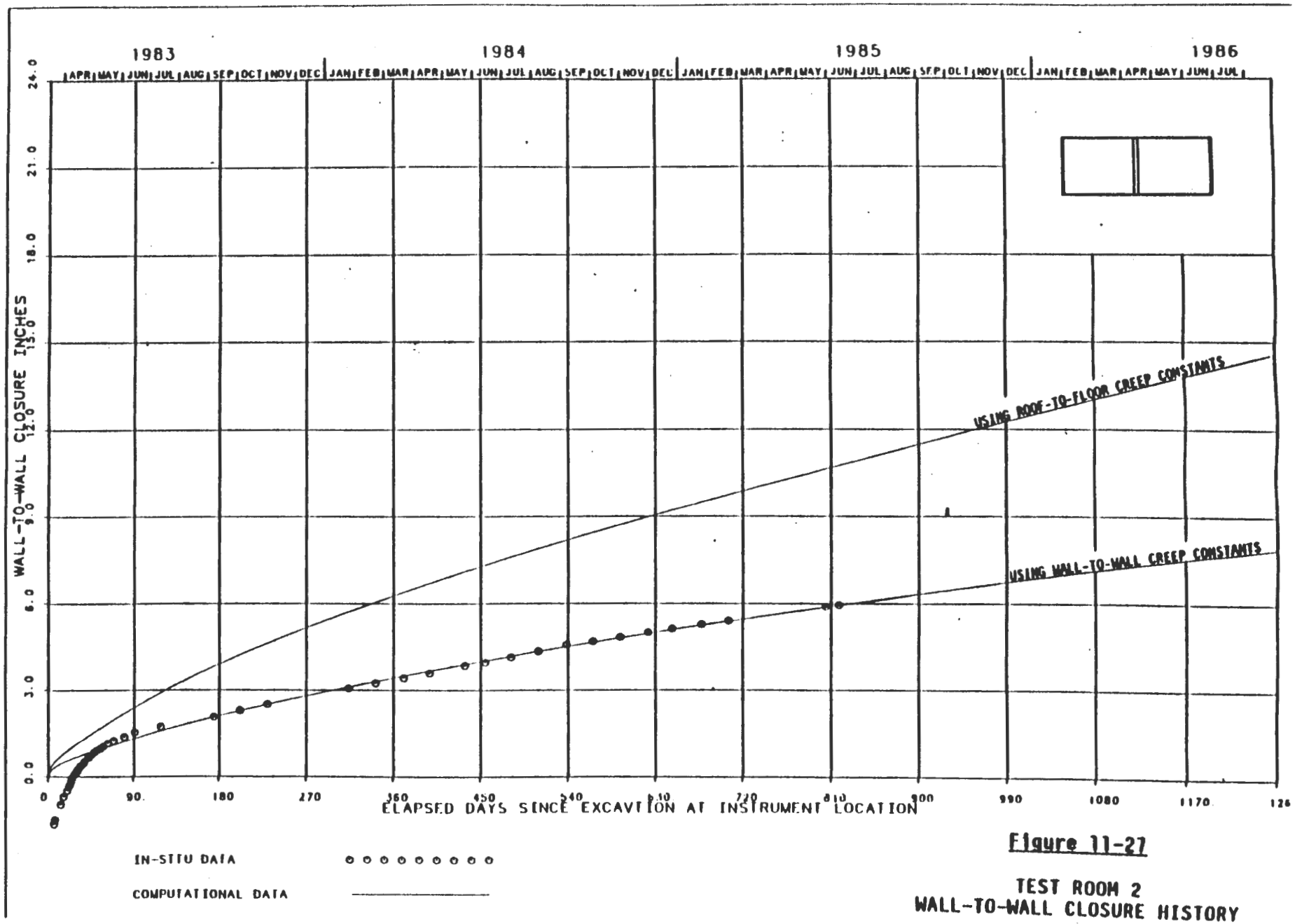


**Figure 11-27**

TEST ROOM 2
WALL-TO-WALL CLOSURE HISTORY

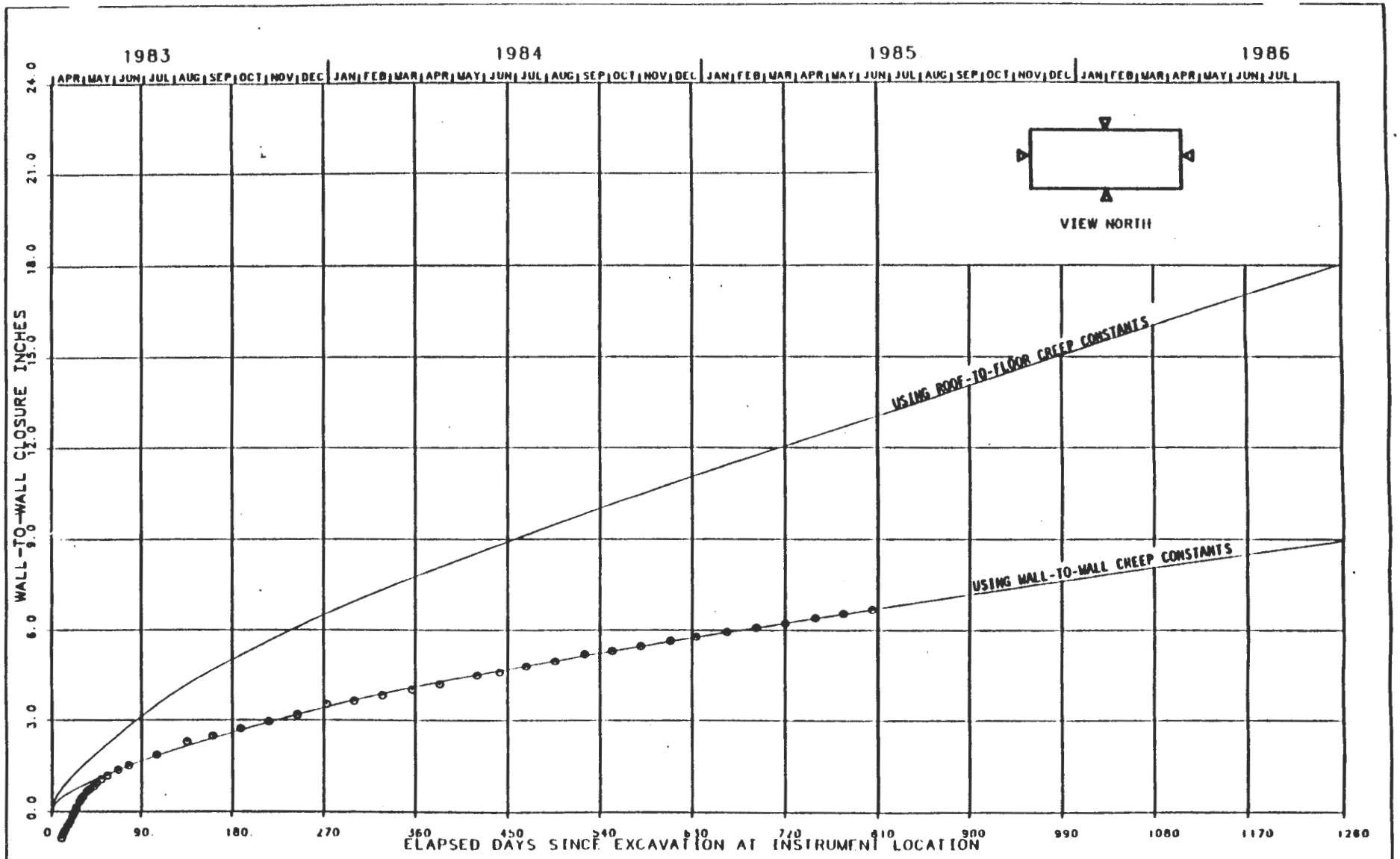


**Figure 11-28**

**TEST ROOM 3**
**WALL-TO-WALL CLOSURE HISTORY**

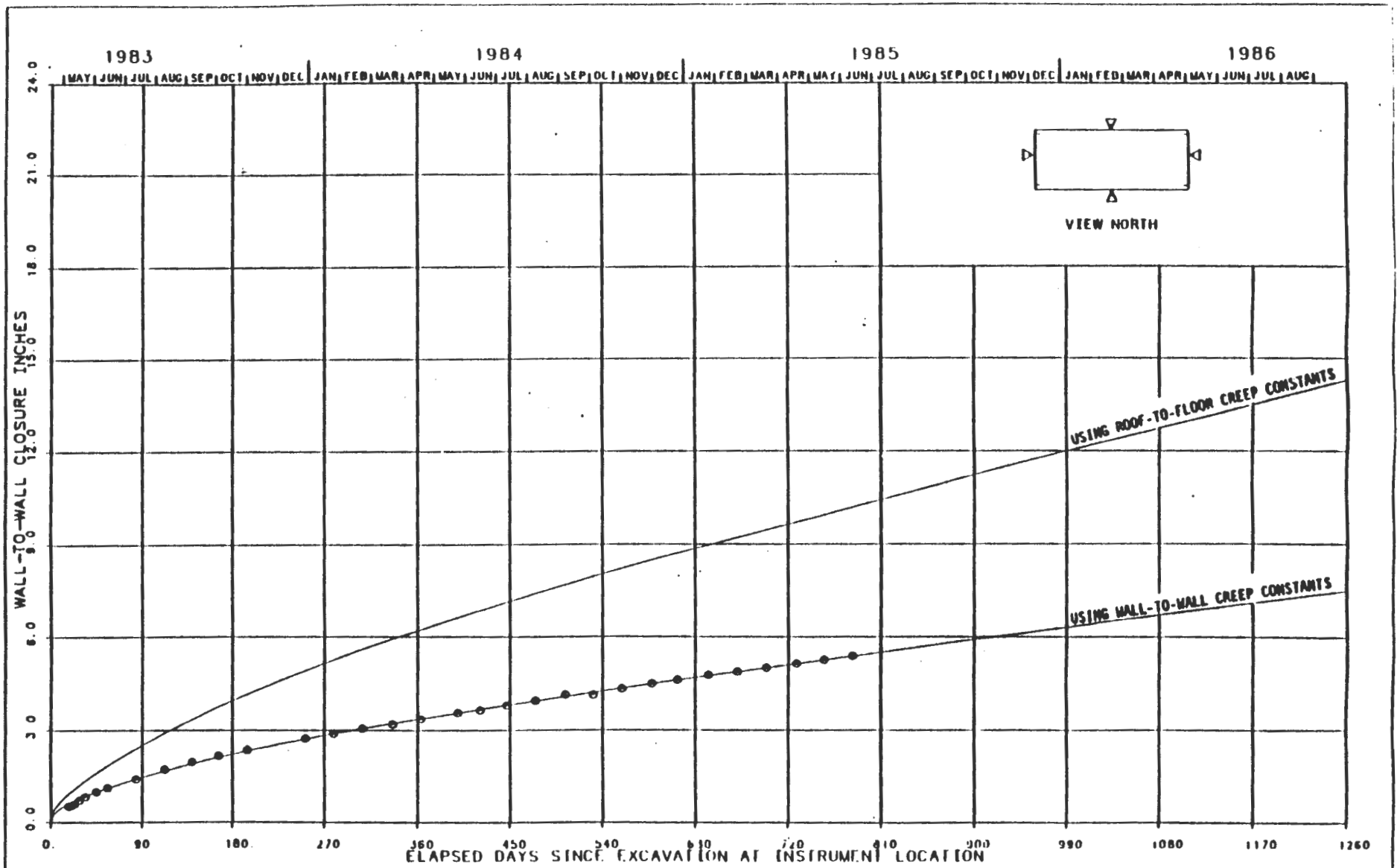


**Figure 11-29**

TEST ROOM 4
WALL-TO-WALL CLOSURE HISTORY

Table 11-13

TEST ROOM CREEP PARAMETERS
DETERMINED FROM WALL-TO-WALL CLOSURES

| Test Room | C ($ksf^{-4.9}sec^{-1}$) | A | z ($sec^{-1}$) |
|---|---|---|---|
| 1 | $2.054 \times 10^{-21}$ | 1.502 | $6.810 \times 10^{-8}$ |
| 2 | $0.850 \times 10^{-21}$ | 1.630 | $2.476 \times 10^{-8}$ |
| 3 | $1.095 \times 10^{-21}$ | 1.920 | $4.464 \times 10^{-8}$ |
| 4 | $1.444 \times 10^{-21}$ | 1.419 | $5.276 \times 10^{-8}$ |
| Mean $\bar{X}$ (Rooms 1 thru 4) | $1.361 \times 10^{-21}$ | 1.618 | $4.757 \times 10^{-8}$ |
| Mean $\bar{X}$ (Rooms 1 & 4) | $1.749 \times 10^{-21}$ | 1.461 | $6.043 \times 10^{-8}$ |
| Mean $\bar{X}$ (Rooms 2 & 3) | $0.973 \times 10^{-21}$ | 1.775 | $3.470 \times 10^{-8}$ |

As shown in Tables 11-12 and 11-13, the creep parameters obtained for the test rooms using roof-to-floor closure values vary significantly from the values obtained using wall-to-wall closure values. To illustrate these variations, the upper curves on Figures 11-26 through 11-29 show the wall-to-wall finite element responses using creep parameters determined from roof-to-floor numerical correlations. The discrepancy may be partly due to material anisotropy of the salt which is not taken into account in the constitutive relationship for the salt. However, the most important contributor to the discrepancy may be the behavior of the clay seams and anhydrite beds. The model also does not include the complete effects of anisotropic creep behavior due to the combination of different layers in the actual stratigraphy. This behavior, due to anisotropic geometry, can be shown using a simple one-dimensional model similar to the one used by Branstetter et. al. (ref. 11-3). Consider a block of halite containing N horizontal layers with equal thickness. The creep law for each of the layers is assumed to be

$$\dot{\varepsilon}_c = f_i(t)\sigma^{-n} \qquad i = 1, 2, \ldots\ldots N \qquad (11\text{-}12)$$

The equivalent vertical creep function computed by considering only the creep relation in the vertical direction can be expressed as

$$f_v(t) = \frac{\sum_{i=1}^{N} f_i(t)}{N} \qquad (11\text{-}13)$$

However, the equivalent horizontal creep function computed by considering only the horizontal direction becomes

$$f_h(t) = [\sum_{i=1}^{N} f_i(t)^{-\frac{1}{n}}]^{-n} N^n \qquad (11\text{-}14)$$

It was found that, for any problem in which $f_i(t)$ varies, the value of the equivalent creep function in the horizontal direction, based on

equation 11-14, is lower than the value in the vertical direction, based on equation 11-13.

Replication of in situ creep behavior by the finite element model would require extensive research into the existing constitutive equations and perhaps modification of the MARC Finite Element Program. It is believed that the present methodology can adequately predict the roof-to-floor and wall-to-wall closures within acceptable engineering accuracy and that further work into anisotropic creep behavior is not justified for design validation.

One method of determining the structural adequacy of the salt is by using the effective strain. Model simulation of Test Room 2 behavior showed that the effective strain reached a maximum value at the intersections of the walls with the roof and floor. As discussed in subsection 11.3.2.4, bay strains in the vertical direction, determined from roof and floor extensometer data, are on the order of 5 percent through June 1986. Field observations of the test room walls have not found any structural failure at these strain values. Occasional minor, shallow spalls are a continuing occurrence, especially along the upper portion of geologic map unit 4.

Based on the results of the model simulation of Test Room 2, the maximum effective strain at the roof and wall intersection will be 6 percent about 15 years after excavation. The corresponding average vertical strain over a 2-foot thickness of salt will be 15 percent. However, effective strain is not directly measurable. At best, only vertical or horizontal strains can be determined from multiple-point borehole extensometer measurements. A comparison of the predicted vertical strain with the vertical strain determined from the relative displacement between the collar and anchor A of the roof extensometers has been made. Because the collar and anchor A are 5 feet apart, the strain calculated from the relative displacements will be an average value. Similarly, the strain from three elements spanning the collar to anchor A interval were summed and averaged for comparison.

Figure 11-30 shows the comparison for the average vertical strain at the roof and wall intersection. Although the relation is expressed in terms of t*, the relationship between t* and the real time t is approximately linear. The strain determined from the collar to anchor A readings indicates that the rate is currently decreasing with time.

Figure 11-31 shows the relationship for the center of the roof. This rate is also decreasing with time, even though the numerical analysis shows a constant rate.

11.3.2.6 Effectiveness of Model Simulation

The procedure discussed in the previous subsection and in Chapter 5 used roof-to-floor closure data for the test rooms to calculate the creep parameters C, A and z. Extrapolation of creep behavior was then accomplished using these derived creep parameters.

The numerical analysis gives the displacements of nodal points and stresses within the elements. The effectiveness of the model used can be checked by comparing measurement data other than roof-to-floor closure with the magnitude predicated by the model. For example, relative displacements between anchor points in multiple-point borehole extensometers may be compared with predicted relative displacements between appropriate nodes of the model. Such a comparison will be helpful to assess the effectiveness of model simulation.

Because a symmetrical two-room model representing four rooms was used for model simulation, the relative displacement between the collar and the deepest anchor of the central roof extensometers in Test Rooms 1 and 4 were calculated for an interval of 60 days, and the average value determined. The real time t was converted to the normalized time t* using equation C.4-17 in Appendix C. This is because the numerical analysis was performed in terms of the normalized time. The vertical displacements of appropriate nodes in the finite element model, which approximately duplicate the collar and the deepest anchor of the roof extensometers, were compiled. If the nodes did not exactly match the

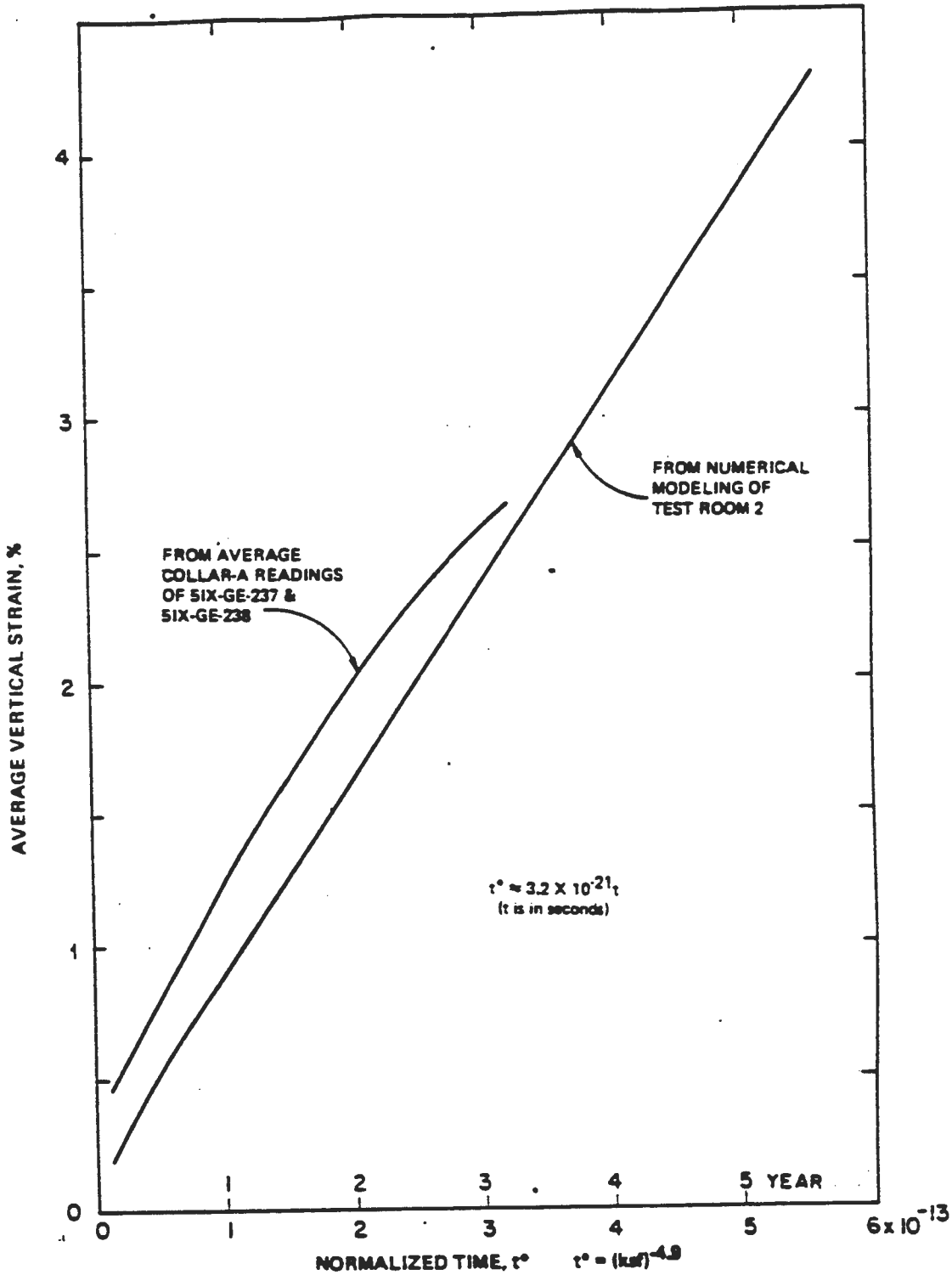


Figure 11-30

TEST ROOM 2
VERTICAL STRAIN AT ROOF AND PILLAR CORNER

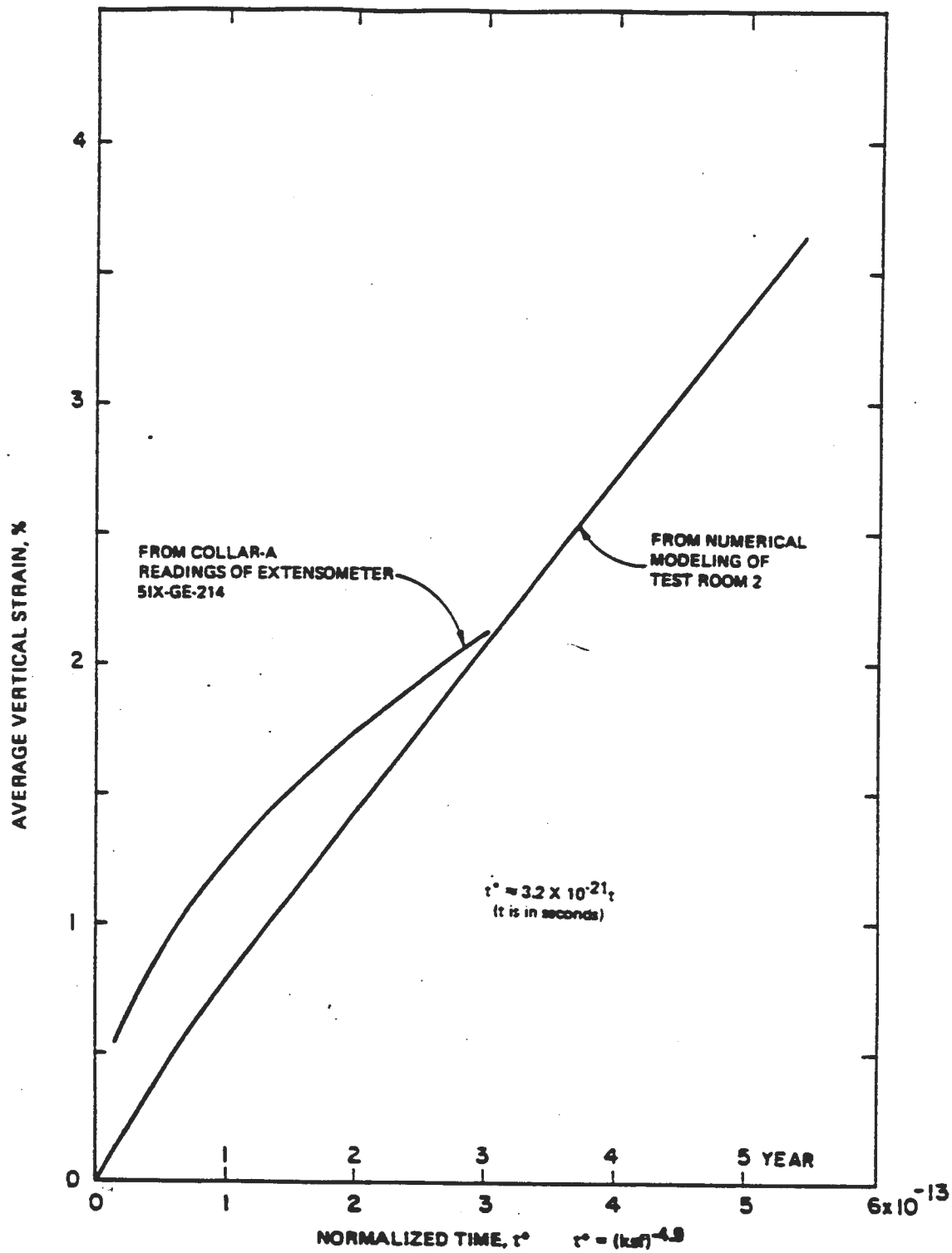


Figure 11-31

TEST ROOM 2
VERTICAL STRAIN AT ROOF CENTER

location of the deepest anchor, then linear interpolation was used to determine the displacement of salt at the required location.

Figure 11-32 compares the average relative displacement between the collar and the deepest anchor for the central roof extensometers 51X-GE-00207 and 51X-GE-00218, with the relative displacement between appropriate nodal points computed from the numerical model. A normalized time t* of $37.07 \times 10^{-14}$ is equivalent to an elapsed time of nearly 3 years since the completion of excavation at the instrument location. The discrepancy between the measured and calculated relative movements is nearly 2 inches in 3 years.

For large values of t, the normalized time is approximately proportional to the real time, since the exponential term in equation C.4-17 in Appendix C approaches unity. For large values of t* (and t), the calculated relative displacement rate will be approximately 44 percent higher than the measured relative displacement rate if the current rate is maintained. A similar analysis was made for Test Rooms 2 and 3. Figure 11-33 compares the measured values with the values obtained from numerical modeling. The discrepancy in this case is 27 percent with respect to the measured value at nearly 3 years of elapsed time.

A comparison of salt heave measurement data from a floor extensometer in Test Room 4 was made with the values computed from numerical modeling. Figure 11-34 shows the results of this comparison. The numerical model underestimates the salt heave in the floor by approximately 70 percent of the measured value. This discrepancy is probably due to the assumption in the model that MB-139, 4.8 feet below the floor, is elastic and has infinite strength. Measurements from the floor extensometer and observations of fracturing indicate that MB-139 cannot be strictly considered as elastic. As discussed in subsection 11.3.2.1, borehole P4X-84 indicates the presence of lateral displacements and vertical separations in MB-139 beneath the floor of Test Room 4. This indicates that stresses in parts of the anhydrite bed may have reached the failure state.

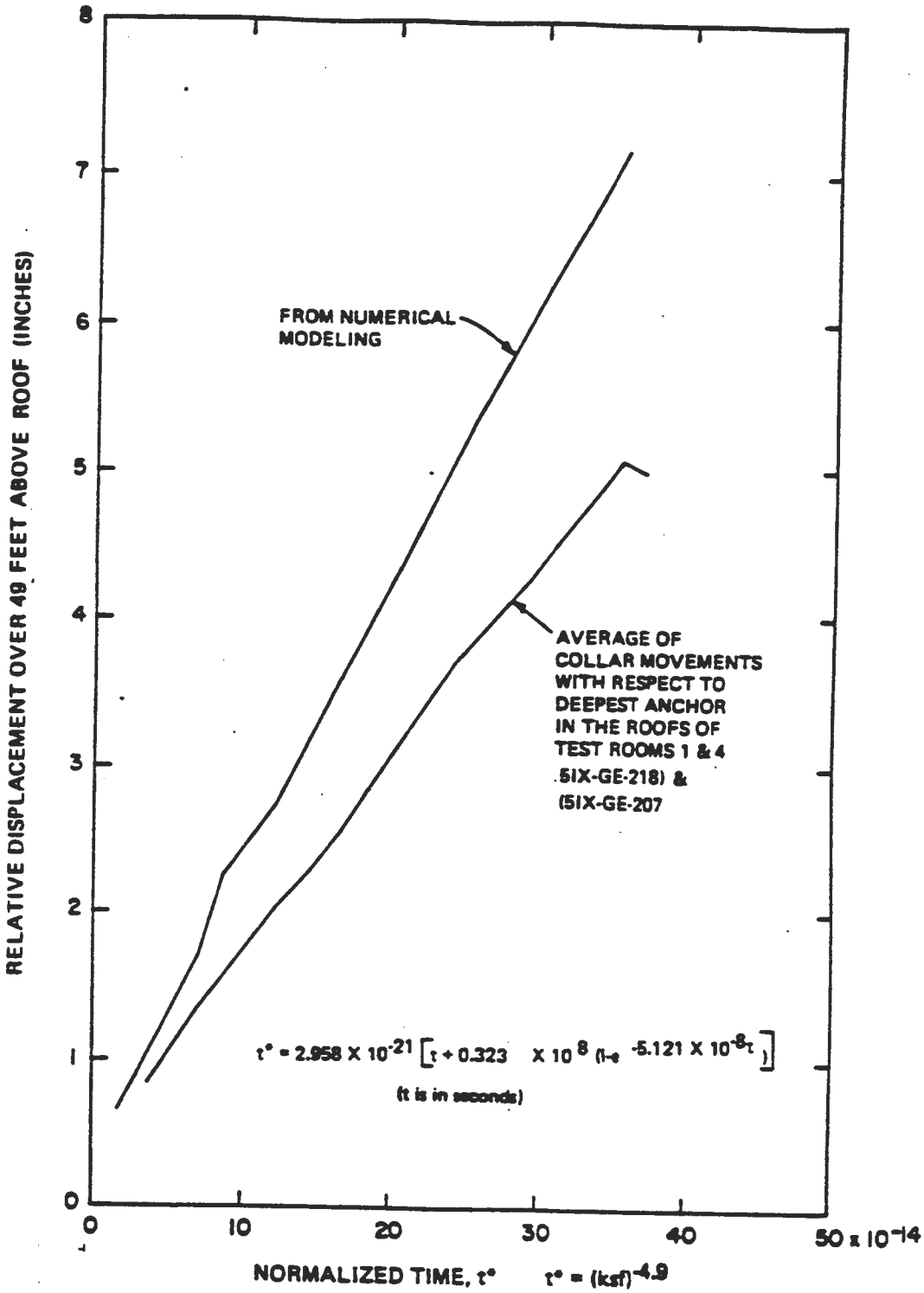


Figure 11-32

TEST ROOMS 1 AND 4 ROOF EXTENSOMETERS
NUMERICAL MODELING VERSUS IN SITU MEASUREMENT DATA

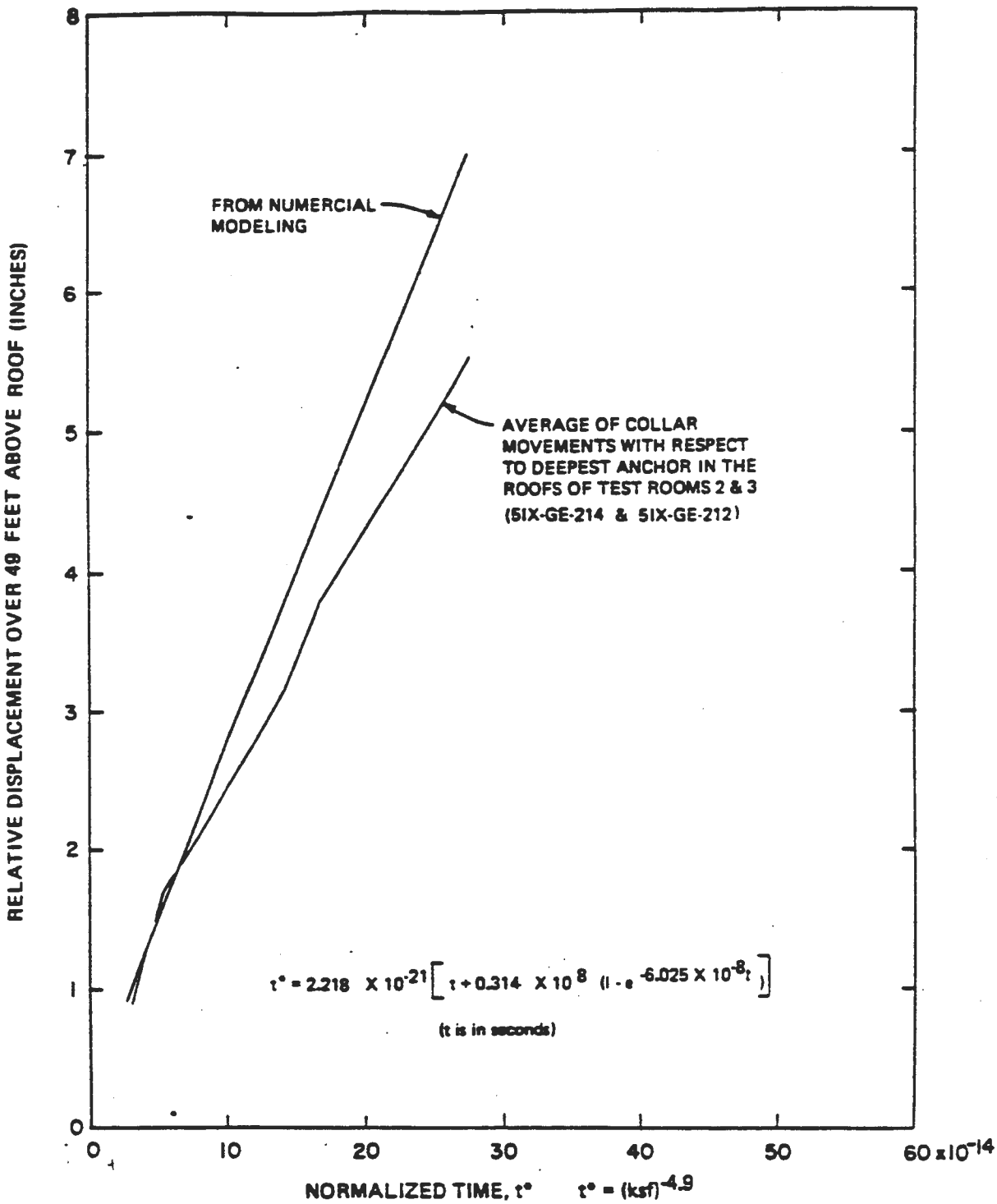


Figure 11-33

TEST ROOMS 2 AND 3 ROOF EXTENSOMETERS
NUMERICAL MODELING VERSUS IN SITU MEASUREMENT DATA

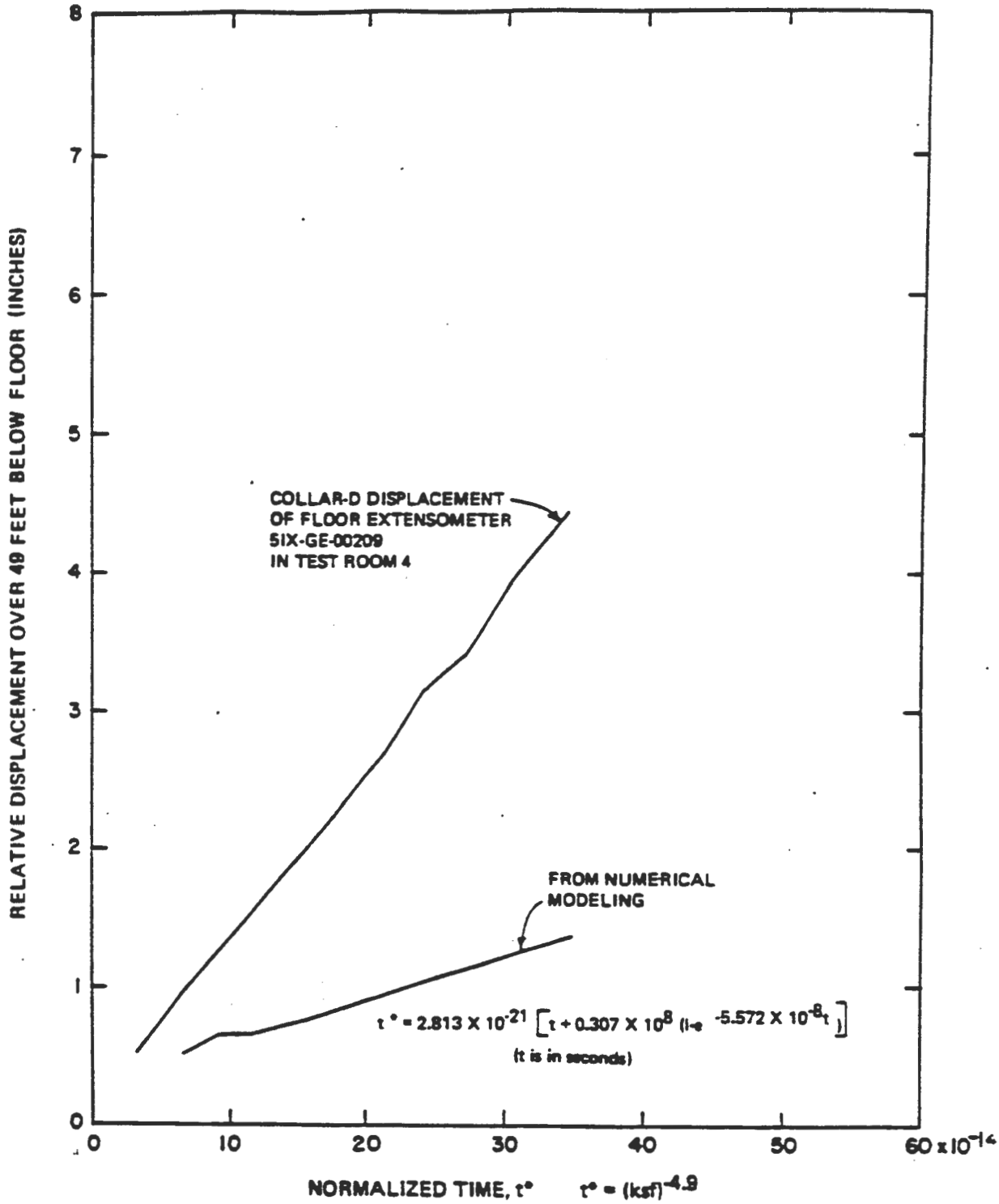


Figure 11-34

TEST ROOM 4 FLOOR EXTENSOMETER
NUMERICAL MODELING VERSUS IN SITU MEASUREMENT DATA

Another possibility is that the fractures might have developed prior to excavation of the test rooms (ref. 6-6). In either case, assumptions of linear elasticity for the anhydrite bed become untenable. Modifications to the material characterization of this anhydrite material will be required to better represent its deformational behavior.

The basic philosophy of the model simulation developed in this report is that in situ measurement data are utilized to back calculate the creep parameters of the salt mass with the attendant discontinuities such as clay seams and anhydrite beds. For the model simulation technique, the in situ roof-to-floor closure data have been used to extract the creep parameters and predict future behavior using these creep parameters. This is because the roof-to-floor closure is deemed critical to evaluate the adequacy of the room dimensions for the effective storage and retrieval of waste. The discussions in the previous paragraphs indicate that there are discrepancies between measured and predicted quantities for variables other than roof-to-floor closure, such as deformations within the salt mass. Such discrepancies are not due exclusively to any inadequacy of the numerical modeling procedure but are also due to differences in the actual and assumed stratigraphy, variations in creep parameters with space and time, and inadequate representation of the stress-strain behavior of the anhydrite bed. However, it has been demonstrated that the model can predict, with sufficient accuracy for engineering purposes, the roof-to-floor closure behavior of the test rooms. A similar model simulation analysis was made for wall-to-wall closure and independent creep parameters were developed. Extrapolation of wall-to-wall closure with time was achieved using these creep parameters. This model simulation technique using in situ data was employed because the more detailed approach using material properties derived from laboratory tests may not produce more accurate results, as discussed in Chapter 5, subsection 5.4.3.

#### 11.3.2.7 Computational Analysis Using Laboratory Test Creep Data

The reference design was based on computations for a single room rather than for multiple rooms. It was assumed that, with a low extraction ratio, the rooms with 100-foot pillars would not have as much early interaction as that which has developed in the four-room test panel. In Figure 11-35 the two lower curves show the computational results of roof-to-floor closure predictions for a 13 x 33-foot room using creep constants obtained from laboratory tests. The bottom curve represents the computational results from reference 11-4, dated August 1982, while the middle curve represents the updated result from reference 11-5, dated March 1985, which used revised creep parameters and an updated reference stratigraphy. In situ closure data for all four test rooms, including adjustments for their early closure, are plotted on the same figure for comparison. Interaction effects may be partly responsible for the discrepancy.

## 11.4 CONCLUSIONS AND RECOMMENDATIONS

### 11.4.1 Conclusions

The determination of the closure behavior of the WIPP underground openings using creep constants derived from laboratory experiments underestimated the actual closure. The measured roof-to-floor closure in the test rooms has exceeded 12 inches in the 3 years since the end of their excavation. This does not comply with the design criteria vertical closure allowance of 12 inches in 5 years.

Average vertical strains at roof and wall intersections, as determined from extensometer readings, were close to 3 percent in June 1986 and the strain rate was decreasing. Maximum vertical strain by numerical modeling occurs at roof and wall intersections and compares well with the value determined from in situ measurements.

Spalling from the roofs and walls, and fractures in the pillars and at pillar corners have been observed. Displacements and minor separations have been observed at clay seams and in the underlying halite in

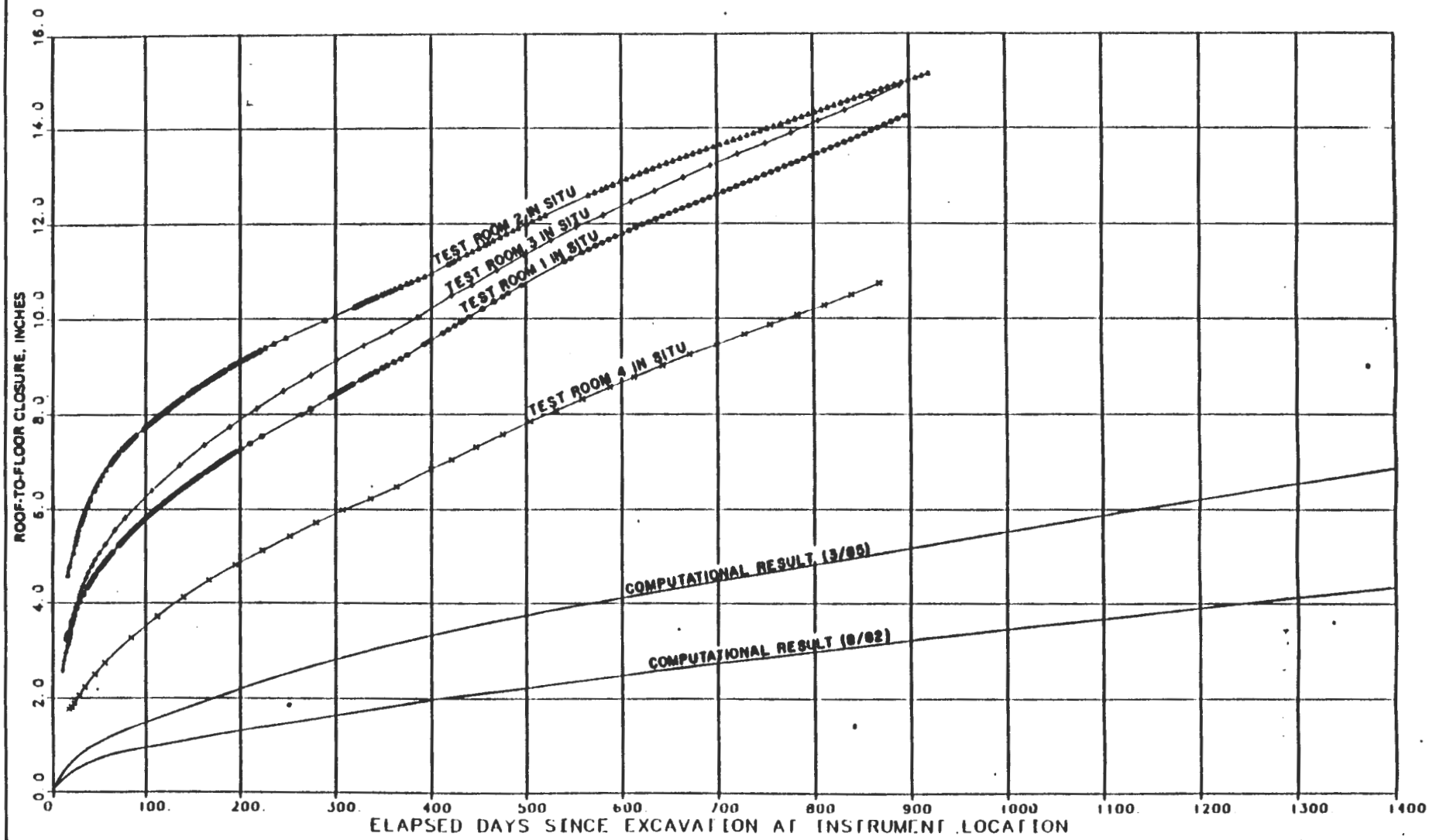


**Figure 11-35**

**TEST ROOMS**
**COMPARISON OF LABORATORY VERSUS IN SITU DATA**

boreholes that penetrate the roofs. These occurrences are expected to continue. Periodic maintenance of the roof and wall surfaces will be required.

Floor fracturing is well developed in the south half of Test Room 3 (Room T). Floor fracturing also occurs to a minor degree in the other test rooms and in a few areas in the drifts. Because the prominent floor fracturing occurring in Test Room 3 has not been found in any other rooms or drifts, it is considered to be anomalous to the underground facility. It is possible that the number and size of the 22 large-diameter holes in Test Room 3 exacerbated the pre-existing fractures. If floor fracturing occurs in the storage rooms, it is not expected to cause any operational or storage problems. As discussed in Chapter 3, Section 3.2, the WIPP project participants agreed, in a meeting on February 13, 1986, that the underground conditions do not require moving the facility level (ref. 3-2).

### 11.4.2 Recommendations

Observations and geomechanical instrumentation measurements should continue in the test rooms. Because they are the models for the determination of storage room behavior, trimming, rock bolting and other maintenance in the test rooms should be kept to the minimum required for safety, and the rooms allowed to deform.

It is recommended that Test Room 2, in particular, be preserved. It is the only test room that has not been physically altered. This room will then serve as a model for the storage rooms as they will exist prior to waste emplacement. Test Room 2 should not be trimmed or supported except as anticipated for the storage rooms. Additional instrumentation may be installed and small-diameter holes should be drilled in the roof and floor to observe the development of displacements, separations and fracturing. Large-diameter drilling should be prohibited and the room should be closed to all other activities. Continued observations of Test Room 2 behavior will

provide valuable data on anticipated storage room performance for the period between room excavation and the emplacement of waste.

A program of drilling, testing and geologic mapping should be continued to determine the development and extent of fracturing beneath the test room floors. When this has been determined, several monitoring stations should be established to document the behavior of the fractures. This program should also include monitoring roof displacements and separations. Arrays of small-diameter holes should be drilled in a few locations in each test room as soon as possible to document movement above the roof. However, drilling in Test Room 2 should be kept to a minimum.

Additional efforts are needed to refine constitutive laws for the creep behavior of salt as well as the representation of stratigraphy. The stress-strain-time behavior of anhydrite beds should be more accurately represented.

THIS PAGE LEFT BLANK INTENTIONALLY

# CHAPTER 12

# STORAGE AREA

## 12.1 INTRODUCTION

The storage area encompasses all rooms, drifts and crosscuts that will be used for the permanent storage of CH and RH TRU wastes. The storage area is located south of the waste shaft station, from S1600 to S3664 (see Chapter 1, Figure 1-2, and this chapter, Figure 12-1, for location and layout). The storage area is arranged to provide a system in which CH and RH TRU wastes can be efficiently and safely handled and stored. A panel of four full-scale test rooms was excavated to determine the adequacy of the opening configuration and dimensions (Chapter 11). Evaluation of in situ data from these test rooms were utilized to predict the closures of, and stresses and strains around, the future storage area rooms and drifts.

This chapter presents information on the reference design of the storage area rooms and drifts, the design validation process, conclusions regarding the suitability of the reference design based on the findings of the validation process, and recommendations for modifications to the storage area design configurations that will, if implemented, result in a validated reference design.

## 12.2 DESIGN

This section presents the design criteria, design bases and reference design configurations that were used for the WIPP storage area rooms and drifts.

### 12.2.1 Design Criteria

The Design Criteria, RMC-IIA, for the storage area (ref. 2-8) is summarized in Chapter 2, Table 2-1. This table presents the major criteria that governed the WIPP underground opening reference design, including those criteria that require evaluation as part of the design validation process. The following discussion presents a description of

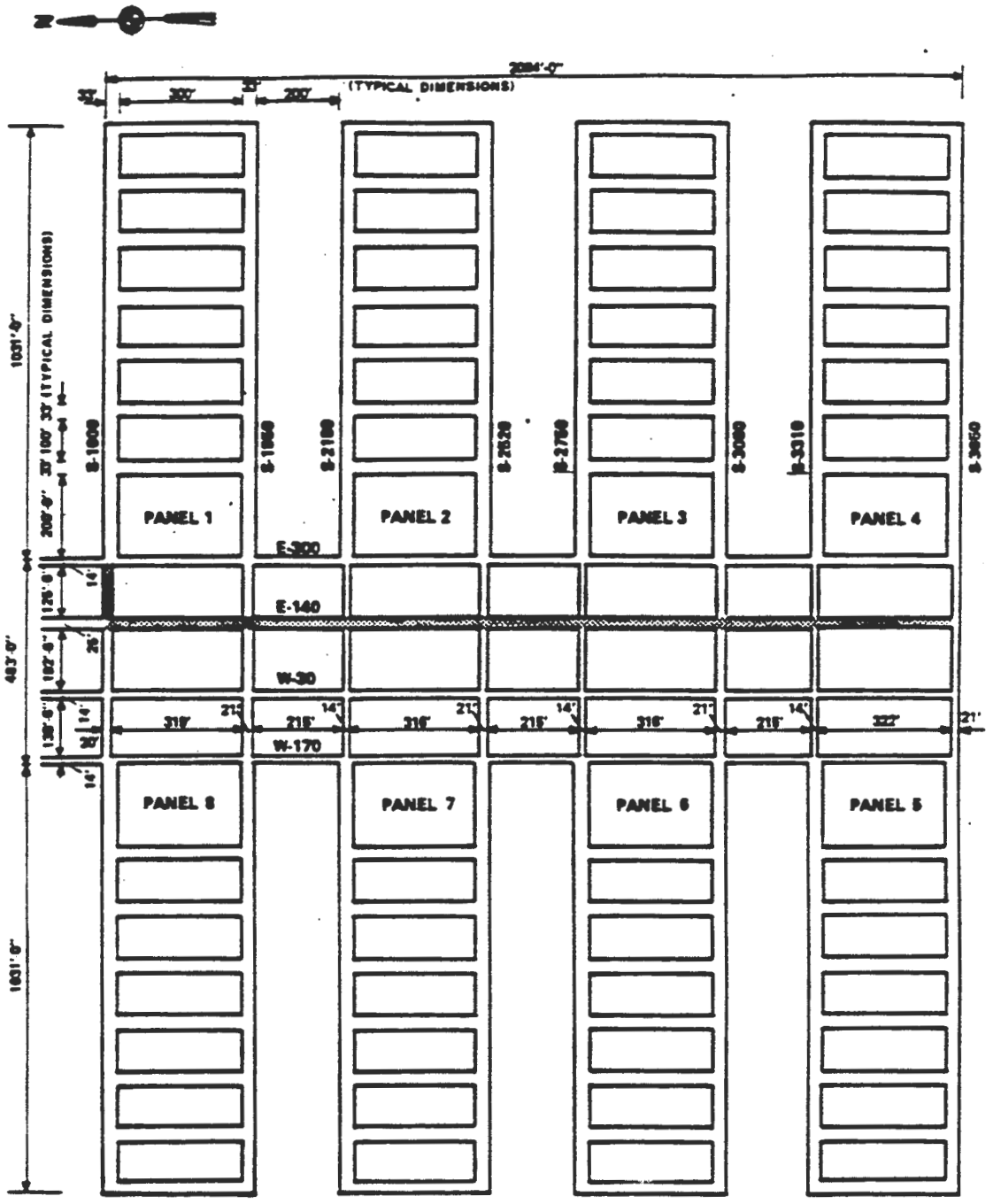


Figure 12-1

STORAGE AREA
REFERENCE DESIGN PLAN

the three design criteria pertaining to the storage area that require evaluation for validation of the reference design.

The first criterion requires that the excavation dimensions of the storage area rooms and drifts include an allowance for creep closure sufficient to prevent container breaching by creep-induced stresses during the retrievability period. The second criterion states that each storage room shall allow for salt creep and shall be sized to minimize breaching of the CH waste containers for a period of 10 years. The third criterion states that the underground storage rooms and access drifts shall be designed to be compatible with the waste transport vehicle, with the waste container sizes, shapes, weights, and stacking configurations, and with the waste handling and backfilling equipment requirements.

Other criteria that apply to the storage area reference design also apply to the drifts and were discussed in Chapter 10.

### 12.2.2 Design Bases

The design bases describe the specific dimensional requirements used to develop the reference design for the storage area drift and room configurations (Figures 12-2 and 12-3). The Design Basis, Underground Excavations (ref. 2-18) contains the bases used for the storage area reference design. The major elements from this Design Basis document are summarized in the following discussion. Although other design bases were also used, they did not have a direct impact on design validation. The specific design bases requiring evaluation during the validation process are presented in Table 12-1.

The design bases specify that the reference design shall provide an underground storage area in which CH and RH TRU wastes can be efficiently handled and stored. The reference design of the waste storage area shall permit simultaneous storage of CH and RH TRU wastes. To the extent possible, the configuration of the storage area shall minimize haulage distances for excavated salt and waste storage.

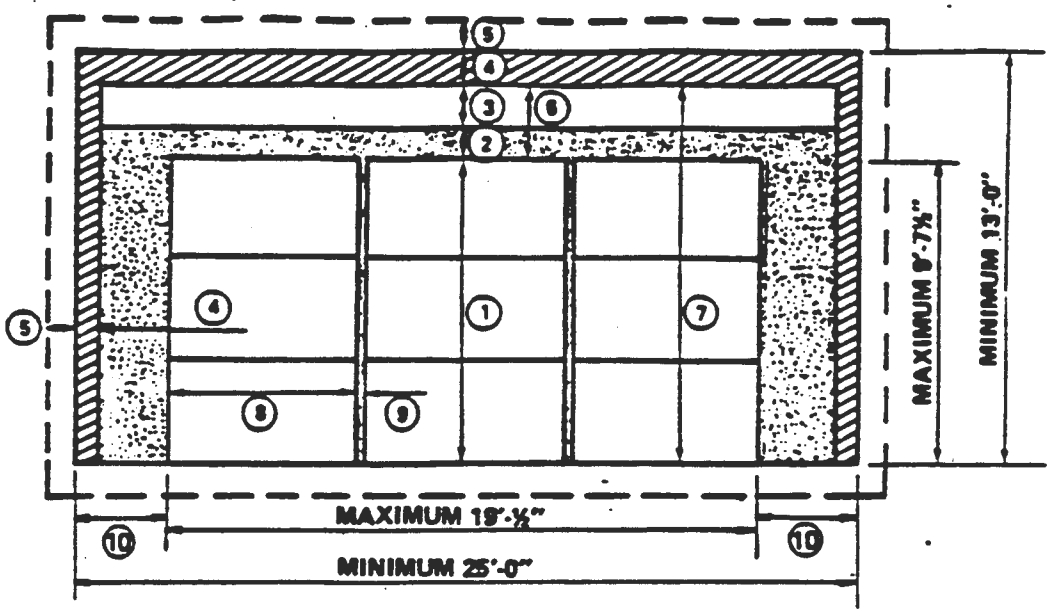


## EXPLANATION

(1) HEIGHT OF WASTE PACKAGES STACKED THREE HIGH: 9'-7 1/2" FOR BOXES; 9'-0" FOR SIX PACKS.

(2) SALT COVER: 1' TO 2'; LEVEL OF SALT IS MAINTAINED AT 10'-8" ABOVE THE FLOOR.

(3) VENTILATION SPACE: 1'-4" MINIMUM UNTIL ROOM OR PANEL IS FILLED AND PLUGGED.

(4) SALT CREEP ALLOWANCE: 1'-0" ROOF; 4 1/2" EACH WALL (ASSUMED TO BE ADEQUATE FOR 5 YEARS).

(5) CONSTRUCTION TOLERANCE: +6". THE CONTRACTOR MUST MAINTAIN THE MINIMUM ROOM DIMENSIONS.

(6) BACKFILLING CONVEYOR CLEARANCE: 2'-4" ABOVE WASTE PACKAGES.

(7) HEADROOM: 12'-0" FOR CH BOXES AND RH TRANSPORTER.

(8) WASTE PACKAGE WIDTH: 6'-2 1/2" FOR BOXES; 6'-1 1/2" FOR SIX PACKS.

(9) STACKING TOLERANCE: 2 1/2" BETWEEN WASTE PACKAGES.

(10) SALT BACKFILL: 3'-0" BETWEEN WASTE PACKAGES AND WALL.

Figure 12-2

STORAGE AREA
DRIFT REFERENCE DESIGN DIMENSIONS

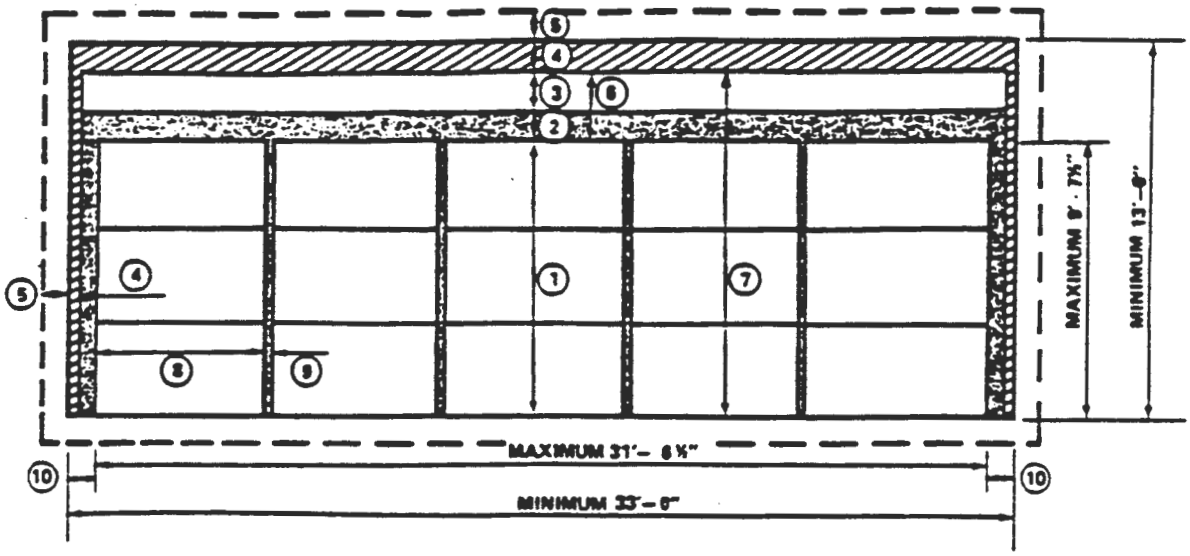


## EXPLANATION

(1) HEIGHT OF WASTE PACKAGES STACKED THREE HIGH: 9'-7 1/2" FOR BOXES; 9'-0" FOR SIX PACKS.

(2) SALT COVER: 1' TO 2'; LEVEL OF SALT IS MAINTAINED AT 10'-8" ABOVE THE FLOOR.

(3) VENTILATION SPACE: 1'-4" MINIMUM UNTIL ROOM OR PANEL IS FILLED AND PLUGGED.

(4) SALT CREEP ALLOWANCE: 1'-0" ROOF; 4 1/2" EACH WALL (ASSUMED TO BE ADEQUATE FOR 5 YEARS).

(5) CONSTRUCTION TOLERANCE: +6". THE CONTRACTOR MUST MAINTAIN THE MINIMUM ROOM DIMENSIONS.

(6) BACKFILLING CONVEYOR CLEARANCE: 2'-4" ABOVE WASTE PACKAGES.

(7) HEADROOM: 12'-0" FOR CH BOXES AND RH TRANSPORTER.

(8) WASTE PACKAGE WIDTH: 6'-2 1/2" FOR BOXES; 6'-1 1/2" FOR SIX PACKS.

(9) STACKING TOLERANCE: 2 1/2" BETWEEN WASTE PACKAGES.

(10) SALT BACKFILL: 8 3/4" BETWEEN WASTE PACKAGES AND WALL.

Figure 12-3

STORAGE AREA
ROOM REFERENCE DESIGN DIMENSIONS

Table 12-1

VALIDATION ELEMENTS OF STORAGE AREA DESIGN BASES

(1) Operational requirements

a. The storage area rooms, drifts and crosscuts shall be designed to allow for retrieval of all CH and RH waste stored for a period of up to 5 years after the initial emplacement of each waste species.

b. Excavation dimensions in the waste storage area shall be to a uniform height of 13 feet.

(2) Essential features

Provide 1 foot vertical and 9 inches horizontal allowance for creep closure to maintain the minimum design dimensions up to 5 years after initial emplacement.

(3) Safety design requirements

A minimum opening of 16 inches shall be left at the top of the rooms and drifts for air passage above the waste and backfill.

Construction and storage operations shall be physically separated and performed during different shifts.

Each storage room is to be filled with waste containers consisting of six-packs of CH TRU waste storage drums and/or boxes of CH TRU waste. The containers shall be stacked three high and five wide, stored with their longest dimension across the opening. A 2 1/2-inch stacking tolerance shall be allowed between waste packages. All rooms, drifts and crosscuts in the storage area may be used to store CH waste containers stacked three high. For this reason, excavation shall be to a uniform height of 13 feet throughout the waste storage area.

The underground storage area shall provide for the horizontal emplacement of 1,000 RH canisters. The RH canisters, nominally 10 feet long and 26 inches in diameter, shall be stored in the salt pillars. Emplacement holes shall be perpendicular to the walls, approximately midway between the floor and ceiling and evenly spaced laterally. Canister spacing shall be based on the assumption that the average heat output per canister will be 60 watts or less. Thermal loading in the RH waste storage area shall not exceed 10 kilowatts (kw) per acre. Allowing 12 inches for salt creep, RH waste emplacement machinery shall be designed to operate in an effective room height of 12 feet, including all required clearances.

The storage area floor shall be approximately 2,150 feet below the ground surface. The final level of the excavations shall be as determined by the DOE Contracting Officer.

Four parallel entries shall be provided from the shafts to the waste storage area. These entries shall provide separate channels for air intake and exhaust, salt removal, and waste storage.

Excavation dimensions shall include an allowance for salt creep of 1 foot in the vertical direction and 9 inches in the horizontal direction for all rooms for up to 5 years. The tolerance for excavation of roof,

floor and wall surfaces shall be no greater than plus 6 inches. In no case shall the finished cross section dimensions be less than the design dimensions.

Provision shall be made for the expansion of the storage area within the boundaries of Zone II (Chapter 1, Figure 1-1) if required in the future. The area extraction ratio in the storage area shall not exceed 25 percent.

The stored CH TRU waste packages shall be covered with a layer of salt backfill (3/8 inch or less in grain size) for fire protection. The volume of stored CH TRU waste in any one compartment without a vertical fire barrier shall be limited to a maximum of 500,000 cubic feet. For ventilation above the backfilled waste, a minimum opening of 16 inches shall be provided.

No personnel may work in air that has passed over the stored CH TRU waste. However, personnel may work in air that has passed through an opening where RH TRU waste has been emplaced provided that canister holes have been sealed with plugs. Personnel may not work in air that has passed through openings where RH TRU waste is being emplaced.

### 12.2.3 Design Configuration

The reference design of the storage area was developed in accordance with the design criteria and the design bases. The design configuration is based on the stratigraphy determined from borehole ERDA-9 and on salt creep performance determined from laboratory tests on core extracted from ERDA-9. The ERDA-9 exploratory hole was the only hole within the underground development area which was permitted to penetrate the Salado formation to the underground facility horizon.

The storage area reference design configuration (Figures 12-1, 12-2 and 12-3) consists of eight panels with seven rooms each. The rooms are 13 feet high, 33 feet wide and 300 feet long. The panel entries are also 13 feet high and 33 feet wide. The rooms are separated in each panel

by 100-foot wide pillars and the panels are separated by 200-foot wide pillars. The test rooms discussed in Chapter 11 were designed to be the same size as the storage rooms. The test rooms were constructed to monitor salt performance, permit observations of opening stability, and to permit validation of the storage room reference design.

The reference design provides for the storage of CH waste in one room while RH waste is stored in another room. Emplacement of RH waste canisters into horizontal holes is depicted on Figure 12-4. After the RH waste canisters are emplaced in the walls of the storage room a shield plug is placed in the wall sleeve. When the emplacement of RH waste canisters is completed in the storage room, CH waste can be stored in the same room. During the 5-year demonstration period, the RH waste canisters are stored in steel sleeves in the first room of Panel 1. During permanent storage, they are emplaced in pillars throughout the storage area as dictated by the receival rate of the waste.

The RH waste canisters (with a heat output of 60 watts or less) are placed in horizontal holes spaced so that the local storage area thermal loading does not exceed the design basis limit of 10 kw/acre. For the reference design, and for this report, the thermal effects on storage room behavior were not considered significant. The reference design for RH waste is subject to the results of the ongoing WIPP experimental program.

The reference design configuration also defines stacking configurations and tolerances for ventilation, backfill and salt creep. These tolerances are shown on Figures 12-2 and 12-3 for the storage area drifts and rooms, respectively. In order to meet these requirements, the reference design configuration incorporates a reference operating procedure. This procedure is based on the waste receipt rates, emplacement rates, and retrieval rates stipulated by the design criteria. This operating procedure is part of the storage room reference design and is incorporated in construction package EP-01X.

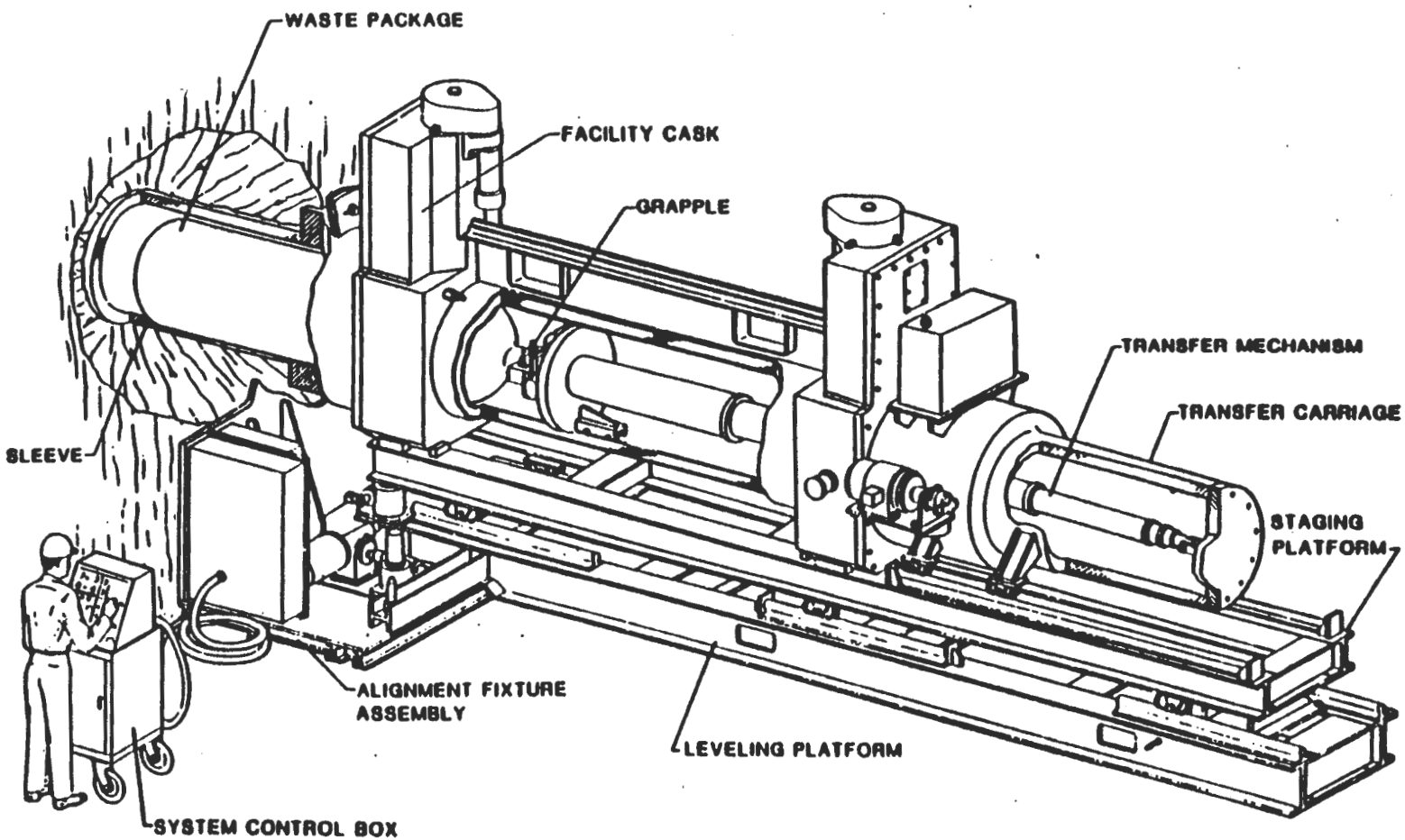


Figure 12-4

STORAGE AREA
HORIZONTAL EMPLACEMENT OF RH WASTE

This package contains the design documents that will be used to operate the WIPP.

## 12.3 DESIGN VALIDATION PROCESS

The design validation process for the storage area consists of the evaluation of numerical modeling and data analysis from the drifts and test rooms (Chapters 10 and 11) and its application to the reference design of the storage area drifts and rooms. The predicted future performance of the storage area openings was compared to the performance of existing openings having comparable dimensions. This was then used as the upper bound for validating the reference design.

### 12.3.1 Data Collection

Geomechanical instrumentation data collected from the test rooms were used to compute the creep parameters of the surrounding salt. Geologic mapping and drill cores from the underground facility were used to confirm the stratigraphy of the storage area. Test room instrumentation data and the computation of creep parameters are presented in Chapter 11. Chapter 6 presents information on the geologic mapping, drill cores and development of the reference stratigraphy.

The geomechanical instruments in the test rooms have provided deformation measurements and response data on the excavated openings. Periodic visual inspections of the rooms have provided observational data with which to further evaluate the response of the surrounding salt. Geologic mapping and core drilling in the E140 drift south of the waste shaft have provided information on the stratigraphy in the storage area.

### 12.3.2 Analysis and Evaluation

#### 12.3.2.1 Storage Rooms

Analysis and evaluation of the storage room reference design have been performed using data collected from the test rooms. The adequacy of

the reference design was evaluated by analysis of the geomechanical behavior, including stress, strain and deformation, which could be expected to occur over the operating life of each room. The operating life is defined as the period of time from initial excavation of the room until retrieval operations are completed, if the decision to retrieve is made, or until the storage operation for each panel is completed.

Evaluation of the geologic mapping and drill cores from the E140 drift south of the waste shaft has confirmed the continuity of the stratigraphy 50 feet above and below the storage area (refs. 4-1 and 4-2).

Based on an engineering approach (Chapter 5), numerical analyses were performed based on creep parameters determined from test room data and the stratigraphy surrounding the facility level. Because the extrapolation of the in situ closure data for the drifts and test rooms indicates that more than four rooms in a storage panel could influence the total closure and overall creep rate, a mathematical model was developed to estimate the upper bound responses. This requires assuming an infinite array of equally spaced storage rooms such that the centerline of a typical room and the centerline of any one of its pillars form axes of symmetry. In addition, the rooms were assumed to be infinitely long.

Figure 12-5 shows the finite element model that was used to determine the responses for an infinite array of infinitely long storage rooms. The model has 94 nodes and consists of 59 plane strain elements, with gap/friction link elements having a friction coefficient of 0.4 to model a clay seam. Because test room creep parameters are used in predicting the responses of the storage rooms, this model uses the same comparative element sizes and external loads as those used in the test room model described in Chapter 11, Section 11.3. The boundaries on both sides of the model were taken as vertical axes of symmetry to represent the pillar centerlines and consist of horizontal restraints.

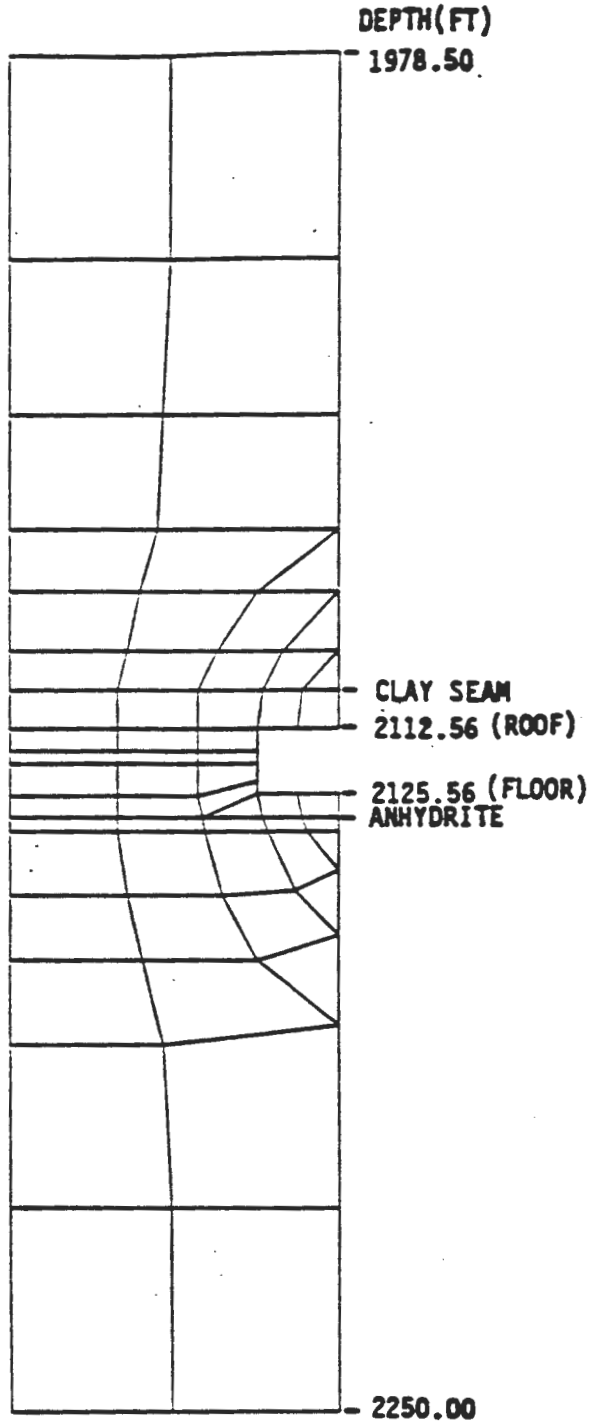


Figure 12-5

STORAGE AREA
ROOM FINITE ELEMENT MODEL

Elevations at the top and bottom of the model, the clay seam, the anhydrite bed, and the roof and floor of the room are based on the reference stratigraphy and are identical to those used in the test room finite element model.

The analyses were performed using the MARC General Purpose Finite Element Program discussed in Chapter 6. The average values of the creep parameters were derived from test room roof-to-floor and wall-to-wall in situ closure data. Using these computed creep parameters, previously presented in Chapter 11, Tables 11-10 and 11-11, the predicted future responses of the storage rooms were computed. The results of the analyses are presented below.

#### 12.3.2.2 Storage Area Drifts

Analysis and evaluation of the 13 x 25-foot drift design for the storage area have been performed using data collected from the existing 8 x 25-foot drifts. The same finite element model used for the 8 x 25-foot drifts (Chapter 10) was used for the larger drifts. A removable floor section extending 5 feet vertically downward from the original floor level was integrated into the model so that this group of elements could be removed at the appropriate stage in the analysis to simulate floor excavation. A coefficient of friction of 0.0 was assumed for the gap/friction elements to model a clay seam. The time between initial excavation and the subsequent floor excavation was assumed to be 2 years. Therefore, all results presented in the following subsection are directly affected by these assumptions. Figure 12-6 shows the model after removal of the floor elements.

### 12.3.3 Prediction of Future Behavior

#### 12.3.3.1 Storage Rooms

Because the room size and panel configuration of the four test rooms is similar to the design of the proposed storage rooms, the behavior of the storage rooms was computed using the measured data from the test rooms, as presented in Chapter 11. The results of the storage room

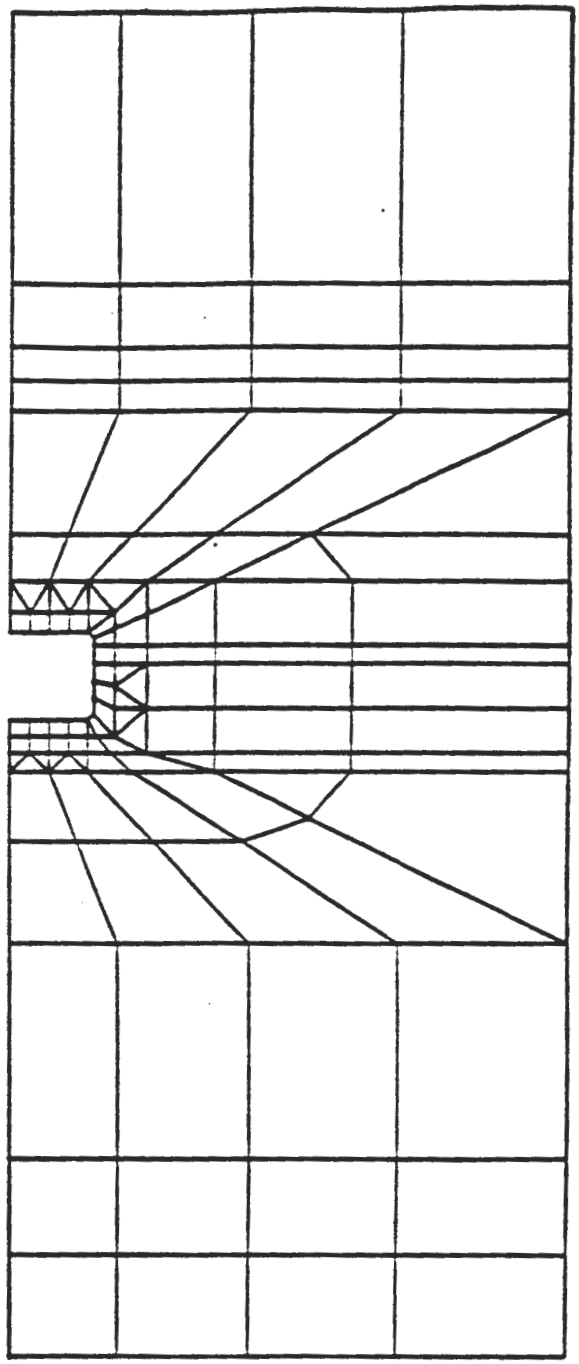

Figure 12-6

STORAGE AREA
DRIFT FINITE ELEMENT MODEL - AFTER FLOOR LOWERING

analyses were plotted at various integration time steps. These integration steps correspond to real times immediately after excavation, 1 year and 10 years after excavation. The horizontal and vertical stresses, effective stresses, effective creep strains, principal stresses and the deformed shapes were plotted at these times based on the mean value of the averaged wall-to-wall and roof-to-floor creep parameters presented in Tables 11-12 and 11-13 in Chapter 11. A closure calculation considering the effects at a room intersection was performed utilizing the values from these tables. Roof-to-floor and wall-to-wall closure predictions for the storage room were then plotted.

Horizontal and Vertical Stresses. The computed horizontal stress distributions in the storage rooms are plotted on selected elements of the finite element mesh immediately after excavation and at times of 1 year and 10 years after excavation (Figures 12-7 through 12-9). A contour interval of 250 ksf was chosen and 10 contour increments were used to span a stress range from 0 to 2,500 ksf compression.

Horizontal stresses immediately after excavation are totally compressive throughout the selected elements of the model. Most of the changes in horizontal stresses in the salt around the opening occur within the first year after excavation and remain practically constant even 10 years after excavation. The walls and the underlying anhydrite bed (MB-139), near the center of the room, have the largest compressive stresses, with values between 250 and 500 ksf compression. As the opening slowly deforms, horizontal stresses tend to become more compressive in the anhydrite bed near the room's vertical centerline. In the anhydrite bed far from the room centerline, the horizontal stresses are relatively low.

The vertical stress distribution was also plotted for time periods immediately after excavation and at times of 1 year and 10 years after excavation (Figures 12-10 through 12-12). The contour interval and stress range are the same as those used for the horizontal stress plots.

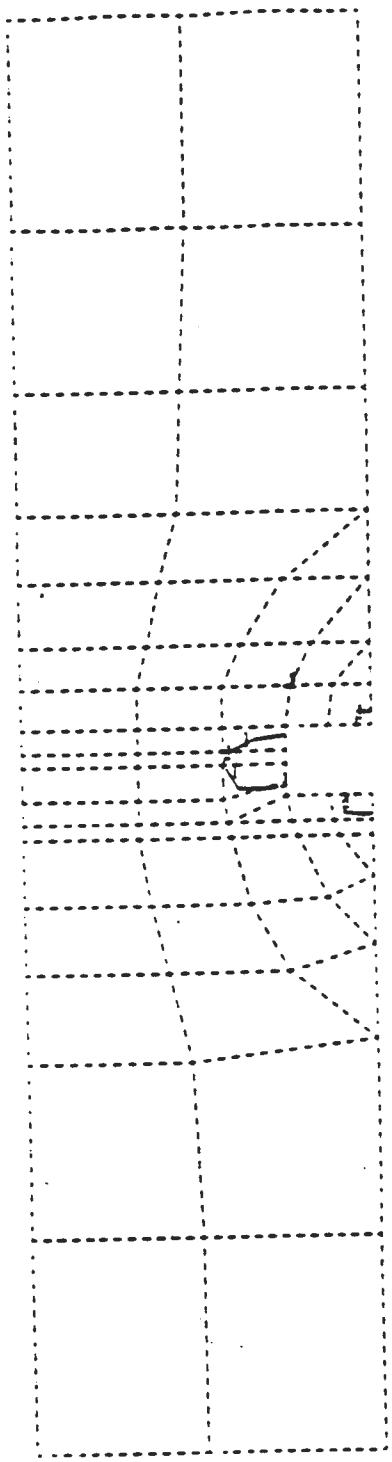

| CONTOUR | $\sigma_h$(ksf) |
|---|---|
| 1 | 250 |
| 2 | 500 |
| 3 | 750 |
| 4 | 1000 |
| 5 | 1250 |
| 6 | 1500 |
| 7 | 1750 |
| 8 | 2000 |
| 9 | 2250 |
| 10 | 2500 |

Figure 12-7

STORAGE ROOMS
HORIZONTAL STRESS DISTRIBUTION IMMEDIATELY AFTER EXCAVATION

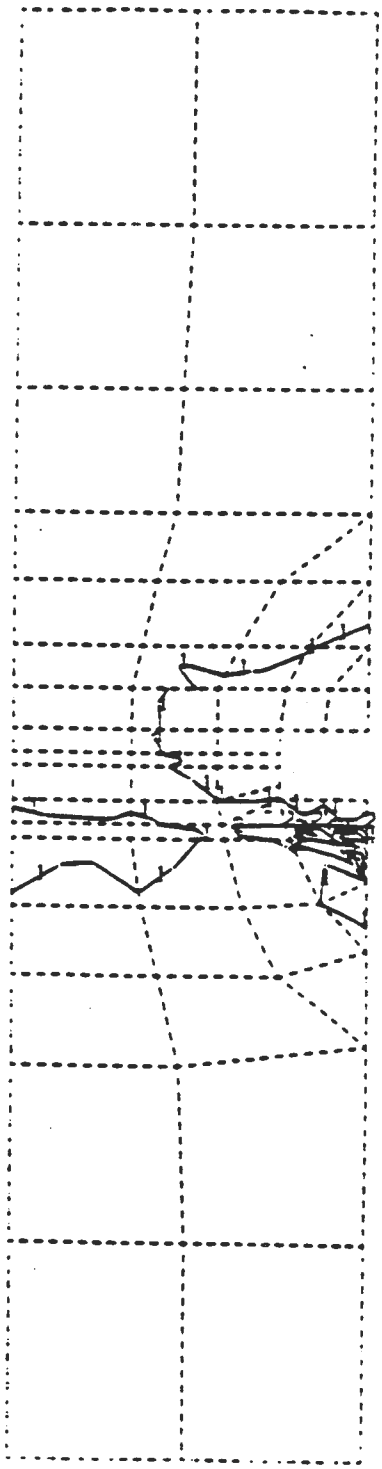

| CONTOUR | $\sigma_h$(ksf) |
|---|---|
| 1 | 250 |
| 2 | 500 |
| 3 | 750 |
| 4 | 1000 |
| 5 | 1250 |
| 6 | 1500 |
| 7 | 1750 |
| 8 | 2000 |
| 9 | 2250 |
| 10 | 2500 |

Figure 12-8

STORAGE ROOMS
HORIZONTAL STRESS DISTRIBUTION 1 YEAR AFTER EXCAVATION

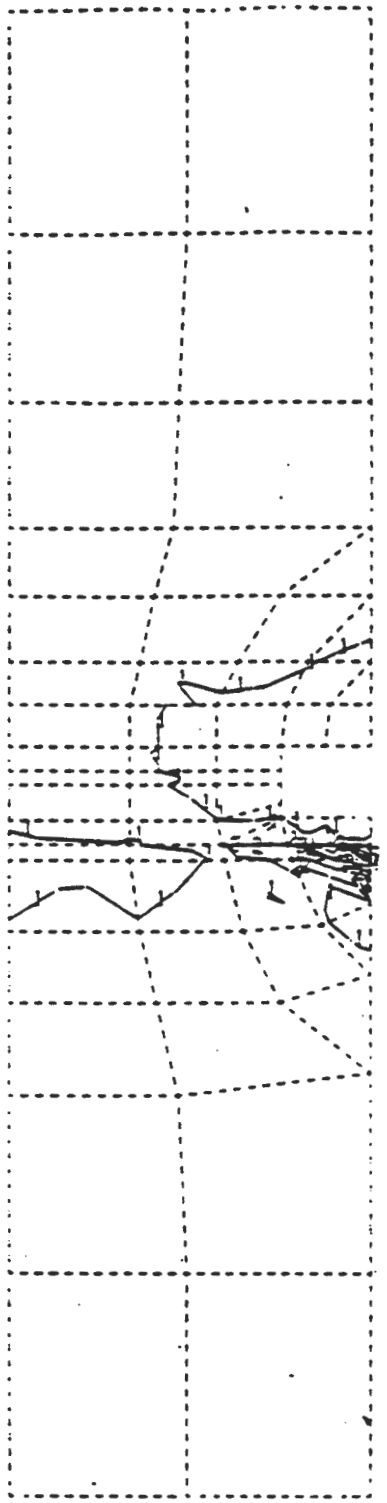

| CONTOUR | $\sigma_h$(ksf) |
|---|---|
| 1 | 250 |
| 2 | 500 |
| 3 | 750 |
| 4 | 1000 |
| 5 | 1250 |
| 6 | 1500 |
| 7 | 1750 |
| 8 | 2000 |
| 9 | 2250 |
| 10 | 2500 |

Figure 12-9

STORAGE ROOMS
HORIZONTAL STRESS DISTRIBUTION 10 YEARS AFTER EXCAVATION

Figure 12-10 shows a vertical stress in the wall near the room opening immediately after excavation of between 500 and 750 ksf compression. This stress is approximately twice the original lithostatic stress before excavation and clearly shows the expected stress concentrations around the opening immediately after excavation. As the opening deforms, the vertical stress is redistributed around the opening and reduced to between 250 and 500 ksf compression.

Figures 12-11 and 12-12 show very small differences from 1 year through 10 years after excavation. That is, the vertical stress is relatively constant throughout that period with most of the halite roof beam having low stress in the vertical direction. Likewise, the uppermost level of elements in the room's floor has relatively low stress in the vertical direction due to its lack of vertical confinement.

The anhydrite bed (MB-139) below the storage room is, in general, subjected to low vertical stresses; however, some compressive vertical stress is indicated under the pillars.

Effective Stresses and Effective Creep Strains. Figures 12-13 through 12-15 show the computed effective stress distribution in those elements of the finite element model near the room opening. Ten contour increments, each having an interval of 250 ksf, were chosen to span a stress range from 0 to 2,500 ksf. The effective stress plot immediately after excavation shows a relatively low stress concentration in the anhydrite bed below the floor and no stresses greater than 500 ksf in the halite beds.

At 1 year and 6.5 years after excavation, the computed effective stresses have increased and concentrated in the anhydrite bed and overlying halite. Because the anhydrite was modeled as being elastic until failure and stiffer than halite, it supports more stress, which results in a large effective stress gradient in the anhydrite. The maximum computed effective stress is 2,600 ksf, concentrated in the anhydrite bed near the room centerline.

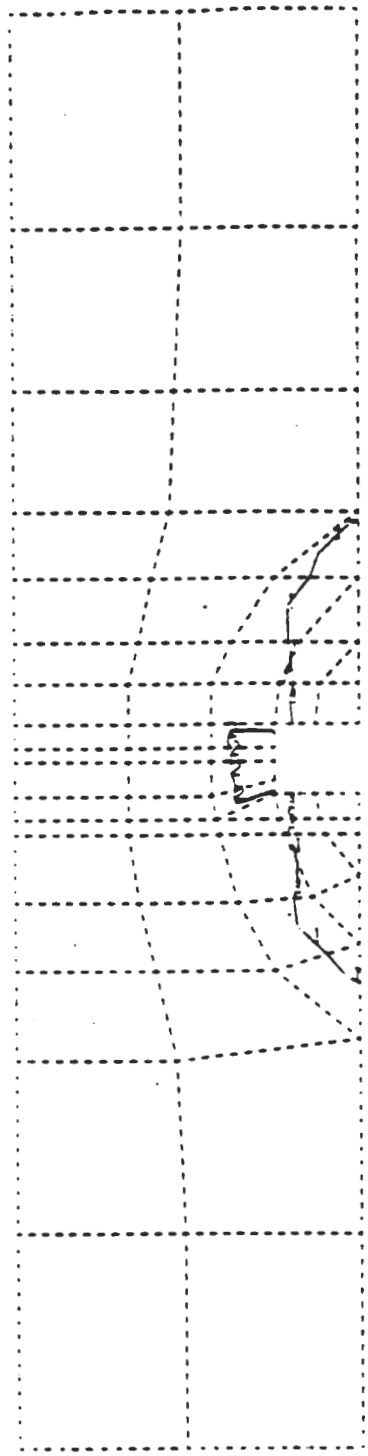

| CONTOUR | $\sigma_v$ (ksf) |
|---|---|
| 1 | 250 |
| 2 | 500 |
| 3 | 750 |
| 4 | 1000 |
| 5 | 1250 |
| 6 | 1500 |
| 7 | 1750 |
| 8 | 2000 |
| 9 | 2250 |
| 10 | 2500 |

Figure 12-10

STORAGE ROOMS
VERTICAL STRESS DISTRIBUTION IMMEDIATELY AFTER EXCAVATION

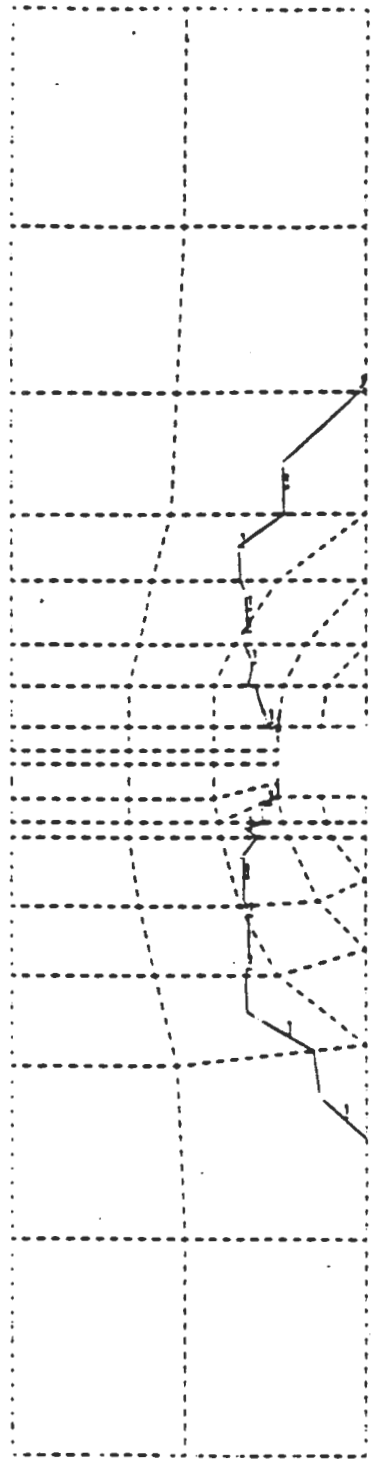

| CONTOUR | $\sigma_v$(ksf) |
|---|---|
| 1 | 250 |
| 2 | 500 |
| 3 | 750 |
| 4 | 1000 |
| 5 | 1250 |
| 6 | 1500 |
| 7 | 1750 |
| 8 | 2000 |
| 9 | 2250 |
| 10 | 2500 |

Figure 12-11

STORAGE ROOMS
VERTICAL STRESS DISTRIBUTION 1 YEAR AFTER EXCAVATION

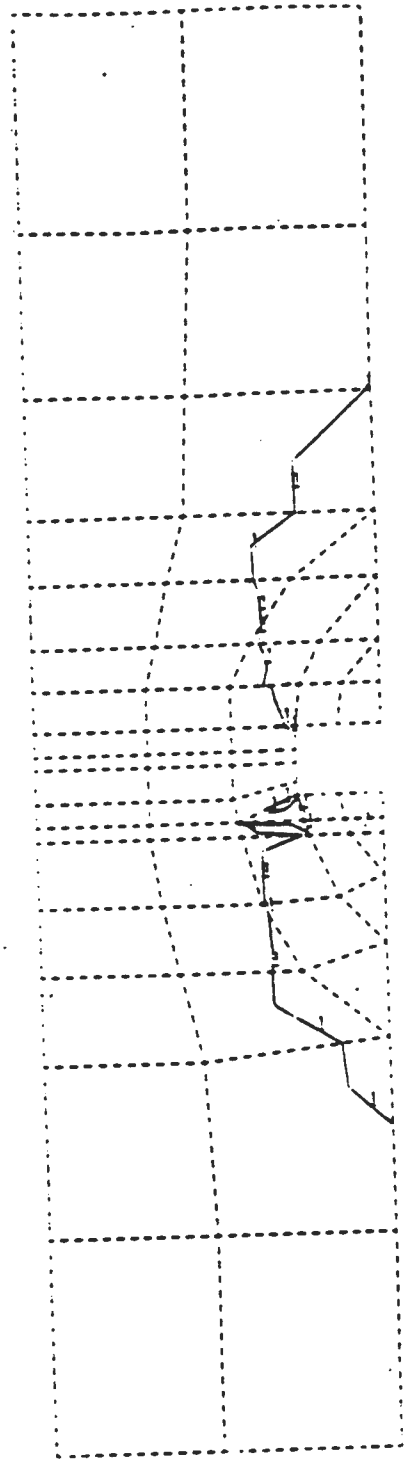

| CONTOUR | $\sigma_v$(ksf) |
|---|---|
| 1 | 250 |
| 2 | 500 |
| 3 | 750 |
| 4 | 1000 |
| 5 | 1250 |
| 6 | 1500 |
| 7 | 1750 |
| 8 | 2000 |
| 9 | 2250 |
| 10 | 2500 |

Figure 12-12

STORAGE ROOMS
VERTICAL STRESS DISTRIBUTION 10 YEARS AFTER EXCAVATION

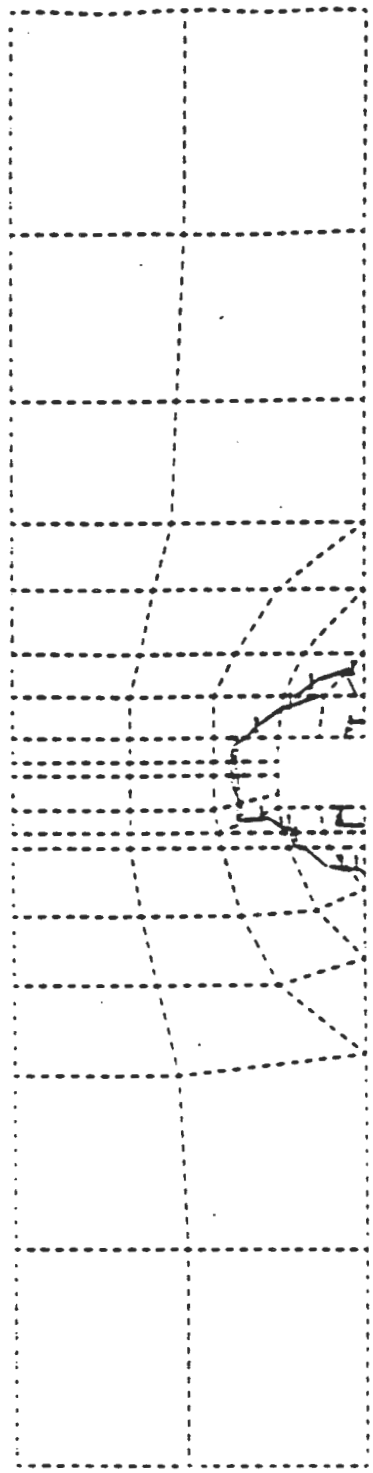

| CONTOUR | $\bar{\sigma}$(ksf) |
|---|---|
| 1 | 250 |
| 2 | 500 |
| 3 | 750 |
| 4 | 1000 |
| 5 | 1250 |
| 6 | 1500 |
| 7 | 1750 |
| 8 | 2000 |
| 9 | 2250 |
| 10 | 2500 |

Figure 12-13

STORAGE ROOMS
EFFECTIVE STRESS DISTRIBUTION IMMEDIATELY AFTER EXCAVATION

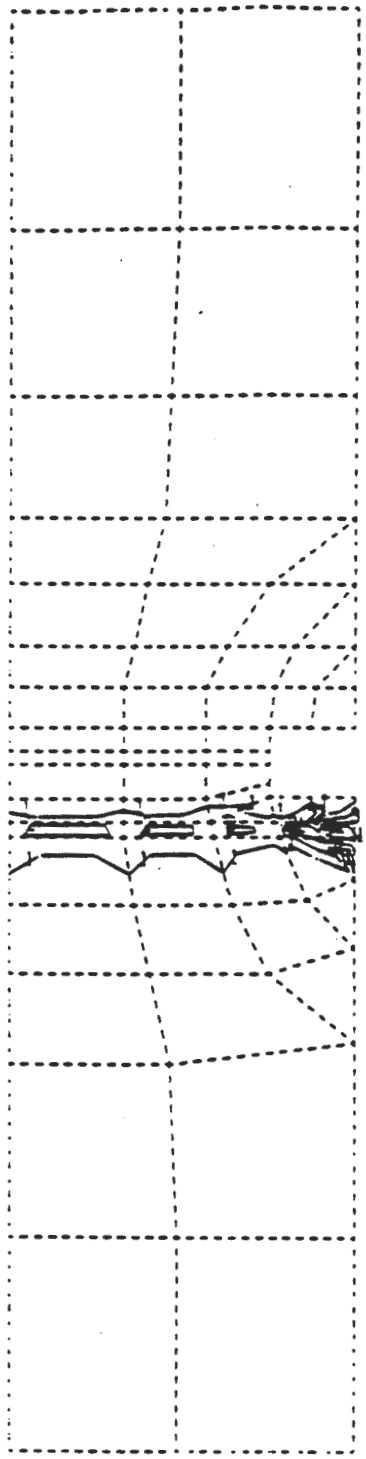

| CONTOUR | $\bar{\sigma}$(ksf) |
|---|---|
| 1 | 250 |
| 2 | 500 |
| 3 | 750 |
| 4 | 1000 |
| 5 | 1250 |
| 6 | 1500 |
| 7 | 1750 |
| 8 | 2000 |
| 9 | 2250 |
| 10 | 2500 |

Figure 12-14

STORAGE ROOMS
EFFECTIVE STRESS DISTRIBUTION 1 YEAR AFTER EXCAVATION

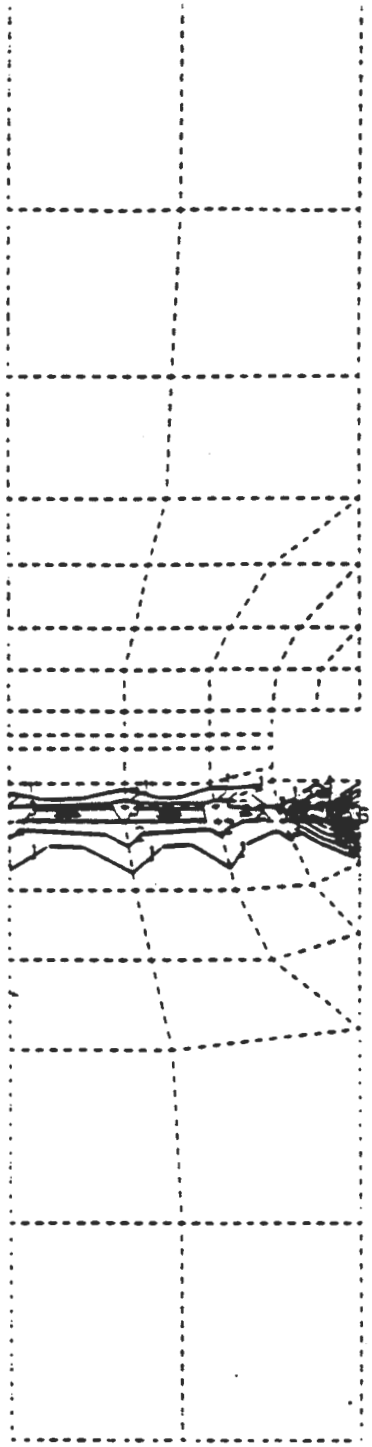

| CONTOUR | $\bar{\sigma}$ (ksf) |
|---|---|
| 1 | 250 |
| 2 | 500 |
| 3 | 750 |
| 4 | 1000 |
| 5 | 1250 |
| 6 | 1500 |
| 7 | 1750 |
| 8 | 2000 |
| 9 | 2250 |
| 10 | 2500 |

Figure 12-15

STORAGE ROOMS
EFFECTIVE STRESS DISTRIBUTION 10 YEARS AFTER EXCAVATION

Because the model does not include failure criteria for the anhydrite bed, an analysis for potential failure in this bed was performed separately. In Chapter 6, the failure criterion

$$\sqrt{J_2'} = 752 - 0.279J_1 \quad \text{(stress in ksf)} \tag{12-1}$$

was defined for the anhydrite bed based on laboratory tests. Rewriting this equation in terms of the effective stress at failure $\bar{\sigma}_f$ and the first stress invarient at failure $(J_1)_f$:

$$\bar{\sigma}_f(\text{ksf}) = 1302.5 - 0.483\ (J_1)_f \tag{12-2}$$

From the results of the numerical modeling, the average effective stress stress at a point close to the center of the room exceeds $\bar{\sigma}_f$ at about 8.5 years since excavation. This does not mean catastrophic failure will occur. Instead, there will be a redistribution of stress in the anhydrite bed which the model cannot consider.

Computed effective creep strain distributions were plotted on selected elements of the deformed mesh at 1 year and 6.5 years after excavation (Figures 12-16 and 12-17). Ten strain increments with an interval of 0.01 were used to span a strain range from 0 to 0.100.

At 1 year after excavation, effective creep strains have concentrated in the region around the room opening. At 6.5 years after excavation, the effective creep strains have further intensified around the room opening and in the region above the anhydrite bed near the room centerline.

Based on laboratory creep tests on samples of halite, a failure criterion has been proposed (equation 6-5 in Chapter 6). Based on this criterion, the failure effective strain for halite is a function of the mean normal stress intensity and reaches a maximum magnitude of nearly 16 percent at a mean stress intensity of 125 ksf.

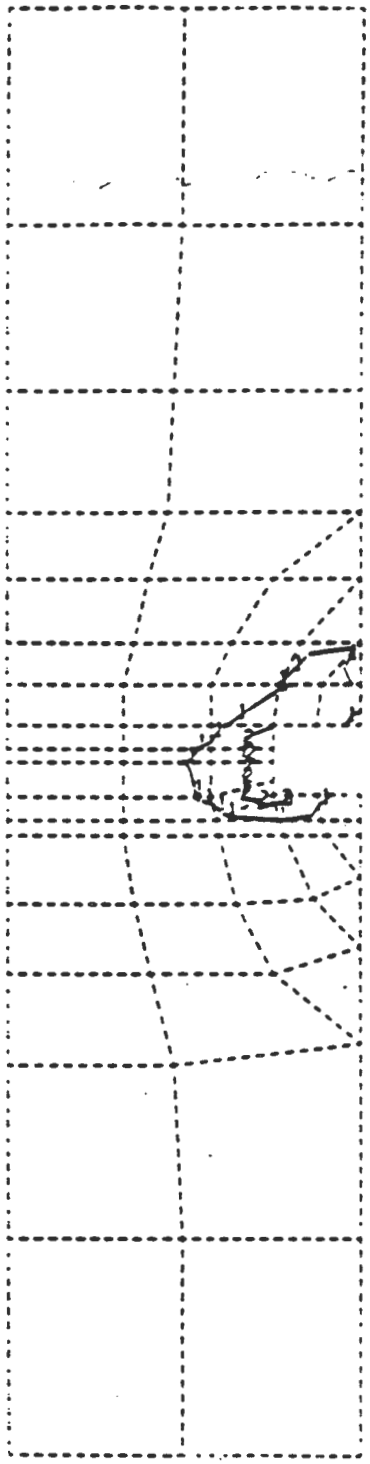

| CONTOUR | $\bar{\epsilon}$ |
|---|---|
| 1 | 0.01 |
| 2 | 0.02 |
| 3 | 0.03 |
| 4 | 0.04 |
| 5 | 0.05 |
| 6 | 0.06 |
| 7 | 0.07 |
| 8 | 0.08 |
| 9 | 0.09 |
| 10 | 0.10 |

Figure 12-16

STORAGE ROOMS
EFFECTIVE CREEP STRAIN DISTRIBUTION 1 YEAR AFTER EXCAVATION

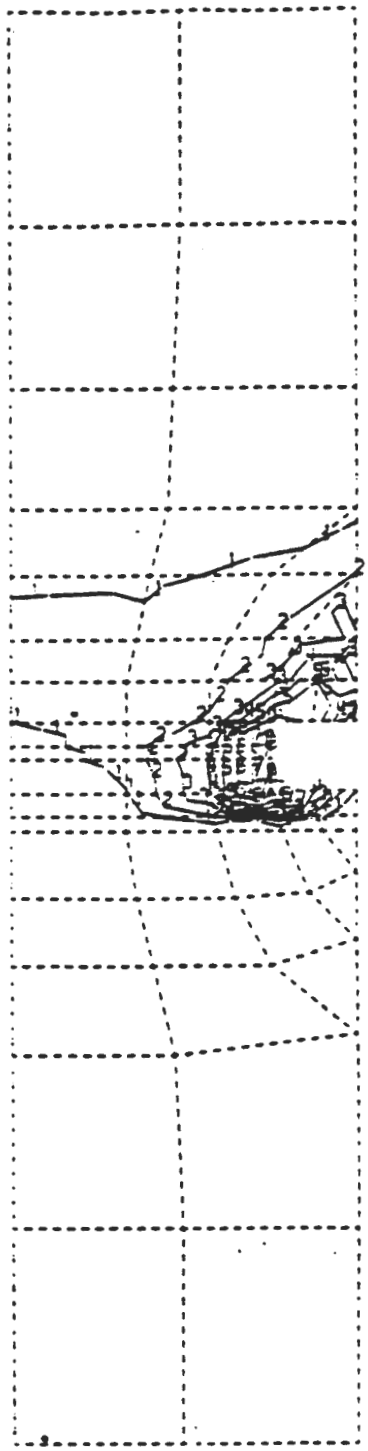

| CONTOUR | $\bar{\epsilon}$ |
|---|---|
| 1 | 0.01 |
| 2 | 0.02 |
| 3 | 0.03 |
| 4 | 0.04 |
| 5 | 0.05 |
| 6 | 0.06 |
| 7 | 0.07 |
| 8 | 0.08 |
| 9 | 0.09 |
| 10 | 0.10 |

Figure 12-17

STORAGE ROOMS
EFFECTIVE CREEP STRAIN DISTRIBUTION 10 YEARS AFTER EXCAVATION

Based on the computed values of effective creep strain up to 6.5 years since excavation, and by linear extrapolation beyond 6.5 years, failure will be initiated in the halite about 12 years after the completion of excavation. The failure will be initiated at floor and wall intersections.

However, the numerical modeling also shows that effective strain decreases rapidly with distance away from the opening. Thus, the failure is expected to be confined very close to the opening. This will require periodic scaling and trimming.

Principal Stresses. The computed principal stresses on the plane of a section across the storage rooms are presented in a qualitative manner on Figures 12-18 through 12-20. The magnitudes of the two principal stresses are proportional to the lengths of the corresponding lines which are plotted, perpendicular to each other, at the centroid of each of the elements.

Immediately after excavation, the magnitudes of the principal stresses are relatively large in the corners of the room and in the anhydrite bed. As the room opening deforms, the principal stresses concentrate in the anhydrite bed near the room centerline.

The plots of the principal stresses also show the stress arch which forms around the room due to the transfer of loads around the room opening. The stress arch tends to become enlarged with time and migrates away from the room.

Deformation and Closure. Figures 12-18 through 12-20 also show the predicted deformed shapes of a typical storage room at different times. The dashed lines represent the outline of the deformed shape of the storage room.

Immediately after excavation, deformation starts around the opening. After 1 year of creep, the halite roof beam deforms noticeably at its

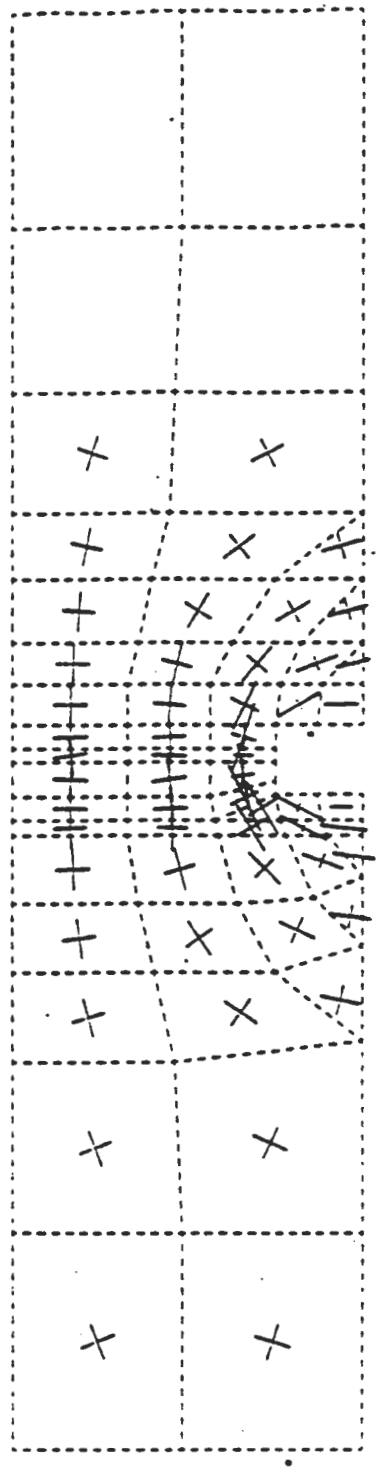

Figure 12-18

STORAGE ROOMS
PRINCIPAL STRESSES AND DEFORMED SHAPE
IMMEDIATELY AFTER EXCAVATION

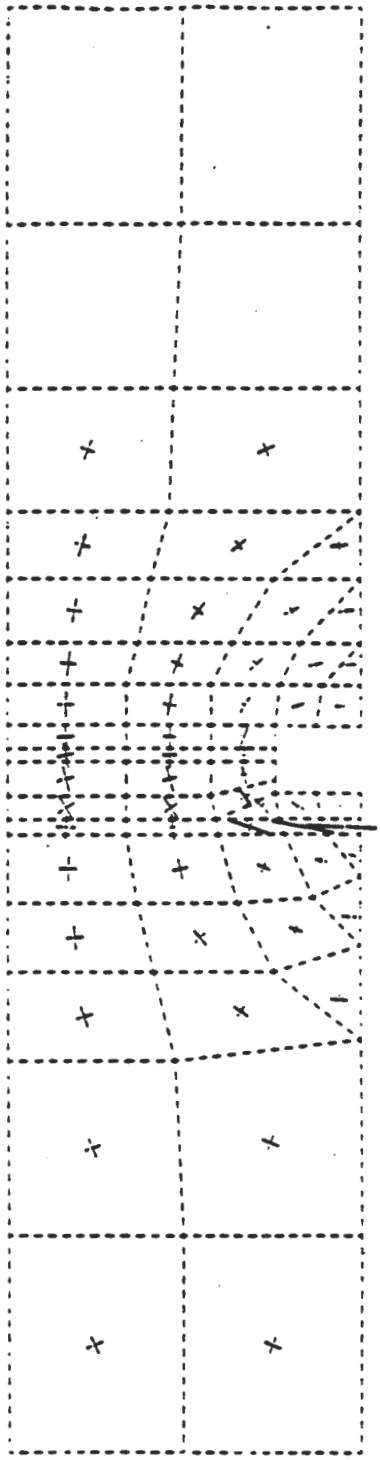

Figure 12-19

STORAGE ROOMS
PRINCIPAL STRESSES AND DEFORMED SHAPE
1 YEAR AFTER EXCAVATION

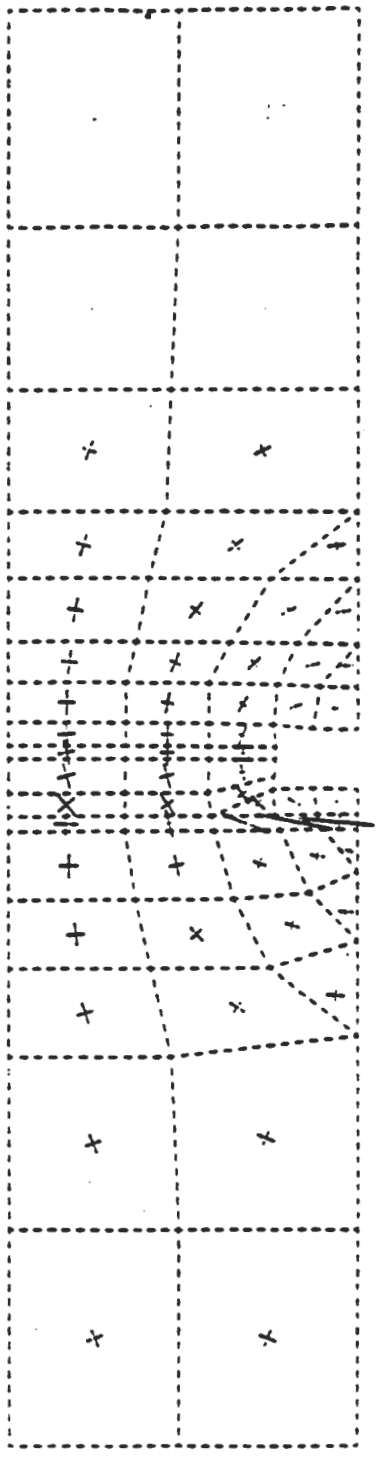

Figure 12-20

STORAGE ROOMS
PRINCIPAL STRESSES AND DEFORMED SHAPE
10 YEARS AFTER EXCAVATION

centerline and the predicted wall deformation is nearly as large. However, the floor heave is still very small. Also, some slippage has occurred along the clay seams. This is graphically depicted as a slight horizontal disjointing of the lines that form the element boundaries along a clay seam.

At 6.5 years after excavation, the predicted deformed shape of the storage room shows much downward deformation in the roof beam at its centerline. The floor has heaved slightly upward, with the upward displacement being somewhat more noticeable in the center of the room. The analysis shows very little deformation in the anhydrite bed even after 10 years. Based on the small amount of floor heave, it appears that the stiff anhydrite bed diminishes the amount of floor creep by supporting a large amount of lateral pressure. However, because there is a potential for the anhydrite bed to fail locally at about 8.5 years after excavation, it may not be able to support this large amount of lateral pressure. This may result in a higher creep rate in the floor than predicted by the model.

As discussed in Chapter 11, laboratory derived creep constants underpredicted actual closure in the test rooms. Thus, back calculation of average creep parameters was made using either measured roof-to-floor or wall-to-wall closure data. The effectiveness of the model simulation techniques used to derive the creep parameters and extrapolate closure behavior were discussed in detail in Chapter 11, subsection 11.3.2.5. Because MB-139 was assumed to be linearly elastic with infinite strength, the numerical modeling underpredicted floor heave but overpredicted roof sag. However, the overall roof-to-floor closure is reasonably well predicted by the model.

In order to show the effect of geometry and extraction on the closure rate, extrapolations of the in situ closure histories for the test rooms and various size drifts, as well as the calculated roof-to-floor and wall-to-wall closures for the storage rooms were plotted for comparison (Figures 12-21 and 12-22). Similar calculations were made using the

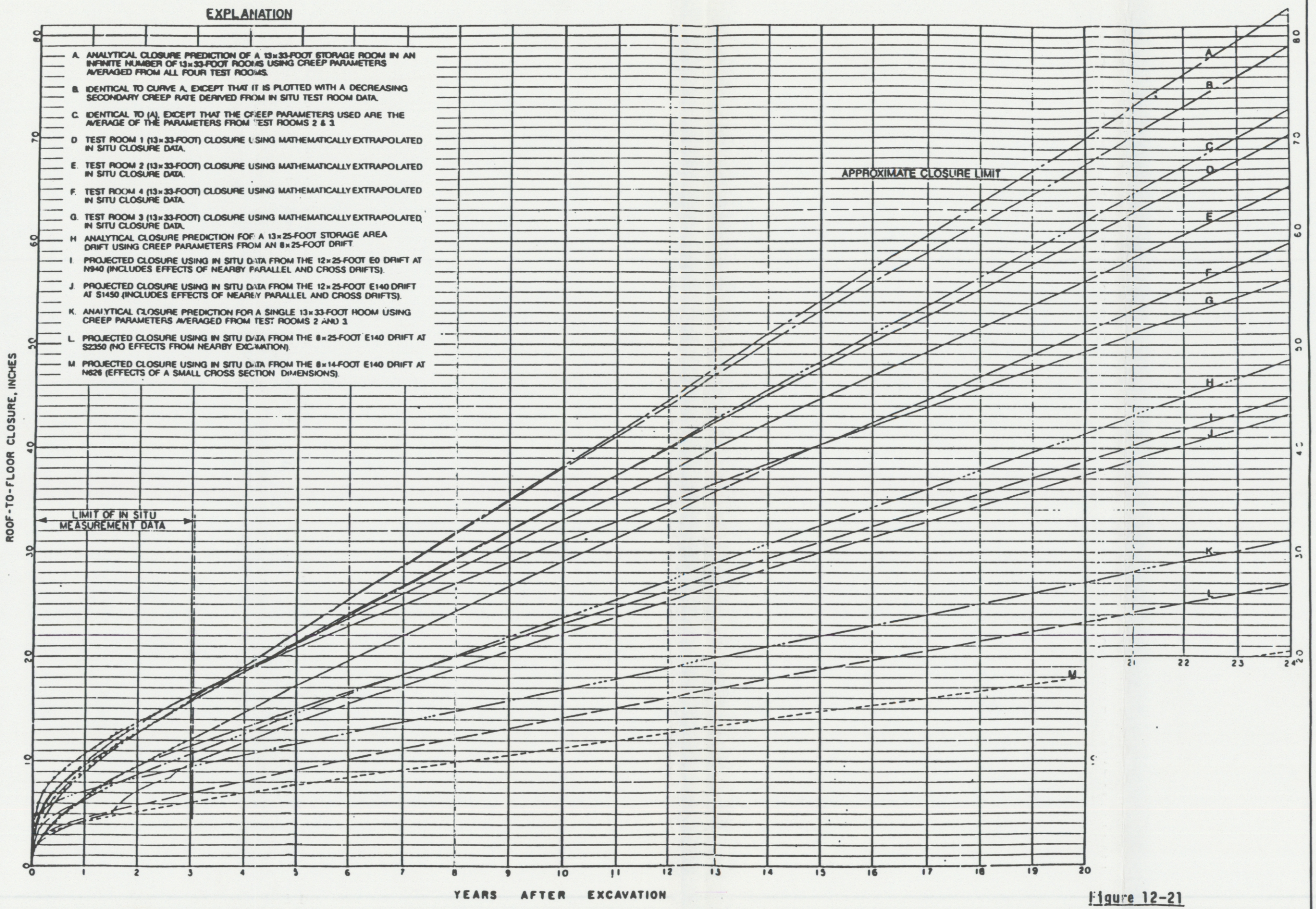


Figure 12-21

ROOF-TO-FLOOR CLOSURE
GEOMETRY AND EXCAVATION EFFECTS

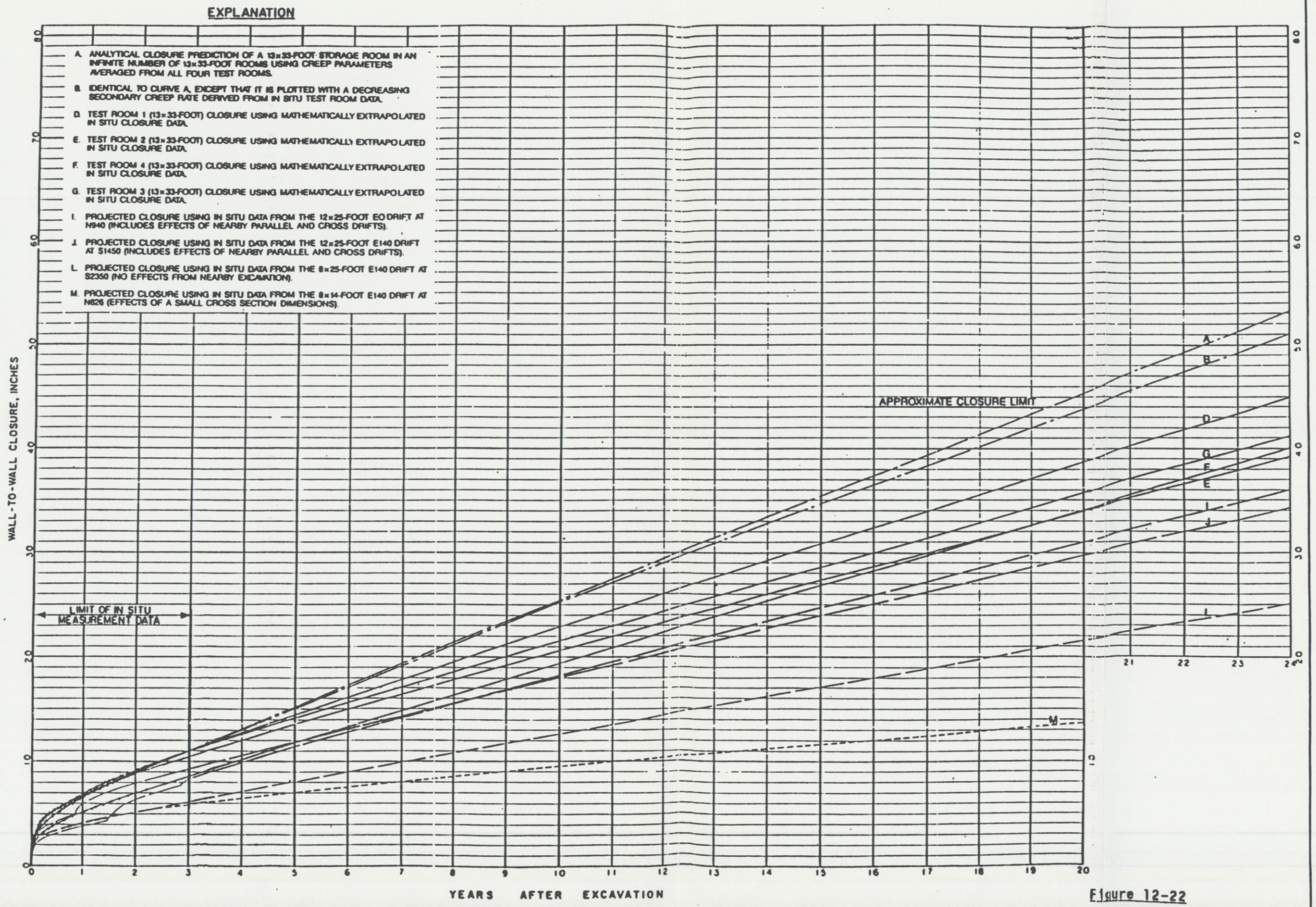


Figure 12-22

WALL-TO-WALL CLOSURE
GEOMETRY AND EXCAVATION EFFECTS

average creep parameters for the two interior 13 x 33-foot test rooms and using an infinite array of rooms to indicate the sensitivity of the value of the parameters. The same parameters were also used in the calculations of a single 13 x 33-foot room model to determine the effects of extraction on the number of rooms in an array. The descriptions of the closure curves plotted on Figures 12-21 and 12-22 are as follows:

(A) Analytical closure prediction of a 13 x 33-foot storage room in an infinite number of 13 x 33-foot rooms using creep parameters averaged from all four test rooms.

(B) Identical to curve A, except that it is plotted with a decreasing secondary creep rate derived from in situ test room data.

(C) Identical to curve A, except that the creep parameters used are the average of the constants from Test Rooms 2 and 3.

(D) Test Room 1 closure using mathematically extrapolated in situ closure data.

(E) Test Room 2 closure using mathematically extrapolated in situ closure data.

(F) Test Room 4 closure using mathematically extrapolated in situ closure data.

(G) Test Room 3 closure using mathematically extrapolated in situ closure data.

(H) Analytical closure predicted for a 13 x 25-foot storage area drift using creep parameters from an 8 x 25-foot drift.

(I) Projected closure using in situ data from the 12 x 25-foot E0 drift at N940 (includes effects of nearby parallel and cross drifts).

(J) Projected closure using in situ data from the 12 x 25-foot E140 drift at S1450 (includes effects of nearby parallel and cross drifts).

(K) Analytical closure prediction for a single 13 x 33-foot room using creep parameters averaged from Test Rooms 2 and 3.

(L) Projected closure using in situ data from the 8 x 25-foot E140 drift at S2350 (no effects from nearby excavation).

(M) Projected closure using in situ data from the 8 x 14-foot E140 drift at N626 (effects of small cross section dimensions).

As expected, the two interior test rooms (Test Rooms 2 and 3) had more closure and higher closure rates during the first year than the outer rooms (Test Rooms 1 and 4). This is due to the fact that Test Rooms 2 and 3 were excavated before Test Rooms 1 and 4. However, Test Rooms 1 and 4 exhibit higher closure rates during the secondary creep stage. This is consistent with the stress arch principle.

An evaluation of these 13 closure curves indicates that geometry and extraction ratio strongly impact the total closure in a seven-room panel within an eight-panel storage area and that the rate of closure will be faster than the extrapolated curves for a test room within the four-room test panel. For conservatism, Curve A (Figures 12-21 and 12-22) is used for storage room analysis, prediction and validation.

Curve A on Figure 12-21 represents the roof-to-floor closure prediction using the average creep parameter values for Test Rooms 1 through 4. These values were previously presented in Chapter 11, Table 11-12. In

the first year following excavation, the roof-to-floor closure curve is non-linear. The primary creep closure rate is very fast, as shown by the steeply sloped region in the first 3 months. Two and one half inches were added to the measured closure values to compensate for the lack of early closure data (Chapter 11). During secondary creep, the curve flattens and becomes approximately linear with a closure rate of approximately 3 inches per year. This closure prediction shows a closure of approximately 22 inches at 5 years after excavation and 54 inches at 15 years after excavation.

Curve A on Figure 12-22 represents the wall-to-wall closure prediction using the average creep parameter values for Test Rooms 1 through 4. These values were previously presented in Chapter 11, Table 11-13. As with the roof-to-floor closure, the wall-to-wall closure is non-linear in the first year following excavation. Again, the closure rate due to primary creep is initially very fast in the first 3 months as shown by the steep slope of the curve. Two inches were added to the measured closure values, as discussed in Chapter 11, to compensate for the lack of early closure data. The curve eventually flattens during the secondary creep phase and becomes approximately linear with a closure rate of about 2 inches per year. The wall-to-wall closure prediction shows a closure of approximately 15 inches at 5 years after excavation and 36 inches at 15 years after excavation.

When the storage rooms are fully occupied by waste and backfill material, the closure of the room will be limited by the ability of the contents to be compacted. Assuming that the volume of the waste container can be compacted by 40 percent and the volume of the backfill material by 15 percent, the roof-to-floor closure is predicted to have a maximum value of 66 inches and the wall-to-wall closure a maximum value of 44 inches. This maximum closure would occur after about 18 years for vertical closure and 19 years for horizontal closure (Figures 12-21 and 12-22). A reduction in the closure rate after the wall and roof surfaces begin compacting the backfill material and exerting pressure on the waste containers has not been considered.

Curve A on Figures 12-21 and 12-22 represents the most conservative estimates of storage room closure. Therefore, values from these curves were used in evaluating the reference design against the design criteria and design bases requirements. The design bases allow up to 12 inches of closure in the first 5 years after excavation in order to maintain a 16-inch space for ventilation and backfill equipment and to maintain a 12-foot minimum clearance for storage equipment. The estimated vertical closure in 5 years using curve A is about 22 inches. This 10 inch increase over the design basis limit could be accommodated by increasing the reference design room height from 13 feet to 13 feet 10 inches. This would be satisfactory for permanent storage. Another way to accommodate the increased closure and still maintain the 16-inch ventilation space (Figure 12-3) is to eliminate the backfill or reduce its thickness covering the CH containers to 6 inches or less. Deleting the salt backfill would require a change in the design criteria.

The solution to the increased vertical closure is not so simple for permanent storage, however. If at the end of the 5-year demonstration period, a decision is made requiring the stored waste to be retrieved, the design criteria assume that it will take twice as long to retrieve waste as it took to store it. This would result in a room being an additional 10 years old before retrieval is completed. Under these circumstances, a 15-year old room would have a closure of 54 inches, based on Curve A. Assuming that a storage room was excavated to the maximum allowable height of 14 feet, the closure would be 14 inches more than could be accommodated (24 inches for closure allowance, including 12 inches allowed by the design basis and 12 inches for the increase in room height from 13 feet to 14 feet, and 16 inches for ventilation space). This would result in the backfill being compressed and in the possible crushing and breaching of the waste containers. Because this scenario does not comply with the design criteria requirements, other alternatives must be considered.

These alternatives, including modification of the design criteria, are presented in subsection 12.6.2. Two considerations must be addressed here, however, to support the recommendations. First, the 10 year maximum retrieval period assumed by the design criteria is very conservative. Should retrieval be conducted on a three shifts per day basis, rather than the assumed one shift per day, no room would be older than 7 years by the time its waste was retrieved. Based on Curve A, a 7 year old room, from the time of initial excavation, would have a closure of about 28 inches. Assuming a room was excavated to the 14-foot high maximum and allowing 24 inches for closure, the waste containers will not be crushed or breached. However, the ventilation space will be reduced to 12 inches. This could be tolerated because the maximum 28-inch closure will be at the room centerline; additional ventilation space will be gained closer to the room walls. Alternatively, the thickness of the salt backfill over the containers could be reduced or eliminated to maintain the ventilation.

The second consideration supporting the recommendations is that a reduction in room closure can be gained by modifying the excavation technique. A panel of rooms could be excavated to the reference design dimension of 13 to 14 feet high. After a year of closure, these openings will be closing at the rate determined by secondary creep. At this time the rooms could be trimmed to 14 feet high. Trimming will remove the salt that has moved into the room during the year and provide a full dimensioned room that will close at the rate determined by secondary creep. Based on an average secondary creep closure rate of 3 inches per year, the rooms would have the following predicted closures after trimming:

| | |
|---|---|
| 5 years | 15 inches |
| 7 years | 21 inches |
| 10 years | 30 inches |
| 15 years | 45 inches |

Should the retrieval be effected within 7 years after trimming, a

trimmed 14-foot high room with 21 inches of closure would meet all of the retrieval requirements without further modification.

In order to gain the reduced closure benefits of secondary creep, the amount of trimming must be kept to a minimum. The rooms should initially be excavated as close to the 14-foot high maximum dimension as possible. The trimming operation a year later should remove no more salt from the floor than necessary to enlarge the room height to 14 feet. This small amount of trimming will minimize the increase in closure that typically follows major re-excavation, as has already been experienced at the WIPP during floor lowering in some drifts (Chapter 10, Figure 10-6, and this chapter, Figure 12-21, Curve J). This is discussed in detail in the next subsection.

The width of the storage rooms presents similar problems. The reference design specifies a minimum room width of 33 feet and a maximum width of 34 feet. Again, Curve A on Figure 12-22 represents the most conservative estimate of horizontal closure. The design basis allows 9 inches of horizontal closure in the first 5 years (4 1/2 inches for each wall). The space between the wall and the waste containers (Item 10, Figure 12-3), for the storage area reference design, will be backfilled with loose salt.

The predicted wall-to-wall closure in 5 years, using Curve A, is about 15 inches. This closure will result in compaction of the salt backfill and possibly in the crushing and breaching of some containers. This condition is suitable for permanent storage. Should retrieval be required, the predicted closure for a 15-year old room would be 36 inches. If it is assumed that the room is excavated to its maximum dimensions, as discussed earlier, the room would be 34 feet wide with the waste containers 15 inches from each wall. This 30 inches of horizontal clearance is not adequate to meet the design criteria requirements for the crushing and breaching of containers, even if backfill were not required. In order to meet the intent of the design criteria, the reference design must be modified. The five alternatives presented in subsection 12.6.2 include modifications to accommodate this horizontal closure.

As is the case with vertical closure in the storage rooms, timing of retrieval operations and two-stage excavation can be used to reduce the wall-to-wall closure. Should three shifts per day be used during retrieval and if the rooms are a maximum of 7 years old, then wall-to-wall closure would be about 20 inches. If the storage operation is conducted on a first emplaced/first retrieved basis and retrieval is effected before a room exceeds an age of 6 years, horizontal closure would be further reduced to 18 inches. Both of these operational changes would decrease the possiblity of crushing or breaching the waste containers.

Two-stage excavation gains additional closure benefits. If a room is initially excavated to the maximum design width of 34 feet and after a year of closure trimmed to 34 feet, closure would be controlled by secondary creep. Based on a wall-to-wall secondary creep closure rate of 2 inches per year, the rooms would have the following predicted closures after trimming:

| | |
|---|---|
| 5 years | 10 inches |
| 7 years | 14 inches |
| 10 years | 20 inches |
| 15 years | 30 inches |

This will further minimize crushing or breaching of the waste containers.

It is expected that increasing the distance between the waste canisters and the wall by increasing the room to the maximum design width of 34 feet, thereby increasing the amount of loose salt backfill in this space, will increase the time it takes for horizontal closure to consolidate the backfill and transfer sufficient load to crush the waste canisters. This, coupled with the faster retrieval schedules discussed previously and the fact that the backfill will not be completely confined, will minimize crushing and breaching of the canisters as required by the criteria. How much it will be minimized

cannot be determined until the results from in situ experiments dealing with backfill consoldiation and container stability become available.

12.3.3.2 Storage Area Drifts

The results of the analysis of the storage area drifts with dimensions of 8 x 25 feet were plotted at various integration time steps. These integration steps correspond to real times immediately after floor lowering and 5 years after initial excavation. The effective stress and effective creep strain, principal stresses, and deformed shape were plotted at these times based on the roof-to-floor creep parameters for a representative station (Chapter 10).

Effective Stresses and Effective Creep Strains. Figures 12-23 and 12-24 show the calculation for effective stress distribution in those elements of the finite element model near the drift opening. As with similar plots for the 8 x 25-foot drifts discussed in Chapter 10, each contour increment represents an effective stress interval of 100 ksf.

The plot of effective stress immediately after floor lowering shows the impact on the stress distribution as a result of the drift height modification. This change in effective stress precipitates a concomitant increase in the creep rate. This appears as a sharp but short increase in slope on the roof-to-floor closure versus time curve (Chapter 10, Figure 10-6, and this chapter, Figure 12-21, Curve J).

At the end of 5 years, the anhydrite bed shows a very large effective stress gradient from top to bottom in the vicinity of the drift floor due to the stiffness of the bed. Maximum effective stresses are in excess of 1,000 ksf.

The effective creep strains have concentrated in the region around the drift opening and intensify with time. A rough linear extrapolation of effective creep strain beyond 5 years indicates that the maximum

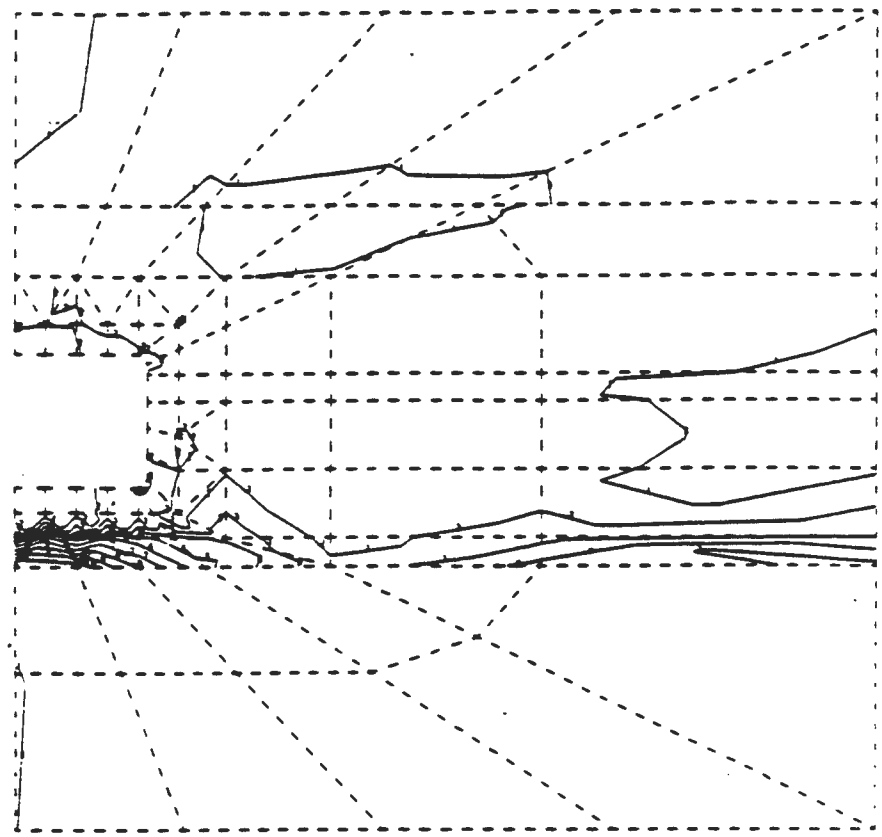

| CONTOUR | $\bar{\sigma}$(ksf) |
|---|---|
| 1 | 100 |
| 2 | 200 |
| 3 | 300 |
| 4 | 400 |
| 5 | 500 |
| 6 | 600 |
| 7 | 700 |
| 8 | 800 |
| 9 | 900 |
| 10 | 1000 |

Figure 12-23

STORAGE AREA DRIFTS
EFFECTIVE STRESS DISTRIBUTION IMMEDIATELY AFTER FLOOR LOWERING

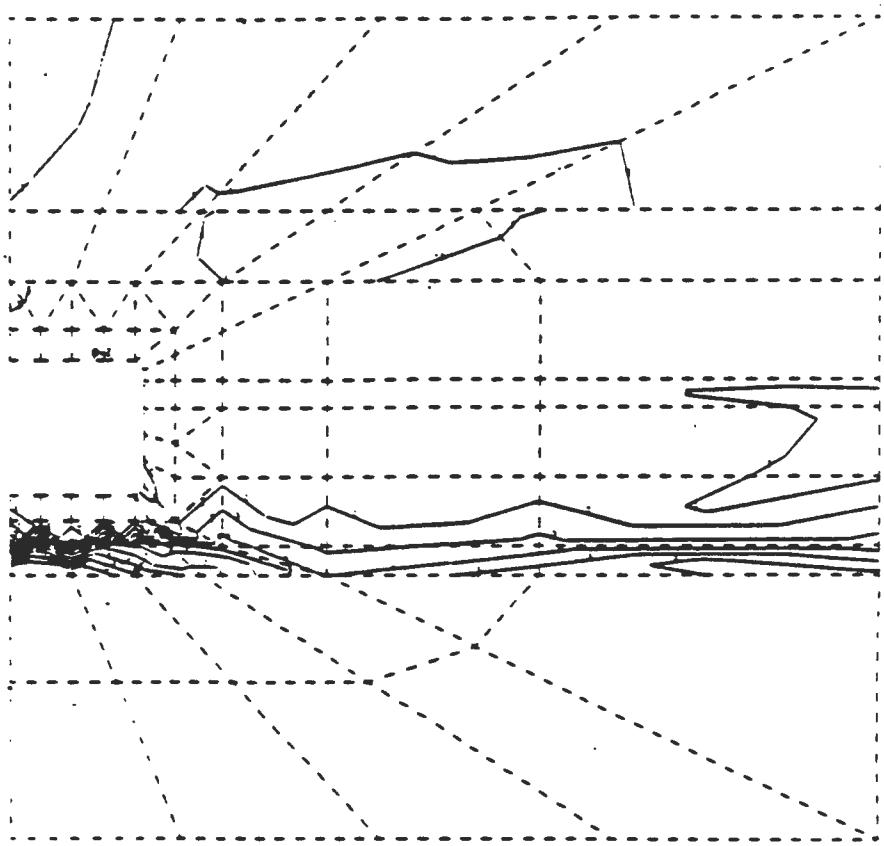

| CONTOUR | $\bar{\sigma}$(ksf) |
|---|---|
| 1 | 100 |
| 2 | 200 |
| 3 | 300 |
| 4 | 400 |
| 5 | 500 |
| 6 | 600 |
| 7 | 700 |
| 8 | 800 |
| 9 | 900 |
| 10 | 1000 |

Figure 12-24

STORAGE AREA DRIFTS
EFFECTIVE STRESS DISTRIBUTION 5 YEARS AFTER EXCAVATION

average effective creep strain may reach 16 percent at about 20 years after excavation. Based on failure criteria for halite obtained from laboratory test data (Chapter 6), failure in halite may start at about 15 percent. However, the numerical modeling indicates that the effective creep strain drops off sharply away from the opening. It is therefore expected that high effective strain would not result in a large scale failure in halite.

Principal Stresses. The plots of principal stresses (Figures 12-25 and 12-26) consistently show the "arch" pattern which develops around the drift in order to transfer loads past the drift opening. The arch is shown to migrate away from the opening with time. As expected, the magnitude of major principal stress is greater in the corners of the drift and in the underlying anhydrite bed. The anhydrite in particular is subjected to large stresses because it is the only material that has been assumed in the model to not creep; it therefore "stores" a large amount of energy in the form of elastic strain.

Deformation and Closure. Figure 12-27 shows the deformed shape 5 years after drift excavation, or approximately 3 years after floor lowering. It should be noted that, while both the roof and walls are creeping inward, the upward floor heave is small by comparison. This phenomenon is due to the stiffening effect of the underlying anhydrite bed.

The stress redistribution that occurs as a result of modifying the drift height is the driving force behind the large roof and wall deflections that are the most prominent features of the plot at 5 years. A close examination of the 5-year deformed plot shows that clay seam slippage has occurred. The most noticeable slippage has occurred in the clay seam located about 8 feet above the existing roof. Here, the maximum horizontal relative displacement across the seam is approximately 3 1/2 inches. Actual relative displacement will be lower because the clay seams have a finite friction coefficient.

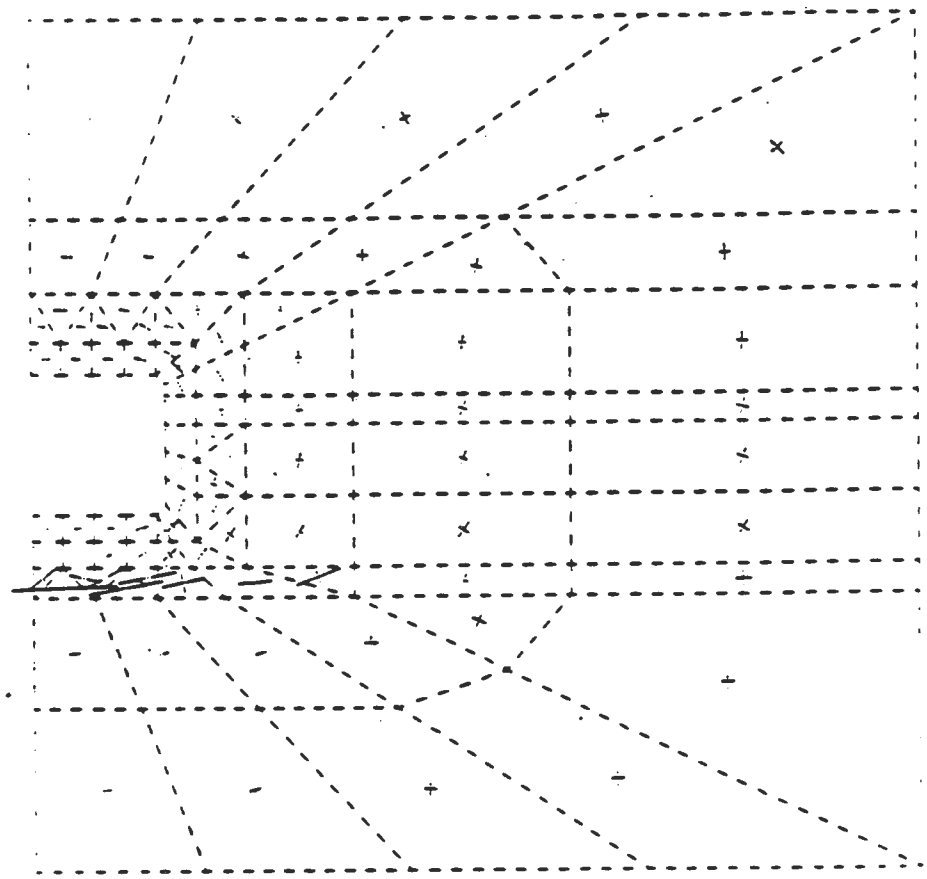

Figure 12-25

STORAGE AREA DRIFTS
PRINCIPAL STRESSES IMMEDIATELY AFTER EXCAVATION

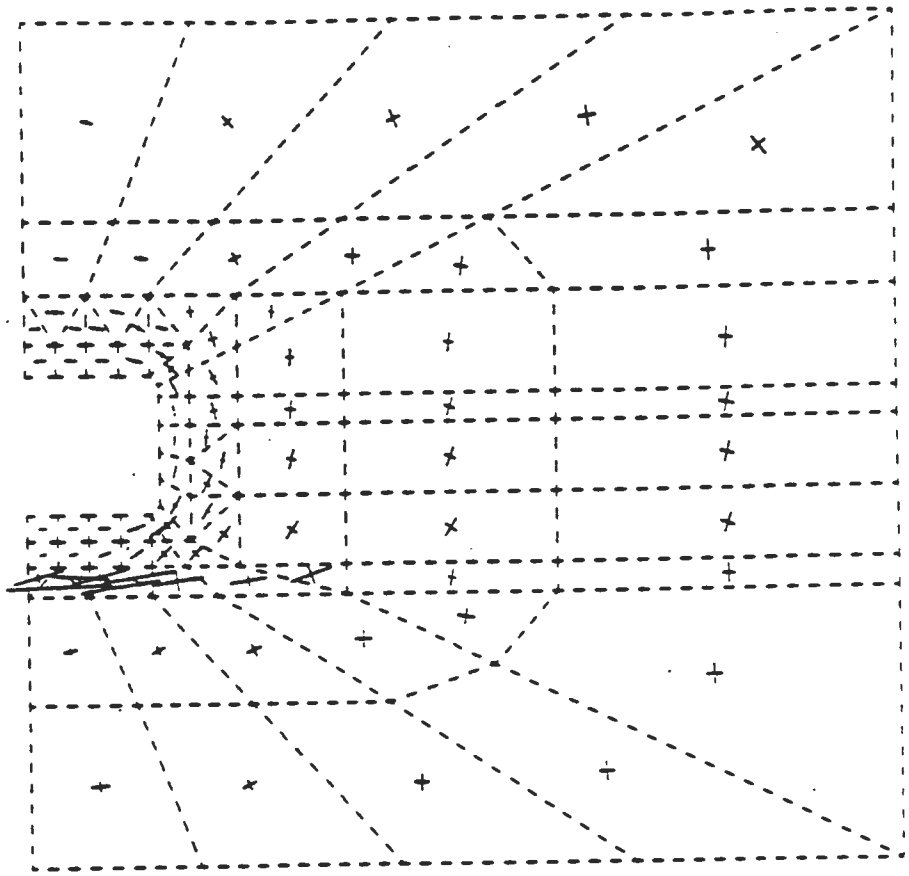

Figure 12-26

STORAGE AREA DRIFTS
PRINCIPAL STRESSES 5 YEARS AFTER EXCAVATION

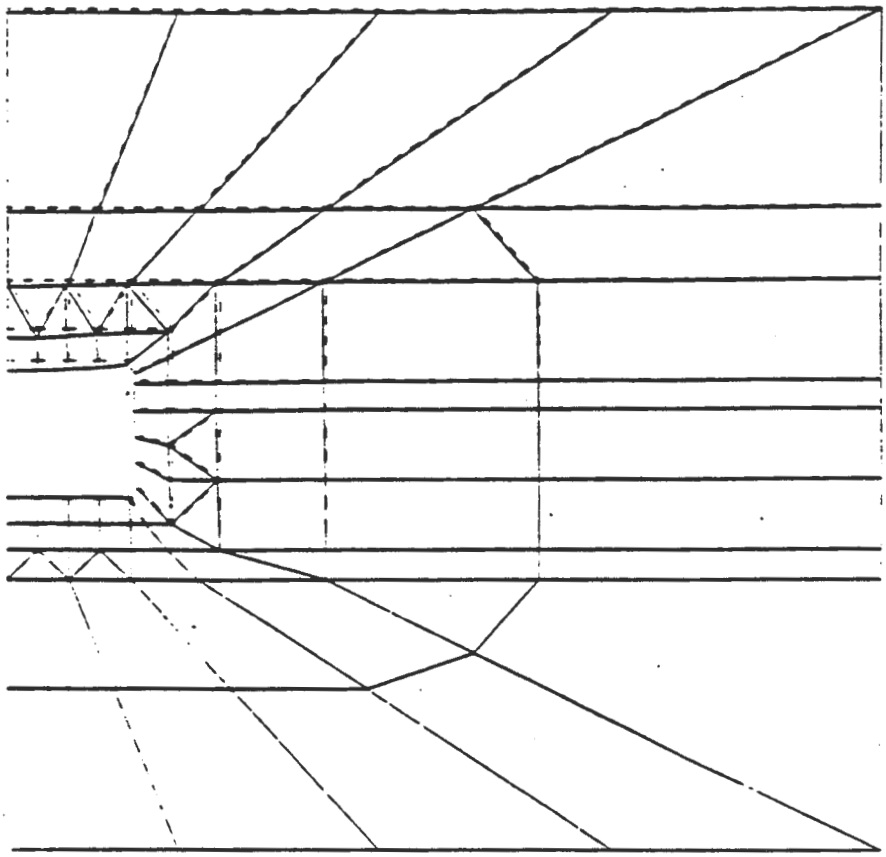

Figure 12-27

STORAGE AREA DRIFTS
DEFORMED SHAPE 5 YEARS AFTER EXCAVATION

Figure 12-28 demonstrates the effect of increasing the vertical dimension of a storage area drift at some point after initial excavation. The finite element model is calibrated with in situ data. It models an 8 x 25-foot drift that has its height increased to 13 feet by excavating an additional 5 feet from the floor. The 8 x 25-foot drift exhibits typical closure; that is, the curve shows high rate of closure during primary creep and a nearly constant closure rate during secondary creep. When the floor is lowered (in this case 2.3 years after excavation), primary creep is temporarily reinitiated. The secondary creep phase is eventually re-established, but with some difference. The slope of the curve during secondary creep after floor lowering is slightly steeper than the secondary creep prior to floor lowering. The rate of closure does not return to the initial rate, but rather reflects the new, larger dimension of the drift. In this model, the modified drift has 11 inches of vertical closure 5 years after initial excavation.

The same computation included wall-to-wall closure. The effects of floor lowering were the same as for roof-to-floor closure. After floor lowering, primary creep was reinitiated and followed by a new secondary creep phase with a slightly higher closure rate. Five years after initial excavation, the predicted horizontal closure is about 8 inches.

A rough extrapolation of the predicted roof-to-floor and wall-to-wall closures based on model simulation and resulting secondary creep closure indicates the following:

| Time (Years) | Roof-to-Floor Closure at 2.0 inches/year (inches) | Wall-to-Wall Closure at 1.6 inches/year (inches) |
|---|---|---|
| 10 | 20 | 16 |
| 15 | 30 | 24 |
| 20 | 40 | 32 |
| 25 | 50 | 40 |

The maximum effective strain around the drift opening reaches 6 percent about 8 years after excavation. Based on in situ observations and the

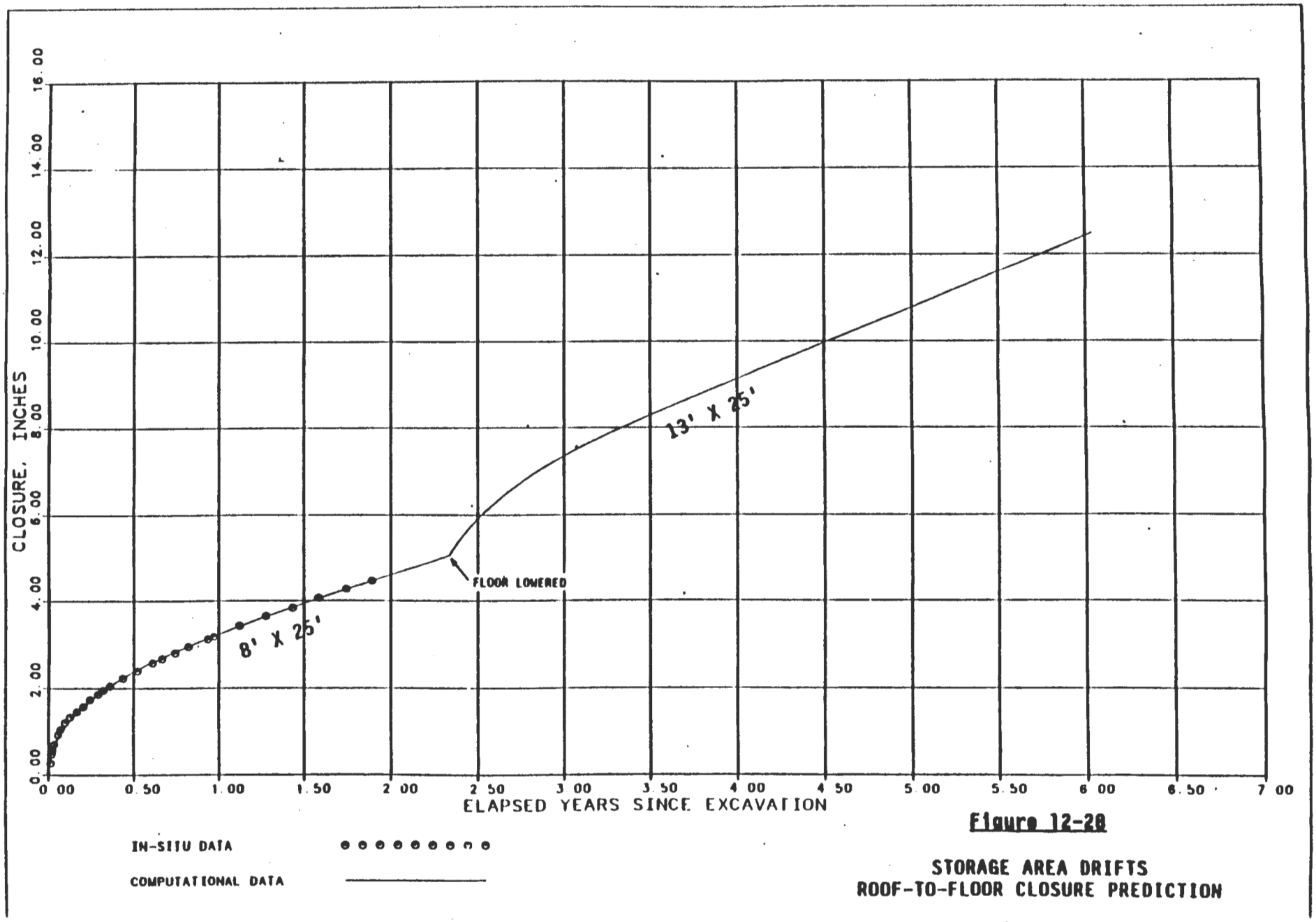


**Figure 12-20**

**STORAGE AREA DRIFTS**
**ROOF-TO-FLOOR CLOSURE PREDICTION**

results of modeling the test rooms, this effective strain of 6 percent may not result in instability of the drifts. However, in 15 years the effective strain at the excavation surface will exceed 10 percent locally and the roof-to-floor closure will be nearly 30 inches. According to the failure criterion, based on laboratory tests on samples of halite (Chapter 6), the halite is supposed to fail at about 16 percent effective strain. Therefore, minor surface deterioration can be expected and some trimming will be required to permit operation of the waste storage equipment. Because the effective strain decreases rapidly within the salt, trimming on the order of only a few feet may be needed after 20 years.

The storage drifts, as with the storage rooms, must accommodate greater than predicted closure. The reference design provides for waste storage in the storage area drifts only after all of the main storage rooms are filled. Since this would occur toward the end of the operating phase, waste in these drifts would not be subject to retrieval under the provisions governing the 5-year demonstration period. Waste stored in the drifts would be on a permanent basis.

Increased closure does impact waste emplacement and emplacement machinery. In the reference design, the greatest age a drift would reach before waste was emplaced would be about 15 years. At this age, based on the calculated closure for a 13 x 25-foot drift, the predicted roof-to-floor closure would be about 25 inches and the predicted wall-to-wall closure would be about 20 inches. The storage drifts would have to be trimmed to permit proper storage and equipment clearance. Similarly, the storage drifts and crosscuts less than 25 feet wide would also require trimming.

#### 12.3.3.3 Intersections

The modeling of intersections is an expensive, three-dimensional analysis. However, to estimate closures at a storage room intersection, a simplified method can be utilized in place of a

three-dimensional analysis. The following discussion develops the mathematical relationship for computing the roof-to-floor closure at the intersections.

When normalized time is sufficiently large, analytical results have consistently shown that room closure in the normalized time domain can be estimated by the following equation:

$$u = u^*_o + \dot{u}^*_f \, t^* \qquad \text{when: } t^* > 1\text{x}10^{-11} \text{ ksf}^{-4.9} \qquad (12\text{-}3)$$

where: $t^* = C[t + \frac{A}{z}(1 - e^{-zt})]$ is the normalized time;

$u^*_o$ is a constant; and

$$\dot{u}^*_f = \lim_{\Delta t \to 0} \frac{\Delta u}{\Delta t^*}$$

Closure for the storage room intersections, in normalized time, was calculated using the creep parameters discussed in Chapter 11 and in situ data collected near the intersections of the N1420 drifts with Rooms L1 and L2. As expected, the closure history follows equation 12-3 when the normalized time is greater than $8.0\text{x}10^{-12}$ ksf$^{-4.9}$. The average values of $u^*_o$ and $\dot{u}^*_f$ for Rooms L1 and L2 were calculated to be 0.0450 feet and $1.967\text{x}10^{12}$ ksf$^{-4.9}$, respectively.

After determining the values of $u^*_o$ and $\dot{u}^*_f$, equation 12-3 can be utilized for computing the closure at a storage room intersection. Figure 12-29 shows the roof-to-floor closure prediction at a storage room intersection.

## 12.4 STORAGE AREA PLUGS

The design criteria require that the storage area reference design contain provisions for the isolation of the waste storage panels from each other. The reference design contains recommended locations for plugs which would provide this isolation. It does not, however,

provide a specific design for the plugs. The design of the plugs is currently under investigation by SNL (ref. 12-8).

The recommended locations for the plugs are shown on Figure 12-30. The plugs will be constructed in the entry drifts to each panel. The four main access drifts to the storage area will also contain plugs. The section of the entry drifts leading from the access drifts to the first storage room is 200 feet long. The reference design contains provisions for the construction of approximately 100-foot long plugs centered in this 200-foot section of each entry drift.

Originally, the reference design contained entry drift cross section dimensions of 13 feet high and 33 feet wide. These dimensions are the same as those for the storage room reference design and were chosen based on waste container stacking considerations. This design was modified as the result of a meeting between the DOE and all project participants (ref. 3-2). The reference design modification was based on the necessity to minimize the cross section area of the plugs while maintaining sufficient room for the excavation and waste storage equipment.

The reference design modification for the entry drifts is shown on Figure 12-31. The 100-foot long section containing the plug has been reduced in cross section to 13 feet high and 14 feet wide for the exhaust drift and 20 feet wide for the intake drift. However, the operating contractor may further modify these dimensions to accommodate equipment. The four main access drifts will retain their original cross section dimensions in the areas of the planned plugs.

The plug shown on Figure 12-31 would consist of multiple components as described in reference 12-8. These components include a central core of bentonite or bentonite-based mix, salt-brick bulkheads, and cement-based bulkheads. Prior to constructing the multiple-component plug in an entry drift, the operating contractor must investigate the disturbed zone surrounding the drift. In particular, the occurrence of any fractures within and above MB-139, beneath the floor, and any

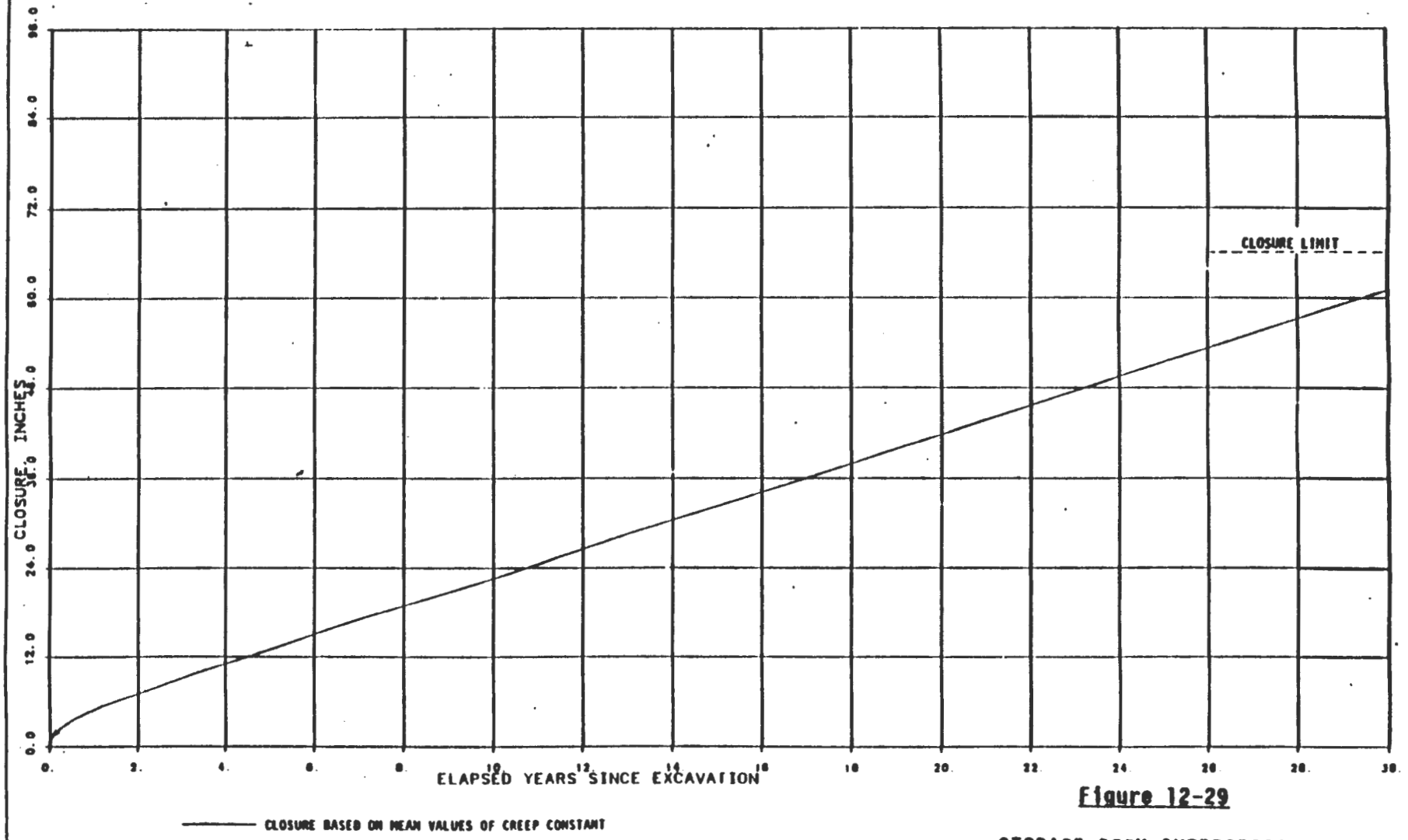


Figure 12-29

STORAGE ROOM INTERSECTION
ROOF-TO-FLOOR CLOSURE PREDICTION

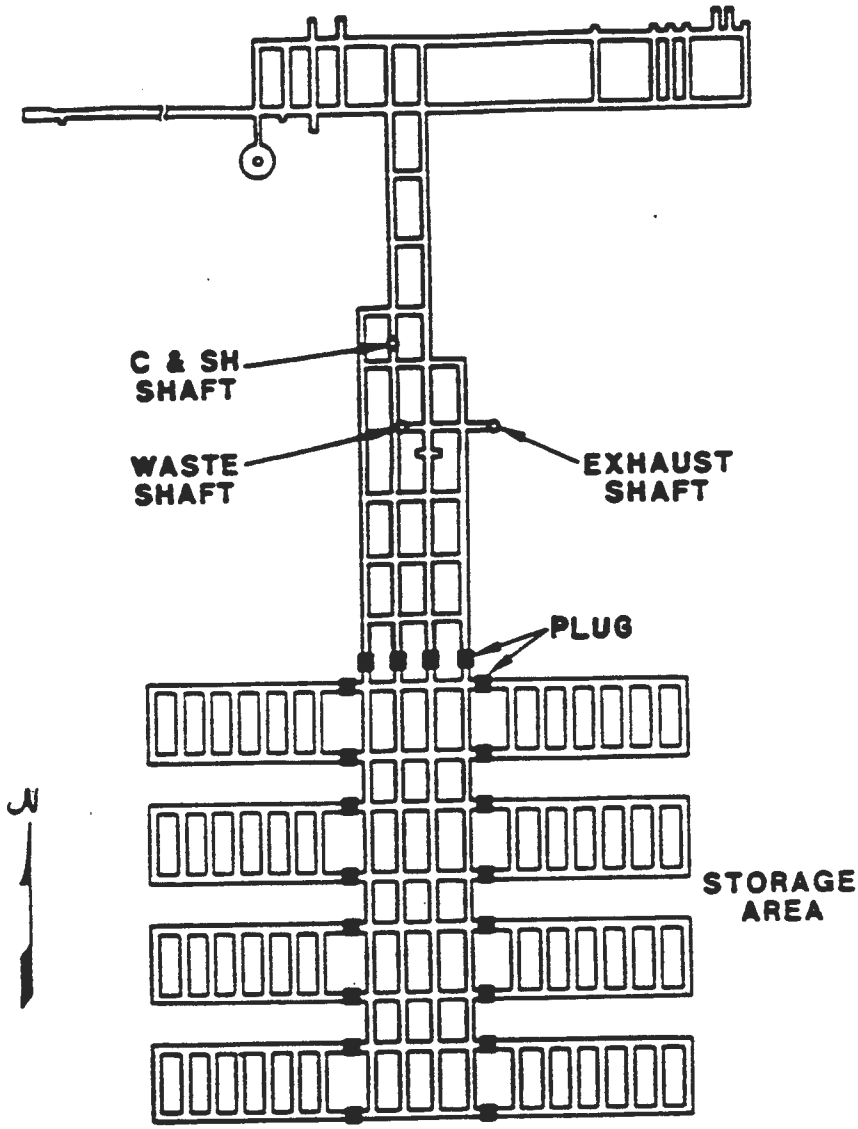


Figure 12-30

STORAGE AREA
PLUG LOCATIONS

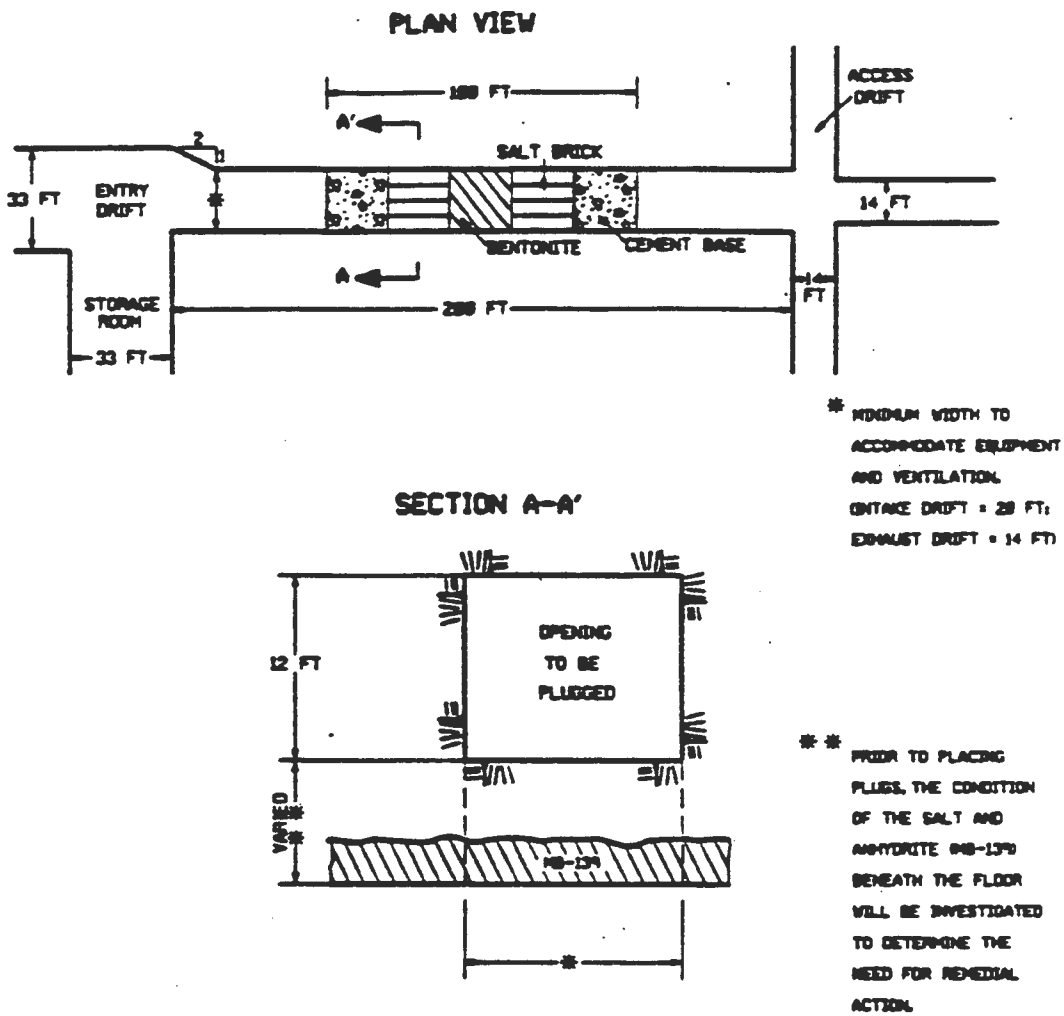


Figure 12-31

STORAGE AREA
PROPOSED PANEL PLUG REFERENCE DESIGN

separations at clay seams above the roof will need to be evaluated. If zones of unacceptable permeability are detected in the floor, the plug area should be lowered to remove the fractured zone and MB-139. Similarly, should any separations be found at clay seams above the entry drift, the roof should be excavated up through the highest seam exhibiting separation.

If the disturbed zone effects are not substantial, low-pressure grouting may be considered as an alternative remedial action. This would permit retention of the minimum cross section for the plug area. In addition, pressure grouting could be used in conjunction with excavation to treat deeper fractures, if present.

## 12.5 STORAGE ROOM BACKFILL

In accordance with the design criteria, the storage room reference design includes backfilling the rooms with crushed salt after waste emplacement. The storage area drift and room dimensional requirements are shown on Figures 12-2 and 12-3. The thickness of the salt backfill covering the waste packages shown on these figures is 1 to 2 feet. This is to be the thickness of the salt after placement and does not take into account backfill consolidation during room closure.

The only purpose for backfilling presented in the criteria is to provide fire protection in the storage rooms based on an accident scenario in which spontaneous ignition of the contents of a CH TRU waste container results in fire propagation to adjacent containers. Recent studies concerning the potential for spontaneous ignition in CH TRU waste containers have indicated that this is not a credible scenario. Although backfill is a design criteria requirement and therefore must be incorporated into the reference design, the results of these studies indicate that backfill will not be necessary for fire protection.

## 12.6 CONCLUSIONS AND RECOMMENDATIONS

The following subsections present conclusions pertaining to validation of the WIPP storage area reference design and recommendations for design modifications to achieve validation of the reference design. These are based on a comparison of the design criteria, design bases and reference design configurations with the results of the analysis and evaluation of data collected during the design validation process.

### 12.6.1 Conclusions

The most significant finding of the design validation program is the difference between closure predicted from laboratory test data and the closure actually occurring in the underground facility. The storage area reference design configurations were designed before long-term in situ data were available. Closure rates were estimated using creep constants derived from the laboratory analyses of salt cores from borehole ERDA-9. These estimates resulted in the establishment of a closure limit of 12 inches in the first 5 years following excavation. Evaluation of the in situ data demonstrates that this closure limit is insufficient. The predicted closure based on laboratory analyses underestimates the actual closure at 3 years by about a factor of three (Figure 11-35). Establishing the causes for this underprediction of closure requires additional study and research and is beyond the scope of this report.

Vertical and horizontal closure demonstrated by the in situ data will not allow the reference design to meet the design criteria requirements. The waste containers will most likely be crushed and breached. Furthermore, because of the in situ closure the waste container stacking configurations and transport vehicle would not be compatible with the reference design room and drift configurations. In order for the reference design to comply with the design criteria, the storage area design configurations or the design criteria will have to be modified. Five alternative modifications are presented in the next subsection.

The analytical results for the storage area show the redistribution of stresses around the openings due to the effects of creep. Based on the computed vertical, horizontal and effective stresses, the magnitude of stresses immediately adjacent to the openings decreases and the stress arch around the openings migrates away with time. The maximum stress occurs immediately after excavation and is followed by relaxation due to creep behavior. Therefore, the stresses will not cause a future stability problem in the storage area except in MB-139, where a gradual buildup of stress may cause local failure of the anhydrite. This failure is expected to be in the form of floor slabbing and should not affect the structural performance of the openings nor hinder the waste storage operations. Investigations of the test room floors indicate that major fracturing has occurred only in the south half of Test Room 3 (Room T). All other floor fracturing has been minor.

The analysis shows the locations of effective creep strain concentrations at different times around the openings. Based on the predicted values of effective creep strain and the strain limit discussed in Chapter 6, effective creep strain may locally exceed the critical strain which is based on laboratory test data. However, this is not expected to disturb the overall structural stability within the limits required for safety during the 5-year demonstration period and permanent storage. Minor spalls and failures on the wall surfaces, similar to the ones discussed in Chapter 11, are expected to occur and can be easily identified and monitored. Scaling of tnese minor failures, when necessary, is considered a normal maintenance operation.

The facility stratigraphy is continuous and uniform. No anomalous conditions have been encountered that would jeopardize facility operations or waste storage integrity. The fracturing that is occurring beneath the test room floors may develop to some degree beneath the storage rooms. These fractures are not considered to be deleterious to storage room performance. There have been no occurrences of gas or brine in quantities that would adversely affect waste storage operations.

The storage area has been designed to accommodate panel plugs as required by the criteria. The reference design for the panel entry drifts contains a reduced cross section in the plug area. The minimum dimensions for the plug area will be dictated by operating requirements. The dimensions may also require alteration if disturbed zone effects are present that necessitate additional excavation.

An independent study has concluded that spontaneous combustion in the waste containers is not a credible event. In this case, crushed salt backfill will not be required for fire protection. Because it has been determined that the storage rooms will close at a rate faster than originally anticipated, deletion of the backfill requirement will provide additional allowance for vertical closure. This has favorable implications in terms of recommended modifications discussed in the next subsection.

### 12.6.2 Recommendations

The reference design will be validated when any of the following alternative modifications or combinations thereof are incorporated:

(1) Maintain the reference design room dimensions (13 to 14 feet high and 33 to 34 feet wide), retain the salt backfill but reduce the volume of waste to be stored and modify the waste stacking configuration in each room and entry drift (Figure 12-32). These changes would be required only during the 5-year demonstration period. Revise the criteria to require that retrieval operations be accomplished within 7 years of excavating each room. This will assure that the waste containers will not be crushed or breached. However, it will require a significant number of additional rooms during and after the demonstration period.

(2) Maintain the reference design room dimensions and the waste storage volume. Revise the criteria to delete the requirement for salt backfill and to require that if the

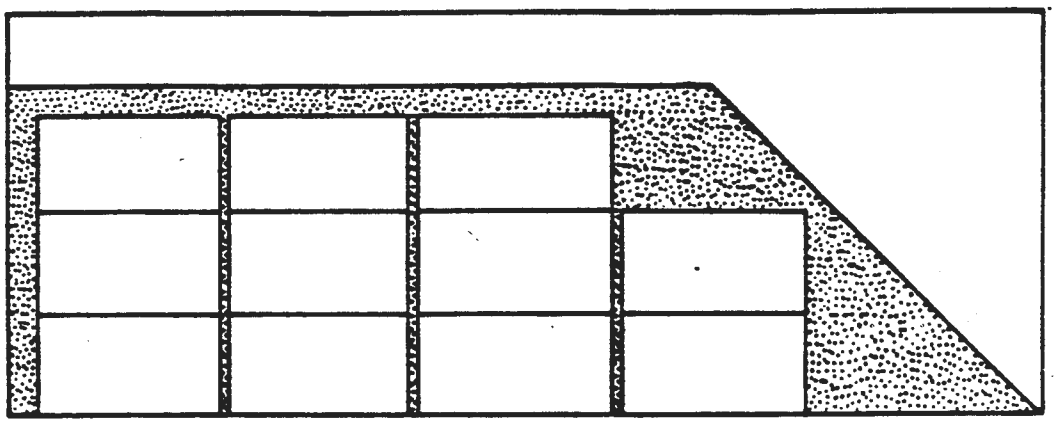

Figure 12-32

STORAGE AREA
MODIFIED WASTE STACKING CONFIGURATION

waste is to be retrieved it shall be done before the age of any room in which waste is being retrieved reaches 7 years. This will preclude the possibility of crushing and/or breaching any waste containers and will make retrieval easier and more rapid. No additional rooms will be required.

(3) Maintain the reference design room dimensions, the waste storage volume, and the salt backfill. Revise the storage operations during the 5-year demonstration period so that the waste stored first can be retrieved first. Excavate the rooms to 14 x 34 feet initially and then trim them to 14 x 34 feet a year later. Rooms having waste retrieved will not be older than 6 years and the wall-to-wall closure will be approximately 12 inches. This would minimize the crushing and breaching of the waste containers. The criteria are to be revised as stated under (5) of these recommendations. However, due to the first-in/first-out recommendation, more rooms will be required during the 5-year demonstration period to accommodate the expected volume of waste. Trimming to the final dimensions will also increase operating costs. The total number of rooms required will be the same as provided by the reference design.

(4) For the 5-year demonstration period, reduce the storage room width from 33 feet to 28 feet, maintain the 13 to 14-foot height, and reduce the pillar width to 84 feet. Maintain the first room for RH emplacement at 33 feet to 34 feet wide and 13 feet to 14 feet high as provided in the reference design. Reduce the volume of waste to be stored in each room and maintain the salt backfill. Excavate the rooms to 14 x 28 feet then, after approximately 1 year, trim them to 14 x 28 feet again. Provide for first-in/first-out emplacement and retrieval during the 5-year demonstration period. This will reduce the rate of creep to approximately

the rate for the 13 x 25-foot drifts. The potential for crushing and breaching of the waste containers will be minimized and the stability should be better than that for a 33-foot wide room. The total volume of excavation will be approximately the same. If this alternative is selected, additional engineering evaluation will be required.

(5) Maintain all of the features of the reference design. That is, maintain the storage room configuration of 13 feet high and 33 feet wide, maintain the salt backfill, maintain the planned volume of waste to be stored in each room and drift, and maintain the same optimized excavation plan for the 5-year demonstration period and permanent storage. Revise the design criteria to allow crushing and breaching of the CH waste containers during the 5-year demonstration period as well as during permanent storage. Also, revise the criteria requiring a demonstration of waste package handling to include a demonstration of the retrieval of crushed and breached containers prior to receiving waste. This alternative will not only demonstrate the safe retrieval of waste if required during the 5-year demonstration period but also at any time during permanent storage.

In addition to these recommended alternative modifications, the following modifications are recommended:

(6) The drifts used for storage will have to be maintained and trimmed to provide the required equipment and storage clearances. The closure rates are not critical for storage because these drifts will be used only for permanent storage near the end of the permanent storage period.

(7) Add additional rooms to compensate for the space occupied by the plugs in the entry drifts.

(8) Install instrumentation in the storage rooms to obtain in situ data to monitor storage room behavior.